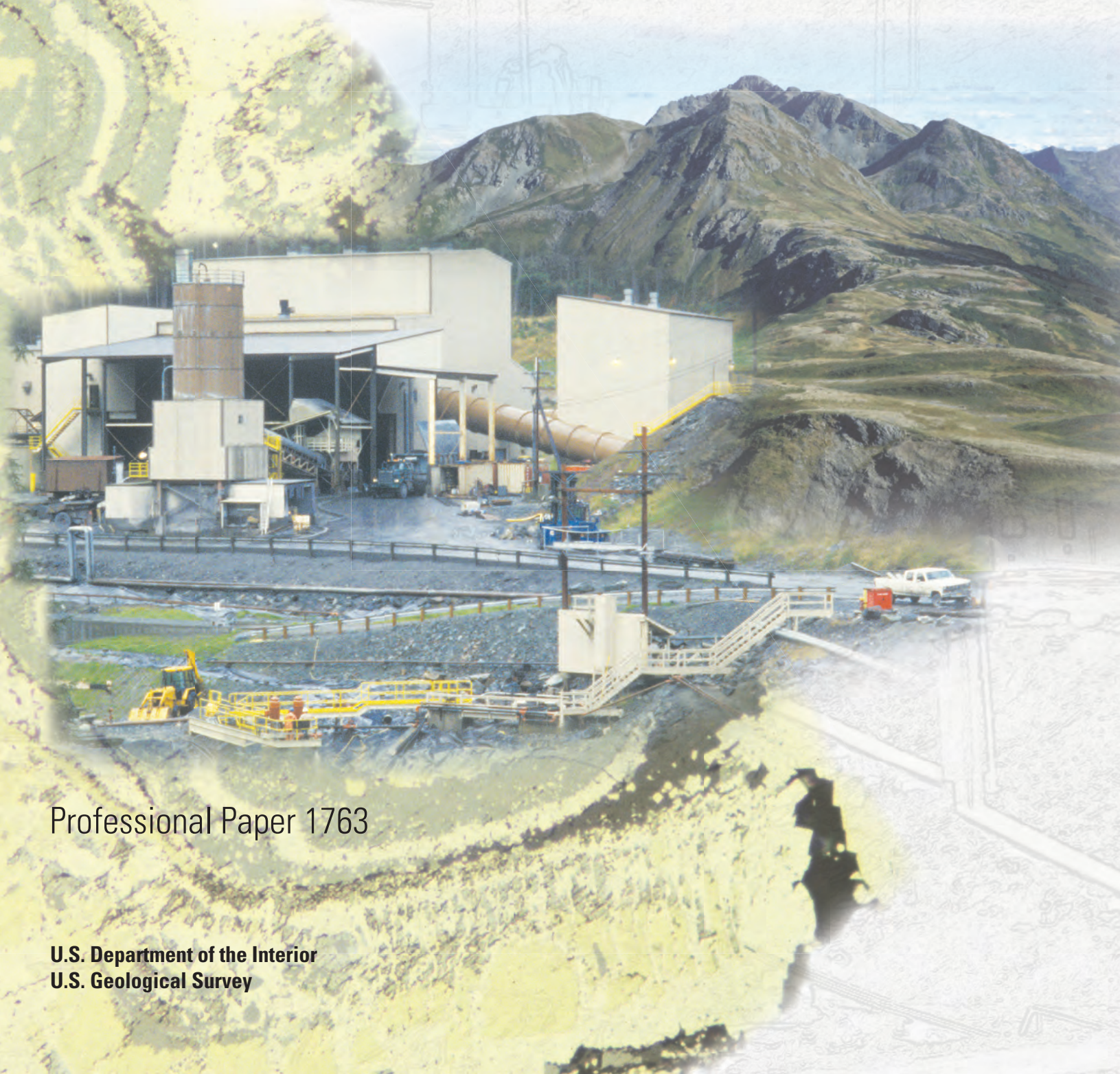




Prepared in cooperation with Kennecott Greens Creek Mining Company

Geology, Geochemistry, and Genesis of the Greens Creek Massive Sulfide Deposit, Admiralty Island, Southeastern Alaska



Professional Paper 1763

U.S. Department of the Interior
U.S. Geological Survey

Geology, Geochemistry, and Genesis of the Greens Creek Massive Sulfide Deposit, Admiralty Island, Southeastern Alaska

Edited by Cliff D. Taylor and Craig A. Johnson

Prepared in cooperation with Kennecott Greens Creek Mining Company

Professional Paper 1763

**U.S. Department of the Interior
U.S. Geological Survey**

U.S. Department of the Interior
KEN SALAZAR, Secretary

U.S. Geological Survey
Marcia K. McNutt, Director

U.S. Geological Survey, Reston, Virginia: 2010

For product and ordering information:
World Wide Web: <http://www.usgs.gov/pubprod>
Telephone: 1-888-ASK-USGS

For more information on the USGS—the Federal source for science about the Earth, its natural and living resources, natural hazards, and the environment:
World Wide Web: <http://www.usgs.gov>
Telephone: 1-888-ASK-USGS

Any use of trade, product, or firm names is for descriptive purposes only and does not imply endorsement by the U.S. Government.

Although this report is in the public domain, permission must be secured from the individual copyright owners to reproduce any copyrighted materials contained within this report.

Suggested citation:
Taylor, C.D., and Johnson, C.A., editors, 2010, Geology, geochemistry, and genesis of the Greens Creek massive sulfide deposit, Admiralty Island, southeastern Alaska: U.S. Geological Survey Professional Paper 1763, 429 p., 7 plates on CD.

Library of Congress Cataloging-in-Publication Data

Geology, geochemistry, and genesis of the Greens Creek massive sulfide deposit, Admiralty Island, Southeastern Alaska / edited by Cliff D. Taylor and Craig A. Johnson ; prepared in cooperation with Kennecott Greens Creek Mining Company.

p. cm. -- (Professional paper ; 1763)

Includes bibliographical references.

ISBN 978-1-4113-2622-4 (pbk.)

1. Sulfide minerals--Alaska--Greens Creek. 2. Geochemistry--Alaska--Greens Creek. I. Taylor, Cliff D. II. Johnson, Craig A. III. Kennecott Greens Creek Mining Company.

QE389.2.G46 2010

549'.32097982--dc22

2010033687

Volume Contents

1. Introduction and Overview of the U.S. Geological Survey–Kennecott Greens Creek Mining Company Cooperative Applied Research Project at the Greens Creek Mine	3
By Cliff D. Taylor and Craig A. Johnson	
2. The Late Triassic Metallogenic Setting of the Greens Creek Massive Sulfide Deposit in Southeastern Alaska	13
By Cliff D. Taylor, John Philpotts, Wayne R. Premo, Alan L. Meier, and Joseph E. Taggart, Jr.	
3. The History of Greens Creek Exploration	65
By Andrew W. West	
4. Geology of the Greens Creek Mining District.....	93
By Norman A. Duke, Paul A. Lindberg, and Andrew W. West	
5. The Airborne Geophysical Survey of the Greens Creek Area	109
By James Fueg	
6. Geology and Metal Zoning of the Greens Creek Massive Sulfide Deposit, Southeastern Alaska	125
By Cliff D. Taylor, Andrew W. West, Kerry G. Lear, Tim E. Hall, and John M. Proffett	
7. Geologic Structure of the Greens Creek Mine Area, Southeastern Alaska.....	141
By John M. Proffett	
8. Geochemistry of Metasedimentary Rocks in the Hanging Wall of the Greens Creek Massive Sulfide Deposit and of Shales Elsewhere on Admiralty Island	163
By Craig A. Johnson, Cliff D. Taylor, Joel S. Leventhal, and Katja Freitag	
9. Mineralogical, Textural, and Metal Residence Studies of Primary, Recrystallized, and Remobilized Ores of the Greens Creek Deposit.....	187
By Cliff D. Taylor, Steven J. Sutley, and Frederick E. Lichte	
10. Sulfur and Lead Isotope Characteristics of the Greens Creek Polymetallic Massive Sulfide Deposit, Admiralty Island, Southeastern Alaska	241
By Cliff D. Taylor, Wayne R. Premo, and Craig A. Johnson	
11. Microfossil and Radioisotopic Geochronological Studies of the Greens Creek Host Rocks	287
By Wayne R. Premo, Cliff D. Taylor, Lawrence W. Snee, and Anita G. Harris	
12. Radiogenic Isotopic Characterization and Petrogenesis of Host Rocks to the Greens Creek Deposit.....	339
By Wayne R. Premo and Cliff D. Taylor	
13. Structure of the Lower Southwest Orebody, Structural Comparison to Neighboring Orebodies, and Tectonic Model for the Greens Creek Deposit	371
By Katja Freitag	
14. Three-Dimensional Modeling and Visualization of Greens Creek Drill-hole Data	405
By Gregory K. Lee and Cliff D. Taylor	
15. A Genetic Model for the Greens Creek Polymetallic Massive Sulfide Deposit, Admiralty Island, Southeastern Alaska.....	417
By Cliff D. Taylor, Kerry G. Lear, and Steven R. Newkirk	

Plates

- 4-1. Geology of the Greens Creek mine area.
- 7-1. Geologic map of the surface, Greens Creek mine, Alaska.
- 7-2A. Greens Creek mine, Alaska, Cross Section 3000.
- 7-2B. Greens Creek mine, Alaska, Long Section 4800.
- 7-3. Map of the surface, Greens Creek mine, Alaska; F2, S2, L2, and S2/bedding intersections.
- 7-4. Map of underground workings, Greens Creek mine, Alaska; F2, L2, and S2/bedding intersections.
- 7-5. Map of the surface, Greens Creek mine, Alaska; F3, S3, L3, F4, S4, L4.

USGS Contributors to the Professional Paper

Harris, Anita G.
Johnson, Craig A.
Lee, Gregory K.
Leventhal, Joel S.
Lichte, Frederick E.
Meier, Alan L.
Philpotts, John A.
Premo, Wayne R.
Snee, Lawrence W.
Sutley, Steven J.
Taggart, Joseph E., Jr.
Taylor, Cliff D.*

*Principal contact:

U.S. Geological Survey – Mineral Resources Program
Box 25046 Federal Center, MS-973
Denver, CO 80225-0046 USA
303-236-2499
ctaylor@usgs.gov

Kennecott Greens Creek Mining Company Contributors to the Professional Paper

Hall, Tim E.
Lear, Kerry G.
Newkirk, Steven R.
West, Andrew W.
Kennecott Greens Creek Mining Company
P.O. Box 32199
Juneau, AK 99803
(Newkirk now at Department of Earth Sciences, University of Memphis, Memphis, TN 38152)

Other Contributors to the Professional Paper

Duke, Norman A.
Department of Earth Sciences
University of Western Ontario
London, Ontario, Canada N6A 5B7

Fueg, James
Chugiak, AK 99567-0236

Lindberg, Paul A.
Sedona, AZ 86336

Proffett, John M.
Eagle River, AK 99577-7124

Freitag, Katja
Department of Geology and Geological Engineering
Colorado School of Mines
Golden, CO 80401
(now at McKinsey & Company, Johannesburg, South Africa)

Introduction and Overview of the U.S. Geological Survey–Kennecott Greens Creek Mining Company Cooperative Applied Research Project at the Greens Creek Mine

By Cliff D. Taylor and Craig A. Johnson

Chapter 1 of

Geology, Geochemistry, and Genesis of the Greens Creek Massive Sulfide Deposit, Admiralty Island, Southeastern Alaska

Edited by Cliff D. Taylor and Craig A. Johnson

Professional Paper 1763

**U.S. Department of the Interior
U.S. Geological Survey**

Contents

Background.....	3
Geology and Geophysics.....	3
Geochemistry.....	4
Models.....	6
Final Comment.....	7
Reference Cited.....	7

Introduction and Overview of the U.S. Geological Survey—Kennecott Greens Creek Mining Company Cooperative Applied Research Project at the Greens Creek Mine

By Cliff D. Taylor and Craig A. Johnson

Background

In 1996, a memorandum of understanding was signed by representatives of the U.S. Geological Survey and Kennecott Greens Creek Mining Company to initiate a cooperative applied research project focused on the Greens Creek massive sulfide deposit in southeastern Alaska. The goals of the project were consistent with the mandate of the U.S. Geological Survey Mineral Resources Program to maintain a leading role in national mineral deposits research and with the need of Kennecott Greens Creek Mining Company to further development of the Greens Creek deposit and similar deposits in Alaska and elsewhere. The memorandum enumerated four main research priorities: (1) characterization of protoliths for the wall rocks, and elucidation of their alteration histories, (2) determination of the ore mineralogy and paragenesis, including metal residences and metal zonation within the deposit, (3) determination of the ages of events important to ore formation using both geochronology and paleontology, and (4) development of computer models that would allow the deposit and its host rocks to be examined in detail in three dimensions.

The work was carried out by numerous scientists of diverse expertise over a period of several years. The written results, which are contained in this Professional Paper, are presented by 21 authors: 13 from the U.S. Geological Survey, 4 from Kennecott Greens Creek Mining Company, 2 from academia, and 2 from consultants.

Geology and Geophysics

The first six papers in the Professional Paper summarize a large body of geologic and geophysical information starting at the regional scale and ending at the scale of the Greens Creek mine and immediate vicinity. The lead-off paper, by Taylor and others (chap. 2), describes the regional setting for Greens Creek on the eastern margin of the Alexander terrane in southeastern Alaska. The deposit lies in what Taylor and others (chap. 2) term the Alexander Triassic Metallogenic Belt (ATMB), a 200–800-m-thick sequence of conglomerates,

limestones, marine clastic sediments, and tuffs with overlying and intercalated pyroclastic rocks and flows that can be traced some 600 km along strike. Fossil evidence suggests that the sequence spans Anisian to late Norian time (Middle Triassic to Late Triassic). In addition to Greens Creek, numerous other sulfide deposits are within the belt, most notably Windy Craggy, which is the largest volcanogenic massive sulfide deposit known in North America.

Within the ATMB, there are along-strike changes in the nature of the sulfide deposits and the depositional setting of the host rocks. From south to north, sulfide deposits change from structurally controlled Pb+Zn+Ag±Cu veins or pods or small stratiform lenses, to stratiform sulfosalt-bearing Zn-Pb-Ag deposits (Greens Creek), to stratiform copper-rich deposits (Windy Craggy). The host rocks also change from felsic volcanics with overlying oolitic limestones to mafic and ultramafic phyllites with overlying argillites or mafic volcanics. Taylor and others (chap. 2) suggest that the change in host rocks reflects a change in depositional environment from shallower waters on the flanks of the Alexander volcanic arc to deeper waters in a back-arc or intra-arc basin. A modern analog for the ATMB may be the southern projection of the Lau Basin, from Valu Fa Ridge to the Taupo Volcanic Zone on the North Island of New Zealand.

West (chap. 3) documents the exploration programs that focused attention on northern Admiralty Island and then defined and expanded the Greens Creek ore reserve. In 1973, Noranda Exploration, Marietta Resources, Exhalas Resources, and Texas Gas Exploration formed a partnership, Pan Sound Joint Venture, to explore for base and precious metals in the northern part of southeastern Alaska, in the Prince William Sound area, and on the Kenai Peninsula. That same year, extensive stream-sediment sampling across northern Admiralty Island revealed high concentrations of zinc and copper in the Cliff Creek drainage, just east of the present-day mine site, and near Hawk Inlet, northwest of the mine site. The following year, a large exposure of unvegetated ferricrete was discovered and dubbed the “Big Sore,” and geophysics and soil geochemistry surveys of the area were carried out. The first drill hole, which was completed in 1975, recovered an 89-foot interval of massive pyrite and base metal sulfides.

The first production from the Greens Creek mine was in 1989, following a development stage that was greatly complicated by the Alaska National Interest Lands Conservation Act of 1980. Throughout the development of the mine, and in subsequent exploration programs, the understanding of the geology of the deposit and the preferred model for ore genesis have evolved considerably. The stratabound nature of the mineral deposits was recognized early on. Although the ores were first thought to be brine pool deposits and the host rocks to be volcanic tuffs and hydrothermal precipitates (exhalites) that had accumulated on the Devonian sea floor, subsequent interpretations favored sulfide precipitation in Triassic time in association with intense hydrothermal alteration of preexisting volcanic and plutonic rocks. It was suggested also that the heat source for the hydrothermal system was ultramafic magmas that were emplaced along faults, and that the ores formed epigenetically by replacement of Triassic sedimentary rocks. The understanding of post-ore deformation has also evolved. An accurate model of the structural geology is considered critical for mine planning and continuing exploration.

Duke and others (chap. 4) and Fueg (chap. 5) report on surface geologic mapping and results of an airborne geophysical survey, respectively, of the greater Greens Creek area. The geologic and geophysical coverages are nearly the same and can be conveniently compared. The data are displayed as maps that cover a 10–12-mile-long segment of the northwest-trending phyllite belt that hosts the Greens Creek deposit.

Greens Creek is in the low-grade metamorphic core of the Admiralty subterrane of Alexandria. The overall tectonostratigraphic setting is back-arc basement of late Paleozoic age overlain by flood basalts of Late Triassic age. The Admiralty back-arc basin is represented by Devonian greenstones of the Retreat Group, overlying Mississippian to Permian siliciclastics and dolomite-chert facies of the Cannery Formation, and the Lower Permian Pybus Formation. Amalgamation of the Alexander and Wrangellia terranes resulted in subaerial exposure of the region, and the formation of an unconformity. Rifting commenced in Late Triassic time leading to the accumulation of the Hyd Group, which is dominated by black argillite and flood basalts. Compressional tectonism in mid-Cretaceous time caused fold and thrust imbrication. Dextral transpression on the Denali transform system in the Tertiary caused strike-slip faulting.

The Greens Creek sulfide bodies are located at the unconformity between the Retreat and Hyd Groups. At the mine site, the Retreat Group contains serpentinite and metagabbro in addition to greenstone; hydrothermal alteration of this assemblage has given rise to phyllitic rocks (termed mine phyllite following common usage by Kennecott Greens Creek geologists; see also Proffett, chap. 7). The Hyd Group consists of a basal breccia/conglomerate, a medial argillite (termed mine argillite by Kennecott Greens Creek geologists; see also Proffett, chap. 7), and an upper basalt member.

The airborne geophysics has proven to be a valuable guide to stratigraphy and structure in the area. Ultramafic units appear as magnetic highs, and the argillite-phyllite contact, which is the mineralized horizon, is revealed as a sharp

gradient in the electromagnetic data (contrast between low and high resistivities, respectively). The Greens Creek sulfide deposit is not apparent in the electromagnetic data mainly because the bulk of it is buried.

The geology of the mine site is described by Taylor and others (chap. 6), who focus on the ores and their immediate wall rocks, and Proffett (chap. 7), who focuses on the structural geology. The Greens Creek ore deposit is a series of massive sulfide bodies that lie along the contact between altered mafic-ultramafic phyllites and stratigraphically overlying Upper Triassic argillites. There are three main orebodies, East, West, and Southwest, that are themselves segmented by faults or attenuated zones. Within individual orebodies there is a common stratigraphic sequence in which white ores (less than 50 percent sulfides) give way upward to pyritic massive ores, and then to base-metal-rich massive ores (both greater than 50 percent sulfides). The global reserve, for a cutoff grade of zero percent metal, is estimated to be 21.9 million metric tonnes with grades of 13.9 weight percent zinc, 5.1 weight percent lead, 19.2 troy ounce per metric tonne silver, and 0.15 troy ounce per metric tonne gold.

Restoration of offsets along the Maki and Klaus faults, the two major ore-displacing faults, suggests that the mineral deposit was originally a single continuous horizon that was thickest in the Central West orebody and thinned to the north, east, and south. It appears that, in general, the ores change from Cu+Fe-rich against the footwall phyllites, to Zn-rich, to Zn+Pb-rich, to Ag-rich and polymetallic against the hanging-wall argillites. The absence of concentric metal zoning in plan view suggests that the sulfide-bearing mineral deposits may have formed above multiple centers of hydrothermal upwelling, or a broad zone of diffuse upwelling, rather than a single pipe-like vent.

The host rocks show the effects of hydrothermal alteration, lower greenschist facies metamorphism, and multiple deformations. In the footwall, mafic rocks are higher in silica content and richer in sericite at the ore contact and become richer in chlorite and carbonate away from ore. Ultramafic rocks are either serpentinitized or carbonate altered. In the hanging wall, the argillites are massive or slaty and can contain graphite, dolomite, or calcite. Carbonate rocks occur locally at or near the ore contact.

The complex distribution of ore at Greens Creek results mainly from the complex deformation history of the area. The earliest structures are schistosity (S1 and S1.5) that are apparent only in Paleozoic rocks. Three cleavage-forming folding events (F2–S2, F3–S3, F4–S4) affected both ores and wall rocks. Ductile shear zones are present above and below the ore zone; these formed between F2 and F3. Brittle faulting postdated the youngest folding event (F4).

Geochemistry

Next in the Professional Paper are five papers on geochemical topics. Johnson and others (chap. 8) report on the organic geochemistry, major and trace element geochemistry, and stable isotope geochemistry of sedimentary rocks in the hanging wall

of the Greens Creek deposit and of shales elsewhere on Admiralty Island. The sedimentary section immediately overlying the ores ranges from carbonate-poor shale to nearly pure dolomite. Some samples resemble normal marine shales in their base and precious metal contents, sulfur-to-organic carbon ratios, and degree-of-pyritization values. These sediments were laid down during periods when the overlying water column was oxic; the only suggestion of hydrothermal venting is a slight enrichment in barium. More commonly the hanging-wall samples are high in sulfur, metals, and degree of pyritization. This could reflect metal accumulation beneath an anoxic metalliferous brine pool but could also be explained by epigenetic emplacement of sulfur and metals during massive sulfide formation or during Cretaceous regional metamorphism as a consequence of mobilization from the neighboring sulfide bodies.

The carbon and oxygen isotopic compositions of hanging-wall carbonates are indistinguishable from the compositions of dolomite in the sulfide ores. The compositional ranges suggest precipitation from a single fluid over a temperature range of 200° to 350°C, which overlaps the range that has been inferred independently for formation of the adjacent massive sulfides (see Taylor and others, chap. 10). However, the compositions may also be consistent with dolomite formation from mixtures of hydrothermal and marine fluids. Whatever the dolomite precipitation mechanism, the isotopic similarity of hanging-wall and ore dolomites is strong evidence that the Greens Creek hydrothermal system persisted until after the hanging-wall sediments had been laid down.

Carbonate carbon isotopes show a negative correlation with the sulfur content of the rocks, which suggests that the oxidation of organic matter, or of methane produced therefrom, was linked to sulfate reduction to form hydrogen sulfide. During growth of the framboidal pyrite forms, sulfate reduction was probably microbially mediated, whereas during formation of base-metal sulfides, sulfate reduction could have been microbial or abiotic. Thus, at least some sulfate reduction took place during early diagenesis beneath the sediment/seawater interface. Limited isotopic data from Hyd Group shales elsewhere on Admiralty Island suggest that the same hydrothermal fluid that formed the Greens Creek massive sulfide deposit may also have interacted with basin-floor sediments several kilometers distant from Greens Creek.

The mineralogy, mineral chemistry, and textures of Greens Creek ores are described by Taylor and others (chap. 9). For mapping purposes, the ores have been divided into massive sulfide ores (greater than 50 percent sulfides), which can be either pyrite- or base-metal-rich, and white ores (less than 50 percent sulfides), which can contain carbonate, silica, or barite. Veining, brecciation, and faulting are also recognized giving rise to subdivisions of the main ore types. In the cores of individual orebodies, white ore gives way stratigraphically upward to massive pyritic ore, which gives way upward and laterally to massive base-metal-rich ore.

Ore with primary textures, which constitutes an estimated 30 percent of the deposit, contains pyrite with framboidal, colloform, dendritic, or “spongy” forms intergrown with

sphalerite, galena, tetrahedrite, chalcopyrite, free gold, and various Pb-Sb-As(-Hg-Tl) sulfosalts. The textures exhibited by pyrite are consistent with formation during diagenesis from bacterial hydrogen sulfide and support a similar inference based on sulfur isotopic analyses (see Taylor and others, chap. 10). The remaining 70 percent of the ores show the effects of secondary processes including recrystallization and coarsening of sulfides, formation of atoll structures, and formation of secondary minerals in late fractures, veinlets, and matrix interstitial to euhedral pyrites. Common secondary minerals include chalcopyrite, low-iron sphalerite, galena, free gold, electrum, antimony-rich tetrahedrite, pyrrargyrite, and numerous sulfosalts. Recrystallization also resulted in higher pyrite purity. A process akin to zone refining is inferred, causing recrystallization of large volumes of ore and the migration of lead, zinc, and precious metals outward toward the lower temperature margins of individual orebodies.

Sulfur and lead isotope analyses of Greens Creek sulfides and of hanging wall and footwall rocks provide information on the sources of these two ore constituents (Taylor and others, chap. 10). Ore pyrite ranged in $\delta^{34}\text{S}$ from -38 to 2 permil, and chalcopyrite, sphalerite, and galena were mostly between -16 and -11 permil. The lower values are strong evidence for sulfur acquisition from bacterial hydrogen sulfide, which was produced from seawater sulfate within the pore waters of argillaceous sediments. The higher values suggest that sulfur may have been derived also from mafic and ultramafic rocks beneath the sulfide deposit. Analyses of barite gave $\delta^{34}\text{S}$ values of 13 to 22 permil, which is consistent with sulfate derivation from Triassic seawater. The sulfur isotopic difference between coexisting sphalerite and galena suggests that the minerals equilibrated at temperatures of 276–313°C. It is uncertain whether this equilibration occurred during hydrothermal metal emplacement or during Cretaceous regional metamorphism.

Lead isotope analyses of Greens Creek samples and of sulfide minerals from elsewhere on Admiralty Island suggest that the lead represents mixtures from multiple sources. Ore sulfides display linear arrays on $^{208}\text{Pb}/^{204}\text{Pb}$ versus $^{206}\text{Pb}/^{204}\text{Pb}$ and $^{207}\text{Pb}/^{204}\text{Pb}$ versus $^{206}\text{Pb}/^{204}\text{Pb}$ plots that are consistent with mixing of less radiogenic lead from a source resembling enriched midocean-ridge-type basalt (EMORB) and more radiogenic lead from an older crustal source. Analyses of host rocks suggest that the less radiogenic source could have been Upper Triassic basalts and gabbros, select phyllites, or Cannery Formation argillites. The more radiogenic source may have been the hanging-wall argillites, although the lack of obvious depletions in lead and other metals immediately above the Greens Creek deposit (Johnson and others, chap. 8) suggests that the source argillites would have been distal to the site of massive sulfide formation. For other sulfide localities on Admiralty Island, there appear to have been contributions from different sources. These include an older or less radiogenic source for the Kennecott Rand, Pyrola, Killer Creek, and Mt. Robert Barron localities that may correspond to Retreat Group sedimentary rocks, and a more highly radiogenic source for the Mammoth Claims, Cascade Creek, Portage, and Cub

Creek localities, as well as to a minor extent at Greens Creek, that may correspond to metasomatic additions of lead during the Cretaceous metamorphic event.

The last two geochemical papers cover age determinations from radiogenic isotopes and biostratigraphy and radiogenic isotope geochemistry of the Greens Creek wall rocks. Premo and others (chap. 11) report on conodonts from calcareous argillites that were obtained from mine workings and outcrops. The most age-restrictive index species is *Metapolygnathus primitius*, which lived during a narrow time interval at the Carnian-Norian boundary for which the estimated age is 220.7 ± 4.4 Ma (Gradstein and others, 1995). The CAI (color alteration index) of most Greens Creek conodonts is 5 or 5–5.5, which implies that the samples experienced temperatures of 300° to 350°C . The general consistency of CAI values within individual samples, and from one sample to another, suggests that the values reflect a low-grade metamorphic event. Less common higher CAI values of 5.5–6 and 6.5–7 reflect higher temperatures or more prolonged heating locally, most likely due to contact metamorphism near basaltic flows or intrusions, or interaction with hydrothermal fluids. The conodont-bearing argillites were hemipelagic basinal deposits with additions of storm- or wave-generated siliciclastic and carbonate muds from shallow-water platforms or other near-surface submarine edifices that were transported and redeposited in deeper marine environments.

Measurements of whole-rock lead, neodymium, and strontium isotopic compositions gave scattered results for some sample suites implying post-depositional disturbance, but gave apparent isochrons for other suites. The U-Pb results for a suite of Hyd Group basalts gave an apparent isochron age of 218 ± 16 Ma, which is consistent with their eruption after argillite sedimentation (220.7 ± 4.4). A suite of altered gabbros that intruded both Hyd Group argillites and Hyd Group basalts gave ages of 206 ± 35 Ma (U-Pb) and 200 ± 27 Ma (Sm-Nd) consistent with the crosscutting relationships. Numerous sericite and fuchsite samples were dated by the $^{40}\text{Ar}/^{39}\text{Ar}$ technique, but most showed evidence for argon loss during Cretaceous time and thus were of limited value in dating hydrothermal mineral growth. However, fuchsite from an altered ultramafic rock at Gambier Bay yielded an undisturbed age of 210.3 ± 0.3 Ma. Taken together, the geochronological data suggest that the lifetime of the Greens Creek hydrothermal system was between 0.4 and 15.1 million years. For some sample suites the U-Pb, Sm-Nd, Rb-Sr, and $^{40}\text{Ar}/^{39}\text{Ar}$ systematics appear to have been perturbed in the time period 110–85 Ma, which corresponds to the Cretaceous metamorphic event.

Premo and Taylor (chap. 12) present whole-rock U-Th-Pb, Rb-Sr, and Sm-Nd isotope data for metabasalts, metagabbros, serpentinites, phyllites, argillites, and crosscutting diabases from the vicinity of the Greens Creek deposit. The metabasalts and metagabbros yield Pb-Pb, Sm-Nd, and Rb-Sr systematics that are consistent with Triassic emplacement ages and with magma production in a depleted mantle source region within a volcanic arc setting. Phyllites show more compositional scatter, suggesting U-Pb fractionation

during hydrothermal alteration and interaction with seawater or marine carbonate rocks. The hanging-wall argillites give Pb-Pb apparent ages consistent with sedimentation during Triassic time of detritus derived in part from an older, more radiogenic source region. The Rb-Sr isotope systematics of the argillites show evidence of disruption in Cretaceous time. Serpentinites also show disrupted isotope systematics. Values of epsilon-Nd increase through the stratigraphy from metabasalts to mafic volcanics and gabbroic plutons to Hyd Group basalts at the top of the Triassic section. The increase implies progressive depletion of magma source regions, which is consistent with the opening of preexisting crust in a rift setting.

The Greens Creek wall rocks span wider lead isotopic ranges than the ores. A comparison of ore and wall-rock compositions suggests that the ore lead was derived mainly from basaltic and gabbroic lithologies with a lesser contribution from the hanging-wall argillites. The isotopic uniformity of the orebody implies that the lead was homogenized prior to being deposited in sulfide minerals.

Models

The final three chapters in the Professional Paper (chaps. 13, 14, 15) describe models for the Greens Creek deposit. The first paper, by Freitag (chap. 13), presents a model for the geometry and structural development of the Lower Southwest orebody. The model is based on rib and plan maps that were prepared for the Lower Southwest orebody and for parts of the Upper Southwest, 244 West Bench, and 200 South orebodies. Similarities are apparent between the structures revealed in the deposit and the structures that have been observed regionally (see Proffett, chap. 7). Thus, the model may provide guidance for exploration away from the mine as well as for continued development within the mine.

Syn depositional normal faults were inferred from north-south-trending accumulations of sulfide and mineralized dolomite that appeared on isopach maps created from palispastic reconstructions. The accumulations are believed to represent thicker sulfide sections that developed above fault-controlled fluid conduits. Next in the structural history were ladder veins that developed perpendicular to bedding in argillaceous rocks; these were later offset by pressure solution seams. Compressional tectonics associated with terrane accretion in Late Jurassic to Cretaceous time caused small thrust faults, and then resulted in south-southwest- to southeast-plunging, open-to-isoclinal folds and southeast-plunging open folds. The effects of the folding events were more pronounced in less competent, thinner sulfide sections leading to greater fold frequencies and fold amplitudes, and more varied orientations of foliations and cleavages. The folding events were followed by a transition to a more brittle deformation style that produced gentle folds and thrust faults. Wrench tectonics in Eocene time led to high-angle faulting, in some cases along reactivated thrust faults.

Next, Lee and Taylor (chap. 14) present three-dimensional depictions of the orebodies, major workings, faults, shear

zones, and assay values for zinc, silver, gold, and antimony. The basis of the depictions is lithologic, structure, and assay data for 1,895 core holes that were drilled in the vicinity of the mine. The results are displayed relative to the mine grid, which is rotated 26.5651 degrees counterclockwise from due north. Mine coordinate elevations are 60 ft higher than above-sea-level elevations. The depictions allow readers to visualize and quickly appreciate a number of important aspects of the deposit and the mine, including the topography of the area, the complexity of the ore distribution, the influence of faults on the ore distribution, and the spatial relationship between zinc mineralization and precious metal mineralization.

In synthesizing the results of the entire cooperative research project, Taylor and others (chap. 15) point out that the Greens Creek deposit is not easily classified because it displays features characteristic of volcanogenic massive sulfide (VMS) deposits, features characteristic of sedimentary exhalative (SEDEX) sulfide deposits, and features characteristic of Mississippi Valley-type (MVT) sulfide deposits. Among the VMS characteristics are an association with abundant volcanic rocks (footwall phyllites), the existence of an alteration profile beneath the mineralized horizons, a metal endowment (Zn-Pb-Ag-Au-Cu) resembling Kuroko- or bimodal-felsic-type VMS deposits, and a mineral deposit type (white ores) that resembles the white smoker deposits found on the modern sea floor in areas of active volcanism. SEDEX characteristics include an association with carbonaceous sedimentary rocks (hanging-wall argillites), the presence of a broad chromium-barium-carbonate alteration halo, the lack of a hydrothermal root beneath the ores, and the diagenetic/bacterial origin of sulfide sulfur. The MVT characteristics are less compelling from a classification standpoint, but they include the local presence of epigenetic sulfide mineralization in carbonate rocks in the deposit footwall.

The tectonic setting for the Greens Creek deposit was a rift basin that developed in the Alexander terrane following a period of shale accumulation in open basins and carbonate platform development, and subsequent emergence and erosion of the Alexander landmass. Rifting commenced in Late Triassic time. Arc-contaminated tholeiites and minor alkaline basalts were extruded, probably subaqueously, in the Greens Creek area. Subsequently, a thin carbonate platform developed within the rift during a period of quiescence. Resumption of rifting caused the carbonate platform to founder, and it was at this time that the Greens Creek hydrothermal system was initiated. Shallowly emplaced mafic and ultramafic magmas supplied the requisite heat for the development of hydrothermal circulation. The first hydrothermal products to be formed were precious-metal-bearing silica-barite-carbonate deposits that formed at or just beneath the sea floor by mixing of metalliferous fluids with sulfate-bearing seawater. The accumulation of organic-rich sediments in the subsiding basin resulted in bacterial sulfate reduction within the sediment column, and possibly also within stagnant basin waters. Base-metal and iron sulfide minerals were formed where hydrothermal fluids encountered bacterial hydrogen sulfide, resulting in the replacement of both unlithified shale and preexisting silica-barite-carbonate

deposits. The deposit underwent a process akin to zone refining during prograde hydrothermal heating, causing precious metals, antimony, mercury, and other metals to migrate upward and outward within the deposit. Hydrothermal activity and shale accumulation were followed by the eruption of voluminous basalts. Heating and deformation during Cretaceous greenschist facies metamorphism recrystallized sulfide minerals and thickened the ore horizon locally.

Greens Creek is a hybrid deposit intermediate between more typical VMS and SEDEX deposits. Deposit characteristics suggest formation in a transitional environment within a rift that was propagating from dominantly oceanic crust toward the core of the Alexander terrane where the crust was increasingly continental. The change in crustal character along the strike of the propagating rift is thought to explain the change in metal endowments from copper-dominant at Windy Craggy to zinc-lead-silver-dominant at Greens Creek. Whereas the Windy Craggy hydrothermal system scavenged metals predominantly from copper-rich, lead- and zinc-poor ocean ridge basaltic rocks, the Greens Creek hydrothermal system scavenged metals from mafic and ultramafic rocks that were richer in zinc and lead because they had assimilated the evolved basement of the Alexander terrane.

Final Comment

As the reader proceeds through this Professional Paper, it will become clear that some research priorities set out in the original memorandum of understanding proved to be quite fruitful, whereas others proved to be less so. This is perhaps inevitable for a complex project with an ambitious work plan and a wide diversity of participants. In particular, attempts to characterize the protoliths and alteration histories of the footwall rocks were only partially successful because, as the data of Premo and Taylor (chap. 12) demonstrate, it is difficult to see backward through the multiple thermal and metasomatic overprints to determine original chemical and isotopic properties. On the other hand, the discovery of disturbed isotope systematics provides strong support for the conclusion that the Greens Creek footwall was intensely altered by throughgoing hydrothermal fluids. Overall, there is no question that the U.S. Geological Survey–Kennecott Greens Creek Mining Company cooperative research project was highly worthwhile; the final product—this Professional Paper—far exceeds what the individual organizations could have accomplished working in isolation.

Reference Cited

Gradstein, F.M., Agterberg, F.P., Ogg, J.G., Hardenbol, Jan, Van Veen, Paul, Thierry, Jacques, and Huang, Zehui, 1995, A Triassic, Jurassic, and Cretaceous time scale, *in* Geochronology time scales and global stratigraphic correlation: SEPM Special Publication No. 54, p. 95–126.

The Late Triassic Metallogenic Setting of the Greens Creek Massive Sulfide Deposit in Southeastern Alaska

By Cliff D. Taylor, John Philpotts, Wayne R. Premo, Alan L. Meier, and Joseph E. Taggart, Jr.

Chapter 2 of

Geology, Geochemistry, and Genesis of the Greens Creek Massive Sulfide Deposit, Admiralty Island, Southeastern Alaska

Edited by Cliff D. Taylor and Craig A. Johnson

Professional Paper 1763

**U.S. Department of the Interior
U.S. Geological Survey**

Contents

Abstract.....	13
Introduction.....	13
Terrane Relationships	21
Stratigraphy of Host Rocks to Late Triassic Mineral Occurrences and Correlation Throughout Southeastern Alaska.....	22
Geochemistry of Upper Triassic Basalts and Rhyolites of Southeastern Alaska	31
The Geochemistry and Significance of Late Triassic Hypabyssal Mafic-Ultramafic Intrusive Rocks	38
Late Triassic Mineral Occurrences in Southeastern Alaska.....	39
Mineral Occurrences in the Southern ATMB	39
Mineral Occurrences in the Northern ATMB.....	42
Mineral Occurrences in the Central ATMB.....	43
Discussion.....	52
References Cited.....	55

Figures

1. Generalized map of southeastern Alaska showing the locations of mines, mineral deposits, and mineral occurrences and other features discussed in the text, in relation to the Alexander Triassic Mineral Belt (ATMB) and insets showing detailed maps	14
2. Tectonostratigraphic terranes of southeastern Alaska	23
3. Stratigraphy and correlation of Upper Triassic host rocks in southeastern Alaska and adjacent British Columbia	24
4. Composite stratigraphic column of the Upper Triassic section on Annette Island	25
5. Composite stratigraphic column of the Upper Triassic section on Gravina Island	25
6. Composite stratigraphic column of the Upper Triassic section in the Keku Strait area	26
7. Photograph of the basal Upper Triassic conglomerate in Nehenta Bay, Gravina Island	27
8. Composite stratigraphic column of the Middle and Upper Triassic section in the Duncan Canal area.....	28
9. Composite stratigraphic column of the Upper Triassic section on the north shore of Gambier Bay, southern Admiralty Island	28
10. Composite stratigraphic column of the Upper Triassic section at the Greens Creek mine, northern Admiralty Island	29
11. Composite stratigraphic column of the Upper Triassic section in the Mt. Henry Clay area, northern southeastern Alaska and northwestern British Columbia	30
12. Photograph of pillowed basalt flow near the base of the Upper Triassic section on the north shore of Gambier Bay, southern Admiralty Island.....	31
13. Composite stratigraphic column of the Upper Triassic section at the Windy Craggy deposit, northwestern British Columbia.....	33

14.	Accuracy and precision of blind standards plotted on the diagrams used in the text as compared to accepted values.....	34
15.	Volcanic rock classification diagram of Winchester and Floyd (1977) based on immobile-element ratios, showing the composition of southeastern Alaska Upper Triassic volcanic rocks analyzed for this study.....	35
16.	Discrimination diagrams showing compositions of southeastern Alaska Upper Triassic basalts and rhyolites analyzed for this study.....	37
17.	MORB-normalized abbreviated immobile-trace-element and REE plots of data for samples from locations throughout the ATMB corresponding to the samples and locations shown on the discriminant plots.....	40
18.	Photographs of outcrops throughout the ATMB demonstrating the spatial relationship between mineral occurrences and mafic-ultramafic hypabyssal sills, dikes, and intrusions	44
19–22.	Photographs of outcrops and polished rock slabs from mineral occurrences in the southern portion of the:	
19.	Southern portion of the ATMB	46
20.	Northern portion of the ATMB	47
21.	Central portion of the ATMB.....	50
22.	Central and northern portion of the ATMB	53
23.	Schematic drawing showing a cross-sectional view of the Upper Triassic metallogenic setting of mineral deposits and occurrences in southeastern Alaska	54

Tables

1.	Summary whole-rock geochemical data for Upper Triassic basaltic rocks at key locations in southeastern Alaska	32
2.	Whole-rock geochemical data for igneous rocks collected throughout the ATMB in southeastern Alaska and British Columbia.....	on CD-ROM

The Late Triassic Metallogenic Setting of the Greens Creek Massive Sulfide Deposit in Southeastern Alaska

By Cliff D. Taylor, John Philpotts, Wayne R. Premo, Alan L. Meier, and Joseph E. Taggart, Jr.

Abstract

The Alexander terrane of southeastern Alaska contains a belt of unusual volcanogenic massive sulfide (VMS) deposits along its eastern margin. The deposits occur within a lithologic sequence that is exposed discontinuously along its 600-kilometer strike length and consists of a 200–800-meter thickness of conglomerate, limestone, marine clastic sediment, and tuff with intercalated and overlying mafic pyroclastic rocks and pillowed flows. The rocks range in age from Anisian (Middle Triassic) to late Norian (middle Late Triassic). Major deposits within the belt, which is referred to herein as the Alexander Triassic Metallogenic Belt (ATMB), are Greens Creek, the most economically significant VMS deposit in Alaska, and Windy Craggy, the largest VMS deposit known in North America.

The VMS deposits vary in structural appearance, chemistry, and stratigraphic setting along strike within the ATMB, which suggests spatial or temporal changes in the tectonic environment. In the southern portion of the belt, the deposit host rocks are felsic volcanics and overlying shallow-water limestones. In the central portion of the belt, a pebble conglomerate appears at the base of the section, suggesting higher energy deposition in a near-slope or basin-margin setting. In the north, the felsic volcanics, limestones, and conglomerates give way to deeper water sediments and mafic volcanic rocks. There is an accompanying change in the sulfide deposits from dominantly structurally controlled Pb-Zn-Ag-Ba±Cu deposits in the south (for example, west of Ketchikan), to sulfosalt-bearing VMS deposits (for example, Greens Creek on Admiralty Island), to larger Cu-Zn±Co±Au VMS deposits in the north (for example, Windy Craggy in northeastern British Columbia).

Igneous activity in the ATMB was characterized by bimodal volcanism and hypabyssal emplacement of mafic-ultramafic magmas. Analyses of immobile trace elements and rare earth elements suggest that the felsic rocks change from calc-alkaline rhyolites in the southern ATMB to peralkaline rhyolites in the middle part of the belt. The capping basaltic rocks have compositions consistent with variable assimilation of mature island arc crust by more primitive, midocean ridge-type or intraplate-type basaltic melts. Radiogenic isotope data for the capping basalts and associated gabbros support the

variable assimilation hypothesis (epsilon-Nd=+4–+9, initial $^{206}\text{Pb}/^{204}\text{Pb}$ =18.42–18.92, initial $^{87}\text{Sr}/^{86}\text{Sr}$ =0.7037–0.7074).

Overall, the regional geology and geochemistry are consistent with sulfide deposition in the south having occurred in shallow, subaqueous environments on the flanks of the Alexander terrane, and sulfide deposition farther north having occurred in progressively deeper environments in an evolving back-arc or intra-arc rift. In their ore and host-rock geochemistry and sulfide mineralogy, the ATMB deposits resemble deposits that have been found at active sea-floor hydrothermal vents (white smokers) associated with back arcs of the southwest Pacific Ocean. A modern analog for the ATMB may be the southward projection of the Lau basin, from the active sea-floor hydrothermal vents of the Valu Fa Ridge to the Taupo Volcanic Zone of the North Island, New Zealand.

Introduction

Numerous papers (compilations by Cobb, 1972, 1978; Berg and Grybeck, 1980; Goldfarb and others, 1987; Taylor and others, 1992; Newberry and Brew, 1997, 1999; Newberry and others, 1997; Taylor and others, 2008) over the last few decades have identified a series of unusual polymetallic volcanogenic massive sulfide (VMS; see reviews by Franklin and others, 1981, and Large, 1992) deposits hosted in an Upper Triassic sequence of volcano-sedimentary rocks that stretch the length of southeastern Alaska (fig. 1). Assuming that correlations among host rocks are correct, these deposits constitute a metallogenically important belt that comprises the easternmost and youngest portion of the Alexander terrane (fig. 2). With the notable exception of the world-class Greens Creek mine having estimated reserves of 21.9 million metric tonnes of ore at 13.9 percent zinc, 5.1 percent lead, 4.8 grams per metric tonne gold, and 599 grams per metric tonne silver at zero cutoff, these are generally small deposits (less than 1 million metric tonnes) dominated by Ba-Zn-Pb-Ag ± Cu-Au, or Cu-Zn ± Au. From south to north, they occur on Annette and Gravina Islands near Ketchikan (fig. 1, inset a), through Keku Strait (fig. 1, inset c) and Duncan Canal–Zarembo Island area west of Petersburg (fig. 1, inset b), through Admiralty Island south of Juneau (fig. 1, inset d), and on and near Mt. Henry Clay west of Haines (fig. 1, inset f). If correlation to

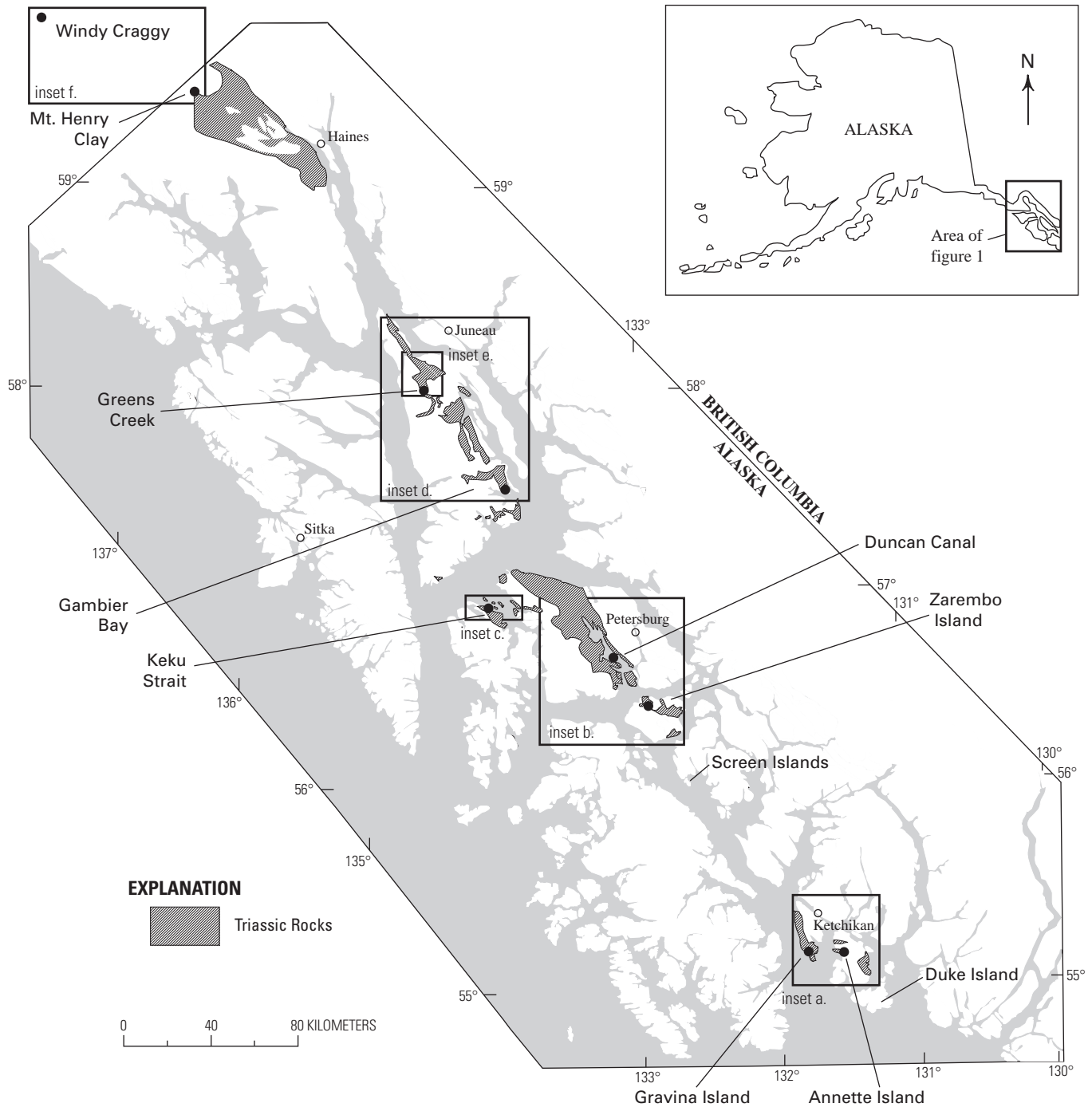


Figure 1. Generalized map of southeastern Alaska (modified from Gehrels and Berg, 1992) showing the locations of mines, mineral deposits, and mineral occurrences (all shown as solid circles) and other features discussed in the text, in relation to the Alexander Triassic Mineral Belt (ATMB). (Inset a) Detailed map of the southern ATMB showing the locations of mines, mineral deposits, and mineral occurrences and other features discussed in the text on Annette and Gravina Islands. (Inset b) Detailed map of the central ATMB showing the locations of mines, mineral deposits, and mineral occurrences and other features discussed in the text in the Duncan Canal area and on Woewodski and Zarembo Islands. (Inset c) Detailed map of the central ATMB showing showing the locations of mines, mineral deposits, and mineral occurrences and other features discussed in the text in the Keku Strait area. (Inset d) Detailed map of the central ATMB showing the locations of mines, mineral deposits, and mineral occurrences and other features discussed in the text on Admiralty Island. (Inset e) Detailed map of the Greens Creek mine area on northern Admiralty Island showing the locations of mines, mineral deposits, and mineral occurrences and other features discussed in the text. (Inset f) Detailed map of the northern ATMB showing the locations of mines, mineral deposits, and mineral occurrences and other features discussed in the text between the Mt. Henry Clay area and Windy Craggy.

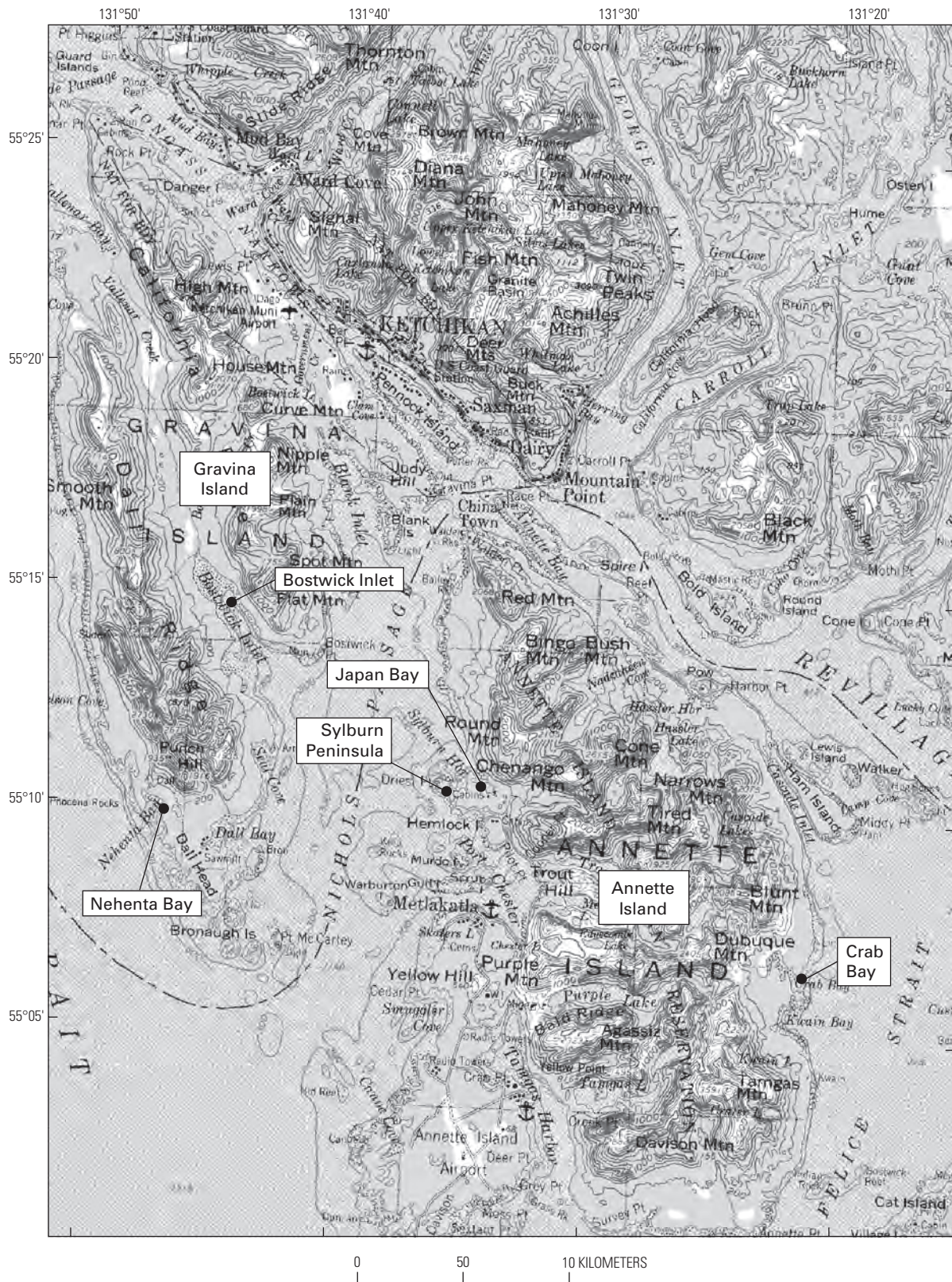


Figure 1, inset a. Detailed map of the southern ATMB showing the locations of mines, mineral deposits, and mineral occurrences and other features discussed in the text on Annette and Gravina Islands.

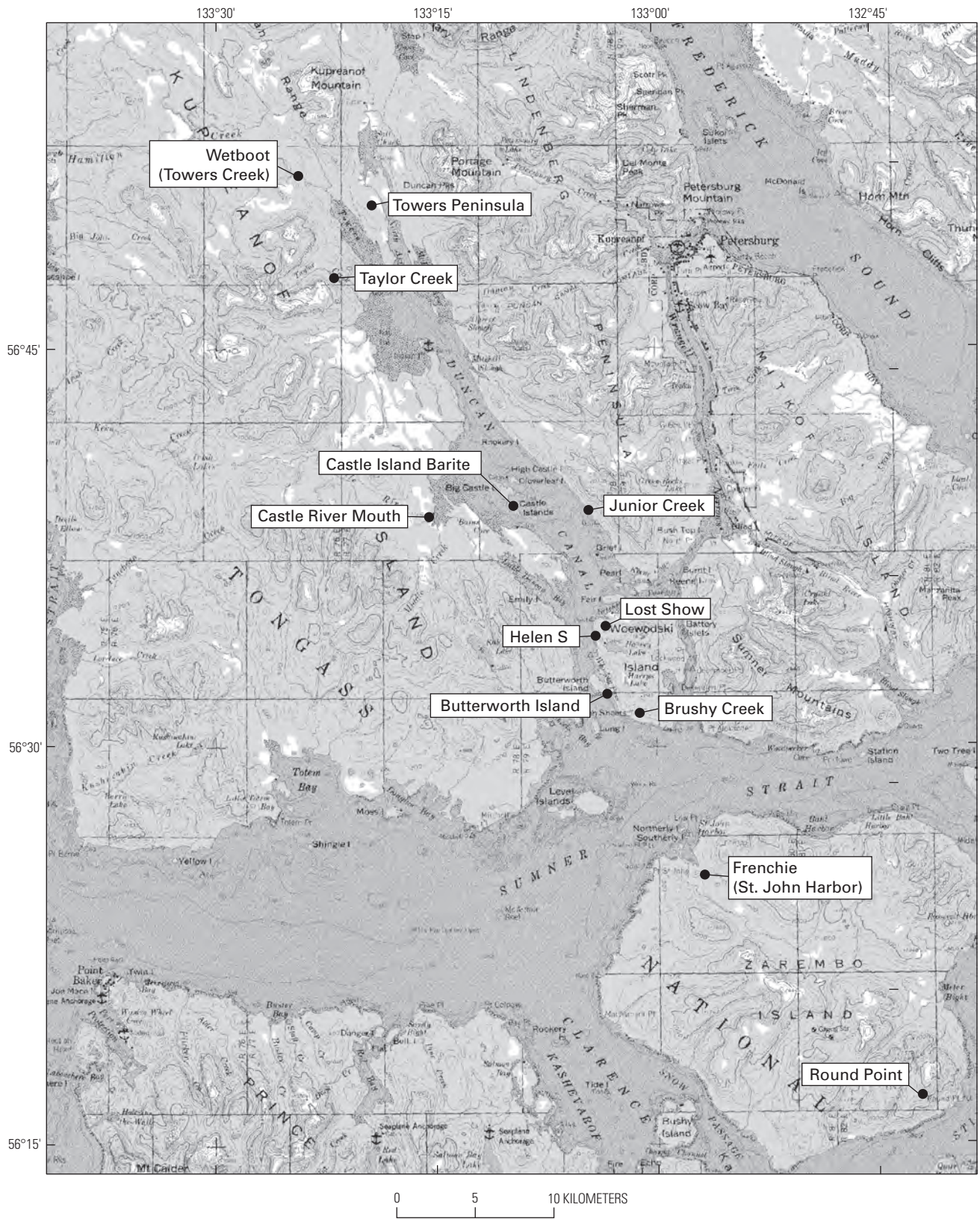


Figure 1, inset b. Detailed map of the central ATMB showing the locations of mines, mineral deposits, and mineral occurrences and other features discussed in the text in the Duncan Canal area and on Woewodski and Zarembo Islands.

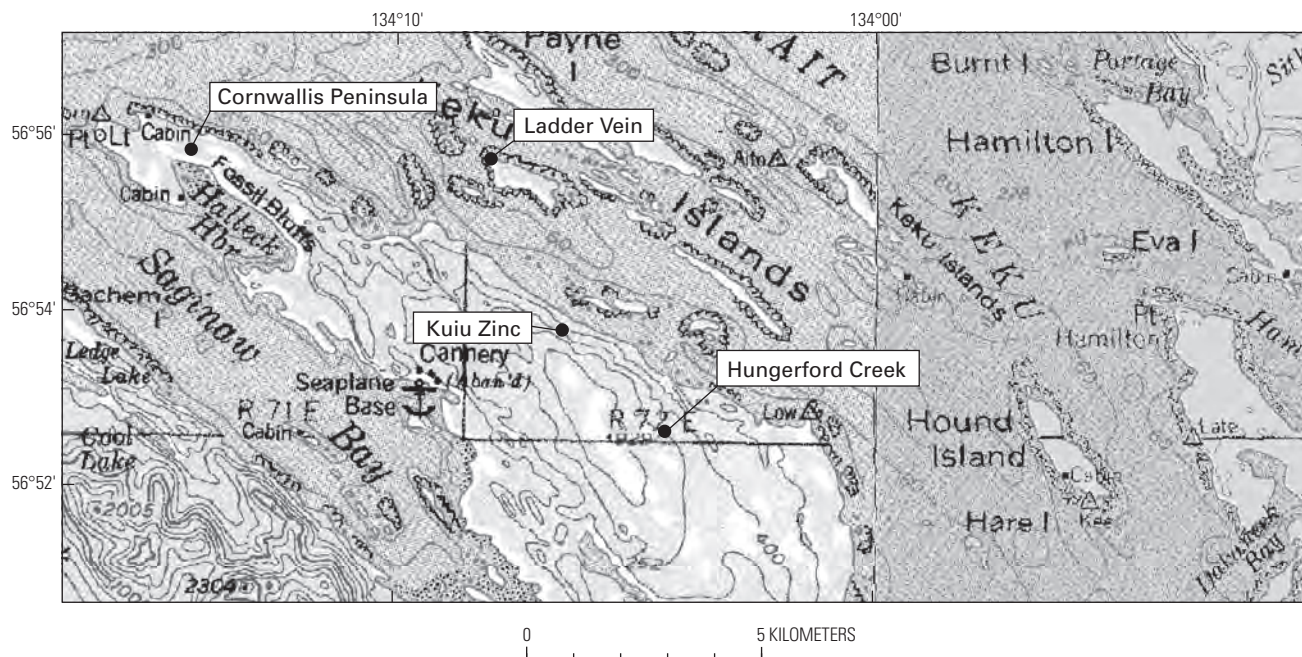


Figure 1, inset c. Detailed map of the central ATMB showing showing the locations of mines, mineral deposits, and mineral occurrences and other features discussed in the text in the Keku Strait area.

the Windy Craggy deposit (reserves estimated at 297.4 million metric tonnes at 1.38 percent copper, 0.07 percent cobalt, 0.2 gram per metric tonne gold, and 3.8 grams per metric tonne silver; Peter and Scott, 1999) to the north is correct, then a belt approximately 600 kilometers in length is defined that contains the largest Besshi-type VMS deposit (see review by Slack, 1993) in the world and the leading producer of silver in the United States. This metallogenic belt is herein referred to as the Alexander Triassic Metallogenic Belt (ATMB).

Host lithologies identify a distinctive geologic setting. The VMS deposits are nearly uniformly hosted within a thin package of structurally dismembered Upper Triassic (Norian) rocks characterized by bimodal volcanics and abundant flysch-type sediments. Mafic volcanic rocks predominate and commonly are volcanoclastics or flow breccias with lesser pillowed and massive flows. At larger, more obviously stratiform occurrences, sediments tend to be basinal in appearance, with high proportions of graphitic argillite and thin lenses of pyrite. Metamorphic grade varies from prehnite-pumpellyite to mid-greenschist. The base of the package is typically marked by the presence of angular to rounded polymictic conglomerate with clasts composed of the immediately underlying unit. In places, discrete packages of conglomerate occupy flow channels that migrate laterally and vertically within a short distance. High-angle faults of probable normal displacement are common and tend to mark changes in lithology, such as from sedimentary to volcanic rocks. Thin carbonate units are common as well and are generally dolomitic. Small outcrops of serpentinized mafic/ultramafic rock also tend to be spatially associated with deposits throughout the ATMB.

From south to north, a distinct variation in both the nature of the deposits and the host rocks is evident. At the southern end of the ATMB, the felsic component of the bimodal volcanic rocks is significant and becomes more rare or even absent northwards. The volcanic stratigraphy on both Annette and Gravina Islands is characterized by a thick sequence of rhyolitic volcanoclastics and tuffs low in the Upper Triassic section, which give way to voluminous mafic volcanoclastics and flows in the upper portion of the section. On the Cornwallis Peninsula in the Keku Strait area, minor mafic volcanic rocks constitute the base of the package and are overlain by a thick sequence of rhyolitic volcanoclastics and flows. Felsic volcanic rocks are rare north of Keku Strait. The northernmost occurrence of felsic volcanic rocks is on Mt. Henry Clay where thin flows of trachyandesite and quartz-sericite-pyrite altered rhyolite and rhyolitic tuffs are associated with the occurrences (Green and others, 2003). Additional but perhaps less obvious regional changes in the host rocks are an increase in the percentage of volcanic to sedimentary rocks to the north, and possibly an increase in metamorphic grade.

A noticeable change in the nature of the deposits parallels the change in host rock lithology. The deposits in the south are predominantly zinc-lead-silver bearing with large amounts of barite. In fact, some of the deposits such as on the Sylburn Peninsula on Annette Island and the Castle Island barite deposit in the Duncan Canal area are composed primarily of barite with minor sphalerite, galena, and tetrahedrite. These deposits share many similarities with Kuroko-type ores (for example, Franklin, 1986, 1993). From the latitude of about Petersburg to the north, deposits appear that contain

18 Geology, Geochemistry, and Genesis of the Greens Creek Massive Sulfide Deposit, Admiralty Island, Alaska

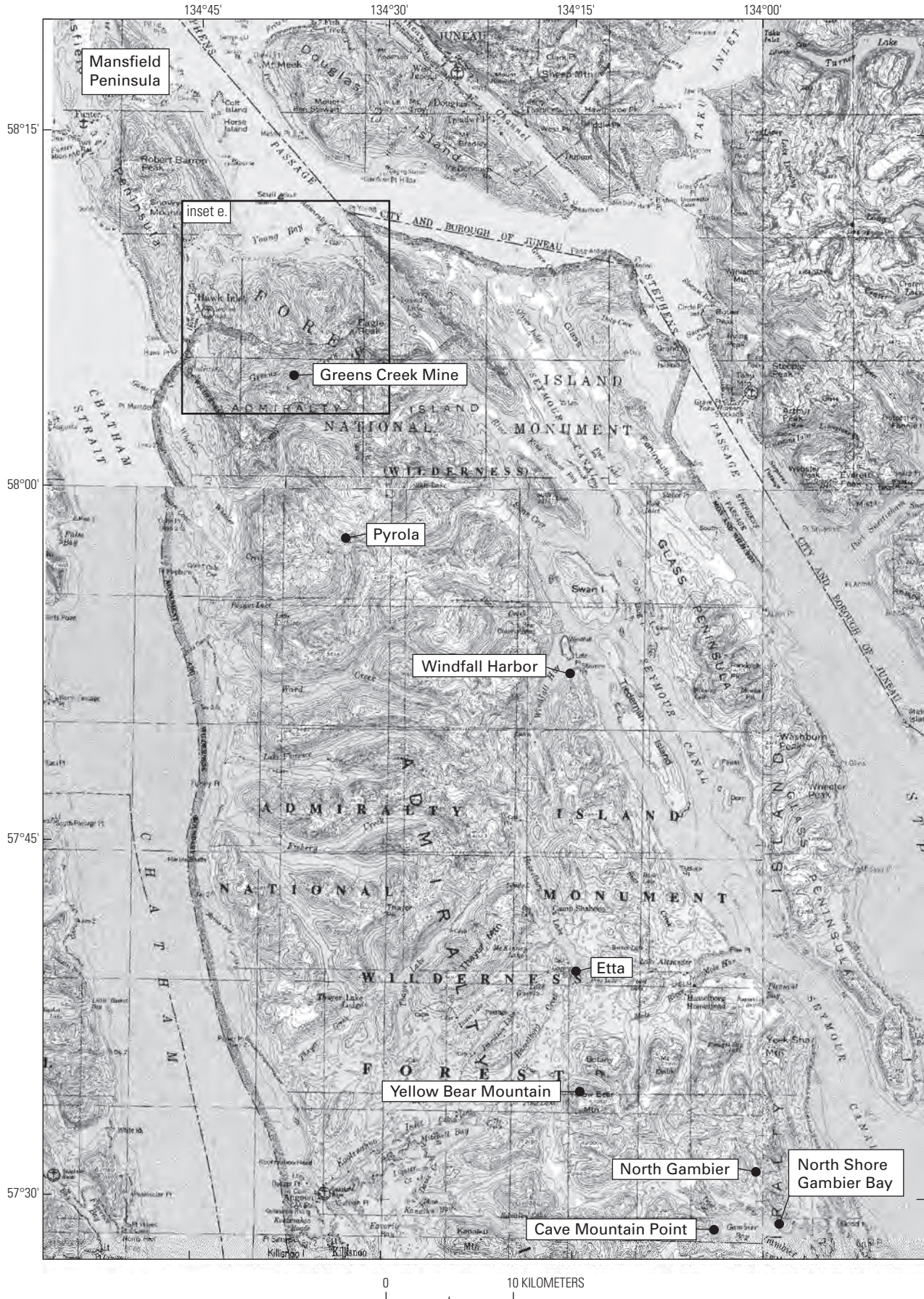


Figure 1, inset d (facing page). Detailed map of the central ATMB showing the locations of mines, mineral deposits, and mineral occurrences and other features discussed in the text on Admiralty Island.

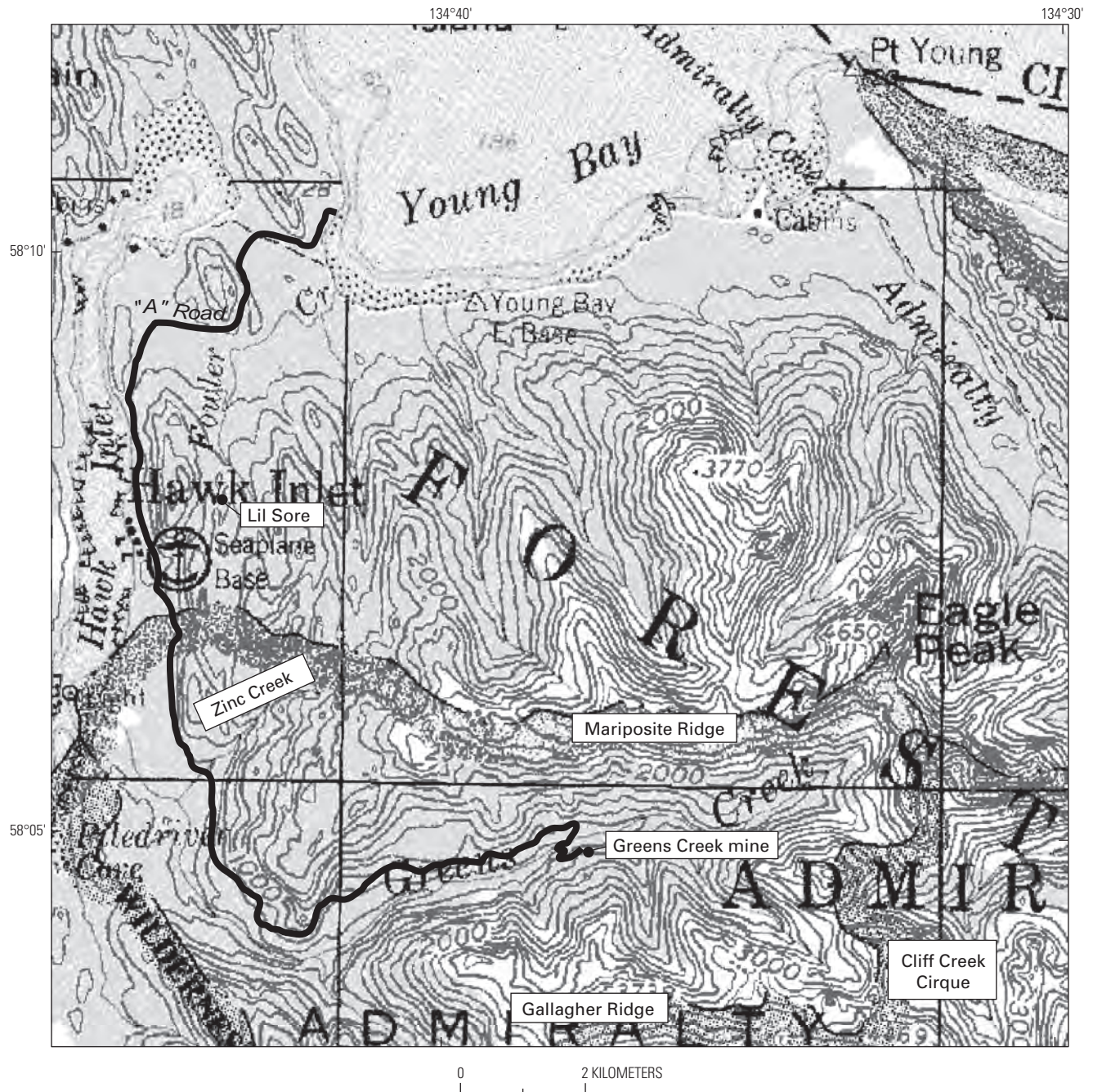


Figure 1, inset e. Detailed map of the Greens Creek mine area on northern Admiralty Island showing the locations of mines, mineral deposits, and mineral occurrences and other features discussed in the text. (Inset f) Detailed map of the northern ATMB showing the locations of mines, mineral deposits, and mineral occurrences and other features discussed in the text between the Mt. Henry Clay area and Windy Craggy.

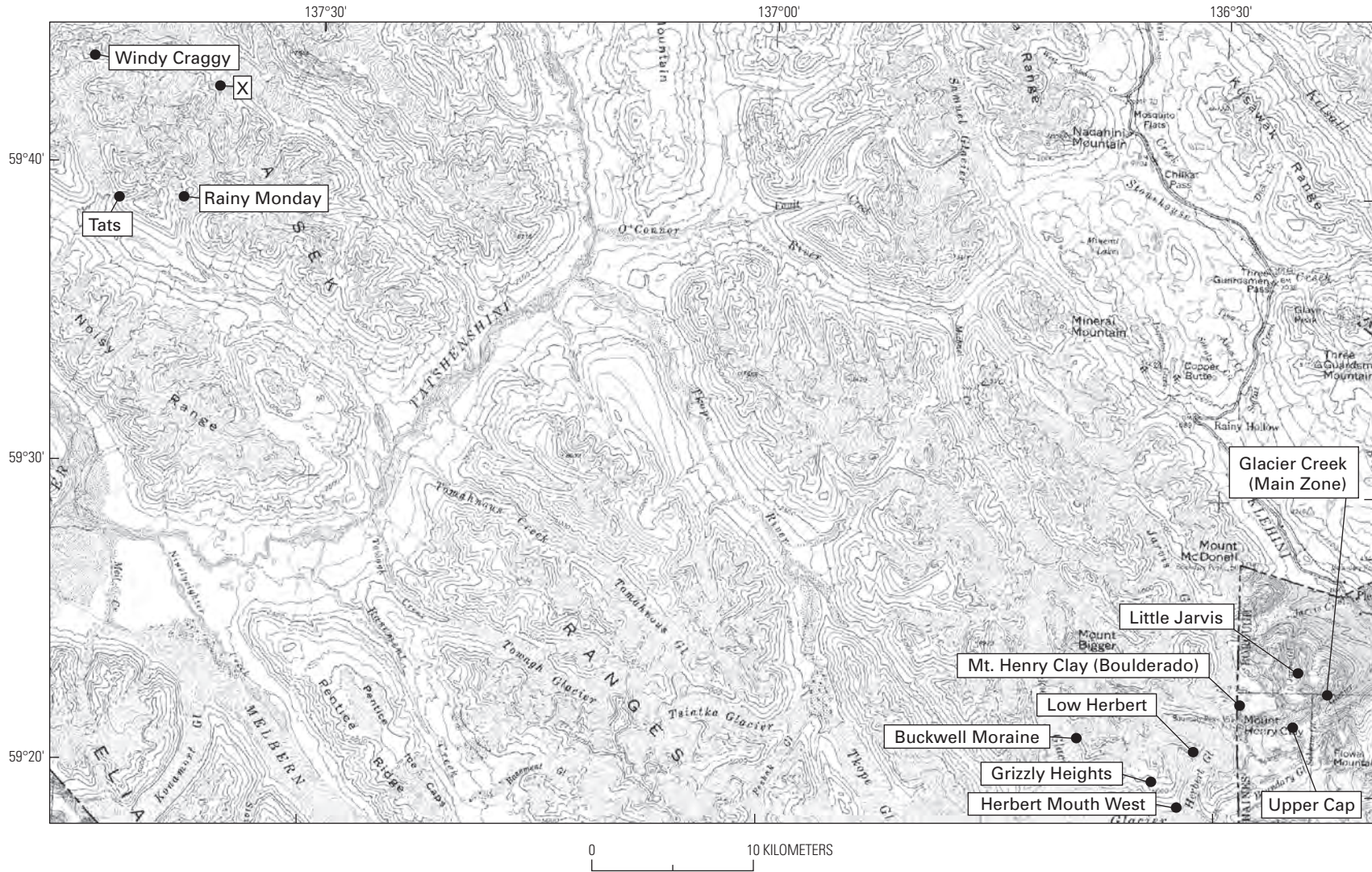


Figure 1, inset f. Detailed map of the northern ATMB showing the locations of mines, mineral deposits, and mineral occurrences and other features discussed in the text between the Mt. Henry Clay area and Windy Craggy.

Cu-Zn ± Au-Co-Ni and are similar to many Besshi-type ores (for example, Slack, 1993). The Frenchie VMS occurrence (St. John's Harbor) may be the southernmost of this type, and deposits of both descriptions occur on either side of the international border in the Mt. Henry Clay area. By the latitude of about the Tatshenshini River, the majority of the deposits are Besshi-like with Windy Craggy being the notable example. The Greens Creek deposit itself is unusual in that it exhibits a range of syngenetic, diagenetic, and epigenetic features that are transitional between VMS, sedimentary exhalative (SEDEX; see review by Goodfellow and others, 1993), and Mississippi Valley-type (MVT; see review by Leach and Sangster, 1993) genetic models (Taylor and others, 1999).

In the several locations where the host rocks of the ATMB have been studied, data uniformly suggest that the environment of deposition was some type of intra-arc or back-arc setting. Trace and REE chemistry of the mafic volcanics is transitional between midocean ridge basalt (MORB) and island-arc basalt (IAB), with discriminant plots based on immobile elements showing tectonic environments from MORB to within-plate basalts. Radiogenic isotopic data are indicative of a juvenile (mantle ?) source for the basalts. The several tectonic settings suggested to have produced these host rocks are variably: a brief episode of Late Triassic rifting prior to final docking of outboard terranes to the continental margin, small pull-apart basins in response to transpressive motion along the margin, or a failed rift.

Under close examination, however, the correlation of host rocks throughout the 600-km-long ATMB is problematic. Traditionally, the central strip of Upper Triassic volcanics, from Annette Island to at least the latitude of mid-Admiralty Island, was placed in the Alexander terrane. The Upper Triassic rocks on the mainland to the east were assigned to the Taku terrane, and the strip of Upper Triassic greenstones at Goondip to the west were placed in the Wrangellia terrane (for example, Berg and others, 1972, 1978; Churkin and Eberlein, 1977; Gehrels and Berg, 1994). Tentative correlation of the Hyd Group rocks on Admiralty Island with the informally named Jarvis basalts at Mt. Henry Clay, and with the informally named Tatshenshini basalts on the Canadian side of the border, would extend the central strip of rocks at least as far north as Windy Craggy within the Alexander terrane. However, correlation of the basalts at Chilkat in the central strip with the basalts at Taku of the eastern strip near Juneau (Ford and Brew, 1993; Gehrels and Barker, 1993) and with possible Hyd Group-equivalent rocks on the north end of Admiralty Island (Ford and Brew, 1993), raises the possibility that all of the Upper Triassic rocks of the composite Alexander-Wrangellia terrane are genetically related and formed during the same igneous event.

As originally defined, the distinguishing difference between the Alexander and Wrangellia terranes is the age and character of the Upper Triassic volcanic rocks. Wrangellia terrane basalts, as exemplified by the Nikolai Greenstone, basalts at Chilkat, greenstones at Goondip, and Karmutsen Formation, are voluminous, subaerial to shallow subaqueous, flood basalts of Carnian (230 Ma) age that were extruded over

a period of about 5 million years (Panuska, 1990; Richards and others, 1991). In contrast, the basalts of the Alexander terrane, as exemplified by the Hyd Group, the Hound Island Volcanics of the Hyd, and possibly the Jarvis basalts of the Mt. Henry Clay area and the Tatshenshini basalts of northern British Columbia, are much thinner flows of Norian (210 Ma) age that are intercalated with graywacke and graphitic/pyritic mudstone. Several competing models for the production of the basalts of the Wrangellia terrane include an episode of volcanism related to intra-arc or back-arc rifting (Barker and others, 1989; Sampson and others, 1991; Barker, 1994), or to production of an oceanic plateau flood-basalt province in response to initiation of a mantle plume beneath the Paleozoic arc (Richards and others, 1991). The Alexander terrane basalts have generally been ascribed to formation during a period of intra-arc or back-arc rifting.

Since the recognition that Pennsylvanian plutons stitch the two terranes into one Wrangellia supercontinent (Gardner and others, 1988), distinctions between the Alexander and Wrangellian Upper Triassic rocks have been glossed over, and they are generally regarded as probable lateral facies of the same extensive unit. The extreme structural dismemberment and juxtaposition of parallel strips of rocks in southeastern Alaska, and thus the rapid variation in thickness of the Upper Triassic section and the associated variation in the percentage of volcanic to sedimentary rock, are explained as having occurred primarily in the Tertiary as a result of lateral transport of terranes northward along the continental margin. Alternatively, the volcanism could have occurred at multiple sites of rifting during discrete intervals from Carnian to Norian time.

Whereas the lumping of all of the Triassic volcanic rocks into one related package of rift- or plume-related rocks is convenient, it leaves unanswered the important question of why the belt of VMS deposits is only associated with basalts of the Alexander terrane. In this chapter we document the geology, stratigraphic setting, and mineral and host-rock geochemistry at a number of mineral occurrences within the ATMB. Our goal is to assemble a coherent metallogenic framework for the ATMB that will serve as a foundation for the more detailed chapters that follow on the Greens Creek deposit. This chapter treats a topic that was covered in a previous publication (Taylor and others, 2008), but it reports a greatly expanded chemical and isotopic database, many new figures, and extended descriptions and discussions.

Terrane Relationships

Host rocks to the ATMB are within the Admiralty and Craig subterrane of the Alexander terrane (Berg and others, 1972, 1978; Churkin and Eberlein, 1977). Terrane relationships in southeastern Alaska are shown in figure 2. The general evolution of the Alexander terrane has been discussed by Sampson and others (1989), who suggested that it has the characteristics of a wholly oceanic island arc. The terrane is

an allochthonous, continent-sized fragment of island arc crust that began forming in latest Precambrian time in low latitudes. It consists of as much as 35,000 feet of predominantly marine sedimentary and volcanic strata and plutonic rocks of latest Precambrian(?) to Middle(?) Jurassic age (Gehrels and Saleeby, 1987; Gehrels and Berg, 1994). By Devonian time the terrane had gone through two orogenies and a protracted period of quiescence marked by erosion and formation of extensive carbonate platforms. Paleomagnetic, paleontologic, and detrital zircon studies (Hillhouse, 1987; Hillhouse and Gromme, 1984; Haeussler and others, 1992; Bazard and others, 1994; Gehrels and others, 1994; Savage, 1994) suggest that by middle Permian time the terrane was outboard of a continental landmass and that depositional environments were characterized by shallow, tropical marine, possibly evaporitic, conditions.

Rift-fill stratigraphic sequences and bimodal volcanism along the eastern edge of the terrane (MacIntyre, 1986; Gehrels and others, 1986, 1987; Taylor and others, 2008) mark the beginning of an extensional tectonic event in the Late Triassic that either split the terrane or separated it from its low-latitude, offshore position and transported it to its present location on the western North American continental margin (Gehrels and Berg, 1994). The allochthonous Wrangellia terrane of Pennsylvanian to Late Triassic age (Jones and others, 1977), which is also of oceanic arc derivation (Sampson and others, 1990), adjoins the Alexander terrane on its western, northern, and northeastern sides. These terranes were stitched together by Middle Pennsylvanian plutons in southern Alaska (Gardner and others, 1988) to form the Wrangellia superterrane. Accretion of the Wrangellia superterrane may have commenced by the Early or Middle Jurassic (McClelland and Gehrels, 1990) or the Late Jurassic (Saleeby, 1994) and was complete by about middle Cretaceous time, as indicated by the intrusion of subduction-related, magmatic-epidote-bearing plutons and the development of the Jurassic-Cretaceous Chugach accretionary prism outboard of the superterrane.

Collision resulted in regional metamorphism and deformation related to underthrusting of the continental margin. This event produced relatively flat-lying, northwest-vergent thrust faults identified underground and in surface outcrops on Admiralty Island and throughout southeastern Alaska. Mapping of regional metamorphic facies by Dusel-Bacon (1994) places Triassic and older rocks in southeastern Alaska within the lower to middle greenschist facies. In early Tertiary time (Goldfarb and others, 1991; Miller and others, 1994), oblique subduction changed to right-lateral transcurrent motion along the margin, imparting the present structural grain to the country rocks and causing the formation of numerous, subparallel, high-angle, strike-slip faults that dismember the outboard terranes.

Stratigraphy of Host Rocks to Late Triassic Mineral Occurrences and Correlation Throughout Southeastern Alaska

The host rocks to the mines, deposits, and mineral occurrences examined during the course of this study are discontinuously exposed for approximately 600 kilometers along the eastern margin of the Alexander terrane, from Annette Island in the south, northward to Windy Craggy. In general, the stratigraphy within the ATMB consists of a 200–800-m-thick sequence of conglomerate, limestone, marine clastic sediment, volcanic rock, and tuff that are intercalated with and overlain by a distinctive unit of mafic pyroclastic rocks and pillowed flows (fig. 3). Faunal data bracket the age of the host rocks between Anisian (Middle Triassic) and late Norian (middle Late Triassic) time.

On Annette (fig. 4) and Gravina Islands (fig. 5) at the southern end, and in Keku Strait (fig. 6) in the middle portion of the ATMB, the base of the section is marked by a distinctive pebble conglomerate indicative of high-energy deposition in a near-slope or basin-margin setting. Clasts are polymictic, extremely immature, and are locally derived from the immediately underlying rocks. Features of the conglomerates indicate changing proximity to the source area. The median size and sorting of the clasts as well as the thickness and continuity of the units substantially change to the north. On Annette and Gravina Islands the dominant clast lithology is Silurian trondhjemite derived from the extensive pluton that underlies most of Annette Island and the south end of Gravina Island (Berg, 1972, 1973; Karl, 1992). Clast sizes range from pebbles to boulders 3 meters in diameter in continuous conglomerate sheets 30–45 meters thick (fig. 7). In Keku Strait clasts are dominantly composed of dolomite and chert from the underlying Pybus and Cannery Formations. Clasts are pebble- to boulder-sized (maximum of 0.3 m in long dimension) and occur in thin (0–6 m) discontinuous outcrops. In places, most notably on the northern shore of Hamilton Island, conglomerates occupy discrete scour channels that migrate laterally and vertically in a graywacke host.

A profound change in the character of the Upper Triassic stratigraphy occurs between Keku Strait and Duncan Canal. Both the sedimentary and volcanic units that comprise the section transition into rock types indicative of a position more distal to the Late Triassic rift margin. Whether this simply reflects a more seaward Late Triassic relative position of the Duncan Canal area to the east of Keku Strait or whether juxtaposition by faulting or folding of the two areas has occurred is not resolvable, given the current state of mapping and the

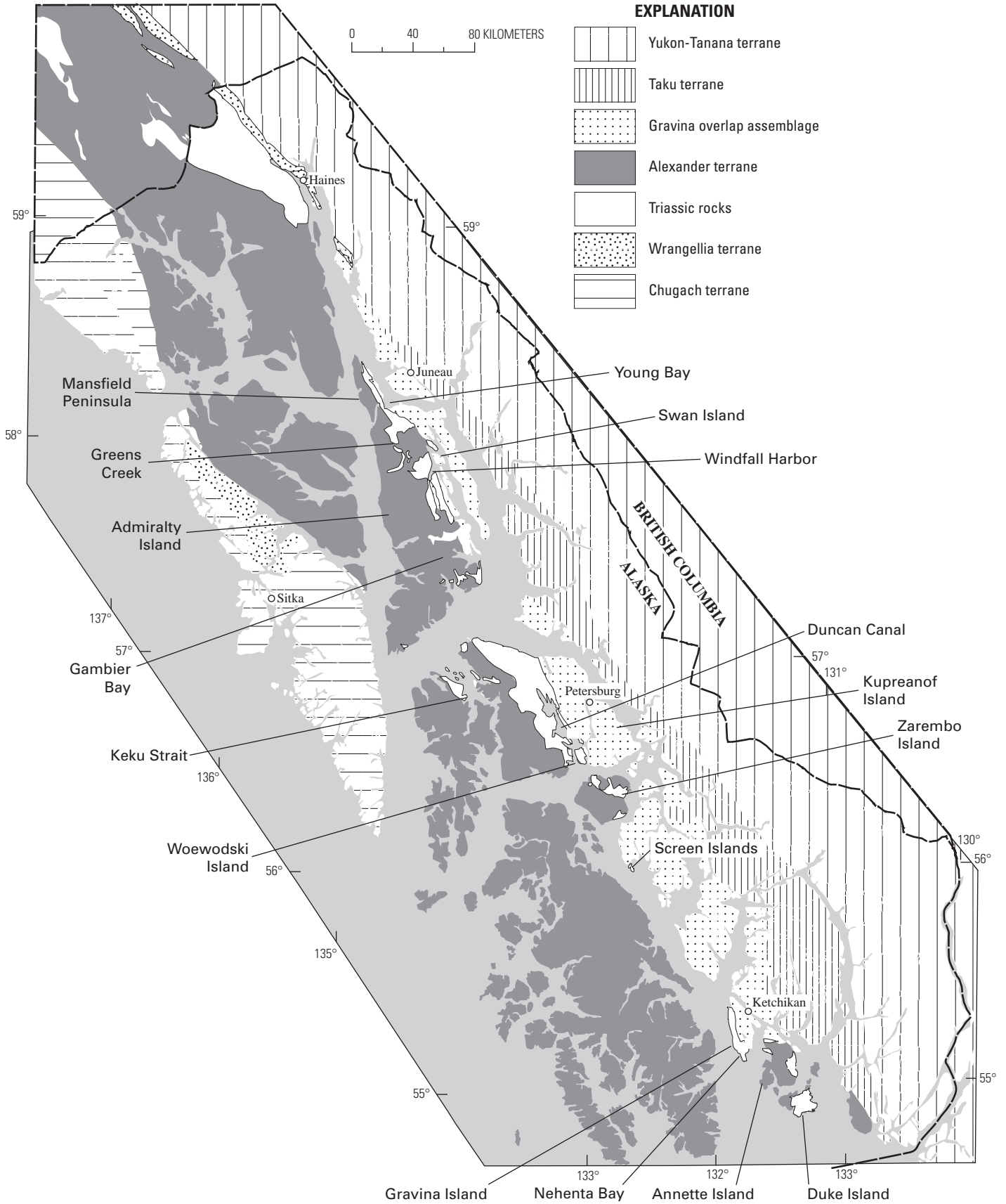


Figure 2. Tectonostratigraphic terranes of southeastern Alaska.

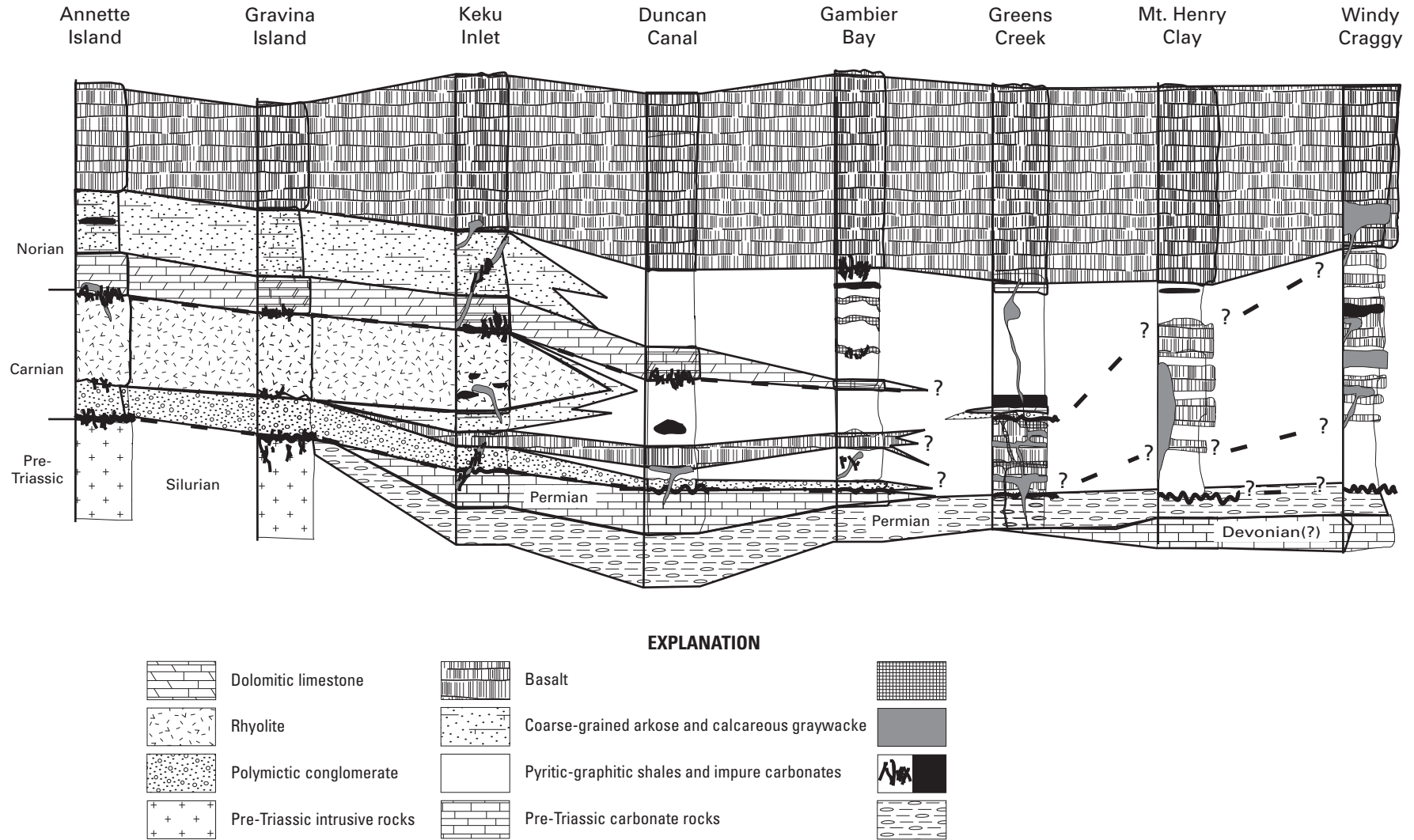


Figure 3. Stratigraphy and correlation of Upper Triassic host rocks in southeastern Alaska and adjacent British Columbia.

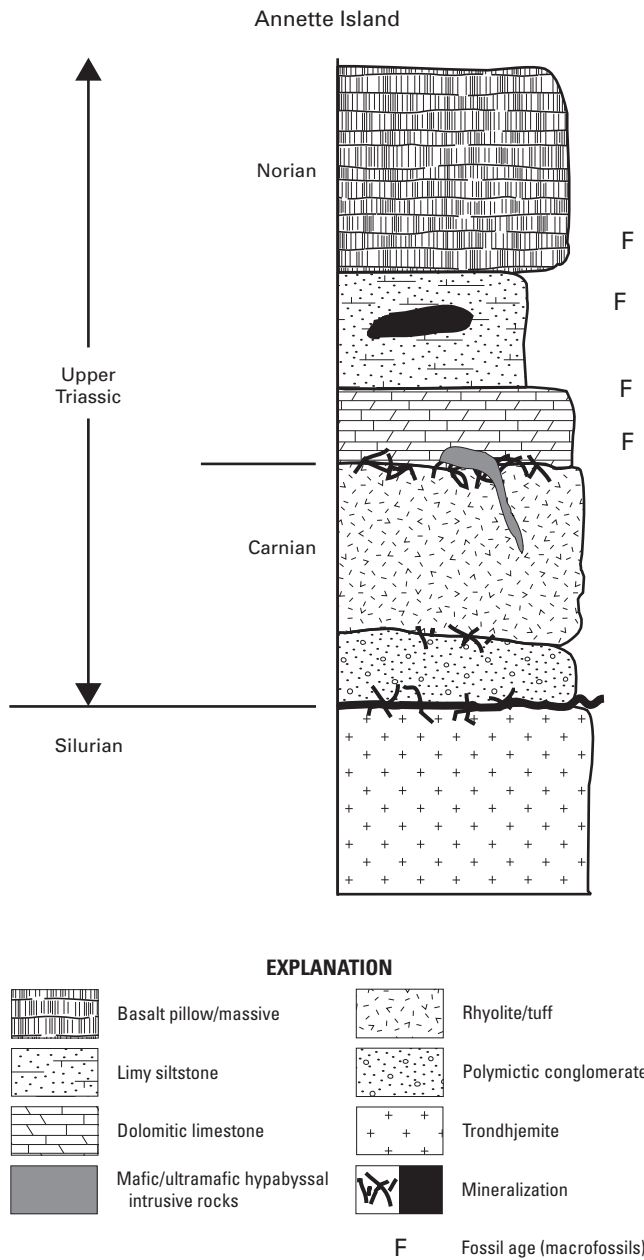


Figure 4. Composite stratigraphic column of the Upper Triassic section on Annette Island. Interpretation is based on Berg (1972), Gehrels and others (1987), Karl (1992), and this study.

generally poor exposure on most of Kupreanof Island. Tectonic shortening of a former basin is consistent with the synclinal structure proposed for the Keku Strait (Muffler, 1967) and is also compatible with the pattern of open folding and northwest-vergent thrusting documented by recent mapping in the Duncan Canal area (Karl and others, 1999a). Alternatively, juxtaposition of seaward (Duncan Canal) and landward (Keku Strait) areas of a northward-deepening rift basin may have resulted due to northward transport of the southern portion of the ATMB during Tertiary margin-parallel faulting.

When present, the basal polymictic conglomerate in Duncan Canal (fig. 8) reflects the character of a debris flow

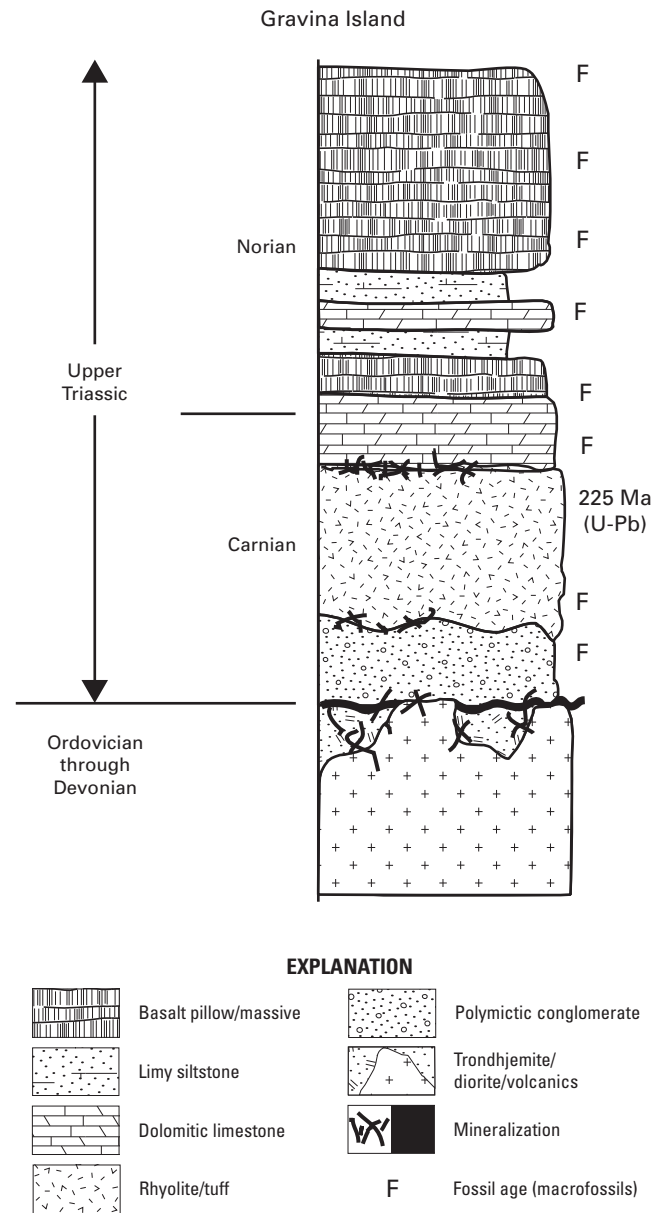


Figure 5. Composite stratigraphic column of the Upper Triassic section on Gravina Island. Interpretation is based on Berg (1973), Gehrels and others (1987), and this study.

that is distal to its source. Clasts are millimeters to several centimeters in size and occur in thin (0–10 meters) discontinuous outcrops. However, clasts appear to be subrounded and somewhat more sorted than conglomerates to the south. Clasts are dominantly composed of white quartz pebbles and chert with a lesser but important component of black shale chips that are probably derived from the underlying Cannery Formation. In two outcrops examined, one on the northwestern shore of Woewodski Island and a second on the west side of Duncan Canal north of the Castle River, the clasts are stretched considerably and the sericitic matrix appears drawn out by shearing. This deformation, related to movement in the

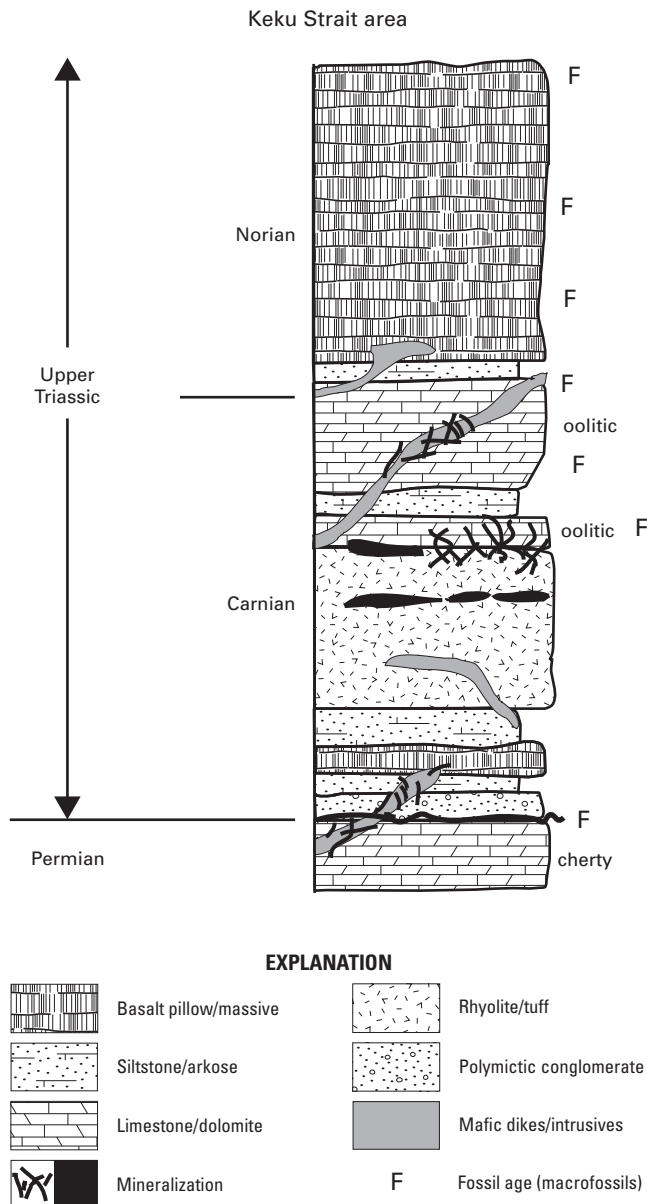


Figure 6. Composite stratigraphic column of the Upper Triassic section in the Keku Strait area. Interpretation is based on Muffler (1967), and this study.

Duncan Canal shear zone (McClelland and Gehrels, 1990; Haeussler and others, 1999), has imparted a platy, fissile character to the conglomerates not observed at the previously described locations.

By the latitude of Gambier Bay and Windfall Harbor on Admiralty Island the basal polymictic conglomerate is only locally present (fig. 9). Clasts are mostly pebble to cobble sized and are dominantly composed of chert and dolomite, derived from the underlying Permian units. Individual conglomerate horizons are no thicker than about 3 meters. Although thin and discontinuous conglomerate horizons

occur in the northern half of Admiralty Island, their stratigraphic positions within the Triassic section are uncertain. In most cases, they are thought to be above the base of the section within the shales that constitute the middle sedimentary portion of the Triassic stratigraphy. Additionally, these midsection conglomerates are similar in clast composition and maturity to the more distal-looking conglomerates in the Duncan Canal area. Notable examples are the thin quartz pebble-rich horizons in the 720 access ramp underground at the Greens Creek mine (fig. 10), and the 2-m-thick horizon immediately west of the drill pad at the Little Sore prospect several kilometers north of the mine. The stretched quartz-pebble-rich conglomerate near Young Bay along the A-road may be an additional example.

The northernmost occurrences of a conglomerate “marker horizon” at the base of the Triassic section are on the eastern shore of Windfall Harbor immediately overlying the siliceous black shales of the Cannery Formation, and the debrisite in Zinc Creek, described by Duke and others (chap. 4, the term debrisite is used here to connote debris-flow deposits, following Warme and Kuehner, 1998). Our examination of this unit shows it to be a very poorly sorted, proximally derived polymictic conglomerate, composed of angular fragments of the immediately underlying lithologies. Abundant pyrite and iron carbonate in the matrix suggest the unit has been mineralized. Similarity to angular conglomerates in the footwall stratigraphy at the North Gambier pyritic copper-zinc-silver-barite occurrence (Taylor and others, 1992) suggests local fault control on the distribution of the basal conglomerates and on hydrothermal fluid flow. North of Admiralty Island, the basal conglomerate is absent, and no midstratigraphy conglomerate lenses are reported in the Triassic section.

In the southern end of the ATMB, dominantly felsic volcanic rocks immediately overlie the basal conglomerate. Thin basaltic flows are variably present as well near the bottom of the section and tend toward alkali basalt compositions. Massive and pillowed basalt flows occur within the sedimentary portion of the section on Gravina Island overlying the Puppets Formation. In the Keku Strait area we place thin basaltic flows within an interval of arkosic sediments immediately below the Keku Volcanics. Muffler (1967) also described mafic flows intercalated with the Keku Volcanics. On Annette and Gravina Islands the rhyolites are continuous, massive, flow-banded units; the cliff exposure of the Puppets Formation in Nehenta Bay is on the order of 150 meters thick. Berg (1973) estimated the unit to be 165 meters thick. On the Cornwallis Peninsula the Keku Volcanics is of uncertain thickness due to structural complexities but occupies an eastward-dipping belt 1.5 to 5 kilometers wide (Muffler, 1967). Drilling on the peninsula in 1995 by Sealaska Corporation was collared in the Keku Volcanics and penetrated over 366 meters of massive, flow-banded, volcanoclastic, and tuffaceous rhyolite without encountering a bottom contact. The position low in the section beneath the sedimentary and overlying mafic volcanic rocks, as well as the distinctive chemistry of the Keku Volcanics (discussed in succeeding



Figure 7. Photograph of the basal Upper Triassic conglomerate in Nehenta Bay, Gravina Island. Note abundance of light-colored clasts of Silurian trondhjemite derived from the pluton that underlies much of Annette and southern Gravina Islands.

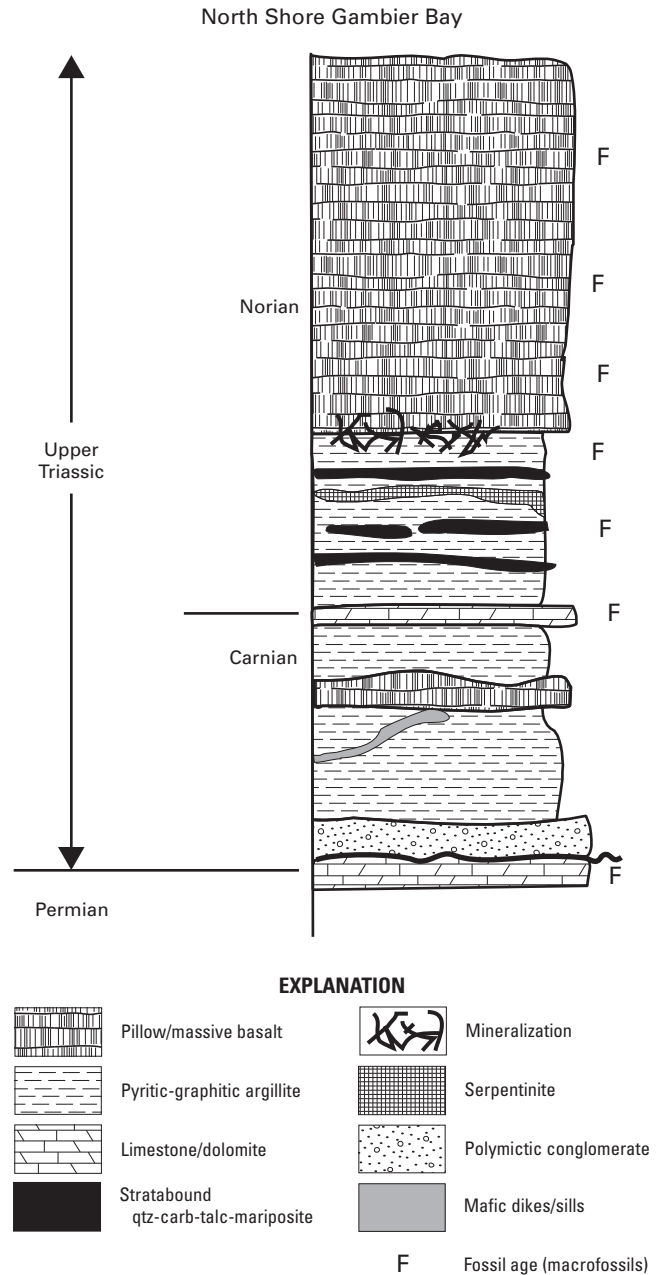
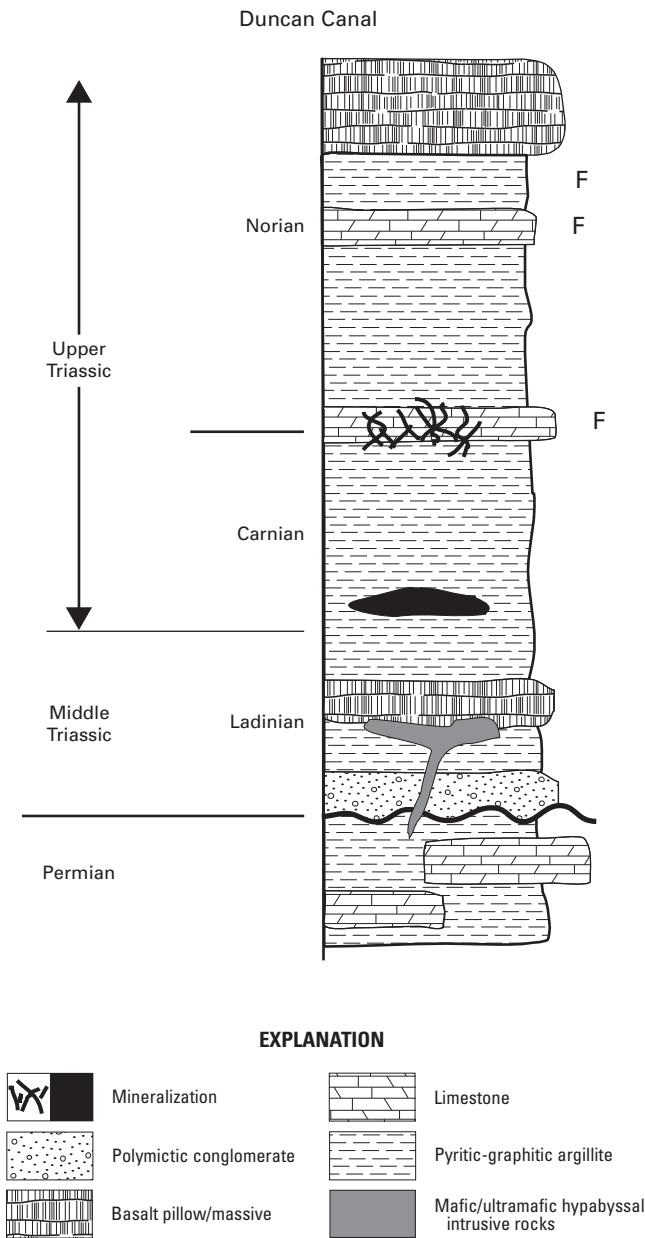


Figure 8. Composite stratigraphic column of the Middle and Upper Triassic section in the Duncan Canal area. Present interpretation is based on McClelland and Gehrels (1990), Karl and others (1999b), and this study.

Figure 9. Composite stratigraphic column of the Upper Triassic section on the north shore of Gambier Bay, southern Admiralty Island. Interpretation is based on Loney (1964), Taylor and others (1992), and this study.

paragraphs), strongly suggest origins as bimodal volcanic rocks that were produced during the initiation of rifting.

In the Duncan Canal area, the stratigraphy is poorly constrained due to poor exposure. Rhyolites are largely absent north of Keku Strait, and their place low in the section is occupied instead by minor basalt flows interbedded with black shale. At the mouth of Castle River on the west side of Duncan Canal, thin (~4-m-thick) columnar-jointed basalt flows occupy a stratigraphic position just above the

conglomerates. Similarly, pillowed basalt flows are present on the north tip of Little Castle Island immediately west of (underlying ?) the Castle Island barite deposit. On the northwest shore of Woewodski Island, a thin basalt flow lies immediately beneath a stretched pebble conglomerate lens that we interpret to be the Upper Triassic basal conglomerate. Black shales immediately overlying the conglomerate contain several 15-cm-thick horizons of pyritic felsic tuff. To the south on Woewodski Island, several crudely stratiform

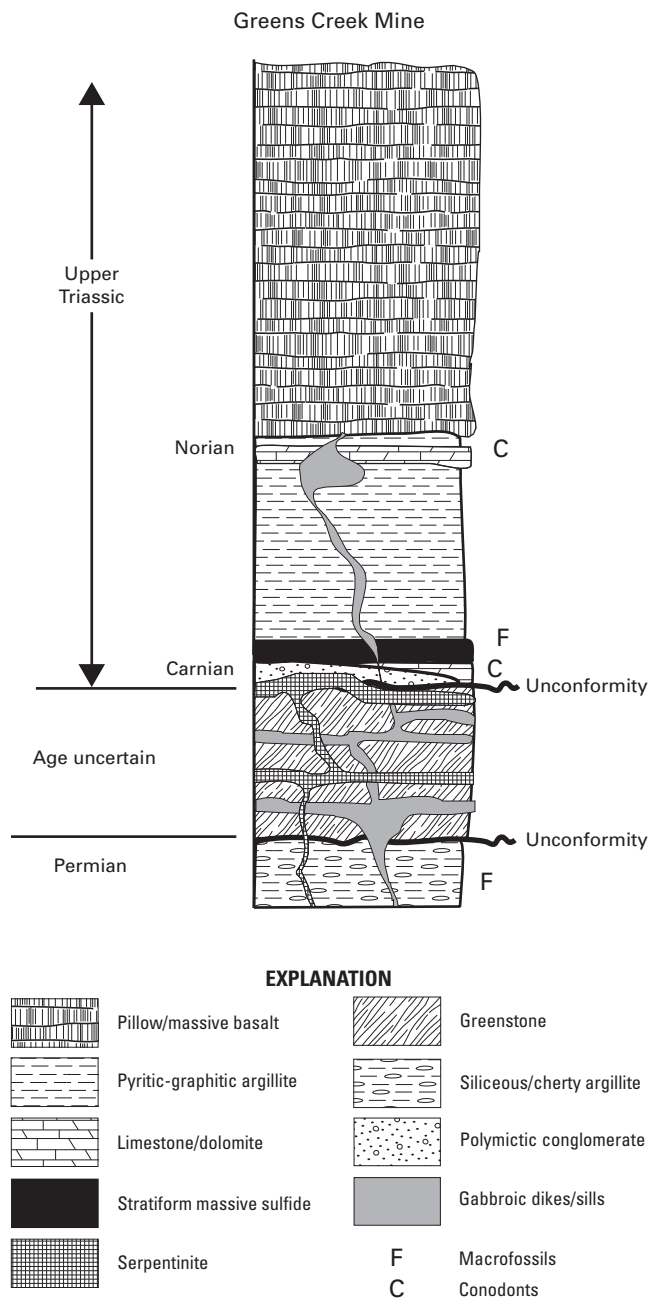


Figure 10. Composite stratigraphic column of the Upper Triassic section at the Greens Creek mine, northern Admiralty Island. Interpretation is based on this study.

mineral occurrences of probable Late Triassic age (for example, Lost Show and Brushy Creek) are hosted in highly altered volcanic rocks. Although protoliths are obscured, it is unlikely that the altered volcanics were rhyolites. Their chemistry (for example, 98DC-33, table 2) and mineralogy is most consistent with altered mafic volcanic rocks. Less altered country rocks consist of mafic volcanic, volcanoclastic, and tuffaceous rocks. Highly altered tuffaceous rocks at Brushy Creek and sericite schist in creek exposures several hundred

meters south of the occurrence could represent felsic tuffs. Poor exposure precludes assignment of these volcanic rocks to a specific position within the Upper Triassic stratigraphy.

On Zarembo Island, Upper Triassic rocks occur in a northwest-trending swath of flat topography that limits exposures to creek banks and borrow pits along logging roads. Absence of a recognizable stratigraphic marker horizon at the Frenchie pyritic massive sulfide deposit prevents distinguishing the stratigraphic position. However, the host rock immediately overlying the Frenchie deposit is a 6- to 10-meter-thick unit of pyritic quartz-sericite schist; the immediate footwall contains a thin lens of muscovite schist overlying graphitic pyritic argillite. Relationships at the Round Point mineral occurrence to the southeast are similarly obscure. Like the volcanic-hosted deposits on Woewodski Island, Round Point is hosted in altered volcanic rocks of probable mafic parentage.

Felsic volcanic rocks in the ATMB north of the felsic tuffs on the northwest shore of Woewodski Island and the Keku Volcanics in Keku Strait are rare. Recent mapping (S.M. Karl, oral commun., 2004) has identified outcrops of rhyolite of probable Triassic age on central Admiralty Island along the shoreline of Seymour Canal west of Swan Island, and vicinity. Thin units of quartz-sericite-pyrite altered trachyandesite, rhyolite, and felsic tuffaceous rocks associated with the RW zone (also called the Little Jarvis occurrence) of the Glacier Creek (Main) deposit (fig. 11) (Green and others, 2003) constitute the northernmost occurrence of Upper Triassic felsic volcanic rocks.

North of the Duncan Canal area, the position low in the Triassic section occupied by the rhyolites is filled by mafic lava flows. On the north shore of Gambier Bay, at least two separate pillowed flows are present in graphitic sediments above the basal conglomerate (fig. 12). Similarly, an outcrop of pillow basalt is present between the conglomerates and sediments in the footwall section of the North Gambier occurrence, 2.5 kilometers to the north (Taylor and others, 1992). At Greens Creek, the age of the footwall phyllites remains the major unanswered question of the current research effort. The position of the phyllites immediately below and in apparent conformable contact with the argillites suggest that they represent a locally thickened accumulation of mafic volcanics low in the section, as observed in Gambier Bay and elsewhere. The presence of the conglomerate horizons, both in the footwall and in the immediate hanging wall as previously described, does little to clarify the problem, as they are not clearly identifiable as the locally derived, polymictic conglomerate marker horizon commonly present at the base of the section. The highly altered and foliated nature of the footwall phyllite also distinguishes it from other mafic volcanics low in the section and invites comparison to other, older mafic units that display similar styles of deformation. Current mapping by Duke and others (chap. 4) assigns the footwall phyllites to the Middle(?) Devonian Retreat Group. Karl and others (S.M. Karl, oral commun., 2004) map a metamorphic unit of mixed lithologies including black phyllite, greenschist, and Devonian metalimestone on the north side of Greens Creek, stratigraphically beneath the Cannery Formation

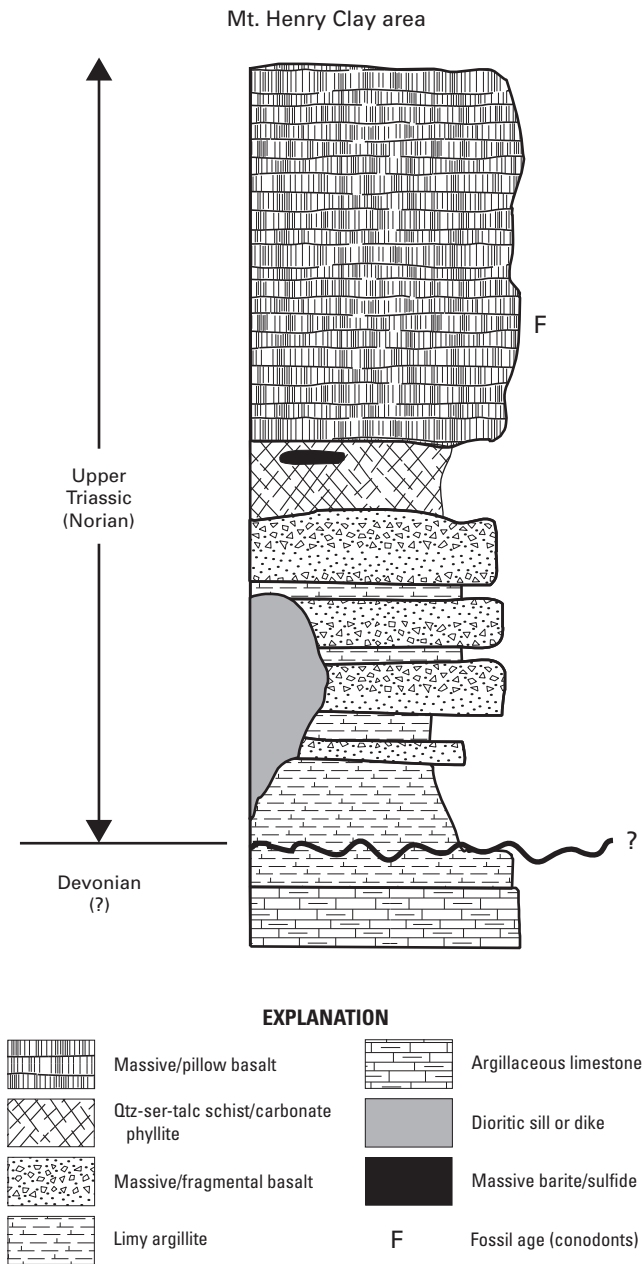


Figure 11. Composite stratigraphic column of the Upper Triassic section in the Mt. Henry Clay area, northern southeastern Alaska and northwestern British Columbia. Modified from MacIntyre and Schroeter (1985).

and Hyd Group. We note the evidence to suggest a Late Triassic age for the footwall; however, in the absence of direct evidence of a Late Triassic age we assign the footwall to an uncertain Late Triassic, Permian, or older lithologic association (fig. 10). At both Mt. Henry Clay and Windy Craggy (fig. 13), felsic volcanic rocks are absent, and their position low in the section is occupied by mafic volcanic rocks (MacIntyre and Schroeter, 1985; Forbes and others, 1989; Peter and Scott, 1999).

In the southern portion of the ATMB the rhyolites are overlain by dolomitic limestones that in places contain ooids (Muffler, 1967) and abundant fossils (Muffler, 1967; Berg, 1973), indicative of a shallow marine depositional environment (Muffler, 1967). The carbonate portion of the section also contains carbonate turbidites and carbonate breccias with fining-upwards sequences (for example, Nehenta Bay of Gravina Island, Screen Islands) indicative of the destruction of a shallow carbonate ramp during the onset of rifting. The limestones are present as 15-meter-high cliffs on the Cornwallis Peninsula, but thin substantially northward. They occur discontinuously in the Duncan Canal area and across Admiralty Island. In Gambier Bay the limestones are present as a locally exposed carbonate/dolomite breccia near the base of the section. In the Cliff Creek Cirque and in several locations along Gallagher Ridge immediately south of the Greens Creek mine, thin carbonate beds lie just below and are intercalated with the capping Hyd basalts. Underground at Greens Creek, thin discontinuous beds of fossiliferous limestone with *Halobia* fragments establish a Late Triassic age for carbonates in the footwall of the orebody and represent additional evidence for a Triassic age of the underlying phyllites. Unfortunately, the highly altered nature of the footwall carbonate rocks and their commonly brecciated texture yields uncertainty regarding the nature of the phyllite-carbonate contact. The footwall carbonate rocks may well be carbonate debris flows and thus could be stratigraphically equivalent to the basal conglomerate. North of Admiralty Island, discrete limestone units appear to be missing from the section.

The disappearance of the limestones from the section is accompanied by a corresponding increase in carbonaceous shales, indicative of deeper water settings. As far north as Keku Strait, the middle portion of the section is composed of very limy, arkosic sediments characteristic of a proximal, carbonate-rich source on the flanks of the Alexander terrane. From Zarembo Island northward the sediments contain more graphitic, pyritic black shale, indicative of an anoxic to euxinic, sediment-starved depositional environment distal to the flanks of the rift. At Greens Creek the shales (argillites) are intercalated with dolomitic limestone, and at Windy Craggy the black shales are markedly calcareous (Peter and Scott, 1999).

Most everywhere throughout southeastern Alaska and adjacent British Columbia the Triassic stratigraphy is capped by a thick (200–600 m) sequence of basalts. These basalts are massive to pillowed and commonly show spectacular volcanoclastic textures. In hand specimen and thin section, the basalts are vesicular and mostly aphanitic; minor porphyritic-aphanitic varieties contain relict phenocrysts of clinopyroxene, plagioclase, hornblende, and rare olivine. Compared to the generally foliated Paleozoic greenstones of the Alexander terrane, these Norian-age basalts are relatively undeformed. In the absence of the basal conglomerates, the thick sequence of greenstones overlying the sedimentary portion of the section is the most distinguishing feature of the Upper Triassic stratigraphy. Although the basalts have a variety of names throughout the ATMB—Chapin Peak Formation of Hyd Group on



Figure 12. Pillowed basalt flow near the base of the Upper Triassic section on the north shore of Gambier Bay, southern Admiralty Island.

Gravina Island (Berg, 1973); Hound Island Volcanics in the Keku Strait (Muffler, 1967); Hyd Group basalts on Admiralty Island (Latham and others, 1965); Jarvis basalts (informal) in the Mt. Henry Clay area (Forbes and others, 1989); Tatshenshini basalts (informal) of northwestern British Columbia (MacIntyre and Schroeter, 1985)—they are all related by similar age, chemistry, and stratigraphic position.

Geochemistry of Upper Triassic Basalts and Rhyolites of Southeastern Alaska

Whole-rock geochemical data for Upper Triassic igneous rocks at mineral occurrences and unmineralized outcrops throughout southeastern Alaska were obtained in order to evaluate the petrogenetic setting of the ATMB. Major, minor, and trace-element abundances were determined by XRF, lithium metaborate fusion ICP–MS, and ICP–AES in the USGS laboratories in Denver. Summary data for a number of key locations are given in [table 1](#); all the data are presented in [table 2](#). General analytical methods and information on accuracy and precision of each method are described in Taggart

(2002). Specific information on the lithium metaborate fusion ICP–MS analytical method used to obtain rare-earth and high field-strength elemental data critical to the tectonic discriminant analysis presented herein is available in Meier and Slowik (2002). Lower limits of detection (LOD) are represented in [table 2](#) as less-thans and are 3 sigma values that are calculated for each instrument run based on multiple analyses of reagent blanks. Multiple analyses of internal laboratory standards are used to calibrate the instrument response, and then accuracy and precision of the analyses are verified to be within published limits by analysis of several USGS standard reference materials that are included in each run. Due to the nature of the ICP–MS technique, lower limits of detection vary between analytical runs. Also, there was an instrumentation change during the course of this study, with a resulting order-of-magnitude increase in instrument sensitivity for analyses performed after 1994. Variation in LOD for most of the elements reported in [table 2](#) are due to these factors and are a normal feature of ICP–MS analyses (P.J. Lamothe, oral commun., 2004). Additional discussion of the use of ICP–MS analysis for the determination of trace elements in igneous rocks is available in Longerich and others (1990), Jenner and others (1990), and Jenner (1996).

Table 1. Summary whole-rock geochemical data for Upper Triassic basaltic rocks at key locations in southeastern Alaska.

Location	Annette Island	Gravina Island	Gravina Island	Keku Strait	Duncan Canal	Gambier Bay	Central Admiralty Island	Greens Creek south	Greens Creek north	Mansfield Peninsula	Mt. Henry Clay	Windy Craggy
Lithology	basalt	basalt	gabbro	basalt	basalt	basalt	basalt	basalt	basalt	basalt	basalt	basalt
Number (n)	7	2	2	7	21	6	7	13	4	5	9	3
SiO ₂	50.1	44.3	44.4	45.8	48.4	45.7	52.1	51.9	46.6	47.3	48.9	42.9
Al ₂ O ₃	17.6	14.3	17.4	14.8	13.6	15.4	15.0	15.8	16.4	14.6	14.0	16.1
Fe ₂ O ₃	10.2	10.8	11.1	13.4	13.1	10.4	10.9	10.1	11.4	11.4	12.0	14.3
MgO	3.6	4.3	8.7	6.1	6.1	5.1	6.9	6.4	6.6	6.7	4.9	10.1
CaO	6.5	12.3	10.1	7.5	9.1	11.8	5.3	4.4	6.6	11.0	7.3	4.7
Na ₂ O	3.7	3.0	2.4	3.3	3.1	2.9	3.1	4.3	2.8	2.3	2.7	2.9
K ₂ O	2.2	1.1	0.3	0.8	0.7	0.6	1.0	1.3	1.9	0.9	0.8	0.4
TiO ₂	0.9	2.0	1.3	2.4	1.9	1.2	1.1	0.8	1.4	1.6	1.1	1.0
P ₂ O ₅	0.3	0.6	0.2	0.4	0.2	0.2	0.2	0.2	0.3	0.2	0.2	0.5
MnO	0.2	0.2	0.2	0.2	0.2	0.2	0.1	0.2	0.2	0.2	0.2	0.1
CO ₂	1.7			1.6	0.9	2.7						
Total H ₂ O	3.3			4.9	3.1							
LOI	4.1	6.5	3.9	4.8	2.7	5.7	3.8	4.1	5.6	3.4	7.0	6.2
Sum	100.2	99.4	99.9	101.1	100.4	101.9	99.5	99.4	99.8	99.4	99.1	99.0
La	11.4	17.4	5.4	13.4	9.3	9.4	10.6	11.9	8.6	7.1	9.3	24.7
Ce	25.6	43.0	15.0	31.0	22.2	21.5	22.4	22.8	22.0	18.4	20.4	48.7
Pr	3.4	6.4	2.4	4.5	3.2	3.1	3.0	2.7	3.4	2.7	2.6	5.5
Nd	15.1	31.0	11.5	20.0	15.3	14.2	13.0	11.4	16.0	13.0	11.5	21.3
Sm	3.5	7.8	3.4	5.2	4.2	3.7	3.3	2.6	4.4	3.6	3.0	3.8
Eu	1.0	2.6	1.3	1.8	1.4	1.1	1.0	0.8	1.5	1.3	1.0	0.9
Gd	3.5	8.9	3.9	6.5	5.0	4.2	3.8	3.1	4.6	4.4	4.0	3.9
Tb	0.6	1.4	0.6	1.1	0.9	0.7	0.7	0.5	0.8	0.7	0.7	0.6
Dy	3.8	8.3	3.8	6.5	5.0	4.1	3.9	3.4	4.5	4.4	4.5	3.8
Ho	0.8	1.8	0.8	1.2	1.0	0.9	0.8	0.8	0.9	0.9	1.0	0.8
Er	2.4	4.9	2.1	3.7	2.8	2.5	2.4	2.3	2.6	2.6	2.9	2.4
Tm	0.4	0.7	0.3	0.6	0.4	0.4	0.4	0.3	0.4	0.4	0.5	0.4
Yb	2.4	4.5	1.8	3.6	2.8	2.4	2.4	2.5	2.4	2.3	3.0	2.3
Hf	2.3	4.3	1.9	4.7	3.6	2.3	3.2	2.3	2.8	3.2	2.7	3.3
Ta	0.4	0.6	0.4	0.7	0.8	0.5	1.3	0.4	0.6	0.6		
Rb	43.6	19.5	4.3	14.5	14.5	16.0	20.5	19.6	53.1	14.4	18.1	5.7
Y	21.0	42.0	17.5	34.0	28.5	22.5	23.4	19.4	22.5	22.6	25.2	24.0
Zr	54.0	205.0	90.0	140.3	124.1	78.8	134.0	85.3	109.8	105.0	69.7	88.7
Nb	3.4	5.3	2.2	11.8	7.2	4.8	7.1	5.7	4.8	5.6	6.0	20.0
Ba	562.9	270.0	140.0	1017.1	956.4	791.8	378.6	633.8	467.8	174.0	397.8	178.0
Th	2.7	3.2		1.1	1.1	0.9	1.8	2.6	1.1	0.8	3.9	4.1
Sc	28.3	27.0	27.0	37.6	41.5	29.2	31.0	28.4	30.5	33.8	37.6	28.7
V	268.6	219.5	255.0	358.6	434.5	333.3	295.7	222.3	307.5	382.0	303.3	196.7
Cr	53.7	120.0	97.0	121.3	185.6	578.0	200.7	314.6	875.0	770.0	49.6	336.7
Ni	19.4	51.0	142.5	43.3	71.9	46.5	47.3	44.2	67.3	70.6	30.7	118.3
Co	29.6	52.0	68.0	44.4	50.1	45.0	39.0	38.7	44.5	47.6	39.2	33.3
Cu	123.4	48.5	62.5	59.7	167.3	219.5	45.8	83.5	80.3	107.4	112.0	249.7
Zn	174.6	135.0	90.0	115.6	112.0	84.3	130.9	111.1	92.0	92.2	336.7	51.0
Ga	20.7			24.0	21.0	17.0					17.7	25.0
Sr	727.1	425.0	365.0	468.6	307.2	773.3	152.9	146.6	330.0	362.0	240.3	251.0
Cs	0.5	0.4	0.3	0.9	0.5	1.4	1.2	0.8	2.0	0.4		
Pb	12.3	3.2		27.0	3.8	6.5	5.3	8.0	4.7	5.2	10.9	4.3
Sn		2.5	0.9	2.0	2.4	0.9	3.5	3.7	0.7	1.4		
W	0.1	0.4	0.3	2.3	2.3	1.4	0.9	0.8	0.3	0.4		
U	0.3	0.7	0.1	0.6	0.4	0.2	0.7	0.7	0.4	0.4		

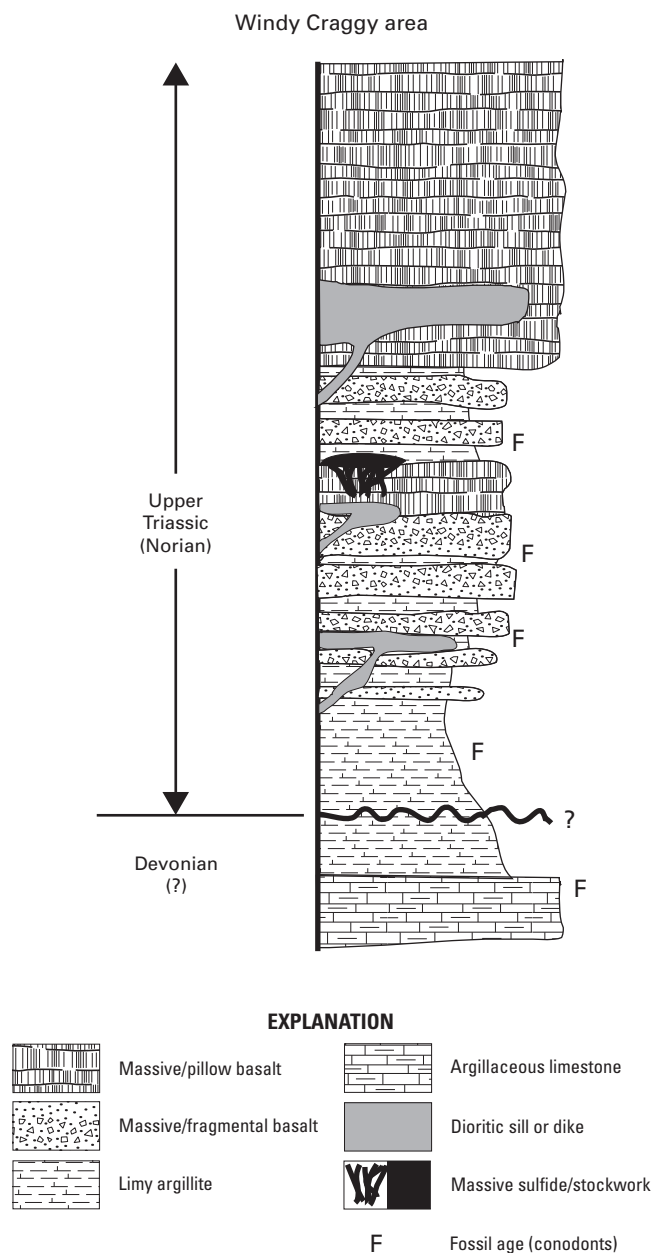


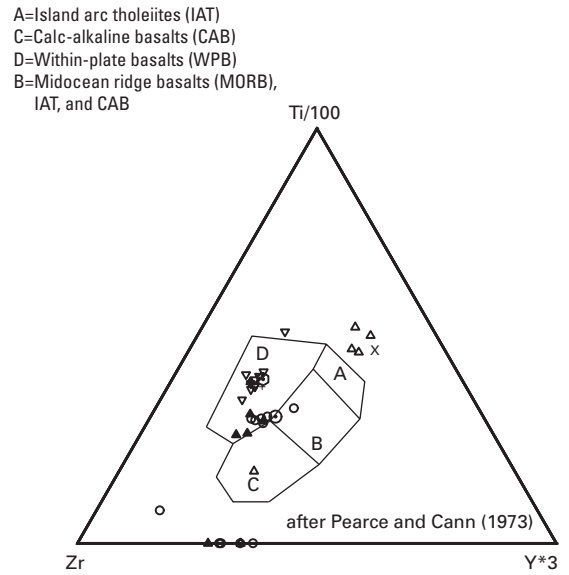
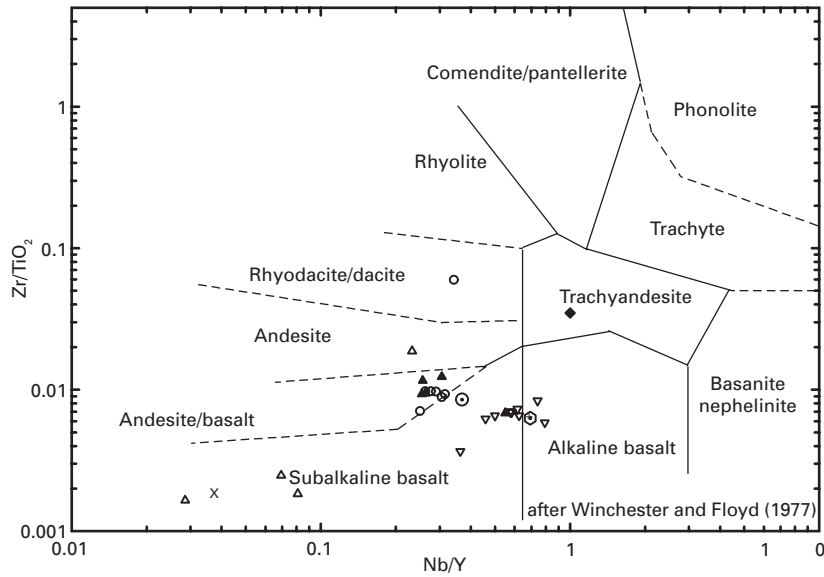
Figure 13. Composite stratigraphic column of the Upper Triassic section at the Windy Craggy deposit, northwestern British Columbia. Modified from MacIntyre and Schroeter (1985).

In the presentation that follows we attempt to shed additional information on the nature of the tectonic setting of the ATMB through the use of immobile-element-based tectonic discriminant diagrams. In general, we have followed the recommendations and cautions regarding the use of such diagrams as explained by Pearce (1996). The literature is full of examples of the use and misuse of discriminant diagrams (for example, Wood, 1980; Arculus, 1987; Dudas, 1992; Rollison, 1993) in developing petrogenetic models for the origin of suites of igneous rocks. Our purpose is not to attempt rigorous

petrogenetic modeling but rather to make a first-order assessment of tectonic settings suggested by the immobile-element geochemistry of igneous rocks of the ATMB, and to look for consistency with the volcanosedimentary, metallogenic, and radiogenic isotopic characteristics that we describe here and in later chapters of this volume.

In acknowledgment of the difficulty of obtaining reliable data at the low abundance levels of the immobile elements commonly used in discriminant diagrams, we have made every effort to be conservative in the representation of our geochemical data. After removing all obviously veined, mineralized, altered, and nonigneous rocks, the data set was stripped of all potential sediments and cumulate rocks using the geochemical criteria of Pearce (1996). The primary geochemical compositions of the volcanic host rocks have been modified by sea-floor alteration as well as by middle-greenschist-facies regional metamorphism during collision and underthrusting of the Alexander terrane with the North American continental margin. The resulting moderate to extreme alteration (loss on ignition-LOI, commonly 4–10 weight percent and as high as 30 weight percent) precludes the use of major element data for identification and tectonic discrimination of the volcanic rocks. Therefore, in order to maximize the utility of the immobile-element chemistry, all extremely altered samples with LOI greater than 10 weight percent also were removed from the database. An additional conservative control was placed on our use of the data by selecting a plotting routine that assigns a null value to all data at the LOD; thus, only data at abundances above the LOD are considered during the discriminant analysis. As a final check on the utility of our data, we have plotted the analyses of the USGS basalt standards BIR-1, BCR-2, and BHVO-2 and of two replicate standards that were inserted as blind standards throughout the duration of the study (fig. 14) onto the suite of discriminant diagrams used in this analysis. We note the acceptable size of the error ellipses relative to the various discriminant fields (Dudas, 1992) and suggest that these plots demonstrate the sufficiency of our data for discriminant analysis.

For plotting purposes, the data in table 2 have been organized by rock type, by known or inferred age (for example, Triassic vs. Triassic(?)), and by principal location. Figure 15 shows the known Upper Triassic igneous whole-rock data plotted on the immobile-element classification diagram of Winchester and Floyd (1977). The most important feature of the data is that a bimodal suite of rocks is clearly distinguishable. Further, basalt-rhyolite suites are evident on Annette Island and on the Cornwallis Peninsula, the latter constituting the western shore of Keku Strait. North of Keku Strait, rhyolites are absent and the volcanic rocks are entirely basaltic. Such bimodal suites of volcanic rocks are a common feature of rift-related tectonic environments worldwide (Wilson, 1989) and are commonly associated with VMS mineral districts (Lentz, 1998; Barrett and MacLean, 1999). These compositions provide first-order evidence of the rift-related origin of the Upper Triassic volcanic rocks of the ATMB. The basaltic rocks (fig. 15) mainly plot in the subalkaline basalt and basaltic andesite fields, with a few examples of alkaline basalts.



AI=WP Alkali basalt
 AII=WP Alkali basalt and WP tholeiite
 B=E-MORB
 C=WP tholeiite and VAB
 D=N-MORB and VAB

A=N-MORB
 B=E-MORB and WP tholeiite
 C=alkaline WPB
 D=VAB

EXPLANATION

- ⊙ BCR-1 published values
- + BHVO-1 published values
- X BIR-1 published values
- ◆ blind standard 93KK-37 altered Keku rhyolite
- ▲ blind standard 93KK-66 Hound Island basalt
- blind standard BCR-2
- ⊕ BHVO-2 published values
- ▽ blind standard BHVO-2
- △ blind standard BIR-1

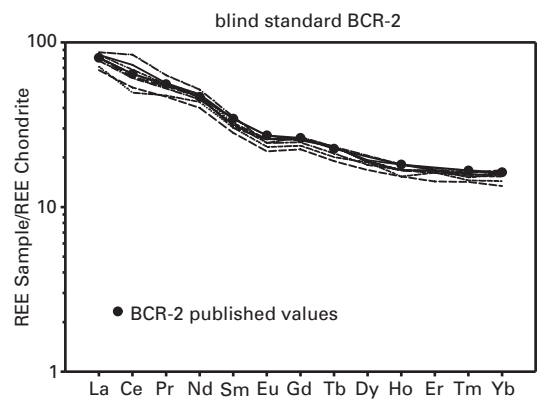
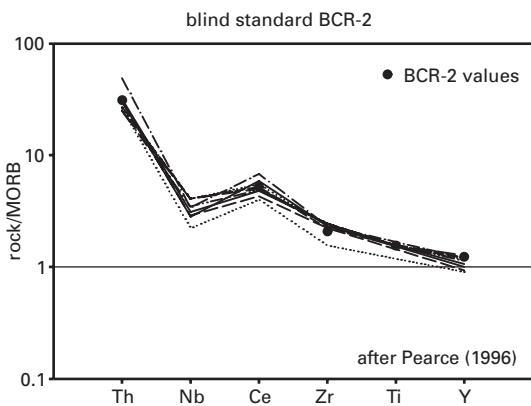
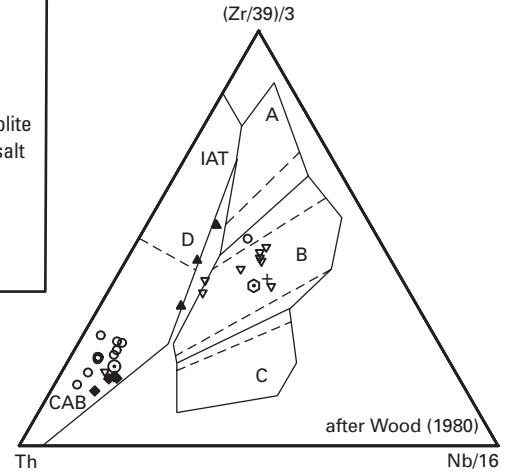
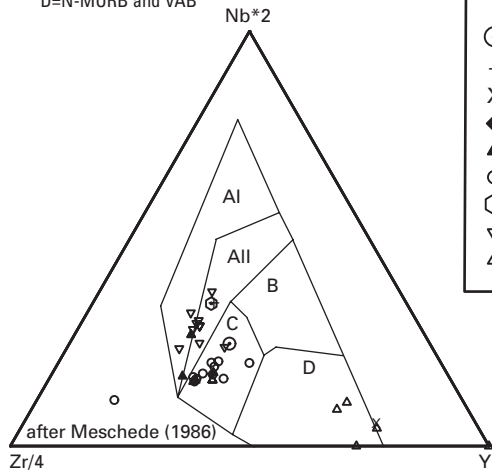


Figure 14 (facing page). Accuracy and precision of blind standards plotted on the diagrams used in the text as compared to accepted values. Multiple analyses of the USGS standards BIR-1, BHVO-2, and BCR-2 inserted as blinds into analytical batches throughout the duration of the study are shown on the immobile-element-based rock type diagram of Winchester and Floyd (1977) and on the tectonic discriminant diagrams of Pearce and Cann (1973), Meschede (1986), and Wood (1980). Multiple analyses of BCR-2 are also shown on the MORB-normalized, abbreviated trace-element plot of Pearce (1996) and on a standard chondrite-normalized REE diagram (using the chondrite values of Boynton, 1984). Note the acceptably small size of the data clusters for a given standard relative to the discriminant fields of the diagrams. Acceptable accuracy and precision are also demonstrated by multiple analyses of BCR-2 on the trace and REE plots.

The felsic volcanic rocks on Annette and Gravina Islands are typical calc-alkaline rhyolites with bulk compositions similar to those of island arc rocks. However, data for the rhyolitic rocks at Keku Strait (Cornwallis Peninsula–Keku Strait area, fig. 15) consistently fall into the comendite/pantellerite to trachyte fields of Winchester and Floyd (1977). Whereas the peralkaline composition of the Keku Volcanics rhyolites is difficult to confirm due to a high degree of brecciation and alteration, at least some of the samples approach the excess of $\text{Na}_2\text{O} + \text{K}_2\text{O}$ over Al_2O_3 that characterizes such rocks (Cole, 1978). This is an important observation due to the relatively distinctive tectonic setting of such rocks, which commonly occur in rift-related environments and are often the indicators of incipient rifting (for example, Mayor Island in the Bay of Plenty, New Zealand, and the D’Entrecasteaux Islands west of the Woodlark Basin, Papua, New Guinea, Smith and others, 1977; Smith and Johnson, 1981; also Civetta and others, 1984; Mahood and Baker, 1986; Pin and Paquette, 1997). The occurrence of felsic volcanism prior to basaltic volcanism throughout the southern portion of the ATMB and the peralkaline composition of the rhyolites of Keku Strait are typical features of intra- and back-arc rifts. The transition from calc-alkaline rhyolites to

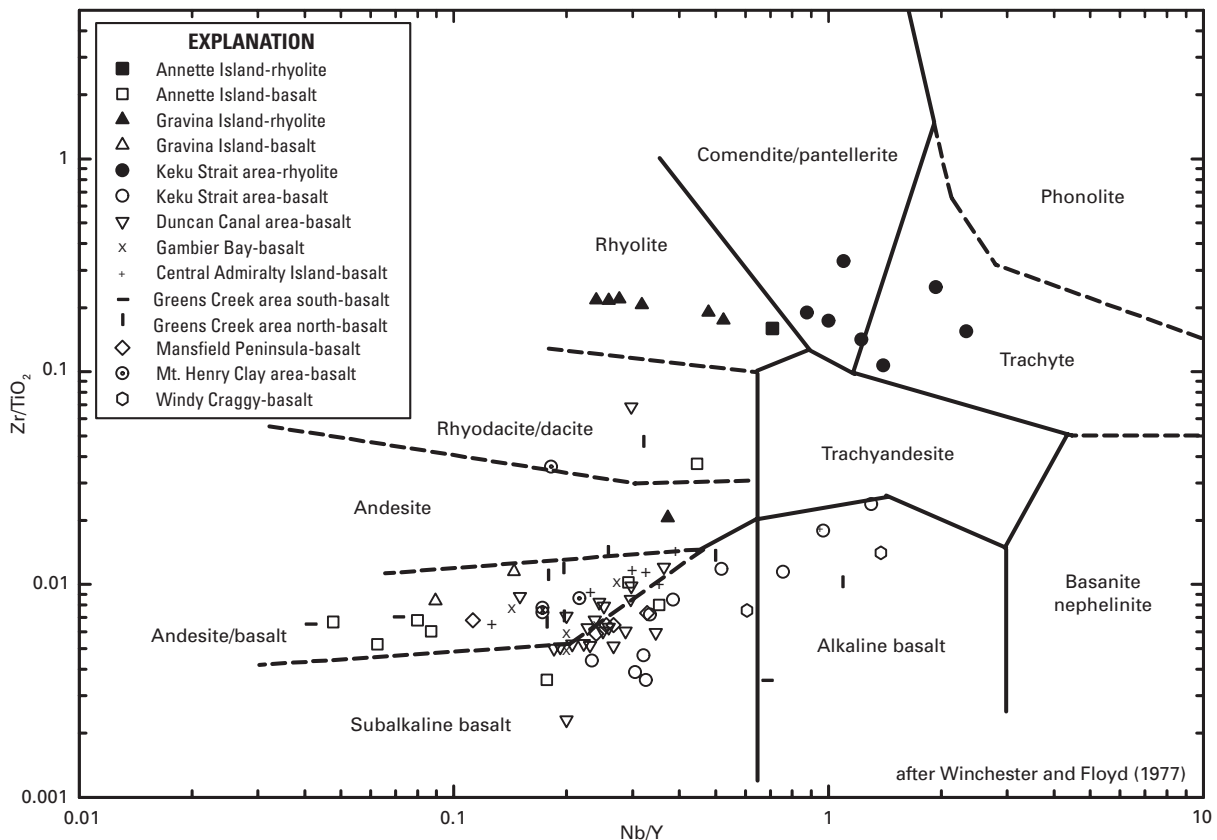


Figure 15. Volcanic rock classification diagram of Winchester and Floyd (1977) based on immobile-element ratios, showing the composition of southeastern Alaska Upper Triassic volcanic rocks analyzed for this study. Note the distinctly bimodal basalt-rhyolite distribution of data, and the comendite-pantellerite to trachytic compositions of the Keku Volcanics rhyolites (Cornwallis Peninsula suite).

peralkaline rhyolites northward along the ATMB is also consistent with a shift from a proximal-arc to an arc-slope or basin-margin setting. The peralkaline Keku rhyolites are indicative of small degrees of partial melting of a deep, garnet-bearing source during the earliest stages of rifting, followed by extreme fractionation and eruption from a shallow magma chamber (for example, Smith and Johnson, 1981; Mahood and Baker, 1986).

Application of discriminant analysis to the basaltic rocks of the ATMB provides additional information regarding their petrotextonic origins. We use a progression of three ternary plots based upon the immobile elements Ti, Zr, Th, Nb, and Y (fig. 16 a–f), and follow with the MORB-normalized trace-element plot recommended by Pearce (1996) and chondrite-normalized REE plots (fig. 17 a–v). The diagram of Pearce and Cann (1973), which is shown in figures 16a and d, is most effective for separating within-plate basalts (WPB) from those showing either destructive plate margin (volcanic arc basalt—VAB, including both calc-alkaline and tholeiitic trends; CAB and IAT, respectively) or MORB compositions. This discriminant is based largely on the effect of melting and residual enrichment of yttrium in a mantle garnet lherzolite source. Thus, WPB compositions on this diagram are suggestive of small degrees of melting from a deep source. In contrast, compositions in the MORB–VAB fields are largely controlled by partial melting at shallower levels of a spinel lherzolite source. Transitional processes such as attenuation of continental lithosphere cause trends from the WPB to the MORB field (due to progressively shallower and increased degrees of partial melting), and assimilation of upper crust results in trends from these compositions toward the CAB field (Pearce, 1996). The Meschede plot (1986), which is shown in figures 16b and e, is similar to the first plot but has the advantage of providing a discriminant between normal and enriched (or transitional) MORB compositions.

The discriminant diagram of Wood (1980), which is shown in figures 16c and f, is most efficient at separating VAB from MORB–WPB compositions and at separating calc-alkaline and tholeiitic VAB trends. As with the previous two diagrams, complex tectonic settings result in transitional data arrays between fields. Lavas erupted on attenuated continental lithosphere are perhaps the most problematic as they occupy overlapping fields in the center of the diagram. Syn- and postcollision zone magmas define a field that stretches from the center of the diagram toward the CAB end of the VAB field, reflecting the assimilation of upper crust by enriched MORB or intraplate magmas. Petrogenetic vectors toward or away from the zirconium apex from the within plate fields of the diagram are controlled by variations in the degree of partial melting and enrichment or depletion of the mantle source. Mantle enrichment and/or low degrees of partial melting shift basalt compositions toward lower zirconium abundances. VAB compositions are controlled by the characteristic depletion in niobium with increasing input of a subduction component reflected by vectors moving toward the thorium apex (Pearce, 1996).

Data for volcanic rocks from the ATMB fall most readily into two basic groups based on how they plot on this series

of discriminants. Lavas from locations predominantly in the central portion of the ATMB (Keku Strait to the Mansfield Peninsula) show a transitional nature with compositions characteristic of WPB that exhibit a spread between variably enriched or depleted MORB and CAB. The second group is composed of rocks from the southern and northern ends of the ATMB and the area immediately surrounding the Greens Creek mine (Annette Island, Greens Creek area south, and Mt. Henry Clay area). This group plots in arrays suggestive of compositions transitional between CAB and variably enriched MORB. Several areas along the ATMB (Gravina Island, Gambier Bay, Greens Creek area north, and the Mansfield Peninsula) exhibit examples of both groups. Notable exceptions are the rocks from Keku Strait which exhibit a shift toward alkaline intraplate compositions on the Wood (1980) diagram, and the consistent display of NMORB to EMORB or alkaline intraplate compositions of the Windy Craggy rocks.

Trace and REE plots of the basaltic rocks of the ATMB (fig. 17 a–v) generally support the division of rocks into two groups. The first group of rocks that plot in the transitional WPB/EMORB to CAB array exhibit the gently sloping profile from enriched thorium, niobium, and zirconium, to depleted yttrium that is characteristic of intraplate rocks and of complex tectonic settings. Similarly, the REE patterns show uniformly smooth slopes without negative europium anomalies. The second group of rocks that exhibit an array transitional between CAB and NMORB on the discriminant plots are all characterized by depletions in niobium, zirconium, titanium, and yttrium that are the hallmark of destructive margin basalts. The REE profiles of these rocks generally have steeper LREE profiles and a slight negative europium anomaly, which probably indicates separation of plagioclase and input of a subduction component to the melt.

We note that there is some consistency in the tectonic environments suggested by the discriminant diagrams and trace and REE plots. On both the Pearce and Cann (1973) and the Wood (1980) plots, the first group of rocks occupy fields that are characteristic of attenuated continental lithosphere, whereas the second group occupy fields defined by rocks produced in syn- and postcollisional environments (Pearce, 1996). In both cases, the data form arrays that are best described as transitional and are indicative of tectonic settings that are more complex than the midocean ridge, intraplate, or destructive margin settings that compose the fields of most of discriminant diagrams. We know that the pre-Jurassic history of the Alexander terrane involved the formation and transport of a continent-sized fragment of island-arc crust to a position just outboard of a subduction zone prior to the Late Triassic. Whether collision and partial subduction (or obduction) of the Alexander terrane occurred is uncertain; however, by Late Triassic the production of ATMB volcanic rocks indicate that a period of crustal relaxation outboard of the destructive margin had occurred, resulting in lithospheric extension and incipient rifting in the Alexander terrane. We suggest that the Alexander terrane must have been thick enough that initial rifting resulted in deep melting of a relatively enriched mantle and that the first melt products

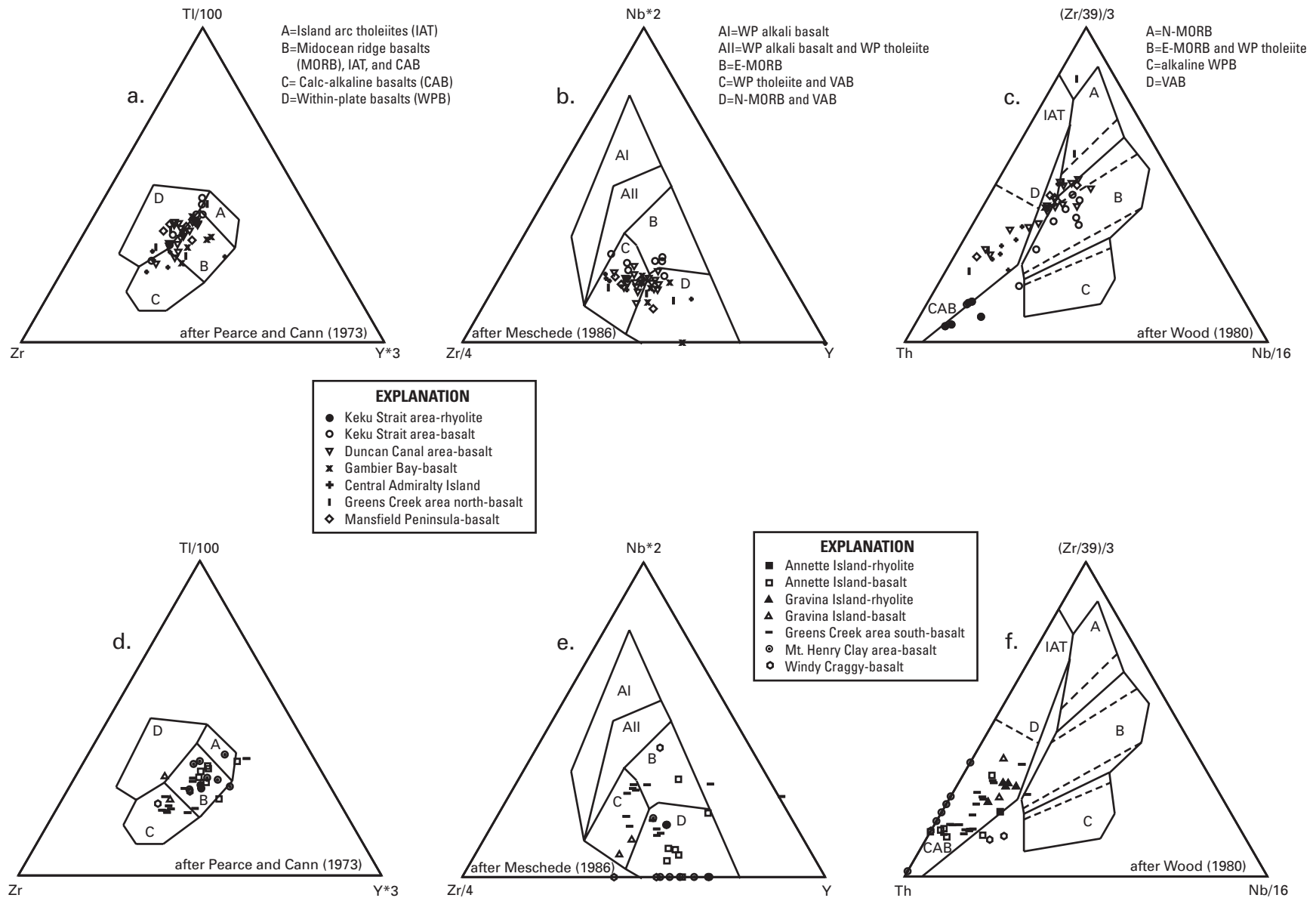


Figure 16 a-f. Discrimination diagrams showing compositions of southeastern Alaska Upper Triassic basalts and rhyolites (on the Wood, 1980, diagram only) analyzed for this study. Diagrams a-c show data from locations within the central ATMB and are characterized by transitional chemistry that reflects a stronger intraplate signature than samples from the north and south end of the ATMB and from the ridge south of the Greens Creek mine as shown in diagrams d-f. The second set of diagrams indicate chemistries transitional between that of WPB and/or EMORB and CAB.

thus have chemistry similar to WPB and EMORB depending upon how much assimilation of the overlying island-arc crust occurred. In places where attenuation or rifting of the crust was more pronounced, shallower melting of variably enriched mantle at variable degrees of partial melting produced the data array between arclike CAB and NMORB of the second group. Thus the transitional chemistry of the ATMB volcanic rocks are a product of a combination of variable depths and degrees of partial melting beneath the rifting Alexander landmass and of variable amounts of crustal assimilation (to achieve the CAB signature).

As with previous radiogenic isotopic studies (Sampson and others, 1989, 1990, 1991), Sr-Nd-Pb isotope analyses of pre-Triassic rocks of the Alexander terrane (Premo and Taylor, unpub. data, 2004) and of footwall host rocks at Greens Creek (chap. 11) suggest derivation from a depleted mantle source and are consistent with isotopic signatures of oceanic island arcs. Initial niodymium compositions at 215 Ma (average age of host rocks) of metabasalts and gabbros vary between $\epsilon_{Nd} = +4$ to $+9$, and initial $^{206}Pb/^{204}Pb$ and $^{87}Sr/^{86}Sr = 18.45$ to 18.92 and 0.7037 to 0.7074 , respectively, and are enriched compared to MORB or oceanic island basalt (OIB) sources. Isotopic data for Permian and Triassic argillites are similarly enriched and indicate derivation from an island-arc terrane with input of older, more radiogenic source material. Interestingly, radiogenic isotopic data on footwall phyllites at Greens Creek are bimodal ($\epsilon_{Nd} \sim +8$ and $+2$), which we interpret to indicate the intrusion of Late Triassic gabbroic sills into the footwall basaltic pile. Hyd Group basalts exhibit a relatively primitive isotopic signature ($\epsilon_{Nd} = +8$ to $+9$) consistent with derivation from a mantle source (chap. 12).

Results of the tectonic discriminant analysis, in combination with the fairly primitive and transitional trace, REE, and radiogenic isotopic geochemical signatures, are consistent with rift-related basalt produced in an incipient intra-arc or back-arc setting. We note that basalts at several locations, especially in the southern end of the ATMB, the Greens Creek area, and at Mt. Henry Clay, have compositions that are similar to those of relatively unfractionated calc-alkaline basalts formed in an oceanic volcanic arc, whereas those in others, most notably in the central portion of the ATMB, display transitional chemistry consistent with derivation from EMORB or OIB sources and variable assimilation of preexisting arc crust. Similar to the trends for the mafic volcanic rocks, the felsic volcanic rocks show a transition from more arclike compositions in the southern end of the ATMB to intraplate compositions in the center of the ATMB. The most MORB-like rock compositions in the ATMB are displayed by Tats Group basalts at Windy Craggy. Consistent with the extensive geochemical data of Peter and Scott (1999) we note elevated LREE compositions and lower ϵ_{Nd} compositions for the Tats Group as compared to Triassic basalts to the south. Peter and Scott (1999) interpret the tectonic setting at Windy Craggy at the time of ore formation as a mature back-arc basin.

The Geochemistry and Significance of Late Triassic Hypabyssal Mafic-Ultramafic Intrusive Rocks

An important and largely unrecognized feature of many of the mineral occurrences that has important genetic implications is their spatial and temporal relationship to a mafic-ultramafic suite of hypabyssal (probably rift-related) intrusions. Throughout the ATMB there are numerous mapped outcrops of gabbros, microgabbros, and less commonly, ultramafic intrusive rocks of either Triassic or uncertain age. Notable examples are the Duke Island ultramafic complex lying immediately south of Annette Island, and the microgabbros on the southwestern shore of Bostwick Inlet on Gravina Island. Microgabbros on Hare Island, just west of Hound Island in Keku Strait, are mapped as Cenozoic igneous rocks; however, we note the similar geochemical compositions of these rocks to those of the Upper Triassic basalts of Hound Island Volcanics. More strikingly perhaps is the growing realization that a significant portion of the capping Triassic basaltic unit throughout the ATMB is composed of gabbroic sills and that immediately underlying serpentinite bodies are probably the residual cumulate sources of these voluminous flows. Both serpentinite and gabbro bodies are commonly intersected by underground mine workings and are seen to crop out at Greens Creek (chaps. 6, 7). Similarly, the stratigraphic sequence at Windy Craggy is composed of interbedded gabbro sills, sediments, and basalts (MacIntyre and Schroeter, 1985).

Even more compelling is the observation that many of the mineral occurrences are within, or are in close proximity to, barite-sulfide-mineralized mafic sills and dikes that have strikingly similar chemistry to the overlying basalts. Figure 18A is a photograph of a heavily carbonate altered gabbroic sill hosted in late Upper Triassic sedimentary rocks at a mineral occurrence (Berg #17, Berg, 1972) on the Sylburn Peninsula of Annette Island. The altered sill sits immediately beneath a large, discontinuous pod of barite accompanied by minor sphalerite, and galena. Similarly, the Ladder vein occurrence (Muffler, 1967) in the Keku Strait and at least two other similar occurrences represent instances of mineralized basaltic intrusions that are spatially associated with Late Triassic mineral occurrences. The Ladder vein (fig. 18B) consists of a basaltic dike cutting Permian and Triassic(?) conglomerates and sedimentary rocks that have distinctive, associated, 2.5-cm-thick, massive sphalerite veins crosscutting the dike and occurring along its margins. A similar sill several hundred meters to the south exhibits peperitic margins with the host (upper Upper Triassic?) sedimentary strata, indicating that the sediments were unlithified and water saturated at the time of intrusion (fig. 18C).

Some of the best examples of both mineralized basaltic dikes and mineralized and altered ultramafic intrusions are in Gambier Bay (fig. 1, inset d). In the southwest arm of the bay at Cave Mountain Point, several 1–2-meter-wide basaltic dikes (fig. 18D) intrude Devonian limestone and Upper Triassic

sedimentary rocks. Veins up to 15 centimeters wide consisting of barite, quartz, iron carbonate, chalcopyrite, sphalerite, and galena are present along the dike margins, locally forming replacement bodies in the limestone. Outcrops of altered serpentinite sills are a striking feature of the Upper Triassic section on the north shore of Gambier Bay and occur as distinctive, orange-weathered outcrops consisting of green and white quartz, magnesite, iron carbonate, sericite, and bright green fuchsite (fig. 18E). Often misidentified as exhalite beds or altered dolomite bodies, the presence of relict chromian spinel and olivine in the altered rocks, the compositionally distinct mafic-ultramafic element suite, and the preservation of serpentinite enclaves and breccia clasts within the altered bodies identify them as heavily carbon dioxide-metasomatized serpentinites. Although attempts to directly date relict serpentinite enclaves (fig. 18F) within these altered ultramafic bodies were unsuccessful, they are thought to be part of the mafic-ultramafic hypabyssal intrusive event related to Triassic rifting (chap. 11). An $^{40}\text{Ar}/^{39}\text{Ar}$ isotopic age for fuchsite separated from a quartz-iron carbonate-fuchsite altered body in Gambier Bay yielded an apparent plateau age of 210.3 ± 0.3 Ma (chap. 11), thus demonstrating that emplacement had occurred by the Late Triassic, and suggesting that alteration and mineralization of the intrusives were nearly synchronous. This relationship and the presence of skarn minerals in the aureoles of serpentinites in the Greens Creek area (N.A. Duke, oral commun., 1997), suggest that the precursor ultramafic rocks were emplaced hot in the shallow subsurface during Late Triassic time. Associated mineralization includes barite, pyrite, chalcopyrite, sphalerite, galena, tetrahedrite, siegenite, nickel bloom, and anomalous gold values, further suggesting that the ultramafic precursor intrusives drove hydrothermal circulation and in the process were themselves altered. Similar examples of mineralized and altered mafic-ultramafic hypabyssal intrusions occur on Zarembo and Woewodski Islands, and in Duncan Canal (Taylor, 2003), and at numerous locations across Admiralty Island, notably at the North Gambier occurrence, Yellow Bear Mountain, Etta prospect, Mariposite Ridge just north of Greens Creek (fig. 18G), and at several localities on the Mansfield Peninsula.

Late Triassic Mineral Occurrences in Southeastern Alaska

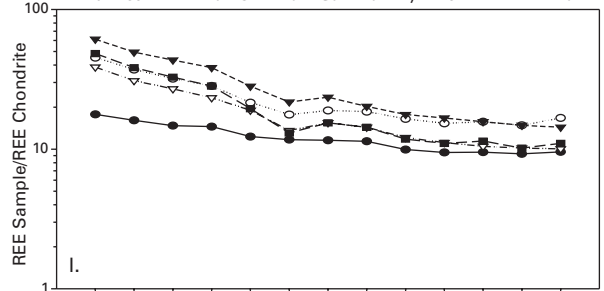
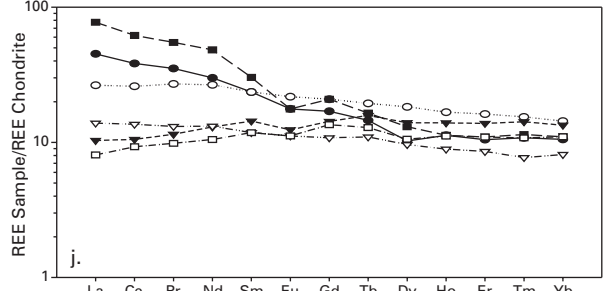
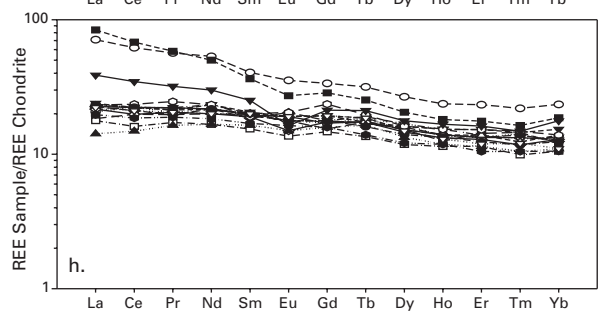
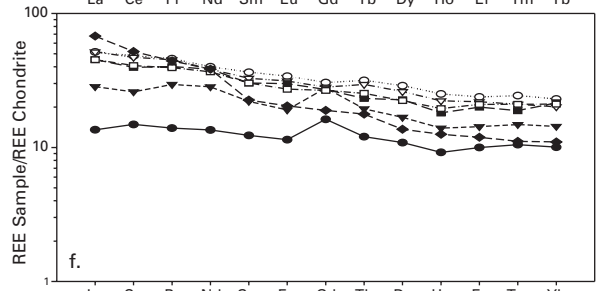
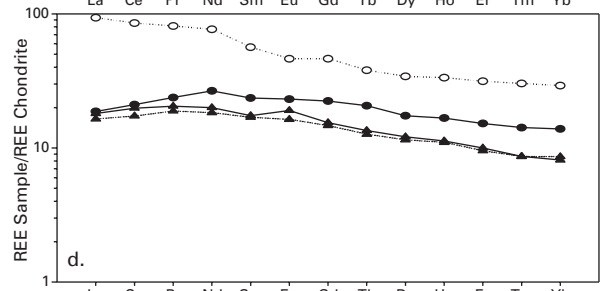
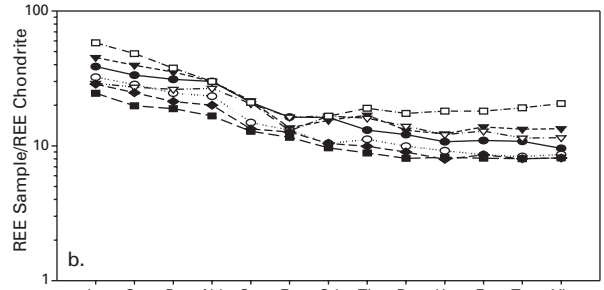
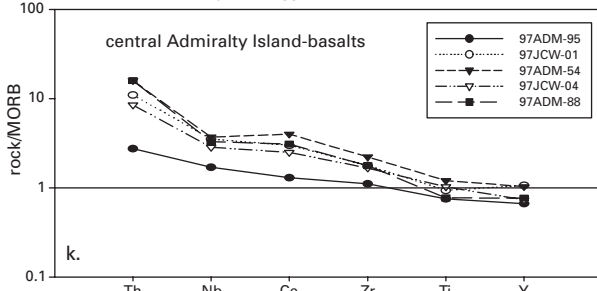
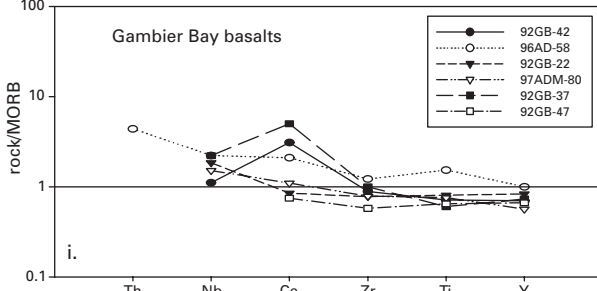
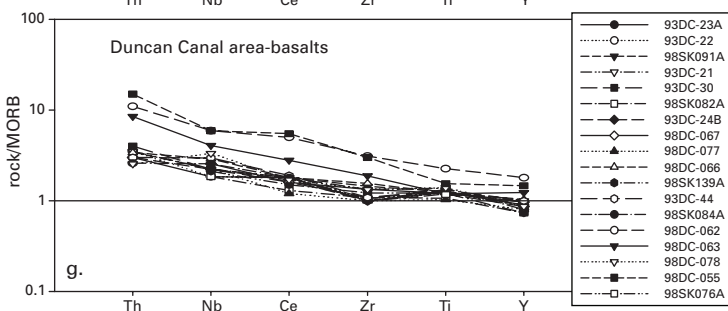
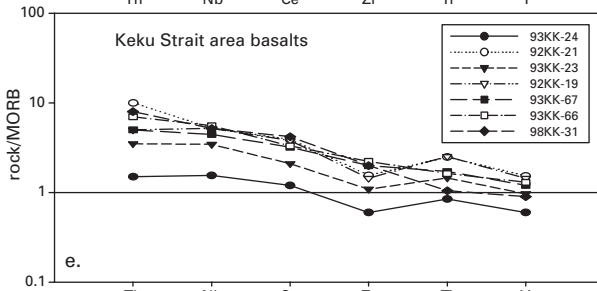
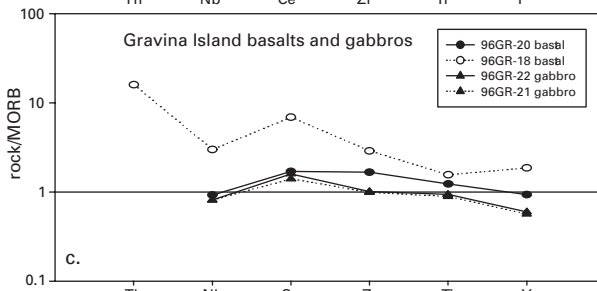
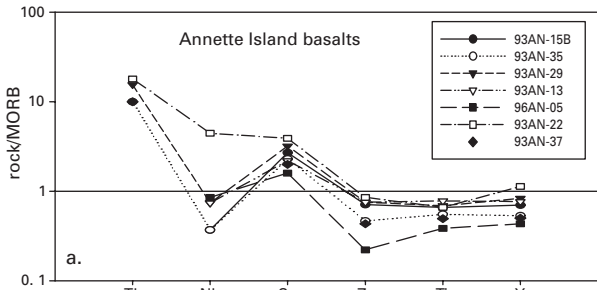
The northward change in depositional environment and volcanic host-rock chemistry in Upper Triassic strata is accompanied by a northward transition from epithermal-type base-metal occurrences having a relatively simple mineralogy, to sulfosalt-enriched polymetallic VMS occurrences, and finally to larger copper-cobalt-bearing deposits with more clearly stratiform morphologies. In the following sections we describe some of the more important mineral occurrences that demonstrate the evolving nature of the Late Triassic metallogeny from south to north in the ATMB.

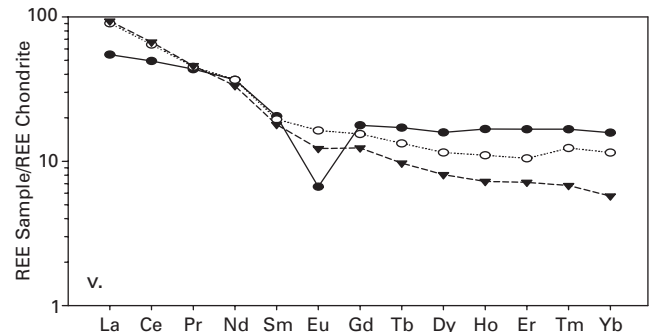
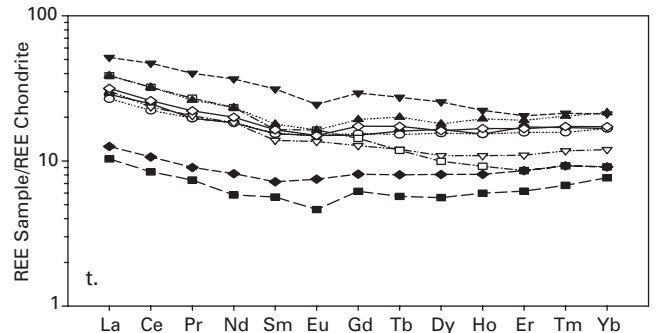
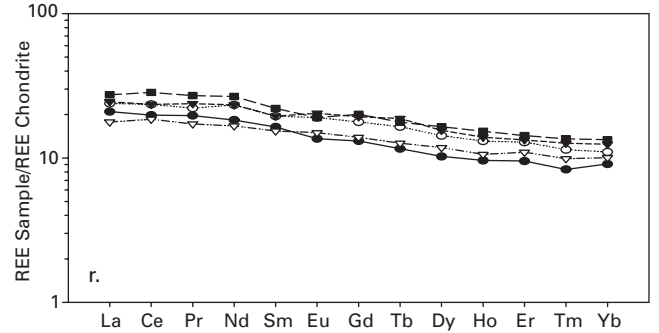
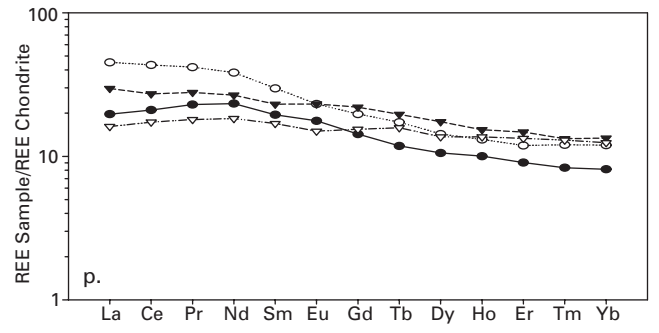
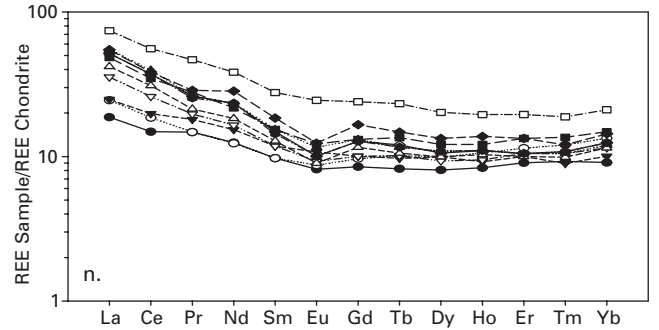
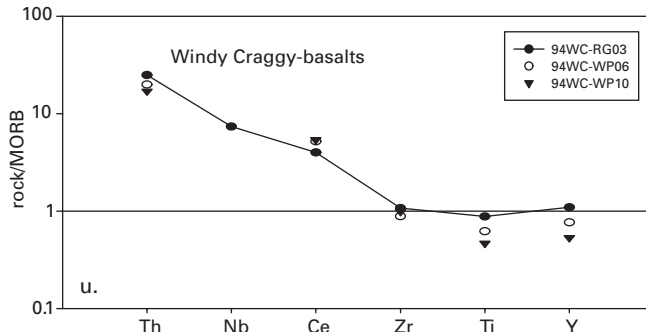
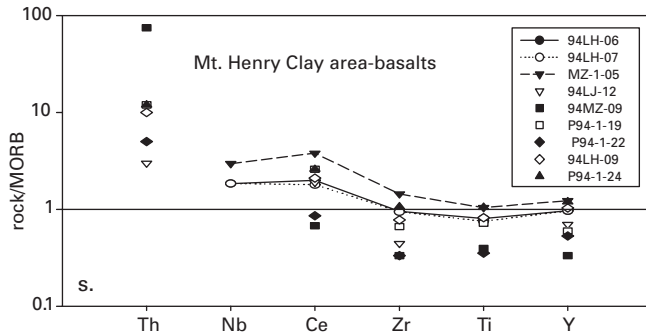
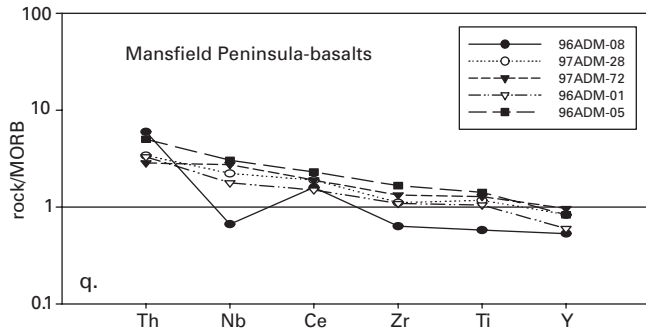
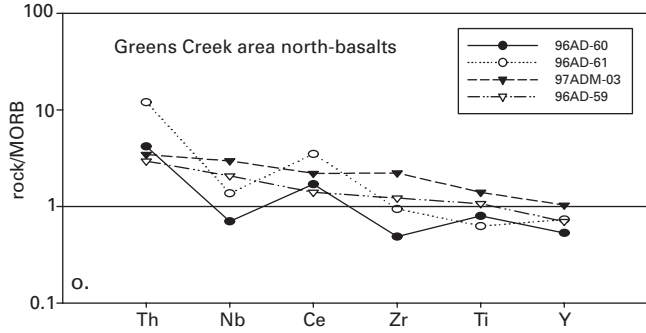
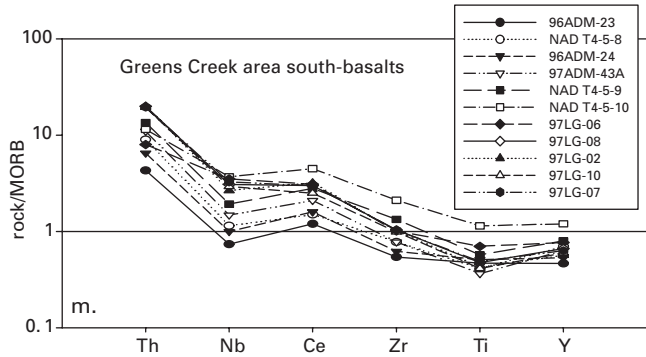
Mineral Occurrences in the Southern ATMB

Occurrences on Annette and Gravina Islands are typified by structurally controlled, discontinuous veins, breccias, and pod-shaped bodies, and less commonly, by small stratiform lenses. The occurrences are Pb-Zn-Ag-Ba-(Cu)-enriched with a relatively simple sulfide mineralogy, at or near the contact between felsic volcanic rocks and overlying fossiliferous and locally oolitic limestone. In places, the limestone is dolomitized and brecciated. A pervasive orange to black, iron- and manganese-rich hydrothermal alteration locally colors the otherwise medium gray dolomite (for example, Nehenta Bay on Gravina Island; fig. 19A). Where this alteration is most intense, the matrix of the dolomite breccia consists of quartz and iron-rich dolomite cement with sparsely disseminated sulfides. Solution cavities are present and commonly have inward-projecting euhedral crystals of quartz, late dolomite, and sulfides. Texturally, the hydrothermal features exhibited in such outcrops of shallow platform carbonates are similar to those in Mississippi Valley-type deposits of the U.S. midcontinent region (Leach and Sangster, 1993).

Examples of the pod-shaped and veinlike occurrences are numerous, especially on Annette Island, and include the previously described barite-chalcopyrite-sphalerite-galena pods (fig. 18A) associated with the altered gabbroic dike at Berg #17 (Berg, 1972). Another weakly mineralized, pod-shaped barite occurrence at Japan Bay on the Sylburn Peninsula (Berg #18) has a similar mineralogy, and botryoidal textures suggestive of growth in open space or in unlithified sediments during early diagenesis (fig. 19C). Interestingly, in 1976, 181.4 meters of diamond core was drilled in five holes at three different locations on the Sylburn Peninsula to test for the presence of minable quantities of barite and Pb-Zn-Ag. Of these, four holes at two locations intersected low-grade stratabound barite-sulfide intervals dipping west under the peninsula at 25 degrees. At

Figure 17 a–v (following pages). MORB-normalized abbreviated immobile-trace-element (after Pearce, 1996) and REE plots of data for samples from locations throughout the ATMB corresponding to the samples and locations shown on the discriminant plots. Chondrite values from Boynton (1984). Note that arc-type trace-element patterns and steeper LREE patterns with slight to moderate negative europium anomalies characterize the samples from the northern and southern ATMB and the ridge south of the Greens Creek mine, consistent with data shown on the discriminant diagrams. Trace-element patterns consistent with transitional mixtures of intraplate rocks and CAB, as are often seen in areas of attenuated lithosphere and in syn- and postcollision settings, are exhibited by samples from locations in the central ATMB. Corresponding REE patterns are generally flatter and do not exhibit europium anomalies.





the first location (Berg #18, previously described), geochemical analyses indicate the presence of a 14.6- to 15.5-meter-thick interval grading 25.8- to 38.3-percent barite with minor lead, zinc, and silver. At the second location 120 meters to the south, drilling revealed a structurally complicated, lower grade mineralized section that may also dip 25 degrees to the west. Geochemical analyses indicate a 21.3-meter-thick interval having an average grade of 16 percent barite and minor lead, zinc, and silver. Within this interval is a 5.8-meter-thick section grading 45.2 percent barite, 3.4 percent lead, and 34 parts per million silver (D.C. McCrillis, written commun., 1976; Berg and Clautice, written commun., 1982). Estimation of size and grade based on the drilling results and the persistence of soil geochemical anomalies indicate a 1–2 million metric tonne deposit averaging 32 percent barite, 2–3 percent combined lead and zinc, and 28 grams per metric tonne silver could be present (A.L. Eng, written commun., 1983; Taylor, 1993). A second, very small stratabound occurrence was noted during this study at the mouth of Nehenta Bay, Gravina Island, enclosed within the gritty limestone sequence overlying the basal conglomerate. Several stacked horizons of bladed barite up to 7 cm thick and 10 m long are present and provide additional evidence for stratabound, early diagenetic if not exhalative mineralization (fig. 19C).

Clearly epigenetic, veinlike mineral occurrences are also common on Annette and Gravina Islands and are typified by occurrences in the Crab Bay area on the east side of Annette Island. As on the Sylburn Peninsula, mineralization occurs predominantly at and near the contact of rhyolitic volcanoclastic rocks and locally dolomitized limestone. Discontinuous and generally small ribbon and ladder quartz veins occurring as an echelon sets tens to 100 meters long are best developed within the limestone (Hawley and Associates, written commun., 1975). They contain sphalerite, galena, and rare chalcopyrite, malachite, tetrahedrite, barite, and possibly stibnite. Most of the veins in the Crab Bay area are too discontinuous and poorly mineralized to be of economic interest (Hawley and Associates, written commun., 1975; A.L. Eng, written commun., 1983; Taylor, 1993). The largest vein is 0.45 meter thick and contains 30 to 50 percent sulfides over an exposed length of 6 meters. A minor amount of galena and sphalerite also is disseminated locally within the limestone. In general, mineral occurrences in the southern end of the ATMB, regardless of morphology, are characterized by an anomalous geochemical signature of Pb, Zn, Cu, Au, Ag, Ba, and minor Sb, As, Cd, Bi, and Ni (Taylor, 1993). Comparison of this geochemical suite to that which characterizes the Greens Creek deposit (chap. 6) demonstrates their similarity and possible genetic relationship.

Mineral Occurrences in the Northern ATMB

Relative to the southern end, the northern end of the ATMB is characterized by larger and more clearly stratiform occurrences of pyrite-pyrrhotite-(chalcopyrite-sphalerite) with Cu-Zn-(Co-Au)-enrichments. They are hosted by thick sections of argillite intercalated with basaltic flows and sills, or

by the uppermost Triassic sequence of mafic volcanic rocks. The best example is the giant Windy Craggy massive sulfide deposit in northwestern British Columbia, approximately 100 km north of the international border. Published data for Windy Craggy indicate a minable resource of 297 million metric tonnes at 1.38 percent copper, 0.07 percent cobalt, 0.2 gram per metric tonne gold, and 3.8 grams per metric tonne silver (Peter and Scott, 1999). The total resource estimate is thought to be in excess of 500 million metric tonnes (Gerald Harper, oral commun., 1995). Currently regarded as the largest Besshi-type VMS deposit in the world (Peter and Scott, 1999), Windy Craggy is hosted in a rift-succecion (Mihalynuk and others, 1993) of mafic flows, sills, and argillites (fig. 20A) which, based on the presence of Norian conodonts both below and immediately above the massive sulfide lenses, can be confidently correlated with the ATMB in southeastern Alaska. Windy Craggy consists of three stratiform massive sulfide lenses composed predominantly of pyrite and pyrrhotite with lesser and variably distributed chalcopyrite, sphalerite, marcasite, galena, digenite, arsenopyrite, an unidentified bismuth telluride, cobaltite, cubanite, electrum, and native gold and silver. Each sulfide lens is associated with a well-developed sulfide stringer zone (Peter and Scott, 1999). Typical massive ore consists of fine- to medium-grained (about 50–500 micrometers) primary-textured to variably recrystallized pyrite and pyrrhotite in a volumetrically minor gangue of quartz, calcite, and siderite gangue (fig. 20B). In striking contrast to many of the Late Triassic occurrences to the south, tetrahedrite-bearing, gangue-rich white ores are absent at Windy Craggy, and barite only occurs in trace amounts. Interestingly, hydrothermal sediments (exhalites) are present at the base of the massive sulfide lenses and suggest that hydrothermal fluids breached the sediment/water interface early in the ore-forming process (Peter and Scott, 1999). Early fluid exhalation may also have occurred at Greens Creek (chap. 15).

Numerous other deposits in the northern end of the ATMB consist of similar stratiform accumulations of pyrite-pyrrhotite massive sulfide characterized by Cu-Zn (-Au-Co-Ag) enrichments. The Tats, X, and Rainy Monday occurrences (Peter and Scott, 1999; Mihalynuk and others, 1993) in the vicinity of Windy Craggy, and several others on the Canadian side of the border in the Mt. Henry Clay area such as the Herbert Mouth West, Grizzly Heights, and Buckwell Moraine (MacIntyre and Schroeter, 1985), all display features similar to Windy Craggy. Notably, they are all hosted in Upper Triassic strata dominated by distal turbiditic sediments, and by mafic sills and flows with transitional chemistry indicative of rifting. At Mt. Henry Clay on the U.S. side of the border, the stratigraphic setting is similar to that in the Windy Craggy area; however, occurrences mostly consist of stratiform lead-zinc-silver-barite deposits such as Glacier Creek (Main) and upper Cap. The Little Jarvis occurrence on the opposite side of the ridge from the Glacier Creek deposit contains pyrite-pyrrhotite-chalcopyrite-sphalerite-bearing semimassive sulfides that may be more similar to the northern group of occurrences. Massive sulfide boulders at the Mt. Henry Clay (Boulderado)

occurrence are difficult to place in stratigraphic context due to their occurrence as float on a moraine. However they are mineralogically and texturally (fig. 20C) more like Windy Craggy than the stratiform lead-zinc-silver-barite occurrences in the Mt. Henry Clay area and to the south.

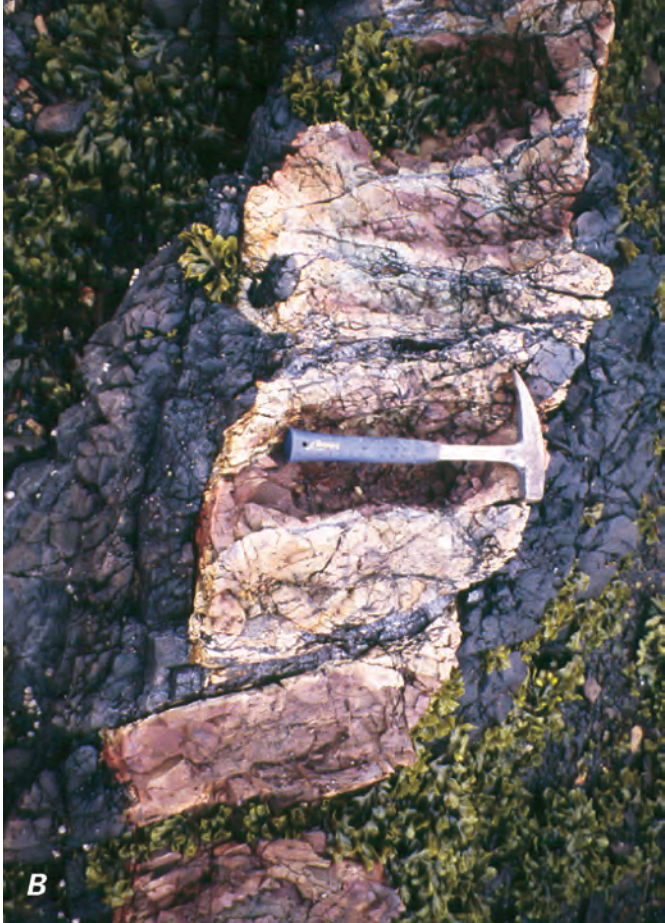
The southernmost occurrences of the northern type may be the numerous small stratiform pyritic bodies in the Duncan Canal and Woewodski and Zarembo Islands area in the central portion of the ATMB. The Junior Creek occurrence on the eastern shore of Duncan Canal consists entirely of semimassive pyrite lenses hosted in Upper Triassic graphitic argillites. On the west side of Woewodski Island, a 0.5- to 1-m-thick pod of pyritic massive sulfide is sandwiched between apparently conformable footwall and hanging-wall rocks composed of highly altered greenschist at the Helen-S occurrence (Taylor, 2003). As described herein, the Frenchie deposit on Zarembo Island is difficult to place in stratigraphic context. It is one of the larger and more clearly stratiform deposits within the ATMB, however, and has mineralogical and textural features most closely associated with the pyritic deposits in the Mt. Henry Clay and Windy Craggy areas. The Frenchie deposit consists of a 2–3-m-thick, ~250-m-long massive sulfide lens (fig. 20D) composed primarily of pyrite with lesser and variable chalcopyrite, sphalerite, and barite (fig. 20E; Taylor, 2003), much like the Windy Craggy and Mt. Henry Clay (Boulderado) deposits. At the adit the massive sulfide lens is approximately 3 meters thick and consists predominantly of coarsely recrystallized pyrite with minor chalcopyrite and sphalerite in a siliceous quartz-carbonate gangue. Along strike 50 to 100 meters upstream, the lens becomes semimassive and then dies out into the hanging-wall quartz-sericite schist. Along strike in the down-creek (westerly) direction for approximately 75 meters the lens maintains its thickness. However, over this interval the massive sulfide becomes finely crystalline, more sphalerite rich, and exhibits a footwall to hanging-wall zonation. Minor barite was observed in the footwall margin of the lens 45 meters west of the adit. Massive sulfide overlying the barite is sphalerite rich compared to the massive pyrite at the adit. The center of the lens becomes more pyritic and then grades into more galena-rich pyritic massive sulfide toward the hanging wall. Remobilization of ductile sulfides into fractures in the immediately overlying, more brittle quartz-sericite schist has caused local chalcopyrite and galena accumulations in the hanging wall. The massive sulfide lens is truncated by a fault oriented N. 65° E., 60° N. (Buddington, 1923) 75 meters downstream from the adit, and then reappears in the north creek bank approximately 150 meters downstream from the adit. The lens is continuous downstream for approximately another 100 meters and is approximately 2 meters thick. Samples collected from the downstream end of the lens in the south bank and from the downstream end of the portion of the lens in the north bank become increasingly sphalerite rich, indicating that a proximal-distal zonation exists as well. From the adit (proximal) to the distal downstream end, the massive lens is zoned from copper-gold to zinc. From footwall to hanging wall the lens is zoned from Zn-Mn-Ba, to Fe-Cu-

Au, to Pb. In addition to the zonation described, the Frenchie occurrence has a geochemical signature containing Fe, Zn, Cu, Au, Fe, (Hg, Ag, As, Cd, Mo, Pb, and Sb; Taylor, 2003).

Mineral Occurrences in the Central ATMB

Mineral occurrences in the middle of the ATMB are transitional and define an overlap area between structurally controlled types that we believe formed in a shallow water, near-arc setting, to those having a more stratiform appearance, reflecting a deeper water, rifted basin-margin setting. Examples of structurally controlled mineral occurrences, similar to those described as characteristic of the southern end of the ATMB, extend northward to about the latitude of Keku Strait, Woewodski Island, and southern Admiralty Island. They include galena-sphalerite breccias in limestone at the contact with felsic volcanics, and galena-sphalerite-bearing mafic dikes on the Cornwallis Peninsula, weakly stockwork-mineralized tuffaceous mafic volcanics at the Lost Show and Brushy Creek on Woewodski Island, and similarly mineralized mafic dikes and chalcopyrite-bornite-tetrahedrite-barite-bearing, quartz-carbonate stockwork veins in mafic volcanics in the Gambier Bay area. Stratiform deposits in this transition region tend to be Pb-Zn-Ag-Ba (-Cu-Au)-rich and are typified by Greens Creek, described in detail in this volume. Other examples of these increasingly larger, polymetallic, silica-barite-carbonate gangue-rich, more obviously stratiform occurrences include silica-barite-sulfide-sulfosalt-rich occurrences on Zarembo Island (Frenchie occurrence described previously) and Woewodski Island, Duncan Canal, Pyrola, Greens Creek, as well

Figure 18 A–G (pages 44–45). Photographs of outcrops throughout the ATMB demonstrating the spatial relationship between mineral occurrences and mafic-ultramafic hypabyssal sills, dikes, and intrusions. (A) Altered gabbroic sill beneath barite-sulfide pod. Berg # 17 occurrence, Sylburn Peninsula, Annette Island. (B) The Keku Islet Ladder vein occurrence. Altered basaltic dike intrudes Permian-Triassic conglomerates and sedimentary rocks and is cut by dark reddish-brown sphalerite veins. (C) Peperitic margin of altered dike intruding Permian-Triassic sedimentary rocks on Keku Islet, south of the Ladder vein occurrence. (D) Basaltic dike cutting Devonian limestone and Upper Triassic sedimentary rocks and basalts in the south arm of Gambier Bay, southern Admiralty Island. Barite-quartz-carbonate-sulfide veins occupy the selvages of the dike and also cut the dike. (E) Quartz-iron carbonate-magnesite-fuchsite-altered ultramafic sills intruding the Upper Triassic sedimentary sections on the north shore of Gambier Bay, southern Admiralty Island. (F) Relatively unaltered enclave of serpentinite within a large body of altered ultramafic rock on the north shore of Gambier Bay, southern Admiralty Island. (G) Quartz-iron carbonate-magnesite-fuchsite-altered ultramafic intrusion on Mariposite Ridge 1 kilometer north of the Greens Creek mine.



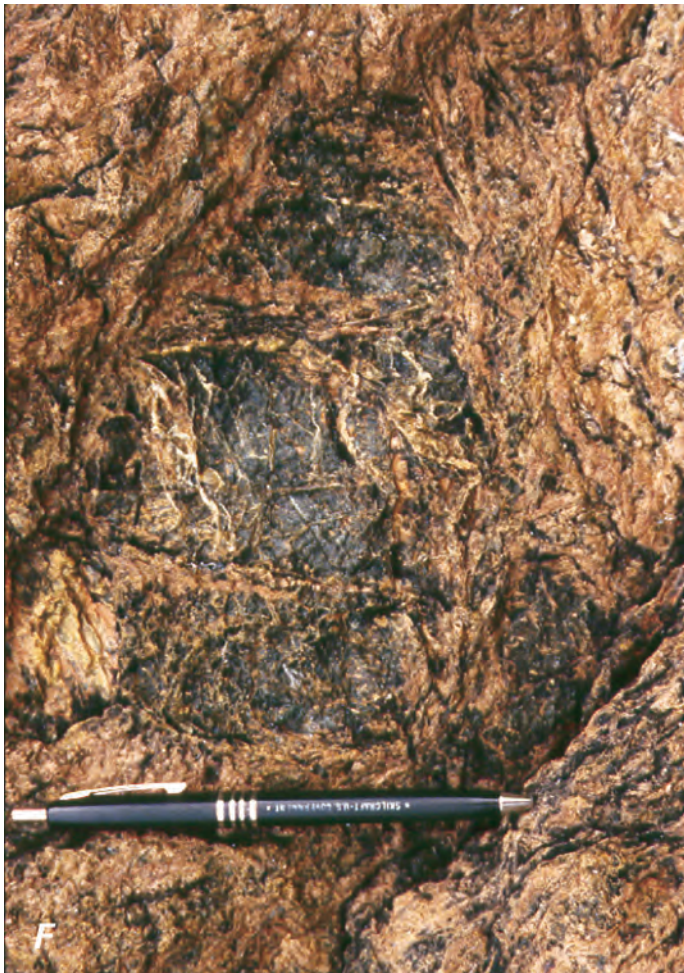




Figure 19 A–C. Photographs of outcrops and polished rock slabs from mineral occurrences in the southern portion of the ATMB. (A) Pervasive orange-black, hydrothermal iron and manganese alteration of the Nehenta Formation limestone and carbonate debris flows in Nehenta Bay, southern Gravina Island. Note pod-shaped occurrence of bladed white barite and minor sulfides to the right of the hammer. (B) Stratiform horizons of bladed barite in iron- and manganese-altered calcareous sedimentary rocks of the Nehenta Formation near the mouth of Nehenta Bay, southern Gravina Island. (C) Massive botryoidal barite and galena from the Berg # 18 occurrence in Japan Bay of the Sylburn Peninsula, Annette Island. Texture of the barite and the fine-scale galena bands suggest growth in open space or into unconsolidated sediments during diagenesis.





Figure 20 A-E. Photographs of outcrops and polished rock slabs from mineral deposits in the northern portion of the ATMB. (A) South side of Windy Peak at the Windy Craggy deposit in northwestern British Columbia. Light and dark subhorizontal layering composes intercalated mafic sills and flows with calcareous black argillites. (B) Typical pyritic massive sulfide with minor pyrrhotite and chalcopyrite in a quartz-carbonate gangue, from the north crosscut of the Windy Craggy deposit in northwestern British Columbia. The black elongate

inclusion in the lower right part of the sample is an argillite clast. (C) Pyrite- and sphalerite-rich massive sulfide from a boulder found at the Mt. Henry Clay (Boulderado) occurrence in northern southeastern Alaska. (D) Massive sulfide lens at the Frenchie deposit on Zarembo Island, central southeastern Alaska. Timbers in the adit are about 2 meters high and are holding up a hanging wall of graphitic quartz-sericite schist. (E) Massive sulfide from the Frenchie deposit. Top sample is dominantly pyritic and characterizes the majority of the sulfide lens. The center sample is more sphalerite- and galena-rich; the bottom sample has significant barite. As shown, the three samples mimic the ore stratigraphy in the distal downstream portion of the lens.

as the Glacier Creek (Main), upper Cap, and other deposits on either side of the border in the Mt. Henry Clay area described.

Numerous small, clearly epigenetic barite-sphalerite-galena (-chalcopyrite) occurrences dot the islets and shoreline of the Cornwallis Peninsula in the Keku Strait area. The majority of the occurrences consist of weakly mineralized, irregular pods and veins composed of massive to bladed, pink to white barite with minor sulfides. Less commonly, colloform banded textures suggestive of mineral growth in open space or in unlithified sediments are observed (fig. 21A), similar to the textures in the barite-rich occurrences on Annette Island. The colloform banded vein shown in figure 21A also exhibits a close spatial relationship with a 1-m-wide mafic dike that contains 1-cm-thick galena veins along its margins.

With few exceptions these occurrences are localized at the contact between the Keku Volcanics and the overlying Cornwallis Limestone. Two of the more highly mineralized occurrences are at the rhyolite/limestone contact along creeks roughly 300 meters from the shoreline. One is generally referred to as the Kuiu zinc deposit, the second is an undescribed occurrence located about half way up the second tributary entering Hungerford Creek south from its mouth. Both occurrences are characterized by stockwork- and breccia-textured Cornwallis Limestone cemented and replaced by sphalerite, galena, and pyrite (fig. 21B). A similar breccia composed of greenstone clasts in a matrix of pink barite, dolomite, and fine bands of galena occurs in the creek bed at the mouth of Hungerford Creek. Whereas all of the occurrences in the Keku Strait area are clearly epigenetic in style, it is worth noting that iron- and manganese-rich hydrothermal alteration is widespread at the rhyolite/limestone contact, which in many places is marked by clastic sediments and thin chert horizons (Muffler, 1967; this study).

A nearly identical style of mineralized limestone breccia associated with mafic dikes is present at the Taylor Creek occurrence on the west side of Duncan Canal. The occurrences are hosted entirely in a massive to thin-bedded, fractured, buff-colored to light gray dolomitic limestone. The limestone is in depositional contact with and overlies a penetratively foliated greenstone composed predominantly of a chlorite-calcite- (muscovite-quartz) phyllite. The units strike northwest to west-northwest and dip shallowly to moderately steeply to the northeast. Numerous north- to north-northeast-striking dikes of probable Tertiary-Quaternary age intrude the country rock.

A Carnian (early Late Triassic) age is firmly established for the limestone at Taylor Creek by a series of conodont samples collected by Kennecott Exploration and identified by Anita Harris (chap. 11). Sampling sites are identified on the recent geologic map of the Duncan Canal-Zarembo Island area (Karl and others, 1999a). Carnian conodonts were recovered from a sample of limestone located on strike about 2.5 kilometers northwest of the creek occurrences; collections from the immediate vicinity of the open cut were barren. Two samples containing latest Early Permian conodonts, located on the ridge a mile to the southwest, and south of the mouth of

Taylor Creek along strike a mile to the southeast, respectively, support the younging-to-the-northeast stratigraphic interpretation of early workers (Kerns, 1950). These conodont samples also bracket the permissive age of the pillowed basaltic volcanics and phyllitic greenstone located on the ridge southwest of the occurrence and in the footwall of the Taylor Creek occurrence, respectively, between late Early Permian and early Late Triassic time.

Mineralized rock in the creek bank exposures of Taylor Creek has two distinct styles. The first and most prevalent consists of irregularly distributed veins, patches, and pods of disseminated to locally abundant pyrite, sphalerite, and galena in a matrix of opaque, light gray to white dolomite gangue (fig. 21C). Marcasite has been reported at Taylor Creek (Kerns, 1950); however, X-ray diffraction analysis of suspected marcasite identified only pyrite in a dolomite and ankerite gangue (S.J. Sutley, U.S. Geological Survey, written commun., 1999). Pyrite forms millimeter- to centimeter-sized clots and rounded aggregates in white dolomite or in a fine crystalline groundmass of a dark gray sulfide and yellow-orange sphalerite. Galena occurs as fine crystalline blebs and streaks, and less commonly as coarse crystalline remobilized clots. Although not visually identified, the strong silver-antimony enrichment of this assemblage described below suggests the presence of antimonian tetrahedrite, a common mineral in Late Triassic mineral deposits throughout the ATMB. This style appears to be a replacement of the host limestone. However, the presence of rounded grains of pyrite is not a typical texture of epigenetic replacement deposits in carbonate strata and raises the possibility that the present textural form is a result of remobilization. The best example of this style of mineralization is in the south bank of Taylor Creek in a 1.6-meter-thick subhorizontal band over the top of the discovery trench (Taylor, 2003).

The second style of mineralization has only recently been recognized (Taylor, 2003) and may provide critical evidence of genetic process at Taylor Creek. This style consists of matrix- to grain-supported, rounded nodules of pyrite up to several centimeters in diameter in a dolomite matrix, and irregular botryoidal crusts of pyrite growing in and on dolomitic limestone. Locally, orange sphalerite and galena are present as a fine-grained crystalline matrix and as sparse, coarse crystalline clots. The best example of this textural style is in the north creek bank about 200 meters upstream from the open cut. A stratiform(?) horizon about 12 meters long and roughly parallel to the creek consists predominantly of this nodular pyrite "pudding stone" (fig. 21D). Conspicuously absent are common indicators of epigenetic styles of mineralization such as discrete quartz-dolomite-sulfide veins or mineralized breccias. The nodular and botryoidal pyrite textures are likely a result of early diagenetic replacement of limestone during carbonate sedimentation. The nodular pyrite textures and intercalations of dolomitic limestone with sulfidic limy phyllite are similar to those observed at the Wetboot occurrence in Towers Creek (Taylor, 2003) except the former are on a larger scale. Significantly, identical nodular

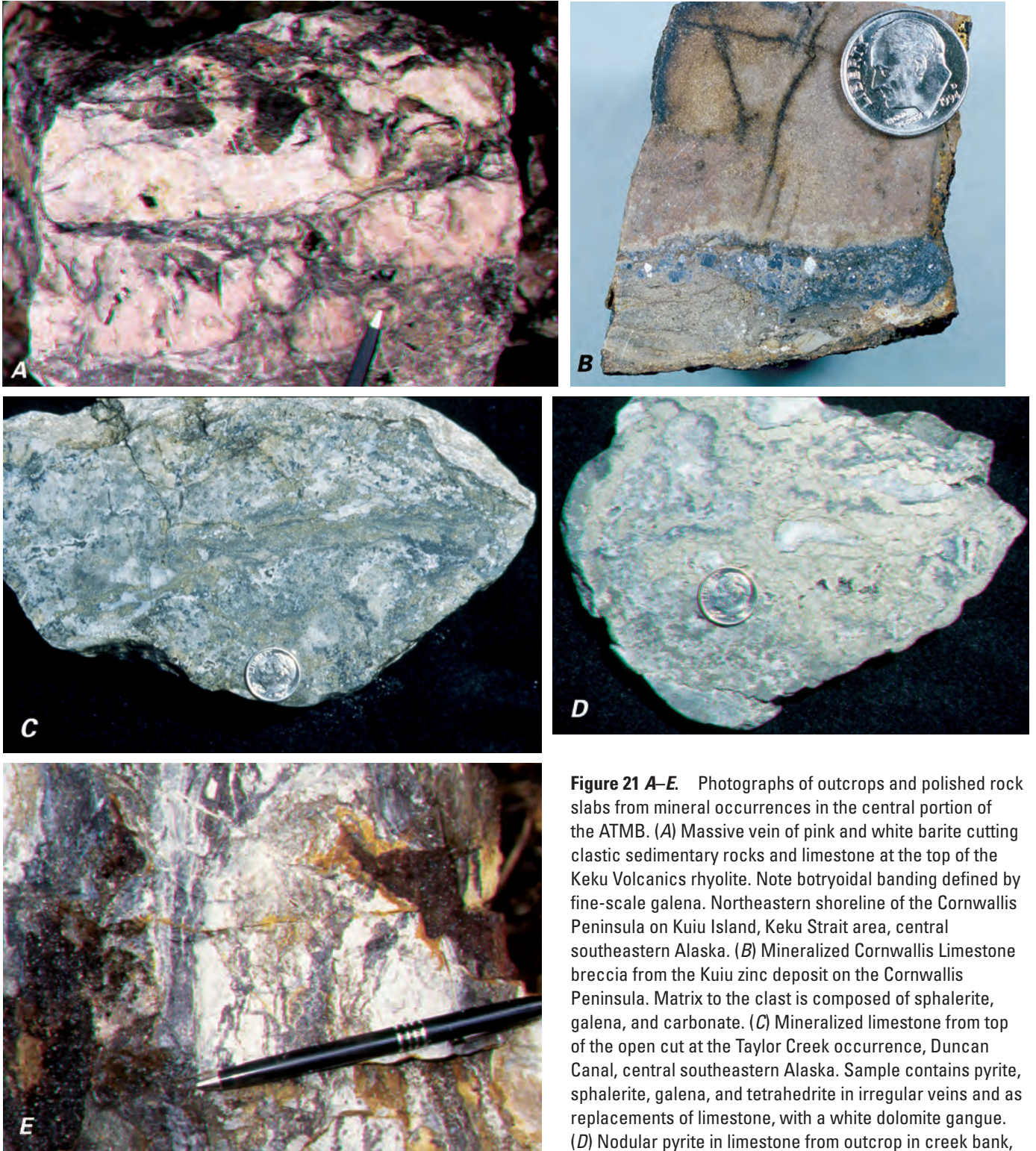


Figure 21 A–E. Photographs of outcrops and polished rock slabs from mineral occurrences in the central portion of the ATMB. (A) Massive vein of pink and white barite cutting clastic sedimentary rocks and limestone at the top of the Keku Volcanics rhyolite. Note botryoidal banding defined by fine-scale galena. Northeastern shoreline of the Cornwallis Peninsula on Kuiu Island, Keku Strait area, central southeastern Alaska. (B) Mineralized Cornwallis Limestone breccia from the Kuiu zinc deposit on the Cornwallis Peninsula. Matrix to the clast is composed of sphalerite, galena, and carbonate. (C) Mineralized limestone from top of the open cut at the Taylor Creek occurrence, Duncan Canal, central southeastern Alaska. Sample contains pyrite, sphalerite, galena, and tetrahedrite in irregular veins and as replacements of limestone, with a white dolomite gangue. (D) Nodular pyrite in limestone from outcrop in creek bank, upstream from the Taylor Creek open cut. This texture is interpreted to be the result of early diagenetic replacement of carbonate mud. (E) Semimassive sulfide in a quartz-carbonate-chlorite-altered greenstone at the Lost Show occurrence, near the northwest shore of Woewodski Island in Duncan Canal, central southeastern Alaska. Dark reddish-brown streaks of sphalerite are prevalent, and sulfides fill vuggy open cavities.

pyrite textures are present in footwall carbonate units and in massive pyritic ore at the Greens Creek mine (chap. 9; see also figs. 4C and D in chap. 11). The Taylor Creek occurrences have a geochemical signature consisting of Fe, Zn, Pb, Ag, Sb, Hg, Cd, Mn (Au, As, Cu, and Mo) (Taylor, 2003).

An additional style of structurally hosted, discontinuous, and vein or stockwork-like occurrences are also present in the central portion of the ATMB. These are typified by Lost Show and Brushy Creek on Woewodski Island and by the North Gambier occurrence in Gambier Bay of Admiralty Island. The Lost Show occurrence is located in the northeast quadrant of Section 22 of the Petersburg C-4 15-minute quadrangle, less than a kilometer from the northwest point of Woewodski Island. The occurrence consists of an east-west-trending low ridge of rock on the north side of a small lake. Two trenches have been cleared over the occurrence, exposing its width at the center and at the west end of the low ridge.

The Lost Show occurrence consists of a single, near vertically dipping, 3–4-m-wide stratiform lens of silicified greenstone. The silicified horizon contains as many as six bands (1–30 cm in thickness) of pyrite- and sphalerite-rich, semi-massive to massive sulfide in the center trench, which coalesce into thicker bands in the west trench. The lens is continuous along strike for at least 40 meters between the two trenches. Continuity of the lens to the east and west is unknown but likely, based on its consistent thickness over 40 meters. The thickest and best-mineralized massive sulfide is in the western trench and appears to be zoned somewhat across the width of the lens. Massive sulfide against the north side of the lens is sphalerite rich and grades into more silica-pyrite-rich massive sulfide toward the southern edge of the lens. Where massive, the sulfides comprise a fine-grained mixture of pyrite, dark red sphalerite, and minor amounts of a dark gray mineral, possibly galena or tetrahedrite. Semimassive sulfides are texturally similar, with a gangue of gray to white silica. Breccia fragments of quartz, minor vug-fillings of euhedral pyrite, and pyrite veinlets cutting silicified breccia fragments suggest tectonic disruption of the lens and redistribution of sulfides (fig. 21E). The occurrence is characterized by a geochemical signature containing Zn, Fe, Cd, Hg, Ag, Sb (Pb, Au, Cu, and Mn) (Taylor, 2003).

The Brushy Creek occurrence is in the southwestern quadrant of section 1 of the Petersburg C-4 15-minute quadrangle, on the southern end of Woewodski Island. Two mineralized open cuts in the southeast bank of the creek are located approximately 50 meters apart, and evidence of weak mineralization is present intermittently for at least 250 meters downstream. Country rock exposed in the creek bank is entirely composed of a brecciated, heavily altered, and weakly foliated mafic metavolcanic or volcanoclastic rock. A small side drainage flowing into Brushy Creek from the southeast contains exposures of thin-bedded, calcareous, quartz-sericite schist with bands of semimassive sulfide. Precursor of the schist is uncertain but could have been a felsic tuff (Taylor, 2003).

The mineral occurrences at Brushy Creek consist of irregularly distributed stockwork calcite-quartz-sulfide veins within brecciated mafic volcanic rock. Two shallow pits in the creek bank each expose 2–3-meter-wide areas crisscrossed by veins. Similar areas of stockwork veining are intermittently exposed in the creek bank downstream for approximately 200 meters. Texturally, all of the sulfides are fine to medium crystalline aggregates of pyrite, dark-reddish sphalerite, and lesser galena. Gangue consists of white quartz and calcite. In slightly more foliated rocks, the clasts are stretched and flattened and the sulfides appear as irregular bands and wisps millimeters to one centimeter in width. In more competent volcanoclastic rocks, sulfides are clearly paragenetically earlier than brecciation of the host rock as the clasts are mineralized and are rotated within the unmineralized matrix and are cut by late quartz-calcite veinlets. In addition to rotation of mineralized clasts, individual bands or stockwork veins are folded. The geochemical signature of the Brushy Creek occurrence consists of Fe, Zn, Ag, Hg, Pb, Sb, Cd, Mn (Au, As, Cu, Co, Ni, and V) (Taylor, 2003).

The barite-quartz-carbonate polymetallic veins and semimassive sulfides at the North Gambier occurrence described in detail by Taylor and others (1992) compose perhaps the northernmost structurally controlled, clearly epigenetic mineral occurrence within the ATMB. The occurrence predominantly consists of sulfide-rich quartz-carbonate-barite veins at the transition between sedimentary rocks and spilitized mafic volcanics. Mineralization occurs primarily within sheared and brecciated zones. Chalcopyrite and barite are the major constituents with lesser bornite, pyrite, sphalerite, galena, covellite, and silver-rich tetrahedrite. Chalcopyrite occurs as clots up to several centimeters in diameter with associated coarsely crystalline bladed, white barite, as millimeter-sized grains disseminated in the greenstone, and as massive, flow-banded material that is intimately intergrown with bornite, covellite, tetrahedrite, and fine-grained pyrite and quartz. Covellite occurs as fine, hairlike needles and laths within the bornite. Tetrahedrite forms small blebs and fracture fillings within the chalcopyrite-bornite assemblage. The dominance of chalcopyrite at the North Gambier occurrence is unusual for the ATMB as is the relatively major proportion of bornite. However, mineralized samples contain 0.1–1 percent copper, 0.1 percent zinc, several parts per million silver, and highly anomalous concentrations of Mn, As, Cd, Mo, Pb, Sb, and Hg, similar to the Greens Creek geochemical signature that occurs consistently throughout the ATMB.

Mineral occurrences that typify the progression to larger, more stratiform morphologies with mineralogical and geochemical features like Greens Creek are also present in the central area of the ATMB and persist northward to the latitude of Mt. Henry Clay. The Butterworth Island occurrence is located just south of the southeastern corner of section 34, in the Petersburg C-4 15-minute quadrangle, just west of Woewodski Island. The occurrence is located below the high tide line in the small spit of land that separates the southeastern

end of Butterworth Island from the small islet to the south. Rocks exposed at low tide between the islands consist of foliated, reddish, highly altered siliceous schist. Immediately to the north, and forming the southern shoreline of Butterworth Island, the siliceous schist is in sharp contact with massive, fractured, unfoliated Cretaceous(?) diorite. Southward the schist grades into a sequence of rocks mapped as Mesozoic volcanics (Brew, 1997). The altered schist hosting the mineral occurrence grades southward into greenschist and moderately foliated mafic metavolcanic rocks that have been intruded by sills of Cretaceous(?) diorite. The diorite contains xenoliths of gabbro probably incorporated from the Mesozoic gabbroic intrusive body that crops out on the northern one-third of Butterworth Island (Brew, 1997).

The Butterworth Island occurrence consists of several subparallel 1–10-cm-thick, semimassive to massive sulfide bands that are conformable with foliation and occur over a width of approximately 4 meters. The mineralized bands are traceable along foliation across the entire width of the low-tide land bridge. The better, more massive sulfide bands are located at low tide on the east side. The best single band is a 10-cm-thick layer of massive pyrite, dark red sphalerite, galena, and probable tetrahedrite. Texturally, the sulfides are fine crystalline and equigranular and appear to form a matrix to clasts of white quartz or chert pebbles and very elongate fragments of thoroughly altered rock. The geochemical signature of the massive sulfide is characterized by very high values of Zn, Fe, Pb, Ag, Hg, Cd, Sb, Co, Mn, (Cu, Au, Mo, and V).

The Castle Island barite deposit is, or was, located in a group of small islands in the middle of Duncan Canal, several kilometers east of the mouth of Castle River. The deposit consisted of a small island almost entirely composed of barite just east of, and connected by a small spit of land to, “Little” Castle Island, the small islet immediately south of Big Castle Island. Little Castle Island is composed from west to east of massive, volcanoclastic, and pillowed mafic volcanic rocks that grade into phyllitic greenstone, which in turn grade into a thin layer of phyllitic pebble conglomerate. Orange-weathering iron-carbonate-altered rock marks a distinctive sheared fault zone running the length of the island that is exposed along the east shoreline. The eastern shore south of the former ore-loading pad consists of a sequence of phyllitic calcareous mudstone, silty limestone, and possibly interbedded gray-wacke; this sequence is approximately 100 meters southeast of the loading pad along strike and likely represents the footwall rocks to the deposit that are now covered. A small knob in the tide zone south of the loading pad and east of the Little Castle Island shoreline is composed of the calcareous phyllite and is cut by poddy and discontinuous, sulfide-bearing, quartz-carbonate veins, centimeters to 0.7 meter thick. Sulfides are disseminated euhedral grains of coarse crystalline pyrite, green (low iron) sphalerite, and minor galena. Geochemical analyses of the veins indicate that the carbonate is iron and manganese rich, as are carbonate alteration minerals associated with mineral occurrences throughout the ATMB

(C.D. Taylor, this study and unpublished data). These veins are probably the metamorphosed feeders to the Castle Island barite deposit.

Previously published records indicate that the Castle Island barite deposit was approximately 95 meters long, 63 meters wide, and extended below sea level to a depth of 47 meters (Grybeck and others, 1984). Maximum elevation of the barite outcrop was between 11 and 18.5 meters above sea level. Enclosing rocks strike northwesterly and dip 50 to 60 degrees to the northeast. A premining estimate based on drilling of the size of the deposit down to 12.5 meters below sea level was 218,000 metric tonnes with a true thickness of the main barite body of 25 to 31 meters (Burchard, 1914; Williams and Decker, 1932). These reports also suggest that the footwall to the deposit consisted of 3–6 meters of “baritic greyschist and limestone” above black slaty argillite, all of which rested on “dark volcanic rocks” that are probably equivalent to the basalt exposed on the islet to the west. Such a stratigraphy is consistent with exposures of presumed footwall sediments to the southeast of the deposit, as previously described. Cross sections based on drilling data suggest that the deposit was essentially a single massive lens dipping eastward, conformably with the enclosing sediments, into Duncan Canal. A horse composed of impure barite, calcite, and schist is indicated at depth near the hanging wall. Sparse exposures of hanging-wall lithologies suggest phyllitic schist and volcanic tuff. The northern limit of the deposit was defined by drilling; the southern boundary was not determined. The barite body was thought to “rake somewhat to the southeast and extend southerly beyond the southern tip of the island” (Williams and Decker, 1932, p. 3), consistent with the general southeast plunge direction of fold axes in Triassic rocks of the area (P.J. Haeussler, written commun., 2000).

Grybeck and others (1984) reported a total production for the Castle Island barite deposit of approximately 0.68 million metric tonnes of barite based upon undocumented sources. Their reinterpretation of unpublished drilling data and cross sections led them to suggest that the deposit “occurred along the trough of a symmetrical open syncline trending about N. 70° W. and centered on the now mined-out island, with limbs dipping 30 to 45 degrees.” Grybeck and others (1984) also reported that drilling “indicated a considerable tonnage of lower grade barite interbedded with ‘gray schist’ (metafelsite?), ‘chert,’ and ‘graphitic schist,’ and indications of at least one more high-grade barite lens offshore.” Texturally, samples of the barite are massive, sugary, and white to light gray, with millimeter-scale bands and discontinuous wisps of fine crystalline sulfides (fig. 22A). Examination of thin sections indicates the presence of disseminated sphalerite, galena, pyrite, pyrrotite, bornite, tetrahedrite-tennantite, and chalcopyrite occurring as equant grains 5–300 micrometers in size (Berg and Grybeck, 1980; Grybeck and others, 1984).

Numerous assays of composite drill-core samples and surface chip samples established an average grade of 89

percent barite and 4.5 percent silica, with 0.5–2.5 percent zinc, 0.5–1 percent lead, 1–2 percent iron, 0.5–2.0 troy ounces per ton silver, and traces of gold (Williams and Decker, 1932; Race, 1963; Grybeck and others, 1984). The geochemical signature of the massive barite consists of Ba, Zn, Pb, Ag, Fe, Cd, Sb, Sr (Cu, Au, and Mo). Quartz-carbonate-sulfide veins in the footwall have a similar signature with the notable addition of manganese, arsenic, mercury, and a mafic-ultramafic suite consisting of cobalt, chromium, nickel, and vanadium (Taylor, 2003).

The Pyrola deposit is located in the north-central part of Admiralty Island within a sequence of greenschist-facies rocks correlated with the Retreat Group schists and unconformably overlying limestone, argillite, and mafic volcanic rocks. This sequence of lithologies bears a strong resemblance to the sequence that characterizes the Hyd Group and, although the age of the Pyrola host rocks are not known with certainty, Van Nieuwenhuysse (1984) suggested that they are either Permian or Triassic. The deposit consists of stratiform layers of interbedded barite and massive sulfide hosted in graphitic sediments. A siliceous disseminated pyritic stockwork zone is also present and contains precious metals. The deposit is underlain by a large, semiconformable chlorite-carbonate alteration halo, which is overprinted in the immediate footwall by intense sericite-quartz-pyrite altered rock. The ore mineralogy consists of pyrite, sphalerite, galena, minor chalcopyrite, jamesonite, and boulangerite (Van Nieuwenhuysse, 1984). In addition to the many geological similarities to Greens Creek and other barite-rich polymetallic deposits in the central portion of the ATMB, at Pyrola both sulfur and lead isotopic values of galena are very similar to values at Greens Creek (chap.10).

The Glacier Creek (Main) deposit and the nearby Upper Cap occurrence are on the U.S. side of the border in the Mt. Henry Clay area. They are both stratiform, barite-rich, polymetallic deposits of Late Triassic age that represent the northernmost examples characteristic of the central, transitional portion of the ATMB. The Glacier Creek deposit consists of a 20–30-m-thick, 600-m-long layer of highly altered quartz-sericite schist that contains lenses of massive barite accompanied by bands of sphalerite, galena, and chalcopyrite (MacIntyre and Schroeter, 1985). The deposit is underlain by mafic flows and sedimentary rocks and is overlain by massive pillow lavas (fig. 22B). The Upper Cap occurrence, located several kilometers up Glacier Creek, displays similar features to the Glacier Creek deposit. The occurrence consists predominantly of a 3-m-thick, silica-barite lens with minor amounts of pyrite, sphalerite, galena, and tetrahedrite (fig. 22C; MacIntyre and Schroeter, 1985). The footwall is largely covered by ice; the hanging wall consists of massive basalt flows. Reports of ruby silver (Ag-sulfosalt) at Upper Cap (Merrill Palmer, oral commun., 1994) suggest mineralogical similarities to Greens Creek. X-ray diffraction analysis of reddish-black crystals in silica-barite identified the lead-antimony sulfide mineral geocronite, which also occurs at Greens Creek (chap. 9).

Discussion

We propose, based on the transitional features of the ATMB just described, that the Late Triassic rift in southeastern Alaska formed by oblique propagation into the Alexander terrane resulting in a metallogenic environment setting common both to VMS and to SEDEX environments. Recent work relating the specific nature of both ancient (Barrett and MacLean, 1999) and modern (Hannington and others, 1986; Halbach and others, 1993; Binns and others, 1993; Fouquet and others, 1993; Stoffers and others, 1999) VMS deposits to the location (continental margin, oceanic) and maturity level of the hosting rift basins helps to explain the variations in the mineral occurrences of the ATMB in southeastern Alaska. For example, deposits that form at the tip of rifts propagating into mature arcs (the western Woodlark basin propagating into Papua New Guinea [Binns and others, 1993]; the southern Lau Basin propagating into the North Island of New Zealand from the Valu Fa Ridge to the Taupo volcanic zone [Fouquet and others, 1993]) or where nascent intracontinental rifts split arcs (Japan [Barrett and MacLean, 1999]) are generally of the Kuroko type and are associated with arc-type or heavily calc-alkaline contaminated transitional lavas such as E-MORB (Barrett and MacLean, 1999; cf. the bimodal-mafic division of Barrie and Hannington, 1999). Deposits landward of the propagating rift, or deposits that form on land in the early stages of rifting, display an epithermal or hot-springs style of mineralization (for example, Stoffers and others, 1999; cf. deposits of the Taupo volcanic zone, White, 1981; Hedenquist and Henley, 1985). Deposits that form in the deeper, seaward portion of propagating rifts or in mature rifts are more likely to have a dominantly copper-zinc rich metal assemblage and may be associated with distal clastic sediments (for example, Windy Craggy [Peter and Scott, 1999]; and the Besshi deposits [Slack, 1993]). The deposits occurring in the mature rift settings are usually generally associated with primitive mafic melts that are forming segments of new oceanic crust and may or may not show contamination by melting and incorporation of the rifted crust (Barrett and MacLean, 1999; cf. the mafic-siliciclastic division of Barrie and Hannington, 1999). That such a variation of deposit styles, associated with predictably varying suites of igneous rocks, can be found in a single rift propagating into a mature arc or continental margin provides confirmation for the lithochemical and deposit variability of the mineral occurrences in southeastern Alaska. Figure 23 depicts a cross-sectional view through such a tectonic setting showing the various subaerial to deepwater settings of the southeastern Alaska Late Triassic mineral occurrences in the ATMB.

The segment of a propagating oceanic rift that we believe is analogous to the Greens Creek tectonic setting is that portion seaward of the propagating tip of a rift basin and landward of the point at which new oceanic crust begins to form. Within this segment, bimodal volcanism is characterized by peralkaline rhyolites and variably enriched basalts that exhibit chemistry similar to intraplate rocks and varying degrees of crustal contamination (for example, Smith and others, 1977; Smith and Johnson, 1981). Moving seaward, rhyolites disappear from



Figure 22 A–C. Photographs of outcrops and polished rock slabs from mineral occurrences in the central and northern portion of the ATMB. (A) Barite-galena-rich float collected on the loading pad at the Castle Island barite mine in the Duncan Canal area, central southeastern Alaska. (B) Glacier Creek (Main) deposit in the Mt. Henry Clay area, northern southeastern Alaska. The central, orange-white stripe consists of quartz-sericite-carbonate schist with lenses of massive barite and lesser sulfides. Outcrop above and below consists of massive and pillowed basalt flows. (C) Barite-sulfide lens at the Upper Cap occurrence in the Mt. Henry Clay area, northern southeastern Alaska. Rocks overlying the lens are massive basalt flows.

landmass of wholly oceanic affinities, cored by sialic Proterozoic and lower Paleozoic crust. At the latitude of Greens Creek, rifting resulted in the formation of a small (second order?), restricted, anoxic, and very organic-rich sedimentary basin, which was intruded by rift-related mafic-ultramafic intrusive rocks. This SEDEX-like metallogenic setting occurred within a propagating rift, which on a larger scale is more similar to the metallogenic setting common to many VMS deposits.

References Cited

- Aitchison, J.C., and Flood, P.G., 1995, Gamilaroi Terrane—A Devonian rifted intra-oceanic island-arc assemblage, NSW, Australia, *in* Smellie, J.L., ed., *Volcanism associated with extension at consuming plate margins*: Geological Society Special Publication no. 81, p. 155–168.
- Arculus, R.J., 1987, The significance of source versus process in the tectonic controls of magma genesis: *Journal of Volcanology and Geothermal Research*, v. 32, p. 1–12.
- Barker, Fred, 1994, Some accreted volcanic rocks of Alaska and their elemental abundances, *in* Plafker, G., and Berg, H.C., eds., *The geology of Alaska: Boulder, Colorado, Geological Society of America, Decade of North American Geology*, v. G–1, p. 555–587.
- Barker, Fred, Sutherland-Brown, A., Budahn, J.R., and Plafker, G., 1989, Back-arc with frontal-arc component origin of Triassic Karmutsen basalt, British Columbia, Canada: *Chemical Geology*, v. 75, p. 81–102.
- Barrett, T.J., and MacLean, W.H., 1999, Volcanic sequences, litho-geochemistry, and hydrothermal alteration in some bimodal volcanic-associated massive sulfide systems, *in* Barrie, C.T., and Hannington, M.D., eds., *Volcanic-associated massive sulfide deposits—Processes and examples in modern and ancient settings*: Society of Economic Geologists Reviews in Economic Geology, v. 8, p. 101–127.
- Barrie, C.T., and Hannington, M.D., 1999, Classification of volcanic-associated massive sulfide deposits based on host-rock composition, *in* Barrie, C.T., and Hannington, M.D., eds., *Volcanic-associated massive sulfide deposits—Processes and examples in modern and ancient settings*: Society of Economic Geologists Reviews in Economic Geology, v. 8, p. 1–11.
- Bazard, D.R., Butler, R., Gehrels, G., and Soja, C.M., 1994, New constraints for Late Silurian-Devonian paleogeography of the Alexander terrane, southeastern Alaska: *Geological Society of America Abstracts with Programs*, v. 26, p. A384.
- Berg, H.C., 1972, Geologic map of Annette Island, Alaska: U.S. Geological Survey Miscellaneous Investigations Series Map I-684, scale 1:63,360.
- Berg, H.C., 1973, The geology of Gravina Island, Alaska: U.S. Geological Survey Bulletin 1373, 41 p.
- Berg, H.C., and Grybeck, D., 1980, Upper Triassic volcanogenic Zn-Pb-Ag-(Cu-Au)-barite mineral deposits near Petersburg, Alaska: U.S. Geological Survey Open-File Report 80-527, 9 p.
- Berg, H.C., Jones, D.L., and Coney, P.J., 1978, Map showing pre-Cenozoic tectono-stratigraphic terranes of southeastern Alaska and adjacent areas: U.S. Geological Survey Open-File Report 78-1085, 2 sheets, scale 1:1,000,000.
- Berg, H.C., Jones, D.L., and Richter, D.H., 1972, Gravina-Nutzotin belt—Tectonic significance of an upper Mesozoic sedimentary and volcanic sequence in southern and southeastern Alaska: U.S. Geological Survey Professional Paper 800-D, p. D1–D24.
- Binns, R.A., Scott, S.D., Bogdanov, Y.A., Lisitzin, A.P., Gordeev, V.V., Gurvich, E.G., Finlayson, E.J., Boyd, T., Dotter, L.E., Wheller, G.E., and Muravyev, K.G., 1993, Hydrothermal oxide and gold-rich sulfate deposits of Franklin Seamount, western Woodlark basin, Papua New Guinea: *Economic Geology*, v. 88, p. 2122–2153.
- Boynton, W.V., 1984, Cosmochemistry of the rare earth elements—Meteorite studies, *in* Henderson, P., ed., *Rare earth element geochemistry*: Amsterdam, Elsevier, p. 63–114.
- Brew, D.A., 1997, Reconnaissance geologic map of the Petersburg C-4 quadrangle, southeastern Alaska: U.S. Geological Survey Open-File Report 97-156-J, 21 p., 1 sheet, scale 1:63,360.
- Buddington, A.F., 1923, Mineral deposits of the Wrangell district: U.S. Geological Survey Bulletin 739, p. 51–75.
- Burchard, E.F., 1914, A barite deposit near Wrangell: U.S. Geological Survey Bulletin 592, p. 109–117.
- Churkin, Michael, Jr., and Eberlein, G.D., 1977, Ancient borderland terranes of the North American Cordillera—Correlation and microplate tectonics: *Geological Society of America Bulletin*, v. 88, p. 769–786.
- Civetta, Lucia, Cornette, Y., Crisci, G., Gillot, P.Y., Orsi, G., and Requejos, C.S., 1984, Geology, geochronology and chemical evolution of the island of Pantelleria: *Geological Magazine*, v. 121, no. 6, p. 541–562.
- Cobb, E.H., 1972, Metallic mineral resources map of the Petersburg quadrangle, Alaska: U.S. Geological Survey Miscellaneous Field Studies Map MF-415, 1 sheet, scale 1:250,000.
- Cobb, E.H., 1978, Summary of references to mineral occurrences (other than mineral fuels and construction materials) in the Petersburg quadrangle, Alaska: U.S. Geological Survey Open-File Report 78-870, 52 p.

- Cole, J.W., 1978, Tectonic setting of Mayor Island volcano: *New Zealand Journal of Geology and Geophysics*, v. 21, p. 645–647.
- Dadd, K.A., 1998, Incipient backarc magmatism in the Silurian Tumut Trough, new South Wales—An ancient analogue of the early Lau Basin: *Australian Journal of Earth Science*, v. 45, p. 109–121.
- Dudas, F.O., 1992, Petrogenetic evaluation of trace element discrimination diagrams, *in* Bartholomew, M.J., Hyndman, D.W., Mogk, D.W., and Mason, R., *Basement tectonics 8—Characterization and comparison of ancient and Mesozoic continental margins—Proceedings of the 8th International Conference on Basement Tectonics* (Butte, Montana, 1988): Dordrecht, The Netherlands, Kluwer Academic Publishers, p. 93–127.
- Dusel-Bacon, Cynthia, 1994, Metamorphic history of Alaska, *in* Plafker, G., and Berg, H.C., eds., *The geology of Alaska: Boulder, Colorado, Geological Society of America, Decade of North American Geology*, v. G1, p. 495–533.
- Forbes, R.B., Gilbert, W., and Redman, E., 1989, Geologic setting and petrology of the metavolcanic rocks in the northwestern part of the Skagway B-4 quadrangle, southeastern Alaska: *Alaska Division of Geological and Geophysical Surveys, Public-Data File 89–14*, 43 p.
- Ford, A.B., and Brew, D.A., 1993, Geochemical character of upper Paleozoic and Triassic greenstone and related metavolcanic rocks of the Wrangellia terrane in northern southeastern Alaska, *in* Dusel-Bacon, Cynthia, and Till, A.B., eds., *Geologic studies in Alaska by the U.S. Geological Survey, 1992: U.S. Geological Survey Bulletin 2068*, p. 197–217.
- Fouquet, Yves, Von Stackelberg, U., Charlou, J.L., Erzinger, J., Herzig, P.M., Muhe, R., and Wiedicke, M., 1993, Metallogensis in back-arc environments—The Lau basin example: *Economic Geology*, v. 88, p. 2154–2181.
- Franklin, J.M., 1986, Volcanic-associated massive sulphide deposits—An update, *in* Andrew, C.J., Crowe, R.W.A., Finlay, S., Pennel, W.M., and Pyne, J.F., eds., *Geology and genesis of mineral deposits in Ireland: Irish Association for Economic Geology*, p. 49–69.
- Franklin, J.M., 1993, Volcanic-associated massive sulphide deposits, *in* Kirkham, R.V., Sinclair, W.D., Thorpe, R.I., and Duke, J.M., eds., *Mineral deposit modeling: Geological Association of Canada, Special Paper 40*, p. 315–334.
- Franklin, J.M., Lydon, J.W., and Sangster, D.F., 1981, Volcanic-associated massive sulfide deposits, *in* Skinner, B.J., ed., *Economic geology—Seventy-fifth anniversary volume, 1905–1980: El Paso, Texas, The Economic Geology Publishing Company*, p. 485–627.
- Gardner, M.C., Bergman, S.C., Cushing, G.W., MacKevett, E.M., Jr., Plafker, G., Campbell, R.B., Dodds, C.J., McClelland, W.C., and Mueller, P.A., 1988, Pennsylvanian pluton stitching of Wrangellia and the Alexander terrane, Wrangell Mountains, Alaska: *Geology*, v. 16, p. 967–971.
- Gehrels, G.E., and Barker, G., 1993, Reconnaissance geochemistry of Permian and Triassic basalts of the Taku and Wrangellia terranes, southeastern Alaska, *in* Dusel-Bacon, Cynthia, and Till, A.B., eds., *Geologic studies in Alaska by the U.S. Geological Survey, 1992: U.S. Geological Survey Bulletin 2068*, p. 218–227.
- Gehrels, G.E., and Berg, H.C., 1992, Geologic map of southeastern Alaska: *U.S. Geological Survey Miscellaneous Investigations Series Map I-1867*, scale 1:600,000.
- Gehrels, G.E., and Berg, H.C., 1994, Geology of southeastern Alaska, *in* Plafker, George, and Berg, H.C., eds., *The geology of Alaska: Boulder, Colorado, Geological Society of America, Decade of North American Geology*, v. G1, p. 451–468.
- Gehrels, G.E., Dickinson, W.R., Ross, G.M., Stewart, J.H., and Howell, D.G., 1994, Provenance of detrital zircons in strata of the Cordilleran miogeocline and selected outboard terranes: *Geological Society of America Abstracts with Programs*, v. 26, p. A384.
- Gehrels, G.E., Dodds, C.J., and Campbell, R.B., 1986, Upper Triassic rocks of the Alexander terrane, SE Alaska, and the Saint Elias Mountains of B.C. and Yukon: *Geological Society of America Abstracts with Programs*, v. 18, p. 109.
- Gehrels, G.E., and Saleeby, J.B., 1987, Geologic framework, tectonic evolution, and displacement history of the Alexander terrane: *Tectonics*, v. 6, p. 151–173.
- Gehrels, G.E., Saleeby, J.B., and Berg, H.C., 1987, Geology of Annette, Gravina, and Duke Islands, southeastern Alaska: *Canadian Journal of Earth Sciences*, v. 24, p. 866–881.
- Gill, James, and Whelan, P., 1989, Early rifting of an oceanic island arc (Fiji) produced shoshonitic to tholeiitic basalts: *Journal of Geophysical Research*, v. 94, no. B4, p. 4561–4578.
- Goldfarb, R.J., Nelson, S.W., Berg, H.C., and Light, T.D., 1987, Distribution of mineral deposits in the Pacific Border Ranges and Coast Mountains of the Alaska Cordillera, *in* Elliot, I.L., and Snee, B.W., eds., *Geoexpo/86—Exploration in the North American Cordillera: Vancouver, B.C., Association of Exploration Geochemists*, p. 19–41.
- Goldfarb, R.J., Snee, L.W., Miller, L.D., and Newberry, R.J., 1991, Rapid dewatering of the crust deduced from ages of mesothermal gold deposits: *Nature*, v. 354, p. 296–298.

- Goodfellow, W.D., Lydon, J.W., and Turner, R.J.W., 1993, Geology and genesis of stratiform sediment-hosted (SEDEX) zinc-lead-silver sulphide deposits, *in* Kirkham, R.V., Sinclair, W.D., Thorpe, R.I., and Duke, J.M., eds., Mineral deposit modelling: Geological Association of Canada, Special Paper 40, p. 201–251.
- Green, Darwin, MacVeigh, J.G., Palmer, M., Watkinson, D.H., and Orchard, M.J., 2003, Stratigraphy and geochemistry of the RW Zone, a new discovery at the Glacier Creek VMS prospect, Palmer Property, Porcupine mining district, southeastern Alaska, *in* Clautice, K.H., and Davis, P.K., eds., Short notes on Alaska geology 2003: Alaska Division of Geological and Geophysical Surveys, Professional Report 120, p. 35–51.
- Grybeck, D.J., Berg, H.C., and Karl, S.M., 1984, Map and description of the mineral deposits in the Petersburg and eastern Port Alexander quadrangles, southeastern Alaska: U.S. Geological Survey Open-File Report 84–837, 87 p., 1 sheet, scale 1:250,000.
- Haeussler, P.J., Coe, R.S., and Onstott, T.C., 1992, Paleomagnetism of the Late Triassic Hound Island Volcanics—Revisited: *Journal of Geophysical Research*, v. 97, p. 19617–19639.
- Haeussler, P.J., Karl, S.M., Mortensen, J.K., Layer, P., and Himmelberg, G.R., 1999, Permian and mid-Cretaceous deformation of the Alexander terrane on Admiralty and Kupreanof Islands, southeastern Alaska: *Geological Society of America Abstracts with Programs*, v. 31, no. 6, p. A–60.
- Halbach, Peter, Pracejus, B., and Marten, A., 1993, Geology and mineralogy of massive sulfide ores from the central Okinawa trough, Japan: *Economic Geology*, v. 88, p. 2210–2225.
- Hannington, M.D., Peter, J.M., and Scott, S.D., 1986, Gold in sea-floor polymetallic sulfide deposits: *Economic Geology*, v. 81, p. 1867–1883.
- Hedenquist, J.W., and Henley, R.W., 1985, Hydrothermal eruptions in the Waiotapu geothermal system, New Zealand—Their origin, associated breccias, and relation to precious metal mineralization: *Economic Geology*, v. 80, p. 1640–1668.
- Hillhouse, J.W., 1987, Accretion of southern Alaska, *in* Kent, D.V., and Krs, M., eds., Laurasian paleomagnetism and tectonics: *Tectonophysics*, v. 139, p. 107–122.
- Hillhouse, J.W., and Gromme, C.S., 1984, Northward displacement and accretion of Wrangellia—New paleomagnetic evidence from Alaska: *Journal of Geophysical Research*, v. 89, p. 4461–4477.
- Jenner, G.A., 1996, Trace element geochemistry of igneous rocks—Geochemical nomenclature and analytical geochemistry, *in* Wyman, D.A., ed., Trace element geochemistry of volcanic rocks—Applications for massive sulfide exploration: Geological Association of Canada, Short Course Notes, v. 12, p. 51–77.
- Jenner, G.A., Longerich, H.P., Jackson, S.E., and Fryer, B.J., 1990, ICP-MS—A powerful tool for high-precision trace-element analysis in earth sciences—Evidence from analysis of selected U.S.G.S. reference samples: *Chemical Geology*, v. 83, p. 133–148.
- Jones, D.L., Silberling, N.J., and Hillhouse, J., 1977, Wrangellia—A displaced terrane in northwestern North America: *Canadian Journal of Earth Sciences*, v. 14, p. 2565–2577.
- Karl, S.M., 1992, Map and table of mineral deposits on Annette Island, Alaska: U.S. Geological Survey Open-File Report 92–690, scale 1:63,360, 57 p.
- Karl, S.M., Haeussler, P.J., and McCafferty, A., 1999a, Reconnaissance geologic map of the Duncan Canal/Zarembo Island area, southeastern Alaska: U.S. Geological Survey Open-File Report 99–168, 23 p.
- Karl, S.M., Haeussler, P.J., Mortenson, J.K., Layer, P., Savage, N., Wardlaw, B., Harris, A., Murchey, B., and Blome, C., 1999b, New stratigraphic and isotopic constraints on the depositional and deformational history of the Alexander terrane, southeastern Alaska: *Geological Society of America Abstracts with Programs* v. 31, no. 6, p. A–68.
- Kerns, W.H., 1950, Investigation of Taylor Creek lead-zinc deposit, Kupreanof Island, Petersburg, Alaska: U.S. Bureau of Mines Report of Investigations 4669, 13 p.
- Large, R.R., 1992, Australian VHMS deposits—Features, styles, models: *Economic Geology*, v. 87, p. 471–510.
- Lathram, E.H., Pomeroy, J.S., Berg, H.C., and Loney, R.A., 1965, Reconnaissance geology of Admiralty Island, Alaska: U.S. Geological Survey Bulletin 1181–R, 48 p.
- Leach, D.L., and Sangster, D.F., 1993, Mississippi Valley-type lead-zinc deposits, *in* Kirkham, R.V., Sinclair, W.D., Thorpe, R.I., and Duke, J.M., eds., Mineral deposit modeling: Geological Association of Canada, Special Paper 40, p. 289–314.
- Lentz, D.R., 1998, Petrogenetic evolution of felsic volcanic sequences associated with Phanerozoic volcanic-hosted massive sulphide systems—The role of extensional geodynamics: *Ore Geology Reviews*, v. 12, p. 289–327.
- Loney, R.A., 1964, Stratigraphy and petrography of the Pybus-Gambier area, Admiralty Island, Alaska: U.S. Geological Survey Bulletin 1178, 103 p.
- Longerich, H.P., Jenner, G.A., Fryer, B.J., and Jackson, S.E., 1990, Inductively coupled plasma-mass spectrometric analysis of geological samples—A critical evaluation based on case studies: *Chemical Geology*, v. 83, p. 105–118.
- MacIntyre, D.G., 1986, The geochemistry of basalts hosting massive sulfide deposits, Alexander terrane northwest British Columbia: British Columbia Ministry of Energy, Mines, and Petroleum Resources, Geological Fieldwork, 1985, Paper 1986–1, p. 197–210.

- MacIntyre, D.G., and Schroeter, T.G., 1985, Mineral occurrences in the Mt. Henry Clay area: British Columbia Ministry of Energy, Mines and Petroleum Resources, Geological Fieldwork, 1984, Paper 1985-1, p. 365-379.
- Mahood, G.A., and Baker, D.R., 1986, Experimental constraints on depths of fractionation of mildly alkalic basalts and associated felsic rocks—Pantelleria, Strait of Sicily: *Contributions to Mineralogy and Petrology*, v. 93, p. 251-264.
- McClelland, W.C., and Gehrels, G.E., 1990, Geology of the Duncan Canal shear zone—Evidence for Early to Middle Jurassic deformation of the Alexander terrane, southeastern Alaska: *Geological Society of America Bulletin*, v. 102, p. 1378-1392.
- Meier, A.L., and Slowik, T., 2002, Chapter K, Rare earth elements by inductively coupled plasma-mass spectrometry, in Taggart, J.E., Jr., ed., *Analytical methods for chemical analysis of geologic and other materials: U.S. Geological Survey Open-File Report 2002-223*, 10 p.
- Meschede, Martin, 1986, A method of discriminating between different types of mid-ocean ridge basalts and continental tholeiites with the Nb-Zr-Y diagram: *Chemical Geology*, v. 56, p. 207-218.
- Mihalynuk, M.G., Smith, M.T., MacIntyre, D.G., and Deschenes, M., 1993, Tatshenshini project, northwestern British Columbia—Part B, Stratigraphic and magmatic setting of mineral occurrences: British Columbia Ministry of Energy, Mines and Petroleum Resources, Geological Fieldwork 1992, Paper 1993-1, p. 189-202.
- Miller, L.D., Goldfarb, R.J., Gehrels, G.E., and Snee, L.W., 1994, Genetic links among fluid cycling, vein formation, regional deformation, and plutonism in the Juneau gold belt, southeastern Alaska: *Geology*, v. 22, p. 203-206.
- Muffler, L.J.P., 1967, Stratigraphy of the Keku Islets and neighbouring parts of Kuiu and Kupreanof Islands, southeastern Alaska: *U.S. Geological Survey Bulletin* 1241-C, 52 p.
- Newberry, R.J., and Brew, D.A., 1997, The Upper Triassic Greens Creek VMS (volcanogenic massive sulfide) deposit and Woewodski Island VMS prospects, southeastern Alaska—Chemical and isotopic data for rocks and ores demonstrate similarity of these deposits and their host rocks: *U.S. Geological Survey Open-File Report 97-539*, 49 p.
- Newberry, R.J., and Brew, D.A., 1999, Chemical and isotopic data for rocks and ores from the Upper Triassic Greens Creek and Woewodski Island volcanogenic massive sulfide deposits, southeastern Alaska, in Kelley, K.D., ed., *Geologic studies in Alaska by the U.S. Geological Survey, 1997: U.S. Geological Survey Professional Paper 1614*, p. 35-55.
- Newberry, R.J., Crafford, T.C., Newkirk, S.R., Young, L.E., Nelson, S.W., and Duke, N.A., 1997, Volcanogenic massive sulfide deposits of Alaska, in Goldfarb, R.J., and Miller, L.E., eds., *Mineral deposits of Alaska: Economic Geology Monograph 9*, p. 120-150.
- Panuska, B.C., 1990, An overlooked world class Triassic flood basalt event: *Geological Society of America Abstracts with Programs*, v. 22, p. A168.
- Pearce, J.A., 1996, A user's guide to basalt discrimination diagrams, in Wyman, D.A., ed., *Trace element geochemistry of volcanic rocks—Applications for massive sulfide exploration: Geological Association of Canada, Short Course Notes*, v. 12, p. 79-113.
- Pearce, J.A., and Cann, J.R., 1973, Tectonic setting of basic volcanic rocks determined using trace element analyses: *Earth and Planetary Science Letters*, v. 19, p. 290-300.
- Peter, J.M., and Scott, S.D., 1999, Windy Craggy, northwestern British Columbia—The world's largest Besshi-type deposit, in Barrie, C.T., and Hannington, M.D., eds., *Volcanic-associated massive sulfide deposits—Processes and examples in modern and ancient settings: Society of Economic Geologists Reviews in Economic Geology*, v. 8, p. 261-295.
- Pin, Christian, and Paquette, J.-L., 1997, A mantle-derived bimodal suite in the Hercynian Belt—Nd isotope and trace element evidence for a subduction-related rift origin of the Late Devonian Brevenne metavolcanics, Massif Central (France): *Contributions to Mineralogy and Petrology*, v. 129, p. 222-238.
- Race, W.H., 1963, Property examination report, Castle Island barite deposit, Duncan Canal, Alaska, Petersburg quadrangle: State of Alaska Division of Mines and Minerals, 13 p.
- Richards, M.A., Jones, D.L., Duncan, R.A., and DePaolo, D.J., 1991, A mantle plume initiation model for the Wrangellia flood basalt and other oceanic plateaus: *Science*, v. 254, p. 263-267.
- Rollison, Hugh, 1993, Using geochemical data—Evaluation, presentation, interpretation: New York, Longman Scientific and Technical, 352 p.
- Saleeby, J.B., 1994, Tectonic history of the Insular Suture Zone, southeastern Alaska: *Geological Society of America Abstracts with Programs*, v. 26, p. A384.
- Sampson, S.D., McClelland, W.C., Patchett, P.J., Gehrels, G.E., and Anderson, R.G., 1989, Evidence from neodymium isotopes for mantle contributions to Phanerozoic crustal genesis in the Canadian Cordillera: *Nature*, v. 337, p. 705-709.

- Sampson, S.D., Patchett, P.J., Gehrels, G.E., and Anderson, R.G., 1990, Nd and Sr isotopic characterization of the Wrangellia terrane and implications for crustal growth of the Canadian Cordillera: *Journal of Geology*, v. 98, p. 749–762.
- Sampson, S.D., Patchett, P.J., McClelland, W.C., and Gehrels, G.E., 1991, Nd and Sr isotopic constraints on the petrogenesis of the west side of the northern Coast Mountains batholith, Alaska and Canadian Cordillera: *Canadian Journal of Earth Science*, v. 28, p. 939–946.
- Savage, N.M., 1994, Terrane affinities of Middle and Late Devonian conodonts from the Wadleigh limestone, southeastern Alaska: *Geological Society of America Abstracts with Programs*, v. 26, p. A158.
- Slack, J.F., 1993, Descriptive and grade-tonnage models for Besshi-type massive sulphide deposits, *in* Kirkham, R.V., Sinclair, W.D., Thorpe, R.I., and Duke, J.M., eds., *Mineral deposit modeling: Geological Association of Canada, Special Paper 40*, p. 343–371.
- Smith, I.E.M., Chappell, B.W., Ward, G.K., and Freeman, R.S., 1977, Peralkaline rhyolites associated with andesitic arcs of the southwest Pacific: *Earth and Planetary Science Letters*, v. 37, p. 230–236.
- Smith, I.E.M., and Johnson, R.W., 1981, Contrasting rhyolite suites in the Late Cenozoic of Papua New Guinea: *Journal of Geophysical Research*, v. 86, no. B11, p. 10257–10272.
- Stern, R.J., Lin, P.-N., Morris, J.D., Jackson, M.C., Fryer, P., Bloomer, S.H., and Ito, E., 1990, Enriched back-arc basin basalts from the northern Mariana Trough—Implications for the magmatic evolution of back-arc basins: *Earth and Planetary Science Letters*, v. 100, p. 210–225.
- Stoffers, Peter, Hannington, M., Wright, I., Herzig, P., de Ronde, C., and Shipboard Scientific Party, 1999, Elemental mercury at submarine hydrothermal vents in the Bay of Plenty, Taupo volcanic zone, New Zealand: *Geology*, v. 27, p. 931–934.
- Taggart, J.E., Jr., ed., 2002, Analytical methods for chemical analysis of geologic and other materials, U.S. Geological Survey Open-File Report 2002–223, variously paginated.
- Taylor, C.D., 1993, Summary of geochemical data—Annette Islands Reserve, southeast Alaska, *in* Godwin, L.H., and Smith, B.D., eds.: *Northwest Mining Association special symposium 1993 on economic mineral resources of the Annette Islands Reserve, Alaska*, p. 77–82.
- Taylor, C.D., 2003, Descriptions of mineral occurrences and interpretation of mineralized rock geochemical data in the Stikine geophysical survey area, southeastern Alaska: U.S. Geological Survey Open-File Report 2003–154, 51 p.
- Taylor, C.D., Cieutat, B.A., and Miller, L.D., 1992, A follow-up geochemical survey of base metal anomalies in the Ward Creek/Windfall Harbor and Gambier Bay areas, Admiralty Island, S.E. Alaska, *in* Bradley, D.C., and Dusel-Bacon, C., eds., 1991 *Geologic Studies in Alaska: U.S. Geological Survey Bulletin 2041*, p. 70–85.
- Taylor, C.D., Newkirk, S.R., Hall, T.E., Lear, K.G., Premo, W.R., Leventhal, J.S., Meier, A.L., Johnson, C.A., and Harris, A.G., 1999, The Greens Creek deposit, southeastern Alaska—A VMS-SEDEX hybrid, *in* Stanley, C.J., and others, eds., *Mineral deposits—Processes to processing: Rotterdam, Balkema*, p. 597–600.
- Taylor, C.D., Premo, W.R., Meier, A.L., and Taggart, J.E., Jr., 2008, The metallogeny of Late Triassic rifting of the Alexander Terrane in southeastern Alaska and northwestern British Columbia: *Economic Geology*, v. 103, p. 89–115.
- Van Nieuwenhuysse, R.E., 1984, *Geology and geochemistry of the Pyrolo massive sulfide deposit, Admiralty Island, Alaska: Tucson, University of Arizona, unpublished Master's thesis*, 170 p.
- Warme, J.E., and Kuehner, H-C., 1998, Anatomy of an anomaly—The Devonian catastrophic Alamo impact breccia of southern Nevada, *in* Ernst, W.G., and Nelson, C.A., eds., *Integrated earth and environmental evolution of the southwestern United States: Boulder, Colo., Geological Society of America*, p. 80–110.
- White, D.E., 1981, Active geothermal systems and hydrothermal ore deposits, *in* Skinner, B.J., ed., *Economic geology—Seventy-fifth anniversary volume, 1905–1980: El Paso, The Economic Geology Publishing Company*, p. 392–423.
- Williams, J.A., and Decker, P.A., 1932, *Exploring Castle Island barite deposit by diamond drilling, a compilation—Unpublished report available from the Juneau office of the U.S. Bureau of Land Management, listing # MR 117–1*, 46 p.
- Wilson, Marjorie, 1989, *Igneous petrogenesis—A global tectonic approach: London, Unwin Hyman*, 466 p.
- Winchester, J.A., and Floyd, P.A., 1977, Geochemical discrimination of different magma series and their differentiation products using immobile elements: *Chemical Geology*, v. 20, p. 325–343.
- Wood, D.A., 1980, The application of a Th-Hf-Ta diagram to problems of tectonomagmatic classification and to establishing the nature of crustal contamination of basaltic lavas of the British Tertiary Volcanic Province: *Earth and Planetary Science Letters*, v. 50, p. 11–30.

The History of Greens Creek Exploration

By Andrew W. West

Chapter 3 of

**Geology, Geochemistry, and Genesis of the Greens Creek Massive
Sulfide Deposit, Admiralty Island, Southeastern Alaska**

Edited by Cliff D. Taylor and Craig A. Johnson

Professional Paper 1763

**U.S. Department of the Interior
U.S. Geological Survey**

Contents

Abstract.....	65
Introduction.....	65
Pan Sound Joint Venture, 1973–78.....	65
1975 Program.....	67
1976 Program.....	69
1977 Program.....	70
Initial Underground Development and Land Battles, 1978–80.....	71
Driving of 1350 Drift.....	72
Federal Proclamations.....	72
1980 Exploration Program.....	73
Race to “Perfect” Claims and Predevelopment, 1981–85.....	73
1981 Exploration Program.....	73
1982 Drill Program.....	74
1983 Feasibility Study.....	75
1983 Exploration Program.....	75
1984 Exploration Program.....	76
1985 Surface Exploration Program.....	77
Land Strategies and Negotiations, 1983–85.....	78
Ownership Changes and Consolidation, Development, 1986–89.....	80
1986 Surface Exploration Program.....	80
1987 Surface Exploration Program.....	81
1988 and 1989 Surface Exploration Projects.....	82
Continuing Underground Exploration, Production to Shutdown to Reopening, 1990–95.....	82
1991 Exploration Program.....	83
1992 Exploration Program.....	83
1993 Closure.....	84
1994 Exploration.....	84
Land Exchange Act and Continuing Production and Exploration, 1995–Present.....	85
1996 Exploration and Reopening.....	85
1997 Exploration.....	86
Discovery of the 200 South Ore Zone.....	86
1998 Exploration.....	87
1999 Exploration Program.....	87
2000 Surface Exploration.....	88
Conclusion.....	88
Reference Cited.....	88

Figures

1. Map of northern Admiralty Island showing the Greens Creek mine and other localities discussed in the text.....	66
2. Ownership and exploration timeline.....	68
3. Chart showing proven and probable reserves compared to total (cumulative) production.....	79

The History of Greens Creek Exploration¹

By Andrew W. West

Abstract

The exploration history of the Greens Creek mine and district includes not only battles fought on the steep and intimidating terrain of Admiralty Island, but also in Washington, D.C., and the Oval Office of the White House. The Greens Creek mine is unique in that it is completely enclosed within a national monument. The time period that began with the initial discovery, in 1974, of the “Big Sore” ore suboutcropping and ended with the underground definition drilling of the orebody, overlapped with the largest national conservation movement of this century that ultimately led to congressional approval of Alaska National Interest Land Claims Act (ANILCA) in 1980. Not only did this legislative act have a profound effect on the subsequent exploration of the district and eventual production of Greens Creek, ANILCA shaped the economic life of Alaska as a whole.

Introduction

The Greens Creek mine (fig. 1) went from initial discovery to predevelopment and production in a fairly orderly, yet untimely manner. The Pan-Sound Joint Venture (JV), charged with mineral exploration in southeast Alaska in 1973, intersected ore in the very first “discovery” drill hole in 1975. The timeline for the project, which is shown in figure 2, demonstrates that despite nearly continuous exploration and/or predevelopment work, production did not begin until February 1989. During this 16-year period, many changes occurred both within and between the joint venture partners. The conservation movement in the late 1970s also had a huge effect on the Greens Creek project, culminating in the passage of the Alaska National Interest Lands Conservation Act (ANILCA) in 1980. Exploration during the first years of production was successful in increasing reserves; however declining metal prices precipitated a shutdown of production in April 1993. Exploration and definition drilling of the

higher grade Southwest Ore Zone from 1993 to 1994 resulted in a new feasibility study that was accepted by the joint venture partners, Kennecott Minerals and Hecla Mining. The mine reopened in 1996. National legislation reentered the picture when President Clinton signed the Land Exchange Bill in August of 1996. This unique piece of legislation allows for exploration and grants subsurface mineral rights to much of what was the original unpatented claim block that existed prior to ANILCA. The 7,301 acres of prospective ground allows Greens Creek to continue exploration activities aimed at increasing the life of the mine.

Pan Sound Joint Venture, 1973–78

The Pan Sound Joint Venture was formed in 1973 as a grass-roots exploration program to find base and/or precious metal deposits in the northern part of southeast Alaska, the Prince William Sound area, and the Kenai Peninsula. The original partners were Noranda Exploration (29.73 percent), Marietta Resources (29.73 percent), Exhalas Resources (29.73 percent), and Texas Gas Exploration (10.81 percent). The rationale behind the exploration program in Alaska was fourfold: (1) exploration was risky in other parts of the world due to unfavorable politics; (2) exploration opportunities in the rest of North America were dwindling; (3) the geology of Alaska was seen as being highly favorable for economic deposits; and (4) the ongoing national energy crisis was underscoring the importance of a healthy domestic natural resource industry (L.M. Klingmueller and G.G. Bigelow, Watts, Griffis and McQuat, Inc., written commun., 1973). Watts, Griffis and McQuat (WGM) of Anchorage was contracted by the Pan Sound JV to carry out an extensive stream silt-sampling project in southeast Alaska. Their 1973 survey yielded anomalous zinc and copper stream silt samples collected from Cliff Creek (east of Big Sore Creek) and just southeast of Hawk Inlet (fig. 1). The sample from Cliff Creek contained 0.13 percent zinc and appeared to be associated with mineralized (disseminated pyrite and chalcopyrite) float from the Triassic Hyd basalt that forms the major cliff above Cliff Creek. Inclement weather prevented any followup work, but an intensive followup survey was recommended for the Cliff Creek drainage as well as first-pass coverage of the areas north and south of Greens Creek. WGM did not stake any claims in the Greens Creek area.

¹ Much of the information conveyed in this chapter was first documented in memoranda or reports to Kennecott Greens Creek Mining Company or its antecedents. Because they are unavailable to the public, these documents are cited in text only.

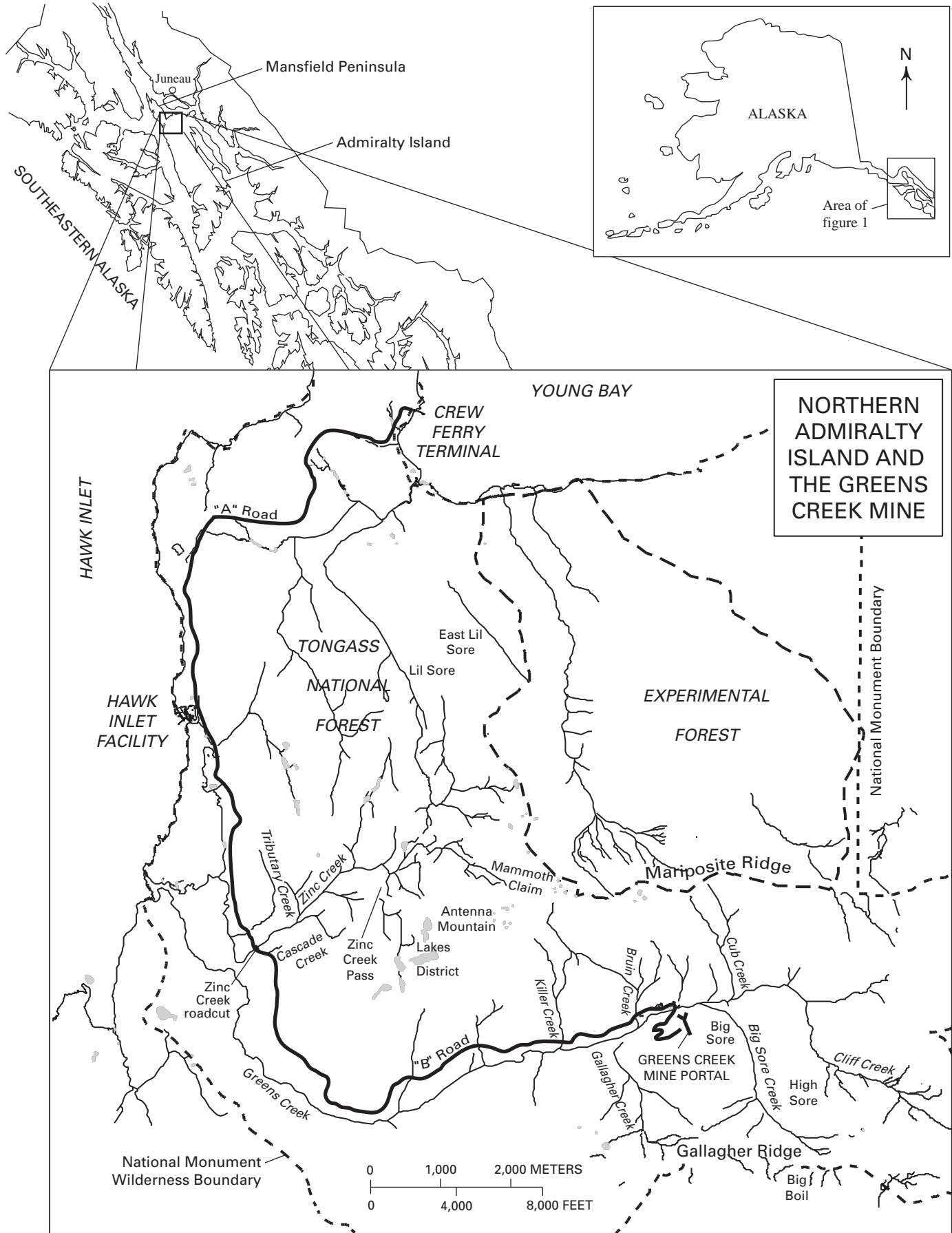


Figure 1 (facing page). Map of northern Admiralty Island showing the Greens Creek mine and other localities discussed in the text.

WGM geologists Bill “Boomer” Block and Joe Dreschler discovered the Greens Creek orebody in 1974 when they observed a large ferricrete kill zone from the air during the followup program (T.E. Andrews and others, Watts, Griffis and McQuat, Inc., written commun., 1975). Dubbed the “Big Sore,” this area (fig. 1) quickly became the focal point of exploration. A soil geochemistry grid laid out over the Big Sore delineated numerous silver-zinc anomalies on the order of 100 parts per million (ppm) silver and up to 1.7 percent zinc. WGM completed a Crone shootback electromagnetic (CEM) geophysical survey over 19,800 feet of gridline and a surface magnetometer survey totaling 12,500 feet. The CEM survey detected a partial conductor roughly coincident with soil anomalies. Two magnetic highs were identified in the lower reaches of Killer Creek. The WGM geologists postulated that the source of the CEM conductor was a mapped graphitic quartz-mica schist (T.E. Andrews and others, Watts, Griffis and McQuat, Inc., written commun., 1975). The magnetic anomalies were due to magnetite-bearing sulfide layers discovered in Killer Creek. A float sample believed to be from the same unit assayed for more than 10 percent copper. These two items generated additional interest in Killer Creek. Most of the exposed mineralization found by WGM, other than the Big Sore itself, was from the Killer Creek area.

WGM staked 134 lode claims, named the Big Sore claims, to establish the land position. The claims stretched from the southeast corner of Cliff Creek across the Greens Creek valley to the northeast corner of Upper Zinc Creek. WGM suggested that the land on the north, east, and south sides also be staked. There was concern that the large claim block would attract attention from various competitors (T.E. Andrews and others, Watts, Griffis and McQuat, Inc., written commun., 1975). Until 1974, very little competitor activity was noted for Admiralty Island except for a small backpack-supported survey of Northern Chicagof and Admiralty Islands by Placid Oil. Also, Resource Associates of Alaska (RAA) and Urangellschaft were exploring parts of Northern Admiralty Island.

The 1974 exploration results led WGM and the Pan Sound JV to believe that the “strongest reconnaissance potential for the discovery of a stratabound massive sulfide is considered to be within the Paleozoic schists located north and south of the Greens Creek discoveries on Admiralty Island” (T.E. Andrews and others, Watts, Griffis and McQuat, Inc., written commun., 1975). WGM recommended additional soil sampling, extension of the CEM survey, detailed geologic mapping, and diamond drill testing of the main Big Sore anomaly. They believed that the Big Sore and Killer Creek areas had the potential to host one or more copper-lead-zinc sulfide body(s) of unknown grade with greater than 1,000 feet of strike length.

1975 Program

The Big Sore project and a detailed reconnaissance of Admiralty Island were two of three projects that the 1975 Pan Sound JV undertook. The third project was followup work on a copper prospect of Latouche Island in Prince William Sound. The 1975 Big Sore project was the most ambitious thus far with more than 1,000 soil, rock, and stream silt samples taken; 80,000 feet of CEM and magnetometer surveys; initial detailed geologic mapping; and trenching and blasting to outline drill targets. Diamond drilling also commenced with three holes completed before the end of the field season. The Big Sore project began on June 4 with a camp at Big Sore Creek. The project demobilized on September 20 when the drilling program finished.

Results from expanding the Big Sore soil grid led the WGM geologists to believe that the stratabound mineralization occurred along three to five stratigraphic horizons within Devonian units (T.E. Andrews and others, Watts, Griffis and McQuat, Inc., written commun., 1976). They believed that soil sampling was the best tool to establish drill targets because of the thick glacier till, the vegetation cover, and the difficulty in defining the stratigraphy. However, WGM did not associate the geochemical and electromagnetic (EM) signatures with a chlorite-carbonate-schist and graphitic schist contact (determined later to be the mineralized horizon).

The three completed diamond drill holes totaled 997 feet. The first drillhole, DDH-1 (later renamed PS-1), was drilled about 150 feet above the Big Sore to test the high-order soil anomaly and the coincident CEM anomaly. The “discovery” hole intersected 89 feet of continuous pyrite and base-metal massive sulfide beginning at 138 feet downhole. This hole remains the longest continuous intersection of massive sulfide mineralization drilled from the surface at Greens Creek. The interval averaged 0.123 troy ounce per ton gold, 5.77 troy ounces per ton silver, 2.04 percent lead, 8.03 percent zinc, and 0.43 percent copper. A marked increase in pyrite and decrease in chlorite-muscovite near the massive sulfide interval was noted. The hole terminated at 296 feet in dolomitic graphite-quartz-mica schist, with local bands of massive sulfide. Holes DDH-1 and DDH-2 were both lost due to caving ground, a harbinger for drilling problems to come. Hole DDH-1 was not able to test the two lower targets identified from the soil sampling.

Hole DDH-2 (PS-2) was collared about 500 feet to the south-southeast of hole DDH-1, downhill from the graphite schist contact. The hole intersected graphitic schist with two massive sulfide bands containing 4.86 percent zinc and 4.3 troy ounces per ton silver over 12 feet, and 6.32 percent zinc, 7.2 troy ounces per ton silver, and 0.275 troy ounce per ton gold over 29.5 feet. The hole was lost due to poor ground conditions before it reached its target horizon. DDH-3 (PS-3) was collared 200 feet downhill from DDH-2 to test the previously untested lower soil anomaly. No visible base-metal sulfides were intersected to the termination depth of 635 feet, despite the presence of “fresh” massive sulfide float and high multi-element soil values directly below the hole.

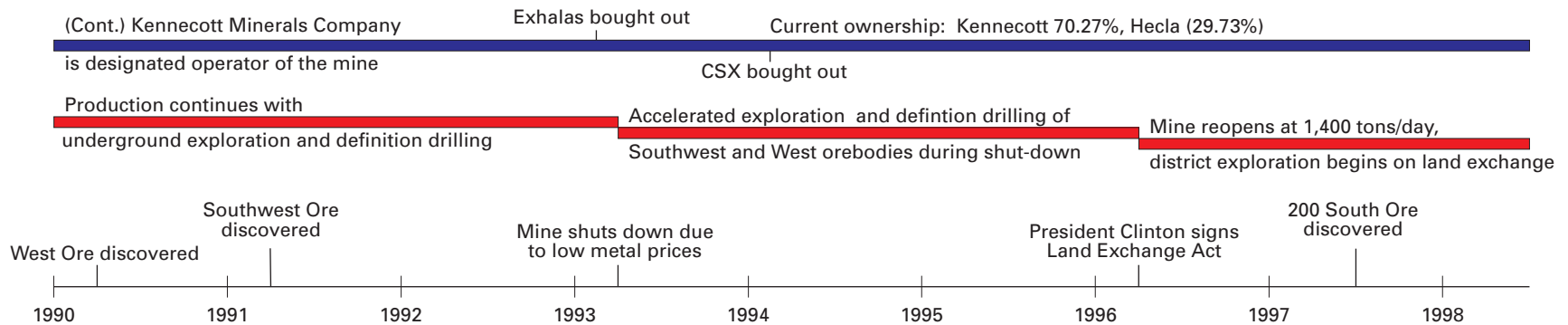
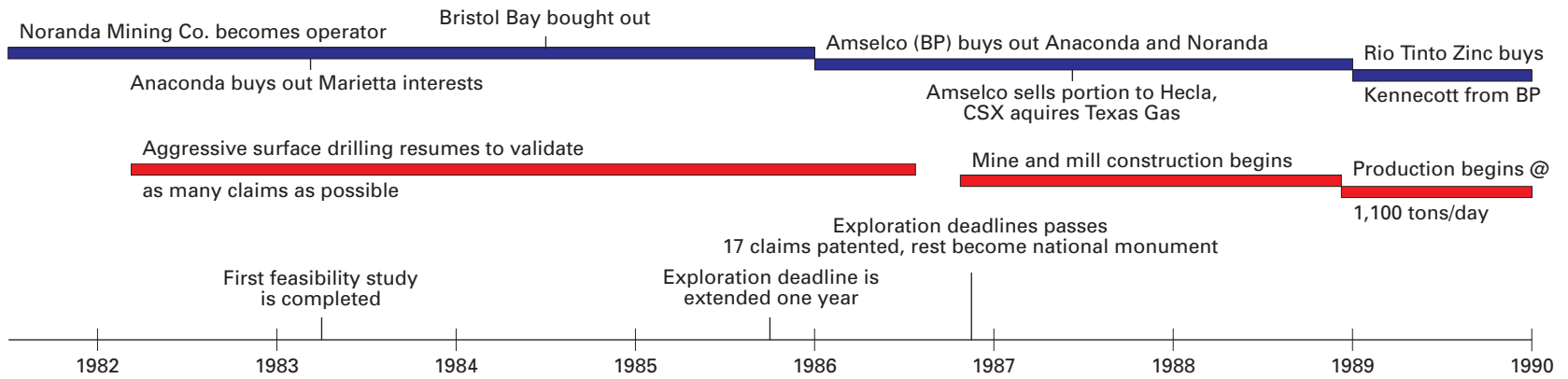
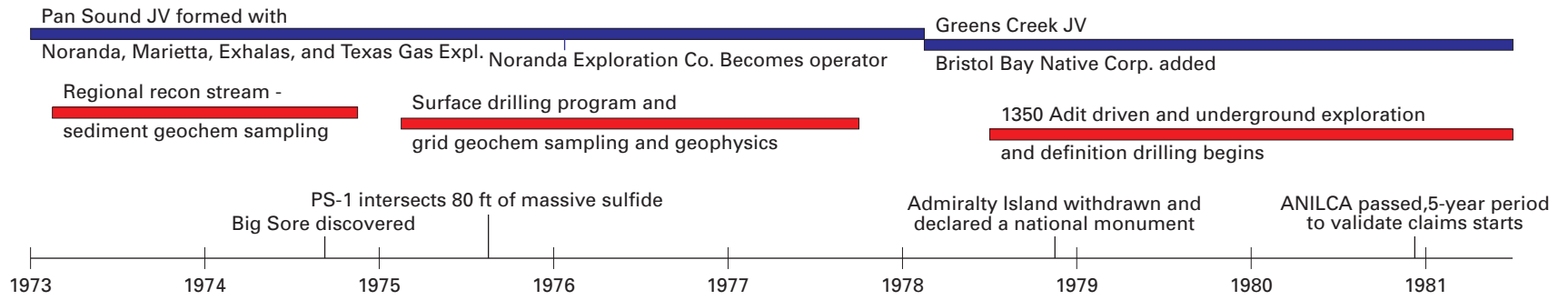


Figure 2 (facing page). Ownership (blue) and exploration (red) timeline.

Correlation of the above drill holes and soil anomalies led the WGM geologists to believe there were at least four, and maybe more, separate mineralized horizons to target (T.E. Andrews and others, Watts, Griffis and McQuat, Inc., written commun., 1976). DDH-3 displayed wildly fluctuating foliation orientations, but folding of the mineralized horizon was not considered. Using the drill-hole results and a tonnage factor of 12, WGM estimated an inferred metal “inventory” of 2 to 20 million tons of greater than 1.5 percent lead, 6.0 percent zinc, 0.1 troy ounce per ton gold, and 6.0 troy ounces per ton silver (T.E. Andrews and others, Watts, Griffis and McQuat, Inc., written commun., 1976). WGM recommended an aggressive (>10,00-foot) drilling program to rapidly bring the Big Sore Prospect to a development decision. They believed that the 1976 drilling program would place the inventory into “exploration” or “possible” reserves category, “barring unusual structural, facies complexity, or external factors” (T.E. Andrews and C. Bigelow, Watts, Griffis and McQuat, Inc., written commun., 1975).

Exploration work was also carried out in the Gallagher Creek, Killer Creek, and North Ridge (Mariposite Ridge) areas (fig. 1). Highlights include the discovery of massive sulfide float and outcrops in Gallagher Creek containing up to 31 percent zinc and 2.1 troy ounces per ton silver (T.E. Andrews and C. Bigelow, Watts, Griffis and McQuat, Inc., written commun., 1976). The outcrops contain sulfide veins up to 2 inches wide over a mineralized interval approximately 100 feet thick. Various mineralization styles were described, sampled, and mapped from the North Ridge, mostly in the vicinity of the Mammoth claims (see next paragraph). “Impressive” values were returned for gold, silver, lead, and zinc. Preliminary sampling and mapping did not provide sufficient data to determine the structural or stratigraphic setting of the mineralization.

The land status was further enhanced surrounding the Big Sore prospect during 1975. An additional 150 claims were added to the Big Sore claim group in all directions. The claim block was extended to the north, overlapping the four patented Mammoth claims that were originally staked in 1889 and patented in 1915. The overlapping claims were not to “jump” the existing claims but to ensure no area was left open between the two claim groups (fig. 1) (T.E. Andrews and C. Bigelow, Watts, Griffis and McQuat, Inc., written commun., 1975). An abandoned adit exists on the Mammoth claim that was excavated about 1904 along a massive galena-sphalerite band. WGM suggested that the owner, Herman Meiners of Juneau, be approached to see if the property could be leased or bought outright before the increased activity at Greens Creek increased the asking price.

The separate reconnaissance program of Admiralty Island completed much of its work near Greens Creek. The Tom claims were staked (a total of 52) to the east of Hawk Inlet within the lower Greens Creek and Zinc Creek drainages (T.E.

Andrews and C. Bigelow, Watts, Griffis and McQuat, Inc., written commun., 1976). WGM sampled Big Sore-type mineralization in graphitic quartz-mica schist, greenstones, and quartz-chlorite-carbonate schists with mariposite. In addition, work was done near ferricrete “sores” in a prospect named Kit Creek (now Lil Sore, fig. 1). The north-northwest-trending sores that contain up to 9,500 ppm zinc were postulated as representing a stratabound zinc sulfide body at moderate depth cut by permeable faults or fractures. No claims were staked during the field season because the land was nominated for Native Selection but was later withdrawn. Other prospects or claims explored included the Scull, Eagle Peak, and Jimbo to the northeast of Greens Creek, the Wheeler and Pyrola to the south and southwest of Greens Creek, and the JS and Barron on Mansfield Peninsula. As a result of the reconnaissance program, 472 new claims were staked on these new prospects. The Big Sore prospect was the standard with which the other prospects were compared, based on type of mineralization present and similar stratigraphy.

1976 Program

Noranda became the operator of the Big Sore program in 1976 for the Pan Sound JV. The program was composed of two projects again, one project concentrating on continued reconnaissance of Northern Admiralty Island, looking for other Greens Creek-type targets, while the other project continued exploration on the Big Sore and Tom claims. The principal objectives at Big Sore were to define the extent of the mineralized horizon intersected in DDH-1 and determine the geologic and geochemical nature of the mineralized zone (John Dunbier, Noranda Exploration, Inc., written commun., 1976). A geochemical grid with CEM and magnetic surveys was oriented north to south along Gallagher and Killer Creeks. The existing grid system was reoriented to trend N. 30° W. and center the baseline on the discovery hole. Two drill rigs were used for the program. A Longyear-34 hydraulic drill rig operated by Diamond Drill Contractors completed the deeper holes. A much smaller Winkie drill, owned and operated by Noranda, drilled 1.197-inch-diameter (AQ) core to penetrate the overburden and determine the lithology of the bedrock in areas of no outcrop. An additional 400+ claims were staked to fill in the gap between the Tom and Big Sore claims.

The diamond drilling program was successful in extending the known mineralized zone to the south-southeast, north-northwest, and slightly downdip (John Dunbier, Noranda Exploration, Inc., written commun., 1976). Three of the five holes drilled with the Longyear-34 intersected low- to high-grade ore along the contact between sericite-quartz phyllite (identified as “tuffites”) and the graphitic schist unit. The other two holes intersected minor mineralization in the tuffites (the hanging wall). Hole PS-3-76 intersected 11 feet of 0.042 troy ounce per ton gold, 22.7 troy ounces per ton silver, 5.9 percent lead, and 14.6 percent zinc to extend the known mineralized zone about 300 feet to the south-southeast of the discovery hole. PS-4-76 intersected a lower grade, yet thicker 12-foot

interval grading 9.9 troy ounces per ton silver and 3.45 percent zinc about 320 feet to the north-northwest. PS-7-76 extended the envelope even farther to the north-northwest (600 feet) with a 6-foot intercept of 29.3 troy ounces per ton silver and only 1.7 percent zinc.

The Winkie drill program consisted of eight holes. Only two of the holes intersected mineralization within the hanging-wall rocks while testing soil anomalies to the northwest of PS-1. One hole, PSW-4, was later followed up by hole PS-7-76 (mentioned previously). Two of the holes were unable to penetrate the overburden. Two large-diameter holes and one Winkie drill hole were drilled in Gallagher Creek. PS-1-76 and PS-2-76 intersected only minor mineralization of up to 4.4 percent zinc over 5 feet.

Noranda Exploration initiated a geologic mapping project carried out by one of their geologists, M.D. Bingham. Noranda anticipated taking a more active role in the Big Sore prospect and wanted to gain firsthand familiarity of the project (M.D. Bingham, Noranda Exploration, Inc., written commun., 1977). His mapping outlined three units favorable for massive sulfide mineralization: the chlorite-carbonate schist, a quartz carbonate (sericitic phyllite), and a quartz graphite schist (differentiated from the graphitic schist unit intersected immediately below the ore horizon in DDH-1).

Noranda attempted to better define and describe the lithologic units, geological and structural setting, and mineralization style of the Big Sore deposit in the 1976 year-end report. The hanging wall was described as chlorite and sericitic tuffites representing volcanoclastics of a mafic to felsic cycle. The footwall rocks were described as epiclastic perigenic conglomerates and carbonaceous argillites (formerly the graphitic schist unit). The pyritic and high-sphalerite ore zones and carbonaceous cherts were classified as exhalative rocks. Essentially, Noranda was trying to pigeonhole Greens Creek into a Kuroko-type deposit. All of the lithologic units were interpreted as grading into one another. Noranda estimated that the mineralized zone contained ± 0.5 million tons of ore (John Dunbier, Noranda Exploration, Inc., written commun., 1976).

An effort was made to determine the age of the described units. Despite the lack of any fossil control or unambiguous small-scale sedimentary structure (that is, graded bedding), Noranda correctly believed that the section was inverted (Noranda Exploration, Inc., written commun., 1977). The circumstantial evidence cited was the observed mafic to felsic volcanic cycle (incorrect), volcanic to sedimentary cycle, paleorelief features, and lithological and geochemical zonation within the exhalites similar to Kuroko-type deposits.

Structurally they observed that minor folds were very common, but no tight or isoclinal folds were found except within the carbonaceous argillites. The rare appearance of fault gouge, tectonic breccias, and slickensides did not allow for any major faults to be identified in the drill sections. However, evidence for intense deformation was described between the mineralized zone and footwall argillites, thought to be the result of adjustments induced by flexuring of units due to a major recumbent fold.

Noranda envisioned the Big Sore deposit as occurring in a predominantly sedimentary basin associated with a nearby mafic to felsic volcanic system. The quiescent submarine environment received ash but no intrusive or extrusive rocks from the volcanic system. The volcanic system did, however, give rise to hydrothermal systems and possible explosive exhalations (as evidenced by the conglomerates near the ore interface). Brines from the hydrothermal system settled into depressions and precipitated chemical sediments (sulfides, cherts, and carbonates). Noranda compared Greens Creek to "artesian" exhalative deposits similar to Iron King in Arizona, Faro in the Yukon, and Sullivan and Rosebury in Tasmania (Noranda Exploration, Inc., written commun., 1977). These geologic observations and deductions formed the working geologic framework for exploration work at Greens Creek and Northern Admiralty Island for the next 10 years.

1977 Program

The 1977 exploration program in the Greens Creek area included two projects; the Big Sore drilling program was the primary project, and detailed exploration of Mariposite Ridge, Gallagher, Killer, and Zinc Creeks was the other project. Noranda continued as the operator of both programs. Surface drilling included 22 holes totaling 8,810 feet, primarily along the Big Sore mineralization trend, but also in Gallagher and Killer Creeks. Soil grids were extended or established for all the prospects/areas mentioned herein. The second project was the most ambitious for the area surrounding the Big Sore prospect to date, and remained so until the passage of the Land Exchange Act spurred the exploration programs of 1996 to 1999.

Surface geologic mapping to the south and southwest outlined the carbonaceous argillite unit as wrapping around the tuffite units. The argillite unit was believed to be the upper limb of an overturned fold (John Dunbier, Noranda Exploration, Inc., written commun., 1977). A new soil grid of five lines oriented at N. 60° E.-S. 60° W. was emplaced over the upper limb contact zone. The soil anomalies generated were more erratic than those of the overturned limb, but local silver and zinc anomalous zones along the contact were delineated. A CEM geophysical survey delineated the argillite unit but did not generate any drill targets.

The 1977 drill program at Big Sore was a success in extending the known mineralized zone along strike and down-dip. Eight diamond drill holes were drilled, totaling 4,446 feet, plus 1,415 feet of Hydra-Wink drilling. PS-4-77 (PS-23) intersected a 75-foot section that averaged 12.6 troy ounces per ton silver with a 3-foot high-grade section of 92.2 troy ounces per ton silver. This hole was located 900 feet to the southeast of PS-1. In addition, PS-5-77 (PS-28) intersected 6.5 feet of mineralized material about 300 feet downdip from PS-4-77. The mineralized zone was extended another 800 to 1,000 feet northwest of PS-6-76 by holes PS-6-77 (8.1 feet of 17 percent zinc and 12.25 troy ounces per ton silver) and PS-W1-77 (28 feet of 18.2 percent lead, 32.75 percent zinc,

and 10.2 troy ounces per ton silver). PS–8–77 (PS–27) intersected 20 feet of ore 300 feet downdip from PS–3–76.

The total strike length of mineralized rock along the overturned limb now totaled 3,500 feet and was open on both ends (Noranda Exploration, Inc., written commun., 1977). However, future surface drilling did not extend the mineralized zone farther along strike in either direction. The mineralized interval also extended at least 500 feet downdip on many of the sections tested. The Noranda geologist (Dunbier) realized that the main mineralized zone was at the lithologic contact between the argillites and tuffites. The calculated, geologically indicated resource was 2.1 million tons with an NSR (net smelter return) value of about \$90/ton (John Dunbier, Noranda Exploration, Inc., written commun., 1977).

Dunbier's recommendation for 1978 was to verify the geologically indicated resource with an underground drill program augmented with Hydra-Wink drilling from the surface. Drill hole PS–W1–77 showed that the Winkie drill was capable of piercing the overburden and the mineralized zone. The current 300-foot drill spacing was considered inadequate for ore reserve calculations, and it was recommended that the underground holes be drilled at regular spacings between the surface holes. Additional reserves could be added by downdip testing of the mineralized zone, drilling along strike to the south-south-east, and surface exploration of the upper limb contact (John Dunbier, Noranda Exploration, Inc., written commun., 1977).

Exploration continued within the Gallagher Creek prospect to follow up on the previous CEM and geochemical soil surveys and to test the massive sulfide outcrops and float. The Noranda geologists thought the rocks in Gallagher Creek were part of the upper (upright) limb of the Big Sore fold (Noranda Exploration, Inc., written commun., 1977). One Hydra-Wink hole was drilled on the west side of the creek and intersected weakly mineralized tuffites with one 5-foot zone of 10.2 percent zinc. The contrasting sections intersected by this hole and the two 1976 drill holes led them to believe that a fold or shear (later to be mapped as the Gallagher fault, a significant right-lateral fault) ran along Gallagher Creek.

Killer Creek was also extensively explored in 1977. The 1976 Gallagher–Killer Creek soil grid was extended, and a new grid with a baseline oriented southeast-northwest was surveyed in middle Killer Creek. The new Killer Creek grid generated 16 primary soil anomalies. Noranda identified three types of mineralization associated with the anomalies, which were tested by drilling. PS–77–1 (PS–20) tested below surface exposures of stringers, veins, and clots of coarse sphalerite with pyrite, magnetite, galena, and chalcopyrite within a talc-serpentine-chlorite-carbonate rock. No significant mineralized rock was intersected. A stratiform massive chalcopyrite, pyrite, and pyrrhotite band within greenstone in Upper Killer Creek was tested by two Hydra-Winkie holes, PS–W4 and PS–W5–77 (PS 32 and PS–33). Both holes intersected copper-bearing mineralized rock with grades up to 2.3 percent. Two other holes were attempted in lower Killer Creek to test stratiform sphalerite-galena sulfide bands, but the attempts failed to drill through the thick glacier till overburden.

Noranda recognized the Killer Creek sequence of rocks as distinct lithologies from Big Sore, consisting mostly of andesites, andesitic tuffs, and three types of serpentinites (one described as being a magnesium-rich exhalite) (Noranda Exploration, Inc., written commun., 1977). Noranda envisioned Killer Creek as a tectonic hinge zone, next to a subsiding sedimentary basin (Big Sore and Gallagher prospects), with active faulting, mafic volcanism, and associated exhalative activity. Noranda looked favorably upon the results and estimated that Killer Creek had the potential for 1–3 high-grade (greater than 10 percent zinc) deposits of more than 50,000 tons, at least one deposit of 2–5 percent zinc greater than one million tons, and one to three 1.5 percent copper deposits of greater than 100,000 tons.

Soil surveys, CEM and magnetic geophysical surveys, and geologic mapping were also carried out on the Zinc Creek and Mariposite Ridge prospects. The results from Zinc Creek were not encouraging: only weakly anomalous soil samples (as compared to Big Sore and Killer Creek grids) and no finite geophysical anomalies. On the other hand, the Mariposite grid generated nine soil anomalies associated with vein, disseminated stratiform, and massive stratiform lead-zinc mineralization within, or along the contacts of, the mariposite-carbonate unit. The Noranda geologists believed this unit was a metacarbonate (Noranda Exploration, Inc., written commun., 1977). Noranda suggested that the joint venture attempt to purchase the Mammoth claims not only for its mineral potential, but because its “main value would be as bargaining chips during land negotiations with federal bureaucrats” (Noranda Exploration, Inc., written commun., 1977).

The 1977 exploration program identified many targets and prospective areas outside the immediate Big Sore prospect and recommended continued work, including drilling at Gallagher and Killer Creeks and Mariposite Ridge. However, the urgency of proving-up the Big Sore deposit and events in Washington, D.C., worked against any further work until 1982.

Initial Underground Development and Land Battles, 1978–80

The Pan Sound Joint Venture was dissolved in 1978 and the Greens Creek Joint Venture formed in its place. The Pan Sound Joint Venture was redrafted in part due to the addition of Bristol Bay Native Corporation. The members of the Greens Creek Joint Venture decided in January of 1978 to begin underground diamond drilling and initiate an environmental baseline study after carefully analyzing the political, environmental, geological, and economic aspects of the project (Ernest Simmons, memorandum to W.W. Holmes, 1978). The Greens Creek Joint Venture agreed to a plan to drive a 4,200-foot drift from which to drill about 30,000 feet of core. The environmental baseline study began April 1 and was carried out by VTN Consulting.

The project's first legal battle came on May 2, 1978. The Southeast Alaska Conservation Council (SEACC), with the legal aid of the Sierra Club, appealed the Regional Forest Supervisor's decision to approve the exploration operation plan. They believed that public involvement was not adequately sought in the process. They cited the overwhelming opposition to the planned ferry dock on the north side of Douglas Island and the public's overall negative sentiment toward Noranda (Ernest Simmons, memorandum to W.W. Holmes, 1978). SEACC was also concerned with recent turbidity measurements in Greens Creek that violated USDA Forest Service regulations. Their appeal was denied by the Regional Forest Supervisor on grounds that public involvement is not necessary for an exploration plan and that Noranda was taking the proper steps to mitigate the turbidity exceedances caused by heavy rains.

Driving of 1350 Drift

Noranda contracted the Mining Company of Denver, Colorado, to drive an exploration drift (1350 Drift) at the 1,350-foot elevation mark. Glacial overburden was removed from the portal site by July 13, 1978, and the initial bench round was drilled out on July 14 (Ernest Simmons, memorandum to W.W. Holmes, 1978). By the end of the year, 1,667 feet of drift had been driven, including drill station cutouts at 150-foot spacings. Work continued through the winter and spring months (with a 45-day weather shutdown in February and March) in an effort to complete the 1350 Drift (T.A. Butler, memorandum to S. Nakata, 1979). The drift was finished in November 1979. A total of 4,190 feet of drifting with a 219-foot rise was completed along with 24 diamond drill stations, assorted sumps, and an underground shop. All work was completed using helicopter support and a camp located just below the portal. The total cost for the 1978–79 drifting and drill program was \$5.05 million (Noranda Exploration, Inc., written commun., 1980).

The initial underground drilling program began in October 1978 and finished in December 1979. Drilling took place on an intermittent basis as new drill stations were cut, and water and power became available from the drifting program. Fifty holes (GC-1 to GC-50) were drilled during this period, totaling 20,240 feet (Noranda Exploration, Inc., written commun., 1980). Most of the drill stations (14 out of 24) were drilled out to help confirm the 2,750 feet of strike length of mineralized rock. The fifty drill holes encountered 59 ore intercepts. Noranda estimated the drill indicated reserves to be about 3 million tons with an approximate grade of 10–16 troy ounces per ton silver, 0.1 troy ounce per ton gold, 7–10 percent zinc, 2–2.5 percent lead, and 0.5 percent copper. The ore zone was still believed to be open downdip and along strike to the southeast (Noranda Exploration, Inc., written commun., 1980).

Noranda performed a base cash-flow model for Greens Creek to estimate the economics of the project. The order of magnitude estimates indicated that the project had a DCF–ROR

(discounted cash flow – rate of return) of 39.3 percent, NPV (net profit value) of \$22.6 million, with payback in 1.8 years (Noranda Exploration, Inc., written commun., 1980). Assumptions and criteria used for the estimate included metal prices at \$300 per troy ounce gold and \$10 per troy ounce silver, a production rate of 800 tons per day (TPD), \$18.4 million in preproduction costs, \$65 per ton operating costs, and 15.75-year mine life. However, Noranda concluded that “Political imponderables far exceed the technical unknowns insofar as the Greens Creek project is concerned” (Noranda Exploration, Inc., written commun., 1980).

The land status of the Greens Creek property changed greatly during the underground drifting and drilling program. Nineteen Big Sore claims were surveyed for patent in July and submitted to the Cadastral Survey Office in April 1979 (T.A. Butler, memorandum to S. Nakata, 1979). The Greens Creek Joint Venture employed the law firm of Pruitt and Gushee of Salt Lake City to aid in the intricate patenting process. An additional 27 lode claims were staked during 1978: 23 to the south of the Big Sore group to cover the downdip projection of the current orebody, three on the southwest to cover an area dubbed the “football field” that was a potential tailings site, and one to cover an open area that developed as a result of the patent survey. A total of 136 mill-site claims were staked to the south and east of the Hawk Inlet Cannery site between November 27 and December 1. The latter date, December 1, proved to be a very fateful day that would change the whole scope of the project and have repercussions throughout the entire State of Alaska.

Federal Proclamations

Federal land-management policy in Alaska was one of the hotly debated topics during the 95th Session of the United States Congress. The Alaska Native Claims Settlement Act (ANCSA) of 1971 provided an 8-year time limit for Federal action on protecting or otherwise designating use of “special national interest lands” that up to 1978 were termed “d-2” lands. The largest conservation lobby ever assembled along with politicians like Congressman Morris Udall and Secretary of the Interior Cecil Andrus were concerned with the fast-approaching 8-year deadline of December 18, 1978 (Nash, 1982). They were worried that if no protective action were taken, there would be a huge “land grab” by mining companies and other developers within pristine parts of Alaska. They felt once the deadline was passed, State, Native, and private parties would be able to stake claims on Federal land, which constituted 99 percent of Alaska. If this happened, they reasoned it would be hopelessly complicated to establish any new national parks or wilderness areas. Bill HR-39, which would have protected 92 million acres of Federal land in Alaska, passed through the House of Representatives by a wide margin. However, Alaska Senator Mike Gravel's threatened filibuster of any bill that withdrew or placed restrictions on Federal land in Alaska stalled the bill in the Senate (Nash, 1982).

The Carter administration took action once it was evident that Congress was not going to pass any Alaska land bill by the end of the congressional session. Interior Secretary Andrus withdrew 110 million acres of Federal lands in Alaska from all forms of development for 3 years on November 16. He used the 1976 Federal Land Policy and Management Act to authorize this action. This act was controversial, and many thought it to be unfair since it was made before the close of the comment period (November 20) on the draft Environmental Supplement (T.E. Butler, written commun., 1978). The Environmental Supplement was to document, in part, the impact on Alaska citizens of the closing to development of land in Alaska. The lands withdrawn included most of Admiralty Island, including Greens Creek.

The big move came on December 1, 1978, when President Jimmy Carter declared 56 million acres of Federal land, including most of Admiralty Island, as national monuments under the authority of the 1906 Antiquities Act, which was designed to protect places of historical interest. Never before had the act been used on such a colossal scale (Nash, 1982). This move was applauded by the numerous conservation and environmental organizations and by the American public in general. Most Alaskans reacted with shock and outrage. The national monument status still had to be approved by Congress, giving the Greens Creek Joint Venture time to formulate a strategy to lobby Congress.

Immediately the land position of the Greens Creek Joint Venture was in jeopardy. The Greens Creek Joint Venture felt that their prior existing rights to the claims would be honored (T.E. Butler, memorandum to S. Nakata, 1979). However, there was a question as to whether a mine could be established within a designated monument, since there was no legal precedent. The 1979 Minerals Availability System Deposit Summary Report by the Bureau of Mines listed the land environmental factor as "prohibitive" until the status is legislatively determined in court (T.E. Butler, memorandum to S. Nakata, 1979). Claims could no longer be staked, nor could any surface construction activities not already approved under the 1978 Exploration Work Plan take place until the USDA Forest Service validated those claims. Considerable energy and resources were expended during the next 2 years to gain legislative relief from the Carter administration decision.

The next 2 years saw extensive lobbying by both sides. Noranda and the Joint Venture partners were actively lobbying Congress for a less restrictive designation for the Greens Creek drainage. One such group that the JV helped fund was the Citizens for Management of Alaska Lands (T.E. Butler, memorandum to S. Nakata, 1979). On the other side of the fence was the Alaska Coalition made up of the Nation's five leading conservation groups (Sierra Club, Wilderness Society, the National Audubon Society, Friends of the Earth, and the National Parks and Conservation Association), the largest and most powerful conservation group ever assembled in American history (Nash, 1982). The House passed Bill HR-39 in May of 1980, which would have recognized the Greens Creek deposit but would have surrounded it with land designated

as wilderness. The Senate passed a much less restrictive bill (S-9) sponsored by Alaska Senator Ted Stevens that excluded Greens Creek from the national monument. House leaders initially did not wish to compromise on their bill, but on November 4 Ronald Reagan was elected president and they realized they had only a small window of opportunity left to pass a bill that would not be vetoed (Nash, 1982). The compromised bill was named the Alaska National Interest Land Conservation Act (ANILCA).

President Carter signed ANILCA into law on December 2, 1980. The act set aside 104 million acres of Federal land in Alaska for permanent protection. The Greens Creek deposit was included in the newly created Admiralty Island National Monument but was excluded from wilderness classification. It was decided legislatively that the Greens Creek project should proceed. Section 504 of ANILCA allowed for exploration on previously located, unpatented claims that fell within three-quarters of a mile of a valid mineral discovery. However, exploration would have to cease in 5 years and any claims not "perfected" would revert to national monument status. Thus the Joint Venture had until December 2, 1985, to perfect any of the 127 claims that fell within the 0.75-mile radius.

1980 Exploration Program

Exploration work was limited while the above political and legislative battles took place. Restrictions were placed on surface activities, and the previously approved plan of operation was only valid until May 31, 1980. Resources were directed toward finishing the environmental impact statement (EIS), which was taken over by International Environmental Consultants. Thirty-three drill holes (GC-51 to GC-83) were completed by the end of March (Noranda Mining, Inc., written commun., 1981). Another 35 feet of drifting intersected the footwall argillite at the south end of the 1350 exploration drift. An important milestone in 1980 was the USDA Forest Service Mineral Examiner's report that recognized valid discoveries on seven Big Sore claims (Noranda Exploration, Inc., and Noranda Mining, Inc., written commun., 1981). These seven claims formed the core claims with surface and subsurface rights.

Race to "Perfect" Claims and Predevelopment, 1981–85

1981 Exploration Program

With the political situation clarified by the passage of ANILCA, the Greens Creek Joint Venture members approved the appointment of Noranda Mining, Inc., as the operator, replacing Noranda Exploration. This change emphasized the point that Greens Creek was passing from the exploration

stage to development. Much of the activity in 1981 reflected this change in status. The primary emphasis was on environmental and engineering studies of various components of the project. The various projects completed included road alignment surveys from Young Bay to the Hawk Inlet Cannery, drilling and geophysical investigations of the tailings site near the cannery, and boat transportation study. The draft EIS was completed by December (Noranda Exploration, Inc., and Noranda Mining, Inc., written commun., 1981).

No surface exploration work was documented for the 1981 summer season. Despite the fact that the clock was already ticking on the 5-year exploration limit, Noranda chose to work on development issues. The USDA Forest Service approved the exploration permit in April; thus, the permit was not the limiting factor for exploration. Noranda lost one valuable season for perfecting claims as they pursued other studies of the project.

Underground development continued in 1981. A 424-foot crosscut was driven from the 1350 adit to expose the ore zone. The drifting continued along the ore to the north and south for a distance of 176 feet (Noranda Mining, Inc., written commun., 1981). This provided material for a 4,200-pound bulk sample for metallurgical bench flotation tests in Salt Lake City. The first exposure of the ore zone in three dimensions provided a "quantum leap" in the knowledge of the deposit (Noranda Mining, Inc., written commun., 1981). The exposure helped to confirm that three types of ore (Massive, White, and Black) were present and relatively lithologically discrete from each other. Vein mineralization, especially with regard to precious metal upgrading, was found to be more prevalent than thought from data obtained from the diamond drill core. Coarse visible gold was intersected in several areas. Overall, the Noranda geologists believed that the original reserve and grade estimates were too conservative based on the precious metals intersected and the inability of the LHDs (load, haul, dump equipment) to carry a full bucket of ore (Noranda Exploration, Inc., and Noranda Mining, Inc., written commun., 1981). A tonnage factor of 9 cubic feet per ton was more realistic than the original estimate of 11 cubic feet per ton. The crosscut also exposed ubiquitous intermediate scale folds (25–75-foot wavelengths) oriented normal to the interpolated large-scale folds that would have great implications for mining methods and grade, tonnage, and dilution estimates.

More legal difficulties arose in 1981. The Southeast Alaska Conservation Council (SEACC) and the Sierra Club challenged the USDA Forest Service's granting of the exploration permit for a second time. They appealed the granting of the exploration permit to the Chief Forester on the basis that the original claims were not valid as of December 1, 1978 (Noranda Exploration, Inc., and Noranda Mining, Inc., written commun., 1981). They argued that the Greens Creek deposit did not pass the marketability test, and no reclamation costs were included in the study. The Regional and Chief Foresters sustained the previous decisions, stating that the mineral inspector used the correct criteria for determining that the seven core claims contained valid mineral discoveries.

1982 Drill Program

Noranda shifted emphasis back to surface exploration and drilling in 1982. The goal was to validate unperfected claims and add to the total mineral inventory. Noranda Exploration, Inc., led by Joe Drechsler, was contracted by Noranda Mining, Inc., to manage the program (J.S. Drechsler, Jr., and others, Noranda Mining, Inc., written commun., 1982). Noranda drilled 12 holes totaling 11,210 feet during the summer field season. Nine of those holes were in the Big Sore area, two in Gallagher Creek, and one in Bruin Creek, on the north side of Greens Creek.

The Big Sore drilling program successfully intersected discoveries on unperfected claims. Three holes were drilled to test the northwest strike extension of the orebody on claims 1107 and 1108. All three intersected only minor mineralization, and the lack of chert buildup (siliceous alteration) along the argillite/phyllite contact suggested that the ore pinches out to the north (J.S. Drechsler, Jr., and others, Noranda Mining, Inc., written commun., 1982). On the south side of the orebody, only argillite was contacted in hole GC-82-9 (PS-50) targeting claim block 901. Holes GC-82-2 (PS-43) and GC-82-7 (PS-48) tested the downdip extent of the argillite/phyllite contact. Both holes intersected thin (4-foot) ore intercepts with high-grade silver up to 26.7 troy ounces per ton. The ore intercepts in these two holes were at a higher level (about 500 feet) than expected from projections from previous holes, indicating flattening of the ore horizon due to folding or faulting. Holes GC-82-8 and GC-82-10 (PS-49 and PS-51) were drilled from claim 1106. GC-82-8 intersected 12 feet of 26.7 troy ounces per ton silver and 11.93 percent zinc. The other hole intersected a barren contact. The final hole of the season, GC-82-12 drilled from claim 1107, intersected a 6-foot interval of argillite running 6.22 troy ounces per ton silver, 3.75 percent lead, and 4.10 percent zinc. Noranda did not make clear in the yearly report which of these intersections would qualify for discovery and claim validation.

The two holes in Gallagher Creek attempted to better outline the mineralization present there from intercepts from the 1976–77 drilling program and test for Greens Creek-type stratigraphy. Drill hole GC-82-5 (PS-46) was successful in intersecting 15 feet of high-grade zinc mineralization (10.22 percent). The hole was located on claim 1304 at the western edge of the 0.75-mile limit. The other hole, GC-82-11 (PS-52) located farther south, intersected minor zinc enrichment. The Bruin Creek hole GC-82-6 (PS-47) was drilled on claim 1213 and intersected several 3–5 foot sections of chert-carbonate rock containing up to 1 percent zinc. However, Noranda did not view the results as being favorable for discovering any significant sulfide occurrences in the area (J.S. Drechsler, Jr., and others, Noranda Mining, Inc., written commun., 1982).

Noranda still saw Greens Creek as being open along strike to the northwest and downdip, with the potential of another 2–5 million tons of ore (J.S. Drechsler, Jr., and others, Noranda Mining, Inc., written commun., 1982). Noranda felt

that five of the holes drilled on unperfected claims intersected mineralization of sufficient quality and quantity to be considered "discoveries." However, section 504(e)(1) of ANILCA left some doubt as to what constituted a valid discovery; whether the standards applied would be those of the USDA Forest Service Mineral Examiners or the stricter Bureau of Land Management (BLM) requirements for issuance of a patent (which appeared to be how the section was worded) was unclear. An unofficial draft of the Mineral Examiner's report stated that claims 1304 and 1305 in Gallagher Creek contained valid mineral discoveries, but claim 1605 in Killer Creek did not. Noranda maintained that drillcore of 2.3 percent copper is a valid discovery, but their legal counsel suggested that this interpretation would not hold up in court (J.S. Drechsler, Jr., and others, Noranda Mining, Inc., written commun., 1982).

Noranda and the JV partners reviewed other options and strategies to protect the exploration potential of Greens Creek. The alternatives to the current aggressive discovery-oriented drill program included a minor boundary change putting Greens Creek outside the national monument, a land swap, or extension of the 5-year period to prove the claims (J.S. Drechsler, Jr., and others, Noranda Mining, Inc., written commun., 1982). The first choice was to lobby the USDA Forest Service for a minor boundary adjustment, a power the USDA Forest Service had under one of the provisions of ANILCA. The other two choices were less attractive because a land swap would be costly and an extension would only delay resolution of the problem.

The cost of the drill program was becoming a concern for Noranda. More definition drilling was necessary to bring the "new" 1982 geologically inferred reserves into indicated reserves (J.S. Drechsler, Jr., and others, Noranda Mining, Inc., written commun., 1982). Even at 400-foot spacings, it would require about 11,000 feet of surface drilling to validate indicated reserve status, leaving very little funds for perfecting claims. Drilling on 150-foot centers, which was preferred, would be extremely expensive. Underground drilling would be less expensive, but the platforms did not exist and would be best established simultaneously with mine development and mining, still years away. Underground and surface drilling both would require helicopter support, adding to the cost. Drilling would be much less expensive after road construction, but road construction might not be possible until after the expiration of the permit period due to political and budget constraints. Noranda was faced with either continuing drilling at a higher expense or pursuing the above-land options and risk losing potential mineral assets.

Noranda Exploration geologist Daryl Scherkenbach completed a geologic mapping project at a scale of 1 inch=500 feet for the Greens Creek area. This work was the basis for his geologic model of the Greens Creek deposit. He suggests that the Big Sore orebody formed within a second- or third-order extensional basin (D.A. Scherkenbach, written commun., 1983). In his model, tectonic extension was accompanied by mafic and ultramafic volcanics and shallow intrusives. The serpentinization of these rocks is a strong indicator of hydrothermal activity that caused the metal transportation.

The effusive vents for the hydrothermal fluids manifested themselves as slump breccias, as mapped within the footwall tuffites. These vents formed fault scarp basins, in which the metalliferous brines could settle and deposit metals. The massive ores accumulated near the vents while black ores accumulated distally, hundreds of meters from the vent. The white ores represented remobilized sulfides as the solutions migrated around sulfide-clogged vent areas. Scherkenbach thought the difference between the sericitic and chloritic tuffites/sediments was due to different source areas or modes of deposition. The highly negative δS isotope values for the argillite and black ore indicate biogenic reduction of seawater sulfate. The less negative values for the remaining ore types and tuffites suggest a mixing with magmatic sulfur.

1983 Feasibility Study

Noranda completed a feasibility study in 1983 that outlined the economic viability of the project. The study was based on probable and possible reserves (including dilution due to mining method) of 2.84 million tons at 0.093 troy ounce per ton gold, 14.42 troy ounces per ton silver, 2.93 percent lead, and 8.56 percent zinc located above the 950-foot level. An additional geologic reserve of 1.45 million tons was estimated to be below that level (Noranda Mining, Inc., written commun., 1983). Noranda envisioned using conventional cut and fill mining methods utilizing jacklegs within "captured" stopes. Five to six separate levels/portals on 200-foot spacings would be connected by a winze and raises. Rail haulage would take place on all levels. Noranda preferred this method to mechanized cut and fill to reduce the amount of ramp development and allow for more selective mining where the ore is too narrow for rubber tire equipment. Mining rates were estimated at 1,200 tons per day (TPD) with dilution at 17 percent and mining recovery at 90 percent. Carbon, lead, and zinc concentrates would be produced over the estimated 20-year mine life (including development time). The mine would have a workforce of 344 people. The economic/cash-flow model given these parameters required a 1987 silver price of \$22.95 for a 15 percent DCF-ROR. The estimated capital investment was \$254.3 million with an operating cost of \$151.85 per ton (Noranda Mining, Inc., written commun., 1983). This was a huge contrast from the 1980 estimate of 39.3 percent DCF-ROR and \$65 per ton operating costs.

1983 Exploration Program

The objectives of the 1983 program were much the same as before, to validate peripheral claims and continue detailed definition drilling of the southern end of the orebody. The management of the program fell back to Noranda Mining, Inc., with Edwin Harrison supervising. The decision to proceed with the drill program did not come until July 7, and the four crews required for the work were not completely mobilized until August 1 (E.D. Harrison, Noranda Mining, Inc., written commun., 1983).

A total of 17 holes were drilled during the season. Most of the holes (15) were drilled from the southern core claims (902, 903, and 904). The aim was to upgrade the southernmost part of the resource to measured reserves status. Noranda viewed the south end as being critical to the initial mine design and development, and they needed a better understanding of the fold closure (E.D. Harrison, Noranda Mining, Inc., written commun., 1983). Three holes drilled updip from the 1982 ore crosscut intersected white, massive, and black ore of economic length and grade. One hole drilled at the southernmost known limits of the orebody intersected 12 feet of high-grade precious metals (0.644 troy ounce per ton gold and 55 troy ounces per ton silver). This hole also tested the upper limb argillite but intersected no mineralization. The remaining nine holes were in-fill drillholes of which five intersected significant ore intervals. The in-fill holes helped "prove" the continuity of ore in the south end of the designed mine plan and helped define the major fold closure controlling the ore to the south (E.D. Harrison, Noranda Mining, Inc., written commun., 1983).

Many high-grade intercepts were assayed during the drill program. A 2-foot interval from PS-62 assayed greater than 11 troy ounces per ton gold, which was confirmed by numerous re-assays. Noranda considered the question of cutting high gold/silver assays for reserve calculations. They felt this idea should be studied closely and put into practice (E.D. Harrison, Noranda Mining, Inc., written commun., 1983).

Little effort was made in proving unperfected claims in 1983. Only two holes were drilled and an older hole was reentered and wedged in a different direction. PS-70 was drilled on claim 1107. Perfecting this claim was a high priority because the 1350 portal, mine camp, and waste dump were all located there. The hole intersected a short (1-foot) but high-grade (109 troy ounces per ton silver) mineralized zone deemed sufficient to prove the claim. The attempt to prove claim 1003 was an expensive ordeal (E.D. Harrison, Noranda Mining, Inc., written commun., 1983). The target was a recumbent drag fold intersected just outside of the claim by PS-48 (1982). An attempt was made to reenter that hole and place a directional wedge to deflect the hole onto claim 1003. The wedge failed to deflect the hole. A new hole, PS-54, was collared at the same site. Despite orienting the hole to compensate for the expected deviation, downhole surveys showed the hole was going to miss the projected contact to the northeast. Poor weather forced the postponement of the drill program before another mechanical wedge could be used to correct the hole. Thus, a valid discovery was made on only one unperfected claim in 1983, with only 2 years remaining on the exploration permit.

The first change within the Greens Creek Joint Venture partners occurred in 1983. Anaconda purchased all of Martin-Marietta's interest in the Greens Creek Joint Venture in March of 1983 after first approaching them in December of 1982 (Anaconda Minerals Company, written commun., 1984). Anaconda already had exploration experience in southeast Alaska, including the Pyrola claims to the south of Greens Creek. Anaconda's Project Evaluation Report

in January of 1984 justified their purchase on the basis of Noranda's prefeasibility study. They believed that Noranda's approach was too conservative and estimated the minable reserve greater by 0.5 million tons with higher silver (16 rather than 14.4 troy ounces per ton) and gold (0.11 rather than 0.093 troy ounce per ton) grades. In addition, they thought that utilizing the mechanized cut and fill mining method would reduce capital costs for full production by 20 percent from Noranda's conventional cut and fill proposal.

Anaconda saw many potential problems with the project. They were concerned with the marketability of the concentrates produced due to the high level of contaminants (cadmium, arsenic, antimony, and mercury). Other concerns were the limited size and accessibility of Juneau, making it difficult to obtain and keep experienced personnel. They felt the lower levels of the deposit lacked the necessary drilling for production to be justified. Anaconda foresaw future delays in the project due to political and environmental factors. However, they did not see the pending exploration deadline and land issues as having an adverse effect on the base case economics. Anaconda's preferred solution to the land situation was a land exchange with the Federal Government (Anaconda Minerals Company, written commun., 1984).

1984 Exploration Program

The 1984 drill program budget was \$3.3 million, a five-fold increase from the \$0.655 million budget of the previous year (E.D. Harrison and others, Noranda Mining, Inc., written commun., 1984). The increased budget, and the primary objective of the 1984 drill program to extend the proven claim block to the north and south, underscored the increasing pressure of the exploration deadline. The northern claims were tested to the 0.75-mile limit by surface holes while the southern claims could only be tested practically by underground drilling. Surface holes would be too long as a result of the increase in topography and southeast-plunging ore zone. An 847-foot-long drift (1984 crosscut) was driven to the edge of the unperfected claims, with drill-cuts along the way for detailed ore reserve drilling.

The secondary objective of the 1984 program was to increase the downdip potential of the previously defined ore zones. The deposit was now divided into three ore zones, the North, South, and Central zones. The drilling took place from the 1350 drift and the new 1984 crosscut. Much rehabilitation work had to be completed on the 1350 drift due to numerous ground falls since 1981 before drilling took place.

The farthest north and northwest drilling in Gallagher Creek (PS-83), Killer Creek (PS-82, PS-86), and Bruin Creek (PS-76 to PS-81 and PS-84) failed to intersect mineralization sufficient to perfect claims. Likewise, hole PS-75 located near the camp on claim 1108 did not intersect mineralization along the argillite/phyllite contact. Drillholes closer to the core claims were more successful. PS-72 and PS-73 extended the now-named North Ore zone downdip another 250 and 350 feet, respectively, although the intersections occurred on

already perfected claims. PS-74 intersected the North Ore zone at the 400-foot level with a 7-foot interval of 17 troy ounces per ton silver and 5 percent zinc. This was the deepest ore intersection to date and perfected claim 1105. Another hole, PS-85, tested claim 1106 and intersected the North Ore zone and 9.4 feet of "black" ore mineralization. This hole perfected claim 1106.

Most of the barren surface holes intersected chloritic sediments or mudstones instead of cherty sericitic tuffites above the argillite contact. Noranda believed that the chloritic rocks were not very conducive to Greens Creek-type ore mineralization, though they did not state any geologic reasoning for their conclusion (E.D. Harrison and others, Noranda Mining, Inc., written commun., 1984).

No claims were perfected on the south end of the ore trend. Three holes were attempted from the southern end of the 1984 crosscut, and all three terminated within 220 feet of the collar due to poor drilling conditions caused by a major northwest-trending fault (later defined as the Maki fault). Another attempt was made to perfect claim 901 to the south by drilling from a station farther back in the crosscut. However that hole, GC-91, intersected a barren contact within that claim. The in-fill drilling was very successful in increasing the reserves. Two stations were drilled from the new 1984 crosscut to test the downdip potential of the South Ore zone while one station was drilled from the 1350 exploration drift to test the downdip potential of the Central Ore zone. Hole GC-86 intersected numerous fold-repeated ore intervals, the lowest of which was located within the southeast corner of unperfected claim 1003. Noranda thought that the 5.9 feet of 16 troy ounces per ton silver would be sufficient to perfect this claim (E.D. Harrison and others, Noranda Mining, Inc., written commun., 1984). Two holes drilled in the South Ore zone, GC-88 and GC-94, intersected ore of higher precious metal grade, coarser grain size, and silica-baritic groundmass that had not been identified previously. Noranda thought that they might be approaching the primary vent to the south and that the grades might continue to increase downdip and to the south (E.D. Harrison and others, Noranda Mining, Inc., written commun., 1984).

The underground drilling program was successful in delineating more reserves below the 950-foot level and provided more insight to fold and fault structures, especially in the southern part of the deposit. Noranda did not add these new reserves to the "probable" category because they were not drilled on 150-foot centers (E.D. Harrison and others, Noranda Mining, Inc., written commun., 1984). However, they believed that the number of good ore intercepts supported the assignment of these areas into the geologic resource category. Thus, they classified the preliminary estimate of 670,000 tons to the "possible" category, with the majority of the tons in the North and South Ore zones. The increase in possible reserves, especially for the North Ore zone, was expected to have a large effect on the mine plan.

Other work included mining of ore underground for two bulk samples, one to be tested by Noranda and the other

by Anaconda. Noranda geologist Floyd Branson initiated a trenching program in an attempt to expose the productive contact and patent claims 1007 and 1107. "Discovering" mineralization on the surface would allow the Greens Creek Joint Venture to exert extralateral rights under the Apex Rule (E.D. Harrison and others, Noranda Mining, Inc., written commun., 1984). The work was very difficult and expensive due to the difficulty in locating the contact under the thick glacier overburden.

Tom Crafford of Anaconda began his active role in the project by completing an extensive geologic mapping project to the north and east of the Greens Creek core claims. Crafford's surface mapping included defining two northwest-trending faults, one on Mariposite Ridge just west of the Mammoth claims, and the other at the head of Big Sore Creek. He believed that these faults were the same structure (T.C. Crafford, written commun., 1984). Sampling of mineralization on the Mammoth claims showed ore-grade material within mariposite-carbonate rocks, which Crafford thought might represent a link between that alteration style and the mineralizing event. Several rock samples were taken for conodont analysis for age determinations, as there was a debate whether the age of the Greens Creek orebody was Paleozoic or Triassic. However, these samples were barren. He also mapped to the northeast of the mine to determine whether or not the overturned limb of the Big Sore anticline reappeared on the surface, but he found no evidence of a fold repeat.

Some of Crafford's ideas expressed in his report were contrary to Noranda's view of the geology. He did not agree with the tuffite designation for the footwall rocks. He viewed these rocks as hydrothermally altered mafic rocks that were proximal to vents (T.C. Crafford, written commun., 1984). He was also doubtful of the large-scale anticline hypothesis.

The end of the year saw a change in the ownership of the Greens Creek Joint Venture. Anaconda and Noranda equally bought out Bristol Bay Native Corporation's properties at Hawk Inlet for a cash payment and a 0.28-percent net smelter royalty. The land would revert back to Bristol Bay upon termination of the Greens Creek Joint Venture.

1985 Surface Exploration Program

The objectives remained much the same as previous years for the 1985 drill program, the final year of the exploration permit granted under ANILCA. The surface drilling of 10 holes totaling 12,266 feet was designed to perfect as many claims as possible. The underground drill program involved definition drilling on 150-foot centers to place 1984's "possible" tons into the probable reserve category. This was the largest underground drill program to date, totaling 47 holes and 34,749 feet of drilling.

PS-87 was the only surface hole successful in perfecting a claim. The hole was drilled vertically from the northwest corner of claim 1206 to test the area between Gallagher Creek to the west and the North Ore zone to the east. The hole intersected 11.3 feet of "black ore" averaging 0.114 troy

ounce per ton gold, 16.88 troy ounces per ton silver, and 4.9 percent zinc (E.D. Harrison and M. Severson, Noranda Mining, Inc., written commun., 1985). The intercept was 40 feet inside claim 1207 due to hole deviation. A wedged hole off of PS-87 also intersected 5.6 feet of ore-grade material, but it too missed claim 1206. Ed Harrison recognized this intersection as a separate orebody that to this day is still isolated from the nearest defined orebody by about 1,000 feet. PS-88 through PS-92 were drilled from already perfected claims 1106 and 1107 to define the eastern edge (or upper shelf) of the North Ore zone. PS-92 was the first and only hole drilled on the east side of Big Sore Creek, above the High Sore, another ferricrete kill zone (fig. 1). Highly fractured and deformed argillite was the only lithology encountered in PS-92. The remaining four holes were drilled on claims 1207, 1208, and 1209 to follow up the ore intercept in PS-87. None of these holes intersected significant mineralization.

The underground drill program was successful in delineating more reserves in all three ore zones. Noranda nearly doubled the probable reserves, adding another 1.33 million tons to the already identified 1.333 million tons (fig. 3). The total tonnage of 2.663 million at 0.13 troy ounce per ton gold, 22.24 troy ounces per ton silver, 3.49 percent lead, and 9.00 percent zinc exceeded their original goal of 2.1 million tons (Noranda Mining, Inc., written commun., 1985). Noranda was very optimistic due to the fact that the grades were increasing with depth and all three ore zones were still open at depth. Hole GC-139, drilled from the southern end of the 1984 crosscut, succeeded in perfecting claim 1002 with numerous 8- to 13-foot ore-grade intercepts. Four holes were attempted from the same station to perfect claims 901 and 1001 to the south. They were all abandoned or lost, however, due to poor drilling conditions in the fault zone where three drill holes were lost in 1984.

The Greens Creek Joint Venture's land position was augmented in 1985 with the signing of an exploration/development agreement with the owners of the Mammoth claims. The agreement was a 10-year lease with a drill commitment and royalty payment due to the owners on any production (E.D. Harrison and M. Severson, Noranda Mining, Inc., written commun., 1985). The old "Mammoth Tunnel #2" was cleared and mapped. Other old pits and trenches were sampled. A grab sample of a tetrahedrite-bearing outcrop just above the portal assayed at 0.778 troy ounce per ton gold, and 17.91 troy ounces per ton silver. An additional 85 claims were staked to the north of the Mammoth claims, just outside the monument boundary, to cover ground not claimed by the Lil Sore claim group controlled by the Norbritex Venture. The crew spent more than 3 weeks staking claims, enduring snow depths up to 12 feet (E.D. Harrison and M. Severson, Noranda Mining, Inc., written commun., 1985).

The south face of the 1981 ore crosscut was advanced to test the ability of the miners and grade-control geologists to stay on the ore and to test the lateral variability of the ore types. This experience left Noranda feeling that it would be a face-to-face requirement of the production geologist to follow the

highly deformed ore (E.D. Harrison and M. Severson, Noranda Mining, Inc., written commun., 1985). A United Nuclear's silver probe was successfully tested as a grade control tool in estimating silver content of drill-core and face chip samples.

Land Strategies and Negotiations, 1983-85

While the exploration projects tried to perfect as many claims as possible before the December 2, 1985, deadline, efforts were underway to find a legal solution or compromise to the dilemma. Just prior to the deadline, the Greens Creek Joint Venture filed proof of discovery of nine additional claims (1002, 1003, 1004, 1005, 1105, 1106, 1107, 1207, and 1304) to add to the original eight core claims (E.D. Harrison and M. Severson, Noranda Mining, Inc., written commun., 1985). The Greens Creek Joint Venture was concerned that the accelerated exploration was too costly and risky, and other avenues needed to be explored to remedy the land situation. The three separate avenues that were explored are discussed in the following paragraphs.

The first option was a boundary change regarding the Admiralty Island National Monument (AINM) and wilderness areas. ANILCA (section 103b) allowed for the Forest Service to make minor boundary adjustments to the various land selections. This idea was being pursued as early as 1983. The Greens Creek Joint Venture was hoping to exchange 18,174 acres of private land in the Young Bay/Young Lakes area for 17,225 acres within the Greens Creek area. However, the Sierra Club was against the boundary change even if it meant no net loss to the AINM because it would set a precedent for boundaries based on economics. Attorneys for Noranda thought any changes in boundaries were unlikely because the USDA Forest Service would be named as the defendant in any litigation, threatening their power to grant minor boundary changes (J.P. Tangen, esq., memorandum to P. Richardson, 1983). In addition, Noranda would not be involved directly in the litigation, thus losing control of the nature and timing of any solution.

The second option that was pursued was legislative relief through extension of the exploration permit (J.P. Tangen, esq., memorandum to P. Richardson, 1983). Representative Don Young, Alaska's sole representative, introduced bill H.R. 2651 on June 3, 1985, to amend section 504 of ANILCA. The amendment would allow the Greens Creek Joint Venture to renew the 5-year exploration permit up to six times so exploration could continue until December 2, 2020. Senator Murkowski of Alaska introduced an identical bill as S. 1330. These bills would only provide for exploration within the 0.75-mile limit. However, neither bill made it out of committee.

The third option was a proposed land exchange involving Sealaska, the southeast Alaska Native corporation. The first iteration of the land-exchange proposal called for Sealaska to exchange subsurface mineral rights in the Cube Cove area for subsurface rights in the Greens Creek area. This land was

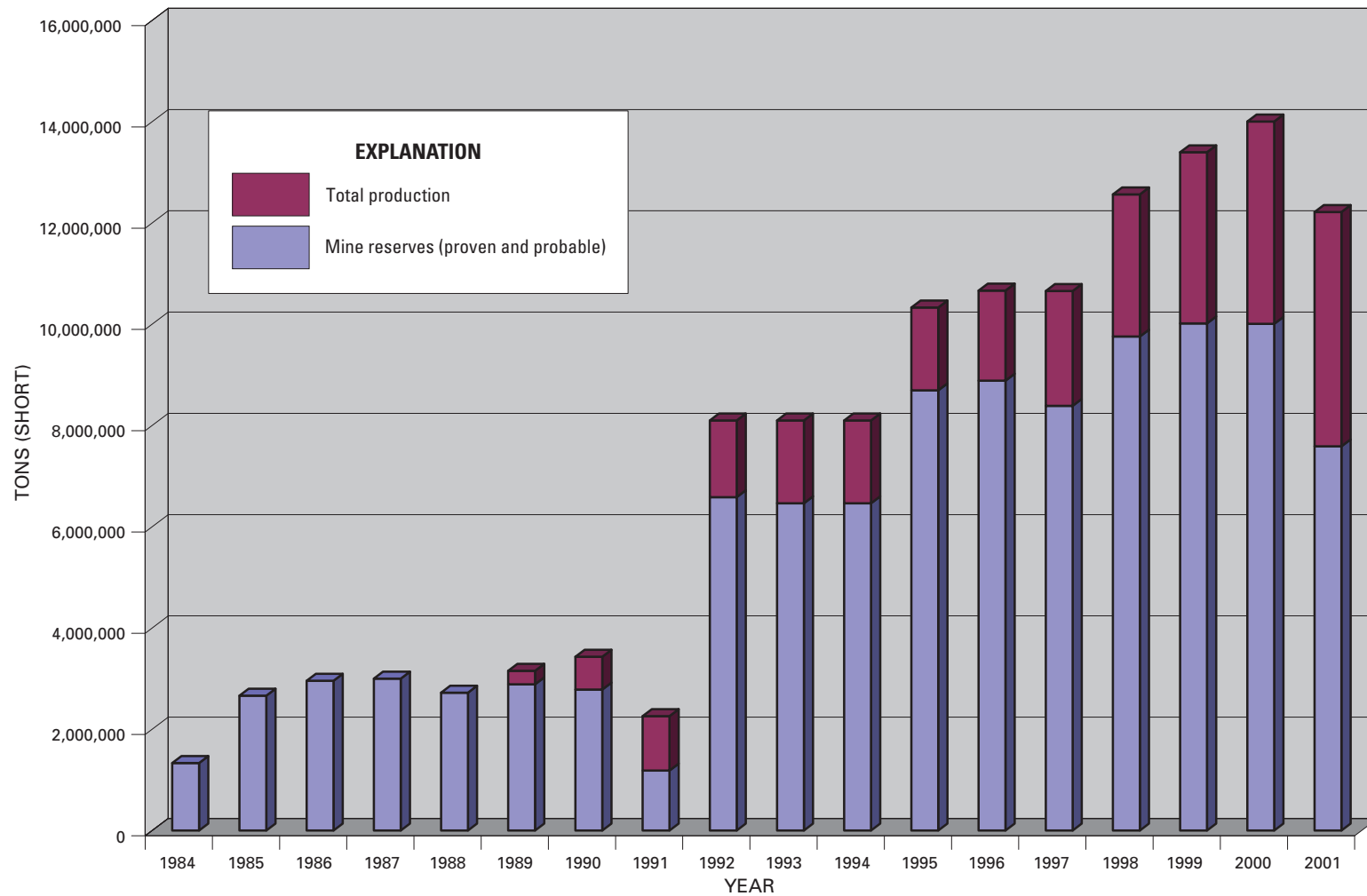


Figure 3. Chart showing proven and probable reserves compared to total (cumulative) production (Kennecott Greens Creek Mining Company, written commun., 2001).

selected by Sealaska under ANCSA. The tentative agreement reached in November of 1985 called for Sealaska to lease these rights to the Greens Creek Joint Venture in return for a yearly lease fee to be negotiated and a 3.5-percent net smelter return royalty on any ore mined outside the existing core and perfected claims and extralateral rights from those claims. The lease would have a life of 25 years with mandatory work commitments made by the Greens Creek Joint Venture for each year. Sealaska saw themselves as a “passive” landowner (Birch, Horton, Bittner, Pestinger, and Anderson, written commun., 1985). This agreement hinged on at least a one-year extension of the exploration permit deadline to allow Sealaska adequate time to complete the land exchange.

The exchange with Sealaska Corporation was seen as the best option. The attorneys employed by Sealaska believed that the various environmental groups would support only this option. Litigation was unlikely since Sealaska, a Native corporation, was involved. Sealaska and the Sierra Club were trying to link the Greens Creek land exchange with another land-management dispute on Admiralty Island. The Shee Atika Native corporation was planning to harvest trees on the land at Cube Cove for which Sealaska owned the mineral rights. This clearcutting plan had the Sierra Club up in arms. Sealaska thought that the Sierra Club and the Forest Service would support a plan that halted the imminent harvesting (Birch, Horton, Bittner, Pestinger, and Anderson, written commun., 1985). However, Greens Creek wanted the issues resolved separately so that no additional complications would arise. Many groups, including the Shee Atika, the Alaskan congressional delegation, and the Greens Creek Joint Venture, were becoming increasingly dubious about Sealaska and their actions (Steven Silver, memorandum to P. Richardson, 1985).

The exploration permit was extended by one year in 1985. This allowed for continuing negotiations with Sealaska and further exploration to prove additional claims. By 1988 the USDA Forest Service rendered a decision denying the land-exchange proposal. The land exchange still could be completed if the agreement involved the surface rights to the Cube Cove land. This would require a direct agreement with the Shee Atika owners. Despite these problems, the Greens Creek Joint Venture felt that a land exchange opening the remainder of the Greens Creek area to subsurface mineral development was just a matter of time (T.C. Crafford, memorandum to H. Griffith, 1988).

Ownership Changes and Consolidation, Development, 1986–89

A major ownership change occurred at the beginning of 1986. Amselco (parent company, BP) purchased Noranda’s and Anaconda’s (which had just been liquidated by its parent company, ARCO) interest in the Greens Creek Joint Venture. That gave Amselco 70 percent of the total interest in Greens Creek, and they became the operators of the property. The geology staff did not change.

1986 Surface Exploration Program

The 1986 surface exploration program drilled surface and subsurface drill holes in an attempt to perfect four claims. Two of the claims (1001 and 1208) would be considered strike extension claims that Amselco believed, if allowed to patent, would extend their extralateral rights to the north and south (E.D. Harrison, Greens Creek Mining Company, written commun., 1986). The other two claims, 1104 and 1206, were believed to be covered under existing extralateral rights but were drilled anyway to test for downdip mineralization. Three surface holes were completed, totaling 4,694 feet, and one underground exploration hole was drilled to 1,271 feet.

The first hole drilled, PS–97, was the only one of major success. Two ore intervals were intersected consisting of mineralized gray chert and massive to semimassive sulfides. The lower intercept was at an elevation of 760 feet and was 25.9 feet long, averaging 0.08 troy ounce per ton gold, 16.68 troy ounces per ton silver, and 6.2 percent zinc. The rocks were unusual in that the mineralized chert was complexly folded and(or) interfingered with argillite, and the contact was 500 feet above the projection of the ore horizon in holes from the North and lower Central Ore zones. Ed Harrison believed the mineralization was continuous (E.D. Harrison, Greens Creek Mining Company, written commun., 1986); however, later drilling would define this as a separate ore zone, the Upper Southwest. The claim line between 1103 and 1104 had not been accurately surveyed and the ore horizon was right along the apparent boundary, thus making it difficult to prove the claim. The other two surface holes, PS–98 and PS–99, did not intersect mineralization on claims 1208 or 1206, respectively.

An underground hole was yet another attempt to prove claims to the south (1001) by drilling through the major fault at the end of the exploration drift. For the first 250 feet of hole GC–143, which corresponded to the faulted zone, 3.25-inch-diameter (PHR) core was taken, and then 2.5-inch diameter (HHR) core was taken to 411.3 feet. The core diameter was reduced to 1.875 inches (NQ) to 1,271 feet. The hole intersected ore grade intervals (up to 16.4 troy ounces per ton silver and 23.7 percent zinc), 3 to 100 feet wide, of mostly faulted white baritic ore (WBA) within argillite. This hole extended the known mineralization of the South Ore zone another 300 feet to the south into an unperfected claim.

Surface mapping and exploration were mostly limited to the Mammoth and Mariposite claim groups. The first occurrence of silver sulfides on Greens Creek Joint Venture lands was sampled in a 10-foot zone just to the north outside of the Mammoth claims. The sample assayed at 53.75 troy ounces per ton silver. Four diamond drill targets were outlined for drilling in 1987 on the Mammoth claims, as specified in the work commitment spelled out in the lease agreement (E.D. Harrison, Greens Creek Mining Company, written commun., 1986).

Tom Crafford’s 1986 map and report outlined his ideas and conclusions concerning Greens Creek geology. He verified through field evidence that the linear aerial photography

features do represent major faults of probable right-lateral movement with possible oblique or reverse slip components (T.C. Crafford, written commun., 1987). The youngest cleavage identified (now defined as S_3) within the Greens Creek rock package is a fracture cleavage related to the above major faults. He believed the first structural event is manifested by the recumbent isoclinal folds (later described as the D_2 event). He further refined the Mammoth claim geology and thought that the previously exhalative explanation for the QCM (quartz-carbonate-mariposite) unit was incorrect. Field evidence supports the idea of the altered mafic tuffs grading into the QCM unit, thus being serpentinized mafics (T.C. Crafford, written commun., 1987).

Four EM and magnetic survey lines were flown over the Greens Creek area piggybacked on Amselco's Mansfield aerial geophysical survey. No magnetic anomalies were identified from the survey. However, 6 of the 11 EM anomalies coincided with soil geochemical anomalies in the Big Sore area (E.D. Harrison, Greens Creek Mining Company, written commun., 1986).

Underground work continued to define the orebody in greater detail and to test different drifting and grade-control practices. A footwall drift was extended 94 feet from the east rib of the 1981 ore crosscut. The 9-foot-wide by 8-foot-high drift driven by jacklegs tested for mining problems within argillite. Four 1.432-inch diameter (BX) core holes were drilled using a CP-65 pneumatic drill rig from the new footwall drift. Two holes were drilled from the 1981 ore crosscut. These holes were drilled at tight 10- to 15-foot spacings along the contact to obtain more detailed structural data than from the drilling at 150-foot spacings. Detailed sampling of this core was carried out to determine the actual ore-waste boundary. The contact between the ore and hanging-wall argillite was the most important contact to define because most of the high-grade precious metals were found within 6 to 18 inches of that contact (E.D. Harrison, Greens Creek Mining Company, written commun., 1986).

1987 Surface Exploration Program

The exploration permit for the Big Sore and Tom claim groups was not extended another year by legislative means. The Greens Creek Joint Venture lost all rights to the Big Sore claims except for the eight core claims and the nine additional perfected claims. Negotiations were continuing with the USDA Forest Service and Sealaska to work out a land-exchange agreement.

The 1987 program concentrated on prospects away from the Greens Creek mine area. The Mammoth claims received the bulk of the attention and funds. Four diamond drill holes were completed, totaling 1,441 feet (W.C. Meyers, written commun., 1988). Three of the holes tested the mineralization seen on the ridgetop exposure of the QCM unit, and one hole targeted the lower QCM band. All holes intersected minor mineralization over short (less than 3-foot) intervals, assaying up to 0.236 troy ounce per ton gold, 1.72 troy ounces per

ton silver, and 3.8 percent zinc. The mineralization occurred within the QCM units for the ridge trend holes, while the mineralization occurred with the graphitic schist unit in the lower band. Six additional holes were outlined for drilling in 1988, mostly along strike of the graphitic schist/QCM contact.

Exploration work also was completed within the Fowler, Lil Sore, and Mariposite claim blocks. The first two claim groups were part of the original Norbritex Joint Venture. This joint venture was formed by Noranda, Bristol Bay, and Texas Gas in 1980 to explore lands outside of the Big Sore and Tom claim groups in which the other members of the Greens Creek Joint Venture did not wish to participate. Norbritex drilled one hole in Lil Sore that intersected a quartz-sericite unit overlying a graphitic unit, both thought to be part of the mine stratigraphy (W.C. Meyers, written commun., 1988). Soil sampling and CEM geophysics were carried out on soil grids to outline possible Greens Creek-type volcanogenic massive sulfide (VMS) targets or epithermal gold targets. Six anomalous soil geochemical zones were outlined, two of which occurred proximal to, or over, a sericitized pyrite breccia unit. Some of the soil anomalies had coincident CEM conductors. Additional soil sampling (in-fill), mapping, and trenching were recommended for these three claim groups.

The Greens Creek Joint Venture recognized the need for a better understanding of the structural geology of the mine, especially for mine planning. Three structural geology consultants (John Proffett, Ken McClay of the University of London, and Brian Marten of BP Minerals International) were contracted to perform separate structural studies. Marten's study was the first undertaken in early April of 1987. Marten deemed his results to be very preliminary by himself after he discovered that the 2 weeks he allotted for the study were "totally inadequate due to the unexpected structural complexity that was found" (B.E. Marten, BP Minerals International, written commun., 1987). He concluded that at least two intense penetrative shear deformational events were present that have been refolded by a third fold phase (D_1 through D_3). Marten believed that the first deformation had the greatest effect on the massive sulfides and result in milling, brecciation, and plastic flow. The hanging-wall breccia was also a result of this intense shearing (not phreatoclastic). He stated that the ore zone was likely a major shear zone. He expressed concern that the previous quantity and quality of structural observations underground, in drill core, and on surface were woefully inadequate for ore reserve calculations and mine planning (B.E. Marten, BP Minerals International, written commun., 1987).

John Proffett largely agreed with Marten's observations, though he did not see direct evidence for the first deformation event and he added a fourth, open-fold event (J.M. Proffett, written commun., 1987). He saw the second event to be the most intense, giving rise to S_2 axial planar to steeply plunging isoclinal F_2 folds. Gently south-southeast-plunging F_3 folds in turn fold F_2 . He thought that the S_2 was nearly parallel to bedding. The S_2 foliation is the dominant foliation seen in all rock types (compositional banding within the phyllites and ore,

and the slaty cleavage in argillite). He found no evidence for major thrust faulting along the ore/argillite contact. In addition, he mapped local F_4 folds that plunge nearly parallel to F_3 . The structural nomenclature suggested by Marten and refined by Proffett is still accepted and used by mine geologists at Greens Creek. McClay also largely agreed with Marten and Proffett. He adds a later D_5 event to describe the later brittle faulting (K.R. McClay, University of London, written commun., 1987). His conclusion mirrored Marten's that the current structural database was inadequate, and more detailed work was necessary for ore reserve calculations and mine planning (K.R. McClay, University of London, written commun., 1987). Despite the inherent structural complexities at Greens Creek, all three geologists agreed on a structural framework that still stood in 2001.

1988 and 1989 Surface Exploration Projects

Development and preproduction projects took priority over the next 2 years. Greens Creek management was waiting for the finalization of a land-exchange agreement with Sealaska (Greens Creek Mining Company, written commun., 1988). The minimum assessment work was completed on the various claim blocks in 1988, mostly consisting of mapping and trenching. Work on the Mammoth claims included the completion of one diamond drill hole. MRD-5 was drilled 600 feet southeast of hole MRD-4, testing for sulfides along the quartz-carbonate/graphitic schist contact. The hole did intersect minor disseminated galena and sphalerite, though no assay numbers are reported.

The Greens Creek Life of Mine Plan was released on March 25, 1988. The plan called for the startup of production operations in early 1989 with concentrate being produced by that February. Full-production rate was expected to be 1,000 tons per day (TPD) operating 355 days a year. The mine life was expected to be 11 years. Total capital expenditures necessary for development and startup were reported as \$105.8 million, with another \$12.1 million expected over the life of mine.

This plan proved workable. The Greens Creek mill processed the first ore from the mine on February 5, 1989. This was achieved despite the ferry dock being severely damaged by a winter storm on January 30 (Greens Creek Mining Company, written commun., 1989). Crews were transported to and from the mine by way of helicopters and float planes until a temporary dock was installed on February 7. The mill processed 8,150 tons of ore during the first month of operations.

Surface exploration activities consisted of two holes drilled from Big Sore claim 1105, targeting downdip of the North Ore zone. PS-100 was abandoned after 456 feet due to poor drilling conditions. PS-101, drilled from the northwest corner of the claim, reached 2,106 feet and intersected three barren contacts. No record exists of any assessment work done on the outlying claims. One significant underground drilling discovery was made. Hole GC-265, drilled along section 33, intersected 235 feet of ore-grade massive sulfide at a lower elevation than that of the North Ore zone. This was an apparent new ore trend in a previously untested area (Greens Creek

Joint Venture, written commun., 1994). This zone was later defined as the (Central) West zone.

Continuing Underground Exploration, Production to Shutdown to Reopening, 1990-95

The 1990 surface exploration campaign was very active after two summers of mostly minimum assessment work during startup. Diamond drilling took place on validated and unvalidated claims to the west of the established orebody. Drilling was allowed off the validated claims and within the national monument nonwilderness after the USDA Forest Service determined the Greens Creek Joint Venture had sufficient claim of extralateral rights (William Edwards, written commun., 1990). This final effort to validate claims to the west of the core claim group was the largest surface drilling project to date (10 holes totaling 23,287 feet).

The first hole, PS-102, was drilled at the same site as PS-100, which was abandoned the previous year. This hole did not intersect any economic mineralization. However, the next three holes all intersected ore from widely scattered drillpads. PS-103 was collared along the very southern edge of claim 1105 to test the possible southwest extension of the North Orebody. The hole intersected three ore-grade intervals along a contact between a siliceous breccia and argillite. The bottommost 5.5-foot intercept included visible electrum that ran 0.524 troy ounce per ton gold and 86.4 troy ounces per ton silver (J.G. Baughman, memorandum to T. Crawford, 1990). PS-104 was drilled 1,200 feet to the southeast of PS-103 and intersected two ore intervals, including 24 feet of 0.102 troy ounce per ton gold, 35.99 troy ounces per ton silver, and 9.1 percent zinc at the 860-foot level. PS-105, 500 feet from PS-103, tested the northwest extension of this mineralized interval. This hole intersected ore-grade massive sulfide at the 950- and 500-foot levels. The drill program geologists believed that the mineralization was continuous for over 1,600 feet, but they could not confidently correlate it with other recognized orebodies (J.G. Baughman, memorandum to T. Crawford, 1990). PS-103 and PS-105 were the first holes to intersect the Northwest West Ore zone on the west side of the Maki fault. The underground drilling program intersected significant base-metal intervals in hole GC-502, drilled from the 33 Exploration drift. This hole helped to define the Central West Ore zone as a separate orebody (Greens Creek Joint Venture, written commun., 1994). PS-104 intersected the top of what was later defined as the Southwest Ore zone.

Three more surface holes tested the extent of the mineralization intersected by GC-502: PS-108 and PS-110 to the south, and PS-109 to the west. Only hole PS-110 and a wedge drilled off the hole (PS-110a) intersected significant mineralization. A 16.1-foot-long ore-grade interval (2.11 troy ounces per ton silver, 16.69 percent zinc) was intersected deep (2,050 feet) in the hole. This pierced the 5250 orebody (a somewhat

continuous satellite of the West Orebody). The other two holes of the 1990 summer program, PS-106 and PS-107, tested downdip (to the southwest) of the intersections in PS-103 and PS-105, respectively. Both holes intersected only stratigraphic footwall (phyllite) rocks.

The 1990 surface drilling program intersected three new orebodies: the Central West, the Northwest West, and the Southwest. Much more drilling from underground was needed before most of the structural complications could be solved and the three new orebodies roughly defined. The following 2 years involved a very aggressive underground drill program to define the Central West Ore zone on 100-foot centers. By the end of 1990, underground drilling had increased the indicated reserves from 3.6 million tons to 6.9 million tons (Greens Creek Joint Venture, written commun., 1990) of which 2.8 million tons were in the probable category (Kennecott Greens Creek Mining Company, written commun., 2001). No additional surface drilling took place until the passage of the Land Exchange Act in 1996.

Assessment work continued on the claim groups to the north, and minor geologic mapping and geochemical sampling took place within the AINM boundary. Two soil geochemistry grids were completed in Fowler Creek and the “L” zone along the Maki fault (Upper Zinc Creek), south of the Lil Sore grid. Only the “L” zone showed any geochemical anomalies (D.L. Lorge and others, written commun., 1990). Previously unidentified mineralization was sampled on Antenna Mountain, Zinc Creek Pass, and the Zinc Creek roadcut south of the Zinc Creek bridge (fig. 1). The latter was the most significant at 8.07 percent lead and 22.86 percent zinc.

A different geologic model for the Greens Creek deposit emerged from the geologic mapping and sampling completed during the summer. The surface crew consisting of David Lorge, Eric Lalechuer, and William McClelland felt that all the anomalous soils and surface mineralization occurred along major faults (D.L. Lorge and others, written commun., 1990). Their new deposit model envisioned these faults (presumably the northwest-trending Maki-type faults) as being the main ore control and horizons. They interpreted the faults as forming during metamorphism and formation of the S_2 foliation. These faults were structural channels for the intrusion of ultramafic plutons and replacement mineralization. In a separate report, McClelland (W.C. McClelland, written commun., 1990) suggests that the Greens Creek deposit is a replacement of Upper Triassic sediments associated with a hydrothermal system driven by Upper Triassic volcanic rocks and (or) Late Triassic hypabyssal mafic to ultramafic intrusions. He cited the presence of an Upper Triassic *Halobia* fossil within an ore-enclosed concretion as evidence of replacement of the surrounding sediments. He described that much of the mineralization observed in core and on surface was controlled by veins that crosscut the S_2 foliation. All of the workers felt confident that additional massive sulfide deposits could be discovered within the Upper Triassic units with exploration concentrated along suspected northwest-trending faults (D.L. Lorge and others, written commun., 1990).

1991 Exploration Program

Underground exploration and continued production were emphasized in 1991. Only the minimum amount of assessment work necessary for claim maintenance was completed on the surface. Underground drilling to define the West Orebody was successful and resulted in subdividing it into three distinct zones (Greens Creek Joint Venture, written commun., 1994). Drilling to the south and west of the projected trend of the West Orebody intercepted high-grade intervals in holes GC-738, GC-739, and GC-753 that further defined the Southwest Ore zone. Continued definition and exploration drilling underground to the south was given an additional boost when the Forest Service’s mineral examiner and council gave positive comments during a preliminary meeting discussing extralateral rights to the south of the Big Sore claim block (Greens Creek Joint Venture, written commun., 1991). The 1991 definition drilling campaign increased the ore resource to 13.0 million tons, an increase of 6.1 million tons (Kennecott Greens Creek Mining Company, written commun., 1991). The proven and probable reserves, however, dropped to 1.2 million tons (Kennecott Greens Creek Mining Company, written commun., 2001).

On-Line Exploration from Anchorage was contracted to complete the assessment work required for claim maintenance. Their work concentrated on the leased Mammoth claims and unpatented Mariposite claim block. A soil geochemistry grid just north of the Mammoth claims yielded two minor discoveries. The first was a barite-bearing outcrop with visible gold (J.E. Adler and others, On-Line Exploration Services, Inc., written commun., 1991). However, assays did not confirm anomalous gold. The other discovery was disseminated sphalerite, galena, and chalcopyrite within a quartz vein. Both mineralized occurrences had slight soil geochemical expressions. On-Line Exploration recommended drill testing on the “L” zone pyrite, previously mapped and sampled within the Mammoth claims (J.E. Adler and others, On-Line Exploration Services, Inc., written commun., 1991).

1992 Exploration Program

The 1992 surface exploration program consisted of diamond drilling to fulfill the annual assessment work requirements. Wink Drilling of Juneau was contracted to drill 2,000 feet on unpatented claims north of the AINM boundary (Greens Creek Joint Venture, written commun., 1992). Two drill holes, MC-1 and MC-2, tested a weak silver-zinc soil anomaly on the Mariposite claim group defined by the 1991 program. Both holes were abandoned before reaching the target depth and did not intersect any mineralized intervals. Drilling was completed on the HI East and HI West claims leased from NERCO on the Mansfield Peninsula with no success. The underground drilling program completed drilling of most of the West Ore zone on 100-foot centers.

Ed Harrison recommended dropping the Mansfield claim groups in order to focus resources on the Fowler, Lil Sore,

Mariposite, and Big Sore claim groups. Harrison also advocated continued drilling on the Mariposite block and forming a Greens Creek joint venture exploration company with a separate budget from the mine because Kennecott Greens Creek Mining Company finances lacked the necessary funds to mount an effective exploration campaign (E.D. Harrison, memorandum to C. Davis, 1992).

Negotiations began on a new land-exchange proposal that only involved Greens Creek and the Forest Service. Greens Creek submitted a "bare-bones" proposal to the Forest Service in September of 1992. The proposal called for Kennecott Greens Creek Mining Company to purchase \$1,375,000 worth of private land in-holdings on Admiralty Island and other areas of the Tongass National Forest and convey the land to the Forest Service in exchange for the subsurface mineral rights to 6,875 acres surrounding the core claims (Steven Silver, memorandum to R. Pierce and C. Davis, 1992). The agreement also called for a net smelter interest paid to the Forest Service for any minerals produced from the area. This item proved to be the most contentious in the negotiations. Congressional approval was necessary for any land exchange involving a national monument. Greens Creek finally received title to the 17 core claims and one millsite claim after the USDA Forest Service and Bureau of Land Management approved the final validity test in December, 14 years after the process had been initiated (Greens Creek Joint Venture, written commun., 1992).

1993 Closure

Kennecott announced in February 1993 that production mining and milling operations would cease by mid-April. The primary cause of the closure was low metal prices (Greens Creek Joint Venture, written commun., 1993). Greens Creek lost \$2.2 million during the month of February alone. Milling ceased on April 10 and all but 24 employees were laid off by April 30 (Greens Creek Joint Venture, written commun., 1993). The remaining personnel were involved in the maintenance of permits and in development of the West Ore zone to satisfy the Forest Service's requirement of "use" of the property.

Underground diamond drilling began on July 17 to explore and define the Southwest Ore zone. The drilling occurred mostly from the 36 Exploration drift, which was being driven to the west of the 920 Main Haulage at the same time. Tim Hall was hired as the new Chief Geologist, and Deborah Apel returned to supervise the drilling program in November. A total of 30,261 feet was drilled along 200-foot spacings from section 3200 to 2400.

1994 Exploration

The Greens Creek Joint Venture agreed on November 17, 1993, that the Southwest Ore zone would require drilling at tighter (50-foot) spacings to adequately define the resource

(Greens Creek Joint Venture, unpub. data, 1993). They approved a 120,000-foot drill program and initiated a feasibility program to explore and develop the Southwest Ore zone. Development continued in the 36 Exploration Drift to provide platforms for drilling. The drift passed through the southern boundary of the claim block in February. It was not until April that the Forest Service confirmed the assertion of extralateral rights that included the Southwest Ore zone (Greens Creek Joint Venture, written commun., 1994).

By the end of 1994, 130,803 feet of diamond drilling had been completed, mostly within the Southwest Ore zone (Greens Creek Joint Venture, written commun., 1994). Most of the drilling was accomplished on 50-foot spacings and centers. At the end of 1994 the recoverable ore reserve for the Southwest Ore stood at 2.4 million tons at 0.244 troy ounce per ton gold, 32.86 troy ounces per ton silver, 5.91 percent lead and 12.35 percent zinc (Greens Creek Joint Venture, written commun., 1994). The feasibility report called for startup of the mill by January 1, 1997, at a rate of 1,320 TPD using the higher grade Southwest ore. The plan also called for expansion to 2,000 TPD by 1999, with additional lower grade ore sourced from the West Ore zone.

The land-exchange agreement with the USDA Forest Service was signed in Washington, D.C., on December 17, 1994, after much bargaining over a sliding royalty scale based on net smelter return (NSR). A compromise was reached in September when Greens Creek accepted the Forest Service's sliding royalty of 3.0 percent for ore greater than \$120/ton in exchange for reducing the \$1.5 million in-holding purchase amount to \$1.0 million (Greens Creek Joint Venture, written commun., 1994). A royalty of 0.5 percent was imposed on ore between \$80/ton and \$120/ton. The next step was to gain congressional approval through legislation.

Very little surface activity took place in 1994. Geologists from Kennecott Exploration completed a reconnaissance sampling program in the mine area and on Mariposite Ridge. Paul Lindberg began a 4-year stint as a consulting geologist to work on various projects, including geologic investigation of the Southwest Ore zone and interpretations and reconstructions along the Maki fault and other shears. Lindberg's interpretation of drillcore from the Southwest Ore zone led him to believe that much of the ore horizon was rooted in the argillite section and not at the argillite/phyllite contact (P.A. Lindberg, written commun., 1994). He also (re)identified the Klaus fault, which he believed decapitated the Southwest Orebody, displacing the top 700 feet to the northwest (P.A. Lindberg, written commun., 1994). The imminent completion of the land exchange led Lindberg to comment on future exploration. He proposed allowing a great deal of lead time to compile and digitize historical exploration data and maps that had been essentially archived for the past 4-plus years (P.A. Lindberg, written commun., 1994). Other ideas for initiating the exploration program were airborne geophysical and photometric surveys and liaising of the new exploration personnel with current geology staff.

The leased claims in HI East and HI West with NERCO were dropped as the area of Joint Venture was reduced to the lands south of Young Bay and east of Hawk Inlet (Greens Creek Joint Venture, written commun., 1994). The Joint Venture changed when Kennecott bought out CSX (Exhalas was bought out by the three remaining partners in 1993). The ownership split was 70.27 percent Kennecott and 29.73 percent Hecla.

Land Exchange Act and Continuing Production and Exploration, 1995–Present

The Greens Creek Land Exchange bill was introduced to the Resource Committee of the U.S. House of Representatives on March 16, 1995. The bill was cosponsored by Don Young (R-Alaska) and George Miller (D-California), who were usually on the opposite side of an issue from each other. The bill did not make it out of committee in 1995. Greens Creek employees received good news when the Kennecott Board of Directors, on April 5, 1995, approved the allocation of \$87.3 million to reopen Greens Creek with production at 1,320 TPD (Greens Creek Joint Venture, written commun., 1995).

Paul Lindberg and Norm Duke of the University of Western Ontario completed a preliminary geologic mapping and sampling project in and around the Greens Creek mine in the summer of 1995 while the Greens Creek Land Exchange bill was in legislative limbo. They spent 2 weeks traversing various parts of the property, including the Mammoth claims, Cliff Creek (the area of the original geochemical anomaly leading to the discovery of Greens Creek), Gallagher Creek, Killer Creek, and along the road corridor. Duke concluded that the Greens Creek orebody was upgraded by remobilization of syngenetic lead-zinc-silver from the argillites (SEDEX model) and gold sourced from the strongly carbonitized mafic and ultramafic rocks (N.A. Duke, written commun., 1996). Duke subsequently refined and redefined his model based on his regional geologic mapping.

1996 Exploration and Reopening

The 12-year battle for gaining exploration rights to the original claim group finally ended on April 1, 1996, when President Bill Clinton signed the Greens Creek Land Exchange Act. Work began immediately on purchasing \$1.0 million of private in-holdings, primarily from a list of preferred properties compiled by the USDA Forest Service. This process took nearly 2 years to complete.

Steve Newkirk was hired during the winter of 1995 to resurrect an active surface exploration program after a 7-year hiatus. Staking and filing 213 Federal lode claims in unclaimed holes south of Young Bay further refined the land picture. In addition, 15 State tideland claims were staked along

upper Hawk Inlet. However, the State of Alaska also selected the land for potential community development and thus its status remains in limbo. The 10-year lease of the Mammoth claims expired at the end of 1995. Negotiations took place over several months with the owner, Herman Meiners, to renew the lease or to purchase the claims outright. However, Meiners did not budge from his high asking price and evidently shopped the property around to other potential buyers with no results (S.R. Newkirk, written commun., 1996). No further negotiations took place.

Surface diamond drilling was limited to the patented claim block until the land-exchange lands were fully conveyed. The Forest Service would allow only nonimpact activities such as helicopter landings, soil and rock sampling, airborne and ground geophysical surveys, and geologic mapping. The 1996 program initially involved one drill rig operated by Connors Drilling. However, poor advance rates due to poor ground conditions, frequent mechanical failures, and driller inexperience with Greens Creek-type conditions necessitated mobilizing a second drill rig.

Nine holes totaling 7,755.5 feet were completed. The first three holes, PS-111, PS-112a (abandoned after 487 feet), and PS-112, were collared from the 1350 adit access road and targeted the possible northwest extension of the North Ore zone. Neither completed hole intersected significant mineralization. PS-113 through PS-117 were drilled from three drillpads targeting the Upper Plate Extension of the Northwest West Ore zone (the Maki offset on the west side of the West Ore zone). This thin, flat-lying mineralized horizon had been intersected in a few holes from underground but was not systemically explored. PS-115 had the only significant intercept, a 1.5-foot interval of ore running 0.16 troy ounce per ton gold, 19.44 troy ounces per ton silver, 3.4 percent lead and 6.8 percent zinc. PS-118 targeted the possible north extension of the West Ore, first intersected by PS-87 in 1984. The hole was located 600 feet north-northeast of PS-87 and did not intersect mineralization.

Numerous geophysics methods were tested at Greens Creek to determine which might be more effective in surface exploration. Airborne EM, radiometric, and magnetometer surveys were completed in conjunction with Kennecott Exploration's Mansfield project. The surveys, carried out by Aerodat, flew more than 1,200 kilometers of line that covered the entire Greens Creek area, including the land exchange. Distinct magnetic anomalies corresponded with already mapped ultramafic bodies (for example, Killer Creek serpentinite). The EM survey proved useful in identifying graphitic rocks, such as the Hyd argillite. Underground and surface gravity surveys were completed. The underground survey, extending from the portal to the end of the 36 Exploration drift, detected a subtle ~1.5-Mgal anomaly over the West Ore zone. The surface survey over the Northwest West Ore zone failed to detect any coincident anomaly. Two test lines over the West and Northwest West Ore zones were surveyed by the CSAMT (controlled source audio-magnetotelluric) method. A resistivity low associated with the Northwest West Ore zone

and Maki fault was detected, but the West Ore zone was not. A time-domain electromagnetic (TEM) survey was also completed over eight lines in the same area and measured a strong response from the West Ore. Downhole TEM surveys were completed on surface and underground holes. GC-1530, an underground exploration hole, produced a strong EM anomaly within the West Ore. This geophysical test work was done to develop the tools for a multiyear exploration program (S.R. Newkirk and others, written commun., 1996).

Norm Duke and Paul Lindberg completed reconnaissance and detailed geologic mapping and sampling within the land-exchange boundary. Their work culminated in a completely revised 1 inch=1,000 foot scale district map and numerous 1 inch=200-foot scale mine geologic maps. The prospective mine stratigraphy was traced to the south and north (S.R. Newkirk and others, written commun., 1996). The land-exchange boundary survey was finalized in November. Kennecott Greens Creek Mining Company developed a cooperative research agreement with Cliff Taylor of the USGS for a program to focus on many of the outstanding geologic problems of the Greens Creek mine (reported in this volume).

The work completed in 1996 was designed to lay the groundwork for a multiyear exploration program. The geologic mapping and research agreement was to refine the geologic model for the deposit. A GIS system, using ArcView software, was set up to aid in organizing the 20+ years of data. Historical geologic maps and geochemistry were digitized for the GIS project during the summer and fall.

Underground exploration was limited to definition drilling in the Northwest West and 5250 Ore zones. Preproduction drilling, consisting of horizontal fans of short (100- to 400-foot) holes, was carried out from various ore accesses in the Southwest Ore zone. These holes drilled on 10- to 25-foot centers aided in stope planning. The recommissioned mill began running ore from the Southwest orebody in July 1996. Kennecott Greens Creek Mining Company produced about 143,000 tons of ore averaging 0.108 troy ounce per ton gold, 23.80 troy ounces per ton silver, 4.84 percent lead, and 10.3 percent zinc. Almost all of the ore was sourced from the Southwest Ore zone.

1997 Exploration

Surface exploration activities were accelerated on the land-exchange property. Seven new grids totaling 230,000 linear feet, were cut and sampled within the Greens Creek Joint Venture lands. The grids within the land exchange included High Sore, Bruin, Lower Zinc, Upper Zinc, and Gallagher. The "A" Road and East Lil Sore (fig. 1) were cut within the unpatented claim groups north of the land exchange. Detailed work along each grid included soil sampling, gravity, magnetic and TEM geophysical surveying, and geologic mapping. No high-priority, near-surface coincident gravity and TEM anomalies (possible shallow massive-sulfide bodies) were identified (S.R. Newkirk and others, written commun., 1997). Soil sampling and geologic mapping outlined drill targets

or areas for detailed followup work in Bruin, Gallagher, and Lower Zinc Creeks. The "A" Road prospect was discovered in 1995 during the road traverse of Paul Lindberg and was thought to be a possible distal "mine" horizon with exhalative quartz, barite, and pyrite (P.A. Lindberg, written commun., 1997). Work in 1997 defined soil anomalies coincident with the exhalative horizon, but convincing evidence was not found to determine whether or not it was the mine horizon. Norm Duke and Paul Lindberg completed reconnaissance scale and detailed geologic mapping. John Proffett returned for the first time since 1987 and carried out structural mapping. Lindberg completed detailed mapping of the road corridor and borrow pits, all of which was compiled in a 15-sheet map folio (P.A. Lindberg, written commun., 1997).

Four diamond drill holes totaling 6,316 feet were completed in 1997. All were drilled from pads constructed on patented Big Sore claims because the land exchange had not been conveyed. Hole PS-119 targeted the lower phyllite-over-argillite contact 800 feet to the northwest of hole PS-87. Only scattered zinc mineralization was intersected in the phyllite, and two argillite intervals intersected were clearly fault-bounded and nonmineralized. PS-120 targeted the same contact, except to the north-northeast (200 feet due east of PS-118). The hole did not intersect the contact, but a downhole TEM survey mapped a steeply dipping conductor to the southwest of the hole and a subhorizontal conductor 200 feet below the hole. This hole was reentered in 1998 to test the deeper conductor but did not intersect an interval corresponding to the conductor. PS-121 and PS-122 were collared in Big Sore claims 1305 and 1304, respectively, in the Gallagher Creek grid/prospect. Both holes intersected semimassive to massive pyrite and sphalerite zones with up to 9 percent zinc over 2-foot intervals. Mineralization in PS-122 occurred at and below a contact between graphitic phyllite and chloritic phyllite, which was thought to represent a new mineralized horizon at a different stratigraphic horizon (S.R. Newkirk and others, written commun., 1997). The surface drill program was cut short by a new discovery underground.

Discovery of the 200 South Ore Zone

Preproduction drilling continued to be a major portion of the underground drilling program. During December 1996, a preproduction fan was drilled from the 200 Ore Access, targeting the 164-foot level. The southernmost hole, PP0204, intersected ore widths showing that the orebody was still open to the south of cross section 18, previously modeled as the end of the Southwest Ore zone. No additional preproduction holes were drilled to the south to find the terminus of the ore because of the oblique drilling angle. The 200 South stope (at the 164-foot level) began mining from the ore crosscut shortly afterwards. The 200 South stope reached section 18, the end of the ore reserve for that level, but still showed a full face of ore. Expecting the ore to terminate at any time, mining continued on a round-by-round basis for another 300 feet. At the same time, exploration drilling to the south commenced

from the 480 Exploration drift. Hole GC–1632, drilled along section 16, intersected a 42-foot interval of zinc-rich massive ore about 200 feet below the 200 South stope. Kennecott Greens Creek Mining Company geologists quickly realized that the 200 South stope was the proverbial tip of the iceberg. Four drill rigs (including a diesel-powered surface drill rig) were mobilized to quickly define this new ore zone, named the 200 South orebody. Two drill rigs were positioned in the 480 Exploration drift and the other two in the 200 South stope, to drill the zone from the inside out. Long-section drilling from the face of the stope indicated that the ore zone continued to at least section 11. Drilling from the south extension of the 480 Exploration (4711 Drift) continued from 1998 through 2000 and defined a reserve of 2.08 million tons at 0.189 troy ounce per ton gold, 21.29 troy ounces per ton silver, 5.15 percent lead, and 12.50 percent zinc. Discovery and definition of the 200 South orebody drastically changed the mining schedule of the various ore zones. Due to the higher grade of the 200 South ore, it was mined ahead of the more accessible West Ore zone(s). The 200 South orebody accounted for 42 percent of the total mine production from 1998 to 2000.

1998 Exploration

The 1998 exploration program was boosted with the completion of the land exchange on August 5, 1998. The combined holdings of the Greens Creek Joint Venture now included 445 unpatented lode mining claims, 58 unpatented millsite claims, 17 patented lode claims, 1 patented millsite claim, and land-exchange lands totaling 17,617 acres. Drilling was completed on lands off of the validated claim block or extralateral rights assertions for the first time since 1985. Four holes (PS–124 through PS–127) were drilled in Bruin Creek, targeting the downdip potential of the north-striking phyllite-over-argillite contact. PS–124 and PS–125 were drilled from the same site as PS–47 and tested downdip and updip, respectively, from the semimassive sulfides intersected near an argillite/phyllite contact in that hole. Both holes intersected only minor mineralization in the upper phyllite unit. Both holes terminated in altered ultramafic rocks below a carbonate-rich contact zone with argillite. PS–126 was drilled near treeline in upper Bruin Creek to test coincident soil and TEM anomalies. The hole intersected a barren phyllite/argillite contact at 1,275 feet and terminated in a gabbro at 1,724 feet. PS–127 was drilled from the site of PS–81, drilled in 1984 by Noranda. This hole intersected two fault-controlled blocks of argillite with no sulfides. The only other hole drilled (besides the reentry of PS–120) was PS–123 in Gallagher Creek, testing the phyllite stratabound zinc-rich zone intersected in PS–46 and PS–122. Minor sphalerite and chalcopyrite were intersected, but to a lesser degree than in holes PS–46 and PS–122, indicating that the mineralization decreases to the southwest (A.W. West and others, written commun., 1999).

One new grid (Upper Big Sore) and extensions of three 1997 grids (Lower Zinc, Bruin, and “A” Road) were geochemically sampled and geophysically surveyed in 1998.

The work outlined numerous multielement anomalies with coincident TEM anomalies, but none were significant enough to warrant immediate drilling (A.W. West and others, written commun., 1999).

John Proffett extended his 1997 mapping in the Big Sore area toward the 920 portal and west of the Maki fault. He also reviewed surface drill core from both sides of the Maki fault. He found evidence for a major shear zone (Upper Shear Zone) that juxtaposes nonmine-type slates, silts, and phyllites of uncertain age over mine-type argillites, phyllites, and ultramafic rocks (J.M. Proffett, written commun., 1998). Subsequent work in 1999 defined a deeper shear zone (Lower Shear Zone). These two shear zones bracket the mine stratigraphy (J.M. Proffett, written commun., 1999). The amount and direction of offset along the two shear zones and the stratigraphic position of the upper-plate rocks remain outstanding and important questions for surface exploration.

1999 Exploration Program

1999 was the first exploration season entirely focused in the land exchange. However, the season began poorly when the contracted Bell-206 helicopter crashed into the mill during takeoff on the first day of service. Fortunately, no one was seriously hurt. Two new geochemical grids were completed and one extended. A large grid was surveyed in Killer Creek, spanning 8,000 feet from the “B” Road to the Mammoth claims. Numerous high-rank, multielement soil anomalies were defined, and numerous sulfide-bearing outcrops and gossan zones were sampled and mapped. A new grid was cut in Cub Grid, just east of Bruin Creek. Two sets of major right-slip faults repeat the argillite/phyllite contact several times in Cub Creek. Anomalous geochemistry was coincident with an inferred contact zone in upper Cub Creek, near the land-exchange boundary (A.W. West and others, written commun., 2000). The Upper Zinc grid of 1997 was extended to the west. No significant discoveries were made in Upper Zinc Creek. However, two significant base-metal mineralized outcrops were sampled and mapped by Norm Duke to the southwest in the Lakes District prospect (N.A. Duke, written commun., 1999). One of the occurrences is near the contact between chlorite phyllite and possible Triassic carbonate rocks.

Ten diamond drill holes were completed totaling 12,715 feet. Seven of the holes were drilled in Bruin Creek. PS–128, PS–129, and PS–130 were drilled from the back-slope directly behind (north of) the 920 administrative building. A shallow southwest-dipping barren phyllite-over-argillite contact was intersected in all three holes. PS–128 drilled through Proffett’s Lower Shear Zone and into more than 1,000 feet of ultramafic rocks. PS–131, PS–133, PS–137, and PS–138 were collared from two different pads on the west side of the mapped contact in middle Bruin Creek, about 1,000 feet east of the 1998 drill holes. Only PS–137 intersected conformable argillite/phyllite contacts. PS–136 was collared on the east side of the contact and also

intersected the contact. In both holes, the contact was intersected multiple times, but no indication of mineralization was found. Three holes were drilled in Killer Creek. The first two holes, PS-132 and PS-134, were collared from the site of PS-20, drilled in 1977. Both holes intersected long intervals of semimassive to massive pyrite bands with minor sphalerite up to 15 feet wide within greenstones and serpentinites. PS-132 also intersected a deep (800 feet below the surface), fault-bounded, 3.6-foot band of massive chalcopyrite that ran 4.2 percent copper. PS-135 was drilled from a pad constructed above Pit 405, at mile 7.6 of the "B" Road. This hole intersected long intervals (up to 15 feet) of patchy zinc mineralization in chloritic phyllites.

2000 Surface Exploration

Two new prospects were drilled in 2000. Two pads were constructed in Cub Creek to test soil anomalies coincident with the phyllite/argillite contact. The targets were further refined by a CSAMT geophysical survey along three lines in Bruin and Cub Creek (three lines were also surveyed in Killer Creek). Results from the survey were of better quality than the 1996 survey due to better location of the transmitter line. The four holes drilled in Cub Creek (PS-144, PS-145, PS-147, and PS-151) did not intersect any significant metal enrichment along the contacts intersected. Data collected from these holes and two others (PS-147 and PS-148) in East Bruin Creek aided in the interpretation of the Bruin and Cub Creek regions. A large-scale recumbent syncline (cored by argillite) that closes to the west-southwest was found to be the dominant structure (A.W. West and others, written commun., 2001). The nearly isoclinal fold has mineral potential along both upper and lower limbs.

The Lower Zinc Creek prospect was drill tested for the first time from a pad constructed at the 2.8-mile mark of the "B" Road. Holes PS-152 and PS-153 were drilled to the northeast, targeting the mine contact. The contact intersected in both holes was strongly silicified and sulfidized (massive bands of pyrite). The geochemical results were highly anomalous in Ag, As, Hg, Ba, and Tl. Due to the mine lithologies intersected, abundant pyrite, silica alteration, and a distal geochemical signature, the potential of the Lower Zinc Creek prospect was upgraded (A.W. West and others, written commun., 2001).

Five holes were drilled in Killer Creek. The first two holes, PS-139 and PS-142, targeted a northwest-striking zone of zinc-rich, poorly exposed gossan. Both holes were abandoned in a wide fault zone (middle Gallagher fault) before reaching their target depth. Three holes drilled from two platforms in middle Killer Creek targeted a deep phyllite-over-argillite contact inferred from the CSAMT survey. None of the holes intersected argillite. However, all three did intersect fault-controlled secondary mineralization within 400 feet of

their collars. Four moderately southwest-dipping zones with silver and zinc enrichment were defined with assays as high as 22.4 troy ounces per ton silver and 9.62 percent zinc (A.W. West and others, written commun., 2001). The intervals did not have sufficiently consistent grades or widths to be of economic significance.

Conclusion

For more than three decades, exploration, development, and production at the Greens Creek mine has been challenging. Fourteen years passed between the discovery drill hole intersecting over 80 feet of massive sulfide and the mill processing the first ore. During that time Greens Creek nearly became a casualty of a large conservation movement that included the White House and Congress. This movement culminated in the passage of ANILCA, which at first threatened to kill the project and then severely limited the land position at Greens Creek. Greens Creek emerged from this situation as an apparent incongruity: a mine within a national monument bordering a wilderness area. However, exploration for new orebodies from the surface effectively ceased. After 12 years of negotiations on local, State, and Federal levels, the land position was remedied in 1996 with signing of the Land Exchange Act. This unique act supported by conservation/environmental groups and industry alike increased Greens Creek's land position to what it was previous to ANILCA and added to the federally protected lands in the Admiralty Island National Monument and elsewhere in Alaska.

Exploration from the surface and underground has been successful in adding to Greens Creek's known reserves during the life of the mine. The nearly constant changes in ownership, personnel, and geologic models did not prevent new orebodies or extensions from being discovered. When low metal prices temporarily closed the mine in 1993, the high-grade Southwest Ore zone was discovered and drilled out. This new orebody allowed Greens Creek to reopen profitably in 1996. Since reopening, new reserves have kept pace with production, adding nearly 4 million tons of ore. The mine's proven and probable reserves, as of the end of 2001, are 7.6 million tons grading 0.133 troy ounce per ton gold, 16.67 troy ounces per ton silver, 4.57 percent lead, and 11.63 percent zinc (Kennecott Greens Creek Mining Company, written commun., 2001). The newly (re)acquired land-exchange lands provide abundant opportunities for future discoveries.

Reference Cited

Nash, Roderick, 1982, *Wilderness and the American mind*, 3d ed.: New Haven, Conn., Yale University Press, 425 p.

Geology of the Greens Creek Mining District

By Norman A. Duke, Paul A. Lindberg, and Andrew W. West

Chapter 4 of

Geology, Geochemistry, and Genesis of the Greens Creek Massive Sulfide Deposit, Admiralty Island, Southeastern Alaska

Edited by Cliff D. Taylor and Craig A. Johnson

Professional Paper 1763

**U.S. Department of the Interior
U.S. Geological Survey**

Contents

Abstract.....	93
Introduction.....	93
Regional Geotectonic Framework	94
Structural Framework within the Greens Creek Domain	95
Tectonostratigraphic Assemblages.....	96
Retreat Group	96
Cannery Formation.....	97
Serpentine.....	97
Black Phyllite	98
Hyd Group.....	98
Basal Hyd Group Breccia/Debrisite/Conglomerate Deposits	98
Restricted Mine Argillite Troughs	99
Upper Hyd Group Gabbro Sills/Flood Basalts	99
Mine Site and Prospect Geology	100
Prospects in the Greens Creek District.....	100
Upper Cliff Creek	101
Gallagher Creek.....	101
West End	101
Cub Creek/Lower Bruin Creek	101
Upper Bruin Creek/Mammoth Ridge	101
Mammoth Pyritic Massive Sulfide Deposit	102
Killer Creek.....	102
Cascade Creek	102
Lakes District.....	102
Zinc Creek	103
Lil Sore Creek.....	103
A-Road Barite	103
Metallogeny	104
Conclusion.....	105
Acknowledgment.....	105
References Cited.....	105

Figures

1. Lodging facilities at Hawk Inlet.....	94
2. Big Sore, the discovery site of the Greens Creek deposit.....	94
3. Mine argillite exposed at mile 2.2 on the B-access road.....	95
4. Convolute-folded black dolomite beds in massive sulfide, M120-S200 Ext	96
5. Hyd Group basalt capping the South Ridge at the headwall of Gallagher Creek.....	101
6. Surface drill site in upper Cub Creek.....	101
7. P. Lindberg examining green carbonate on Mammoth Ridge	102

8. The trace of the Maki fault system north of Gunsight Pass	102
9. Silicified rock developed below the Killer Creek serpentinite	102
10. Basal Hyd Group phyllite breccia exposed in upper Zinc Creek.....	103
11. Basal Hyd Group heterolithic debrisite exposed in lower Zinc Creek.....	103
12. A. West examining mine argillite exposed in Lil Sore Creek.....	103

Plate

[on CD-ROM]

- 4-1. Geology of the Greens Creek mine area.

Geology of the Greens Creek Mining District

By Norman A. Duke, Paul A. Lindberg, and Andrew W. West

Abstract

The Greens Creek polymetallic sulfide deposit occurs within the low-grade metamorphic core of the Admiralty subterrane of Alexandria. Local tectonostratigraphic assemblages constitute late Paleozoic back-arc basement and its Upper Triassic flood basalt cover sequence. The Admiralty back-arc basin was volcanically active into the Devonian, giving rise to Retreat Group greenstones. The Upper Devonian through Lower Permian Cannery Formation includes older deep marine siliciclastics and a younger shallow marine dolomite-chert facies. The uppermost Pybus Formation signals the termination of back-arc sedimentation through shoaling accompanying the amalgamation of Alexandria and Wrangellia by the mid-Permian. The post-amalgamation unconformity ended with Late Triassic rifting driven by the Nikolai plume: the Carnian Nikolai Greenstone and Norian Hyd Group flood basalt provinces, occurring respectively in Wrangellia and Alexandria, overlap in time. The Greens Creek deposit is hosted within Carnian/Norian-age black argillite occurring below the Hyd basalts.

Protracted compressional tectonism attended the suturing of the Wrangellian superterrane to continental North America. Mid-Cretaceous collision resulted in fold and thrust-style imbrication, while dextral transpression on the Tertiary Denali transform system caused severe strike-slip dislocation of the imbricated stratigraphic package. The back-arc assemblage and its flood basalt cover were decoupled, resulting in a stacked series of inversely metamorphosed thrusts south of the mine. The Greens Creek deposit occurs in low-grade phyllites, which make up the lowest exposed thrust plate. This mineralized domain is bound by major ductile faults bordering on Hawk Inlet and Young Bay. Brittle northwest-southeast fault fracture systems are common; the Maki fault through the immediate mine site dextrally offsets the mineralization about 1,800 feet.

The Hyd Group is subdivided informally into basal growth-fault-related breccia/conglomerate, medial mine argillite, and upper basalt members. At the mine, the Retreat Group greenstone substrate to mine argillite is interleaved with sheets of serpentinite and lesser metagabbro. Intense hydrothermal alteration of this rock association forms the informal mine phyllite in the stratigraphic footwall of the ore. Widespread occurrence of barian mariposite ties hydrothermal alteration of serpentinite to massive baritic ores capping mine phyllite. High-grade laminated ores at the

base of mine argillite are capped by bedded pyrite, and thin, cherty, black manganoan dolomite beds persist into overlying slaty argillite.

Greens Creek is unique in that it comprises high-grade zinc-lead-silver-gold ores at a major unconformity in a juvenile arc setting. The deposit is linked to an active rift segment plumbed by serpentinite/gabbro and filled with euxenic pyritic-graphitic argillite. Gabbro sills intruding mine argillite have the same geochemistry as the upper Hyd Group basalt, thus tying rifting to the Nikolai plume. Although somewhat of a volcanogenic massive sulfide/sedimentary exhalative hybrid, the Greens Creek setting lacks the felsic volcanics that characterize polymetallic Kuroko-type volcanogenic massive sulfide districts. The link to a growth-fault-controlled, starved sedimentary trough makes it more appropriate to classify Greens Creek as a sedimentary exhalative deposit.

Introduction

The Greens Creek polymetallic (Zn-Pb-Ag-Sb-As-Cu-Au-Ba) sulfide deposit, the location of which is shown on plate 1 (plate 1 in digital form only), occurs in complexly deformed, low-grade phyllites exposed between Hawk Inlet and Young Bay on northern Admiralty Island. The mine is situated in the upper reaches of Greens Creek, outcropping as a gossanous kill zone on the west wall of the Big Sore tributary. This chapter describes the district geology of the Greens Creek mining area, extending from the cirque headwall of Cliff Creek, approximately 3 miles southeast of the mine, through the Zinc Creek drainage northeastward to the isthmus separating Hawk Inlet and Young Bay. The geological overview covers an approximate 10-mile-long segment of the northwest-trending phyllite belt on strike with the mine. The road connecting the mine to accommodation facilities on Hawk Inlet and docking facilities on Young Bay provides the most accessible transect through the complex tectonostratigraphy of the area (fig. 1). Because the mine is within the Admiralty Island National Monument, surface exploration is restricted to lands specified by a Federal land-exchange agreement dating from 1995, together with the area immediately to the north through the Lil Sore Creek drainage that is covered by Federal Mining Lode Claims. A total of 119 square miles is open to mineral exploration.



Figure 1. Lodging facilities at Hawk Inlet.

Geological mapping in this area is severely hampered by rugged mountainous topography, a near-complete veneer of glacial till, and dense vegetation below ridge crests. Ridges provide the best exposures, with common rocky knobs outcropping through thin, clayey basal till. The steep U-shaped valley walls and heavy foliage, including patches of devils club wherever sunshine penetrates the canopy formed by old-growth stands of hemlock and spruce, restrict helicopter access largely to ridge crests. Muskegs that develop over the larger serpentinite bodies offer a few additional landing sites. The thickness of till cover increases downslope, with almost no bedrock exposure except on truncated spurs forming cliff faces and along deeply incised stream courses. Although creek traverses from ridge crests to valley floors are physically taxing, these provide the most effective means of attaining bedrock information.

The district geological map (plate 1) is based on 1-inch to 500-foot scale mapping carried out over most of the area shown and documented in unpublished Greens Creek Mining Company reports. The compilation incorporates data collected since the discovery of the Greens Creek deposit in the mid-1970s (fig. 2). This information has been reinterpreted in the light of airborne geophysical surveys carried out in 1995–96. The core of the area, including upper Cliff Creek, the Greens Creek mine site, Mammoth Ridge to Killer Creek, and the Zinc Creek and Lil Sore Creek drainages, has been mapped in greatest detail. The geology shown for outlying areas is less detailed but is included to provide a broader context for situating the mine stratigraphy.

This chapter describes the district geological setting of the Greens Creek ore deposit. Results from limited supporting microscopy and geochemistry are reported; however, lithological subdivision is based essentially on field observations. We refine the Retreat-Cannery-Hyd tectonostratigraphic grouping based on earlier reconnaissance mapping by the U.S. Geological Survey (Lathram and others, 1965). The main objective is to define the structural/stratigraphic controls of the Greens Creek ores. The second section of this chapter presents a regional geotectonic framework for the district. The third section provides brief lithological descriptions and an overview



Figure 2. Big Sore, the discovery site of the Greens Creek deposit.

of the local structural/stratigraphic relationships of the various rock units. The fourth section describes the mine-site geology and places several prospects within their geological framework. The fifth section offers a number of hypotheses concerning the genesis of the Greens Creek deposit, based on observed ore/host-rock relationships.

Regional Geotectonic Framework

Admiralty Island occupies a central position in the Alexander Archipelago and is the type locale for the Admiralty subterrane of the Alexander terrane (Alexandria). Alexandria formed as a Late Proterozoic-Paleozoic oceanic island arc system somewhat older than the late Paleozoic Wrangellian oceanic island arc system with which it had amalgamated by the Permian (Berg and others, 1978; Gehrels and Saleeby, 1987a; Gardner and others, 1988; Karl and others, 1999a). On Admiralty Island, 265-Ma (mega-annum) metamorphic dates (Karl and others, 1999b; Haeussler and others, 1999) and a regional mid-Permian to Late Triassic unconformity record the time of amalgamation. The 50-Ma period of nondeposition following this event ended in the Middle to Late Triassic with rift-related flood basalt volcanism caused by the Nikolai Greenstone plume (Richards and Jones, 1991).

Recent geochronology (S.M. Karl, oral commun., 2002) identifies substrate on Admiralty Island dating back to the Late Proterozoic, thus linking the Admiralty subterrane to the Craig subterrane, which includes similar-aged Late Proterozoic and Paleozoic arc volcanics on Prince of Wales Island (Gehrels and Saleeby, 1987b). The deep-water, black argillite-chert-pillow basalt assemblage forming the Middle Ordovician Hood Bay Formation on southern Admiralty Island (Carter, 1977) indicates that the Admiralty subterrane developed back arc to the frontal Craig volcanic chain. The Admiralty back-arc setting was still volcanically active in the late Paleozoic, with regional deposition of the Retreat Group greenstones, locally incorporating Devonian/Mississippian-age reefal carbonates. The Middle(?) Devonian through Lower Permian stratigraphic

succession, constituting the Retreat Group and overlying Cannery Formation, appears to be more or less continuous on Admiralty Island. The Upper Devonian through Lower Permian Cannery Formation includes both an older, deep-water siliciclastic assemblage and a younger, shallow-marine chemical/clastic dolomite-chert facies (Loney, 1964). The Lower Permian Pybus Formation chert member signifies termination of back-arc sedimentation under shoaling conditions accompanying the amalgamation of Alexandria and Wrangellia. The welding together of these two juvenile oceanic settings may have imparted the penetrative S_1 metamorphic segregation foliation that characterizes the Retreat Group.

The post-amalgamation unconformity ended with Middle to Late Triassic rifting related to the Nikolai plume. The Wrangellian Nikolai Greenstone and Admiralty Hyd Group flood basalt provinces overlap in time, although the Nikolai basalts are dominantly Carnian and the Hyd basalts Norian in age (fig. 3). As discussed in this paper, the Greens Creek ore deposit is hosted within Hyd Group rocks, specifically occurring at the base of the informal mine argillite member immediately underlying upper Hyd basalts. Conodont studies demonstrate that the mine argillite was deposited at the Carnian/Norian transition between 225 and 221 Ma (chap. 11). Following the Nikolai rifting event, a Jurassic-Cretaceous arc/trench system developed between the Wrangellian superterrane and the North American craton, accounting for the flysch of the Seymour Canal Formation and the Douglas Island Volcanics occurring on the eastern side of Admiralty Island. Arc/craton collision driven by eastward subduction along the leading Wrangellian foredeep culminated in mid-Cretaceous through early Tertiary Coast Range plutonism.

The prolonged period of late Mesozoic compressional tectonism, an expression of the Laramide in the northern Cordillera, led to polyphase deformation in the Greens Creek mining area. The dominant regional tectonic grain relates to D_2 thrusting. That the Retreat Group and Cannery Formation lithologies are penetratively foliated by S_2 , that mine argillite is isoclinally folded by F_2 , but that upper Hyd Group flood basalts only show strong S_2 development along their basal contact, indicates that the Upper Triassic deposits were ramped at relatively shallow crustal levels. Following the D_2 overprint, the accreted complex was subjected to protracted transpression, giving rise to upright chevron-style F_3 folding and related steeply dipping shear zones that strongly disrupt the regional D_2 structural/stratigraphic framework. Reactivation of D_2 thrusts post- D_3 produced shallow-dipping D_4 shears that locally overprint S_3 . Mid- to late-Tertiary dextral transform faulting along the Denali transform system, with major strands following Chatham Strait and Gastineau Channel, occurring respectively west and east of Admiralty Island, caused brittle D_5 faults, such as the Maki system cutting through the immediate Greens Creek mine site. The similar orientations of D_3 -ductile and D_5 -brittle structures indicate that the D_3 structural grain was reactivated in D_5 . The late dextral fault strands locally develop complementary interior sinistral fault/fracture sets of minimal displacement.



Figure 3. Mine argillite exposed at mile 2.2 on the B-access road.

Structural Framework within the Greens Creek Domain

The Greens Creek domain is defined as comprising the low-grade metamorphic assemblages which occur between major north- to northwest-striking shear zones bordering Hawk Inlet and Young Bay. Hyd Group rocks east of the Young Bay shear zone are at epidote-amphibolite hornfels facies, suggesting proximity to a Coast Range pluton such as the one mapped on the northeast corner of Admiralty Island. The mafic metavolcanic rocks occurring southwest of the Greens Creek thrust are overprinted by regional epidote-amphibolite facies metamorphism. These amphibolites may include amygdaloidal Retreat greenstones as well as Hyd-age metagabbro sills. The uppermost thrust forming the Cliff Creek headwall at the southeast corner of the map is a garnet-amphibolite facies. Recent U/Pb dates demonstrate the presence of Hyd-age metadiorite intrusions (S.M. Karl, oral commun., 2002). These garnet amphibolite gneisses are strongly injected by mid-Cretaceous(?) ferrodiorite and pegmatite dikes. The stacking of higher grade amphibolites structurally above the low-grade Greens Creek domain suggests that the area was strongly telescoped in a subductionlike setting typified by hot over cold metamorphic plates. The low greenschist facies domain hosting mineralization forms the structurally lowest plate, and the ambient metamorphic overprint within the Greens Creek domain is below biotite stability. Limited Ar/Ar work on white mica identifies a mid-Cretaceous age for the low greenschist facies metamorphic conditions (Brew and others, 1992; Haeussler and others, 1999).

The gross distribution of lithological units in the Greens Creek domain reflects dome-and-basin structural egg-crating. The prominent bluff of Retreat Group marble surrounded by Retreat Group greenstone that is shown in the central-northwest portion of the map area is identified as an F_2 isocline preserved on the nose of an F_3 anticline. The serpentinite-cored area of Retreat greenstone, extending westerly from the mine site through the Killer Creek drainage, is another basement high interrupting the Zinc Creek/Lil Sore Creek and Gallagher

Ridge tracts of mine argillite. The undifferentiated Cannery Formation sedimentary rocks on the eastern side of the map area and transected by the Young Bay shear zone form a subtly developed structural high. These domal elements are bordered by peripheral black phyllite. The more restricted tracts of mine argillite are tectonically imbricated with Retreat greenstone. In its regional context the Greens Creek domain comprises a window of complexly deformed low-grade phyllites exposed beneath Hyd flood basalts, forming nearly complete cover along the southern margin and a continuous belt along the northeastern boundary of the mapped area.

Tectonic imbrication, dome-and-basin interference patterns, and major northwest-trending faults collectively indicate that the area of the Greens Creek deposit has been subjected to polyphase deformation. There is evidence of five deformational events. The dominant penetrative S_2 schistosity trends approximately east-west and dips moderately $20\text{--}40^\circ$ south. An earlier S_1 segregation foliation within Retreat greenstone forms isoclinal microfold closures in S_2 . The thin-bedded mine argillite exhibits isoclinal F_2 folding; spaced S_2 cleavage in these rocks is axial planar to exceptionally appressed F_2 folds, which are particularly well exposed at mile 2.2 on the B-access road and in the underground workings. S_2 is more or less penetrative in all lithologies in the Greens Creek domain except for massive serpentinite, metagabbro, and the black dolomite beds, which occur within mine argillite. The ultramafic/mafic intrusions escaped this deformation through strain partitioning into marginal shears, while the black dolomite beds deformed brittlely, giving rise to ubiquitous ladder quartz veining (fig. 4). D_2 accounts for the structural imbrication of the serpentinite-cored panels of Retreat greenstone north of the Killer Creek serpentinite body as the shallow to moderate, south-dipping lithological contacts paralleling S_2 are clearly overprinted by high-angle D_3 fabrics.

D_3 gave rise to northwest-southeast-trending shears and variably tight, upright, chevron-style folding of S_2 . This fabric is only penetrative within the bounding Young Bay shear zone and the north-trending Hawk Inlet high strain zone. S_3 intensifies along the numerous northwest-trending brittle/ductile fault zones. Most of the deformation along these topographic linears appears ductile, stress being accommodated largely by ductile stratal thinning rather than through brittle fault failure. D_4 relates to late (post- S_3) low-angle shearing and intensifies southward toward the base of the thrust plates of amphibolite. S_4 is rather common in the immediate mine area (for example, the Klaus fault), causing low-angle transposition of the steeply dipping S_3 cleavage sets. It is notable that D_2 thrusts and D_4 shears both show broadly coincident orientation and vergence, suggesting reactivation of D_2 thrusts late in the history of transpressional D_3 shearing. All rocks have been displaced by late northwest-southeast-trending brittle faults showing dextral displacement—the Gallagher and Maki fault/fracture systems through the area of the mine show on the order of 1,000 and 1,800 feet of dextral west-side-up displacement, respectively. Complementary sinistral fault splays have only minor displacements; but where present, these make tracing geological units very difficult.



Figure 4. Convolute-folded black dolomite beds in massive sulfide, M120-S200 Ext. Photograph by N.A. Duke, University of Western Ontario.

Tectonostratigraphic Assemblages

Retreat Group

Three lithotypes are differentiated in the Retreat Group: greenstone, black phyllite, and marble. The only map-scale unit of Retreat marble is restricted to Limestone Bluff. Fossils collected by the USGS suggest that the marble is Silurian or Devonian (D.A. Brew, oral commun., 2002), which is consistent with the Middle(?) Devonian age assignment for this unit proposed by Lathram and others (1965). Limestone units occurring on strike to the north on the west shore of Hawk Inlet have been identified as Middle Devonian on the basis of recent conodont determinations (A.G. Harris, oral commun., 2001). The marble at Limestone Bluff is gray- to buff-weathering and composed essentially of coarsely crystalline calcite. Primary bedding is only weakly discernible, with buff dolomitic and siliceous layers slightly more resistant to weathering. Transecting shears weather brown and have limited quartz vein development. Lustrous gray to black phyllite forms thick units interlayered with the Retreat greenstones. That these monotonous “black shale” units have intimately interstratified greenstone panels suggests that they represent background sedimentation coincident with Retreat mafic volcanism. Also, like the Retreat greenstone units, these tracts of lustrous black phyllite retain no primary bedding features due to an intense S_1 schistosity that developed prior to overprint by the regionally penetrative S_2 -crenulation cleavage.

Units of Retreat Group greenstone are dominated by monotonous green chloritic phyllite with variable interlayering of lustrous gray phyllite after graphitic shale and rare thin gray to white marble bands. Retreat Group greenstone is without doubt the most enigmatic lithology in the district. This greenstone is everywhere characterized by streaky light/dark green layering of tectonic origin. The S_1 overprint was so severe that neither flow nor intrusive contacts were observed. Rare relict amygdules in samples collected north of Limestone Bluff, in the Lakes District, and at the west end of Gallagher Ridge

indicate a flow origin. Contacts with bordering units appear entirely tectonic; the streaky-foliated greenstone panels are structurally interleaved with gray phyllite and massive serpentinite. Greenstone contacts against graphitic units are strongly carbonatized. Contacts with interleaved serpentinites are extremely slivered, with greenstone/serpentinite sheeting on the meter scale. At the mine site, variably intense hydrothermal alteration of greenstone/serpentinite protoliths gives rise to voluminous mine phyllite in the stratigraphic footwall of the Greens Creek ore horizon (discussed herein and in Chap. 6). Limited geochemical work on Retreat greenstone broadly indicates that the protolith was compositionally similar to midocean-ridge basalt. Based on the present level of mapping, Retreat Group greenstone forms the primary flooring for the Hyd Group at the site of the Greens Creek mineralization. The S_1 foliations indicate that this substrate was extremely tectonically attenuated prior to S_2 deformation. The mine phyllite enveloping serpentinite may have been radically thinned at the time of serpentinite emplacement.

Cannery Formation

Although the map shows the Cannery Formation as essentially undivided, the separate areas mapped as Cannery show marked lithological differences. The main domical exposure transected by the Young Bay shear zone is dominated by low-grade phyllites after core dolomitic arenite, medial dolomitic siltstone, and peripheral phyllitic chert. The outer phyllitic chert likely accounts for the on-strike cherty white phyllite units interleaved with black phyllite east of the mine. This same siliceous white phyllite accounts for the slaty siliceous sediments capping northerly trending spurs off the east-west-trending Gallagher Ridge of Hyd Group basalt south of the mine. These isolated white phyllite domains form klippen overlying the immediate mine stratigraphy at the Gallagher Creek headwall. This cherty white phyllite unit in the Greens Creek area is tentatively correlated to the Pybus Formation that caps the Cannery Formation regionally. Weathering of Pybus Formation accounts for common chert pebbles in basal Hyd Group conglomerate over Admiralty Island.

The metasedimentary rocks bordering on Retreat Group greenstone at Limestone Bluff are dominantly lustrous black and white siliceous schist. The more siliceous (cherty) units in this package form the prominent ridge crests paralleling Hawk Inlet. The Cannery Formation exposed along the shore of Hawk Inlet at the Cannery and along the A-road to Young Bay comprises varicolored gray-green-white-black banded schists, in part graphitic (black), in part marly (green) and in part dolomitic (white). The graphitic units are locally rich in nodular pyrite. The thin-banded character of these siliceous units is in part attributed to high D_3 -strain overprinting a compositionally varied deep marine siliciclastic facies. This assemblage is interpreted as an older (Carboniferous?) component of the Cannery Formation. It is possible that some black phyllite now identified as Retreat Group sediment may include infolds of Carboniferous(?) siliceous rock. The Retreat "black schists" mapped

below the serpentinite of Killer Creek and the Mammoth Ridge green carbonate are strongly silicified, thus showing lithological similarity to the siliceous schists mapped as Cannery. The masking of lithotype by silicification is even more extreme in the Lakes District where considerable thicknesses of silica rock could be protolithed in either Retreat black phyllite or the Cannery siliceous sedimentary rocks. The lower Cascade Creek section is somewhat transitional in lithology between Retreat phyllite and Cannery siliceous-graphitic-pyritic schist. This particular section is classed as Cannery on the basis that it is somewhat more lithologically varied than is typical for the units mapped as black phyllite of the Retreat Group.

Serpentinite

The largest single serpentinite mass in the map area is the Killer Creek body, located 1.5 miles west-northwest of the mine site. This unit is strongly sheared on its upper and lower contacts against variably altered Retreat greenstone. Serpentinite-injected greenstone forming substrate to mine argillite is strongly carbonatized. The panel of Retreat greenstone in the immediate footwall of mine argillite is variably sulfidized, with pyrite-pyrrhotite-chalcopyrite forming patchy disseminations and locally massive replacement pods of meter scale. The northern contact of the serpentinite of Killer Creek has occasional talc-sericite-carbonate shears with associated zinc-lead-silver disseminations. The faulted southeast nose, exposed in Killer Creek at the B-road bridge, has associated massive magnetite-pyrite skarn mineralization.

Although the margins of the Killer Creek serpentinite are strongly deformed and mineralized, the interior is massive nonfoliated serpentinite. Limited microscopic study shows coarse honeycomb-textured serpentine outlined by the distribution of fine magnetite (up to about 10 modal percent). Ubiquitous disseminated magnetite in massive serpentinite accounts for coincident magnetic anomalies. The massive serpentinite of Killer Creek is a striking airborne magnetic anomaly, as are structural repeats at the mine site and in the upper reaches of Zinc Creek. However, serpentinite replaced by green carbonate (listwanite) is not magnetic, indicating magnetite breakdown during pervasive carbonatization. Extreme carbonatization of serpentinite is accompanied by formation of spaced waxy green foliations defined by barian mariposite. Limited microprobe work on green carbonate collected from Mammoth Ridge identifies paragenetically early magnesite and later species within the ankerite-kutnahorite solid solution series. Barite, barian mica, and barian feldspar species are also present. In some panels, like the one in upper Zinc Creek, green carbonate locally retains relict metagabbroic textures. Green micas in these domains are chromium-poor and barium-rich (oellacherite), indicating similar carbonate-barite replacement of the gabbroic injections into serpentinite. The best locale for demonstrating that sheeted gabbro dikes locally inject serpentinite is at Serpentine Gulch, the most northeasterly green carbonate body exposed on the Bruin Creek/Cub Creek ridge crest. Here, massive serpentine appears rather fresh, while numerous phases of

gabbro with preserved multiple chill margins are pervasively retrograded to green-brown mica, complex magnesium-iron-manganese carbonates, and pumpellyite (Reich, 1996). The mixed serpentinite/green carbonate sheet exposed in the uppermost tributaries of Lil Sore Creek shows considerable lithological affinity to the serpentinite/gabbro complex at Serpentine Gulch.

In the more highly sheared and altered serpentinite/green carbonate sheets north of the main Killer Creek body there is ample evidence for structurally controlled talc-carbonate replacement of massive serpentinite. Toward sheared margins the massive serpentine becomes increasingly transected by brown carbonate fracture sets. Tectonic milling of serpentinite blocks results in talc-carbonate schist enveloping “knockers” of massive serpentine. Within green-yellow talc schist, slips of green barian mariposite progressively replace serpentinite smears. Talc-mariposite-barite veins crosscutting carbonated serpentinite and associated green carbonate are themselves deformed in S_2 , clearly indicating that serpentinite emplacement/replacement predated regional D_2 metamorphism. Common occurrence of green carbonate clasts in basal Hyd debriite (debriite is used here to connote debris-flow deposits, following Warme and Kuehner, 1998) conclusively ties serpentinite emplacement, alteration, and exposure to basal Hyd times. On the basis of detailed structural/stratigraphic evidence, the emplacement of serpentinite, with limited associated sheeted gabbro, can thus be linked to the initial stages of Hyd rifting. It is hypothesized that the serpentinite sheets were injected into growth faults that controlled the deposition of the mine argillite member of the Hyd Group.

Black Phyllite

The extensive tracts of black phyllite that occupy the structural lows between the domains of Retreat greenstone and the Cannery metasedimentary rocks present a critical stratigraphic problem within the Greens Creek mining area. It is somewhat unclear to which unit they should be assigned; as mapped, they may include similar lithology of differing ages. The fact that the panels of Retreat Group greenstone are interlayered with panels of lustrous black phyllite indicates that black phyllite is a major member of the Retreat Group. However, that black phyllite also occurs peripheral to siliceous schist domains tentatively correlated with Pybus Formation suggests a black phyllite member that is younger than the uppermost member of the Cannery Formation. This problem is exacerbated by the difficulty of differentiating slaty to phyllitic facies of mine argillite from the more regionally extensive tracts of younger black phyllite. As currently shown on the map, the contact between black phyllite and mine argillite is a rather arbitrary boundary placed between (a) euxenic argillite with easily discernible black dolomite beds and (b) monotonous gray to black phyllite lacking recognizable bedding. At the current level of mapping, the tracts of undifferentiated black phyllite are considered primarily to postdate the Cannery Formation and, at least in part, to show stratigraphic

continuity with the mine argillite—the youngest black phyllite may occur on the weak sides and restricted mine argillite buttressing against fault blocks of Retreat greenstone on the strong downthrown sides of half grabens.

Hyd Group

Unlike the Retreat Group and Cannery Formation in which detailed stratigraphy remains but poorly resolved due to complex regional metamorphic overprinting, the Upper Triassic Hyd Group, postdating the mid-Permian amalgamation of Wrangellia, can be clearly subdivided into basal growth fault-related breccia/debriite/conglomerate deposits, medial argillite, and upper basalt members. Other units include local argillaceous limestones at the base of the upper basalt and gabbro sills within medial mine argillite. Gabbro sill-argillite complexes occur below the upper Hyd basalts capping the Gallagher Ridge south of the mine, in the Lakes District, and in lower Lil Sore Valley south of Young Bay.

Basal Hyd Group Breccia/Debriite/ Conglomerate Deposits

The primary significance of the occurrence of extensive basal Hyd fragmental units is that these stratigraphically tie the Hyd Group to Retreat substrate. Most importantly, the lithological diversity of basal Hyd growth-fault-related rocks identifies the specific nature of the Hyd rift just prior to the deposition of mine argillite, host to the high-grade Greens Creek ores. The deepest seated manifestation of growth-fault lithotypes comprises 10–100-meter-thick zones of silicified mylonite (mapped as Trhsr—siliceous rock) closely affiliated with carbonate-altered serpentinite. There is a semicontinuous siliceous band striking from the immediate mine site along the length of Mammoth Ridge. The silicified rock delineating this structural unit is derived primarily through intense silicification of greenstone protolith, accounting for finely disseminated leucoxene. Not shown are associated alteration zones grading outward from siliceous rocks into tan sericite-leucoxene phyllite, sericite-chlorite-ankerite phyllite, and chlorite-calcite phyllite into greenstone. These various hydrothermal alteration zones overprinting Retreat greenstone collectively make up the mine phyllite occurring in the stratigraphic footwall of the Greens Creek ore deposit. As this zoning is best developed at the mine site, it is described in more detail in the section below on mine geology. The silica rock that forms a series of benches in the Lakes District is thought to represent a major sheet of silicification related to the emplacement of the Killer Creek serpentinite.

By far the best exposures of basal fault-breccia and debriite are found in outcrops following Zinc Creek and forming a near-continuous unit extending northeast along the Lil Sore drainage. The best development of nonbedded fault breccia is in the lower and middle reaches of Zinc Creek. These

areas are dominated by massive heterolithic phyllite breccia protolithed wholly in mine phyllite and green carbonate-altered serpentinite. The fact that no fresh greenstone and only rare serpentinite clasts are observed in these breccias, despite their provenance in greenstone/serpentinite-altered equivalents, unequivocally links the formation of basal Hyd fault breccia to hydrothermal alteration of active fault structures controlling the deposition of mine argillite.

The first appearance of mine argillite clasts in fault breccia approximates the transit from poorly layered breccia to bedded debriite. Significantly, the most readily identifiable mine phyllite clasts in bedded debriite tend to be the most highly altered sericite-mariposite phyllite and green carbonate clasts. The matrix of debriite adjacent to basal mine argillite is typically crystalline quartz-carbonate, signifying a hydrothermal silica-dolomite cementing agent. Nodular pyrite, with or without barite, is relatively common. The contact between basal Hyd debriite and medial Hyd mine argillite is placed at the transition from dolomite-clast debriite, which comprises cryptocrystalline black dolomite clasts in a crystalline carbonate matrix, to coherently bedded black dolomite interlayered within slaty black pyritic argillite. North of the Zinc Creek/Lil Sore Creek divide, resedimented argillaceous grit overlies non- to poorly layered mine phyllite pebble debriite. The unit of Hyd Group conglomerate (Trhc) traced from exposures on the A-road southeasterly to the mouth of Lil Sore Creek on Young Bay is also poorly layered but contains a greater variety of clasts—the red jasper clasts are weathered from Pybus Formation while the green carbonate clasts indicate a source in mine phyllite. The Hyd conglomerate unit shown at the headwall of Greens Creek separates black phyllite and Hyd flows; that is, no mine argillite is recognized at this locale. This particular conglomeratic unit includes upper Hyd Group basalt clasts, indicating that deposition postdated the initiation of the flood basalt volcanism.

Restricted Mine Argillite Troughs

The occurrence of well-bedded black argillite/black dolomite overlying debriite deposits of the same lithological makeup conclusively ties mine argillite stratigraphically to the basal Hyd Group fault-controlled breccia/debriite/conglomerate deposits. Using dolomite beds as a defining characteristic of mine argillite restricts its distribution to (1) the faulted margins against altered Retreat greenstone (mine phyllite) and (2) the immediate base of upper Hyd flood basalt. At the mine, the high-grade laminated zinc-lead-silver ores form a basal mine argillite facies that immediately overlies massive white carbonate-barite ores capping mine phyllite. Here, the well-bedded mine argillite overlies only minor basal Hyd fault breccia/chert conglomerate, indicating the juxtaposition of a coherent panel of intensely hydrothermally altered Retreat greenstone almost directly against slump-folded mine argillite.

In the Zinc Creek trough, the Greens Creek ore horizon occurs well below the base of coherently bedded black dolomite interlayered with pyritic slaty argillite. Given the setting

at the mine site, ore should occur below the first appearance of black dolomite clasts within debriite stratigraphy. Thin (decimeter scale) black dolomite interbeds persist vertically through mine argillite even where this unit is apparently thickest, as in the Lil Sore Valley and on Gallagher Ridge. That no significant mineralization is known to occur much above the basal contact suggests that hydrothermal activity and ore deposition coincided with the collapse that initiated restricted trough-controlled mine argillite sedimentation.

The upper termination of mine argillite is represented by a thin, discontinuous argillaceous limestone member deposited immediately below the upper Hyd flood basalts. Conodont specimens from basal ores to the capping limestone identify a relatively short time span for mine argillite deposition (220.7 ± 4.4 Ma, chap. 11). The variable yet considerable thickness of mine argillite (locally up to a few hundred meters) may be attributed to chemical precipitation within hydrothermally active troughs keeping pace with tectonic subsidence; that is, the host mine argillite to the Greens Creek ore may represent a highly reduced hydrothermal brine pool lithofacies.

Upper Hyd Group Gabbro Sills/Flood Basalts

The Greens Creek District includes only the basal members of the upper Hyd Group: the gabbro sills intruding into the medial Hyd mine argillite and the immediately overlying, similarly metagabbroic-textured massive flows, flow breccias, and minor pillow basalt. Intense swarms of gabbro sills intrude white phyllites (a Pybus equivalent?) in upper Cliff Creek and mine argillite south of the mine, in the Lakes District, and in Lil Sore Valley. These gabbros are medium grained and nonfoliated and exhibit relict gabbroic to diabasic textures. They are completely hydrated, being composed essentially of uralitized pyroxene and saussuritized plagioclase. The limited petrographic work carried out to date has not identified any relict primary pyroxene or plagioclase. Observed fining of grain size toward sill margins indicates that the secondary mineralogy faithfully pseudomorphs the primary igneous textures. The massive metagabbroic units overlying mine argillite in the Lakes District are fine to medium grained and could include massive flows capping the medial Hyd argillite. Upper Hyd flows capping Gallagher Ridge and traced to the headwall of Cliff Creek immediately overlie a discontinuous limestone unit occurring at the top of the mine argillite. These may show the same metagabbroic textures as the sills into underlying mine argillite but are retrograded to greenschist facies chlorite-albite-calcite mineral assemblages. The Hyd Group basalts of upper Cliff Creek are dominantly flow breccias. Rare pillowed flows in the lowermost volcanic units indicate initial eruption into locally submarine conditions. Hydrothermal breccias crosscutting the basal flows have associated minor chalcopyrite-pyrite mineralization.

Little information is presently available for the superjacent garnet amphibolite facies mafic gneisses in upper Cliff Creek. The boundary between the greenschist and amphibolite facies rocks is a sharp, moderately south-dipping thrust

surface along which amphibolitic gneisses are juxtaposed over greenschist facies metavolcanics. The amphibolitic gneisses are characterized by metamorphic layering and common ferrodiorite and pegmatite diking. Only one dike of ferrodiorite was observed on the Gallagher Creek headwall below the Cliff Creek thrust. Notably, similar ferrodiorite dikes have also been intersected locally in the underground mine workings where they clearly crosscut S_2 , but both inject and are overprinted by D_3 cleavages. The relation of the garnet amphibolite facies gneisses at the base of the Cliff Creek thrust to epidote-actinolite amphibolite occurring at the base of the central Greens Creek thrust is unknown. The strong airborne magnetic anomaly associated with this latter boundary may relate to basal serpentinite and/or a pyrite to pyrrhotite metamorphic conversion.

Mine Site and Prospect Geology

Bedrock exposures at the Greens Creek mine site are limited, and the specific geological setting of the ores is best deciphered on the basis of underground mapping and drill sections. Only features that place the mineralization within the regional structural/stratigraphic framework and bearing most directly on the origin of the high-grade ores are considered here. Following a brief review of the mine-site geology, selected known mineral prospects are described to illustrate the metal endowment of the district as a whole.

The Greens Creek ore horizon outcrops near the eastern nose of Retreat greenstone cored by the Killer Creek serpentinite. This nose of greenstone is intensely altered, forming mine phyllite proximal to the mineralization. The host structure has the geometry of an F_2 anticline. Given the subtle but significant change from structurally lower mine argillite to structurally overlying black phyllite on the limbs, it is possible that the core of greenstone may have originated as a basement horst, sidewall to a mine argillite trough. Cross-folding causes marked structural egg-crating and accounts for symmetrical hour-glass pinchouts of the immediate mine stratigraphy on the opposing limbs. The Greens Creek ores are specifically sited on the overturned eastern limb. Offsets postdating F_3 folding caused by the Klaus and Maki fault systems severely hamper stratigraphic reconstructions. Nevertheless, the detailed exploratory work clearly demonstrates that ore is confined to the immediate mine argillite/mine phyllite contact. The Greens Creek ore horizon is sandwiched between structural-hanging-wall mine phyllite, derived from hydrothermal alteration of Retreat greenstone, and structural-footwall mine argillite, on the lower overturned F_2 fold limb. The original host-rock stratigraphy had mine argillite deposited against pervasively hydrothermally altered Retreat greenstone (the mine phyllite). Mine phyllite comprises chlorite-calcite phyllite, chlorite-sericite-ankerite phyllite, tan sericite-leucoxene phyllite, and silica rock developed through increasingly intense hydrothermal alteration of an already S_1 -foliated greenstone protolith, as well as

green barian mariposite-talc-carbonate-barite phyllite developed through alteration of serpentinite and lesser gabbro.

At the mine portal, mine argillite is separated from the mine phyllite by a thin interval of dolomitic phyllite/cherty dolomite. This assemblage has lithological kinship to the white phyllite occurring south and west of the mine and is tentatively correlated with the Cannery Formation (PDcpw on plate 1). Both underground and surface drilling have commonly intersected impure dolomitic to phyllitic cherts below a persistent black and white banded chert marker. Where this impure chert/dolomite sequence stratigraphically underlies the high-grade ores, it carries appreciable pyrite and may contain up to 2 percent zinc. Massive bodies of white dolomite-barite, capping mine phyllite and at least partly derived through hydrothermal replacement of greenstone protolith, can locally constitute high-grade zinc (20 percent), lead (8 percent), silver (20 troy ounces per ton), and gold (0.5 troy ounce per ton) "White Ore." The very high-grade zinc (30 percent), lead (10 percent), and silver (>50 troy ounces per ton) laminated "Black Ore" occurs at the base of anoxic graphitic argillite peripheral to massive, non- to poorly bedded "mounds" of framboidal textured pyrite. The highest grade ores are essentially restricted to the base of the mine argillite. Immediately above ore, the mine argillite is characterized by dense, cherty, black dolomite interbeds that are moderately manganeseiferous (2 percent MnO_2). Away from mineralization, the host mine argillite tends to be limy rather than graphitic and dolomitic, suggesting waning of hydrothermal input away from zones of discharge.

The stratigraphic position of the Greens Creek ores at the Retreat Group/Hyd Group contact places the site of the mineralization at the regional mid-Permian to Upper Triassic unconformity. Where preserved, the footwall cherts are commonly hydrothermally silicified and brecciated and are locally conglomeratic. These sometimes-graded chert pebble beds represent erosional lags of the Pybus Formation and therefore identify the basal Hyd unconformity. The affiliation of silicified conglomerates with limited, growth-fault-controlled mine phyllite breccia indicates that Greens Creek mineralization accompanied the initial collapse of the Hyd rift, the deposition of the overlying high-grade black ores coinciding with restricted marine incursion.

Prospects in the Greens Creek District

A number of prospects have been discovered during ongoing surface exploration efforts in the Greens Creek district. The following brief descriptions of selected targets illustrate the character of mineralization away from the immediate mine site. Prospects are listed from the south extension of the land exchange northward; the primary aim is to situate various mineralized sites within their local geological environment.

Upper Cliff Creek

Mine argillite underlies the upper Hyd basalt in the headwall of Cliff Creek. Numerous Hyd gabbro sills are injected into white cherty phyllite immediately below argillite. Geochemically anomalous but weak sulfide mineralization is associated with the sill margins. The absence of footwall mine phyllite after altered Retreat greenstone suggests that this is a distal, non-fault-controlled contact where the mine argillite overlapped Pybus Formation.

Gallagher Creek

The Gallagher Creek area overlies the downdip extension of the mine (fig. 5). Just as the Maki fault cuts through the underground workings, the Gallagher fault system cuts through the Gallagher Creek area. The mineralization exposed in lower Gallagher Creek consists of pyrite-pyrrothite-sphalerite-impregnated mine phyllite. This is interpreted as footwall alteration to the Greens Creek ore horizon. Polymetallic sulfide mineralization occurs within the isoclinal F_2 infold of mine argillite overlying a substantial thickness of basal Hyd debriite. This is identified as a structural repeat of the Greens Creek ore horizon. The Gallagher infold occurs immediately below a shallow, south-dipping, late D_2 thrust in central Gallagher Creek. The upper-plate rocks consist of black phyllite and sericitic siliceous sediment, which is in turn overlain by gabbro-silled mine argillite and the upper Hyd basalt flows, forming the ridge crest. Lithologies making up the upper plate are broadly correlative to the Cliff Creek section.

West End

The West End prospect is at the western termination of the prominent Gallagher Ridge southwest of the mine. At West End, mine argillite overlies a thin interval of debriite developed on a serpentinite-plumbed panel of mine phyllite. Though structurally thin, the upright mine argillite/mine phyllite section at West End is basically lithologically similar to the overturned section hosting the Greens Creek ore.

Cub Creek/Lower Bruin Creek

Mine phyllite structurally overlies mine argillite between Cub and Bruin Creeks, the same overturned structural/stratigraphic setting as the mine (fig. 6). Anomalous geochemistry and evidence of growth-fault breccia at the phyllite/argillite contact are positive indicators for occurrence of Greens Creek type ores.



Figure 5. Hyd Group basalt capping the South Ridge at the headwall of Gallagher Creek.



Figure 6. Surface drill site in upper Cub Creek.

Upper Bruin Creek/Mammoth Ridge

The Mammoth Ridge green carbonate and related mariposite phyllite association represents the most highly altered ultramafic/mafic rocks in the district. This rock package has considerable lithological similarity to California Mother Lode-type gold systems. Despite the intensity and magnitude of alteration, the adjacent mine argillite is less “sooty” and more “phyllitic” than the host argillite at the mine site. A possible explanation is that Mammoth Ridge was a topographic high at the time of fluid expulsion and is juxtaposed against argillite deposited stratigraphically above or lateral to the restricted sooty facies of argillite hosting the ore.

Mammoth Pyritic Massive Sulfide Deposit

The Mammoth pyritic massive sulfide deposit is hosted in lustrous black schist immediately below the green carbonate altered serpentinite that extends the length of Mammoth Ridge (fig. 7). Bands of massive pyrite interleaved with schist are exposed over about 200 feet of elevation, with the central 50 feet of the interval dominated by massive pyrite bands of meter scale. These central bands are the most massive and have the finest grained textures. Grab samples reveal chalcopyrite-rich breccia clasts in pyrite-quartz-barite gangue. Like the Greens Creek deposit, the Mammoth deposit is intersected by the Maki fault system (fig. 8). Although more highly recrystallized, the Mammoth pyrite deposit may be akin to the barren pyrite centers developed within the Greens Creek deposit.



Figure 7. Examining green carbonate on Mammoth Ridge.

Killer Creek

The Killer Creek serpentinite is a south-dipping sheet overlying strongly sulfidized chlorite phyllite developed from Retreat greenstone (fig. 9). Local zones of sericite-talc phyllite with patchy sub-ore grade silver values lie along this basal contact at surface. However, mapping has yet to identify host mine argillite in the section. Exploratory work suggests a foot-wall feeder system with the serpentinite mass occurring where the Greens Creek ore zone would be expected.



Figure 8. The trace of the Maki fault system north of Gunsight Pass.

Cascade Creek

Several zinc prospects are in the Cascade Creek drainage. These take the form of patchy disseminations of sphalerite along phyllite/greenstone contacts. The sphalerite mineralization has been overprinted by S_2 foliations, suggesting zinc remobilization into the strongly S_1 -sheared margins of greenstone units bordering on graphitic-pyritic phyllite. These contacts tend to be strongly carbonatized, silicified and, more locally, sulfidized. The occurrence of stringery sphalerite in this environment suggests that the Retreat black phyllite/greenstone association is a preferred reservoir for the Greens Creek pay metals.

Lakes District

Extensive stockwork mineralization occurs in strongly brecciated quartz-graphite schist below gabbro-silled mine argillite at the northwest termination of the Killer Creek serpentinite in the Lakes District. Mineralization includes veinlets of pyrite-sphalerite-chalcopyrite and patchy, semi-massive, coarsely granular aggregates cemented by galena-sphalerite-tetrahedrite. Well-mineralized samples have also been collected from the immediate contact of the mine argillite overlying mine phyllite. Anomalous zinc-lead-silver is associated with overlying gabbro sill/argillite contacts. The Lakes District is a prime target for the preservation of a satellite Greens Creek-type deposit.



Figure 9. Silicified rock developed below the Killer Creek serpentinite.

Zinc Creek

As the name indicates, the Zinc Creek drainage is characterized by anomalously high zinc in stream geochemical surveys. The creek cuts across the southern culmination of the Zinc Creek/Lil Sore Creek trough of mine argillite. In lower Zinc Creek, thick phyllite breccia capped by heterolithic debriite underlies strongly sulfidic mine argillite (figs. 10, 11), with meter-scale intervals containing 30 to 40 percent laminated pyrite with associated barite. This facies of argillite is lithologically identical to mineralized slaty argillite in the mine stratigraphy. Underlying crystalline-carbonate cemented debriite is also sulphidic with trace to minor disseminated chalcopyrite. In places, the debriite is wholly replaced by crystalline carbonate-barite lithologically similar to dolomitic massive argillite hosting white ores in the mine series.



Figure 10. Basal Hyd Group phyllite breccia exposed in upper Zinc Creek.



Figure 11. Basal Hyd Group heterolithic debriite exposed in lower Zinc Creek.

Lil Sore Creek

The mine argillite/phyllite breccia contact in lower Zinc Creek extends northward into argillite/phyllite debriite following the Lil Sore drainage (fig. 12). Like Zinc Creek, Lil Sore Creek is geochemically anomalous, attributed to the fact that this stream course runs along the basal argillite/debriite contact. Geochemical sampling surveys carried out over the Lil Sore mine argillite trough also identify weak sulfide mineralization related to gabbro sills in argillite well above the basal contact.

A-Road Barite

This roadside outcrop exposes a baritic chert horizon occurring near or at the contact between quartz schist and very highly sheared black phyllite. A strongly carbonatized gabbro sill intrudes the immediate contact. This prospect may be a baritic member of the Pybus Formation or demark the distal tail-end of the Greens Creek ore horizon.

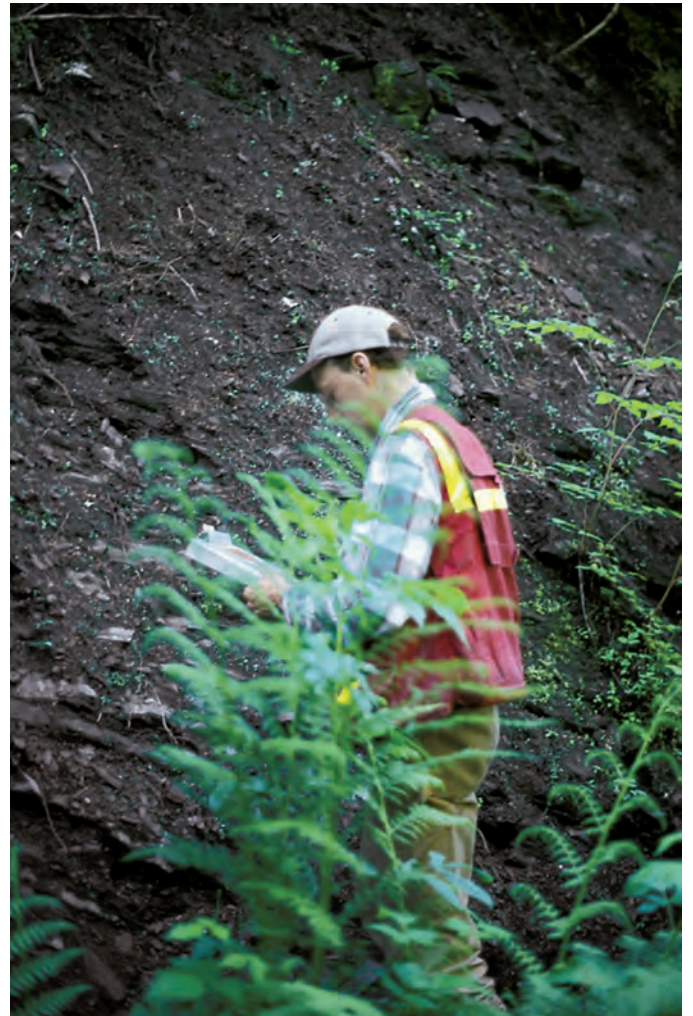


Figure 12. Examining mine argillite exposed in Lil Sore Creek.

Metallogeny

Although the high-grade Zn-Pb-Ag-Au-Ba ores at Greens Creek are similar to Kuroko-type volcanogenic massive sulfide (VMS) deposits, and the mine is located in an island arc system, the absence of associated felsic volcanics argues against any direct application of a Kuroko-VMS model. Similarly, although the metal signatures at Greens Creek are also consistent with shale-hosted sedimentary-exhalative (SEDEX) mineralization of the Mount Isa type, application of the model is made problematic by the juvenile arc setting at Greens Creek—SEDEX mineralization is generally held to relate to intercontinental to continental-margin rift settings. Based on the foregoing overview of the regional geological setting and of the deposit itself, it is here proposed that Greens Creek is a unique type of polymetallic sulfide mineralization, with the ores being essentially SEDEX in origin but linked to rifting within a juvenile arc system.

The most unusual feature of the immediate host-rock stratigraphy at Greens Creek is the evidence it presents for a 150-Ma time gap between the origin of the Retreat greenstone, protolith to mine phyllite, and the deposition of polymetallic ores at the base of the mine argillite. This time gap may be attributed to uplift of the Retreat Group after deposition of the Lower Permian Pybus Formation, accounting for the occurrence of chert pebble conglomerates below the Upper Triassic zinc-lead-silver-gold ores. These lag deposits represent the weathering of the Pybus Formation cover sequence. The absence of the full Cannery Formation at the mine suggests that the site of mineralization may have been a mid-Permian high, with uparched Retreat greenstone being overlapped only by impure dolomitic cherts capping the Cannery Formation regionally.

The ongoing conodont dating program of mine argillite has confirmed that the Greens Creek ore was deposited at 220.7 ± 4.4 Ma at the Carnian/Norian transition (chap. 11). This age, falling between the Carnian-age Nikolai flood basalts in Wrangellia and the Norian-age Hyd flood basalts in Alexandria, is key for linking arc rifting to the effects of the Nikolai plume. The thinness of juvenile back-arc crust may account for the association of Greens Creek ore with massive serpentinite. Serpentine emplacement is intimately associated with dewatering along growth-fault structures that controlled deposition of the mine argillite. There is a strong spatial relationship between the serpentinite sheeting and the wholesale hydrothermal alteration of Retreat greenstone to mine phyllite. Occurrence of footwall mine phyllite breccia and debris deposits irrefutably ties the host mine argillite stratigraphically to altered Retreat Group greenstone substrate. The green carbonate clasts developed from altered serpentinite, which are common in basal Hyd phyllite breccia/debriite units, indicate that the serpentinite must have (a) been present in the controlling growth-fault structures, (b) participated in fault-focused hydrothermal alteration, and (c) been exposed on fault scarps prior to ore deposition. More study is needed to address the origin of the associated serpentinite and its function in fluid evolution. Certainly the widespread occurrence of barian mariposite in green carbonate altered serpentinite ties this

alteration to the baritic replacement ores hosted in footwall mine phyllite. The similarity of this green carbonate to that occurring in the California Mother Lode mesothermal gold district is striking—so much so, in fact, that one wonders if the Greens Creek ores could in some fashion be a surface manifestation of a mesothermal gold system at depth, perhaps in some way accounting for its richness in precious metals.

At Greens Creek, the host mine argillite overlies massive crystalline barite-carbonate bodies developed in part by hydrothermal replacement of mine phyllite; these bodies locally comprise white ores. The occurrence of such ores low in a mineralized system capped by stratiform high-grade black ores with the same metal signature strongly suggests that the ores formed proximally within an environment of active hydrothermal venting. The fact that the stratiform ores were deposited at the base of a considerable thickness of anoxic black argillite interlayered with thin dolomite beds indicates that they represent initial deposits related to marine inundation of restricted, hydrothermally active trough environments at the time of rift collapse. The widespread occurrence of growth-fault breccia and debriite signifies considerable mass wasting from hydrothermally altered fault scarps prior to mine argillite deposition. The evidence thus points to hydrothermal fluid expulsion in a dynamic growth-fault-controlled depositional regimen. Fault control is clearly indicated by the fact that the Greens Creek ore horizon coincides with a “silica rock” structural marker that extends from the mine site for several kilometers and runs the length of Mammoth Ridge. Farther north, in the Zinc Creek/Lil Sore Creek trough of mine argillite, this same structural/stratigraphic position is occupied by considerable thicknesses of phyllite breccia and debriite, indicating preservation of the surficial “depositional” growth-fault environment.

Both mine phyllite and the related phyllite breccia/debriite deposits are locally replaced by siliceous dolomite variably rich in pyrite and barite. This “hydrothermal dolomite” may have kinship to footwall copper orebodies that accompany several large SEDEX deposits, suggesting that yet undiscovered copper ores may well occur deeper in the Greens Creek system. The debriite deposits themselves are cemented by crystalline carbonate and zones of quartz-pyrite-ankerite-barite, indicating dynamic hydrothermal plumbing. Primary hydrothermal textures are common in the overlying stratiform ores as well. Porous-textured framboidal pyrite forming massive centers of mineralization is variably recrystallized into compact euhedral forms. Analytical work reveals that the most primitive porous pyrite species coexisting with colloform sphalerite and galena are enriched in arsenic-antimony-silver-gold (Bennett, 1999). Perhaps some form of zone refining of both precious and semiprecious metals toward the margins of growing framboidal pyrite mounds was instrumental in concentrating the unusually high grade zinc-lead-silver ores. To what extent recrystallization was induced by heat buildup due to capping of the hydrothermal system and to what extent it is related to the Late Cretaceous metamorphic overprint has yet to be determined. The Greens Creek ores have certainly not undergone complete metamorphic

recrystallization since they retain many original depositional textural features. Nevertheless, some features of the deposit are best accounted for by secondary remobilization during metamorphic and later structural overprinting. In particular, the erratic distribution of the ruby silvers and of silver-rich electrum signifies marked precious metal mobility.

Conclusion

Geological mapping in the Greens Creek district broadly supports a dynamic growth-fault-controlled depositional environment for the Greens Creek ores. The specific contact relationships within the immediate mine stratigraphy are subject to dynamic change. Adjacent Retreat greenstones may show no hydrothermal alteration, altered contacts have been subjected to variable mass wasting, and the basal “sooty” facies of mine argillite is commonly missing. It seems probable that the high-grade stratiform ores represent the front of an anoxic marine transgression into dynamic restricted trough settings. The ores ponded against hydrothermally active fault scarps plumbed by serpentinite accompanied by limited sheeted gabbro dike. The serpentinite and gabbro dike association suggests development of active igneous fissure segments at the inception of Late Triassic rifting. The Killer Creek serpentinite body may have provided a sustained heat source within uparched Retreat Group greenstone essentially denuded of its Permian-Carboniferous cover. In contrast to classic SEDEX systems, the Greens Creek setting is therefore one in which “igneous” heat may have had a more formative function in driving a dynamic hydrothermal fluid cell, perhaps initiating a component of fluid recharge from surface, above and beyond discharge of formational brine. That the Greens Creek ores occupy the profound regional mid-Permian to Late Triassic unconformity that characterizes the geological record on Admiralty Island suggests that the Greens Creek fluid reservoir may well have tapped evaporitic brines from the surface.

Acknowledgment

This chapter benefited from constructive reviews by Sue Karl and David Brew.

References Cited

- Bennett, Cora, 1999, A SIMS study of framboidal pyrite at the Greens Creek mine, southeast Alaska: Unpublished Bachelor of Science thesis, University of Western Ontario, London, Canada, 87 p.
- Berg, H.C., Jones, D.L., and Coney, P.J., 1978, Pre-Cenozoic tectonostratigraphic terranes of southeastern Alaska and adjacent areas: U.S. Geological Survey Open-File Report 78-1085, 2 sheets, scale 1:1,000,000.
- Brew, D.A., Himmelberg, G.R., Loney, R.A., and Ford, A.B., 1992, Distribution and characteristics of metamorphic belts in the southeastern Alaska part of the North American Cordillera: *Journal of Metamorphic Geology*, v. 10, p. 465–482.
- Carter, Claire, 1977, Age of the Hood Bay Formation, Alaska, *in* Sohl, N.F., and Wright, W.B., eds., *Changes in stratigraphic nomenclature by the U.S. Geological Survey, 1976*: U.S. Geological Survey Bulletin 1435-A, p. A117–A118.
- Gardner, M.C., Bergman, S.C., Cushing, G.W., Mackevett, E.M., Plafker, G., Cambell, R.B., McClelland, W.C., and Mueller, P.A., 1988, Pennsylvanian pluton stitching of Wrangellia and the Alexander terrane, Wrangell Mountains, Alaska: *Geology*, v. 16, p. 967–971.
- Gehrels, G.E., and Saleeby, J.B., 1987a, Geological framework, tectonic evolution and displacement history of the Alexander terrane: *Tectonics*, v. 6, p. 151–173.
- Gehrels, G.E., and Saleeby, J.B., 1987b, Geology of southern Prince of Wales Island, southeastern Alaska: *Geological Society of America Bulletin*, v. 98, p. 123–137.
- Haeussler, P.J., Karl, S.M., Mortensen, J.K., Layer, Paul, and Himmelberg, G.R., 1999, Permian and mid-Cretaceous deformation of the Alexander terrane on Admiralty and Kupreanof Islands, southeastern Alaska: *Geological Society of America Abstracts with Programs* v. 31, no. 6, p. A–60.
- Karl, S.M., Haeussler, P.J., Layer, P., Soja, C., and Himmelberg, G.R., 1999a, Incremental Paleozoic amalgamation of the composite Alexander/Wrangellia/Taku terrane, southeast Alaska, *in* Evenchick, C.A., Woodsworth, G.C., and Jorgens, R., eds., *Terrane Paths 99—Circum-Pacific Terrane Conference, Vernon, British Columbia, 1999*, Abstracts with Program: Vancouver, Geological Survey of Canada, p. 44.
- Karl, S.M., Haeussler, P.J., Mortenson, J.K., Layer, P., Savage, N., Wardlaw, B., Harris, A., Murchey, B., and Blome, C., 1999b, New stratigraphic and isotopic constraints on the depositional and deformational history of the Alexander Terrane, southeastern Alaska: *Geological Society of America Abstracts with Programs*, v. 31, no. 6, p. A–68.
- Lathram, E.H., Pomeroy, J.S., Berg, H.C., and Loney, R.A., 1965, Reconnaissance geology of Admiralty Island Alaska: U.S. Geological Survey Bulletin 1181-R, 48 p.
- Loney, R.A., 1964, Stratigraphy and petrography of the Pybus-Gambier Bay area, Admiralty Island, Alaska: U.S. Geological Survey Bulletin 1178, 100 p.
- Reich, Michael, 1996, Ultramafic/mafic protoliths to massive carbonate replacement bodies at the Greens Creek Zn-Pb-Ag-Au deposit, Southeast Alaska: Unpublished Bachelor of Science thesis, University of Western Ontario, London, Canada, 120 p.

Richards, M.A., and Jones, D.L., 1991, A mantle plume initiation model for the formation of Wrangellia (and other flood basalt plateaus): Geological Society of America Abstracts with Programs, v. 23, no. 2, p. 92.

Warne, J.E., and Kuehner, H-C., 1998, Anatomy of an anomaly—The Devonian catastrophic Alamo impact breccia of southern Nevada, *in* Ernst, W.G., and Nelson, C.A., eds., Integrated earth and environmental evolution of the southwestern United States: Boulder, Colo., Geological Society of America, p. 80–110.

The Airborne Geophysical Survey of the Greens Creek Area

By James Fueg

Chapter 5 of

**Geology, Geochemistry, and Genesis of the Greens Creek Massive
Sulfide Deposit, Admiralty Island, Southeastern Alaska**

Edited by Cliff D. Taylor and Craig A. Johnson

Professional Paper 1763

**U.S. Department of the Interior
U.S. Geological Survey**

Contents

Abstract.....	109
Introduction.....	109
Geology.....	109
Physical Properties.....	109
Airborne Survey Parameters	110
Results	111
Conclusions.....	121
Reference Cited.....	121

Figures

1. Total magnetic field	112
2. Magnetics—calculated vertical gradient.....	113
3. 800-hertz apparent resistivity	114
4. 4,000-hertz apparent resistivity	115
5. Topography	116
6. Radiometrics—Potassium	117
7. Radiometrics—Thorium	118
8. Radiometrics—Uranium.....	119
9. Radiometrics—Potassium over thorium.....	120

Tables

1. Resistivity and chargeability of Greens Creek area rocks.....	110
2. Airborne geophysical survey parameters.....	110

The Airborne Geophysical Survey of the Greens Creek Area

By James Fueg

Abstract

An airborne geophysical survey of the Greens Creek massive sulfide deposit was flown in 1996 to collect magnetic, radiometric, and five frequencies of electromagnetic (EM) data. Results of a physical properties study conducted prior to the survey showed the mineralization to be strongly conductive, and with the lithologies showing a wide range in both conductivity and susceptibility.

The magnetic response of the area was dominated by the highs associated with the ultramafic units, while the EM data were useful in mapping out the argillite/phyllite (low/high resistivity) contact. Large numbers of EM anomalies were picked from the data, but none of those checked corresponded to mineralization. The count rates of the radiometric data were extremely low, and the effects of topography dominated the response. The survey provided valuable structural and stratigraphic data, but selection of valid exploration targets in this environment cannot be done using geophysics alone.

Introduction

A combined helicopter-borne electromagnetic (EM), magnetic, and radiometric survey was flown over the Greens Creek area in September 1996. The objective of the survey was twofold:

1. To attempt direct detection of additional Greens Creek-style mineralization.
2. To assist in the mapping of stratigraphy and structure throughout the area.

Results have shown that the magnetic and apparent resistivity maps produced from the survey were probably the most useful products produced. A large number of conductors were identified in the survey, mostly formational conductors associated with the more graphitic argillite units.

Geology

Greens Creek is a high-grade massive sulfide deposit with a global resource that is estimated to be 21.9 million

metric tonnes of ore at 13.9 percent zinc, 5.1 percent lead, 4.8 grams per metric tonne gold, and 599 grams per metric tonne silver at zero cutoff (chap. 2). The deposit can be regarded as a hybrid volcanogenic massive sulfide/sedimentary exhalative (VMS/SEDEX) deposit, as it exhibits characteristics of both categories of deposit (Taylor and others, 1999; chap. 15).

Host rocks to the Greens Creek deposit lie within a 600-km-long belt of Triassic-aged conglomerates, limestones, marine clastic sediments, tuffs and intercalated mafic pyroclastics, and pillowed flows that form the eastern margin of the Alexander terrane. Deposits within this belt include Greens Creek and Windy Craggy (chap. 2). The deposit is located at the contact between a footwall sequence consisting predominantly of various categories of phyllite and a hanging-wall sequence of massive and slaty black argillites (chap. 6). Deformation in the area is extremely complex and involves at least four periods of folding, one of semiductile shearing, and two of faulting (chap. 7).

Ore lithologies at Greens Creek are broken into two main groups of massive sulfide ores and semimassive or gangue-rich "white" ores. The massive ores contain greater than 50 percent sulfides and consist of massive fine- to very fine grained ore in which base-metal sulfides are greater than pyrite and massive medium- to very fine grained pyrite-rich ore in which pyrite predominates. The white ores are a group of mineralized lithologies that contain less than 50 percent sulfides and are defined by their principal gangue mineral. There are three types: white carbonate ore, white siliceous ore, and white baritic ore (chap. 6).

Physical Properties

During 1996, 18 rock samples from the Greens Creek area, including both drill-core and hand samples, were sent to Zonge Engineering and Research Organization for physical properties testing. Samples were tested for the induced polarization response (time-domain) and resistivity. The samples were vacuum impregnated with distilled water and the induced polarization measurements were made using an 8-second cycle time. The data are listed in table 1.

Table 1. Resistivity and chargeability of Greens Creek area rocks.

[ohm-m, ohm-meters; msec, millisecond]

Description	Source	Resistivity (ohm-m)	Chargeability (msec)
Massive very fine grained base-metal sulfides	Drill core	4.7	289.5
Massive fine-grained base-metal sulfides	Drill core	2.1	202.0
Massive fine-grained base-metal sulfides	Drill core	2.7	291.6
Massive fine-grained base-metal sulfides	Drill core	4.7	174.3
Pyritic semimassive sulfide	Hand specimen	20.1	44.0
Sericitic phyllite	Drill core	134	74.2
Siliceous sericitic phyllite	Drill core	191	83.0
Chloritic phyllite	Drill core	200	110.0
Mineralized sericitic phyllite	Drill core	1,446	121.8
Sericitic phyllite	Drill core	1,470	10.9
Laminated black argillite	Hand specimen	272	110.8
Slaty argillite	Drill core	9.9	117.5
Slaty argillite	Drill core	458	14.6
Slaty argillite	Drill core	572	28.0
Contorted black argillite	Hand specimen	862	65.5
Baritic sericitic schist	Hand specimen	610	23.4
Chloritic serpentinite	Drill core	1,604	6.3
Chloritic serpentinite	Drill core	1,187	2.9

Analysis of the results shows that the massive sulfide samples are strongly conductive (less than 5 ohm-m), the argillites vary from conductive to resistive (9 to 860 ohm-m) depending on the amount of shearing and carbon, and the phyllites range from resistive to highly resistive (130 to 1,600 ohm-m). See table 1.

These results initially suggested to us that not only should it be possible to directly detect Greens Creek-style zones of massive sulfide mineralization using airborne EM (provided the zones are large enough, not too deep, and not masked by other conductive material such as graphitic argillite), but there should also be sufficient resistivity contrast between many of the Greens Creek-area lithologies to allow them to be discriminated in the apparent resistivity maps produced from the EM data.

Susceptibility measurements on core and hand samples were also done at Greens Creek using a hand-held Exploranium KT-9 susceptibility meter. As expected, results showed that the more mafic rocks (serpentinite, gabbro, chloritic phyllite) have susceptibilities at least one or two orders of magnitude greater than the more silicic units (silicic phyllite, chert), the dolomitic units, the argillites, and also the massive sulfides. Clearly, the Greens Creek ore would not be directly detectable using aeromagnetic data, and the contrast between some of the more important lithologies in the area is not as well defined as in the resistivities. The results nevertheless suggested that aeromagnetic data would be of use in mapping lithologies in the area.

The possibility of elevated potassium levels in some of the altered volcanics around Greens Creek suggested that radiometric data might be of use in mapping these units. Obvious concerns existed with the high rainfall, the dense nature of the vegetation cover, and the amount of swamp-covered areas that could potentially mask the radiometric response of the various lithologies. However, it was relatively inexpensive to add this technique to the planned survey.

Airborne Survey Parameters

Based on the previous analysis, it was decided that a combined airborne electromagnetic, magnetic, and radiometric survey should be flown over the property. The contract to fly the survey was awarded to Aerodat, and it was completed over a 5-day period in late September 1996. A total of 1,227 line kilometers of data were collected. Some of the data over the northern part of the Mansfield Peninsula remain proprietary and have not been included in this report. The survey parameters and instrumentation are shown in table 2.

Table 2. Airborne geophysical survey parameters.

[m, meter; EM, electromagnetic; Hz, hertz; GPS, global positioning system]

Survey elements	Parameter or instrumentation
Line direction	070°
Line spacing	200 m (100 m over immediate GC area)
Survey altitude	60-m crystal, 45-m magnetometer, 30-m EM
Survey aircraft	Aerospatiale SA 315B Lama
EM system	Aerodat 5 frequency; coplanar 865, 4175, 32k Hz; coaxial 935, 4,600 Hz @ 10 Hz
Magnetometer	Scintrex H8 Cs sensor @ 10 Hz
Spectrometer	Exploranium GR-820 (16.81) recording 4 channels @ 1 Hz (TC, K, U, Th)
Navigation	Differential GPS

Results

Figures 1 through 9 are images of the various data sets collected, including total magnetic field, calculated vertical gradient of the magnetic field, 4,000-Hz and 800-Hz apparent resistivity, topography, the potassium, thorium, and uranium spectrometer channels, and a ratio of the potassium and thorium spectrometer channels. All images were gridded at a 50-m cell size and sunshaded at an inclination of 45° from the northeast.

The magnetic response of the Greens Creek area is dominated by a series of circular and irregularly shaped magnetic highs (with amplitudes up to 500 nanoteslas) immersed within a relatively quiet background. Most of the highs correspond with mapped mafic and ultramafic rock units. A predominantly northwest trending structural grain is visible in the magnetic data, and several structures offsetting magnetic features can be identified in the data. North of Hawk Inlet the character of the data changes substantially and consists primarily of northwest-trending linear magnetic features.

Comparison of the apparent resistivity data with mapped geology (chap. 4) reveals a distinct correlation between areas

of low resistivity and mapped argillite and more resistive areas and mapped phyllite. In the mine area the main phyllite/argillite contact can clearly be tracked in the resistivity data. The Greens Creek mineralization itself is not visible in the data, primarily due to the depth of burial of the bulk of the ore. Analysis of the EM profile data by Aerodat processing staff resulted in the picking of about 3,100 "EM anomalies." The bulk of these occur within the low-resistivity zones associated with the argillites and probably represent more graphitic zones within the metasediments. The large number of anomalies made impractical the ground followups of all the identified bedrock conductors, but field visits to some of the best-ranked conductors did not result in any obvious targets being identified.

The average count rate for all four channels of the radiometric data is extremely low. The radiometric response is dominated by the effects of topography, with most anomalous areas correlating to topographic highs. These are zones of little or no vegetation, in strong contrast to the heavily forested slopes and muskeg-covered lowlands. Count rates are generally so low that even ratio maps such as potassium/thorium show little consistency outside the topographic highs.

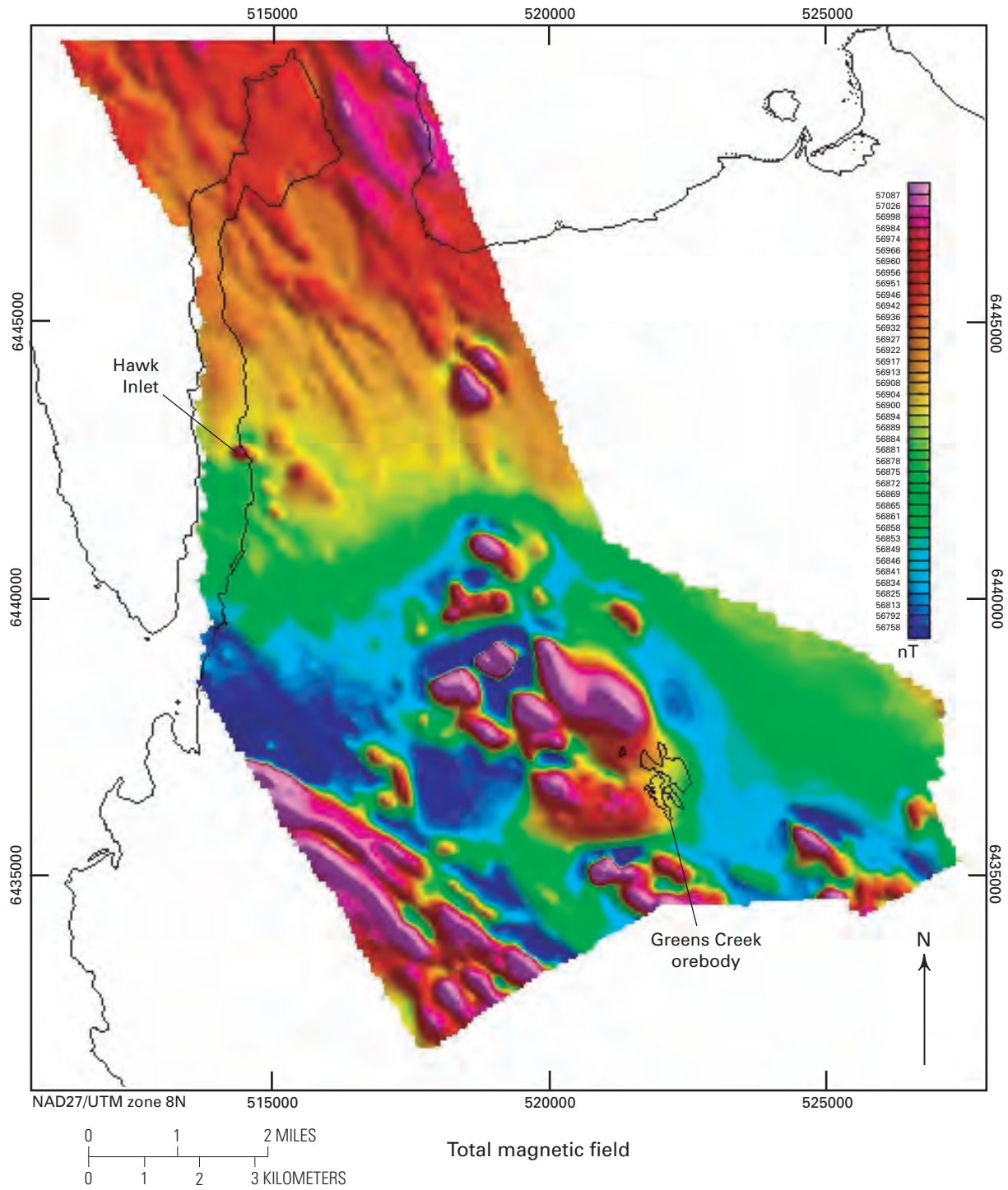


Figure 1. Total magnetic field.

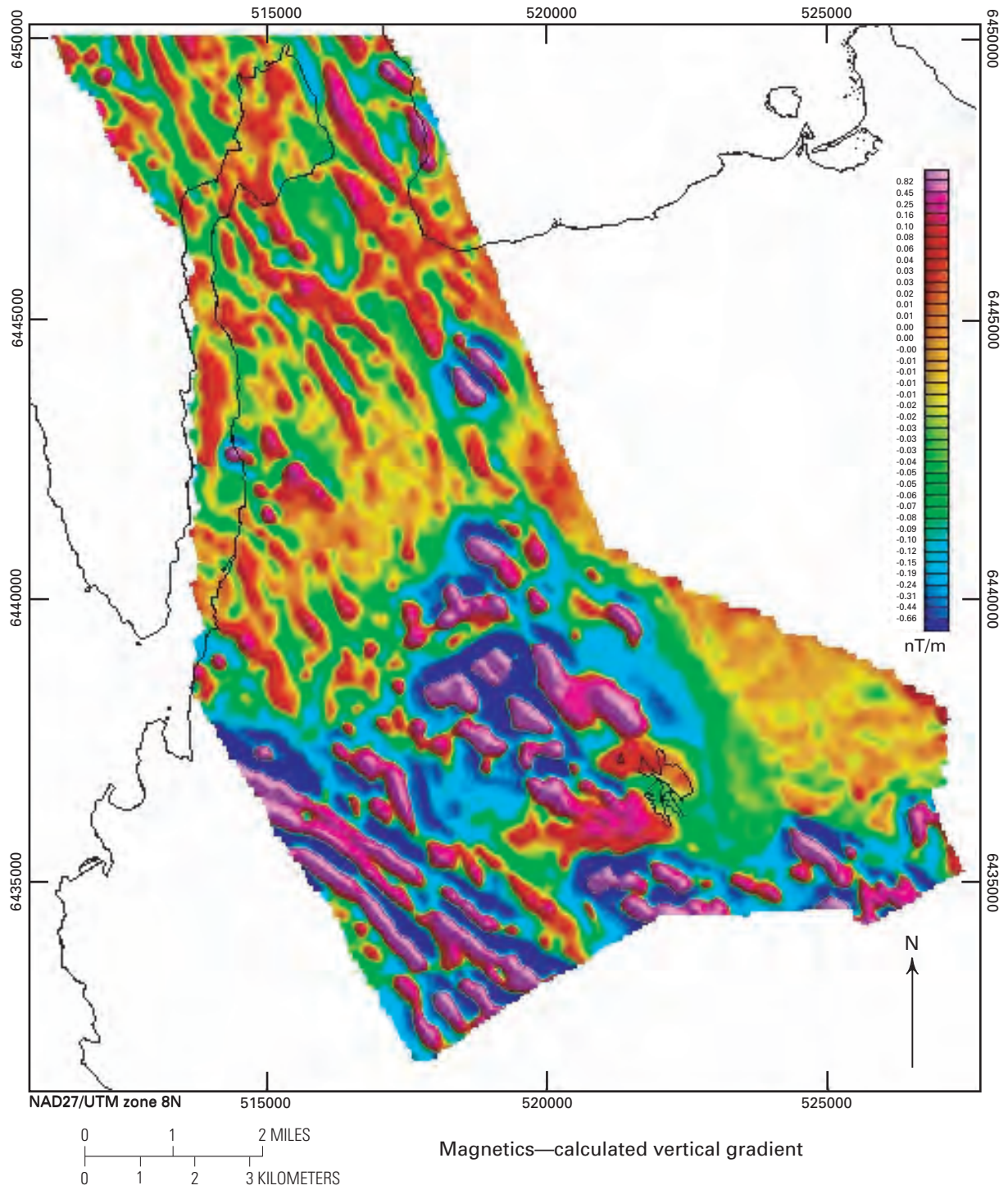


Figure 2. Magnetics—calculated vertical gradient.

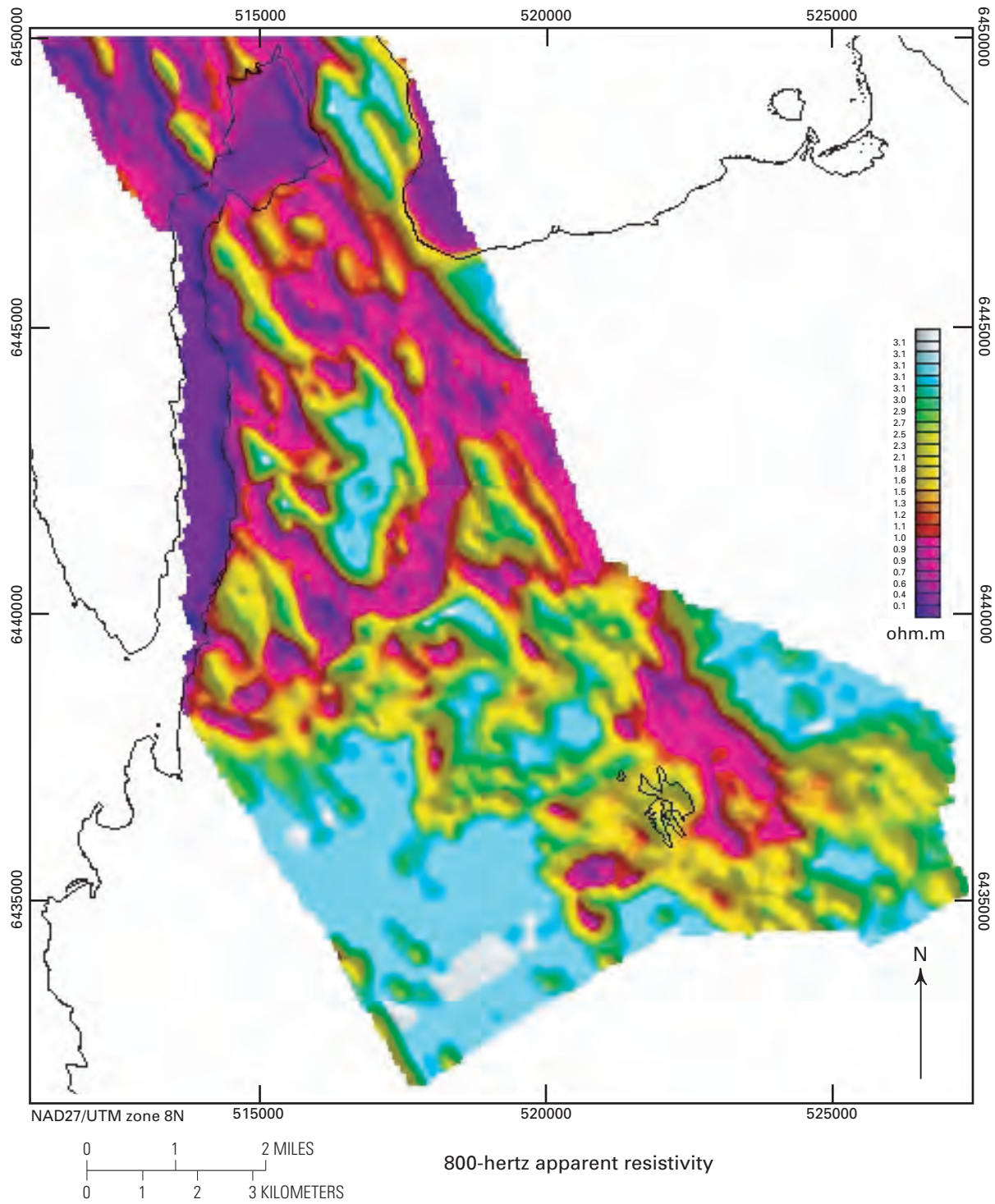


Figure 3. 800-hertz apparent resistivity.

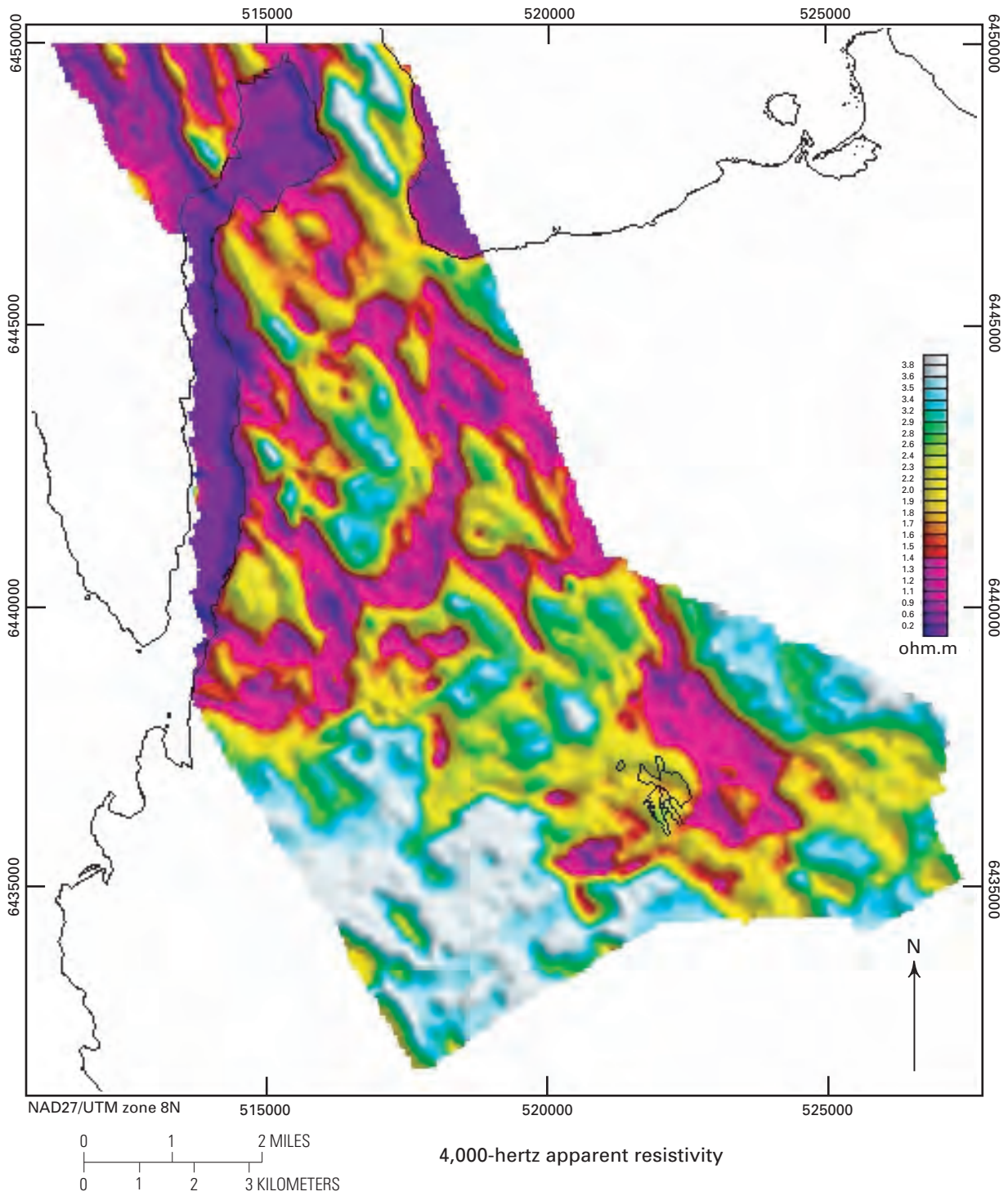


Figure 4. 4,000-hertz apparent resistivity.

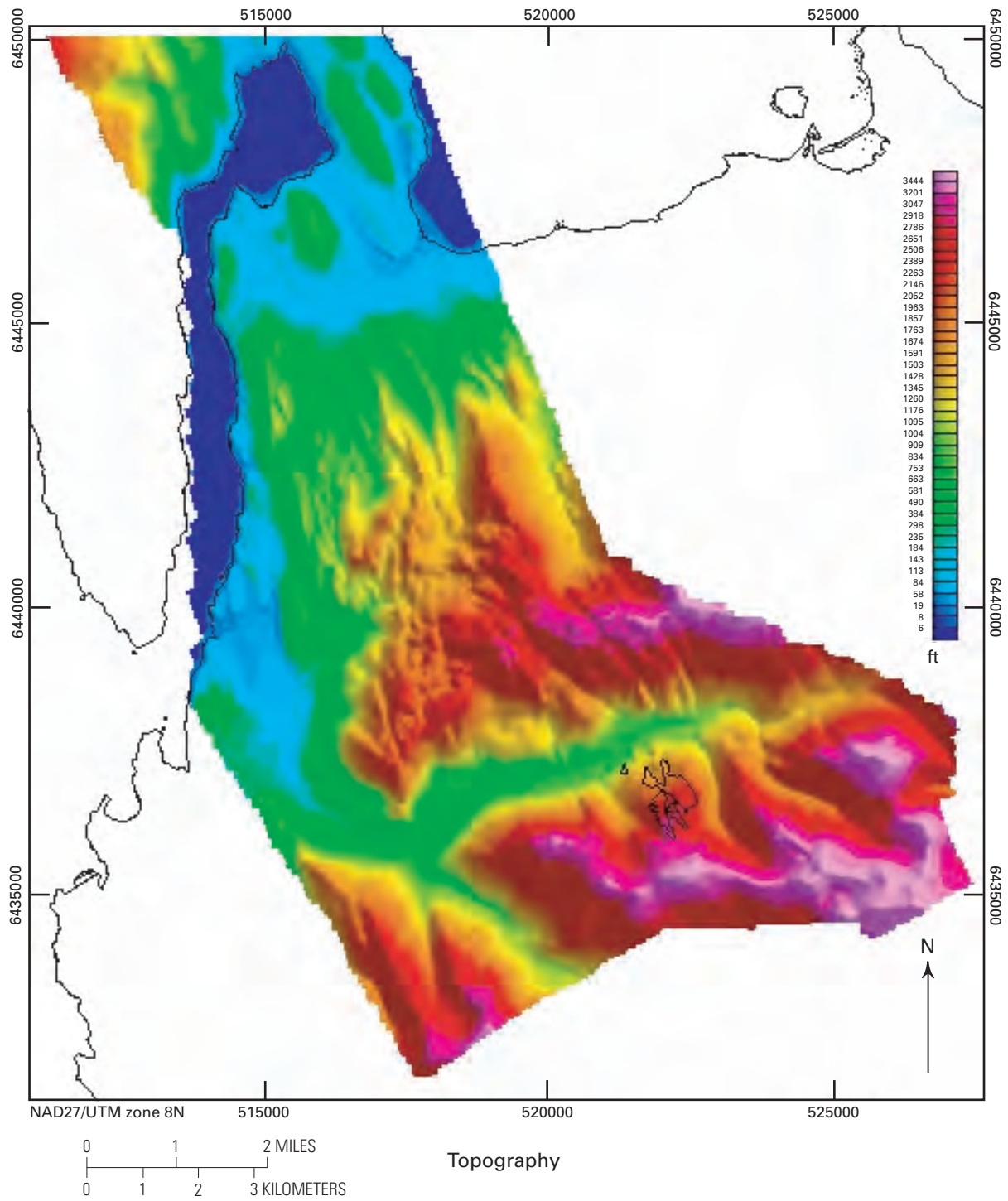


Figure 5. Topography.

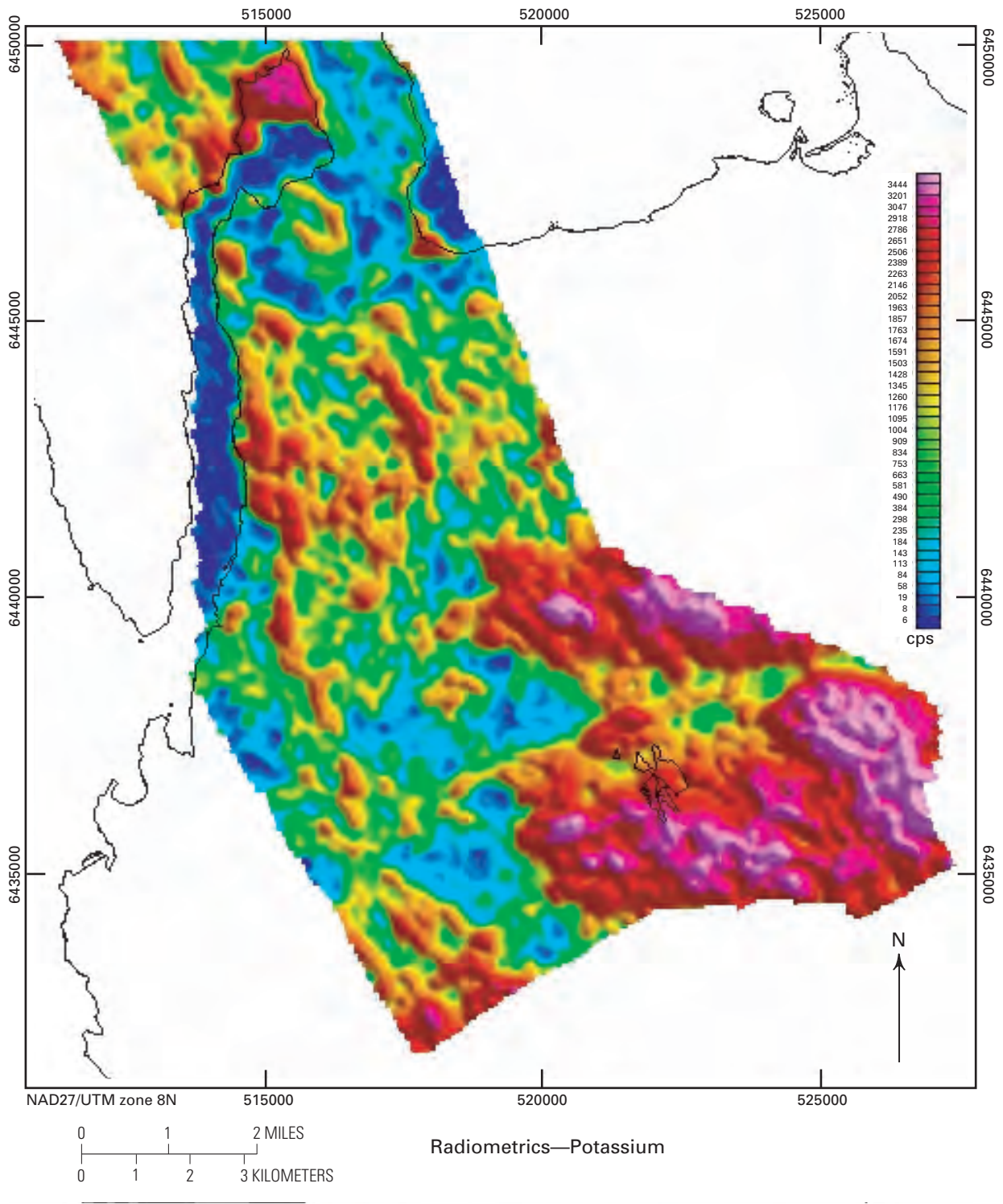


Figure 6. Radiometrics—Potassium.

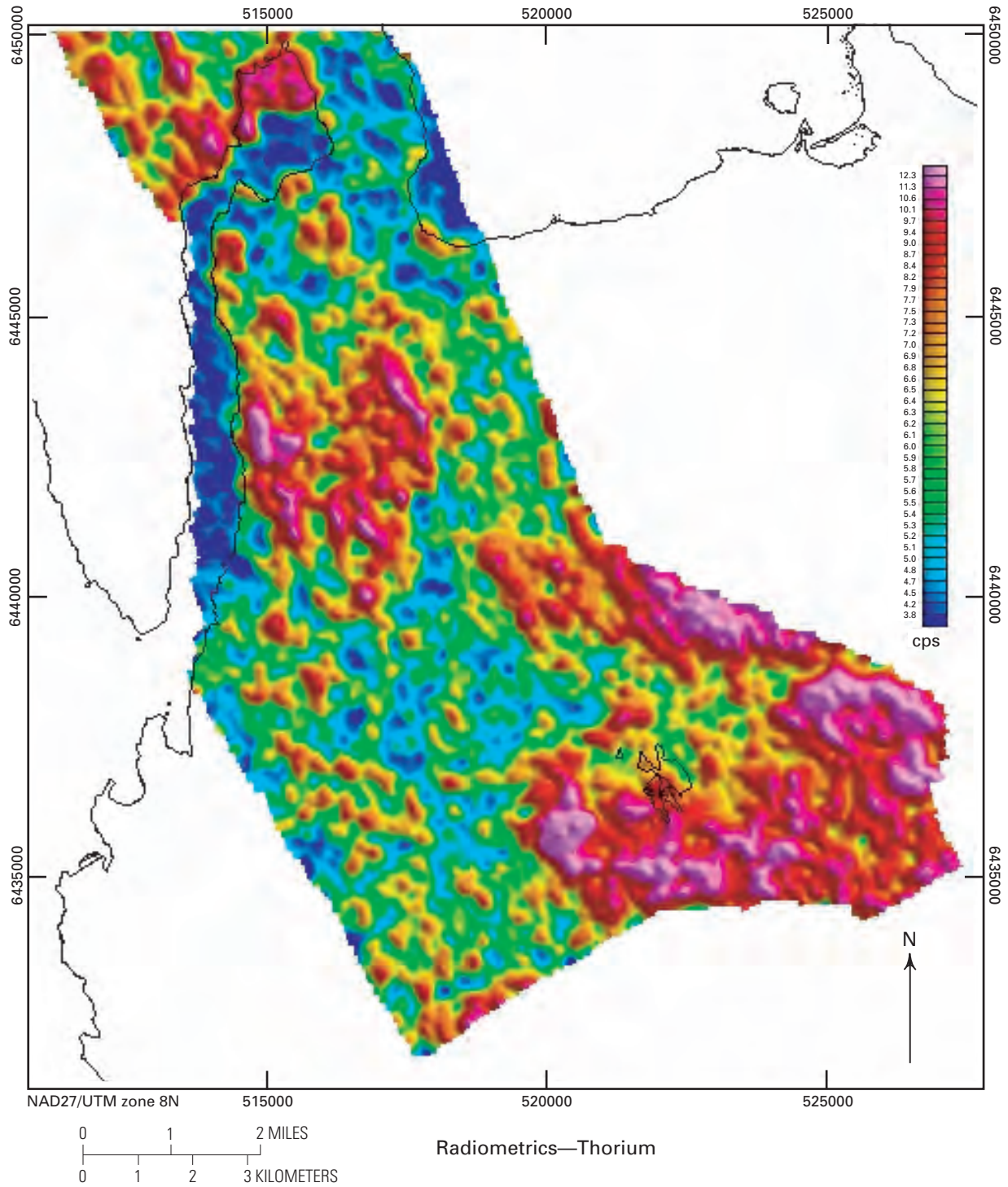


Figure 7. Radiometrics—Thorium.

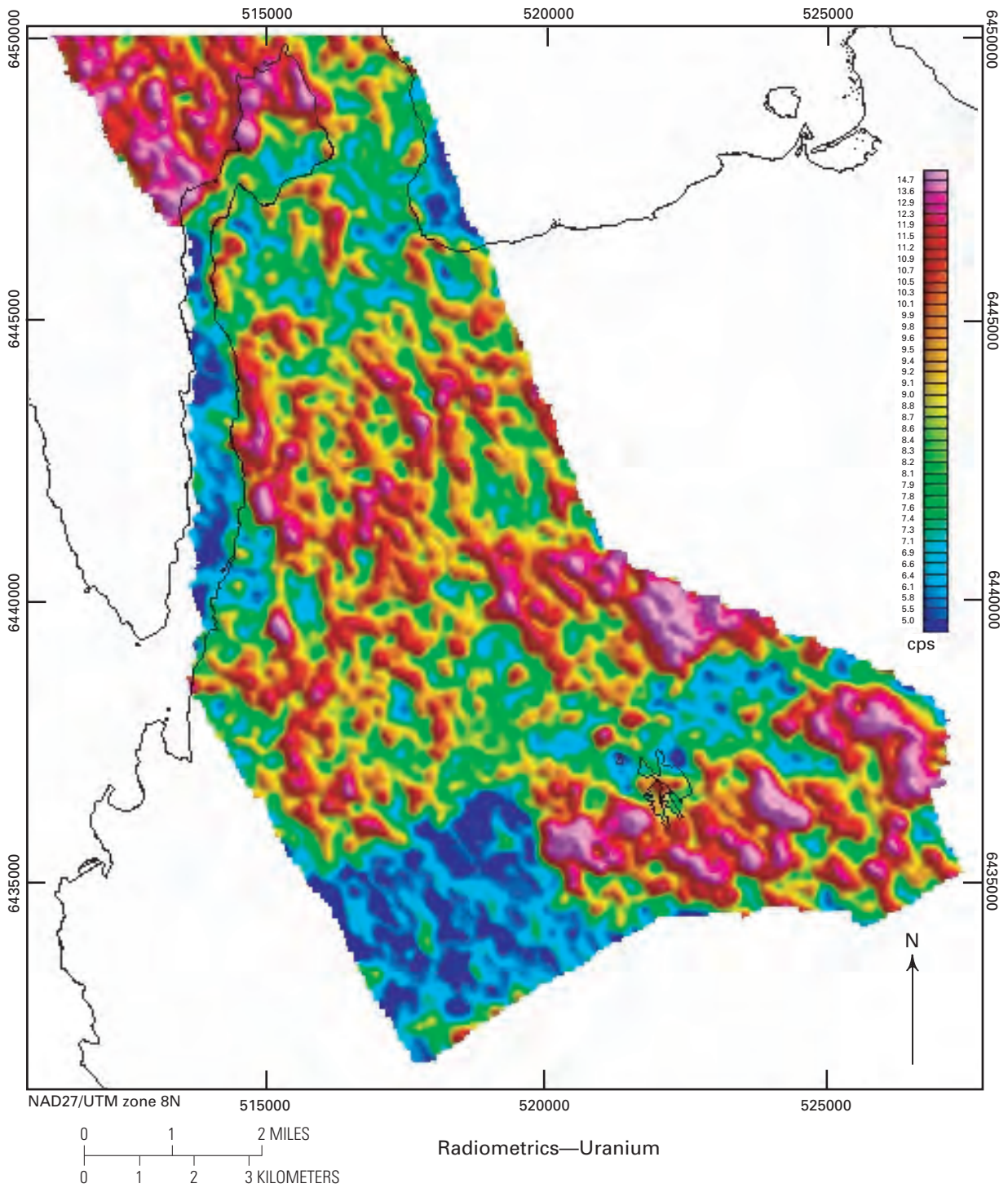


Figure 8. Radiometrics—Uranium.

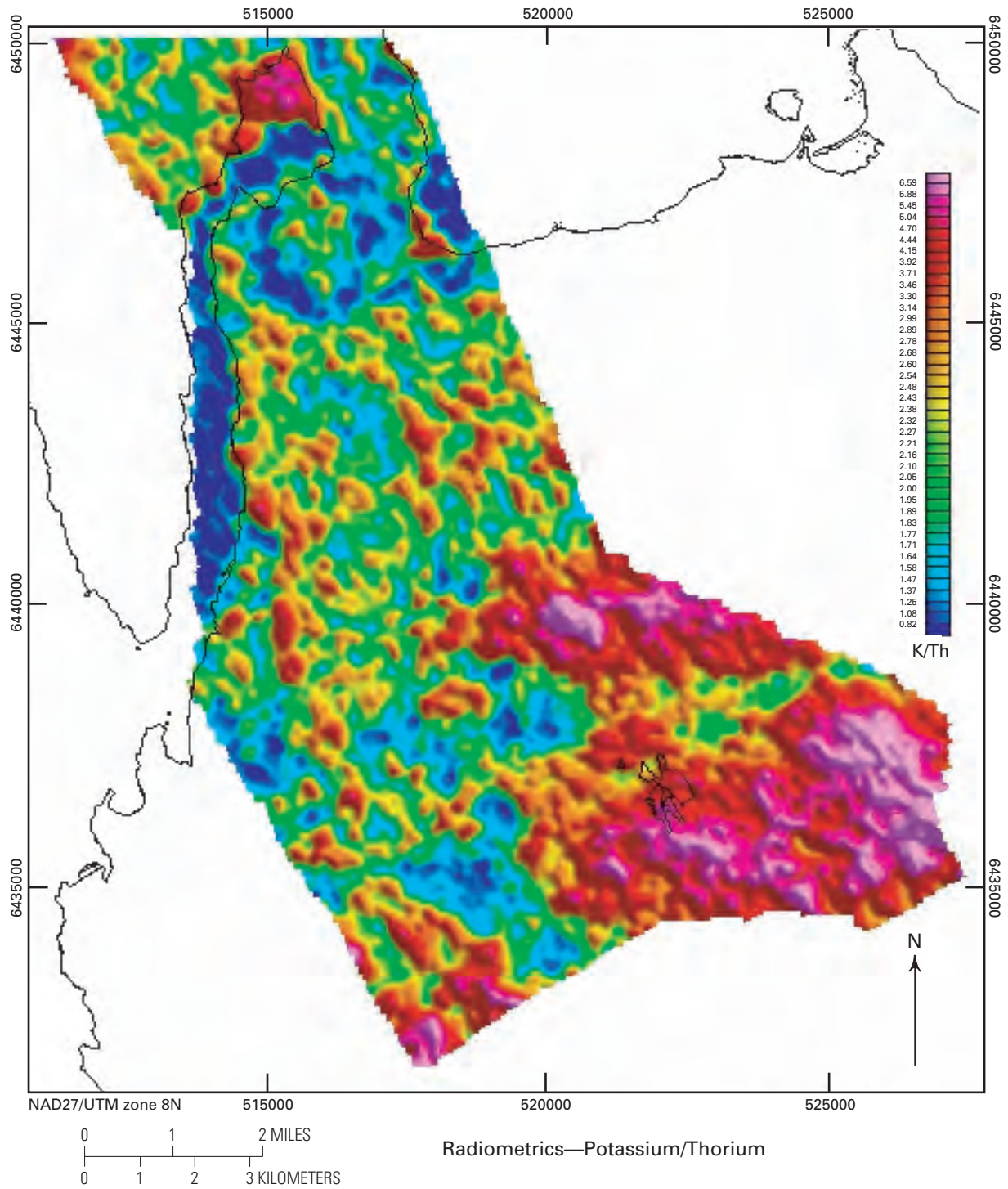


Figure 9. Radiometrics—Potassium over thorium.

Conclusions

The Greens Creek airborne geophysical survey was successful in providing valuable stratigraphic and structural information about the area. The most useful products of the survey were the apparent resistivity and magnetic maps produced, as may be expected given the range of physical properties in table 1. The radiometric data did not provide much useful information, primarily due to the effects on the data of ground cover, which dominated the response. The EM data produced a large number of anomalies, most of which are associated with graphitic metasediments. Identification of valid exploration targets within these conductive zones cannot be done using geophysics alone.

Reference Cited

Taylor, C.D., Newkirk, S.R., Hall, T.E., Lear, K.G., Premo, W.R., Leventhal, J.S., Meier, A.L., Johnson, C.A., and Harris, A.G., 1999, The Greens Creek deposit, southeastern Alaska—A VMS-SEDEX hybrid, in Stanley, C.J., and others, eds., *Mineral deposits—Processes to processing*: Rotterdam, Balkema, v. 1, p. 597–600.

Geology and Metal Zoning of the Greens Creek Massive Sulfide Deposit, Southeastern Alaska

By Cliff D. Taylor, Andrew W. West, Kerry G. Lear, Tim E. Hall, and
John M. Proffett

Chapter 6 of

**Geology, Geochemistry, and Genesis of the Greens Creek Massive
Sulfide Deposit, Admiralty Island, Southeastern Alaska**

Edited by Cliff D. Taylor and Craig A. Johnson

Professional Paper 1763

**U.S. Department of the Interior
U.S. Geological Survey**

Contents

Abstract.....	125
Introduction.....	125
Description of the Wall Rocks	127
Stratigraphic Footwall.....	127
Breccia and Conglomeratic Rocks of the Footwall and Hanging Wall.....	129
Stratigraphic Hanging Wall.....	129
Description of the Ores.....	130
Geometry of the Ore Zones	132
East Orebody.....	132
West Orebody.....	132
Central West.....	132
9A.....	132
Northwest West.....	133
5250.....	133
Southwest Orebody.....	134
200 South.....	134
Metal Zoning.....	135
References Cited.....	136

Figures

1. Map of southeastern Alaska showing the location of the Greens Creek mine	127
2. Geologic cross section through the Lower Southwest ore zone, which lies at the contact between phyllites of the stratigraphic footwall and argillites of the stratigraphic hanging wall	127
3. Schematic distribution of ore types within an individual Greens Creek orebody prior to deformation.....	130
4. Photographs of representative samples of Greens Creek ore	131
5. Surface projections of the Greens Creek ore zones	133
6. North-looking cross section showing, in black, the East, 9A, 5250, Lower Southwest, and 224 West Bench ore zones	134
7. Metal zoning observed in the core of the Central West ore zone	135

Geology and Metal Zoning of the Greens Creek Massive Sulfide Deposit, Southeastern Alaska

By Cliff D. Taylor, Andrew W. West, Kerry G. Lear, Tim E. Hall, and John M. Proffett

Abstract

The Greens Creek deposit is a series of massive sulfide bodies that lie along the contact between altered mafic-ultramafic rocks and stratigraphically overlying Upper Triassic argillites. Both the deposit and its enclosing rocks show the effects of lower greenschist facies metamorphism and multiple episodes of deformation. In the footwall, mafic rocks are enriched in silica and have abundant sericite at the ore contact; they become richer in chlorite and carbonate away from ore. Ultramafic rocks in the footwall are either serpentinized or carbonate altered. The hanging-wall argillite is massive or slaty and contains graphite, dolomite, or calcite. Locally, nongraphitic carbonate rocks are present at or near the ore contact. Geologic mapping in the underground workings and examination of drill core have revealed a common stratigraphic sequence in which white ores (less than 50 percent sulfides) give way upward to pyritic massive ores and then base-metal-rich massive ores (both greater than 50 percent sulfides).

The deposit consists of three main orebodies, East, West, and Southwest, that are themselves segmented by faults or attenuated zones that are too thin to mine. The global reserve, for a cutoff grade of zero percent metal, is estimated to be 24.2 million tons with grades of 13.9 weight percent zinc, 5.1 weight percent lead, 19.2 troy ounces per ton silver, and 0.15 troy ounce per ton gold. It is likely that continuing exploration will lead to additional discoveries that will increase the size estimate for the deposit.

Restoration of offsets along the Maki and Klaus faults, the two major ore-displacing faults, suggests that the mineralization was originally a single continuous horizon that was thickest in the Central West ore zone and thinned to the north, east, and south. The Central West zone shows a progression from a copper-iron zone against the footwall phyllites, to a zinc zone, to a zinc-lead zone, and finally a silver-polymetallic zone against the hanging-wall argillites. Similar footwall-to-hanging-wall progressions are apparent in the East and Southwest orebodies, although these orebodies are not yet completely characterized, and in some locations the metal progression appears to be different. The absence of mine-scale concentric metal zoning suggests that the Greens Creek deposit may have formed above multiple centers of hydrothermal upwelling, or a broad zone of diffuse upwelling, rather than above a single vent.

Introduction

The Greens Creek mine, which is located on Admiralty Island 29 km south of Juneau, Alaska (fig. 1), is surrounded by the Admiralty Island National Monument, an entity created in 1980 by the Alaska National Interest Land Conservation Act. The mine site is accessed by a 14-km road that leads southeast from a permanent port and camp facility at Hawk Inlet. A second road joins Hawk Inlet and Young Bay, 4 km to the north, where miners are ferried to and from Juneau.

For two decades mining activity was a joint venture between Kennecott Minerals Co. (70.27 percent), a wholly-owned subsidiary of Rio Tinto, and Hecla Mining Co. (29.73 percent), but in early 2008 Hecla acquired Kennecott Minerals' share of the operation and became sole owner. At the present time a work force numbering about 300 people mines and mills about 2,000 tons of ore per day. Mining has been by selective overhand cut and fill, drift and fill, and, most recently, long-hole stoping with ore transport to the surface by rubber-tired vehicles using ramps. Separate zinc, lead, and bulk concentrates are prepared using conventional flotation techniques, and gold is recovered using a gravitational circuit. The concentrates are loaded onto ocean-going vessels at Hawk Inlet for transportation to smelters around the world. About half the mill tailings are mixed with cement and used as back-fill in the underground workings, and the remainder is placed in a dry tailings pile near Hawk Inlet.

The Greens Creek deposit lies in a narrow belt of rift-related volcanic and sedimentary rocks that stretches the length of Admiralty Island and continues both north and south (chaps. 2, 4). The mineral deposit is stratiform and lies along the contact between Triassic argillites of the Hyd Group and stratigraphically underlying greenschist phyllites of uncertain age. Ore crops out at a locality referred to as the Big Sore kill zone. This 20-m by 40-m iron-oxide gossan was first seen from the air in 1974 by geologists investigating stream-sediment zinc anomalies. The first drill hole at the property, which was collared in 1975, contacted more than 25 m of massive sulfide material. Exploration and development activities involved numerous changes in property ownership and in the interpretation of the geology (chap. 3). The first ore was milled in 1989.

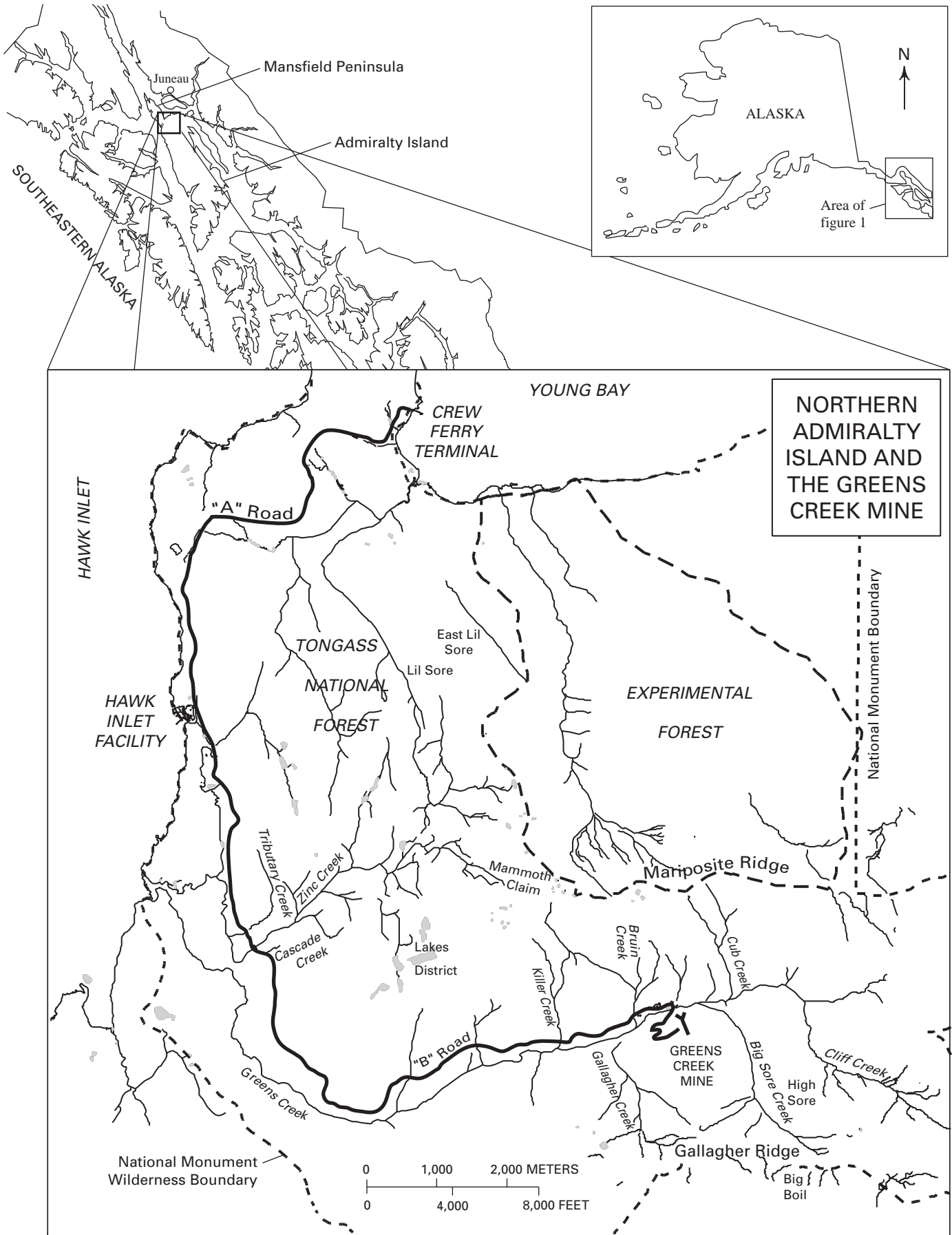


Figure 1 (facing page). Map of southeastern Alaska showing the location of the Greens Creek mine.

The purpose of this chapter is to describe the ores and their immediate wall rocks. The lithologic descriptions are based on core logging, underground and surface mapping, and limited petrographic studies that were carried out by a number of different geologists over a number of years. Information is also given on the geometry of the ore zones and on the metal zoning within them. Much of the information was first documented in reports to the Kennecott Greens Creek Mining Company or its antecedents. The structural geology referred to in this paper is described in detail in chapter 7. For more complete descriptions of the mineralogy and mineral chemistry of the ores, the reader is referred to chapter 9.

Description of the Wall Rocks

The Greens Creek ores occur at the contact between altered and metamorphosed mafic/ultramafic rocks and stratigraphically overlying argillites. Figure 2 is a geologic cross section through the Southwest orebody that serves to illustrate the stratigraphy and structure of the wall rocks.

Stratigraphic Footwall

The stratigraphic footwall to the Greens Creek mineral deposit consists of variably altered mafic to ultramafic volcanics, minor clastic sediments, and hypabyssal sills and intrusions. For the purpose of underground and surface mapping in the mine area, these rocks are classified by their metamorphic

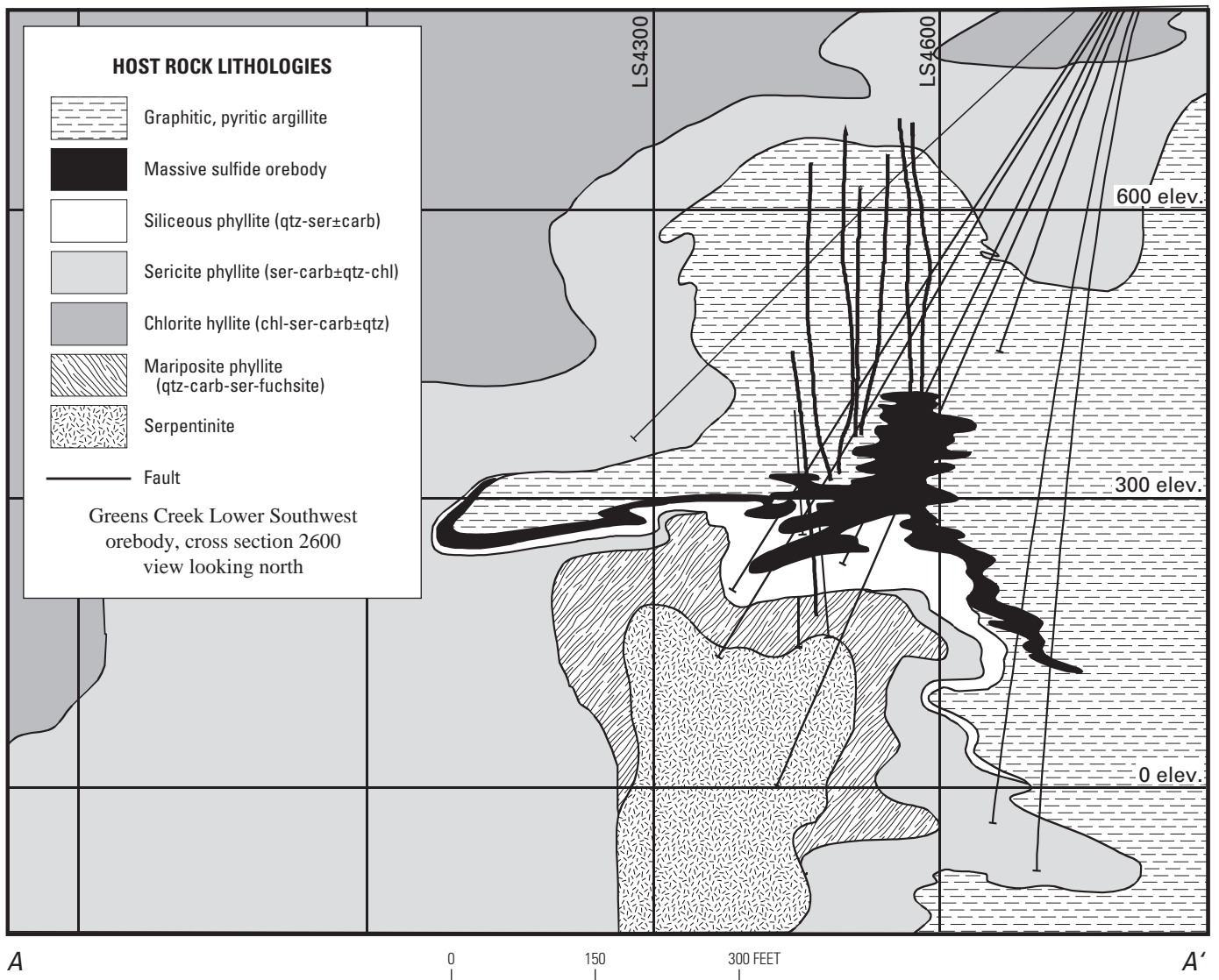


Figure 2. Geologic cross section through the Lower Southwest ore zone, which lies at the contact between phyllites of the stratigraphic footwall and argillites of the stratigraphic hanging wall. Line of section (A–A') is shown in figure 5. Elevations are in feet relative to sea level; long sections are labeled in feet according to the mine grid. Abbreviations are: qtz, quartz; ser, sericite; carb, carbonate; chl, chlorite.

or alteration mineralogy. The mafic lithologies are subdivided into siliceous phyllite, which typically occurs adjacent to ore, sericite phyllite, which is more distal, and chlorite phyllite, which is found farthest from ore. Mariposite (chromian phengite) phyllite, which is also believed to have a mafic protolith, is less abundant and less regular in its distribution. The ultramafic lithologies are subdivided into serpentinite and quartz-carbonate-mariposite phyllite, which is believed to be an alteration of serpentinite. Diabase dikes and highly altered gabbros have also been identified, but they are less common.

Siliceous phyllite is white to dark gray and dense and displays a broadly spaced foliation (S2). The rock is composed of cryptocrystalline quartz with minor sericite and medium-grained euhedral pyrite. By definition, siliceous phyllite contains 80 weight percent or more silica. Clasts of angular to rounded quartz or chert are common; these are believed to be tectonic breccias in some locations and sedimentary conglomerates in others.

The protolith for siliceous phyllite is thought to be a mafic volcanic rock that had been enriched in silica and potassium by metasomatism related to ore formation (see also Newberry and Brew, 1999). However, it is also possible that the protolith was a sediment that had formed prior to ore formation from hydrothermal fluids exhaled onto the sea floor.

Sericite phyllite, which is the most abundant footwall lithology, is tan to greenish gray. It is strongly foliated (S2) and commonly displays a crenulation cleavage (S3). Quartz, sericite, and carbonate are the main constituents. The rock can also contain minor chlorite, leucoxene, chromian phengite, serpentine, or graphite. Pyrite is present as disseminations and massive bands, generally increasing in abundance toward ore where it can attain 40 volume percent or more. Sphalerite, galena, and chalcopyrite disseminations are also common (1–3 volume percent). Bands of sphalerite, pyrite, galena, and chalcopyrite occur sporadically, most commonly in the 200 South ore zone where they are interpreted to be feeders for the mineralizing fluids. Remobilized sulfides and remobilized tetrahedrite are present in quartz-carbonate veins adjacent to ore zones.

The original fabrics of the sericite phyllite protolith are no longer evident because they were obliterated by hydrothermal alteration and metamorphism. Consequently, the unit is subdivided on the basis of alteration mineralogy and is mapped using the modifiers siliceous, graphitic, chloritic, carbonate-rich, and tan (leucoxene). Siliceous sericite phyllite contains quartz-graphite segregations that are believed to represent original quartz-rich sedimentary layers. Where graphite exceeds quartz, the rock is referred to as graphitic. Chloritic sericite phyllite contains 15 volume percent or more chlorite along foliation segregations and grades into chlorite phyllite, a separate unit that is described in a subsequent paragraph. Carbonate-rich sericite phyllite is composed of massive dolomite or ankerite with minor quartz and sericite. The carbonate-rich lithology was formed by alteration of footwall mafic or ultramafic rocks, and it commonly grades into quartz-carbonate-mariposite phyllite or highly sheared rocks of the Upper Shear

Zone (chap. 7). Carbonate-rich sericite phyllite can also occur against the hanging-wall argillites where it is believed to be a replacement of an original debris-flow carbonate rock. Tan sericite phyllite contains 0.5- to 10-cm-thick bands of leucoxene wisps that, by definition, make up 15 volume percent or more of the rock.

The age of the sericite phyllite is not known. Radiometric methods have yielded Cretaceous dates indicative of metamorphic resetting (chap. 11). The carbonate-rich and graphitic sericite phyllites, which are thought to have sedimentary protoliths, are not fossiliferous. Duke and others (chap. 4) and Proffett (chap. 7) have proposed a Devonian age based on the identification within both sericite phyllite and siliceous phyllite of an early foliation that may correlate with a late Paleozoic metamorphic event that has been documented elsewhere on Admiralty Island and on Kupreanof Island (Hauessler and others, 1999).

Chlorite phyllite is medium to dark green and thinly to broadly foliated. The rock contains 60 volume percent or more chlorite in addition to quartz veins and segregations, sericite, carbonate, leucoxene, and magnetite. Far from ore, chlorite phyllite can be massive granular chlorite and calcite. Bull quartz and quartz-carbonate veins are common with thicknesses up to 20 cm. Locally, these veins contain sphalerite, galena, pyrite, chalcopyrite, and rare silver sulfides and sulfosalts. A subdivision of chlorite phyllite, termed diorite gabbro, is composed of chlorite, relict pyroxene phenocrysts (2–3 mm), and disseminated pyrite (up to 15 volume percent). The presence of phenocrysts indicates that the protolith was a cumulate or intrusive rock.

Mariposite phyllite is a banded to foliated, gray-green to brilliant green rock. It is named for its distinctive green mica, which has been referred to by the varietal names mariposite and fuchsite (for example, Newberry and Brew, 1999; Anderson and Taylor, 2000) but is most appropriately classified as chromian phengite according to the scheme of Bailey (1984). A survey of representative examples has shown chromium to be characteristically high, reaching 3 weight percent Cr_2O_3 , and barium to be occasionally high, reaching 11 weight percent BaO (C.D. Taylor, U.S. Geological Survey, unpub. data, 2008). Other minerals are quartz, sericite, carbonate, leucoxene, and locally chlorite. Mariposite phyllite is found near most of the Greens Creek ore zones (for example, fig. 2), and also where the footwall/hanging-wall contact is unmineralized. Mariposite phyllite is concordant with the mafic stratigraphy and is believed to have had a mafic or ultramafic protolith (see also Newberry and Brew, 1999).

The most abundant ultramafic lithology is serpentinite, which is a light to dark green and is typically sheared or crudely foliated. Locally, the rock can be massive. The mineralogy is serpentine, chlorite, carbonate (normally ankerite), and talc, with minor leucoxene and chromian phengite. Serpentinite is not consistently associated with ore but rather occurs as large masses or irregularly shaped bodies within shear zones, fault zones, or fold noses (for example, fig. 2). It

is clear from field observations that considerable strain was localized within this ductile lithology.

Quartz-carbonate-mariposite phyllite, which has not been identified in the cross section shown in figure 2, is massive to crudely foliated and can be white, orange, green, or lavender. The rock is composed of quartz, ankerite, and chromian phengite with local occurrences of a lavender phyllosilicate that is believed to be chromian chlorite. In underground exposures this lithology forms massive irregular pods adjacent to serpentinite or dolomitic massive argillite. The same lithology outcrops north of the mine on Mammoth Ridge where it has been mapped as green carbonate by Duke and others (chap. 4). The protolith is believed to have been an altered ultramafic rock.

Diabase dikes crosscut both the footwall and the hanging wall. They are most common in the southern portion of the mine near the 200 South ore zone. The dikes are medium to dark gray, aphanitic to fine-grained granular, and range from less than 1 centimeter to 1 m in thickness. Plagioclase, pyroxene, and hornblende are phenocrysts. Thicker dikes have well-developed, chilled margins. The dikes are less altered than the surrounding country rock and have not been affected by the D2 deformation that was defined by Proffett (chap. 7). Whether they have been affected by the D3/S3 deformation of Proffett (chap. 7) is uncertain. The dikes are not mineralized themselves, but near ore their emplacement remobilized sulfides, sulfosalts, and rare electrum and native silver along selvages.

Breccia and Conglomeratic Rocks of the Footwall and Hanging Wall

The Greens Creek footwall contains 30-m-thick lenses of dense, white to gray, silicified, quartz+carbonate or chert clasts in a siliceous matrix. The clasts are generally 1–10 cm in diameter, and their mineralogy suggests that they were derived from the underlying phyllites and, less commonly, footwall carbonates. In some locations the clasts are subrounded and the rock appears to be a polymict breccia. These occurrences are believed to be debris flows that formed during rifting in Late Triassic time. More commonly, the clasts are subangular and the rock appears to be a monomict breccia. These occurrences, which are typically near silica-altered rocks, are believed to be tectonic breccias that formed by post-ore fracturing of brittle siliceous lithologies. Some tectonic breccias display prominent S2 and S3 foliations; these are mapped separately as foliation breccias.

A third breccia type has been observed underground in the stratigraphic hanging wall. This breccia is polymict and consists of 1–5-cm rounded white quartz and argillite clasts in a matrix of fine-to-coarse subhedral pyrite. Good exposures are found within argillite 20–30 m from ore on the 720 access ramp to the Upper Southwest ore zone (for location see plate 4 in chap. 7). These breccias are thought to be mineralized debris-flow conglomerates.

Beyond indicating depositional environments, the sedimentary breccias and conglomerates serve as a marker horizon

for regional stratigraphic correlation. South of Greens Creek, a polymict conglomerate underlies the lower volcanic member of the Hyd Group (chap. 4). This conglomerate is believed to be correlative to the sedimentary breccias and conglomerates at Greens Creek, and to record rifting in the area.

Stratigraphic Hanging Wall

Hanging-wall rocks at Greens Creek are broadly categorized as either massive argillite or slaty argillite. Locally, rocks of both categories can approach dolostone. Massive argillite is light gray to black with 1–50-cm-thick beds separated by slaty intervals. Where it is graphite-rich, the rock tends to be finer grained than where it is carbonate-rich. Fractures are commonly filled with quartz±calcite or quartz±dolomite.

Slaty argillite is light gray to black. This rock exhibits a prominent slaty cleavage (S2) as well as a crenulation cleavage (S3) near fold hinges (F3). Quartz±calcite or quartz±dolomite lightning veins follow and also crosscut foliation planes. Thin-section study reveals that slaty argillite is composed of fine quartz, feldspar, muscovite, and lesser dolomite in a carbonaceous matrix. The predominance of silicates over dolomite distinguishes this rock unit from massive argillite in which dolomite is more abundant.

Dolomitic massive argillite is characterized by light to medium gray, 1- to 2-m-thick beds of medium to coarse dolomite separated by thin micaceous bands. Graphite is absent. Peloidal textures are common, as are poorly preserved fossil fragments that include crinoid stems and rare occurrences of the Triassic indicator fossil *Halobia*. Premo and others (chap. 11) used conodonts from this unit to establish a minimum age for the Greens Creek deposit of latest Carnian/earliest Norian.

Dolomitic massive argillite can grade into carbonate-bearing ore, particularly in the Lower Southwest ore zone. Here, dolomitic massive argillite directly overlies phyllite and forms the footwall to ore. Weakly dolomitized areas are cut by stockwork and gash veins containing pyrite, sphalerite, galena, tetrahedrite, chalcopyrite, white quartz, and white dolomite, suggesting that dolomitization preceded sulfide emplacement. In other ore zones, dolomitic massive argillite can be absent in favor of greater thicknesses of silica rock, which may be a replacement of original carbonate rock.

Dolomitic slaty argillite contains dolomite, quartz, sericite, graphite, and coarse pyrite (15 volume percent or more). Discontinuous siliceous lenses, 1 to 25 cm in length, are common. Pyrite can be massive adjacent to the stratigraphic footwall. The occurrence of this lithology adjacent to ore, and its high content of pyrite, both suggest that dolomitization of slaty argillite occurred during sulfide emplacement.

A systematic stratigraphy has not been recognized in the argillites. However, some spatial variations are evident. Sericite can be abundant near major faults, and there are indications that sericite increases in abundance upsection. Massive argillite is more abundant nearer to the ores, where this lithology can also be enriched in silica. The silica-enriched massive

argillite grades locally into gray-green or olive-brown chert. The occurrence of precious metals in this chert suggests that the silica enrichment was caused by ore-associated hydrothermal alteration, but petrographic study has also revealed primary depositional cryptocrystalline quartz chert, which suggests a sedimentary origin for the silica.

Sulfide mineralization in the hanging-wall argillite includes ubiquitous pyrite as fine disseminations, stringers, bands, and framboidal clots. Base-metal sulfides are rare except near ore. Precious metals can be abundant locally (>1 troy ounce per ton gold, >500 troy ounces per ton silver) within meters of ore as microfracture-hosted acanthite, electrum, or native silver. This mineralization can be difficult to recognize in hand specimen.

Description of the Ores

For mapping purposes, the Greens Creek sulfide deposits have been divided by mine geologists into massive ore in which sulfides exceed 50 volume percent and white ore in which sulfides are below 50 volume percent. Massive ores are subdivided depending on the relative abundance of base-metal sulfides (sphalerite plus galena) and pyrite, whether the grain size is fine or very fine, and whether there is intercalated graphitic argillite. This gives rise to six map units: massive fine-grained base-metal ore; massive very fine grained base-metal ore; massive fine-grained base-metal ore with graphite, massive fine-grained pyrite ore, massive very fine-grained pyrite ore, and massive fine-grained pyrite ore with graphite. White ore is subdivided into three map units according to whether the dominant gangue mineral is carbonate, barite, or quartz (silica).

Ore types tend to have a consistent distribution within individual orebodies. This is illustrated in figure 3, which shows a schematic cross section generalized from detailed maps of several individual Greens Creek orebodies. In general, siliceous phyllite is stratigraphically overlain by white ore, followed by massive pyritic ore, and then massive base-metal ore. In the core of the orebody, the white ore tends to be siliceous, giving way laterally to carbonate-rich and then baritic equivalents.

An example of massive fine-grained base-metal ore is shown in figure 4A. The rock is metallic gray, blue gray, or dull tannish yellow depending on the relative abundance of sphalerite, galena, and pyrite. Layering is often apparent in which 1–5-mm-thick bands are distinguished by different relative abundances of the sulfides. Gangue minerals are quartz, sericite, barite, and chromian phengite. Silver contents vary widely, particularly in the Lower Southwest ore zone where assays range from 5 to more than 200 troy ounces per ton.

Massive fine-grained pyrite ore (fig. 4B) is yellow-bronze to metallic brown, is coarser than massive fine-grained base-metal ore, and lacks visible banding. Quartz is the dominant gangue mineral in veins or in the matrix. Base-metal sulfides range from a few disseminated grains to segregations that collectively approach the abundance of pyrite. Precious metals can exceed 50 troy ounces per ton silver and 0.5 troy ounce per ton gold. Massive fine-grained pyrite ore is not generally mined because the ore metal content is insufficient.

Very fine grained massive ores (fig. 4C) lack megascopic sulfides and have a polished appearance in drill core. Graphitic varieties contain 15 percent or more argillite as massive bands, slaty intervals, or deformed rip-up clasts. In some locations argillite and massive sulfide appear to have been codeposited, and in other locations the lithologies appear to have been mixed tectonically. Graphitic massive ore is characteristically high in precious metals.

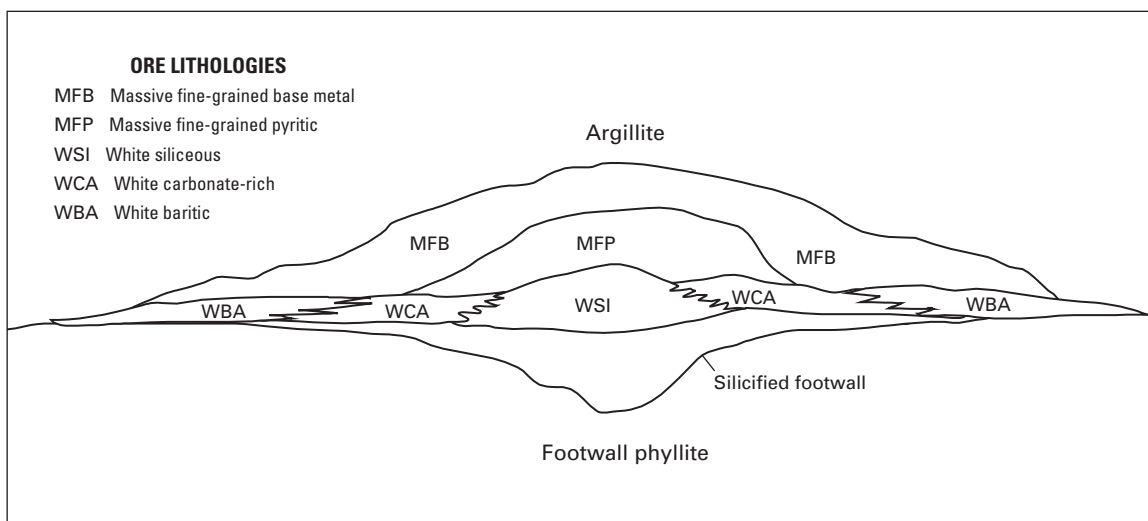


Figure 3. Schematic distribution of ore types within an individual Greens Creek orebody prior to deformation. Generalized from detailed maps of several individual Greens Creek orebodies. Ore types that do not appear in this section (very fine grained, graphitic) are less abundant and have less regular distributions.

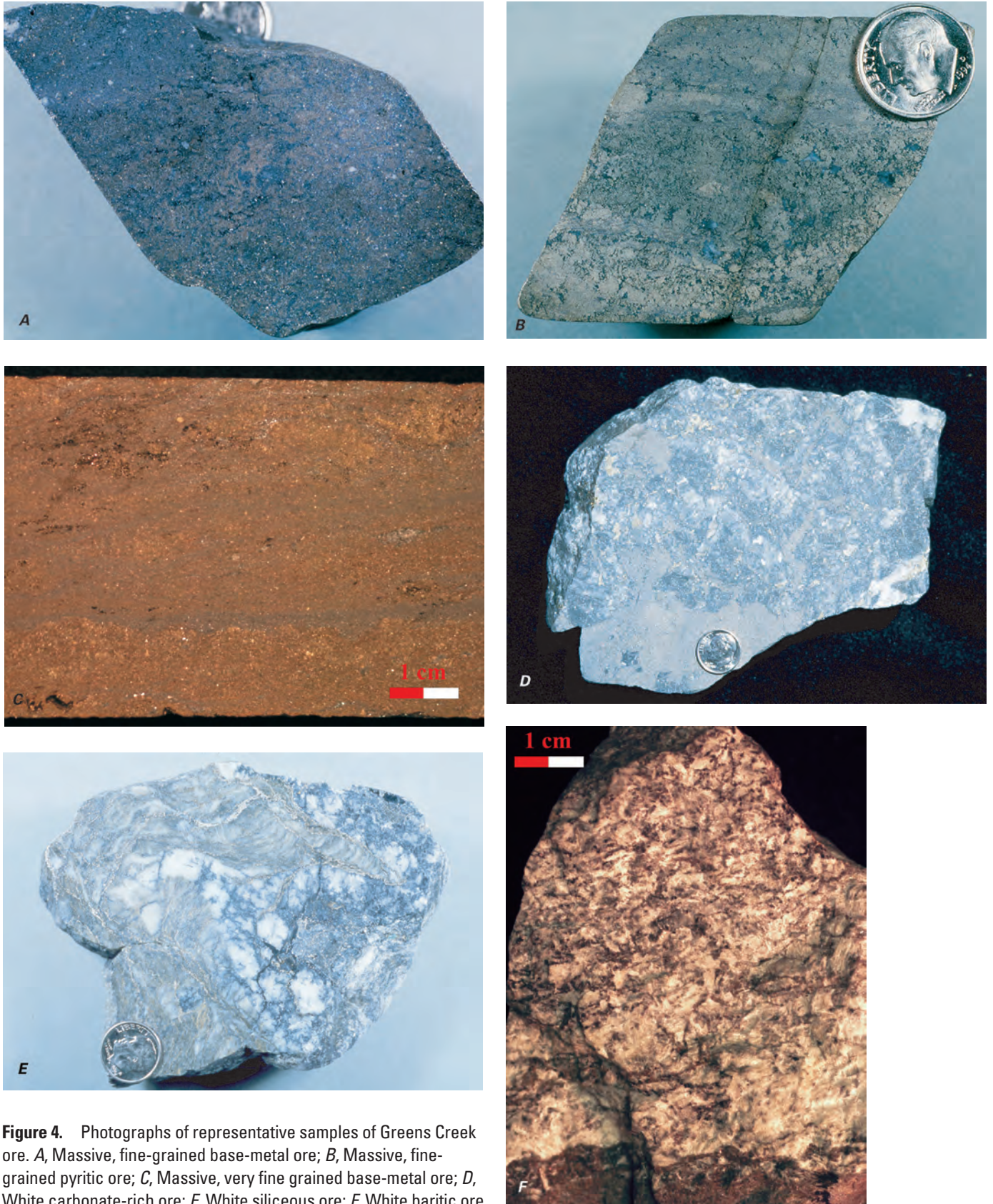


Figure 4. Photographs of representative samples of Greens Creek ore. *A*, Massive, fine-grained base-metal ore; *B*, Massive, fine-grained pyritic ore; *C*, Massive, very fine grained base-metal ore; *D*, White carbonate-rich ore; *E*, White siliceous ore; *F*, White baritic ore.

Among the white ores the carbonate-rich variety is most abundant. White carbonate ore is massive and white to light gray (fig. 4D). It is composed of granular dolomite with disseminated and banded sulfides. Quartz- and carbonate-filled fractures are ubiquitous. White carbonate ore can grade into massive ore, particularly in the West orebody where nearly pure sulfide bands 1 to 50 cm thick are interlayered with carbonate. The sulfide assemblage in these rocks includes pyrite, sphalerite, galena, bornite, and, locally, chalcopyrite. Argentiferous tetrahedrite is present within quartz-carbonate veins as sub-centimeter blebs. Acanthite, electrum, native silver, and native gold are rare, as are gangue minerals other than carbonate.

White siliceous ore (fig. 4E) is found in all of the known orebodies, although it is usually minor. The silica is dominantly cryptocrystalline hydrothermal quartz with lesser vein quartz and chert, but there can also be appreciable carbonate, sericite, chromian phengite, or graphite. The rock is highly variable in texture, sulfide content, and gangue content and can show precious metal grades exceeding 1,000 troy ounces per ton silver and 4 troy ounces per ton gold.

White baritic ore (fig. 4F) is thinly laminated to massive and contains fine sulfides as disseminations or stringers. This lithology is easily identified by its sugary texture and high specific gravity. White baritic ore tends to be base metal sulfide-poor (typically less than 5 volume percent), but silver-rich. Higher grade examples contain disseminated bright red pyrrargyrite/proustite. In many locations white baritic ore is too low in metal content to be mined.

Locally, all of the ore types can be veined, brecciated, or crosscut by gouge or rubble zones as a consequence of post-ore faulting or folding. Veining is most common in the white ores. Vein-associated remobilization and recrystallization have resulted in spectacular concentrations of native gold and silver sulfosalts. Good examples are found in the Upper Southwest ore zone where quartz veins contain coarse remobilized sulfides, native gold, electrum, native silver, and argentite/acanthite. Brecciated ores in some cases formed by slumping of massive sulfide, often into weakly mineralized surrounding sediments. In other cases brecciated ores formed by postdepositional faulting and shearing. Solution-collapse breccias have also been identified, particularly in the white carbonate ores.

Geometry of the Ore Zones

At the Greens Creek mine site, sulfide mineralization is nearly continuous along the phyllite/argillite contact. The major sulfide accumulations, which are shown projected to the surface in figure 5, are the East orebody, the West orebody (including the Central West, 9A, Northwest West, and 5250 zones), and the Southwest orebody (including the Upper and Lower Southwest, 224 West Bench, 200 West Bench, and 200 South zones). The boundaries between orebodies and ore zones are defined by faults, shear zones, or changes in the thickness of the mineralized horizon.

East Orebody

The East orebody crops out at the Big Sore kill zone (fig. 6) where the stratigraphy is inverted by folding with phyllite overlying argillite. The deposit forms a sheet 3 to 12 m thick that strikes N. 15° E. for 920 m. At the surface the mineralization dips 60–80° to the west, but the dip shallows with depth to near horizontal as a result of F3 folding. The deeper portion of the orebody consists of two parallel flat-lying panels that were affected by the shallowly dipping Klaus shear. North of the Big Sore kill zone, the updip boundary of the East orebody is the Upper Shear Zone, which displaced massive sulfide an unknown distance to the west (chap. 7). To the south, the mineralized horizon rotates to an east-west strike before truncation by the Maki fault.

Folding produced three lobes within the East orebody that are thick enough to mine: the North, Central, and South zones. The Greens Creek mine was capitalized on an East orebody reserve of 2.7 million tons at 9.7 weight percent zinc, 3.9 weight percent lead, 14.7 troy ounces per ton silver, and 0.111 troy ounce per ton gold, with an additional resource of 522,000 tons at the same grades.

West Orebody

The West orebody, which was originally the downdip extension of the East orebody, is subdivided into the Central West, 9A, Northwest West, and 5250 zones (figs. 5, 6). Through the year 2000, the West orebody had produced 379,000 tons of ore grading 14.2 weight percent zinc, 4.1 weight percent lead, 0.180 troy ounce per ton gold, and 17.2 troy ounces per ton silver. At that time reserves were 6.62 million tons grading 12.0 weight percent zinc, 4.3 weight percent lead, 13.7 troy ounces per ton silver, and 0.119 troy ounce per ton gold, with an additional resource of 2.6 million tons at slightly lower grades.

Central West

The Central West zone lies beneath the Klaus fault and between the East orebody and the Maki fault (figs. 5, 6). At its eastern boundary the mineralized horizon is near vertical and 3–6 m thick. The horizon shallows to the west due to F3 folding becoming horizontal and then east-dipping (10–20°). Here the east-dipping ore band forms the upper limb of a recumbent F2 fold, the lower limb of which contains a 100-m thickness of ore. The unusual thickness of the sulfide accumulation is interpreted to reflect a greater primary buildup as well as structural thickening due to F2 folding.

9A

The Maki fault marks the transition from the Central West to the 9A ore zone (fig. 5). The 9A zone extends for 600 m along strike and measures 150 m perpendicular to

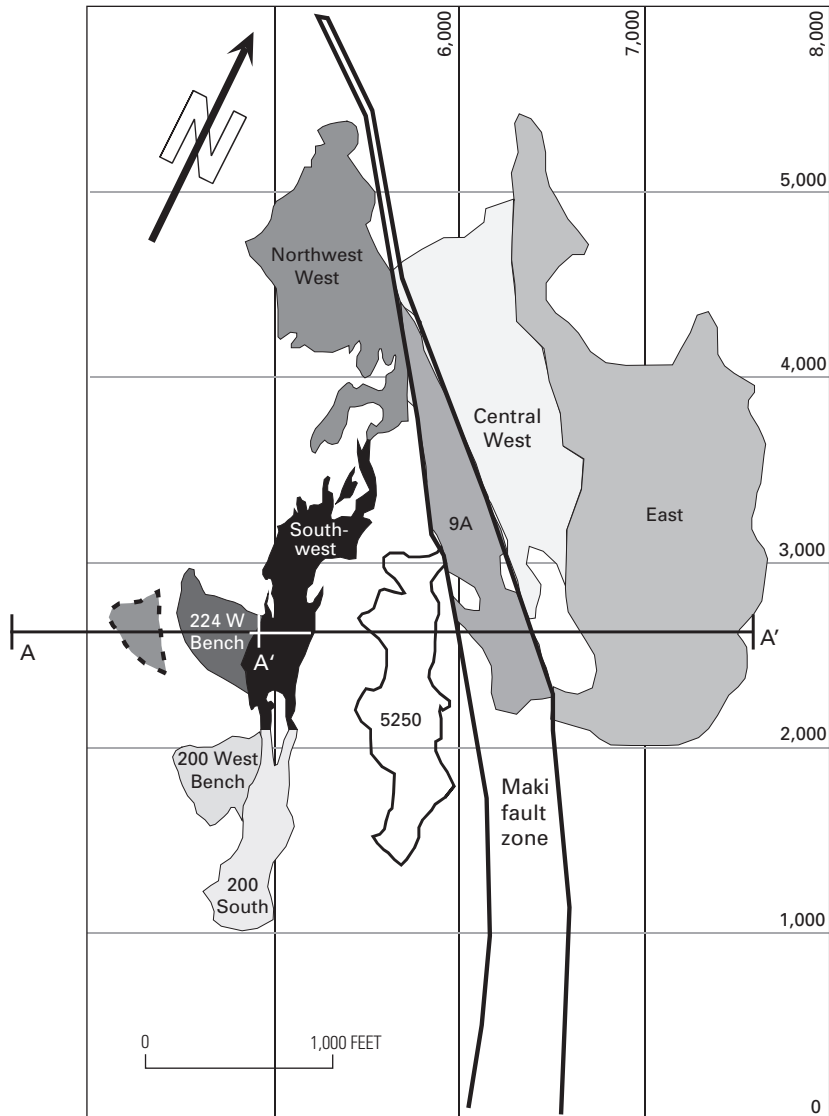


Figure 5. Surface projections of the Greens Creek ore zones. A–A' is the line of section for figure 2; A–A' is the line of section for figure 6.

strike. It is composed of numerous fault blocks, all of which display the characteristic stratabound nature of Greens Creek ore. Restoration of the movement along the Maki fault reveals that the 9A zone represents the southwesterly, down-plunge extension of the East orebody and Central West ore zone. Throughout the 9A zone, grain-size reduction during faulting has yielded gouge with millimeter- to centimeter-sized clots of electrum that are rich in gold, silver, and base metals.

Northwest West

The Northwest West zone is an extension of the Central West that was offset along the Maki fault. The structure is dominated by a pair of recumbent F2 folds that form an acute S-shape in cross section, the upper fold an argillite-cored syncline, and the lower fold a phyllite-cored anticline. The

axial planes of these folds were affected by south-southeast-plunging F3 folds (J.M. Proffett, written commun., 1998). The main part of the ore zone lies on the lower limb of the syncline.

5250

The 5250 ore zone is a portion of the East orebody that was offset by the Maki fault (figs. 5, 6). The mineralization continues for 550 m along a north-northwest strike and extends 100 m perpendicular to strike. The intensity of F2 folding increases to the north where the Klaus shear may affect the mineralization. In the southern portion of the zone, the ore horizon dips more regularly at 60° to 70° to the west and plunges 20° south. The 5250 zone is atypical among the Greens Creek ore zones in containing a high proportion of white baritic ore. This zone is base-metal poor and has not yet been mined.

Southwest Orebody

The Southwest orebody is an extension of the Northwest West ore zone along the lower F2 fold. An upper zone extends 260 m along a N. 20° W. strike with a plan width of 210 m. A lower zone extends 360 m along a northerly strike and has a plan width of 240 m. The transition between the upper and lower zones, which lies at an elevation of about 120 m above sea level, is marked by conspicuous changes in structure and style of mineralization.

The Upper Southwest zone is characterized by vertical, tight, south-closing F2 folds that are phyllite cored. The overall geometry of the ore is that of a “ripple-fall.” The “falls” are the near-vertical F2 fold limbs, some of which extend to 50 m in height. The “ripple” areas, which show undulations on scales of a few meters or less, dip shallowly to the west as a consequence of F3 folding. The intense folding produced remobilizations with high precious-metal grades.

The Lower Southwest zone lies mainly along the limb of a major F2 fold. The overall geometry is a phyllite-cored upright anticline with a steeply dipping eastern limb and a flat, undulating western limb (fig. 6). The ore is up to 25 m thick in the core of the anticline. Along the eastern limb, mineralization thins to less than 3 m before it is truncated by a series of moderately to steeply dipping faults that are thought to be a western strand of

the Maki fault with right-lateral displacement of several hundred feet. The ore zone is cut by other steeply dipping right-lateral faults as well as by low-angle shears.

The Southwest orebody is smaller than the West orebody, but its higher precious-metal grades offer a premium that was important in the 1996 reopening of the mine. Through the year 2000, total production from the Upper and Lower Southwest zones was 1.3 million tons at 11.3 weight percent zinc, 5.2 weight percent lead, 25.8 troy ounces per ton silver, and 0.189 troy ounce per ton gold. At that time the remaining reserve was 554,000 tons at 10.1 weight percent zinc, 4.8 weight percent lead, 24.1 troy ounces per ton silver, and 0.190 troy ounce per ton gold. Continued exploration downdip and along strike has resulted in the discovery of the 224 West Bench, 200 West Bench, and 200 South zones (figs. 5, 6). At the time of writing of this chapter, sufficient development work has been carried out in the 200 South zone such that a general description can be given.

200 South

The 200 South zone displays the same general anticlinal geometry as the Lower Southwest zone with a steeply dipping eastern limb and a flat-lying western limb. Mineralization continues for 340 m along a strike of N. 15° W. The plan

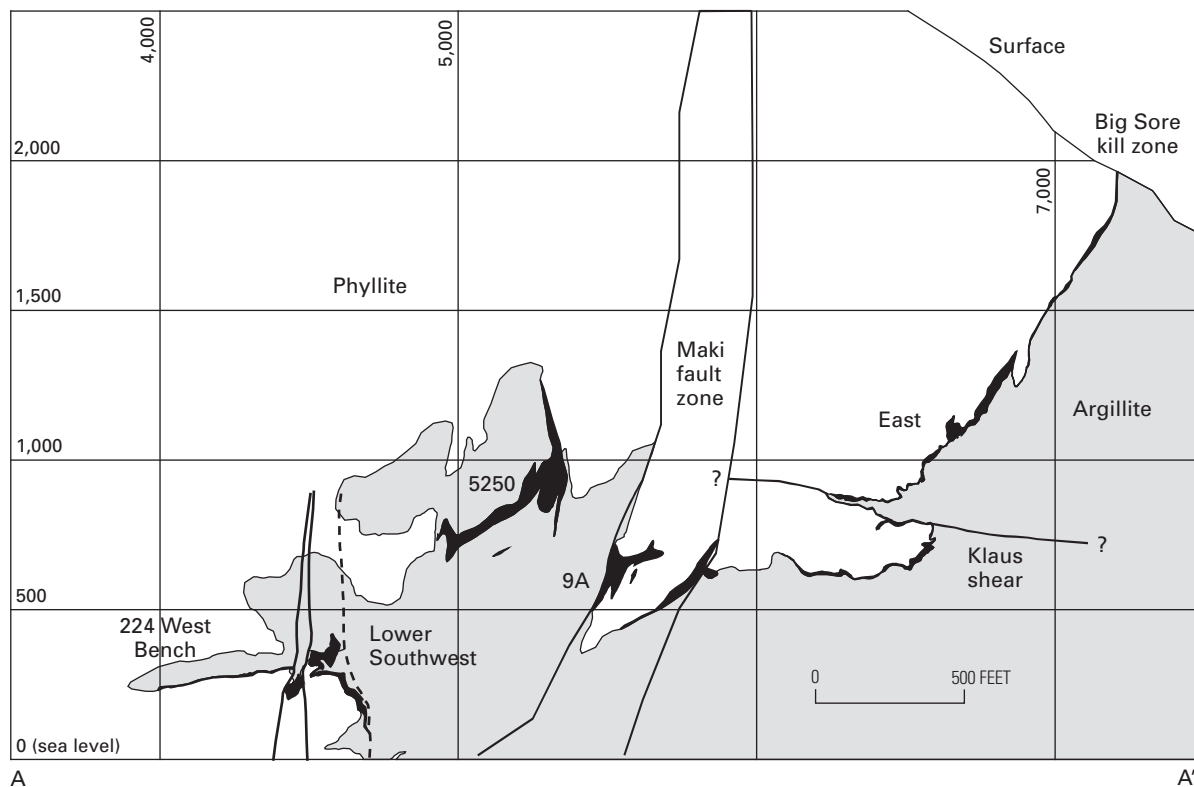


Figure 6. North-looking cross section showing, in black, the East, 9A, 5250, Lower Southwest, and 224 West Bench ore zones. Line of section is shown in figure 5. The East orebody crops out at the Big Sore kill zone.

width is 60 m with an additional 140 m westward extension of bench-style mineralization. The mineralized horizon is 45 m thick in the crest of the anticline and tapers downdip and to the south, although the Greens Creek reserve is currently open to the south.

The 200 South zone extends from 160 m below sea level to 65 m above. There appears to be at least one major F2 anticline in the core of the deposit that has been affected by an F3 fold with east-dipping axial plane. Mineralization is bounded on the east by a steep, brittle fault zone (a strand of the Maki fault) that offsets the ore horizon several hundred feet in a dextral sense.

The 200 South extension is atypical in showing the highest silver grades adjacent to the footwall phyllite. Production through 2000 was 352,000 tons at 14.6 weight percent zinc, 6.0 weight percent lead, 22.2 troy ounces per ton silver, and 0.237 troy ounce per ton gold. At that time the remaining reserve was 1.15 million tons at 12.9 weight percent zinc, 5.2 weight percent lead, 21.0 troy ounces per ton silver, and 0.184 troy ounce per ton gold.

Metal Zoning

As they are presently known, the distributions of ore types and the shapes and thicknesses of the major mineralized zones suggest that the Central West zone was a major center of sulfide precipitation. Drilling in this area has outlined a large, coherent block of massive sulfide and barite-poor white ore with a systematic metal zoning from the footwall phyllites to the hanging-wall argillites. The zoning is illustrated in figure 7. Adjacent to the phyllite lies a copper/iron zone that is composed of pyrite-rich massive to semimassive ores with silica as the dominant gangue. More copper-rich areas are 0.7–4 weight percent copper whereas more iron-rich areas are 0.2–0.7 weight percent copper. Ratios of iron to zinc (weight basis) are 5–10. Relative to average Greens Creek ore, silver, lead, and mercury concentrations are low and arsenic/antimony is high. (Note that As/Sb is high only on a relative basis; in Greens Creek ores generally antimony dominates arsenic.) The copper/iron zone is presently uneconomic.

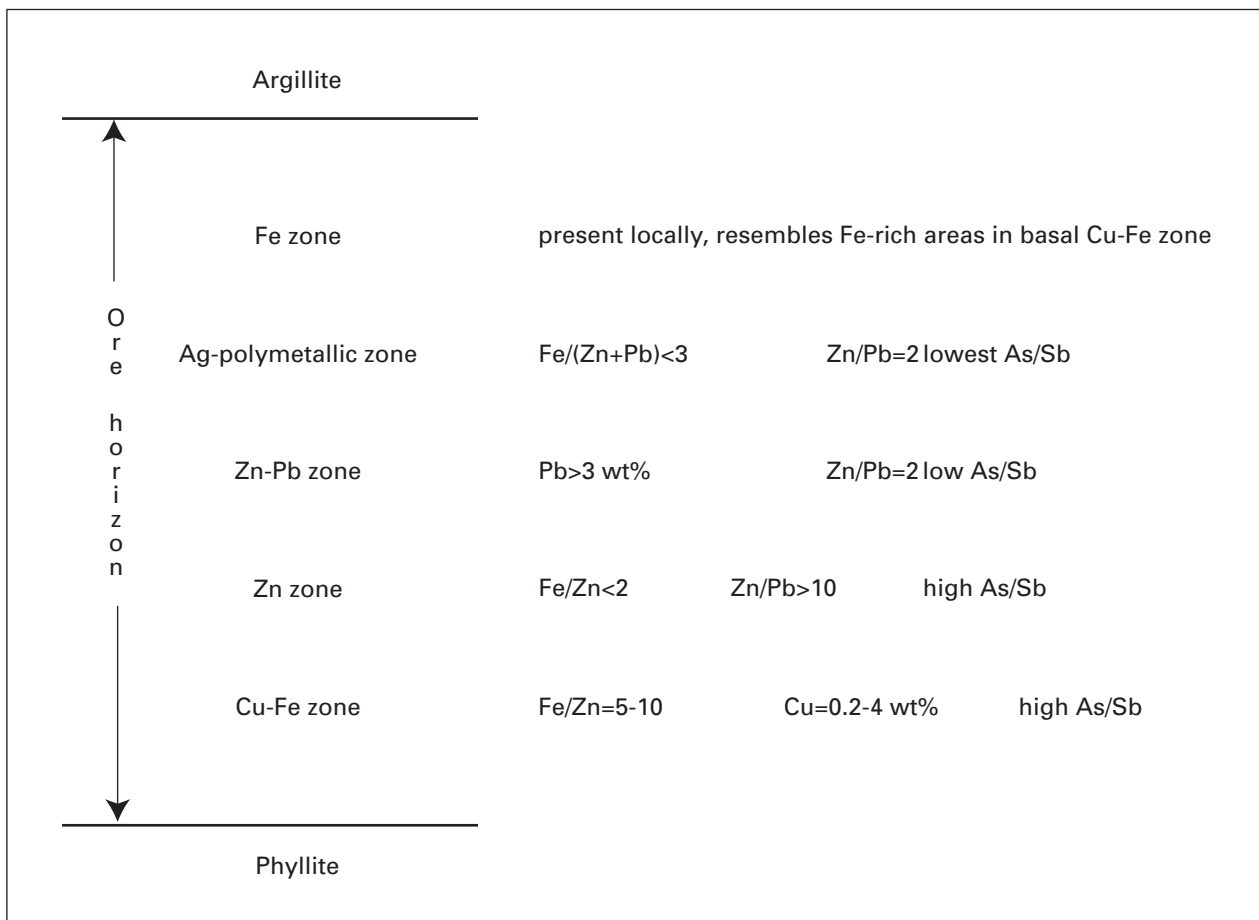


Figure 7. Metal zoning observed in the core of the Central West ore zone. Broadly similar patterns have been identified in the Northwest West, East, 200 South, and 5250 ore zones. Note that high arsenic:antimony in the zinc and copper/iron zones is relative to other zones. Most everywhere in the Greens Creek deposit, antimony exceeds arsenic.

Stratigraphically overlying the copper/iron zone is a zinc zone where iron to zinc ratios are less than 2 and zinc to lead ratios are greater than 10. Mercury concentrations are 2–10 times the concentration in the copper/iron zone, and arsenic/antimony is relatively high.

Above the zinc zone is a zinc/lead zone. Here, lead is 3 weight percent or higher, zinc to lead ratios are about 2, and mercury concentrations are 10–15 times the concentrations in the copper/iron zone.

A silver/polymetallic zone typically occurs adjacent to argillite or within the cores of synclines. This zone is characterized by Fe/(Zn+Pb) of 3 or less, zinc/lead of 2, relatively high concentrations of arsenic and antimony, and the lowest arsenic/antimony ratios of all the zones. Gold concentrations are slightly elevated.

In some locations, an iron-rich, zinc- and lead-poor zone can be found between the silver/polymetallic zone and the hanging-wall argillite. Metal concentrations resemble those in iron-rich portions of the basal copper/iron zone.

Restoration of the displacement along the Maki fault places the high-copper pyritic ores of the Central West ore zone adjacent to copper/iron-rich mineralization of the Northwest West ore zone. Detailed metal zoning studies of the Northwest West have not been carried out, but a cursory investigation indicates a pattern similar to that in the Central West zone, but overlying a thicker sequence of siliceous phyllite in the footwall.

The East orebody (particularly the steeply dipping portion of the South zone), the 200 South zone, and the 5250 zone show metal zoning patterns similar to the Central West and Northwest West zones. However, the understanding of metal distributions in these locations is incomplete, and locally the zoning can differ from the Central West. As it is presently understood, the overall Greens Creek metal distributions do not show the concentric zoning pattern that would be expected if the sulfide mineralization formed above a single hydrothermal center. Thus, despite the fact that the ore horizon thins away from the Central West ore zone as if this were the principal vent for the metalliferous fluids, the metal zoning patterns suggest instead that hydrothermal upwelling was from multiple centers or was diffuse across a broad area.

References Cited

- Anderson, V.M., and Taylor, C.D., 2000, Alteration mineralogy and zonation in host rocks to the Greens Creek deposit, southeastern Alaska [abs.]: Geological Society of America Abstracts with Programs, v. 32, p. A–2.
- Bailey, S.W., 1984, Classification and structure of the micas: Reviews in Mineralogy, v. 13, p. 1–12.
- Haeussler, P.J., Karl, S.M., Mortensen, J.K., Layer, Paul, and Himmelberg, G.R., 1999, Permian and mid-Cretaceous deformation of the Alexander terrane on Admiralty and Kupreanof Islands, southeastern Alaska [abs.]: Geological Society of America Abstracts with Programs v. 31, p. A–60.
- Newberry, R.J., and Brew, D.A., 1999, Chemical and isotopic data for rocks and ores from the Upper Triassic Greens Creek and Woewodski Island volcanogenic massive sulfide deposits, southeastern Alaska, *in* Kelley, K.D., ed., Geologic studies in Alaska by the U.S. Geological Survey, 1997: U.S. Geological Survey Professional Paper 1614, p. 35–55.

Geologic Structure of the Greens Creek Mine Area, Southeastern Alaska

By John M. Proffett

Chapter 7 of

**Geology, Geochemistry, and Genesis of the Greens Creek Massive
Sulfide Deposit, Admiralty Island, Southeastern Alaska**

Edited by Cliff D. Taylor and Craig A. Johnson

Professional Paper 1763

**U.S. Department of the Interior
U.S. Geological Survey**

Contents

Introduction.....	141
Rock Units and Their Distribution	141
Regional Rock Units.....	141
Paleozoic Rocks.....	141
Triassic Rocks.....	142
Jurassic and Cretaceous	143
Intrusive Rocks.....	143
Rock Units of the Greens Creek Mine Area	143
Graphitic Quartz Mica Schist (Retreat? Group).....	143
Ultramafic Rocks.....	143
Mafic Rocks.....	143
Conglomerate/Breccia.....	143
Argillites and Mafic Rocks	144
Graphitic Slates and Sericitic Slaty Sediments	145
Geologic Structure.....	145
Pre-Hyd Group Deformation (S1 and S1.5)	147
F2 Folding and S2 Foliation.....	147
Ductile Shear Zones (S2.5).....	149
Upper Shear Zone.....	149
Klaus Shear.....	152
Lower Shear Zone	152
Possible F2.5 Folds (?)	152
F3 Folding and S3 Foliation.....	154
S3 Shear Zones	154
F4 Folding.....	154
Brittle Faults.....	154
Low-Angle Faults	154
Northwest-Striking Right-Slip Faults.....	156
North-Northeast-Trending Left-Slip Faults.....	156
Relationship Between Ore and Structure.....	156
References Cited.....	157

Figures

1. Diagrammatic 3-dimensional sketch showing relationships between the different stages of ductile deformation at the Greens Creek mine	142
2. Photographs of Greens Creek rocks	144
3. Photographs of F2 related structures in the Greens Creek mine	147
4. Map of 344 stope and 350 ore access crosscut (344–354-foot mine elevation)	148
5. Map of 524 stope and 530 ore access crosscut (524–532-foot mine elevation)	150
6. Fence section, looking north and down at 60°, showing variation in orientation of F2 axes in West orebody between 28XS to 32XS.....	151

7. Three-dimensional sketch of northern part of Central West orebody, diagrammatically showing interpretation of F2 folds refolded by F3, east of Maki fault	152
8. Diagrammatic plan view, showing relationships between bedding, F2/S2, and F3/S3 in the main part of the Mine Plate	152
9. <i>A</i> , Photograph of shear foliated quartz-sericite-(carbonate) phyllite (a mylonite), showing asymmetric tails on quartz pods that suggest top-to-the-west sense of shear. <i>B</i> , Thin section of <i>A</i> , crossed polarizers, showing preferred orientations of flattened quartz grains oblique to shear foliation, also indicating top-to-the-west sense of shear	153
10. Photographs. <i>A</i> , Steeply west-dipping beds of argillite, with massive sulfide layers, on the east limb of a large-scale F3 synform. <i>B</i> , Cherty argillite with massive base-metal sulfide layers and pyritic beds, folded in an F3 antiform. <i>C</i> , S2, and quartz veins parallel to S2, in tan phyllite, folded by F3 and refolded by F4	155

Plates

[on CD-ROM]

- 7-1. Geologic map of the surface, Greens Creek mine, Alaska.
- 7-2A. Greens Creek mine, Alaska, Cross Section 3000.
- 7-2B. Greens Creek mine, Alaska, Long Section 4800.
- 7-3. Map of the surface, Greens Creek mine, Alaska; F2, S2, L2, and S2/bedding intersections.
- 7-4. Map of underground workings, Greens Creek mine, Alaska; F2, L2, and S2/bedding intersections.
- 7-5. Map of the surface, Greens Creek mine, Alaska; F3, S3, L3, F4, S4, L4.

Geologic Structure of the Greens Creek Mine Area, Southeastern Alaska

By John M. Proffett

Introduction

This chapter discusses the surface and subsurface structural geology of the Greens Creek mine and surrounding area. It is based on detailed geologic mapping of selected mine workings at a scale of 1 inch = 20 feet and 1 inch = 40 feet, and of surface outcrops at 1 inch = 200 feet and 1 inch = 40 feet (J.M. Proffett, written commun., 1987, 1997, 1998, 1999, 2000, 2001, 2002). The mapping was supplemented with detailed logging of drill core at various scales. In addition to field work by the writer, drill logs and underground maps by numerous Greens Creek geologists have been essential to developing the present understanding of the geologic structure. Work by others on various aspects of the structural and regional geology at Greens Creek, including Brian Martin, Thomas Crafford, Klaus Triebel, Paul Lindberg, Norman Duke, Kerry Lear, Andrew West, Brian Erikson, Peter Powers, and Christian Schrader, have also been helpful.

Greens Creek geology is extremely complicated due to complex structure and a wide variety of metaigneous and metasedimentary rock units, many of which have undergone hydrothermal alteration. Regionally, the rock units can be divided into a Late Triassic (and younger?) age group and a Paleozoic (and older?) age group. The ore at the Greens Creek mine lies mostly near the base of the Triassic rocks. The earliest structures (S1 and S1.5) are known only from the older rocks and do not affect the ores. Three major folding-cleavage-forming events (F2–S2, F3–S3, and F4–S4) overprint the Upper Triassic rocks and ore, as well as older rocks (fig. 1). Major ductile shear zones, between F2 and F3 in age, occur above and below the ore zone, and one or more periods of brittle faulting, involving at least three sets of faults, postdate the youngest (F4) folding event. Understanding this complex geology is essential not only for directing exploration and interpreting results for resource estimates and mine planning, but also for planning and interpreting work directed toward understanding the genesis of the Greens Creek ore deposit. This paper will begin with a brief review of rock units, which is essential to understanding the discussion of structures that follows.

Rock Units and Their Distribution

Rock units, as defined regionally (Loney, 1964; Lathram and others, 1965; Muffler, 1967), have been used somewhat

differently from those used for more detailed geologic work in the mine and vicinity. Regional units are discussed first, followed by a discussion of mine units and how they may correlate with regional units. More detailed discussions of rock units are provided in chapters 2, 4, and 6 of this volume.

Regional Rock Units

The Greens Creek region is underlain by several Paleozoic and Upper Triassic metasedimentary and metavolcanic rock units. Upper Jurassic to Lower Cretaceous metasedimentary and metavolcanic rock units are known to the north and east (Lathram and others, 1965). Paleozoic rocks are separated from Upper Triassic rocks by what appears to be a major unconformity (Lathram and others, 1965; Brew and Karl, 1988). Mafic and ultramafic intrusive rocks also are present in the mine area.

Paleozoic Rocks

A sequence of dark gray, graphitic, quartz-mica schists (fig. 2A) and interlayered white, pale yellow to pale green quartz-muscovite schists (fig. 2B) is exposed along Hawk Inlet and for a variable distance inland. Rare marble units interlayered with these rocks in the north part of Hawk Inlet have yielded conodonts of Late Devonian age (collected by Russ Franklin and Duane Olsen; identified by Anita Harris, chap. 11). Calcite marble on the ridge east of Hawk Inlet has yielded a Devonian or Silurian megafossil (Brew and Ford, 1985) and is probably part of this sequence. These rocks were called the Retreat Group by Lathram and others (1965).

Metacherts and siliceous metasedimentary rocks of Late Devonian to Early Permian age, assigned to the Cannery Formation, occur on southern Admiralty Island and adjacent areas (Muffler, 1967; Jones and others, 1981). Early Permian megafossils southwest of Eagle Peak (3 miles northeast of the Greens Creek mine) indicate the presence of Cannery Formation partial equivalents there (Lathram and others, 1965).

Stratigraphy and structure in these older rocks are not well understood in the Greens Creek area, and it is not known whether or not the “Retreat Group” and the Cannery Formation in the Greens Creek area belong to the same sequence. Clasts of the deformed and metamorphosed Paleozoic rocks occur in Triassic conglomerates at Greens Creek (fig. 2C)

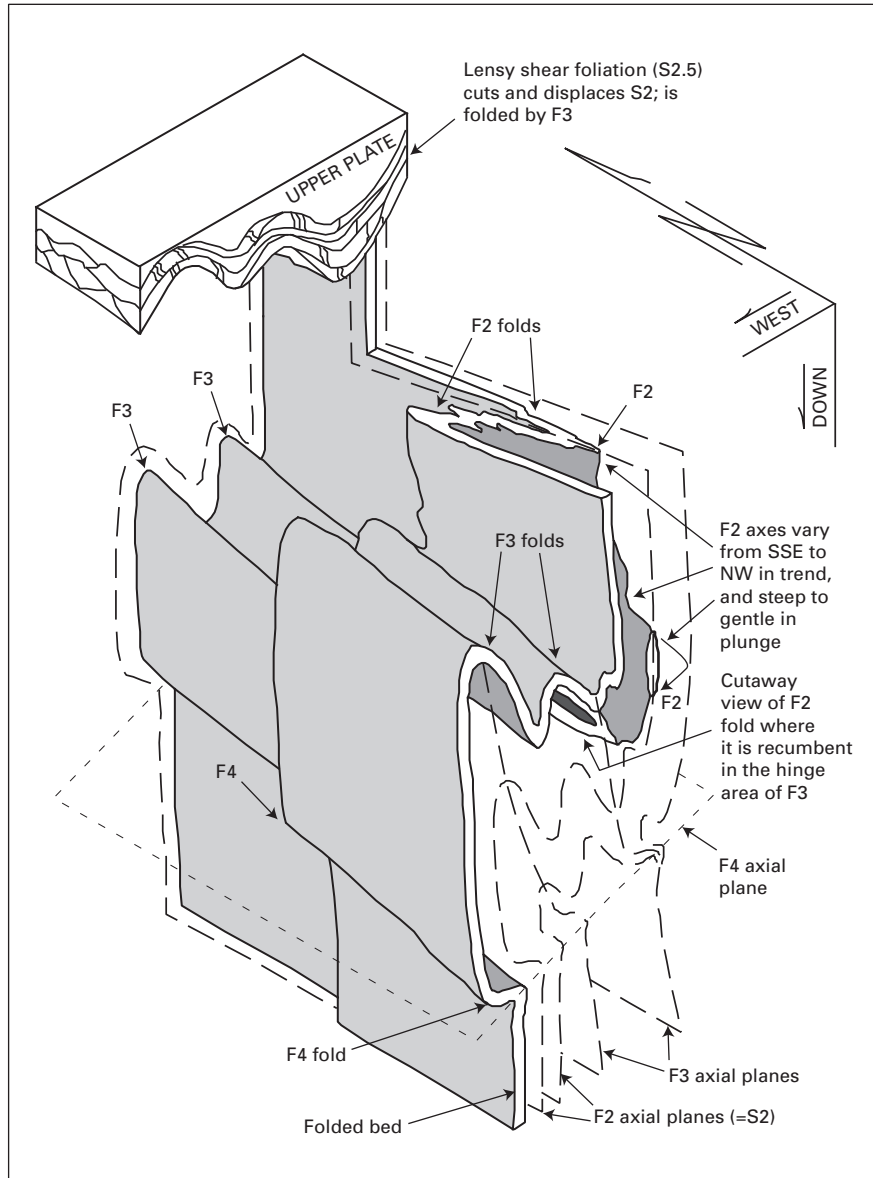


Figure 1. Diagrammatic 3-dimensional sketch showing relationships between the different stages of ductile deformation at the Greens Creek mine.

and near Young Bay. $^{40}\text{Ar}/^{39}\text{Ar}$ cooling ages of about 265 m.y. on metamorphic white mica and hornblende from the Paleozoic rocks of Admiralty Island (Haeussler and others, 1999) indicate a deformational and metamorphic event prior to late middle Permian time.

Triassic Rocks

The Upper Triassic Hyd Group of Admiralty Island and vicinity consists of locally derived conglomerate and sedimentary breccia, black slaty, calcareous, and dolomitic argillite, limestone, dolomite, and metabasalt. The conglomerate and

sedimentary breccia (fig. 2C) are near or at the base of the section in most areas near Greens Creek. The overlying argillite section, which contains the Greens Creek orebodies near its base, has yielded conodonts of late Carnian to earliest Norian age (chap. 11). Metabasalts on Gallagher Ridge, just south of the Greens Creek mine, conformably overlie argillite, contain late Carnian to earliest Norian conodonts (chap. 11), and have a U/Pb isochron age of 218 ± 16 Ma and a Sm/Nd age of 215 ± 95 Ma (chap. 11). Argillite with *Monotis subcircularis*, a late Norian pelecypod, reported from farther south on Admiralty Island (Loney, 1964; Lathram and others, 1965), indicates that the Hyd Group includes rocks younger than those dated in the mine area.

Jurassic and Cretaceous

Sedimentary rocks with Late Jurassic and Early Cretaceous fossils and interbedded volcanic rocks (the Seymour Canal Formation) occur in a belt along the east side of Admiralty Island, 4 miles northeast of Greens Creek (Loney, 1964; Lathram and others, 1965; Cohen and Lundberg, 1993). Rocks along the southwestern side of this belt, nearest to Greens Creek, consist mainly of dark gray slate and slaty graywacke. Contacts between the Seymour Canal Formation and the Triassic rocks were not observed during this study. However, Barker (1957) indicates that observed contacts between these units appear conformable (Barker's Barlow Cove Formation is apparently partly equivalent to the Triassic Hyd Group and his Symonds Formation (abandoned by Lathram and others, 1965) is equivalent to the Seymour Canal Formation). Fossils suggest a significant nondepositional hiatus between the Hyd Group and the Seymour Canal Formation. Structures observed during this study in the Hyd Group and in the lower part of the Seymour Canal Formation are similar, which is interpreted to suggest that a major metamorphic or deformational event did not occur during this hiatus.

Intrusive Rocks

Intrusive rocks include middle Cretaceous quartz diorite plutons 11 to 15 miles east of Greens Creek (Haeussler, 1992) and ultramafic and mafic rocks near the Greens Creek mine and to the northwest. The ultramafic and mafic rocks are of uncertain age, but fragments of some of them in basal Hyd Group conglomerates at Greens Creek indicate that they are at least in part older than Upper Triassic Hyd Group and therefore are at least in part older than ore.

Rock Units of the Greens Creek Mine Area

Rock units in the mine area are briefly summarized here for use in the following discussion. More detailed descriptions can be found in chapter 6 of this volume. The units are grouped according to whether they are stratigraphically below or above the ore horizon. Those stratigraphically below the ore horizon include deformed and metamorphosed ultramafic and mafic rocks and their intensely altered, deformed, and metamorphosed equivalents, which comprise a group collectively referred to as "phyllites." Conglomerate and sedimentary breccia, with clasts of the mafic and ultramafic rocks and of phyllites, lie above these rocks and below the ore horizon. Rocks stratigraphically above the ore horizon are argillites, metabasalts, and minor metagabbros of the Upper Triassic Hyd Group and slaty siltstones and lithic sandstones that are either part of the Hyd Group or part of a younger unit.

Graphitic Quartz Mica Schist (Retreat? Group)

Outcrops of graphitic quartz mica schist and phyllite are in the northern part of the Bruin Creek area, near the 1350 portal, just east of the mouth of Gallagher Creek, and in a

few other localities (pl. 7–1). These are highly deformed, commonly graphitic, quartz-rich metasedimentary rocks that resemble the Paleozoic rocks referred to as "Retreat Group" (Lathram and others, 1965) along Hawk Inlet. In the mine area, these rocks lie structurally below the altered mafic rocks discussed herein, but in the Bruin Creek area they locally lie structurally above these rocks, though below the conglomerate and sedimentary breccia (pl. 7–1).

Ultramafic Rocks

Ultramafic rocks include serpentinite (\pm chlorite) (SC), and its hydrothermally altered, deformed equivalent, carbonate (magnesite, ankerite or dolomite)- \pm mariposite- \pm chlorite- \pm talca(?)- \pm quartz- \pm leucoxene phyllite.

Mafic Rocks

Most mafic rocks are strongly altered and deformed, but where alteration and deformation are least intense, relict textures generally indicate the rock is gabbro (DG). Relict textures indicative of basalt are generally rare to absent within the phyllites of the mine area. However, if basalts had been present, their textures may have been destroyed because of the finer grain size. Altered, deformed equivalents of the mafic rocks, in order of increasing alteration intensity, are chloritic rock or phyllite (CR), chlorite-sericite- \pm quartz-pyrite- \pm carbonate-leucoxene phyllite (SPc), sericite-quartz- \pm carbonate-pyrite- \pm leucoxene phyllite (SP), and siliceous rock (SR, essentially alteration silica with pyrite, \pm minor sericite). Phyllites representing the most intense alteration are most commonly found stratigraphically directly below the ore. These rocks are discussed in more detail in chapter 6 of this volume.

Conglomerate/Breccia

A unit of strongly deformed conglomerate and sedimentary breccia is commonly present at the top of the phyllites. Coarse sandstone is present locally and may be bedded (fig. 2C). West of Gallagher Creek (16675N, 17150E, pl. 7–1) conglomerate and coarse sandstone are interbedded with the lower part of the argillite unit. Throughout the mine area clasts mostly consist of various metamorphic rocks of types found in the Paleozoic section and of altered, deformed, and metamorphosed mafic and ultramafic rocks, like those they overlie. Due to the intense deformation, it is not always certain whether the altered mafic/ultramafic clasts were altered before or after becoming clasts. In a few exposures, however, such as west of Gallagher Creek (16788N, 17193E, pl. 7–1), the presence of carbonate-mariposite-quartz (probable altered ultramafic) clasts adjacent to serpentine clasts in a serpentine-rich clastic matrix suggests at least some alteration took place before deposition of the conglomerate. Except for the presence of clasts, the conglomerates closely resemble sericitic phyllites and siliceous rock of the underlying "phyllites" and when clasts are difficult to see, these rocks are usually mapped as

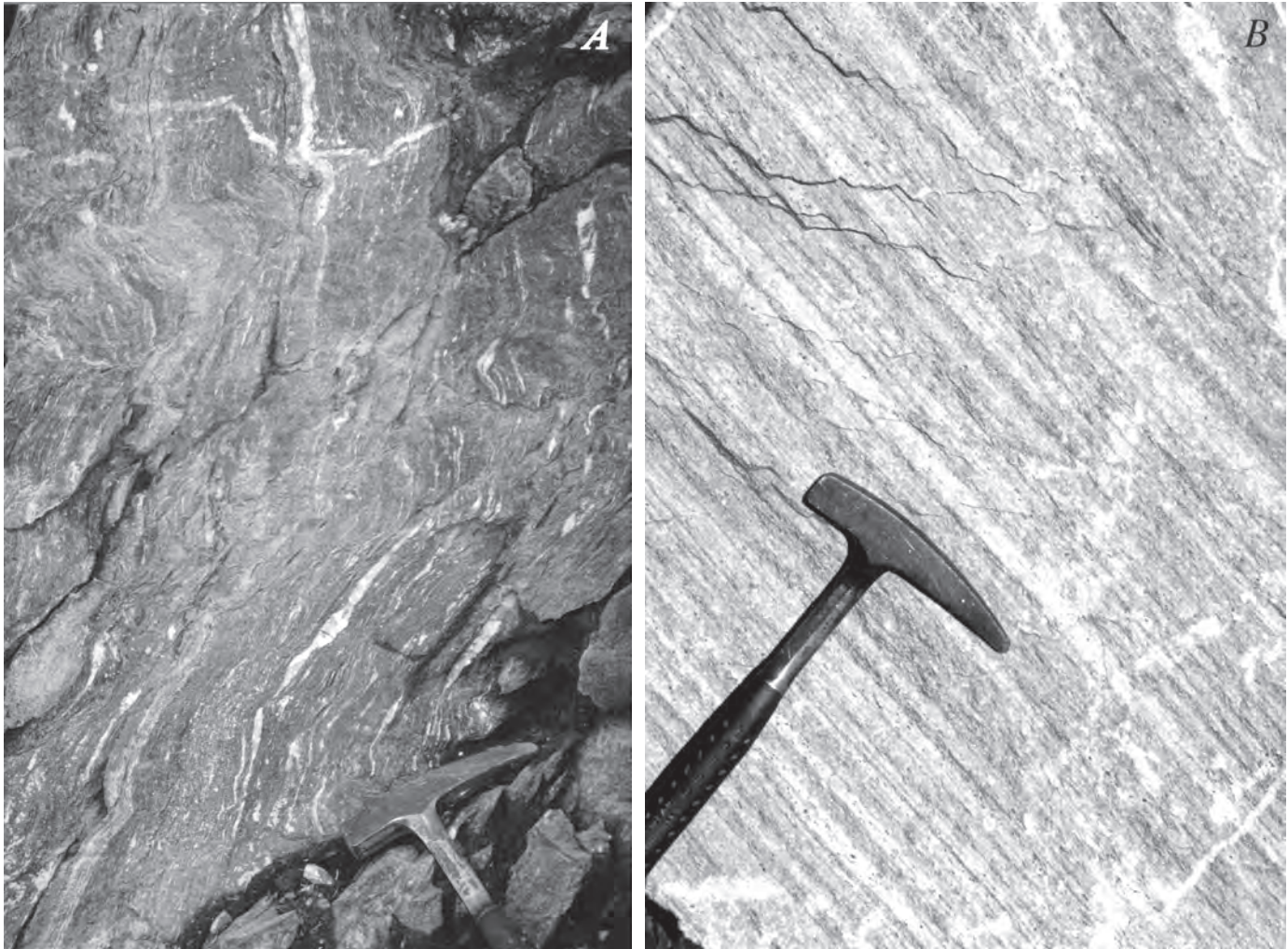


Figure 2 (above and facing page). Photographs of Greens Creek rocks. *A*, Graphitic quartz-mica phyllite or schist of Paleozoic Retreat(?) Group, 3.4 mile “B” road, 3.6 miles (5.9 km) west-northwest of Greens Creek mine. White to pale gray lenses are mainly highly deformed vein quartz of predeformation origin. *B*, White to pale greenish quartz-muscovite schist of Retreat(?) Group, Pit 7, “A” road, 6.5 miles (10.5 km) northwest of Greens Creek mine. White layers are mainly quartz; gray (actually greenish) is muscovite. *C*, Angular pebble conglomerate with faintly bedded sandstone in upper right. White dashes show contact between conglomerate and sandstone and are parallel to bedding; black dashes show orientation of S₂. Some fragments contain a preconglomerate foliation and metamorphic segregation at various angles to each other and to S₂, and some fragments contain preconglomerate quartz veins. Matrix and sandstone largely pyritized. From 720 ore access (17250N, 20300E, 718-foot elevation), looking N. 27 W., with up indicated by white arrow in upper left.

part of the phyllite package. However, the presence of Paleozoic metamorphic clasts indicates that they are probably part of the conglomerate unit near the base of the Upper Triassic Hyd Group.

Clasts of mafic and ultramafic metaintrusive rocks and of their phyllitic altered equivalents in the conglomerate indicate that at least some mafic and ultramafic rocks are of pre-Hyd age, older than Greens Creek ore, and may not be related to the Hyd basalts. Alternatively, they may, at least in part, have been emplaced early in a protracted igneous episode that included later ore deposition and still later Hyd basalts.

Argillites and Mafic Rocks

Most ore occurs in the basal part of the argillite unit of the Upper Triassic Hyd Group. The main lithologies in this unit are black to dark gray, slaty argillite (SA) and gray to brown, dolomitic and calcareous, massive argillite (MA). Massive argillite occurs in beds that vary from about 2 cm to 20 cm (rarely up to a meter) thick. They are characterized by abundant white ladder veins or “lightning veins” (fig. 3A). Some massive argillite beds mainly consist of fine dark silica, but it is not known if this is primary chert or the result of silicification of carbonate beds.



Massive argillite beds are generally separated by interbeds of slaty argillite and occur in sequences up to tens of meters thick (for example, fig. 4). Sequences of slaty argillite with few or no massive argillite beds are also common and seem to become more abundant in the upper part of the section. Locally minor, thinly laminated, pale gray to pinkish chert is associated with the ore horizon (for example, fig. 5).

Conodonts from two localities near the base of the argillite in the mine have yielded Late Triassic ages with possible ranges from late Carnian through about middle Norian (chap. 11). Two samples, one from the mine and one from Big Sore Creek, from argillite farther from the phyllite contact (presumably higher in the section?) have yielded possible age ranges of late Carnian through earliest Norian (chap. 11). Conodonts from a limestone bed at the phyllite/argillite contact west of Gallagher Creek are also latest Carnian through earliest Norian (chap. 11).

On Gallagher Ridge south of the Greens Creek mine, a sequence of Hyd metabasalts overlies typical argillite in conformable depositional contact. Conodonts from limestone interbedded with the lowermost two or three flows also are of late Carnian through earliest Norian age. Gabbro sills in the underlying argillite may be related to feeders for the flows and are discussed further in chapter 12.

Graphitic Slates and Sericitic Slaty Sediments

Above the Greens Creek mine, a sequence of metasedimentary rocks of uncertain correlation with other rock units in the area overlies a major low-angle ductile shear zone (see pl. 7-1; shear zone described in “Geologic Structure” section). Although these rocks are strongly deformed, a few graded beds suggest they are mostly right-side-up. The lowermost part of the sequence consists of black to pale gray, graphitic, slaty sedimentary rocks with rare beds of calcareous or dolomitic argillite a few centimeters thick. Some of the calcareous or dolomitic beds have lightning veins, and the sequence somewhat resembles parts of the argillite sequence above the orebodies. However, sequences with abundant massive argillite beds, such as are common above the ore, have never been observed in this upper sequence. Upwards in the section, the few beds of massive argillite are absent, and the rocks resemble argillite above the orebodies even less. The graphitic slaty sedimentary rocks are overlain by greenish to pale gray, sericitic, slaty rocks. These consist of siltstones and lithic sandstones that are commonly well bedded and which may locally be interbedded with rocks similar to those of the underlying graphitic unit. A few beds are very fine grained and siliceous, but it has not been determined if these are primary cherts or silicified siltstones. Rare dolomitic beds are also present.

More than 20 samples of calcareous and dolomitic beds from the graphitic slaty sedimentary unit and the sericitic slaty sedimentary unit were sampled for conodonts, but all were barren (chap. 11). Possibilities for correlation of these two units are: (1) They represent an upper part of the Upper Triassic Hyd Group well above the ore horizon; (2) they may correlate with parts of the Upper Jurassic and Lower Cretaceous Seymour Canal Formation, which they somewhat resemble, except for the slightly stronger deformation, alteration, and metamorphism; or (3) they may be part of an unrecognized post-Hyd unit.

Geologic Structure

Structural features are described in the following subsections from oldest to youngest; the younger structures have had important effects on the distribution and orientation of older structures. Northwest-trending strike-slip faults are the youngest features and divide the area into several major blocks. The best known blocks are those on each side of the Maki fault; structure and stratigraphy are readily correlated across the fault (pl. 7-1). Other blocks occur within and southwest from the Gallagher fault system, southwest of the mine (pl. 7-1). In addition, all blocks are further subdivided by major low-angle ductile shear zones of post-F2, pre-F3 age. The best known is the “Upper Shear Zone” above the mine workings, which separates the geology within the mine (“Mine Plate” or footwall of Upper Shear Zone) from the geology exposed on the surface along Big Sore Ridge (“Upper Plate” or hanging wall of Upper Shear Zone) above the mine (pl. 7-2A, B). Also, a less well known “Lower Shear Zone” lies below the mine workings; the footwall rocks (“Lower Plate”) are poorly known (pl. 7-2A, B).

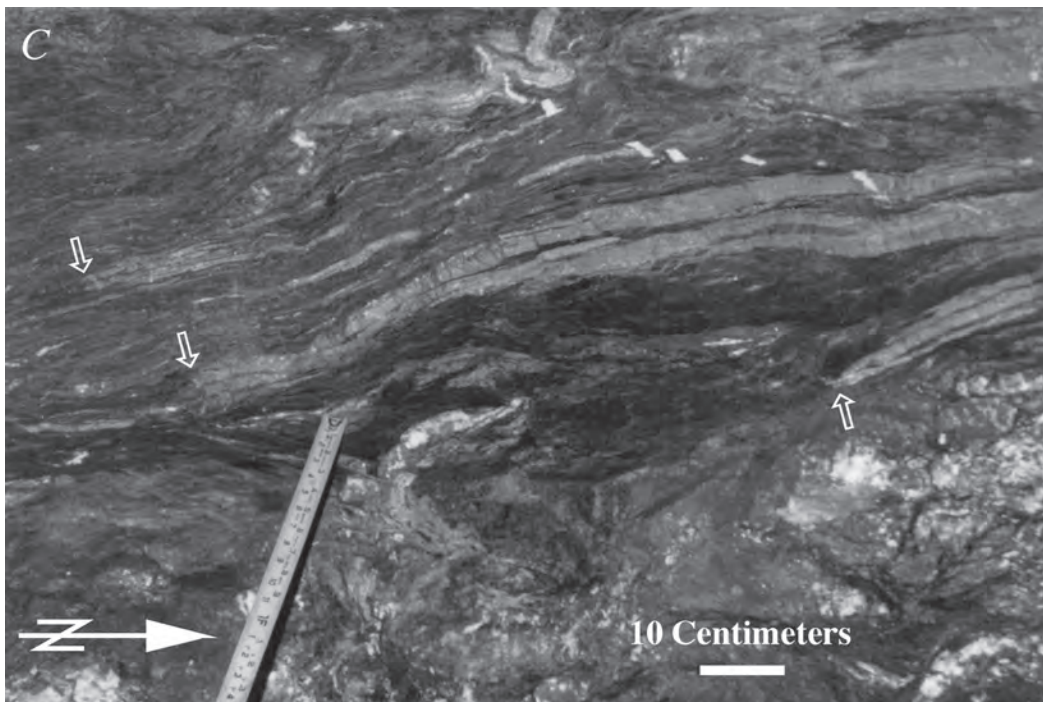


Figure 3 (facing page). Photographs of F2 related structures in the Greens Creek mine. *A*, Tight F2 fold in massive argillite beds, looking down plunge (N. 58 W., 67°). F2 axial plane (white dashed lines) and axial planar S2 foliation in slaty interbeds are slightly refolded by F3. Ladder veins are at a high angle to S2 and are not folded by F2, even in the tight F2 hinge zone, but are folded by the small F3 fold. 580 ore access, 17450N, 20355E, 584-foot elevation. *B*, S2 foliation plane, showing L2 (half-barbed arrow) and small F4 folds (full arrow). 1350 tunnel, 73 feet from portal, northeast rib, looking N. 60 E. (20085N, 19995E, 1,365-foot elevation). *C*, Layers of massive sulfides (lighter colored bands in upper half of photograph) in slaty argillite, tightly folded by F2 (open arrows point to hinges). Strong, penetrative S2 is subparallel to the tightly folded layers, and many S2 planes appear to have accommodated shearing. Lower part of photograph is massive argillite. 344S stope, view of back, looking up (16905N, 20392E, 360-foot elevation).

Pre-Hyd Group Deformation (S1 and S1.5)

Pre-Hyd Group deformation is represented by foliation in metamorphic clasts in the conglomerate/sedimentary breccia unit (fig. 2C), and by foliations observed in outcrops of the graphitic quartz mica schists and phyllites correlated with the Retreat(?) Group (see section “Rock Units of the Greens Creek Mine Area”). The most common type of early foliation, in outcrops and in clasts, is a prominent metamorphic, segregation-type layering, in which quartz-rich layers, 1–10 mm thick, alternate with thinner, gray to black, sericitic layers. This layering is here referred to as S1.5. Although S2 foliation (described in the following subsection) overprints this layering and is commonly parallel to the layering, outcrops can be found in which S2 is at an angle to the layering, and the layers are folded by F2. Rare outcrops can also be found (pl. 7–1, 23880N, 18820E) in which the layering is truncated at the basal contact of the conglomerate/sedimentary breccia unit. In conglomerate, the metamorphic layering is restricted to clasts, is of different orientations in different clasts, and is truncated by the conglomerate matrix (fig. 2C). Clasts, metamorphic layering within clasts, and conglomerate matrix are all overprinted by S2 foliation (fig. 2C).

Within the quartz-rich layers of the graphitic sericitic schists and phyllites, a relict foliation at an angle to the layering can be observed locally (pl. 7–1, just east of the mouth of Gallagher Creek, and in the Bruin Creek area). This relict foliation, here referred to as S1, is defined by grain size, grain shape, and by white to dark gray colored layers, in quartz and associated carbonate. Rarely, micas are parallel to this relict foliation, but in most rocks mica has been reoriented parallel to S2 or S1.5.

Muscovite that defines S1 or S1.5 is commonly coarser grained than that which defines S2 or younger foliations (fig. 2B). Layers rich in leucoxene, carbonate, chlorite, or other silicates may define S1.5 or S1 in mafic and ultramafic rocks.

It is likely that S1.5 and possibly S1 were formed as part of the Permian metamorphic event documented by the 265-m.y. cooling ages reported by Haeussler and others (1999). This event likely involved structural features other than these foliations but has not yet been studied in detail in the Greens Creek area.

F2 Folding and S2 Foliation

F2 folding at Greens Creek and related S2 foliation represent the oldest deformation known to have affected rocks of the Upper Triassic Hyd Group and overprint all older rocks. Folding and foliation that appear to be similar to F2 and S2 at Greens Creek, with regard to its characteristics and age relationships, are well developed in the surrounding region, extending at least from Hawk Inlet to Young Bay. At Young Bay the folding and related foliation overprint Hyd Group rocks as well as rocks of at least the lower part of the Upper Jurassic to Lower Cretaceous Seymour Canal Formation. Therefore, this deformation is tentatively considered to be an early phase of the middle Cretaceous deformation that occurred in a belt along the east margin of the Alexander terrane in southeastern Alaska (Haeussler and others, 1999).

F2 folds in the Greens Creek mine area are extremely tight and are isoclinal in many places (figs. 3A, 3C, 4, 5). S2, which is axial planar to these folds, is very strongly developed and is usually penetrative. In most of the phyllites, S2 is the dominant structural fabric (for example, see fig. 10C) and S2 is also well developed in most argillites. A lineation, L2, is common on S2 planes. In metasedimentary rocks, L2 is commonly a color streaking due to S2-bedding intersections and, in these cases, is essentially parallel to F2 fold axes. In phyllites, L2 is commonly a color streaking or, in some cases, is defined by small, hard ridges and grooves (fig. 3B). L2 in phyllites is commonly, but not always, subparallel to fold axes. L2 may be the result of the intersection of S2 with various features in the phyllite, such as altered relict primary mineral grains, fragments, or small veinlets, that have been elongated subparallel to fold axes or flattened subparallel to axial planes during deformation.

F2 folds have highly variable orientations, at least partly because they have been strongly refolded by F3 folds. F2 axial planes and S2 planes generally strike north-northwest and dip steeply on the east limbs of F3 synforms, dip gently in most F3 hinge zones, and dip gently to moderately easterly on west limbs of F3 synforms (fig. 1). With the effects of F3 folding removed, it appears that the average S2 orientation would have dipped moderately to the southwest. F2 axes also vary greatly in orientation within the refolded F2 axial planes (fig. 6). In most of the Mine Plate, F2 axes, L2, and bedding-S2 intersections (pl. 7–3, 7–4) plunge mostly steeply where S2 is steep, and have a northeast-southwest to west-northwest–east-southeast orientation where S2 dips gently. There are many exceptions, however, and many F2, L2, and bedding-S2 intersections also plunge gently northerly or southerly. In the Upper Plate, F2 orientation is also

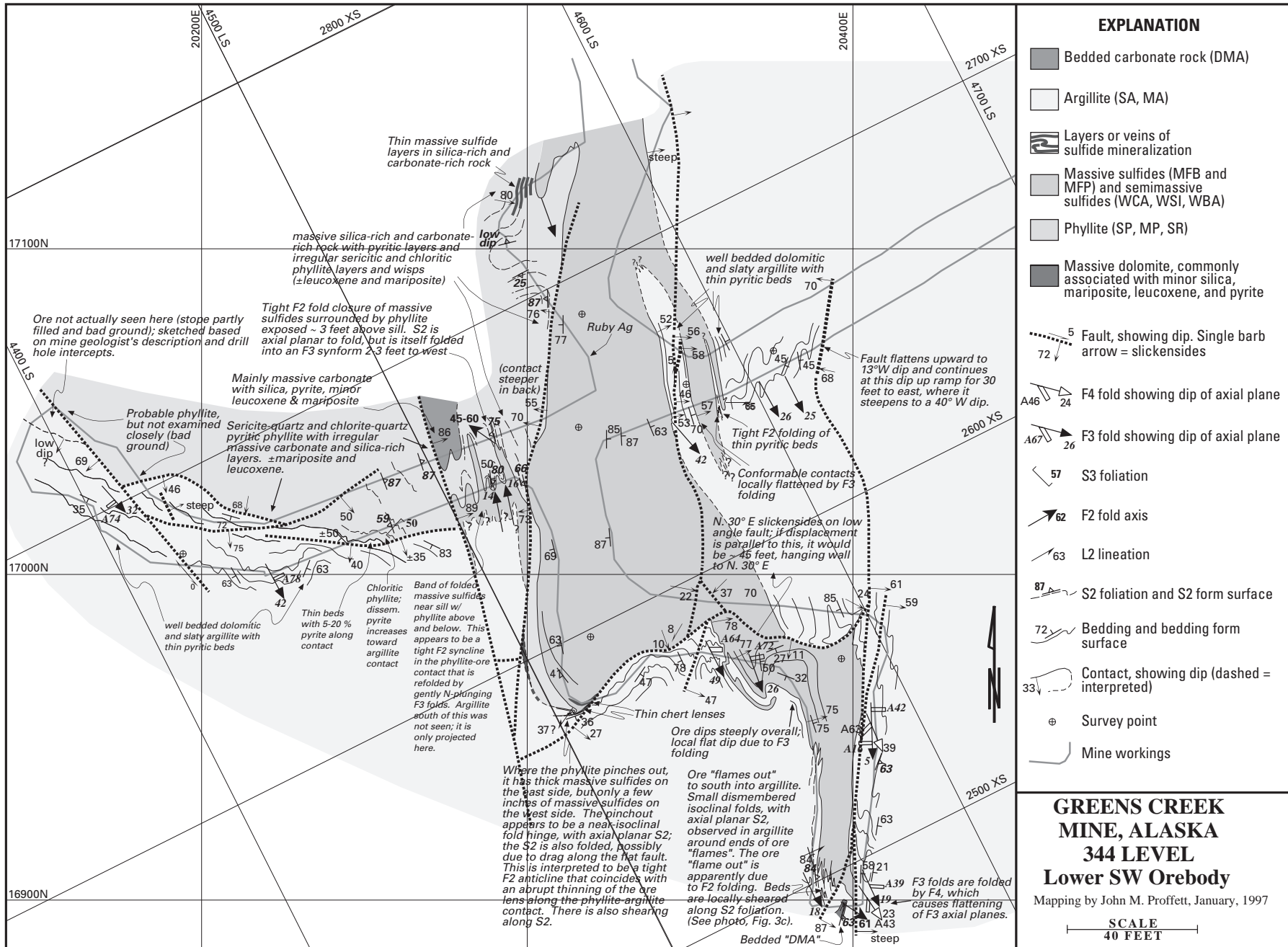


Figure 4. Map of 344 stope and 350 ore access crosscut (344-354-foot mine elevation).

highly variable (pl. 7–3), but here F2 has a tendency to trend south-southeast at gentle to moderate plunges, especially in the southern part of the area.

The variability of measured axial orientations is also reflected in direct observations of F2 folds in outcrops and mine workings. Axes are observed to bend more than 60 degrees across a few feet of mine workings.

Although much of the variability of F2 axis orientations is due to refolding by F3, observations suggest that some variability may be due to causes other than later folding. Possible causes are F2 folding of previously deformed rocks, possibly the result of pre-F2 folding or faulting that is not yet understood, or nonhomogeneous deformation, resulting in amplitude variations along fold axes. Nonhomogeneity is not uncommon in strong deformation, such as F2.

In phyllites, S2 is defined by oriented sheet silicates and, in some cases, by layers or lenses rich in quartz and/or carbonates that alternate with layers rich in sheet silicates. Generally, minerals that define S2 are finer grained than those that define S1.

Most massive argillite beds have white ladder veins of quartz and calcite (“lightning veins”). Generally these are oriented at a high angle to S2 but are parallel to, or within a few tens of degrees of, F2. They have not been observed to be folded by F2, but are folded by F3 (fig. 3A). The veins are interpreted to have formed as tension fractures more or less perpendicular to the lengthening direction that was perpendicular to F2 shortening.

In mine workings many F2 folds have been mapped that have amplitudes of up to several tens of feet, and in some cases up to 200 feet (fig. 5). Based on correlation between various workings and drill holes, larger F2 folds with up to several hundred feet amplitude are interpreted. In the eastern and northern parts of the mine, most F2 anticlines (that is, folds with phyllite cores and argillite outer parts) close southward and have long eastern limbs and short western limbs (when viewed looking downward where the F2 folds are exposed on steep east limbs of F3 synforms; see figs. 7, 8). Overall, with F3 unfolded, it appears this zone would have been the overturned lower limb of a major, inclined, south- or southeast-closing F2 anticline, with older rocks above and to the west (fig. 8). The hinge and west (right-side-up) limb of this anticline is mostly truncated upward by the Upper Shear Zone, but parts of the west limb are exposed just below the Upper Shear Zone east of the mouth of Gallagher Creek (pl. 7–1, ~18800N., 17300E.).

Several F2 folds, with geometries consistent with location on the overturned lower limb of a major F2 anticline, cross through the West orebody (see pl. 7–4 for orebody locations). Their axes can be traced southwestward through the north part of the Central West orebody (fig. 7) to where they are displaced 1,750 feet northwestward across the Maki fault to the Northwest West orebody. They trend southward through the Northwest West orebody, where they bend to the southeast and, at the south end of this orebody, are again cut by the Maki fault and displaced southeast back to the south part of

the Central West orebody (fig. 6). Here they trend southeast, and as they are followed southeastward, they again bend to the south (fig. 6).

The Upper Southwest and Lower Southwest orebodies appear to be situated on a large F2 anticline (pl. 7–2A). The eastern part of the Lower Southwest orebody is mostly on the steep east limb of the anticline (fig. 4) and flat-lying ore is on the west limb. The Upper Southwest orebody consists of several tight anticlines within the hinge zone of the main anticline (fig. 5) that have been refolded by F3. These anticlines appear to define an overall axial zone that plunges moderately to the south.

In surface exposures above the Upper Shear Zone, most F2 anticlines also appear to close to the south, but with long west limbs and short east limbs, and with older rocks apparently exposed below and to the east. Overall, this area appears to be on the upright lower limb of a major, inclined, F2 syncline, with older rocks below. The hinge zone of this major F2 syncline is exposed west of Gallagher Creek (pl. 7–1, 7–3, ~17650N, 15000E).

Where examined in detail, beds are sometimes found to end abruptly at S2 planes, especially in areas of strongest F2 deformation. Apparently, cleavage plane shearing has taken place, but it is not certain if this was part of the F2 deformation process or related to the S2.5 ductile shearing event that followed (described below).

Ductile Shear Zones (S2.5)

Upper Shear Zone

The Upper Shear Zone is a major ductile shear zone exposed above the uppermost mine workings, on the surface, and in several drill holes (pl. 7–1, 7–2A, 7–2B). This zone dips gently and separates the geology of the mine (Mine Plate) from the somewhat different geology exposed on the surface above (Upper Plate).

The shear zone is tens to several hundred feet thick, and rocks within this zone are overprinted by a strong shear foliation (fig. 9). Immediately below the zone in the mine area are mafic and ultramafic rocks and their altered equivalents, mostly phyllites consisting of carbonates and sheet silicate. Rocks immediately above the zone are black graphitic slates and slaty argillites with rare carbonate or siliceous massive argillite interbeds. In parts of the shear zone, shear-foliated equivalents of rocks above and below can be recognized, but intensely shear-foliated rocks of uncertain origin also are present within the shear zone. These latter rocks consist of quartz and/or carbonate with minor sericite and other sheet silicates (qsc unit—see pl. 7–1, 7–2A, 7–2B; fig. 9). The protoliths for the quartz-rich rocks probably were siliceous metasedimentary rocks and/or phyllites, and the protoliths for the carbonate-rich rocks probably were altered ultramafic and mafic rocks.

The shear foliation consists of slightly undulating, bifurcating, thin, discrete layers rich in sheet silicates, that separate thin, lens-shaped layers relatively rich in quartz and/or

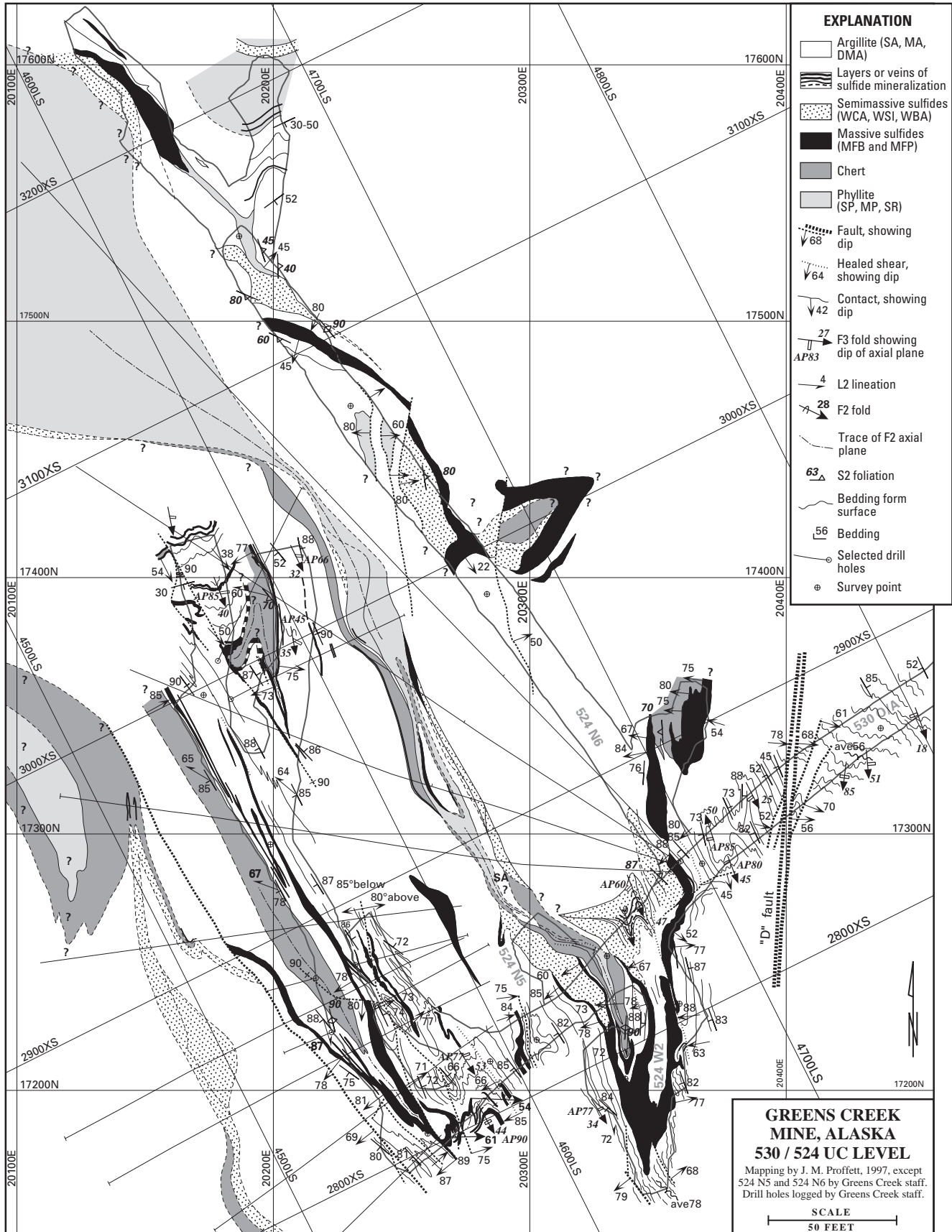


Figure 5. Map of 524 stope and 530 ore access crosscut (524–532-foot mine elevation).

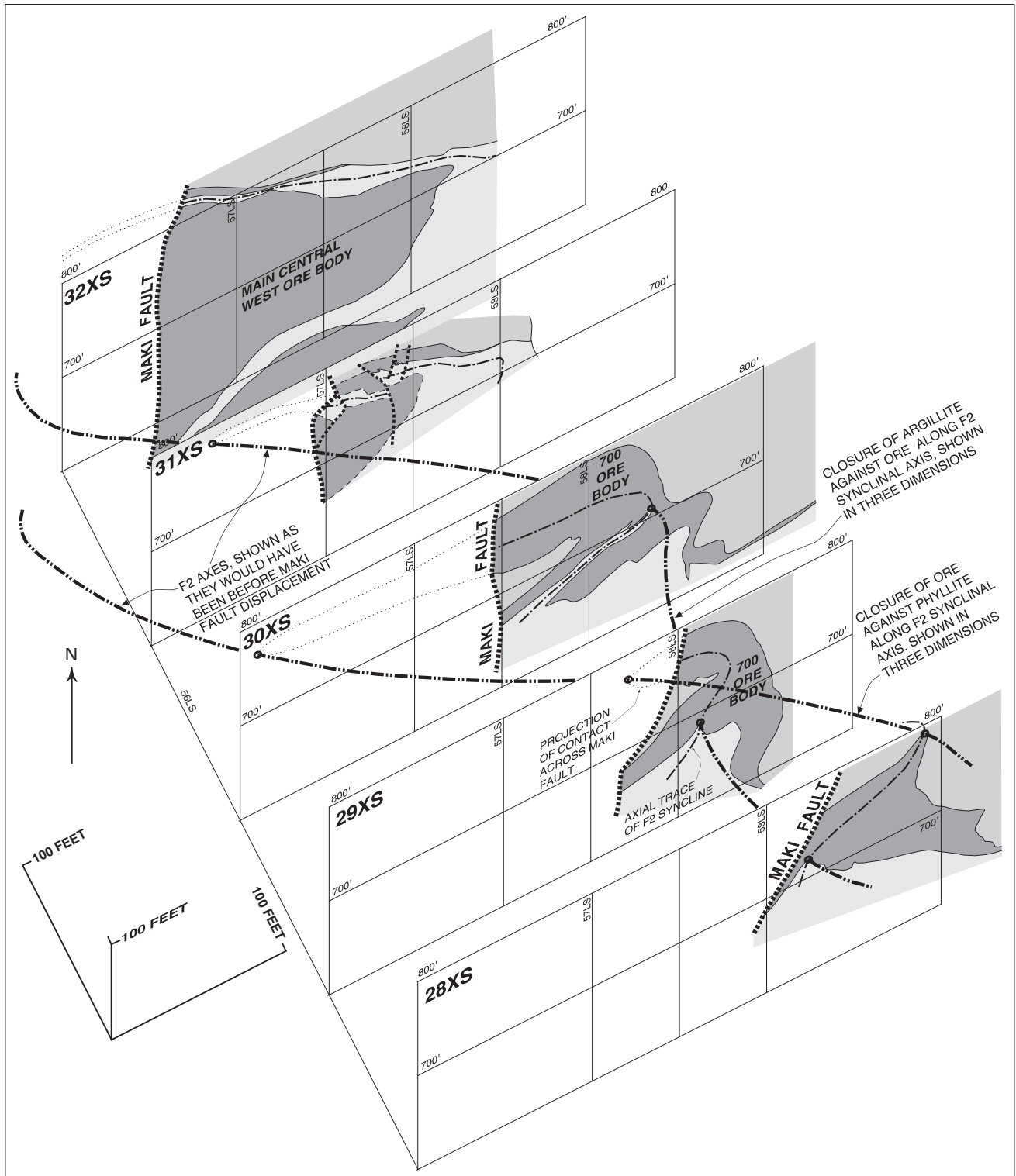


Figure 6. Fence section, looking north and down at 60°, showing variation in orientation of F2 axes in West orebody between 28XS to 32XS. The axial trace of the uppermost F2 fold is shown as a dot-dash line on each section. F2 fold axes for this fold are shown in three dimensions as they would have projected across both sides of the Maki fault, as double-dot-dash lines connecting the sections, one showing the hinge for the argillite/ore contact, and one showing the hinge for the ore/phyllite contact. The ore horizon is interpreted as thickest on the east limb of this F2 fold south of 31XS, resulting in the 700 orebody, and as thicker on the west limb of the fold north of 31XS, resulting in the main Central West orebody. The shape of orebodies on the sections appears flattened because of the perspective resulting from the view looking down at a 60° angle (compare the center section, 30XS, with the same area on pl. 7-2A (in CD), which shows a slightly more detailed interpretation).

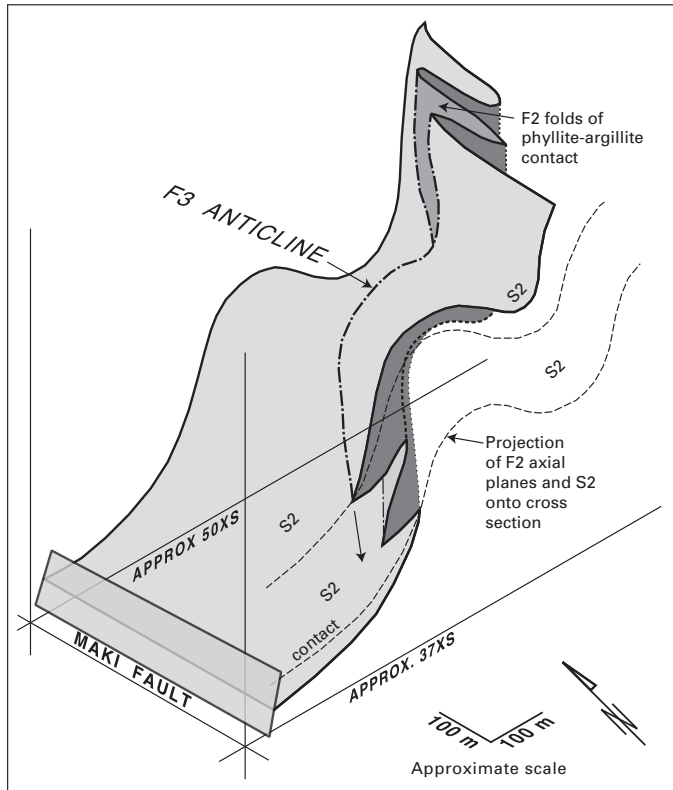


Figure 7. Three-dimensional sketch of northern part of Central West orebody, diagrammatically showing interpretation of F2 folds refolded by F3, east of Maki fault.

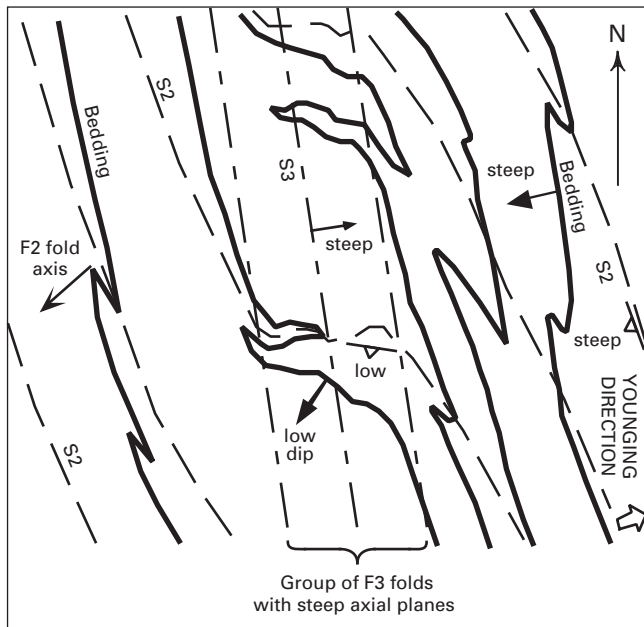


Figure 8. Diagrammatic plan view, showing relationships between bedding, F2/S2, and F3/S3 in the main part of the Mine Plate. South-closing F2 folds (which are anticlines here) have short west limbs and long east limbs. Bedding and S2 are locally folded by groups of F3 folds with axial planar S3.

carbonates (fig. 9). A stretching or mineral lineation (L2.5) is usually present on shear foliation surfaces, and the quartz/carbonate-rich lenses between shear-foliation planes are elongate parallel to the lineation. The lenses are thus ribbonlike, with length to width to thickness ratios of as much as 50:10:1.

Shear foliation (S2.5) postdates F2 and predates F3; it displaces and deforms S2 foliation but is folded by F3.

Zones of breccia, or partly brecciated wall rock, are present along the shear zone (pl. 7-2A, 7-2B) and are overprinted by the shear foliation. Therefore, it appears that the shear zone began as a brittle fault zone, which became ductile with time.

Direction and amount of displacement across the Upper Shear Zone are uncertain. Although some generalized stratigraphic units can be matched across the shear zone, complex F2 structure and limited exposures have precluded establishment of a satisfactory match. Displacement direction is likely in the direction of the shear lineation previously described, which in most outcrops measured trends E-W to WNW-ESE. Rare megascopic shear-sense indicators suggest top-to-the-west (fig. 9A) as does limited petrographic work (fig. 9B), but more work is needed. Effects on shear sense indicators of F3 and of other postshearing deformations are still being evaluated. Top-to-the-west displacement would be consistent with the apparent younging directions in the Mine Plate and Upper Plate (pl. 7-2A).

Klaus Shear

The Klaus shear, first noted by Klaus Triebel (written commun., 1992), is a low-angle healed fault that displaces the argillite/phyllite contact in the east part of the mine (pl. 7-2A). A displacement of a few hundred feet of hanging wall northwest has been estimated by Lindberg (P.A. Lindberg, written commun., 1994). This shear zone appears to correlate with one mapped in the 1350 tunnel (J.M. Proffett, written commun., 1987), which is associated with ductile shear foliation and is folded by F3. The Klaus shear could, therefore, be part of the same deformational event as the Upper Shear Zone.

Lower Shear Zone

Evidence for another shear zone has been found in a few deep drill holes below the mine (pl. 7-2A, 7-2B). In most holes, argillite is juxtaposed against underlying phyllites. Ductile shearing fabrics similar to those in the Upper Shear Zone occur in the Lower Shear Zone, as do zones of breccia and partly brecciated wall rock that are overprinted by shear foliation.

Possible F2.5 Folds (?)

A few folds have been found that appear to fold S2 but are overprinted and transected by S3. These are not common, but their age relationships suggest they could be related to the ductile shearing event.

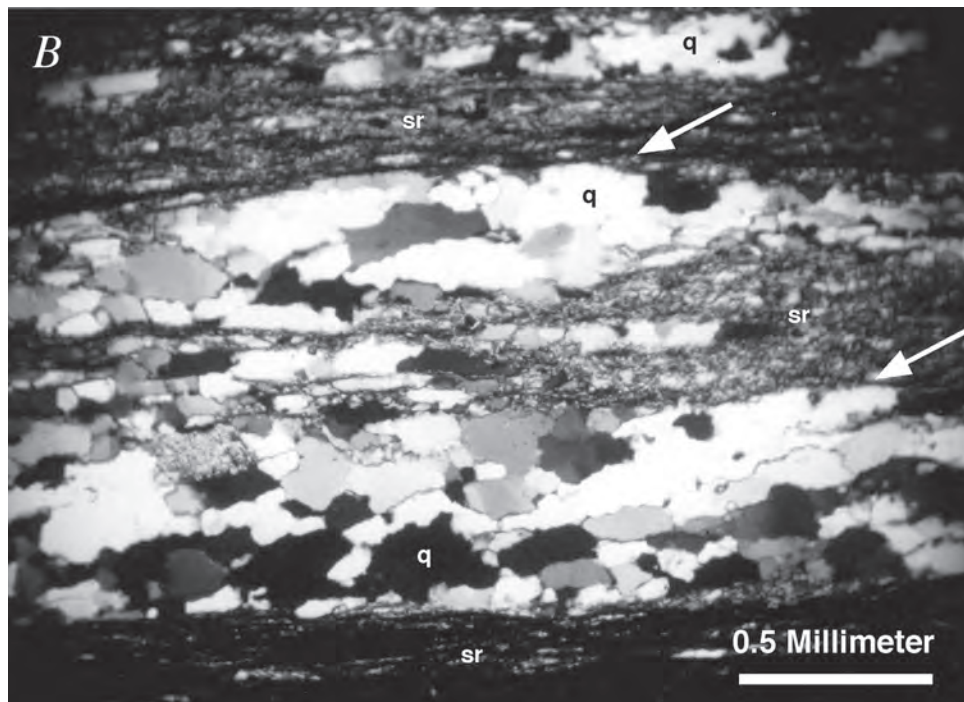
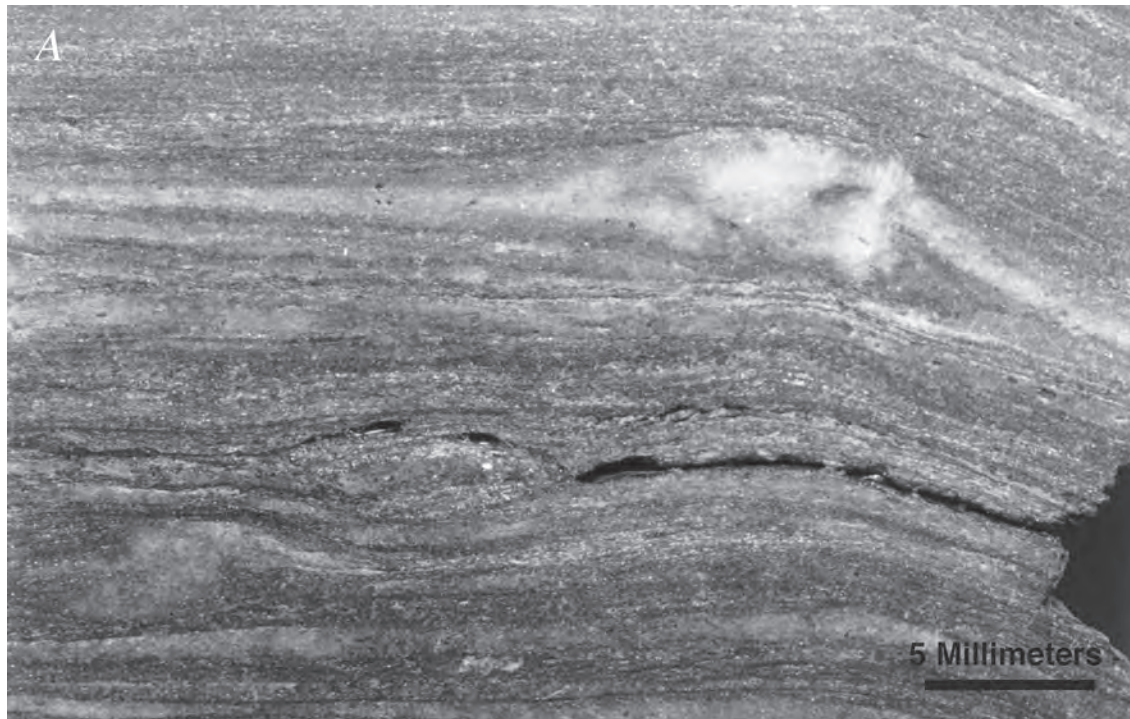


Figure 9. *A*, Photograph of shear foliated quartz-sericite-(carbonate) phyllite (a mylonite), showing asymmetric tails on quartz pods that suggest top-to-the-west sense of shear. *B*, Thin section of *A*, crossed polarizers, showing preferred orientations of flattened quartz grains (white arrows) oblique to shear foliation (which is parallel to bottom and top edges of photograph), also indicating top-to-the-west sense of shear (Simpson and Schmid, 1983; Lister and Snoke, 1984). Quartz-rich lenses indicated by "q," sericite-rich areas by "sr." Top of both photographs is top in the field; both photographs looking south; view is of a plane cut perpendicular to foliation (S2.5) and parallel to lineation (L2.5); location: 18681N, 21137E, surface, 1,952-foot elevation.

F3 Folding and S3 Foliation

F3 folds are generally tight to open upright folds and are the most common and obvious folds in the mine (fig. 10A, B). They clearly fold S2 as well as bedding and shear foliation and are refolded by F4 (fig. 10C). Where not affected by post-F3 structural events, F3 axial surfaces generally strike north-northwest in the northern and eastern part of the area, gradually bend to an approximate north-south strike farther south, and to a south-southwest to southwest strike in the southwest part of the area (pl. 7–5). Most axial surfaces dip moderately to steeply eastward throughout the area. There are many local exceptions to these general trends. Where refolded by F4, the F3 axial surfaces commonly dip gently eastward overall (fig. 1). Locally, axial surfaces dip near vertically, or steeply west, which could also be due to F4 refolding.

F3 fold axes generally plunge gently to the south in the plane of the axial surface, but locally they plunge gently northward (pl. 7–5). In rare cases, they plunge quite steeply north or south. In the 530 Ore Access in the Upper Southwest orebody, F3 changes from a 50°N plunge to a 45°S plunge across a 15-foot-wide crosscut (fig. 5). This could be due to bedding that was previously deformed rather than to refolding of F3.

F3 synforms generally have steeply dipping east limbs (fig. 10A) and moderately east dipping west limbs. The mine area includes several large-scale F3 folds with wavelengths of several hundred feet. Hinge zones of these larger scale folds are characterized by numerous smaller scale F3 folds (fig. 10B) with wavelengths and amplitudes of a few inches to a few feet. These smaller scale folds are less common on the limbs of the larger scale folds. Most of the upper east part of the mine is on the east limb of a large synform (see pl. 7–2A), with an antiform and another synform west of this. Much of the Upper Southwest orebody is in an F3 antiformal hinge zone with abundant smaller scale folds, and the eastern part of the Lower Southwest orebody is on the west limb of this same anticline (pl. 7–2A).

S3 foliation is axial planar to F3 folds, is usually spaced, and usually crenulates S2 (fig. 10B). In some areas it is not developed, especially in massive rocks such as massive argillite. It is most strongly developed in rocks that have abundant fine sheet silicates, such as many of the phyllites and some of the slaty argillites. In a few areas, S3 can be very strongly developed, especially where F3 hinge zones occur in rocks with abundant fine sheet silicates, locally causing complete reorientation of S2. In such areas, it is possible to distinguish S3 from S2 only by mapping the structures into an area where the S3 overprinting is less strong. L3 is a crenulation lineation, generally consisting of small-scale (millimeter scale) folding of S2 foliation planes (fig. 3B).

In general, F2 folds tend to change in orientation irregularly through the mine and on the surface from a roughly southwest trend in the north to a more or less south-southeast trend in the south, whereas F3 folds appear to do the opposite (pl. 7–3, 7–4, 7–5).

S3 Shear Zones

Apparent displacement of older structures or rock units is commonly observed across certain S3 foliation planes. In most cases apparent displacements are only a few centimeters, and many of these could be the result of rock dissolution along cleavage planes. Others are on the scale of mine workings and can locally displace ore and other rock units several feet. At the northern end of the map (pl. 7–1 and 7–5, 24300N, 17900E) the Upper Shear Zone and rock units above and below are displaced by a north-northwest-trending shear zone that is parallel to strongly developed S3. Where exposed, this shear zone forms the contact between graphitic sericitic phyllite to the southwest and carbonate-altered ultramafic rock to the northeast. The contact zone consists of several centimeters of sericitic phyllite, strongly foliated parallel to S3, but no late fault gouge. The vertical component of displacement of the Upper Shear Zone by this S3 shear zone (which is the minimum possible displacement) is 300–400 feet, northeast-side-down. The net direction and total amount of displacement are not known.

F4 Folding

F4 folds and axial planar S4 cleavage are locally developed throughout the mine and surface (fig. 10C). They are abundant in certain areas near the 1350 portal and in the upper part of Big Sore Ridge (pl. 7–5).

F4 folds, which are usually open, have axial planes that generally dip gently southerly and axes that plunge southwest to south (pl. 7–5). They are commonly nearly coaxial with F3, but F4 axial planes generally are at high angles to F3 axial planes (fig. 1). Where F4 and F3 occur together, F3 axial planes are folded by F4 folds (fig. 10C), and the folded F3 axial planes commonly are flattened to an overall gentle east dip. S4 cleavage is only locally developed and is either a spaced fracture cleavage or a crenulation cleavage.

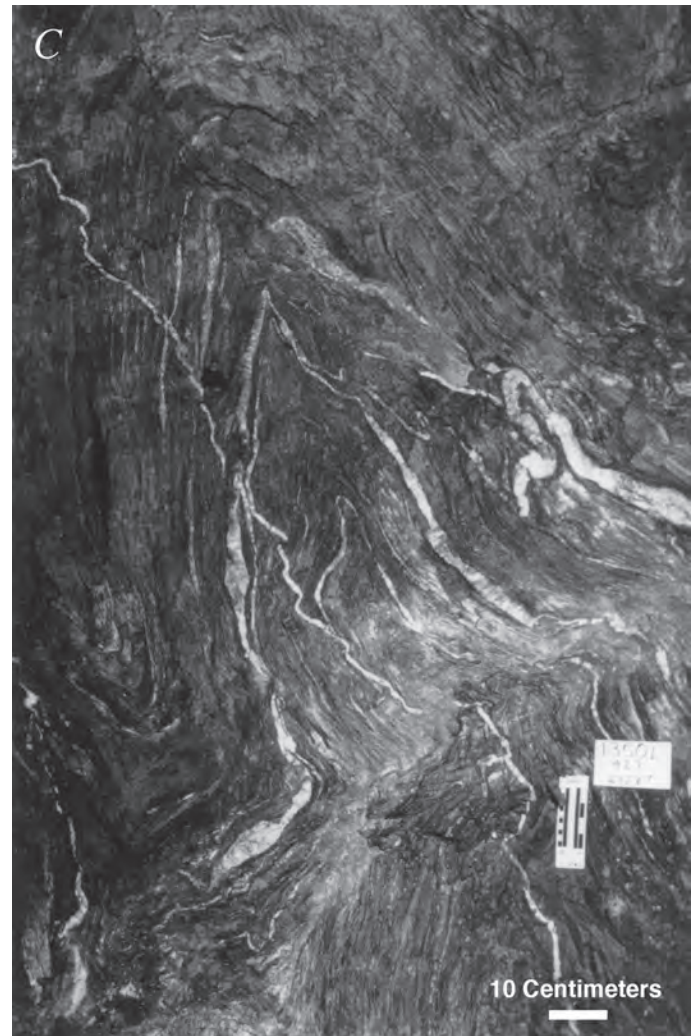
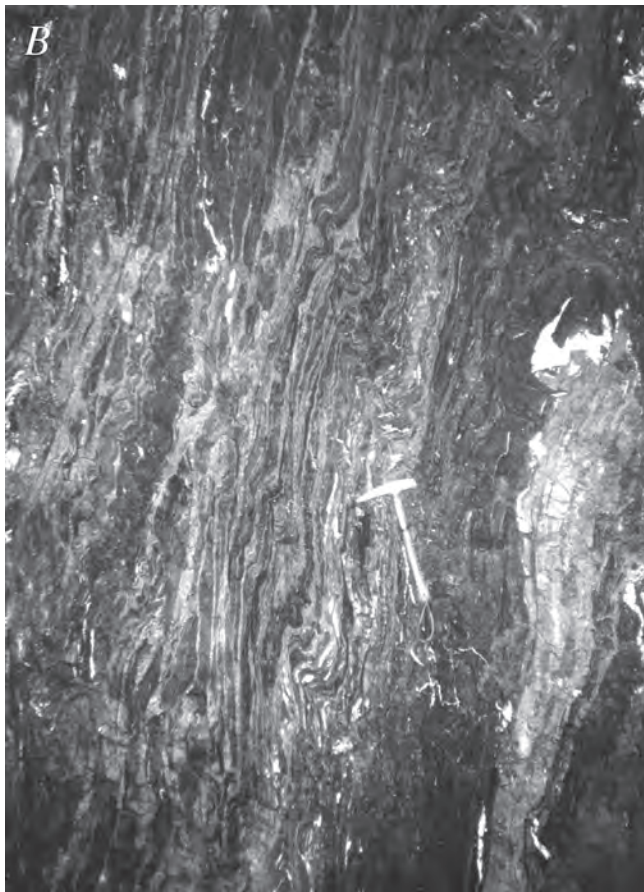
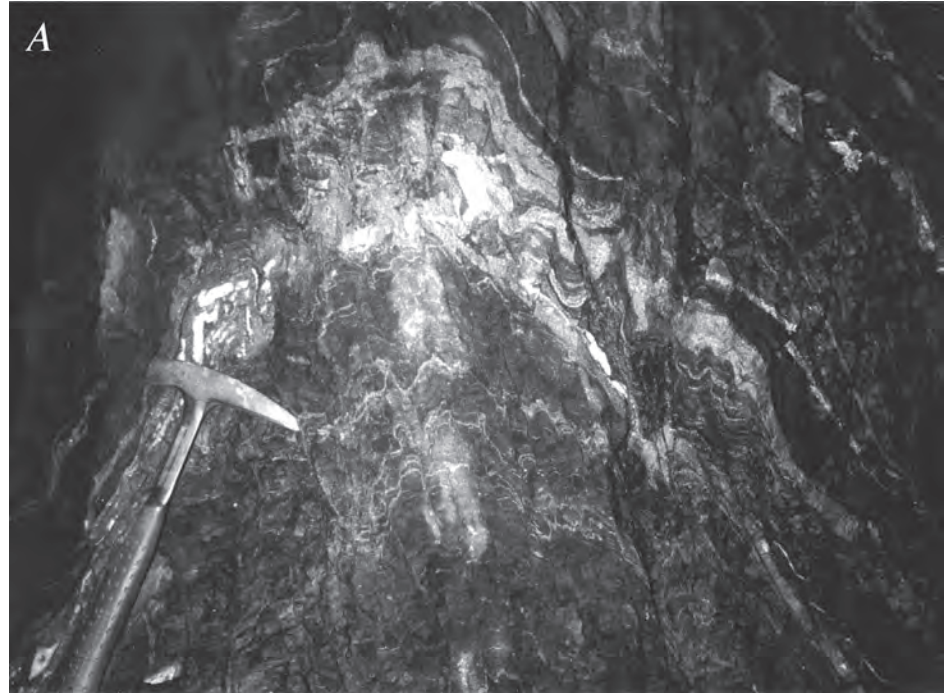
The nearly coaxial orientation of F3 and F4 folds suggests they may be related to the same period of deformation. However, the age relationships and differing orientations of these two fold sets is consistent throughout the mine area, as well as in other areas, such as along the access road (2.5 mi “B” road) just east of Hawk Inlet. In the 1350 tunnel (450 feet southeast of portal), where F4 refolds F3, a quartz vein cuts an F3 axial plane without being folded by F3, but is folded by F4 (fig. 10C). Therefore, these two periods of folding were separated by a fracturing and veining event.

Brittle Faults

Low-Angle Faults

Small, gently dipping faults occur in several parts of the mine. Many of these are healed by white quartz and calcite vein material, and some have been refractured and have dark clay gouge. Other faults consist mainly of clay gouge. These

Figure 10. Photographs. *A*, Steeply west-dipping beds of argillite, with massive sulfide layers, on the east limb of a large-scale F3 synform. Note that bedding is flattened only where crossed by rare F3 folds, such as along hammer handle and 1 foot left of hammer. 580E stope, looking north-northwest (17520N, 20395E, 580-foot elevation). *B*, Cherty argillite with massive base-metal sulfide layers and pyritic beds, folded in an F3 antiform. Note spaced S3 cleavage parallel to axial plane. 580E stope looking north-northwest (17502N, 20385E, 580-foot elevation). *C*, S₂ and quartz veins parallel to S₂, in tan phyllite, folded by F3 and refolded by F4. Note later quartz vein that cuts across F3 axial plane without being folded, but which is folded by F4. 1350 tunnel at 423 feet from portal, NE rib, looking N. 20 W., up plunge (19912N, 20275E, 1,407-foot elevation).



low-angle faults truncate F3 folds, but their relationship to F4 folds has not been established. Many seem to be closely related to strike-slip faults (described below) and may represent bends in strike-slip fault planes or connecting faults between different strike-slip faults. None of these faults are known to have large displacement. For example, the fault shown in figure 4 appears to have about 45 feet of north-north-east displacement of the hanging wall.

Northwest-Striking Right-Slip Faults

The most important brittle faults in the mine area are northwest-striking right-slip faults. These dip steeply, generally to the southwest. The best known is the Maki fault, which separates the east and west parts of the mine (pl. 7-1, 7-4). This fault was defined by T.C. Crafford (written commun., 1986), and an estimate of about 1,800 feet of right slip was made by P.A. Lindberg (written commun., 1994). Correlation of axes of large F2 folds and thickened ore in the Central West ore zone east of the fault with similar structures and thickening in the Northwest West ore zone on the west indicates 1,755 feet (535 meters) of right slip, with 110 feet (34 meters) of west-side-up slip, closely confirming Lindberg's estimate.

The Maki fault consists of several strands within a zone nearly 200 m wide in the southern part of the mine. Northward, the strands merge to a zone about 10 m wide in the north part of the mine. The fault strands consist mainly of soft, sheared, clay-rich gouge and breccia. The Maki fault is also exposed on the surface above and southeast of the mine and can be traced across the district as a prominent topographic lineament.

The Gallagher fault in the Gallagher Creek area west of the mine (see pl. 7-1) is similar to the Maki fault. It consists of at least two main branches, referred to as the East Gallagher fault and the Middle Gallagher fault (P.A. Lindberg, written commun., 1998). Each branch may have up to a few hundred feet of displacement. Topographic lineaments and mapping to the north (for example, T.C. Crafford, written commun., 1987) suggest that another northwest-trending right-slip fault may occur to the northeast of the mine, northeast of Big Sore Creek.

North-Northeast-Trending Left-Slip Faults

Steep, north- to northeast-trending faults with left slip occur in a few areas of the mine. Like the northwest-trending strike-slip faults, these also have brittle clay gouges and breccias. An example is the "D" fault in the Southwest orebody area (fig. 5), which has tens of feet of displacement. Several such faults occur on the surface near the headwaters of Gallagher Creek (pl. 7-1). These have from a few feet to about 250 feet of left slip, with a possible north-side-down component. Some strands displace branches of the Middle Gallagher fault, but it is possible that the left-slip faults are displaced by the East Gallagher fault. Another set of northeast-trending faults, possibly

with left slip and north-side-down displacement, are interpreted to cut the rocks west of the Maki fault about 1,700 feet south of the 1350 portal (see pl. 7-1) based on drill-hole intercepts and surface outcrop patterns.

The similarity of gouges on northwest-trending right-slip faults and northeast-trending left-slip faults, and the apparent mutual crosscutting relationship between the two sets, suggest that they are related. They may be a complementary set, and would indicate regional north-south shortening. Haeussler (1992) found similar relationships and came to similar conclusions in the Seymour Canal Formation rocks to the east.

Relationship Between Ore and Structure

Ore minerals replace matrix and clasts in conglomerate, which contains clasts in which S1.5 is truncated by the conglomerate matrix, and base-metal-bearing veins cut the conglomerate. Mineralization is therefore younger than S1.5. Orebodies are clearly folded by F2 and overprinted by S2 foliation. The S2 foliation near F2 hinges is sometimes refracted where it passes from slaty host rocks into ore, but S2 is not well developed in ore except where ore contains patches of sheet silicates. Many sulfide-bearing veinlets in sericitic phyllite and siliceous rock adjacent to ore are also folded by F2 and overprinted by S2. Sericite and chlorite of the phyllite, which are part of the alteration halo of the ore, are strongly recrystallized and reoriented along S2, and these minerals along with the quartz, carbonate, and sulfides of the phyllite are in many cases segregated along S2 foliation planes. Thus, the mineralization predated F2 events.

Small tension fractures related to F2 folding, or in some cases F3 folding, commonly cut the ore. These may be filled with various ore minerals, such as chalcopyrite, bornite, galena, silver-sulfosalts, or electrum, which apparently formed by remobilization of certain ore elements during deformation (see also chap. 9).

Essentially all alteration minerals, especially sheet silicates, have been strongly affected by S2 deformation and probably recrystallized during related greenschist facies metamorphism. In F2 hinge zones, such as most of the Upper Southwest orebody, most ore appears to have been largely recrystallized. Even in the least-deformed, least-recrystallized ore on the limbs of F2 folds, such as in much of the Lower Southwest orebody, most primary ore components have been modified, though up to 30 percent of the ore components appear to retain primary textures, mineralogy, and trace-element distributions (chap. 9). The age of gangue and ore mineral recrystallization and other modification is tentatively considered to be middle Cretaceous, based on the tentative age assignment of F2 (previously discussed).

In addition to effects on the ore itself, the intense nature of F2 deformation makes the original overall geometry of the Greens Creek deposit extremely difficult to decipher. To

arrive at even a rudimentary understanding of the distribution of such features as possible syndepositional faults or feeders, location of intrusive or volcanic units, sedimentary facies distribution, original mineral or alteration zoning, or other features that might be of interest would require detailed understanding of all F2 and younger structure, as well as stratigraphic younging directions. Such a study would require very careful lithologic and structural mapping and analysis of essentially all workings in the mine and of most available drill core.

References Cited

- Barker, Fred, 1957, *Geology of the Juneau B-3 quadrangle, Alaska*: U.S. Geological Survey map GQ-100, scale 1:63,360.
- Brew, D.A., and Ford, A.B., 1985, Preliminary reconnaissance geologic map of the Juneau, Taku River, Atlin, and part of the Skagway 1:250,000 quadrangles, southeastern Alaska: U.S. Geological Survey Open-File Report 85-395, 23 p.
- Brew, D.A., and Karl, S.M., 1988, A reexamination of the contacts and other features of the Gravina belt, southeastern Alaska: U.S. Geological Survey Circular 1016, p. 143-146.
- Cohen, H.A., and Lundberg, N., 1993, Detrital record of the Gravina arc, southeastern Alaska—Petrology and provenance of Seymour Canal Formation sandstones: *Geological Society of America Bulletin*, v. 105, p. 1400-1414.
- Haeussler, P.J., 1992, Structural evolution of an arc-basin—The Gravina belt in central southeastern Alaska: *Tectonics*, v. 11, no. 6, p. 1245-1265.
- Haeussler, P.J., Karl, S.M., Mortensen, J.K., Layer, P., and Himmelberg, G.R., 1999, Permian and mid-Cretaceous deformation of the Alexander terrane on Admiralty and Kupreanof Islands, southeastern Alaska: *Geological Society of America Abstracts with Programs*, v. 31, no. 6, p. A-60.
- Jones, D.L., Berg, H.C., Coney, P., and Harris, A., 1981, Structural and stratigraphic significance of Upper Devonian and Mississippian fossils from the Cannery Formation, Kupreanof Island, southeastern Alaska: U.S. Geological Survey Circular 823-B, p. B109-B112.
- Lathram, E.H., Pomeroy, J.S., Berg, H.C., and Loney, R.A., 1965, Reconnaissance geology of Admiralty Island, Alaska: U.S. Geological Survey Bulletin 1181-R, 48 p.
- Lister, G.S., and Snoke, A.W., 1984, S-C mylonites: *Journal of Structural Geology*, v. 6, p. 617-638.
- Loney, R.A., 1964, Stratigraphy and petrography of the Pybus-Gambier area, Admiralty Island, Alaska: U.S. Geological Survey Bulletin 1178, 103 p.
- Muffler, L.J.P., 1967, Stratigraphy of the Keku Islets and neighboring parts of Kuiu and Kupreanof Islands, southeastern Alaska: U.S. Geological Survey Bulletin 1241-C, 52 p.
- Simpson, Carol, and Schmid, S.M., 1983, An evaluation of criteria to deduce the sense of movement in sheared rocks: *Geological Society of America Bulletin*, v. 94, p. 1281-1288.

Geochemistry of Metasedimentary Rocks in the Hanging Wall of the Greens Creek Massive Sulfide Deposit and of Shales Elsewhere on Admiralty Island

By Craig A. Johnson, Cliff D. Taylor, Joel S. Leventhal, and Katja Freitag

Chapter 8 of

**Geology, Geochemistry, and Genesis of the Greens Creek Massive
Sulfide Deposit, Admiralty Island, Southeastern Alaska**

Edited by Cliff D. Taylor and Craig A. Johnson

Professional Paper 1763

**U.S. Department of the Interior
U.S. Geological Survey**

Contents

Abstract.....	163
Introduction.....	163
Sampling and Analytical Methods.....	164
Samples.....	164
Chemical Analysis.....	164
Degree of Pyritization.....	165
Rock-Eval.....	165
Stable Isotope Analysis.....	165
Results.....	165
Major-Element Chemical Compositions.....	165
Rock-Eval.....	166
Carbon-Sulfur-Iron Relationships.....	166
Metals.....	167
Stable Carbon and Oxygen Isotopes.....	169
Effects of Cretaceous Regional Metamorphism.....	172
Implications of Whole-Rock Chemical Compositions.....	177
Implications of Carbonate Isotopic Compositions.....	177
Conclusions.....	180
References Cited.....	181

Figures

1. Plot of aluminum compared to carbonate carbon illustrating that the metasediments in the Greens Creek hanging wall span a broad lithologic range from carbonate-poor shale to nearly pure carbonate, and exhibit variable contents of quartz or chert.....	166
2. Comparison of the calcium and magnesium contents of hanging-wall samples with the ratio characteristic of dolomite.....	167
3. Plot of organic carbon (C) (determined by Rock-Eval) compared to sulfur (S) for hanging-wall samples.....	169
4. Plot of organic carbon (C) (total carbon minus carbonate carbon) compared to sulfur (S) for Hyd Group, Cannery Formation, Gambier Bay Formation, and Retreat Group samples.....	170
5. Plot of degree-of-pyritization compared to organic carbon (C) for Hyd Group, Cannery Formation, and Retreat Group samples.....	170
6. Concentrations of several metals in hanging-wall shales (only those samples that contain less than 15 percent carbonate) compared with the concentrations in (A) average black shale and (B) average Hyd Group shale (table 1).....	171
7. Correlations in hanging-wall samples of various elements with organic carbon (C _{org}) compared to the correlations of the same elements with sulfur (S), expressed as correlation coefficients (R-values).....	172
8. Plots of degree-of-pyritization (DOP) compared to (A) lead and (B) zinc (Zn) for hanging-wall samples.....	173

9.	(A) The carbon isotopic compositions of coexisting carbonate (filled symbols) and organic matter (open symbols) in hanging-wall samples, (B) The carbon isotopic compositions of Hyd Group, Cannery Formation, and Retreat Group (squares) samples	174
10.	Carbon isotopic compositions of organic matter	175
11.	The carbon and oxygen isotopic compositions of carbonate minerals in hanging-wall rocks, white carbonate-rich ore, Hyd Group, and Cannery Formation samples	175
12.	Comparison of the isotopic compositions of carbonate in the hanging-wall rocks (filled circles) with dolomite in white carbonate-rich ore	178
13.	Plot of the carbon isotopic composition of coexisting carbonate and organic matter in hanging-wall rocks	179
14.	Plot of the carbon (C) isotopic composition of carbonate relative to the sulfur (S) content of hanging-wall rocks.....	180

Tables

1.	Chemical analyses.....	on CD-ROM
2.	Average chemical compositions of Admiralty Island shales compared with average shale and average black shale	168
3.	Rock-Eval analyses of hanging-wall samples	176
4.	Stable isotopic compositions of carbonate minerals and organic matter.....	176
5.	Chemical analyses of hanging-wall samples with low sulfur: organic carbon and low degree-of-pyritization (DOP) values	177

Geochemistry of Metasedimentary Rocks in the Hanging Wall of the Greens Creek Massive Sulfide Deposit and of Shales Elsewhere on Admiralty Island

By Craig A. Johnson, Cliff D. Taylor, Joel S. Leventhal, and Katja Freitag

Abstract

Metasedimentary rocks in the hanging wall of the Greens Creek massive sulfide deposit span a lithologic range from carbonate-poor shale to nearly pure dolomite, and have organic carbon contents higher than average shale, but lower than average black shale. Rock-Eval analyses of the organic matter reveal that the rocks have undergone heating beyond the oil and gas generation stages, and that carbon-oxygen-hydrogen volatiles have been released. Some hanging-wall samples have sulfur-to-organic carbon ratios and degree-of-pyritization values similar to normal marine shales. These same samples also have base- and precious-metal contents like normal shales but are somewhat enriched in barium. The data are evidence that the depositional history of the hanging-wall sediments included periods where the overlying water column was oxic, with only a slight barium enrichment as possible evidence for venting of hydrothermal fluids to the basin waters. More commonly, hanging-wall samples are high in sulfur, high in metals, and high in degree-of-pyritization, consistent either with (1) sediment accumulation beneath an anoxic water column strongly affected by hydrothermal venting, (2) epigenetic hydrothermal sulfur and metal emplacement, or (3) sulfur and metal release from the underlying massive sulfide body during the Cretaceous regional metamorphism.

The carbon and oxygen isotopic compositions of hanging-wall carbonates appear to have been unaffected by the Cretaceous regional metamorphism, and they are indistinguishable from the isotopic compositions of dolomite in the underlying massive sulfide ores. This observation provides strong evidence that the Greens Creek hydrothermal system continued operating until after the hanging-wall sequence was laid down. The isotopic variations in both the hanging-wall rocks and the ores are consistent with dolomite precipitation from a single carbonate-bearing fluid over the temperature range 200–350°C, or dolomite precipitation from mixed marine and hydrothermal fluids. Carbonate $\delta^{13}\text{C}$ correlates positively with organic matter $\delta^{13}\text{C}$, which suggests that carbonate precipitation was accompanied by oxidation of the ambient organic matter or organic-matter-derived methane.

Carbonate $\delta^{13}\text{C}$ correlates negatively with the sulfur content of the rocks, which suggests that organic-matter or methane oxidation was accompanied by reduction of dissolved sulfate to produce hydrogen sulfide. Some sulfate reduction, but not necessarily all, was microbially mediated and took place during early diagenesis beneath the sediment/seawater interface. Limited isotopic data from Hyd Group shales elsewhere on Admiralty Island, which are thought to be distal equivalents of the hanging-wall section, suggest that the same hydrothermal fluid that formed the Greens Creek massive sulfide may also have interacted with basin-floor sediments at distances of several kilometers from the Greens Creek deposit.

Introduction

The metasedimentary rocks in the hanging wall of the Greens Creek massive sulfide deposit have been variously referred to as argillites, calc-argillites, metasiltstones, metashales, and argillaceous limestones (for example, Newberry and others, 1997; Taylor and others, 1999, 2000; Freitag, 2000). Common to all descriptions of these rocks has been the observation that they contain abundant reduced carbon, presumably sedimentary organic matter that has been depleted in hydrogen and oxygen by postdepositional heating. Carbonaceous sediments can be critical to the development of sulfide ores because they can supply metals to ore-forming fluids, or they can supply the reduced sulfur necessary to form sulfide minerals (Tourtelot, 1979; Leventhal, 1993). Simple mass-balance calculations demonstrate that it is not unreasonable to hypothesize that these shales and their distal equivalents were the primary metal source for the Greens Creek hydrothermal system. For example, the zinc content of the presently defined Greens Creek reserve could have been obtained by hydrothermal scavenging from a geologically reasonable volume of shale measuring 5 km³ if the metal concentration was the same as in average black shale. Carbonaceous sediments can also act to preserve sulfide ores because the anoxic conditions that led to their formation can protect underlying sulfide minerals from destruction by seawater oxidation (Goodfellow and others, 1993; Eastoe and Gustin, 1996).

The purpose of this paper is to report on the organic geochemistry, major and trace-element geochemistry, and stable isotope geochemistry of the hanging-wall rocks at Greens Creek in order to examine their function in the genesis of the underlying ore deposit. Also reported are data from Hyd Group shales collected elsewhere on Admiralty Island, which are presumed to be stratigraphic equivalents of the hanging-wall section (chap. 4), and data from shales that occur lower in the Admiralty Island section, in the Retreat Group (Devonian?), the Gambier Bay Formation (Devonian), and the Cannery Formation (Permian). For descriptions of the Admiralty Island stratigraphy, the reader is referred to chapters 4, 7, and 11. Chapter 7 also gives photographs and descriptions of typical exposures of the rocks.

Sampling and Analytical Methods

Samples

In the immediate mine area hanging-wall rocks were obtained from drill core and from underground workings. An effort was made to obtain a variety of samples from the two main lithologic groups that have been recognized in the mine area: massive argillite and slaty argillite (chap. 6). Petrographic observations have indicated that the massive argillites are characteristically richer in dolomite with abundant included organic matter (the field term that is used for this material is graphite), whereas the slaty argillites are richer in quartz and feldspar (up to 50 volume percent) commonly with rhombic dolomite overgrowths. Samples were taken from (1) core GC1136, which intersected a 275-foot section of wall rock overlying the Lower Southwest orebody; (2) core GC1530, which intersected a 675-foot section of wall rock overlying the Northwest orebody; (3) core GCPP173, which was collared on the 350 level and intersected a 150-foot section of wall rock above the Lower Southwest orebody; (4) core GCPP177, which was also collared on the 350 level and intersected a 280-foot section of wall rock above the Lower Southwest orebody; (5) cores PP-198 and PP-204, which were collared on the 170 level above the Lower Southwest orebody; and (6) core PS-50, which was collared at the surface due south of the South zone of the East orebody. Hand specimens were collected on the 350 level in the 2650 crosscut from rocks overlying the Lower Southwest orebody (96GC prefixes in table 1, on CD-ROM), and from the exposure at the 920 portal (GCPF-1).

The hanging-wall samples included specimens with varying degrees of veining, shearing, and fracturing and also specimens showing none of these features. In all cases, the entire sample was crushed and ground for geochemical analysis. The reasons for this are threefold. First, in most cases it is not clear from the textures whether chemical transport to or from veins occurred on length scales exceeding the size of a typical hand specimen (none of the analyzed samples approached 100 percent of what was clearly vein material). Thus, analysis of entire samples may be a more appropriate measure of

original whole-rock compositions than analysis of material between veins. Second, any longer range remobilizations that did occur during either a protracted hydrothermal history or later metamorphism/deformation event were thought to be best characterized by comparing whole-rock analyses of veined or fractured samples with those of unveined samples. Third, analysis of entire samples has been the common practice in geochemical studies of sediment-hosted mineralization at other similar deposits (Williams, 1978, and references therein); thus, comparisons to other occurrences are best made using data that include samples with textural evidence of remobilization.

Shales and related sedimentary rocks also were sampled elsewhere on Admiralty Island from surface exposures of the Retreat Group (Devonian?), Gambier Bay Formation (Devonian), Cannery Formation (Permian), and Hyd Group (Triassic). Sample locations are given in table 1. In all cases efforts were made to obtain fresh rock minimally affected by weathering, but some samples probably experienced pyrite oxidation and sulfur loss, as noted below.

Chemical Analysis

For whole-rock chemical analysis, samples were analyzed either by a protocol referred to as U or by a protocol referred to as A, depending on the analytical services that were available at the time of sample collection. In the U protocol, 50–100 mg of rock was passed through a jaw crusher and then through a pulverizer equipped with ceramic plates. Splits of the resulting powders were decomposed in a mixture of hydrochloric, nitric, perchloric, and hydrofluoric acids, and the solutions were analyzed for Ag, Al, As, Au, Ba, Be, Ca, Cd, Ce, Co, Cr, Cu, Eu, Fe, Ga, Hg, K, La, Li, Mg, Mn, Mo, Na, Nb, Nd, Ni, P, Pb, Sc, Sn, Sr, Ta, Th, Ti, U, V, Y, Yb, and Zn by inductively coupled plasma atomic emission spectrometry using procedures described by Arbogast (1996). Some minerals are known to resist dissolution in the acid mixture, including barite and chromite. Because the shales studied here may contain these two minerals, the results reported for barium and chromium may be too low. Apart from this potential difficulty, the analytical results are considered on the basis of data reported in Arbogast (1996) to be accurate to within ± 10 percent of the amount of the element present, except for beryllium, molybdenum, and phosphorus, which are considered to be accurate to within ± 20 percent. As part of this same protocol, gold was analyzed by fire assay, mercury was analyzed by vapor extraction using a Leeman PS200 analyzer, carbonate carbon was analyzed by coulometric titration after digestion in perchloric acid, and total carbon and total sulfur were analyzed by high temperature (LECO) combustion. Analyses of standard materials indicate that these methods give results that are generally accurate to within ± 10 percent (Arbogast, 1996).

In the A protocol, rock samples were crushed and passed through a pulverizer equipped with steel plates. Splits of the resulting powders were analyzed by instrumental neutron activation (INAA) for Au, As, Ba, Ce, Co, Cr, Eu, Fe, Hg, La, Na, Nd, Sc, Sn, Ta, Th, U, W, and Yb. Splits also

were dissolved in a mixture of hydrochloric, nitric, perchloric, and hydrofluoric acids, and the resulting solutions were analyzed by inductively coupled plasma mass spectrometry (ICP-MS) for Al, Ag, Be, Bi, Ca, Cd, Cu, K, Mg, Mn, Mo, Ni, Pb, Sr, Ti, V, Y, and Zn. Incomplete dissolution of the acid-resistant minerals barite and chromite would have no effect on the barium and chromium values reported for these samples because only the INAA results were used. However, the ICP-MS results for strontium might be low for samples containing barite. As part of this same protocol, carbonate carbon was analyzed by acid digestion, and total carbon and total sulfur were analyzed by high temperature (LECO) combustion. Analyses of standard materials indicated that these methods give results that are generally within ± 10 percent of the accepted concentrations, except for silver, cadmium, nickel, and vanadium, which have greater uncertainties. Results for these latter elements are not tabulated in this paper, but correlations among them are noted assuming that the relative concentrations were determined more accurately than the absolute concentrations.

For some hanging-wall samples there is evidence that the carbonate carbon values were erroneously low, probably due to the presence of dolomite which is known to be more resistant to acid digestion than calcite. Thus, the carbonate carbon results given for hanging-wall rocks in table 1 should be considered minima. For the Hyd Group, Cannery Formation, and Gambier Bay Formation samples, carbonate is present at lower concentrations, and the carbonate mineral is probably calcite. The carbonate carbon results for these rocks are believed to be accurate due to the greater reliability of the coulometric titration method for calcite. For these samples, organic carbon was determined by taking the difference between total carbon and carbonate carbon (table 1).

Degree of Pyritization

Degree of pyritization (DOP), which is defined as

$$\text{DOP} = \text{Fe}_{\text{pyrite}} / (\text{Fe}_{\text{pyrite}} + \text{Fe}_{\text{reactive}}),$$

was determined using methods that have been described by Leventhal and Taylor (1990). The parameter $\text{Fe}_{\text{pyrite}}$ was calculated from the measured sulfur contents of the samples after correcting for sulfur contained in sphalerite, galena, and chalcopyrite using the equations

$$S_{\text{pyrite}} = S_{\text{total}} - 0.490 (\text{Zn}) - 0.155 (\text{Pb}) - 1.009 (\text{Cu}),$$

and

$$\text{Fe}_{\text{pyrite}} = 0.871 (S_{\text{pyrite}}).$$

In some rocks, sulfur is also contained in barite. However, the barium contents of the samples analyzed in this study are low enough that the correction to S_{pyrite} for barite sulfur is insignificant (table 1). The parameter $\text{Fe}_{\text{reactive}}$ was determined by measuring the amount of iron leached from the samples by a 1N HCl solution at room temperature in a 24-hour period (Leventhal and Taylor, 1990).

Rock-Eval

Rock-Eval analyses were carried out using the standard pyrolysis procedure (Tissot and Welte, 1984), and the results were used to calculate total organic carbon content (TOC), the parameter T_{max} , the hydrogen index (HI), and the oxygen index (OI). Because the organic matter in the rocks is mature and possibly graphitic (see Rock-Eval results, and the conodont color alteration indices reported in chapter 11), the pyrolysis reactions may have been incomplete, resulting in erroneously low values for total organic carbon content. However, prior experience with similar types of samples (J.S. Leventhal, unpub. data, 2001) suggests that the underreporting is no more than 5–10 percent. Conclusions that will be drawn herein from the total organic carbon data are insensitive to errors of this magnitude.

Stable Isotope Analysis

Carbonate minerals were converted to carbon dioxide for isotopic analysis by treating whole-rock powders with phosphoric acid as described by McCrea (1950). All samples were reacted for 2 days at 25°C to ensure that yields were complete whether the carbonate mineral was dolomite or calcite. Isotopic compositions of the gases were determined using a Finnigan MAT 252 isotope ratio mass spectrometer equipped with a dual viscous inlet system. The acid fractionation factor for dolomite was used to calculate the oxygen isotopic compositions (Friedman and O'Neil, 1977). For samples containing calcite, which probably include the Hyd, Cannery, Retreat, and Gambier Bay samples, this has resulted in $\delta^{18}\text{O}$ values that are 0.8 permil too low. This potential error is small enough to have no effect on our conclusions. Carbon isotopic compositions determined by the phosphoric acid method do not depend on carbonate mineralogy.

For isotopic analysis of organic matter, powders were treated with 6N HCl to remove all carbonate carbon and then rinsed in deionized water. The solid residues were combusted in an elemental analyzer to convert the remaining carbon to carbon dioxide gas, which was admitted directly to a Micro-mass Optima mass spectrometer for determination of isotopic compositions by the continuous flow method.

Isotopic data are reported in δ -notation relative to Vienna Standard Mean Ocean Water (VSMOW) for oxygen and Vienna Pee Dee belemnite (VPDB) for carbon. Reproducibility was typically ± 0.1 permil or better for $\delta^{13}\text{C}$, and ± 0.2 permil or better for $\delta^{18}\text{O}$.

Results

Major-Element Chemical Compositions

The hanging-wall samples span a wide range of chemical compositions corresponding to lithologic variation from carbonate-free shale to nearly pure carbonate rock (table 1). Elements normally found in detrital silicates or clays, such as aluminum, potassium, and sodium, generally show inverse

relationships with elements normally found in carbonate minerals, such as calcium, magnesium, and carbon. An example is shown in figure 1 where aluminum and carbonate carbon are shown to span the entire range from typical shale or black shale to silicate-poor carbonate. Also evident in figure 1 are samples low in both aluminum and carbonate carbon, presumably due to an abundance of quartz or chert (silicon was not analyzed in this study). The calcium:magnesium ratios for many samples are within analytical error of the dolomite ratio (fig. 2), which is strong evidence that dolomite is the predominant host mineral for these two elements. Organic carbon in samples analyzed by Rock-Eval ranges from 0.5 to 5.0 percent, averaging 1.9 percent (table 2). This is higher than the values that have been proposed for average shale (Blatt and others, 1972; Krauskopf, 1979) but lower than the 2–10 percent range characteristic of black shales (Tourtelot, 1979). The dark appearance of the Greens Creek rocks probably reflects the graphitization of the organic matter due to heating rather than a particularly high organic content (Leventhal, 1993).

Chemical compositions are more restricted for other shale units on Admiralty Island, and the data are summarized as averages in table 2. The Cannery and Gambier Bay samples have major element compositions within the ranges characteristic of shales (Blatt and others, 1972), but the Hyd Group and Retreat Group samples are lower in aluminum. The carbonate carbon values are no higher for these units, so we infer that they contain a greater proportion of quartz or chert relative

to feldspars and clay minerals. This inference conflicts with observations made during field mapping (chap. 4) that the Hyd Group is less siliceous than the Cannery Formation. However, other observations from field mapping are borne out by the chemical data. The observation that the Hyd Group is more pyritic than the Cannery Formation is confirmed by higher sulfur contents (1.7 versus 0.7 wt%), and the observation that the Hyd Group is more graphitic than the Cannery Formation is borne out by higher organic carbon (1.9 versus 0.7 wt%).

Rock-Eval

Rock-Eval results for hanging-wall samples are given in table 3. The HI and OI values are generally low, and the T_{max} values generally are greater than 500, indicating that the samples are overmature with respect to oil and gas generation, having been heated to temperatures exceeding 150°C. For comparison, black shales from unmetamorphosed localities elsewhere typically display HI values of 300–500, OI values of 50–100, and T_{max} below 460 (Leventhal, 1998).

Carbon-Sulfur-Iron Relationships

Most hanging-wall samples have sulfur:organic carbon ratios well above the value of ~0.36 that is characteristic of normal marine shale (for example, Berner and Raiswell, 1983)

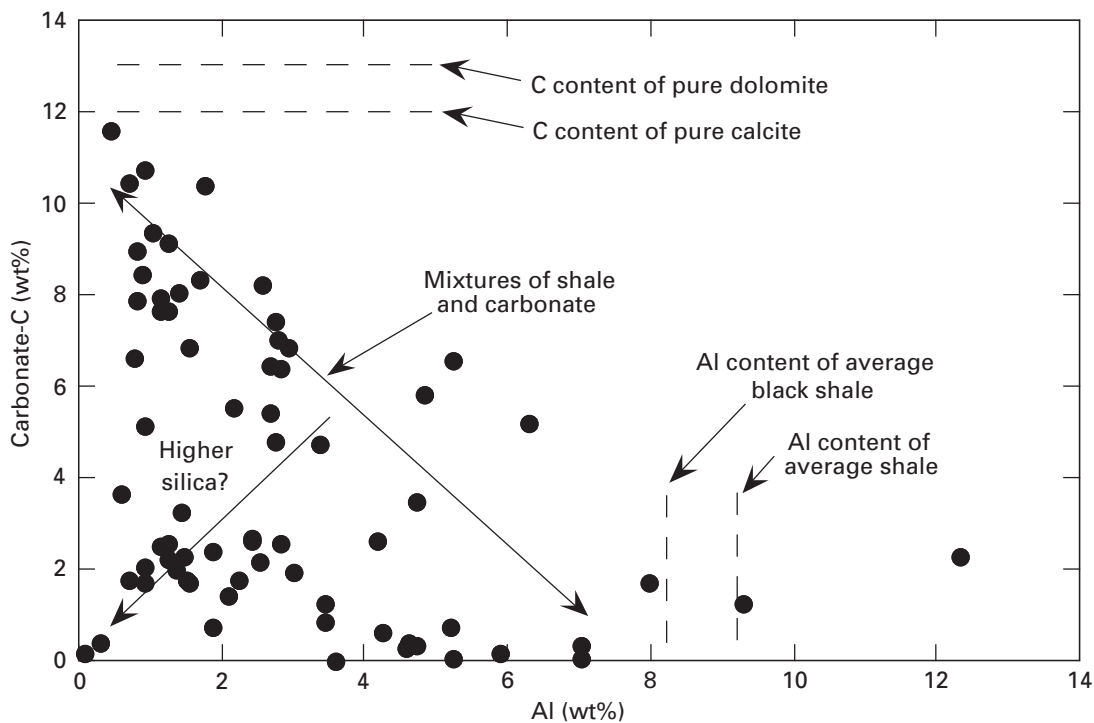


Figure 1. Plot of aluminum compared to carbonate carbon illustrating that the metasediments in the Greens Creek hanging wall span a broad lithologic range from carbonate-poor shale to nearly pure carbonate, and exhibit variable contents of quartz or chert. Aluminum (Al) contents of average shale and average black shale are from Krauskopf (1979) and Quinby-Hunt and others (1989), respectively. wt%, weight percent.

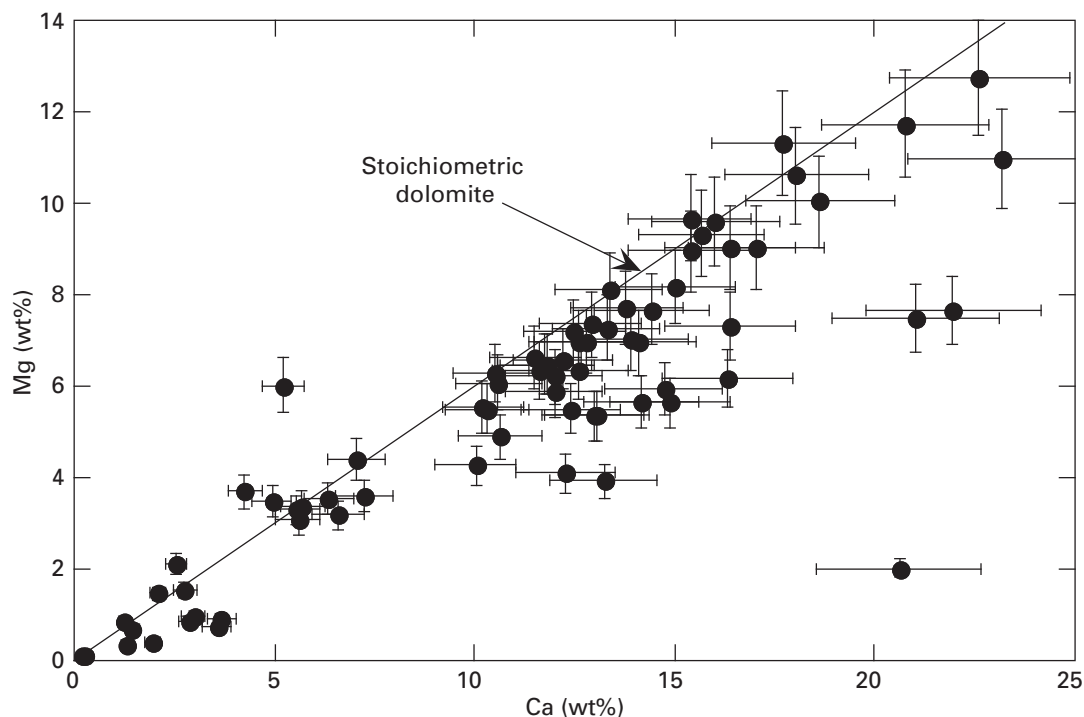


Figure 2. Comparison of the calcium and magnesium contents of hanging-wall samples with the ratio characteristic of dolomite. The close correspondence suggests that dolomite is the dominant host mineral for these elements. Ca, calcium; Mg, magnesium; wt%, weight percent.

in which diagenetic sulfide has been formed in anoxic sediment overlain by an oxic water column (fig. 3). The high ratios could be a consequence of organic matter loss during postdepositional heating, but the sulfur contents of many samples would require organic contents far higher than ordinary marine shales. Sulfide precipitation within an anoxic, hydrogen sulfide-bearing water column could also explain the high sulfur content of the rocks, but this typically preserves a positive- or zero-slope correlation between organic carbon and sulfur (Leventhal, 1983; Raiswell and Berner, 1985), a feature that is not apparent in the hanging-wall data. Epigenetic introduction of sulfur is a third mechanism that can lead to high sulfur:organic carbon ratios (Leventhal, 1995). The very high degree-of-pyritization values determined for many hanging-wall samples (table 1) is consistent with this process.

The Hyd Group and Cannery Formation samples also span wide ranges of sulfur:organic carbon (fig. 4). However, the very low sulfur contents and very low DOP values (less than 0.2, see Leventhal, 1993) displayed by many samples (fig. 5) are strong evidence that the chemical compositions of Admiralty Island surface outcrops have been affected by weathering. The fact that a few Hyd Group and Cannery Formation samples extend to high sulfur contents and high DOP values (figs. 4 and 5) suggests that at least some experienced substantial sulfur addition. Whether epigenetic sulfur addition is widespread in these units cannot be determined from the limited number of fresh samples that were available for this study.

Metals

For most of the listed metals, the agreement between Hyd Group samples analyzed by the A protocol and Hyd Group samples analyzed by the U protocol is reasonably good (table 2). However, for chromium and barium the results obtained using the A protocol are higher, possibly reflecting incomplete dissolution of chromite and barite in the U protocol, or chromium contamination from steel pulverizer plates in the A protocol.

The hanging-wall rocks show extremely broad ranges of metal contents (table 1). For samples that are true shales, which is defined here as samples containing less than 15 percent carbonate, the concentrations of iron and cobalt are the same as average black shale, copper and zinc are the same or slightly higher than in average black shale, and lead, gold, barium, and arsenic are higher than in average black shale (fig. 6A).

A comparison of metal concentrations in the hanging-wall shales with concentrations in their stratigraphic equivalents, the Hyd Group shales, is shown in figure 6B. The concentrations of cobalt, iron, and molybdenum are similar in the two units, and for each of the other elements the hanging-wall analyses overlap the Hyd average and extend to higher concentrations. No strong evidence exists in the data for metal depletions in the exposed Hyd Group rocks, as might be expected if this unit were the main metal source for the Greens Creek massive sulfide deposit.

With regard to chemical variations within the entire hanging-wall shale + carbonate package, cobalt, chromium, nickel, and vanadium were found to correlate with organic

Table 2. Average chemical compositions of Admiralty Island shales compared with average shale and average black shale.[#]

[<, less than; -, no data; Gp., Group; Fm.; Formation; Ave., average]

Element	Hyd (A) Gp.	Hyd (U) Gp.	Cannery Fm.	Gambier Bay Fm.	Retreat Gp.	Ave. shale ^{@@}	Ave. black shale [^]
Al ₂ O ₃	7.6	-	11.4	16.8	8.3	17	15.5
CaO	0.8	-	1.0	0.1	0.01	3.5	2.4
FeO*	3.6	-	4.8	4.4	2.0	6.0	4.7
K ₂ O	1.6	-	2.0	3.4	2.2	3.0	3.6
MgO	1.5	-	2.2	1.5	2.0	2.3	1.7
Na ₂ O	1.0	-	1.6	0.9	0.03	1.2	0.7
TiO ₂	0.3	-	0.5	0.6	0.4	0.8	0.7
S	1.7	1.1	0.7	0.9	0.01	0.25	1
C _{org} **	1.9	-	0.7	2.3	0.5	0.8	3.2
U	4	-	-	-	-	3.5	15.2
Mo	6	14	7	<2	<2	2	65
V	-	196	206	181	82	130	500
Ni	-	35	36	38	13	80	50
Cu	20	31	37	25	17	50	70
Cr	130 [@]	43 ^{***}	36	68	16	100	111
Co	5	8	9	5	<2	20	17
As	23	-	-	18	<10	10	29
Pb	32	16	18	29	9	20	20
Ba	2,078	1,539 ^{***}	2,327	810	4,083	600	1,120
Zn	81	85	119	81	49	90	310
Ag	-	<2	<2	<2	<2	0.1	0.1
Cd	-	<2	<2	<2	<2	0.3	-
P	-	570	717	500	233	750	-
Mn	-	191	479	97	189	850	383
no. samples	9	33	17	1	3	-	-

[#]Oxides in percent, elements in parts per million.

*Total iron as iron (II) oxide.

**Organic carbon from Rock-Eval for mine argillite, from difference between total carbon and carbonate carbon for all others.

[@]May be high by this method (see text).^{***}May be low by this method (see text).^{@@}Krauskopf (1979), except for organic carbon which is from Leventhal (unpub. data, 2001).[^]Quinby-Hunt and others (1989), except for lead, organic carbon, nickel, copper, which are from Vine and Tourtelot (1970), and sulfur and silver, which are from Leventhal (unpub. data, 2001).

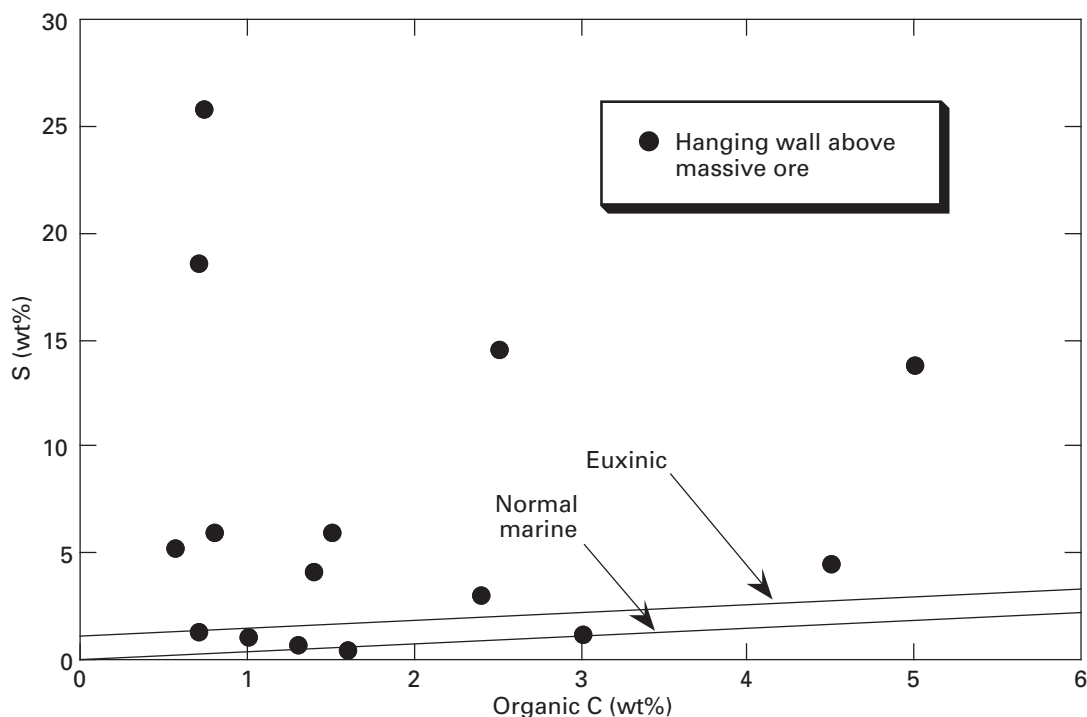


Figure 3. Plot of organic carbon (C) (determined by Rock-Eval) compared to sulfur (S) for hanging-wall samples. The lines marking normal marine sediments and sediments deposited in euxinic environments were taken from Leventhal (1995). wt%, weight percent.

carbon with R-values of around 0.7 (fig. 7). Silver, As, Au, Cd, Cu, Fe, Mo, Pb, and Zn were found to correlate only weakly with organic carbon (R-values less than 0.4), but more strongly with sulfur (R-values of 0.4–0.5 for cadmium, silver; 0.5–0.6 for copper, molybdenum, lead; about 0.7 for gold, arsenic, zinc; 0.9 for iron) (fig. 7). Figure 8 illustrates that samples with intermediate degree-of-pyritization values have lead and zinc contents that are typical of shale or black shale, but samples with higher degree-of-pyritization values have substantially higher metal contents. Barium falls in neither of the two suites of metals shown in figure 8, displaying a fair correlation with organic carbon, but no correlation with sulfur. This may imply that barium was added during sedimentation or diagenesis.

Stable Carbon and Oxygen Isotopes

The stable isotopic compositions of carbonates and total organic carbon are given in table 4. Hanging-wall carbonates have an average $\delta^{18}\text{O}$ of 18 permil and an average $\delta^{13}\text{C}$ of -6 permil. Both values are significantly lower than marine limestones and dolomites of Triassic age (Veizer and others, 1999). Organic carbon isotopic compositions are -25.9 ± 0.9 ($1-\sigma$) permil, which is intermediate between the compositions characteristic of the two kerogen types found in Phanerozoic sedimentary rocks (Lewan, 1986). Thermal maturation can cause an upward shift in organic matter $\delta^{13}\text{C}$ values of as much as 3 permil (Schidlowski, 1987). Thus the hanging-wall

organic matter may originally have had isotopic compositions resembling *l* (italic “el”)-amorphous kerogen (Lewan, 1986). The isotopic fractionations between carbonate carbon and organic carbon are 19.9 ± 0.8 ($1-\sigma$) permil across a wide range of organic carbon:carbonate carbon ratios (fig. 9A).

Fewer analyses were made of the Cannery Formation and Hyd Group shales (fig. 9B). The isotopic compositions of Hyd carbonates resemble those of the hanging-wall carbonates, whereas three Cannery samples have compositions spanning a wide $\delta^{13}\text{C}$ range of -13 to -2 permil. Organic carbon $\delta^{13}\text{C}$ values for the Hyd Group and Cannery Formation are very similar to the hanging-wall samples, although two Hyd samples extend to significantly higher $\delta^{13}\text{C}$ (fig. 10). Of note is the low carbonate $\delta^{13}\text{C}$ value and the small carbonate-organic carbon fractionation in Cannery sample Ard-02, which suggest that there may have been isotope exchange between carbonate minerals and organic matter during a postdepositional heating event. The fact that isotopic exchange is apparent in this Permian unit, but neither in the mine argillite nor in the Hyd Group, both of which are Triassic, may mean that the exchange was a consequence of the Early Permian low-grade metamorphic event that affected some areas on Admiralty Island (Haeussler and others, 1999; Karl and others, 1999).

On a plot of $\delta^{18}\text{O}$ and $\delta^{13}\text{C}$ (fig. 11) the hanging-wall carbonates display a broad linear trend with a regression slope of 0.6. The Hyd samples conform closely to this trend, but two Cannery samples do not. This observation may imply a genetic

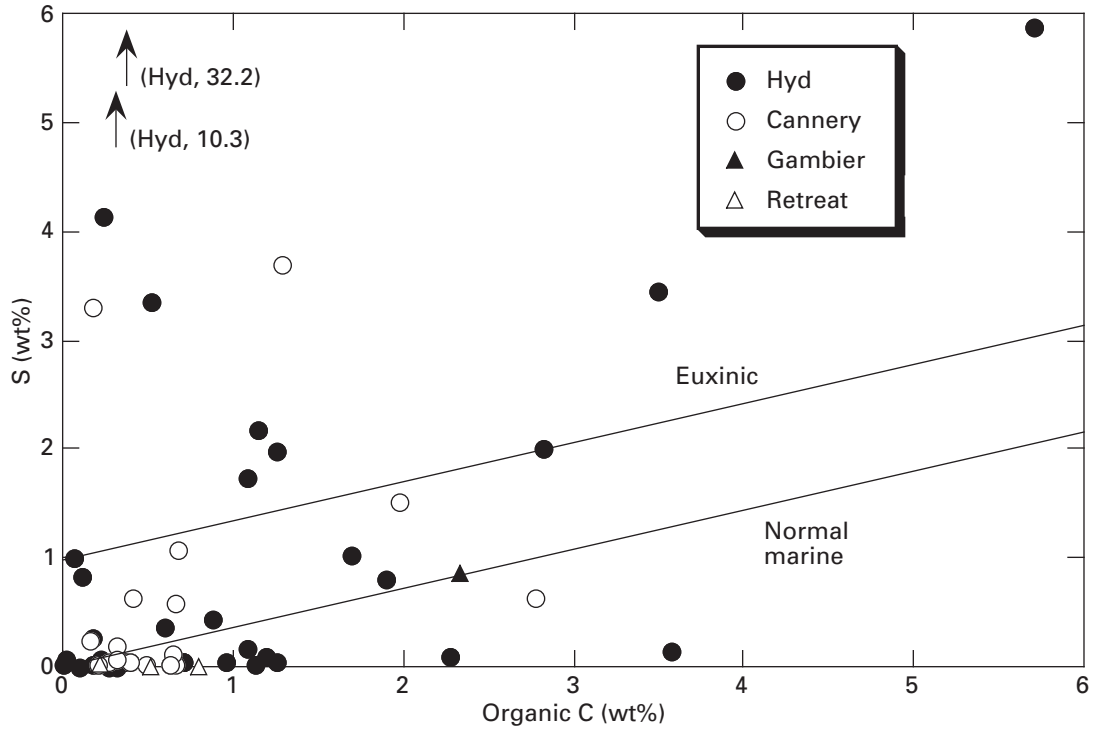


Figure 4. Plot of organic carbon (C) (total carbon minus carbonate carbon) compared to sulfur (S) for Hyd Group, Cannery Formation, Gambier Bay Formation, and Retreat Group samples. wt%, weight percent.

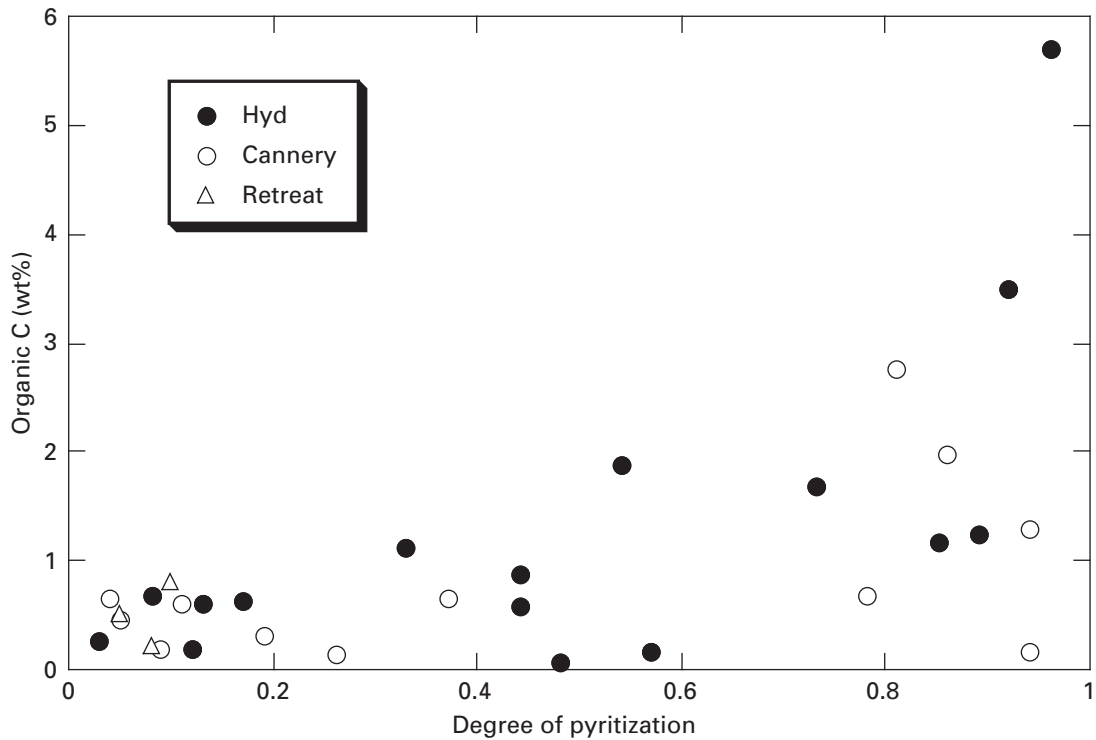


Figure 5. Plot of degree-of-pyritization compared to organic carbon (C) for Hyd Group, Cannery Formation, and Retreat Group samples. wt%, weight percent.

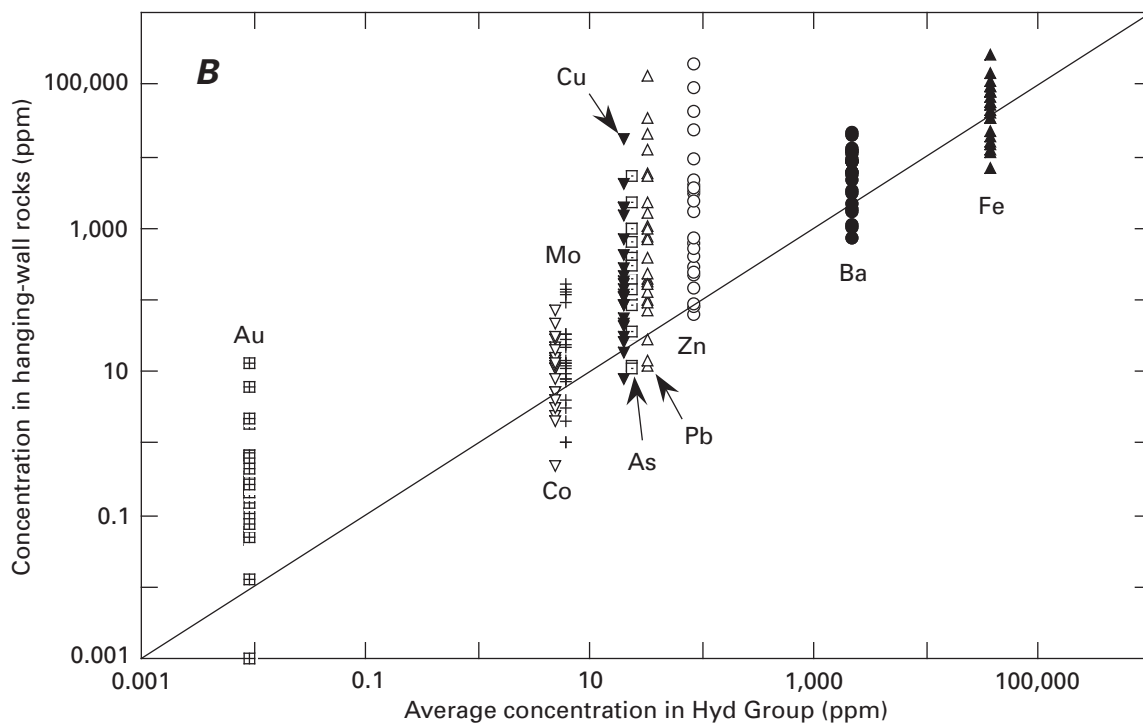
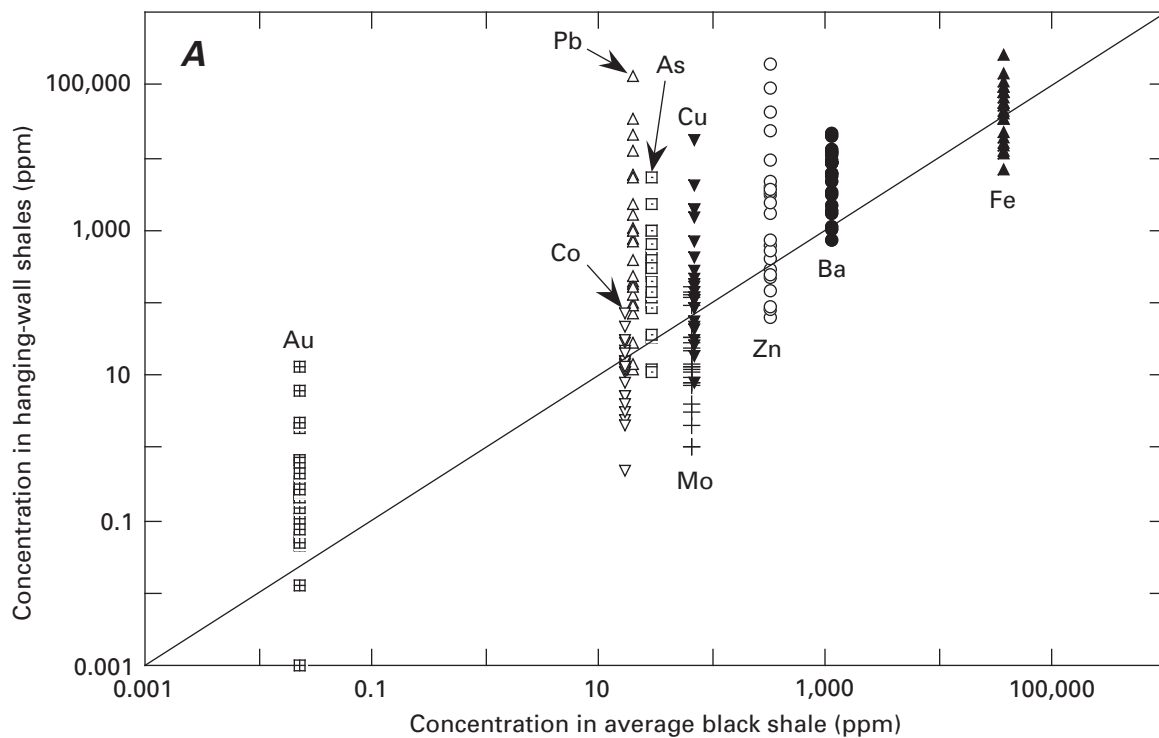


Figure 6. Concentrations of several metals in hanging-wall shales (only those samples that contain less than 15 percent carbonate) compared with the concentrations in (A) average black shale (Quinby-Hunt and others, 1989) and (B) average Hyd Group shale (table 1). The Hyd average includes only those samples analyzed by the same protocol used for the hanging-wall samples (see text). ppm, parts per million.

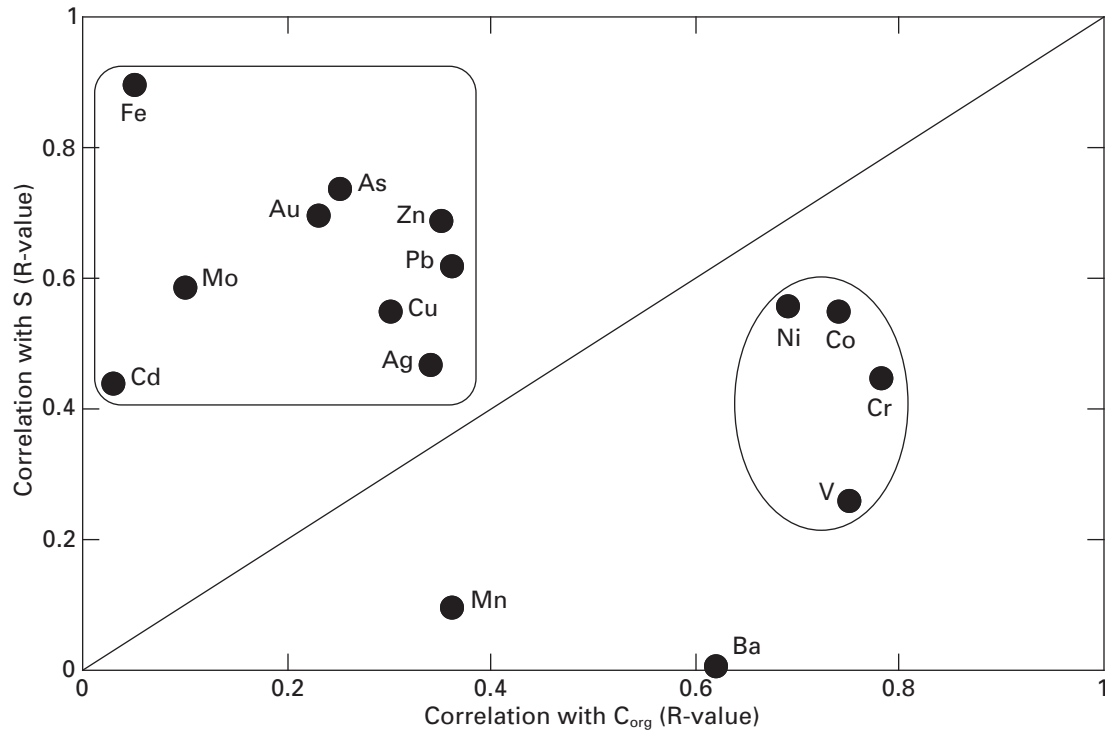


Figure 7. Correlations in hanging-wall samples of various elements with organic carbon (C_{org}) compared to the correlations of the same elements with sulfur (S), expressed as correlation coefficients (R-values). Base metals, precious metals, iron, molybdenum, and arsenic show a higher correlation with sulfur than with organic carbon, and the reverse is true for cobalt, chromium, nickel, and vanadium, suggesting that different processes were responsible for the emplacement of these two groups of elements.

link between the carbonate minerals in the hanging-wall rocks and those in Hyd Group rocks found several kilometers to the northwest near Hawk Inlet (see succeeding discussion).

Effects of Cretaceous Regional Metamorphism

The regional metamorphic-deformation event that affected Admiralty Island in Cretaceous time could have caused significant changes in the hanging-wall rocks, and it is important that any such changes be considered so that primary features can be discriminated from any secondary metamorphic features. In underground exposures and in drill core, there is clear textural evidence for remobilization of metals and sulfur, including crosscutting sulfide veinlets, and fractures and shears with sulfide minerals dispersed along them. Whether these remobilizations were caused by a protracted hydrothermal event or by the Cretaceous metamorphism-deformation is uncertain, in much the same way that remobilization textures within the underlying massive sulfide bodies are of uncertain origin (chap. 9).

Volatile species would very likely have been released from the hanging-wall section during regional metamorphism. Kerogen is known to lose methane starting at around 120°C

(Tissot and others, 1974), and clays begin to dehydrate at 100–200°C (Fyfe and others, 1978). The Rock-Eval results (table 3) are consistent with these types of prograde reactions because they indicate carbon-oxygen-hydrogen volatile loss at temperatures greater than 150°C. On the other hand, any pre-Cretaceous heating event, including the metal-depositing event itself, could also explain the Rock-Eval data. The production and movement of fluids during low-grade metamorphism could have led to redistribution of volatile species within the rocks and may be partly responsible for the wide variation in sulfur:organic carbon ratios observed in the hanging-wall samples (fig. 3). Because the metamorphic event was regional, the same phenomenon might also explain the wide variation in sulfur:organic carbon ratios observed in the Hyd Group and Cannery Formation rocks. The fact that the hanging-wall rocks have systematically high degree-of-pyritization values indicates that aqueous sulfide or hydrogen sulfide was abundantly available at some time during the history of these rocks, possibly during the Cretaceous metamorphism when hydrogen sulfide-bearing fluids may have been released from the nearby massive sulfide bodies. For the Hyd Group and Cannery Formation, the wide range in degree-of-pyritization values indicates that reduced sulfur was abundantly available at some locations but was never available at others, presumably due to heterogeneity of flow paths and bulk permeability.

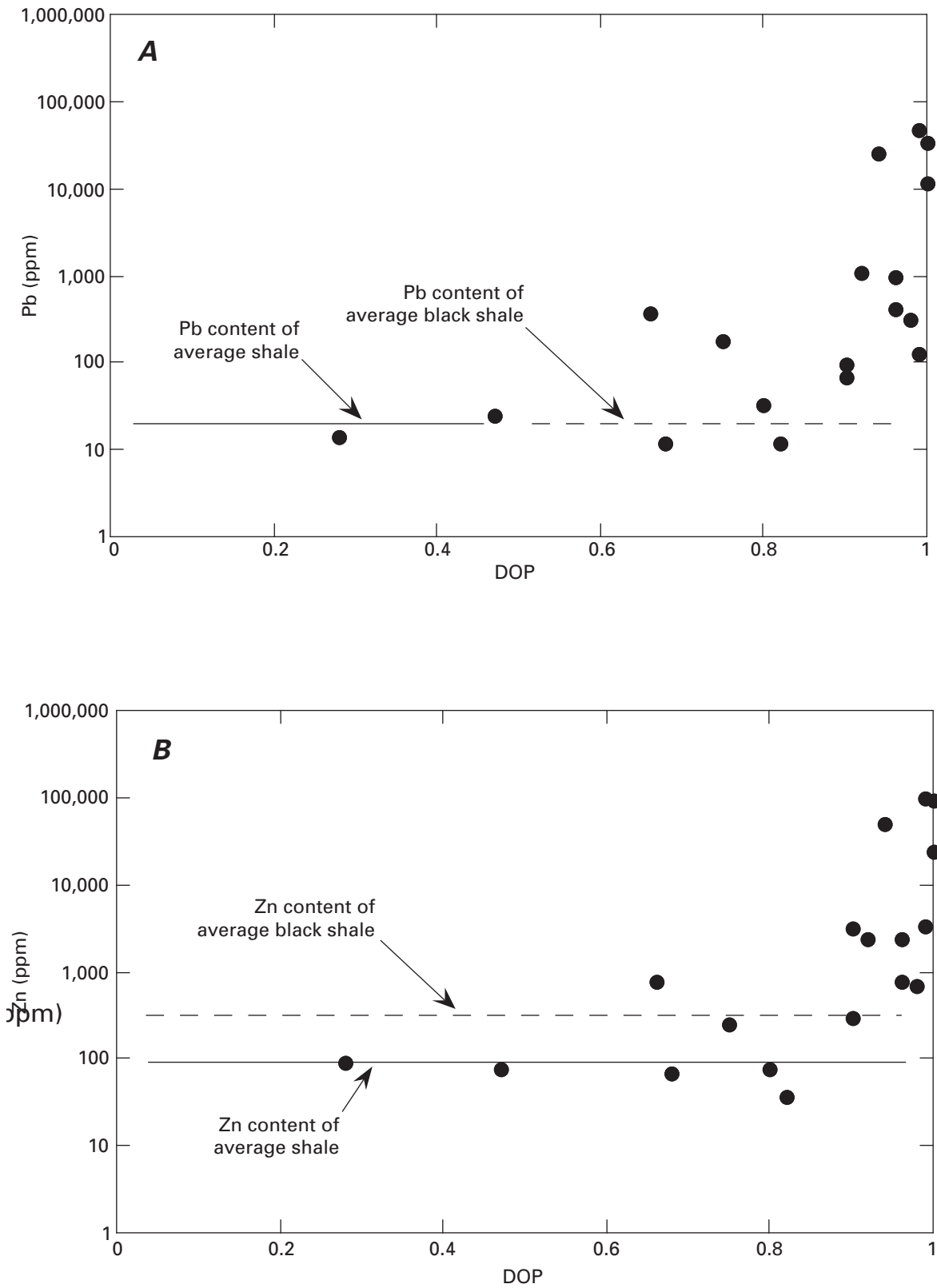


Figure 8. Plots of degree-of-pyritization (DOP) compared to (A) lead and (B) zinc (Zn) for hanging-wall samples. ppm, parts per million.

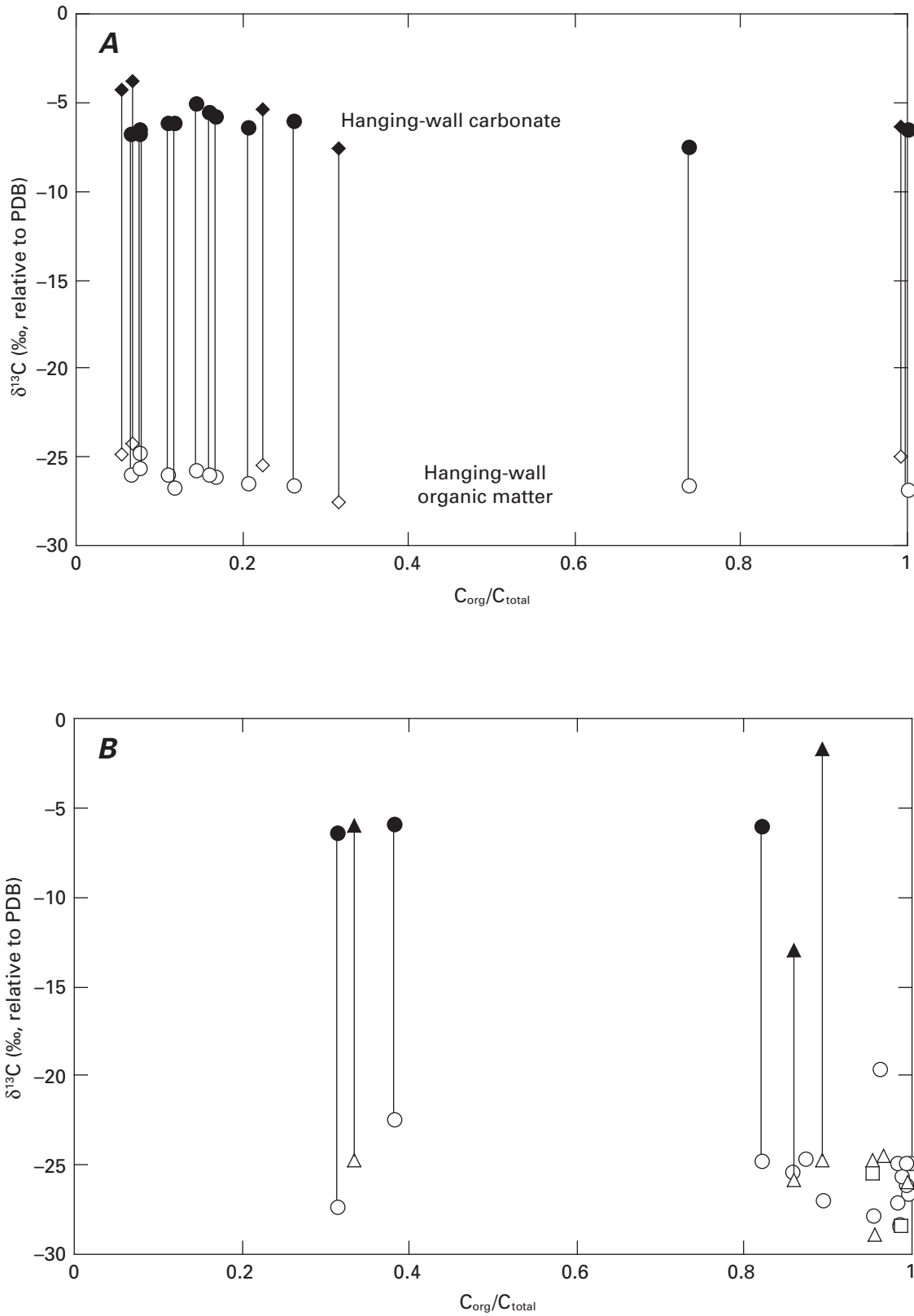


Figure 9. (A) The carbon isotopic compositions of coexisting carbonate (filled symbols) and organic matter (open symbols) in hanging-wall samples. Diamonds indicate samples for which organic carbon was calculated by difference and could be erroneously low. (B) The carbon isotopic compositions of Hyd Group (circles), Cannery Formation (triangles), and Retreat Group (squares) samples. PDB, Pee Dee Belemnite.

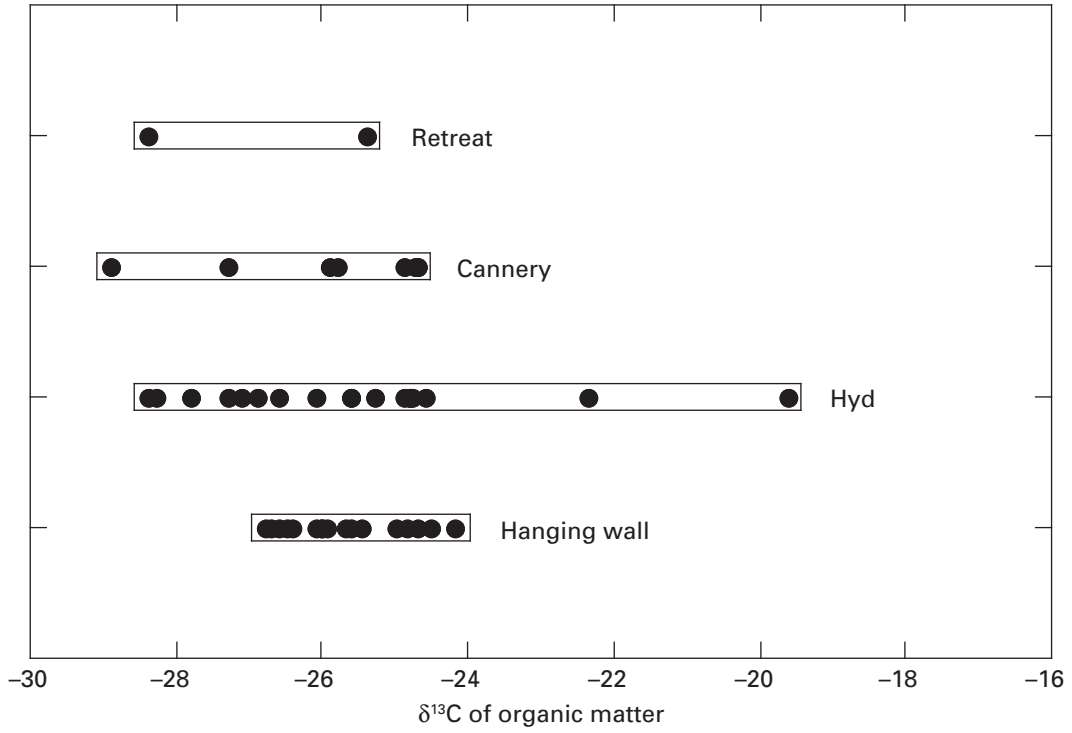


Figure 10. Carbon isotopic compositions of organic matter.

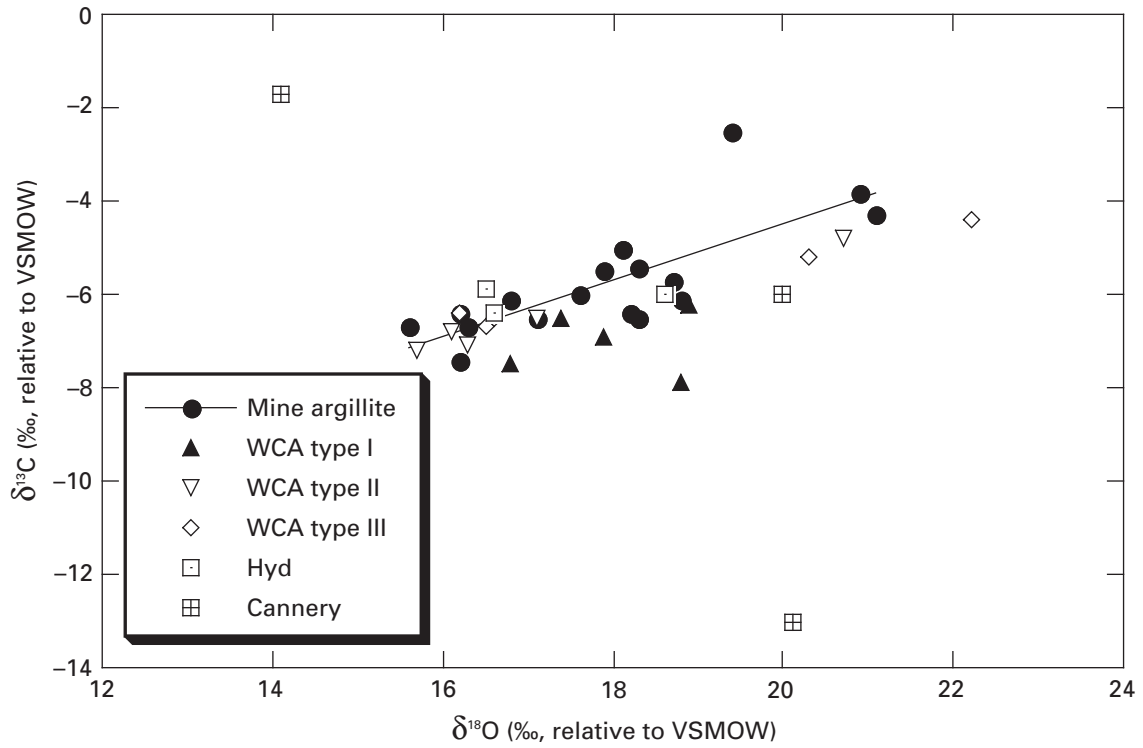


Figure 11. The carbon and oxygen isotopic compositions of carbonate minerals in hanging-wall rocks, white carbonate-rich ore, Hyd Group, and Cannery Formation samples. VSMOW, Vienna Standard Mean Ocean Water.

Table 3. Rock-Eval analyses of hanging-wall samples.

Sample	T _{max} *	TOC**	HI	OI
1136-4	519	3.01	6	3
1136-5A	501	1.62	3	12
1136-8	533	5.04	2	0
1136-12	494	4.48	2	1
1136-26	564	1.02	2	12
1136-27	502	0.75	4	36
1136-13	566	0.7	7	20
1136-16	583	1.26	4	10
96GC-5	527	1.41	2	14
96GC-7	521	2.4	4	6
96GC-9	571	2.48	12	2
96GC-14	514	1.53	9	8
96GC-28	546	0.8	41	36
96GC-37	496	0.56	62	30

*T_{max} is an instrumental, not geologic, temperature. T_{max} < 420 is immature relative to petroleum generation (geologic less than about 70°C), T_{max} = 420–440 is oil generation (geologic 80–100°C), T_{max} = 440–460 is gas generation (geologic 100–150°C), T_{max} > 460 is anthracite rank coal equivalent proceeding to amorphous graphite with higher temperature.

**Total organic carbon.

Metamorphic heating also could cause exchange of carbon isotopes between organic matter and carbonate minerals, and this phenomenon could be argued to explain the low carbonate δ¹³C values in the hanging-wall rocks compared with typical marine carbonates of Triassic age. However, low-grade metamorphism does not always cause significant exchange (Kitchen and Valley, 1995) due to differences in the duration of heating or to variable exchange kinetics from one locality to another. The work of Himmelberg and others (1995) in the Juneau area on the same metamorphic event that affected the Greens Creek area (their M₁ metamorphism) suggests that the event was characterized by rapid burial, limited duration of heating, and rapid uplift, all of which would have minimized isotope exchange among coexisting minerals.

Two observations suggest that isotope exchange was not important for the Greens Creek rocks and that the carbonates have retained their premetamorphic compositions. First, the carbonate carbon–organic carbon isotopic fractionations are very uniform, quite different from the wide variability observed in other low-grade metamorphic localities reflecting different degrees of isotopic reequilibration from one hand specimen to another (for example, Arneeth and others, 1985). The second observation is that the carbonate carbon–organic carbon fractionation does not vary with the relative proportions of the two carbon reservoirs, as would be required by isotope mass balance in systems approaching isotopic equilibrium (Gregory and others, 1989).

Table 4. Stable isotopic compositions of carbonate minerals and organic matter.

Sample	Unit	δ ¹⁸ O _{carb}	δ ¹⁸ C _{carb}	δ ¹⁸ C _{org}
96GC-5	hanging wall	18.7	-5.7	-26.1
96GC-7	hanging wall	17.6	-6.0	-26.5
96GC-14	hanging wall	16.2	-6.4	-26.4
96GC-28	hanging wall	15.6	-6.7	-24.7
96GC-37	hanging wall	16.3	-6.7	-26.0
GC1136-4	hanging wall	18.2	-6.4	-25.0
GC1136-5	hanging wall	18.1	-5.0	-25.7
GC1136-8	hanging wall	16.2	-7.4	-26.6
GC1136-12	hanging wall	17.1	-6.5	-26.8
GC1136-13	hanging wall	18.3	-6.5	-25.6
GC1136-16	hanging wall	18.8	-6.1	-26.0
GC1136-26	hanging wall	17.9	-5.5	-26.0
GC1136-27	hanging wall	16.8	-6.1	-26.7
PP204-01	hanging wall	18.3	-5.4	-25.5
PS50-01	hanging wall*	19.0	-7.6	-27.8
PS50-02	hanging wall	21.1	-4.3	-24.9
PS50-03	hanging wall	20.9	-3.8	-24.2
GCPF-1	hanging wall	19.4	-2.5	-24.5
96ADM7	Hyd			-26.9
96ADM19	Hyd			-28.3
97ADM27	Hyd	16.6	-6.4	-27.3
Brd-01	Hyd	18.6	-6.0	-24.8
Brd-02	Hyd			-24.6
Brd-03	Hyd			-19.6
Brd-04	Hyd	16.5	-5.9	-22.4
NAD T9-1	Hyd			-27.8
NAD T9-6B	Hyd			-28.4
NAD T16-7	Hyd			-26.6
NAD T17-3	Hyd			-24.8
97LG11	Hyd			-25.3
97LG14	Hyd			-26.1
97LG57	Hyd			-25.6
97LG60	Hyd			-25.6
97LG65	Hyd			-24.9
97LG66	Hyd			-24.8
97LG75	Hyd			-27.1
97ADM6	Cannery	14.1	-1.7	-24.7
Ard-02	Cannery	20.1	-13.0	-25.8
Ard-03	Cannery	20.0	-6.0	-24.7
Ard-01	Cannery			-24.9
Ard-04	Cannery			-28.9
96ADM13	Cannery			-25.9
97LG25	Cannery			-24.7
97ADM22	Retreat			-28.4
97LG76	Retreat			-25.4

*This sample is from what may be a separate lithologic unit overlying the hanging-wall unit.

That premetamorphic isotopic compositions might be preserved is somewhat surprising given the ladder veins of quartz and carbonate evident in many hanging-wall rocks (chap. 7) that formed by mobilization of chemical constituents into tension fractures during Cretaceous time (the F2 folding event described in chap. 7). The preservation of isotopic compositions may be due to the sample-selection protocol that was used for the carbonate isotopic work in which rocks with abundant carbonate veining were generally avoided. However, the isotopic results for sample 96GC-37, which did contain megascopic carbonate veins, were indistinguishable from those for other hanging-wall samples (table 4), which suggests that the ladder veins may have been local redistributions (compare Ramsay, 1980; Hobbs, 1986) that did not significantly alter the $\delta^{13}\text{C}$ value of the carbonate.

It is noteworthy that the smallest observed carbonate carbon-organic carbon isotopic fractionations are in a Hyd Group sample collected 6 km west-northwest of the mine site (Brd-04) and a Cannery Formation sample collected 10 km northwest of the mine site (Ard-02) (table 4). If these fractionations reflect exchange between organic matter and carbonate minerals on heating, then the highest temperatures (whether hydrothermal or metamorphic), or the longest duration of heating, or the most favorable exchange kinetics were not in the vicinity of the mine but rather to the west and northwest nearer Hawk Inlet.

Implications of Whole-Rock Chemical Compositions

The overall high sulfur:organic carbon ratios and high degree-of-pyritization values found for many hanging-wall samples are strong evidence for epigenetic sulfur addition in much of the section, and the close correlation of lead, zinc, and other metals with sulfur is evidence for epigenetic metal addition as well. However, there are hanging-wall samples that were collected in close proximity to ore that have sulfur:organic carbon ratios and degree-of-pyritization values characteristic of normal marine sediments. In these samples (table 5), the concentrations of zinc, gold, and silver are no greater than in average black

shale or average shale, and lead is higher than in average black shale or shale in only one of five samples. Barium is systematically high at about twice the average black shale value. Thus, for at least part of the depositional history of the hanging-wall section, the accumulating sediment appears to have been overlain by an oxic water column with dissolved metal contents that were for the most part like normal seawater. The twofold enrichment in barium suggests enhanced barite precipitation in the water column, which could have been a consequence of elevated barium. This might reflect a hydrothermal fluid flux to the basin producing a geochemical fingerprint in the sediment similar to that observed in the barite-rich, precious metal-rich, base metal-poor, earliest stages of massive sulfide mineralization (chap. 6). Thus, there is some evidence, albeit weak, for hydrothermal venting to the basin waters during the most normal marinelike periods of sediment accumulation. A substantial hydrothermal flux, or a standing brine pool, at the Greens Creek vent site is ruled out during sedimentation of these samples (table 5).

On the other hand, during deposition of the more common metal- and sulfur-rich samples, a hydrothermal brine could have been a significant component of the overlying water column. Many hanging-wall samples show very strong enrichments in sulfur, lead, arsenic, and gold with respect to normal black shales, but these same samples are not enriched in cobalt, nor, for the most part, in copper and zinc (fig. 6A). Thus, even if the accumulating sediments were overlain by a brine pool or a hydrothermally impacted water column, evidence is lacking for the basaltic or ultramafic metal source that influenced the metal abundances of the underlying massive sulfide deposit and its alteration envelope in the footwall phyllites.

Implications of Carbonate Isotopic Compositions

Isotopic data from hanging-wall carbonates are compared with data from dolomite in white ore (Freitag, 2000) in figure 11. The hanging-wall compositions are indistinguishable from the compositions of Freitag's (2000) dolomite types I, II, and III. Textural evidence indicates that dolomite types II and III

Table 5. Chemical analyses of hanging-wall samples with low sulfur:organic carbon (C_{org}) and low degree-of-pyritization (DOP) values.[#]

[<, less than; -, no data; S, sulfur; Ba, barium; Pb, lead; Zn, zinc; Au, gold; As, arsenic]

Sample	DOP	C_{org}	S	S: C_{org}	carbonate C	Ba	Pb	Zn	Au	As
96GC1136-3	-	3.00	1.19	0.39	2.31	3,500	142	222	31	15
5	0.68	1.60	0.48	0.30	1.74	1,200	12	68	13	11
16	0.82	1.30	0.69	0.53	2.59	2,200	12	37	40	17
PS-50-01	0.28	-	0.36	-	1.29	1,900	14	93	<2	3.9
PS-50-03	0.47	-	1.14	-	6.42	1,700	25	78	19	11
Average black shale	0.6	3.2	1	0.3	-	1,120	20	310	23	28.8
Average shale	0.5	0.8	0.25	0.3	-	600	20	90	3	10

[#] C_{org} , S, and carbonate C in percent; Ba, Pb, Zn, and As in parts per million; Au in parts per billion.

filled open spaces and that type III coprecipitated with sphalerite, galena, and silver sulfosalts (Freitag, 2000). The isotopic similarity is strong evidence that the carbonate contained in the hanging-wall rocks precipitated from the same fluid that deposited metals in the underlying massive sulfide deposit. Thus, hydrothermal activity at Greens Creek must have persisted until after the hanging-wall sediments had been laid down, a finding which is consistent with the sulfur isotopic evidence that the main sulfur source for the massive ores was bacterial reduction of pore-water sulfate in overlying anoxic sediments (chap. 10).

There are two possible explanations for the carbonate isotopic data shown in figure 11. The first is that the trend reflects variable mixtures of two different carbonate types. One possible end-member is any marine carbonate that may have been present during hydrothermal activity. Evidence for the existence of such an end-member is the platform carbonate rocks that occur discontinuously on Admiralty Island at the same stratigraphic position as the Greens Creek massive sulfide deposit (chap. 2). Triassic marine carbonates would be expected to have $\delta^{18}\text{O}$ values of about 30 permil and $\delta^{13}\text{C}$ values of about 2 permil (Veizer and others, 1999), compositions which lie along the upper extension of the hanging-wall array

shown in figure 11. The low- $\delta^{18}\text{O}$, low- $\delta^{13}\text{C}$ end-member might reasonably be hypothesized to be a hydrothermal precipitate.

The second possible explanation for the isotopic trend is that it reflects carbonates precipitated from a single hydrothermal fluid over a range of temperatures. Shown in figure 12 are two curves that define the isotopic compositions of dolomite precipitated from two different hypothetical fluids at temperatures ranging from 150 to 350°C, a range that includes the temperatures inferred for sulfide precipitation in the massive sulfide body (chap. 15). Both fluids were assigned a $\delta^{18}\text{O}_{\text{H}_2\text{O}}$ value of 10.4 permil on the basis of visual best-fit. The upper curve corresponds to a fluid in which the carbon species is carbonic acid (H_2CO_3) with a $\delta^{13}\text{C}$ value of -4.2 permil, and the lower curve corresponds to a fluid in which the carbon species is also H_2CO_3 , but with a $\delta^{13}\text{C}$ value of -6.2 permil. These $\delta^{13}\text{C}$ values were chosen so that the curves would enclose the majority of the hanging-wall and ore data. The development of the dolomite curves follows Rye and Williams (1981), to which the reader is referred for the underlying details and assumptions.

The slope of the model curves corresponds quite well to the trend of the data (fig. 12). Variation of the fluid $\delta^{13}\text{C}$ value from -4.2 permil to -6.2 permil could be explained by

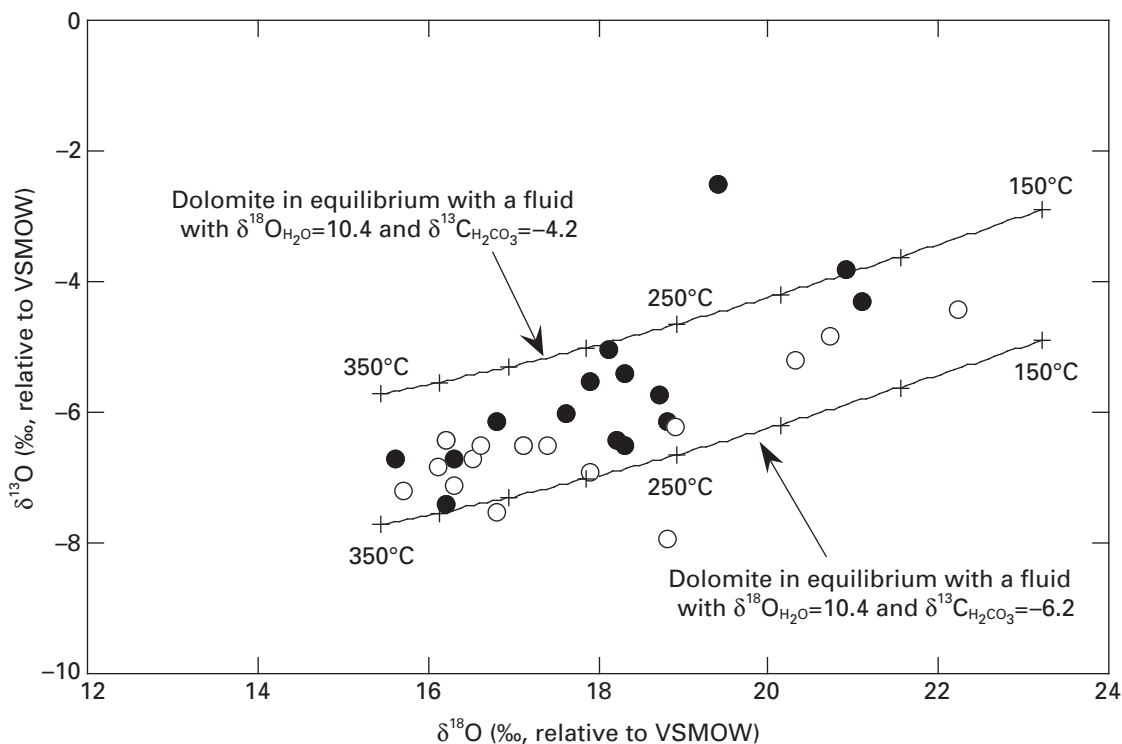
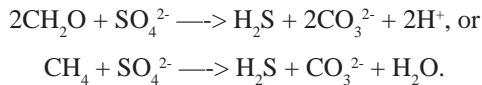


Figure 12. Comparison of the isotopic compositions of carbonate in the hanging-wall rocks (filled circles) with dolomite in white carbonate-rich ore (open circles, Freitag, 2000). Freitag's (2000) tabulated $\delta^{18}\text{O}$ values have been reduced by 0.8 permil to correct for the difference between the acid fractionation factors for calcite and dolomite (Friedman and O'Neil, 1977; Rosebaum and Sheppard, 1986; Swart and others, 1991). Also plotted are curves showing the dolomite compositions that would be predicted for precipitation from a hydrothermal fluid with $\delta^{18}\text{O}_{\text{H}_2\text{O}}$ value of 10.4 permil and $\delta^{13}\text{C}_{\text{H}_2\text{CO}_3}$ value of either -4.2 or -6.2 permil over a temperature range of 150–350°C, the same range that has been inferred for formation of the underlying massive sulfide deposit. VSMOW, Vienna Standard Mean Ocean Water; ‰, permil.

progressive precipitation of dolomite, which would have the effect of depleting the fluid in the heavy isotope and driving the $\delta^{13}\text{C}$ value of dissolved H_2CO_3 downward over time, or by oxidation of organic matter or methane, which would contribute isotopically light carbon also driving the $\delta^{13}\text{C}$ value of H_2CO_3 downward (Rye and Williams, 1981).

Two observations suggest that oxidation of organic matter or methane was an important process during deposition of the hanging-wall section. The first is that the $\delta^{13}\text{C}$ values of carbonate and organic matter are correlated (fig. 13), consistent with carbonate production by oxidation of ambient organic carbon or of methane produced by thermal maturation of organic matter. The fact that the carbonate $\delta^{13}\text{C}$ values are much higher than the organic carbon $\delta^{13}\text{C}$ values implies that organic matter or methane oxidation was a minor carbonate source compared with higher $\delta^{13}\text{C}$ marine carbonate rocks or marine fluids. The second observation suggesting that organic matter or methane oxidation was important is that carbonate $\delta^{13}\text{C}$ values and sulfur contents of the hanging-wall rocks are correlated (fig. 14). This relationship suggests that hydrogen sulfide was produced from sulfate by reaction with low- $\delta^{13}\text{C}$ reduced carbon compounds by chemical pathways such as:



The subsequent reaction of hydrogen sulfide with iron or other metals then caused the reduced sulfur to become fixed in the sediments.

The links illustrated in figures 13 and 14 between sulfide sulfur and carbonate carbon, and between carbonate carbon and organic carbon are strong evidence that sulfide minerals formed, at least in part, during early diagenesis beneath the sediment/seawater interface. Whether any of the hanging-wall sulfides represent true syngenetic accumulations on the ancient sea floor cannot be determined from the observations made in this study.

Also uncertain is the relative importance of microbially mediated and inorganic reactions during formation of the hanging-wall section. The abundance of framboidal pyrite in many of the rocks (chap. 9) and the low and variable $\delta^{34}\text{S}$ values of the hanging-wall pyrite (ave. $\delta^{34}\text{S}$ is -17 permil, range is -29 to 1 permil ($n=12$), chap. 10) are evidence that microbial sulfate reduction was important during this paragenetic stage, but the $\sim 300^\circ\text{C}$ mineralization temperatures that have been inferred for the formation of the base-metal sulfides within the orebody (chap. 10) is high enough that inorganic sulfate reduction could also have been important (compare Orr, 1974; Kiyosu, 1980; Powell and Macqueen, 1984).

The fluid isotopic compositions implied by the model curves (fig. 12), $\delta^{18}\text{O}=10.4$ permil and $\delta^{13}\text{C}=-5.2\pm 1$ permil, should be viewed as approximate. They are within the isotopic ranges expected for fluids that had undergone isotopic exchange with the shale + carbonate + basalt stratigraphic package in which the Greens Creek deposit sits, but they do not rule out magmatic fluids associated with the Triassic mafic/ultramafic magmatism in the region.

The isotopic data for Hyd Group and Cannery Formation carbonates are compared with the hanging-wall data in

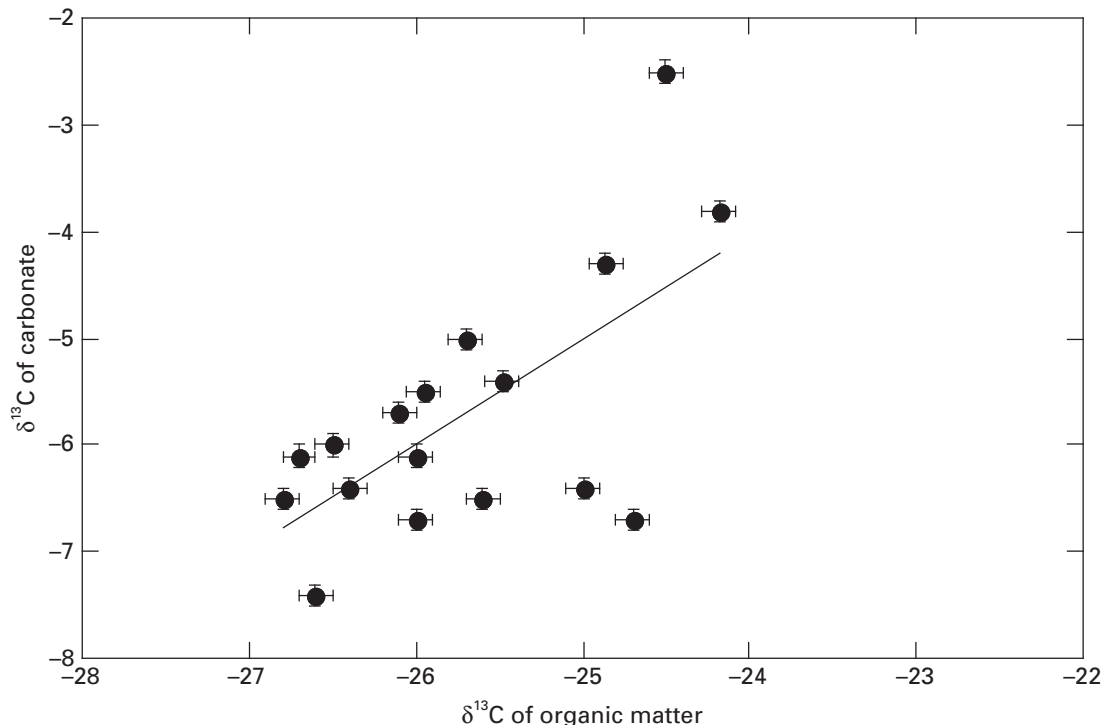


Figure 13. Plot of the carbon isotopic composition of coexisting carbonate and organic matter in hanging-wall rocks. The two parameters show a weak but significant positive correlation ($R=0.64$).

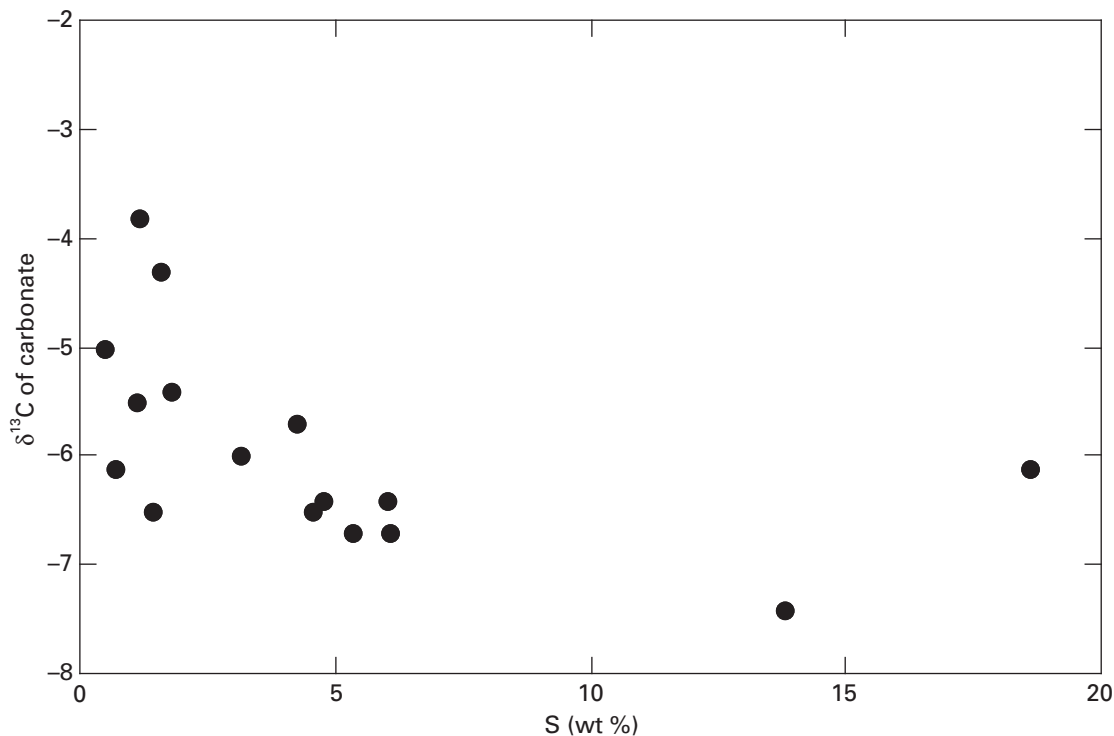


Figure 14. Plot of the carbon (C) isotopic composition of carbonate relative to the sulfur (S) content of hanging-wall rocks. The negative correlation is evidence that the reduction of sulfate to form hydrogen sulfide, which subsequently combined with metals to form sulfide minerals, was accompanied by oxidation of low $\delta^{13}\text{C}$ organic matter or methane. wt%, weight percent.

figure 11. The Hyd samples conform quite well to the hanging-wall array, but the Cannery Formation samples do not. The implication of the hanging wall–Hyd Group correspondence is that both units were exposed to the same fluid over approximately the same temperature range. This finding is consistent with hydrothermal metal scavenging from the Hyd Group sediments but could also be explained by flushing of Hyd sediments by spent hydrothermal fluids after metals had been precipitated. The absence of obvious metal depletions in the Hyd Group occurrences analyzed for this work would seem to favor the spent hydrothermal fluid alternative. The poor correspondence between the hanging-wall and Cannery data suggests that the hydrothermal fluid did not encounter the Cannery section. The Cannery results also support our conclusion that the carbonate isotopic compositions of Admiralty Island shales were not significantly affected by the Cretaceous metamorphism because the three analyzed samples show neither similar isotopic compositions nor a consistent isotopic trend as they might if isotopic exchange had occurred among minerals or between minerals and fluids during regional prograde heating.

Conclusions

Several conclusions arising from this study have implications for the genesis of the Greens Creek ores. First, large

volumes of the hanging-wall sediments experienced epigenetic sulfur addition with associated addition of Ag, As, Au, Cd, Cu, Fe, Mo, Pb, and Zn. However, Co, Cr, Ni, and V show no evidence for similar addition; their abundances appear to be related to the syngenetic accumulation of organic matter.

Second, for at least part of the time that the hanging-wall sediments were accumulating, the overlying water column was oxic, with evidence for possible water column hydrothermal enrichment only in barium. For the remainder of the accumulation history, a hydrothermal component in the overlying water column is neither proved nor disproved. Whatever the exact nature of the overlying water column, there is no clear evidence in the hanging-wall sediments for the basaltic or ultramafic metal source that appears to have been important for the underlying massive sulfide deposit and its alteration envelope in the footwall phyllites.

Third, the isotopic variations of carbonate minerals in both the hanging wall and the white ores are consistent with precipitation from a single hydrothermal fluid over a temperature range of 200 to 350°C, essentially the same temperature range that has been inferred from other observations for formation of the underlying massive ores, or with precipitation from mixed marine and hydrothermal fluids. Whatever the exact dolomite formation mechanism, the close similarity of the compositions in the hanging-wall metasediments and in the white carbonate-rich ores implies deposition from the same fluid by the same mechanism and thus provides strong evidence that hydrothermal

fluid flow at Greens Creek persisted until after the hanging-wall sediments were laid down. The carbonaceous sediment cap may have been an important feature that protected the underlying massive sulfide body from destruction by seawater oxidation.

Fourth, carbonate precipitation was accompanied by, and perhaps driven by, oxidation of organic matter or organic-derived methane. These same reactions resulted in reduction of sulfate to hydrogen sulfide which then reacted with iron and other metals to form sulfide minerals. During growth of framboidal pyrite, sulfate reduction was probably microbially mediated. During formation of base-metal sulfides, sulfate reduction could have proceeded inorganically. Thus, some sulfide minerals, but not necessarily all, formed during early diagenesis beneath the sediment/seawater interface.

Fifth, Hyd Group sediments several kilometers west and northwest of the Greens Creek deposit may have been exposed to hydrothermal fluids either before sulfide mineral precipitation, in which case the fluids may have scavenged metals from Hyd sediments, or after sulfide precipitation from hydrothermal fluids that were spent. The absence of obvious metal depletions in these Hyd rocks suggests that the fluids were spent. Older Cannery Formation shales do not appear to have been exposed to these fluids, although the number of Cannery samples that were studied is too small to exclude this possibility on a regional basis.

References Cited

- Arbogast, B.F., ed., 1996, Analytical methods manual for the Mineral Resource Surveys program: U.S. Geological Survey Open-File Report 96-525, 149 p.
- Arneth, J.D., Schidlowski, M., Sarbas, B., Goerg, U., and Amstutz, G.C., 1985, Graphite content and isotopic fractionation between calcite-graphite pairs in metasediments from the Mgama Hill, southern Kenya: *Geochimica et Cosmochimica Acta*, v. 49, p. 1553-1560.
- Berner, R.A., and Raiswell, R., 1983, Burial of organic carbon and pyrite sulfur in sediments over Phanerozoic time—A new theory: *Geochimica et Cosmochimica Acta*, v. 47, p. 855-862.
- Blatt, Harvey, Middleton, G., and Murray, R., 1972, *Origin of sedimentary rocks*: Englewood Cliffs, New Jersey, Prentice-Hall, 634 p.
- Eastoe, C.J., and Gustin, M.M., 1996, Volcanogenic massive sulfide deposits and anoxia in the Phanerozoic oceans: *Ore Geology Reviews*, v. 10, p. 179-197.
- Freitag, Katje, 2000, *Geology and structure of the lower southwest orebody, Greens Creek mine, Alaska*: Golden, Colorado School of Mines, Ph.D. dissertation, 248 p.
- Friedman, Irving, and O'Neil, J.R., 1977, *Compilation of stable isotope fractionation factors of geochemical interest*: U.S. Geological Survey Professional Paper 440-KK, 12 p.
- Fyfe, W.S., Price, N.J., and Thompson, A.B., 1978, *Fluids in the Earth's crust*: Amsterdam, Elsevier, 383 p.
- Goodfellow, W.D., Lydon, J.W., and Turner, R.J.W., 1993, *Geology and genesis of stratiform sediment-hosted (SEDEX) zinc-lead-silver deposits*: Geological Association of Canada Special Paper 40, p. 201-252.
- Gregory, R.T., Criss, R.E., and Taylor, H.P., Jr., 1989, Oxygen isotope exchange kinetics of mineral pairs in closed and open systems—Applications to problems of hydrothermal alteration of igneous rocks and Precambrian iron formations: *Chemical Geology*, v. 75, p. 1-42.
- Haeussler, P.J., Karl, S.M., Mortensen, J.K., Layer, P., and Himmelberg, G.R., 1999, Permian and mid-Cretaceous deformation of the Alexander terrane on Admiralty and Kupreanof Islands, southeastern Alaska: *Geological Society of America Abstracts with Programs*, v. 31, no. 6, p. A-60.
- Himmelberg, G.R., Brew, D.A., and Ford, A.B., 1995, Low-grade, M_1 metamorphism of the Douglas Island volcanics, western metamorphic belt near Juneau, Alaska, in Schiffman, P., and Day, H.W., eds., *Low-grade metamorphism of mafic rocks*: Boulder, Colorado, Geological Society of America Special Paper 296, p. 51-66.
- Hobbs, B.E., 1986, Principles involved in mobilization and remobilization: *Ore Geology Reviews*, v. 3, p. 37-45.
- Karl, S.M., Haeussler, P.J., Mortensen, J.K., Layer, P., Savage, N., Wardlaw, B., Harris, A., Murchey, B., and Blane, C., 1999, New stratigraphic and isotopic constraints on the depositional and deformational history of the Alexander terrane, southeastern Alaska: *Geological Society of America Abstracts with Programs*, v. 31, no. 6, p. A-68.
- Kitchen, N.E., and Valley, J.W., 1995, Carbon isotope thermometry in marbles of the Adirondack Mountains, New York: *Journal of Metamorphic Geology*, v. 13, p. 577-594.
- Kiyosu, Yasuhiro, 1980, Chemical reduction and sulfur-isotope effects of sulfate by organic matter under hydrothermal conditions: *Chemical Geology*, v. 30, p. 47-56.
- Krauskopf, K.B., 1979, *Introduction to geochemistry* (2d ed.): New York, McGraw-Hill, 617 p.
- Leventhal, J.S., 1983, An interpretation of carbon and sulfur relationships in Black Sea sediments as indicators of environments of deposition: *Geochimica et Cosmochimica Acta*, v. 47, p. 133-137.
- Leventhal, Joel, 1993, Metals in black shales, in Engel, M.H., and Macko, S.A., eds., *Organic geochemistry*: New York, Plenum Press, p. 581-592.
- Leventhal, J.S., 1995, Carbon-sulfur plots to show diagenetic and epigenetic sulfidation in sediments: *Geochimica et Cosmochimica Acta*, v. 59, p. 1207-1211.

- Leventhal, J.S., 1998, Metal-rich black shales—Formation, economic geology and environmental considerations, *in* Schieber, J., Zimmerle, W., and Sethi, P., eds., *Shales and mudstones II: Stuttgart, E. Schweizerbart'sche Verlagsbuchhandlung (Nägele u. Obermiller)*, p. 255–282.
- Leventhal, Joel, and Taylor, C., 1990, Comparison of methods to determine degree of pyritization: *Geochimica et Cosmochimica Acta*, v. 54, p. 2621–2625.
- Lewan, M.D., 1986, Stable carbon isotopes of amorphous kerogens from Phanerozoic sedimentary rocks: *Geochimica et Cosmochimica Acta*, v. 50, p. 1583–1591.
- McCrea, J.M., 1950, On the isotope chemistry of carbonates and a paleotemperature scale: *Journal of Chemical Physics*, v. 18, p. 849–857.
- Newberry, R.F., Crafford, T.C., Newkirk, S.R., Young, L.E., Nelson, S.W., and Duke, N.A., 1997, Volcanogenic massive sulfide deposits of Alaska, *in* Goldfarb, R.J., and Miller, L.D., eds., *Economic geology monograph 9—Mineral deposits of Alaska: Littleton, Colorado, Economic Geology Publishing Company*, p. 120–150.
- Orr, W.L., 1974, Changes in sulfur content and isotopic ratios of sulfur during petroleum maturation—Study of Big Horn basin Paleozoic oils: *American Association of Petroleum Geologists Bulletin*, v. 58, p. 2295–2318.
- Powell, T.G., and Macqueen, R.W., 1984, Precipitation of sulfide ores and organic matter—Sulfate reactions at Pine Point, Canada: *Science*, v. 224, p. 63–66.
- Quinby-Hunt, M.S., Wilde, P., Orth, C.J., and Berry W.B.N., 1989, Elemental geochemistry of black shales—Statistical comparison of low-calcic shales with other shales: *U.S. Geological Survey Circular 1037*, p. 8–15.
- Raiswell, R., and Berner, R.A., 1985, Pyrite formation in euxinic and semi-euxinic sediments: *American Journal of Science*, v. 285, p. 710–724.
- Ramsay, J.G., 1980, The crack-seal mechanism of rock deformation: *Nature*, v. 284, p. 135–139.
- Rosebaum, Joseph, and Sheppard, S.M.F., 1986, An isotopic study of siderites, dolomites and ankerites at hightemperatures: *Geochimica et Cosmochimica Acta*, v. 50, p. 1147–1150.
- Rye, D.M., and Williams, N., 1981, Studies of the base metal sulfide deposits at McArthur River, Northern Territory, Australia, III. The stable isotope geochemistry of the H.Y.C., Ridge and Cooley deposits: *Economic Geology*, v. 76, p. 1–26.
- Schidowski, Manfred, 1987, Application of stable carbon isotopes to early biochemical evolution on Earth: *Annual Review of Earth and Planetary Sciences*, v. 15, p. 47–72.
- Swart, P.K., Burns, S.J., and Leder, J.J., 1991, Fractionation of the stable isotopes of oxygen and carbon in carbon dioxide during the reaction of calcite with phosphoric acid as a function of temperature and technique: *Isotope Geoscience*, v. 12, p. 89–96.
- Taylor, C.D., Leventhal, J.S., Johnson, C.A., and Lear, K.G., 2000, The Greens Creek massive sulfide deposit, southeastern Alaska—Stable isotopic evidence for the involvement of biogenic sulfate reduction in the formation of ores and carbonates, *in* Gemmell, J.B., and Pongratz, J., eds., *Volcanic environments and massive sulfide deposits: Program and Abstracts, Special Publication 3, Centre for Ore Deposits Research, Hobart, University of Tasmania*, p. 209–210.
- Taylor, C.D., Newkirk, S.R., Hall, T.E., Lear, K.G., Premo, W.R., Leventhal, J.S., Meier, A.L., Johnson, C.A., and Harris, A.G., 1999, The Greens Creek deposit, southeastern Alaska—A VMS-SEDEX hybrid, *in* Stanley, C.J., and others, eds., *Mineral deposits, processes to processing: Rotterdam, Balkema*, p. 597–600.
- Tissot, B.P., and Welte, D.H., 1984, *Petroleum formation and occurrence (2d ed.)*: Berlin, Springer-Verlag, 699 p.
- Tissot, B., Durand, B., Espitalie, J., and Combaz, A., 1974, Influence of the nature and diagenesis of organic matter on the formation of petroleum: *American Association of Petroleum Geologists Bulletin*, v. 58, p. 499–506.
- Tourtlot, H.A., 1979, Black shale—Its deposition and diagenesis: *Clays and Clay Minerals*, v. 27, p. 313–321.
- Veizer, Jan, Ala, D., Azmy, K., Bruckschen, P., Buhl, D., Bruhn, F., Carden, G.A.F., Diener, A., Ebner, S., Godderis, Y., Jasper, T., Korte, C., Pawellek, F., Podlaha, O.G., and Strauss, H., 1999, $^{87}\text{Sr}/^{86}\text{Sr}$, $\delta^{13}\text{C}$ and $\delta^{18}\text{O}$ evolution of Phanerozoic seawater: *Chemical Geology*, v. 161, p. 59–88.
- Vine, J.D., and Tourtelot, E.B., 1970, Geochemistry of black shale deposits—A summary report: *Economic Geology*, v. 65, p. 253–272.
- Williams, Neil, 1978, Studies of the base metal sulfide deposits at McArthur River, Northern Territory, Australia—II. The sulfide-S and organic-C relationships of the concordant deposits and their significance: *Economic Geology*, v. 73, p. 1036–1056.

Mineralogical, Textural, and Metal Residence Studies of Primary, Recrystallized, and Remobilized Ores of the Greens Creek Deposit

By Cliff D. Taylor, Steven J. Sutley, and Frederick E. Lichte

Chapter 9 of

**Geology, Geochemistry, and Genesis of the Greens Creek Massive
Sulfide Deposit, Admiralty Island, Southeastern Alaska**

Edited by Cliff D. Taylor and Craig A. Johnson

Professional Paper 1763

**U.S. Department of the Interior
U.S. Geological Survey**

Contents

Abstract.....	187
Introduction.....	187
Mine Location, General Host Rocks, Metamorphic History, Deposit Morphology, and Structural History	189
Previous Mineralogical and Mineral Geochemical Studies.....	191
Ore Types.....	194
Primary Ore Mineralogy and Textures	196
Recrystallized and Remobilized Ore Mineralogy and Textures.....	196
Free Gold—Mineralogy and Textures.....	199
Paragenetic Relationships—Physical and Chemical Modification of Ores	200
LA–ICP–MS Mineral Chemistry Studies	204
Methods.....	204
Results	209
Discussion.....	230
Conclusions.....	234
References Cited.....	234

Figures

1. Maps of northern Admiralty Island showing the location of the Greens Creek mine and other features mentioned in the text.....	191
2. Plan and cross-sectional views of the Greens Creek deposit showing features described in the text.....	192
3. Photographs of hand samples illustrating the various massive sulfide and white ore types.....	194
4. Photographs of hand samples illustrating textures present in various ore types	197
5. Photomicrographs of polished thin sections showing primary mineral textures	198
6. Photomicrographs of polished thin sections showing recrystallized ore textures	201
7. Photomicrographs of arsenian pyrite and arsenopyrite in polished thin sections	205
8. Photographs and photomicrographs of free gold (Au) in hand samples and polished sections.....	207
9. LA–ICP–MS traverses across heavy concentrate grains recovered from the Greens Creek mill.....	208
10. Photographs and photomicrographs showing textural relationships in Greens Creek ores.....	210
11. Summary LA–ICP–MS data on sulfide ore minerals in the Greens Creek deposit. Box plots of percentiles shows the log ₁₀ concentration range for primary, recrystallized, and remobilized ore textures for each of 19 elements.....	212
12. Single element plots of LA–ICP–MS data showing the range of elemental abundances of metals in primary and recrystallized pyrite and sphalerite, and in primary, recrystallized, and remobilized galena.....	221

Tables

1. Greens Creek ore mineralogy—minerals identified	188
2. Trace-element composition of primary pyrite as determined by Laser Ablation–Inductively Coupled Plasma—Mass Spectroscopy analyses	213
3. Trace-element composition of recrystallized pyrite as determined by Laser Ablation–Inductively Coupled Plasma—Mass Spectroscopy analyses	214
4. Trace-element composition of arsenian pyrite as determined by Laser Ablation–Inductively Coupled Plasma—Mass Spectroscopy analyses	215
5. Trace-element composition of galena as determined by Laser Ablation–Inductively Coupled Plasma—Mass Spectroscopy analyses	215
6. Trace-element composition of sphalerite as determined by Laser Ablation–Inductively Coupled Plasma—Mass Spectroscopy analyses	216
7. Trace-element composition of tetrahedrite as determined by Laser Ablation–Inductively Coupled Plasma—Mass Spectroscopy analyses	217
8. Trace-element composition of mixed primary-textured mineral aggregates as determined by Laser Ablation–Inductively Coupled Plasma—Mass Spectroscopy analyses	218
9. Trace-element composition of recrystallized mixed mineral aggregates as determined by Laser Ablation–Inductively Coupled Plasma—Mass Spectroscopy analyses	219
10. Trace-element composition of remobilized mixed mineral aggregates as determined by Laser Ablation–Inductively Coupled Plasma—Mass Spectroscopy analyses	220

Mineralogical, Textural, and Metal Residence Studies of Primary, Recrystallized, and Remobilized Ores of the Greens Creek Deposit

By Cliff D. Taylor, Steven J. Sutley, and Frederick E. Lichte

Abstract

The Greens Creek deposit is a 24.2-million-ton polymetallic massive sulfide with a diverse base- and precious-metal-rich mineralogy, which has been subjected to regional lower greenschist facies metamorphism. Roughly 30 percent of the ores retain primary mineralogy and mineral textures as well as gross original ore stratigraphy. Ore lithologies fall into two groups: massive sulfide ores (greater than 50 percent sulfides) and semimassive or disseminated sulfide gangue-rich “white” ores (less than 50 percent sulfides). There are two types of massive ore: massive pyritic and massive base-metal-rich ore. The white ores are of three types: white carbonate and white siliceous ores (common), and white baritic ore. All the ore types can be further subdivided on the basis of modification by veins, breccias, and gouge or rubble zones produced during faulting or folding. Veining due to metamorphic remobilization and recrystallization can result in enrichment of free gold and a variety of silver-sulfosalt minerals. The ore stratigraphy at Greens Creek is characterized by proximal copper-arsenic-gold-enriched massive pyritic ores centered over white siliceous ores and silicified footwall. Laterally, the white siliceous ores grade outward into white carbonate and barite ores. White ores are overlain by massive pyritic ores that change upward and outward toward lower copper-gold grades. Proximal ores transition to increasingly higher grade zinc-lead-silver-(gold)-rich, massive, fine-grained, base-metal-rich ores toward the argillite hanging wall and the margins of the deposit. Distal ore commonly is characterized by carbonate- and barite-rich white ores against footwall phyllites, which grade into massive, fine-grained, base-metal-rich ores toward the hanging wall. This progression of ore types is the most common throughout the mine.

Primary mineral textures are characterized by framboidal, colloform, dendritic, and “spongy” pyrite intergrown with base-metal sulfides and sulfosalts. Primary assemblages also include sphalerite, galena, tetrahedrite, chalcopyrite, free gold, and a variety of lead-antimony-arsenic (-mercury-thallium) sulfosalts. The abundance of polyframboidal, colloform, and nodular pyrite textures coupled with their $\delta^{34}\text{S}$ -depleted isotopic signature provides strong evidence that the main stage

of massive sulfide mineralization at Greens Creek occurred primarily during early diagenesis, synchronous with accumulation of the hanging-wall sediments. The early development of framboid-derived, atoll-shaped textures in the ores may indicate that a zone-refinement process occurred in the presence of colloidal base-metal-sulfide gels. Metamorphic recrystallization produced advanced atoll-shaped structures in the ores and resulted in much coarser textures and the formation and(or) remobilization of secondary, precious-metal-enriched minerals. Secondary minerals are present as matrix to pyrite euhedra and in late fractures and veinlets. Secondary mineralogy includes chalcopyrite, sphalerite (low iron), galena, free gold, electrum, tetrahedrite (antimony-rich), pyrrargyrite, and many other sulfosalt minerals. Metamorphism resulted in visible cleaning and coarsening of the ore mineralogy and caused local trace-element redistribution and upgrading of the ores.

Introduction

The Greens Creek deposit is a mineralogically diverse, polymetallic (zinc-lead-silver-gold-copper) massive sulfide of Late Triassic age and unusually high silver content. The global resource is currently 24.2 million tons at an average grade of 13.9 percent zinc, 5.1 percent lead, 0.15 troy ounces per ton gold, and 19.2 troy ounces per ton silver. Twenty-nine ore sulfide minerals have been reported, 18 of which are silver bearing (table 1). In addition to the metals of economic interest, the ores are enriched in trace elements such as As, Sb, Hg, Tl, Ni, Co, Cr, and Mo. These metals and minerals are contained in a suite of five ore types, which define an ore stratigraphy that progressed from early white ores to main-stage massive sulfide ores during the growth of the system. This progression (see chap. 15 for a more thorough description) is thought to have started at low temperature, at or very near the sediment/water interface in a basin containing oxygenated seawater, and then evolved to higher temperature within a growing sulfide blanket that formed in and beneath a progressively thickening layer of black shales. As deposition progressed, pore fluids in the shales and probably the overlying water column gradually became anoxic. These early and main-stage ore-forming

Table 1. Greens Creek ore mineralogy—minerals identified.

Mineral name	Mineral formula	How identified	Reference
silver	Ag	XRD, LA--ICP--MS	this study
acanthite	Ag ₂ S	electron microprobe, XRD	C.J. Carter (written commun., 1994)
proustite	Ag ₃ AsS ₃	optical microscope, XRD, electron microprobe	this study
jalpaite	Ag ₃ CuS ₂	electron microprobe	C.J. Carter (written commun., 1994); T.K. Bundtzen (written commun., 1996)
pyrargyrite	Ag ₃ SbS ₃	optical microscope, electron microprobe	T.C. Crafford (written commun., 1989)
stephanite	Ag ₅ SbS ₄	electron microprobe	T.C. Crafford (written commun., 1989)
argyrodite	Ag ₈ GeS ₆	electron microprobe	K.G. Lear (oral commun., 2000)
stromeyerite	AgCuS	electron microprobe	E.U. Peterson (written commun., 1991)
realgar	AsS	optical microscope, XRD	this study
pearceite	(Ag,Cu) ₁₆ As ₂ S ₁₁	electron microprobe	E.U. Peterson (written commun., 1991)
antimonpearceite	(Ag,Cu) ₁₆ Sb ₂ S ₁₁	optical microscope, XRD, electron microprobe	K.G. Lear (oral commun., 2000)
polybasite	(Ag,Cu) ₁₆ Sb ₂ S ₁₁	electron microprobe	T.C. Crafford (written commun., 1989)
mckinstryite	(Ag,Cu) ₂ S	electron microprobe	E.U. Peterson and D. Chirban (written commun., 1994)
freibergite	(Ag,Cu,Fe) ₁₂ (Sb,As) ₄ S ₁₃	optical microscope, electron microprobe	T.C. Crafford (written commun., 1989)
gold	Au,(Ag)	optical microscope, LA-ICP-MS	T.C. Crafford (written commun., 1989); this study
electrum	Au,Ag,(Hg)	optical microscope, LA-ICP-MS	T.C. Crafford (written commun., 1989); E.U. Peterson (written commun., 1991); this study
chalcocite - Ag-bearing	Cu ₂ S +Ag	electron microprobe	E.U. Peterson (written commun., 1991)
bornite	Cu ₅ FeS ₄	optical microscope	E.U. Peterson (written commun., 1991)
bornite - Ag-bearing	Cu ₅ FeS ₄ +Ag	electron microprobe	E.U. Peterson (written commun., 1991)
chalcopyrite	CuFeS ₂	optical microscope	T.C. Crafford (written commun., 1989); E.U. Peterson (written commun., 1991)
tennantite	(Cu,Fe) ₁₂ As ₄ S ₁₃	optical microscope, XRD, electron microprobe	this study
tetrahedrite	(Cu,Fe) ₁₂ Sb ₄ S ₁₃	optical microscope, electron microprobe, XRD	T.C. Crafford (written commun., 1989); E.U. Peterson (written commun., 1991)
covellite	CuS	optical microscope	E.U. Peterson (written commun., 1991)
covellite-acanthite mineral	CuS-Ag ₂ S	electron microprobe	E.U. Peterson (written commun., 1991)
unknown (possibly thalcosite)	CuTlS (Tl ₂ (Cu,Fe) ₄ S ₄)	electron microprobe	K.G. Lear (oral commun., 2000)
arsenopyrite	FeAsS	electron microprobe, XRD	C.J. Carter (written commun., 1994)
marcasite	FeS ₂	optical microscope	C.J. Carter (written commun., 1994)
pyrite	FeS ₂	optical microscope	T.C. Crafford (written commun., 1989); E.U. Peterson (written commun., 1991)
geocronite	Pb ₁₄ (As,Sb) ₆ S ₂₃	electron microprobe	K.G. Lear (oral commun., 2000)
jordanite	Pb ₁₄ (As,Sb) ₆ S ₂₃	optical microscope, XRD, electron microprobe	this study
boulangerite	Pb ₅ Sb ₄ S ₁₁	electron microprobe	K.G. Lear (oral commun., 2000)
galena	PbS	optical microscope	T.C. Crafford (written commun., 1989); E.U. Peterson (written commun., 1991)
cassiterite	SnO ₂	electron microprobe	K.G. Lear (oral commun., 2000)
sphalerite	ZnS	optical microscope	T.C. Crafford (written commun., 1989); E.U. Peterson (written commun., 1991)

Spelling of mineral names and mineral formulas follows the usage of Blackburn and Dennen, 1997.

KGCMC, Kennecott Greens Creek Mining Company; XRD, X-ray diffraction; LA-ICP-MS, laser ablation-inductively coupled plasma-mass spectrometry.

processes produced a trace-element-rich orebody with a diverse silver- and base-metal-rich mineralogy, primarily by replacement of shale, early sulfides, and silica-barite gangue. Remnants of primary mineral textures are represented by fine- to very fine grained aggregates of framboidal, dendritic, and colloform or botryoidal pyrite intimately intergrown and banded with base-metal sulfides and the diverse suite of trace-element and silver-bearing sulfides.

Following the cessation of mineral deposition in latest Triassic time, the deposit was buried by continued shale sedimentation, which effectively prevented sea-floor oxidation of the newly formed sulfides. During the next 215 million years the deposit went through at least three phases of deformation (see chap. 7) and a regional subgreenschist to lower greenschist facies metamorphic event (see chap. 2) that reached temperatures of 275–350°C (see chap. 12) and buried host rocks in the Greens Creek area to a depth of about 17–18 kilometers (Himmelberg and others, 1995). Although the metamorphism and multiple deformation of the orebody resulted in pronounced structural dismemberment, folding, recrystallization, and remobilization of the ores, large areas of the deposit preserve primary mineralogy, textures, and chemistry. A range of preservation states exists, from pristine to completely modified. This fortuitous situation presents an opportunity to study the effects of deformation and metamorphism upon massive sulfide mineral textures and to understand the details of mineral residence of specific trace elements and their redistribution as a result of textural modification.

Most of the initial mineral identifications, descriptions of ore textures, and preliminary determinations of mineral chemistry are contained in unpublished mining company reports (see “Previous Mineralogical and Mineral Geochemical Studies” section). In particular, electron microprobe mineral-chemistry studies were conducted to improve the beneficiation of various mill products, and metal zonation studies of tetrahedrites were conducted in an attempt to obtain geochemical vectors within ore assemblages. We summarize these unpublished reports, compile their mineral identifications and textural observations, and significantly extend the petrographic descriptions and geochemistry of the various ores at Greens Creek.

Here we describe the five principal ore types in detail and the mineralogy and mineral textures present in these ores. We then discuss the paragenesis of the ores and the progressive modification of the mineralogy and mineral textures as a result of deformation and metamorphism. We follow the descriptive portion of the chapter with the presentation of preliminary Laser Ablation–Inductively Coupled Plasma–Mass Spectroscopy (LA–ICP–MS) mineral geochemical studies of the ores. The LA–ICP–MS studies provide mineral-specific geochemical data in support of the petrographic observations. These data demonstrate that the specific mineral residence and concentrations of trace elements in the ores change as a result of recrystallization and remobilization, in addition to the resulting mineralogical and textural modifications. Based on the petrographic observations and mineral chemistry presented, we propose a sequence of events that explain the formation and modification of the

mineralogy, textures, metal endowments, and zonation of the ores throughout the deposit. The chapter concludes with a discussion of the mobility of metals in deformed massive sulfide deposits and a comparison of Greens Creek mineralogy and chemistry to modern and ancient analogs.

Mine Location, General Host Rocks, Metamorphic History, Deposit Morphology, and Structural History

The Greens Creek mine is 29 km south of Juneau, Alaska, near the northern end of Admiralty Island and within Admiralty Island National Monument (fig. 1). The deposit is located at the contact between a footwall sequence of predominantly phyllitic mafic volcanic rocks and mafic-ultramafic hypabyssal sills and intrusions, and a hanging wall of black argillites. Geochronologic studies (chap. 11) have established that the hanging-wall argillites have an age of 220 Ma and are thus part of the sedimentary portion of the regionally extensive Hyd Group of latest Triassic (Norian) age. Less precise age controls suggest strongly that the mafic-ultramafic intrusive suite in the footwall is also of Late Triassic age and are the parent rocks to the Hyd Group basalts that cap the argillites. Uncertainty remains as to the age and identity of the footwall phyllites. They are most likely either of middle Permian or of Late Triassic age.

Constraints on the metamorphic history of the host rocks and ore at Greens Creek are few. The Late Triassic and older rocks of most of Admiralty Island are within the Admiralty Island Metamorphic Belt of Brew and others (1992), which refers to most of the island west of the Glass Peninsula. Within this region, mineral assemblage data are limited, no isograds have been mapped, and no thermobarometric data are available. No clear trends in the metamorphic pattern are discernible, and rocks from subgreenschist through amphibolite facies are present, produced during post-Triassic metamorphism and deformation (Brew and others, 1992). Loney (1964) suggested there is a westward decrease in metamorphic grade present in correlative rocks on the southern portion of Admiralty Island. Regional mapping of metamorphic units (Dusel-Bacon, 1994) places the Admiralty Island Metamorphic Belt in the greenschist facies; descriptions of Late Triassic and younger rock units within this belt in the area around the mine (Lathram and others, 1965; S.M. Karl, written commun., 2003) suggest subgreenschist to lower greenschist facies metamorphic grade. Limited petrographic and electron microprobe work conducted during this study on Hyd Group basalt samples from the immediate vicinity of the mine suggest a dominantly chlorite-albite-epidote-quartz-sericite-calcite assemblage with occasional relict clinopyroxene and(or) hornblende phenocrysts. Tentative petrographic and electron microprobe identification of minor pumpellyite may indicate that the Late Triassic and younger rocks of the mine area are near the prehnite-pumpellyite to lower greenschist facies transition.

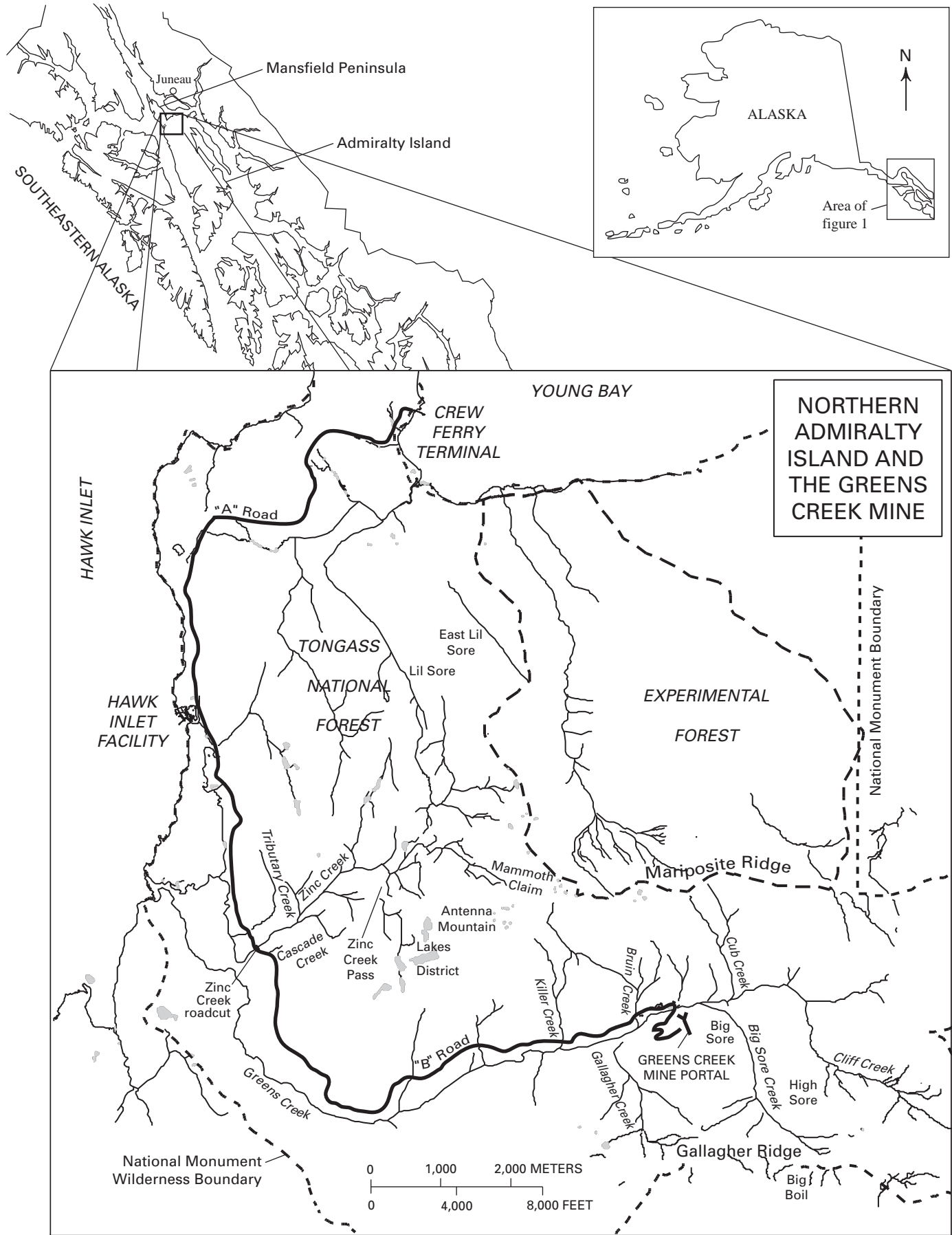


Figure 1 (facing page). Maps of northern Admiralty Island showing the location of the Greens Creek mine and other features mentioned in the text.

In general, the metamorphic history of Permian and younger rocks in the mine area is thought to be similar to the better-studied western metamorphic belt, the western edge of which is located several kilometers northeast of the mine. The western metamorphic belt is part of the Coast plutonic-metamorphic complex (Brew and others, 1989) of western Canada and southeastern Alaska that developed during the collision of the Alexander terrane and Gravina overlap assemblage with the Stikine terrane (Brew and others, 1989, 1992; Himmelberg and others, 1994, 1995). The western metamorphic belt is about 30 kilometers wide in the vicinity of Juneau and is characterized by Barrovian metamorphism. Multiple periods of deformation, metamorphism, and plutonism occurred from about 120 to 50 Ma, with the earliest, a regional dynamothermal event termed M_1 , constrained by fabrics that predate intrusion of 110-Ma mafic-ultramafic rocks (Brew and others, 1989, 1992; Himmelberg and others, 1994, 1995). Himmelberg and others (1995) conducted a mineral chemistry and phase equilibria study of the M_1 event in subgreenschist to lower greenschist facies Douglas Island volcanics along the western edge of the western metamorphic belt. They concluded that thermal peak metamorphism of pumpellyite-bearing assemblages occurred at about 325°C and 2 to 4.8 kbar, equal to a maximum burial depth, assuming a normal geothermal gradient, of about 17–18 kilometers (Himmelberg and others, 1995). They also argued that in order to preserve the M_1 mineral assemblage observed at the western edge of the belt given a structurally and metamorphically continuous 120- to 50-Ma event, that rapid burial, a limited extent of thermal pulse (from the 70-Ma intrusive event along the Coast batholith), and rapid uplift must have occurred. They suggest that uplift rates of 6 km/10⁶ years are required, which implies exhumation of the western edge of the belt in as little as several hundred thousand years.

A variety of indirect constraints on temperature (⁴⁰Ar/³⁹Ar closure temperature of 2 M_1 muscovite, conodont color alteration indices of 5 to 5.5, lack of carbonate and organic carbon isotopic reequilibration, sphalerite-galena sulfur isotope pairs; chaps. 8, 10, 11) at Greens Creek suggest that maximum temperature during either the mineralizing event or Cretaceous regional metamorphism was no greater than about 275–350°C. These various lines of evidence coupled with the limited petrographic and microprobe data previously described are consistent with metamorphic conditions near the prehnite-pumpellyite to lower greenschist transition in the Greens Creek area. The preservation of primary isotopic and geochemical features of the deposit as well as the primary textural features of the ores described in this chapter further suggest that the M_1 metamorphic event was neither pervasive nor long lived.

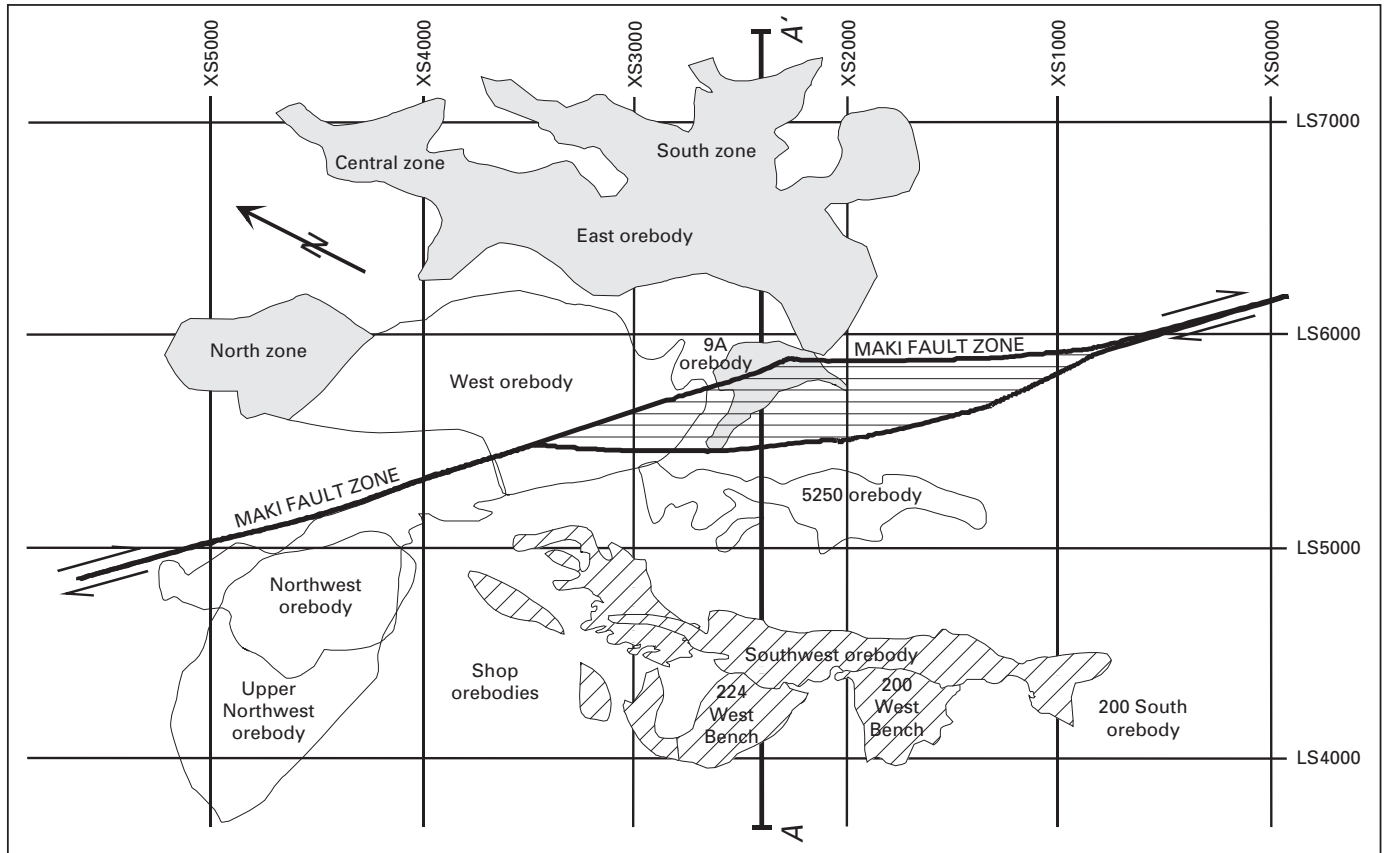
Ore is nearly continuous along the phyllite/argillite contact and consists of three main orebodies—the East, West, and Southwest—and three extensions (fig. 2). The East orebody outcrops near the northeastern edge of the property, plunges shallowly to the southwest, and dips steeply west, flattening out gradually into the West orebody. The Klaus thrust fault separates the East and West orebodies approximately halfway through the flat. West of the flat, the West orebody continues beneath the Klaus fault as a thin horizontal layer, which dips to near vertical and then swells into a multiply folded and thickened mass that occupies a trough-shaped depression in the phyllite/argillite contact. A southward extension of the West orebody is hosted entirely within the hanging-wall argillites. The Northwest extension is a dextral fault translation of the western portion of the West orebody along the Maki fault, a major, near-vertical, strike-slip fault that cuts the property in two.

The Southwest orebody extends from the West/Northwest orebody in a complex helical fold that plunges shallowly to the southwest. Like the southward extension of the West orebody, the upper portion of the Southwest orebody transgresses the phyllite/argillite contact into the argillites. Maximum separation is about 35 m. The 200 South orebody is a southward extension of the Southwest orebody.

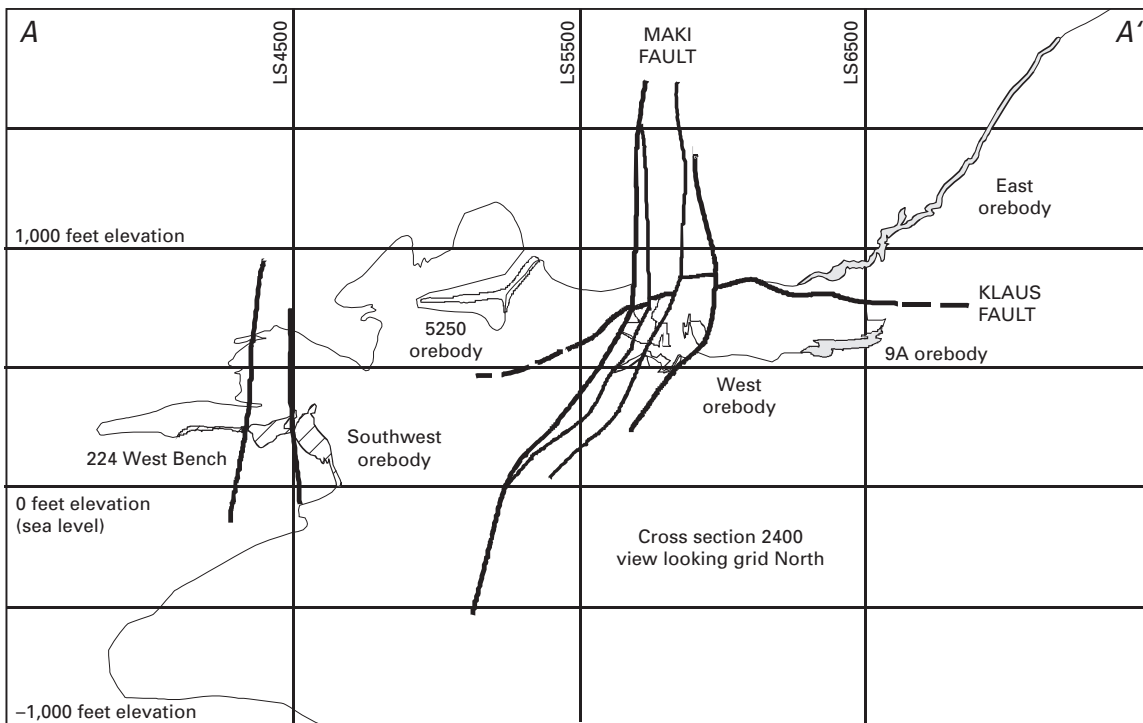
Deformation at Greens Creek is extremely complex and involves at least four periods of folding, one period of semiductile shearing, and two periods of faulting (see chap. 7). Continuity of the orebodies is interrupted by numerous thrusts and strike-slip faults on and parallel to the Klaus and Maki faults. The four phases of folding have further modified the deposit morphology. However, with few exceptions the ore horizon is traceable along the phyllite/argillite contact throughout the mine. Restoration of 600 m of movement along the Maki fault and 200 m of movement along the Klaus fault (P.A. Lindberg, written commun., 1994) results in a single orebody with a thickened central core in the West/Northwest orebody, which thins to the north, east, and south. The only indication that stacked orebodies may be present is the separate occurrence of ore above and south of the main ore concentration in the 5250 orebody (fig. 2).

Previous Mineralogical and Mineral Geochemical Studies

The earliest report on the mineralogy of Greens Creek ores of which we are aware consists of a brief summary and petrographic descriptions of six samples from the East orebody (George Alorno, written commun., 1987). Two samples of phyllite, one argillite, one white ore that probably would be currently classified as a white carbonate ore type, and two massive sulfide ores are described in detail. The major conclusions were that (1) variable deformation and degree of recrystallization between the phyllites and argillites indicate that the ore horizon is a tectonic contact, (2) massive sulfides



PLAN VIEW OF THE GREENS CREEK DEPOSIT.



CROSS-SECTIONAL VIEW OF THE GREENS CREEK DEPOSIT.

Figure 2. Plan and cross-sectional views of the Greens Creek deposit showing features described in the text.

show a mix of primary and intensely granulated textures but no evidence for ductile deformation, and (3) the white ore sample contains abundant cymrite (hydrous barium aluminosilicate) and probably barian muscovite. Importantly, Alorno (written commun., 1987) also noted that the ore sulfides, particularly tetrahedrite, were confined to veinlets in the white ore and were not part of the “early assemblage.” Both polycrystalline quartz and rotated dolomite porphyroblasts were observed in the phyllites, establishing a predeformation age of silica-carbonate alteration, similar to the findings of this study (V.M. Anderson and C.D. Taylor, unpub. data, 2000), and compositional layering in the phyllite occasionally was truncated against pyrite bands. If so, this observation suggests the presence of a premineralization fabric in the phyllites that is probably equivalent to the S_1 foliation of current usage (see chap. 7). Alorno’s report documents the occurrence of all of the currently known major sulfide minerals as well as gangue graphite, rutile, ilmenite, “green mica,” and the postulated barian muscovite. Although cymrite may be present, it has not been documented in any of the later studies. He notes the presence of delicate botryoidal features in pyrite-tetrahedrite-sphalerite bands, describes either cataclasis or the lack of deformation features in pyrite, and “granoblastic,” “annealed,” and “flame” textures in galena and sphalerite. Paragenetically, Alorno (George Alorno, written commun., 1987) notes the remobilization of tetrahedrite and galena into fractures in, and as matrix to, pyrite and refers to “pseudoframboidal” pyrite features produced by replacement of base-metal sulfides by pyrite. Additionally, he makes the important observation that early primary textured pyrite is commonly overgrown by euhedral pyrite.

The next and most significant effort at understanding the mineralogy and mineral chemistry of the ores at Greens Creek is contained in a series of internal mining company reports. These reports detail the results of three major phases of work. The first phase consists of three reports that describe the mineralogy and mineral chemistry, as determined by electron microprobe analysis, on a variety of mill products drawn from East orebody ore: mill head; lead (Pb), zinc (Zn), and bulk concentrates; tails; and final tails (E.U. Petersen, written commun., 1991, 1992a, b). These early studies recognized the complexity of the silver (Ag) mineralogy at Greens Creek (see table 1) and placed some preliminary constraints on the mineral chemistry of a few of the major phases. East orebody sphalerite was shown to have fairly homogeneous low iron (Fe) content (less than 1.0 percent) and measurable cadmium (Cd), mercury (Hg), copper (Cu), and manganese (Mn) (less than 1.0 percent combined). Analyses of tetrahedrite showed them to be the zinc-antimony-rich, iron-arsenic-poor end member, with measurable cadmium. Silver in tetrahedrite ranged from about 0.5 to 6.5 percent with several exceptionally silver-rich analyses up to 15.9 percent. E.U. Petersen (written commun., 1992) also noted the common occurrence of an unknown silver-rich mineral (up to 44 percent silver), previously identified as covellite, which plots along the covellite (CuS) – acanthite (Ag₂S) join.

Results of the second phase of mineralogical research at Greens Creek are contained in a series of memorandums from Chris J. Carter to the Greens Creek mine staff (C.J. Carter, written commun., 1994a, b, c, d). In these memorandums, Carter presents a reevaluation of Petersen’s concentrate microprobe data and a preliminary evaluation of microprobe data from a set of 12 samples collected from the Southwest orebody. A report containing detailed descriptions and assay data provides context for the 12 hand samples (Debra Apel, written commun., 1993). Carter’s evaluation of Petersen’s data focuses on the variation of silver content in tetrahedrite and the possible utility of using silver as a vector for exploration. He suggests that the broad range of silver/copper values determined for tetrahedrites from East orebody concentrates indicates that original metal zoning features have probably been preserved and thus might provide a useful exploration criterion.

Petrographic and geochemical studies of mineralogy in the Southwest orebody samples noted a broad range of sulfide textures and grain sizes. Four distinct textural varieties of pyrite were observed: euhedral, spongy, colloform, and framboidal. Minor to moderate amounts of arsenopyrite also were observed, and microprobe data on pyrite, arsenian pyrite, and arsenopyrite indicated measurable gold and nickel (Ni). Galena was noted to be weakly argentiferous and thus not a significant contributor to the silver budget. The antimony content of tetrahedrite was shown to vary greatly from about 13 percent (expressed as the molar ratio Sb/[Sb+As]) to about 81 percent, demonstrating that a series of tetrahedrite-tennantite minerals are present in the Southwest orebody. These tetrahedrites also have three times the average silver content (expressed as the molar ratio Ag/[Ag+Cu]) than those in the East orebody (17.6 versus 5.2 percent), lower zinc content, and higher iron and cadmium content. They also report silver-rich minerals belonging to the proustite-pyrargyrite series, jalpaite, and an unidentified mineral with 86 weight percent silver (C.J. Carter, written commun., 1994). Ag/Ag+Cu versus Sb/Sb+As plots of tetrahedrite analyses were interpreted as having three distinct trends, indicating three distinct starting fluid compositions may have contributed to the ore-forming process (C.J. Carter, written commun., 1994). Sphalerite iron content was observed to be as homogeneous as in East orebody sphalerites with perhaps a slightly higher average value (0.9 weight percent).

The potential use of iron in sphalerite and Ag-Cu versus Sb-As trends in tetrahedrites as exploration tools led to a third phase of mineralogical research. E.U. Petersen and D. Chirban (written commun., 1994) conducted a study aimed at characterizing the mineralogical and chemical zoning of the Greens Creek deposit based on tetrahedrite chemistry. Tetrahedrites in 44 samples primarily from drill holes on the 2400 cross section of the Lower Southwest orebody, representing four major ore types, were analyzed by electron microprobe (Denise Chirban, written commun., 1995; Denise Chirban and E.U. Petersen, written commun., 1996).

The concentration of silver in tetrahedrite was found to vary from 2.45 to 20.95 weight percent and was accompanied by large variations in all three solid solutions as expressed by

X_{Ag} (Ag atoms/[Ag+Cu]), X_{Sb} ($100 \times$ Sb atoms/[Sb+As+Bi]), and X_{Zn} ($100 \times$ Zn atoms/[Zn+Fe]). The silver index, X_{Ag} , ranged from 0 to 0.4, the antimony index, X_{Sb} , ranged from 0.1 to 1, and the zinc index, X_{Zn} , ranged from 0.1 to 1. They determined that the chemical variation within a sample was much less than the variation between samples, indicating that the average of several spot analyses of a sample is a good representation of the tetrahedrite composition for that location. This also implies that zoning patterns, if present, should be discernible between samples. They applied this to cross-stratigraphic variations in ore types on the 2400 cross section and concluded that each ore type has its own “mini-stratigraphy” with all of the above index ratios increasing stratigraphically upward. Each ore type was found to have characteristic tetrahedrite compositions, which define a trend. However, these trends were not sufficient to identify an ore type based on inspection of single spot analyses (Denise Chirban and E.U. Petersen, written commun., 1996). Their work on the high-silver sulfosalt minerals demonstrated that tetrahedrite could coexist with, or occur independently of, the covellite-acanthite solid solution, mckinstryite, or jalpaite. Data from one pulp sample also indicates that these silver-rich minerals may occur independently from tetrahedrite.

Finally, electron microprobe results were reported for a single sample of native-silver-bearing, high-grade white siliceous ore from the 764N1 stope of the Upper Southwest orebody (T.K. Bundtzen, written commun., 1996). The data indicate the presence of coarse grains of jalpaite occurring as bluish rims around native silver and that the silver contains less than 0.1 percent gold. The sample also contained euhedral crystals of gangue celsian or harmotome.

Ore Types

Ore lithologies at Greens Creek are broken into two main groups of massive sulfide ores and semimassive or disseminated sulfide gangue-rich “white” ores. The group of massive ores contain greater than 50 percent sulfides and consist of two types: (1) massive fine- to very fine grained ore in which base-metal sulfides are greater than pyrite (hereinafter referred to by the ore lithology code MFB, for Massive, Fine-grained, Base-metal-rich, and MVB, for Massive, Very fine grained, Base-metal-rich ores, respectively), and (2) massive medium- to very fine grained pyrite-rich ore in which pyrite predominates (hereinafter referred to as MFP and MVP, respectively). The distinction between the fine- and very fine grained ore types is subjective and based on the visual appearance of grain sizes in drill core. In general, the very fine grained ore types are so designated when individual sulfide grains cannot be seen with the naked eye. The MFBs are a medium to dark metallic gray to blue-gray (fig. 3A); the MFPs are bronze to metallic brown (fig. 3B). The MVBs and MVPs are similar in color to the coarser grained ore types with two notable variations. MVBs occasionally take on a distinct yellow-orange hue due to high concentrations of low-iron sphalerite (fig. 3C), and

MVPs take on a light creamy bronze color due to increased content of arsenian pyrite. All the massive ores have variable subordinate gangue of quartz, dolomite, sericite, barite, and fuchsite. Graphite is a less ubiquitous but locally abundant gangue mineral. The massive sulfide ores constitute the main stage of ore formation.

The white ores are a group of mineralized lithologies that contain less than 50 percent sulfides and are defined by their principal gangue mineral. They commonly contain base- and precious-metal enrichments and are usually, but for core logging purposes are not required to be, of ore grade. The three types are (1) white carbonate ore (WCA) and (2) white siliceous ore (WSI), which are most common, and (3) white baritic ore (WBA). The WCAs are characterized by granular textured, medium- to coarse-grained dolomite (fig. 3D). Accessory gangue minerals are present but less abundant than in WSIs. WSIs are dominated by massive cryptocrystalline aggregates of hydrothermal quartz or chert and regularly contain significant dolomite, sericite, fuchsite, and barite (fig. 3E). WBAs are characterized by coarse, sugary, massive barite and other gangue (as above) (fig. 3F). They commonly are not ore grade despite their inclusion as an ore lithology. The white ores constitute the early stage of ore formation and precede the main stage of massive sulfide ores.

All the ore types previously mentioned include subtypes that are modifications resulting from veins, breccias, and gouge or rubble zones produced during faulting or folding. Veining due to secondary metamorphic remobilization and accompanying recrystallization can result in spectacular enrichments of free gold and a variety of silver-sulfosalt minerals, which are described herein. Ore breccias appear to be both primary sedimentary breccias produced by slumping of the massive sulfides and inclusion of clasts of the underlying as well as overlying host rocks, and tectonic breccias produced during deformation. Solution brecciation may also be present, particularly in the WCAs.

Figure 3 (facing page). Photographs of hand samples illustrating the various massive sulfide and white ore types: (A) typical MFB with primary-textured pyrite (py) in a matrix of sphalerite (sph) and galena (gn) (drill-core sample GC127-18, 1007', ST-2 84 crosscut East orebody); (B) typical MFP (drill-core sample GC1136-05, 602', Lower Southwest orebody), note the breccia texture caused by the brittle failure of massive pyrite; (C) typical MVB (drill-core sample GC1643-10, 272', 200 South orebody), the orange color is due to the very high proportion of sphalerite in the sample and the low iron content of the sphalerite; (D) typical WCA (rib sample 164 crosscut, 82', Lower Southwest orebody); (E) typical WSI (rib sample from East orebody); (F) typical WBA (rib sample from the 164 crosscut, 164N1 stope, Lower Southwest orebody).



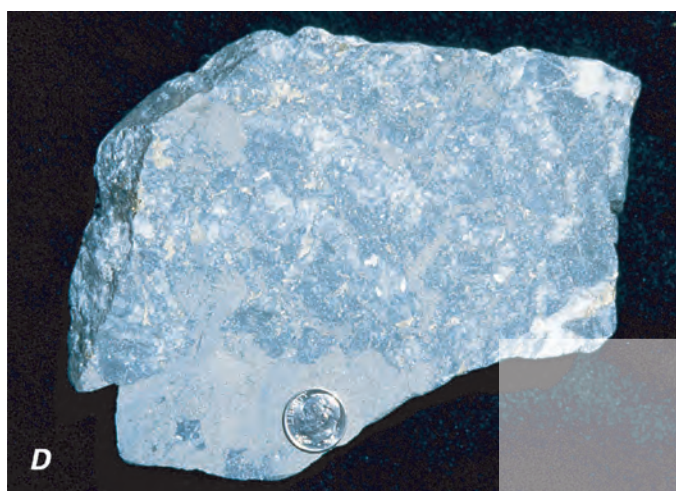
A



B



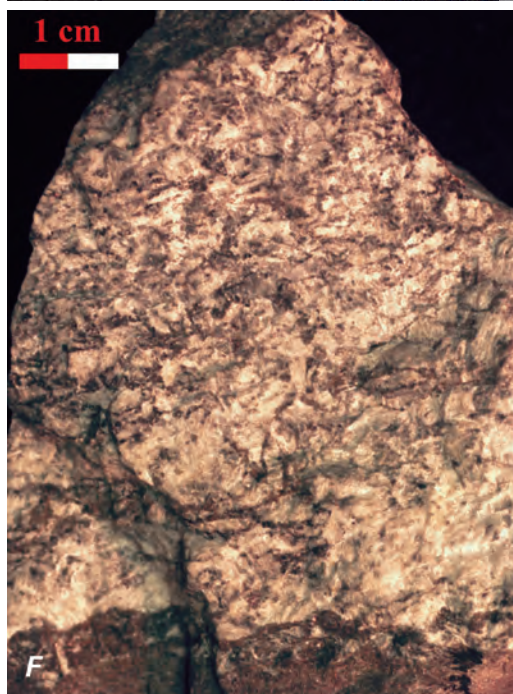
C



D



E



F

Primary Ore Mineralogy and Textures

Roughly 30 percent of the Greens Creek ores retain primary mineralogy and textures. With one notable exception, primary features are present in massive, homogeneous, fine-grained MFPs that usually contain a high percentage of silica gangue. Apparently, large, cohesive blocks of pyritic ore have acted as undeformed nuclei around which the more ductile MFBs have flowed during deformation. Brecciation of the MFPs is a common feature within these cohesive blocks, resulting in angular to subangular, tectonically milled clasts of primary-textured MFP in a sheared sulfide matrix consisting mostly of more ductile and recrystallized base-metal sulfides (fig. 4A). Clear evidence for primary depositional layering of sulfides is lacking. However, mineralogically banded massive ores are common and are composed of entirely recrystallized sulfides (fig. 4B).

Within primary-textured MFPs, framboidal, colloform, and dendritic-textured pyrite is common and is intimately intergrown with a variety of base-metal sulfides and sulfosalts. Framboids are commonly in the 1–5 micrometer (μm) size range and are as large as 30 μm (figs. 5A–C). Colloform-textured areas can be millimeters in size (fig. 5D), with individual mineral bands ranging from less than 1 to 10 μm in width (fig. 5E). Mineral bands are most commonly composed of pyrite interbanded with sphalerite, galena, tetrahedrite, and a lead-antimony sulfosalt mineral (fig. 5F). Rarely, chalcopyrite replaces pyrite or infills bands between pyrite layers in the more copper-rich orebodies (fig. 5G). Dendritic-textured areas of pyrite are less common, only occur in MFP, and can have individual dendrites in the 100–200 μm size range (fig. 5H). Common accessory mineralogy in the primary textured ores includes sphalerite, galena, tetrahedrite, chalcopyrite, free gold, and a variety of Pb-Sb-As (-Hg-Tl) sulfosalts.

Primary-textured sulfides are also present in WCAs. Rounded grains of pyrite up to a centimeter in diameter with radial growth textures occur in a matrix of massive, coarse crystalline dolostone. These features produce a “pudding stone” texture and are reminiscent of diagenetic pyrite nodules (fig. 4C). Similar nodular pyrite textures, fragments of nodules, pyrite rinds, and concentrations of framboidal and colloform pyrite intergrown with base-metal sulfides also occur in association with concentrations of white, hydrothermal dolomite that typically cuts more massive, coarse crystalline dolostone. These textures are clearly linked to hydrothermal veining and in some cases may be produced by solution brecciation of footwall dolostones and WCAs followed by precipitation of dolomite and quartz cements in the resulting cavities (fig. 4D).

Recrystallized and Remobilized Ore Mineralogy and Textures

Recrystallization of the primary textures in individual hand samples ranges from 20 percent to 100 percent and results in a range of textures. Incipient recrystallization results in the

formation of polyframboidal aggregates (rogenpyrite; fig. 6A), “spongy” textured pyrite, and atoll-shaped pyrite. Spongy texture is most common in the massive ores in millimeter- to centimeter-scale areas of massive and aggregated pyrite. These areas often show relict framboidal and colloform textures. The pyrite itself commonly appears quite “clean” or monomineralic. However, the spongy areas are full of micrometer-scale inclusions of other sulfides, sulfosalts, and gangue minerals (fig. 6B). The centers of euhedral pyrite crystals larger than about 100 μm also tend to have spongy texture. As recrystallization progresses, atoll-shaped pyrite forms at the expense of framboids and colloform pyrite (fig. 6C). The larger aggregates of polyframboids and spongy textures coalesce further into large areas of inclusion-rich anhedral to subhedral pyrite (fig. 6D).

The major effects of more advanced recrystallization is much coarser grain sizes and the formation and(or) remobilization of secondary, precious-metal-enriched minerals (fig. 6E). Pyrite recrystallization is characterized by development of euhedral crystals and polygonal textured masses that appear to be unzoned and free of mineral inclusions (fig. 6F). Recrystallization of pyrite tends to roughly double the grain size; for example, pyrite euhedra in areas of 1–5- μm framboids are 5–10 μm in size. In recrystallized aggregates or massive areas of pyrite with development of polygonal texture, individual grains are commonly in the 50–100- μm range. In MFPs that have been entirely recrystallized, pyrite euhedra are commonly in the 0.1- to 1-mm size range or larger (fig. 6G). Secondary minerals occur as discrete rounded inclusions within pyrite grains (figs. 6H and I), as growth zones within, and as margins to, pyrite (figs. 6J and K), and as matrix to pyrite euhedra. Subhedral to euhedral sphalerite occurs in recrystallized MFB, usually in a matrix of anhedral galena (figs. 6L and M). Secondary mineralogy includes chalcopyrite, sphalerite (low iron), galena, free gold, electrum, tetrahedrite (antimony-rich), bornite, covellite, pyrargyrite, and a host of other sulfosalt minerals. Rare realgar has been identified (by X-ray diffraction) in the WBAs of the 200 South orebody. Base-metal sulfides in recrystallized ores most commonly occur as anhedral intercrystalline masses of secondary sphalerite, galena, chalcopyrite, tetrahedrite, and pyrargyrite. Individual anhedral crystals are commonly 50–200 μm in size (fig. 6N). Secondary sulfides also commonly occur in late fractures and veinlets millimeters wide and centimeters long (figs. 6O and P).

An interesting and potentially genetically important modification that affects MFPs in proximal, copper-arsenic-gold-rich areas of the deposit is the occurrence of subhedral to euhedral, light creamy yellow to white, arsenian pyrite (FeS_2 with variable substitution of arsenic for iron) and arsenopyrite (FeAsS , 46 percent arsenic). These phases appear to replace primary pyrite (figs. 7A–C) or form as overgrowths on primary-textured pyrite masses (figs. 7D and E). They are present in trace amounts to as much as 50 percent of a sample. Powder X-ray diffraction analyses of two MFP ores, each with approximately 50 percent of this sulfide visible in polished thin section, confirmed the presence of arsenopyrite, but only in trace to minor amounts. In both cases the major

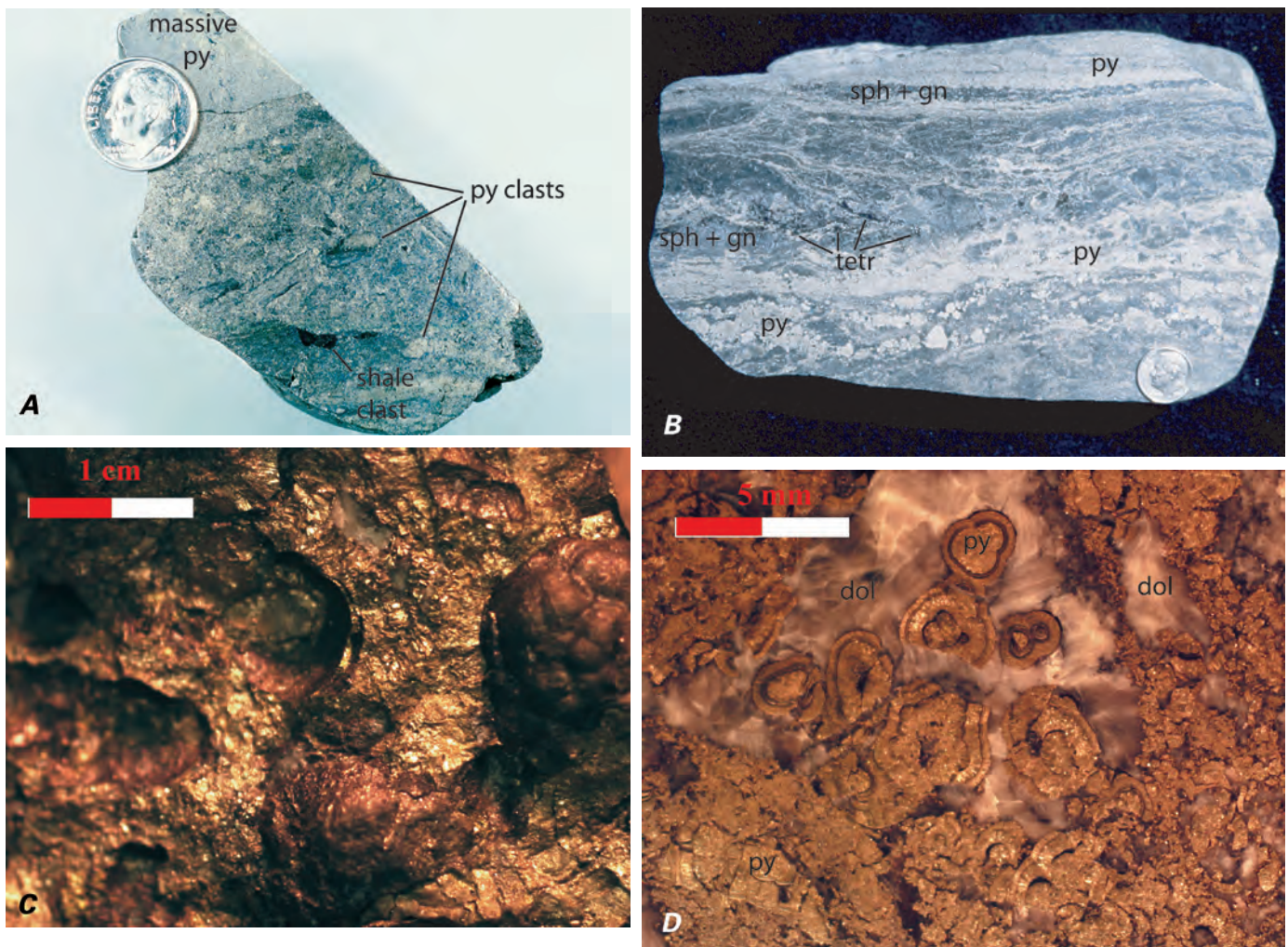


Figure 4. Photographs of hand samples illustrating textures present in various ore types: (A) brecciated MFP consisting of angular to subangular, tectonically milled clasts of siliceous, primary-textured, fine-grained, pyritic massive ore in a sheared sulfide matrix consisting mostly of more ductile and recrystallized base-metal sulfides (drill-core sample GC1136-04, 594.5', Lower Southwest orebody); (B) tectonically banded MFB (rib sample from the 764 crosscut, 764N1 stope, Upper Southwest orebody); (C) nodular diagenetic pyrite texture in MFP (rib sample from the 2250 crosscut, 215 stope, Lower Southwest orebody); and (D) closeup photograph of WCA showing nodular pyrite textures, fragments of nodules, pyrite rinds, and concentrations of framboidal and colloform pyrite intergrown with base-metal sulfides in association with concentrations of white, hydrothermal dolomite usually cutting more massive, coarse crystalline dolostone (drill-core sample GC1092-02, 711', Lower Southwest orebody). py, pyrite; sph, sphalerite; gn, galena; dol, dolomite; tetr, tetrahedrite.

phase identified was pyrite, indicating that the majority of the creamy white mineral observed must be arsenian pyrite. Rarely, euhedral arsenopyrite has been observed in a silica-dolomite matrix (fig. 7F).

Physical remobilization of the more ductile base-metal sulfides is indicated by fractured masses of pyrite filled with flow-textured anhedral chalcopyrite, galena, and tetrahedrite (fig. 6E). Flow-textured galena is characterized by the near total absence of the triangular pits usually observed in unstrained galena (fig. 6L). Physical remobilization and recrystallization in tectonized ores is probably responsible for creating the mineralogically segregated layers in banded ores. Creation of base-metal-rich veinlets and infilling of fractures

by physical remobilization is an important process of metals redistribution in ores on a hand-sample scale and is ubiquitous in the more thoroughly recrystallized and tectonized ores. It is distinguished from the process of chemical remobilization by the lack of associated gangue minerals in the base-metal-rich fractures, veinlets, and piercement structures.

Chemical remobilization and reprecipitation of base-metal sulfides is also a locally important process and is characterized by the formation of paragenetically late veinlets and veins of chalcopyrite, sphalerite, galena, tetrahedrite, and pyrrargyrite usually in association with quartz and dolomite (figs. 6Q and R). Occasionally, sericite and fuchsite gangue are present as well. Yellow and silvery-white gold is present

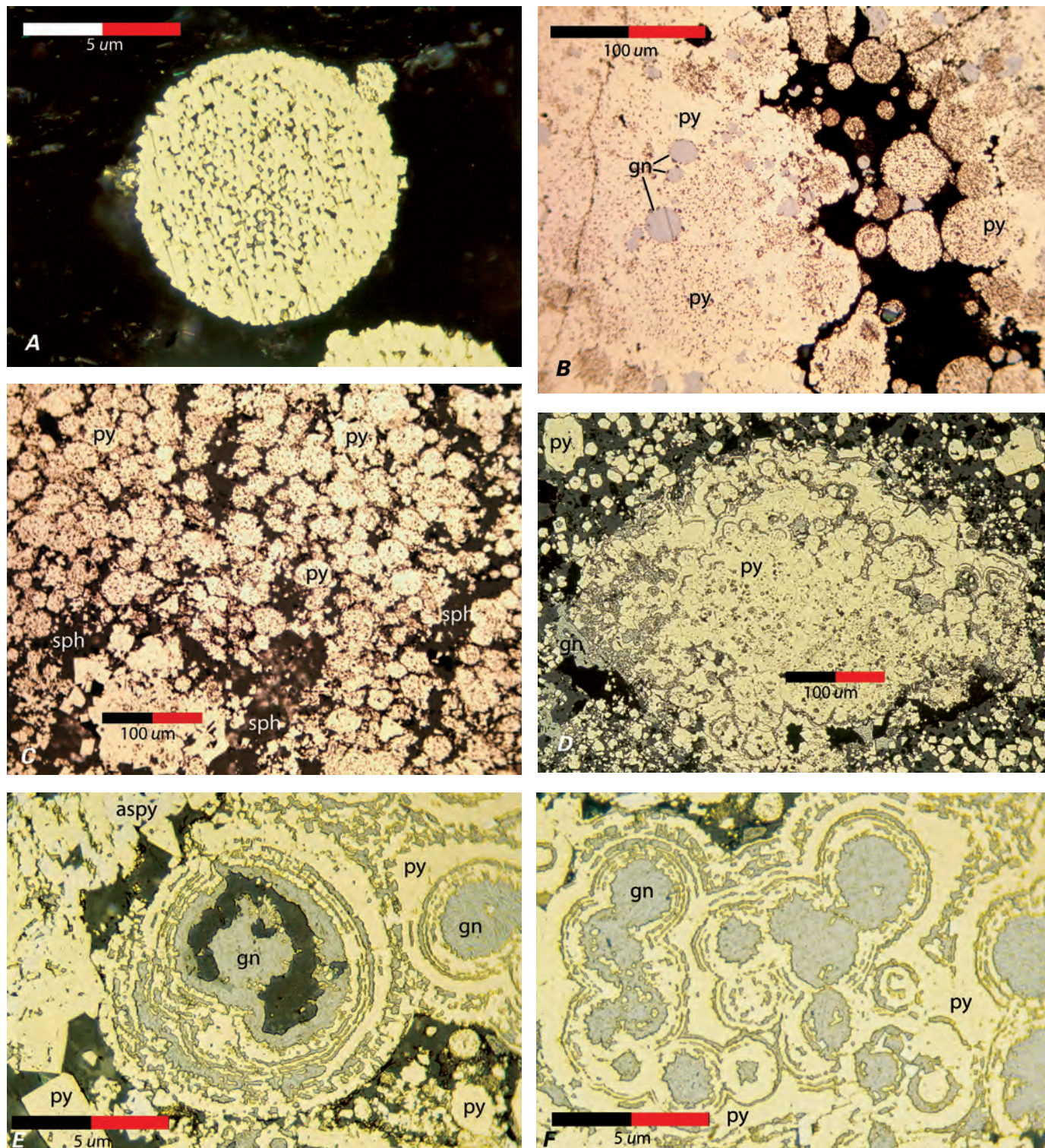


Figure 5 (above and facing page). Photomicrographs of polished thin sections showing primary mineral textures: (A) framboidal pyrite (rib sample 96GC-14, 31', 344 crosscut, Lower Southwest orebody); (B) pyrite (py) framboids and galena (gn) spheres in spongy-textured to massive pyrite (drill-core sample GC1643-04, 75' 200 South orebody); (C) aggregated pyrite framboids in a matrix of sphalerite (sph) (drill-core sample GC1643-03, 54', 200 South orebody); (D) colloform-textured aggregate of pyrite with a spongy-textured interior and growth zones composed of sphalerite, galena, and tetrahedrite (rib sample 96GC-12, 21.5', 344 crosscut, Lower Southwest orebody);

in chemically remobilized veins and is particularly abundant in association with late quartz-carbonate-pyrargyrite veins. Concentrations of these precious metal enriched veins usually occur in or within close proximity to areas of primary-textured ore and account for the highest grade ores in the mine, with total metal values reaching \$10,000/ton.

Free Gold—Mineralogy and Textures

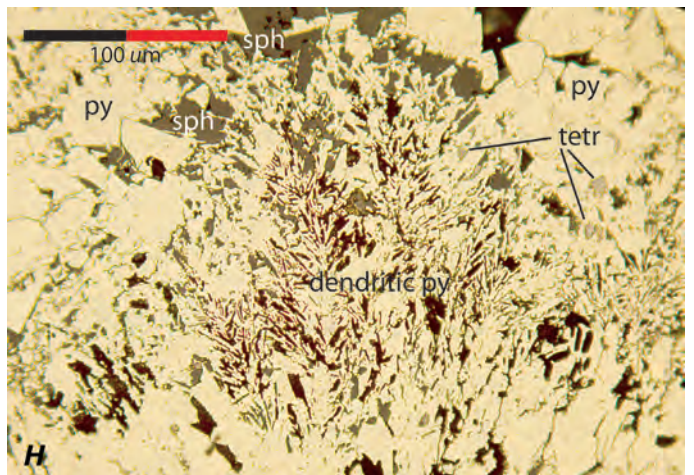
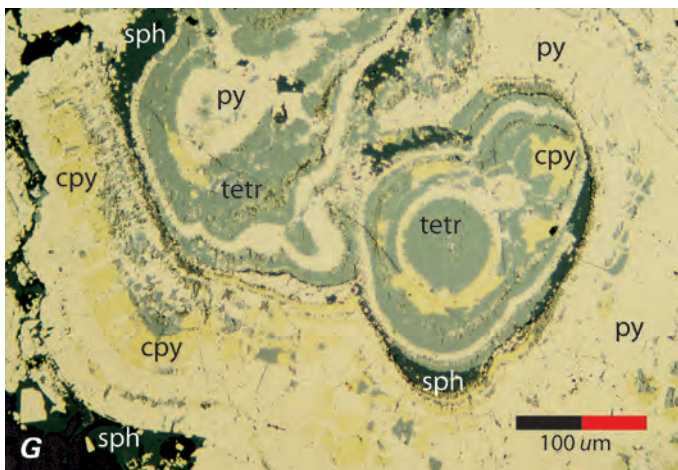
Free gold is a relatively common feature at Greens Creek and has been found in a wide variety of both ore and host-rock lithologies. Two types are visually distinguishable, and a third was identified during LA-ICP-MS analysis. Bright yellow gold of high fineness occurs in thin section as rounded blebs and inclusions from 5 to 100 μm in size, although the most common size is about 5 to 20 μm (fig. 8A). Most of the grains are in cracks in pyrite and in the matrix to pyrite grains in association with secondary chalcopyrite, sphalerite, galena, tetrahedrite, and pyrargyrite (figs. 8B and C). Most gold grains are in contact with either pyrite or arsenian pyrite (fig. 8D); however, a few grains were observed included within coarse-grained subhedral to euhedral pyrite (fig. 8E). Yellow gold is most commonly seen in the large blocks of MFP ore but also has been observed in all of the ore types at the mine and in both hanging-wall and footwall rocks, usually in association with quartz-carbonate veins.

The second type of free gold is silvery white and occurs predominantly as a thin foil coating late fractures and shear

planes in underground exposures and hand samples (figs. 8F and G). In thin section, white gold appears as thin veinlets and spaced sheets that occupy fractures up to 0.5 millimeter wide. These fractures are paragenetically late and appear to be tension gashes and piercement structures that occur at high angles to S_2 foliation (fig. 8H). Geochemical data suggest this is a gold-silver electrum.

Free gold occurs in ores that exhibit a high degree of recrystallization and remobilization of the more ductile sulfides and are usually in close proximity to areas of primary-textured ores. Exceptions include yellow gold that occurs in quartz-carbonate veins in the host rock and rare instances of white gold foil in highly sheared and fractured argillites in the immediate hanging wall. These electrum-bearing quartz-carbonate veins typically are within 1–2 m of high-grade primary ores. Yellow gold has also been observed in association with chalcopyrite and tetrahedrite in hairline fractures cutting late diabase dikes in the 200 South portion of the Lower Southwest orebody. This relationship thus requires remobilization of gold at some time after emplacement of the dikes.

The two types of gold, as well as native silver, are easily distinguished based upon LA-ICP-MS geochemical studies of free gold separates recovered from the mill (figs. 9A–D). Laser traverses across 0.5- to 1.0-mm-sized grains recovered from heavy concentrates, represented as time versus elemental intensity plots, clearly indicate the presence of nearly pure gold grains with a high ratio of gold to silver (figs. 9A, D–F). Other grains that appear silvery-white on polished surfaces show lower gold-to-silver ratios and consistently elevated mercury, demonstrating that the silvery white gold is actually a



(E) colloform banded spheres in pyrite with growth bands filled with galena or perhaps lead-antimony sulfosalts minerals (rib sample 96GC-13, 25.5', 344 crosscut, Lower Southwest orebody); (F) aggregate of colloform shapes in pyrite (rib sample 96GC-13, 25.5', 344 crosscut, Lower Southwest orebody); (G) chalcopyrite (cpy) infilling or replacing bands between pyrite layers in colloform-textured MFP (drill-core sample GC1527-09, 402.5', Northwest orebody); and (H) dendritic-textured pyrite fronds in massive pyrite (rib sample 96GC-16, 43.5', 344 crosscut, Lower Southwest orebody).

gold-silver-mercury amalgam (figs. 9B and C). A few traverses suggest that some of the gold grains may also incorporate significant copper (fig. 9G). Silver grains either contain irregular inclusions of gold or are relatively pure (figs. 9H and I). The silver quickly tarnishes to a dirty, bluish-gray color, enabling visual identification in slides of the mill separates.

Paragenetic Relationships—Physical and Chemical Modification of Ores

Two major processes govern paragenetic relationships in Greens Creek ores. Primary ores are dominated by textures indicative of rapid crystallization, very early infilling of void spaces, and replacement of one sulfide by another during growth of the massive sulfide body, whereas the secondary ores are the product of recrystallization and remobilization of primary ores during zone refinement and metamorphism. In primary ores, framboidal and colloform pyrite are the earliest formed sulfides. Sphalerite, galena, tetrahedrite, and lead-antimony sulfosalts appear to be coeval and form the matrix of framboidal aggregates (figs. 10A; 3A; 5C; 6A) as well as the intervening bands in colloform-textured pyrite (figs. 5D–F). Bands of pyrite are nearly always present in colloform-textured ores; in the few cases where successive bands of base-metal sulfides without intervening pyrite bands occur, they are present as colloform growths within predominantly pyritic primary-textured masses (figs. 10B; 5G). These primary-textured, pyrite- and base-metal-sulfide-rich masses appear to undergo modification early in the growth of the massive sulfide bodies by a process of zone refinement. Early, porous masses, composed of framboidal and colloform pyrite with a high percentage of sphalerite, galena, and lead-antimony sulfides (figs. 5A, D–F; 6A), progress into more densely packed pyrite-chalcopyrite-arsenopyrite-rich masses through a combined process of pyrite coalescence and replacement of the base-metal sulfides. The resulting ores exhibit a progression of textures characterized by the destruction of discrete frambooids (figs. 5B; 6B) and the formation of polyframboidal (figs. 6A; 10A) and spongy-textured (figs. 5D; 6C, I) pyrite aggregates, atoll-shaped and subhedral pyrite grains (figs. 6J, K), and subhedral to euhedral arsenian pyrite and arsenopyrite (figs. 7A–F). Chalcopyrite generally occurs as matrix in the resulting pyritic masses along with a much lower percentage of sphalerite, galena, and tetrahedrite (figs. 6E, G). Replacement of the base-metal sulfides presumably results in expulsion of lead, zinc, and other trace elements upward and outward to form the MFBs. Rarely, in copper-rich primary-textured MFPs, chalcopyrite has been observed, partially replacing bands of other base-metal sulfides in colloform ores (fig. 5G). Several examples of frambooids composed of chalcopyrite crystallites in a matrix of pyrite have been observed; however, it is questionable whether such examples indicate a paragenetically early position of chalcopyrite relative to pyrite (fig. 10C). Frambooids composed of sphalerite or other base-metal sulfides have not been observed in this study.

Graphite is a ubiquitous feature of primary ores and occurs as fine disseminations in the matrix between frambooids and colloform-textured masses (fig. 5C) and in association with dendritic and spongy-textured pyrite (fig. 5H).

The formation of light creamy yellow to white, arsenian pyrite and arsenopyrite (figs. 7A–F) is a paragenetically important feature of the primary-textured ores and is of uncertain origin. It is most commonly observed in association with primary ores that have undergone incipient to moderate recrystallization. As the “dirty” trace-element-rich primary-textured pyrites undergo recrystallization, the stoichiometric reorganization of the pyrite mineral structure expels excess trace elements from its structure, including arsenic. Liberated arsenic is then available to form new arsenian pyrite or arsenopyrite. However, both arsenian pyrite and arsenopyrite are concentrated in areas of primary-textured ores where permeability is greater, either due to presence of abundant spongy-textured pyrite, loose packing of framboidal aggregates, or the presence of veining. This relationship suggests that arsenian pyrite and arsenopyrite may have formed early in the paragenesis, after the formation of primary-textured sulfides but prior to advanced recrystallization of the ores. A possible explanation is that these minerals represent a hotter, more reducing period of fluid circulation and mineral formation by replacement of earlier formed minerals during a zone-refining stage of sulfide mound growth.

Nonprimary-textured ores exhibit a range of features that suggest a progression from incipient through complete recrystallization and physical as well as chemical remobilization as a result of metamorphism. Incipient recrystallization causes individual frambooids to coalesce into atoll-shaped grains, with centers filled with base-metal sulfides and rims of clean, bright pyrite (figs. 10D; 5E–G; 6C, J). Aggregates of frambooids develop into large spongy-textured masses with numerous discrete inclusions of base-metal sulfides and graphite (figs. 10E; 6D, H, I). Graphite tends to recrystallize into felty concentrations of needle- or lath-shaped crystals that are aligned subparallel to S2 foliation (fig. 10F). As recrystallization progresses, large areas of inclusion-free pyrite form with relict framboidal shapes preserved in the interiors of the masses. Euhedral-shaped growth zones are defined by thin bands of sphalerite or galena (figs. 10G; 6J). Fully recrystallized pyritic ores are characterized by very large areas of inclusion-free, monomineralic pyrite with polygonal grain boundaries (figs. 10H; 6F). Matrix between the large areas of pyrite is filled with anhedral masses of sphalerite, galena, and tetrahedrite, which are generally also inclusion free (fig. 6G). Bright yellow free gold is most commonly seen in partially to fully recrystallized MFPs as inclusions within recrystallized pyrite grains (fig. 8E) and in matrix with base-metal sulfides (figs. 8A–D). In recrystallized MFBs, clean, euhedral pyrite and euhedral to subhedral sphalerite are contained in a matrix of anhedral galena and tetrahedrite (figs. 6L–N). Areas of macroscopically banded ore in thin section alternate between pyrite-rich and base-metal-sulfide-rich layers that are texturally as previously described (fig. 4B). Recrystallization of chalcopyrite-rich MFPs generally

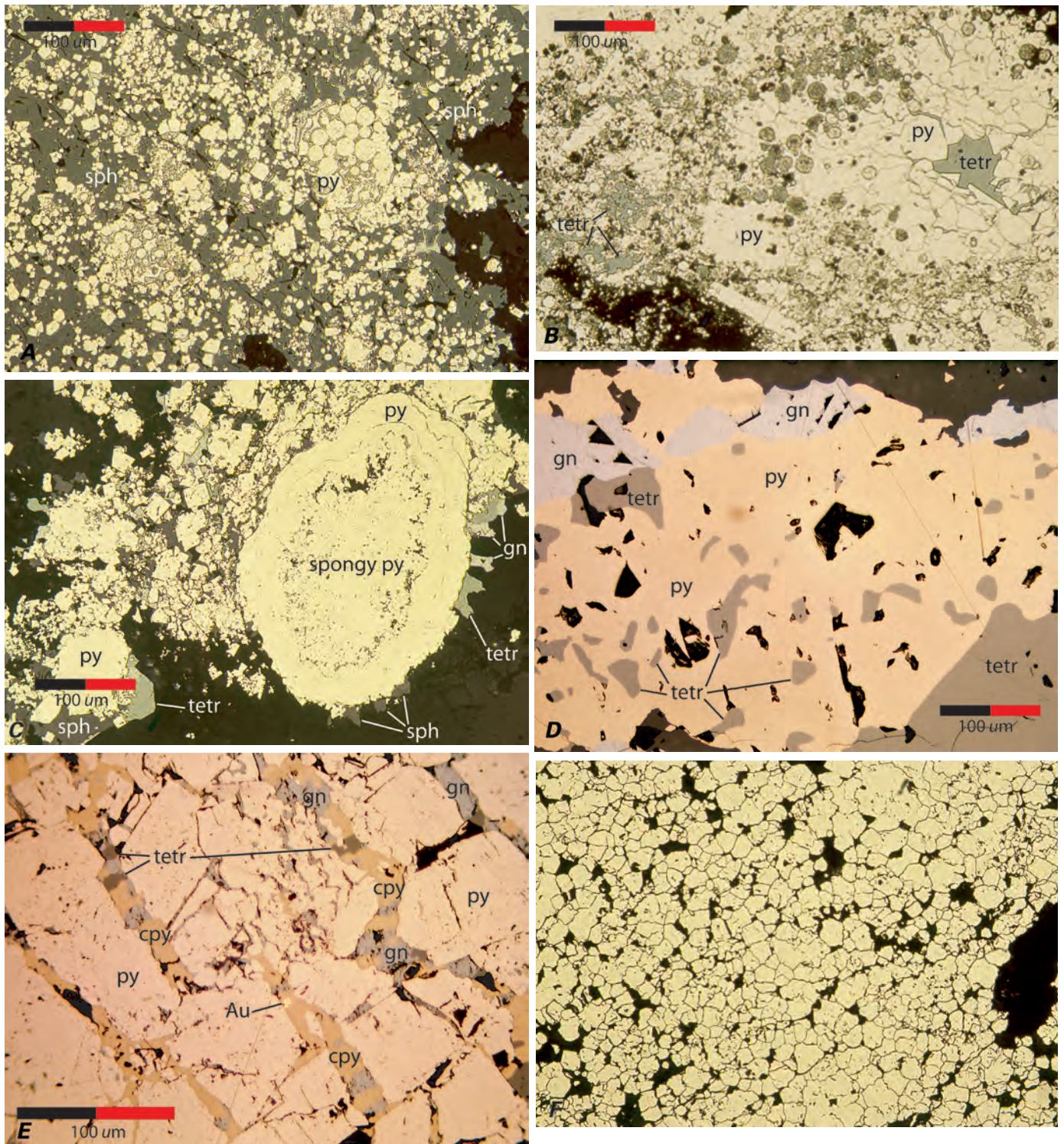
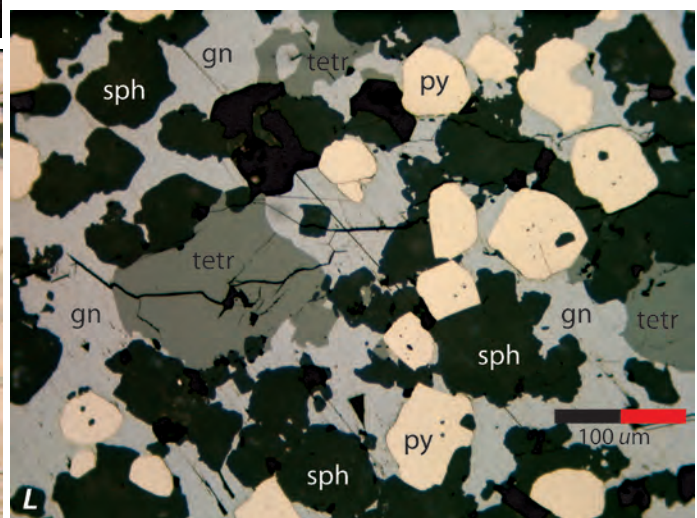
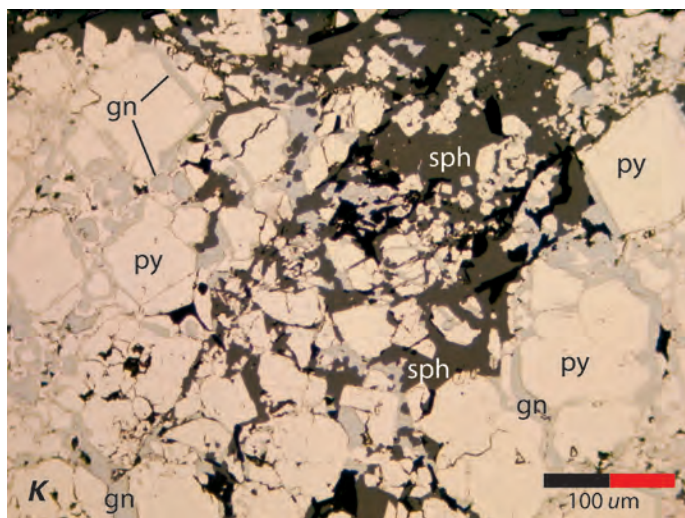
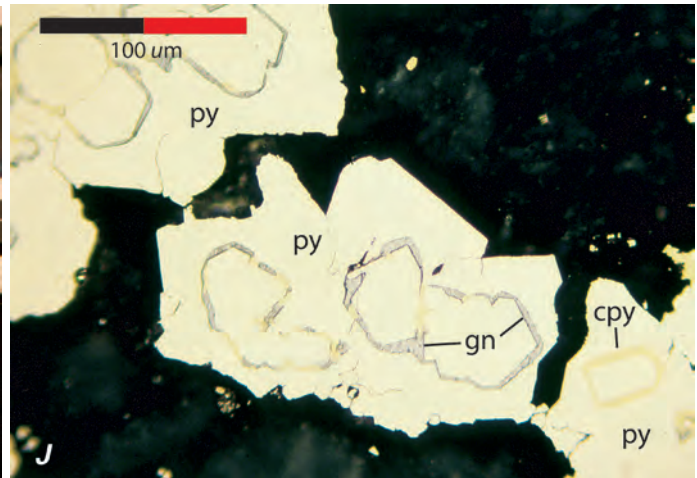
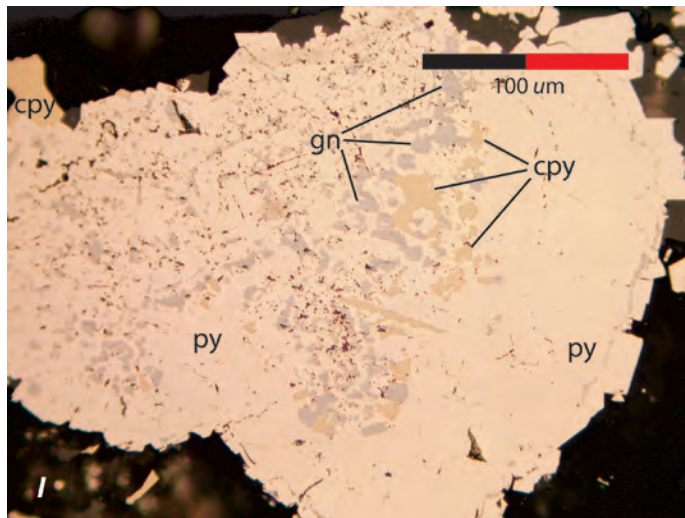
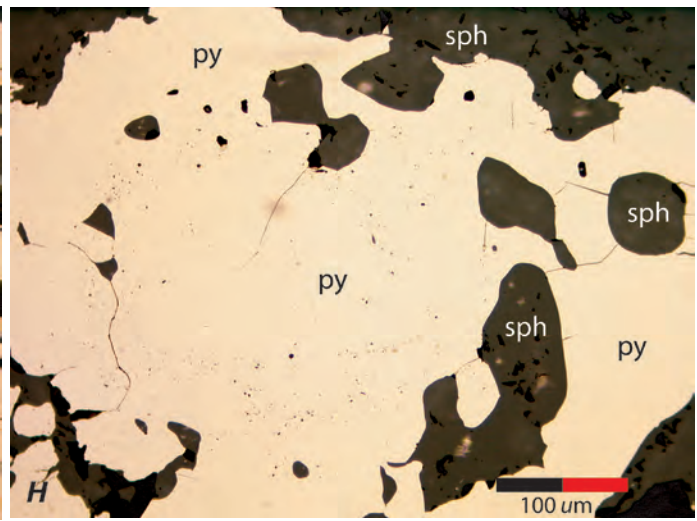
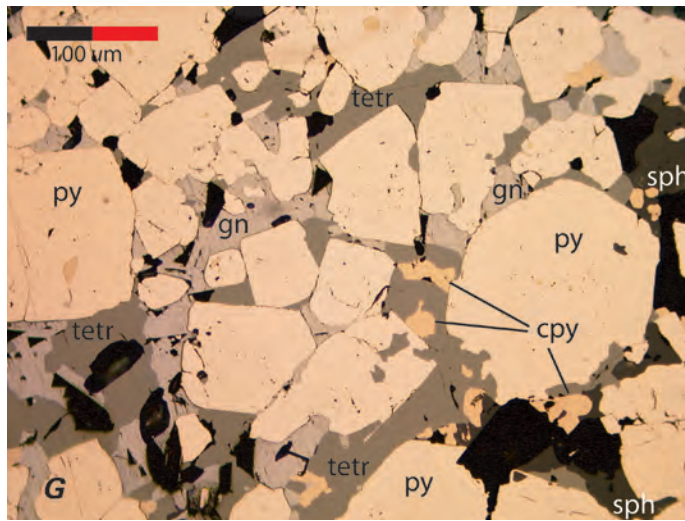
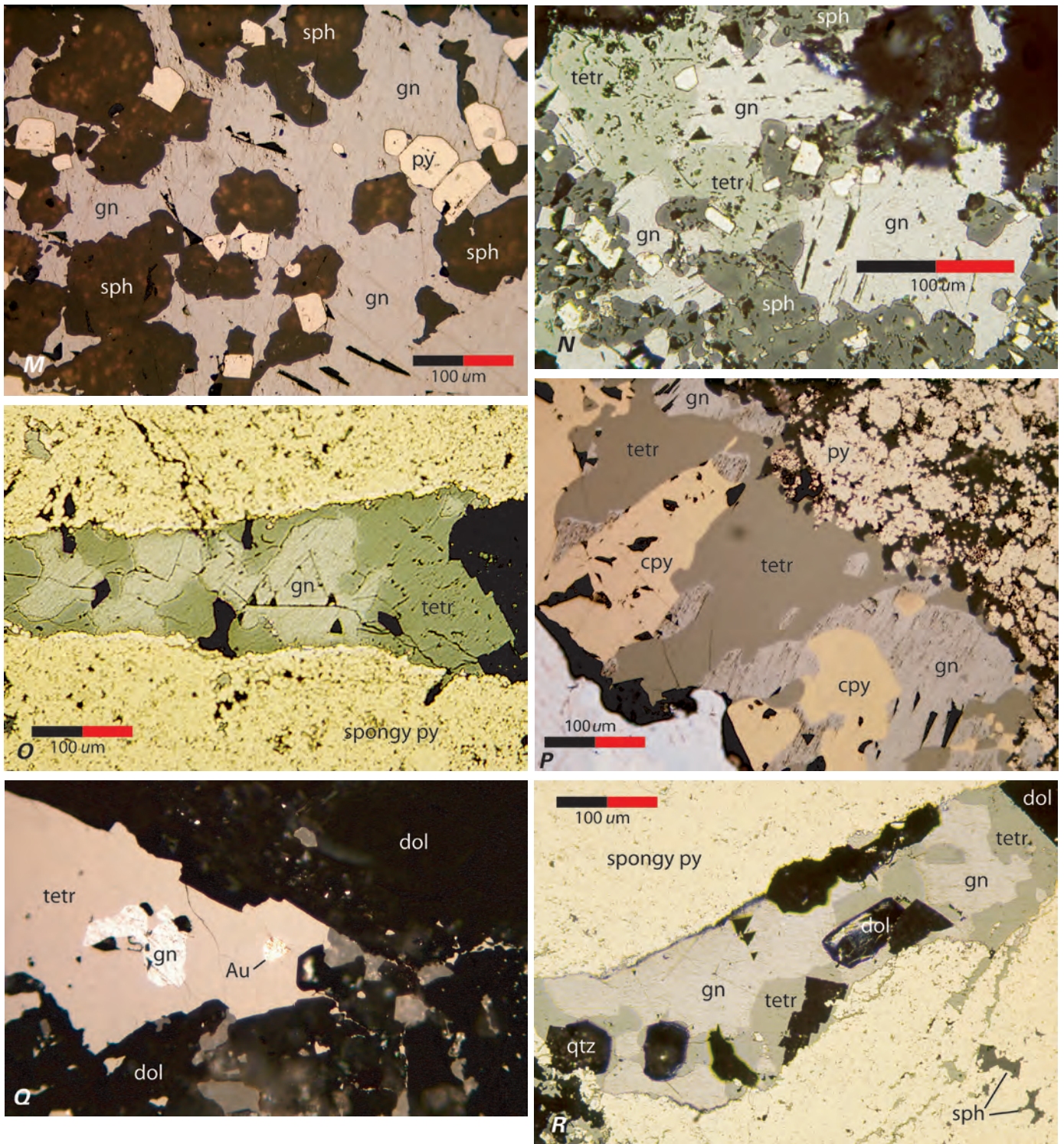


Figure 6 (pages 15–17). Photomicrographs of polished thin sections showing recrystallized ore textures: (A) growth of polyframboidal clusters in a matrix of sphalerite (sph) (rib sample 96GC-12, 21.5', 344 crosscut, Lower Southwest orebody); (B) spongy-textured pyrite (py) with relict framboidal and colloform shapes, and numerous inclusions of sulfides, sulfosalts, and gangue (rib sample 96GC-18, 51', 344 crosscut, Lower Southwest orebody); (C) atoll structure of clean recrystallized pyrite forming around a grain of spongy-textured pyrite (rib sample 96GC-13, 25.5', 344 crosscut, Lower Southwest orebody); (D) clean anhedral pyrite with numerous rounded inclusions of tetrahedrite (tetr) and galena (gn) (drill-core sample GC1643-06, 119.5', 200 South orebody); (E) veinlets of chalcocyanite (cpy), tetrahedrite (tetr), galena (gn), and yellow gold (Au) cutting recrystallized pyrite (drill-core sample GC1643-05, 100.5', 200 South orebody); (F) clean, completely recrystallized, polygonal-textured pyrite (rib sample 96GC-14, 31', 344 crosscut, Lower Southwest



orebody); (G) recrystallized pyrite euhedra in a matrix of chalcopyrite, galena, tetrahedrite, and sphalerite (drill-core sample GC1643-08, 147.5', 200 South orebody); (H) clean, recrystallized anhedral pyrite with rounded inclusions of sphalerite (drill-core sample GC1643-08, 147.5', 200 South orebody); (I) partially recrystallized spongy pyrite with rounded inclusions of chalcopyrite and galena (drill-core sample GC1643-07, 143.5', 200 South orebody); (J) clean, recrystallized pyrite with discrete, atoll-shaped growth zones of chalcopyrite and galena GC1527-08, 397.5', Northwest orebody); (K) recrystallized pyrite with rims of galena (drill-core sample GC1643-11, 438', 200 South orebody); (L) recrystallized euhedral pyrite and sphalerite in a matrix of anhedral tetrahedrite and galena (drill-core sample



GC1643-01, 11.7', 200 South orebody); (*M*) recrystallized euhedral sphalerite in galena matrix (drill-core sample GC1643-10, 272', 200 South orebody); (*N*) inclusion-free, euhedral pyrite with anhedral sphalerite, galena, and tetrahedrite as matrix (rib sample 96GC-10, 18.5', 344 crosscut, Lower Southwest orebody); (*O*) late galena and tetrahedrite veinlet cutting spongy-textured pyrite (rib sample 96GC-15, 39', 344 crosscut, Lower Southwest orebody); (*P*) late chalcopyrite, galena, and tetrahedrite veinlet cutting framboidal pyrite (drill-core sample GC1643-03, 54', 200 South orebody); (*Q*) remobilized veinlet of tetrahedrite, galena, and yellow gold in dolomite (drill-core sample GC1643-06, 119.5', 200 South orebody); and (*R*) veinlet of anhedral sphalerite, galena, chalcopyrite, and tetrahedrite, and pyrrargyrite cutting recrystallized pyrite (rib sample 96GC-17, 49', 344 crosscut, Lower Southwest orebody).

progresses from spongy-textured masses of pyrite with chalcopyrite in the matrix and numerous small chalcopyrite inclusions to clean, monomineralic, polygonal-textured masses of pyrite with grain boundaries and intercrystal spaces filled with anhedral, monomineralic chalcopyrite (fig. 10I).

Physical remobilization of the ductile sulfides and electrum is a feature of the ores that is clearly related to Cretaceous deformation (figs. 6E, O, P; 8B, C). Evidence for flow-textured sulfides is most pronounced in areas of well-developed fabric where F2 and F3 folding can be discerned, as described by Proffett (chap. 7). Chemical remobilization and reprecipitation of sulfides is also a paragenetically late feature as indicated by the formation of veinlets and veins that cross-cut the metamorphic fabric (figs. 6Q, R).

LA-ICP-MS Mineral Chemistry Studies

Methods

The LA-ICP-MS analytical technique is a relatively new and rapidly evolving method of solid sample microanalysis that holds great promise for the study of ore mineral chemistry. A focused laser beam directed onto the surface of a mineral grain is used to excavate, or "ablate," a small volume of sample. The ablated material, in the form of micrometer-size fragments and condensed droplets, is transported by a carrier gas into the induction port of an ICP where the solids are melted, dissociated, and ionized. The ions are then focused into a quadrupole mass spectrometer where detection of a broad range of elemental masses occurs. The technique offers a wide dynamic range with trace and ultratrace detection limits coupled with simultaneous major-element determinations. However, the introduction of solid sample material to the instrument as opposed to the usual solution creates a new set of complexities. The mechanical, chemical, and physical factors involved in laser ablation and transport of the sample to the instrument result in a variety of fractionation effects (Ludden and others, 1995). Elemental fractionation occurs primarily because of secondary heating of the sample crater following the laser shot and thus, consequently, is of particular concern in infrared laser determinations. Elements more volatile than the host material can be volatilized from the area surrounding the crater and carried to the plasma, resulting in erroneously high element concentrations. For an element such as mercury this can be as much as 30-percent error in a poorly designed experiment. For this study, we used the Q-switched mode of an Nd/YAG laser with a shot duration of approximately 4 nanoseconds. Most sulfide minerals measured for this study have similar melting and boiling points, which should also minimize the fractionation effects reported in the literature. A second constraint on the accuracy of LA-ICP-MS analyses is the paucity of well-characterized reference materials for use in calibration and as secondary standards (Ridley, 2000). To date, only a handful of studies

report quantitative analyses of solid mineral species (Norman and others, 1996). The only previous study of trace-element content in sulfides, using the LA-ICP-MS system in the Denver laboratory under operating conditions using a free-running laser with a 100-msec pulse duration, reported semiquantitative elemental concentrations (Viets and others, 1996). For the purposes of this study, a brief description of the Denver LA-ICP-MS system is given below and followed by a rough estimation of the accuracy and precision of the resulting analyses. For an in-depth review of the method, the instrumentation involved, and a detailed evaluation of the various fractionation factors, development of solid standards, and sources of analytical error, see Ridley and Lichte (1998), Ridley (2000), and references therein.

At the time the analyses of the Greens Creek ores were made, instrumentation in the Denver laboratory consisted of a CETAC laser, controlled by CETAC computer software, coupled to an ELAN 5000 ICP-MS. The Nd/YAG laser was operated in the Q-switched mode at a quadrupled frequency resulting in an ultraviolet wavelength of 266 nanometers, with a maximum energy output of about 3 millijoules. Analyses were performed on minerals previously identified by optical methods in standard (30 mm) polished thin sections. Thin sections were placed in a cylindrical Plexiglas sample cell driven by computer-controlled x-y-z stepper motors capable of movement in 0.05-mm steps. Laser spot selection was provided by a zoomable color video camera with 15–1500X magnification. After some experimentation to optimize the instrument response to the amount of sample ablated and the delivery to the ICP-MS, a beam diameter of 50 μ m was selected. Individual mineral grains were sampled with two laser pulses per spot spaced by one second to allow the crater to cool and to offer a wider window for the analysis of the vapor cloud by the ICP-MS.

Calibration was performed using a combination of external standards. The ICP-MS was initially calibrated using in-house solution standards that use lutetium as an internal standard. The LA-ICP-MS system was then calibrated against an external glass standard (either NIST612 or GSE, an in-house standard) and checked against an experimental natural sulfide before, during, and after sample analyses. The natural sulfide standard used was a centimeter-sized crystal of pyrite from the Groundhog mine in southwest New Mexico (Hawksworth and Meinert, 1990). This pyrite was selected due to its large range of measurable trace elements and its relative homogeneity based on rastered laser analysis as compared to the solution ICP-MS method. By conducting routine analysis of the Groundhog pyrite during a session, instrument performance and major variations in transport efficiency were monitored.

All reduction of raw ICP-MS data was performed in a spreadsheet using linear relationships. The instrument mass counts for a given element were converted to an absolute concentration by normalization to an "ablation efficiency factor." The ablation efficiency factor was calculated for each analysis by ratio of the measured sum of all concentrations to 100 percent or in some cases by ratio of the measured concentration of a single major element (such as iron) based on the assumption

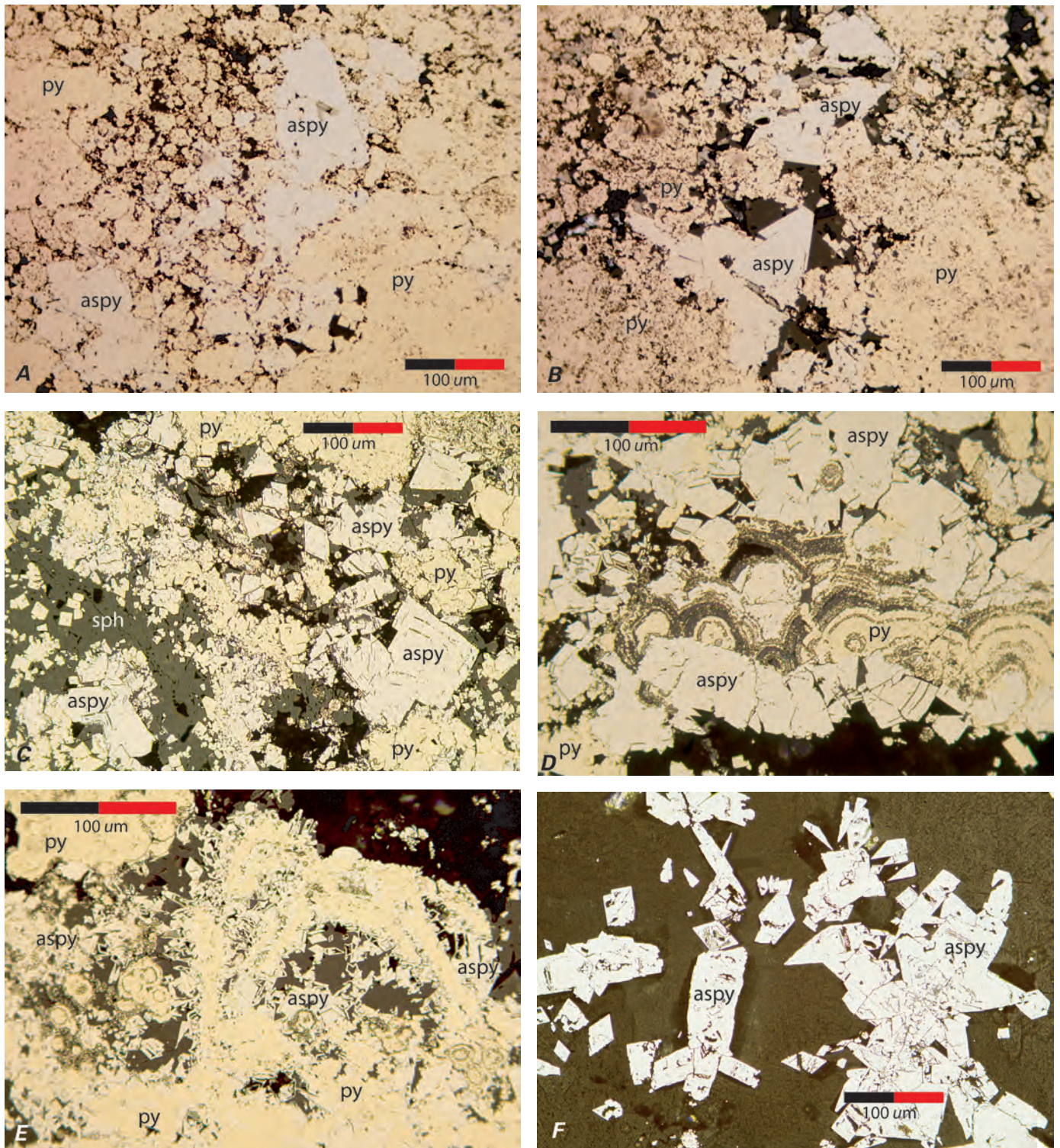
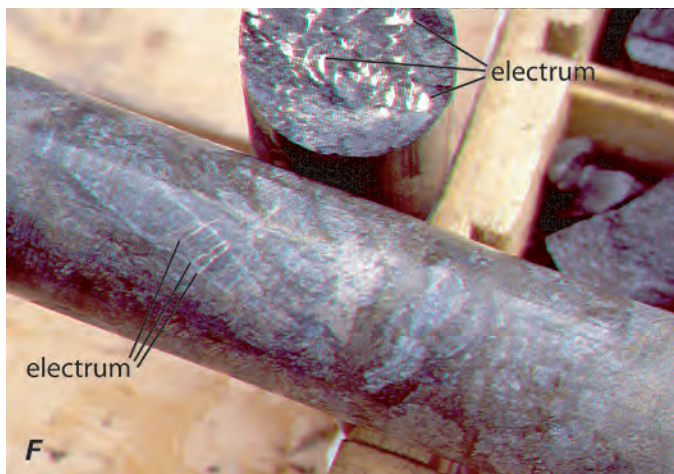
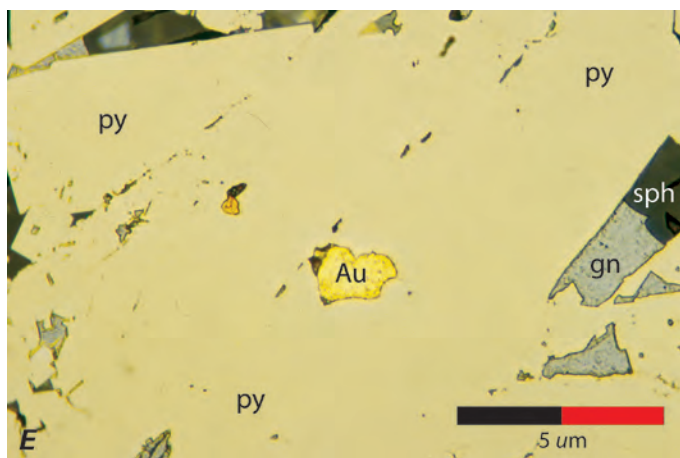
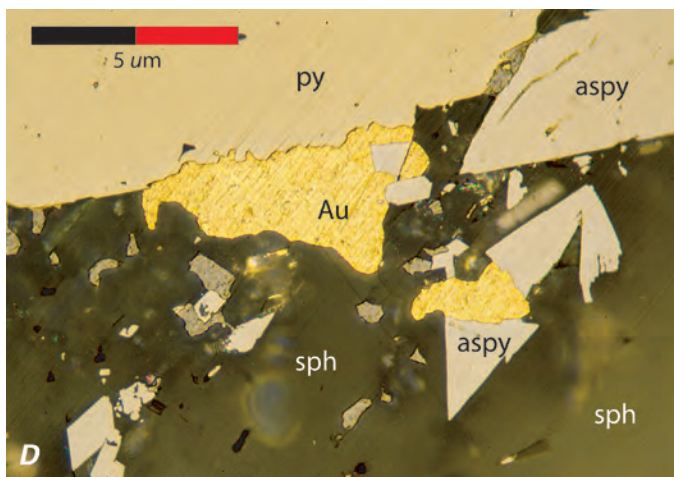
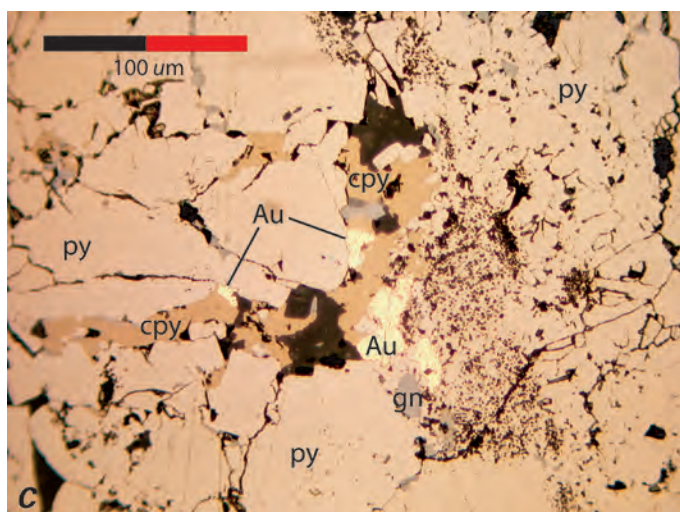
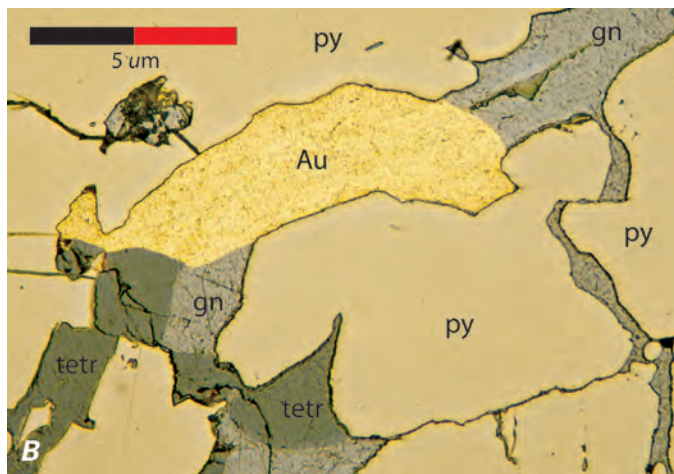
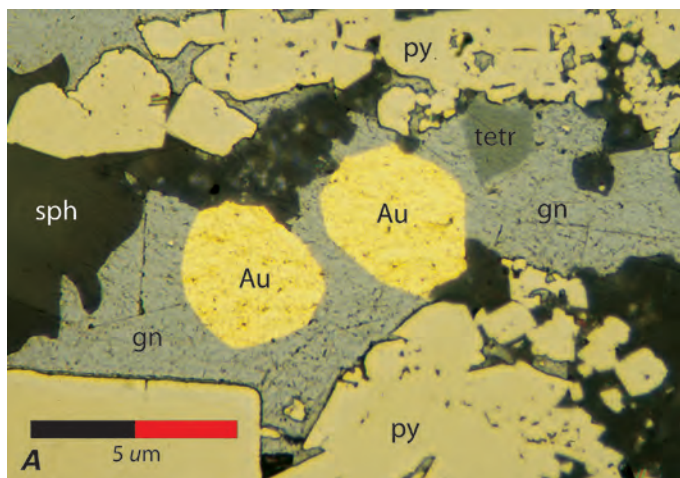


Figure 7. Photomicrographs of arsenian pyrite and arsenopyrite in polished thin sections: (A–C) euhedral arsenian pyrite and arsenopyrite (aspy) replacing framboidal and spongy-textured pyrite (A and B: drill-core sample GC1643–03, 119.5', 200 South orebody, C: rib sample 96GC–17, 49', 344 crosscut, Lower Southwest orebody); (D) subhedral to euhedral crystals of arsenian pyrite and arsenopyrite overgrowing colloform pyrite (rib sample 96GC–17, 49', 344 crosscut, Lower Southwest orebody); (E) euhedral arsenian pyrite and arsenopyrite overgrowing and replacing framboidal and atoll-shaped pyrite (rib sample 96GC–17, 49', 344 crosscut, Lower Southwest orebody); and (F) euhedral arsenopyrite in silica and dolomite matrix (rib sample 96GC–18, 51', 344 crosscut, Lower Southwest orebody).



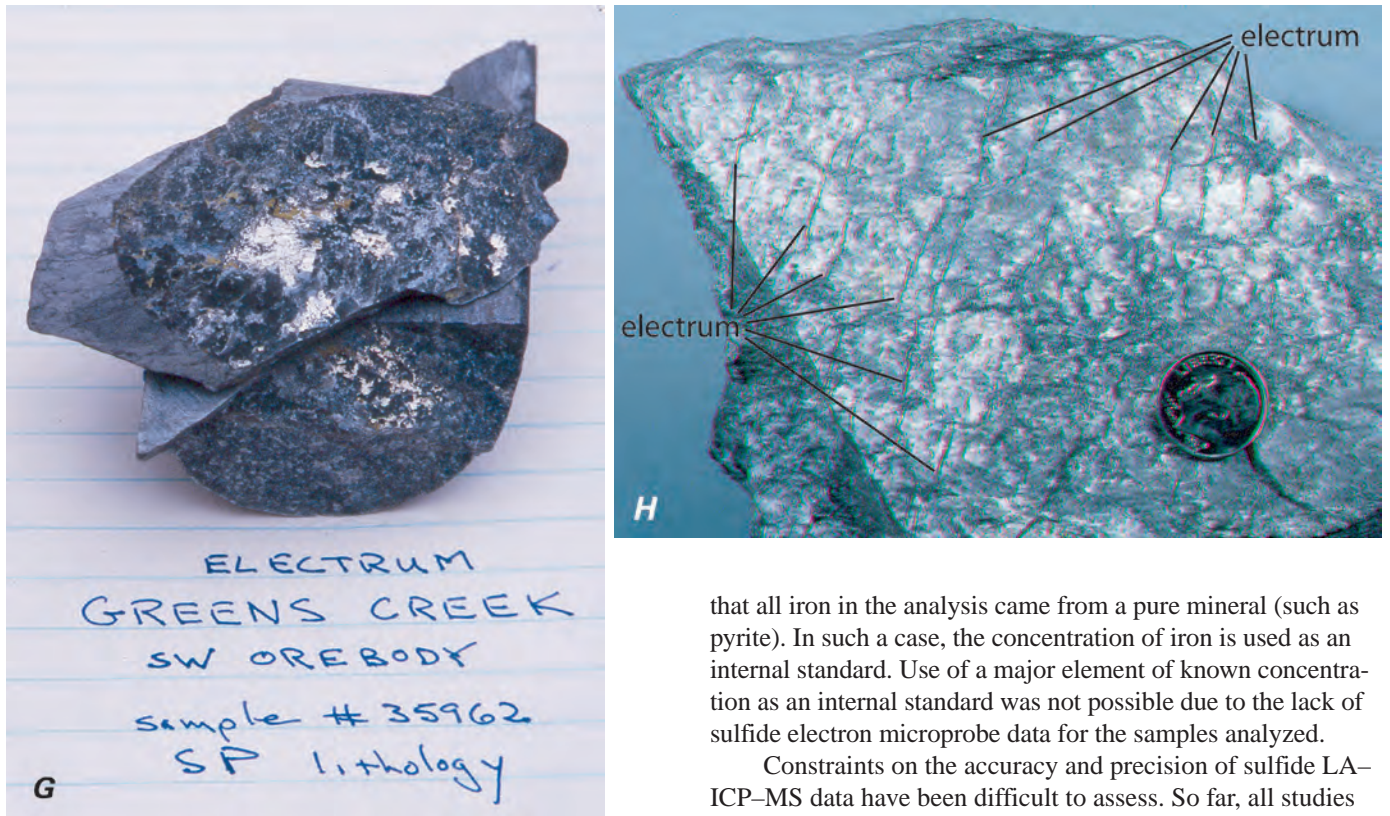


Figure 8 (above and facing page). Photographs and photomicrographs of free gold (Au) in hand samples and polished sections: (A) rounded grains of yellow gold in matrix of sphalerite (sph), galena (gn), and tetrahedrite (tetr) (rib sample 96GC-13, 25.5', 344 crosscut, Lower Southwest orebody); (B) large grain of yellow gold, and galena and tetrahedrite filling crack in massive recrystallized pyrite (rib sample 96GC-16, 43.5', 344 crosscut, Lower Southwest orebody); (C) bright yellow gold, chalcopyrite, sphalerite, and galena in a veinlet cutting recrystallized pyrite (drill-core sample GC1643-06, 119.5', 200 South orebody); (D) grains of yellow gold in contact with pyrite and arsenopyrite (aspy) (rib sample 96GC-19, 53', 344 crosscut, Lower Southwest orebody); (E) yellow gold included within clean, recrystallized pyrite (rib sample 96GC-13, 25.5', 344 crosscut, Lower Southwest orebody); (F and G) silver-white electrum filling fractures and coating fracture surfaces in drill core (GC1155, 319.5', Lower Southwest orebody); and (H) hand sample showing electrum in thin veinlets and spaced sheets that occupy fractures up to 0.5 millimeter wide (rib sample, 30 East decline, 650' level, East orebody). These fractures are paragenetically late and appear to be tension gashes and piercement structures that occur at high angles to S_2 foliation.

that all iron in the analysis came from a pure mineral (such as pyrite). In such a case, the concentration of iron is used as an internal standard. Use of a major element of known concentration as an internal standard was not possible due to the lack of sulfide electron microprobe data for the samples analyzed.

Constraints on the accuracy and precision of sulfide LA-ICP-MS data have been difficult to assess. So far, all studies on natural sulfides report data as semiquantitative (Watling and others, 1995; Viets and others, 1996; Butler and Nesbitt, 1999; J.L. Houghton, W.C. Shanks, and W.E. Seyfried, written commun., 2003). Major reasons for this include poorly quantified differences in ablation efficiency of different sulfides, a near universal lack of appropriate natural or synthetic sulfide calibration standards, and poorly characterized matrix effects that arise as a result of using glass or pressed powder standards. Careful work on glass standards using microprobe data to provide internal standard elemental concentrations has demonstrated that current LA-ICP-MS instrumentation is capable of 2–5 percent accuracy and precision (Norman and others, 1996). Similar careful studies of trace elements in NiS beads, a matrix similar to natural sulfides, document much wider error limits; Shibuya and others (1998) report better than 17 percent accuracy for platinum-group elements and gold, and Guo and Lichte (1995) report between 2 and 12 percent accuracy for chalcophile elements. For an excellent discussion of error analysis of LA-ICP-MS data, see Norman and others (1996).

The data in this study are preliminary and, although absolute concentrations are presented, the results should be evaluated semiquantitatively. Major sources of uncertainty in these data include the lack of independently determined internal element concentrations, thus requiring the assumption of pure mineral species, the reliance on glass standards for calibration, the unknown volume of ablated material, the various differences in elemental fractionations and mineral ablation efficiencies, and finally, the uncertainty of target mineral purity due to the relatively large size of the ablation crater compared with the size of many of the mineral grains. This last feature is perhaps the largest of all the uncertainty factors.

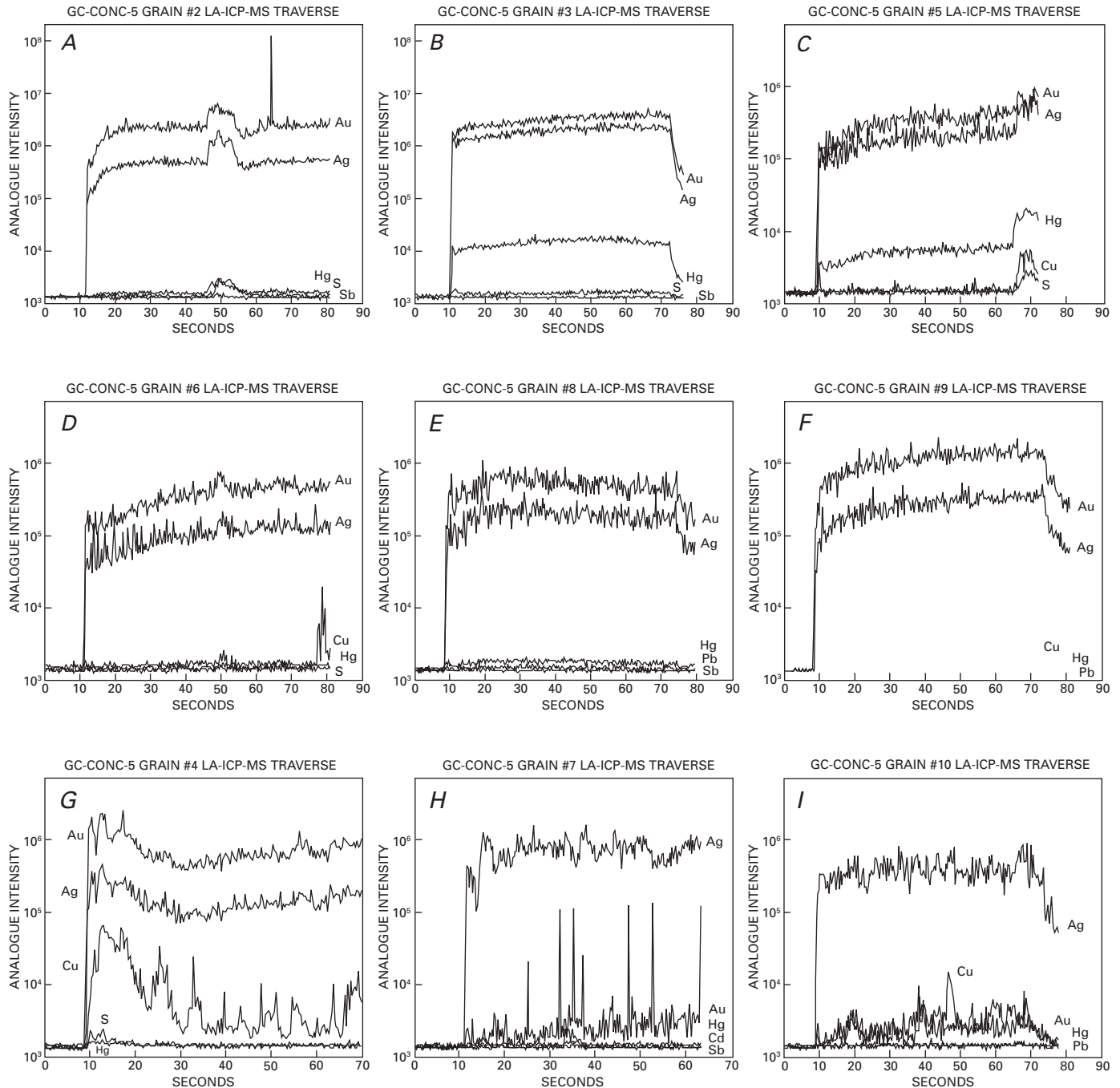


Figure 9. LA-ICP-MS traverses across heavy concentrate grains recovered from the Greens Creek mill. All grains analyzed are from the coarsest fraction of sample GC-CONC-5. Each profile was obtained by operating the laser in continuous mode across a traverse of approximately 100 micrometers with the ICP-MS detectors set to record the relative abundances, measured as the \log_{10} of analogue intensity, of five selected elements. Each plot exhibits the relative abundances of the elements selected and shows the variation in relative concentration with time (distance along the traverse). Note that plots A and B have a greater y-axis range than plots C-I. Plots A and B exhibit the two types of gold identified at Greens Creek: yellow gold of high fineness and silver-white electrum composed of an amalgam of gold, silver, and mercury. Plot C is an example of electrum, plots D-F are analyses of yellow gold grains, plot G represents a possible copper-rich variant of yellow gold, and plots H and I are examples of nearly pure native silver grains. (A) grain #2, Au and Ag only, high Au/Ag; (B) grain #3, Au, Ag, and Hg, lower Au/Ag; (C) grain #5, Au, Ag, and Hg, lower Au/Ag; (D) grain #6, Au and Ag, high Au/Ag; (E) grain #8, Au and Ag, high Au/Ag; (F) grain #9, Au and Ag, high Au/Ag; (G) grain #4, Au, Ag, and Cu, high Au/Ag; (H) grain #7, nearly pure Ag; and (I) grain #10, nearly pure Ag.

Results

Progressive recrystallization of the primary-textured ores and the remobilization of base-metal sulfides have had a profound effect on the siting of trace elements in the ores. LA-ICP-MS studies indicate that a wide range of trace elements is present in the major primary-textured sulfide minerals at relatively high concentrations (fig. 11). As the recrystallization process progresses, trace-element abundances decrease in later formed pyrites and increase predictably in recrystallized and remobilized base-metal sulfides. A second result of the metamorphic refining process is a decrease in the variety of intermediate solid solution sulfosalt minerals and the formation of a less diverse mineral assemblage with a greater proportion of the trace elements contained in discrete end-member mineral phases such as sphalerite and tetrahedrite.

The data from the LA-ICP-MS analyses are presented in tables 2–7. These tables contain data on selected trace-element abundances in primary-textured pyrite, recrystallized pyrite, arsenian pyrite, galena, sphalerite, and tetrahedrite. Plots showing the changes in major- and trace-element concentrations in pyrite, sphalerite, and galena with modification from primary to recrystallized and remobilized textures are shown in figures 12a–ay. Tables 8–10 contain data on primary-textured, recrystallized, and remobilized mixed mineral aggregates. Even though these data are considered semiquantitative for the reasons discussed, the order of magnitude differences in trace-element concentrations within these data reflects usable information on the relative abundances and siting of trace elements in minerals and on the range of trace-element abundances in the various major types of ores present at Greens Creek. These data are discussed below.

Typical trace-element abundances in primary-textured ores as determined by LA-ICP-MS are difficult to interpret due to the fine-scale banding and grain sizes present in the framboidal aggregates and colloform textures. In most cases, the 50-mm beam size of the instrument is incapable of acquiring data from single phases within these ores. Smaller beam size would result in higher limits of detection because the amount of material sampled varies with the square of the crater diameter. Thus, there is a tradeoff between detectability and sampling integrity for these fine-grained minerals. However, data from a limited number of analyses of primary-textured pyrite (mostly spongy pyrite; table 2) and primary-textured ores of mixed mineralogy (table 8) provide a baseline against which to compare analyses of discrete recrystallized or remobilized grains. Typical trace-element abundances in primary-textured pyrite and mixed primary-textured ores are: gold at <240 parts per billion (ppb), silver commonly in the hundreds of parts per million (ppm) and as high as 19,400 ppm, and arsenic at 0.1–4.8 percent. Antimony is clearly the dominant trace element present ubiquitously in the primary-textured pyritic ores near the 1 percent level, and rises to the 9 percent level. Thallium is present in primary ores in the hundreds of parts per million and rises as high as 2,300 ppm. Molybdenum is present from the hundreds to several thousand parts per million and rises as high as 11,930 ppm.

LA-ICP-MS analyses of recrystallized and remobilized phases demonstrate that trace elements are predictably concentrated in fewer, more stoichiometrically ordered minerals. After free gold, the next consistently high concentrations of gold, up to 2,613 ppb, occur in arsenian pyrite (table 4). Gold is inhomogeneously distributed, tends to be concentrated near the edges of euhedral grains, and is probably present as discrete, submicrometer inclusions within the recrystallized pyrite/arsenopyrite. The next most obvious residence of gold, at the 0–700-ppb range with a high of 5,401 ppb, is in the secondary masses of sphalerite and tetrahedrite (table 9). The relatively uniform distribution of gold in these phases suggests that it forms a solid solution rather than occurring as inclusions (fig. 12y). Silver is present in pyrargyrite and in secondary tetrahedrite at 2.9 to 6.7 percent (table 7). Grains of other secondary silver-bearing minerals known to be present at Greens Creek of a size large enough to analyze were not found. Other silver-bearing minerals are recrystallized and remobilized “clean” crystals of pyrite, arsenian pyrite/arsenopyrite, and galena that typically contain hundreds of parts per million and as high as 3,740 ppm (table 5; fig. 12ao). The silver content of sphalerite is extremely variable but generally low. Copper is present in chalcopyrite and in tetrahedrite up to 47 percent, and zinc is present in tetrahedrite at 2.4–7.7 percent (table 7). Arsenic is present in arsenian pyrite/arsenopyrite at the 19–24 percent level (table 4), and in late tetrahedrite in the 2.4–10.2 percent range. Recrystallized pyrite and large secondary anhedral grains of sphalerite and galena typically have less than 0.5 percent arsenic, with maximum values of 1.9 percent. Antimony is a major component of tetrahedrite, is present at 7.6–28 percent and is clearly the dominant and ubiquitous trace element present in Greens Creek ores. It is present at more than 1,000 ppm in every mineral examined with the exceptions of recrystallized pyrite and secondary sphalerite (figs. 12f, w, and aj). Mercury is present at the 58–2,390-ppm level in secondary sphalerite and tetrahedrite and is lowest in secondary galena and arsenian pyrite (figs. 12i, z, and aq). Thallium is present in secondary galena to just less than 1.2 percent (table 5, fig. 12ar). Cadmium is present in sphalerite up to 2,731 ppm. Chromium, cobalt, and nickel are ubiquitous and appear to be associated. These elements occur routinely at levels of tens to hundreds of parts per million in all minerals and ore types. Note that their concentrations are very similar in primary and recrystallized phases but tend to drop to low abundances in the remobilized phases (figs. 12n, o, p, ae, af, ag, av, aw, and ax; tables 8–10). Bismuth, a trace element that is commonly enriched in sulfosalt-bearing massive sulfide deposits, occurs in notably low concentrations in Greens Creek ores. Selenium occurs in all ore types up to 6,000 ppm and is present at 1.1 percent and 1.8 percent in recrystallized pyrite and sphalerite, respectively. Interestingly, the distribution of selenium is generally antithetic to that of antimony, which is notably low in recrystallized pyrite and sphalerite. Selenium shares a distribution similar to chromium, cobalt, and nickel.

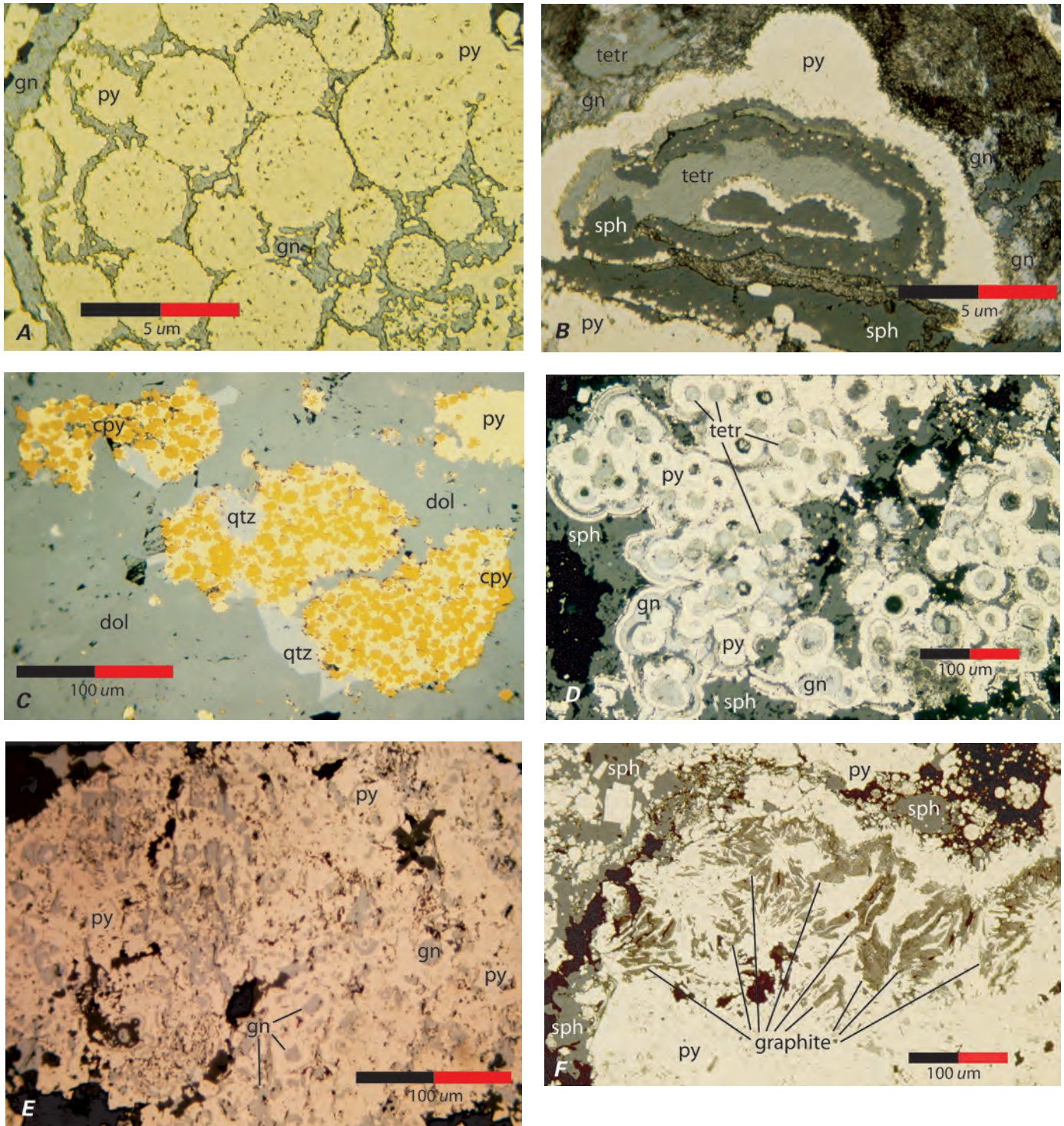
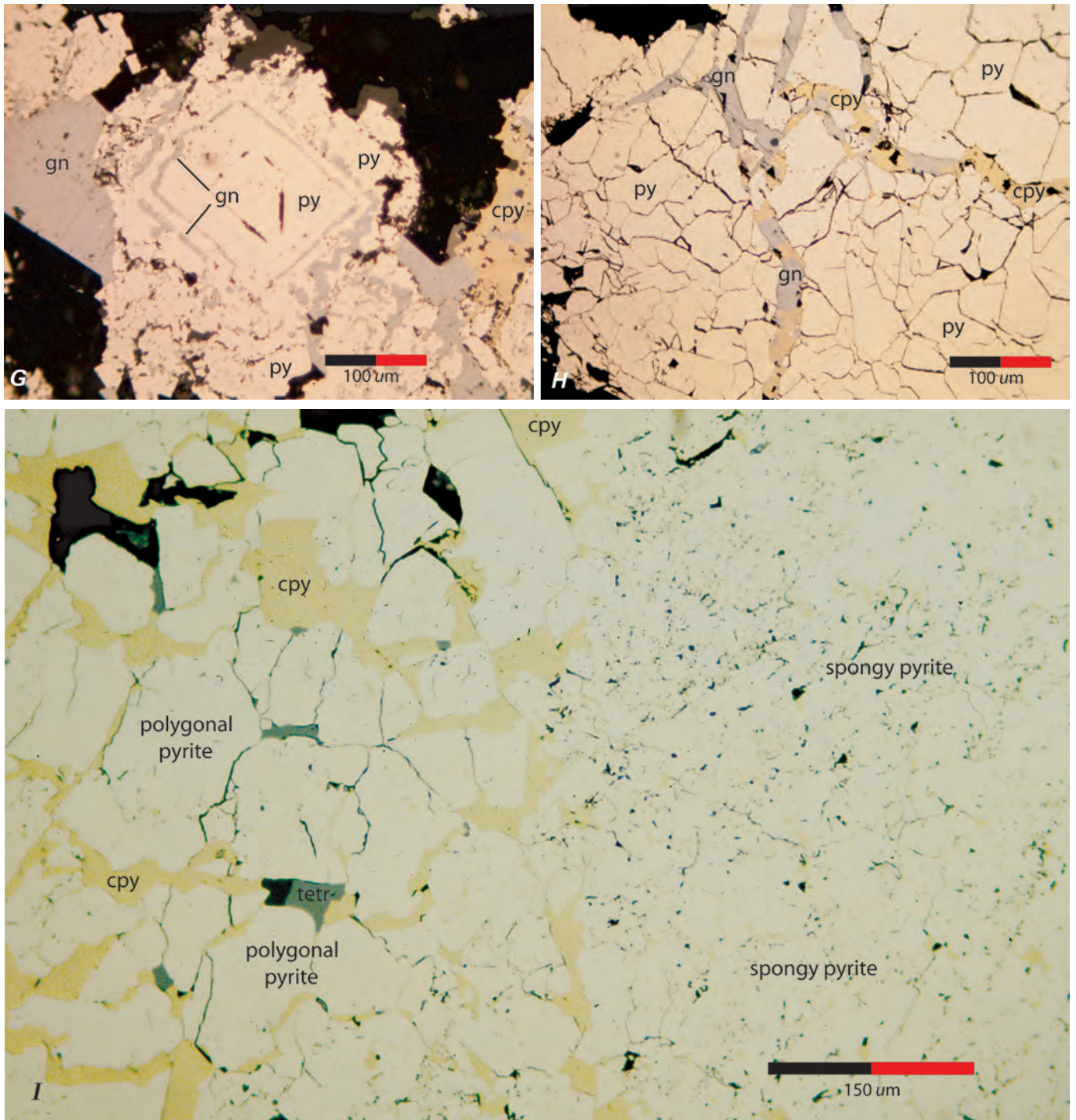


Figure 10 (above and facing page). Photographs and photomicrographs showing textural relationships in Greens Creek ores: (A) polyframboidal pyrite aggregate in galena or lead-antimony sulfosalt matrix (rib sample 96GC-12, 21.5', 344 crosscut, Lower Southwest orebody); (B) successive bands of colloform-textured base-metal sulfides without intervening pyrite bands, within predominantly pyritic primary textured masses (rib sample 96GC-16, 43.5', 344 crosscut, Lower Southwest orebody); (C) framboids composed of chalcopyrite crystallites in a matrix of pyrite, quartz, and dolomite (drill-core sample GC1527-15, 454.2', Northwest orebody); (D) incipient recrystallization of individual framboids resulting in atoll-shaped grains, with centers filled with base-metal sulfides and rims of clean, bright pyrite (drill-core sample GC1527-09, 402.5', Northwest orebody); (E) an aggregate of framboids developed into a large, spongy-textured mass with numerous discrete inclusions of base-metal sulfides and graphite (drill-core sample GC1643-05, 100.5', 200 South orebody); (F) a felty concentration of



needle- or lath-shaped crystals of recrystallized graphite that are aligned subparallel to S2 foliation (rib sample 96GC-16, 43.5', 344 crosscut, Lower Southwest orebody); (G) progressive recrystallization showing a large area of inclusion-free pyrite with relict framboidal shapes preserved in the interior of the mass and euhedral-shaped growth zones defined by thin bands of galena (drill-core sample GC1643-07, 143.5', 200 South orebody); (H) fully recrystallized pyritic ore showing very large areas of inclusion-free, monomineralic pyrite with polygonal grain boundaries cut by chalcopyrite-galena-tetrahedrite veinlets (drill-core sample GC1643-04, 75', 200 South orebody); and (I) chalcopyrite-rich MFP showing the progression from spongy-textured masses with chalcopyrite matrix and numerous small chalcopyrite inclusions on the right, to clean, monomineralic, polygonal-textured masses of pyrite with grain boundaries and intercrystal spaces filled with anhedral, monomineralic chalcopyrite on the left (drill-core sample GC1527-14, 447.2', Northwest orebody).

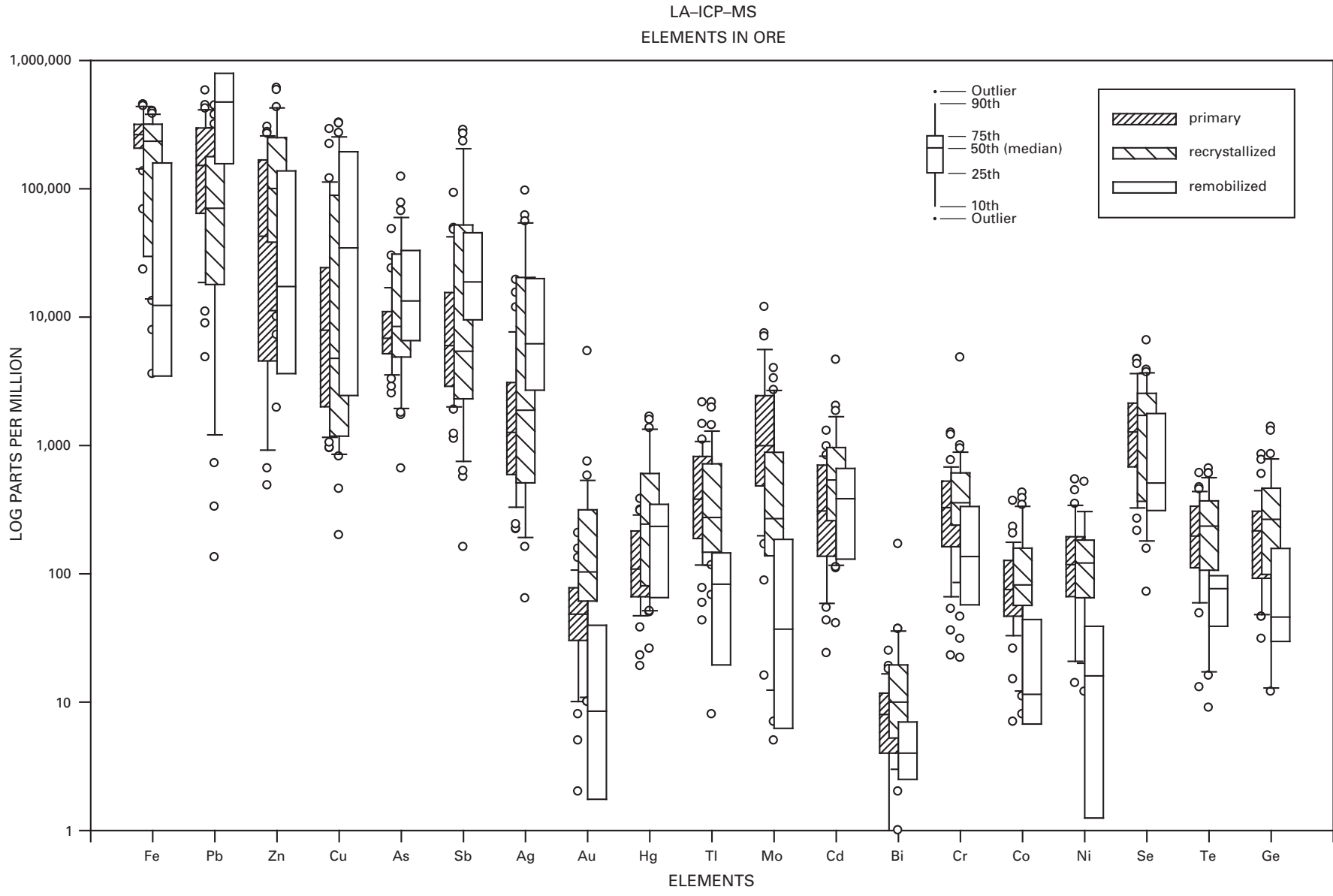


Figure 11. Summary LA-ICP-MS data on sulfide ore minerals in the Greens Creek deposit. Box plots of percentiles shows the \log_{10} concentration range for primary, recrystallized, and remobilized ore textures for each of 19 elements. All elements measured in parts per million, except gold, which is in parts per billion. Horizontal lines within each box show the geometric mean (median value). Each box extends from the 25th to the 75th percentile, whiskers extend out to the 5th and 95th percentiles, and the open or closed circles show individual outlier values. Data plotted from data in tables 2–10.

Table 2. Trace-element composition of primary pyrite as determined by Laser Ablation–Inductively Coupled Plasma–Mass Spectroscopy analyses.

Sample #	Fe %	Pb %	As %	Sb %	Zn ppm	Cu ppm	Ag ppm	Au ppb	Hg ppm	Tl ppm	Mo ppm	Cd ppm	Bi ppm	Cr ppm	Co ppm	Ni ppm	Se ppm
96GC-25	34.8	16.9	0.6	0.2	25,166	4,400	765	49	66	591	2,585	77	6	81	101	280	670
96GC-25	44.1	1.1	0.7	0.6	1,484	13,826	1,929	45	85	107	48	31	3	146	0	119	1,081
96GC-25	35.4	19.9	0.3	0.1	538	683	2,400	39	65	2,304	524	26	1	181	39	221	127
96GC-25	30.9	17.8	0.8	1.1	46,813	23,025	3,217	74	123	1,067	2,703	167	9	96	78	216	0
96GC-25	32.3	16.3	1.1	0.4	56,832	7,009	1,302	47	129	1,072	2,284	196	2	199	102	387	0
96GC-25	44.8	1.3	0.1	0.1	12,694	1,193	338	240	71	37	235	49	12	137	71	123	1,157
96GC-25	24.8	35.0	0.6	0.5	15,711	12,122	2,101	55	45	535	2,562	80	15	411	262	251	3,565
96GC-25	36.6	10.6	1.3	0.8	17,645	22,264	4,027	82	123	1,433	1,747	136	8	848	185	240	446
96GC-25	35.7	17.4	0.6	0.3	3,201	6,242	1,310	124	37	1,270	2,396	146	20	566	248	369	3,411
96GC-25	42.9	4.1	1.5	0.3	862	223	291	31	30	690	115	118	3	598	125	256	1,662
mean	36.2	14.1	0.8	0.4	18,095	9,099	1,768	79	77	911	1,520	103	8	326	121	246	1,212
std. deviation	6.3	10.3	0.4	0.3	19,758	8,469	1,220	63	36	675	1,145	59	6	264	86	88	1,316
maximum	44.8	35.0	1.5	1.1	56,832	23,025	4,027	240	129	2,304	2,703	196	20	848	262	387	3,565
minimum	24.8	1.1	0.1	0.1	538	223	291	31	30	37	48	26	1	81	0	119	0

Table 3. Trace-element composition of recrystallized pyrite as determined by Laser Ablation–Inductively Coupled Plasma–Mass Spectroscopy analyses.

Sample #	Fe %	As %	Pb ppm	Zn ppm	Cu ppm	Sb ppm	Ag ppm	Au ppb	Hg ppm	Tl ppm	Mo ppm	Cd ppm	Bi ppm	Cr ppm	Co ppm	Ni ppm	Se ppm
96GC-18	45.8	0.4	1,076	2,031	541	948	307	33	42	109	78	78	14	476	60		2,438
96GC-18	45.7	0.1	53	1,513	2,003	228	518	0	25	30	235	52	15	610	467		9,864
96GC-18	43.4	1.5	2,230	6,211	553	9,743	850	222	190	1,109	194	228	0	990	181		11,136
96GC-18	46.1	0.2	708	1,239	902	435	76	50	24	37	155	49	14	340	0		1,783
96GC-18	45.3	0.3	2,292	521	399	8,945	126	20	212	1,080	120	70	5	484	212		4,855
96GC-18	44.8	0.3	744	2,790	700	6,995	687	103	146	912	253	223	29	912	447		10,589
96GC-18	45.7	0.5	95	0	224	229	360	66	0	36	41	119	39	326	330		6,427
96GC-19	44.0	1.7	11,570	9,812	55	330	100	54	23	123	62	51	9	195	10		890
96GC-19	46.3	0.1	786	1,474	446	0	80	20	32	50	170	114	5	255	118		1,350
96GC-19	45.5	0.6	7,563	1,141	349	49	110	45	31	91	84	44	12	392	96		3,108
96GC-19	46.3	0.1	1,430	0	721	94	123	0	23	68	38	45	2	416	115		2,378
96GC-19	46.3	0.3	584	1,121	153	60	78	16	32	26	40	487	18	466	48		342
96GC-19	43.9	0.4	4,704	28,550	2,578	156	66	56	47	0	0	270	12	549	105		350
mean	45.3	0.5	2,603	4,339	740	2,170	268	53	64	282	113	141	13	493	169	0	4,270
std. deviation	1.0	0.5	3,423	7,778	737	3,697	263	58	70	432	82	130	11	233	155	0	3,964
maximum	46.3	1.7	11,570	28,550	2,578	9,743	850	222	212	1,109	253	487	39	990	467	0	11,136
minimum	43.4	0.1	53	0	55	0	66	0	0	0	0	44	0	195	0	0	342

Table 4. Trace-element composition of arsenian pyrite as determined by Laser Ablation–Inductively Coupled Plasma–Mass Spectroscopy analyses.

Sample #	Mineral texture	Fe %	Zn %	As %	Sb %	Pb ppm	Cu ppm	Ag ppm	Au ppb	Hg ppm	Tl ppm	Mo ppm	Cd ppm	Bi ppm	Cr ppm
96GC-18	recrystallized	25.0	3.3	24.1	0.5	4,285	1,258	361	95	59	24	4,061	233	7	296
96GC-19	recrystallized	30.9	0.8	18.9	0.2	647	349	2,478	2,613	9	32	158	71	9	571
96GC-19	recrystallized	26.8	2.3	23.0	0.3	620	577	225	1,172	14	48	1,566	256	10	564
mean		27.6	2.1	22.0	0.4	1,851	728	1,021	1,294	27	35	1,928	187	9	477
std. deviation		3.0	1.3	2.7	0.2	2,109	473	1,264	1,263	28	12	1,977	101	2	157
maximum		30.9	3.3	24.1	0.5	4,285	1,258	2,478	2,613	59	48	4,061	256	10	571
minimum		25.0	0.8	18.9	0.2	620	349	225	95	9	24	158	71	7	296

Table 5. Trace-element composition of galena as determined by Laser Ablation–Inductively Coupled Plasma–Mass Spectroscopy analyses.

Sample #	Mineral texture	Pb %	Sb %	Fe ppm	Zn ppm	Cu ppm	As ppm	Ag ppm	Au ppb	Hg ppm	Tl ppm	Mo ppm	Cd ppm	Bi ppm	Cr ppm	Co ppm	Ni ppm	Se ppm
96GC-26b	primary	75.7	3.2	3,513	36,069	176	14,015	234	12	56	124	27	47	3	143	38	20	894
96GC-26b	primary	78.3	3.0	2,767	619	4,810	6,435	37	11	22	327	35	24	3	103	47	56	495
96GC-19	recrystallized	84.1	0.3	4,557	845	79	114	891	19	16	11,724	30	12	4	269	91		2,364
96GC-19	recrystallized	84.8	0.3	687	888	117	135	773	10	16	11,558	19	31	2	244	90		2,047
96GC-19	recrystallized	85.5	0.2	153	420	76	331	518	5	11	8,515	28	29	3	166	52		1,263
96GC-19	recrystallized	85.5	0.3	0	271	122	232	749	8	11	8,275	31	24	4	174	57		1,419
96GC-19	recrystallized	85.4	0.3	97	512	137	266	761	3	14	8,654	46	26	4	257	45		1,412
96GC-19	recrystallized	85.4	0.3	418	271	114	498	640	22	15	8,597	18	0	2	175	44		920
96GC-19	recrystallized	85.2	0.3	903	480	62	556	791	2	14	8,655	36	35	2	177	63		1,508
96GC-26b	remobilized	86.5	0.2	196	84	154	728	222	1	60	11	3	13	2	41	7	15	282
96GC-26b	remobilized	79.4	4.1	270	75	83	18,801	97	9	49	237	5	52	1	5	4	2	345
96GC-26b	remobilized	79.9	3.6	3,102	1,252	95	14,793	85	3	23	152	27	14	1	19	6	6	157
96GC-26b	remobilized	82.9	0.7	2,151	3,012	10,970	5,118	3,740	6	88	11	17	55	1	40	6	18	191
mean		83.0	1.3	1,447	3,446	1,307	4,771	734	9	30	5,142	25	28	2	139	42	20	1,023
std. deviation		3.5	1.5	1,565	9,832	3,181	6,719	955	6	25	4,935	12	16	1	91	30	19	719
maximum		86.5	4.1	4,557	36,069	10,970	18,801	3,740	22	88	11,724	46	55	4	269	91	56	2,364
minimum		75.7	0.2	0	75	62	114	37	1	11	11	3	0	1	5	4	2	157

Table 6. Trace-element composition of sphalerite as determined by Laser Ablation–Inductively Coupled Plasma–Mass Spectroscopy analyses.

Sample #	Mineral texture	Zn %	Fe ppm	Pb ppm	Cu ppm	As ppm	Sb ppm	Ag ppm	Au ppb	Hg ppm	Tl ppm	Mo ppm	Cd ppm	Bi ppm	Cr ppm	Co ppm	Ni ppm	Se ppm
96GC-25	primary	35.4	159,769	98,166	3,170	4,939	1,813	650	41	58	161	1,899	376	5	163	66	34	661
96GC-25	primary	35.1	155,144	68,913	30,489	5,855	8,637	2,637	50	742	42	368	396	6	671	51	33	1,031
96GC-19	recrystallized	62.6	7,064	18,788	100	843	314	588	375	371	314	247	2,729	41	2,021	556		13,751
96GC-19	recrystallized	62.7	7,673	12,170	454	404	474	645	365	401	245	154	2,570	9	1,629	571		16,271
96GC-19	recrystallized	65.8	4,780	152	822	219	270	98	601	1,115	277	119	2,707	27	543	151		0
96GC-19	recrystallized	62.0	9,138	16,250	589	779	392	821	448	521	342	346	2,731	23	1,692	745		18,277
96GC-19	recrystallized	63.4	2,702	5,517	4,100	5,199	9,766	1,256	644	1,142	361	133	2,438	20	603	246		5,615
96GC-19	recrystallized	65.3	5,546	169	556	272	179	262	697	1,301	347	224	2,227	24	805	144		4,674
96GC-19	recrystallized	65.5	5,420	78	0	0	99	187	717	1,184	350	175	2,292	15	1,366	127		3,199
96GC-19	recrystallized	57.1	19,407	128	646	504	176	78,422	772	1,351	304	117	1,301	4	706	198		2,106
96GC-25	recrystallized	62.4	12,227	15,494	4,968	1,320	7,562	1,734	55	1,581	36	57	625	10	225	101	126	885
96GC-26b	recrystallized	64.6	1,589	17,558	962	685	558	86	94	2,390	58	87	1,045	22	593	165	97	2,383
mean		58.5	32,538	21,115	3,905	1,752	2,520	7,282	405	1,013	236	327	1,786	17	918	260	72	5,738
std. deviation		11.1	58,545	30,718	8,534	2,194	3,756	22,416	285	639	128	504	962	11	606	230	46	6,529
maximum		65.8	159,769	98,166	30,489	5,855	9,766	78,422	772	2,390	361	1,899	2,731	41	2,021	745	126	18,277
minimum		35.1	1,589	78	0	0	99	86	41	58	36	57	376	4	163	51	33	0

Table 7. Trace-element composition of tetrahedrite as determined by Laser Ablation–Inductively Coupled Plasma–Mass Spectroscopy analyses.

Sample #	Mineral texture	Fe %	Zn %	Cu %	As %	Sb %	Ag %	Pb ppm	Au ppb	Hg ppm	Tl ppm	Mo ppm	Cd ppm	Bi ppm	Cr ppm	Co ppm	Ni ppm	Se ppm
96GC-18	recrystallized	3.9	2.4	37.5	2.9	21.1	6.2	270	429	804	141	35	805	2	71	52		1,382
96GC-19	recrystallized	1.5	4.0	33.4	2.7	27.5	5.9	226	311	485	92	48	990	5	167	83		831
96GC-19	recrystallized	5.3	3.7	32.9	4.1	21.2	4.6	145	474	566	152	67	931	11	546	136		5,174
96GC-19	recrystallized	1.8	3.3	34.3	2.9	27.1	5.5	892	291	513	132	16	981	3	344	43		1,261
96GC-19	recrystallized	1.4	4.9	33.9	2.4	27.2	5.3	183	243	416	123	80	954	4	282	23		1,081
96GC-19	recrystallized	1.6	3.7	34.0	2.5	27.8	5.5	162	301	545	95	22	984	8	286	57		854
96GC-19	recrystallized	2.0	3.6	36.5	4.1	22.9	5.0	98	409	506	163	111	730	11	606	164		6,009
96GC-19	recrystallized	1.9	3.8	35.8	4.2	23.4	5.1	146	472	600	223	127	838	5	811	220		3,703
96GC-25	recrystallized	3.1	4.1	38.3	7.7	13.0	6.7	6,741	58	879	67	71	808	3	32	18	9	114
96GC-25	recrystallized	3.1	4.2	40.5	9.7	10.7	4.4	3,542	16	775	51	391	980	4	0	28	50	480
96GC-25	recrystallized	3.6	4.6	38.5	10.2	8.9	4.2	28,714	32	781	47	164	903	2	119	17	68	494
96GC-25	recrystallized	1.7	7.7	47.1	6.5	7.6	2.9	10,519	97	1,273	93	66	210	5	79	67	68	207
96GC-25	remobilized	2.8	4.0	38.1	7.0	12.9	5.7	34,783	20	894	24	40	1,144	0	370	40	103	2,565
mean		2.6	4.2	37.0	5.2	19.3	5.2	6,648	242	695	108	95	866	5	286	73	60	1,858
std. deviation		1.2	1.2	3.8	2.8	7.6	1.0	11,653	178	237	55	99	224	3	247	63	34	1,935
maximum		5.3	7.7	47.1	10.2	27.8	6.7	34,783	474	1,273	223	391	1,144	11	811	220	103	6,009
minimum		1.4	2.4	32.9	2.4	7.6	2.9	98	16	416	24	16	210	0	0	17	9	114

Table 8. Trace-element composition of mixed primary-textured mineral aggregates as determined by Laser Ablation–Inductively Coupled Plasma–Mass Spectroscopy analyses.

Sample #	Mineralogy	Fe %	Pb %	Zn %	Cu %	As %	Sb %	Ag ppm	Au ppb	Hg ppm	Tl ppm	Mo ppm	Cd ppm	Bi ppm	Cr ppm	Co ppm	Ni ppm	Se ppm
96GC-25	?	31.6	20.1	0.4	1.1	1.0	4.0	1,203	60	38	399	4,973	43	1	139	62	174	677
96GC-25	?	22.6	33.8	2.5	3.0	1.3	1.6	5,871	47	86	768	11,930	223	6	195	42	130	782
96GC-25	?	29.1	28.2	0.4	1.2	0.9	0.4	2,097	55	105	979	7,026	143	19	764	368	541	4,295
96GC-25	gn-gcr	22.0	42.0	1.2	0.7	0.5	0.3	1,425	91	23	633	3,533	54	10	246	131	128	2,058
96GC-26b	gn-py-tetr-sph	14.6	41.0	6.4	6.2	1.4	0.9	3,125	5	88	157	169	417	8	383	38	34	1,719
96GC-25	gn-tetr	2.3	58.0	0.9	12.0	3.0	3.7	15,427	11	314	77	16	218	0	23	7	14	446
96GC-25	gn-tetr	27.0	20.1	1.7	11.0	0.6	0.8	3,605	78	66	324	3,704	163	8	419	70	288	694
96GC-25	py-gn	34.3	17.5	0.5	1.9	0.8	0.8	5,224	32	56	1,059	898	62	3	53	106	445	351
96GC-25	py-gn	31.3	16.2	3.6	0.9	0.7	4.8	1,764	70	86	693	2,092	158	8	105	36	60	267
96GC-25	py-gn	26.0	36.6	0.1	0.5	0.5	0.2	936	64	19	174	210	61	3	287	81	78	555
96GC-25	py-gn-qtz	27.2	35.0	0.0	0.1	0.6	0.1	644	81	53	839	618	75	7	159	46	118	215
96GC-26b	py-gn-sph	20.3	36.2	7.7	0.2	0.6	1.4	670	28	81	240	1,248	250	2	238	46	0	843
96GC-26b	py-gn-sph	16.5	30.3	17.5	1.2	0.5	0.7	2,371	41	189	612	492	731	7	534	52	78	912
96GC-26b	py-gn-tetr-sph	19.4	28.0	12.4	2.2	1.1	1.7	2,663	2	250	232	458	617	12	594	82	67	2,889
96GC-26b	py-gn-tetr-sph	22.1	13.6	20.0	2.5	0.8	1.1	2,999	16	215	270	990	834	10	1,250	108	81	4,695
96GC-25	py-qtz	31.8	18.2	0.4	4.3	1.3	1.3	5,271	156	85	2,155	804	135	6	285	156	204	729
96GC-25	py-sph	31.1	7.9	14.5	0.6	0.5	0.3	998	49	121	312	4,293	387	10	1,202	127	331	2,703
96GC-25	py-sph-gn	28.2	14.1	14.4	0.5	0.4	0.2	846	43	164	429	1,736	347	6	160	42	153	669
96GC-26b	py-sph-gn	14.8	44.6	8.8	0.3	0.5	1.8	690	15	165	312	435	370	8	369	58	66	996
96GC-26b	py-sph-gn	34.9	5.9	11.4	0.2	0.3	0.3	487	32	113	134	606	392	11	381	51	190	1,569
96GC-26b	py-sph-gn	27.3	11.3	17.8	0.2	0.4	0.5	578	39	206	301	1,037	817	4	482	53	199	1,289
96GC-26b	py-sph-gn	22.8	7.1	26.7	0.3	0.7	0.6	834	32	381	995	2,562	980	13	642	49	141	1,886
96GC-26b	py-sph-gn	26.4	12.0	18.5	0.1	0.3	0.4	518	48	163	364	1,530	746	1	463	15	184	2,340
96GC-26b	py-sph-gn	22.5	7.6	27.6	0.2	0.4	0.5	723	8	263	159	1,003	754	15	446	231	105	1,691
96GC-26b	py-sph-gn	26.4	5.1	24.0	0.1	0.6	0.4	501	30	216	169	674	589	16	555	136	112	2,725
96GC-26b	py-sph-gn	24.9	6.2	25.4	0.1	0.3	0.3	457	77	265	1,106	821	740	16	170	69	94	1,881
96GC-26b	py-sph-gn	18.1	11.3	30.3	0.2	0.7	0.7	368	22	278	153	221	1,295	25	599	127	31	3,345
96GC-25	py-tetr	38.7	4.9	4.9	1.4	0.8	0.4	1,322	63	72	1,461	7,427	820	0	156	107	349	388
96GC-25	py-tetr	41.2	1.1	3.5	2.2	0.7	0.6	2,639	62	66	43	88	215	6	380	119	97	1,212
96GC-18	py-tetr-gn	45.1	0.9	0.1	0.2	0.7	0.3	224	132	84	913	3,553	128	4	281	151		1,260
96GC-18	py-tetr-gn	43.7	2.9	0.2	0.2	1.2	0.2	221	96	67	729	1,914	24	18	200	164		2,160
96GC-18	py-tetr-gn	45.1	0.5	0.0	0.1	1.1	0.1	242	96	51	268	756	177	16	508	205		4,652
96GC-25	py-tetr-gn	13.6	27.1	1.4	22.2	2.4	3.2	11,825	96	309	719	1,230	270	1	72	26	62	769
96GC-25	py-tetr-gn-sph	24.3	14.2	6.6	5.1	1.4	9.2	5,350	31	158	636	1,831	417	6	217	109	230	0
96GC-25	py-tetr-qtz	43.9	2.2	0.1	1.1	0.7	0.3	1,438	66	53	891	332	106	11	590	82	168	1,307
96GC-25	tetr-gn	6.9	25.9	1.3	29.0	4.8	4.9	19,399	207	237	59	481	418	10	36	63	0	1,577
mean		26.6	19.1	8.7	3.1	1.0	1.4	2,915	58	144	549	1,991	394	9	377	95	150	1,571
std. deviation		10.2	14.7	9.6	6.2	0.9	1.9	4,274	43	95	451	2,510	319	6	283	70	124	1,228
maximum		45.1	58.0	30.3	29.0	4.8	9.2	19,399	207	381	2,155	11,930	1,295	25	1,250	368	541	4,695
minimum		2.3	0.5	0.0	0.1	0.3	0.1	221	2	19	43	16	24	0	23	7	0	0

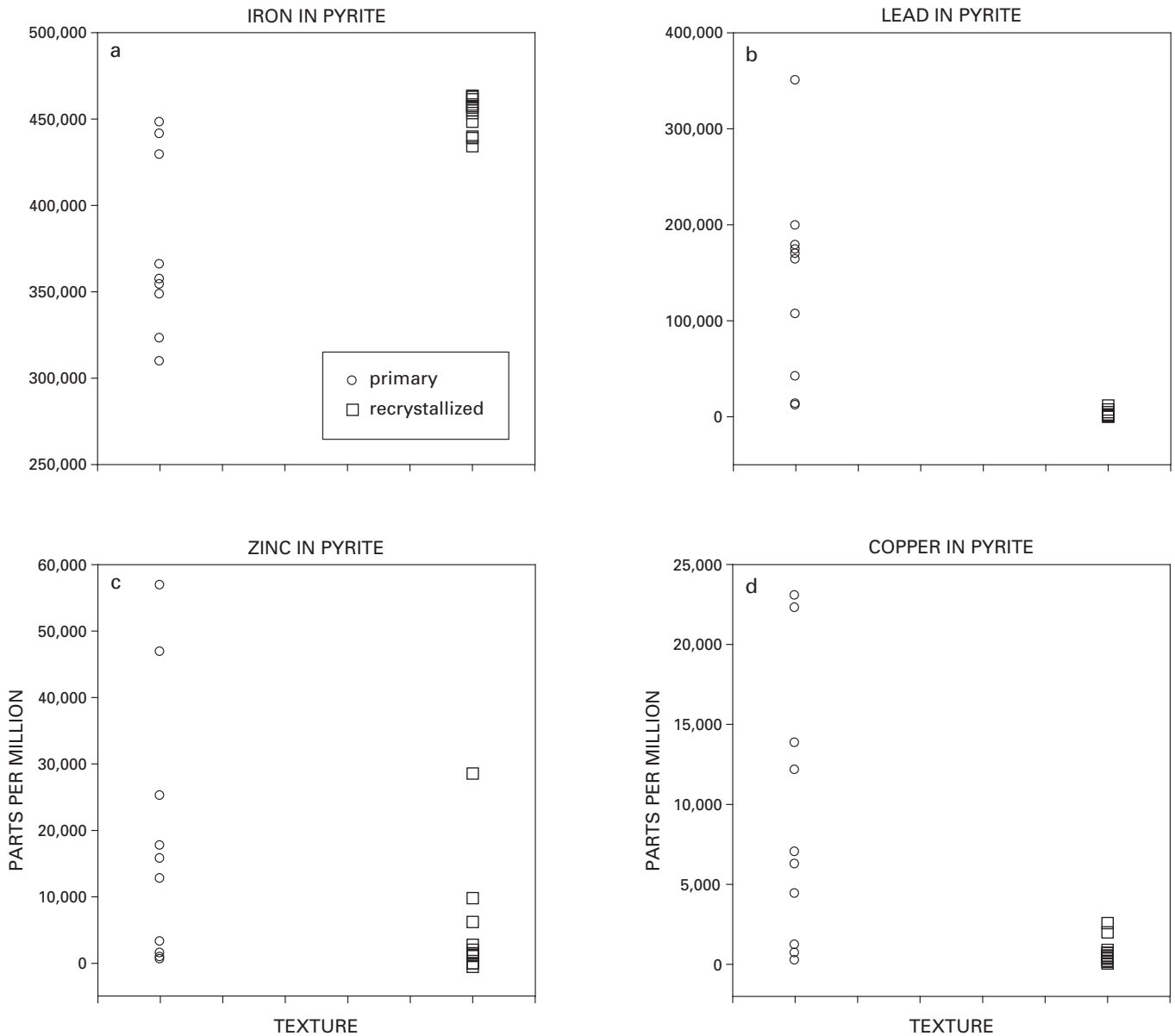
Table 9. Trace-element composition of recrystallized mixed mineral aggregates as determined by Laser Ablation–Inductively Coupled Plasma– Mass Spectroscopy analyses.

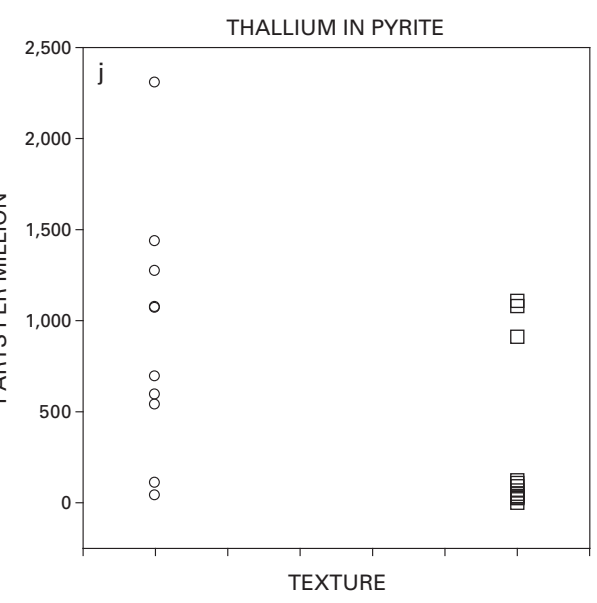
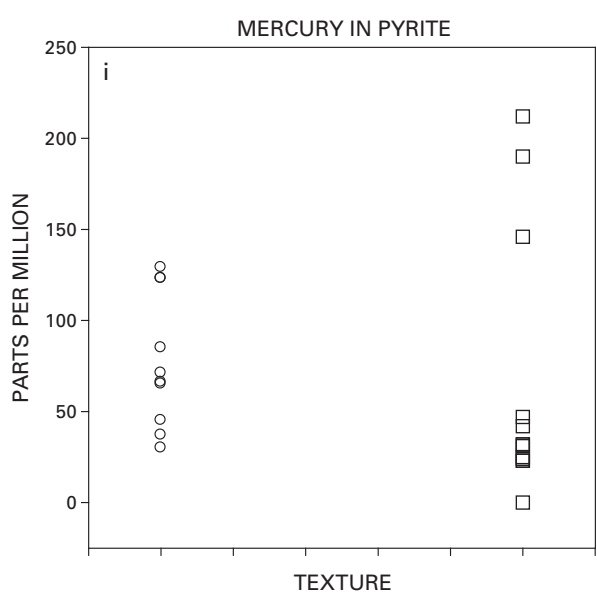
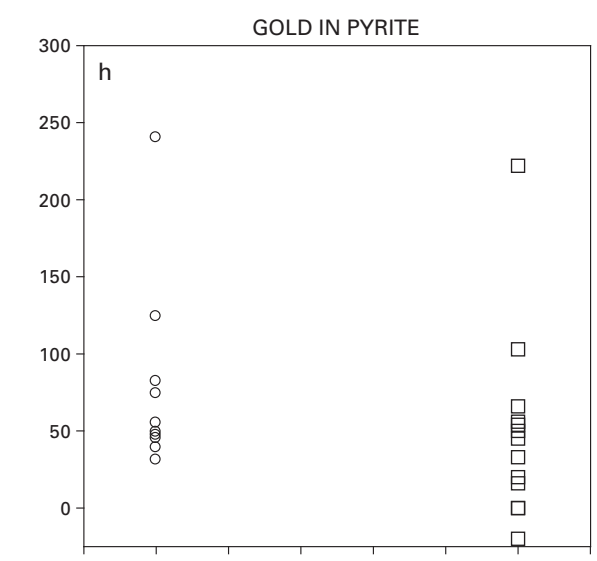
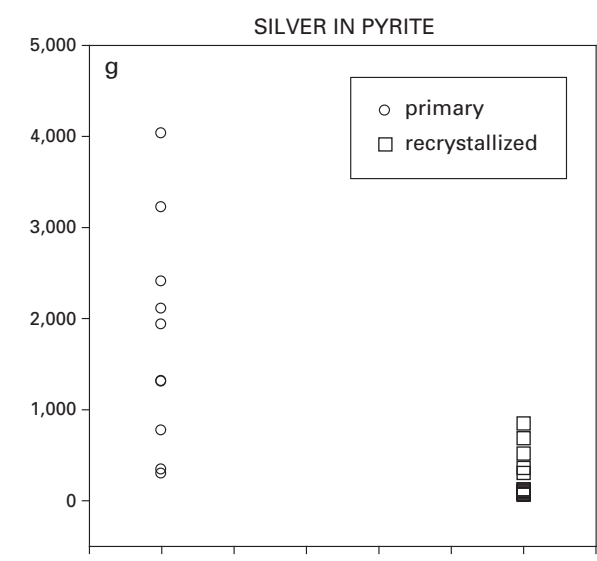
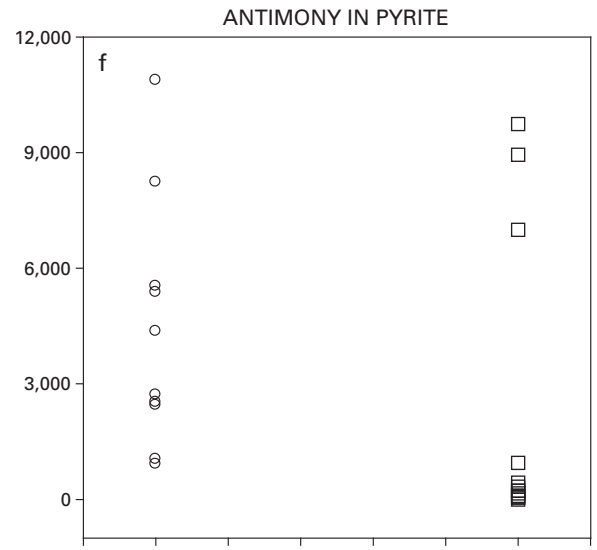
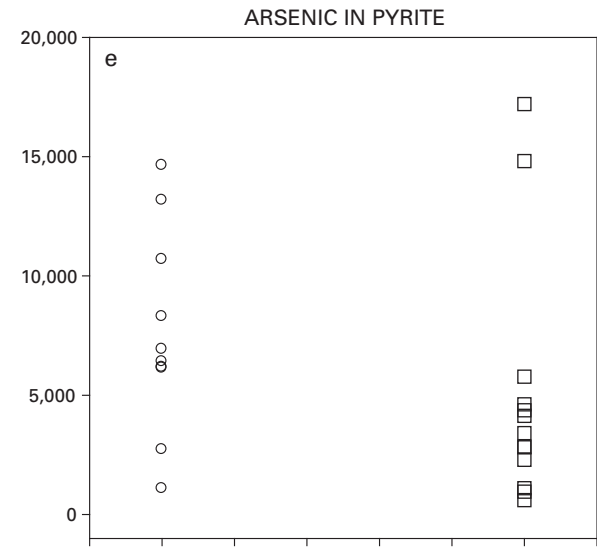
Sample #	Mineralogy	Fe %	Pb %	Zn %	Cu %	As %	Sb %	Ag ppm	Au ppb	Hg ppm	Tl ppm	Mo ppm	Cd ppm	Bi ppm	Cr ppm	Co ppm	Ni ppm	Se ppm
96GC-18	aspy-gn	21.0	25.8	0.7	1.5	12.3	0.5	494	196	79	2158	1601	1191	37	420	150		6571
96GC-25	gn-sph-dolo	29.9	2.3	10.6	0.3	0.6	0.2	23952	164	109	651	2680	546	33	722	278	518	2016
96GC-25	gn-tetr	1.3	44.3	1.4	21.5	4.3	5.3	23107	10	306	8	7	321	1	31	11	12	366
96GC-19	py-gn	33.0	12.6	1.0	0.1	7.7	0.3	861	76	26	743	538	41	3	259	112		290
96GC-19	py-gn	37.5	11.4	2.8	0.0	1.1	0.1	64	32	51	756	194	182	14	312	161		2384
96GC-26b	py-gn-sph	13.4	31.6	19.9	0.9	0.8	1.6	1749	13	247	290	574	464	11	178	86	66	1999
96GC-26b	py-gn-sph	31.2	18.8	5.3	0.1	0.9	1.3	532	88	76	122	168	225	13	275	52	213	1038
96GC-26b	py-gn-sph	27.3	14.8	14.0	0.3	0.9	1.0	887	136	209	360	1695	709	170	365	56	131	2041
96GC-25	py-qtz	24.4	37.5	0.2	1.4	0.7	0.5	2013	86	60	1960	231	110	10	233	59	112	916
96GC-18	py-sph	32.1	0.3	19.8	0.2	0.2	0.1	374	411	173	68	341	657	9	218	251		3,867
96GC-19	py-sph	38.0	3.6	9.5	0.0	0.1	0.0	0	34	50	230	135	515	21	419	43		1,690
96GC-19	py-sph-gn	39.7	2.9	3.4	0.6	3.2	0.2	505	65	53	160	253	437	20	671	20		1,736
96GC-19	py-sph-gn	38.1	2.1	6.1	0.1	3.9	0.1	263	10	66	165	285	450	18	630	101		72
96GC-26b	py-sph-gn	29.1	20.5	8.5	0.1	0.2	0.4	3,126	10	86	895	516	179	4	46	15	62	293
96GC-26b	py-sph-gn	13.7	24.8	26.5	0.3	0.6	0.6	4,075	43	133	316	597	623	7	350	77	146	443
96GC-26b	py-sph-gn	23.6	7.4	26.4	0.1	0.3	0.5	487	87	241	305	3,316	874	15	277	-12	51	993
96GC-26b	py-sph-gn	23.3	14.2	20.9	0.4	0.5	0.5	1,166	72	248	158	1,334	968	7	228	76	282	1,246
96GC-26b	py-sph-gn	40.2	4.2	4.6	0.2	0.5	0.2	2,781	176	264	203	382	112	16	995	197	170	2,755
96GC-26b	py-sph-gn	34.3	6.8	11.6	0.1	0.2	0.4	161	118	655	164	217	127	37	942	71	145	1,753
96GC-18	py-sph-gn-tetr	29.5	7.3	8.1	5.1	0.6	5.0	10,149	70	158	764	3,989	531	23	289	387		2,466
96GC-25	py-tetr	31.0	6.3	4.9	7.0	3.9	1.0	17,964	119	284	970	2,688	239	5	427	128	279	678
96GC-26b	sph-dolo	2.8	1.0	60.8	0.2	0.3	0.2	557	89	1,667	116	180	1,843	9	223	125	73	3,590
96GC-26b	sph-py-gn	20.1	9.0	30.4	0.1	0.3	0.4	636	60	357	401	870	491	10	403	78	73	0
96GC-18	sph-tetr	1.9	0.0	43.0	8.1	0.7	14.0	1,422	579	1,359	260	147	4,631	4	438	319		3,696
96GC-19	sph-tetr	0.8	0.0	41.8	12.7	1.0	11.6	21,153	353	549	117	25	1,283	8	648	103		237
96GC-19	sph-tetr	0.4	1.4	58.5	2.2	0.8	3.4	4,566	745	1,283	396	0	2,022	28	757	342		3,631
96GC-19	tetr-gn	1.8	0.2	3.6	32.1	2.8	28.5	55,492	428	698	140	60	947	10	380	71		1,911
96GC-19	tetr-gn	1.5	13.7	3.2	27.1	2.5	23.3	51,249	307	566	1,431	56	864	5	289	72		2,570
96GC-19	tetr-gn	1.7	0.1	4.6	32.6	2.8	26.7	61,569	346	618	144	5	1,060	3	551	65		2,986
96GC-25	tetr-sph	3.6	1.7	27.7	16.2	4.2	7.2	96,112	169	1,573	124	117	501	6	294	97	173	269
96GC-25	tetr-sph	8.1	6.0	16.5	18.1	6.7	9.5	34,892	318	942	303	889	1,133	13	4,826	427	86	372
96GC-26b	tetr-sph-gn	9.4	24.4	20.5	9.1	1.0	4.4	13,988	5,401	128	193	178	710	2	22	8	21	156
mean		20.1	11.2	16.1	6.2	2.1	4.6	13,636	338	416	471	758	781	18	535	126	145	1,720
std. deviation		14.2	11.8	16.3	9.9	2.7	7.9	22,893	941	466	525	1,041	849	30	819	114	122	1,488
maximum		40.2	44.3	60.8	32.6	12.3	28.5	96,112	5,401	1,667	2,158	3,989	4,631	170	4,826	427	518	6,571
minimum		0.4	0.0	0.2	0.0	0.1	0.0	0	10	26	8	0	41	1	22	-12	12	0

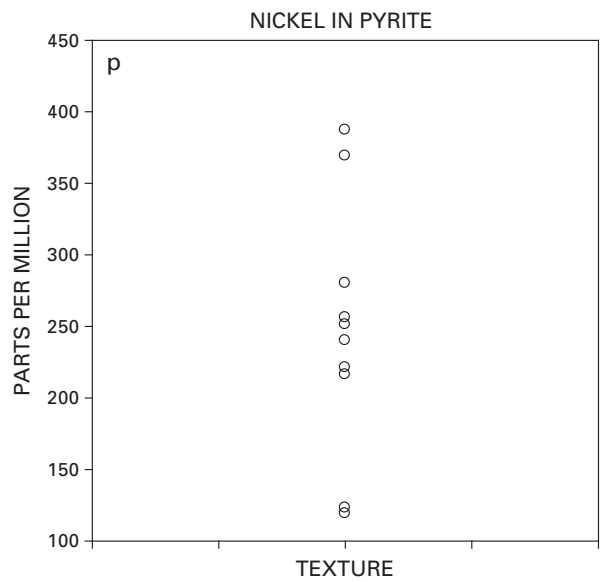
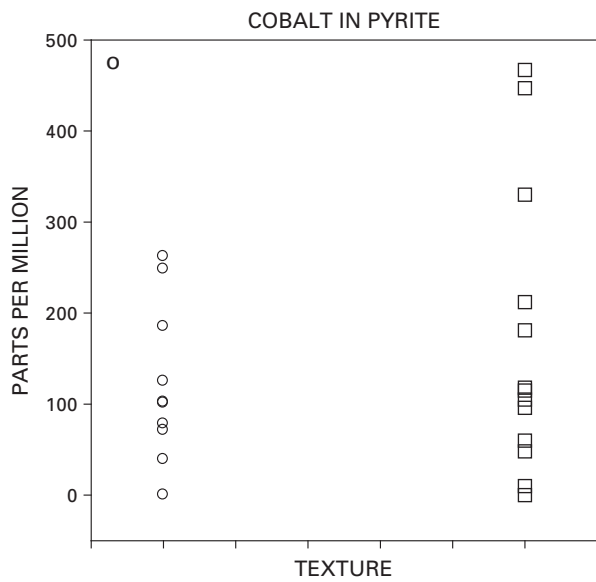
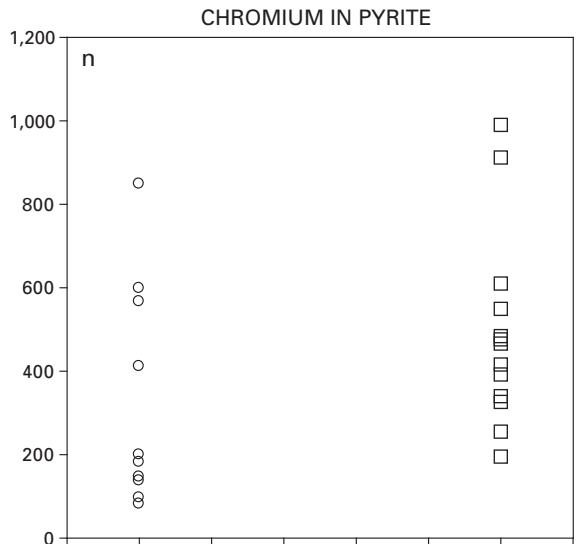
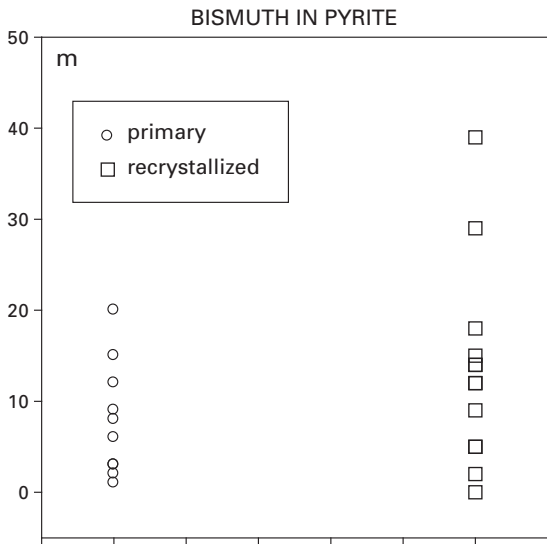
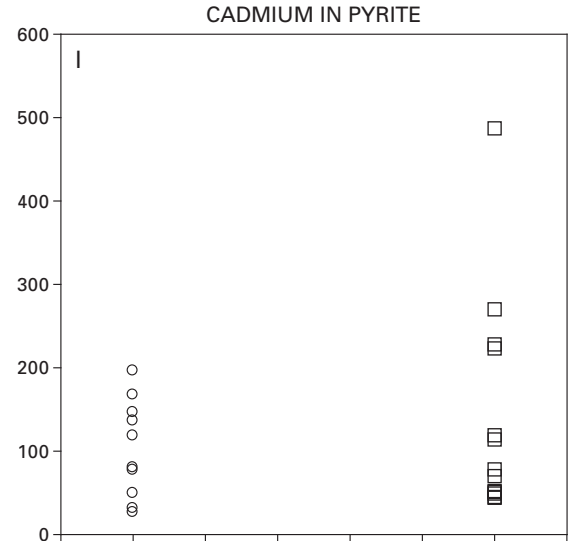
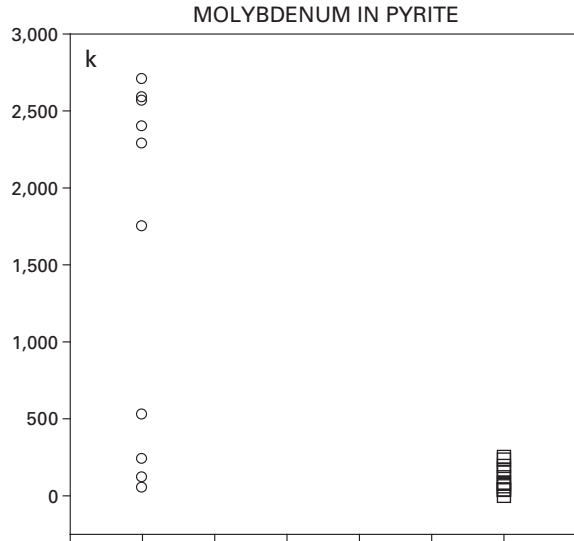
Table 10. Trace-element composition of remobilized mixed mineral aggregates as determined by Laser Ablation–Inductively Coupled Plasma–Mass Spectroscopy analyses.

Sample #	Mineralogy	Fe %	Pb %	Zn %	Cu %	As %	Sb %	Ag ppm	Au ppb	Hg ppm	Tl ppm	Mo ppm	Cd ppm	Bi ppm	Cr ppm	Co ppm	Ni ppm	Se ppm
96GC-26b	gn-tetr	0.2	81.2	0.3	2.2	0.7	0.8	4,483	1	111	10	6	104	4	97	9	6	532
96GC-26b	gn-tetr	0.0	81.1	0.0	0.0	1.3	3.4	77	1	21	157	5	7	2	82	6	0	202
96GC-26b	gn-tetr	0.7	74.4	0.6	4.7	1.4	2.1	7,903	10	209	10	7	208	4	32	6	26	339
96GC-26b	gn-tetr	0.9	58.8	1.3	11.5	2.9	4.9	20,229	7	310	48	21	468	4	176	13	5	1,054
96GC-26b	py-gn-sph	16.6	32.0	16.3	0.6	0.6	0.6	3,307	46	50	597	206	301	1	49	10	45	302
96GC-26b	sph-py-gn	13.7	10.2	37.4	0.1	0.1	1.7	2,497	21	920	71	365	606	10	763	41	17	2,016
96GC-26b	tetr-gn	1.6	36.1	2.2	22.1	4.4	8.9	37,439	4	360	95	53	680	4	260	45	27	2,064
96GC-26b	tetr-py-sph-gn	18.0	4.6	6.1	29.4	3.4	1.5	19,174	79	259	110	123	2,095	8	359	254	43	487
mean		6.5	47.3	8.0	8.8	1.9	3.0	11,889	21	280	137	98	558	5	227	48	21	874
std. deviation		8.1	31.0	13.1	11.2	1.5	2.8	12,804	28	286	192	129	664	3	244	85	17	764
maximum		18.0	81.2	37.4	29.4	4.4	8.9	37,439	79	920	597	365	2,095	10	763	254	45	2,064
minimum		0.0	4.6	0.0	0.0	0.1	0.6	77	1	21	10	5	7	1	32	6	0	202

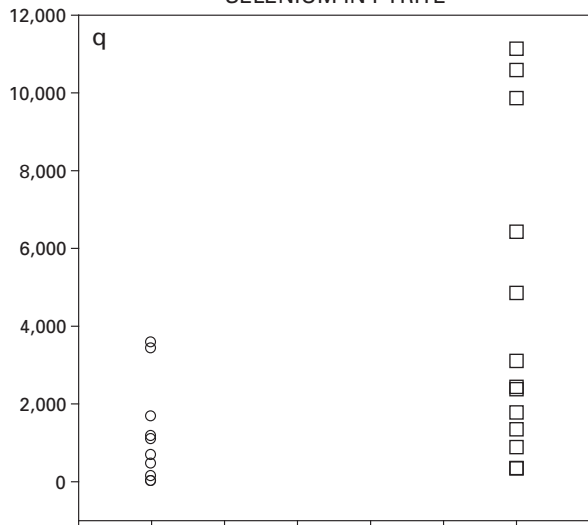
Figure 12. Single element plots of LA-ICP-MS data showing the range of elemental abundances of metals in primary and recrystallized pyrite (a–q) and sphalerite (r–ah), and in primary, recrystallized, and remobilized galena (ai–ay). (a) Fe in pyrite, (b) Pb in pyrite, (c) Zn in pyrite, (d) Cu in pyrite, (e) As in pyrite, (f) Sb in pyrite, (g) Ag in pyrite, (h) Au in pyrite, (i) Hg in pyrite, (j) Tl in pyrite, (k) Mo in pyrite, (l) Cd in pyrite, (m) Bi in pyrite, (n) Cr in pyrite, (o) Co in pyrite, (p) Ni in pyrite, (q) Se in pyrite, (r) Fe in sphalerite, (s) Pb in sphalerite, (t) Zn in sphalerite, (u) Cu in sphalerite, (v) As in sphalerite, (w) Sb in sphalerite, (x) Ag in sphalerite, (y) Au in sphalerite, (z) Hg in sphalerite, (aa) Tl in sphalerite, (ab) Mo in sphalerite, (ac) Cd in sphalerite, (ad) Bi in sphalerite, (ae) Cr in sphalerite, (af) Co in sphalerite, (ag) Ni in sphalerite, (ah) Se in sphalerite, (ai) Pb in galena, (aj) Sb in galena, (ak) Fe in galena, (al) Zn in galena, (am) Cu in galena, (an) As in galena, (ao) Ag in galena, (ap) Au in galena, (aq) Hg in galena, (ar) Tl in galena, (as) Mo in galena, (at) Cd in galena, (au) Bi in galena, (av) Cr in galena, (aw) Co in galena, (ax) Ni in galena, (ay) Se in galena. Pyrite data plotted from tables 2 and 3. Galena data plotted from table 5. Sphalerite data plotted from table 6.



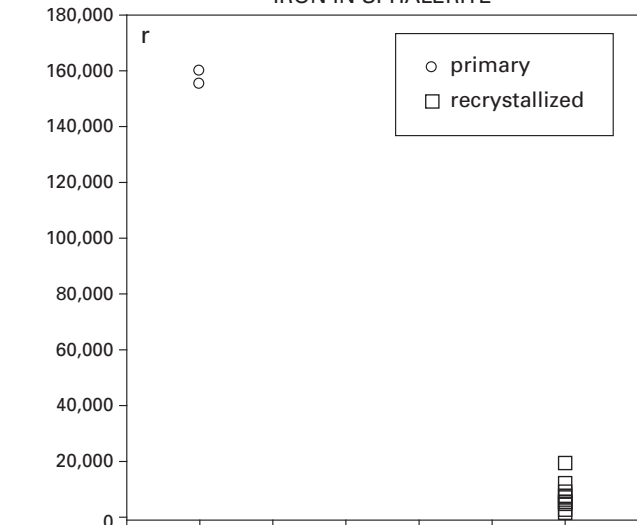




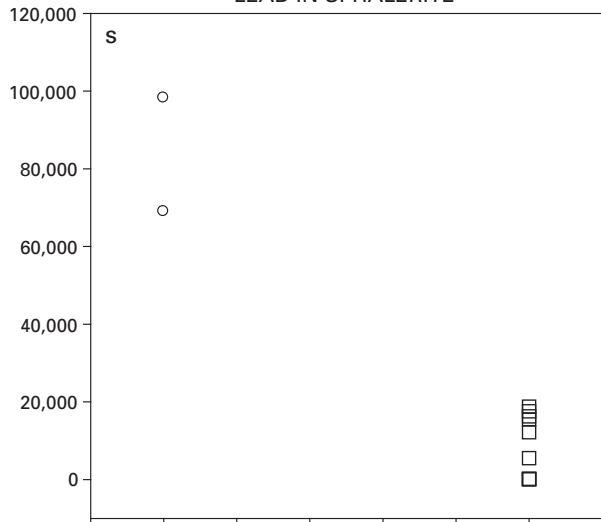
SELENIUM IN PYRITE



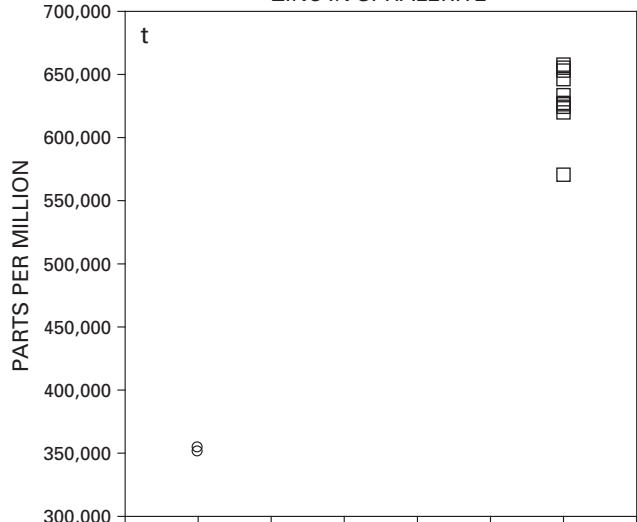
IRON IN SPHALERITE



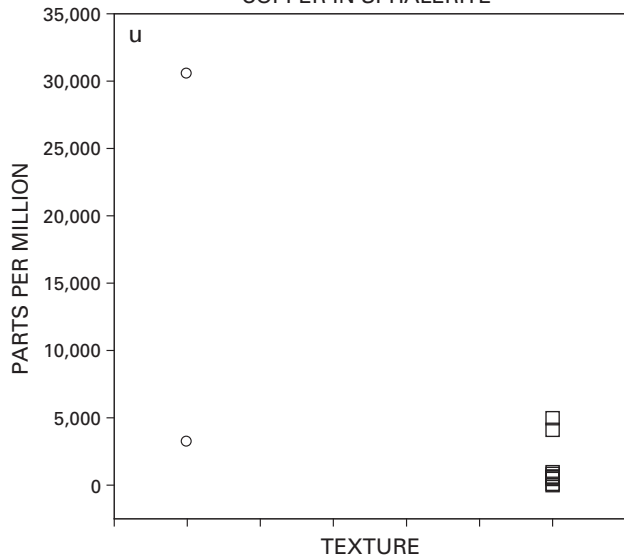
LEAD IN SPHALERITE



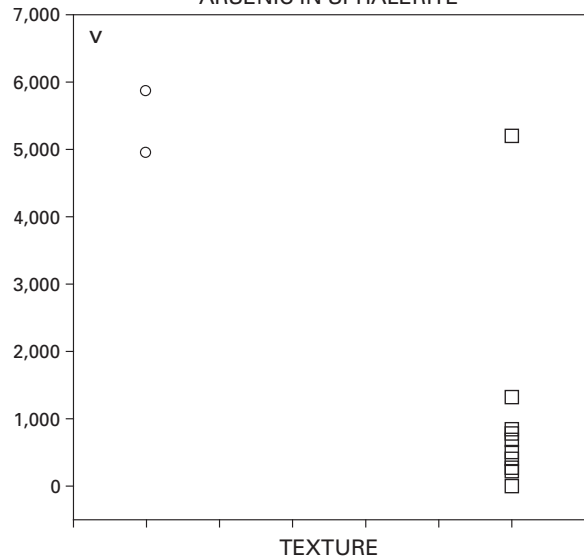
ZINC IN SPHALERITE

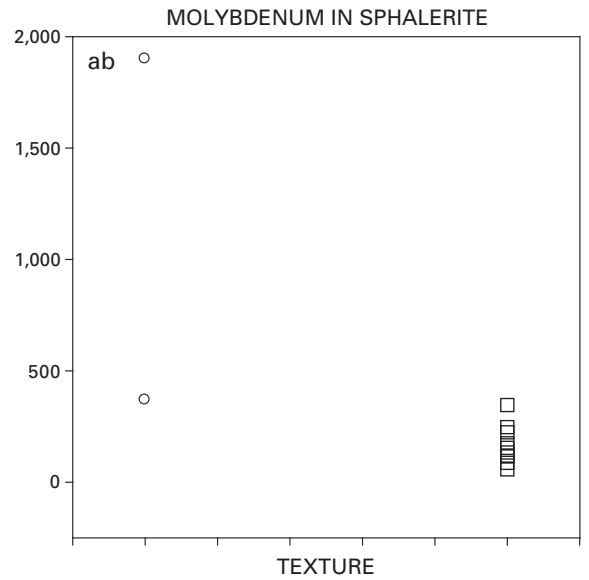
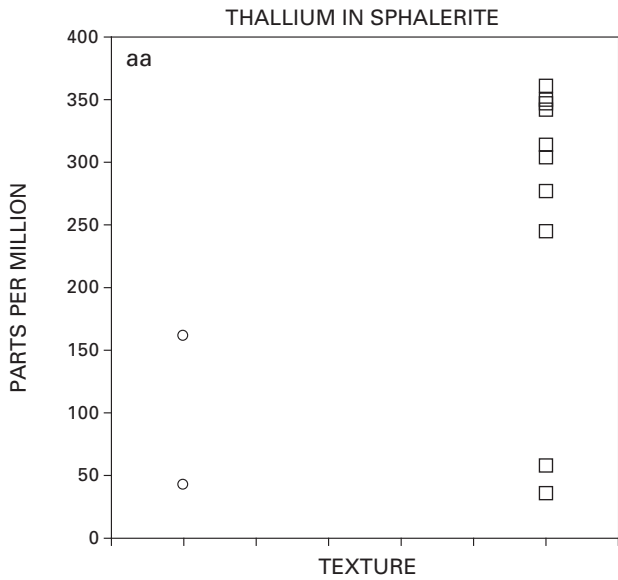
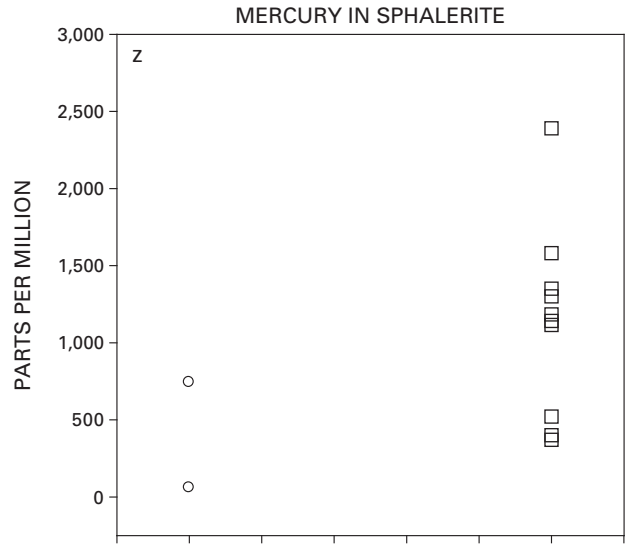
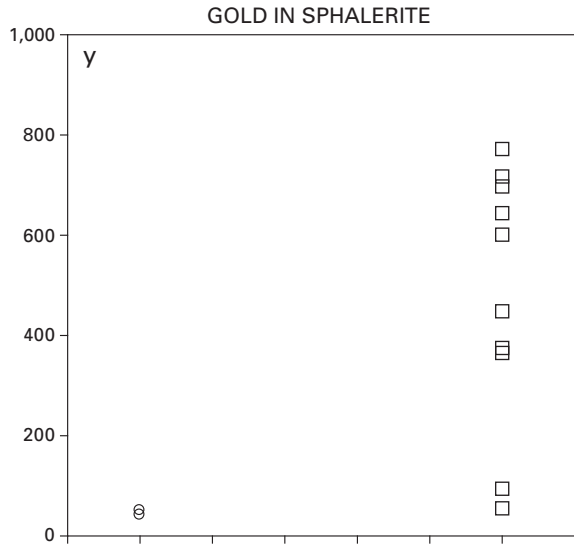
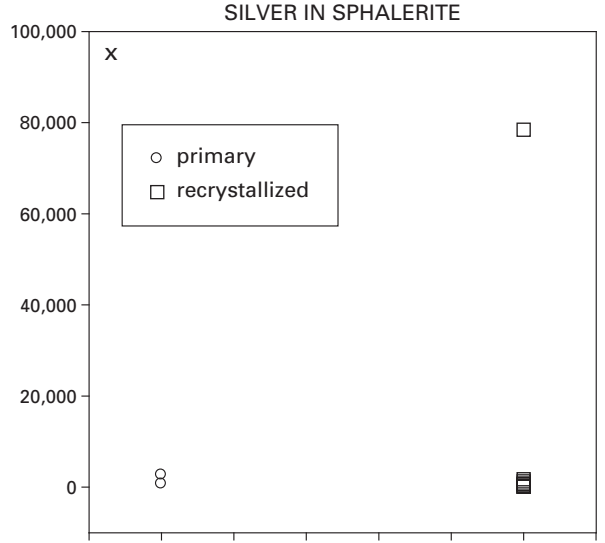
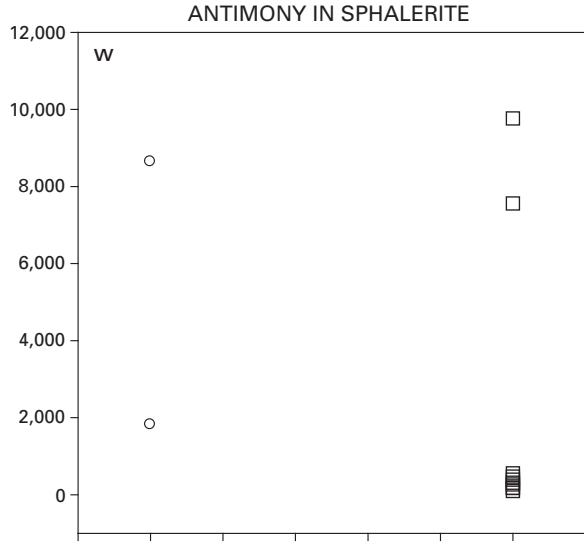


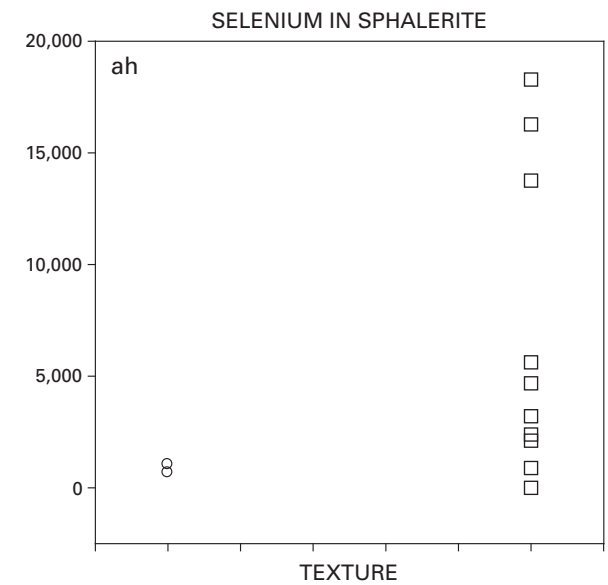
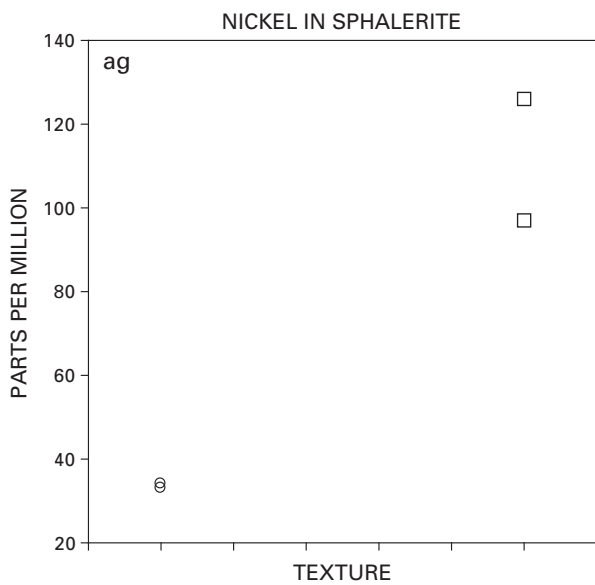
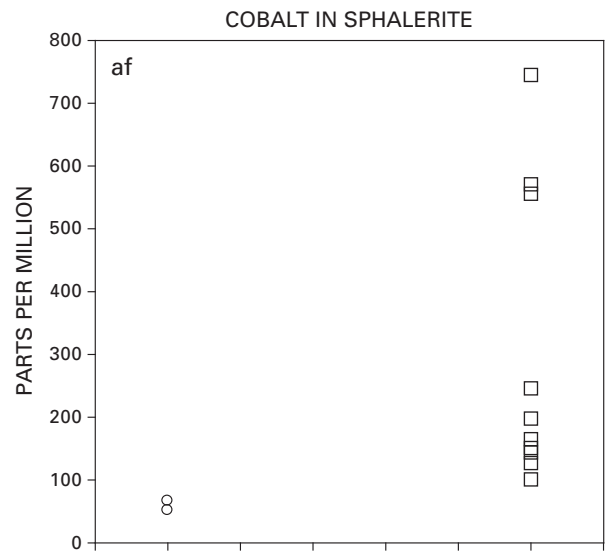
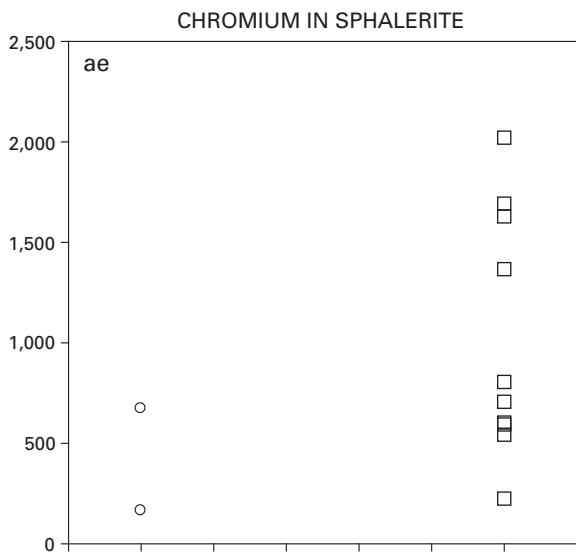
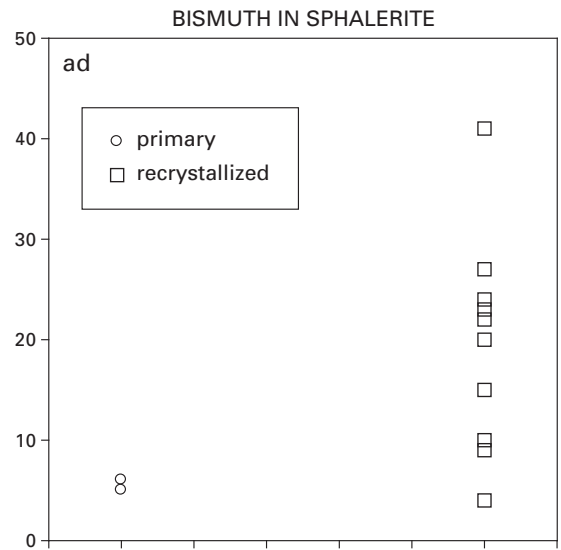
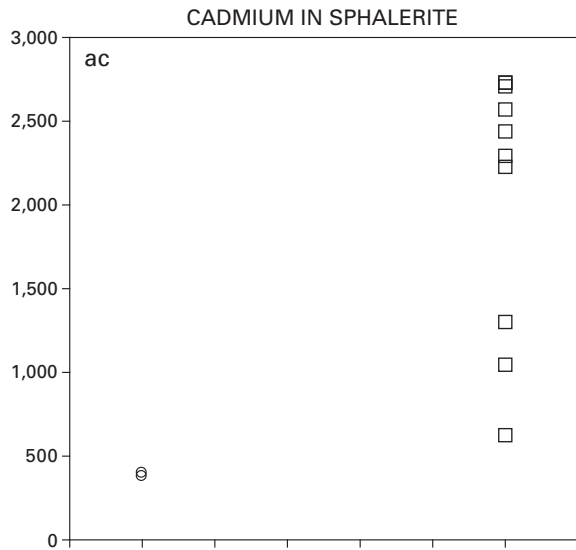
COPPER IN SPHALERITE

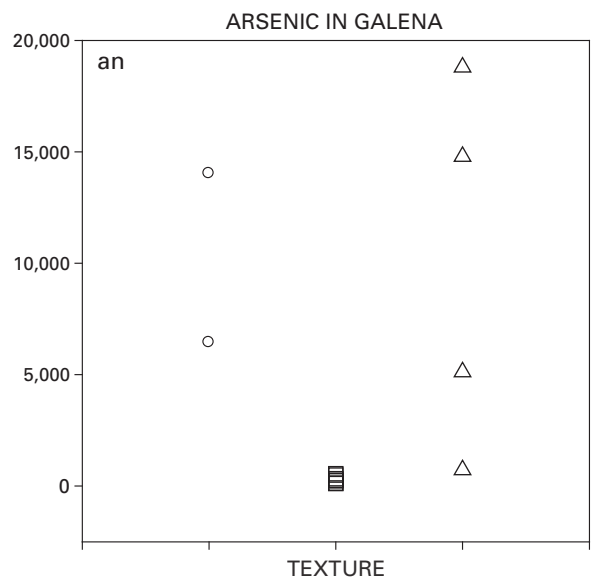
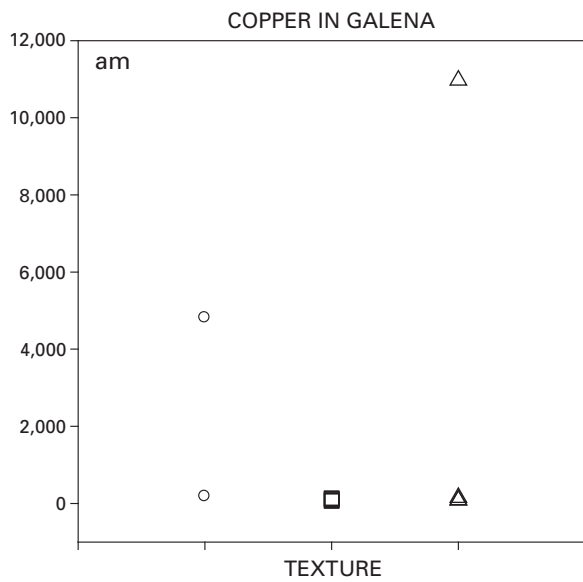
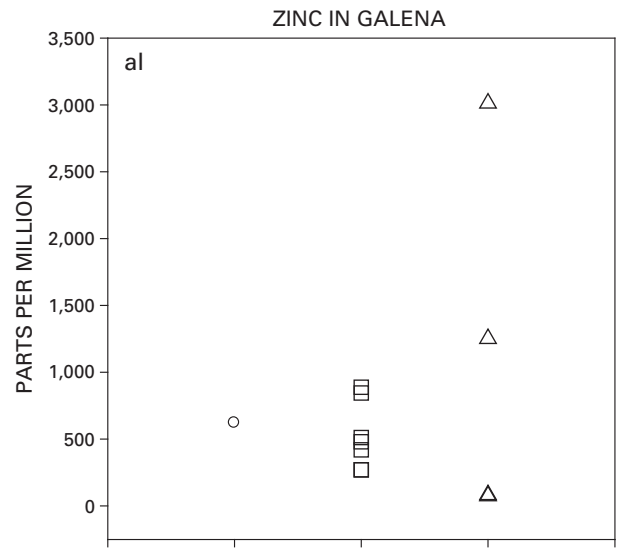
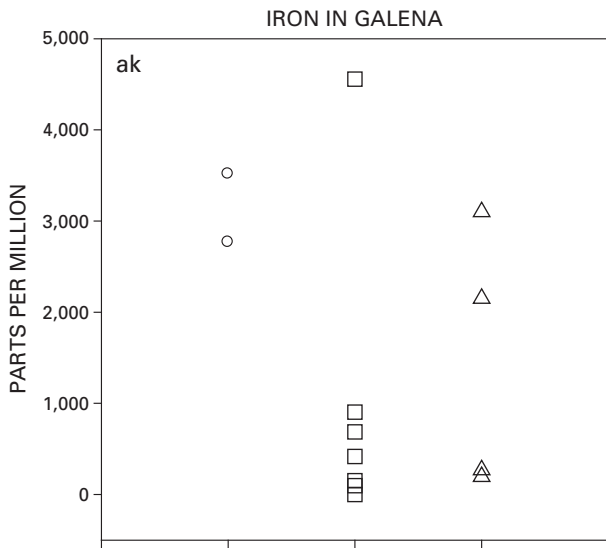
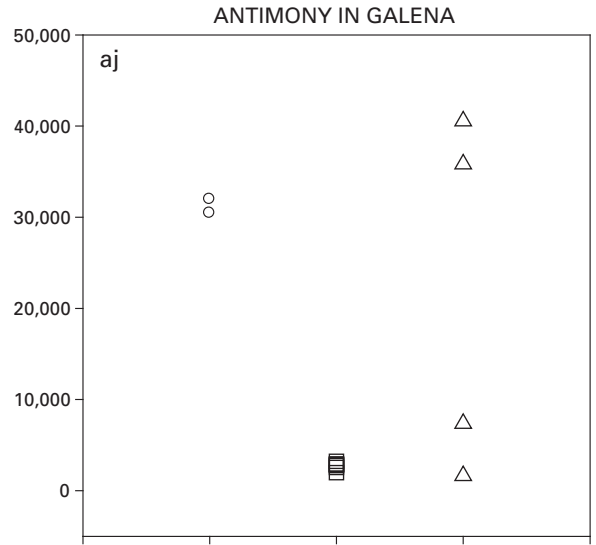
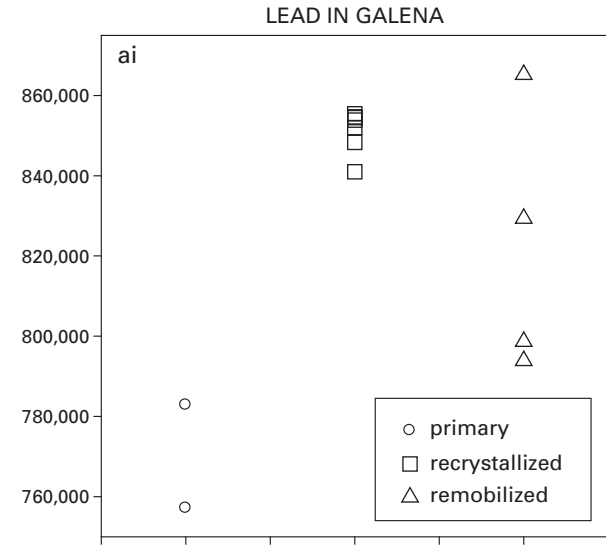


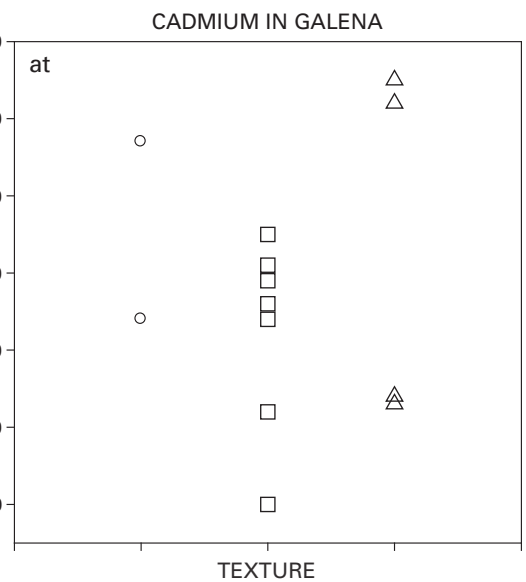
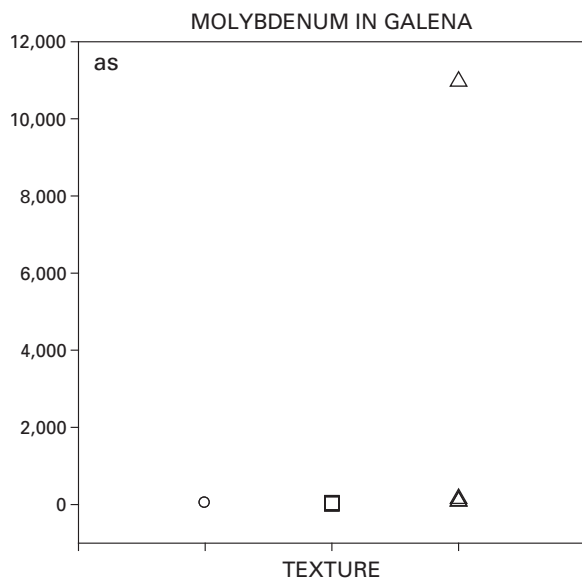
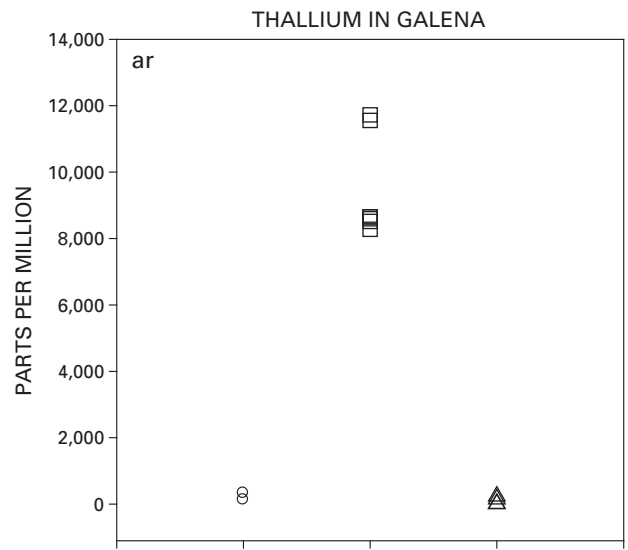
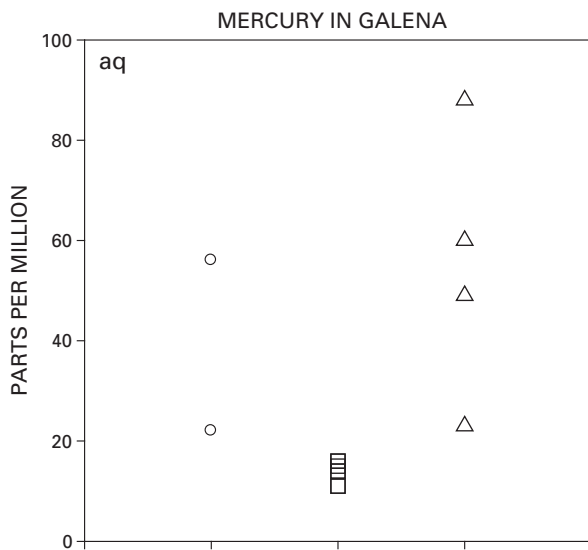
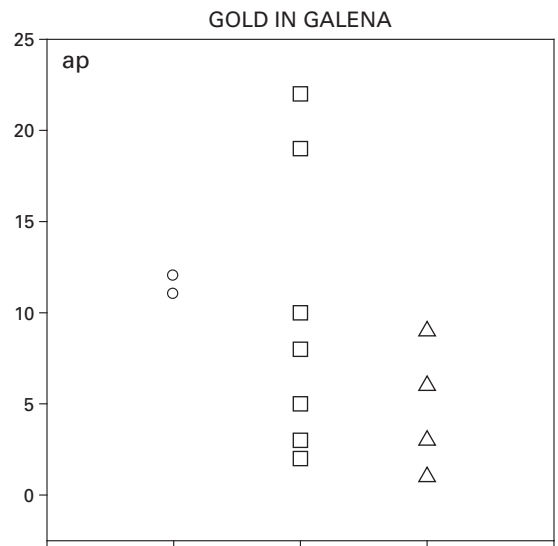
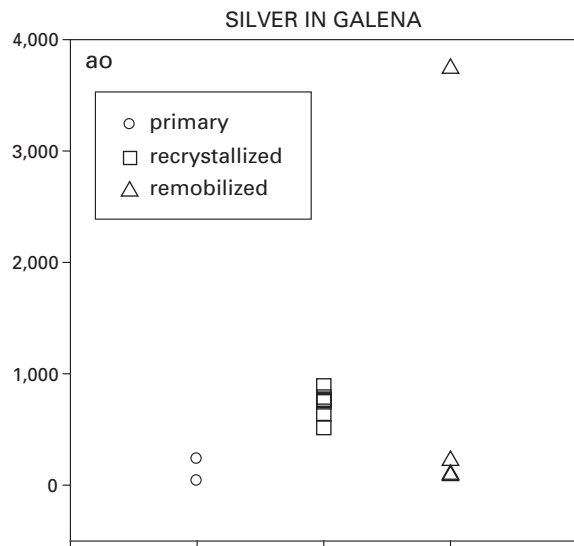
ARSENIC IN SPHALERITE

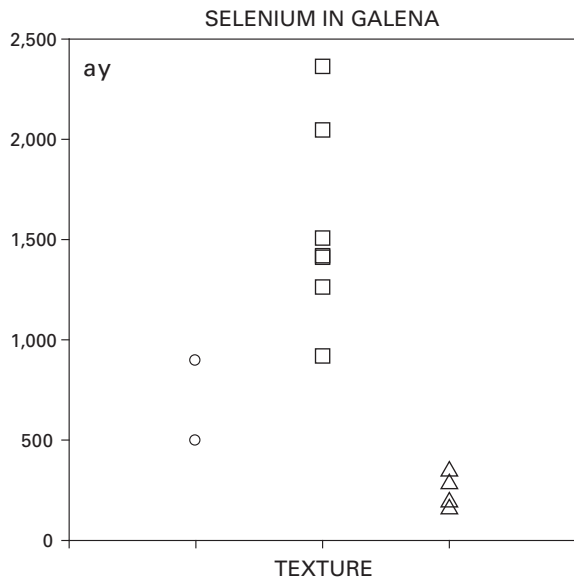
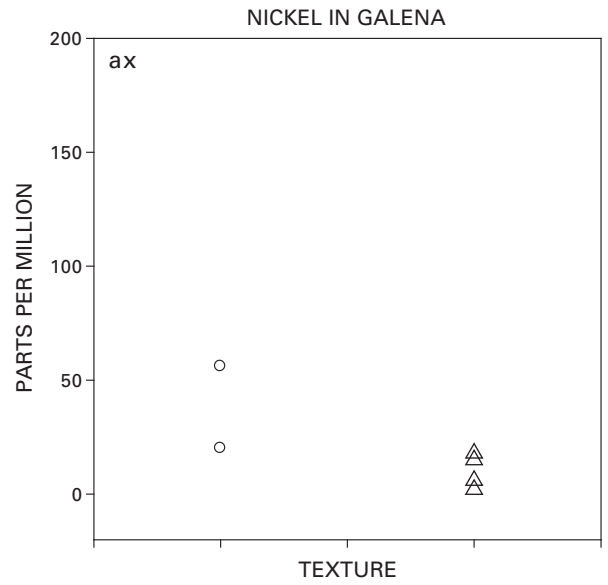
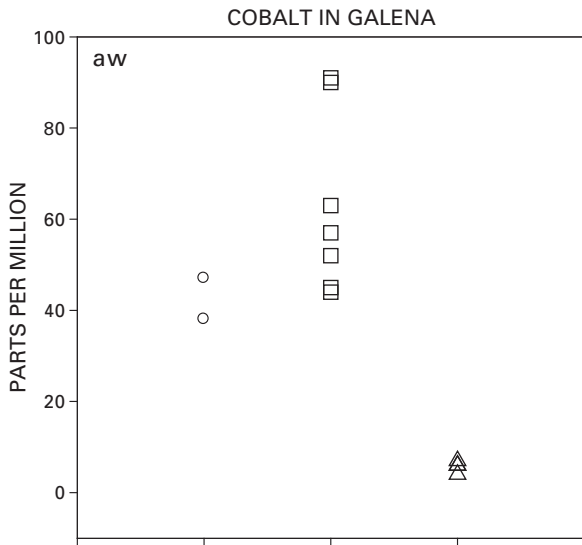
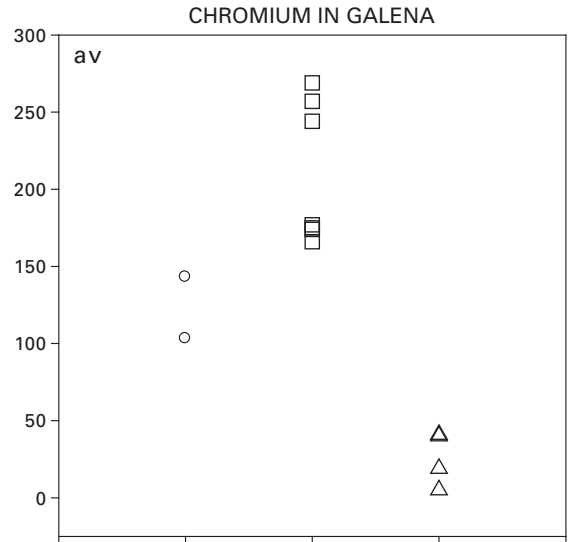
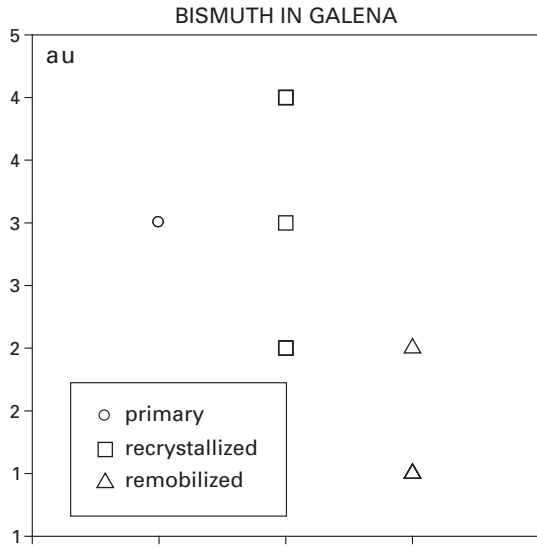












Discussion

There are a number of mineralogical, textural, and geochemical features of the ores as described herein that bear directly on elucidating the genetic processes of formation leading to the Greens Creek deposit and its subsequent modification during regional deformation. We will concentrate first on characteristics of the primary ores and whether their textures and geochemistry yield useful information regarding their origin. We will then discuss the subsequent deformation of the ores and whether specific textures are indicative of the timing or physical parameters of the deformation event. Finally, we will look at the nature and the extent of both solid- and liquid-state remobilization of minerals and metals in the ores and the effect of remobilization on the distribution and grade of the ores.

Pyrite provides the most complete textural record of mineral formation and subsequent modification due to its ubiquity in all ores and host rocks throughout the deposit and as the hardest ore mineral, as indicated by its resistance to texture-obliterating plastic deformation. The paragenetically earliest pyrites have framboidal and colloform banded textures with layers of sphalerite, galena, tetrahedrite, and probably other complex lead-antimony sulfides, and dendritic textures. These textures are preserved in relatively undeformed blocks of massive pyritic ore or in clasts within blocks of MFP that display abundant evidence of brittle failure and cataclasis. Similar textures are commonly preserved in ancient massive sulfide deposits and are usually referred to as primary depositional textures that are taken as evidence of ore deposition on or near the sea floor as a result of rapid cooling and mixing of a hydrothermal fluid with cold seawater (Leitch, 1981; Eldridge and others, 1983; Yui, 1983; McClay, 1991; Craig and Vokes, 1992; Gaspar and Pinto, 1993; Larocque and Hodgson, 1995; Hannington and others, 1999). Numerous observations of identical textures forming in active sea-floor systems worldwide (Graham and others, 1988; Koski and others, 1988, 1994; Paradis and others, 1988; Binns and others, 1993; Halbach and others, 1993; Duckworth and others, 1995; Knott and others, 1995; Krasnov and others, 1995) would seem to confirm the sea-floor origin of such textures.

Detailed studies of active systems, however, indicate that a substrate is necessary upon which such primary textures form by replacement of amorphous silica and cementation of porosity. Two likely substrates include a biotic framework of tubeworms and filamentous bacteria (Knott and others, 1995; Juniper and others, 1992) or a porous boxwork of silica-anhydrite-barite formed by early low-temperature venting of fluids (Haymon, 1983). Once a substrate is established, sulfide mound growth occurs within this substrate initially by constructional growth of spheroidal, colloform, and dendritic pyrite with lesser sphalerite and galena, and then by replacement of the early colloform textures by euhedral forms. Growth of the sulfide body proceeds by high-temperature replacement of previously formed lower temperature phases

and outward metal displacement or "zone refinement." Even the earliest formed sulfides in most active sea-floor massive sulfides form by replacement processes and rapidly evolve to exhibit euhedral mineral textures. Therefore, the earliest mineral textures at Greens Creek likely represent formation beneath the sediment/water interface.

An additional feature of the primary mineral textures at Greens Creek indicates that the hanging-wall shales were being deposited early in the ore-forming process. We note that the majority of the primary-textured pyrite that has survived metamorphism exhibits polyframboidal and spongy pyrite textures. These textures suggest that large masses of MFP were formed by coalescence of framboids and infilling of porosity by precipitation of additional pyrite. Because true framboids are generally thought of as products of early iron sulfide diagenesis in sediments, their presence as the major precursor to spongy-textured massive pyrite indicates the shales were in place and undergoing early diagenesis during the main-stage ore-forming event. True framboids are distinguished from the colloform- and spheroidal-textured sulfide grains commonly seen in both modern and ancient massive sulfides by their characteristic raspberry-like appearance. They typically consist of spherical aggregates, 5–40 mm in size, of 0.2–5-mm pyrite crystallites. Crystallites exhibit ordered or disordered packing with intercrystallite spaces left void or infilled with later sulfides, quartz, and(or) carbonate (England and Ostwald, 1993). The presence of abundant framboids in all Greens Creek ores with relict primary texture is consistent with the sulfur, carbon, and oxygen isotope data that support the origin of the main stage ores by biogenic sulfate reduction in and beneath an accumulating shale cap (chaps. 8, 10).

Direct evidence of widespread replacement of shales by sulfide minerals is generally lacking. This may indicate that growth of main stage ore happened primarily at the phyllite/argillite contact or by inflation of a previously formed silica-barite-sulfide framework, as is often indicated for actively forming systems today (Haymon, 1983; Paradis and others, 1988; Binns and others, 1993; Petersen and others, 2000). Another possibility is that we do not have the undisturbed mesoscale exposures necessary to observe sulfide replacement fronts in the hanging-wall shales at the margins of the ore-bodies. In general the ore/hanging-wall contact is sharp, but in many places the sulfide content of the argillite is gradational over several meters. The ore/hanging-wall contact is commonly a zone of strong deformation due to the tendency for the shales to accommodate strain and the usual superposition of the shales against the ductile massive base-metal-rich ores. The MFBs at this contact are generally tectonically banded with near-complete destruction of primary textures, and the ore/argillite contact can be a slip surface exhibiting graphite-rich, polished gouge. Thus, direct observational evidence for sulfide replacement of argillites is inconclusive.

We suggest, based largely on ore stratigraphic and geochemical considerations, that the earliest mineral precipitation at Greens Creek was exhalative, silica-barite-carbonate-rich material that acted as the substrate within which the later,

main-stage massive sulfide grew. Discontinuous massive and debris-flow carbonate units in the immediate footwall exhibit both nodular-colloform pyrite and late dolomite cement textures that are indicative of diagenetic and epigenetic formation in fractures and dissolution cavities. These features, reminiscent of mineral textures common in Mississippi Valley-type (MVT) deposits (Leach and Sangster, 1993), demonstrate that hydrothermal fluids traversed through the carbonates on route to the site of ore formation. Primary textures similar to those observed in the MFPs are occasionally preserved in the more competent WSIs and support the idea that growth of main-stage mineralization occurred primarily by sulfide replacement of the white ores. Additionally, the association of occasional grains of free gold and electrum and elevated precious metal grades within these WSIs supports the suggestion that the early fluids were hydrogen sulfide and precious metal rich and base metal poor. The absence of well-developed WCAs and WBAs directly beneath proximal accumulations of WSI and MFP and the presence of these barite-carbonate-rich white ores beneath and lateral to massive sulfide ores in distal portions of the mine further indicates that main-stage ore transgressed and obliterated much of the early white ores. The less competent WCAs and especially the WBAs usually do not preserve evidence of primary mineral textures.

Several features suggest that as main-stage massive sulfide mineralization progressed, the Greens Creek system went through a process of zone refinement as described in many ancient and modern VMS systems (Eldridge and others, 1983; Goldfarb and others, 1983; Huston and Large, 1989; Large and others, 1989; Hannington and others, 1986; Petersen and others, 2000). Most compelling is the typical pattern of metal zonation observed at Greens Creek. Where the complete ore stratigraphy is present, metal zonation progresses from proximal copper-gold-arsenic rich, to zinc-lead-silver rich, to more lead, silver, and gold-enriched zinc-lead-silver ores at the margins. Such a pattern is identical to that expected due to selective remobilization of metals by a hydrothermal fluid from the interior of a growing sulfide accumulation, transport of metals toward the margins of the accumulation, and reprecipitation along a temperature-solubility gradient (Huston and Large, 1989). Thus, despite considerable subsequent remobilization of metals and deformation of the ores as a result of the Cretaceous metamorphism, we believe Greens Creek preserves an original mineral and metal zonation that is attributable to early sulfide replacement and zone refining within a growing sulfide accumulation.

A more circumstantial feature indicative of zone refinement is indicated by early replacement textures within proximal, primary-textured ores. In the proximal copper-rich ores of the Northwest West orebody, chalcopyrite has been found replacing pyrite within concentrically banded spheroids and colloform pyrite-sphalerite-galena-rich structures (fig. 5G). Close examination shows that chalcopyrite cuts across banding and engulfs remnants of other sulfide minerals, demonstrating that the paragenetic order of chalcopyrite succeeds the primary-textured sulfides. Similar observations have been used to establish the paragenetic position of chalcopyrite in the

undeformed ores of the Kuroko deposits (Eldridge and others, 1983). Also, in one instance, framboidal-textured crystallites of chalcopyrite occur within a pyrite matrix that is surrounded by dolomite (fig. 10C). This sample may represent a rare case of primary chalcopyrite framboids. However, if all modern framboids are composed of pyrite (England and Ostwald, 1993), then this occurrence demonstrates replacement of pyrite by chalcopyrite. Replacement must have occurred prior to metamorphism and probably during the zone-refining stage.

Euhedral arsenian pyrite and arsenopyrite crystals in proximal MFPs (figs. 7A–F) appear to be another textural feature that occurs as a secondary modification of primary ores prior to metamorphism. When present, arsenian pyrite is always in spatial association with primary-textured pyritic ores and tends to be concentrated along the margins of, or in passageways through, areas of massive sulfide where original porosity would have been greatest. It always exhibits unstrained subhedral to euhedral shapes, does not show a preferred orientation, and is generally clean and free of inclusions of other minerals. Elevated nickel, arsenic, and gold contents of the arsenian pyrite suggest a high-temperature metal association (for example, note similarity to the high-temperature metal assemblage at Kidd Creek in Hannington and others, 1999) as does the generally proximal position of these arsenic-rich pyritic ores and their close association to chalcopyrite-rich MFPs with elevated copper-gold contents. Thus, arsenian pyrite appears to have formed in the high-temperature proximal areas of the deposit by replacement of trace-element-rich, primary-textured pyrite. Though we cannot demonstrate conclusively that arsenian pyrite is not a product of metamorphic remobilization of constituents out of the primary ores, the lack of (1) strained crystals, (2) location in pressure shadows, or (3) evidence of solution creep, suggests formation after the primary ores in areas unaffected by metamorphism. Additionally, the observation that some of the most ^{34}S -depleted sulfur isotope values are from arsenian pyrite-rich ores (see chap. 10) is consistent with formation when supply of isotopically light sulfur from the hanging wall was at a maximum, presumably during main-stage ore formation. The extreme $\delta^{34}\text{S}$ depletion of the arsenic-rich ores also demonstrates the lack of a homogenized sulfur isotope signature that might be expected of a sulfide produced as a result of metamorphic remobilization and further demonstrates the association of light sulfur with the main-stage massive sulfides (chap. 10). Koski and others (1994) document the formation of arsenopyrite-lollingite “fronts” during zone refining of black smoker chimneys in the Escanaba Trough.

One of the most interesting textural features of the primary-textured ores is the abundance of pyrite framboids, polyframboids (rogenpyrite), nodules, and a variety of spheroidal and atoll-shaped structures that appear to be modifications of originally framboidal grains. Collectively, these features provide strong evidence for the concurrence of main-stage ore formation at Greens Creek with the accumulation and early diagenetic history of the hanging-wall sediments. Examination of polished thin sections provides evidence for a complete textural evolution from early

framboidal and colloform features, through intermediate stages where coalescence of atoll-shaped and spheroidal aggregates occurs, to a final spongy-textured pyrite stage with abundant inclusions of other ore and gangue minerals. Such an origin and evolutionary process has been described by England and Ostwald (1993) for syngenetic and vein-type massive sulfides of the Lachlan Fold Belt of Eastern Australia. Several points emphasized in their work have significance for the origin of such textures at Greens Creek. First, they conclude that the presence of framboids and subsequently derived atoll structures is indicative of early diagenetic processes in anoxic sediments. Second, they suggest that the recrystallization and crystal growth of polyframboid aggregates and the subsequent development of atoll structures requires the presence of a gel-like substance such as colloidal silica, chalcopyrite gel, or other base-metal-sulfide gels through which iron and sulfur can diffuse to the framboidal growth centers. If England and Ostwald (1993) are correct, the presence of framboid-derived textures at Greens Creek constitutes additional compelling evidence for our suggestion that the main-stage ores formed predominantly during and after deposition of the hanging wall, that is, during early diagenesis. If a gel-like medium is required for the diffusion of iron and sulfur into polyframboid aggregates to create atolls and spongy-textured massive pyrite, this implies that diffusion of other metals also may occur at this time and has important implications for the zone refinement process. Simply based on mineralogical and textural observations, the process of framboid agglomeration, coalescence, and recrystallization described herein appears to result in a migration of base metals out of the predominantly pyritic masses. This results in spongy pyritic masses with elevated copper, arsenic, and gold and a spatial association with euhedral arsenian pyrite, which we previously suggested is a product of zone refinement. It seems reasonable that the zone-refinement process would be facilitated if the process occurred within a growing sulfide accumulation that was partially colloidal gel and partially a crystalline silica-sulfide framework, and by the presence of unlithified sediments. Perhaps the presence and coalescence of framboid-derived textures at Greens Creek and other massive sulfide deposits represent textural evidence of a zone-refinement process and link the timing of ore formation to early diagenesis of the enclosing sediments.

In the massive sulfide ores studied by England and Ostwald (1993), chalcopyrite was the major phase associated with the more evolved framboid-derived pyrite textures, leading these workers to suggest chalcopyrite gel was the primary diffusion media. We note that at Greens Creek chalcopyrite only rarely occurs in association with framboid-derived structures and then only as a clearly replacive and (or) infilling phase. However, in all cases where atoll-shaped grains occur, they are associated with other base-metal sulfides such as sphalerite, galena, tetrahedrite, and probably other more complex lead-antimony sulfides. The association of atolls with base-metal-sulfide matrix is consistent with the suggestion of England and Ostwald (1993) that the presence

of a gel-like diffusion media is required for the growth of more texturally evolved pyrite structures.

We also note the abundant documentation of the zone-refinement process in chimney structures on the modern sea floor (Graham and others, 1988; Paradis and others, 1988; Krasnov and others, 1995; Duckworth and others, 1995; Knott and others, 1995; Petersen and others, 2000). Many of these chimneys occur in nonsedimented settings or project well above any sediment cover. Clearly these examples demonstrate that early diagenetic processes in enclosing sediments are not a requirement for zone refinement to occur. However, these do not invalidate the notion that zone refinement may be enhanced by the presence of gel sulfides in the porous framework of the chimneys.

Also, we note that although spherical, framboidlike textures are described in the modern sea-floor sulfide literature and that true framboids have been documented from a wide variety of massive sulfide deposit types, including veins, and VMS deposits not associated with sediments (Leitch, 1981; Eldridge and others, 1983; England and Ostwald, 1993; Hannington and others, 1999), they are far more ubiquitous in deposits associated with sediments such as MVT, SEDEX lead-zinc, and sedimentary copper deposits (Schouten, 1946; Croxford and Jephcott, 1972; Chen, 1978; Leach and Sangster, 1993; Large and Walcher, 1999). A literature search also indicates that, while spheroidal and colloform textures are common in modern massive sulfides, true framboids are described only from sediment-covered sites (Koski and others, 1988, 1994; Peter and Scott, 1988). We suggest that true framboids are relatively uncommon in nonsediment-associated modern and ancient massive sulfide deposits and that when present, they indicate early diagenetic mineral formation. The presence of framboid-derived textures at Greens Creek and in numerous other, more typical VMS deposits suggests that early diagenetic ore formation may be more common than has been previously recognized. The presence of true framboid-derived textures is not common in most VMS and is ubiquitous in SEDEX (sedimentary exhalative) deposits, reflecting the diagenetic origin of most of the latter.

While the textures described above are striking and provide us with information regarding the earliest events at Greens Creek through possibly late diagenetic modifications to the ores, they represent only about 30 percent of the deposit and are skewed heavily toward features in pyritic ores. Most of the deposit shows the effects of Cretaceous metamorphism and polyphase deformation that was destructive to primary ore textures. In general, sulfide textures in the metamorphosed ores are characterized by cataclasis, annealing recrystallization, pressure solution, and solution creep that are consistent with lower greenschist facies dynamic metamorphism (Cox, 1987; Gilligan and Marshall, 1987; Marshall and Gilligan, 1987). Intramineral translocation and diffusional features such as dislocation glide, kinking, twinning, nabbarro-herring creep, and coble creep, indicative of deformation at higher metamorphic grades, are absent or have not been observed. None of the various etching techniques useful for elucidating such textures were used during the course of this study.

As previously mentioned, pyrite, due to its hardness, exhibits the greatest range of mineral textures. The most obvious and widespread pyrite texture that can be attributed to deformation of the deposit is the abundant instances of cataclasis exhibited by the more competent MFP ores. Especially where gangue silica content is high, large blocks of MFP have acted as deformation-resistant buttresses around which the softer ores and host rocks have flowed. When deformation does occur, it is usually manifested by brittle failure, resulting in a cataclastic breccia composed of angular, primary-textured pyrite clasts in a matrix of smaller pyrite fragments and ductile sulfides. In cases where deformation has shattered and transposed the MFP enough to impose a fabric, pyrite clasts of widely varying size become strung out in cataclastic trails. Clasts in these strings commonly exhibit pressure shadows filled with galena, tetrahedrite, chalcopyrite, and gangue minerals. In cases where the primary-textured fragments are precious metal enriched, pressure shadows can be occupied by native gold, electrum, pyrargyrite, and other exotic secondary silver minerals. Another brittle failure texture commonly seen in association with cataclastically deformed pyritic ores is intragranular extension microfractures in pyrite crystals that also become filled by secondary remobilized phases.

The other dominant texture present in pyrite as well as in base-metal sulfides is annealing recrystallization. As with the gradational development described above for the production of spongy pyrite, the annealing recrystallization produced a spectrum of textures. In incipient stages, the texture is characterized by inclusion-free areas in otherwise spongy-textured pyrite masses. Intermediate stages are characterized by masses of relatively clean, inclusion-free pyrite with subhedral grain boundaries. When other minerals are present, they occur within the clean pyrite as rounded, irregular inclusions or as fillings within extensional microfractures. We also have observed more advanced stages of framboid-derived atoll-shaped structures as described by England and Ostwald (1993). Relict rounded shapes within otherwise clean, monomineralic pyrite (figs. 6B, 10E) are common, as are euhedral-crystal-shaped sphalerite-, galena-, or tetrahedrite-filled growth zones (atolls) within subhedral to euhedral pyrite grains (figs. 6J, K; 10D, G). The presence of such textures in ores that show evidence of progressive metamorphism seems to confirm the suggestion of England and Ostwald (1993) that additional heat energy beyond that supplied during diagenesis is required to develop advanced atoll-shaped textures in sulfides. In their most advanced textural state, fully annealed pyritic ores exhibit the typical close-packed polygonal grain-boundary shapes (foam texture) commonly seen in higher grade metamorphosed massive sulfides. At this stage of deformation the pyritic ores are monomineralic with the exception of remobilized minerals that occupy late veinlets and extension microfractures (figs. 6F, 10H).

With the exception of the minor amounts of sphalerite, galena, tetrahedrite, and chalcopyrite that appear as bands, infillings, and matrix in the primary-textured ores, 95 percent of these minerals exhibit either recrystallization

or remobilization textures. Of the base-metal sulfides, only sphalerite displays subhedral to euhedral crystal development, probably as a result of annealing recrystallization. When present, subhedral to euhedral crystals of sphalerite (fig. 6L, M) occur usually in a galena matrix or in a mixed base-metal-rich assemblage of annealed (?) sphalerite-galena-tetrahedrite-(pyrite). In extremely high grade zinc-rich MFBs (fig. 3C), nearly monomineralic aggregates of sphalerite have formed that exhibit rounded and bulging grain boundaries with anhedral galena. The prominence of recrystallization, as opposed to ductile flow, as a major process in Greens Creek ores is difficult to assess. The near universal absence of the characteristic triangular cleavage pits common to unstrained galena may be indicative of widespread recrystallization.

The complete absence of euhedral or even subhedral crystal shapes of tetrahedrite, chalcopyrite, and in most cases galena suggests that their occurrence in Greens Creek ores is largely the result of either physical (solid state) or chemical (fluid state) remobilization. The ubiquitous occurrence of these three minerals in extension microfractures and in pressure shadows of harder grains supports this contention. In well-banded MFBs it appears as though the primary means of mineral layer segregation is by ductile flow of the softer sulfides. Similarly, some fractures appear to have ductile sulfides injected into the open space. In such cases, quartz, dolomite, or other gangue minerals do not accompany the physically remobilized phases.

Instances of fluid-state remobilization over distances of millimeters to several meters are much more prevalent and easier to document. In such cases, grains of tetrahedrite, galena, chalcopyrite, and especially pyrargyrite and other exotic silver minerals clearly occupy veinlets (figs. 6Q, R; 5A) and veins that cut the massive ores. Fluid-state remobilization also appears to cause remobilization and concentration of free gold and electrum into late quartz veins and silica-flooded WSIs.

Overall, the process of metamorphic recrystallization and micro- to mesoscale remobilization of primary-textured ores has a visible (fig. 10I) as well as geochemical cleaning effect. As determined by LA-ICP-MS analyses, the relatively uniform low-level concentrations of trace elements in the primary-textured ores is consistent with redistribution of trace elements into predictable mineral phases based on free energy considerations. Specific trace elements are selectively partitioned into specific secondary mineral phases based on the size of the trace-element cations that are expelled from the trace-element-rich and poorly ordered primary ores into the appropriate-sized lattices of new phases. Thus, recrystallized sphalerite has high cadmium and mercury content but very low antimony and silver content, whereas remobilized tetrahedrite displays the opposite relationship. This metamorphic cleaning of primary ore and remobilization of metals into new mineral assemblages is a feature that has been documented at other massive sulfide deposits in metamorphic terranes (for example, the Sulitjelma deposit, Norway, Cook, 1996; nickel deposits of the Yilgarn craton, Australia, McQueen, 1987; Marshall and others, 2000).

Conclusions

The mineralogy, mineral textures, and mineral geochemical relationships at Greens Creek present the relatively unusual case of a trace-element-rich polymetallic massive sulfide deposit that has been subjected to partial metamorphic modification at low to moderate grade. The resulting array of textures spans the range from pristine primary features that provide insight into the genetic origins of the deposit through completely recrystallized and remobilized metamorphic features that provide an excellent opportunity to document the textural and chemical evolution of the deposit during its subsequent diagenetic and metamorphic history.

We believe that textures preserved in the primary ores exhibit an overwhelming preponderance of features attributable to formation of main-stage sulfide mineralization during early diagenesis of the accumulating hanging-wall sediments. These framboidal, colloform, and nodular pyrite textures also appear to preserve an early phase of coalescence and replacement, possibly enhanced by colloidal base-metal-sulfide gels, that marks the textural development of zone refinement in the growing sulfide accumulation. Subsequently, these same textures were modified to varying degrees by at least two periods of deformation related to the Cretaceous dynamic metamorphism that affected the region. This resulted in the continued development of more advanced atoll-shaped textures at the expense of polyframboid aggregates and spongy-textured pyrite. Progressive metamorphism of most of the ores resulted in recrystallization and remobilization of minerals and trace elements. The major effect of metamorphism was mineralogical cleaning of the ores resulting in redistribution and local upgrading of specific metals into predictable and more stoichiometrically ordered minerals.

References Cited

- Binns, R.A., Scott, S.D., Bogdanov, Y.A., Lisitzin, A.P., Gordeev, V.V., Gurvich, E.G., Finlayson, E.J., Boyd, T., Dotter, L.E., Wheller, G.E., and Muravyev, K.G., 1993, Hydrothermal oxide and gold-rich sulfate deposits of Franklin Seamount, western Woodlark basin, Papua New Guinea: *Economic Geology*, v. 88, p. 2122–2153.
- Blackburn, W.H., and Dennen, W.H., 1997, *Encyclopedia of mineral names: The Canadian Mineralogist*, Special Publication 1, 360 p.
- Brew, D.A., Ford, A.B., and Himmelberg, G.R., 1989, Evolution of the western part of the Coast plutonic-metamorphic complex, southeastern Alaska, U.S.A.—A summary, *in* Daly, S.R., Cliff, R.A., and Yardley, B.W., eds., *Evolution of metamorphic belts*: London, Blackwell, Geological Society Special Publication 43, p. 447–451.
- Brew, D.A., Himmelberg, G.R., Loney, R.A., and Ford, A.B., 1992, Distribution and characteristics of metamorphic belts in the southeastern Alaska part of the North American Cordillera: *Journal of Metamorphic Geology*, v. 10, p. 465–482.
- Butler, I.B., and Nesbitt, R.W., 1999, Trace element distributions in the chalcopyrite wall of a black smoker chimney—Insights from laser ablation inductively coupled plasma mass spectrometry (LA-ICP-MS): *Earth and Planetary Science Letters*, v. 167, p. 335–345.
- Chen, T.T., 1978, Colloform and framboidal pyrite from the Caribou deposit, New Brunswick: *Canadian Mineralogist*, v. 16, p. 9–15.
- Cook, N.J., 1996, Mineralogy of the sulphide deposits at Sulitjelma, northern Norway: *Ore Geology Reviews*, v. 11, p. 303–338.
- Cox, S.F., 1987, Flow mechanisms in sulphide minerals: *Ore Geology Reviews*, v. 2, p. 133–171.
- Craig, J.R., and Vokes, F.M., 1992, Ore mineralogy of the Appalachian-Caledonian stratabound sulfide deposits: *Ore Geology Reviews*, v. 7, p. 77–123.
- Croxford, N.J.W., and Jephcott, S., 1972, The McArthur River lead-zinc-silver deposit, NT, *in* Newcastle Conference 1972, Proceedings: Parkville, Victoria, Australasian Institute of Mining and Metallurgy, p. 1–27.
- Duckworth, R.C., Knott, R., Fallick, A.E., Rickard, D., Murtton, B.J., and Van Dover, C., 1995, Mineralogy and sulphur isotope geochemistry of the Broken Spur sulphides, 29°N, Mid-Atlantic Ridge, *in* Parson, L.M., Walker, C.L., and Dixon, D.R., eds., *Hydrothermal vents and processes: Geological Society Special Publication no. 87*, p. 175–189.
- Dusel-Bacon, Cynthia, 1994, Metamorphic history of Alaska, *in* Plafker, G., and Berg, H.C., eds., *The geology of Alaska: Boulder, Colorado, Geological Society of America*, v. G1, p. 495–533.
- Eldridge, S.E., Barton, P.B., Jr., and Ohmoto, H., 1983, Mineral textures and their bearing on formation of the Kuroko orebodies: *Economic Geology Monograph 5*, p. 241–281.
- England, B.M., and Ostwald, J., 1993, Framboid-derived structures in some Tasman fold belt base-metal sulphide deposits, New South Wales, Australia: *Ore Geology Reviews*, v. 7, p. 381–412.
- Gaspar, O.C., and Pinto, A., 1993, Neves-Corvo, a Kuroko type deposit in the Iberian Pyrite Belt: *Resource Geology Special Issue*, no. 17, p. 249–262.
- Gilligan, L.B., and Marshall, B., 1987, Textural evidence for remobilization in metamorphic environments: *Ore Geology Reviews*, v. 2, p. 205–229.

- Goldfarb, M.S., Converse, D.R., Holland, H.D., and Edmond, J.M., 1983, The genesis of hot springs deposits on the East Pacific Rise, 21°N: *Economic Geology Monograph* 5, p. 184–197.
- Graham, U.M., Bluth, G.J., and Ohmoto, H., 1988, Sulfide-sulfate chimneys on the East Pacific Rise, 11° and 13°N latitudes, part I—Mineralogy and paragenesis: *Canadian Mineralogist*, v. 26, p. 487–504.
- Guo, Xun, and Lichte, F.E., 1995, Analysis of rocks, soils, and sediments for the chalcophile elements by laser ablation—inductively coupled plasma mass spectrometry: *Analyst*, v. 120, p. 2707–2711.
- Halbach, Peter, Pracejus, B., and Marten, A., 1993, Geology and mineralogy of massive sulfide ores from the central Okinawa trough, Japan: *Economic Geology*, v. 88, p. 2210–2225.
- Hannington, M.D., Bleeker, W., and Kjarsgaard, I., 1999, Sulfide mineralogy, geochemistry, and ore genesis of the Kidd Creek deposit—Part I. North, Central, and South orebodies: *Economic Geology Monograph* 10, p. 163–224.
- Hannington, M.D., Peter, J.M., and Scott, S.D., 1986, Gold in sea-floor polymetallic sulfide deposits: *Economic Geology*, v. 81, p. 1867–1883.
- Hawksworth, M.A., and Meinert, L.D., 1990, Alteration and fluid inclusion study of the Groundhog mine vein system, Central mining district, New Mexico: *Economic Geology*, v. 85, p. 1825–1839.
- Haymon, R.M., 1983, Growth history of hydrothermal black smoker chimneys: *Nature*, v. 301, p. 695–698.
- Himmelberg, G.R., Brew, D.A., and Ford, A.B., 1994, Petrologic characterization of pelitic schists in the western metamorphic belt, Coast plutonic-metamorphic complex, near Juneau, southeastern Alaska: *U.S. Geological Survey Bulletin* 2074, 18 p.
- Himmelberg, G.R., Brew, D.A., and Ford, A.B., 1995, Low-grade, M_1 metamorphism of the Douglas Island Volcanics, western metamorphic belt near Juneau, Alaska, in Schiffman, P., and Day, H.W., eds., *Low-grade metamorphism of mafic rocks: Boulder, Colorado*, Geological Society of America Special Paper 296, p. 51–66.
- Huston, D.L., and Large, R.R., 1989, A chemical model for the concentration of gold in volcanogenic massive sulphide deposits: *Ore Geology Reviews*, v. 4, p. 171–200.
- Juniper, S.K., Jonasson, I.R., Tunnicliffe, V., and Southward, A.J., 1992, Influence of a tube-building polychaete on hydrothermal chimney mineralization: *Geology*, v. 20, p. 895–898.
- Knott, Richard, Fallick, A.E., Rickard, D., and Backer, H., 1995, Mineralogy and sulfur isotope characteristics of a massive sulfide boulder, Galapagos Rift, 58°55'W, in Parson, L.M., Walker, C.L., and Dixon, D.R., eds., *Hydrothermal vents and processes: Geological Society Special Publication* no. 87, p. 207–222.
- Koski, R.A., Benninger, L.M., Zierenberg, R.A., and Jonasson, I.R., 1994, Chapter 16, Composition and growth history of hydrothermal deposits in Escanaba Trough, southern Gorda Ridge, in Morton, J.L., Zierenberg, R.A., and Reiss, C.A., eds., *Geologic hydrothermal and biologic studies at Escanaba Trough, Gorda Ridge, offshore northern California: U.S. Geological Survey Bulletin* 2022, p. 293–324.
- Koski, R.A., Shanks, W.C. III, Bohrson, W.A., and Oscarson, R.L., 1988, The composition of massive sulfide deposits from the sediment-covered floor of Escanaba Trough, Gorda Ridge—Implications for depositional processes: *Canadian Mineralogist*, v. 26, p. 655–673.
- Krasnov, S.G., Cherkashev, G.A., Stepanova, T.V., Batuyev, B.N., Krotov, A.G., Malin, B.V., Maslov, M.N., Markov, V.F., Poroshina, I.M., Samovarov, M.S., Ashadze, A.M., Lazareva, L.I., and Ermolayev, I.K., 1995, Detailed geological studies of hydrothermal fields in the North Atlantic, in Parson, L.M., Walker, C.L., and Dixon, D.R., eds., *Hydrothermal vents and processes: Geological Society Special Publication* no. 87, p. 43–64.
- Large, Duncan, and Walcher, E., 1999, The Rammelsberg Cu-Zn-Pb-Ba deposit, Germany—An example of sediment-hosted, massive sulfide mineralization: *Mineralium Deposita*, v. 34, p. 522–538.
- Large, R.R., Huston, D.L., McGoldrick, P.J., and Ruxton, P.A., 1989, Gold distribution and genesis in Australian volcanogenic massive sulfide deposits and their significance for gold transport models: *Economic Geology Monograph* 6, p. 520–536.
- Larocque, A.C.L., and Hodgson, C.J., 1995, Effects of greenschist-facies metamorphism and related deformation on the Mobern massive sulfide deposit, Quebec, Canada: *Mineralium Deposita*, v. 30, p. 439–448.
- Latham, E.H., Pomeroy, J.S., Berg, H.C., and Loney, R.A., 1965, Reconnaissance geology of Admiralty Island, Alaska: *U.S. Geological Survey Bulletin* 1181-R, 48 p.
- Leach, D.L., and Sangster, D.F., 1993, Mississippi Valley-type lead-zinc deposits, in Kirkham, R.V., Sinclair, W.D., Thorpe, R.I., and Duke, J.M., eds., *Mineral deposit modeling: Geological Association of Canada, Special Paper* 40, p. 289–314.
- Leitch, C.H.B., 1981, Mineralogy and textures of the Lahanos and Kizilkaya massive sulfide deposits, northeastern Turkey, and their similarity to Kuroko ores: *Mineralium Deposita*, v. 16, p. 241–257.
- Loney, R.A., 1964, Stratigraphy and petrography of the Pybus-Gambier area, Admiralty Island, Alaska: *U.S. Geological Survey Bulletin* 1178, 103 p.

- Ludden, J.N., Feng, R., Gauthier, G., Stix, J., Shi, L., Francis, D., Machado, N., and Wu, G., 1995, Applications of LAM-ICP-MS analysis to minerals: *Canadian Mineralogist*, v. 33, p. 419-434.
- Marshall, Brian, and Gilligan, L.B., 1987, An introduction to remobilization—Information from ore-body geometry and experimental considerations: *Ore Geology Reviews*, v. 2, p. 87-131.
- Marshall, Brian, Vokes, F.M., and Larocque, A.C.L., 2000, Chapter 2, Regional metamorphic remobilization—Upgrading and formation of ore deposits, *in* Spry, P.G., Marshall, B., and Vokes, F.M., eds., *Metamorphosed and metamorphogenic ore deposits: Reviews in Economic Geology*, v. 11, p. 19-38.
- McClay, K.R., 1991, Deformation of stratiform Zn-Pb (-barite) deposits in the northern Canadian cordillera: *Ore Geology Reviews*, v. 6, p. 435-462.
- McQueen, K.G., 1987, Deformation and remobilization in some western Australian nickel ores: *Ore Geology Reviews*, v. 2, p. 269-286.
- Norman, M.D., Pearson, N.J., Sharma, A., and Griffin, W.L., 1996, Quantitative analysis of trace elements in geological materials by laser ablation ICPMS—Instrument operating conditions and calibration values of NIST glasses: *Geostandards Newsletter*, v. 20, p. 247-261.
- Paradis, Suzanne, Jonasson, I.R., Le Cheminant, G.M., and Watkinson, D.H., 1988, Two zinc-rich chimneys from the Plume site, southern Juan de Fuca Ridge: *Canadian Mineralogist*, v. 26, p. 637-654.
- Peter, J.M., and Scott, S.D., 1988, Mineralogy, composition, and fluid-inclusion microthermometry of seafloor hydrothermal deposits in the Southern Trough of Guaymas Basin, Gulf of California: *Canadian Mineralogist*, v. 26, p. 567-587.
- Petersen, Sven, Herzig, P.M., and Hannington, M.D., 2000, Third dimension of a presently forming VMS deposit, TAG hydrothermal mound, mid-Atlantic ridge, 26°N: *Mineralium Deposita*, v. 35, p. 233-259.
- Ridley, W.I., 2000, The ICP-MS laser microprobe—A new geochemical tool: *Trends in Geochemistry*, v. 1, p. 1-14.
- Ridley, W.I., and Lichte, F.E., 1998, Chapter 11, Major, trace, and ultratrace element analysis by laser ablation ICP-MS, *in* McKibben, M.A., Shanks III, W.C., and Ridley, W.I., eds., *Application of microanalytical techniques to understanding mineralizing processes: Reviews in Economic Geology*, v. 7, p. 199-215.
- Schouten, Cornelius, 1946, The role of sulphur bacteria in the formation of the so-called sedimentary copper ores and pyritic orebodies: *Economic Geology*, v. 41, p. 517-538.
- Shibuya, E.K., Sarkis, J.E.S., Enzweiler, J., Jorge, A.P.S., and Figueiredo, A.G., 1998, Determination of platinum group elements and gold in geologic materials using an ultraviolet laser ablation high-resolution inductively coupled plasma mass spectrometric technique: *Journal of Analytical Atomic Spectrometry*, v. 13, p. 941-944.
- Viets, J.G., Leach, D.L., Lichte, F.E., Hopkins, R.T., Gent, C.A., and Powell, J.W., 1996, Paragenetic and minor- and trace-element studies of Mississippi Valley-type ore deposits of the Cracow-Silesia district, southern Poland: *Prace Panstwowego Instytutu Geologicznego*, v. 154, p. 51-71.
- Watling, R.J., Herbert, H.K., and Abell, I.D., 1995, The application of laser ablation-inductively coupled plasma-mass spectrometry (LA-ICP-MS) to the analysis of selected sulphide minerals: *Chemical Geology*, v. 124, p. 67-81.
- Yui, Shunzo, 1983, Textures of some Japanese Besshi-type ores and their implications for Kuroko deposits: *Economic Geology Monograph* 5, p. 231-240.

Sulfur and Lead Isotope Characteristics of the Greens Creek Polymetallic Massive Sulfide Deposit, Admiralty Island, Southeastern Alaska

By Cliff D. Taylor, Wayne R. Premo, and Craig A. Johnson

Chapter 10 of

**Geology, Geochemistry, and Genesis of the Greens Creek Massive
Sulfide Deposit, Admiralty Island, Southeastern Alaska**

Edited by Cliff D. Taylor and Craig A. Johnson

Professional Paper 1763

**U.S. Department of the Interior
U.S. Geological Survey**

Contents

Abstract.....	241
Introduction.....	241
Regional and District Setting	242
Terrane Relationships	242
District Geology.....	242
Deposit Geology.....	243
Mine Sequence Nomenclature and Stratigraphy	243
Ore Types and Ore Mineralogy.....	244
Ore Distribution: Ore-Type Zonation and Metal Zoning.....	245
Previous Sulfur and Lead Isotope Studies	246
Methods.....	247
Lead Isotope Analyses.....	247
Sulfur Isotope Analyses.....	247
Isotopic Data.....	247
Sulfur Isotopes	247
Lead Isotopes	261
Interpretation of Sulfur Isotopes.....	271
Interpretation of Lead Isotope Data	276
Conclusions.....	280
Acknowledgments.....	280
References Cited.....	280

Figures

1. Composite stratigraphic column of the Upper Triassic section at the Greens Creek mine, northern Admiralty Island	243
2. Plan view map of the Greens Creek mine showing the spatial distribution of major orebodies and major structures	245
3. Histogram showing the distribution of all sulfide and sulfate $\delta^{34}\text{S}$ values obtained from the Greens Creek deposit.....	248
4. Greens Creek sulfide sulfur isotope data sorted by: (A) mineral texture, (B) mine location, and (C) type of host rock.....	249
5. Comparison of sulfide sulfur isotope data in footwall versus hanging-wall lithologies.....	260
6. Sulfide sulfur isotope data sorted by mineralogy and ore type.....	263
7. Sulfide and barite sulfur isotope data from host rocks and occurrences elsewhere on Admiralty Island.....	263
8. Plot showing the range of galena lead isotopic compositions from Greens Creek ore and several occurrences on Admiralty Island	268
9. Plot showing the range of lead isotopic compositions of pyrrargyrite and tetrahedrite from Greens Creek ore, and compared to galena from Greens Creek (shaded field) and from several occurrences on Admiralty Island	269

10.	Plot showing the range of lead isotopic compositions of sphalerite and pyrite from Greens Creek ore, and compared to galena from Greens Creek (shaded field) and from several occurrences on Admiralty Island.....	270
11.	Plot showing the range of lead isotopic compositions of pyrrhotite, chalcopyrite, and several ore bands from Greens Creek, and compared to galena from Greens Creek and from several occurrences on Admiralty Island.....	272
12.	Plots showing $\delta^{34}\text{S}$ versus $^{207}\text{Pb}/^{204}\text{Pb}$ and $^{206}\text{Pb}/^{204}\text{Pb}$ isotopic data for ores and sulfides in the Greens Creek deposit and for sulfides from Late Triassic and other mineral occurrences on Admiralty Island.....	273
13.	Figure showing calculated ranges of various major processes of sulfate reduction compared to the histogram showing the range of all sulfide and sulfate $\delta^{34}\text{S}$ analyses from the Greens Creek deposit	275
14.	Plot comparing Greens Creek sulfide lead data with initial lead values at 215 Ma for argillites as well as many of the metabasalts and metagabbros of the area, including other Admiralty Island host rock samples, presumably of the same age.....	277
15.	Plot ($^{206}\text{Pb}/^{204}\text{Pb}$ versus $^{207}\text{Pb}/^{204}\text{Pb}$) showing a comparison of the range of Greens Creek lead isotope values to those from other Alaskan VMS deposits of various ages.....	279

Tables

1.	Greens Creek sulfur isotope data, sample locations, and descriptions for samples from drill core and underground exposures	252
2.	Sulfur isotope data, sample locations, and descriptions for samples from Admiralty Island host rocks and mineral occurrences	258
3.	Uranium-thorium-lead (U-Th-Pb) isotope data, sample locations, and descriptions of ores and sulfide minerals from the Greens Creek mine, and mineral occurrences and host rocks on Admiralty Island.....	264

Sulfur and Lead Isotope Characteristics of the Greens Creek Polymetallic Massive Sulfide Deposit, Admiralty Island, Southeastern Alaska

Cliff D. Taylor, Wayne R. Premo, and Craig A. Johnson

Abstract

Sulfur isotopic analyses were obtained for 221 sulfide mineral separates and bulk ore samples and 14 barite separates taken from the mine workings and underground drill core. Also, 55 sulfide mineral separates and 4 barites from mineral occurrences and country rock elsewhere on Admiralty Island were analyzed. Pyrite $\delta^{34}\text{S}$ values span the range -38 to 2 per mil, and chalcopyrite, sphalerite, and galena values cluster tightly between -11 and -16 per mil. Sphalerite-galena mineral pairs display consistent isotopic fractionations corresponding to an equilibrium temperature of about 300 degrees Celsius. Primary-textured sulfides are generally more ^{34}S -depleted than recrystallized or remobilized sulfides, and the most ^{34}S -enriched values occur in the smaller and more distally located orebodies. On a deposit scale the most ^{34}S -enriched sulfides are near the footwall igneous rocks and white siliceous ores. The progression toward ^{34}S -depleted sulfides roughly follows the ore paragenesis from white ores against the footwall, to massive pyritic, to massive base-metal-rich ores against the hanging wall. Pyrite $\delta^{34}\text{S}$ values in the overlying shales exhibit a wide range of values from -29.0 to 1.1 per mil. Sulfate $\delta^{34}\text{S}$ values fall between 13 and 22 per mil, consistent with global values for Triassic evaporites. The unimodal distribution of both ore-stage pyrite and base-metal sulfide sulfur isotope values suggests a single fluid supply of sulfur from two main sources. The data suggest input of heavy sulfur from the mafic-ultramafic footwall igneous rocks and a dominant source of light sulfur from biogenically reduced seawater sulfate present in pore water and (or) in diagenetic pyrite in the hanging-wall shales.

Seventy-six lead isotopic analyses have been made on 34 sulfides and 9 ores from underground and 15 sulfides from 11 different sites on Admiralty Island. Sulfides analyzed are chalcopyrite, pyrite, sphalerite, galena, tetrahedrite, pyrargyrite, and pyrrhotite. Ore and host-rock lead isotope values indicate derivation of metal from two major sources. Sulfide lead isotopic values define a mixing line on an uraniumogenic plot between a relatively nonradiogenic component similar to slightly enriched E-MOR basalt and a ^{207}Pb -enriched component from an older crustal source. The nonradiogenic end of the mixing

line overlaps the field of Late Triassic age basalts and gabbros. The ^{207}Pb -enriched end is poorly constrained but permissive of lead extraction from the hanging-wall argillites.

Introduction

In this chapter we describe the results of a comprehensive study of the sulfur and lead isotopic characteristics of the Greens Creek ores. We have attempted to sample in such a manner as to allow evaluation of the isotopic variations within the deposit in a spatial as well as temporal/textural context. Thus, we have analyzed all of the major sulfide minerals present in the deposit and have obtained a series of footwall to hanging-wall profiles, primarily in drill core and several underground crosscuts, in each of the six major orebodies of the mine. For each analysis the type of ore or host rock has been noted, as has the primary, recrystallized, or remobilized texture of the sulfide sampled. In a handful of ore samples, two or three coexisting sulfides have been analyzed in an attempt to utilize sulfur isotopes for geothermometry.

Sulfur and lead (Pb) isotopic data on ores can be powerful indicators of the sources of sulfur and metals to the deposit and can help to constrain the possible sulfide precipitation mechanisms that lead to economic ore accumulation. Additionally, if the spatial sampling is sufficient, identification of sulfur isotopic gradients may provide vectors toward thermal centers of fluid upwelling or provide information on the oxidation state and activity of sulfur in the source fluids. Lead isotopic gradients may help identify the proportions of metals contributed to the system from various host rocks. Isotopic variations with respect to ore paragenesis and textural state of the sulfides provide information on how the source fluids and the input of metal to them may have evolved over the lifespan of the system. In the case of the Greens Creek deposit, where lower greenschist facies metamorphism has caused recrystallization and local remobilization of the ores, comparison of isotopic values with respect to sulfide mineral textures provides the opportunity to evaluate the degree to which the isotopic systems may have been reset or modified.

In the following sections we provide brief reviews of the regional and local geology, Greens Creek ore types, mineralogy, and metal zonation in order to provide background for the sulfur and lead isotope discussion that follows. We also review the recent literature for previous sulfur and lead isotope data. We then present the sulfur and lead isotope data obtained from the Greens Creek system as well as a number of other mineralized occurrences elsewhere on Admiralty Island. The regional values are used for comparison of the Greens Creek system to other Triassic-age occurrences on the Island and to contrast the Triassic mineralization against older and younger mineral occurrences. The initial lead-isotope compositions of probable source rocks to the Greens Creek ores are shown in this chapter in the context of the ore lead-isotope systematics. The radiogenic isotopic data on the host rocks and a full discussion of their isotopic character as they relate to petrogenesis and age relationships are presented by Premo, Taylor, and others (chap. 11). Finally, we discuss the data presented in terms of a genetic model for Greens Creek and how it compares with similar data from other major ore districts and deposit types.

Regional and District Setting

Terrane Relationships

Host rocks to the Greens Creek deposit on Admiralty Island are within the Admiralty subterrane of the Alexander terrane (Berg and others, 1972, 1978; Churkin and Eberlein, 1977; see fig. 2 and a more complete presentation of southeastern Alaska terrane relationships in chap. 2). The general evolution of the terrane has been discussed by Samson and others (1989) who suggested, based primarily on whole-rock neodymium-strontium radiogenic isotopic studies, that it has the characteristics of a wholly oceanic island arc (also see chap. 11). The terrane is an allochthonous, continent-sized piece of intraoceanic island-arc crust that began forming in latest Precambrian time in low latitudes. It consists of as much as 35,000 feet of predominantly marine sedimentary and volcanic strata, and plutonic rocks, of latest Precambrian(?) to Middle(?) Jurassic age (Gehrels and Saleeby, 1987; Gehrels and Berg, 1994). Rift-fill stratigraphic sequences and bimodal volcanism along the eastern edge of the terrane (Taylor, 1997; Taylor and others, 1995a and b, 1999a, 2000a) mark the beginning of an extensional tectonic event in latest Triassic time that either split the terrane or separated it from its low-latitude offshore position and transported it to its present position on the western North American continental margin (Gehrels and Berg, 1994). Accretion may have commenced by Early or Middle Jurassic (McClelland and Gehrels, 1990) or Late Jurassic (Saleeby, 1994) and was complete by about middle Cretaceous. Collision resulted in regional metamorphism and deformation related to underthrusting of the margin. This produced relatively flat-lying, northwest-vergent thrust faults identified underground and in

surface outcrops on Admiralty Island (see chaps. 7 and 13). Compilation of regional metamorphic facies by Dusel-Bacon (1994) places Triassic and older rocks on northern Admiralty Island within lower to middle greenschist facies isograds. In early Tertiary time (Goldfarb and others, 1991; Miller and others, 1994), oblique subduction changed to right-lateral transcurrent motion along the margin, imparting the present structural grain to the country rock, and caused the formation of numerous, subparallel, high-angle, strike-slip faults that have dismembered the outboard terranes.

District Geology

The eastern margin of the terrane is marked by a discontinuously exposed, 600-km-long belt of rocks that host numerous polymetallic volcanogenic massive sulfide (VMS) occurrences (see figure 1, inset a in chap. 2), including Greens Creek and Windy Craggy, the most significant VMS deposit in Alaska and the largest in North America, respectively. Stratigraphy within the belt consists of a 200–800-m-thick sequence of conglomerates, limestones, marine clastic sediments, and tuffs that are intercalated with and overlain by a distinctive unit of mafic pyroclastics and pillowed flows (see figure 3 in chap. 2). Faunal data bracket the age of the host rocks between early Carnian (early Late Triassic) and late Norian (middle Late Triassic) time (see chap. 12). Changes in the stratigraphic setting and chemistry of the volcanic rocks from south to north along the belt are accompanied by crude yet systematic changes in the structural appearance, chemistry, and mineralogy of the occurrences. Together, these systematic variations suggest important spatial or temporal changes in the Late Triassic tectonic/metallogenic environment. The geologic setting in the south is consistent with shallow subaqueous emplacement on the flanks of the Alexander edifice. Northward, the setting changes to increasingly deeper subaqueous deposition in an evolving back-arc or intra-arc rift basin (Taylor, 1997; Taylor and others, 1995a and b, 1999a, 2000a, chap. 2).

In the southern end of the belt, felsic volcanic rocks fill the position in the sequence immediately overlying a basal conglomerate. On Annette and Gravina Islands the rhyolites are continuous, massive, flow-banded units with arlike geochemistry. On the Cornwallis Peninsula the Keku Volcanics are approximately 300 meters thick. The position low in the section beneath the overlying mafic volcanics as well as the distinctive peralkaline chemistry of the Keku Volcanics suggest their origins as bimodal volcanics produced during the initiation of rifting. Rhyolites are largely absent north of Keku Inlet, and their place low in the section is occupied by minor basalt flows interbedded with black shales. The occurrence of felsic volcanism prior to basaltic volcanism throughout the southern portion of the belt and the peralkaline composition of the Keku Volcanics are typical features of intra- and back-arc rifts. The transition from calc-alkaline rhyolites to peralkaline rhyolites and finally to basalt northward along the belt is also consistent with a shift from a proximal-arc to an arc-slope or basin

quartz-carbonate-pyrite veined, dark gray to greenish sericite phyllite (SP); and (3) carbonate-pyrite-quartz veined, light to dark green, chlorite phyllite (CR for chloritic rock). Footwall lithologies that have less consistent spatial distribution are: (4) serpentine-chlorite phyllites (SC) and (5) mariposite-phyllites (MP). Rarely, poorly preserved gabbros and post-ore diabase dikes are recognized (Taylor and others, 1999b, 2000a, 2000b; chap. 6).

Hanging-wall rocks are dominated by massive and slaty black argillites (MAs and SAs, respectively). In underground exposures and in hand samples, the MAs are generally dull, very dark gray to black, blocky, and thick bedded. They are composed of very fine silt to mud-sized grains of fine crystalline, organic-rich dolomite, and lesser quartz and feldspar in a matrix of dark organic residue and carbonate (dolomite). The SAs are also dark gray to black but are platy and thin bedded and often have a shine on parting surfaces. In contrast to the MAs, the SAs have fine-grained quartz, feldspar, and muscovite as their major component with lesser fine crystalline organic-rich dolomite in a matrix of dark organic residue. More carbonate-rich variants of these two basic rock types, dolomitic massive and slaty argillites (DMAs and DSAs, respectively), occupy variable stratigraphic positions. These beds represent quiescent periods of carbonate deposition interspersed with dolosiltstone and organic-rich siliciclastic layers characteristic of the distal turbidite sedimentation that formed the MAs and SAs.

A subset of DMAs have the genetically important distinction of being located in the footwall between the phyllites and ore (Taylor and others, 2000a). When present, they occur as a single, discontinuous massive lens of medium to coarse crystalline dolomite, which can contain peloidal textures or even poorly preserved fossil fragments (typically crinoid stems). In a few cases, such footwall DMAs have been observed to contain fragments of the Triassic indicator fossil *Halobia* (J.M. Proffett, oral commun., 1999). Where footwall carbonate bodies grade into white carbonate ore (WCA), the massive dolomite becomes indistinguishable from the hydrothermal quartz-dolomite veins that constitute the majority of the WCAs. Thus, in proximal areas of intense alteration the distinction between a primary, fossil-bearing, depositional carbonate unit and a hydrothermal carbonate body produced during mineralization becomes blurred.

The existence of a thin, discontinuous carbonate platform on the footwall phyllites is an important point both in terms of determining the tectonic setting at Greens Creek just prior to mineralization and providing a time-stratigraphic marker horizon useful for regional correlation. The presence of platform carbonates in the immediate footwall suggests that the depositional environment at Greens Creek just prior to the onset of mineralization was a relatively quiescent, shallow water, marine setting on the flanks of the Alexander edifice. The presence of *Halobia* fragments establishes the age of the carbonate bodies as Norian (Late Triassic) (see chap. 11), consistent with the age of the conodont-bearing layers in the immediate hanging-wall argillites. Additionally, the

stratigraphic position of the carbonate unit low in the sedimentary portion of the Upper Triassic section at Greens Creek is consistent with the stratigraphic position of other similar carbonate units at other Late Triassic occurrences in southeastern Alaska south of Greens Creek (Taylor, 1997; Taylor and others, 1999a, 2000a).

A problematic feature of the footwall at Greens Creek is the discontinuous presence of silicified conglomerates and breccias. When present, they occur as 0–30-meter-thick lenses of dense, white to gray, nonporous accumulations of silicified clasts in a siliceous matrix. The appearance of the clasts suggests that their protoliths were derived primarily from the underlying phyllites and, less prevalently, from the footwall carbonates. Clasts are generally 1–10 cm in size and are distinctly subrounded or subangular, indicating that there may be at least two types of breccias. The first type are polymictic, with subrounded clasts, and are likely conglomeratic breccias that formed as locally derived debris flows in response to the onset of Late Triassic rifting. The second type, subangular breccias that constitute the majority of these footwall accumulations, are monomictic and are spatially associated with the proximal footwall SR lithology. They are probably tectonic breccias produced by fracturing of the SRs after ore formation. A third, less common type of breccia has been observed in a few locations underground. This is a polymictic breccia in the immediate hanging wall that consists of slightly smaller (1–5 cm) clasts of predominantly white quartz pebbles, minor phyllite, and argillite in a matrix of fine to coarse crystalline, subhedral pyrite (also see chap. 7). This breccia, here interpreted as a conglomeratic lens that formed as a debris flow during deposition of the hanging wall, is distinctly different in terms of its stratigraphic position, size and composition of the constituent clasts, and composition of its matrix.

Similar to the footwall carbonates, the breccias have significance both as indicators of the tectonic environment at Greens Creek and as a possible stratigraphic marker horizon. Elsewhere in southeastern Alaska south of Greens Creek the base of the Upper Triassic section is marked by a polymictic conglomerate of local derivation that is thought to mark the onset of Late Triassic rifting. In other locations, this conglomerate is consistently located beneath the lower volcanic member of the Hyd Group, which is in turn overlain by a thin platform carbonate unit. It therefore serves as a correlatable marker horizon at the base of the Upper Triassic section as well as a tectonic indicator of the onset of rifting (Taylor, 1997; Taylor and others, 1999a).

Ore Types and Ore Mineralogy

Ore lithologies at Greens Creek are broken into two main groups: (1) massive sulfide ores and (2) semimassive or disseminated sulfide gangue-rich “white” ores. The massive ores contain greater than 50 percent sulfides and consist of massive, fine- to very fine grained ore in which base-metal sulfides are greater than pyrite (MFB, MVB) and massive, medium- to very

fine grained pyrite-rich ore in which pyrite predominates (MFP, MVP). All the massive ores have variable amounts and proportions of quartz, dolomite, sericite, barite, and fuchsite gangue. Graphite is a less ubiquitous but locally abundant gangue mineral (Taylor and others, 1999b, 2000b).

The white ores are a group of mineralized lithologies that contain less than 50 percent sulfides and are defined by their principal gangue mineral. They commonly contain base metal and spectacular precious-metal enrichments. There are three types: (1) white carbonate ore (WCA) and (2) white siliceous ore (WSI) are most common; and (3) white baritic ore (WBA). The WCAs are characterized by granular-textured, medium- to coarse-grained dolomite. Accessory gangue minerals, as previously mentioned, are present but less abundant than in WSIs. The WSIs are dominated by massive cryptocrystalline aggregates of hydrothermal quartz or chert and regularly contain significant dolomite, sericite, fuchsite, and barite. WBAs are characterized by coarse, sugary, massive barite and other gangue as above. Commonly, they are not ore grade.

All the above ore types include subtypes that are modified by the presence of veins, breccias, and gouge or rubble zones produced during faulting or folding. Veining due to secondary remobilization and accompanying recrystallization during metamorphism can result in spectacular enrichments of free gold and a variety of silver sulfosalt minerals. Breccias appear to be both primary sedimentary breccias produced by slumping of the massive sulfides and inclusion of clasts of the underlying as well as overlying host rocks, and tectonic breccias produced during deformation. Solution brecciation may also be present, particularly in the WCAs. For a more complete presentation of ore types, mineralogy, and ore textures, see chapter 9.

Ore Distribution: Ore-Type Zonation and Metal Zoning

The mineral deposit at Greens Creek (fig. 2) is nearly continuous along the phyllite/argillite contact and consists of three main orebodies—the East, West, and Southwest—and three extensions—the Northwest, 200 South, and 5250. This section is excerpted from chapter 6. See chapter 6 for a more complete presentation. The East orebody outcrops at the Big Sore and is continuous along a north 10°–20° east strike for 920 m to the south. The orebody plunges to the southwest at 20° and dips initially at 60° to 80° to the west and flattens out to near horizontal due to F3 folding. The main Klaus fault bisects the flat, lower portion of the East ore zone so that it appears to form two parallel flat panels. The demarcation line between the East and West orebodies occurs where the ore transitions from the lower flat-lying panel back to near vertical. The width of the East orebody in plan is approximately 460 m with a true thickness of ore of 3 to 12 m.

The West orebody continues to the west beneath the Klaus fault and is subdivided into two subzones and two

extensions: the Central West, and 9A subzones, and the Northwest West and 5250 extensions (fig. 2). The Central West ore zone lies between the East orebody and the Maki fault. The near-vertical portion is referred to as the Wall, which has an average thickness of 3 to 6 m, strikes northwest for 620 m and dips steeply (80° to 90°) to the west for over 90 m of vertical extent. The ore horizon then begins to flatten due to F3 folding. The northern half of the flattened part forms a 3- to 5-meter-thick ore horizon, dipping at 45° to the west, that pinches out to less than 1 m to the north. In the southern half, the intensity of F3 folding is greater and the 2- to 4-m-thick ore becomes flat and then recumbent with 10° to 20° E dips. This band of east-dipping ore forms the upper limb to a nearly isoclinal, recumbent F2 fold. The lower limb is characterized by a marked increase in thickness up to 100 m. The thickened lower limb runs for a strike length of 250 m and varies in thickness from 10 m up to a maximum of 120 m.

The Maki fault marks the transition from the Central West ore zone into the 9A ore zone. The 9A zone is composed of numerous fault blocks of ore, which, when the right-lateral

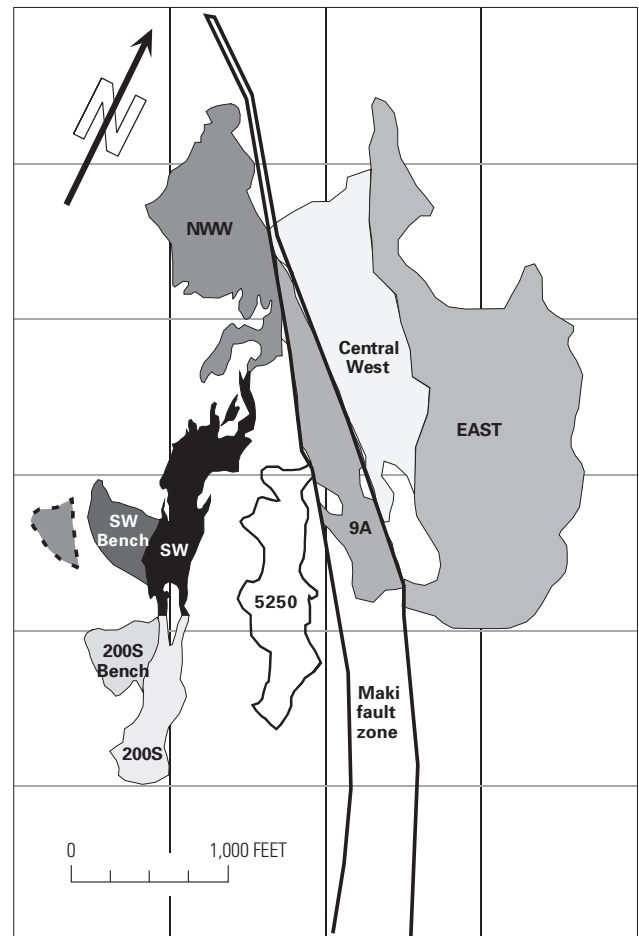


Figure 2. Plan view map of the Greens Creek mine showing the spatial distribution of major orebodies and major structures.

strike-slip motion of the Maki fault zone is removed, represent the continued southwest, down-plunge continuations of the East and Central West ore zone. Individual fault blocks maintain the typical stratabound nature of Greens Creek ores, but detailed structure interpretations are difficult due to complexity of faulting within this zone. The overall strike length of 9A is 600 m with a plan width of 150 m.

The two extensions to the West orebody, the Northwest West and 5250, represent the fault-offset portions of the Central West ore zone and East orebody, respectively. Both zones show the effect of increasing intensity of F2 folding, and the northern 100-m portion of 5250 may be transected by the Klaus fault. The 5250 orebody strikes north-northwest for 550 m and has a plan width of 100 m. To the south, the ore trend becomes more regular with the ore dipping to the west at 60° to 70° and plunging near 20° south. The 5250 zone is atypical of most ore zones at Greens Creek, as the zone contains a high proportion of white baritic ore as compared to the others. The Northwest extension is the dextral fault translation of the Central West. The Northwest shows the continuing development of the F2 folding noted in the Central West. The ore decreases in thickness downdip and to the south from 50 m to less than a few meters. A pair of recumbent F2 folds that form an acute “S” when viewed in cross section dominates the large-scale structure. The upper fold is a west- to northwest-closing syncline (cored by argillite) that lies above an east- to southeast-closing anticline (cored by phyllite) below. The main part of the orebody lies on the lower limb of the syncline.

The Southwest orebody extends from the West/Northwest orebody as a continuation of the trend along the lower F2 fold. The Southwest orebody is subdivided into two zones, the Upper and Lower ore zones, and has one extension, the 200 South. The Upper Southwest ore zone strikes north 20° west for 260 m and has a plan width of 210 m. The Lower Southwest ore zone strikes approximately due north for over 360 m and the main portion of the ore zone has a plan width of 240 m. The vertical extent for the entire Southwest orebody runs from 35 m below sea level to 275 m above with the demarcation line between lower Southwest and upper Southwest being placed at approximately 120 m above sea level.

Exploration downdip and along strike of the Lower Southwest resulted in the discovery of the 200 South extension along strike to the south. The 200 South extension displays the same gross-scale geometry of the Lower Southwest with a steeply dipping eastern limb and a nearly flat-lying western limb. The 200 South extension strikes north 10°–20° west for 340 m. The plan width is 60 m with an additional 140-m width, the 200 South Bench, to the west of the main mass of ore, which is similar to the Lower Southwest thin, flat-lying, SW Bench mineralized trend. The central and upper half of the eastern limb have ore thickness of 45 m. The thickness tapers downdip and along strike to the south until the mineralization becomes too narrow to economically recover. Vertically, the 200 South extension extends from 160 m below sea level to 65 m above.

Due to the polyphase deformation and faulting at Greens Creek, the ore stratigraphy and metal zonation from footwall to hanging wall and from center to margin of an orebody is quite variable and difficult to reconstruct. However, there is a sequence of ores present in most of the orebodies such that an original configuration is suggested (Taylor and others, 1999b, 2000b). Individual orebodies are generally centered over a particularly thick footwall sequence of highly siliceous SRs (see figure 3 in chap. 6). Laterally away from this area of intense alteration the first ore types encountered above the footwall are WSIs followed upward and outward by WCAs and rare WBAs at the extreme lateral edges. These white ores are overlain by MFPs that are copper-rich in proximal core areas and change upward and outward toward lower copper-gold grades and increasing zinc. Ores change gradationally into increasingly higher grade zinc-lead-silver-(gold)-rich MFBs as the argillite hanging wall and the thinned distal edges of the deposit are reached. Distal ore progressions often are characterized by carbonate- and barite-rich white ores against phyllites that transition into MFBs toward the hanging wall. This progression of ore types from white ores against the phyllites grading into massive pyritic ores and then into the massive base-metal-rich ores against the argillites is the pattern most commonly seen throughout the mine (Taylor and others, 1999b, 2000b; see chap. 6, fig. 3). Although this pattern of ore types is highly simplified, and numerous examples can be found to contradict this model, it is broadly consistent at the orebody but not at a deposit scale. There are distinct differences between orebodies such that trying to explain the orebodies as proximal-distal portions of a single deposit is not possible. The implications of this observation is that multiple centers of upwelling may have been active along a paleo-Maki fault but with variable and different fluid chemistry and temperatures (for example, Freitag, 2000). For details of metal zonation in individual orebodies see chapter 6.

Previous Sulfur and Lead Isotope Studies

Very little previous isotopic data are available for the Greens Creek deposit or for other mineral occurrences on Admiralty Island. Newberry and others (1997) display isotopic ranges of both sulfur and lead for Late Triassic-hosted VMS deposits of southeastern Alaska. Sulfide sulfur spans a range of 0 to about –15 per mil $\delta^{34}\text{S}$, and the isotopically light values are attributed to the light isotopic composition of Late Triassic seawater. Ore lead isotope values form an irregular field with $^{206}\text{Pb}/^{204}\text{Pb}$ values of 18.65 to 18.85 and $^{207}\text{Pb}/^{204}\text{Pb}$ values of 15.52 to 15.60 (Newberry and others, 1997). Van Nieuwenhuysen (1984) reported lead isotope values for “composite samples of galena-bearing mineralization” from Pyrola and Glacier Creek and a galena from Greens Creek (exploration core PS-27, 660’). The Greens Creek sample has ratios of $^{206}\text{Pb}/^{204}\text{Pb} = 18.670$, $^{207}\text{Pb}/^{204}\text{Pb} = 15.610$, and $^{208}\text{Pb}/^{204}\text{Pb} =$

38.449. The Pyrola sample has ratios of $^{206}\text{Pb}/^{204}\text{Pb} = 18.520$, $^{207}\text{Pb}/^{204}\text{Pb} = 15.570$, and $^{208}\text{Pb}/^{204}\text{Pb} = 38.224$. On the basis of these analyses, Van Nieuwenhuysse (1984) concluded that the deposits formed in either a primitive arc or oceanic volcanic environment and that the data also support a back-arc or marginal basin environment in which the crust was ensimatic in nature. Newberry and Brew (1999) reported an additional galena lead isotope analysis from Greens Creek with ratios of $^{206}\text{Pb}/^{204}\text{Pb} = 18.635$, $^{207}\text{Pb}/^{204}\text{Pb} = 15.583$, and $^{208}\text{Pb}/^{204}\text{Pb} = 38.239$. They note that this analysis falls within the range of ore-lead previously determined (Newberry and others, 1997) for Triassic-Jurassic VMS deposit of southeastern Alaska and nearby Canada. No sulfur isotopic data for Greens Creek or any other mineral occurrences on Admiralty Island have been reported in the literature.

Methods

Lead Isotope Analyses

Lead isotope samples were obtained either by microdrilling or handpicking slabbed hand samples and core. Mineral separates were checked for purity under a binocular microscope. Each was then hand-ground in an agate mortar to homogenize the sample. Analyses were performed at the U.S. Geological Survey in Denver, Colorado. Galena separates were roughly measured out (about 0.5 to 1 mg) in order to provide a dilute enough concentration of lead by dissolution with ultrapure 7N nitric acid in a precleaned 7-mL-volume, PFA-Teflon vial to produce a 1 to 9V signal during the thermal ionization mass spectrometry. Dissolution of the sulfide fractions were aided by heating on a hot plate overnight. Samples were then evaporated and redissolved in dilute nitric acid. Other sulfide separates (excluding galena) were washed once with ethanol and ultrapure distilled water and then leached once with 1N hydrochloric acid for 10 minutes in an ultrasonic bath and finally rinsed with ultrapure water. The separates were dissolved in 7-mL PFA Teflon vials with ultrapure 2N–6N nitric acid and then spiked with a dilute mixed tracer of ^{205}Pb – ^{233}U – ^{236}U – ^{230}Th . Extraction of lead was achieved using Dowex AG 1-X8 anion-exchange resin in a 0.5–1N hydrobromic acid medium. Uranium and thorium were separated using the same kind of anion resin in a 6N nitric acid medium.

For all samples, lead was loaded onto a single rhenium filament with very dilute phosphoric acid and ionized in the mass spectrometer at currents between 1.7 and 2.3 amps, corresponding to a temperature range of about 1,150 to 1,300°C for which mass fractionation factors were calculated. Uranium and thorium were loaded together onto rhenium side filaments and run in the triple rhenium filament mode at temperatures of about 2,100°C. Lead, uranium, and thorium isotopic ratios were measured using a fully automated, multisample, single-collector, VG Isomass 54R thermal-ionization mass spectrometer. Instrumental bias was monitored using the NBS Common Lead Standard 981 and was found to be negligible.

Lead isotopic ratios were corrected for mass fractionation of 0.08 ± 0.03 percent per atomic mass unit and a laboratory blank of 6 ± 4 picograms total lead (negligible) with an assumed composition of $^{206}\text{Pb}/^{204}\text{Pb} = 18.458 \pm 0.093$, $^{207}\text{Pb}/^{204}\text{Pb} = 15.287 \pm 0.03$, and $^{208}\text{Pb}/^{204}\text{Pb} = 37.54 \pm 0.11$. Raw data were reduced using the programming of Ludwig (1980, 1985) and plotted using Isoplot software of Ludwig (1991).

Sulfur Isotope Analyses

Sulfur isotope samples were obtained by handpicking or microdrilling slabbed hand samples and core, checked for purity under a binocular microscope, and hand-ground in an agate mortar to homogenize the sample. Analyses were made in the stable isotope laboratories of the U.S. Geological Survey in Denver, Colorado. Quantities of a few hundred micrograms of mineral powder were weighed into tin capsules along with 1–2 milligrams of vanadium pentoxide oxidant. The samples were converted to sulfur dioxide gas using a Carlo Erba NA 2500 elemental analyzer, and the gases were admitted directly to a Micromass Optima mass spectrometer. Isotope ratios were measured by isotope ratio monitoring using a method similar to that described by Giesmann and others (1994). Sulfur isotope compositions are reported in δ -notation in units of per mil relative to Cañon Diablo troilite (CDT). Reproducibility was generally within ± 0.2 per mil.

Isotopic Data

Sulfur Isotopes

A comprehensive sulfur isotopic study was conducted on 221 sulfide mineral separates and bulk ore samples and 14 barite separates from samples collected from the mine workings and underground drill core. Fifty-five sulfide mineral separates and four barites from various mineral occurrences and from country rock on Admiralty Island were also analyzed. Figure 3 shows all the sulfide and sulfate $\delta^{34}\text{S}$ results obtained for the Greens Creek deposit. Data for samples from drill core and underground exposures in the mine are contained in table 1. Data for samples from Admiralty Island host rocks and mineral occurrences are presented in table 2. Greens Creek sulfides are strongly ^{34}S -depleted showing a $\delta^{34}\text{S}$ range of -38 to 2 per mil and a distinctly unimodal distribution with the bulk of the analyses between about -9 and -16 per mil. Greens Creek sulfates fall between 13.4 and 21.9 per mil, which is within the range exhibited by seawater sulfate in Triassic time (Strauss, 1997; Claypool and others, 1980). Figures 4 A–C show the sulfur isotope data sorted according to the texture of the sulfide analyzed, the mine location, and the type of host rock or ore lithology, respectively. Primary-textured sulfides are generally more ^{34}S -depleted than recrystallized or remobilized sulfides (see chap. 9 for descriptions and photomicrographs of sulfide

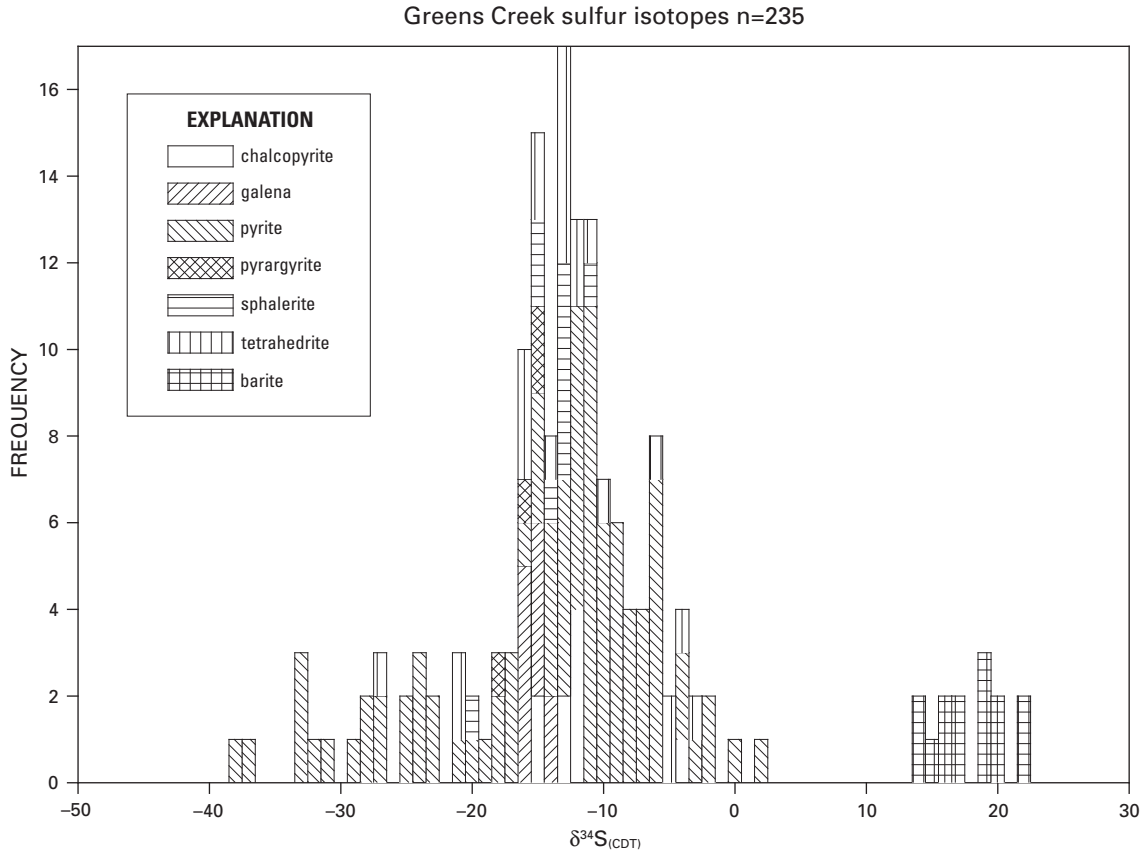


Figure 3. Histogram showing the distribution of all sulfide and sulfate $\delta^{34}\text{S}$ values obtained from the Greens Creek deposit. CDT, Cañon Diablo troilite.

textures); the isotopically heaviest primary-textured sulfide has a value of -10 per mil. Recrystallized sulfides span the isotopic range and have an almost bell-shaped distribution centered between -18 and -4 per mil. The range of remobilized sulfides is more restricted than that of the recrystallized sulfides, with a more restricted distribution as well, clustered between -10 and -16 per mil (fig. 4A).

Spatially, the two largest orebodies (West and Southwest) exhibit sulfur isotope values that span the range. The ^{34}S -enriched values are most likely to occur in the smaller and more distally located orebodies such as the East or 5250 (fig. 4B). On a deposit scale the most ^{34}S -enriched sulfides are in and near the footwall igneous rocks and white siliceous ores. The progression upward and outward toward ^{34}S -depleted sulfides roughly follows the ore paragenesis from white ores against the footwall, to massive pyritic, to massive base-metal-rich ores against the hanging wall. Pyrite $\delta^{34}\text{S}$ values in the overlying shales exhibit a wide range of values (fig. 4C). This comparative ^{34}S enrichment of footwall sulfur isotope values over those in the hanging wall is further demonstrated by the histograms shown in figure 5. Minewide, the average value of sulfide sulfur in the footwall phyllites and white siliceous ore type is -9.9 ± 5.0 per mil $\delta^{34}\text{S}$. The average value of sulfide

sulfur in massive fine grained base-metal-rich ores and in the hanging-wall argillites is -15.5 ± 6.6 per mil $\delta^{34}\text{S}$. Thus, on average, ore stratigraphic profiles at Greens Creek exhibit a 5.6 per mil $\delta^{34}\text{S}$ depletion from footwall to hanging wall.

Figure 6 shows the sulfide sulfur isotope data sorted by mineralogy. Pyrite values span the entire isotopic range, a feature that has been noted at other sediment-hosted massive sulfide deposits (Ohmoto, 1986). Tetrahedrite values also are broadly distributed. In contrast, chalcopyrite, sphalerite, galena, and pyrargyrite cluster tightly between -11 and -18 per mil. Whole rock analyses of MFP and MFB ore types show that they are isotopically indistinguishable, with compositions typically in the range -9 to -18 per mil (fig. 6). Examination of the histogram in figure 6 shows that the average $\delta^{34}\text{S}$ values increase in the order galena-sphalerite-pyrite, consistent with the order expected for equilibrium fractionation (Ohmoto and Rye, 1979). This same ordering was also observed for sulfide separates from individual hand samples. Pyrite-chalcopyrite, pyrite-sphalerite, and pyrite-galena mineral pair geothermometers generally gave extremely high or impossible temperatures. The sphalerite-galena mineral pair geothermometer yielded three relatively consistent and low temperature values with a range of 276 – 313°C .

It is important to note that wherever sulfur isotope determinations were made on multiple base-metal sulfides from the same sample, the minerals displayed textures indicative of recrystallization or remobilization. In most samples where only pyrite was analyzed, the pyrite displayed primary textures or had relict primary features. The base-metal sulfides that coexist with such pyrite were too fine grained and intimately intergrown to separate by conventional techniques. The base-metal sulfides that were of sufficient grain size to sample were always texturally recrystallized or remobilized. In the one sample (GC-164-08) where recrystallized pyrite and coexisting sphalerite were analyzed, the pyrite-sphalerite geothermometer gave an isotopic equilibration temperature of 275°C. These relationships imply that the isotopic fractionations displayed by the ore sulfides may reflect isotopic exchange during the same event that modified the textures of the Greens Creek ores. The critical question is, therefore, whether the recrystallization/remobilization was the result of zone refining (for example, Hannington

and others, 1998) during the mineralization process, or of metamorphism during the Cretaceous deformation.

Isotope analyses of sulfide minerals in host rocks and mineralized occurrences elsewhere on Admiralty Island show trends similar to Greens Creek (fig. 7). The ^{34}S -values of sulfides from known or suspected Triassic-hosted mineral occurrences tend to be very low, whereas those of unknown or non-Triassic-hosted occurrences are generally in a more restricted range near 0 per mil. Analyses of barites from two Triassic mineralized occurrences on and north of the north shore of Gambier Bay (Taylor and others, 1992) range from 12.8 to 14.6 per mil. Analyses of pyrites in Devonian(?)–Triassic greenstones, phyllites, and other metaigneous rocks on Admiralty commonly are 0 to –12 per mil. Pyrite in country-rock argillite of Triassic age, like the hanging-wall argillite, is strongly ^{34}S -depleted, with a range of –30 to –1 per mil. The $\delta^{34}\text{S}$ values of sulfides from older host rocks are noticeably higher than the Greens Creek values.

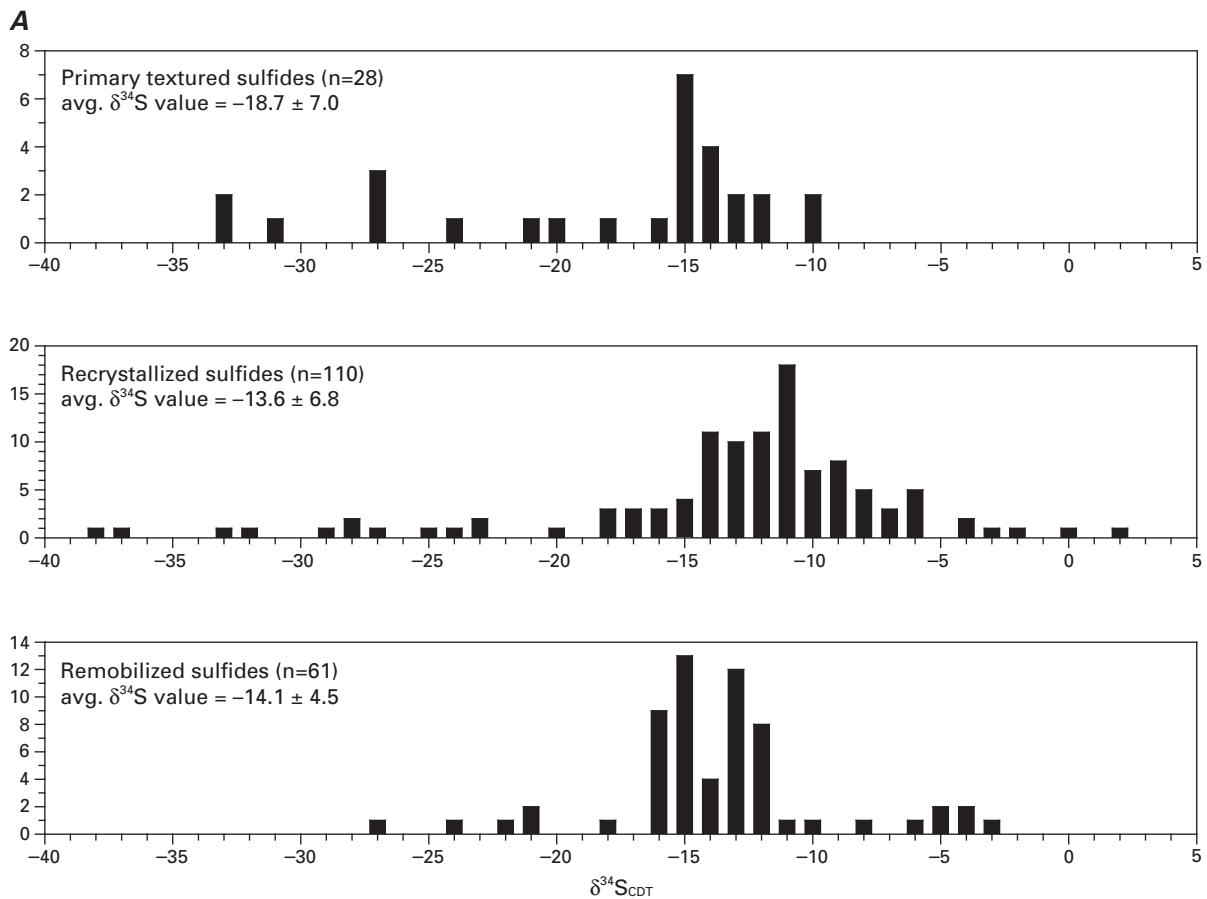


Figure 4. Greens Creek sulfide sulfur isotope data sorted by: (A) mineral texture, (B) mine location, and (C) type of host rock. n, number of samples. CDT, Cañon Diablo troilite.

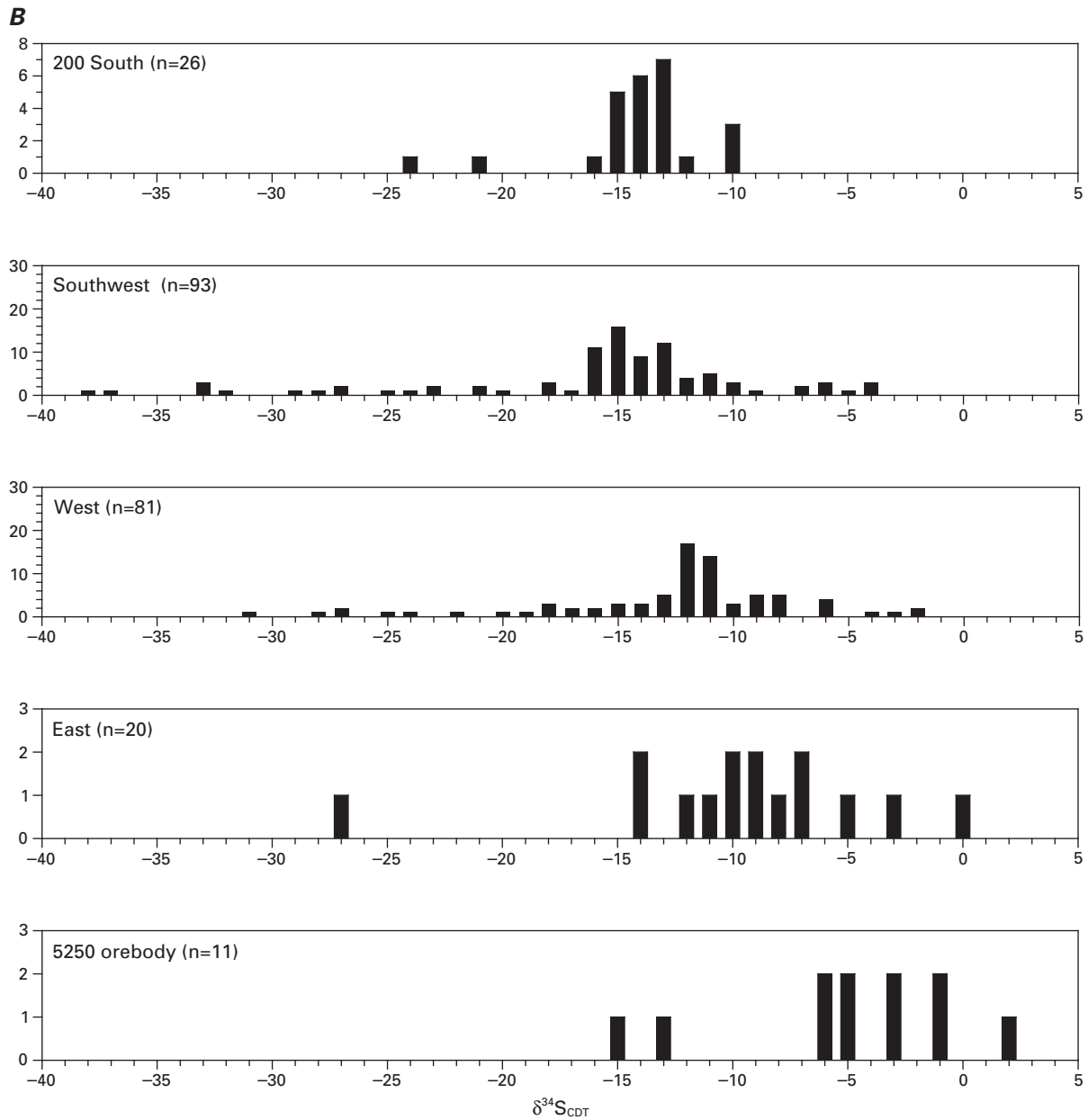


Figure 4. Greens Creek sulfide sulfur isotope data sorted by: (A) mineral texture, (B) mine location, and (C) type of host rock. n, number of samples. CDT, Cañon Diablo troilite.—Continued

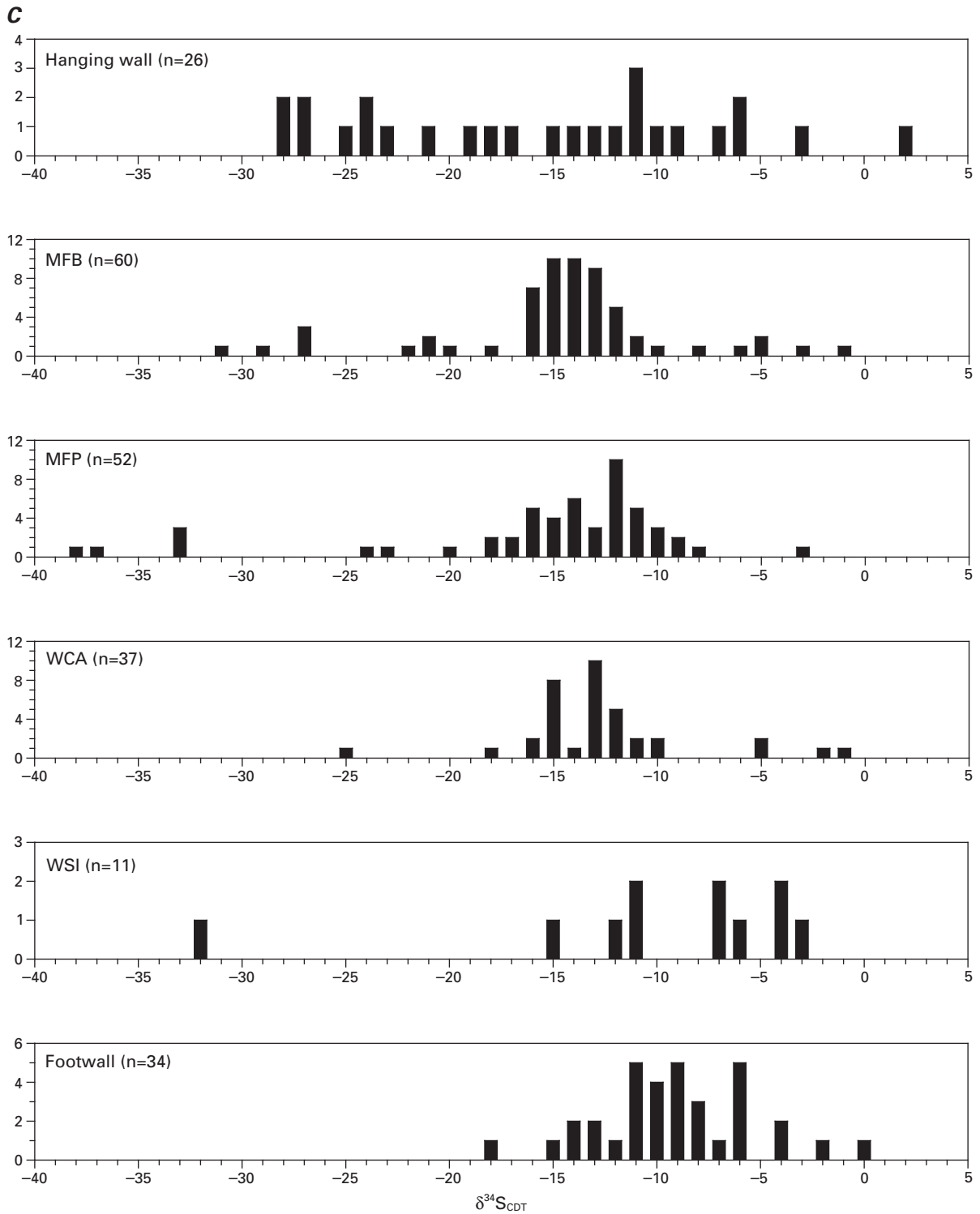


Figure 4. Greens Creek sulfide sulfur isotope data sorted by: (A) mineral texture, (B) mine location, and (C) type of host rock. n, number of samples. CDT, Cañon Diablo troilite.—Continued

Table 1. Greens Creek sulfur isotope data, sample locations, and descriptions for samples from drill core and underground exposures.

Sample id	Mineralogy	$\delta^{34}\text{S}$ value	DH depth	Location	Host rock	Mineral texture	Comments
350-2650	py	-33.3	79	lower SW	MFP	primary	primary textured clasts, very fine grained
350-2650	pyrar	-16.8	79	lower SW	MFP	remobilized	qtz-pyrrar veinlets crosscutting MFP
350-2650 dup	py	-33.9	79	lower SW	MFP	primary	primary textured clasts, very fine grained
764N1A	tetr	-5.6		upper SW	WCA	remobilized	qtz-tetr-electrum veined dolomite
764N1B	cpy	-4.2		upper SW	MCHT	remobilized	coarse tetr-cpy
764N1B	tetr	-5.0		upper SW	MCHT	remobilized	coarse tetr-cpy
88-RN-80D	py	-9.9	103	East	SPgr	recrystallized	clots of qtz-carb-py
88-RN-80H	py	-0.1	200	East	SPgr	recrystallized	coarse pyrite
88-RN-80K	py	-11.9	310	East	SP	recrystallized	coarse pyrite
88-RN-80N	py	-9.7	370	East	SP	recrystallized	coarse py to 1 mm in carb
91-GC-01	gn	-14.7		East	MFB	remobilized	
91-GC-02A	MFP	-14.6		East	MFP	primary?	
91-GC-02B	bt	21.3		East	WBA	coarse xline	
91-GC-04B	bt	13.4		East	WBA	coarse xline	
91-GC-04C	acan	-8.1		East	WBA	remobilized	
91-GC-07	MFB	-10.7		East	MFB	primary?	orange, fine crystalline
91-GC-08A	tetr	-12.7		East	WSI	remobilized	
91-GC-13	tetr	-27.6		East	MA	remobilized	graphite-tetr-qtz vein near hw contact
91-GC-14A	bt	13.9		East	WBA	coarse xline	
91-GC-15	py	-8.0		East	WSI	recrystallized	ground up pyrite separate from Ar/Ar sample
91-GC-16	bt	14.8		East	WBA	coarse xline	dark gray, bedded
91-GC-17	bt	16.5		East	WBA	coarse xline	medium gray, sugary, ser-fuch rich
96-GC-01	pyrar	-18.2	79	lower SW	MFP	remobilized	
96-GC-02	sph	-20.4	62.5	lower SW	MFP	recrystallized	
96-GC-03	pyrar	-15.3	79	lower SW	MCHT	remobilized	
96-GC-08	py	-23.3	16	lower SW	MSA	recrystallized	spongy, subhedral grains, 50-100 μm
96-GC-11	MFP	-18.5	20	lower SW	MFP	recrystallized	bright, euhedral-subhedral, 10-100 μm
96-GC-12	MVB	-11.5	21.5	lower SW	MVB	recrystallized	orange, fine crystalline, euhedral to subhedral
96-GC-13	MFP	-16.7	25.5	lower SW	MFP	clastic	pyrite consists of massive to spongy aggregates
96-GC-14	py	-28.3	31	lower SW	FMSAS	recrystallized	cm-sized broken grains of py
96-GC-15	py	-29.2	39	lower SW	XMFBgr	recrystallized	0.5–1.0-cm pyrites in frambooid-rich graphitic sample
96-GC-17	py-asp	-37.3	49	lower SW	MFP	recrystallized	slightly spongy py with aspy replacement
96-GC-19	py-asp	-33.7	53	lower SW	MFP	recrystallized	equal proportions of euhedral py-asp
96-GC-19	sph	-15.8	53	lower SW	WCA	remobilized	
96-GC-21A	tetr	-16.2	62.5	lower SW	WCA	remobilized	
96-GC-21B	sph	-15.9	62.5	lower SW	WCA	remobilized	
96-GC-23	py-asp	-38.8	67	lower SW	MFP	recrystallized	bright, massive euhedral with minor primary textures
96-GC-24	MFP	-16.8	72	lower SW	MFP	primary	50% recrystallized, 50% frambooidal
96-GC-24	tetr	-21.5	72	lower SW	MFB	remobilized	Clot of tetr in qtz vein
96-GC-24 dup	tetr	-21.2	72	lower SW	MFB	remobilized	Clot of tetr in qtz vein
96-GC-26	MFP	-15.9	79	lower SW	MFP	primary	frambooidal pyrite in sph matrix
96-GC-29	MFP	-14.4	89	lower SW	MFP	recrystallized	clean, euhedral, 0.1-1.0 mm
96-GC-34	py	-7.5	104	lower SW	MDMA	recrystallized	bright, subhedral 50-200 μm
96-GC-38	py	-6.3	148	lower SW	MP	recrystallized	bright, euhedral-subhedral

Table 1. Greens Creek sulfur isotope data, sample locations, and descriptions for samples from drill core and underground exposures.—Continued

Sample id	Mineralogy	$\delta^{34}\text{S}$ value	DH depth	Location	Host rock	Mineral texture	Comments
GC-1093-03	gn	-15.3		lower SW	WCA	remobilized	very coarse grained, monomineralic
GC-1093-05	cpy	-15.0		lower SW	WCA	remobilized	gn-cpy clots in qtz-dol veins adj to MFP
GC-1093-05	gn	-16.9		lower SW	WCA	remobilized	gn-cpy clots in qtz-dol veins adj to MFP
GC-1136-08	py	-14	443	lower SW	MA	recrystallized	highly sheared/foliated
GC-1136-12	py	-24.8	491	lower SW	SA	recrystallized	finely laminated, minor py
GC-1136-21	py	-17.2	541	lower SW	MFP	recrystallized	(sph-rich) MFP bands
GC-1136-29	py	-23.8	583	lower SW	MFP	recrystallized	coarse pyritic
GC-1136-33	py	-14.6	607	lower SW	MFB	recrystallized	Pb-Zn rich
GC-1136-35	py	-13.4	617	lower SW	MFB	recrystallized	graphitic MFB lens in MA
GC-1136-36	py	-25.1	626	lower SW	MA	recrystallized	pyrite stringer (mean of two analyses)
GC-1136-39	py	-7.8	652.5	lower SW	MP	recrystallized	sericitic (mean of two analyses)
GC-1136-40	py	-6.4		lower SW	MP	recrystallized	
GC-1136-42A	py	-13.8	667	lower SW	SCcb	recrystallized	breccia frags of SC in carb-py matrix. Clean py cubes or dodecs
GC-1136-42B	py	-11.2	667	lower SW	SCcb	recrystallized	breccia frags of SC in carb-py matrix. Clean py cubes or dodecs
GC-1136-44	py	-10	680	lower SW	SC	recrystallized	SC phyllite (two identical analyses)
GC-1136-55	py	-4.6	818.5	lower SW	SC	recrystallized	serpentinite (chl-leuc?)
GC-1136-61	py	-14.1	898	lower SW	SC	recrystallized	euhedral to massive, spongy aggregates
GC-127-06	py	-10.0	714.5	East	SP		sparse wisps and clots of py
GC-127-17	MFB	-5.3	1,001	East	MFB	remobilized	
GC-127-18	py	-7.1	1,007	East	WSI		pyritic MFB clot in WSI
GC-127-19	tetr	-3.9	1,010	East	WSI	remobilized	
GC-1514-03	MFB	-16.8	22	Northwest	MFB	recrystallized	fine crystalline py-sph-gn, euhedral
GC-1514-14	py	-8.6	381	Northwest	SP	recrystallized	1-cm-sized clots in dolo-ser
GC-1514-25A	py	-27.2	489.8	Northwest	MFB	primary/recrystallized	1-5-mm clastic grains in gn-rich MFB, spongy
GC-1514-25B	gn-rich MFB	-22.5	489.8	Northwest	MFB	remobilized	gn-rich MFB
GC-1514-34	py	-2.4	636	Northwest	WCA	recrystallized	wispy, in silicified dolo
GC-1514-36	py	-11.7	648	Northwest	MFP	recrystallized	qtz-carb matrix
GC-1514-38	py	-11.5	654	Northwest	MFP	recrystallized	bright, in qtz-carb matrix
GC-1514-40	py	-12.4	676.5	Northwest	MFP	recrystallized	bright, cpy-rich(?)
GC-1514-41	py	-12.4	682	Northwest	MFP	recrystallized	bright, cpy-rich(?)
GC-1514-42	cpy-rich MFP	-12.2	686.5	Northwest	MFP	recrystallized	non-remobilized cpy-rich portion
GC-1514-44	cpy	-13.1	696	Northwest	MFP	remobilized	cpy on fracture
GC-1514-44	cpy-rich MFP	-12.1	696	Northwest	MFP	recrystallized	cpy-rich MFP
GC-1514-45	cpy-rich MFP	-12.6	703	Northwest	MFP	recrystallized	cpy-rich MFP
GC-1514-46	cpy	-12.8	707	Northwest	MFP	remobilized	euhedral cpy and sph on fracture
GC-1514-46	cpy-rich MFP	-12.2	707	Northwest	MFP	recrystallized	cpy-rich MFP
GC-1514-46	sph	-14.1	707	Northwest	MFP	remobilized	euhedral cpy and sph on fracture
GC-1514-46dup	cpy	-12.7	707	Northwest	MFP	remobilized	euhedral cpy and sph on fracture
GC-1514-49	py	-12.5	718	Northwest	SR	recrystallized	wispy, semimassive band, euhedral py, anhedral cpy matrix
GC-1514-52	py	-11.1	735	Northwest	SRcx	recrystallized	cpy-rich clastic py to 1 cm, subhedral-euhedral massive, cpy matrix
GC-1514-53	py	-9.8	737	Northwest	SRcx	recrystallized	cpy-rich clastic py to 1 cm, subhedral-euhedral massive, cpy matrix
GC-1514-57	py	-10.5	779	Northwest	SR	recrystallized	in siliceous chl-carb schist
GC-1527-01	py	-6.8	96	Northwest	SP	recrystallized	subhedral, <1mm disseminated
GC-1527-05	py	-9.5	357.4	Northwest	MSR	recrystallized	

Table 1. Greens Creek sulfur isotope data, sample locations, and descriptions for samples from drill core and underground exposures.—Continued

Sample id	Mineralogy	$\delta^{34}\text{S}$ value	DH depth	Location	Host rock	Mineral texture	Comments
GC-1527-07A	py	-17.6	390.5	Northwest	MDMA	recrystallized	subhedral, dull, bronze colored, fine grained
GC-1527-07B	cpy	-12.3	390.5	Northwest	MMA	remobilized	remobilized cpy in qtz
GC-1527-07C	py	-11.4	390.5	Northwest	MDMA	recrystallized	bright, coarse crystalline
GC-1527-08	cpy	-12.7	397.5	Northwest	WCA	remobilized	2 mm x 1 cm clots, silicified matrix
GC-1527-09	MFB	-13.4	402.5	Northwest	MFB	primary	spectacular framboidal and colloform banded
GC-1527-12	cpy-rich MFP	-3.8	429.7	Northwest	MFP	recrystallized	
GC-1527-13	cpy-rich MFP	-9.7	438.5	Northwest	MFP	recrystallized	spongy to clean massive aggregates
GC-1527-14	cpy	-15.3	447.2	Northwest	WCA	remobilized	cpy remobilized, siliceous, wisps of dull, brassy py
GC-1527-15	py	-11.7	454.2	Northwest	WCA	recrystallized	dull, brassy, fine grained
GC-1527-16	cpy-rich MFP	-11.0	459.8	Northwest	MFP	recrystallized	
GC-1527-18	MFP	-11.5	472.2	Northwest	MFP	recrystallized	euhedral-subhedral, dull, brassy, sph-rich matrix
GC-1527-19	MFP	-9.1	482.5	Northwest	MFP	recrystallized	euhedral-subhedral, bright, bronze colored, moderate cpy
GC-1527-20	MFB	-11.1	491.5	Northwest	MFB	recrystallized	gn-tetr rich, banded with pyritic DMA
GC-1527-21	tetr	-12.1	498	Northwest	MFBgr	remobilized	tetr-acn-cpy veinlets
GC-1527-22	py	-10.9	498	Northwest	MFPgr	recrystallized	fine grained, wispy, euhedral, clean
GC-1527-28	MFB	-11.3	570.4	Northwest	MSAS or MSR	recrystallized	siliceous, secondary cpy
GC-1527-36	py	-8.6	665	Northwest	SP	recrystallized	discrete 2–3-mm subhedral grains in dolo
GC-1527-40	py	-8.5	722	Northwest	SP	recrystallized	subhedral, 1–3-mm py
GC-1530-03	py	-6.2	50.5	Northwest	SP	recrystallized	euhedral, clean, fine-grained py in dolo-rich bands
GC-1530-08	cpy-rich MFB	-12.5	141	Northwest	MFP/MFB	remobilized	streaks of remobilized cpy in silicified matrix
GC-1530-09	gn-rich MFB	-14.1	142.6	Northwest	MFB	remobilized	graphitic MFB/MFP with remobilized galena matrix
GC-1530-11	py	-31.7	148.5	Northwest	MFB	primary	>1-mm pyrite clasts, colloform internal texture
GC-1530-12A	py	-21.0	154.4	Northwest	MFB	primary	>1-mm pyrite clasts
GC-1530-12B	gn-rich MFB	-18.4	154.4	Northwest	MFB	primary	galena-rich bands
GC-1530-13	py	-29.0	164	Northwest	SA	recrystallized	clasts to 1cm in carbonate
GC-1530-19	py	-16.5	222.5	Northwest	MFP	recrystallized/primary	large areas of fractured clasts, spongy
GC-1530-21	py	-27.6	260	Northwest	MA	recrystallized	1-cm clots of py in qtz-carb veins
GC-1530-22	py	-17.5	276.5	Northwest	MFPgr	recrystallized	1-cm clasts in graphitic MFB
GC-1530-28	gn-rich MFB	-15.3	420.2	Northwest	MFB	primary	fine grained, galena-rich
GC-1530-30	MFB	-13.8	440.5	Northwest	MFB	recrystallized	dolo-rich py-sph-gn
GC-1530-30 dup	MFB	-13.8	440.5	Northwest	MFB	recrystallized	dolo-rich py-sph-gn
GC-1530-31	py +cpy	-12.5	449.8	Northwest	WCA	recrystallized	dull, brassy, minor to moderate cpy
GC-1530-34	py	-11.1	476.7	Northwest	MFP	recrystallized	dull, brassy, minor cpy
GC-1530-36	py	-11.5	507.2	Northwest	WCA	recrystallized	wispy, dull, brassy pyrite
GC-1530-39	py	-12.3	541.5	Northwest	WCA	recrystallized	wispy, bright, brassy pyrite
GC-1530-41A	py	-15.6	558.5	Northwest	WCA	primary/recrystallized	dull, brassy, in 3-cm bands with cpy
GC-1530-41B	cpy	-13.2	558.5	Northwest	WCA	remobilized	late veinlets with dolo-tetr
GC-1530-42	py	-9.0	569.7	Northwest	MFP	recrystallized	lemon-yellow colored, in dolo (cpy-rich?)
GC-1530-44	py	-9.1	582.2	Northwest	SR	recrystallized	nonclastic looking, sulfide bands
GC-1530-46	py	-11.1	595	Northwest	SRcx	recrystallized	bright, shiny, clastic, to 1cm
GC-1530-52	py	-4.9	692	Northwest	SRcx	recrystallized	1–2-cm in qtz-carb matrix
GC-1530-59B	MFP	-10.4	781.2	Northwest	MFP	recrystallized	dull, brassy, fine grained
GC-1530-60	bt	15.0	787.4	Northwest	WBA	coarse xline	sugary white barite with py wisps
GC-1530-62A	bt	19.3	802.3	Northwest	WBA	coarse xline	foliated barite minor pyrite

Table 1. Greens Creek sulfur isotope data, sample locations, and descriptions for samples from drill core and underground exposures.—Continued

Sample id	Mineralogy	$\delta^{34}\text{S}$ value	DH depth	Location	Host rock	Mineral texture	Comments
GC-1530-64	MFB	-8.0	825.5	Northwest	MFB	recrystallized	very fine crystalline, euhedral
GC-1530-66	py	-19.1	829.2	Northwest	MA		py-sph along stylolitic contact
GC-1530-66 dup	py	-19.0	829.2	Northwest	MA		py-sph along stylolitic contact
GC-1530-67	py	-24.6	838.2	Northwest	MA	remobilized	crosscutting pyrite vein
GC-1536-02	py	-2.6	233.6	West	SP		qtz-carb-py veins
GC-1536-06	py	-18.5	372	West	SPgr	recrystallized	1–2-mm euhedral py
GC-1536-08B	py	-6.2	489	West	SP		crosscutting fine-grained py vein
GC-1536-09	py	-25.5	529.4	West	WCA		clots of dull py, acid treated
GC-1536-10	sph-rich MFB	-12.0	534.6	West	MFB		fine grained, banded, sph-rich
GC-1536-10 dup	sph-rich MFB	-12.2	534.6	West	MFB		fine grained, banded, sph-rich
GC-1536-13	py	-6.6	548	West	MSA		band of bright py
GC-1536-15	tetr	-11.6	576.2	West	WSI	remobilized	qtz-tetr vein crosscutting DMA
GC-1536-16	sph	-11.5	576.4	West	WSI		large clots of light sph in DMA
GC-1536-18	MFB	-14.3	604	West	MFB		2.5-cm-thick band in SA
GC-1603-03	py	-13.7	233	Fred	DMA		qtz-carb-mp-py veined
GC-1603-05	MFB	-5.5	236.6	Fred	MFB		fine grained
GC-1603-06	tetr	-5.4	237.5	Fred	WCA	remobilized	coarse clots
GC-1603-08	MFB	-6.2	243	Fred	MFB		fine grained, banded
GC-1603-09	py	-3.4	246.5	Fred	SA		dull, wispy
GC-1605-02	py	1.1	115.7	Fred	SA	recrystallized	1-mm-sized, clean
GC-1605-03	MFB	-1.6	118.7	Fred	WCA		MFB band
GC-1605-06	tetr	-6.4	166.1	Fred	SA	remobilized	1-cm clot in qtz vein
GC-1605-08A	MFB	-1.5	171	Fred	MFB		
GC-1605-08B	bt	21.9	171	Fred	WBA	coarse xlline	coarse white barite
GC-1605-09A	MFB	-3.8	173.8	Fred	MFB		very fine grained band
GC-1605-09B	bt	19.8	173.8	Fred	WBA	coarse xlline	coarse white barite
GC-1605-10	bt	18.7	176.5	Fred	WBA	coarse xlline	white, banded, massive, sugary
GC-1605-11	bt	15.8	185.1	Fred	WBA	coarse xlline	gray, massive, sugary
GC-1605-14	py	-15.3	212	Fred	SP		wispy pyrite
GC-164-02	MVP	-15.1	-3	lower SW	MVP	primary	fine-grained pyrite band
GC-164-02 dup	MVP	-15.5	-3	lower SW	MVP	primary	fine-grained pyrite band
GC-164-03	MVP	-28.0	0.5	lower SW	MVB	primary	very fine grained banded
GC-164-03 dup	MVP	-27.9	0.5	lower SW	MVB	primary	very fine grained banded
GC-164-04	gn-rich MVB	-15.5	4.5	lower SW	MVB	remobilized	silver-gray with gn in center of band
GC-164-04	MVB	-15.9	4.5	lower SW	MVB	remobilized	dark gray to shiny black
GC-164-04A	MVP	-14.2	4.5	lower SW	MVB	primary	very fine grained, in dolostone
GC-164-04A dup	MVP	-14.6	4.5	lower SW	MVB	primary	very fine grained, in dolostone
GC-164-04B	tetr	-16.1	4.5	lower SW	MVB	remobilized	dark gray to shiny black
GC-164-04B dup	tetr	-16.3	4.5	lower SW	MVB	remobilized	
GC-164-04B dup	tetr	-15.7	4.5	lower SW	MVB	remobilized	dark gray to shiny black
GC-164-06	gn	-16.2	10.5	lower SW	MVB	remobilized	dull, brassy, fine grained, with large areas of gn
GC-164-06A	MVP	-15.3	10.5	lower SW	MVB	primary	dull, brassy, fine grained
GC-164-06A dup	MVP	-15.1	10.5	lower SW	MVB	primary	dull, brassy, fine grained
GC-164-06B	gn	-16.7	10.5	lower SW	MVB	remobilized	dull, brassy, fine grained, with large areas of gn

Table 1. Greens Creek sulfur isotope data, sample locations, and descriptions for samples from drill core and underground exposures.—Continued

Sample id	Mineralogy	$\delta^{34}\text{S}$ value	DH depth	Location	Host rock	Mineral texture	Comments
GC-164-06B dup	gn	-16.7	10.5	lower SW	MVB	remobilized	dull, brassy, fine grained, with large areas of gn
GC-164-06B dup	gn	-16.5	10.5	lower SW	MVB	remobilized	dull, brassy, fine grained, with large areas of gn
GC-164-08	tetr	-13.3	30	lower SW	WCA	remobilized	in pyritic gray dolostone
GC-164-08B	py	-12.6	30	lower SW	WCA	primary/recrystallized	bands in gray dolostone, minor aspy
GC-164-08B dup	py	-12.1	30	lower SW	WCA	primary/recrystallized	bands in gray dolostone, minor aspy
GC-164-08C	sph	-13.7	30	lower SW	WCA	remobilized	in pyritic gray dolostone
GC-164-08C dup	sph	-13.9	30	lower SW	WCA	remobilized	in pyritic gray dolostone
GC-164-08C dup	sph	-13.7	30	lower SW	WCA	remobilized	in pyritic gray dolostone
GC-164-09	py	-14.2	40	lower SW	WCA	primary	dull, fine grained, wispy
GC-164-10A	py	-13.7	50	lower SW	WCA	primary/recrystallized	dull, fine grained in gray dolostone
GC-164-10B	tetr	-14.0	50	lower SW	WCA	remobilized	in gray dolostone
GC-164-11	gn	-15.9	60	lower SW	WCA	remobilized	
GC-164-11	sph	-13.8	60	lower SW	WCA	remobilized	
GC-164-11	MFP	-18.3	60	lower SW	WCA	recrystallized	
GC-164-11	tetr	-13.8	60	lower SW	WCA	remobilized	
GC-164-11dup	sph	-13.5	60	lower SW	WCA	remobilized	
GC-164-13	py	-32.6	67	lower SW	WSI	recrystallized	0.5–1-cm grains in banded py-sph-gn-tetr rich ore
GC-164-14	gn-rich MFB	-14.5	80	lower SW	MFBgr	recrystallized	graphitic, carb-rich
GC-164-15	cpy-rich MFB	-12.8	85	lower SW	MFB	remobilized	py with abundant remobilized cpy
GC-164-16	MFP	-12.7	88	lower SW	MFP	recrystallized	1–2-mm aggregates in base-metal-rich MFP
GC-164-17A	py	-10.5	90	lower SW	SP	recrystallized	<1 mm grains in wispy veinlets
GC-164-17B	gn-rich MFB	-14.2	90	lower SW	SP	recrystallized	
GC-164-17B	cpy-rich MFP	-11.3	90	lower SW	SP	recrystallized	
GC-164-18	py	-11.8	94	lower SW	MSP	recrystallized	5-mm clots in heavily altered SP
GC-164-19	py	-13.7	100	lower SW	SP	recrystallized	0.5–1-mm clots
GC-1643-02	MFB	-15.4	29	200 South	MFB	recrystallized	fine-grained typical MFB
GC-1643-06	tetr	-15.1	119.5	200 South	WCA	remobilized	clot in white dolomite vein, minor cpy
GC-1643-07	MFP	-14.2	143.5	200 South	MFP	recrystallized	growth banded crystals with gn-cpy
GC-1643-10	sph-rich MFB	-13.8	272	200 South	MFB	recrystallized	orange sph-rich band
GC-1643-10	gn-rich MFB	-14.3	272	200 South	MFB	recrystallized	banded MFB
GC-1643-10 dup	sph-rich MFB	-13.7	272	200 South	MFB	recrystallized	orange sph-rich band
GC-164N1	bt	17.0		lower SW	WBA	coarse xline	white barite
GC-1656-02	py	-21.4	606.5	200 South	SA	primary	
GC-1656-06	MFP	-10.0	911	200 South	MFP	recrystallized	banded MFP/WCA, drilled out MFP band
GC-1656-06	mixed	-16.8	911	200 South	MFP	recrystallized	
GC-1656-11	py	-15.4	987.7	200 South	MFB	recrystallized	MFB with 1–2-mm rounded clots
GC-1656-12	bt	19.0	1,004	200 South	WCA/WBA	coarse xline	white barite
GC-1656-13	gn	-14.7	1,008	200 South	MFB	recrystallized	galena-rich banded MFB/MFP
GC-1656-13	MFP	-13.9	1,008	200 South	MFB	recrystallized	galena-rich banded MFB/MFP
GC-1656-13 dup	MFP	-14.5	1,008	200 South	MFP	recrystallized	galena-rich banded MFB/MFP
GC-1656-15	MFB	-12.0	1,017	200 South	MFB	recrystallized	massive fine grained MFB with areas of WCA
GC-1656-18	MFB	-13.7	1,037	200 South	MFB	recrystallized	
GC-1656-18A	gn-rich MFB	-14.4	1,037	200 South	MFB	recrystallized	fine-grained gn-rich MFB in bands
GC-1656-19A	py	-10.4	1,052	200 South	WCA	primary	light brassy pyrite in carb

Table 1. Greens Creek sulfur isotope data, sample locations, and descriptions for samples from drill core and underground exposures.—Continued

Sample id	Mineralogy	$\delta^{34}\text{S}$ value	DH depth	Location	Host rock	Mineral texture	Comments
GC-1656-19B	tetr	-10.1	1,052	200 South	WCA	remobilized	Clots on white dolomite
GC-1656-20	py	-24.4	1,062	200 South	MFP	primary	dull, brassy, pyritic MFP
GC-1656-20	pyrar	-15.9	1,062	200 South	MFP	remobilized	
GC-1656-20	tetr	-14.0	1,062	200 South	MFP	remobilized	
GC-1656-20 dup	tetr	-13.6	1,062	200 South	MFP	remobilized	
GC-1656-20 dup	tetr	-13.8	1,062	200 South	MFP	remobilized	
GC-1656-21	gn	-15.5	1,071	200 South	MFB	recrystallized	very fine grained, banded, gn-rich
GC-1656-21	sph-rich MFB	-13.2	1,071	200 South	MFB	recrystallized	area of yellow sph-rich MFB
GC-764N3-03	MFB	-11.0		upper SW	MSA	recrystallized	2–3-cm-thick band of carb-MFB
GC-764N3-06	MFB	-15.2		upper SW	SA	recrystallized	1–2-mm thick bands
GC-764N3-07	MFP	-11.0		upper SW	MSA	recrystallized	py-gn-dol-qtz bands to 2 cm
GC-764N3-09	py	-9.2		upper SW	MMA	recrystallized	graphite-py-rich clots to 2 cm
GC-764N3-10	py	-6.6		upper SW	MCHT	recrystallized	banded py-dol in chert
GC-764N3-11	bt	18.0		upper SW	WBA	coarse xline	light gray barite
PP173-06	gn	-15.2	63.5	lower SW	MFB	remobilized	galena-rich MFB

Table 2. Sulfur isotope data, sample locations, and descriptions for samples from Admiralty Island host rocks and mineral occurrences.

Sample id	Location	Mineralogy	$\delta^{34}\text{S}$ value	Host rock	Comments
91- AD-60H	North Gambier occurrence	bt	12.8	basalt	bt-cpy-sph-gn-tetr bearing silicified breccia
92- GB-21	North shore, Gambier Bay	bt	14.6	listwanite	qtz-carb-mp-altered serpentinite with bladed barite and sulfides
92- GB-60	North Gambier occurrence	bt	14.1	limestone at contact with basaltic dike	vein of massive bladed barite and calcite
92- GB-67	North Gambier occurrence	bt	13.8	basalt	bt-sph veined basalt
92- GB-46	North Gambier occurrence	cpy	-5	basalt	1105'; high-graded qtz-carb-cpy-bn stockwork
92- GB-63	North Gambier occurrence	cpy	-4.3	limestone	cpy-bn-qtz-cc veined limestone
97- LG-33	Mammoth claim	gn	-5.5	py-sph-gn mineralized qtz-carbonate	
97- LG-35	Mammoth claim	gn	-5.6	gn-sph-py-bt-carb-rich (light green sph)	
KENNECOTT RAND	Mansfield Peninsula, Kennecott-Rand occurrence	gn	0.4		
NAD-T17-7B	Killer Creek occurrence	gn	-8.3	MFP	py-sph-gn-cpy-qtz-carb
NAD-T17-7D	Killer Creek occurrence	gn	-9.4	WSI	
NAD-T17-7D dup	Killer Creek occurrence	gn	-9.3	WSI	
PY-7-13, 262'	Pyrola deposit	gn	-16.6	massive argillite	2" lens of banded bt-sph-gn-py at base of gray chert interval
PY-7-13, 262' dup	Pyrola deposit	gn	-16.6	massive argillite	2" lens of banded bt-sph-gn-py at base of gray chert interval
PY-7-20, 294'	Pyrola deposit	gn	-16.8	massive argillite	1.5" thick barite-sulfide horizon
PY-7-20, 294' dup	Pyrola deposit	gn	-16.8	massive argillite	1.5" thick barite-sulfide horizon
B-18	B-Road	MFP	-14.2		
97-ADM-67	Mt. Robert Barron profile sta RA-K	po	-5.2	po-rich vein quartz	
92-GB-15	North shore, Gambier Bay	py	-23	listwanite	green qtz-carbonate with sulfides
92-GB-17	North shore, Gambier Bay	py	-15.2	graphitic schist	graphitic schist with bands of white qtz and sulfides
92-GB-25	North shore, Gambier Bay	py	-19.9	sediments	2" thick pyrite horizon
97-ADM-06	A-Road, 3.9 miles	py	-6.0	pyritic argillite	
97-ADM-09A	A-Road occurrence, 3.6 miles	py	-7.1	4' thick bedded bt-py-qtz	
97-ADM-09A dup	A-Road occurrence, 3.6 miles	py	-7.0	4' thick bedded bt-py-qtz	
97-ADM-09C	A-Road occurrence, 3.6 miles	py	-1.4	mineralized graphitic black argillite	
97-ADM-13	B-Road, 1.1 miles, "wide corner"	py	-2.2	pyritic graphitic sericite phyllite	
97-ADM-17	North Gambier occurrence discovery bend	py	-11.7	qtz-flooded volcanic w sph-gn-tetr	
97-ADM-20	North Gambier occurrence VLFsta 200' N	py	-15.9	qtz-sulfide stockwork in hematized basalt	
97-ADM-46	Creek AD-07, Eagle Peak	py	-2.8	green-tan banded phyllite with py-mp-carb	
97-ADM-52	W. of Swan Island occurrence	py	1.3	vein of py-qtz-carb in altered basalt	
97-ADM-66	Mt. Robert Barron profile sta RA-J	py	3.8	metadiorite	
97-ADM-70	Mt. Robert Barron profile sta RA-P	py	3.8	metadiorite with disseminated pyrite	
97-ADM-79	North shore, Gambier Bay, VLF station 5800'	py	-30.1	pyritic bands in mixed argillite/tuff	
97-ADM-91	Etta prospect	py	-2.9	sulfide veined mottled quartz	
97-LG-11	Gallagher Ridge, east end, south side	py	-31.1	pyritic argillite	
97-LG-35	Mammoth claim	py	0.7	gn-sph-py-bt-carb-rich (light green sph)	
97-LG-56	upper Zinc Creek	py	-20.3	SPgr, Fe-stained py-rich sericite phyllite	
A-Rd-02	A-Road, 3.1mi	py	2.6	sheared graphitic argillaceous phyllite	
A-Rd-04	A-Road, 1.9 miles, Pit 7	py	-35.4	argillaceous schist, metacrystic pyrite	
B-18	B-Road	py	-13.3		
B-Rd-02	B-Road, 2.42 miles	py	-13.0	semimassive pyrite in black argillite	
B-Rd-04	B-Road, 3.3 mi, just up from pit	py	-15.5	sericitic carbonated argillite	
B-Rd-04 dup	B-Road, 3.3 mi, just up from pit	py	-15.5	sericitic carbonated argillite	
NAD-T16-11	upper Zinc Creek	py	-8.4	argillite	brecciated argillite with qtz and py-mp clasts
NAD-T17-10A	Killer Creek occurrence	py	-11.0	massive pyrite	
NAD-T17-1B	Killer Creek occurrence	py	-12.3	semimassive graphitic py-qtz-carb	

Table 2. Sulfur isotope data, sample locations, and descriptions for samples from Admiralty Island host rocks and mineral occurrences.—Continued

Sample id	Location	Mineralogy	$\delta^{34}\text{S}$ value	Host rock	Comments
NAD-T17-4B	Killer Creek occurrence	py	-8.2	argillite	semimassive base-metal sulfide
NAD-T17-8B	Killer Creek occurrence	py	-11.7	greenstone	pyritic qtz-carb altered mafic rock (?)
NAD-T17-9A	Killer Creek occurrence	py	-10.0	massive pyrite	
PS-122 721'	mine area	py	-10.3	phyllite	
92-GB-67	North Gambier occurrence	sph	-7.4	basalt	bt-sph veined basalt
97-ADM-17	North Gambier occurrence discovery bend	sph	-4.8	qtz-flooded volcanic w sph-gn-tetr	
97-ADM-67	Mt. Robert Barron profile sta RA-K	sph	-4.5	po-rich vein quartz	
97-LG-33	Mammoth claim	sph	-2.7	py-sph-gn mineralized qtz-carbonate	
CASCADE CR.	B-Road, 3.4 miles	sph	-13.3		
NAD-T17-7D	Killer Creek occurrence	sph	-8.6	WSI	
NAD-T17-7D dup	Killer Creek occurrence	sph	-8.5	WSI	
PORTAGE	Mansfield Peninsula, Portage occurrence	sph	-2.1		
PORTAGE dup	Mansfield Peninsula, Portage occurrence	sph	-2.1		

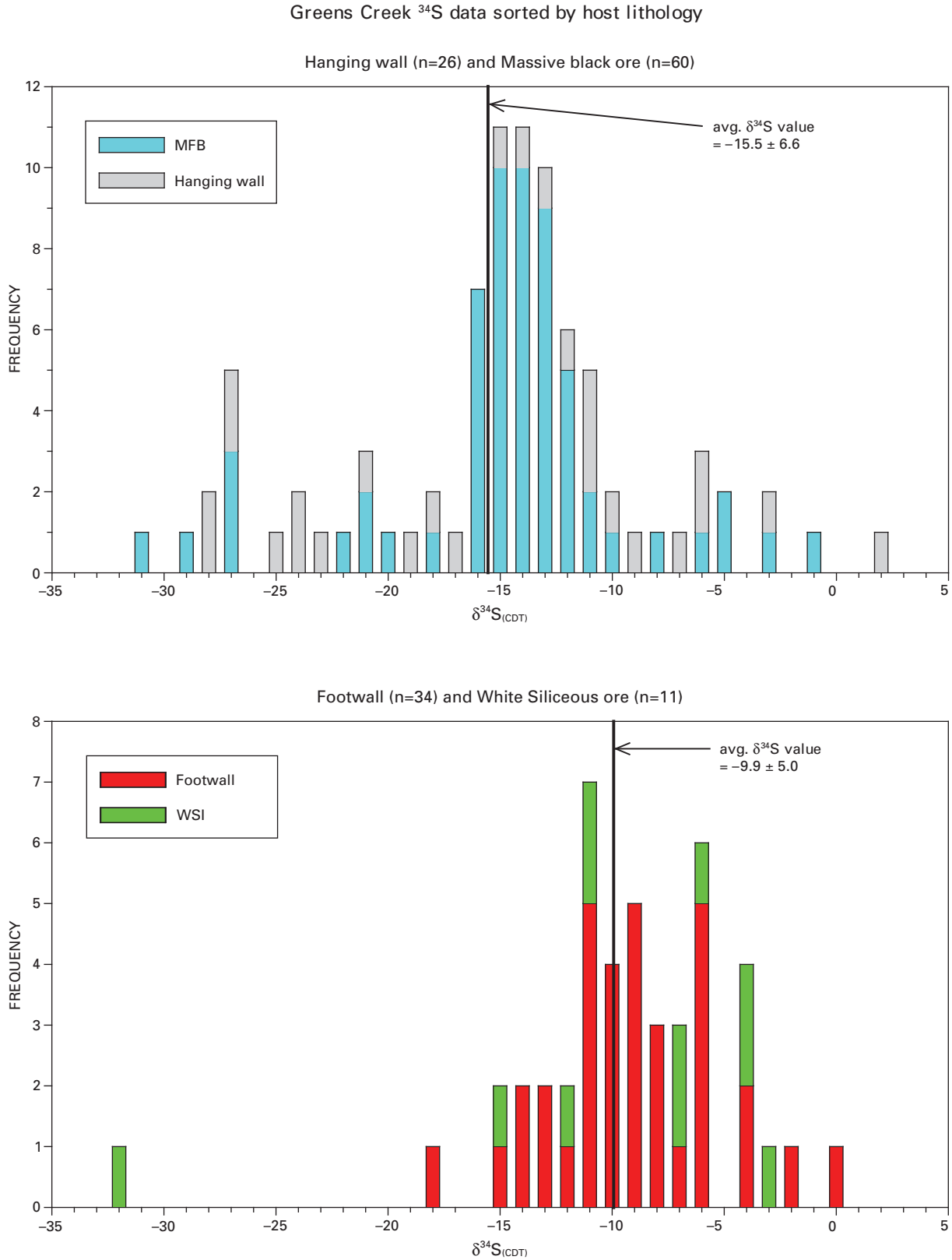


Figure 5. Comparison of sulfide sulfur isotope data in footwall versus hanging-wall lithologies. The upper plot shows all data from the hanging-wall argillites and MFB ore type, with an average value of -15.5 ± 6.6 per mil $\delta^{34}\text{S}$. The lower plot shows all data from the footwall phyllites and WSI ore type, with an average value of -9.9 ± 5.0 per mil $\delta^{34}\text{S}$. Together, the plots demonstrate the minewide ^{34}S -depletion with stratigraphic height through the ore stratigraphy. CDT, Cañon Diablo troilite.

Lead Isotopes

Fifty-five lead isotopic determinations were performed on 46 sulfides and 9 ores from underground, and 15 sulfides from 11 surface sites on Admiralty Island. Sulfides analyzed are chalcopyrite, pyrite, sphalerite, galena, tetrahedrite, pyrrargyrite, and pyrrotite. Data are presented in table 3. Whole-rock uranium-thorium-lead (as well as rubidium-strontium and samarium-neodymium) isotopic analyses were performed on a suite of mafic-ultramafic igneous rocks, argillites, and phyllites from Admiralty Island, and these data are used to characterize host rocks and possible source rocks in the mine area as well as compare host-rock and sulfide lead isotope compositions (see chap. 11).

Figure 8 shows the distribution of galena lead isotopic compositions from Greens Creek ore and several occurrences on Admiralty Island (Mammoth claim, Kennecott Rand, and Pyrola). Data from the Greens Creek galenas define a trend that is very similar to that produced by fractionation of the lead isotopes during ionization in the mass spectrometer. The majority of lead isotopic values for the Greens Creek galena vary between $^{206}\text{Pb}/^{204}\text{Pb} = 18.645$ to 18.708 and $^{207}\text{Pb}/^{204}\text{Pb} = 15.594$ to 15.669 (fig. 8A) and $^{208}\text{Pb}/^{204}\text{Pb} = 38.34$ to 38.625 (fig. 8B). Some of the trend is undoubtedly produced by mass discrimination effects during spectrometry; however, the full isotopic range shown by the galena data appears to be too large (see below). Although none of the Greens Creek galena separates were measured more than once, two analyses for the same Kennecott-Rand sample yielded nearly identical results at $^{206}\text{Pb}/^{204}\text{Pb} = 18.535$, $^{207}\text{Pb}/^{204}\text{Pb} = 15.60$, and $^{208}\text{Pb}/^{204}\text{Pb} = 38.29$, a composition that deviates from the ore-lead trend. Two galenas from the Pyrola occurrence plot on top of each other and also fall off the Greens Creek ore-lead trend, similar to, but slightly more ^{207}Pb and ^{208}Pb depleted than, the Kennecott-Rand galenas. Galena from an occurrence on the Mammoth claim (LG-33) just north of Greens Creek plots slightly off of the Greens Creek ore-lead trend. These data are then compared to average model lead values of the orogene curve of Zartman (1984). A similar average model lead curve for the mantle is out of the scope of this diagram to the lower left corner. Comparisons of the $^{206}\text{Pb}/^{204}\text{Pb}$ and $^{208}\text{Pb}/^{204}\text{Pb}$ data produce very similar relationships (fig. 8B).

Pyrrargyrite and tetrahedrite are compared to the galena ore-lead trend and were found to conform to it (fig. 9), although on average at slightly less radiogenic values. The least radiogenic compositions for these sulfides are $^{206}\text{Pb}/^{204}\text{Pb} = 18.642$ and 18.637 , respectively, $^{207}\text{Pb}/^{204}\text{Pb} = 15.584$ and 15.578 , respectively (fig. 9A), and $^{208}\text{Pb}/^{204}\text{Pb} = 38.343$ and 38.330 , respectively (fig. 9B). One notable exception is the pyrrargyrite from diabase dike GC-1701-01 that plots on the Greens Creek ore-lead trend to the high ^{207}Pb and ^{208}Pb side. Although this analysis deviates from the main cluster, it is presumed to be accurate as multiple runs at differing currents and temperatures of the same tetrahedrite sample, GC-24, vary less than the deviation shown by sample GC-1701-01 from the main cluster (fig. 9). Maximum deviations due to mass

discrimination effects in the lead isotopic ratios for the five GC-24 analyses are $\delta^{206}\text{Pb}/^{204}\text{Pb} = 0.013$, $\delta^{207}\text{Pb}/^{204}\text{Pb} = 0.018$, and $\delta^{208}\text{Pb}/^{204}\text{Pb} = 0.052$ (table 3), corresponding to slopes of $7/6 = 1.4$ and $8/6 = 4$.

Sphalerite and pyrite data are compared with the galena ore-lead trend and are found to deviate in some cases (fig. 10). In both ^{207}Pb - ^{206}Pb and ^{208}Pb - ^{206}Pb correlation diagrams, two sphalerites (Cascade Creek and Portage) and four pyrites (NAD-T13-3c and three samples from drill hole GC-1656) plot with a higher $^{206}\text{Pb}/^{204}\text{Pb}$ value than Greens Creek galena. One obvious explanation is that several of these separates contain measurable uranium that has since produced enough radiogenic lead to evolve the lead isotopic composition to higher $^{206}\text{Pb}/^{204}\text{Pb}$ values. For example, the Portage sphalerite contained significant amounts of uranium such that a correction for radiogenic lead due to in-situ decay of uranium since 215 Ma in the Portage sphalerite results in a composition slightly less radiogenic than Kennecott-Rand galena (fig. 10A).

In contrast, an analysis of sphalerite from Cascade Creek also exhibits a more radiogenic value, $^{206}\text{Pb}/^{204}\text{Pb} = 19.017$, $^{207}\text{Pb}/^{204}\text{Pb} = 15.646$, and $^{208}\text{Pb}/^{204}\text{Pb} = 39.204$ (fig. 10), clearly more enriched and quite different than either the Greens Creek ore-lead trend or the Portage sphalerite, but did not contain enough uranium to produce a significant change in this lead isotopic composition (table 3). Initial lead isotopic compositions for all mineral separates for which uranium was measured are given in table 3.

Another exception is sphalerite lead (97-ADM-17) from the North Gambier occurrence (Taylor and others, 1992) that is less ^{206}Pb -rich, but more ^{207}Pb -rich than the Greens Creek ore-lead trend (fig. 10). Sphalerites from underground are also variable. GC-1514-46 (Northwest West orebody) sphalerite is slightly off the Greens Creek ore-lead trend, whereas sphalerite from GC-19 and GC-164-11 (both lower Southwest orebody) are both on the trend. Sphalerite sample GC-19 was measured five times (fig. 10), again to evaluate deviations due to mass discrimination effects. Maximum deviations in the lead isotopic ratios for the five GC-19 analyses are $\delta^{206}\text{Pb}/^{204}\text{Pb} = 0.035$, $\delta^{207}\text{Pb}/^{204}\text{Pb} = 0.034$, and $\delta^{208}\text{Pb}/^{204}\text{Pb} = 0.102$ (table 3), corresponding to slopes of $7/6 = 1.0$ and $8/6 = 2.9$.

Similar relationships are found in some of the ^{206}Pb - ^{208}Pb data (fig. 10B). However, slight differences can be observed in the pyrite and sphalerite data, indicating slightly different thorium/uranium values for these mineral separates as can be noted from the data in table 3. In particular, Cascade Creek exhibits the highest $^{208}\text{Pb}/^{204}\text{Pb}$ value (39.35), indicating that the lead for this sphalerite was derived from a source with higher thorium/uranium values than other sphalerites.

Pyrite lead data can be found both on and off the Greens Creek galena ore-lead trend. Thirteen of 20 pyrite analyses lie on or very near the ore-lead trend. Exceptions include massive pyrite (NAD-T17-9a) from the Killer Creek occurrence with a composition very similar to the Kennecott-Rand galena (fig. 10). Several other pyrites from Killer Creek and the upper Zinc Creek area plot off the Greens Creek ore-lead

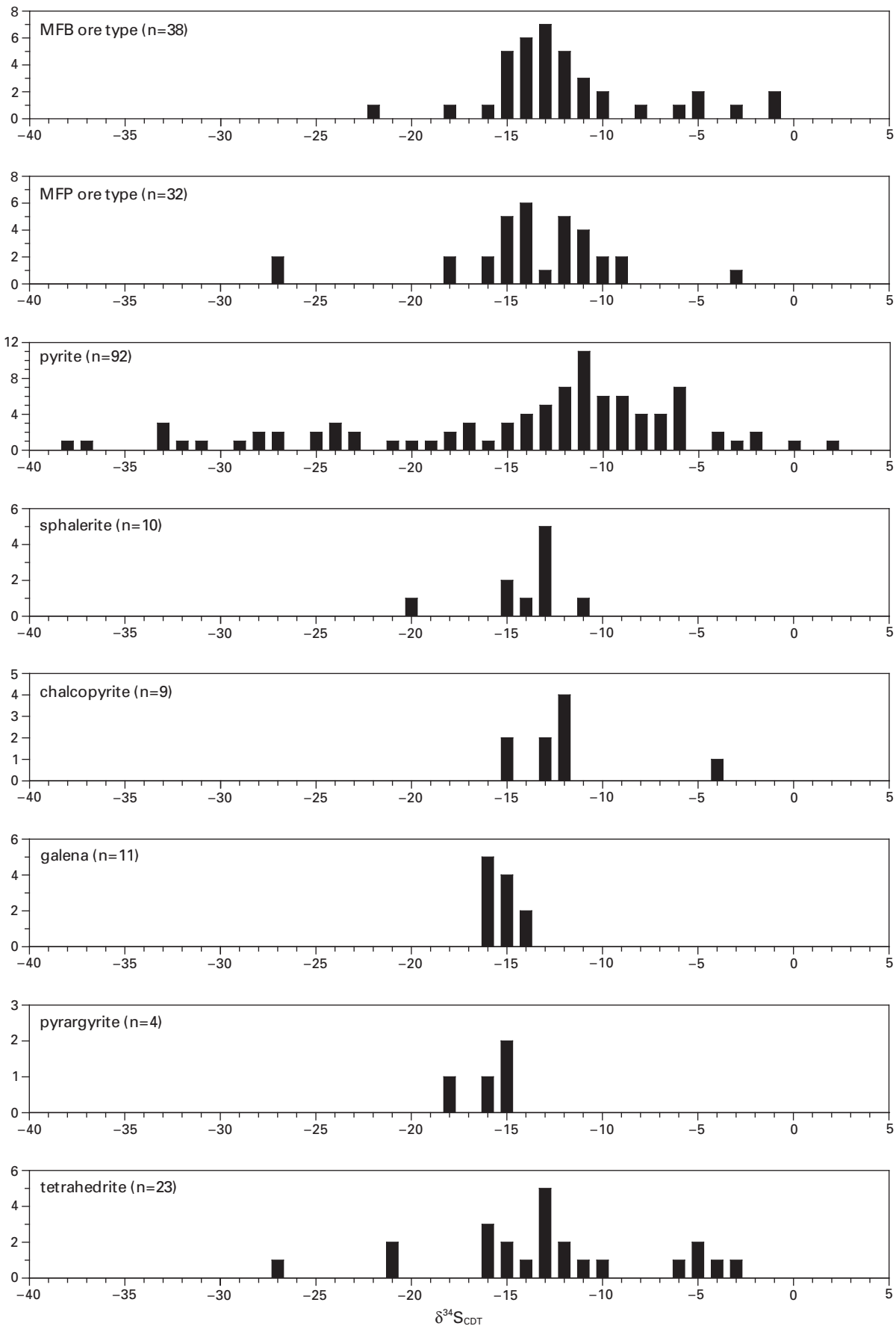


Figure 6 (facing page). Sulfide sulfur isotope data sorted by mineralogy and ore type. MFB, massive fine-grained black ore; WSI, white siliceous ore. CDT, Cañon Diablo troilite.

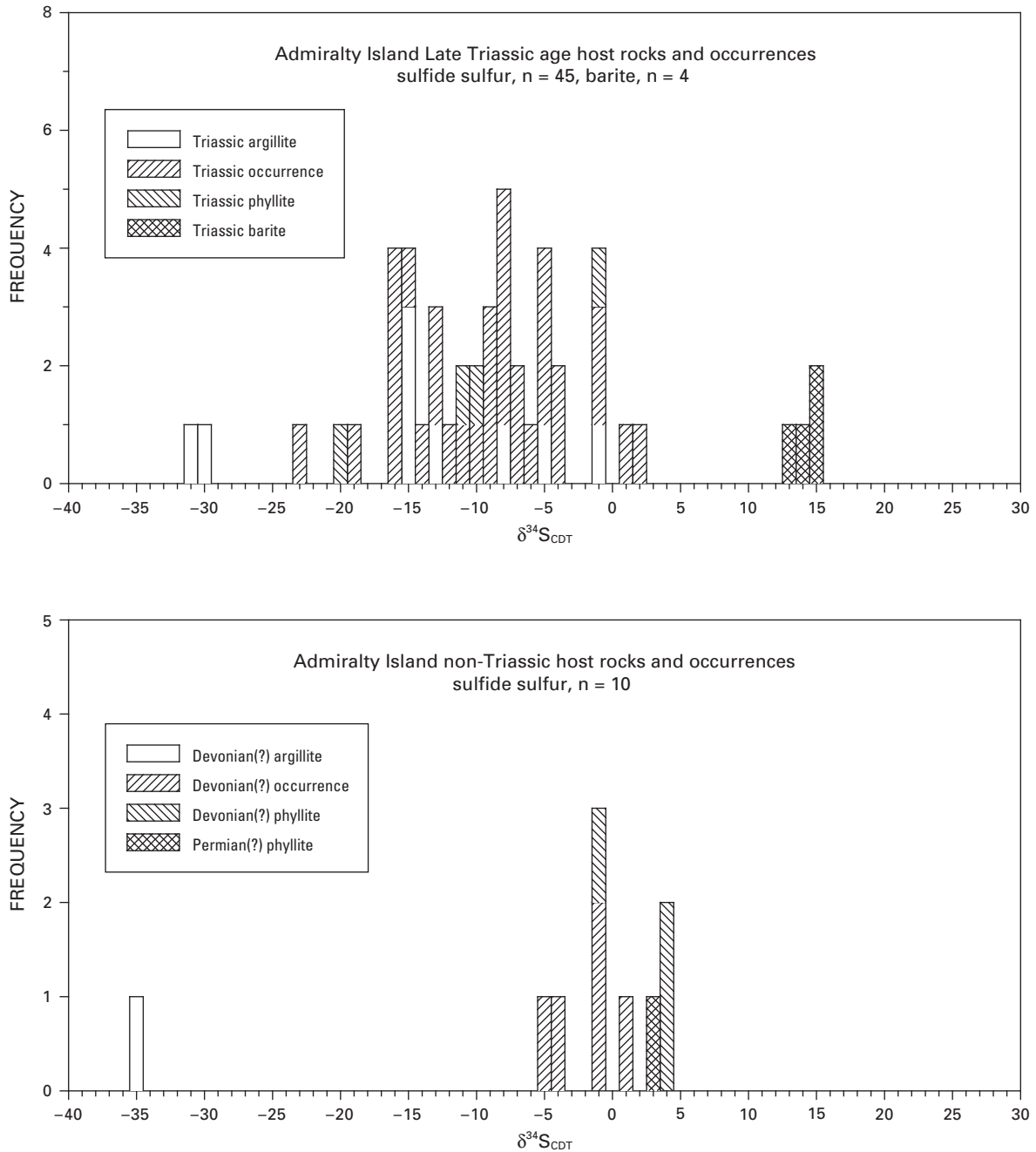


Figure 7. Sulfide and barite sulfur isotope data from host rocks and occurrences elsewhere on Admiralty Island. The upper histogram shows the $\delta^{34}\text{S}$ distribution of sulfide and barite sulfur in Late Triassic age argillites, phyllites, and mineral occurrences on Admiralty Island. The lower histogram shows the $\delta^{34}\text{S}$ distribution of Devonian(?) argillites, phyllites, and mineral occurrences, and Permian(?) phyllites. The histograms demonstrate the strongly ^{34}S -depleted signature of Late Triassic age host rocks and occurrences as compared to the near-zero values of non-Triassic host rocks and occurrences. CDT, Cañon Diablo troilite.

Table 3. Uranium-thorium-lead (U-Th-Pb) isotope data, sample locations, and descriptions of ores and sulfide minerals from the Greens Creek mine, and mineral occurrences and host rocks on Admiralty Island.

Sample name	Mineralogy	Sample wt. (mg)	U (ppm)	Th (ppm)	Pb (ppm)	$^{206}\text{Pb}/^{204}\text{Pb} \dagger$	^{206}Pb % error	$^{207}\text{Pb}/^{204}\text{Pb} \dagger$	^{207}Pb % error	$^{208}\text{Pb}/^{204}\text{Pb} \dagger$	^{208}Pb % error	$^{238}\text{U}/^{204}\text{Pb} \dagger$	$^{238}\text{U}/^{204}\text{Pb}$ % error	$^{232}\text{Th}/^{204}\text{Pb} \dagger$	$^{232}\text{Th}/^{204}\text{Pb}$ % error
GC-1093-05	cpy	4.39	0.013	0.052	1,998	18.6580	0.063	15.6090	0.093	38.4200	0.124	0.00042	2.860	0.00170	2.890
GC-1514-44	cpy	2.37	0.093	0.010	130	18.6850	0.079	15.6050	0.114	38.4070	0.152	0.04590	0.616	0.00483	17.200
GC-1514-46	cpy	3.43	0.294	0.134	66	18.7830	0.067	15.6090	0.096	38.4040	0.124	0.28571	1.130	0.13490	1.700
97-GC164-06	gn	2.88				18.6990	0.043	15.6579	0.070	38.5875	0.096				
97-GC164-08	gn	1.28				18.6598	0.043	15.6075	0.058	38.4173	0.094				
97-LG-33	gn	0.65				18.6808	0.037	15.6145	0.051	38.4258	0.075				
GC-1093-03	gn	5.98				18.7079	0.588	15.6688	0.134	38.6250	0.192				
GC-1093-05	gn	2.16				18.6794	0.048	15.6340	0.058	38.5060	0.078				
GC-164-11	gn	2.08				18.6845	0.027	15.6384	0.038	38.5273	0.039				
GC-1643-06	gn	0.33				18.6626	0.016	15.6116	0.026	38.4420	0.042				
GC-1656-13	gn	1.21				18.6808	0.064	15.6340	0.090	38.5104	0.127				
GC-1656-21	gn	3.75				18.6858	0.064	15.6404	0.121	38.5263	0.127				
Kennecott-Rand	gn	1.06				18.5338	0.022	15.5952	0.038	38.2869	0.047				
Kennecott-Rand #2	gn	1.06				18.5376	0.038	15.5983	0.045	38.2940	0.071				
PP- 173-06	gn					18.6457	0.059	15.5936	0.064	38.3400	0.065				
PS-27 660'	gn					18.6700	0.161	15.6100	0.192	38.4490	0.156				
PY-7-13	gn	0.3				18.5410	0.021	15.5679	0.028	38.1507	0.035				
PY-7-20	gn	0.6				18.5397	0.015	15.5672	0.022	38.1508	0.030				
97-ADM-67	po	11.52	0.024	0.010	948	18.4350	0.180	15.5950	0.232	38.2130	0.235	0.00161	3.850	0.00072	5.230
350-2650	py	4.91			8,048	18.6624	0.064	15.6120	0.090	38.4305	0.122				
96-GC-38	py	1.64	0.202	0.122	10,494	18.6710	0.062	15.6180	0.092	38.4530	0.122	0.00122	0.995	0.00076	2.240
97-ADM-06	py	4.45	0.265	1.240	177	18.6440	0.062	15.5830	0.092	38.3000	0.122	0.09520	0.426	0.45990	0.196
97-ADM-06 #2	py	4.45	0.265	1.240	177	18.6450	0.064	15.5850	0.093	38.3070	0.122	0.09535	0.425	0.46060	0.194
97-LG-64	py	7.61	0.094	0.275	1,233	18.7970	0.079	15.4730	0.111	38.0510	0.135	4.81320	0.352	14.63000	1.210
B-18	py	1.86	0.024	0.134	53	18.6730	0.063	15.6030	0.093	38.3810	0.122	0.02860	2.830	0.16590	1.580
B-18	py	1.8	0.012	0.043	96	18.6730	0.065	15.6180	0.094	38.4360	0.123	0.00830	5.640	0.02965	4.910
GC-1656-02	py	0.54	1.026	0.958	427	18.7520	0.061	15.6040	0.091	38.3620	0.122	0.15291	1.760	0.14760	3.150
GC-1656-02	py	0.94	3.499	0.501	352	18.7170	0.061	15.5920	0.091	38.3360	0.121	0.63329	0.117	0.09377	1.440
GC-1701-01	py	4.75	0.040	0.084	5,859	18.6550	0.063	15.6070	0.094	38.4100	0.123	0.00044	1.720	0.00094	3.520
GC-1136-40	py	2.1	0.893	0.130	4,151	18.6758	0.193	15.6102	0.211	38.4384	0.221	0.01370	0.630	0.00206	1.650
GC-1656-05	py	0.48	23.630	2.098	874	18.7330	0.063	15.6310	0.093	38.4760	0.122	1.72500	0.191	0.15830	2.390
GC-1656-20	py	0.89				18.6662	0.059	15.6152	0.090	38.4389	0.122				
NAD-T16-11	py	1.5	0.029	0.023	582	18.6650	0.065	15.6020	0.095	38.3960	0.124	0.00318	2.870	0.00258	11.100
NAD-T17-1b	py	1.56	0.039	0.033	353	18.6530	0.064	15.5900	0.093	38.3520	0.124	0.00703	2.110	0.00611	7.430
NAD-T17-1b #2	py	1.56	0.039	0.033	353	18.6610	0.061	15.5990	0.091	38.3820	0.121	0.00702	2.110	0.00610	7.430
NAD-T17-8b	py	1.74	0.062	0.416	146	18.6910	0.061	15.6150	0.091	38.4300	0.121	0.02702	1.650	0.18730	0.620
NAD-T17-9a	py	2.52	0.026	0.023	1,708	18.5420	0.089	15.5930	0.111	38.2800	0.143	0.00096	2.350	0.00086	6.670
NAD-T17-9a #2	py	2.52	0.026	0.023	1,708	18.5400	0.061	15.5920	0.091	38.2760	0.121	0.00096	2.350	0.00086	6.670
NAD-T13-3c	py	1.28	0.132	0.255	65	18.8000	0.078	15.6050	0.105	38.4300	0.136	0.12918	0.834	0.25860	2.320
350-2650	pyr	0.88				18.6499	0.040	15.5982	0.045	38.3896	0.060				
96-GC-01	pyr	6.76				18.6788	0.294	15.6224	0.390	38.4485	0.341				
96-GC-03	pyr	15.27				18.6418	0.123	15.5922	0.141	38.3794	0.138				
GC-1656-20	pyr	0.03				18.6418	0.040	15.5836	0.045	38.3431	0.060				
GC-1701-01	pyr	1.14				18.7270	0.080	15.6920	0.107	38.6900	0.138				
96-GC-02	sph	5.03				18.6599	0.064	15.6103	0.089	38.4301	0.130				
96-GC-19	sph	0.7				18.6433	0.345	15.5956	0.356	38.4152	0.368				
96-GC-19 #2	sph	0.7				18.6612	0.064	15.6121	0.090	38.4296	0.122				
96-GC-19 #3	sph	0.7				18.6530	0.060	15.6010	0.091	38.3980	0.120				
96-GC-19 #4	sph	0.7				18.6690	0.061	15.6200	0.091	38.4650	0.121				
96-GC-19 #5	sph	0.7				18.6780	0.061	15.6300	0.091	38.5000	0.121				
97-ADM-17	sph	3.66				18.5596	0.060	15.7732	0.090	38.9713	0.122				

Table 3. Uranium-thorium-lead (U-Th-Pb) isotope data, sample locations, and descriptions of ores and sulfide minerals from the Greens Creek mine, and mineral occurrences and host rocks on Admiralty Island.—Continued

Sample name	Mineralogy	^{206/204} Pb ††	^{207/204} Pb ††	^{208/204} Pb ††	DH depth	Location	Host rock	Mineral texture	Comments
GC-1093-05	cpy					lower SW	WCA	remobilized	gn-cpy clots in qtz-dol veins adj to MFP
GC-1514-44	cpy				696	Northwest	MFP	remobilized	cpy on fracture
GC-1514-46	cpy	18.773	15.609	38.403	707	Northwest	MFP	remobilized	euhedral cpy and sph on fracture
97-GC164-06	gn				10.5	lower SW	MVB	remobilized	dull, brassy, fine grained, with large areas of gn
97-GC164-08	gn				30	lower SW	WCA	primary/recrysta	bands in gray dolostone, minor aspy
97-LG-33	gn					Mammoth claim			py-sph-gn mineralized qtz-carbonate
GC-1093-03	gn					lower SW	WCA	remobilized	very coarse grained, monomineralic
GC-1093-05	gn					lower SW	WCA	remobilized	gn-cpy clots in qtz-dol veins adj to MFP
GC-164-11	gn				60	lower SW	WCA	remobilized	
GC-1643-06	gn				119.5	200 South	WCA	remobilized	clot in white dolomite vein, minor cpy
GC-1656-13	gn				1,008	200 South	MFB	recrystallized	galena-rich banded MFB/MFP
GC-1656-21	gn				1,071	200 South	MFB	recrystallized	very fine grained, banded, gn-rich
Kennecott-Rand	gn					Mansfield Peninsula, Kennecott-Rand occurrence			
Kennecott-Rand #2	gn					Mansfield Peninsula, Kennecott-Rand occurrence			
PP-173-06	gn				63.5	lower SW	MFB	remobilized	galena-rich MFB
PS-27 660'	gn				660	mine area			
PY-7-13	gn								
PY-7-20	gn								
97-ADM-67	po					Mt. Robert Barron profile sta RA-K			po-rich vein quartz
350-2650	py				79	lower SW	MFP	primary	primary-textured clasts, very fine grained
96-GC-38	py				148	lower SW	MP	recrystallized	bright, euhedral-subhedral,
97-ADM-06	py	18.641	15.583	38.295		A-Road, 3.9 miles	argillite		pyritic argillite
97-ADM-06 #2	py	18.642	15.585	38.302		A-Road, 3.9 miles	argillite		pyritic argillite
97-LG-64	py	18.599	15.463	37.862		Gallagher Ridge			
B-18	py					B-Road			
B-18	py					B-Road			
GC-1656-02	py	18.747	15.604	38.360	606.5	200 South	SA	primary	
GC-1656-02	py	18.696	15.591	38.335	606.5	200 South	SA	primary	
GC-1701-01	py					200 South			
GC-1136-40	py					lower SW	MP	recrystallized	
GC-1656-05	py	18.674	15.628	38.474		200 South			
GC-1656-20	py				1,062	200 South	MFP	primary	dull, brassy, pyritic MFP
NAD-T16-11	py					upper Zinc Creek	argillite		brecciated argillite with qtz and py-mp clasts
NAD-T17-1b	py					Killer Creek occurrence			semimassive graphitic py-qtz-carb
NAD-T17-1b #2	py					Killer Creek occurrence			semimassive graphitic py-qtz-carb
NAD-T17-8b	py					Killer Creek occurrence	greenstone		pyritic qtz-carb altered mafic rock (?)
NAD-T17-9a	py					Killer Creek occurrence	massive pyrite		
NAD-T17-9a #2	py					Killer Creek occurrence	massive pyrite		
NAD-T13-3c	py	18.796	15.605	38.427					
350-2650	pyr				79	lower SW	MFP	remobilized	qtz-pyr veinlets crosscutting MFP
96-GC-01	pyr				79	lower SW	MFP	remobilized	
96-GC-03	pyr				79	lower SW	MCHT	remobilized	
GC-1656-20	pyr				1,062	200 South	MFP	remobilized	
GC-1701-01	pyr								
96-GC-02	sph				62.5	lower SW	MFP	recrystallized	
96-GC-19	sph				53	lower SW	WCA	remobilized	
96-GC-19 #2	sph				53	lower SW	WCA	remobilized	
96-GC-19 #3	sph				53	lower SW	WCA	remobilized	
96-GC-19 #4	sph				53	lower SW	WCA	remobilized	
96-GC-19 #5	sph				53	lower SW	WCA	remobilized	
97-ADM-17	sph					North Gambier occurrence discovery bend	basalt		qtz-flooded volcanic w sph-gn-tetr

Table 3. Uranium-thorium-lead (U-Th-Pb) isotope data, sample locations, and descriptions of ores and sulfide minerals from the Greens Creek mine, and mineral occurrences and host rocks on Admiralty Island.—Continued

Sample name	Mineralogy	Sample wt. (mg)	U (ppm)	Th (ppm)	Pb (ppm)	²⁰⁶ Pb/ ²⁰⁴ Pb †	²⁰⁶ Pb/ ²⁰⁴ Pb % error	²⁰⁷ Pb/ ²⁰⁴ Pb †	²⁰⁷ Pb/ ²⁰⁴ Pb % error	²⁰⁸ Pb/ ²⁰⁴ Pb †	²⁰⁸ Pb/ ²⁰⁴ Pb % error	²³⁸ U/ ²⁰⁴ Pb †	²³⁸ U/ ²⁰⁴ Pb % error	²³² Th/ ²⁰⁴ Pb †	²³² Th/ ²⁰⁴ Pb % error
Cascade Ck	sph	20.32	0.928	0.140	2,182	19.0170	0.065	15.6460	0.094	39.2040	0.123	0.02752	2.400	0.00428	2.400
GC-1514-46	sph	3.79	0.024	0.014	77	18.6860	0.063	15.6000	0.093	38.3850	0.122	0.02023	1.500	0.01180	7.310
GC-164-11	sph	3.85	0.020	0.009	1,109	18.6410	0.062	15.5850	0.092	38.3470	0.122	0.00117	2.340	0.00054	11.000
Portage	sph	24.53	2.476	1.495	17.4	18.7900	0.061	15.6090	0.091	38.3500	0.121	9.06880	0.491	5.65600	0.505
96-GC-24	tetr	1.61				18.6441	0.064	15.5894	0.096	38.3544	0.125				
96-GC-24 #2	tetr	1.61				18.6565	0.064	15.6071	0.096	38.4066	0.125				
96-GC-24 #3	tetr	1.61				18.6440	0.060	15.5900	0.090	38.3560	0.120				
96-GC-24 #4	tetr	1.61				18.6470	0.061	15.5940	0.091	38.3710	0.121				
96-GC-24 #5	tetr	1.61				18.6510	0.062	15.5980	0.092	38.3840	0.123				
97-GC164-11	tetr	0.23	0.064	0.322	30,660	18.6636	0.064	15.6133	0.093	38.4420	0.122	0.00013	8.780	0.00069	5.310
GC-164-04	tetr	3.52				18.6371	0.064	15.5782	0.096	38.3302	0.125				
GC-1643-06	tetr	1.52	0.060	0.018	2,112	18.6680	0.065	15.6180	0.094	38.4570	0.126	0.00182	1.540	0.00055	14.300
GC-1656-20	tetr	6.11			9,894	18.6504	0.070	15.5977	0.103	38.3868	0.130				
96-GC-24	MFB	25.27	0.491		703	18.6860	0.134	15.6640	0.242	38.5340	0.435	0.04460	5.000		
GC-1530-64	MFB	1				18.6639	0.032	15.6086	0.045	38.4170	0.065				
GC-1530-64 #2	MFB	1				18.6647	0.032	15.6089	0.045	38.4169	0.065				
GC-1643-10	MFB gn-rich	2.11				18.6418	0.102	15.5918	0.115	38.3730	0.156				
GC-1643-10	MFB sph-rich	2.8				18.6828	0.198	15.6282	0.211	38.4963	0.234				
GC-1643-10 #2	MFB sph-rich	2.8				18.6700	0.062	15.6230	0.093	38.4730	0.122				
GC-1643-10 #3	MFB sph-rich	2.8				18.6780	0.063	15.6300	0.093	38.4900	0.123				
GC-1643-10 #4	MFB sph-rich	2.8				18.6720	0.065	15.6250	0.098	38.4720	0.123				
GC-1643-10 #5	MFB sph-rich	2.8				18.6770	0.074	15.6320	0.105	38.4870	0.129				
GC-164-04	MVB gn-rich	1.52				18.6644	0.032	15.6142	0.051	38.4497	0.088				
96-GC-24	MFP	18.23				18.6698	0.616	15.6292	0.665	38.5115	0.626				
96-GC-24 #2	MFP	18.23				18.6869	0.150	15.6330	0.269	38.5165	0.260				
96-GC-24 #3	MFP	18.23				18.6756	0.016	15.6278	0.032	38.4809	0.029				
GC-1656-06	MFP	28.81				18.7709	0.075	15.7453	0.102	38.8737	0.131				
GC-1656-13	MFP	9.87				18.6756	0.037	15.6301	0.058	38.4910	0.068				
GC-1656-13 #2	MFP	9.87				18.6740	0.037	15.6327	0.058	38.5035	0.068				
GC-1514-44	MFP cpy-rich	18.32				18.6617	0.059	15.5917	0.090	38.3565	0.120				

† - corrected ratios; corrected for Pb mass fractionation (0.08 ± 0.03 % per atomic mass unit) and blank Pb (variable amounts between 5 and 20 pg total Pb; blank composition: $^{206}\text{Pb}/^{204}\text{Pb} = 18.8 \pm 0.6$; $^{207}\text{Pb}/^{204}\text{Pb} = 15.65 \pm 0.2$; and $^{208}\text{Pb}/^{204}\text{Pb} = 38.65 \pm 0.75$); U mass fractionation using a double U spike ($^{233}\text{U}/^{235}\text{U} = 1.018$; and assumed Th fractionation of -0.2 ± 0.5 % per atomic mass unit using the programming of Ludwig (1985). U and Th blanks ranged between 2 - 15 and 7 - 50 pg, respectively.

†† - initial ratio values; corrected for mass fractionation, blank Pb, radiogenic Pb accumulated from the in-situ decay of U and Th over the age of the sample taken to be 215 Ma.

gn = galena, pyr = pyrrhotite, sph = sphalerite, py = pyrite, tetr = tetrahedrite, cpy = chalcopyrite, po = pyrrhotite, aspy = arsenopyrite, MFP = massive fine-grained pyritic ore, MFB = massive fine-grained base-metal-rich ore, MVB = massive very fine grained base-metal-rich ore, qtz = quartz, carb = carbonate, mp = mariposite.

Table 3. Uranium-thorium-lead (U-Th-Pb) isotope data, sample locations, and descriptions of ores and sulfide minerals from the Greens Creek mine, and mineral occurrences and host rocks on Admiralty Island.—Continued

Sample name	Mineralogy	$^{206}\text{Pb}/^{204}\text{Pb}$ ††	$^{207}\text{Pb}/^{204}\text{Pb}$ ††	$^{208}\text{Pb}/^{204}\text{Pb}$ ††	DH depth	Location	Host rock	Mineral texture	Comments
Cascade Ck	sph					B-Road, 3.4 miles			
GC-1514-46	sph				707	Northwest	MFP	remobilized	euhedral cpy and sph on fracture
GC-164-11	sph				60	lower SW	WCA	remobilized	
Portage	sph	18.482	15.593	38.290		Mansfield Peninsula, Portage occurrence			
96-GC-24	tetr				72	lower SW	MFB	remobilized	Clot of tetr in qtz vein
96-GC-24 #2	tetr				72	lower SW	MFB	remobilized	Clot of tetr in qtz vein
96-GC-24 #3	tetr				72	lower SW	MFB	remobilized	Clot of tetr in qtz vein
96-GC-24 #4	tetr				72	lower SW	MFB	remobilized	Clot of tetr in qtz vein
96-GC-24 #5	tetr				72	lower SW	MFB	remobilized	Clot of tetr in qtz vein
97-GC164-11	tetr				60	lower SW	WCA	remobilized	
GC-164-04	tetr				4.5	lower SW	MVB	remobilized	dark gray to shiny black
GC-1643-06	tetr				119.5	200 South	WCA	remobilized	clot in white dolomite vein, minor cpy
GC-1656-20	tetr				1,062	200 South	MFP	remobilized	
96-GC-24	MFB				72	lower SW	MFB	recrystallized	along edges of qtz-tetr vein in MFB banded sample
GC-1530-64	MFB				825.5	Northwest	MFB	recrystallized	very fine crystalline, euhedral
GC-1530-64 #2	MFB				825.5	Northwest	MFB	recrystallized	very fine crystalline, euhedral
GC-1643-10	MFB gn-rich				272	200 South	MFB	recrystallized	gn-rich banded MFB
GC-1643-10	MFB sph-rich				272	200 South	MFB	recrystallized	orange sph-rich band
GC-1643-10 #2	MFB sph-rich				272	200 South	MFB	recrystallized	orange sph-rich band
GC-1643-10 #3	MFB sph-rich				272	200 South	MFB	recrystallized	orange sph-rich band
GC-1643-10 #4	MFB sph-rich				272	200 South	MFB	recrystallized	orange sph-rich band
GC-1643-10 #5	MFB sph-rich				272	200 South	MFB	recrystallized	orange sph-rich band
GC-164-04	MVB gn-rich				4.5	lower SW	MVB	remobilized	silver-gray with gn in center of band
96-GC-24	MFP				72	lower SW	MFP	primary	50% recrystallized, 50% framboidal
96-GC-24 #2	MFP				72	lower SW	MFP	primary	50% recrystallized, 50% framboidal
96-GC-24 #3	MFP				72	lower SW	MFP	primary	50% recrystallized, 50% framboidal
GC-1656-06	MFP				911	200 South	MFP	recrystallized	banded MFP/WCA, drilled out MFP band
GC-1656-13	MFP				1,008	200 South	MFB	recrystallized	galena-rich banded MFB/MFP
GC-1656-13 #2	MFP				1,008	200 South	MFB	recrystallized	galena-rich banded MFB/MFP
GC-1514-44	MFP cpy-rich				696	Northwest	MFP	recrystallized	cpy-rich MFP

† - corrected ratios; corrected for Pb mass fractionation (0.08 ± 0.03 % per atomic mass unit) and blank Pb (variable amounts between 5 and 20 pg total Pb; blank composition: $^{206}\text{Pb}/^{204}\text{Pb} = 18.8 \pm 0.6$; $^{207}\text{Pb}/^{204}\text{Pb} = 15.65 \pm 0.2$; and $^{208}\text{Pb}/^{204}\text{Pb} = 38.65 \pm 0.75$); U mass fractionation using a double U spike ($^{233}\text{U}/^{236}\text{U} = 1.018$; and assumed Th fractionation of -0.2 ± 0.5 % per atomic mass unit using the programming of Ludwig (1985). U and Th blanks ranged between 2–15 and 7–50 pg, respectively.

††- initial ratio values; corrected for mass fractionation, blank Pb, radiogenic Pb accumulated from the in-situ decay of U and Th over the age of the sample taken to be 215 Ma.

gn = galena, pyr = pyrrhotite, sph = sphalerite, py = pyrite, tetr = tetrahedrite, cpy = chalcopyrite, po = pyrrhotite, aspy = arsenopyrite, MFP = massive fine-grained pyritic ore, MFB = massive fine-grained base-metal-rich ore, MVB = massive very fine grained base-metal-rich ore, qtz = quartz, carb = carbonate, mp = mariposite.

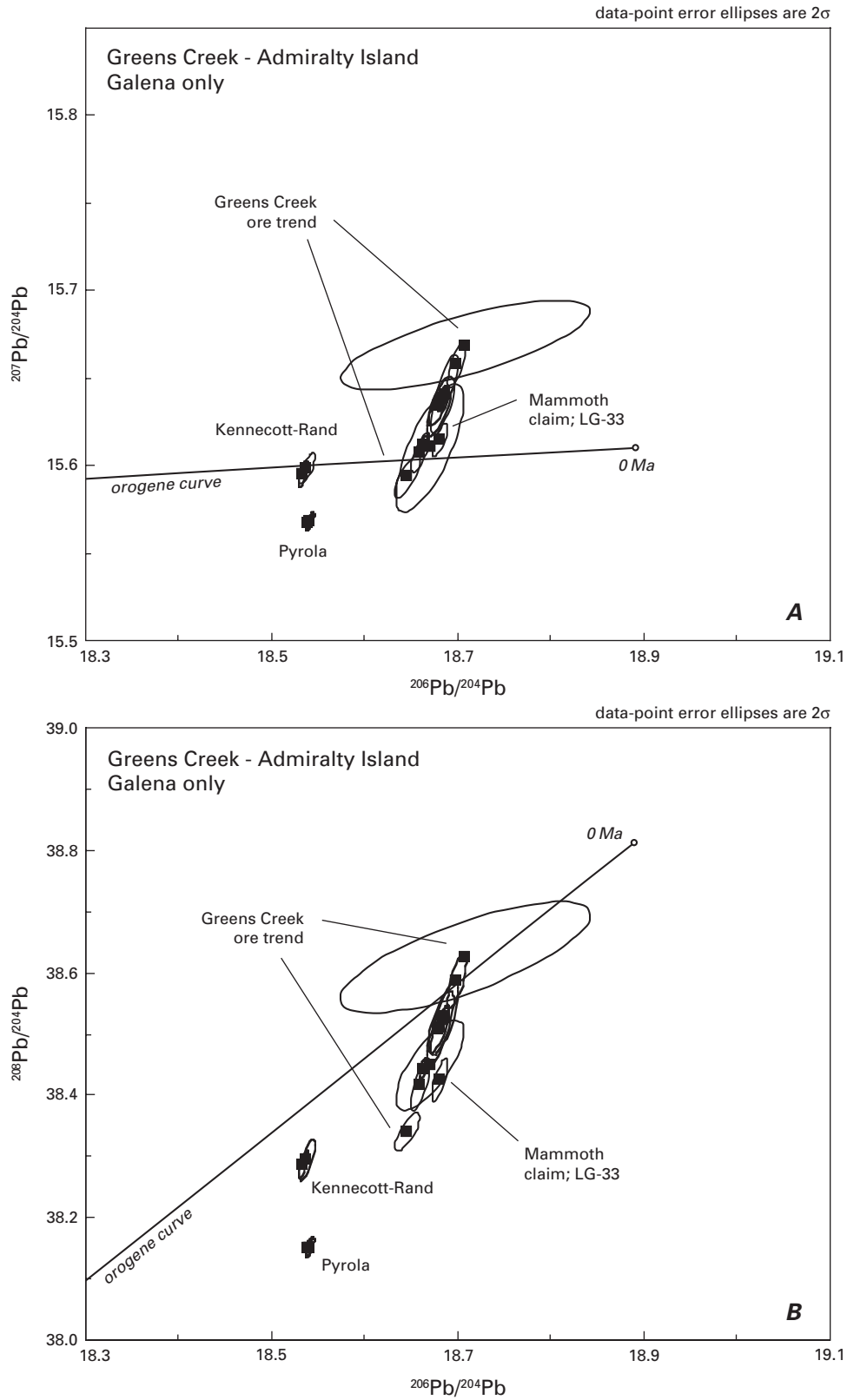


Figure 8. Plot showing the range of galena lead isotopic compositions from Greens Creek ore and several occurrences on Admiralty Island (Mammoth claim, Kennecott-Rand, and Pyrola). (A) $^{206}\text{Pb}/^{204}\text{Pb}$ versus $^{207}\text{Pb}/^{204}\text{Pb}$; (B) $^{206}\text{Pb}/^{204}\text{Pb}$ versus $^{208}\text{Pb}/^{204}\text{Pb}$. Error ellipses are 2σ . Orogene curve is that of Zartman (1984).

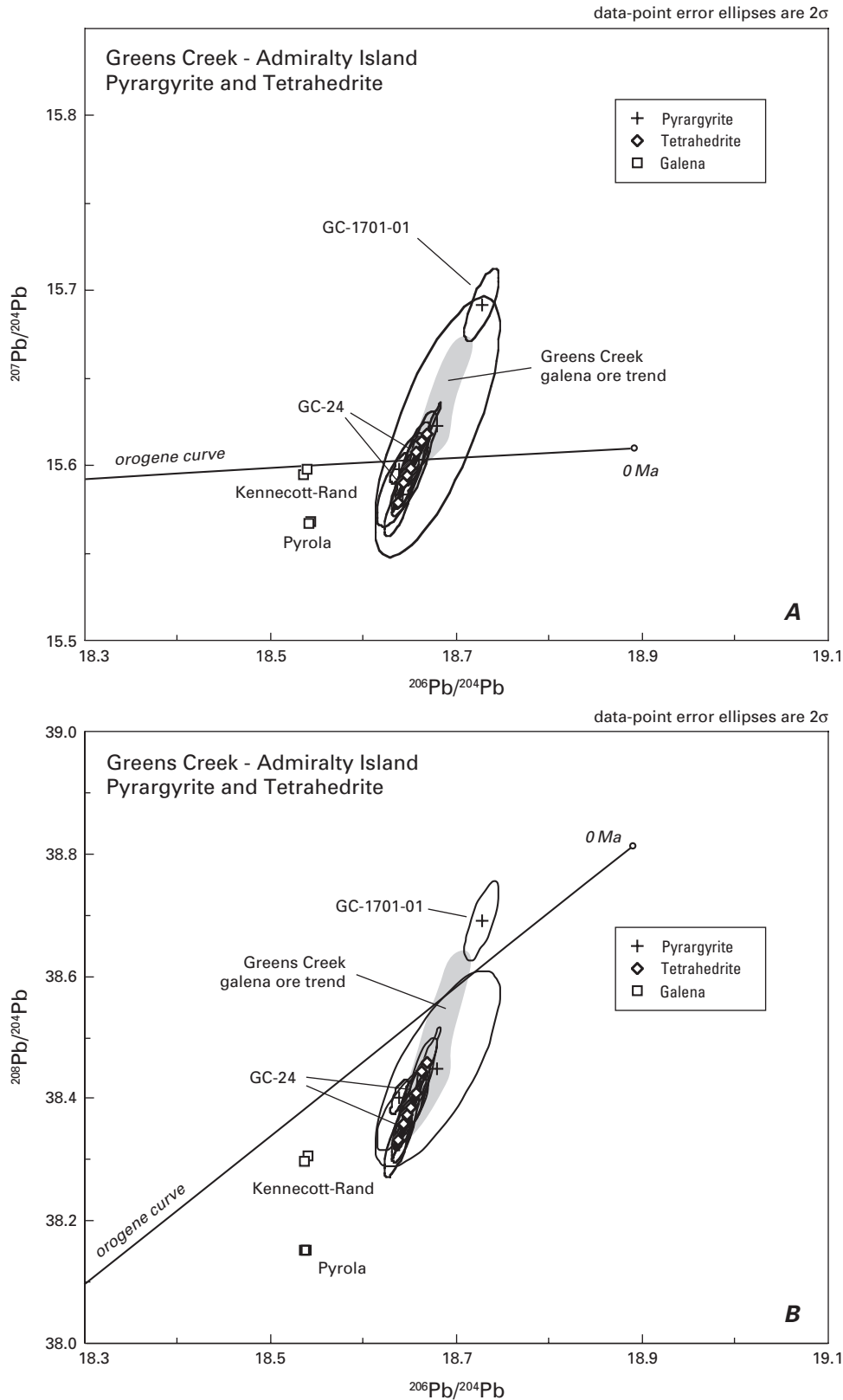


Figure 9. Plot showing the range of lead isotopic compositions of pyrrargyrite (crosses) and tetrahedrite (open diamonds) from Greens Creek ore, and compared to galena from Greens Creek (shaded field) and from several occurrences on Admiralty Island (open squares; Kennecott-Rand and Pyrola). (A) $^{206}\text{Pb}/^{204}\text{Pb}$ versus $^{207}\text{Pb}/^{204}\text{Pb}$; (B) $^{206}\text{Pb}/^{204}\text{Pb}$ versus $^{208}\text{Pb}/^{204}\text{Pb}$. Error ellipses are 2σ . Orogene curve is that of Zartman (1984).

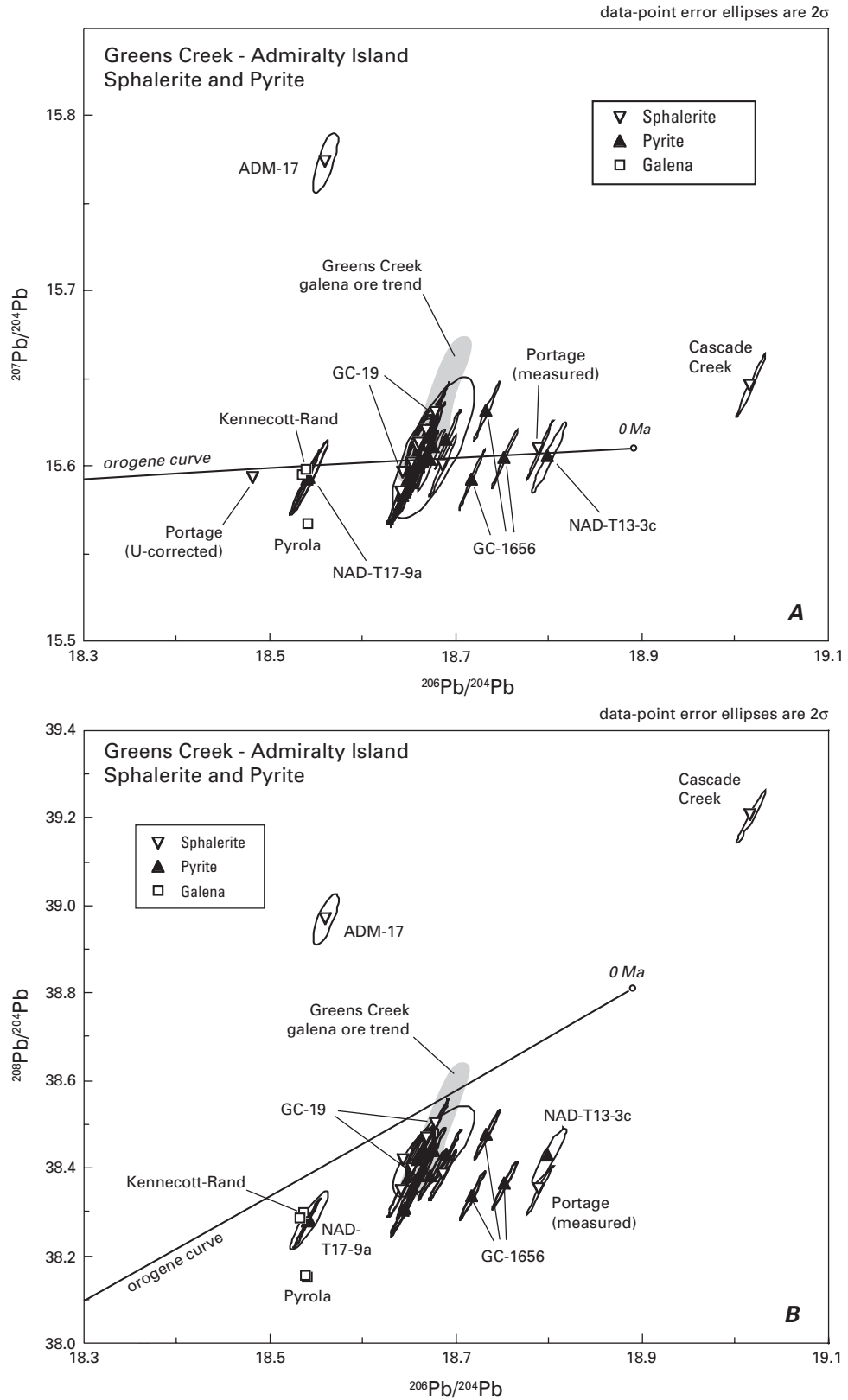


Figure 10. Plot showing the range of lead isotopic compositions of sphalerite (inverted open triangles) and pyrite (solid triangles) from Greens Creek ore, and compared to galena from Greens Creek (shaded field) and from several occurrences on Admiralty Island (open squares; Kennecott-Rand and Pyrola). (A) $^{206}\text{Pb}/^{204}\text{Pb}$ versus $^{207}\text{Pb}/^{204}\text{Pb}$; (B) $^{206}\text{Pb}/^{204}\text{Pb}$ versus $^{208}\text{Pb}/^{204}\text{Pb}$. Error ellipses are 2σ . Orogene curve is that of Zartman (1984).

trend in the high ^{206}Pb -direction. Pyrite in argillite (NAD T13-3c) from the sediments at the head of Cub Creek on Mariposite Ridge has a measured lead isotopic composition similar to that reported for Portage sphalerite. Three pyrites from drill hole GC-1656 in the hanging-wall argillite (2) and from massive ore in the 200 South orebody scatter off the Greens Creek ore-lead trend in the high ^{206}Pb direction. Two of these pyrites had measurable uranium such that a correction for radiogenic lead resulted in slightly less radiogenic values (table 3; fig. 10). One pyrite analysis is corrected to the Greens Creek ore lead trend.

Figure 11 compares analyses of chalcopyrite, pyrrhotite, and ore bands (MFB and MFP) with the galena ore-lead trend. The chalcopyrite generally conforms to the Greens Creek galena ore-lead trend with two exceptions: one chalcopyrite (GC-1514-46) plots on the high- ^{206}Pb trend, very near the Portage sphalerite composition. This chalcopyrite sample is notable because texturally the chalcopyrite occurs as euhedral crystals on a fracture through chalcopyrite-rich, massive pyritic ore. The late chalcopyrite is therefore a remobilized phase, probably as a result of metamorphism or deformation at a time when the massive Greens Creek ore was behaving in a brittle fashion. The other exception, chalcopyrite GC-1514-44, plots slightly higher in $^{206}\text{Pb}/^{204}\text{Pb}$ than the Greens Creek ore-lead trend and coincident with the composition of sphalerite GC-1514-46. The pyrrhotite analysis does not conform to the other lead analyses but is a potentially informative sample as it is from a vein occurrence near Mt. Robert Barron on the Mansfield Peninsula where rocks in the vicinity of this occurrence are mapped as the older, highly metamorphosed Retreat Group sedimentary rocks.

The massive ores conform to the Greens Creek ore-lead trend, and one sample (GC-1656-06), an MFP, extends the trends toward higher ^{207}Pb and ^{208}Pb values of $^{206}\text{Pb}/^{204}\text{Pb} = 18.771$, $^{207}\text{Pb}/^{204}\text{Pb} = 15.745$, and $^{208}\text{Pb}/^{204}\text{Pb} = 38.874$ (fig. 11). Sphalerite-rich MFB sample GC-1643-10 was measured five times, once again to evaluate deviations due to mass discrimination effects. Maximum deviations in the lead isotopic ratios for the five analyses are $\delta^{206}\text{Pb}/^{204}\text{Pb} = 0.013$, $\delta^{207}\text{Pb}/^{204}\text{Pb} = 0.009$, and $\delta^{208}\text{Pb}/^{204}\text{Pb} = 0.024$ (table 3), corresponding to slopes of $7/6 = 1.4$ and $8/6 = 1.8$. In general, like galena and tetrahedrite, the massive ores tend to be enriched in ^{207}Pb and ^{208}Pb relative to chalcopyrite and pyrite.

Finally, figure 12 displays plots of $\delta^{34}\text{S}$ versus $^{206}\text{Pb}/^{204}\text{Pb}$ and $^{207}\text{Pb}/^{204}\text{Pb}$ for sulfides and ores at Greens Creek as well as sulfides in host rocks and other mineral occurrences on Admiralty Island. In general, for Greens Creek sulfide minerals, both plots exhibit a lack of systematic variation of sulfur with lead. In detail there is a rough vertical separation on each plot of mineral species by $\delta^{34}\text{S}$ value, as observed in figure 6. The lack of variation in lead isotope values may indicate that the metal supply to the Greens Creek ore-lead trend was fairly homogeneous. Analyses of sulfides from other occurrences on Admiralty Island tend to group in the upper left quadrant of each diagram. Analyses from Pyrola and Cascade Creek have similarly ^{34}S -depleted sulfur isotope values as Greens Creek sulfides and are less radiogenic. Analyses from the

Kennecott-Rand, Portage, and Mt. Robert Barron occurrences fall within and at the less radiogenic end of the Greens Creek ore-lead trend but have noticeably ^{34}S -enriched sulfur isotope values. This is potentially significant, as all three of these occurrences are on the Mansfield Peninsula and are hosted by the older Retreat Group rocks.

Interpretation of Sulfur Isotopes

The seawater sulfate $\delta^{34}\text{S}$ curve (Strauss, 1997; Claypool and others, 1980) increases rapidly from a low of 10.5 per mil at the end of the Permian to a high of about 19 per mil in the Middle Jurassic. The isotopic similarity to Greens Creek barite, which probably formed in latest Triassic time, suggests that the barite sulfate was derived from early Mesozoic seawater.

The Greens Creek sulfide data are intriguing because they are lower than the $\delta^{34}\text{S}$ values commonly found in either VMS or clastic-hosted SEDEX deposits. Studies of numerous Phanerozoic VMS indicate that sulfide $\delta^{34}\text{S}$ values are 15–25 per mil less than those of coeval seawater sulfate. The total range for over 200 deposits worldwide is between –20 and 27 per mil (fig. 13) with means for individual deposits falling between –5 and 20 per mil (Huston, 1999). These data suggest that for most deposits, inorganic reduction of seawater sulfate by ferrous iron in country rocks is the dominant source of reduced sulfur and thus the dominant mechanism for its fixation in the rocks (Shanks and others, 1981). Another common sulfur source is igneous sulfide from leaching of volcanic host rocks and input of sulfur from degassing magmas.

In clastic-hosted SEDEX deposits, sulfide $\delta^{34}\text{S}$ values show a slightly broader range of values although fewer data are available than for VMS deposits. If the sedimentary pyrite that is commonly associated with SEDEX ores is considered, the total range is between –22 and 43 per mil with values for massive ores between –10 and 28 (fig. 13). In general, these wide ranges of values and typical fractionations of -45 ± 20 per mil from coeval seawater sulfate (Ohmoto and others, 1990) are cited as evidence for biogenically reduced seawater sulfate (Goodfellow and others, 1993; Solomon and Groves, 1994; Lydon, 1996). Strongly ^{34}S -depleted sulfides are thought to form directly from bacterially produced hydrogen sulfide in anoxic stratified bottom waters, from hydrogen sulfide-rich pore fluids in saturated sediments, or from partial dissolution of diagenetic pyrite. The tighter ranges and generally more ^{34}S -enriched values of the base-metal sulfides than for pyrite in most SEDEX deposits can be explained by the addition of a hydrothermal component carrying isotopically heavier sulfur formed by inorganic sulfate reduction (Large, 1980; Ohmoto and others, 1990; many of the northern Australia examples such as HVC and Lady Loretta, the so-called dual-sulfur source model). Clastic-hosted SEDEX deposits also commonly exhibit an increase in sulfide ^{34}S stratigraphically upward through the ore section. This feature is interpreted as evidence of bacterial sulfate reduction in a basin with restricted communication with the open ocean (Large, 1980; Goodfellow and others, 1993). Pyrite profiles that do not become ^{34}S -enriched with increasing

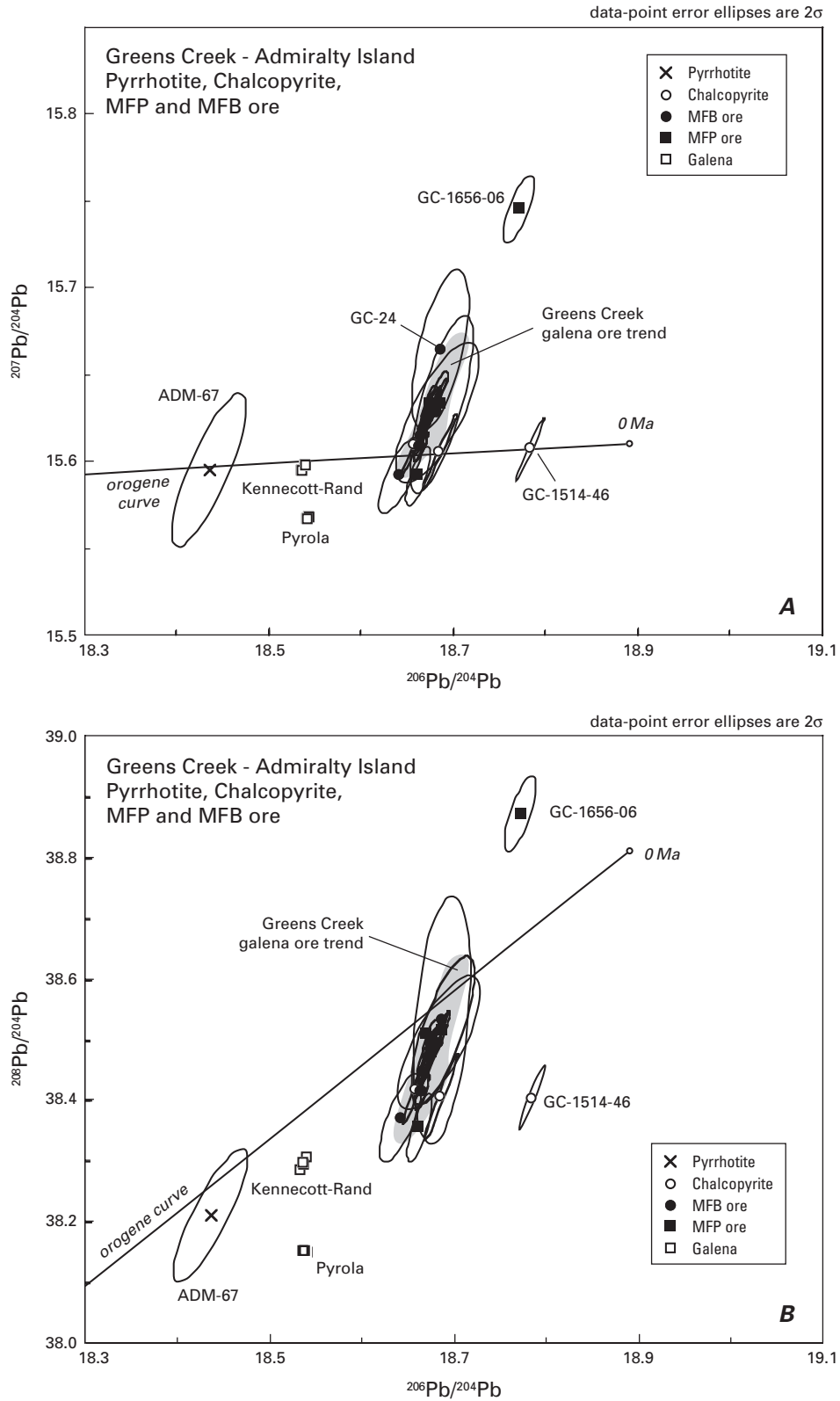


Figure 11. Plot showing the range of lead isotopic compositions of pyrrhotite (X), chalcopyrite (open circles), and several ore bands (MFB, solid circles; MFP, solid squares) from Greens Creek, and compared to galena from Greens Creek (shaded field) and from several occurrences on Admiralty Island (open squares; Kennecott-Rand and Pyrola). (A) $^{206}\text{Pb}/^{204}\text{Pb}$ versus $^{207}\text{Pb}/^{204}\text{Pb}$; (B) $^{206}\text{Pb}/^{204}\text{Pb}$ versus $^{208}\text{Pb}/^{204}\text{Pb}$. Error ellipses are 2σ . Orogene curve is that of Zartman (1984).

Greens Creek and Admiralty Island sulfide sulfur and lead isotope data
 $\delta^{34}\text{S}$ versus $^{207}\text{Pb}/^{204}\text{Pb}$ and $^{206}\text{Pb}/^{204}\text{Pb}$

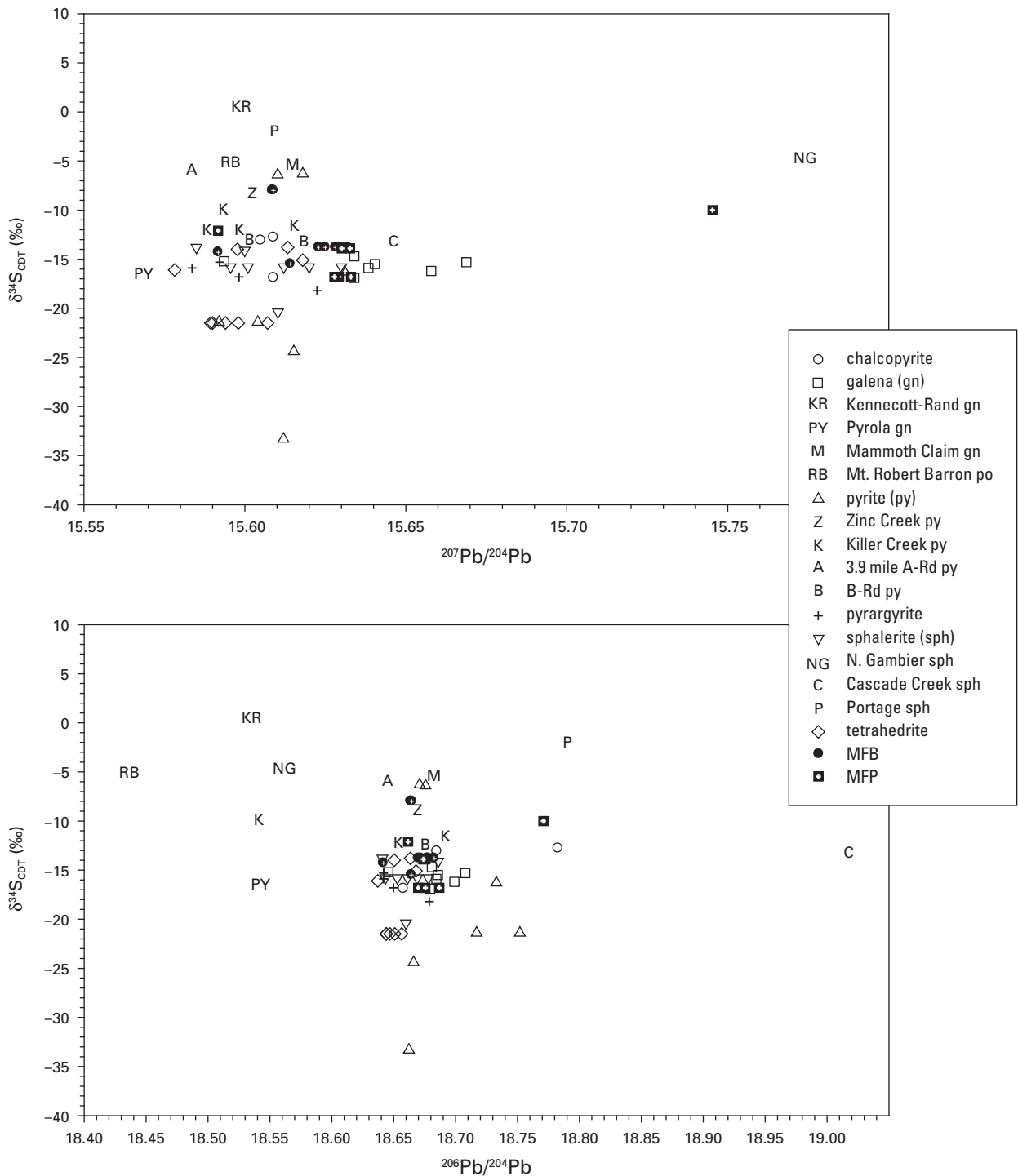


Figure 12. Plots showing $\delta^{34}\text{S}$ versus $^{207}\text{Pb}/^{204}\text{Pb}$ and $^{206}\text{Pb}/^{204}\text{Pb}$ isotopic data for ores and sulfides in the Greens Creek deposit and for sulfides from Late Triassic and other mineral occurrences on Admiralty Island.

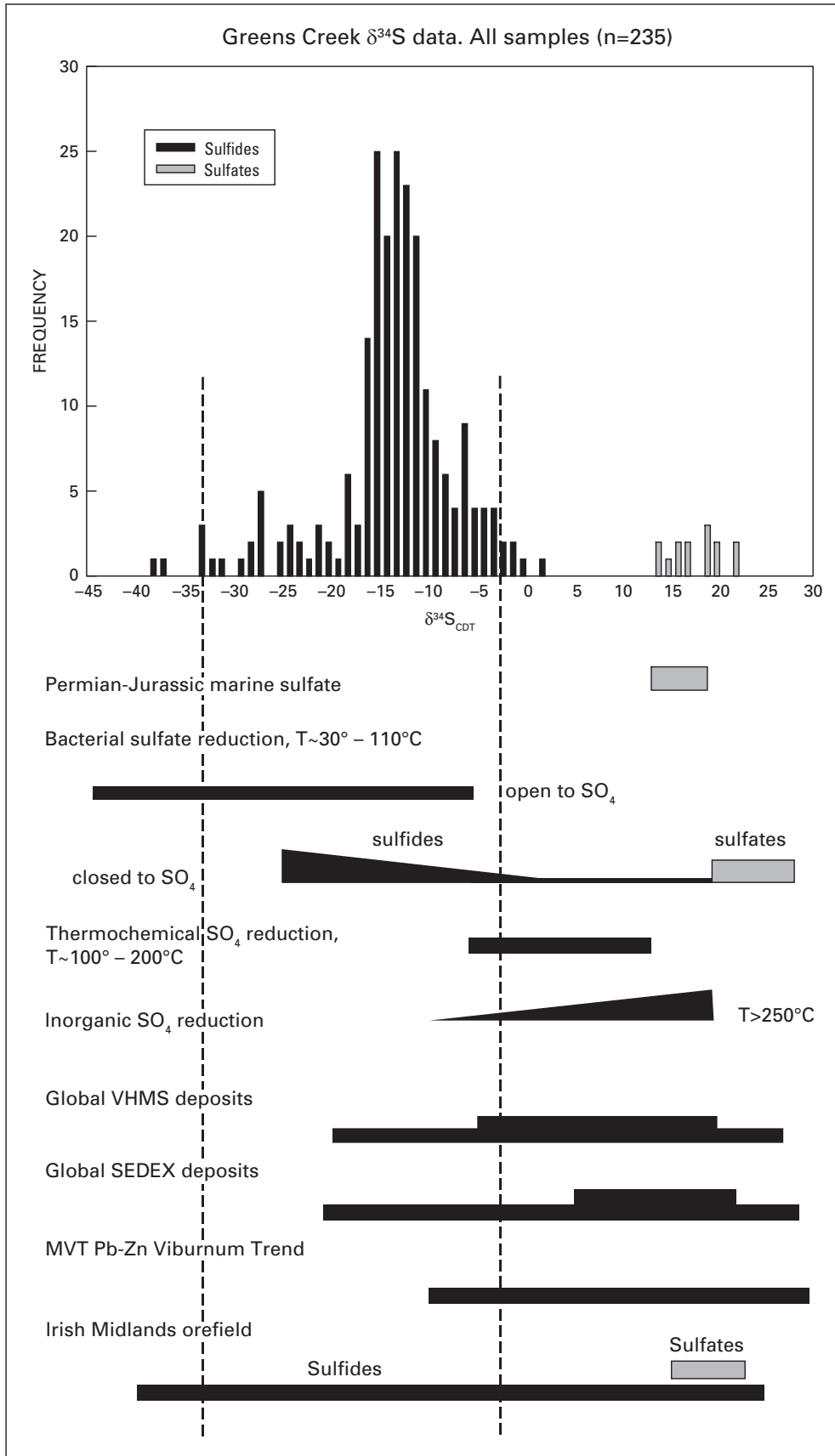


Figure 13 (facing page). Figure showing calculated ranges of various major processes of sulfate reduction compared to the histogram showing the range of all sulfide and sulfate $\delta^{34}\text{S}$ analyses from the Greens Creek deposit. Calculations based on 15–18 per mil $\delta^{34}\text{S}$ seawater sulfate. Also shown is the range of Permian through Jurassic seawater sulfate (Claypool and others, 1980) and summary $\delta^{34}\text{S}$ ranges of four major types of massive sulfide deposits: VMHS deposits, showing the total and most common ranges of values (Huston, 1999); SEDEX pyrite- and base-metal sulfide-sulfur isotope ranges (Large, 1980; Solomon and Groves, 1994); MVT deposits of the Viburnum Trend (Leach and Sangster, 1993) and the Irish-type base-metal deposits, showing range of sulfides and sulfates (Hitzman and Beaty, 1996). CDT, Cañon Diablo troilite.

stratigraphic height suggest open basin settings. The dual source model is invoked when diagenetic pyrite exhibits the upward-increasing ^{34}S profile, but base-metal sulfides show tight and nonsystematic patterns.

One of the important differences between the sulfide sulfur isotopic characteristics of Greens Creek ores and those of typical clastic-hosted SEDEX deposits is the similarity of sulfur in the massive pyritic ores to sulfur in the base-metal sulfide minerals. Recrystallized pyrite in the massive, iron-rich orebodies demonstrates the proper equilibrium relationship to the coexisting base-metal sulfides. While the most ^{34}S -depleted pyrites analyzed formed from hydrogen sulfide dominantly produced by bacterial sulfate reduction, the bulk of the pyrite and associated base-metal sulfides were produced by fluids carrying heavier sulfur derived from the footwall mafic rocks. As the hydrothermal system grew, it incorporated steadily increasing proportions of biogenic sulfur derived from dissolution of diagenetic pyrite or from biogenically reduced hydrogen sulfide in pore fluids of the accumulating shale cap. This mixing of isotopically heavier fluids with a progressively greater biogenic component from the hanging-wall argillites explains the unusual upward progression toward lower sulfur isotope values.

Arsenopyrite at Greens Creek accounts for some of the very lightest values. Texturally, these minerals are not primary framboidal aggregates forming in sediments but are incipient replacements of colloform pyrite (see chap. 9, fig. 4C) in the most proximal, massive pyritic portions of the Greens Creek deposit. The extremely light arsenopyrite sulfur implies that by the time the hydrothermal system had evolved to a zone-refining stage, not only was the fluid probably hotter and more reducing than early in the ore-forming process, but the shale cap was developed and was supplying an abundance of isotopically light sulfur to the hydrothermal system. This sulfur was of biogenic origin, either as hydrogen sulfide from pore fluids or from hydrolysis of diagenetic pyrite forming in the shale cap. The observation that both pyrite and base-metal sulfides follow this footwall-to-hanging-wall progression demonstrates that the bulk of the iron was introduced with the base metals in a single evolving mineralization episode.

This is a markedly different process than the “dual-sulfur source” model (Large, 1980; Ohmoto and others, 1990) invoked in the genesis of many of the classic clastic-hosted SEDEX deposits. The common interpretation for these deposits is early formation of isotopically light diagenetic pyrite, which becomes isotopically heavier with stratigraphic height as sulfate is progressively consumed in a restricted basin. This is followed by the introduction of base-metal sulfides with a heavier and more restricted range of sulfide $\delta^{34}\text{S}$ values. Formation of the later, main-stage base-metal mineralization occurs as a result of hydrothermal fluid circulation, which carries a component of sulfur derived from magma or from volcanic rocks that is abiotically reduced at the site of mineral deposition. In contrast, Greens Creek sulfur isotope relationships indicate mixing of sulfur from a hanging-wall sedimentary source and from a mafic-ultramafic igneous footwall source in differing proportions during a single, evolving hydrothermal episode. As in VMS systems, a component of the sulfur at Greens Creek may have been produced by inorganic reduction of sulfate by interaction with the footwall, especially early in the history of the hydrothermal system. However, the data require that the bulk of the sulfide involved in the formation of both massive pyritic and base-metal sulfides had a dominantly biogenic origin. This conclusion is one of the strongest pieces of evidence available to support the suggestion that the shale cap was present for most of the Greens Creek hydrothermal episode.

The deposits of the Irish Midlands orefield display sulfide isotopic ranges similar to those at Greens Creek. These deposits, which are commonly included in the SEDEX class (Large, 1980; Goodfellow and others, 1993; Solomon and Groves, 1994), are predominantly carbonate hosted and have sulfide $\delta^{34}\text{S}$ values that are more negative than in the clastic-hosted deposits described above. As a whole, the Irish deposits range from –45 to 30 per mil with base-metal sulfides ranging from –36 to 30 per mil (fig. 13). Notably, there is a distinction between deposits with the isotopically lightest sulfides and those with $\delta^{34}\text{S}$ values in the range more commonly seen in the SEDEX literature. The isotopically lightest sulfides are observed from deposits that are hosted by the argillaceous Waulsortian Group sediments. The deposits hosted in carbonates of the Navan Group are uniformly heavier (Hitzman and Beaty, 1996).

The paragenetic order of barite and sulfides at Greens Creek, combined with the consistent values of both sulfates and sulfides, provides additional information about how the hydrothermal system evolved. Early barite with $\delta^{34}\text{S}$ values the same as coeval seawater sulfate were followed by sulfides with $\delta^{34}\text{S}$ values that do not vary or become progressively lighter with stratigraphic height, which suggests that the Greens Creek depositional setting had a plentiful supply of marine sulfate throughout its history. Also, the paragenetic progression from early barite precious-metal-rich ores to later barite-free, base-metal-rich and proximal pyrite-arsenopyrite ores suggests a progression from oxic to anoxic conditions through time. Early in the mineralizing sequence, reduced low-temperature hydrothermal fluids carrying barium, minor amounts of gold,

abiogenic hydrogen sulfide, silver, and base metals from the underlying volcanic rocks mixed with oxygenated, sulfate-rich seawater. As downfaulting and shale sedimentation progressed, the seawater source gradually became anoxic, resulting in cessation of barite precipitation. As the insulating shale cap accumulated, the hydrothermal fluid gradually increased in temperature. Thus, the hydrothermal fluid evolved to carry a greater metal load as a chloride complex to the site of fluid mixing and ore deposition in the accumulating and probably unlithified shales.

Interpretation of Lead Isotope Data

The lead isotopic data from Greens Creek sulfide samples, regardless of mineral species, form a very definite ore-lead trend. Most ore sulfides fall on this tightly constrained, remarkably linear, ^{207}Pb - and ^{208}Pb -enriched trend that unfortunately is coincident with the slope produced by natural mass discrimination of the lead isotopes during mass spectrometry. Three different samples were run five times each through a range of currents and temperatures to evaluate the range or deviation of isotopic values expected during mass spectrometry using our procedures and techniques. $^{206}\text{Pb}/^{204}\text{Pb}$ and $^{207}\text{Pb}/^{204}\text{Pb}$ values were found not to vary more than 0.035 (about 0.19 percent), and $^{208}\text{Pb}/^{204}\text{Pb}$ not more than 0.102 (about 0.26 percent). These deviations are considerably less—approximately 4 to 5 times less—than the maximum range of isotopic values exhibited by the ^{207}Pb – ^{208}Pb trends of the Greens Creek ore: $^{206}\text{Pb}/^{204}\text{Pb}$ about 0.134 (0.72 percent); $^{207}\text{Pb}/^{204}\text{Pb}$ = about 0.167 (1.07 percent); and $^{208}\text{Pb}/^{204}\text{Pb}$ about 0.544 (1.41 percent). Although these maximum deviations are controlled by one datum, that of the massive ore sample GC-1656-06 that extends the mine-ore trend toward highly ^{207}Pb - and ^{208}Pb -enriched values, four other analyses help define the high end of this trend. Barring those analyses, 61 others fall within a smaller range of values: $^{206}\text{Pb}/^{204}\text{Pb}$ about 0.049; $^{207}\text{Pb}/^{204}\text{Pb}$ = about 0.062; and $^{208}\text{Pb}/^{204}\text{Pb}$ about 0.196, still greater than the maximum deviations shown by multiple mass spectrometer runs on the same sample.

These observations lead us to believe that the ^{207}Pb – ^{208}Pb trend of the Greens Creek ore is not an analytical artifact but involves the mixing of at least two sources of different lead isotopic compositions, one at approximately $^{206}\text{Pb}/^{204}\text{Pb}$ = 18.645, $^{207}\text{Pb}/^{204}\text{Pb}$ = 15.594, and $^{208}\text{Pb}/^{204}\text{Pb}$ = 38.34, and a second, undetermined, but a more enriched lead isotopic composition. The massive ore sample GC-1656-06 with ^{207}Pb - and ^{208}Pb -enriched values implies the probability of mixing with an older “crustal” source of lead.

A second, less well defined trend within the ^{206}Pb – ^{207}Pb correlation is delineated by the Cascade Creek sphalerite, chalcopyrite GC-1514-46, and several pyrites—three GC-1656 separates from the mine and NAD-T13-3c, a surface sample—a small number compared to the 61 analyses of the Greens Creek ore-lead trend. These results may indicate a second mixing line of lead isotopic compositions that are strongly influenced by

^{206}Pb . Mixing in this direction implies that the sphalerite lead compositions more radiogenic than the Greens Creek ore-lead trend are derived from younger or more radiogenic (or both) sources and apparently are not related to the main Greens Creek mineralization event. However, this trend is not completely supported within the ^{206}Pb – ^{208}Pb correlation (fig. 10B), indicating that thorium/uranium values for some sources for these mineral separates are not similar. In particular, Cascade Creek exhibits the highest $^{208}\text{Pb}/^{204}\text{Pb}$ value (39.35), indicating that the lead for this sphalerite was derived from a source with higher thorium/uranium than the other sphalerites.

Some of these samples have enough, though small, uranium and thorium contents that lead growth has occurred since the sulfides formed. Correction of these analyses for their radiogenic lead (given in table 3) replots some of them to the galena ore-lead trend, but others do not. For example, the Portage sphalerite, when corrected for radiogenic lead, has a composition similar to that of the Kennecott-Rand galena (fig. 10), suggesting a genetic link between the two or the uranium-lead systematics in this sphalerite sample have been disturbed, and therefore possibly overcorrected. The less radiogenic end of the ^{206}Pb trend is defined by Kennecott-Rand galena and the massive pyrite sample from the Killer Creek occurrence. Other deviates in the lower- ^{206}Pb field are analyses of sphalerite (ADM-17 from the North Gambier occurrence) and pyrrhotite (ADM-67 from an occurrence on the Mansfield Peninsula), both involving different geologic environments than that found at Greens Creek. Again, this is a small number of deviates compared to the bulk of the Greens Creek ore. The deviation of these samples to less radiogenic values than the ore-lead trend implies that the lead in these samples is either older or from a more depleted source, or both, and not related to the main Greens Creek mineralization event.

We evaluate possible sources of lead for the Greens Creek ore deposit by comparing the Greens Creek ore-lead trend to initial lead values of the surrounding host rocks (see chap. 11) at 215 Ma (fig. 14), including samples of the Hyd Group argillites, many of the metabasalts and metagabbros in the mine area, and samples, presumably of the same age, from other occurrences on Admiralty Island (for example, Gambier Bay, Pyrola). If the ore lead was derived from any of these rocks or from a similar source at 215 Ma, then the ore-lead compositions should match the initial lead values of the source rock(s). In order for this comparison to be valid, several assumptions must be met with respect to the data: (1) The lead isotopic compositions of the sulfides/ore have not changed since their formation at about 215 Ma. This assumption applies both to closed system behavior (leads of different composition have not been added) and that ore minerals are nonradiogenic (that is, they do not contain significant amounts of uranium or thorium); and (2) The uranium-lead isotopic systematics of the host whole rocks have not been disturbed since their formation. This assumption is the least likely to be true. States of alteration within these host-source rocks have been evaluated, and some samples were found to be altered enough to expect disturbed whole-rock isotopic behavior (see chap. 11, figs. 6 through 9).

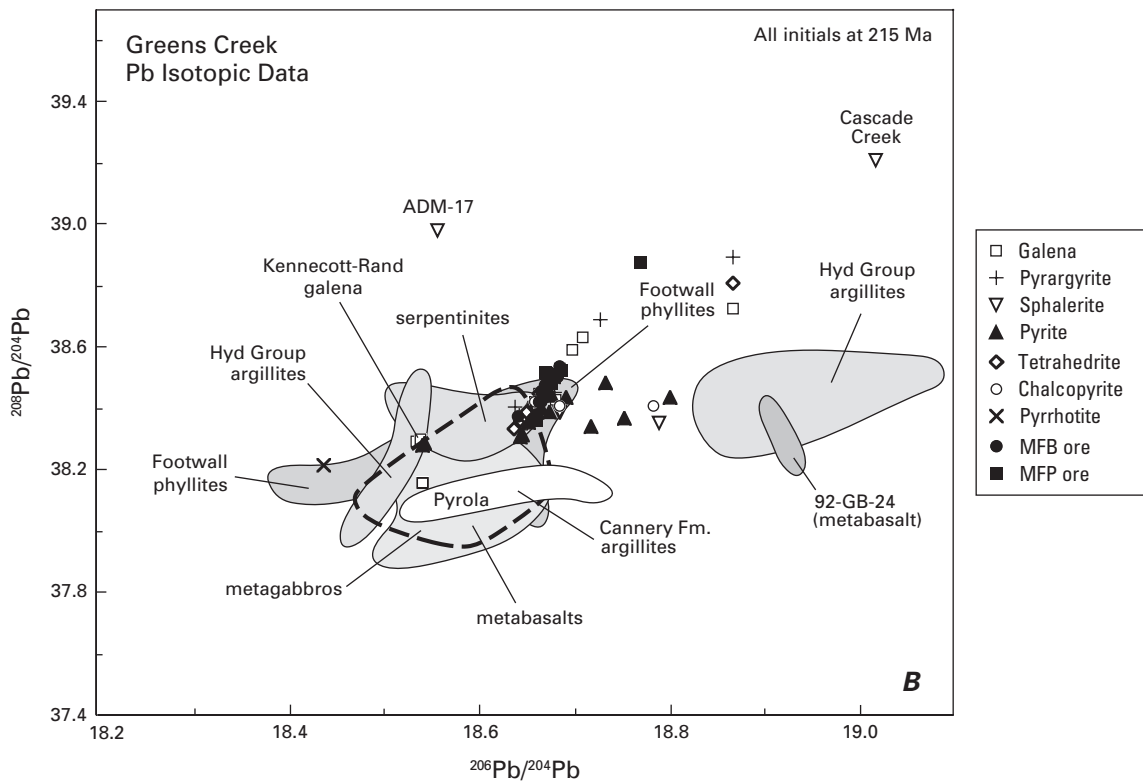
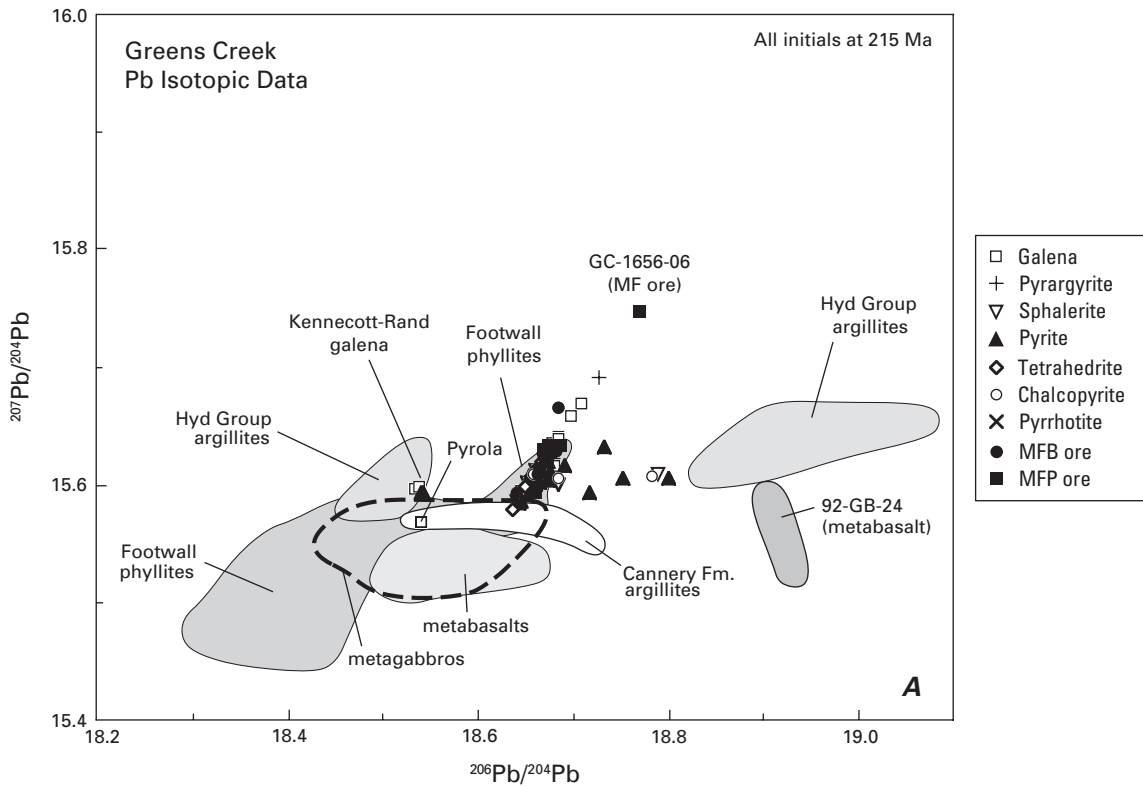


Figure 14. Plot comparing Greens Creek sulfide lead data with initial lead values at 215 Ma for argillites as well as many of the metabasalts and metagabbros of the area, including other Admiralty Island host rock samples, presumably of the same age (for example, Gambier Bay, Pyrola). (A) $^{206}\text{Pb}/^{204}\text{Pb}$ versus $^{207}\text{Pb}/^{204}\text{Pb}$; (B) $^{206}\text{Pb}/^{204}\text{Pb}$ versus $^{208}\text{Pb}/^{204}\text{Pb}$.

Several observations can be made with respect to the ore-lead data and the sources of Greens Creek ore-lead. Greens Creek lead isotopic systematics involve four components, two major and two minor. The first major source is a slightly enriched mantle component (E-MORB), very similar to those values indicative of arc-type environments (Plumbotectonics “orogene” curve; Doe and Zartman, 1979; Zartman, 1984; see chap. 11, fig. 10). The E-MORB component is represented by the vast majority of the metabasaltic and metagabbroic samples, some footwall phyllites, and the three Cannery Formation argillites (see chap. 11, fig. 15). At 215 Ma, the least radiogenic end of the Greens Creek ore-lead trend falls within these fields, indicating their direct connection. The Greens Creek ore-lead trend suggests mixing between the mafic-ultramafic source and a ^{207}Pb -enriched source more radiogenic than the most radiogenic sulfide.

The second major component is a poorly defined high- ^{207}Pb component that controls the position of the radiogenic end of the Greens Creek ore-lead trend. The enrichment of ^{207}Pb relative to ^{206}Pb implies the addition of “older” more radiogenic lead into the system. The high- ^{207}Pb trend suggests that this component incorporated “crustal” lead similar to Ordovician to Devonian model lead compositions (Plumbotectonics “upper crust” curve; for example see chap. 11, fig. 15). An obvious candidate for the source of this ^{207}Pb -enrichment is the hanging-wall argillite. As discussed previously, the sulfur isotope data provide evidence that sedimentation of the shales was occurring during the growth of the Greens Creek system, and the shales were a source of sulfur, if not metals. However, the argillites measured define a broad field of argillite lead that encompasses all of the Greens Creek sulfide lead at and above the line of ^{206}Pb variation. In detail, the argillites are grouped in three distinct clusters: two that plot on either end of the ^{206}Pb trend line and a third, consisting of the three Cannery Formation argillites that plot within the E-MORB field at the depleted end of the Greens Creek ore-lead trend.

Although we believe the actual source for the Greens Creek high- ^{207}Pb component is poorly defined, these results indicate a probable source within the Hyd Group argillites. The ore-lead trend could be produced by homogenization of all lead sources, and the high ^{207}Pb portion actually represents an average of $^{206}\text{Pb}/^{204}\text{Pb}$ compositions for high ^{207}Pb compositions of some Hyd Group argillites.

The third and fourth components are relatively minor compared to the bulk of the data, which lies on the ore-lead trend. These minor components lie at either end of the ^{206}Pb trend. The third component is less radiogenic than the bulk of the data and is found in the Kennecott Rand and Pyrola galenas, a Killer Creek pyrite (NAD-T17-9a), and the Mt. Robert Barron pyrrhotite. These samples plot within the field of least radiogenic argillites and perhaps within the field defined by the Greens Creek footwall phyllites (fig. 14). These least radiogenic samples require that their lead be derived from older or less radiogenic source rocks (or both) than the bulk of the Greens Creek ore lead. We find it compelling that sulfides from the Kennecott-Rand and Mt. Robert Barron occurrences,

both of which are hosted in (Devonian?) Retreat Group rocks, define this third component. Similarly, the Pyrola galenas are hosted in rocks of uncertain age and of possibly older origins than those at Greens Creek. Current mapping (Karl and others, unpub. data, 2000) suggests a possible Devonian age for the Pyrola schist. The composition of the Killer Creek massive pyrite sample is problematic, especially with regard to the other samples from the Killer Creek occurrence, which all plot on the Greens Creek ore-lead trend. However, we note that Duke and others (see chap. 4) map the greenstones associated with Killer Creek as belonging to the (Devonian?) Retreat Group.

Considered as a group, the sulfide analyses that define the less radiogenic end of the ^{206}Pb -trend have derived their lead from source rocks that are older than and distinctly separate from the rocks that supplied the bulk of the lead to the Greens Creek system. Further, we suggest that available age constraints indicate that this older source rock is probably Devonian in age and represents a Paleozoic unit of what is commonly referred to as the medium- to high-grade metamorphosed Retreat Group. Whereas the age of mineralization at these occurrences may have been Late Triassic, as indicated by numerous other similarities of most of these occurrences to Greens Creek, it is clear that the lead in these occurrences was derived from older rocks that are of minor importance to the metal budget at Greens Creek. It is significant that none of the Greens Creek ore sulfides analyzed exhibit lead isotopic compositions coincident with these older, less radiogenic compositions.

The fourth component is the radiogenic end of the ^{206}Pb trend, defined by the Mammoth claim galena, Cascade Creek and Portage sphalerites, a Cub Creek pyrite, a subset of Greens Creek pyrites, and two chalcopyrites. As previously discussed, some of these analyses can be corrected (and possibly over-corrected) for accumulation of radiogenic lead that may or may not result in an initial lead composition on or near the Greens Creek ore-lead trend. Therefore, the high ^{206}Pb component must have a distinctly different source than the Greens Creek ore lead. The only field of host-rock initial lead-isotopic compositions that could be involved in generating the radiogenic ^{206}Pb trend is a group of the most radiogenic Hyd Group argillites (fig. 14). Whereas it is a possibility these ^{206}Pb -rich signatures were generated from these argillites, we believe this component is more likely a younger, perhaps Cretaceous, lead-isotopic signature. The trajectory of the ^{206}Pb trend is consistent with the uranium-thorium-lead isotopic evolution of Greens Creek host rocks and parallel to Doe and Zartman’s (1979) “orogene” growth curve. Additional data on host-rock radiogenic isotopic characteristics presented in chapter 11 demonstrate that Cretaceous lead-isotope compositions are mainly more radiogenic than these radiogenic data for some Greens Creek and Admiralty Island mineral occurrences.

Both pyrite and chalcopyrite from Greens Creek that plot on the ^{206}Pb trend are paragenetically late minerals that were probably remobilized from the main ore mass during Cretaceous metamorphism (see chap. 11) and therefore probably represent mixtures of Greens Creek ore lead with radiogenic lead from surrounding host rock. While the majority of data

presented here and elsewhere suggests that the effects of Cretaceous metamorphism on the geochemistry and isotopic systematics of the Greens Creek orebody were minor, the deviation of these few ore sulfides along a high ^{206}Pb trend may provide evidence for minor incorporation of Cretaceous lead signatures.

Finally, figure 15 compares Greens Creek lead values and other Alaskan ore deposits of various ages with model lead compositions from several major lead reservoirs (for example, mantle, orogene, upper crust; Zartman and Doe, 1981; Zartman, 1984). Readers should bear in mind that these curves are averages and not absolute values for these grand, planet-scale reservoirs. Also, the "upper crust" curve is defined from mostly Phanerozoic data, such that lead from much older (for example, Archean to Proterozoic) crustal sources could yield considerably different lead compositions.

Lead isotopic values from Greens Creek more or less fall within a region defined by analyses from other Late Triassic occurrences within the belt (Newberry and others, 1997; this

study). As is typical of volcanogenic massive sulfide deposits, the range of values from Greens Creek is restricted despite the fact that there are over 43 sulfide lead determinations from Greens Creek compared to less than 10 for any other late Triassic Alaskan ore deposit. There is more isotopic variation between deposits of a given age or district than within a single deposit. Our analyses extend the field of common lead isotope values for Greens Creek and for other late Triassic deposits of southeastern Alaska. However, as suggested by Newberry and others (1997), fields of lead-isotope values for massive sulfide deposits of Alaska fall in discrete positions on lead-isotope plots and can be distinguished generally by age.

The similarity of Greens Creek ore lead to that of the orogene curve, and not the mantle curve, indicates its origin within a primitive arc environment, a conclusion also reached by Van Nieuwenhuysse (1984) and supported by the whole-rock neodymium-strontium-lead isotopic data of Greens Creek host rock (see chap. 11) and adjacent regions (Samson and others, 1989, 1990).

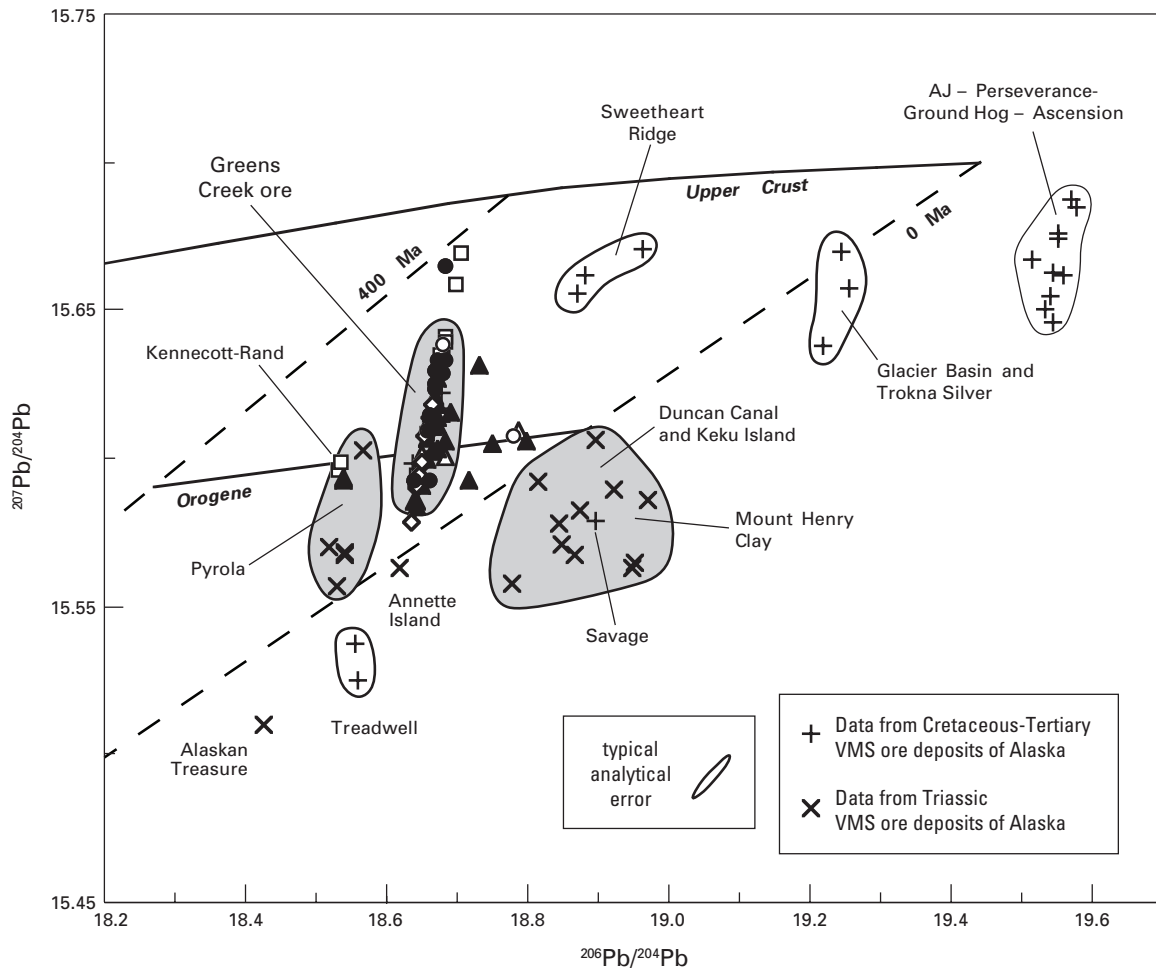


Figure 15. Plot ($^{206}\text{Pb}/^{204}\text{Pb}$ versus $^{207}\text{Pb}/^{204}\text{Pb}$) showing a comparison of the range of Greens Creek lead isotope values to those from other Alaskan VMS deposits of various ages (modified from Newberry and others, 1997). Model lead isotopic evolution curves are from Zartman (1984).

Conclusions

The Greens Creek sulfur isotope data are indicative of a single evolving hydrothermal system that derived sulfur from two major sources. Early in the hydrothermal history, reduced low-temperature fluids leached metals, barium, and sulfur from the footwall mafic igneous rocks and mixed with oxygenated seawater to produce the early white ores. As rifting and down-faulting progressed, leading to isolation of the basin and onset of shale sedimentation, the water column became progressively less oxidizing, resulting in bacterial sulfate reduction, formation of diagenetic pyrite in the shales, and resulting in hydrogen sulfide-rich pore fluids in the unconsolidated sediments. As the shale cap formed, the temperature of the hydrothermal system increased and resulted in greater base-metal solubility as chloride complexes. The hydrothermal fluid also leached a progressively greater component of isotopically light biogenic sulfur from the shales. Ultimately, the lightest sulfides formed late in the hydrothermal history during its peak temperature and most reducing phase. At this point, zone refining occurred, resulting in proximal footwall silicification and replacement/removal of early carbonate-barite assemblages, movement of silver-lead-zinc upward and outward, proximal enrichment of copper-gold, and incipient replacement of colloform sulfides with arsenopyrite. Main-stage ores formed by mixing, cooling, and dilution of a reduced metal-rich hydrothermal fluid with an anoxic seawater column and hydrogen sulfide-rich pore fluids that nevertheless remained in contact with isotopically normal seawater.

Ore and host-rock lead isotope studies indicate derivation of metal from two major sources. Sulfide lead isotopic values define a mixing line on an uraniumogenic lead plot between a non-radiogenic component similar to slightly enriched MORB and a ^{207}Pb -enriched component from an older or more radiogenic source. The nonradiogenic end of the mixing line overlaps the field defined by Late Triassic age basalts and related gabbros, some phyllites, and the Cannery Formation argillites. The ^{207}Pb -enriched end is permissive of lead extraction from the hanging-wall argillites. A second minor ^{206}Pb -trend is present that suggests that an older, less radiogenic lead source is present on Admiralty Island and contributed lead to some of the Late Triassic occurrences but not significantly to Greens Creek. More radiogenic lead compositions were found in some of the Greens Creek ore sulfides, indicating the likelihood of addition of Cretaceous lead to the Greens Creek system during regional metamorphism.

Acknowledgments

The authors would like to thank the Kennecott Greens Creek Mining Company for their cooperation, hospitality, and special equipment during sample collection on Admiralty Island. Also, thanks to all the workers at the USGS that were responsible for the majority of sample preparation and chemical analysis. Special thanks to manuscript reviewers Pat Shanks, Dan Unruh, and Robert Ayuso for their helpful comments and criticisms.

References Cited

- Berg, H.C., 1973, The geology of Gravina Island, Alaska: U.S. Geological Survey Bulletin 1373, 41 p.
- Berg, H.C., Jones, D.L., and Richter, D.H., 1972, Gravina-Nutzotin belt—Tectonic significance of an upper Mesozoic sedimentary and volcanic sequence in southern and southeastern Alaska: U.S. Geological Survey Professional Paper 800-D, p. D1–D24.
- Berg, H.C., Jones, D.L., and Coney, P.J., 1978, Map showing pre-Cenozoic tectono-stratigraphic terranes of southeastern Alaska and adjacent areas: U.S. Geological Survey Open-File Report 78-1085, 2 sheets, scale 1:1,000,000.
- Churkin, Michael, Jr., and Eberlein, G.D., 1977, Ancient borderland terranes of the North American Cordillera—Correlation and microplate tectonics: Geological Society of America Bulletin, v. 88, p. 769–786.
- Claypool, G.E., Holster, W.T., Kaplan, I.R., Sakai, H., and Zak, I., 1980, The age curves of sulfur and oxygen isotopes in marine sulfate and their mutual interpretation: Chemical Geology, v. 28, 199–260.
- Doe, B.R., and Zartman, R.E., 1979, Plumbotectonics, the Phanerozoic, *in* Barnes, H.L., ed., Geochemistry of hydrothermal ore deposits: New York, John Wiley and Sons, p. 22–70.
- Dusel-Bacon, C., 1994, Metamorphic history of Alaska, *in* Plafker, G., and Berg, H.C., eds., The geology of Alaska: Boulder, Colorado, Geological Society of America, v. G1, p. 495–533.
- Freitag, Katja, 2000, Geology and structure of the Lower Southwest orebody, Greens Creek mine, Alaska: Golden, Colorado School of Mines, Ph.D. dissertation, 248 p.
- Gehrels, G.E., and Berg, H.C., 1994, Geology of southeastern Alaska, *in* Plafker, George, and Berg, H.C., eds., The geology of Alaska: Boulder, Colorado, Geological Society of America, v. G1, p. 451–468.
- Gehrels, G.E., and Saleeby, J.B., 1987, Geologic framework, tectonic evolution, and displacement history of the Alexander terrane: Tectonics, v. 6, p. 151–173.
- Giesmann, A., Jasper, H.J., Norman, A.L., Krouse, H.R., and Brand, W.A., 1994, On-line sulfur isotope determination using an elemental analyzer coupled to a mass spectrometer: Analytical Chemistry, v. 66, p. 2816–2819.
- Goldfarb, R.J., Snee, L.W., Miller, L.D., and Newberry, R.J., 1991, Rapid dewatering of the crust deduced from ages of mesothermal gold deposits: Nature, v. 354, p. 296–298.
- Goodfellow, W.D., Lydon, J.W., and Turner, R.J.W., 1993, Geology and genesis of stratiform sediment-hosted (SEDEX)

- zinc-lead-silver sulphide deposits, *in* Kirkham, R.V., Sinclair, W.D., Thorpe, R.I., and Duke, J.M., eds., Mineral deposit modeling: Geological Association of Canada, Special Paper 40, p. 201–251.
- Hannington, M.D., Galley, A.G., Herzig, P.M., and Petersen, S., 1998, Comparison of the TAG mound and stockwork complex with Cyprus-type massive sulfide deposits, *in* Herzig, P.M., Humphris, S.E., Miller, D.J., and Zierenberg, R.A., eds., Proceedings of the ocean drilling program: Scientific Results, v. 158, p. 389–415.
- Hitzman, M.W., and Beaty, D.W., 1996, The Irish Zn-Pb-(Ba) orefield, *in* Sangster, D.F., ed., Carbonate-hosted lead-zinc deposits, 75th Anniversary Volume: Society of Economic Geologists Special Publication Number 4, p. 112–143.
- Huston, D.L., 1999, Stable isotopes and their significance for understanding the genesis of volcanic-hosted massive sulfide deposits—A review, *in* Barrie, C.T., and Hannington, M.D., eds., Volcanic-associated massive sulfide deposits—Processes and examples in modern and ancient settings: Society of Economic Geologists Reviews in Economic Geology, v. 8, p. 261–295.
- Large, D.E., 1980, Geological parameters associated with sediment-hosted, submarine exhalative Pb-Zn deposits—An empirical model for mineral exploration: *Geologisches Jahrbuch*, v. D40, p. 59–129.
- Leach, D.L., and Sangster, D.F., 1993, Mississippi Valley-type lead-zinc deposits, *in* Kirkham, R.V., Sinclair, W.D., Thorpe, R.I., and Duke, J.M., eds., Mineral deposit modeling: Geological Association of Canada, Special Paper 40, p. 289–314.
- Ludwig, K.R., 1980, Calculation of uncertainties of U-Pb data: *Earth and Planetary Science Letters*, v. 46, p. 212–220.
- Ludwig, K.R., 1985, PBDAT200—A Computer Program for processing raw Pb-U-Th isotope data: U.S. Geological Survey Open-File Report 85–547, 54 p.
- Ludwig, K.R., 1991, ISOPLOT—A plotting and regression program for radiogenic-isotope data; version 2.53: U.S. Geological Survey Open-File Report 91–0445, 39 p.
- Lydon, J.W., 1996, Sedimentary exhalative sulphides (Sedex), *in* Eckstrand, O.R., Sinclair, W.D., and Thorpe, R.I., eds., Geology of Canadian mineral deposit types: Geological Society of America, The geology of North America, v. P-1, p. 130–152.
- McClelland, W.C., and Gehrels, G.E., 1990, Geology of the Duncan Canal shear zone—Evidence for Early to Middle Jurassic deformation of the Alexander terrane, southeastern Alaska: *Geological Society of America Bulletin*, v. 102, p. 1378–1392.
- Miller, L.D., Goldfarb, R.J., Gehrels, G.E., and Snee, L.W., 1994, Genetic links among fluid cycling, vein formation, regional deformation, and plutonism in the Juneau gold belt, southeastern Alaska: *Geology*, v. 22, p. 203–206.
- Muffler, L.J.P., 1967, Stratigraphy of the Keku Islets and neighboring parts of Kuiu and Kupreanof Islands southeastern Alaska: U.S. Geological Survey Bulletin 1241–C, 52 p.
- Newberry, R.J., and Brew, D.A., 1999, Chemical and isotopic data for rocks and ores from the Upper Triassic Greens Creek and Woewodski Island volcanogenic massive sulfide deposits, southeastern Alaska, *in* Kelley, K.D., ed., Geologic studies in Alaska by the U.S. Geological Survey, 1997: U.S. Geological Survey Professional Paper 1614, p. 35–55.
- Newberry, R.J., Crafford, T.C., Newkirk, S.R., Young, L.E., Nelson, S.W., and Duke, N.A., 1997, Volcanogenic massive sulfide deposits of Alaska, *in* Goldfarb, R.J., and Miller, L.E., eds., Mineral deposits of Alaska: Economic Geology Monograph 9, p. 120–150.
- Ohmoto, Hiroshi, 1986, Stable isotope geochemistry of ore deposits, *in* Valley, J.W., Taylor, H.P., Jr., and O’Neil, J.R., eds., chapter 14, Stable isotopes in high temperature geological processes: *Reviews in Mineralogy*, v. 16, p. 491–559.
- Ohmoto, Hiroshi, Kaiser, C.J., and Geer, K.A., 1990, Systematics of sulfur isotopes in recent marine sediments and ancient sediment-hosted base metal deposits, *in* Herbert, H.K., and Ho, S.E., eds., Stable isotopes and fluid processes in mineralization: Nedlands, Western Australia, The University of Western Australia, Publication 23, p. 70–120.
- Ohmoto, Hiroshi, and Rye, R.O., 1979, Isotopes of sulfur and carbon, *in* Barnes, H.L., ed., Geochemistry of hydrothermal ore deposits: John Wiley and Sons, New York, p. 509–567.
- Peter, J.M., and Scott, S.D., 1999, Windy Craggy, northwestern British Columbia—The world’s largest Besshi-type deposit, *in* Barrie, C.T., and Hannington, M.D., eds., Volcanic-associated massive sulfide deposits—Processes and examples in modern and ancient settings: Society of Economic Geologists Reviews in Economic Geology, v. 8, p. 261–295.
- Saleeby, J.B., 1994, Tectonic history of the Insular Suture Zone, southeastern Alaska: *Geological Society of America Abstracts* v. 26, p. A384.
- Samson, S.D., McClelland, W.C., Patchett, P.J., Gehrels, G.E., and Anderson, R.G., 1989, Evidence from neodymium isotopes for mantle contributions to Phanerozoic crustal genesis in the Canadian Cordillera: *Nature*, v. 337, no. 23, p. 705–709.
- Samson S.D., Patchett P.J., Gehrels G.E., and Anderson R.G., 1990, Nd and Sr Isotopic characterization of the Wrangellia Terrane and implications for crustal growth of the Canadian Cordillera: *Journal of Geology*, v. 98, p. 749–762.

- Shanks, W.C. III, Bischoff, J.L., and Rosenbauer, R.J., 1981, Seawater sulfate reduction and sulfur isotope fractionation in basaltic systems—Interaction of seawater with fayalite and magnetite at 200–300° C: *Geochimica et Cosmochimica Acta*, v. 48, p. 557–569.
- Solomon, Michael, and Groves, D.I., 1994, *The geology and origin of Australia's mineral deposits*: Oxford, Oxford Science Publications, 951 p.
- Stacey, J.S., and Kramers, J.D., 1975, Approximation of terrestrial lead evolution by a two-stage model: *Earth and Planetary Science Letters*, v. 26, p. 207–221.
- Strauss, Harald, 1997, The isotopic composition of sedimentary sulfur through time: *Palaeogeography, Palaeoclimatology, Palaeoecology*, v. 132, p. 97–118.
- Taylor, C.D., 1997, An arc-flank to back-arc transect—Metallogeny of Late Triassic volcanogenic massive sulfide occurrences of the Alexander terrane, southeastern Alaska and British Columbia: [extended abs.] in *Society of Economic Geologists Neves Corvo Field Conference*, May 7–17, 1997, Lisbon, Portugal, Abstracts and Programs volume, p. 68.
- Taylor, C.D., Cieutat, B.A., and Miller, L.D., 1992, A follow-up geochemical survey of base metal anomalies in the Ward Creek/Windfall Harbor and Gambier Bay areas, Admiralty Island, S.E. Alaska, in Bradley, D., and Dusel-Bacon, C., eds., 1991 *Geologic studies in Alaska*: U.S. Geological Survey Bulletin 2041, p. 70–85.
- Taylor, C.D., Leventhal, J.S., Johnson, C.A., and Lear, K.G., 2000b, The Greens Creek massive sulfide deposit southeastern Alaska—Stable isotopic evidence for the involvement of biogenic sulfate reduction in the formation of ores and carbonates, in Gemmell, J.B., and Pongratz, J., eds., *Volcanic environments and massive sulfide deposits: Program and abstracts*, CODES special publication #3, p. 209–210.
- Taylor, C.D., Newkirk, S.R., Hall, T.E., Lear, K.G., Premo, W.R., Leventhal, J.S., Meier, A.L., Johnson, C.A. and Harris, A.G., 1999b, The Greens Creek deposit, southeastern Alaska—A VMS-SEDEX hybrid, in Stanley, C.J., and others, eds., *Mineral deposits—Processes to processing*: Balkema, Rotterdam, v. 1, p. 597–600.
- Taylor, C.D., Philpotts, J.A., Hall, T.E., and Wakeman, B.W., 1995b, New information on the geochemistry, age, and tectonic history of Late Triassic volcanic host rocks and associated massive sulfide occurrences of the Alexander terrane, southeast Alaska: *Alaska Miners Association Conference Juneau, Program with Abstracts*, p. 31–32.
- Taylor, C.D., Philpotts, J., Sutley, S., Gent, C., Harlan, S., Premo, W., Tatsumoto, M., Emsbo, P., and Meier, A., 1995a, Geochemistry of Late Triassic volcanic rocks and age of alteration associated with volcanogenic massive sulfide occurrences, Alexander terrane, southeast Alaska: *Geological Society of Nevada, Geology and ore deposits of the American cordillera abstracts volume*, p. A74.
- Taylor, C.D., Premo, W.R., and Meier, A.L., 1999a, The Late Triassic metallogeny of the Alexander terrane, southeastern Alaska and British Columbia: *Geological Society of America Abstracts with Programs*, v. 31, no. 6, p. A–101.
- Taylor, C.D., Premo, W.R., and Lear, K.G., 2000b, The Greens Creek massive sulfide deposit—Premier example of the Late Triassic metallogeny of the Alexander terrane, southeastern Alaska and British Columbia: *Geological Society of America Abstracts with Programs*, v. 32, no. 6, p. A–71.
- Van Nieuwenhuysse, R.E., 1984, *Geology and geochemistry of the Pyrola massive sulfide deposit, Admiralty Island, Alaska*: Tucson, Arizona, unpublished Master's thesis, University of Arizona, 170 p.
- Zartman R.E., 1984, Lead, strontium, and neodymium isotopic characterization of mineral deposits relative to their geologic environments, in *Proceedings of the 27th International Geological Congress, Moscow*, v. 12, p. 83–106, *Metallogeneses and Mineral Ore Deposits*: Utrecht, The Netherlands, VNU Science Press.
- Zartman, R.E., and Doe, B.R., 1981, *Plumbotectonics—The model*: *Tectonophysics*, v. 75, p. 135–162.

Microfossil and Radioisotopic Geochronological Studies of the Greens Creek Host Rocks

By Wayne R. Premo, Cliff D. Taylor, Lawrence W. Snee, and Anita G. Harris

Chapter 11 of

**Geology, Geochemistry, and Genesis of the Greens Creek Massive
Sulfide Deposit, Admiralty Island, Southeastern Alaska**

Edited by Cliff D. Taylor and Craig A. Johnson

Professional Paper 1763

**U.S. Department of the Interior
U.S. Geological Survey**

Contents

Abstract.....	287
Introduction.....	287
Geology.....	291
Geochronology.....	293
Paleontology—Conodont Studies.....	293
Conodonts from the Greens Creek Mine Area.....	294
Underground Collections.....	294
Outcrop Collections.....	295
Color Alteration Index (CAI).....	299
Paleoenvironmental and Depositional Controls for Conodont Distribution.....	299
Conodonts from the Mansfield Peninsula and Northern Kupreanof Island.....	299
Radiogenic Isotopic Age Determinations.....	300
⁴⁰ Ar- ³⁹ Ar Age Determinations.....	300
U-Th-Pb, Rb-Sr, and Sm-Nd Ages on Host-Rock Lithologies.....	307
Whole-Rock Compared to Mineral (Internal) Isochron Ages.....	307
Analytical Methods.....	307
Results.....	310
Metabasalts and Phyllites.....	310
Metagabbros.....	311
Argillites.....	320
Serpentinites.....	321
Discussion.....	324
Late Triassic Igneous Activity.....	324
Age of Greens Creek Mineralization.....	324
Isotopic Resetting of the Older Stratigraphy.....	324
Age of Cretaceous Overprinting on Greens Creek Mineralization.....	326
Acknowledgments.....	327
References Cited.....	327
Appendix.....	331

Figures

1. Generalized map of terrane boundaries and major volcanogenic massive sulfide prospects, southeast Alaska, showing the locations of the Late Triassic age volcanogenic massive sulfide (VMS) deposits, including Greens Creek, Pyrola, and Gambier Bay on Admiralty Island.....288
2. Simplified geologic map of Admiralty Island, showing locations for Greens Creek and Pyrola deposits, Gambier Bay, Windfall Harbor, the Mansfield Peninsula, and Staunch Point (locations of some whole-rock samples)289
3. Map of surface sampling sites at and near Greens Creek mine, Admiralty Island.....290
4. Photograph of *Halobia* in clast of siliceous argillite milled into massive sulfide ore.....292

5.	Stratigraphy of the Greens Creek section, Admiralty Island, showing the orebody at the contact between footwall phyllites and hanging-wall argillites	293
6.	Lower and Upper <i>primitius</i> Zone conodonts (latest Carnian-earliest Norian) from the Hyd Group, northern Admiralty Island, Alaska	295
6.	A-I, Pa elements from outcrop in cirque at head of upper Cliff Creek	295
6.	A, B, <i>Metapolygnathus primitius</i> (Mosher), Upper views of two incomplete adult specimens with quadrate platform with five nodes on lateral margins and posterior margin without nodes	295
6.	C, D, <i>Metapolygnathus primitius</i> Upper and lower views of small adult with three lateral nodes on inner margin and four on outer margin	295
6.	H, A <i>Metapolygnathus primitius</i> Pa element bent out of shape	295
6.	I, <i>Metapolygnathus primitius</i> Juvenile with three nodes on lateral margins and midplatform constriction	295
6.	E-G, <i>Metapolygnathus primitius</i> transitional to <i>Epigondolella</i> , well-preserved subadult, lateral, upper, and lower views.....	295
6.	J-O, <i>Metapolygnathus primitius</i> specimens from mine workings at 37 Ramp drift, no. 1 passing bay and within 20 meters of the orebody.....	295
6.	J-M, Juvenile and subadult Pa elements of <i>Metapolygnathus primitius</i> (Mosher).....	295
6.	N, O, <i>Neogondolella</i> sp., Pa element, upper and lower views	295
6.	P-R, Specimens from mine workings in 620-2955 drift and within 15 meters of the orebody.....	295
7.	Carnian-Middle Norian conodont zonation showing age range of biostratigraphically useful and (or) geologically significant conodont collections from Hyd Group host rocks, Greens Creek mine and vicinity, and four collections from the Hyd in the vicinity of the Taylor Creek deposit, northern Kupreanof Island.....	298
8.	Conodont zonation for the Lower and part of the Upper Permian showing age range of conodont collections from the uppermost exposed beds of the Cannery Formation in the vicinity of the Taylor Creek deposit and the Pybus Formation about 15 kilometers farther northwest, northern Kupreanof Island.....	301
9.	$^{40}\text{Ar}/^{39}\text{Ar}$ step-release spectra for four samples: one from the Greens Creek mine, two from other locations on Admiralty Island, and one fuchsite, 92-GB-05, from altered ultramafic rocks on the north shore of Gambier Bay showing a two-step $^{40}\text{Ar}/^{39}\text{Ar}$ plateau date of 210.3 ± 0.3 Ma (1σ)	306
10.	$^{40}\text{Ar}/^{39}\text{Ar}$ spectra for Greens Creek fuchsite and sericite — Spectra that indicate complete resetting of argon in the alteration assemblage prior to 105 – 95 Ma.....	308
11.	Uranium-lead isotopic correlation diagram of data from metabasalt rocks (Hyd Group and Gambier Bay Formation) and footwall phyllites of the Green Creek area.....	311
12.	Samarium-neodymium isotopic correlation diagram of data from metabasalt rocks and footwall phyllites — Greens Creek area	318
13.	Rubidium-strontium isotopic correlation diagram of data from metabasalt rocks and footwall phyllites of the Greens Creek area	319
14.	Uranium-lead isotopic correlation diagram of data from some of the Greens Creek metagabbros, yielding a whole-rock isochron age of 206 ± 35 Ma and initial $^{206}\text{Pb}/^{204}\text{Pb}$ value of 18.61 ± 0.19 , similar to that of the Greens Creek ore	320
15.	Samarium-neodymium isotopic correlation diagram of data from Greens Creek metagabbros.....	321

16. Rubidium-strontium isotopic correlation diagram of whole-rock data from argillites	323
17. Rubidium-strontium isotopic correlation diagram of whole-rock data from serpentinites	323
18. Diagram summarizing the various ages for Greens Creek samples	325

Tables

1. Data for geologically and biostratigraphically significant conodont collections from the Greens Creek mine and immediate vicinity, Alaska	296
2. $^{40}\text{Ar}/^{39}\text{Ar}$ data for samples* from Greens Creek VMS deposit, Admiralty Island, Alaska	302
3. Descriptions and locations for host rock and adjacent samples of the Greens Creek VMS deposit	309
4. Uranium-thorium-lead analytical data for host-rock samples from the Greens Creek VMS deposit	312
5. Initial lead compositions for host-rock samples from the Greens Creek VMS deposit	314
6. Rubidium-strontium and samarium-neodymium analytical data for host-rock and adjacent samples of the Greens Creek VMS deposit	316
7. Age results for various Greens Creek rocks and minerals	326

Microfossil and Radioisotopic Geochronological Studies of the Greens Creek Host Rocks

Wayne R. Premo,¹ Cliff D. Taylor,¹ and Lawrence W. Snee,¹ and Anita G. Harris²

Abstract

Paleontologic and radiometric ages were determined for samples from the Greens Creek strata in order to more precisely date the timing and duration of ore deposition as well as provide an overall chronology at Greens Creek. Conodonts were the biostratigraphic index of choice because of the Triassic age, marine depositional setting, and low-grade metamorphism. Four conodont samples tightly constrain the age of the host rock within the Late Triassic. Two samples from the hanging wall in underground workings yielded an index species that restricts these samples to an interval that includes the Carnian-Norian boundary, which was previously dated at 220.7 ± 4.4 Ma (mega-annum).

⁴⁰Ar/³⁹Ar geochronologic studies of sericite and fuchsite in the mine and of ultramafic bodies in the mine area generated argon age spectra that indicate Cretaceous-Tertiary metamorphic resetting of older minerals. However, one fuchsite separate from the thickest of the alteration zones yielded a two-step ⁴⁰Ar/³⁹Ar plateau age of 210.3 ± 0.3 Ma (1 σ). If this age approximates the age of alteration of the ultramafic bodies, then it also estimates intrusion of Greens Creek mafic-ultramafic heat sources at between 215 and 211 Ma, allowing a few million years for emplacement, crystallization, and cooling. If the ultramafic bodies across the island are coeval and they were altered by hydrothermal fluids related to the Greens Creek ore-forming event, then the age of 210.3 ± 0.3 Ma represents the best constraint available on the age of the Greens Creek orebody.

Minimum and maximum estimates for the lifespan of the Greens Creek hydrothermal system can be calculated by assuming the initiation of mineralization occurred either during emplacement of mafic-ultramafic heat sources at between 215 and 211 Ma, or at the time of shale sedimentation at 220.7 ± 4.4 Ma, and that the ⁴⁰Ar-³⁹Ar age on fuchsite dates the ore-forming event. If either of these scenarios is correct, then the age data indicate that the Greens Creek hydrothermal system had minimum and maximum lifespans of 2.7 ± 2.3 million years and 10.4 ± 4.7 million years, respectively.

Whole-rock uranium-lead (U-Pb), rubidium-strontium (Rb-Sr), and samarium-neodymium (Sm-Nd) isotopic data

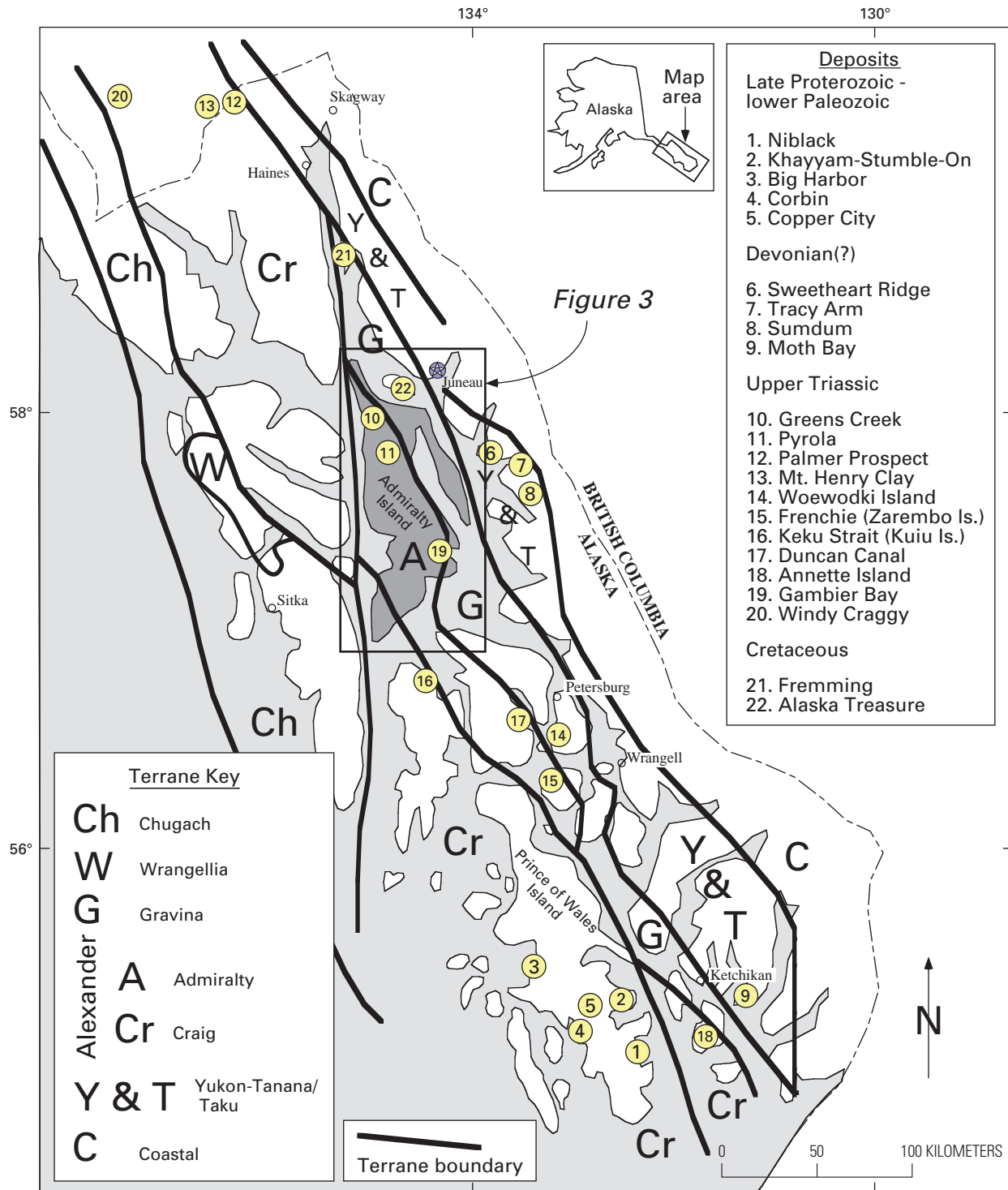
were used to evaluate apparent isochron ages for several sample suites. U-Pb and Sm-Nd isotopic data for most of the Hyd Group metabasalt samples collected from Gambier Bay yielded apparent isochron ages of about 215 Ma. Several apparent Rb-Sr isochron ages agree with partially disturbed ⁴⁰Ar-³⁹Ar ages from fuchsite and sericite that yield total gas ages between 80 and 100 Ma, ages that are consistent with the timing for terrane accretion during the Cretaceous.

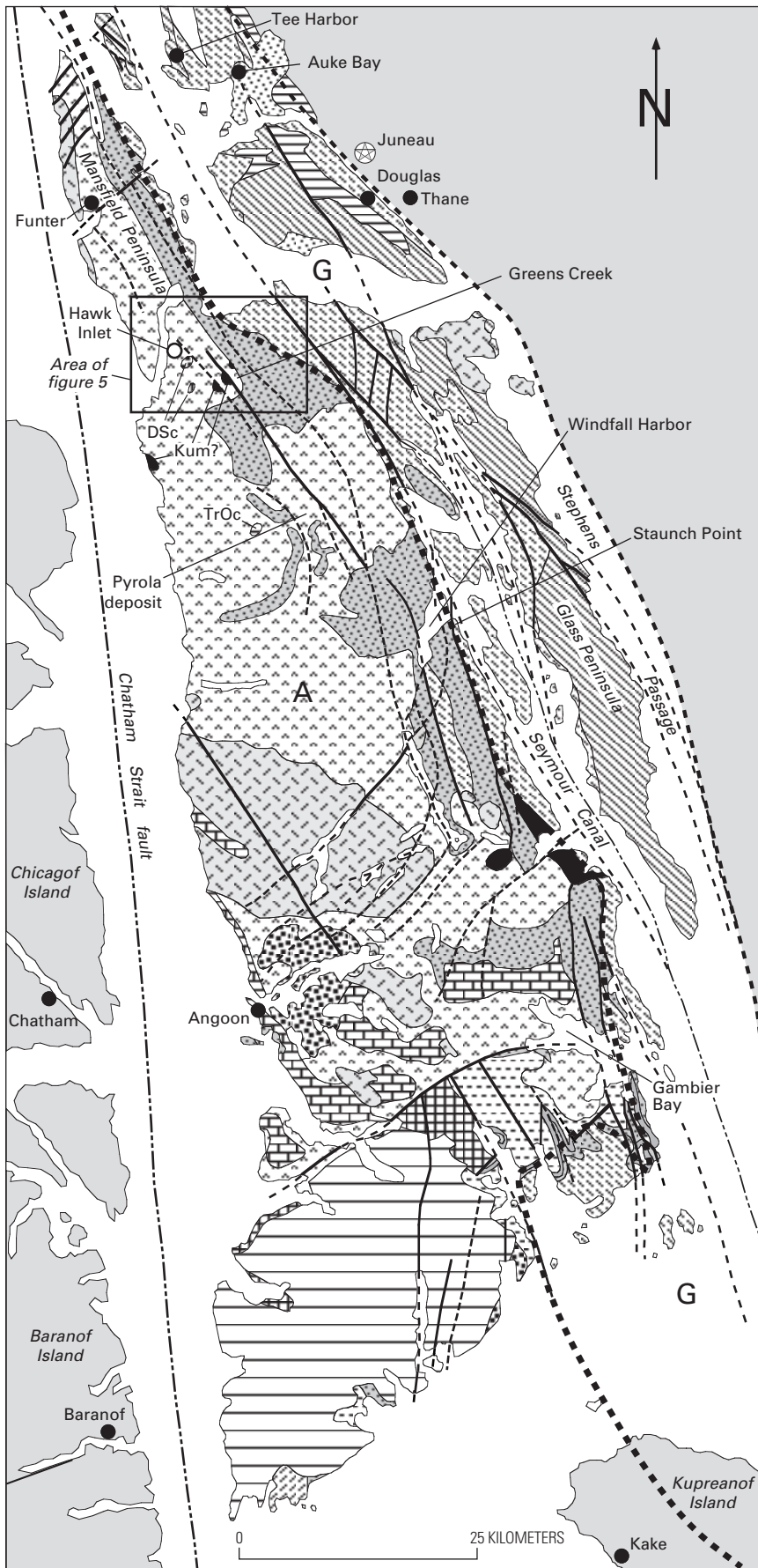
Introduction

The Greens Creek ore deposit, one of many suspected volcanogenic massive sulfide (VMS) deposits in southeastern Alaska (fig. 1), is located at the north end of Admiralty Island (figs. 1 and 2). Age constraints on the host sedimentary rocks and for ore formation at Greens Creek have been conspicuously lacking throughout the existence of the mine and have been a source of uncertainty regarding the tectonic history and style of mineralization. Reconnaissance geologic mapping in the 1960s (Lathram and others, 1965) identified the lithologic units in the vicinity of Greens Creek as the Retreat Group, which at the time was thought to be Devonian in age, and those at the mine portal as belonging to the Permian Cannery Formation (chap. 4). Unaltered ultramafic bodies on Mariposite Ridge north of the mine (fig. 3) were mapped as middle Cretaceous in age, and the quartz-carbonate-fuchsite altered serpentinite body at Bruin Knob was considered to be a Middle Devonian serpentinitized dolomite. As late as 1985, company geologists were uncertain regarding the age of the host rocks within a range of Permian to Late Triassic because Permian macrofossils recovered from a limestone body about 6.5 km from the deposit and its probable association to Greens Creek, assigned by D. Grybeck and H.C. Berg (U.S. Geological Survey), conflicted with Late Triassic *Halobia* faunas found at other southeastern Alaska massive sulfide deposits (Crafford, 1984). Preliminary mapping by the U.S. Geological Survey (Brew and Ford, 1985) showed the mine hosted in the Cannery Formation and revised the age of the Retreat Group to indeterminate Mesozoic lithologies. It was also noted that the ultramafic bodies on the ridge north of the mine are variably altered dunites and peridotites; their age was revised to Mesozoic.

¹U.S. Geological Survey, Denver, Colorado.

²U.S. Geological Survey, Reston, Virginia.





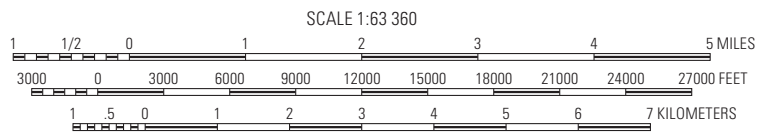
EXPLANATION

- Qs Quaternary surficial sediments
- Tv Tertiary volcanic rocks
- Ts Tertiary sedimentary rocks
- Kg Cretaceous granitoids
- Kum Cretaceous ultramafic rocks
- KJs Cretaceous-Jurassic sedimentary rocks
- KJsv Cretaceous-Jurassic volcanic and sedimentary rocks
- KJv Cretaceous-Jurassic volcanic rocks
- TrPsv Triassic-Permian sedimentary and volcanic rocks, und.
- TrOsv Triassic-Ordovician sedimentary and volcanic rocks, und.
- TrOc Triassic-Ordovician carbonate rocks, und.
- Ps Permian sedimentary rocks
- Pc Permian carbonate rocks
- DSc Devonian-Silurian carbonate rocks
- Ss Silurian sedimentary rocks
- SOs Silurian-Ordovician sedimentary rocks
- Other rocks
- Major fault
- Inferred fault trace
- Terrane boundary

Figure 2. Simplified geologic map of Admiralty Island, showing locations for Greens Creek and Pyrola deposits, Gambier Bay, Windfall Harbor, the Mansfield Peninsula, and Staunch Point (locations of some whole-rock samples). Bold dotted line is approximate boundary between the Alexander (A) and Gravina (G) terranes (after mapping by Gehrels and Berg, 1992).



Figure 3. Map of surface sampling sites at and near Greens Creek mine, Admiralty Island. Single-numbered locations are from the 97-LG-series (for example, “82” is the locations of 97-LG-82, and so forth). PF-series (–09 and –18) are from the Portal Face. Topographic map compiled from USGS Juneau A3 and A2 1:63,360 scale, 1997.



The first important age constraint based on data collected at the mine came in 1988 when, in a rib of the first stope at Greens Creek, Andrew Hawthorne and T.C. Crafford found two fossils in a clast of siliceous argillite interpreted to have been tectonically milled into the massive sulfide ore (Crafford, 1989, oral commun., 2002). One is the shell of the cosmopolitan Middle and Late Triassic flat clam *Halobia* (N.J. Silberling, written commun., 1988; fig. 4); the other is a poorly preserved patelliform gastropod that merely indicates a Silurian to Holocene age (R.B. Blodgett, written commun., 1988). According to T.R. Waller (written commun., 2002), *Halobia* first appears in the Ladinian (late Middle Triassic) of the Tethys sea but has its main occurrence in younger Triassic rocks, so that a Carnian or Norian age would be likely for the Alaskan specimen. Prior to our study, the *Halobia* was the only paleontologic evidence that could be tied to either the mine host rocks or the age of mineralization, and the deposit was assigned a Late Triassic age (Crafford, 1989; Newberry and others, 1990, 1997). Other assignments of a Triassic age for the deposit have been based on the similarity of the geochemical signature, basalt geochemistry, stratigraphic position of the metals, and correlation to other paleontologically dated Late Triassic massive sulfide occurrences in southeastern Alaska and British Columbia (MacIntyre, 1986; Taylor and others, 1995a, b, and 1999; Newberry and Brew, 1997, 1999). Because of uncertainty about the precise age of the *Halobia* from the mine area and the absence of other direct age data for the immediate host rocks or absolute age of mineralization, a concerted effort was made during our study to develop age constraints for the host rocks and to determine the age of ore formation. Accordingly, conodont samples were taken from the immediate hanging wall, $^{40}\text{Ar}/^{39}\text{Ar}$ analyses of sericite and fuchsite alteration from ore and altered footwall phyllites, and construction of U-Pb and Sm-Nd mineral and whole-rock isochrons on specific host lithologies have all been performed to provide usable constraints on the age of ore formation in relationship to the age of the host rocks.

Geology

The detailed geology of Greens Creek is presented elsewhere in this volume so that only a brief summary of the rocks sampled for geochronology is included here.

The stratigraphy at Greens Creek can be summarized in three distinct sections, separated by unconformities. The first section is composed of siliceous to cherty argillite of the Cannery Formation of at least very late Early Permian age (Appendix, localities 8–10), the oldest stratigraphic unit at Greens Creek. These argillites are then unconformably overlain by the second section composed of metabasalts of unknown age (fig. 5). These metabasalts were variably metamorphosed at greenschist to amphibolite grade and subsequently hydrothermally altered (for example, Newberry and others, 1990), producing several types of phyllitic rocks.

It is likely that this phyllitic sequence originally consisted of a composite mafic-ultramafic collection of massive flows and volcanoclastic deposits. Geochemical signatures of many of these phyllites are inconclusive but are consistent with basaltic protoliths, either as a rift-related basalt produced in an intra-arc setting or as a fairly unfractionated calc-alkaline basalt formed in an oceanic volcanic arc. The arc-related signatures could be indicative of variable amounts of assimilation of preexisting island arc crust.

The metabasalts are unconformably overlain by the third section — the Upper Triassic Hyd Group — that consists of a basal conglomerate, overlain by a thick sequence of argillites, and finally capped by a thick sequence of basalts (fig. 5). Such conglomerates are found throughout the southern and middle portions of the Upper Triassic volcano-sedimentary belt throughout southeastern Alaska. Although thin, discontinuous, polymictic, conglomerate horizons occur in the northern half of Admiralty Island, their stratigraphic positions within the Triassic stratigraphy are uncertain. Mostly they are interpreted to be above the base of the section and within the shales that comprise the middle sedimentary part of the Triassic stratigraphy.

A thin, discontinuous, carbonate bed occurs between the conglomerate and the main ore body, and other carbonate beds are found just underlying and intercalated with the capping basalts and related argillites.

Within the Hyd Group, thick sequences of massive to slaty, graphitic, pyritic, black argillite and massive to slaty, carbonate-rich, dolomitic argillite overlie the main orebody and are of Carnian to Norian age based on fossil assemblages within underlying and overlying carbonate beds (fig. 5). Thick sequences of massive to pillowed basalts cap the section at Greens Creek and, like the basal conglomerate, they are a distinctive marker horizon throughout the Upper Triassic stratigraphy of southeastern Alaska.

Serpentinities of uncertain age crosscut the lower sequences of the Permian-Triassic sections at Greens Creek (fig. 5) and may represent the shallow ultramafic source of the metabasaltic protoliths or the overlying mafic volcanic flows of the Hyd Group, perhaps highly altered cumulates left after extraction of mafic melts. Gabbro-clinopyroxenite, both as relatively fresh rock and as highly quartz-carbonate-fuchsite-altered serpentinite, is common in outcrops in the mine area.

Continued emplacement of basaltic magmas at shallow levels accounts for the common occurrence of large gabbroic sills and stocks, particularly well exposed along Gallagher Ridge, south of the mine. These intrusions are thought either to just precede or to be coeval with extrusion of the overlying Hyd Group mafic flows (fig. 5). Continued production of heat in the immediate footwall of the deposit would similarly result in the extreme alteration of the gabbro-basalt pile during hydrothermal convection.

Diabase dikes are observed to crosscut massive ore and are not well understood. Obviously younger and much less deformed and altered, they are thought to be products of Jurassic-Cretaceous resumption of island-arc volcanism.

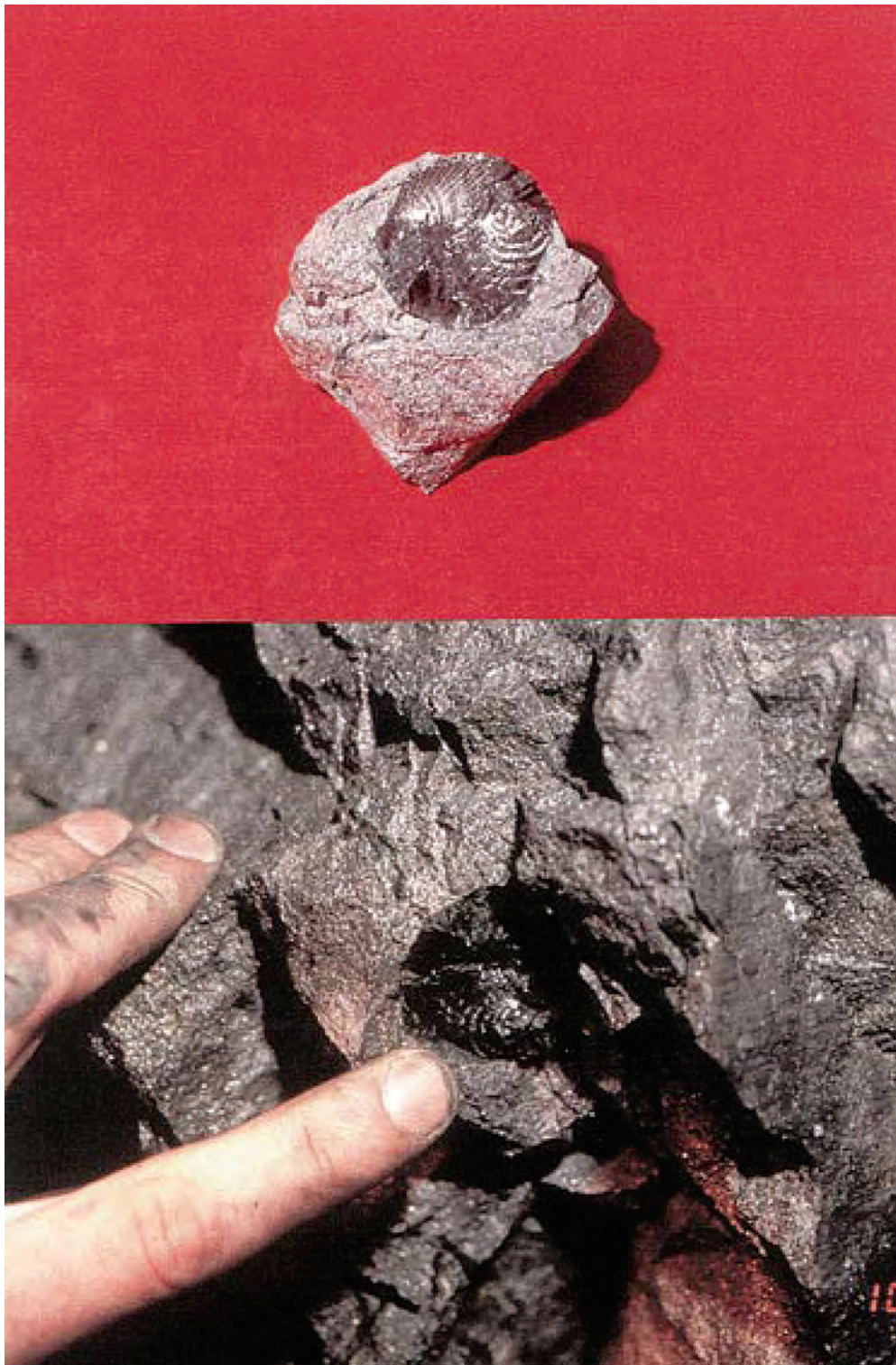


Figure 4. Photograph of *Halobia* in clast of siliceous argillite milled into massive sulfide ore (courtesy of T.C. Crafford). Fingertip is shown for scale.

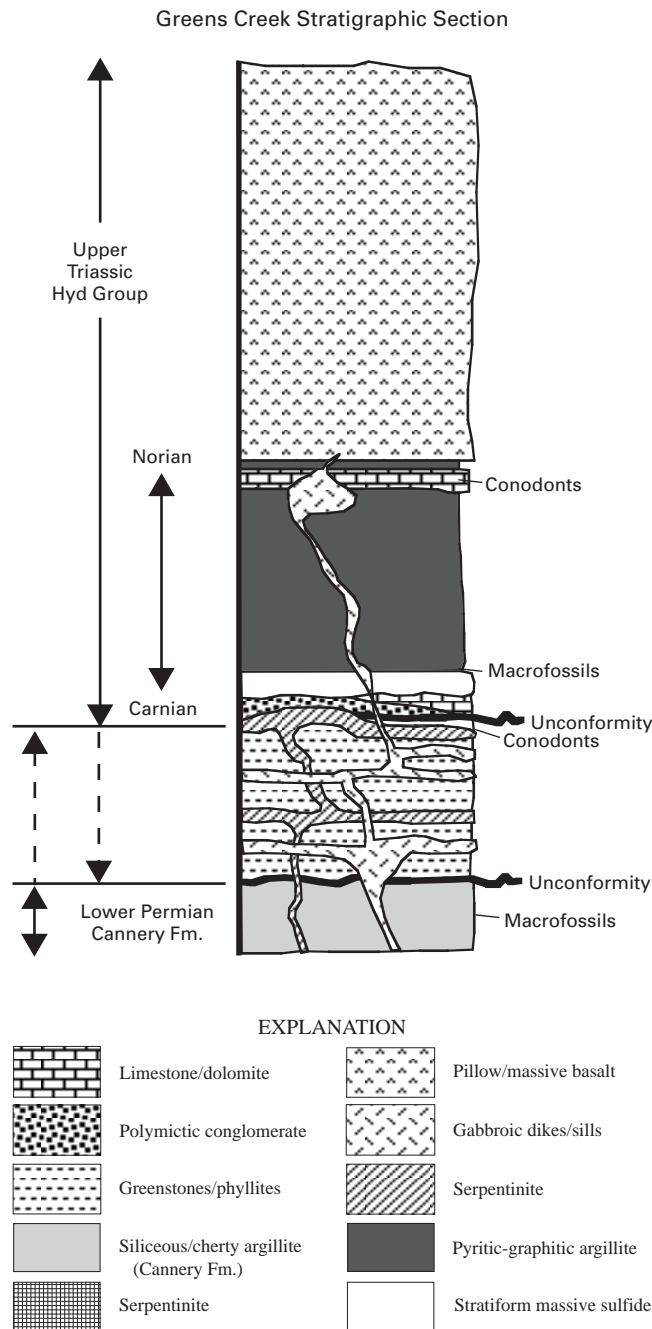


Figure 5. Stratigraphy of the Greens Creek section, Admiralty Island, showing the orebody at the contact between footwall phyllites and hanging-wall argillites (from Taylor and others, 2000).

Geochronology

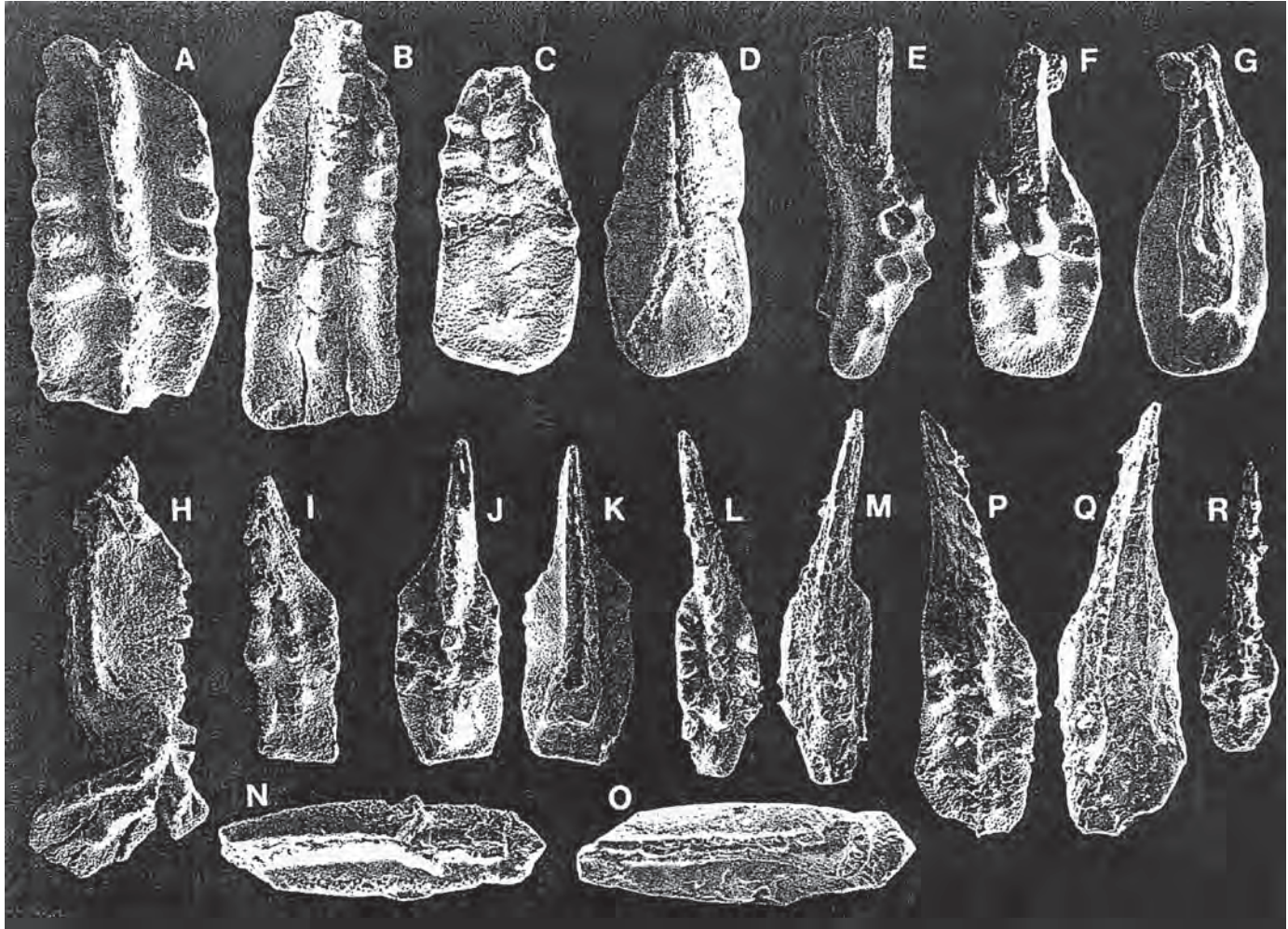
Paleontology—Conodont Studies

In 1997, the U.S. Geological Survey and Kennecott Greens Creek Mining Company joined in an effort to better understand the geologic setting and metallogenesis of the Greens Creek area. To that end, conodont samples were collected to provide higher biostratigraphic resolution for the age of the host rock and timing of mineralization. Conodonts were the fossil of choice because: (1) they are the major micropaleontologic index fossils in marine rocks of Triassic age; (2) they are apatitic and remain identifiable in low- to lower medium-grade metamorphic and hydrothermal regimes (Epstein and others, 1977; Rejebian and others, 1987); and (3) they are most easily recovered from carbonate rocks and had been recovered from Triassic carbonate and metacarbonate rocks throughout Alaska, including Admiralty and Kupreanof Islands (fig. 2 and Appendix).

By the end of 2001, thirty-nine conodont samples from host rocks in the Greens Creek mine and from outcrops of carbonate-bearing strata in the vicinity of the mine had been processed, searched for conodonts, and analyzed in order to refine the age of the host rock and timing of mineralization (table 1; Appendix, localities 23–31). In addition, carbonate samples from exploration areas on the Mansfield Peninsula (fig. 2 and Appendix, localities 1–4) and from the vicinity of the Taylor Creek deposit in the Duncan Canal area, northern Kupreanof Island (Appendix, localities 6–21), were also processed and analyzed.

All of the conodont samples from the immediate vicinity of the Greens Creek mine are from the Hyd Group of Late Triassic age. The group extends the length of Admiralty Island in a relatively narrow belt that parallels the island's eastern margin and also crops out on northern Kupreanof Island (see chap. 2). The Hyd Group is part of the Admiralty subterrane of the Alexander terrane (Gehrels and Berg, 1994). It unconformably overlies the Cannery or Pybus Formations on Admiralty and northern Kupreanof Islands. Conodont collections from northern Kupreanof Island indicate both formations are at least as young as very late Early Permian (Appendix, localities 8–10, and 22). The Hyd Group is mostly low-grade metamorphosed greenstone and phyllites that are hydrothermally altered locally. Crucial for the extraction of conodonts are the carbonate-rich intervals within calcareous and (or) dolomitic, carbonaceous, pyritic black phyllites and argillites and thin carbonate beds intercalated with these rocks (fig. 5).

The taxonomy and biochronology used for species and age determination, particularly for conodonts of late Carnian and earliest Norian age, are based on data from systematic and integrated conodont and ammonoid collections from many Upper Triassic successions in northeast British Columbia and, closer to Greens Creek both geographically and paleogeographically, from the lower part of the Kunga Group (Wrangellia terrane) in the Queen Charlotte Islands



(Orchard, 1991a, b), about 400 km southeast. The Carnian-Norian boundary and the interval of the Lower and Upper *primitius* Zones lie within the lower member of the Peril Formation; the formation ranges in age from late Carnian to late Norian. Both the type section of the Peril and reference sections for the Lower and Upper *primitius* Zones are in northwesternmost Queen Charlotte Islands (Desrochers and Orchard, 1991; Orchard, 1991a).

Conodonts from the Greens Creek Mine Area

Underground Collections

Twenty-seven samples were collected from various levels above the ore zone; some are from the underground workings, within about 50 m of the hanging-wall/ore contact, and others are from drill core taken in the hanging wall. Only four samples yielded conodonts (figs. 6 and 7; table 1, samples 1–4; Appendix, localities 27–31). The results are not as disappointing as the low number of productive samples might imply. Two samples from the underground workings (table 1, samples 1–2) yielded conodonts diagnostic of the Lower and Upper *primitius*

Zones (figs. 6 and 7). Medium-gray, medium-grained dolomite from sample 1 collected about 20 m above the orebody (table 1) yielded the index species *Metapolygnathus primitius* (Mosher) and other less biostratigraphically diagnostic forms including *Neogondolella* sp. (fig. 6, A–D, and I). *M. primitius* restricts the collection to the Lower or Upper *primitius* Zone — a narrow interval that straddles the Carnian-Norian boundary. *M. primitius* is also the only conodont recovered from very dark gray, slightly silty dolomitic lime mudstone and fine-grained dolomite of sample 2 that is only 15 m above the orebody (fig. 6, P and R; table 1). Sample 3, from medium-gray, slightly dolomitic, calcareous phyllitic mudstone, was selected from a drill core that penetrated the stratigraphic package on Big Sore Ridge (fig. 3) immediately above the mine workings. This sample yielded deformed fragments of neogondolellids and *Metapolygnathus?* sp. that indicate a Late Triassic, likely Carnian to very earliest Norian age (the age range of *Metapolygnathus*). The fourth sample from the workings, produced one ramiform conodont element that merely indicates a Triassic age. These four samples confine rocks in the hanging wall close to the ore to the Lower and (or) Upper *primitius* Zone (latest Carnian and (or) earliest Norian).

Figure 6 (facing page). Lower and Upper *primitius* Zone conodonts (latest Carnian-earliest Norian) from the Hyd Group, northern Admiralty Island, Alaska. Collections are from underground workings and outcrop, Greens Creek mine (scanning electron micrographs of carbon-coated specimens, $\times 70$; illustrated specimens deposited in the U.S. National Museum, USNM, Washington, D.C. See table 1 for locality data, sample description, and analysis of faunules).

Figure 6. A-I, Pa elements from outcrop in cirque at head of upper Cliff Creek (table 1, sample 5); USGS colln. Mes. 35007.

Figure 6. A, B, *Metapolygnathus primitius* (Mosher), Upper views of two incomplete adult specimens with quadrate platform with five nodes on lateral margins and posterior margin without nodes (B); USNM 519818, 19.

Figure 6. C, D, *Metapolygnathus primitius* Upper and lower views of small adult with three lateral nodes on inner margin and four on outer margin. Even though the lower surface is corroded, there is still evidence of a bifurcate scar and the pit close to the center of the platform; USNM 519820.

Figure 6. H, A *Metapolygnathus primitius* Pa element bent out of shape. Preservation like this is more typical of specimens in this collection rather than other specimens shown here; USNM 519827.

Figure 6. I, *Metapolygnathus primitius* Juvenile with three nodes on lateral margins and midplatform constriction; USNM 519821.

Figure 6. E-G, *Metapolygnathus primitius* transitional to *Epigondolella*, well-preserved subadult, lateral, upper, and lower views. This specimen already has five nodes on one lateral margin; lateral view shows microreticulation on nodes confirming assignment to *M. primitius* but, like *Epigondolella* (its likely descendant), the pit is centrally located on the platform; USNM 519826.

Figure 6. J-O, *Metapolygnathus primitius* Specimens from mine workings at 37 Ramp drift, no. 1 passing bay and within 20 meters of the orebody (table 1, sample 1); USGS colln. Mes. 35004.

Figure 6. J-M, Juvenile (L, M) and subadult (J, K) Pa elements of *Metapolygnathus primitius* (Mosher), upper and lower views; K shows squared-off scar that is incipiently bifurcate and pit slightly posterior of platform center. J has lateral margins with three nodes whereas L, even though a juvenile, has four nodes on one margin; USNM 519822, 23.

Figure 6. N, O, *Neogondolella* sp., Pa element, upper and lower views; specimen poorly preserved but clearly shows this is a neogondolellid and not a metapolygnathid homeomorph of *Neogondolella*, such as *M. communisti*; USNM 519828.

Figure 6. P-R, Specimens from mine workings in 620-2955 drift and within 15 meters of the orebody (table 1, sample 2); USGS colln. Mes. 35003. Subadult and juvenile complete Pa elements, though poorly preserved, *Metapolygnathus primitius* (Mosher), upper and lower views, USNM 519824, 25.

Outcrop Collections

Conodont samples from outcrops in the mine area were more productive than those from underground as the choices of sampling sites in the Triassic stratigraphy are much greater. Conodonts were found in 7 of the 16 outcrop samples (table 1, samples 5–11; Appendix, localities 24–26). Like the underground samples, the most tightly constrained collections are diagnostic of the Lower and (or) Upper *primitius* Zones; all other productive samples contain conodonts whose range, though not restricted to these zones, includes all or part of the Upper and Lower *primitius* Zones (fig. 7). Sample 5, from an outcrop of medium-gray lime mudstone in the cirque at the head of Cliff Creek yielded at least 100 deformed and (or) fractured conodont fragments, several incomplete though generically identifiable platform elements, and several others identifiable to species (table 1, sample 5); some of the best and one of the worst are shown in figure 6, A–I. Four specimens can be confidently assigned to *Metapolygnathus primitius* (fig. 6, A–D, and I) and two others are transitional between *M. primitius* and *Epigondolella* (fig. 6, E–G).

A sample of calcareous argillite (table 1, sample 6) at Big Sore Creek (fig. 3), produced the most biostratigraphically constrained conodont collection. *M. primitius* and abundant *Neogondolella* spp., including many *N. navicula*, likely restrict this collection to the Upper *primitius* Zone of the earliest Norian. Even though the assignment of one definitive *Metapolygnathus* to a species (*M. primitius*) is uncertain, the occurrence of a definitive ornate *Metapolygnathus* with *N. navicula* restricts the age of the collection to the Upper *primitius* Zone as the first appearance of *N. navicula* marks the base of the Upper *primitius* Zone and *Metapolygnathus* should not extend above that zone. At Lil Sore (fig. 3), another calcareous argillite yielded a juvenile fragment of a metapolygnathid or epigondolellid and a deformed subadult of *M. primitius* or *M. nodosus*. The age range for this sample is no older than the Lower *nodosus* Zone and no younger than the Upper *primitius* Zone. Sample localities 8–11 yielded poorly preserved conodonts that could only be assigned a rather broad age range from or within the early or late Carnian to the earliest or middle Norian, even though one collection, from sample locality 10, has abundant conodonts.

Table 1. Data for geologically and biostratigraphically significant conodont collections from the Greens Creek mine and immediate vicinity, Alaska.

[Conodont zonation and age range of collections shown in figure 7; samples from Juneau A–2 quadrangle; all conodonts analyzed by A.G. Harris. CAI, conodont color alteration index of Epstein and others, 1977, and Rejebian and others, 1987; Pa, platform element; m, meter; mm, millimeter]

Sample no. and location	Stratigraphic unit, lithology, and collector(s)	Conodont fauna and remarks	Zone/Age	CAI	Conodont biofacies and environment
Sample 1 37 Ramp drift, no. 1 passing bay; collection is ~20 meters above orebody, but intervening rocks are structurally complex 58°04'57"N., 134°37'50"W.	Hyd Group Medium-gray, medium-grained dolomite containing abundant pyrite and crosscutting dolomite vein fillings as much as 3 millimeters thick. Collectors: C.D. Taylor and K.G. Lear, 1996	USGS colln. Mes. 35004 Conodonts are poorly preserved. 1 subadult and 1 juvenile Pa elements <i>Metapolygnathus primitius</i> (Mosher) [fig. 6, J–M] 1 anterior half of Pa element <i>Metapolygnathus</i> sp. indet. 1 Pa element <i>Neogondolella</i> sp. indet. [fig. 6, N and O]. Sample also contains phosphatized steinkerns of gastropods and pelecypods.	Lower and Upper <i>primitius</i> Zones (latest Carnian to earliest Norian)	5-5.5	Indeterminate (too few conodonts) but undoubtedly open-marine.
Sample 2 620-2955 drift; 15 meters above orebody 58°04'57"N., 134°37'50"W.	Hyd Group Very dark gray, dolomitic, slightly silty, fine-grained lime mudstone and fine-grained dolomite. Collectors: C.D. Taylor and K.G. Lear, 1996	USGS colln. Mes. 35003 2 (a juvenile and an adult) Pa elements <i>Metapolygnathus primitius</i> (Mosher) [fig. 6, P–R]. The keel and pit on the lower side of the adult specimen is poorly preserved (eroded and (or) corroded).	Lower and Upper <i>primitius</i> Zones (latest Carnian to earliest Norian)	5	Indeterminate (too few conodonts); likely normal marine.
Sample 3 480 South drift; 58°04'57"N., 134°37'50"W.	Hyd Group Medium-gray, slightly dolomitic, calcareous, phyllitic mudstone. Collectors: C.D. Taylor and K.G. Lear, 1996	USGS colln. Mes. 35006 6 deformed Pa element fragments of neogondolellids 2 Pa element fragments <i>Metapolygnathus</i> ? sp. indet. 1 indet. bar fragment. Conodonts are deformed and fractured.	Late Triassic, likely Carnian to very earliest Norian	5	Indeterminate (too few conodonts) but open-marine depositional setting.
Sample 4 PS-112, 1347 ft. Core drilled on Big Sore Ridge, immediately above mine workings 58°04.8'N., 134°38.1'W.	Hyd Group Medium-gray, fossiliferous (crinoid ossicles and other indet. bioclasts), calcareous dolomite containing quartz-filled gashes. Collector: S. Newkirk, 1996	USGS colln. Mes. 35005 1 incomplete M element of Triassic morphotype.	Triassic	5 or 5.5	Indeterminate (too few conodonts).
Sample 5 Cliff-2; Outcrop in cirque at upper Cliff Creek 58°03'35"N., 134°34'03"W.	Hyd Group Medium-gray lime mudstone containing <10% calcite veins. Collectors: N.A. Duke and P.A. Lindberg, 1996	USGS colln. Mes. 35007 83 deformed, fragmented, fractured, and (or) corroded Pa elements. <i>Metapolygnathus nodosus</i> or <i>M. primitius</i> (Mosher) [fig. 6, H]. 4 Pa elements <i>Metapolygnathus primitius</i> (Mosher) [fig. 6, A–D, I]. 2 Pa elements <i>M. primitius</i> (Mosher) transitional to <i>Epigondolella</i> [fig. 6, E–G]. 12 indet. blade fragments 1 ichthyolith. Minor phosphatic and phosphatized bioclasts.	Lower-Upper <i>primitius</i> Zones (latest Carnian to earliest Norian)	5	Post-mortem transport from or within a metapolygnathid biofacies (a normal-marine shelf or platform depositional setting if not hydraulically transported farther seaward after death.)
Sample 6 JMP-131 Outcrop at Big Sore Creek 58°04'47"N. 134°36'53"W.	Hyd Group Calcareous argillite. Collector: J.M. Proffett, 1999	USGS colln. Mes. 35018. Most of the conodonts in this collection are covered with or invaded by organic matter. 1 incomplete Pa element <i>Metapolygnathus primitius</i> (Mosher)? 4 juvenile Pa elements <i>Metapolygnathus</i> sp. indet. and (or) <i>Epigondolella</i> sp. indet. 2 incomplete, fractured and deformed Pa elements <i>Metapolygnathus</i> sp. indet. and (or) <i>Epigondolella</i> sp. indet. 21 Pa elements <i>Neogondolella navicula</i> (Huckriede). 43 Pa element fragments or juveniles of chiefly <i>Neogondolella</i> spp. indet. <i>Neogondolella</i> spp. indet. vicarious elements. 2 Pb, 1 M, 2 Sa, and 2 Sc 14 indet. bar, blade, and juvenile platform fragments.	Lower-Upper <i>primitius</i> Zone, probably Upper <i>primitius</i> Zone (latest Carnian to earliest Norian; probably earliest Norian). This is the most tightly dated conodont collection from the Hyd Group in the Greens Creek mine area (fig. 7).	Most 5; rare 4	<i>Neogondolellid</i> biofacies (most likely basin depositional setting) with post-mortem hydraulic addition of a few <i>Metapolygnathus</i> from a nearby shallow-water carbonate platform or submarine edifice.

Table 1. Data for geologically and biostratigraphically significant conodont collections from the Greens Creek mine and immediate vicinity, Alaska.—Continued

[Conodont zonation and age range of collections shown in figure 7; samples from Juneau A–2 quadrangle; all conodonts analyzed by A.G. Harris. CAI, conodont color alteration index of Epstein and others, 1977, and Rejebian and others, 1987; Pa, platform element; m, meter; mm, millimeter]

Sample no. and location	Stratigraphic unit, lithology, and collector(s)	Conodont fauna and remarks	Zone/Age	CAI	Conodont biofacies and environment
Sample 7 NAD-170 Outcrop at Lil' Sore 58°07'56"N. 134°41'26.5"W.	Hyd Group Calcareous argillite. Collector: N.A. Duke, 1999	USGS colln. Mes. 35051. 1 juvenile Pa element fragment (free blade and small part of anterior end of platform) of a metapolygnathid or epigondolellid. 1 deformed subadult Pa element of <i>Metapolygnathus nodosus</i> (Hayashi) or <i>M. primitius</i> (Mosher).	nodosus Zone through Upper <i>primitius</i> Zone (late Carnian to earliest Norian)	5	Indeterminate (too few conodonts); normal-marine depositional setting.
Sample 8 NAD-2B Outcrop in Lakes District 58°05'23"N. 134°42'04"W.	Hyd Group Black calcareous argillite. Collector: N.A. Duke, 1999	USGS colln. Mes. 35050. Conodonts are deformed, fractured, corroded and mostly incomplete. 6 Pa elements <i>Metapolygnathus</i> sp. 3 poorly preserved neogondolellid Pa element fragments.	Carnian to very earliest Norian	5	Post-mortem transport from or within a normal-marine shelf or platform depositional setting.
Sample 9 NAD-99A Outcrop in Lakes District 58°05'27"N. 134°42'09.6"W.	Argillitic limestone. Collector: N.A. Duke, 1999	USGS colln. Mes. 35022. Conodonts are extremely poorly preserved; the chemical composition of a few was determined using EDAX (energy dispersive X-ray system); results are consistent with conodont composition. 5 Pa elements of <i>Metapolygnathus?</i> sp. indet. or <i>Epigondolella?</i> sp. indet. of Late Triassic age or even <i>Polygnathus?</i> sp. indet. of Middle Devonian-Early Mississippian age. These specimens most resemble Late Triassic metapolygnathids and epigondolellids; the geologic framework favors a Late Triassic age.	Carnian to middle Norian	5	Indeterminate; generic assignment uncertain.
Sample 10 97-LG-05 Outcrop on Gallagher Ridge, 200 m west of top of Big Sore Ridge and above mine workings. 58°03'38"N. 134°37'29"W.	Hyd Group Metalimestone. Collector: C.D. Taylor, 1997	USGS colln. Mes. 35023. All specimens are incomplete, variably deformed, and recrystallized so that species determination is not possible. These specimens are, however, confidently assigned to <i>Metapolygnathus</i> because the lateral marginal nodes are relatively few, the free blade is low, the keel bifurcates posteriorly, and there are no posterior margin nodes. 47 Pa element fragments <i>Metapolygnathus</i> sp. indet. (better preserved specimens have 3–5 marginal nodes). 76 Pa (small fragments) elements <i>Metapolygnathus</i> sp. indet. Minor phosphatic and phosphatized bioclasts.	late Carnian to very earliest Norian (no older than nodosus Zone)	6.5-7	Post-mortem transport within or from a metapolygnathid biofacies; this is likely a post-mortem hydraulic sort (lag concentrate) as only Pa elements are present.
Sample 11 97-LG-09 Outcrop on Gallagher Ridge, 11 m west of interbedded basalt and limestone exposure. 58°03'39"N. 134°37'22"W.	Hyd Group Metalimestone. Collector: C.D. Taylor, 1997	USGS colln. Mes. 35024 1 incomplete, deformed, and fractured Pa element <i>Metapolygnathus?</i> sp. indet.	Probably latest early Carnian to very earliest Norian	5.5-6	Indeterminate (too few conodonts).

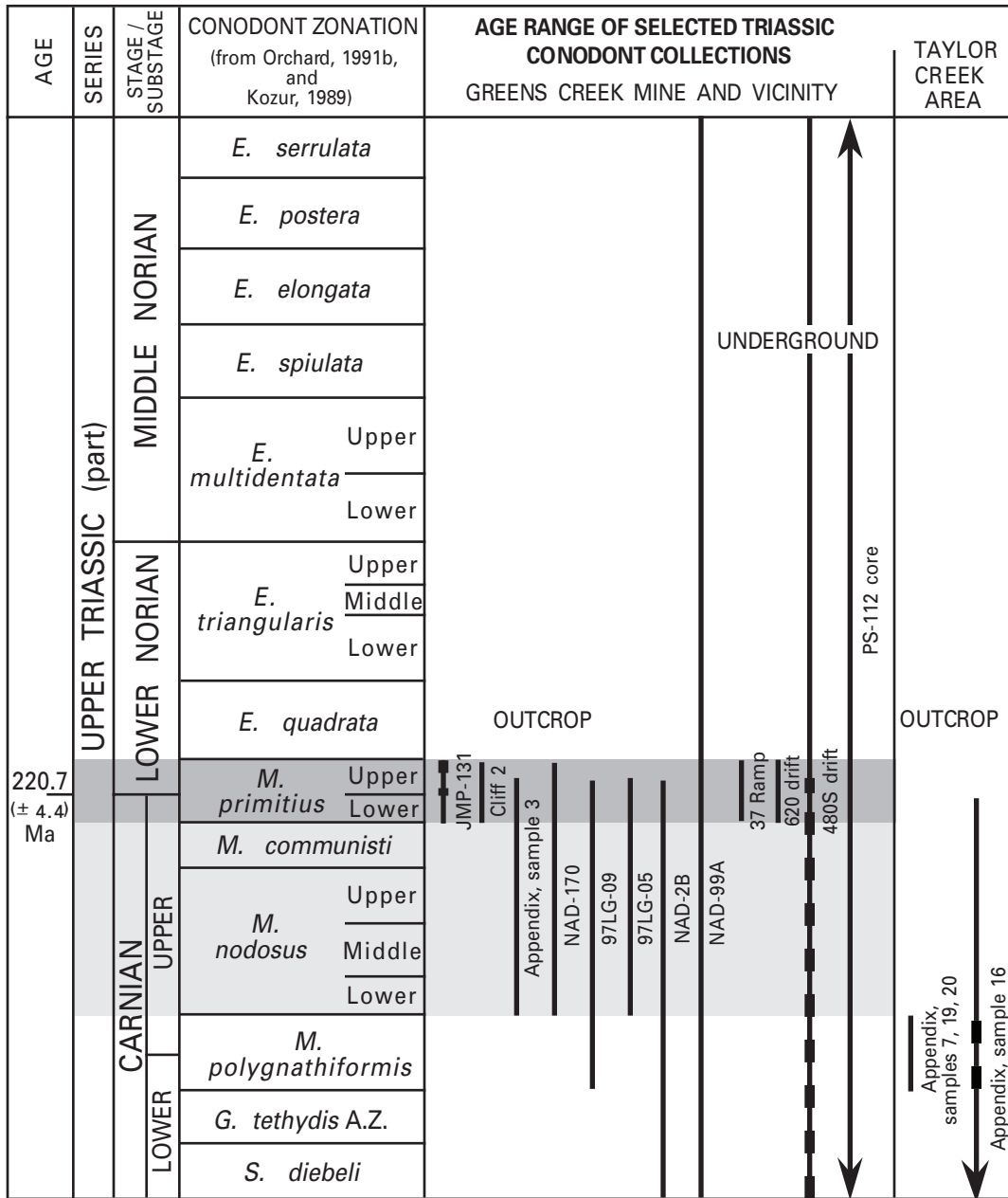


Figure 7. Carnian-Middle Norian conodont zonation showing age range of biostratigraphically useful and (or) geologically significant conodont collections from Hyd Group host rocks, Greens Creek mine and vicinity, and four collections from the Hyd in the vicinity of the Taylor Creek deposit, northern Kupreanof Island. Plain solid bar indicates age range of collection; arrow at either end of bar indicates range extends beyond the Carnian and (or) middle Norian; dashed part of range indicates probable restricted age. The combined light and dark shaded areas indicate the common age of all biostratigraphically useful samples in the Greens Creek area; the narrow dark band marks the range of the four most biostratigraphically diagnostic collections, which is coincident with the boundaries of the Lower and Upper *primitius* Zones. Note that the age range of all collections overlap in the lower part of the Upper *primitius* Zone and that collection JMP-131 is most likely restricted to the Upper *primitius* Zone (see table 1). Radiometric age from Gradstein and others (1995). Abbreviations: A.Z., assemblage Zone; *E.*, *Epigondolella*; *G.*, *Gladigondolella*; *M.*, *Metapolygnathus*; *S.*, *Sephardiella*;

Color Alteration Index (CAI)

The CAI of most Greens Creek area samples is 5 or 5–5.5, indicating the immediate host rock of each conodont sample reached at least 300° (CAI 5) or 350°C (CAI 5–5.5) using the experimental data of Epstein and others (1977) and Rejebian and others (1987). The fracturing and flowage of the conodonts, the consistency of CAI values within a sample and from sample to sample within the area, and the general absence of recrystallization suggest a low-grade metamorphic event. Conodonts from samples 10 and 11, however, have higher CAI values of 5.5–6 and 6.5–7 and, unlike conodonts from other Greens Creek area samples, they are partly recrystallized. Recrystallization of conodont carbonate apatite (approximating francolite) first begins at CAI 5.5 (Königshof, 1992); recrystallization generally increases with increasing CAI as a function of time, temperature, and mineralogy of the host rock as well as the porosity of the host during metamorphism and (or) hydrothermal alteration (Rejebian and others, 1987, their figs. 1 and 2; Königshof, 1992). Sample 11 is from an outcrop on Gallagher Ridge (fig. 3), just 11 m west of exposures of interbedded basalt and limestone. The CAI values of conodonts from sample 11 are higher than CAIs of conodonts from most Hyd samples and were either elevated soon after their deposition as a consequence of contact metamorphism (by basalt flows or intrusions) and (or) hydrothermal alteration associated with the nearby interbedded basalts or at a later time during larger scale metamorphism and contemporaneous or subsequent hydrothermal alteration. Nonetheless, conodonts from sample 11, and the more thermally altered conodonts from nearby sample 10 experienced higher temperatures and (or) contact with low- or high-temperature fluids that produced higher color and textural alteration of these conodonts than of conodonts from other collections in the Greens Creek mine area. Several collections of Permian and Triassic age from northern Kupreanof Island also contain conodonts having a range of high CAI values within a single sample. These are discussed later in this chapter.

Paleoenvironmental and Depositional Controls for Conodont Distribution

The conodonts in the Greens Creek area collections are metapolygnathids and neogondolellids. The former are predominantly tropical to subtropical, cosmopolitan, relatively warm shallow-water open-marine forms (ornate metapolygnathids) that were widespread in the western Cordillera of North America and elsewhere. If well enough preserved to permit species determination, the conodont found from the Greens Creek area includes only one or two species. Six collections contain only metapolygnathids, and of these, only samples 5 and 10 produced relatively abundant conodonts, whereas the other four samples yielded only a few metapolygnathid platform (Pa) elements (table 1). The carbonaceous, calcareous and (or) dolomitic phyllitic mudstones and argillites that preserve these conodonts likely represent mainly hemipelagic

basinal deposits with additions of storm- or wave-generated siliciclastic and carbonate muds from shallow-water platforms or other near-surface submarine edifices that were transported and redeposited in deeper marine environments. In the same way, the metapolygnathid conodont platform elements are also post-mortem hydraulic additions to these basinal deposits. Most conodont animals contained an array of morphologically distinct and functionally specialized conodonts in their feeding apparatus, like the variety of tooth shapes in humans. The conodont apparatus includes fanglike grasping and piercing elements, sawbladelike (ramiform) shredding elements, and more massive, nodose, ribbed, and (or) crenulate platelike (platform) grinding elements (for example, Purnell and Donoghue, 1997, 1998; Sweet, 1989). All conodonts shown in figure 6 are the more massive platform elements, which were the more rapidly evolving and therefore more biostratigraphically useful conodonts in the feeding apparatus. The Hyd Group collections lack the more abundant and lighter ramiform elements of the conodont feeding apparatus; these, being lighter, were probably carried farther basinward from their shallow-water area of origin. The conodont animal was, for the most part, an active predator but was also preyed upon. Well-preserved fossils exist of Late Devonian sharks with their innards filled with the recognizable remains of conodont animals, that is, with indigestible conodont elements (Williams, 1990). Thus, some of the conodonts in the Greens Creek collections may have come from fecal pellets of other marine animals, probably other fish, that fed on conodonts. Conodonts have been reported in phosphatized fecal pellets in acid residues (Lange, 1968) and are commonly observed in associated fecal-pellet-rich areas that litter bedding planes of some black shales. Limestone samples containing abundant metapolygnathids probably originated as calciturbidites from sites closer to a shallow-water carbonate platform (table 1, samples 5 and 10). Sample 6, the most precisely dated collection, contains conodonts that lived in a basinal setting. The conodonts are predominantly deep and (or) cool-water neogondolellids. In this collection, most of the lighter conodont elements of the feeding apparatus have been winnowed away, but more ramiform elements are present here than in any of our other collections. Metapolygnathids make up only a small percentage of this collection and are undoubtedly post-mortem additions.

Conodonts from the Mansfield Peninsula and Northern Kupreanof Island

Conodont samples were also collected from exploration areas on the Mansfield Peninsula, northwestern Admiralty Island (fig. 2), at least 7 km northwest of the mine (Appendix, localities 1–4) and on northern Kupreanof Island, mostly in the vicinity of the Taylor Creek deposit in the Duncan Canal area (Appendix, localities 6–21). Only one collection from the Mansfield Peninsula produced conodonts of Triassic age (Appendix, sample 3). The collection includes nine platform elements of an ornate *Metapolygnathus*, likely *M. primitius* and (or) *M. nodosus*, and six platform elements of either

Neogondolella sp. or *Metapolygnathus communisti*. Most of the conodonts are deformed and (or) incomplete; all are partly corroded and heavily coated with carbonaceous matter. Nonetheless, based on the broadest age interpretation for these conodont species, the collection could range from the *nodosus* Zone through the *primitius* Zone (upper Carnian–lowermost Norian). This range includes the interval of the mostly tightly constrained conodont collections from the immediate vicinity of the Greens Creek mine (table 1, samples 1, 2, and 6; fig. 7).

On northern Kupreanof Island, conodont samples from the Hyd Group and stratigraphically older Cannery and Pybus Formations were collected in the course of this study or collected previously by U.S. Geological Survey personnel involved in geologic mapping or topical studies. Data for all these samples are given in the Appendix.

More than 60 percent of the samples from the vicinity of the Taylor Creek deposit were productive. Samples were taken from the Cannery Formation and Hyd Group and from carbonate-bearing rocks of uncertain stratigraphic assignment. Three samples, from the highest exposed beds of the Cannery, all produced the same conodont species association. The presence of *Mesogondolella idahoensis* in all three collections restricts their age to the Kungurian (late Leonardian; fig. 8). In addition, a sample collected from the Pybus Formation in 1980, about 15 km northwest of the Taylor Creek deposit, produced conodonts of the same age but of greater diversity (Appendix, locality 22). These collections confirm the opinion of Karl and others (1999) that the Pybus is a facies equivalent of the Cannery. Most of the conodonts from the Cannery and Pybus have a range of CAI values within a sample (some from 5 to 6.5). Moreover, a few other collections that contain less biostratigraphically diagnostic conodonts and therefore have longer age ranges also have a range of CAI values within a single sample; these might also be Permian collections (Appendix, localities 13 and 15).

The conodont collections from the Taylor Creek area assigned to the Hyd Group are of latest early to earliest late Carnian age (Appendix, localities 7, 19, and 20). The predominant conodont in these collections is *Metapolygnathus polygnathiformis*, the nominate species of the *polygnathiformis* Zone (fig. 7). These Hyd conodonts from the vicinity of the Taylor Creek deposit are of older Carnian age than any of the well-dated samples from the Greens Creek area. A fourth sample, probably from the Hyd, produced conodonts that can confidently be assigned a late Early to early Late Triassic age. However, some specimens that are less deformed than others could be representatives of *M. polygnathiformis*, so this collection may be the same age as the other collections from the Hyd at Taylor Creek (Appendix, locality 16). The CAI of conodonts from the Hyd is mostly 5 (Appendix, localities 7, 19, and 20); conodonts from locality 16, however, have a range of CAI values from 5.5 to 7. Although stratigraphic levels apparently high in the Cannery and Pybus Formations and locally within the Hyd show effects of hydrothermal activity, and at least three conodont collections from the Hyd are older than the host rock or any Triassic rock thus far biostratigraphically well constrained in the vicinity of

Greens Creek, the paleontologic data available at this time do not necessarily restrict the age of mineralization at Taylor Creek to the latest early or earliest late Carnian. The CAI of conodonts from the Hyd in the Taylor Creek area is mostly the same as that exhibited by conodonts from the Hyd in the vicinity of Greens Creek — 5 or 5–5.5. Higher CAI values occur locally in the Hyd in both areas (table 1, samples 10 and 11; Appendix, locality 16). The Hyd Group likely hosts the mineralization at Greens and Taylor Creeks, but the mineralization may not occur at the same stratigraphic level in both areas. At Greens Creek, the ore lies at or very close to the Carnian-Norian boundary interval (within rocks that are dated as Lower and/or Upper *primitius* Zone). In the vicinity of the Taylor Creek deposits, probably no closer than 3 km, the Hyd strata are of older Late Triassic age. As yet, no conodont samples have been taken in the immediate vicinity of the Taylor Creek deposit.

Radiogenic Isotopic Age Determinations

Radiogenic isotopic systems (for example, U-Pb, Th-Pb, Sm-Nd, Rb-Sr, K-Ca, ^{40}Ar - ^{39}Ar , and Re-Os) are mainly used for age determinations of igneous and metamorphic rocks and for tracing the source(s) of fluids and magmas (for example, Dickin, 1995, and references within). However, these isotopic methods can also be used to determine ages for mineralization or remobilization of ore fluids, interpreted as disturbances to radioisotopic systems (for example, Snee and others, 1988; Hart and Kinloch, 1989; Lambert and others, 1989; Walker and others, 1991; Kerrich, 1991; Brannon and others, 1992, 1996; Chesley and others, 1993, 1994; Kerrich and King, 1993; Christensen and others, 1995a, 1995b; Snee, 2002). To this end, we used (1) the $^{40}\text{Ar}/^{39}\text{Ar}$ dating method to determine either the age of mineralization if it were preserved or the age of a disturbance to this isotopic system, and (2) the U-Pb, Th-Pb, Sm-Nd, and Rb-Sr systems to date mineralization, host rocks, or disturbances.

^{40}Ar - ^{39}Ar Age Determinations

$^{40}\text{Ar}/^{39}\text{Ar}$ geochronologic studies of sericite and fuchsite alteration in the Greens Creek mine and of fuchsite alteration of ultramafic bodies near the mine area were conducted in an attempt to constrain the timing of ore formation. Eight samples yielded data: six samples of sericite, mixed sericite/fuchsite, and fuchsite from ore and altered footwall phyllites, one sample of fuchsite from the Bruin Knob altered ultramafic body in the Mammoth claim area of Mariposite Ridge, and one sample of fuchsite from a similar altered ultramafic body on the Mansfield Peninsula (chap. 4). Unfortunately, all eight samples generated step-release-argon spectra that indicate Cretaceous metamorphic resetting of older minerals. The $^{40}\text{Ar}/^{39}\text{Ar}$ data are presented in table 2 and in figures 9 and 10 that show the age spectra for each sample analyzed. In the simplest case, each of the spectra is the product of gas released from minerals that define the minimum age of the oldest mineral domains and the maximum age of the youngest

SYSTEM/SERIES		SERIES/STAGE		CONODONT ZONES (modified from Mei and Henderson, 2002)
PERMIAN (part)	MIDDLE (pt.)	GUADALUPIAN (pt.)	WORDIAN	<i>J. aserrata</i> Me. phosphoriensis- Me. prolongata
				<i>M. bitteri</i>
			UFIMIAN	<i>M. phosphorensis</i>
		KUNGURIAN	<i>Neostr. newelli - M. serrata</i>	
			<i>Neostr. sulcopicatus</i>	
			<i>Neostr. prayi</i>	
	LOWER (CISURALIAN)	LEONARDIAN	ARTINSKIAN	<i>M. idahoensis</i>
				<i>Neostr. pnevi</i>
				<i>Neostr. pequopensis-Neostr. ruzencevi</i> A.Z.
				<i>M. bisselli-Sw. whitei</i> A.Z.
				<i>Sw. whitei - St. artinski.</i> A.Z.
	WOLFCAMPIAN	SAKMARIAN	<i>St. artin. - Sw. adent.</i> A.Z.	
			<i>M. bisselli-Sw. merrilli-St. simplex</i> A.Z.	
			<i>M. striata-St. simplex</i>	
			<i>St. baskovi-St. constrictus</i>	
		ASSELIAN	<i>St. elongatus-St. simplex-St. wabaunensis</i> A.Z.	

 Cannery Fm. samples 8-10
 Pybus Fm. sample 22

Figure 8. Conodont zonation for the Lower and part of the Upper Permian showing age range of conodont collections from the uppermost exposed beds of the Cannery Formation in the vicinity of the Taylor Creek deposit and the Pybus Formation about 15 kilometers farther northwest, northern Kupreanof Island (Appendix, localities 8–10 and 22). Abbreviations: A.Z., assemblage Zone; *M.*, *Mesogondolella*; *Neostr.*, *Neostreptognathodus*; *St.*, *Streptognathodus*; *Sw.*, *Sweetognathus*.

Table 2. $^{40}\text{Ar}/^{39}\text{Ar}$ data for samples* from Greens Creek VMS deposit, Admiralty Island, Alaska.

[T, temperature; °C, degrees Celsius; %, percent; Ma, mega-annum; mg, milligram]

T (°C)	Radiogenic $^{40}\text{Ar}^+$	K-derived $^{39}\text{Ar}^+$	$^{40}\text{Ar}_R/^{39}\text{Ar}_K$ #	$^{39}\text{Ar}_K/^{37}\text{Ar}_{Ca}$ **	Radiogenic yield (%)	$^{39}\text{Ar}_K$ (%)	Apparent age and error [®] (Ma)
96AD-06, Mammoth claim, fuchsite							
Total-gas date: 97.5±0.2 Ma; No plateau; J=0.007599, +0.1%; wt. 49.4 mg							
600	0.0374	0.0194	1.930	--	24.3	0.3	26.2 ± 0.6
700	0.7494	0.1621	4.623	19	92.1	2.4	62.3 ± 0.2
750	1.9497	0.3238	6.022	4.0	98.7	4.8	80.7 ± 0.2
800	4.3911	0.6496	6.759	4.2	93.7	9.7	90.4 ± 0.1
850	4.9855	0.6976	7.146	28	98.6	10.4	95.4 ± 0.2
900	9.7913	1.3262	7.383	237	99.5	19.8	98.5 ± 0.2
950	10.4570	1.3874	7.537	404	99.6	20.7	100.5 ± 0.2
1,000	7.2248	0.9411	7.677	1045	99.4	14.1	102.3 ± 0.2
1,050	3.8559	0.4917	7.843	265	98.9	7.4	104.4 ± 0.2
1,100	1.8586	0.2359	7.878	217	97.2	3.5	104.9 ± 0.2
1,150	1.4989	0.1901	7.885	235	95.9	2.8	105.0 ± 0.4
1,300	2.0917	0.2634	7.940	124	97.0	3.9	105.7 ± 0.2
96AD-02, Mansfield Peninsula, fuchsite							
Total-gas date: 60.8±0.2 Ma; No plateau; J=0.007579, ±0.1%; wt. 15.5 mg							
600	0.0116	0.0057	2.025	9	15.8	0.3	27.0 ± 4.0
700	0.1991	0.0532	3.743	23	79.2	2.4	50.5 ± 0.7
800	1.0028	0.2278	4.402	4.2	75.9	10.2	59.2 ± 0.1
850	1.4919	0.3199	4.663	26	95.3	14.4	62.7 ± 0.1
950	4.2774	0.9069	4.717	1161	98.6	40.8	63.4 ± 0.1
1,050	1.9078	0.4363	4.372	950	97.0	19.6	58.8 ± 0.2
1,150	0.5167	0.1180	4.378	133	82.3	5.3	58.9 ± 0.1
1,300	0.6486	0.1567	4.140	--	88.1	7.0	55.7 ± 0.2
Greens Creek East orebody, fuchsite							
Total-gas date: 89.0±0.2 Ma; No plateau; J=0.007566, ±0.1; wt. 52.4 mg							
600	0.2318	0.0791	2.929	161	62.6	1.2	39.5 ± 0.3
700	1.6182	0.3235	5.002	129	96.6	4.9	67.0 ± 0.1
750	2.5339	0.4350	5.002	48	97.4	6.6	77.8 ± 0.2
800	5.5079	0.8689	6.339	37	94.5	13.3	84.5 ± 0.1
850	9.3754	1.4021	6.687	169	98.6	21.4	89.0 ± 0.2
900	7.1184	1.0289	6.918	393	98.6	15.7	92.0 ± 0.1
950	5.3942	0.7659	7.043	737	98.5	11.7	93.7 ± 0.1
1,000	4.8071	0.6708	7.166	847	98.6	10.2	95.2 ± 0.1
1,050	2.6971	0.3716	7.258	1331	97.5	5.8	96.4 ± 0.2
1,100	1.7354	0.2369	7.326	342	97.7	3.6	97.3 ± 0.2
1,150	1.8212	0.2451	7.432	609	97.9	3.7	98.7 ± 0.2
1,350	0.9466	0.1255	7.541	230	93.6	1.9	100.1 ± 0.3

Table 2. $^{40}\text{Ar}/^{39}\text{Ar}$ data for samples* from Greens Creek VMS deposit, Admiralty Island, Alaska.—Continued

[T, temperature; °C, degrees Celsius; %, percent; Ma, mega-annum; mg, milligram]

T (°C)	Radiogenic $^{40}\text{Ar}^+$	K-derived $^{39}\text{Ar}^+$	$^{40}\text{Ar}_R/^{39}\text{Ar}_K$ #	$^{39}\text{Ar}_K/^{37}\text{Ar}_{Ca}$ **	Radiogenic yield (%)	$^{39}\text{Ar}_K$ (%)	Apparent age and error [@] (Ma)
Greens Creek east orebody, sericite							
Total-gas date: 77.5 ± 0.1 Ma; No plateau; $J=0.007558, \pm 0.1\%$; wt. 62.3 mg							
500	0.2166	0.0710	3.049	136	40.8	1.0	41.1 ± 0.6
600	0.1743	0.0535	3.258	184	81.5	0.8	43.9 ± 0.6
650	0.3973	0.1043	3.808	261	97.7	1.5	51.2 ± 0.2
700	1.1167	0.2793	3.998	33	95.8	3.9	53.7 ± 0.2
750	1.9110	0.4414	4.330	13	89.2	6.2	58.1 ± 0.1
800	3.2430	0.6784	4.781	79	92.7	9.5	64.0 ± 0.1
850	4.9680	0.9466	5.248	424	98.1	13.3	70.2 ± 0.1
900	4.4801	0.7855	5.703	557	98.2	11.0	76.1 ± 0.1
950	4.8884	0.7948	6.150	658	98.3	11.2	82.0 ± 0.1
1,000	5.4835	0.8411	6.520	584	98.8	11.8	86.8 ± 0.1
1,050	3.6438	0.5462	6.672	584	98.6	7.7	88.8 ± 0.1
1,100	4.3078	0.6418	6.712	392	98.5	9.0	89.3 ± 0.1
1,150	3.6127	0.5298	6.819	261	96.4	7.4	90.7 ± 0.1
1,200	2.2907	0.3282	6.980	154	97.5	4.6	92.7 ± 0.1
1,250	0.5304	0.0691	7.673	32	93.5	1.0	101.7 ± 0.3
1,350	0.1032	0.0103	10.010	2	76.2	0.1	132.0 ± 6.0
96GC-38, Greens Creek lower southwest orebody, fuchsite							
Total-gas date: 83.4 ± 0.2 Ma; No plateau; $J=0.007581, \pm 0.1\%$; wt. 36.8 mg							
600	0.0744	0.0297	2.501	35	33.1	0.7	34.0 ± 1.0
700	0.8166	0.2333	3.501	48	89.7	5.3	47.2 ± 0.1
800	2.0386	0.4062	5.019	21	87.9	9.3	67.4 ± 0.2
850	4.7641	0.7882	6.045	407	98.3	18.0	80.8 ± 0.1
900	4.5305	0.7021	6.452	283	98.9	16.1	86.2 ± 0.2
950	3.6134	0.5406	6.684	513	99.2	12.4	89.2 ± 0.1
1,000	3.7288	0.5501	6.778	232	98.9	12.6	90.4 ± 0.1
1,050	2.3592	0.3451	6.837	463	98.3	7.9	91.2 ± 0.2
1,100	2.5145	0.3674	6.844	292	97.8	8.4	96.2 ± 0.1
1,150	1.6150	0.2332	6.925	152	97.2	5.3	92.3 ± 0.1
1,200	0.8956	0.1287	6.960	183	95.6	2.9	92.8 ± 0.4
1,350	0.3332	0.0491	6.793	2	88.3	1.1	90.6 ± 0.8

Table 2. $^{40}\text{Ar}/^{39}\text{Ar}$ data for samples* from Greens Creek VMS deposit, Admiralty Island, Alaska.—Continued

[T, temperature; °C, degrees Celsius; %, percent; Ma, mega-annum; mg, milligram]

T (°C)	Radiogenic $^{40}\text{Ar}^+$	K-derived $^{39}\text{Ar}^+$	$^{40}\text{Ar}_R/^{39}\text{Ar}_K$ #	$^{39}\text{Ar}_K/^{37}\text{Ar}_{Ca}$ **	Radiogenic yield (%)	$^{39}\text{Ar}_K$ (%)	Apparent age and error [®] (Ma)
29F-heading, north zone, east orebody, fuchsite Total-gas date: 85.4±0.2 Ma; No plateau; J=0.007588, ±0.2%; wt. 28.7 mg							
550	0.0136	0.0070	1.959	26	19.4	0.2	27.0 + 3.0
650	0.2641	0.0639	4.135	123	87.7	1.8	55.7 + 0.9
750	1.1341	0.2377	4.771	72	96.7	6.7	64.2 + 0.1
800	0.9370	0.1769	5.297	94	69.7	5.0	71.1 + 0.2
850	2.3265	0.4040	5.758	202	96.9	11.4	77.2 + 0.2
900	4.9914	0.7810	6.391	203	98.7	22.0	85.4 + 0.1
950	3.2131	0.4716	6.814	162	98.1	13.3	90.9 + 0.1
1,000	3.7706	0.5420	6.957	95	98.6	15.2	92.8 + 0.2
1,050	1.2301	0.1772	6.943	146	97.5	5.0	92.6 + 0.4
1,100	1.0498	0.1512	6.945	74	97.0	4.2	92.6 + 0.2
1,150	1.3104	0.1910	6.861	37	97.2	5.4	91.6 + 0.1
1,300	2.4946	0.3548	7.031	12	97.1	10.0	93.8 + 0.1
PS115, Greens Creek exploration drill hole, mica; Total-gas date: 98.6±1.0 Ma; J=0.007597, ±0.2%; wt. 45.5 mg							
600	0.0440	0.0034	12.93	2.70	22.5	1.3	169.0 ± 8.0
700	0.1375	0.0279	4.94	1.50	53.7	11.0	66.4 ± 0.8
800	0.3475	0.0536	6.48	0.16	55.7	21.1	86.7 ± 0.5
850	0.4348	0.0399	10.91	0.05	68.9	15.7	143.6 ± 0.8
900	0.3841	0.0539	7.13	0.96	86.0	21.2	95.1 ± 0.6
950	0.1651	0.0245	6.73	14.00	82.4	9.7	90.0 ± 0.6
1,000	0.0946	0.0137	6.91	43.00	73.8	5.4	92.0 ± 3.0
1,100	0.1834	0.0257	7.14	20.00	71.4	10.1	95.0 ± 1.0
1,300	0.0871	0.0116	7.52	0.75	36.8	4.6	100.0 ± 3.0
PS111, Greens Creek exploration drill hole, fuchsite; No plateau; J=0.007608, ±0.2%; wt. 29.4 mg							
600	0.1460	0.0477	3.065	7050	37.9	1.1	42.0 + 2.0
700	0.2302	0.0535	4.304	17	84.1	1.2	58.1 + 0.4
750	0.7133	0.1460	4.887	14	91.5	3.4	65.8 + 0.4
800	1.1261	0.2019	5.577	3	71.5	4.7	75.0 + 0.2
850	2.3371	0.3827	6.106	32	95.1	8.8	81.9 + 0.1
900	5.6769	0.8508	6.672	233	98.9	19.6	89.3 + 0.1
950	3.2973	0.4688	7.034	nd	99.2	10.8	94.0 + 0.1
1,000	4.0846	0.5684	7.186	339	99.1	13.1	96.0 + 0.2
1,050	5.1016	0.6932	7.360	408	99.4	16.0	98.3 + 0.2
1,100	3.8179	0.5078	7.518	284	99.0	11.7	100.4 + 0.2
1,150	2.1332	0.2815	7.579	160	98.7	6.5	101.1 + 0.3
1,200	0.8787	0.1141	7.701	37	98.2	2.6	102.7 + 0.7
1,350	0.1821	0.0231	7.875	2	77.5	0.5	105.0 + 1.0

Table 2. $^{40}\text{Ar}/^{39}\text{Ar}$ data for samples* from Greens Creek VMS deposit, Admiralty Island, Alaska.—Continued

[T, temperature; °C, degrees Celsius; %, percent; Ma, mega-annum; mg, milligram]

T (°C)	Radiogenic $^{40}\text{Ar}^+$	K-derived $^{39}\text{Ar}^+$	$^{40}\text{Ar}_R/^{39}\text{Ar}_K$ #	$^{39}\text{Ar}_K/^{37}\text{Ar}_{Ca}$ **	Radiogenic yield (%)	$^{39}\text{Ar}_K$ (%)	Apparent age and error [®] (Ma)
92GB-05, north shore, Gambier Bay, fuchs site							
Total-gas date: 204.6±0.4 Ma; Plateau age: 210.3±0.3 Ma; J=0.007830, +0.2%; wt. 22.1 mg							
500	9.2430	0.6296	14.68	205	96.7	36.1	196.3 ± 0.3
600 ^P	13.2510	0.8376	15.82	238	97.0	48.0	210.7 ± 0.3
650 ^P	3.9534	0.2517	15.71	202	96.6	14.4	209.2 ± 0.5
700	0.1033	0.0080	12.97	1246	86.2	0.5	174.0 ± 2.0
750	0.0476	0.0034	14.15	23	89.1	0.2	190.0 ± 13.0
800	0.0401	0.0033	12.02	329	66.3	0.2	162.0 ± 11.0
1,050	0.1170	0.0105	11.13	18	60.7	0.6	151.0 ± 4.0

*Mineral concentrates were derived from rock samples that were crushed, ground, and sieved to 60–120 mesh size (250–125 micrometers). Concentrates were passed through magnetic separator and heavy liquids and then handpicked to greater than 99 percent purity. All samples then were cleaned with reagent-grade acetone, alcohol, and deionized water and air-dried in an oven at 75°C. Fifteen to 65 mg of mineral were wrapped in aluminum foil packages and encapsulated in silica vials along with neutron-fluence standards prior to irradiation. The standard for this experiment was hornblende MMhb-1 with percent K = 1.555, $^{40}\text{Ar}_R = 1.624 \times 10^{-9}$ mole/gm, and K-Ar age = 520.4 Ma (Samson and Alexander, 1987). For irradiation, an aluminum canister was loaded with six silica vials, each containing samples and standards. Standards were placed between every two samples as well as at the top and bottom of each silica vial. Samples were irradiated in one of three different irradiation packages in the TRIGA reactor at the U.S. Geological Survey in Denver, Colorado. Length of each irradiation was 30 hours. Each irradiation package was rotated at 1rpm during irradiation. All samples and standards were analyzed in the Denver Argon Laboratory of the U.S. Geological Survey using a Mass Analyser Products 215 rare-gas mass spectrometer on a Faraday-cup collector. Each sample was heated in a double-vacuum low-blank resistance furnace for 20 minutes, in a series of 7 to 16 steps, to a maximum of 1,350°C, and analyzed using the standard stepwise heating technique described by Snee (2002). MMhb-1 standards were degassed to release argon in a single step at 1,250°C. For every argon measurement, five isotopes of argon (^{40}Ar , ^{39}Ar , ^{38}Ar , ^{37}Ar , and ^{36}Ar) are measured. Detection limit at the time of these experiments was 2×10^{-17} moles of argon.

⁺ Abundance of “radiogenic ^{40}Ar ” and “K-derived ^{39}Ar ” is measured in volts and calculated to five decimal places. Voltage may be converted to moles using 1.160×10^{-12} moles argon per volt signal. “ $^{40}\text{Ar}_R/^{39}\text{Ar}_K$ ” is calculated to three decimal places. All three are rounded to significant figures using analytical precision.

“ $^{40}\text{Ar}_R/^{39}\text{Ar}_K$ ” has been corrected for mass discrimination. Mass discrimination was determined by calculating the $^{40}\text{Ar}/^{36}\text{Ar}$ ratio of aliquots of atmospheric argon pipetted from a fixed pipette on the extraction line; the ratio during these experiment was between 296.6 and 299.1, which was corrected to 295.5 to account for mass discrimination. “ $^{40}\text{Ar}_R/^{39}\text{Ar}_K$ ” was corrected for all interfering isotopes of argon including atmospheric argon. ^{37}Ar and ^{39}Ar , which are produced during irradiation, are radioactive and their abundances were corrected for radioactive decay. Abundances of interfering isotopes from potassium and calcium were calculated from reactor production ratios determined by irradiating and analyzing pure CaF_2 and K_2SO_4 ; the K_2SO_4 was degassed in a vacuum furnace prior to irradiation to release extraneous argon. Correction for chlorine-derived ^{36}Ar was determined using the method of Roddick (1983). Production ratios for this experiment were determined for ($^{40}\text{Ar}/^{39}\text{Ar}$)_K, ($^{38}\text{Ar}/^{39}\text{Ar}$)_K, ($^{37}\text{Ar}/^{39}\text{Ar}$)_K, ($^{36}\text{Ar}/^{37}\text{Ar}$)_{Ca}, ($^{39}\text{Ar}/^{37}\text{Ar}$)_{Ca}, and ($^{38}\text{Ar}/^{37}\text{Ar}$)_{Ca}; measured values are available upon request.

[®] Apparent ages and associated errors were calculated from raw analytical data then rounded using associated analytical errors. Apparent ages of each fraction include the error in J value (0.11 percent), which was calculated from the reproducibility of splits of the argon from several standards. Apparent ages were calculated using decay constants of Steiger and Jäger (1977). All apparent age errors are cited at 1 sigma. Uncertainties in the calculations for apparent age of individual fractions were calculated using equations of Dalrymple and others (1981).

** To calculate apparent K/Ca ratios, divide the “ $^{39}\text{Ar}_K/^{37}\text{Ar}_{Ca}$ ” by 2. The accuracy of apparent K/Ca ratios is dependent upon fast to thermal neutron ratios in the particular reactor. In the U.S. Geological Survey TRIGA reactor the correction factor has not been determined since Dalrymple and others (1981). Because reactor fuel in the USGS TRIGA has been changed since 1981, this ratio must be viewed as approximate but is internally consistent for each sample and reveals within-sample variability.

^P Fraction included in plateau date. Plateaus determined according to the method of Fleck and others (1977).

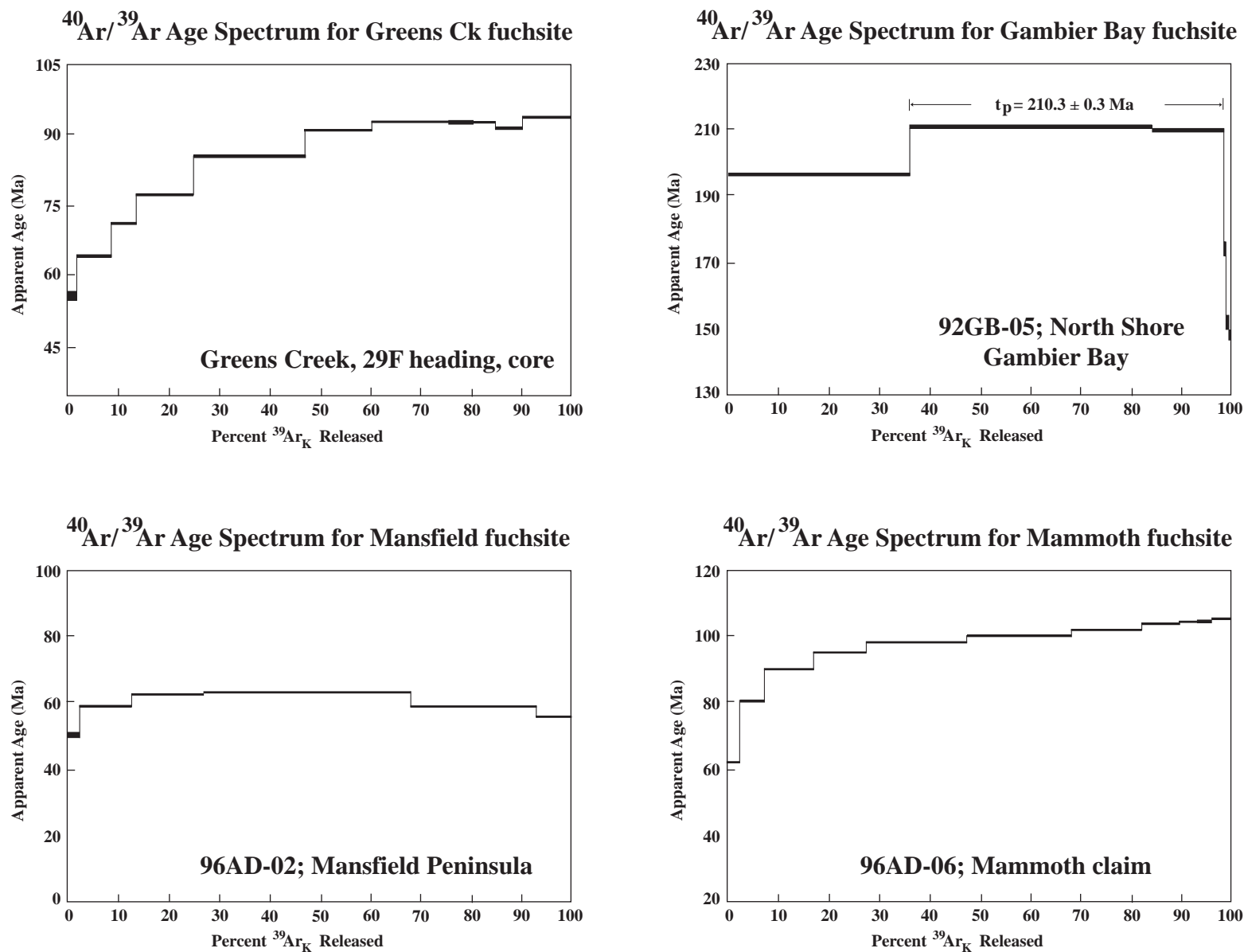


Figure 9. $^{40}\text{Ar}/^{39}\text{Ar}$ step-release spectra for four samples: one from the Greens Creek mine, two from other locations on Admiralty Island, and one fuchsite, 92-GB-05, from altered ultramafic rocks on the north shore of Gambier Bay showing a two-step $^{40}\text{Ar}/^{39}\text{Ar}$ plateau date of 210.3 ± 0.3 Ma (1σ).

mineral domains represented in the sample analyzed. They thus provide information on the minimum time period within which the minerals were reset. The actual age of the alteration mineral is therefore older than the oldest step indicated by each spectra. The five samples from the mine and the sample from Bruin Knob (chap. 4) indicate that complete resetting of argon in the alteration assemblage had occurred prior to about 105–95 Ma. The Mansfield Peninsula sample is interesting in that it appears to indicate a plateau age of 60.8 Ma (fig. 9), consistent with alteration of the ultramafic body during the transition from oblique convergence to margin-parallel motion of the Alexander terrane during the Paleocene.

A ninth sample, reported in Taylor and others (1995a), provides an important age constraint on the Greens Creek hydrothermal system. On the southeastern side of Admiralty Island, on the north shore of Gambier Bay, several mineral occurrences are hosted in Upper Triassic rocks that bear a strong resemblance to those at Greens Creek (Taylor and others, 1992). These occurrences are associated with bodies of altered ultramafic rocks identical to the rocks at Greens Creek. On the north shore they consist of several horizons of graphitic/pyritic sediments, tuffs, and mafic volcanics of the Hyd Group that are 3 to 60 meters wide, conformable, and contain pervasively altered quartz-carbonate-fuchsite. Characteristics that link them to the altered ultramafic rocks near the mine include a similar mineralogy of serpentine, talc, barite, traces of magnesium-chromite, siegenite, pyrite, chalcopyrite, sphalerite, and tetrahedrite and a trace-element geochemical signature that is dominated by As, Cr, Co, Hg, Ni, and Sb. We interpret these altered ultramafics as part of a series of similar occurrences that occur in a linear belt from Gambier Bay to the Mansfield Peninsula that are associated with the Greens Creek ore-forming event.

Geochronologic data from a fuchsite separate from the thickest of these alteration zones yields a two-step $^{40}\text{Ar}/^{39}\text{Ar}$ plateau date of 210.3 ± 0.3 Ma (1σ ; fig. 10) and a total gas age of 204.6 ± 0.4 Ma. The lack of evidence of thermal resetting of this relatively disordered mica ($2M_1$ structure) implies that this portion of the belt, in contrast to the seven analyses from the northern end of the island, has not undergone subsequent thermal events hotter than lower greenschist facies metamorphism since the Late Triassic.

U-Th-Pb, Rb-Sr, and Sm-Nd Ages on Host-Rock Lithologies

Whole-Rock Compared to Mineral (Internal) Isochron Ages

Because all attempts to separate uranium-bearing geochronometers (for example, zircon, baddeleyite, sphene, monazite) from several variably altered gabbros, diorites, and serpentinites in the immediate footwall were unsuccessful, the following age information was extracted from the U-Th-Pb, Sm-Nd, and Rb-Sr isotopic data from host-rock samples used for tracer studies (chap. 12). Although some of these ages can be considered accurate as well as precise,

none are “internal” isochrons; that is, isochrons defined by the isotopic systematics of individual mineral separates (for example, plagioclase, pyroxene, ilmenite) from the same sample (for example, gabbro), as it is highly probable that all were formed from exactly the same melt with exactly the same initial isotopic composition, a criterion necessary to yield a valid isochron age. However, several studies showed that the isotopic systematics in minerals are sometimes disturbed during subsequent alteration and (or) metamorphism, whereas whole-rock systematics often are preserved even under adverse conditions (for example, Fairbairn and others, 1961; Lanphere and others, 1964; Wetherill and others, 1968; Taylor and others, 1980; Moorbath and Taylor, 1981; Whitehouse, 1988; Barovich and Patchett, 1988).

Specific examples of both successful and unsuccessful whole-rock isochron ages from the literature should be a warning that this method of determining ages is not always reliable. Most whole-rock isochron ages that fail, do so because the isotopic composition of the source of the magma(s) is changing slightly over the geologically short duration of magma ascent and emplacement (less than 1 Ma), such that the data yield a mixing line of at least two initial isotopic compositions for the sample suite. In addition, problems in the isotopic systematics can occur during alteration and (or) metamorphism, as this sample suite has undergone (table 3), because of the instability of the elements of either the parent or daughter isotope.

Nonetheless, this is an important exercise because isochrons, if they exist, can help us to evaluate the stability of the isotopic systems and the reliability of their calculated initial values that have important implications on petro-tectonic origins for these rocks (chap. 12).

Analytical Methods

The analytical techniques used for the simultaneous, single dissolution of U-Th-Pb, Rb-Sr, and Sm-Nd analysis on whole-rock and mineral separates were similar to those reported by Tatsumoto and Unruh (1976) and Premo and Tatsumoto (1991, 1992), except that the mineral separates analyzed in this study were washed once with ethanol and ultrapure distilled water and then leached once with 1N hydrochloric acid for 10 minutes in an ultrasonic bath and finally rinsed with ultrapure water.

The whole rocks and separates were dissolved in 7-mL PFA Teflon vials with ultrapure concentrated hydrofluoric and nitric acids and then spiked with a dilute mixed tracer of ^{205}Pb - ^{233}U - ^{236}U - ^{230}Th as well as dilute mixed tracers of ^{84}Sr - ^{87}Rb and ^{150}Nd - ^{149}Sm . Reheating was conducted to achieve isotopic equilibration. Lead was extracted from the dissolved powders using AG 1-X8 anion exchange resin in a dilute hydrobromic acid medium, then loaded in phosphoric acid onto single rhenium filaments, and isotopic ratios measured using a multisample, single-collector, VG Isomass 54R mass spectrometer. Lead isotopic ratios were corrected for a mass fractionation of 0.08 ± 0.03 percent per atomic mass unit

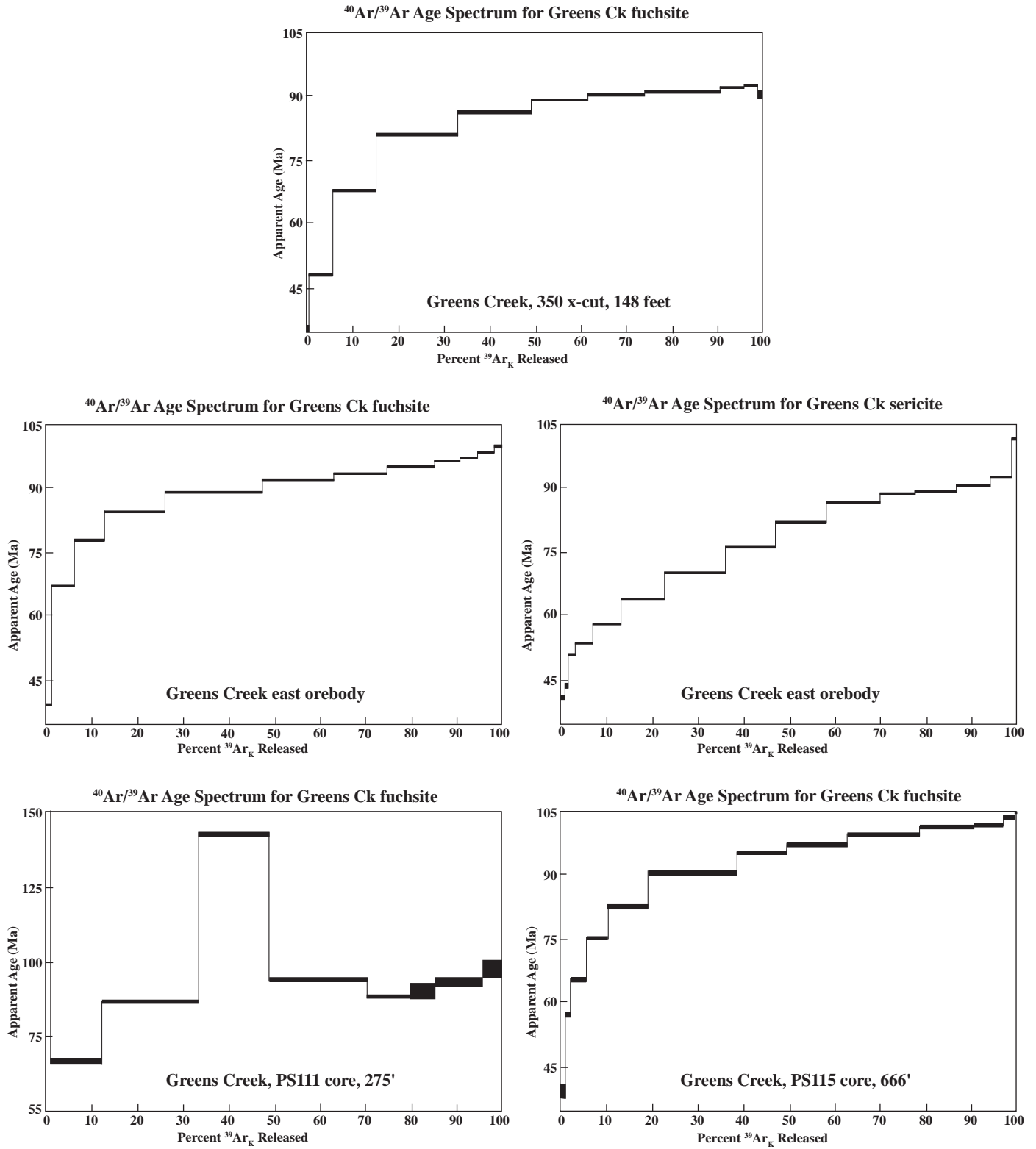


Figure 10. $^{40}\text{Ar}/^{39}\text{Ar}$ spectra for Greens Creek fuchsite and sericite — spectra that indicate complete resetting of argon in the alteration assemblage prior to 105 – 95 Ma.

Table 3. Descriptions and locations for host rock and adjacent samples of the Greens Creek VMS deposit.

Sample/ fraction	Rock type	Sample mode	Sample location	Degree of alteration/ grade of metamorphism	Sample notes, descriptions
<i>Mafic rocks</i>					
<i>Gambier Bay basalts</i>					
92-GB-22	massive basalt	WR powder	Gambier Bay, Admiralty Island	relatively unaltered	Upper Triassic Hyd Group basalt
92-GB-24	metabasalt	WR powder	Gambier Bay, Admiralty Island	greenschist facies, chloritized	Gambier Bay Formation
92-GB-42	massive basalt WR	WR powder	Gambier Bay, Admiralty Island	relatively unaltered	Upper Triassic Hyd Group basalt
92-GB-55	metabasalt	WR powder	Gambier Bay, Admiralty Island	greenschist facies, chloritized	Gambier Bay Formation
92-GB-59	massive basalt WR	WR powder	Gambier Bay, Admiralty Island	relatively unaltered	Upper Triassic Hyd Group basalt
92-GB-80	massive basalt WR	WR powder	Gambier Bay, Admiralty Island	relatively unaltered	Upper Triassic Hyd Group basalt
<i>basalt</i>					
97-LG-17	chlorite-epidote basalt	WR powder	Gallagher Ridge, middle of east GR	highly altered, chlorite- epidote- biotite-carbonate-quartz-feldspar	prominent chalky basalt or gabbro outcrop
<i>serpentinite</i>					
97-LG-19	serpentinite	WR powder	Gallagher Ridge, middle of east GR	highly altered, serpentinitized	
97-LG-20	serpentinite	WR powder	Gallagher Ridge, middle of east GR	highly altered, serpentinitized	
97-LG-32	serpentinite	WR powder	Mariposite Ridge-Mammoth Claim area	altered, relict plag & olivine	
96-GC1136-53	serpentinite	WR powder	Footwall, from southwest orebody	altered, relict plag & oliv + carb	spatially associated with ore
96-GC1136-59	serpentinite	WR powder	Footwall, from southwest orebody	altered, relict plag & oliv + carb	known to be older than 210 Ma
97-ADM-59	serpentinite	WR powder	Gambier Bay, Admiralty Island	highly altered, serpentinitized biotite-carbonate-quartz-feldspar	
<i>gabbro</i>					
97-LG-45	altered gabbro or basalt?	WR powder	Zinc Creek area, north side of hill, west of saddle	massive, highly-altered + carbonate	relict gabbroic textures
97-LG-69	gabbro	WR powder	Gallagher Ridge, immediately to the east side of the lake	altered, hornblde, sericite, albite	hornblende-bearing gabbro
97-LG-70	microgabbro	WR powder	Gallagher Cirque, at base of cliff	altered, hornblde, sericite, albite	pyroxene-hornblende-plagioclase micro- gabbro
97-LG-71 PL	gabbro, plagioclase	mineral sep	Gallagher Cirque, under the face of the cliff	highly altered - sericitic to albitic	
97-LG-71	gabbro	WR powder	Gallagher Cirque, under the face of the cliff	altered, hornblde, sericite, albite	coarse-grained
97-LG-82	hornblende gabbro	WR powder	East Little Sore grid, gabbro cliff	altered, hornblde, sericite, albite	
Gst, NW1/4, Sec 6	altered gabbro or basalt?	WR powder	Mariposite Ridge	altered, hornblde, sericite, albite	from Norm Duke's layered gabbros
<i>other mafic rocks</i>					
96-ADM-01	massive basalt	WR powder	Mansfield Peninsula, Admiralty Island	altered basalt grdmass + carb + qtz	
96-ADM-12	porph. microgabbro	WR powder	Staunch Point, Admiralty Island	highly-altered, ser-chlor-qtz-serpent	
96-AD-58	cemented mafic volcanic	WR powder	North Gambier Bay, Admiralty Island	altered basalt grdmass + carb + qtz + hornblende	
<i>Phyllites</i>					
GC-PF-09	sericitic phyllite	WR powder	Portal Face, footwall	sericite + chlorite + qtz + carb	
GC-PF-18	chlorite-carbonate phyl	WR powder	Portal Face, footwall	sericite + chlorite + qtz + carb	
GC-462-02	sericitic phyllite	WR powder	Footwall, from east ore	sericitic	greenschist of mafic volcanic origin
GC-462-07	sericitic, chloritic	WR powder	Footwall, from east ore	chloritic	
GC-1103-16	sericitic phyllite	WR powder	Footwall, from southwest orebody	sericitic	
GC-1637-44	sericitic phyllite	WR powder	Footwall, from deepest hole sampled to date	unaltered (?)	
<i>Argillites</i>					
A-Rd-03	argillite	WR powder	from 3.66 mi on the A-road	low grade alteration	thought to be Hyd argillite
B-Rd-04	argillite	WR powder	from 3.3 mi on the B-road	low grade alteration	thought to be Hyd argillite
97-LG-78	siliceous argillite	WR powder	from the top of Big Sore Ridge	deformed laminae, siliceous	thought to be Cannery argillite
97-LG-75	graphitic argillite	WR powder	from north-facing slope of Gallagher Ridge, s. of Big Sore	deformed laminae, siliceous (?)	thought to be Hyd argillite
96-GC1136-05	massive	WR powder	Hanging wall, from lower southwest orebody	sericite + feldspar + qtz + carb	known to be mine (Hyd) argillite
PP-204-01	argillite	WR powder	Hanging wall, from level 170, lower southwest orebody	undetermined	known to be mine (Hyd) argillite
97-LG-66	slaty argillite	WR powder	from west side of Gallagher cirque	deformed, siliceous-micaceous clay	thought to be Hyd argillite
97-ADM-29	massive	WR powder	from east Mariposite Ridge	undeformed, siliceous clay + carb	thought to be Cannery argillite
NAD-T4-2	argillite	WR powder	from Cliff Creek cirque	finely laminated, undeformed, siliceous	known to be mine (Hyd) argillite
97-ADM-34	massive	WR powder	from eastern end of east Mariposite Ridge	undeformed, siliceous clay + carb	thought to be Cannery argillite
<i>Crosscutting dikes</i>					
97-LG-64	diorite? dike	WR powder	Gallagher Ridge, moving ~100 m east of LG-63	hornblde-plag (altered), relic pyrox	one of the best preserved samples,
GC-1701-01	diabase dike	WR powder	Greens Creek mine, at 645 ft	sericite-fldspar + chlorite + qtz + carb	
GC-1704-01	diabase dike	WR powder	Greens Creek mine, at 1,335 ft	amphibole-altered plag + carb + pyrox	with LG-64, one of the best preserved samples
<i>Pyrola mine</i>					
PY-5-09	qtz-sericite-schist	WR powder	Pyrola mine site, southern Admiralty Island	highly-altered, chloritic,	

(amu) and a laboratory blank varying between 107 and 242 picograms (pg) (average = 165 pg) total lead with an average measured composition of $^{206}\text{Pb}/^{204}\text{Pb} = 18.681 \pm 0.064$, $^{207}\text{Pb}/^{204}\text{Pb} = 15.432 \pm 0.033$, and $^{208}\text{Pb}/^{204}\text{Pb} = 37.72 \pm 0.12$ (table 4 footnotes). Uranium and thorium were extracted using AG 1–X8 anion exchange resin in a 7N nitric acid medium and residues were loaded onto rhenium filaments using dilute nitric acid. Uranium and thorium ratios were measured in the triple filament mode using the tandem mass spectrometer and were corrected for a mass fractionation of about 0.20 ± 0.03 percent per amu and laboratory blanks ranging between 2 and 15 (average 9) and 7 and 50 (average 25) pg, respectively. Uranium-thorium-lead (U-Th-Pb) isotopic ratios were measured using a fully automated (Ludwig, 1993), multisample, single-collector, VG Isomass 54R mass spectrometer, and corrected using the algorithms and programming of Ludwig (1980, 1985).

The effluent from the U-Th-Pb chemistry was then passed through a large (30 mL resin-volume) column with AG 50W–X8 cation exchange resin, separating Rb, Sr, and rare-earth elements (REE). Samarium was separated from neodymium using AG50W–X8 cation exchange resin and the *a*-isobutyric method of Lugmair and others (1975), and then both were loaded with very dilute phosphoric acid onto tantalum filaments in either the single or triple filament mode and run on the fully automated, multisample, VG Isomass 54R mass spectrometer. Total strontium blanks ranged between 0.03 and 0.3 nanogram (ng), and total neodymium blanks ranged between 0.03 and 0.1 ng. Uncertainties on isotopic ratios are given in tables 4 through 6 and are reported at the 2σ level. See footnotes of the analytical tables for other correction information.

Results

Attempts at producing internal isochron ages using the U-Pb, Rb-Sr, and Sm-Nd isotopic data from whole-rock and mineral separates from several of the least-altered basalts, serpentinites, and metagabbros were unsuccessful, probably due to the advanced state of alteration in nearly every sample (table 3). Therefore, mostly whole-rock U-Pb, Rb-Sr, and Sm-Nd isotopic data are used here to evaluate possible isochron ages for specific groups of host-rock lithologies. Age determinations and diagrams were made using the programming of Ludwig (1998). Surface sampling sites are shown in figure 3.

Metabasalts and Phyllites

Uranium-lead isotopic data for whole-rock samples of metabasalts from Gambier Bay and Greens Creek and phyllites from in and around the mine are relatively scattered and do not form well-defined arrays. These metabasaltic rocks are not the same age and therefore not cogenetic. The phyllites are highly altered metabasalts from the second section of the

Greens Creek stratigraphy known to be older than Carnian (fig. 5), whereas several of the metabasalts at Gambier Bay are samples from the upper horizons of the Hyd Group that caps the stratigraphy and are younger than Norian.

An apparent U-Pb isochron age can be calculated for the best-preserved or least-altered metabasaltic samples from the Hyd Group (97–GB-22, 42, 59, and 80; table 3), and data from three out of four of these whole-rock samples form an array with an isochron age of 218 ± 16 Ma and an initial lead value of 18.515 ± 0.04 (dashed line; fig. 11). This age is interpreted to approximate the timing for extrusion of the Hyd Group basalts at Gambier Bay.

Hyd Group metabasalt 92–GB-59 does not conform to the Hyd Group isochron and appears to contain excess radiogenic lead as is exhibited by both of the chloritized metabasalts 92–GB-24 and 92–GB-55 of the Gambier Bay Formation. Highly altered metabasalt from Gallagher Ridge (97–LG-17) and several mine phyllites (GC–PF-18, GC-1103-16, and GC-1637-44) plot in a cluster near the initial $^{206}\text{Pb}/^{204}\text{Pb}$ value of 18.640 ± 0.032 , which is very similar to the Greens Creek ore lead composition of about 18.64 (chap. 10). The cluster also contains data from a sample of sericitic phyllite (PY-5-09) from Pyrola (fig. 2), another orebody to the south of Greens Creek (chap. 2). These data suggest that the whole-rock, U-Pb isotopic systematics of the highly altered, chloritized metabasalts and phyllites were disturbed and reset, and plot coincident with a 215-Ma reference line (fig. 11).

The Sm-Nd isotopic data (table 6) for metabasalts and associated phyllites are mostly scattered and do not form obvious linear arrays or yield any precise isochron ages. However, several of the Hyd Group metabasalts — the same group used to form a U-Pb isochron above (92–GB-22, 42, and 80) — yielded a poorly defined, apparent Sm-Nd isochron age of 215 ± 95 Ma (dashed line, fig. 12) with an initial ϵ_{Nd} value of +7.4 at 215 Ma. One of the chloritized metabasalts from the Gambier Bay Formation (92–GB-24) and two analyses from phyllite GC–PF-18 yielded data that appear to be coincident with this apparent isochron. The other Hyd Group metabasalt 92–GB-59 yielded a more enriched (lower) Nd isotopic signature (fig. 12), indicating either derivation from a more enriched source, contamination by older crust during ascent and extrusion, or open-system behavior due to exchange of REE with more enriched rocks during subsequent metamorphism and(or) alteration. The other chloritized metabasalt from the Gambier Bay Formation, 92–GB-55, plots very near 97–LG-17, the highly altered metabasalt from Gallagher Ridge, and both data plot near a 215-Ma reference line (dashed, fig. 12) that includes Hyd Group metabasalt 92–GB-59 and Pyrola phyllite PY-5-09. This same association of samples was observed in the U-Pb isotopic data (fig. 11).

Samarium-neodymium analyses from footwall phyllites do not form an array but a field of enriched (lower) Nd isotopic signatures (fig. 12), again indicating either derivation from more enriched sources, contamination by older crust during ascent and extrusion, or open-system behavior due to exchange of REE with more enriched rocks during subsequent metamorphism and(or) alteration.

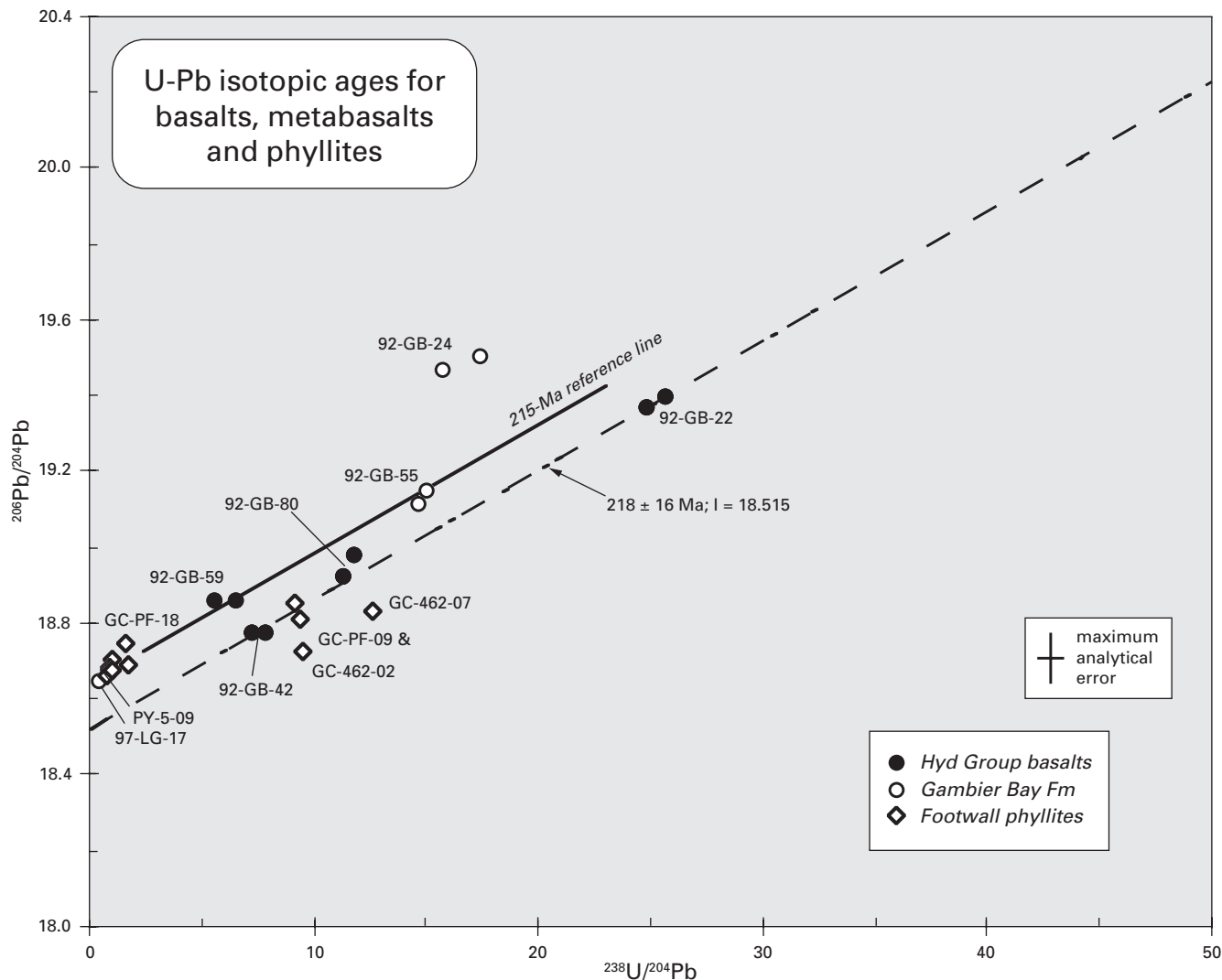


Figure 11. Uranium-lead isotopic correlation diagram of data from metabasalt rocks (Hyd Group and Gambier Bay Formation) and footwall phyllites (altered mafic volcanic rock?) of the Green Creek area. Three whole-rock samples of the Hyd Group metabasalts define a U-Pb isochron age of 218 ± 16 Ma (dashed line). Several other metabasalts that are highly altered and some of the phyllites form a possible isochron (215-My reference line) yielding an initial $^{206}\text{Pb}/^{204}\text{Pb}$ value of 18.640 ± 0.032 , exactly that of the Greens Creek ore.

The same samples were analyzed for their Rb-Sr whole-rock isotopic systematics, and these results appear to be even less stable and more varied than results from the other two isotopic systems. The least-altered Hyd Group metabasalts (92-GB-22 and -80; and 92-GB-42 and -59) appear to form arrays that suggest apparent Rb-Sr ages of about 180 Ma that might be interpreted as disturbed or reset. One Gambier Bay Formation metabasalt, 92-GB-24, has a slightly higher initial $^{87}\text{Sr}/^{86}\text{Sr}$ value of about 0.7052, whereas the other, 92-GB-55, has a lower value and plots along with Hyd Group metabasalts 92-GB-59 and GB-42 that indicate an initial Sr value of about 0.70409 (fig. 13), the lowest observed from this suite of rocks.

Rubidium-strontium isotopic data from footwall phyllites vary widely; some exhibiting elevated initial Sr values

between about 0.706 and 0.707 at 215 Ma, perhaps indicating partial resetting of the Rb-Sr isotopic systematics during Cretaceous metamorphism (for example, Rubin and others, 1990; chap. 12). However, an apparent Rb-Sr isochron age of 182 ± 29 Ma (dashed line, fig. 13) can be calculated using all the data from the phyllites and highly altered metabasalts, implying that the Rb-Sr isotopic systematics were reset in these rocks at about that time.

Metagabbros

Most of the metagabbro data of Greens Creek form an imprecise, apparent U-Pb whole-rock isochron indicating an age of 206 ± 35 Ma with initial $^{206}\text{Pb}/^{204}\text{Pb}$ value of about 18.61 (fig. 14), which excludes analyses from three samples.

Table 4. Uranium-thorium-lead analytical data for host-rock samples from the Greens Creek VMS deposit.

[wgt, weight; g, gram; ppm, parts per million; U, uranium; Th, thorium; Pb, lead]

Sample/fraction	Sample wgt (g)	U (ppm)	Th (ppm)	Pb (ppm)	²⁰⁶ Pb/ ²⁰⁴ Pb ^a	% err 206/204	²⁰⁷ Pb/ ²⁰⁴ Pb ^a	% err 207/204	²⁰⁸ Pb/ ²⁰⁴ Pb ^a	% err 208/204	²³⁸ U/ ²⁰⁴ Pb ^a	% err 238/204	²³² Th/ ²⁰⁴ Pb ^a	% err 232/204
<i>Mafic rocks</i>														
<i>Gambier Bay basalts</i>														
92-GB-22	0.063	0.693	0.401	1.79	19.369	0.076	15.574	0.103	38.339	0.131	24.903	0.173	14.88	0.336
92-GB-22-2	0.176	0.676	0.384	1.69	19.397	0.171	15.592	0.191	38.407	0.202	25.764	0.457	15.11	0.474
92-GB-24	0.052	0.051	0.111	0.19	19.499	0.098	15.622	0.121	38.821	0.150	17.485	0.435	39.13	0.514
92-GB-24-2	0.147	0.042	0.101	0.17	19.464	0.172	15.547	0.251	38.633	0.209	15.783	0.664	39.52	0.292
92-GB-42	0.058	1.030	2.450	8.90	18.772	0.066	15.530	0.095	38.119	0.132	7.348	0.311	18.05	0.200
92-GB-42-2	0.110	1.000	2.330	8.03	18.769	0.064	15.531	0.093	38.121	0.123	7.924	0.232	18.98	0.177
92-GB-55	0.090	0.545	1.560	2.31	19.150	0.066	15.566	0.094	38.500	0.123	15.128	0.202	44.82	0.553
92-GB-55-2	0.149	0.515	failed	2.23	19.114	0.062	15.547	0.092			14.765	0.115	failed	
92-GB-59	0.067	0.231	0.608	2.60	18.856	0.107	15.547	0.130	38.262	0.157	5.659	0.745	15.41	0.264
92-GB-59-2	0.226	0.221	0.557	2.12	18.859	0.065	15.543	0.094	38.253	0.123	6.619	0.109	17.26	0.138
92-GB-80	0.072	0.334	1.090	1.87	18.919	0.074	15.527	0.101	38.401	0.128	11.410	0.537	38.58	0.631
92-GB-80-2	0.131	0.322	1.040	1.74	18.976	0.415	15.581	0.421	38.571	0.429	11.839	0.802	39.45	0.804
<i>basalt</i>														
97-LG-17	0.079	0.067	0.292	5.64	18.598	0.095	15.545	0.116	38.109	0.141	0.746	1.370	3.39	0.914
97-LG-17-2	0.123	0.064	0.244	9.46	18.644	0.152	15.602	0.167	38.285	0.185	0.431	0.669	1.69	0.715
<i>serpentinite</i>														
97-LG-19-2	0.140	0.011	0.032	0.51	18.450	0.695	15.376	0.738	37.829	0.749	1.361	0.984	4.16	1.620
97-LG-20-2	0.155	0.011	0.031	0.54	18.610	1.610	15.568	1.630	38.324	1.620	1.298	2.770	3.82	3.800
97-LG-32	0.080	0.034	0.190	0.65	18.626	0.479	15.596	0.542	38.643	0.535	3.336	1.110	19.29	12.100
96-GC 1136-53	0.104	0.038	0.045	75.48	18.656	0.061	15.603	0.091	38.402	0.121	0.032	1.610	0.04	0.895
96-GC 1136-59	0.176	0.061	0.069	26.48	18.646	0.061	15.589	0.090	38.354	0.120	0.147	0.924	0.17	0.322
97-ADM-59	0.153	0.110	0.949	4.74	18.929	1.200	15.888	1.230	39.057	1.270	1.497	4.190	0.01	6.780
<i>gabbro</i>														
97-LG-45	0.099	0.517	0.602	2.53	18.962	0.062	15.584	0.092	38.332	0.121	13.029	2.370	15.67	0.279
97-LG-45-2	0.186	0.484	0.579	3.03	18.983	0.134	15.638	0.154	38.561	0.171	10.249	0.885	12.67	0.912
97-LG-69-2	0.232	0.288	0.854	0.42	20.127	0.366	15.596	0.384	39.478	0.393	45.468	0.678	139.40	0.684
97-LG-70	0.083	0.081	0.246	0.24	19.312	0.183	15.613	0.196	38.808	0.214	21.580	0.359	67.93	0.354
97-LG-71	0.337	0.308	0.917	0.50	19.634	0.153	15.629	0.168	39.117	0.186	39.900	0.556	122.60	0.692
97-LG-82	0.090	0.424	1.430	0.68	20.021	0.068	15.640	0.096	39.644	0.125	41.048	0.360	143.30	0.239
97-LG-82-2	0.163	0.467	1.430	0.62	20.119	0.070	15.658	0.099	39.731	0.127	49.460	0.215	156.80	0.201
Gst, NW1/4, Sec 6	0.100	0.256	failed	1.03	19.911	0.326	15.705	0.336	38.686	0.343	16.236	0.536	failed	
<i>Admiralty Island</i>														
96-ADM-01	0.104	0.603	0.519	2.14	18.872	0.069	15.611	0.097	38.410	0.125	17.980	0.946	15.97	6.510
96-ADM-01-2	0.156	0.675	0.501	5.30	18.847	0.062	15.610	0.091	38.436	0.121	8.124	0.172	6.24	0.189
96-ADM-12	0.061	0.830	1.990	9.47	18.901	0.089	15.588	0.113	37.773	0.137	5.551	0.286	13.75	0.179
96-ADM-12-2	0.200	0.840	2.010	11.80	18.795	0.238	15.528	0.253	38.301	0.262	4.526	0.468	11.16	0.537
96-AD-58	0.166	0.240	0.737	2.18	18.872	0.073	15.558	0.099	38.377	0.127	7.011	0.283	22.29	0.690

Table 4. Uranium-thorium-lead analytical data for host-rock samples from the Greens Creek VMS deposit.—Continued

[wgt, weight; g, gram; ppm, parts per million; U, uranium; Th, thorium; Pb, lead]

<i>Phyllites</i>														
GC-PF-09	0.124	0.632	1.280	4.37	18.851	0.078	15.597	0.143	38.502	0.247	9.249	0.475	19.39	0.433
GC-PF-18	0.108	0.097	0.402	5.81	18.698	0.062	15.580	0.092	38.088	0.125	1.054	0.886	4.54	0.601
GC-PF-18-2	0.108	0.150	0.485	5.91	18.742	0.069	15.631	0.097	38.513	0.125	1.626	0.203	5.42	0.170
GC-PF-18-3	0.184	0.191	0.550	6.96	18.688	0.062	15.568	0.091	38.285	0.121	1.741	0.348	5.19	0.348
GC-462-02	0.156	1.270	1.580	8.60	18.808	0.117	15.599	0.141	38.309	0.161	9.609	0.646	12.30	0.587
GC-462-02-2	0.156	1.080	9.290	11.90	18.633	0.090	15.464	0.119	37.890	0.139	5.744	3.030	50.89	44.000
GC-462-07	0.165	1.870	2.360	9.42	18.830	0.060	15.579	0.090	38.342	0.120	12.651	0.855	16.47	1.410
GC-1103-16	0.142	0.881	2.370	59.80	18.677	0.061	15.604	0.091	38.420	0.122	0.943	0.399	2.60	0.295
GC-1637-44	0.189	1.350	2.060	97.82	18.657	0.073	15.587	0.101	38.361	0.130	0.881	1.360	1.38	6.340
<i>Argillites</i>														
A-Rd-03	0.073	1.770	4.290	7.93	19.559	0.061	15.677	0.093	38.895	0.124	14.483	0.330	36.30	0.317
B-Rd-04	0.076	2.880	4.110	7.34	19.731	0.077	15.656	0.103	38.678	0.131	25.406	0.249	37.54	0.419
97-LG-78	0.057	1.430	3.010	3.21	19.489	0.071	15.598	0.098	38.667	0.126	28.776	0.446	62.51	0.198
97-LG-75	0.095	1.800	1.000	5.62	19.219	0.062	15.616	0.092	38.371	0.122	20.510	1.450	11.80	0.150
96-GC 1136-05	0.074	1.480	0.244	9.82	18.865	0.062	15.645	0.094	38.487	0.127	9.609	0.218	1.64	0.216
PP-204-01-1	0.147	7.400	1.220	14.50	19.962	0.190	15.668	0.202	38.486	0.221	33.093	1.430	5.62	1.430
97-LG-66	0.191	1.590	0.684	11.60	19.215	0.076	15.672	0.103	38.570	0.131	8.763	0.162	3.90	0.388
97-ADM-29	0.059	2.900	2.080	5.52	19.824	0.092	15.633	0.117	38.443	0.141	33.949	0.309	25.14	0.171
NAD-T4-2	0.236	0.720	1.980	1.70	19.396	0.152	15.627	0.168	38.816	0.185	27.464	0.296	77.92	0.264
97ADM-34	0.201	2.220	4.130	18.85	18.973	0.060	15.563	0.090	38.282	0.120	7.501	0.131	14.46	0.308
<i>Crosscutting dikes</i>														
97-LG-64-2	0.16818	1.220	2.270	4.22	18.923	0.084	15.608	0.110	38.478	0.139	18.479	0.493	35.56	0.481
GC-1701-01	0.084	0.873	2.010	312.80	18.659	0.072	15.612	0.100	38.432	0.133	0.178	7.100	0.42	7.100
GC-1701-01-2	0.136	0.901	2.080	640.40	18.759	0.083	15.745	0.113	38.897	0.154	0.091	3.300	0.22	3.300
GC-1704-01	0.256	0.840	1.650	6.55	18.721	0.072	15.563	0.100	38.274	0.130	8.153	0.469	16.53	0.425
GC-1704-01-2	0.210	0.835	1.620	5.09	18.591	0.134	15.450	0.155	37.991	0.186	10.353	1.150	20.72	1.260
<i>Pyrola mine</i>														
PY-5-09	0.193	2.170	2.525	130.70	18.673	0.061	15.567	0.091	38.183	0.121	1.053	0.721	1.27	0.730

^a – corrected for Pb mass fractionation (0.08 ± 0.03 % per a.m.u.) and blank Pb (variable amounts between 107 and 242 pg total Pb) with average composition:

$$^{206}\text{Pb}/^{204}\text{Pb} = 18.681 \pm 0.064; \quad ^{207}\text{Pb}/^{204}\text{Pb} = 15.432 \pm 0.033; \quad \text{and} \quad ^{208}\text{Pb}/^{204}\text{Pb} = 37.72 \pm 0.12).$$

failed – Some mass spectrometric runs failed and were not reattempted.

Table 5. Initial lead compositions for host-rock samples from the Greens Creek VMS deposit.

[Ma, mega-annum; Pb, lead; U, uranium; Th, thorium; pg, picograms; a.m.u., atomic mass unit]

Sample/fraction	Initial Pb values at 215 Ma		Initial Pb values at 185 Ma		Initial Pb values at 260 Ma		Initial Pb values at 90 Ma		Initial Pb values at 50 Ma	
	$\frac{^{206}\text{Pb}}{^{204}\text{Pb}^a}$	$\frac{^{207}\text{Pb}}{^{204}\text{Pb}^a}$								
<i>Mafic rocks</i>										
<i>Gambier Bay basalts</i>										
92-GB-22	18.524	15.531	18.644	15.538	18.344	15.521	N/A		N/A	
92-GB-22-2	18.523	15.548	18.647	15.555	18.337	15.537				
92-GB-24	18.906	15.592	18.990	15.597	18.779	15.585				
92-GB-24-2	18.929	15.520	19.004	15.524	18.814	15.514				
92-GB-42	18.523	15.517	18.558	15.519	18.470	15.514				
92-GB-42-2	18.500	15.517	18.538	15.520	18.443	15.514				
92-GB-55	18.637	15.540	18.710	15.544	18.527	15.534				
92-GB-55-2	18.613	15.522	18.684	15.526	18.506	15.516				
92-GB-59	18.664	15.537	18.691	15.539	18.623	15.535				
92-GB-59-2	18.635	15.532	18.666	15.533	18.587	15.529				
92-GB-80	18.532	15.507	18.587	15.510	18.449	15.503				
92-GB-80-2	18.574	15.561	18.631	15.564	18.489	15.556				
<i>basalt</i>										
97-LG-17	18.573	15.544	18.576	15.544	18.567	15.543	18.588	15.544	18.592	15.545
97-LG-17-2	18.629	15.601	18.631	15.601	18.626	15.601	18.638	15.602	18.641	15.602
<i>serpentinite</i>										
97-LG-19-2	18.404	15.374	18.410	15.374	18.394	15.373	18.431	15.375	18.439	15.376
97-LG-20-2	18.566	15.566	18.572	15.566	18.557	15.565	18.592	15.567	18.600	15.568
97-LG-32	18.513	15.590	18.529	15.591	18.489	15.589	18.579	15.594	18.600	15.595
96-GC 1136-53	18.655	15.603	18.655	15.603	18.655	15.603	18.656	15.603	18.656	15.603
96-GC 1136-59	18.641	15.589	18.642	15.589	18.640	15.589	18.644	15.589	18.645	15.589
97-ADM-59	18.878	15.885	18.885	15.886	18.867	15.885	18.908	15.887	18.917	15.887
<i>gabbro</i>										
97-LG-45	18.520	15.562	18.583	15.565	18.426	15.556	18.779	15.575	18.861	15.579
97-LG-45-2	18.635	15.620	18.685	15.623	18.561	15.616	18.839	15.631	18.903	15.634
97-LG-69-2	18.585	15.518	18.803	15.530	18.256	15.500	19.488	15.565	19.773	15.579
97-LG-70	18.580	15.576	18.684	15.582	18.424	15.567	19.009	15.598	19.144	15.605
97-LG-71-1	18.281	15.561	18.472	15.571	17.992	15.545	19.073	15.602	19.323	15.614
97-LG-82	18.662	15.572	18.826	15.581	18.332	15.553	19.444	15.612	19.701	15.625
97-LG-82-2	18.481	15.576	18.679	15.586	18.083	15.553	19.424	15.625	19.734	15.640
Gst, NW1/4, Sec 6	19.373	15.678	19.438	15.681	19.243	15.671	19.683	15.694	19.785	15.699
<i>Admiralty Island</i>										
96-ADM-01	18.262	15.580	18.349	15.585	18.132	15.573	18.619	15.599	18.732	15.604
96-ADM-01-2	18.571	15.596	18.610	15.598	18.513	15.593	18.733	15.605	18.784	15.607
96-ADM-12	18.713	15.579	18.739	15.580	18.672	15.576	18.823	15.584	18.858	15.586
96ADM-12-2	18.642	15.520	18.663	15.521	18.609	15.518	18.731	15.525	18.760	15.526
96-AD-58	18.634	15.546	18.668	15.548	18.583	15.543	18.773	15.553	18.817	15.555

Table 5. Initial lead compositions for host-rock samples from the Greens Creek VMS deposit.—Continued

[Ma, mega-annum; Pb, lead; U, uranium; Th, thorium; pg, picograms; a.m.u., atomic mass unit]

<i>Phyllites</i>										
GC-PF-09	18.537	15.581	18.582	15.584	18.470	15.577	18.721	15.591	18.779	15.594
GC-PF-18	18.662	15.578	18.667	15.578	18.655	15.578	18.683	15.579	18.690	15.580
GC-PF-18-2	18.687	15.628	18.695	15.629	18.675	15.628	18.719	15.630	18.729	15.630
GC-PF-18-3	18.629	15.565	18.637	15.565	18.616	15.564	18.664	15.567	18.674	15.567
GC-462-02	18.489	15.583	18.534	15.585	18.421	15.579	18.676	15.593	18.735	15.596
GC-462-02-2	18.438	15.454	18.466	15.456	18.397	15.452	18.552	15.460	18.588	15.462
GC-462-07	18.401	15.557	18.462	15.561	18.309	15.552	18.652	15.570	18.731	15.574
GC-1103-16	18.645	15.602	18.650	15.603	18.638	15.602	18.664	15.603	18.670	15.604
GC-1637-44	18.627	15.585	18.631	15.586	18.621	15.585	18.645	15.586	18.650	15.587
<i>Argillites</i>										
A-Rd-03	19.068	15.652	19.137	15.656	18.963	15.646	19.355	15.667	19.446	15.672
B-Rd-04	18.869	15.613	18.991	15.619	18.685	15.602	19.374	15.639	19.533	15.647
97-LG-78	18.533	15.573	18.671	15.580	18.324	15.561	19.104	15.603	19.265	15.587
97-LG-75	18.523	15.581	18.622	15.586	18.375	15.573	18.931	15.602	19.059	15.608
96-GC 1136-05	18.539	15.629	18.585	15.631	18.470	15.625	18.730	15.639	18.790	15.641
PP-204-01-1	18.840	15.611	18.999	15.620	18.600	15.598	19.497	15.646	19.704	15.656
97-LG-66	18.918	15.657	18.960	15.659	18.854	15.653	19.092	15.666	19.147	15.669
97-ADM-29	18.673	15.575	18.836	15.584	18.427	15.561	19.347	15.610	19.560	15.621
NAD-T4-2	18.465	15.580	18.596	15.587	18.266	15.569	19.010	15.609	19.182	15.617
97-ADM-34	18.719	15.550	18.755	15.552	18.664	15.547	18.868	15.558	18.915	15.560
<i>Crosscutting dikes</i>										
97-LG-64-2	18.296	15.576	18.385	15.581	18.162	15.569	18.663	15.596	18.779	15.601
GC-1701-01	18.653	15.612	18.654	15.612	18.652	15.612	18.657	15.612	18.658	15.612
GC-1701-01-2	18.756	15.745	18.756	15.745	18.755	15.745	18.758	15.745	18.758	15.745
GC-1701-04	18.444	15.549	18.484	15.551	18.385	15.546	18.606	15.558	18.658	15.560
GC-1701-04-2	18.240	15.432	18.290	15.435	18.165	15.428	18.445	15.443	18.510	15.446
<i>Pyrola mine</i>										
PY-5-09	18.637	15.565	18.642	15.565	18.630	15.565	18.658	15.566	18.665	15.567

^a – corrected ratios; corrected for Pb mass fractionation (0.08 ± 0.03 % per a.m.u.) and blank Pb (variable amounts between 5 and 20 pg total Pb; blank composition: $^{206}\text{Pb}/^{204}\text{Pb} = 18.8 \pm 0.6$; $^{207}\text{Pb}/^{204}\text{Pb} = 15.65 \pm 0.2$; and $^{208}\text{Pb}/^{204}\text{Pb} = 38.65 \pm 0.75$); U mass fractionation using a double U spike ($^{233}\text{U}/^{236}\text{U} = 1.02$???); and assumed Th fractionation of $\sim 0.2 \pm 0.5$ % per a.m.u. using the programming of Ludwig (1985). Uranium and thorium blanks ranged between 2-15 and 7-50 pg, respectively.

Table 6. Rb-Sr and Sm-Nd analytical data for host-rock and adjacent samples of the Greens Creek VMS deposit.

[wgt, weight; g, gram; ppm, parts per million; Rb, rubidium; Sr, strontium; Sm, samarium; Nd, neodymium]

Sample name	Sample wgt (g)	Rb * (ppm)	Sr * (ppm)	Sm * (ppm)	Nd * (ppm)	⁸⁷ Rb/ ⁸⁶ Sr †	Rb/Sr abs err	⁸⁷ Sr/ ⁸⁶ Sr †	87/86 abs err	¹⁴⁷ Sm/ ¹⁴⁴ Nd †	147/144 abs err	¹⁴³ Nd/ ¹⁴⁴ Nd †	143/144 abs err	Initial § ⁸⁷ Sr/ ⁸⁶ Sr	εNd(t)
<i>Mafic rocks</i>															
<i>Gambier Bay basalts</i>															
92-GB-22-2	0.176	4.1	233	2.7	7.3	0.050	0.000	0.705	0.000	0.223	0.001	0.513	0.000	0.705	7.31
92-GB-24-2	0.147	0.8	17.5	1.9	4.6	0.136	0.000	0.706	0.000	0.252	0.001	0.513	0.000	0.706	7.94
92-GB-42	0.058	3.6	708	4.6	19.2	0.015	0.000	0.704	0.000	0.146	0.000	0.513	0.000	0.704	7.29
92-GB-55	0.090	25.8	568	4.8	20.6	0.131	0.000	0.705	0.000	0.140	0.000	0.513	0.000	0.704	4.70
92-GB-55-2	0.149	25.0	539	4.3	18.7	0.134	0.000	0.705	0.000	0.139	0.000	0.513	0.000	0.704	4.08
92-GB-59-2	0.226	7.3	122	2.0	7.2	0.174	0.001	0.705	0.000	0.171	0.000	0.513	0.000	0.704	5.22
92-GB-80	0.072	40.9	199	4.6	17.0	0.593	0.002	0.707	0.000	0.162	0.000	0.513	0.000	0.705	7.52
92-GB-80-2	0.131	41.3	198	4.5	16.9	0.603	0.003	0.707	0.000	0.163	0.000	0.513	0.000	0.705	7.46
<i>basalt</i>															
97-LG-17	0.079	41.7	158	0.71	3.0	0.763	0.001	0.707	0.000	0.145	0.000	0.513	0.000	0.705	4.70
97-LG-17-2	0.123	41.4	189	0.75	3.1	0.632	0.002	0.707	0.000	0.145	0.000	0.513	0.000	0.705	5.34
<i>serpentinite</i>															
97-LG-19-2	0.140	0.14	15.9	0.02	0.12	0.025	0.000	0.705	0.000	0.125	0.000	0.513	0.000	0.705	1.79
97-LG-20-2	0.155	0.15	8.3	0.02	0.09	0.052	0.000	0.705	0.000	0.115	0.000	0.512	0.000	0.705	-1.63
97-LG-32-2	0.162	0.25	8.0	0.02	0.13	0.090	0.000	0.706	0.000	0.105	0.000	0.512	0.000	0.705	-12.40
96-GC-1136-53	0.104	32.8	153	0.20	0.70	0.61961	0.001	0.708	0.000	0.195	0.001	0.513	0.000	0.706555	4.15
96-GC-1136-59	0.176	44.5	68.0	0.10		1.89624	0.004	0.710066	0.000	failed				0.704268	
97ADM-59	0.153	0.32	6.8	0.017	2.66	0.137	0.003	0.708	0.000	0.173	0.001	0.513	0.000	0.707	8.35
<i>gabbro</i>															
97-LG-45	0.099	15.1	219	4.4	15.5	0.200	0.000	0.705	0.000	0.174	0.000	0.513	0.000	0.704548	6.04
97-LG-45-2	0.186	15.9	260	4.1	14.5	0.177	0.001	0.705	0.000	0.172	0.000	0.513	0.000	0.705	6.34
97-LG-69	0.109	3.53	318	1.8	6.0	0.032	0.000	0.704	0.000	0.179	0.000	0.513	0.000	0.704	6.03
97-LG-69-2	0.232	3.35	331	1.8	6.2	0.029	0.000	0.704	0.000	0.178	0.000	0.513	0.000	0.704	6.10
97-LG-70	0.083	3.46	151	1.3	3.3	0.066	0.000	0.705	0.000	0.226	0.000	0.513	0.000	0.704	5.58
97-LG-70-2	0.147	3.72	165	1.2	3.2	0.065	0.000	0.705	0.000	0.234	0.000	0.513	0.000	0.705	5.41
97-LG-71 PL-2	0.105			0.5	2.3		failed			0.136	0.000	0.513	0.000		
97-LG-71-1	0.337	23.2	160	1.9	6.8	0.419	0.053	0.705	0.000	0.171	0.000	0.513	0.000	0.704	5.70
97-LG-82	0.090	4.00	238	2.8	10.3	0.049	0.000	0.704	0.000	0.163	0.000	0.513	0.000	0.703862	6.05
97-LG-82-2	0.163	4.00	241	2.7	10.1	0.048	0.000	0.704	0.000	0.175	0.000	0.513	0.000	0.703860	5.23
Gst, NW1/4, Sec 6	0.100			3.0	10.2		failed			0.176	0.000	0.513	0.000	0.704764	6.55
Gst-2, NW1/4, Sec 6	0.10587	0.75	144	3.4	11.6	0.015	0.000	0.705	0.000	0.175	0.000	0.513	0.000	0.704699	6.85
<i>Admiralty Island mafic rocks</i>															
96-ADM-01	0.104	19.9	148	4.5	12.8	0.387	0.003	0.705	0.001	0.212	0.114	0.513	0.001	0.704	4.92
96-ADM-01-2	0.156	20.6	171	3.2	10.9	0.348	0.001	0.705	0.000	0.176	0.000	0.513	0.000	0.704	5.93
96-ADM-12	0.061	17.1	173	4.0	15.8	0.286	0.001	0.706	0.000	0.153	0.003	0.513	0.000	0.705	4.38
96-ADM-12-2	0.200	14.4	146	3.7	14.9	0.284	0.001	0.706	0.000	0.148	0.000	0.513	0.000	0.705	4.22
96AD-58	0.166	8.5	125	4.4	15.4	0.196	0.000	0.705	0.000	0.172	0.000	0.513	0.000	0.704	6.37

Table 6. Rb-Sr and Sm-Nd analytical data for host-rock and adjacent samples of the Greens Creek VMS deposit.—Continued

[wgt, weight; g, gram; ppm, parts per million; Rb, rubidium; Sr, strontium; Sm, samarium; Nd, neodymium]

<i>Phyllites</i>															
GC-PF-09	0.124	47.6	39.7	3.1	12.6	3.472	0.006	0.712	0.000	0.150	0.000	0.513	0.000	0.702	2.75
GC-PF-18-2	0.108	13.3	112	2.9	9.4	0.344	0.001	0.707	0.000019	0.185	0.000	0.513	0.000	0.706	7.34
GC-PF-18-3	0.184	13.3	106	2.7	8.3	0.364	0.000	0.707	0.000	0.193	0.000	0.513	0.000	0.706	7.16
GC-462-02	0.156	1.0	107	0.6	3.1	0.026	0.000	0.705	0.000	0.126	0.000	0.513	0.000	0.705	2.21
GC-462-02-2	0.156	n.d.	108	0.6	3.1	n.d.		0.705	0.000021	0.126	0.000	0.513	0.000		1.61
GC-462-07	0.165			4.0	18.4		failed			0.131	0.000	0.513	0.000		2.81
GC-1103-16	0.142	44.5	65.6	2.3	9.8	1.96433	.00223	0.712	0.000024	0.14357	0.000	0.512666	0.000015	0.706354	2.04
GC-1637-44	0.189	55.3	25.6	3.7	15.7	6.26289	.01838	0.722	0.000025	0.14143	0.000	0.512774	0.000014	0.702935	4.21
<i>Argillites</i>															
A-Rd-03	0.073	n.d.		3.8	18.2	n.d.		0.712	0.000	0.126	0.000	0.512	0.000		-1.15
B-Rd-04	0.076	n.d.		3.4	17.4	n.d.		0.715	0.000	0.118	0.000	0.512	0.000		-5.07
97-LG-78	0.057	n.d.		2.6	13.6	n.d.		0.737	0.000	0.118	0.000	0.513	0.000		2.58
97-LG-75	0.095	1.0	1.8	3.1	18.1	1.607	0.002	0.710	0.000	0.103	0.000	0.512	0.000	0.704797	-1.45
96-GC 1136-05	0.074	7.1	134	0.7	3.2	0.153	0.000	0.708	0.000	0.129	0.000	0.513	0.000	0.707062	0.21
PP-204-01-1	0.147	27.3	130	2.5	11.5	0.606	0.001	0.708	0.000	0.132	0.000	0.513	0.000	0.706619	1.62
97-LG-66	0.191	26.1	1.3	2.2	12.4	59.091	0.058	0.784	0.000	0.108	0.000	0.512	0.000	0.602977	-2.47
97-ADM-29	0.059	31.7	105	2.7	11.1	0.877	0.001	0.707	0.000	0.148	0.000	0.513	0.000	0.704735	2.28
NAD-T4-2	0.236	34.0	13.9	2.1	9.2	7.087	0.011	0.716	0.000	0.138	0.000	0.513	0.000	0.694	2.19
97-ADM-34	0.201	47.1	63.7	1.9	8.1	2.138	0.004	0.709	0.000	0.142	0.000	0.513	0.000	0.702071	1.61
<i>Crosscutting dikes</i>															
97-LG-64-2	0.16818	16.1	678	4.5	21.2	0.06850	0.000	0.703466	0.000022	0.129	0.000	0.513	0.000	0.703257	8.62
GC-1701-01	0.084	7.4	1578	10.3	55.8	0.014	0.000	0.705	0.000	0.112	0.000	0.513	0.000	0.705	6.10
GC-1701-01-2	0.136			10.6	60.3		failed			0.107	0.000	0.513	0.000		5.83
GC-1704-01	0.256	9.9	326	3.9	17.1	0.088	0.000	0.706	0.000	0.139	0.000	0.513	0.000	0.706	8.03
GC-1704-01-2	0.210	10.0	560	3.8	16.4	0.052	0.000	0.704	0.000	0.138	0.000	0.513	0.000	0.703	8.46
<i>Pyrola mine</i>															
PY-5-09	0.193	109.0	676	4.5	24.1	0.467	0.001	0.709	0.000	0.114	0.000	0.513	0.000	0.707	4.86

† Isotopic ratios corrected for blank and mass fractionation, $^{87}\text{Sr}/^{86}\text{Sr}$ data are normalized to $^{86}\text{Sr}/^{88}\text{Sr} = 0.1194$ and adjusted for instrumental bias to $^{87}\text{Sr}/^{86}\text{Sr} = 0.710265$ for NBS SRM 987 standard. The mean value of $^{87}\text{Sr}/^{86}\text{Sr}$ for 30 analyses the Sr standard was 0.710265 ± 10 . Isotopic ratios corrected for blank and mass fractionation, $^{143}\text{Nd}/^{144}\text{Nd}$ data are normalized to $^{146}\text{Nd}/^{144}\text{Nd} = 0.7219$ and adjusted for instrumental bias to $^{143}\text{Nd}/^{144}\text{Nd} = 0.511860$ for the La Jolla Nd standard. The mean value of $^{143}\text{Nd}/^{144}\text{Nd}$ for 30 analyses of the La Jolla Nd standard was 0.511865 ± 10 .

§ Initial $^{87}\text{Sr}/^{86}\text{Sr}$ ratios and initial ϵ_{Nd} values are calculated using an age of 215 Ma; $\lambda = 1.42 \times 10^{-11}/\text{yr}$, $\lambda = 6.54 \times 10^{-12}/\text{yr}$ (Steiger and Jäger, 1977). where present day ($^{143}\text{Nd}/^{144}\text{Nd}$)CHUR = 0.512636, and ($^{147}\text{Sm}/^{144}\text{Nd}$)CHUR = 0.1967; CHUR = chondritic uniform reservoir.

n.d. – Not determined.

failed – Some mass spectrometric runs failed and were not reattempted.

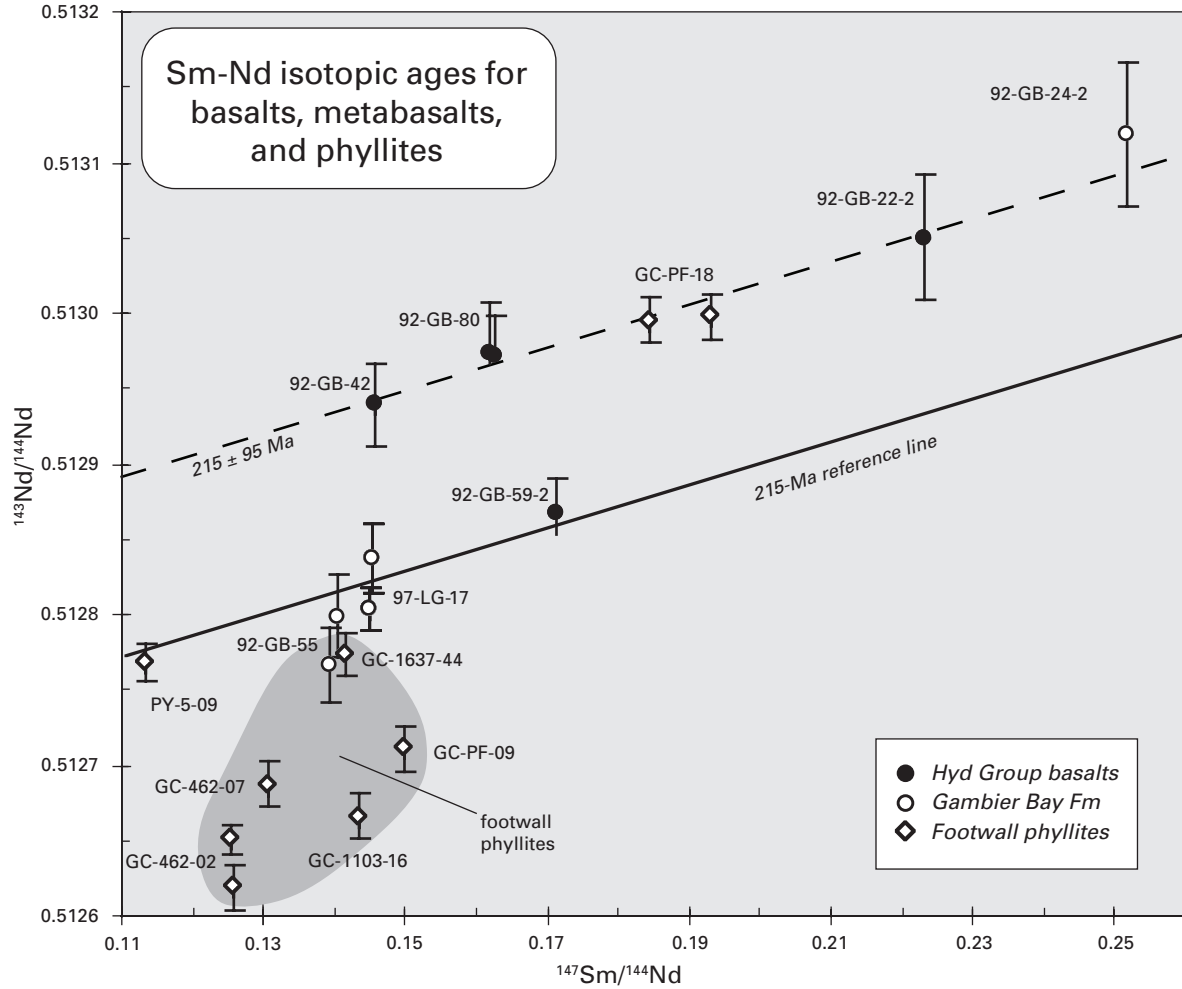


Figure 12. Samarium-neodymium isotopic correlation diagram of data from metabasalts rocks (Hyd Group and Gambier Bay Formation) and footwall phyllites (altered mafic volcanic rock?) — Greens Creek area. The same three Hyd Group metabasalts that yield a U-Pb age of 218 ± 16 Ma, yield a Sm-Nd isochron age of 215 ± 95 Ma ($N = 4$; solid line). Data from a phyllite sample, PF-18, and Gambier Bay metabasalt, 92-GB-24, are coincident with this isochron. Other metabasaltic samples and footwall phyllites did not form linear arrays or yield Sm-Nd age results, but define a field indicating more enriched (lower) Nd signatures, either through differences in their sources or by alteration and (or) metamorphism as many of these samples are highly altered. Gambier Bay metabasalts 92-GB-55 and 59, Gallagher Ridge metabasalt 97-LG-17, and Pyrola phyllite, PY-5-09, appear to form an array approximating an age near 215 Ma. This same association of samples was observed in the U-Pb isotopic data (fig. 8, chap. 12, this volume).

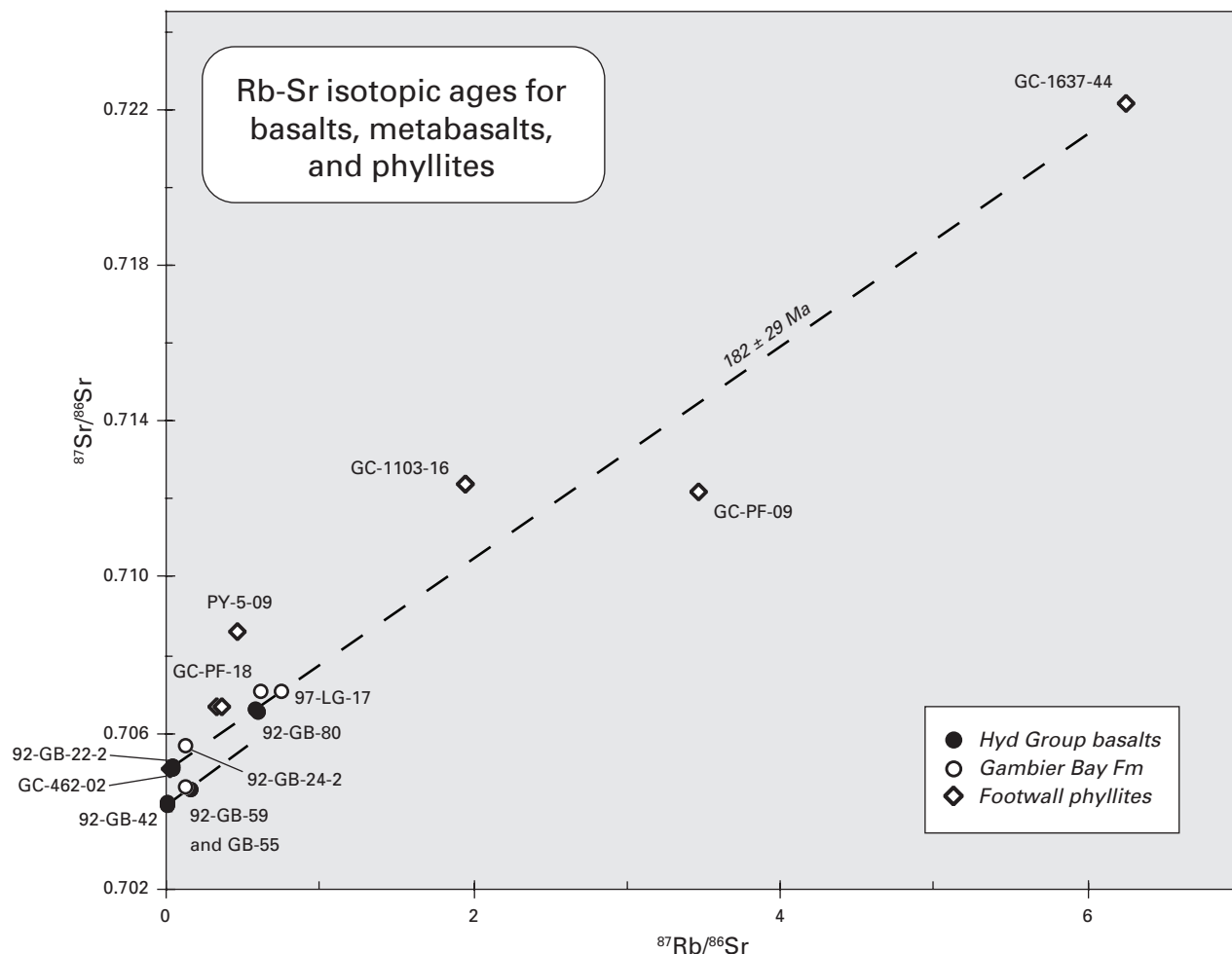


Figure 13. Rubidium-strontium isotopic correlation diagram of data from metabasalts rocks (Hyd Group and Gambier Bay Formation) and footwall phyllites (altered mafic volcanic rock?) of the Greens Creek area. An overall Rb-Sr isochron age for these rocks yielded an age of 182 ± 29 Ma, interpreted as an age for resetting of the Rb-Sr isotopic system.

The three exclusions are GST–NW1/4–Sec 6 from Mariposite Ridge, which is clearly different with respect to its U-Pb systematics; 97–LG–71 from Gallagher Ridge, which appears to have been isotopically disturbed (also see figs. 7, 10, and 11 in chap. 12); and 96–ADM–12, which is from Gambier Bay. This latter sample, although from Gambier Bay, yielded U-Pb data consistent with the Greens Creek metagabbro array. The corresponding initial lead composition defined by the regression of Greens Creek metagabbro data is similar to the Greens Creek ore lead composition as well as that for metabasalt at Gallagher Ridge 97–LG–17 (fig. 14). An age of 216 ± 20 Ma is indicated by two of the three metagabbros at Gallagher Ridge (97–LG–69 and 70), which does not include the isotopically disturbed sample 97–LG–71 (fig. 14). Gallagher Ridge metabasalt 97–LG–17 also lies upon this array.

The Sm-Nd isotopic systematics are equally varied and none of the rock suites form a well-constrained linear array. Whole rocks and a plagioclase separate from adjacent

samples 97–LG–70 and LG–71 from the Gallagher Ridge metagabbro suite yield a Sm-Nd isochron age of 200 ± 27 Ma with $\epsilon_{\text{Nd}} = +5.6$ (fig. 15), consistent with the U-Pb age of 216 ± 20 Ma. These particular analyses are more enriched (lower Nd value) than other Gallagher Ridge metagabbros (fig. 15) that plot between the Hyd Group metabasalt array at $\epsilon_{\text{Nd}} = +7.4$ and the 97LG–70, 71 metagabbro array. For example, sample GST–2–NW1/4–Sec 6 (GST) yielded a depleted ϵ_{Nd} value (+6.7 at 215 Ma) and actually plots closer to the Hyd Group metabasalt array. Two apparent Hyd Group metabasalts, 92–GB–59 and 97–LG–17, plot below but within error limits of the Gallagher Ridge array.

Greens Creek metagabbros and metabasalts span initial ϵ_{Nd} values from +5 to +7, indicating either progressive changes in the Nd isotopic composition of their parental magmas due to contamination by older crustal material or mixing between different isotopic compositions of mantle sources.

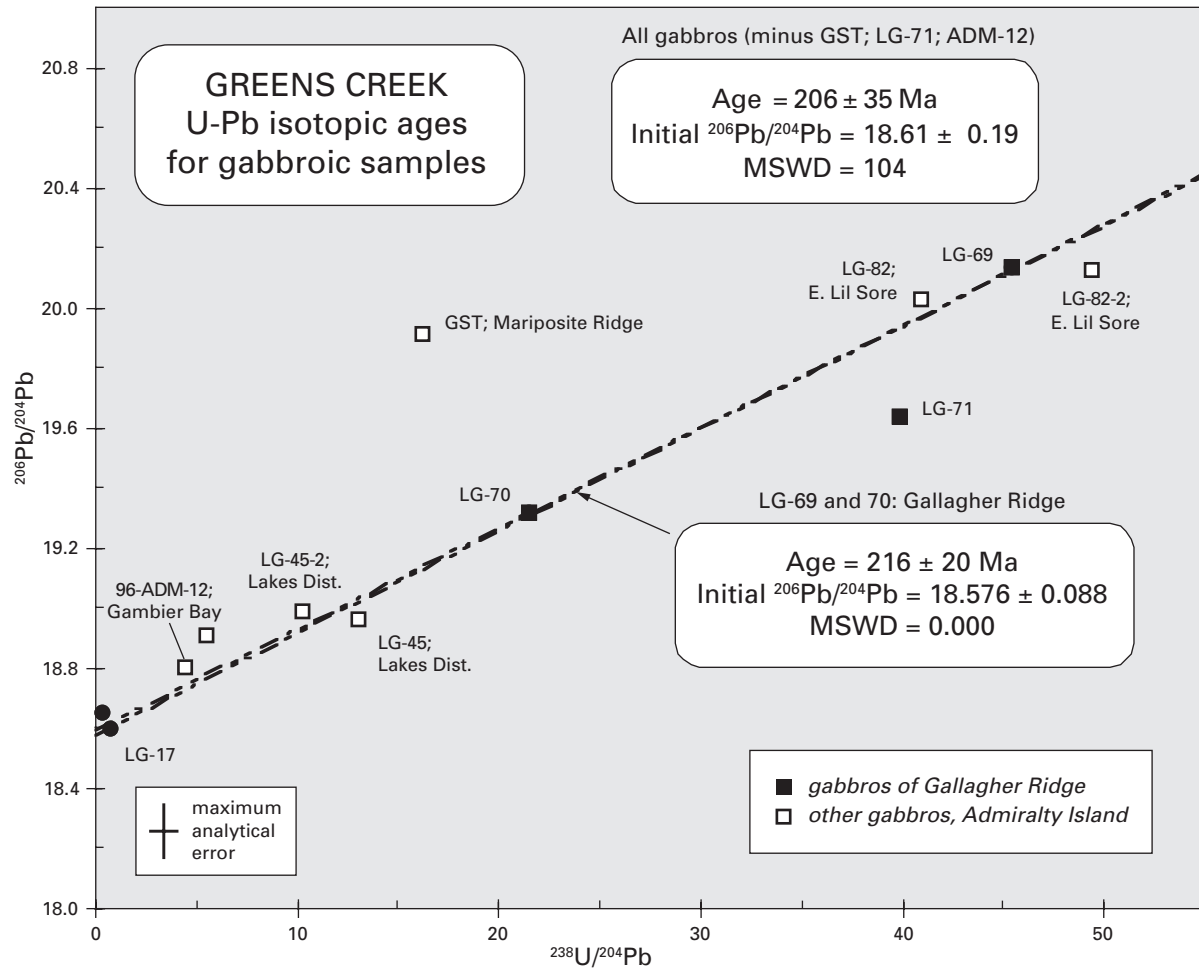


Figure 14. Uranium-lead isotopic correlation diagram of data from some of the Greens Creek metagabbros, yielding a whole-rock isochron age of 206 ± 35 Ma and initial $^{206}\text{Pb}/^{204}\text{Pb}$ value of 18.61 ± 0.19 , similar to that of the Greens Creek ore.

Rubidium-strontium whole-rock isotopic systematics for the Gallagher Ridge metagabbros are equally complex, yielding no definitive arrays. Whole-rock data for these metagabbros indicate that initial $^{87}\text{Sr}/^{86}\text{Sr}$ values can vary between 0.7039 and about 0.7048 at 215 Ma, noticeably lower than the metabasalt-phyllite suite (chap. 12).

Argillites

Argillitic rocks from the Greens Creek area probably represent the erosional products of basalt flow sequences that underlie and host the ore horizon (chap. 8). In the Greens Creek area, argillites have been divided into two formations; the Lower Permian Cannery Formation (97LG-78, ADM-29 and ADM-34) and the Upper Triassic Hyd Group (all other argillite samples — table 3).

The U-Pb isotopic data for the argillites do not yield a well-defined linear array, but rather an elongate field that indicates an age of about 185 Ma. None of the Sm-Nd isotopic data for the argillites yielded any age information.

Rubidium-Sr isotopic age data for the argillite samples suggest a single resetting age of 91.4 ± 2.6 Ma that includes Hyd Group and Cannery Formation alike. It is essentially a three-point isochron controlled by two Hyd Group argillites, 97LG-66 and NAD T4-2, neither of which is carbonaceous. Omission of the Cannery Formation data alters the Rb-Sr isochron age to 90.8 ± 2.2 Ma with initial $^{87}\text{Sr}/^{86}\text{Sr}$ at 0.70733 for the Hyd Group argillites (fig. 16A), a value that approaches the strontium composition of Late Cretaceous seawater (fig. 8 in chap. 12). However, the Hyd Group argillite data are quasi-linear (MSWD = 1104) and basically

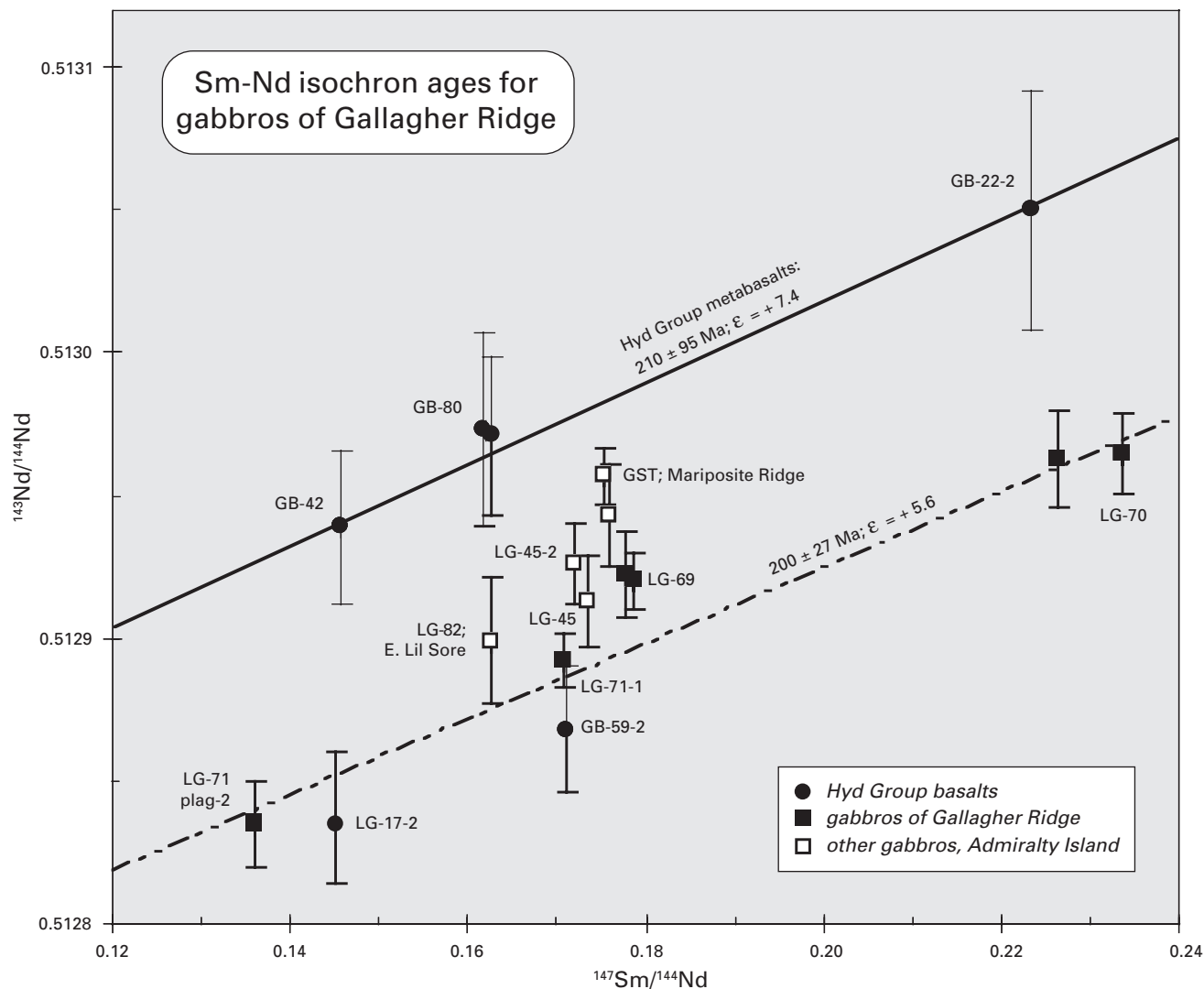


Figure 15. Samarium-neodymium isotopic correlation diagram of data from Greens Creek metagabbros. One array of adjacent Gallagher Ridge samples yielded a whole-rock and plagioclase separate “internal” isochron age of 200 ± 27 Ma and initial ϵ_{Nd} value of $+5.6$; other metagabbros do not lie on this isochron but plot toward Hyd Group metabasalt data at $\epsilon_{Nd} = +7.4$ at 215 Ma.

controlled by the radiogenic strontium from 97–LG–66. An alternate apparent isochron age excluding 97–LG–66 is 81 ± 14 Ma for the other Hyd Group argillites that include two mine argillites with slightly different strontium initial values (fig. 16B). Another alternative isochron age excluding the two mine argillites but including 97–LG–66 (that is, surface argillite samples) is 91 ± 15 Ma (fig. 16B).

Rubidium-Sr data from the two Cannery Formation samples indicate a lower initial strontium value of about 0.7066 and perhaps a younger age, but more analyses are needed in order to verify these indications.

Serpentinites

Neither the U-Pb or Sm-Nd isotopic systematics for serpentinites yield any age data. However, the initial lead signature for two mine serpentinites GC–1136–53 and GC–1136–59 is about 18.65, a value very similar to the Greens Creek ore lead signature (chap. 10). The other serpentinites initial lead signatures vary widely from about 18.4 (97–LG–19) to almost 18.8 (97–ADM–59) consistent with their strong differences in neodymium initial values (fig. 13 in chap. 12).

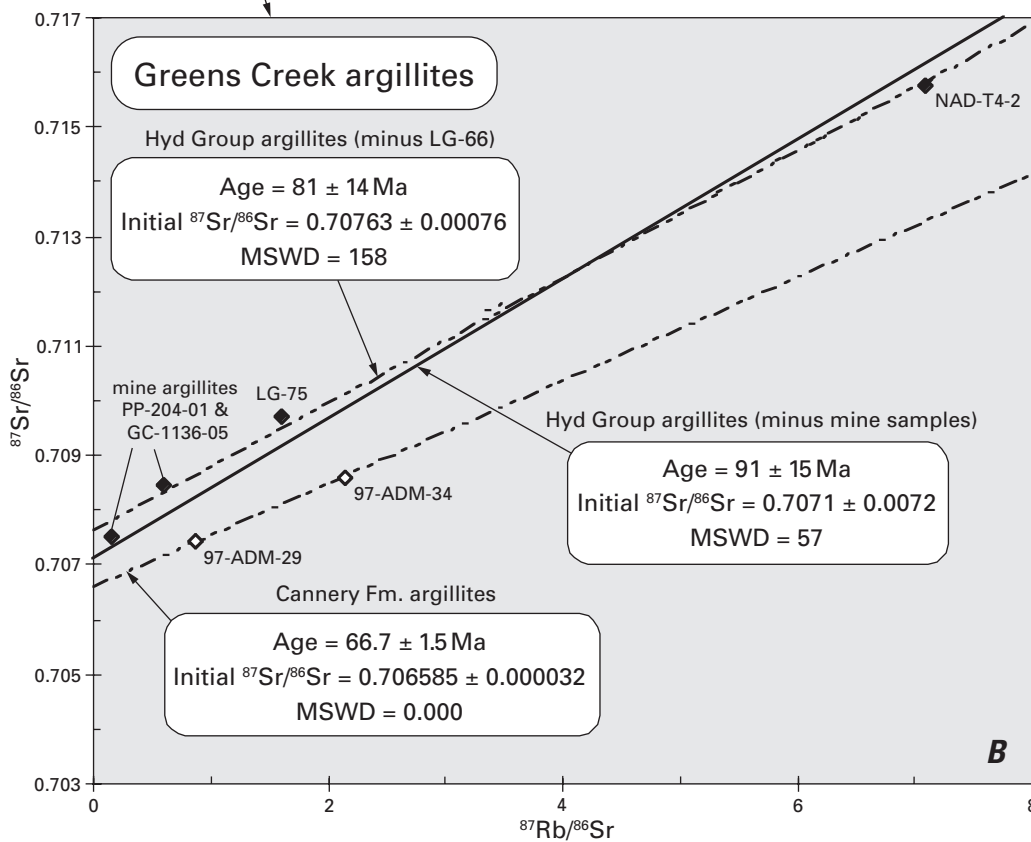
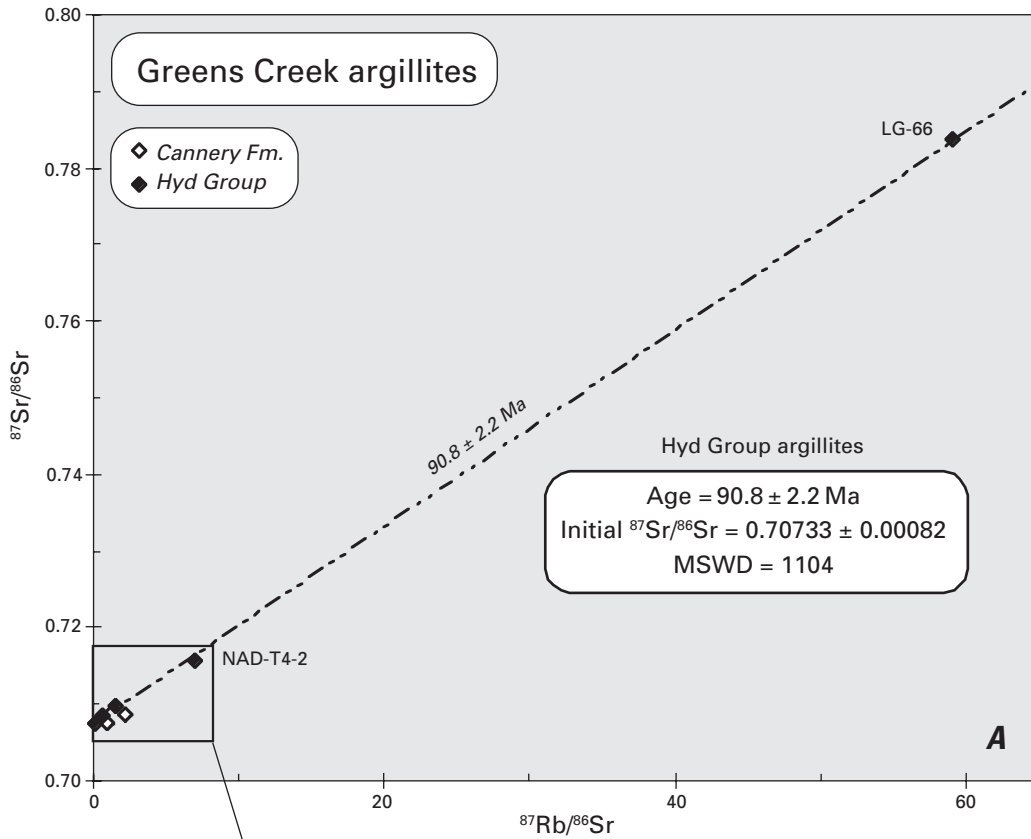


Figure 16. Rubidium-strontium isotopic correlation diagram of whole-rock data from argillites. All data (including Cannery Formation units) yield an isochron age of 91.4 ± 2.6 Ma and initial $^{87}\text{Sr}/^{86}\text{Sr}$ value of 0.70689, indicating that these isotopic systematics have been reset during Late Cretaceous deformation and metamorphism. Omission of the Cannery Formation data alters the Rb-Sr isochron age to 90.8 ± 2.2 Ma and initial $^{87}\text{Sr}/^{86}\text{Sr}$ at 0.70733 for the Hyd Group argillites (table 14.3), a value that approaches Cretaceous seawater strontium composition (see chap. 12). MSWD, mean square of weighted deviates.

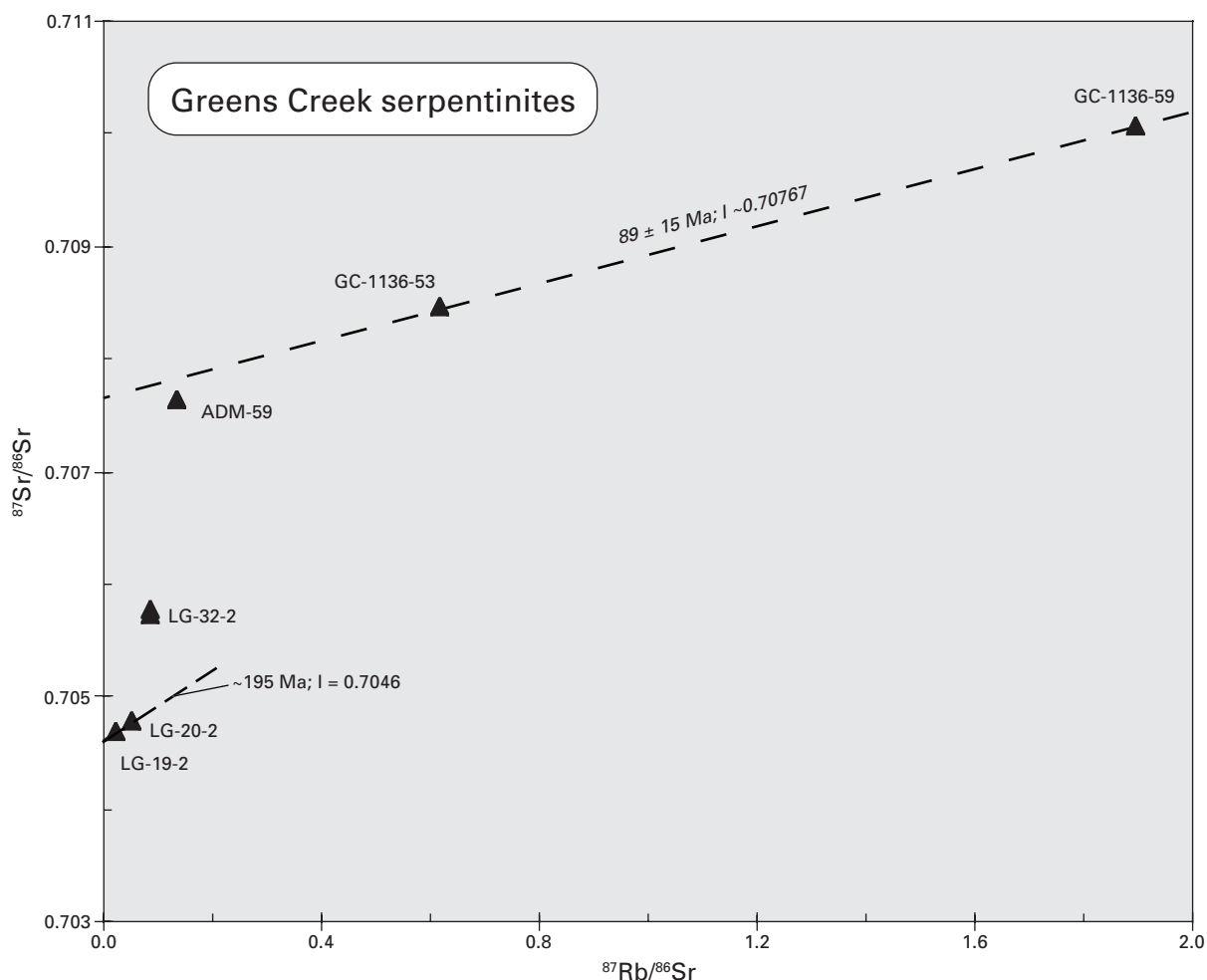


Figure 17. Rubidium-strontium isotopic correlation diagram of whole-rock data from serpentinites. At least two weak isochrons can be constructed through the data. Two samples from the Lakes District (97-LG-19-2 and 97-LG-20-2) plot near the initial $^{87}\text{Sr}/^{86}\text{Sr}$ composition of 0.70461, a value similar to that defined by disturbed isochrons from the metabasalts and suggest an age of about 195 Ma. In contrast, the Rb-Sr data for the two mine serpentinites, GC-1136-53 and GC-1136-59, yield a reset age of 89 ± 15 Ma and initial $^{87}\text{Sr}/^{86}\text{Sr}$ value of 0.70767, very close to the value defined by reset isochron data ($^{87}\text{Sr}/^{86}\text{Sr} = 0.70733$) at 91 Ma for the Hyd Group argillites.

Although the Rb-Sr isotopic data from serpentinite samples are scattered and do not form well-defined isochrons, a very imprecise apparent age of 195 ± 100 Ma is calculated for serpentinites 97-LG-19 and LG-20 from the Upper Zinc Creek area. An initial strontium value of 0.70462 ± 6 is calculated from this age, a value very similar to both metabasalts and some metagabbros.

Another apparent Rb-Sr age of 89 ± 15 Ma (fig. 17) is defined by the two mine serpentinites, GC-1136-53 and GC-1136-59, indicating an initial strontium value of 0.70767, a value very similar to that from the Hyd Group argillites (0.70733) with a Rb-Sr age of resetting at 91 Ma (fig. 16; table 7). Serpentinite 97-ADM-59 from Gambier Bay plots near this possible "reset" isochron.

Discussion

A comparison of the ages obtained both from conodonts and radiogenic isotopes works to constrain the timing of several geologic events at Greens Creek (fig. 18). The conodont age of 220.7 ± 4.4 Ma (Gradstein and others, 1995) provides a sedimentation age for the Hyd Group argillite that contains them and serves as a marker to help interpret other ages.

Late Triassic Igneous Activity

The U-Pb isochron age of 218 ± 16 Ma for several Hyd Group metabasalts is consistent with the stratigraphy and suggests that the capping basalts are only slightly younger than the underlying argillites (fig. 18 and table 7). Samples of massive, yet altered gabbro collected in the vicinity of the mine form whole-rock isochrons with apparent ages of 206 ± 35 Ma (U-Pb) and 200 ± 27 Ma (Sm-Nd) with initial values of 18.61 and +5.6, respectively (table 7). If these ages for the gabbros are accurate, then they are also consistent with crosscutting relationships (fig. 5) as these gabbros (about 206 to 200 Ma) intrude the Hyd Group basalts (about 218 Ma) and the Hyd Group argillites (about 221 Ma).

The ^{40}Ar - ^{39}Ar age of 210.3 ± 0.3 Ma for fuchsite from an altered ultramafic body in Gambier Bay apparently records the timing for argon isotopic closure at less than about 300°C in this particular ultramafic body, and at average cooling rates for upper crustal intrusions, suggests emplacement of this ultramafic body at about 216 to 212 Ma. Obtaining age constraints on the protolith age of altered serpentinites is difficult due to their low trace- and rare-earth-element abundances and their susceptibility to resetting of the U-Pb and Rb-Sr systems. Two mine serpentinites yield a Rb-Sr age suggesting resetting at about 90 Ma (fig. 17). Geological constraints on the probable age of the serpentinites are sparse due to the plasticity and tendency of the original ultramafic magma (protoserpentinite) to move into zones of structural activity. However, the available field data are consistent with a probable Late Triassic age between 221 and 199 Ma for at least

some of these serpentinites (fig. 5). The serpentinite bodies on the north shore of Gambier Bay exhibit baked contacts with the Hyd Group argillites, implying that the ultramafic protoliths were intruded into the sediments while still hot, and contain xenoliths of gabbro. One of the serpentinite bodies on Mariposite Ridge is in contact with, but does not crosscut, the overlying Hyd Group basalt.

Together, the evidence suggests that the gabbros, ultramafic rocks (serpentinites), and Hyd Group basalts in the mine area are contemporaneous and are of Late Triassic age, although some of the gabbros appear to have been emplaced last and therefore could be significantly younger.

Age of Greens Creek Mineralization

The available age constraints suggest that intrusion of mafic-ultramafic heat sources at Greens Creek occurred between 215 and 211 Ma and were then altered and cooled below about 300°C (closure temperature for argon diffusion in fuchsite is assumed to be below about 300°C) by 210.3 ± 0.3 Ma. If intrusion of these mafic-ultramafic heat sources at Greens Creek initiated the ore-forming process and this process ceased when temperatures cooled below the fuchsite argon closure temperature, then the hydrothermal system may have had a lifespan as short as 2.7 ± 2.3 m.y. (that is, a maximum span from 215 to 210 Ma, or 5 m.y., and a minimum span from 211 to 210.6 Ma, or 0.4 m.y.).

Another estimate for the duration of the Greens Creek hydrothermal system, based on the assumption that the initiation of mineralization occurred at or about the time of Hyd Group shale sedimentation, is provided by the conodont age data (220.7 ± 4.4 Ma) and the age of alteration of the serpentinite body in Gambier Bay (210.3 ± 0.3 Ma), again interpreted as the age of cessation of the ore-forming event. If we are correct in the assumption that the altered ultramafic bodies across the island are coeval and that they were altered by hydrothermal fluids related to the Greens Creek ore-forming event, then the age of 210.3 ± 0.3 Ma represents the best constraint available for the formation of the Greens Creek orebody. If we are also correct in our assumption that the onset of mineralization coincided with the onset of sedimentation of the hanging-wall argillites, then these data suggest that the Greens Creek hydrothermal system had a maximum lifespan of 10.4 ± 4.7 m.y. (that is, a maximum span from 225.1 to 210 Ma, or 15.1 m.y., and a minimum span from 216.3 to 210.6 Ma, or 5.7 m.y.). Following these arguments, intrusion of the gabbroic bodies (about 206 to 200 Ma) occurred after cessation of the ore-forming event (about 210 Ma), implying that the heat source for mineralization was supplied by the ultramafic intrusions and not by the gabbroic bodies.

Isotopic Resetting of the Older Stratigraphy

Whole-rock U-Pb and Rb-Sr data from the phyllites and argillites suggest an isotopic disturbance or partial resetting

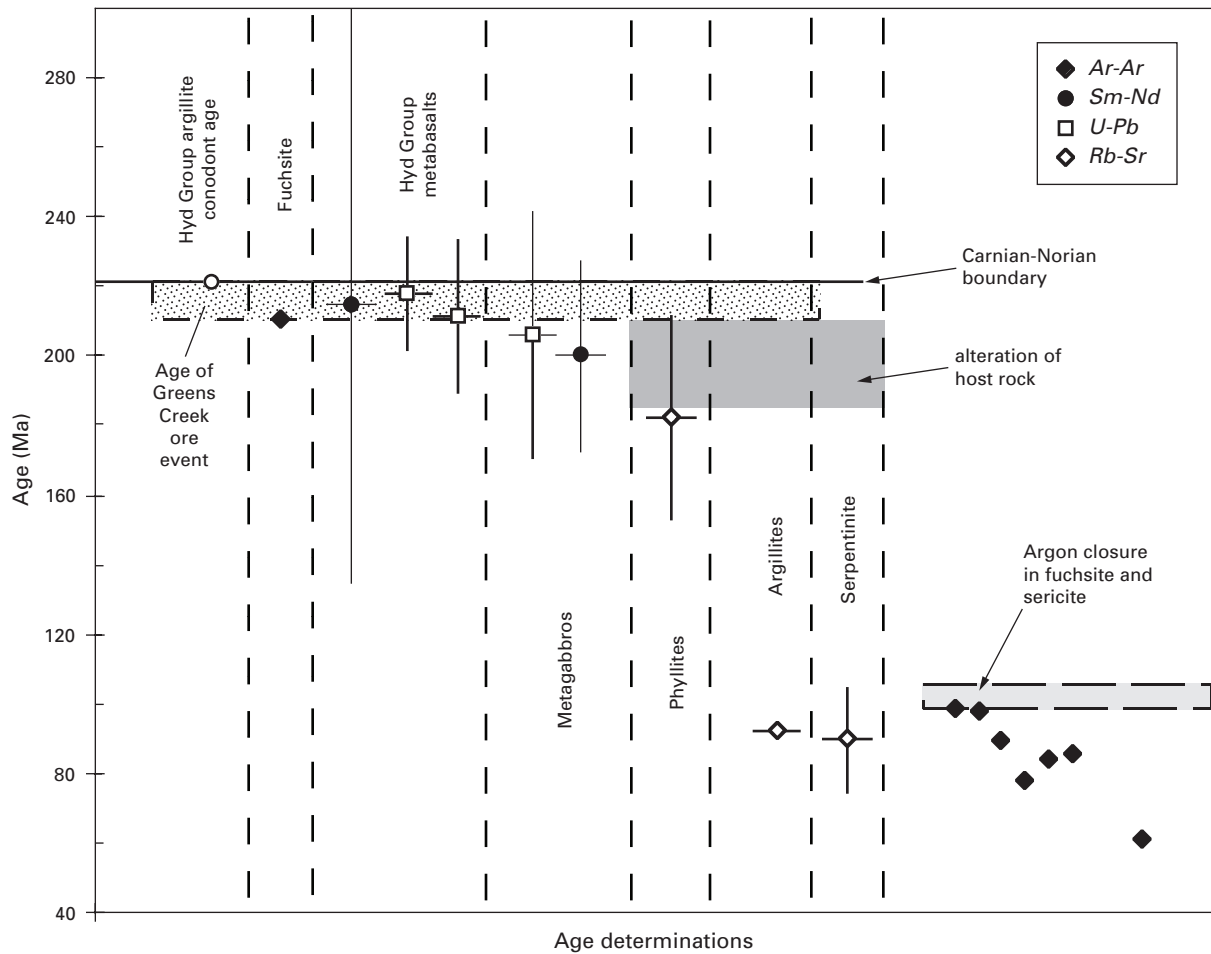


Figure 18. Diagram summarizing the various ages for Greens Creek samples. The isotopic age accompanying the conodont symbol is from Gradstein and others (1995) and dates the Carnian-Norian boundary. The most biochronologically constrained conodont collections from mine workings and outcrops in the Greens Creek mine area are diagnostic of the Lower and (or) Upper *primitivus* Zone(s). The boundary between these zones coincides with the Carnian-Norian boundary (fig. 5). The best ages suggest that the Hyd Group argillites and metabasalts are coeval at 220.7 ± 4.4 Ma and that subsequent intrusion(s) of gabbroic magmas at 206 to 200 Ma, disturbed many of the U-Pb and Rb-Sr isotopic systematics of older rock suites (metabasalt, serpentinite, argillite). The main phase of polymetallic mineralization is constrained to have occurred between these two ages and is confirmed by the $^{40}\text{Ar}/^{39}\text{Ar}$ plateau age of 210.3 ± 0.3 Ma for fuchsite from Gambier Bay. Other U-Pb, Rb-Sr, and $^{40}\text{Ar}/^{39}\text{Ar}$ total gas ages from argillites, sulfides, fuchsite, and sericite define much younger, “reset” ages between 90 and 105 Ma, and also about 61 Ma, consistent with known ages for Late Cretaceous deformation and metamorphism, and Early Tertiary gold mineralization, respectively.

Table 7. Age results for various Greens Creek rocks and minerals.

[Fmn., Formation; Gp., Group; GC, Greens Creek; Pen., Peninsula; OB, orebody]

Location/ stratigraphic unit	Rock/ mineral	Dating technique	Age (Ma)	Error (Ma)	Initial value*	Confidence (Precision)	Interpretation
Cliff Creek	argillite	conodont	220.7	4.4		High (Great)	Age of Hyd Group argillite
Gambier Bay	fuchsite	Ar-Ar	210.3	0.3		High (Great)	Age of argon closure in fuchsite
Hyd Group	metabasalts	Sm-Nd	215	95	7.4	High (Poor)	Age of Hyd Group basalts
Hyd Group	metabasalts	U-Pb	218	16	18.515	High	Age of Hyd Group
Hyd Gp. - Gambier Bay	metabasalts + phyllites	U-Pb	211	27	18.64	High (Poor)	Age of disturbance of metabasalts
Hyd Gp. - Gambier Bay	metabasalts	Rb-Sr	182	29	0.70494	Fair (Poor)	Age of disturbance of metabasalts
Greens Creek area	metabasalts	U-Pb	206	35	18.61	Good (Poor)	Age of gabbros on Gallagher Ridge
Gallagher Ridge		U-Pb	216	20	18.576		
Gallagher Ridge	metabasalts	Sm-Nd	200	27	5.6	Good (Poor)	Age of gabbros on Gallagher Ridge
Hyd Group and Cannery Fm.	argillites	U-Pb	186	100	18.81	Good (Poor)	Age of disturbance of argillites
Hyd Group	argillites	Rb-Sr	90.8	2.2	0.70733	Good (Good)	Age of disturbance of argillites
Greens Creek	serpentinites	Rb-Sr	89	15	0.70767	Fair (Poor)	Age of disturbance of mine serpentinites
GC DC ovr West OB	mica	Ar-Ar	98.6	1			
Mammoth claim	fuchsite	Ar-Ar	97.5	0.2			
GC - east OB	fuchsite	Ar-Ar	89	0.2			
GC - east OB	sericite	Ar-Ar	77.5	0.1			
GC - SW OB	fuchsite	Ar-Ar	83.4	0.2		Total gas ages	Argon closure is interpreted to have occurred between 105 and 95 Ma for these samples
GC 29F N heading	fuchsite	Ar-Ar	85.4	0.2			
Mansfield Pen.	fuchsite	Ar-Ar	60.8	0.2			

* - Initial values for U-Pb ages are $^{206}\text{Pb}/^{204}\text{Pb}$; for Rb-Sr ages, 87 Sr/86Sr; and for Sm-Nd ages, epsilon Nd (ϵ_{Nd}) define as the initial $^{134}\text{Nd}/^{144}\text{Nd}$ value in parts per 10^4 deviation from the CHUR evolution line.

that occurred between 211 and 190 Ma (figs. 11, 13, and 16; table 7), an age range that is coincident with intrusion of the gabbroic suite. Initial $^{206}\text{Pb}/^{204}\text{Pb}$ values near 18.64 for some of these suites of altered rock are very similar to both the initial lead value defined by U-Pb data from Gallagher Ridge metagabbros (figs. 11 and 14) and the Greens Creek ore lead composition, suggesting that alteration and isotopic resetting of the older stratigraphy may be related to intrusion of the Gallagher Ridge gabbroic suite.

Age of Cretaceous Overprinting on Greens Creek Mineralization

Several lines of evidence indicate that the Greens Creek region was isotopically affected by Cretaceous metamorphism at 110 to 85 Ma (Rubin and others, 1990). An apparent Rb-Sr isochron age from argillites indicates a disturbance of this isotopic system at about 90 Ma (table 7 and fig. 16). An imprecise, apparent Rb-Sr age was also found in mine serpentinite,

suggesting ages around 90 Ma. These ages are likewise similar to age results that infer complete resetting of argon in fuchsite and sericite just prior to around 105 to 95 Ma and are consistent with Cretaceous ages for the accretion of the Alexander, Wrangellia, and Gravina terranes with the North American craton (Rubin and others, 1990).

The Mansfield Peninsula sample is interesting in that it appears to indicate a plateau age of 60.8 Ma, consistent with alteration of the ultramafic body during the transition from oblique convergence to margin-parallel motion of the Alexander terrane during the Eocene. The age is also very close to that accepted for mineralization of the Alaskan-Juneau district (about 55 Ma; Goldfarb and others, 1991), only 40 km to the east.

Acknowledgments

The authors would like to thank the Kennecott Greens Creek Mining Company for their cooperation, hospitality, and special equipment during sample collection on Admiralty Island. Also, thanks to all the workers at the USGS that were responsible for the majority of sample preparation and chemical analysis, especially Ross Yeoman and Elaine Gilman. Special thanks to manuscript reviewers J.N. Aleinikoff, M.L. Kunk, and Daniel M. Unruh for their helpful comments and criticisms. And special thanks to Cliff D. Taylor and Craig Johnson, our editors, for having the patience to see this manuscript into review and eventual fruition.

A.G. Harris thanks N.A. Duke, P.A. Lindberg, J.M. Prof-fett, and A.W. West, associates and personnel of Greens Creek Kennecott Mining Company, and C.D. Taylor, U.S. Geological Survey, for collecting the conodont samples, the productive and, less enthusiastically, nonproductive, that made this study possible and successful. Thanks are also due the Greens Creek explorationists who went farther afield to sample on Admiralty and northern Kupreanof Islands to provide broader coverage regionally and stratigraphically.

References Cited

- Barovich, K.M., and Patchett, P.J., 1988, Behavior of isotopic systematics during deformation and metamorphism— A Hf, Nd and Sr isotopic study of mylonitized granite: *Contributions to Mineralogy and Petrology*, v. 109, p. 386–393.
- Brannon, J.C., Podosek, F.A., and McLimans, R.K., 1992, Alleghenian age of the Upper Mississippi Valley zinc-lead deposit determined by Rb-Sr dating of sphalerite: *Nature*, v. 356, p. 509–511.
- Brannon, J.C., Cole, S.C., Podosek, F.A., Ragan, V.M., Coveney, R.M., Jr., Wallace, M.W., and Bradley, A.J., 1996, Th-Pb and U-Pb dating of ore-stage calcite and Paleozoic fluid flow: *Science*, v. 271, p. 491–493.
- Brew, D.A., and Ford, A.B., 1985, Preliminary reconnaissance geologic map of the Juneau, Taku River, Atlin, and part of the Skagway 1:250,000 quadrangles, southeastern Alaska: U.S. Geological Survey Open-File Report 85–395, 23 p.
- Chesley, J.T., Halliday, A.N., Snee, L.W., Mezger, K., Shepherd, T.J., and Scrivener, R.C., 1993, Thermochronology of the Cornubian batholith in southwest England — Implications for pluton emplacement and protracted hydrothermal mineralization: *Geochimica et Cosmochimica Acta*, v. 57, p. 1817–1835.
- Chesley, J.T., Halliday, A.N., Kyser, T.K., and Spry, P.G., 1994, Direct dating of Mississippi Valley-type mineralization — Use of Sm-Nd in fluorite: *Economic Geology*, v. 89, p. 1192–1199.
- Christensen, J.N., Halliday, A.N., Leigh, K.E., Randell, R.N., and Kesler, S.E., 1995a, Direct dating of sulfides by Rb-Sr — A critical test using the Polaris Mississippi Valley-type Zn-Pb deposit: *Geochimica et Cosmochimica Acta*, v. 59, p. 5191–5197.
- Christensen, J.N., Halliday, A.N., Vearncombe, J.R., and Kesler, S.E., 1995b, Testing models of large-scale crustal fluid flow using direct dating of sulfides — Rb-Sr evidence for early dewatering and formation of Mississippi Valley-type deposits, Canning Basin, Australia: *Economic Geology*, v. 90, p. 877–884.
- Crafford, T.C., 1984, Greens Creek-type massive sulfide exploration criteria — Anaconda Minerals Company memorandum to D.A. Heatwole, Anaconda Geological Document Collection: Laramie, American Heritage Center, University of Wyoming, 6 p.
- Crafford, T.C., 1989, The Greens Creek Ag-Au-Pb-Zn massive sulfide deposit, Admiralty Island, southeast Alaska [abs.]: Alaska Miners Association Conference Juneau, Program with Abstracts, p. 27–29.
- Dalrymple, G.B., Alexander, E.C., Lanphere, M.A., and Kraker, G.P., 1981, Irradiation of samples for $^{40}\text{Ar}/^{39}\text{Ar}$ dating using the Geological Survey TRIGA reactor: U.S. Geological Survey Professional Paper 1176, 55 p.
- Desrochers, A., and Orchard, M.J., 1991, Stratigraphic revisions and carbonate sedimentology of the Kunga Group (Upper Triassic-Lower Jurassic), Queen Charlotte Islands, British Columbia, in Woodsworth, G.J., ed., *Evolution and hydrocarbon potential of the Queen Charlotte Basin, British Columbia*: Geological Survey of Canada Paper 90–10, p. 163–172.
- Dickinson, Alan, 1995, *Radiogenic isotope geology*: Oxford, Cambridge Press, 490 p.
- Epstein, A.G., Epstein, J.B., and Harris, L.D., 1977, Conodont color alteration — An index to organic metamorphism: U.S. Geological Survey Professional Paper 995, 27 p.

- Fairbairn, H.W., Hurley, P.M., and Pinson, W.H., 1961, The relation of discordant Rb-Sr mineral and rock ages in an igneous rock to its time of subsequent Sr87/Sr86 metamorphism: *Geochimica et Cosmochimica Acta*, v. 23, p. 135–144.
- Fleck, R.J., Sutter, J.F., and Elliot, D.H., 1977, Interpretation of discordant ⁴⁰Ar/³⁹Ar age spectra of Mesozoic tholeiites from Antarctica: *Geochimica et Cosmochimica Acta*, v. 41, p. 15–32.
- Gehrels, G.E., and Berg, H.D., 1994, Geology of southeastern Alaska, in Plafker, George, and Berg, H.C., eds., *The geology of Alaska: Boulder, Colo., Geological Society of America, The Geology of North America*, v. G-1, p. 451–467.
- Goldfarb, R.J., Newberry, R.J., Pickthorn, W.J., and Gent, C.A., 1991, Oxygen, hydrogen, and sulfur isotope studies in the Juneau gold belt, southeastern Alaska — Constraints on the origin of the hydrothermal fluids: *Economic Geology*, v. 86, p. 66–80.
- Gradstein, F.M., Agterberg, F.P., Ogg, J.G., Hardenbol, Jan, Van Veen, Paul, Thierry, Jacques, and Huang, Zehui, 1995, A Triassic, Jurassic, and Cretaceous time scale, in *Geochronology time scales and global stratigraphic correlation: SEPM Special Publication no. 54*, p. 95–126.
- Hart, S.R., and Kinloch, E.D., 1989, Osmium isotope systematics in Witwatersrand and Bushveld ore deposits: *Economic Geology*, v. 84, p. 1651–1655.
- Karl, S.M., Haeussler, P.J., and McCafferty, Anne, 1999, Reconnaissance geologic map of the Duncan Canal-Zarembko Island area, southeastern Alaska: U.S. Geological Survey Open-file Report 99–168, 29 p., map scale 1:150,000.
- Kerrick, Robert, 1991, Radiogenic isotope systems applied to ore deposits, in Heaman, L., and Ludden, J.N., eds., *Applications of radiogenic isotopes systems to problems in geology: Mineralogical Association of Canada, Short Course 19*, p. 365–421.
- Kerrick, Robert, and King, R., 1993, Hydrothermal zircon and baddeleyite in Val-d'Or Archean mesothermal gold deposits — Characteristics, compositions, and fluid-inclusion properties, with implications for timing of primary gold mineralization: *Canadian Journal of Earth Sciences*, v. 30, p. 2334–2351.
- Königshof, Peter, 1992, Conodont colour alteration index (CAI) in Paleozoic rocks (Middle Devonian to Lower Carboniferous) of the Rhenish Massif — A comparison to vitrinite reflectance: *Courier Forschungsinstitut Senckenberg*, no. 149, 118 p. [in German].
- Kozur, Heinz, 1989, Significance of events in conodont evolution for the Permian and Triassic stratigraphy, in Ziegler, Willi, ed., 1st International Senckenberg conference and 5th European Conodont Symposium (ECOS V), *Contributions III — Papers on Ordovician to Triassic conodonts: Courier Forschungsinstitut Senckenberg*, no. 117, p. 385–408.
- Lambert, D.D., Morgan, J.W., Walker, R.J., Shirey, S.B., Carlson, R.W., Zientek, M.L., and Koski, M.S., 1989, Rhenium-osmium and samarium-neodymium isotopic systematics of the Stillwater Complex: *Science*, v. 244, p. 1169–1174.
- Lange, F.-G., 1968, Conodonten-Gruppenfunde aus Kalken des tieferen Oberdevon: *Geological et Palaeontologica*, v. 2, p. 37–57.
- Lanphere, M.A., Wasserburg, G.J., Albee, A.L., and Tilton, G.R., 1964, Redistribution of strontium and rubidium isotopes during metamorphism, World Beater Complex, Panamint Range, California, in Craig, H., Miller, S.L., and Wasserburg, G.J., eds., *Isotopic and cosmic chemistry: Amsterdam, North Holland Publications*, p. 269–320.
- Lathram, E.H., Pomeroy, J.S., Berg, H.C., and Loney, R.A., 1965, Reconnaissance geology of Admiralty Island, Alaska: U.S. Geological Survey Bulletin 1181-R, 48 p.
- Ludwig, K.R., 1980, Calculation of uncertainties of U-Pb data: *Earth and Planetary Science Letters*, v. 46, p. 212–220.
- Ludwig, K.R., 1985, PBDAT200 — A computer program for processing raw Pb-U-Th isotope data: U.S. Geological Survey Open-File Report 85–547, 54 p.
- Ludwig, K.R., 1993, ANALYST: VER. 2.20 — A computer program for control of a thermal-ionization, single-collector mass spectrometer, user's manual: U.S. Geological Survey Open-File Report 92–543, rev. Dec. 7, 1993, 94 p.
- Ludwig, K.R., 1998, ISOPLOT/Ex, version 1.00, A geochronological toolkit for Microsoft Excel: Berkeley Geochronology Center, Special Publication no.1, 43 p.
- Lugmair, G.W., Scheinin, N.B., and Marti, K., 1975, Sm-Nd age and history of Apollo 17 basalt 75075 — Evidence for early differentiation of the lunar exterior: *Proceedings of the 6th Lunar Science Conference*, p. 1419–1429.
- MacIntyre, D.G., 1986, The geochemistry of basalts hosting massive sulfide deposits, Alexander terrane northwest British Columbia: British Columbia Ministry of Energy, Mines, and Petroleum Resources, *Geological Fieldwork*, 1985, Paper 1986–1, pp. 197–210.
- Mei, S., and Henderson, C.M., 2002, Comments on some Permian conodont faunas reported from southeast Asia and adjacent areas and their global correlation: *Journal of Asian Earth Sciences*, v. 20, p. 599–608.
- Moorbath, Stephen, and Taylor, P.N., 1981, Isotopic evidence for continental growth in the Precambrian, in Kroner, A., ed., *Precambrian plate tectonics: Elsevier*, p. 491–525.
- Newberry, R.J., and Brew, D.A., 1997, The Upper Triassic Greens Creek VMS (volcanogenic massive sulfide) deposit and Woewodski Island VMS prospects, southeastern Alaska — Chemical and isotopic data for rocks and

- ores demonstrate similarity of these deposits and their host rocks: U.S. Geological Survey Open-File Report 97-539, 49 p.
- Newberry, R.J., and Brew, D.A., 1999, Chemical and isotopic data for rocks and ores from the Upper Triassic Greens Creek and Woewodski Island volcanogenic massive sulfide deposits, southeastern Alaska, *in* Kelley, K.D., ed., *Geologic studies in Alaska by the U.S. Geological Survey, 1997: U.S. Geological Survey Professional Paper 1614*, p. 35-55.
- Newberry, R.J., Brew, D.A., and Crafford, T.C., 1990, Genesis of the Greens Creek volcanogenic massive sulfide deposit, S.E. Alaska — A geochemical study [abs.]: *Geological Association of Canada Program with Abstracts*, v. 15, p. A96.
- Newberry, R.J., Crafford, T.C., Newkirk, S.R., Young, L.E., Nelson, S.W., and Duke, N.A., 1997, Volcanogenic massive sulfide deposits of Alaska: *Economic Geology Monograph 9*, p. 120-150.
- Orchard, M.J., 1991a, Upper Triassic conodont biochronology and biostratigraphy of the Kunga Group, Queen Charlotte Islands, British Columbia, *in* Woodsworth, G.J., ed., *Evolution and hydrocarbon potential of the Queen Charlotte Basin, British Columbia: Geological Survey of Canada Paper 90-10*, p. 173-193.
- Orchard, M.J., 1991b, Upper Triassic conodont biochronology and new index species from the Canadian Cordillera, *in* Orchard, M.J., and McCracken, A.D., eds., *Ordovician and Triassic conodont paleontology of the Canadian Cordillera: Geological Survey of Canada Bulletin 417*, p. 299-335.
- Premo, W.R., and Tatsumoto, M., 1991, U-Th-Pb isotopic systematics of lunar norite 78235, *in* *Proceedings of the 21st Lunar and Planetary Science Conference: Houston, The Lunar and Planetary Institute*, p. 89-100.
- Premo, W.R., and Tatsumoto, M., 1992, U-Th-Pb, Rb-Sr, and Sm-Nd isotopic systematics of lunar troctolitic cumulate 76535—Implications on the age and origin of this early lunar, deep-seated cumulate, *in* *Proceedings of the 22d Lunar and Planetary Science Conference*, p. 381-397: Houston, Texas, The Lunar and Planetary Institute.
- Purnell, M.A., and Donoghue, P.C.J., 1997, Architecture and functional morphology of the skeletal apparatus of ozarkodinid conodonts: *Philosophical Transactions of the Royal Society of London, Series B*, v. 352, no. 1361, p. 1545-1655.
- Purnell, M.A., and Donoghue, P.C.J., 1998, Skeletal architecture, homologies and taphonomy of ozarkodinid conodonts: *Palaeontology*, v. 41, part 1, p. 57-102.
- Rejebian, V.A., Harris, A.G., and Huebner, J.S., 1987, Conodont color and textural alteration—An index to regional metamorphism, contact metamorphism, and hydrothermal alteration: *Geological Society of America Bulletin*, v. 99, p. 471-479.
- Roddick, J.C., 1983, High-precision intercalibration of $^{40}\text{Ar}/^{39}\text{Ar}$ standards: *Geochimica et Cosmochimica Acta*, v. 47, p. 887-898.
- Rubin, C.M., Saleeby, J.B., Cowan, D.S., Brandon, M.T., and McGroder, M.F., 1990, Regionally extensive mid-Cretaceous west-vergent thrust system in the northwestern Cordillera — Implications for continent-margin tectonism: *Geology*, v. 18, p. 276-280.
- Samson, S.D., and Alexander, E.C., 1987, Calibration of interlaboratory $^{40}\text{Ar}/^{39}\text{Ar}$ dating standard, MMhb-1: *Isotope Science*, v. 66, p. 27-34.
- Snee, L.W., 2002, Argon thermochronology of mineral deposits—A review: *U.S. Geological Survey E-Bulletin 2194*, 39 p.
- Snee, L.W., Sutter, J.F., and Kelly, W.C., 1988, Thermochronology of economic mineral deposits — Dating the stages of mineralization at Panasqueira, Portugal, by high-precision $^{40}\text{Ar}/^{39}\text{Ar}$ age spectrum techniques on muscovite: *Economic Geology*, v. 83, p. 335-354.
- Steiger, R.H., and Jäger, E., 1977, Subcommission on geochronology — Convention on the use of decay constants in geo- and cosmochronology: *Earth and Planetary Science Letters*, v. 36, p. 359-362.
- Sweet, W.C., 1989, *The Conodonta: Oxford Monographs on Geology and Geophysics no. 10*, 212 p.
- Tatsumoto, Mitsunobu, and Unruh, D.M., 1976, KREEP basalt age — Grain by grain U-Th-Pb systematics study of the quartz monzodiorite clast 15405, 88: *Proceedings of the 7th Lunar and Planetary Science Conference, Houston, The Lunar and Planetary Institute*, p. 2107-2129.
- Taylor, C.D., 1997, An arc-flank to back-arc transect—Metallogeny of Upper Triassic volcanogenic massive sulfide occurrences of the Alexander terrane, southeastern Alaska and British Columbia: [extended abs.] *in* *Society of Economic Geologists Neves Corvo Field Conference, May 7-17, 1997, Lisbon, Portugal, Abstracts and Programs volume*, p. 68.
- Taylor, C.D., Cieutat, B.A., and Miller, L.D., 1992, A follow-up geochemical survey of base metal anomalies in the Ward Creek/Windfall Harbor and Gambier Bay areas, Admiralty Island, S.E. Alaska, *in* Bradley, D., and Dusel-Bacon, C., eds., *1991 Geologic studies in Alaska: U.S. Geological Survey Bulletin 2041*, p. 70-85.
- Taylor, C.D., Philpotts, J., Sutley, S., Gent, C., Harlan, S., Premo, W.R., Tatsumoto, M., Emsbo, P., and Meier, A., 1995a, Geochemistry of Late Triassic volcanic rocks and age of alteration associated with volcanogenic massive sulfide occurrences, Alexander terrane, southeast Alaska, *in*

Geology and ore deposits of the American cordillera — A symposium: Geological Society of Nevada, p. A74.

Taylor, C.D., Philpotts, J.A., Hall, T.E., and Wakeman, B.W., 1995b, New information on the geochemistry, age, and tectonic history of Late Triassic volcanic host rocks and associated massive sulfide occurrences of the Alexander terrane, southeast Alaska: Alaska Miners Association Conference, Juneau, Program with Abstracts, p. 31–32.

Taylor, C.D., Premo, W. R., and Meier, A. L., 1999, The Late Triassic metallogeny of the Alexander terrane, southeastern Alaska and British Columbia: Geological Society of America Abstracts with Programs, v. 31, no. 6, p. A–101.

Taylor, C.D., Premo, W.R., and Lear, K.G., 2000, The Greens Creek massive sulfide deposit — Premier example of the Late Triassic metallogeny of the Alexander terrane, southeastern Alaska and British Columbia: Geological Society of America Abstracts with Programs, v. 32, no. 6, p. A–71.

Taylor, P.N., Moorbath, S., Goodwin, R., and Petrykowski, A.C., 1980, Crustal contamination as an indicator of the extent of early Archaean continental crust—Pb isotopic evidence from the late Archaean gneisses of West Greenland: *Geochimica et Cosmochimica Acta*, v. 44, p. 1437–1453.

Walker, R.J., Morgan, J.W., Naldrett, A.J., and Li C., 1991, Re-Os isotopic systematics of Ni-Cu sulfide ores, Sudbury Igneous Complex, Ontario — Evidence for a major crustal component: *Earth and Planetary Science Letters*, v. 105, p. 416–429.

Wetherill, G.W., Davis, G.L., and Lee-Hu C., 1968, Rb-Sr measurements on whole rocks and separated minerals from the Baltimore Gneiss, Maryland: *Geological Society of America Bulletin*, v. 79, p. 757–762.

Whitehouse, M.J., 1988, Granulite facies Nd-isotopic homogenization in the Lewisian complex of northwest Scotland: *Nature*, v. 331, p. 705–707.

Williams, M.E., 1990, Feeding behavior in Cleveland Shale sharks, in Boucot, A.J., ed., *Evolutionary paleobiology of behavior and coevolution*: Elsevier, Amsterdam, p. 273–287.

Appendix. Data for Permian and Triassic conodont samples from Admiralty and northern Kupreanof Islands, Alaska (exclusive of samples listed in table 1).

[CAI, color alteration index; samples collected by Greens Creek and U.S. Geological Survey personnel. See figures 7 and 8 for Permian and Triassic conodont zonation and range of biostratigraphically useful collections; colln., collection]

Locality no., field no., and USGS Colln. no.	Location	Lithology and stratigraphic unit	CAI	Age
1 AK14701	Juneau A-3 quadrangle 58°09.97'N., 134°46.37'W.	Dark-gray coarsely crystalline dolomite. Barren.		
2 AK14718	Juneau A-3 quadrangle 58°14.05'N., 134°49.7'W.	Not designated. Barren.		
3 AK14747 (Mes. 35016)	Juneau A-3 quadrangle 58°12.60'N., 134°45.36'W.	Not designated; age indicates Hyd Group.	5	late Carnian-very earliest Norian
4 SP-32373	Juneau A-3 quadrangle 58°11.67'N., 134°44.38'W.	Shaly dark-gray limestone, near contact with overlying(?) Hyd Group greenstone; lies structurally above a thick chert-clast conglomerate. Barren.		
5 SP-32356	Sitka D-2 quadrangle 57°57.39'N., 134°32.4'W.	Gray limestone structurally above graphitic argillite that hosts a stratiform, barite-rich massive sulfide. Hyd Group sequence? Barren.		
6 AK14920	Petersburg D-5 quadrangle 56°48.52'N., 133°24.28'W.	Not designated. Barren.		
7 AK14973 (Mes. 35013)	Petersburg D-5 quadrangle 56°48.52'N., 133°24.28'W.	Gray limestone; Hyd Group.	5	<i>polygnathiformis</i> Zone (latest early-earliest late Carnian)
8 AK15066 (33405-PC)	Petersburg D-5 quadrangle 56°46.26'N., 133°23.09'W.	Cherty limestone; Cannery Formation.	5	very late Early Permian (late Leonardian; Kungurian)
9 AK15553 (33486-PC)	Petersburg D-5 quadrangle 56°47.71'N., 133°21.26'W.	Cannery Formation.	5–6.5	very late Early Permian (late Leonardian; Kungurian)
10 AK15554 (33487-PC)	Petersburg D-5 quadrangle 56°47.97'N., 133°21.33'W.	Cannery Formation.	5.5 and minor 5 and 6	very late Early Permian (late Leonardian; Kungurian)
11 AK15601	Petersburg D-5 quadrangle 56°47.65'N., 133°21.66'W.	Not designated.	about 5	Mississippian-Early Triassic

Appendix. Data for Permian and Triassic conodont samples from Admiralty and northern Kupreanof Islands, Alaska.—Continued

[CAI, color alteration index; samples collected by Greens Creek and U.S. Geological Survey personnel. See figs. 7 and 8 for Permian and Triassic conodont zonation and range of biostratigraphically useful collections; colln., collection]

Locality no., field no., and USGS Colln. no.	Location	Lithology and stratigraphic unit	CAI	Age
12 AK15614	Petersburg D-5 quadrangle 56°46.42'N., 133°21.73'W.	Not designated. Barren.		
13 AK15615	Petersburg D-5 quadrangle 56°47.64'N., 133°21.57'W.	Not designated.	6, 6.5, mi- nor 5.5, 7	Permian-Triassic
14 AK15616	Petersburg D-5 quadrangle 56°47.57'N., 133°21.48'W.	Not designated. Barren.		
15 AK15617	Petersburg D-5 quadrangle 56°47.55'N., 133°21.35'W.	Not designated.	5.5-6.5	Early Permian-early Late Triassic
16 AK15618 (Mes. 35017)	Petersburg D-5 quadrangle 56°47.53'N., 133°21.24'W.	Likely Hyd Group.	5.5-6.5 and rare 7	late Early Triassic to early Late Triassic (late Carnian)
17 AK15970	Petersburg D-5 quadrangle 56°47.52'N., 133°20.59'W.	Not designated. Barren.		
18 AK19903	Petersburg D-5 quadrangle 56°47.8'N., 133°23.3'W.	Graphitic phyllite and argillite with limy beds. Barren.		
19 AK19904 (Mes. 35025)	Petersburg D-5 quadrangle 56°47.8'N., 133°23.1'W.	Dark-gray to black silty lime- stone; Hyd Group.	5	<i>polygnathiformis</i> Zone (latest early-earliest late Carnian)
20 AK19912 (Mes. 35026)	Petersburg D-5 quadrangle 56°47.8'N., 133°23.0'W.	Graphitic, phyllitic carbonate; Hyd Group.	5	<i>polygnathiformis</i> Zone (latest early-earliest late Carnian)
21 AK19918	Petersburg D-5 quadrangle 56° 48.0'N., 133°21.8'W.	Light-gray massive dolomite. Barren.		
22 80EK107 (27118-PC)	Petersburg D-6 quadrangle 56°54'46"N., 133°48'30"	Partly dolomitic, chert-bearing limestone; Pybus Formation.	6-6.5	very late Early Permian (late Leonardian; Kun- gurian)
23 600-Wis underground	Juneau A-2 quadrangle 58°04'07"N., 134°37'50"W.	3 samples White, massive dolomite. Bar- ren.		
24 Cliff 1	Juneau A-2 quadrangle 58°03'35"N., 134°34'03"W.	Light-gray, medium-grained do- lomite; Hyd Group. Barren.		
25 JMP-115A, 115B, and 115C	Juneau A-2 quadrangle 58°03.98'N., 134°37.12'W.	3 samples Dark-gray slate with carbonate. Barren.		
26 JMP-126	Juneau A-2 quadrangle 58°04.58'N., 134°36.77'W.	Argillite; Hyd Group. Barren.		

Appendix. Data for Permian and Triassic conodont samples from Admiralty and northern Kupreanof Islands, Alaska.—Continued

[CAI, color alteration index; samples collected by Greens Creek and U.S. Geological Survey personnel. See figs. 7 and 8 for Permian and Triassic conodont zonation and range of biostratigraphically useful collections; colln., collection]

Locality no., field no., and USGS Colln. no.	Location	Lithology and stratigraphic unit	CAI	Age
27 Drill core PP-365 (260-67 ft)	Juneau A-2 quadrangle 58°04.06'N., 134°37.55'W.	Massive dolomitic argillite; Hyd Group. Barren.		
28 Drill core PP-365 (287-303 ft)	Juneau A-2 quadrangle 58°04.06'N., 134°37.55'W.	2 samples Massive dolomitic argillite; Hyd Group. Barren.		
29 Drill core PS-97 (335-53; 360- 66; 371-376 ft)	Juneau A-2 quadrangle 58°04.39'N., 134°37.68'W.	3 samples Likely Hyd Group. Barren.		
30 Drill core PS-108 (from 173- 1161 ft)	Juneau A-2 quadrangle 58°04.23'N., 134°37.58'W.	14 samples Hyd Group. Barren.		
31 Drill core PS116 (763 ft)	Juneau A-2 quadrangle 58°04'57"N., 134°37'50"W.	Medium-gray, fossiliferous (pelmatozoan ossicles and other indeterminate bio- clasts), calcareous dolomite. Barren.		

Radiogenic Isotopic Characterization and Petrogenesis of Host Rocks to the Greens Creek Deposit

By Wayne R. Premo and Cliff D. Taylor

Chapter 12 of

Geology, Geochemistry, and Genesis of the Greens Creek Massive Sulfide Deposit, Admiralty Island, Southeastern Alaska

Edited by Cliff D. Taylor and Craig A. Johnson

Professional Paper 1763

**U.S. Department of the Interior
U.S. Geological Survey**

Contents

Abstract.....	339
Introduction.....	339
Geology.....	341
Sampling.....	346
Results	347
Degree of Stability of the Isotopic Systematics	347
Initial Lead, Strontium, and Neodymium Isotopic Systematics of Greens Creek Host-Rock Lithologies.....	352
Metabasalts.....	354
Metagabbros	355
Phyllites	356
Argillites.....	358
Serpentinites.....	358
Crosscutting Diabases — Diorites	359
Discussion.....	359
Geologic Framework at Greens Creek	359
Petrotectonic Environment of the Greens Creek VMS Deposit	360
Initial Lead Isotopes of Greens Creek Host Rocks Compared to Ore Lead Compositions.....	360
Summary.....	363
Acknowledgments.....	363
References.....	363

Figures

1. Generalized map of terranes boundaries (bold lines) and major volcanogenic massive sulfide prospects southeast Alaska, showing the locations of the Late Triassic-age VMS deposits, including Greens Creek (#10), Pyrola (#11), and Gambier Bay (#19) on Admiralty Island.....340
2. $^{206}\text{Pb}/^{204}\text{Pb} - ^{207}\text{Pb}/^{204}\text{Pb}$ correlation diagram showing the distribution of lead isotopic compositions (fields) for Alaskan volcanogenic massive sulfide (VMS) occurrences compared to model lead evolution curves (“upper crust,” “orogene,” and “depleted mantle”)342
3. Simplified geologic map of Admiralty Island, showing locations for Greens Creek and Pyrola deposits, Gambier Bay, Windfall Harbor, the Mansfield Peninsula, and Staunch Point.....343
4. Stratigraphy of the Greens Creek section, Admiralty Island, showing the orebody at the contact between footwall phyllites and hanging-wall argillites344
5. Map of surface sampling sites at and near Greens Creek mine, Admiralty Island345
6. (A) Geologic cross section, Greens Creek mine.....346
6. (B) Predeformation, cross-sectional model, Greens Creek deposit, based on drill-core logging and underground and surface mapping.....347

7. (A) Plot of uranium (U) concentration versus calculated initial $^{206}\text{Pb}/^{204}\text{Pb}$ at 215 Ma for whole-rock analyses of major Greens Creek host rocks, illustrating the possible isotopic disturbance of some whole-rock samples, probably during alteration.....	348
8. A comparison of calculated initial $^{206}\text{Pb}/^{204}\text{Pb}$ versus initial ϵ_{Nd} for whole-rock analyses from Greens Creek host rocks at 90 Ma	350
9. A comparison of the samarium-neodymium isotopic systematics of Greens Creek host rocks to Hyd Group metabasalt and Gallagher Ridge metagabbro isochrons, showing the extent of isotopic stability or variation within the different lithologic units.....	352
10. Pb-Pb correlation diagram ($^{206}\text{Pb}/^{204}\text{Pb}$ versus $^{207}\text{Pb}/^{204}\text{Pb}$) showing the distribution of initial lead compositions of Greens Creek host rocks relative to model lead evolution curves and fields for modern petrotectonic environments.....	353
11. Pb-Pb correlation diagram ($^{206}\text{Pb}/^{204}\text{Pb}$ versus $^{208}\text{Pb}/^{204}\text{Pb}$) showing the distribution of initial lead compositions of Greens Creek host rocks relative to model lead evolution curves and fields for modern petrotectonic environments.....	354
12. Initial strontium versus initial neodymium correlation diagram showing the distribution of initial Sr-Nd values for Greens Creek host rocks relative to model Sr-Nd fields for modern petro-tectonic environments	356
13. Initial lead versus initial neodymium correlation diagram showing the distribution of initial Pb-Nd values for Greens Creek host rocks relative to model lead-neodymium fields for modern petrotectonic environments	357
14. Initial strontium versus initial neodymium correlation diagram showing the distribution of initial Sr-Nd values for Greens Creek host rocks relative to Sr-Nd fields for previously published Alexander and Gravina terrane rocks	361
15. Pb-Pb correlation diagram ($^{206}\text{Pb}/^{204}\text{Pb}$ versus $^{207}\text{Pb}/^{204}\text{Pb}$) showing the distribution of initial lead compositions of Greens Creek host rocks relative to lead isotopic compositions for Greens Creek sulfides (ore).....	362

Radiogenic Isotopic Characterization and Petrogenesis of Host Rocks to the Greens Creek Deposit

Wayne R. Premo¹ and Cliff D. Taylor¹

Abstract

Samples representing the major host and adjacent lithologies at the Greens Creek deposit, Admiralty Island, were analyzed for their uranium-thorium-lead (U-Th-Pb), rubidium-strontium (Rb-Sr), and samarium-neodymium (Sm-Nd) isotopic systematics in order to provide petrogenetic information. A multisystematic procedure from a single-aliquot dissolution of whole-rock powders provided direct correlation of the isotopic systems in order to (1) characterize the tectonic environment(s) in which these rocks formed and provide a setting for the production of the Greens Creek style mineralization; (2) compare to other radiogenic isotopic results from various Upper Triassic rock suites throughout southeastern Alaska; and (3) compare with lead isotope data from Greens Creek ore (chap. 10) to determine the relationship of ore to host rock. The same set of isotopic data was evaluated for geochronologic purposes in chapter 11.

Initial Nd compositions at 215 Ma (average age for host rocks) of metabasalts and metagabbros varied between $\epsilon_{Nd} = +4$ to $+9$; whereas, initial $^{206}\text{Pb}/^{204}\text{Pb}$ and $^{87}\text{Sr}/^{86}\text{Sr}$ isotopic compositions at 215 Ma for the same suite of samples ranged from 18.45 to 18.92, and from 0.7037 to 0.7074, respectively, and are more enriched than mid-ocean ridge basalt values. These isotopic results are indicative of oceanic magmatic arcs environments and consistent with their derivation from a mostly depleted source(s) at about 215 Ma. Although initial Pb values from phyllite samples mimic those of the metabasaltic rocks, initial Sr and Nd values of phyllites are bimodal, some with $\epsilon_{Nd} = +8$, others with values at $+2$. Argillites have lower initial Nd (ϵ_{Nd} about -2 to $+2$), higher initial $^{206}\text{Pb}/^{204}\text{Pb}$ (18.4 to 19.0), and higher $^{87}\text{Sr}/^{86}\text{Sr}$ (0.705 to 0.707) than other host rocks, values that are typical for shales. These values suggest that the argillites contain some proportion of older, slightly more radiogenic crust. In general, initial Nd-Sr isotopic values for Greens Creek host rocks are comparable to previously published data from samples of the Alexander and Gravina terranes.

These radiogenic isotopic systematics indicate a progressively depleting source for the Upper Triassic Greens Creek rocks, suggesting a rift setting. The oldest argillites have slightly depleted signatures (ϵ_{Nd} about $+1.5$), that are unconformably overlain by a sequence of metabasalts that exhibit

depleted, island-arc-type isotopic signatures ($\epsilon_{Nd} = +4$ to $+5$ with elevated $^{87}\text{Sr}/^{86}\text{Sr}$ and $^{206}\text{Pb}/^{204}\text{Pb}$). The metabasalts are then unconformably overlain by conglomerate, dolomite, and more argillites of the Hyd Group. The Hyd Group argillites have slightly depleted to slightly enriched ϵ_{Nd} between -5 and $+2$, indicating the incorporation of some older, more enriched crustal material. The lower metabasaltic sequences are intruded by ultramafic sills and stocks, represented now as highly altered serpentinites that exhibit a wide range of isotopic signatures (ϵ_{Nd} between -12 and $+8$). Subsequent mafic volcanism and gabbroic plutonism are characterized by more depleted source signatures ($\epsilon_{Nd} = +5$ to $+9$). Hyd Group basalts that cap the Triassic section have even more depleted signatures ($\epsilon_{Nd} = +8$ to $+9$). This progressive sequence of least to most depletion implies opening of preexisting crust in a rift setting, probably within an oceanic arc environment.

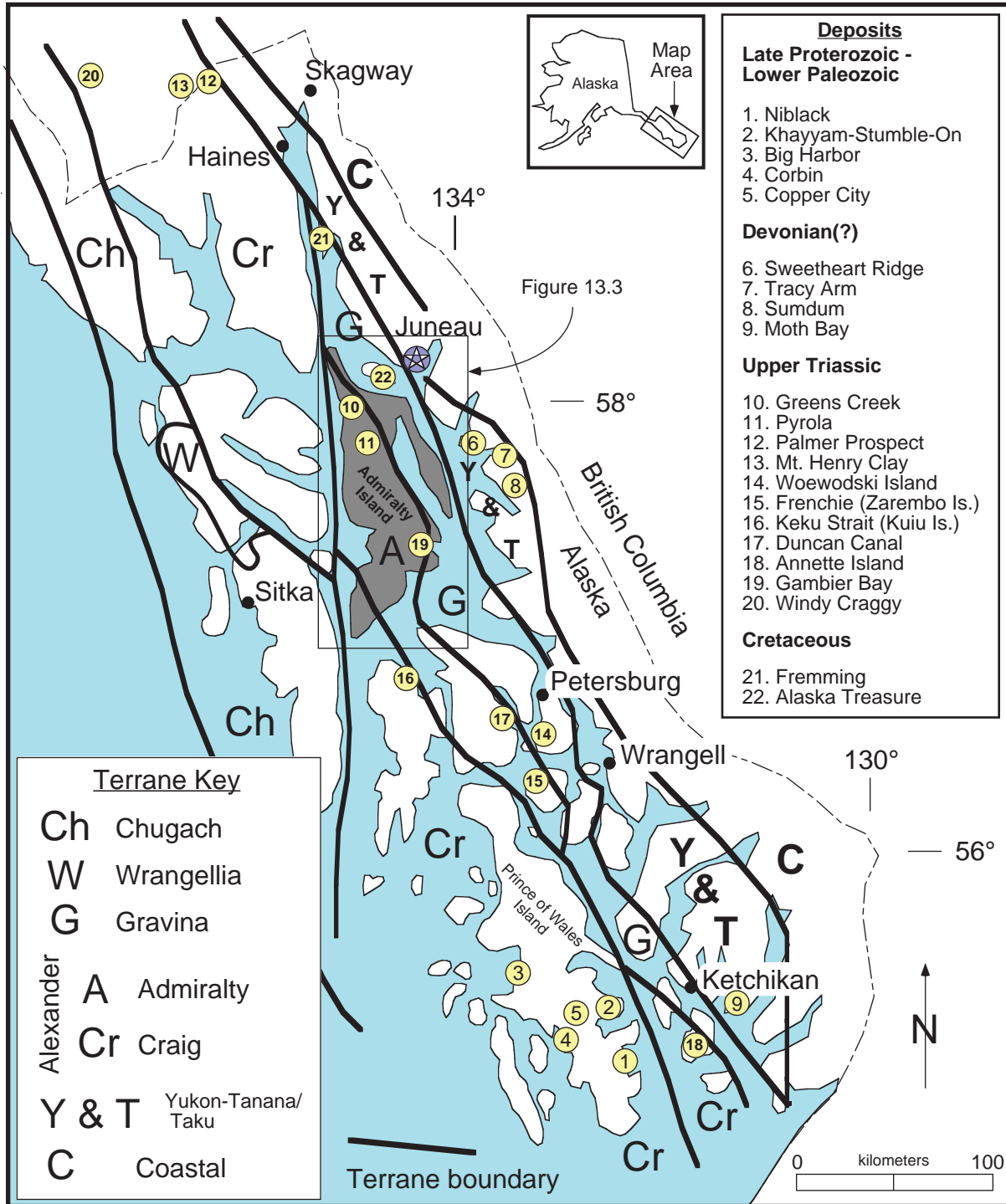
Initial Pb isotopic compositions of Greens Creek host rocks for the most part are not the same as Pb isotopic compositions for Greens Creek galena and other sulfides. However, it is evident that the relatively uniform ore Pb signature may represent a homogenization of Pb derived mainly from host basalt and gabbro, but also including some Pb from hanging-wall argillites, a Pb isotopic trend similar to those documented for volcanogenic massive sulfides (VMS) from modern rift zones and island-arc sequences.

Introduction

Volcanogenic massive sulfide (VMS) deposits are found in many locations and occurrences around the Pacific rim and particularly in Alaska. Their ages and styles vary somewhat, but most in Alaska are thought to originate in or near oceanic island-arc or rift-related settings (Newberry and others, 1997; Newberry and Brew, 1997). The ages for most of the VMS deposits of southeastern Alaska (fig. 1), and particularly within the Alexander terrane, are thought to be the same as their host rock sequences, such that the ore is syngenetic. In general, however, precise ages of mineralization are scarce. In approaching an age and origin for VMS deposits, particularly Greens Creek, radiogenic isotopic systems can be invaluable.

Radiogenic isotopic systems (U-Pb, Th-Pb, Sm-Nd, Rb-Sr, K-Ca, ^{40}Ar - ^{39}Ar , and Re-Os) can be and have been used

¹U.S. Geological Survey, Denver, Colorado.



for shedding light on the source(s) of mineralizing fluids (for example, Allegre and Luck, 1980; DePaolo, 1981; Zartman and Doe, 1981; Burke and others, 1982; Fehn and others, 1983; Zartman, 1984; Hart and Kinloch, 1989; Lambert and others, 1989; Walker and others, 1991; Kerrick, 1991; Martin, 1991; Ayuso and others, 2004). Previous radiogenic isotopic work on Greens Creek and other Late Triassic age VMS deposits of Alaska include lead (Pb) isotopic data of various sulfides, including galena, pyrite, and chalcopyrite (compiled in Gaccetta and Church, 1989, and references within; Newberry and Brew, 1997), and Rb-Sr and(or) Sm-Nd isotopic data from a variety of lithologic units from the Alexander, Stikine, Wrangellia, Gravina, and Taku terranes as well as samples from the Coast Mountains batholith (Samson and others, 1989, 1990, 1991a, 1991b).

An accurate yet simplistic interpretation of the Pb isotopic data for Alaskan VMS ore deposits including Greens Creek is discussed in Newberry and others (1997). These authors suggested that Pb isotopic compositions on sulfides from Alaskan VMS deposits are mixtures of mantle and crustal endmembers that exhibit apparent young model lead ages for ore deposition (fig. 2). Because crustal Pb compositions are typically more radiogenic (enriched ^{206}Pb) than mantle Pb compositions, the sulfide Pb isotopic compositions from various VMS deposits plot beyond the model-Pb evolution isochron at their actual ages. For example, Greens Creek and Pyrola ore Pb plots along the 0-Ma model lead isochron, although these deposits are constrained to have occurred in the Late Triassic (chap. 11). Other deposits exhibit Pb isotopic fields corresponding to futuristic model lead ages (for example, Mt. Henry Clay and Kuiu; figs. 1 and 2). This effect is thought to be the result of mixing between radiogenic crustal Pb and depleted mantle Pb in the source(s) prior to ore deposition. Mixing of these components might occur as continental crustal detritus is subducted beneath ore-producing oceanic island arcs. Whereas it is obvious that Pb isotopic data should not be used for model age determinations, they do hold promise in helping to identify possible source(s) for ore metals.

This explanation for radiogenic Pb signatures is testable using correlated Pb-Sr-Nd isotopic systematics from syngenetic, host-rock lithologies, isotopic signatures that should indicate to what degree crustal source(s) were involved in ore-forming processes as well as help delineate petroTECTONIC origins of various Phanerozoic allochthonous terranes of southeastern Alaska.

Greens Creek is located at the edge of the Alexander and Gravina Belt terranes (#10 in fig. 1), both of early Paleozoic to Jurassic-Cretaceous age. Positive initial ϵ_{Nd} (0 to +9) and low initial $^{87}\text{Sr}/^{86}\text{Sr}$ (0.7028 to 0.7071) isotopic values from volcanic, plutonic, and metasedimentary samples from these two terranes indicate that they were derived mainly from depleted mantle sources (Samson and others, 1989, 1991a) and were interpreted to represent Paleozoic island-arc terranes. Likewise, Sr-Nd isotopic data from samples of the adjacent Wrangellia terrane indicated a largely juvenile, mantle-derived

arc terrane with less than 6 percent Proterozoic crustal input (Samson and others, 1990).

In this chapter, we use several different radioactive decay schemes (U-Pb, Th-Pb, Rb-Sr, and Sm-Nd) to isotopically characterize in detail the host/source rocks of the Greens Creek ore deposit in order to better understand their petroTECTONIC derivation and provide a geologic framework and tectonic setting that produced sulfide deposition. Radiogenic isotopic signatures can further provide clues toward source(s) of ore-forming metals and fluids, helping to develop genetic ore deposit models and aid in the classification and prediction of known and potential deposits.

Geology

The geology at Greens Creek has been covered in detail in other chapters of this volume. Only a brief outline of the geology of the major host/source rocks that have been sampled is included here.

Greens Creek mine is 29 km south of Juneau, in the southeastern coastal region of Alaska, near the northern end of Admiralty Island (figs. 1 and 3). The deposit is located in an 800-km-long belt of volcano-sedimentary rocks interpreted to represent a rift-fill sequence formed during a brief period of intra-arc or back-arc rifting in latest Triassic time (Berg and others, 1972; Taylor, 1997; Taylor and others, 1995a, 1995b, 1999, 2000). Stratigraphy within the belt consists of a 200- to 800-m-thick sequence of conglomerates, limestones, marine clastic sediments, and tuffs that are intercalated with and overlain by a distinctive unit of mafic pyroclastics and pillowed flows (figs. 3 and 4). Faunal data bracket the age of the host rocks between early Carnian (early Late Triassic) and late Norian (late Late Triassic) time (fig. 4 and fig. 5, chap. 11).

At Greens Creek, the stratigraphy includes a Permian-age, siliceous to cherty argillite in the upper part of the Cannery Formation that is unconformably overlain by a sequence of metabasalts of unknown age (fig. 4). These metabasalts are variably metamorphosed at greenschist to amphibolite grade and subsequently altered during hydrothermal metasomatism (for example, Newberry and others, 1990), resulting in several types of phyllitic rocks. Geochemical signatures of many of these phyllites are not conclusive but are consistent with basaltic protoliths, either as a rift-related basalt produced in an intra-arc setting or as a fairly unfractionated calc-alkaline basalt formed in an oceanic volcanic arc. The arc-related signatures probably could be indicative of variable amounts of assimilation of preexisting island-arc crust.

These metabasalts are unconformably overlain by a thin, discontinuous polymictic conglomerate (fig. 4). Such conglomerates are found throughout the southern and middle portions of the Upper Triassic volcano-sedimentary belt at the base of most sections, indicative of high-energy deposition in a near slope or basin margin setting. Although thin and discontinuous conglomerate horizons occur in the northern half of Admiralty Island, their stratigraphic positions within

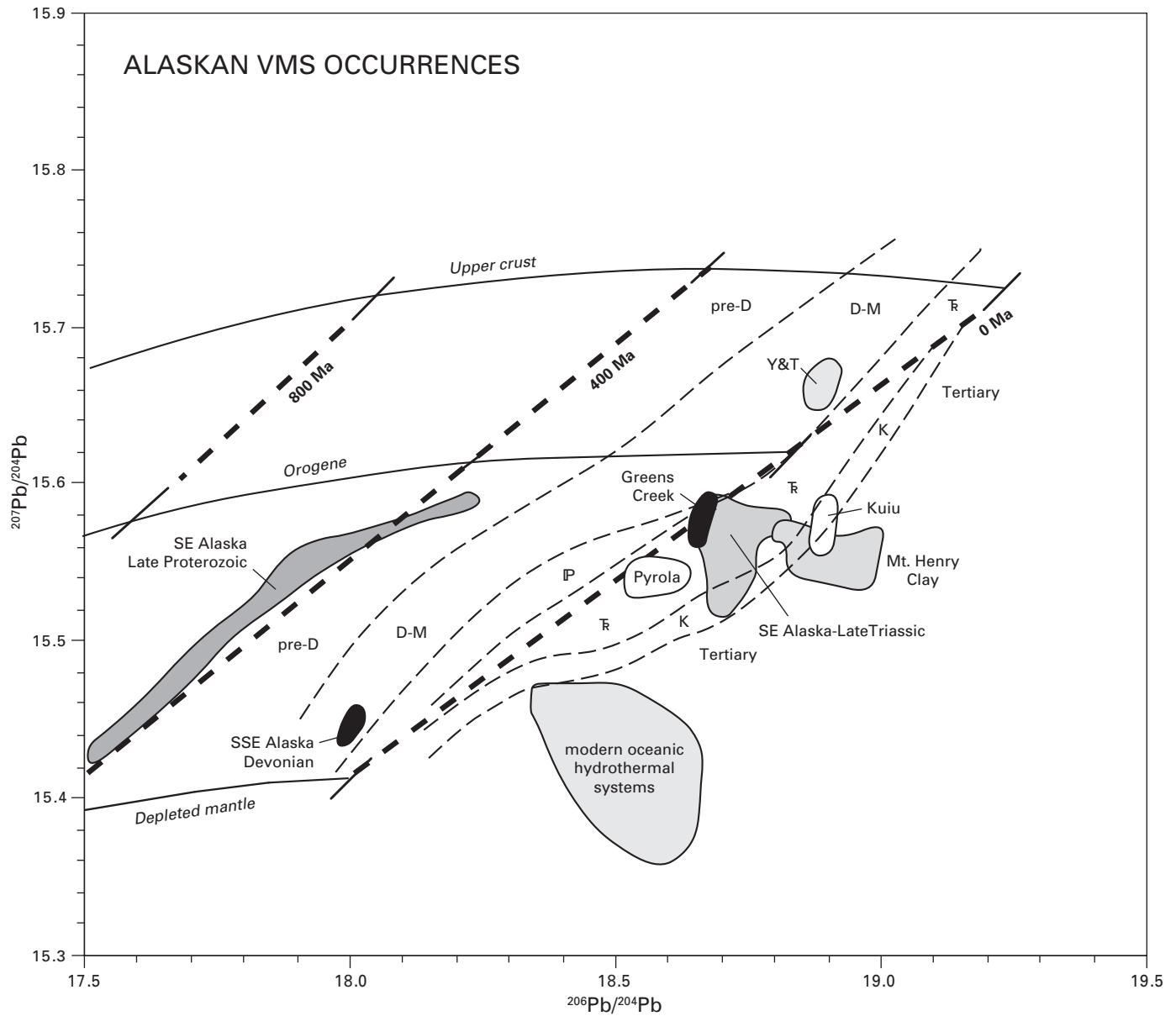
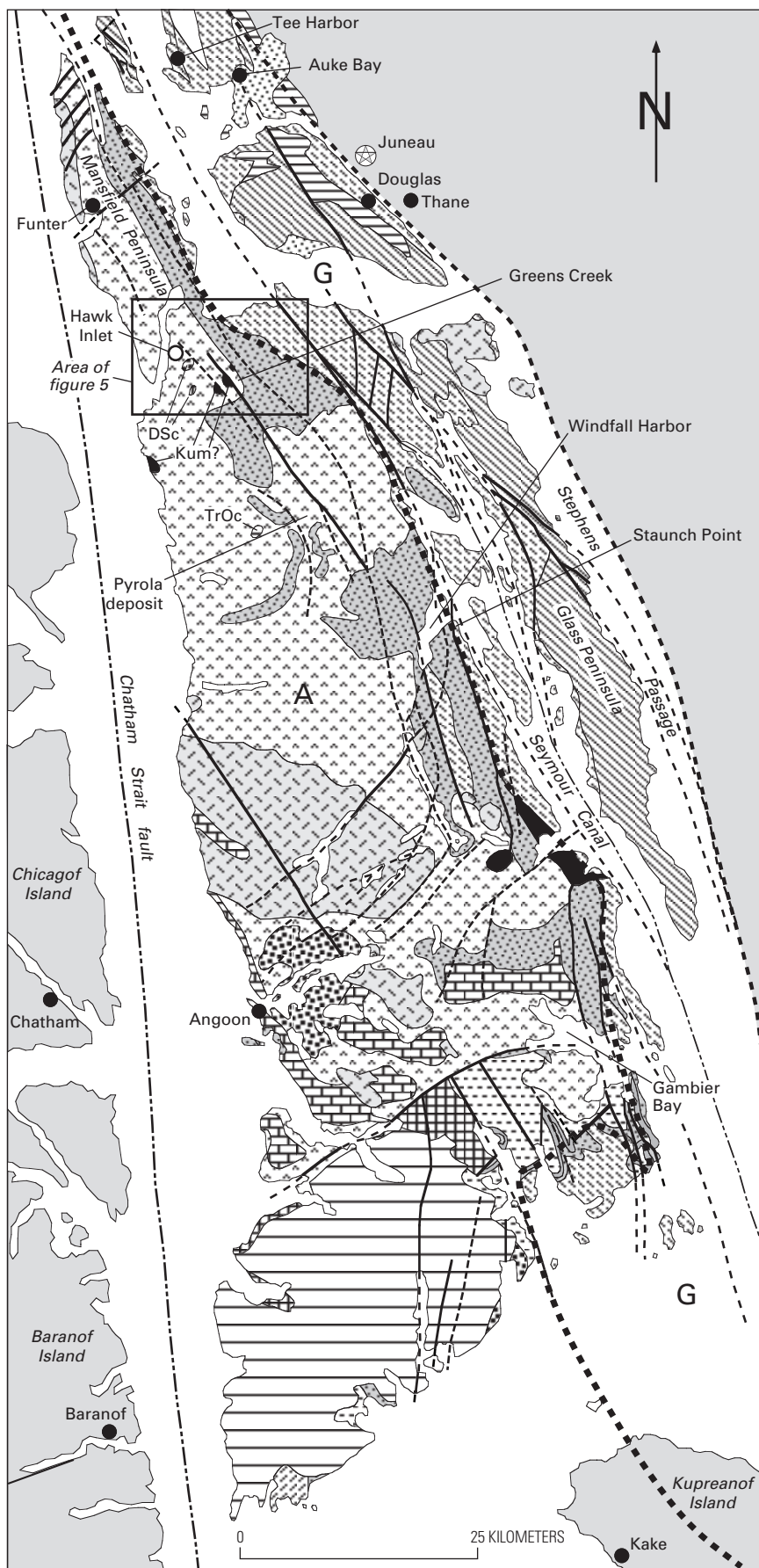


Figure 2. $^{206}\text{Pb}/^{204}\text{Pb} - ^{207}\text{Pb}/^{204}\text{Pb}$ correlation diagram showing the distribution of lead isotopic compositions (fields) for Alaskan volcanogenic massive sulfide (VMS) occurrences compared to model lead evolution curves ("upper crust," "orogene," and "depleted mantle") of Zartman and Doe (1981). Greens Creek ore compositions lie near other Late Triassic deposits such as Pyrola, Kuiu, and Mt. Henry Clay (modified from Newberry and others, 1997), at model lead ages (isochrons shown as bold dashed lines) younger than the actual age of mineralization (separated by lighter dashed lines and labeled; D = Devonian, D-M = Devonian to Mississippian, IP = Pennsylvanian, T = Triassic, K = Cretaceous). Y & T indicates the location of lead isotopic results from ores of the Yukon-Tanana/Taku terrane.



EXPLANATION

- Quaternary surficial sediments
- Tertiary volcanic rocks
- Tertiary sedimentary rocks
- Cretaceous granitoids
- Cretaceous ultramafic rocks
- Cretaceous-Jurassic sedimentary rocks
- Cretaceous-Jurassic volcanic and sedimentary rocks
- Cretaceous-Jurassic volcanic rocks
- Triassic-Permian sedimentary and volcanic rocks, undifferentiated
- Triassic-Ordovician sedimentary and volcanic rocks, undifferentiated
- Triassic-Ordovician carbonate rocks, undifferentiated.
- Permian sedimentary rocks
- Permian carbonate rocks
- Devonian-Silurian carbonate rocks
- Silurian sedimentary rocks
- Silurian-Ordovician sedimentary rocks
- Other rocks
- Major fault
- Inferred fault trace
- Terrane boundary

Figure 3. Simplified geologic map of Admiralty Island, showing locations for Greens Creek and Pyrola deposits, Gambier Bay, Windfall Harbor, the Mansfield Peninsula, and Staunch Point (locations of some whole-rock samples). Bold dotted line is approximate boundary between the Alexander (A) and Gravina (G) terranes (after mapping by Gehrels and Berg, 1992).

the Triassic stratigraphy are uncertain and in most cases are thought to be above the base of the section within the shales that compose the middle sedimentary portion of the Triassic stratigraphy. The northernmost occurrence of a conglomerate “marker horizon” at the base of the section is on the eastern shore of Windfall Harbor (fig. 3) immediately overlying the siliceous black shales of the Cannery Formation.

Thin carbonate beds lie just below and intercalated with the capping Hyd Group basalts and are intercalated with the shales (argillites). North of Admiralty Island, limestones appear to be absent from the section.

Serpentinities are clearly produced by alteration of an ultramafic protolith and probably represent the shallow intrusive sources to the primitive basalt protoliths or to the overlying Hyd Group mafic volcanic flows. Many of these serpentinite bodies were probably cumulates left after extraction of mafic melts. These serpentinites crosscut the older metabasalt and phyllite sequences as well as the basal conglomerate horizon (figs. 3 and 4). Gabbro-clinopyroxenite, both relatively fresh and highly quartz-carbonate-fuchsite-altered serpentinite, is a common outcrop occurrence in the mine area. It is likely that the footwall phyllite pile originally consisted of a composite mafic-ultramafic collection of massive to volcanoclastic textured volcanics.

These mafic/ultramafic rocks are in turn overlain by massive and slaty graphitic, pyritic, black argillites and by carbonate-rich dolomitic massive and slaty argillites of the Hyd Group.

Continued emplacement of basaltic magmas at shallow levels account for the common occurrence of large gabbroic sills and stocks, particularly exposed along Gallagher Ridge, south of the mine (fig. 5), and followed by mafic flows of the overlying Hyd Group (fig. 4). Continued production of heat in the immediate footwall of the deposit would similarly account for the extreme alteration of the gabbro-basalt pile by driving a hydrothermal convection system.

Diabase dikes are observed to crosscut massive ore and are, at this point, not well understood. It is likely that these dikes are the product of Jurassic-Cretaceous resumption of island-arc volcanism. The fact that they crosscut ore and the overlying argillites and themselves are mineralized with a late, precious-metal-enriched mineral assemblage brackets their age between 220 Ma and the 105- to 90-Ma mid-greenschist facies regional metamorphism.

The Greens Creek massive sulfides are located at the contact between a footwall sequence of predominantly mafic volcanic rocks and mafic-ultramafic hypabyssal sills and intrusions, and a hanging wall of black argillites (figs. 4 and 6A). With increasing proximity to ore, footwall lithologies are dominated by chlorite-phyllites, sericite-phyllites, and silicified sericite-phyllites (fig. 6B). Footwall lithologies which have less consistent spatial distribution are serpentine-chlorite phyllites, mariposite-phyllites, and rarely, recognizable gabbros and post-ore diabase dikes. Hanging-wall rocks are dominated by massive and slaty graphitic, pyritic, black argillites and by carbonate-rich dolomitic massive and slaty argillites. Three

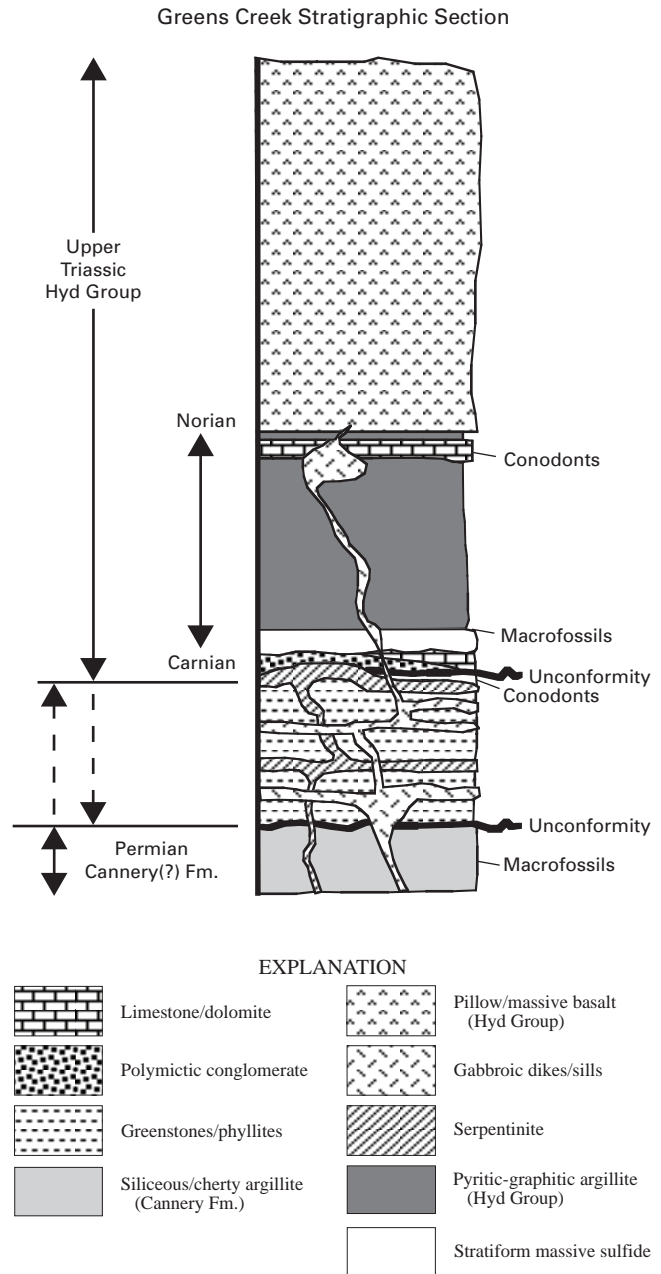
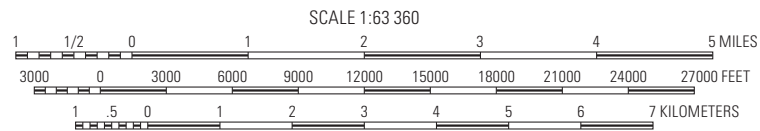


Figure 4. Stratigraphy of the Greens Creek section, Admiralty Island, showing the orebody at the contact between footwall phyllites and hanging-wall argillites (after Taylor and others, 2000).



Figure 5. Map of surface sampling sites at and near Greens Creek mine, Admiralty Island. Single-numbered locations are from the 97-LG series (for example, "82" is the location of 97-LG-82, and so forth). PF-series (-09 and -18) are from the Portal Face. Topographic map compiled from USGS Juneau A3 and A2 1:63,360 scale, 1997.



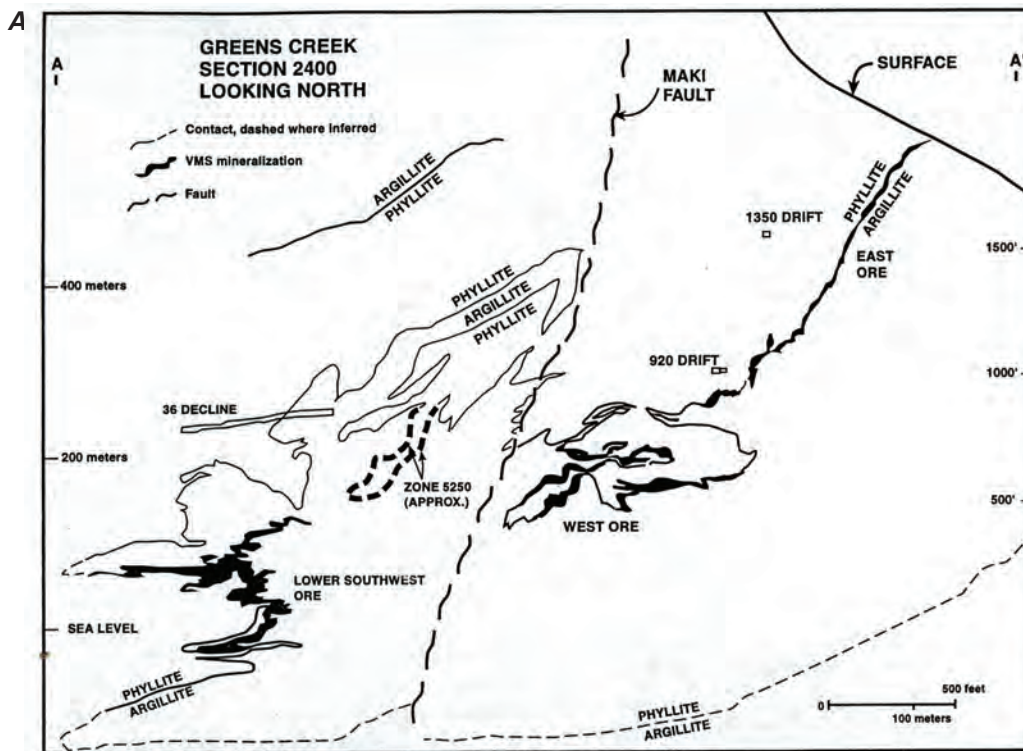


Figure 6. (A) Geologic cross section, Greens Creek mine. Courtesy of T. Hall, senior mine geologist, Kennecott Greens Creek Mining Co., 1995. VMS = volcanogenic massive sulfide (after Newberry and others, 1997), showing the orebody at the contact between footwall phyllites and hanging-wall argillites. Locations are shown for East, West, and the Southwest orebodies where samples of sulfides, host rocks, and alteration minerals for Ar–Ar work were collected.

major contiguous orebodies lie along a single horizon marked by a footwall greenschist and a hanging wall composed of graphitic, pyritic, black argillite. Ores are zoned from silica-, carbonate-, and barite-rich white ores against the footwall, to massive pyritic, and then to base-metal-rich massive sulfide-rich ores against the hanging wall (fig. 6).

Sampling

Ore deposits form from mineralizing fluids that have passed through a sequence of rocks and therefore have had some contact with various lithologies of differing geochemical signatures and isotopic compositions. The result is very likely a mixture of several components. Geochemical and isotopic data for the host/source rocks are therefore critical toward a clear interpretation of the isotopic signature of the ore. In addition, identification of multiple fluids and ore-forming stages can be crucial to evaluating the isotopic information.

Certain geologic conditions can unequally disrupt the stability and therefore the reliability of isotopic results. For example, elemental mobility through alteration and/or metamorphism, can fractionate parent-daughter ratios and disturb the isotopic systematics. In general, a hierarchy of stability during

metamorphism is recognized: Sm–Nd > U–Pb > Rb–Sr; however, extreme alteration can greatly affect any of the systematics.

Consequently, radiogenic isotopic systematics of altered rocks are often disturbed, yielding results that are not easily interpretable — interpretations that are necessary for distinguishing between syndepositional, tectonic, magmatic, or hydrothermal processes. Therefore, careful sampling of both ore and host/source rock is a critical aspect for the successful use of radiogenic isotopic systems on ore deposits.

With these possible difficulties in mind, only the best preserved and most representative samples (listed in table 3, chap. 11) were carefully selected from several hundred other samples for this multisystematic isotopic analysis. U–Th–Pb, Rb–Sr, and Sm–Nd isotopic data from whole-rock powders and mineral separates were collected from Greens Creek host rocks and related units that include (1) a variety of argillites, both from the Cannery Formation and the Hyd Group, collected from inside and outside the mine; (2) various metabasalts including some from the Gambier Bay Formation and the Hyd Group; (3) various metagabbroic to ultramafic intrusives (serpentinites) of Late Triassic age, some perhaps slightly older or younger; (4) associated chloritic to sericitic phyllites that probably represent altered mafic volcanic rocks (Newberry and others, 1990), collected from inside and outside the mine proper; and (5) several crosscutting diabasic to dioritic intrusives of unknown age.

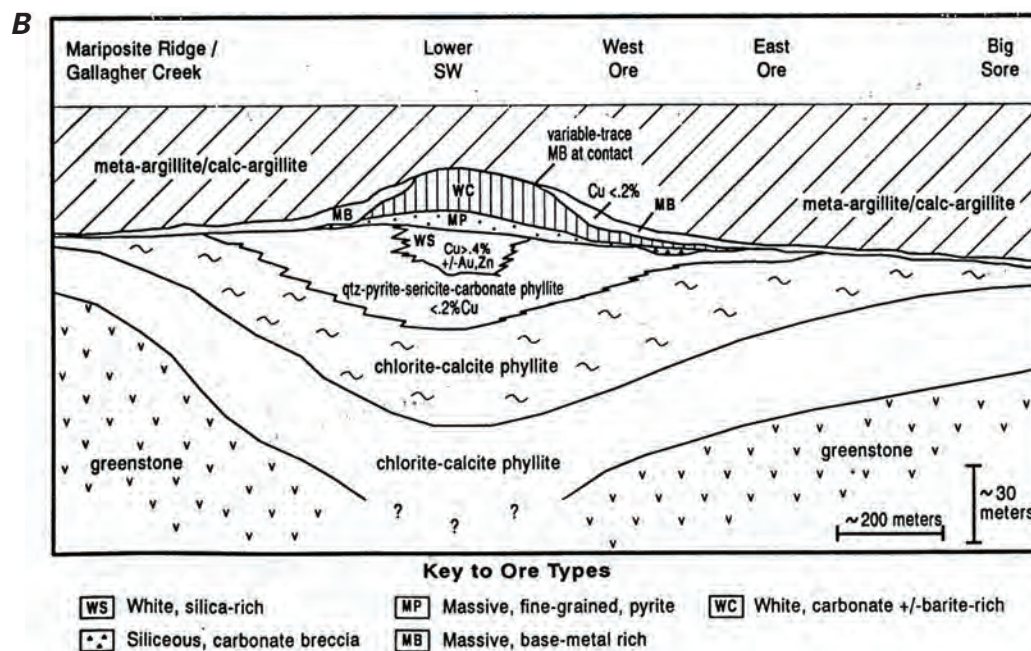


Figure 6. (B) Predeformation, cross-sectional model, Greens Creek deposit, based on drill-core logging and underground and surface mapping (Rainer Newberry, unpub. mapping, 1985–1994; after Newberry and others, 1997), again showing the orebody (mainly MB and MP) at the contact between footwall phyllites and hanging-wall argillites, but also the distribution and relationship of several types of footwall phyllites within the alteration zone of the mine area (see table 3 in chapter 11 for whole-rock sample designations).

Surface sampling sites around the Greens Creek mine are shown in figure 5; mine sample locations are more problematic and are simply stated in table 3 in chapter 11. Locations of samples from other parts of Admiralty Island are not shown but generally given in table 3, chapter 11, by their geographic location (for example, Gambier Bay, Pyrola, Staunch Point). Also, for the full names of samples used for whole-rock isotopic work, the reader is directed to tables 3 through 6, chapter 11, as many of the sample names have been shortened in this text and in the figures by removing the front numbers corresponding to their year of collection (for example, LG-71 in the text is actually 97–LG-71 in the tables).

Results

The data were produced in order to calculate initial Pb-Sr-Nd isotopic compositions that can be compared with known, time-integrated, isotopic fields from different petrotectonic environments. This exercise is intended to delineate the geologic framework and tectonic setting in which Greens Creek and possibly other VMS deposits of southeastern Alaska were formed as well as to contribute to the growing isotopic database for such rocks for use in the scientific community at large. The U-Pb, Rb-Sr, and Sm-Nd isotopic data are

given in tables 4 through 6 in chapter 11, where the same data were evaluated for geochronologic purposes.

The analytical techniques used for the simultaneous, single-dissolution of U-Th-Pb, Rb-Sr, and Sm-Nd analysis on whole-rock and mineral separates were similar to those reported by Tatsumoto and Unruh (1976) and Premo and Tatsumoto (1991, 1992) and are given in detail in chapter 11.

Degree of Stability of the Isotopic Systematics

There is some concern as to whether the isotopic systematics of these whole rocks, which have certainly been altered to some degree (table 3 in chap. 11), have remained stable or undisturbed. The processes of alteration involve mobilization of certain elements, and it is probable that elemental concentrations as well as their corresponding Pb-Sr-Nd isotopic compositions are to some degree disturbed in some samples. However, we expect that the Sm-Nd systematics are less affected than the more mobile and volatile Rb-Sr and U-Pb systematics (for example, Whitehouse, 1988; Barovich and Patchett, 1992).

There is no way to absolutely ascertain to what degree any particular isotopic system is undisturbed or overprinted without fresh, unaltered samples to compare. However, we expect that varying degrees of alteration should reflect the

relative stability of their isotopic systematics. For example, the least-altered samples are the Hyd Group metabasalts from Gambier Bay (fig. 3) and their isotopic systematics are arguably the best preserved and are used to construct several isochron ages (chap. 11). In contrast, the isotopic systematics of highly altered serpentinites vary widely, and little confidence can be held for these results.

In an attempt to evaluate the degree of isotopic disturbance, uranium concentration in parts per million (ppm) is plotted against calculated initial $^{206}\text{Pb}/^{204}\text{Pb}$ values at 215 Ma (taken to be an average estimate of the age of the host-rock strata at Greens Creek; chap. 11) and Rb (ppm) against calculated initial $^{87}\text{Sr}/^{86}\text{Sr}$ values (fig. 7). Because we have defined an isochron age of 218 ± 16 Ma and initial $^{206}\text{Pb}/^{204}\text{Pb}$ value of 18.515 for the Hyd Group metabasalts (chap. 11), this value is taken to represent the Greens Creek host-rock initial lead signature to which all other initial values can be compared (fig. 7A). In addition, the majority of sulfide lead (mainly galena) from the Greens Creek deposit defines a $^{206}\text{Pb}/^{204}\text{Pb}$ isotopic composition of 18.64 ± 0.01 that we interpret to represent that of the mineralizing fluid that probably altered many of the host rocks. Therefore, samples that yielded initial $^{206}\text{Pb}/^{204}\text{Pb}$ values outside of the 18.515 to 18.640 range are suspected of either having some subsequent open-system isotopic disturbance or derivation from a distinctly different isotopic source. In some cases, the calculated initial $^{206}\text{Pb}/^{204}\text{Pb}$ values are unreasonably low such that the addition of uranium or loss of lead during subsequent alteration is suspected (for example, LG-71 and ADM-01; fig. 7A). In some other cases where the calculated initial $^{206}\text{Pb}/^{204}\text{Pb}$ values are significantly higher than 18.64, the addition of lead with a more radiogenic composition is suspected. This situation is reasonable as nearby Cretaceous-Tertiary ore $^{206}\text{Pb}/^{204}\text{Pb}$ signatures are between 19.1 and 19.5 (discussed herein and also in chapter 10) and certainly could have been involved in a partial resetting of the lead isotopic composition of some lithologies (for example, some Hyd Group argillites and sample GST; fig. 7A).

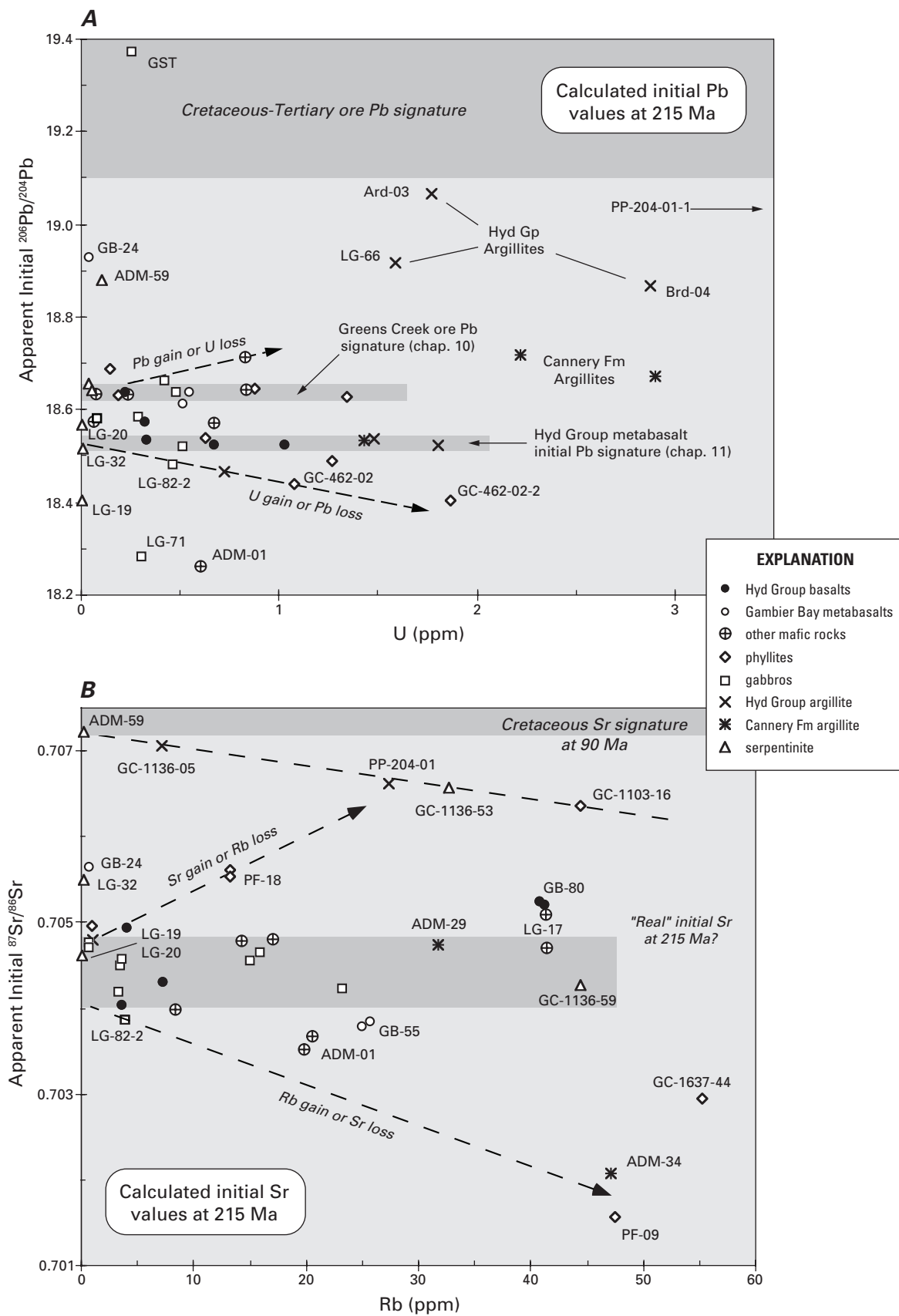
A similar situation can be made in the case of rubidium concentration (ppm) versus calculated initial $^{87}\text{Sr}/^{86}\text{Sr}$ values (fig. 7B). The majority of least-altered mafic samples (for example, Hyd Group metabasalts and metagabbros at Gallagher Ridge) define a range of initial $^{87}\text{Sr}/^{86}\text{Sr}$ values between 0.7038 to 0.7048 that we tentatively regard as the range of the original Greens Creek host-rock initial strontium composition. And all other samples that yielded initial strontium values outside that range, we suspect either have had some subsequent open-system isotopic disturbance or derivation from a distinctly different isotopic source. For example, samples PF-09 and ADM-34 yielded unreasonably low calculated initial $^{87}\text{Sr}/^{86}\text{Sr}$ values (less than 0.7023) and are therefore suspected of having secondary rubidium added during alteration (fig. 7B). This suspicion is reasonable as sericitization would involve alteration to micaceous minerals with the addition of potassium (K) and Rb. Other samples with “low” calculated initial $^{87}\text{Sr}/^{86}\text{Sr}$ values (less than 0.7038) may have had secondary rubidium added to lesser degrees. In cases where the calculated initial $^{87}\text{Sr}/^{86}\text{Sr}$

Figure 7 (facing page). (A) Plot of uranium (U) concentration versus calculated initial $^{206}\text{Pb}/^{204}\text{Pb}$ at 215 Ma for whole-rock analyses of major Greens Creek host rocks, illustrating the possible isotopic disturbance of some whole-rock samples, probably during alteration. The expected range of initial $^{206}\text{Pb}/^{204}\text{Pb}$ values is between 18.515 (Hyd Group metabasalt initial lead (Pb) and 18.64 (Greens Creek ore lead signature). All samples outside of this range are either isotopically disturbed or derived from distinctly different source(s). (B) Plot of rubidium (Rb) concentration versus calculated initial $^{87}\text{Sr}/^{86}\text{Sr}$ at 215 Ma for whole-rock analyses of major Greens Creek host rocks. Similar to the lead results, these strontium results possibly indicate isotopic disturbance within some whole-rock samples. The expected range of initial $^{87}\text{Sr}/^{86}\text{Sr}$ values is indicated by the least altered or best preserved Hyd Group metabasalts that indicate values between 0.7041 and 0.7049, and all samples with initial $^{87}\text{Sr}/^{86}\text{Sr}$ values outside this range are either isotopically disturbed or derived from distinctly different source(s). Ma, mega-annum. See text for further discussion.

values are significantly higher than about 0.7048, the addition of secondary radiogenic strontium is suspected. A likely source for this secondary radiogenic strontium would be seawater alteration at just about any time after formation as all seawater strontium isotopic compositions from the Triassic to the present have been more radiogenic than 0.7065 (Burke and others, 1982; Hess and others, 1986).

In another evaluation of possible alteration or contamination of some of these samples by subsequent elemental and isotopic exchange, calculated initial $^{206}\text{Pb}/^{204}\text{Pb}$ and $^{87}\text{Sr}/^{86}\text{Sr}$ values are plotted against calculated initial ϵ_{Nd} values at 90 Ma (fig. 8). This age corresponds to average ages defined by isochrons from the same isotopic data and similar to Ar-Ar isotopic data from sericite and fuchsite (chap. 11), and the age therefore represents a very likely time that some of the isotopic systems were disturbed. In figure 8A, nearly 6 of 10 argillitic and 3 of 8 metagabbroic samples yielded initial $^{206}\text{Pb}/^{204}\text{Pb}$ values at 90 Ma between 19.1 and 19.55, values that are very similar to lead isotopic compositions of Cretaceous to early Tertiary age, southeastern Alaskan ore deposits (for example, Alaska-Juneau, Ascension, Ground Hog, Perseverance, Trokna Silver, and Glacier Basin; Gaccetta and Church, 1989). These values are also very similar to those measured on the Cretaceous-Tertiary, arc-related, Valdez and Orca Group argillites and phyllites of southern Alaska (Farmer and others, 1993).

The suggestion here is that a Cretaceous-Tertiary lead signature may have overprinted several samples of argillite (ADM-29, Ard-03, PP-204-01, and Brd-04) and/or gabbro (GST, LG-69, LG-82) during the already established Cretaceous accretionary event at ca. 115 to 90 Ma (for example, Rubin and



others, 1990; Rubin and Saleeby, 1992), although alteration at any time after emplacement of these rock sequences may contribute to a disturbance of the U-Pb isotopic systematics. All of these samples yielded calculated $^{206}\text{Pb}/^{204}\text{Pb}$ values at 215 Ma outside the expected range of values (fig. 7A).

Another point of interest, six of nine phyllites and several other mafic samples exhibit calculated $^{206}\text{Pb}/^{204}\text{Pb}$ values at 90 Ma that are similar to the Greens Creek ore lead signature (fig. 8A), suggesting that the lead isotopic compositions of these samples had been overprinted during the Cretaceous. However, many of the better-preserved samples (for example, Hyd Group metabasalts and some metagabbros) yielded expected initial $^{206}\text{Pb}/^{204}\text{Pb}$ values at 215 Ma and keep a tight cluster through time (fig. 8), lending confidence to these whole-rock isotopic data.

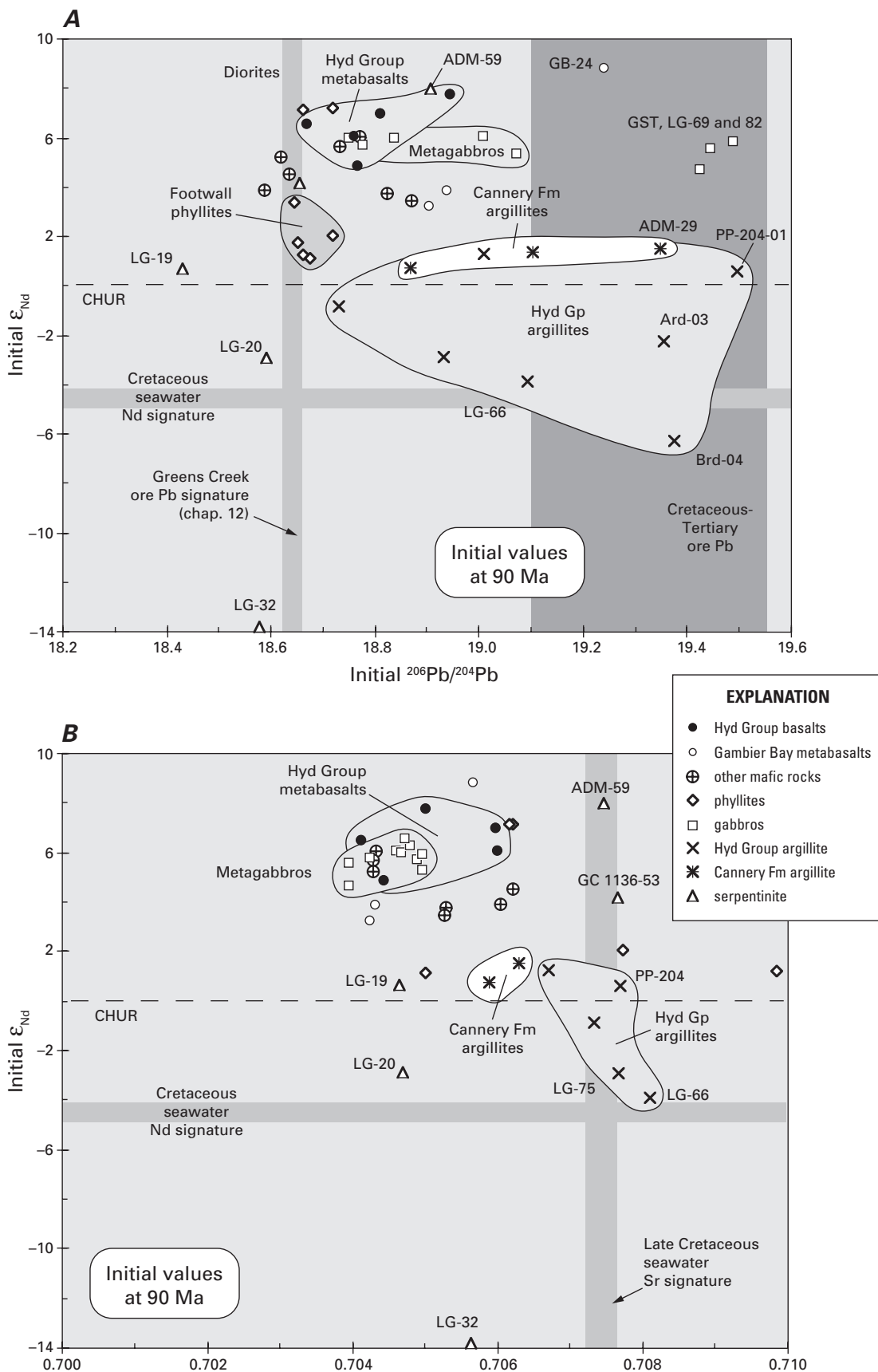
Similar to initial $^{206}\text{Pb}/^{204}\text{Pb}$ values suggestive of Cretaceous resetting, initial $^{87}\text{Sr}/^{86}\text{Sr}$ isotopic compositions for several argillites, phyllites, and serpentinites at 90 Ma (fig. 8B) are similar to the range of Late Cretaceous seawater strontium isotopic compositions (about 0.7074; Burke and others, 1982; Hess and others, 1986). Metagabbros, metabasalts, and other mafic samples appear relatively stable with initial $^{87}\text{Sr}/^{86}\text{Sr}$ values between 0.703 and 0.706, but initial strontium values for serpentinites, phyllites, and argillites vary widely, some remaining similar to those of the igneous suite, and others enriched with values near or at the Cretaceous-Tertiary seawater signature at about 90 Ma (fig. 8B). It may be coincidence that several are similar to this seawater value, but the variation would suggest some disturbance to the strontium isotopic systematics, perhaps due to Rb/Sr fractionations during alteration.

Sm-Nd isotopic systematics can be compared between lithologies and their differences evaluated — caused largely due to source differences and not because of alteration or age effects. Stability of the Sm-Nd isotopic system for some of the better-preserved samples appears to be good (fig. 9, chap. 11), and due to a fortunate spread in parent-daughter ratios, isochrons can be fitted to some of the analyses of two suites of samples. Four out of five Hyd Group metabasalt analyses define an apparent isochron age of 215 ± 95 Ma and four analyses from metagabbro samples LG-70 and LG-71 yielded an isochron age of 200 ± 27 Ma (chap. 11). Metagabbros and metabasalts have elevated $^{143}\text{Nd}/^{144}\text{Nd}$ (corresponding to initial ϵ_{Nd} values of +5.5 to 8) compared to coeval argillitic metasediments and most phyllites (less than 0.5128; initial ϵ_{Nd} = -2.5 to +4). Cannery Formation argillites yield uniform $^{143}\text{Nd}/^{144}\text{Nd}$ values at about 0.51266 (initial ϵ_{Nd} about +2.3) that contrast with Hyd Group argillites signatures (initial ϵ_{Nd} about -5 to +2.2). Serpentinites vary from very low $^{143}\text{Nd}/^{144}\text{Nd}$ (ϵ_{Nd} = -12.5; LG-32) to very high $^{143}\text{Nd}/^{144}\text{Nd}$ (ϵ_{Nd} = +8.4; ADM-59), indicating highly variable crustal to mantle source(s) for the ultramafic equivalents (fig. 9). However, because of very low Sm-Nd abundances in these samples, most of these isotopic analyses were obtained during low ion-beam intensity measurements that could produce results of questionable quality (see table 6, chap. 11). Therefore, the Sm-Nd isotopic differences in the serpentinites are regarded with skepticism and

Figure 8 (facing page). (A) A comparison of calculated initial $^{206}\text{Pb}/^{204}\text{Pb}$ versus initial ϵ_{Nd} for whole rocks analyses from Greens Creek host rocks at 90 Ma. Because the Greens Creek section is known to have undergone at least greenschist metamorphism during the Cretaceous (ca. 115 to 90 Ma; Rubin and others, 1990; Rubin and Saleeby, 1992), initial Pb-Nd values were calculated back to 90 Ma for a comparison with known Late Cretaceous-Tertiary ore lead compositions (for example, Gaccetta and Church, 1989) and contemporaneous arc-related sediments (Farmer and others, 1993). Some whole-rock samples, particularly argillites and three metagabbros, have similar lead isotopic composition to Cretaceous-Tertiary ore deposits at 90 Ma, suggesting the possibility that these samples were overprinted by this lead isotopic composition. It could also be coincidence, although all other whole-rock samples do not plot near this composition at 90 Ma with the possible exception of metabasalt, GB-24. Pb, lead; Nd, neodymium; Ma, mega-annum; CHUR, chondritic uniform reservoir. (B) A comparison of initial $^{87}\text{Sr}/^{86}\text{Sr}$ versus initial ϵ_{Nd} for whole rocks analyses from Greens Creek host rocks at 90 Ma. Again, because the Greens Creek section is known to have undergone at least greenschist metamorphism during the Cretaceous (ca. 115 to 90 Ma; Rubin and others, 1990; Rubin and Saleeby, 1992), initial Sr-Nd values were calculated back to 90 Ma for a comparison with known Late Cretaceous-Tertiary seawater strontium compositions (for example, Burke and others, 1982; Hess and others, 1986). Again, some argillites (but not the same argillites), two phyllites, and two serpentinites appear to have possibly been affected or overprinted by Cretaceous-Tertiary seawater strontium. This observation may only be coincidence. However, in general, only relatively high Rb/Sr rocks show any appreciable variation between 215 and 90 Ma, and these rocks are mostly argillites and phyllites that contain a greater proportion of micaceous minerals. Sr, strontium; Nd, neodymium; Ma, mega-annum; CHUR, chondritic uniform reservoir.

are included here for the sake of completeness and discussion in the event they may be accurate, though imprecise.

Because the Sm-Nd systematics were obtained from whole rocks, some associations can be made: (1) metabasalts GB-22, GB-42, and GB-80, and phyllite PF-18; (2) ADM-01, AD-58, perhaps GB-59, and most of the metagabbros; (3) metabasalts GB-55, ADM-12, perhaps LG-17, phyllite GC-1637-44, and the serpentinite GC-1136-53; (4) phyllites GC-462-02, GC 462-07, and PF-09 with argillites PP-204-01, LG-78, ADM-29, ADM-34, NAD T4-2, and serpentinite LG-19; and (5) argillites Ard-03, LG-75, and serpentinite LG-20. As will be discussed later, these Sm-Nd isotopic differences are largely indicative of source material such that low $^{143}\text{Nd}/^{144}\text{Nd}$ compositions (and correspondingly low or negative ϵ_{Nd} values) indicate contamination from an older, more enriched, crustal source, and that the progression of negative to positive ϵ_{Nd} values may well indicate the evolution of a rifting event within the Alexander terrane.



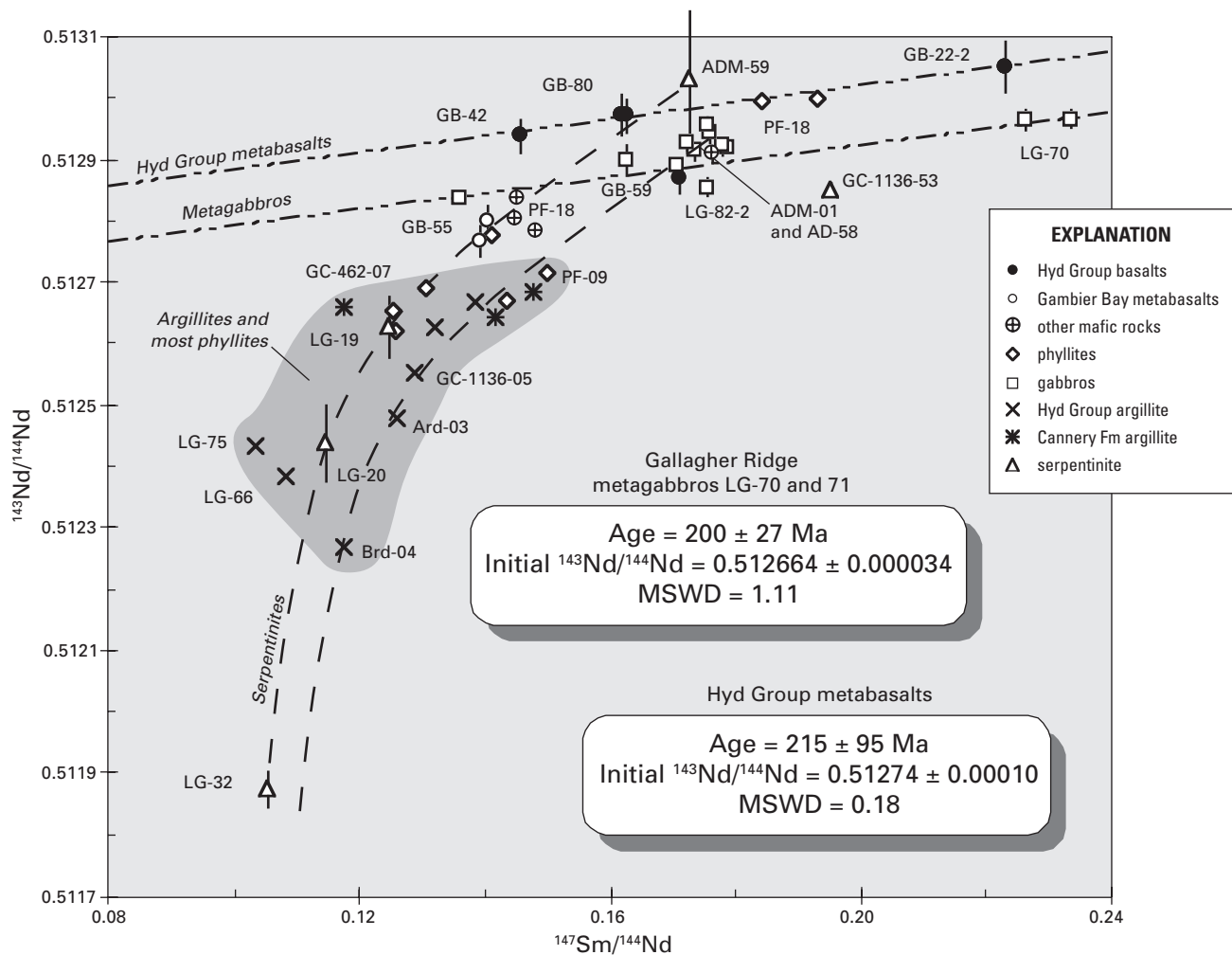


Figure 9. A comparison of the samarium-neodymium isotopic systematics of Greens Creek host rocks to Hyd Group metabasalt and Gallagher Ridge metagabbro isochrons, showing the extent of isotopic stability or variation within the different lithologic units. Argillites and phyllites are significantly more enriched than the metabasalt and metagabbro suites, indicating older crustal input or subsequent alteration. Serpentinites are conspicuously different, initial ϵ_{Nd} ranging from +8 (ADM-29) to -12 (LG-32), indicating distinctly different sources, probably at significantly different ages. MSWD, mean square of weighted deviates.

Initial Lead, Strontium, and Neodymium Isotopic Systematics of Greens Creek Host-Rock Lithologies

In figures 10 and 11, initial lead isotopic values (calculated at 215 Ma, Hyd Group metabasalt age) for Greens Creek host rocks are compared to model lead compositions from several major, planet-scale, lead reservoirs (Zartman and Doe, 1981). The lead isotopic evolution of these lead reservoirs is illustrated by separate curves emanating from a much older reservoir (ca. 4,000 Ma) that underwent planet-scale U/Pb fractionations. Average isotopic compositions of these separate lead reservoirs over the Phanerozoic are labeled “depleted mantle,” “orogene,” “lower crust,” and “upper crust.” Readers should bear in mind that these curves

represent the path of average values and do not convey the ranges of values that are possible for these reservoirs. Also, the “upper crust” curve is defined from mostly Phanerozoic data, such that lead from much older (for example, Archean to Proterozoic) crustal sources could be considerably more radiogenic with much higher $^{207}\text{Pb}/^{204}\text{Pb}$ values at equal $^{206}\text{Pb}/^{204}\text{Pb}$ compositions. Readers are referred to Dickin (1995) for a more detailed discussion of the U-Pb evolution of the Earth and its major reservoirs.

Important advantages can be found in the correlation of the two U-Pb decay schemes; one, they are geochemically similar, eliminating any effects due to natural fractionation processes; and two, their decay constants are different enough to cause a pronounced nonlinear correlation between them, and greater separation and distinction of their lead evolution curves (fig. 10). The

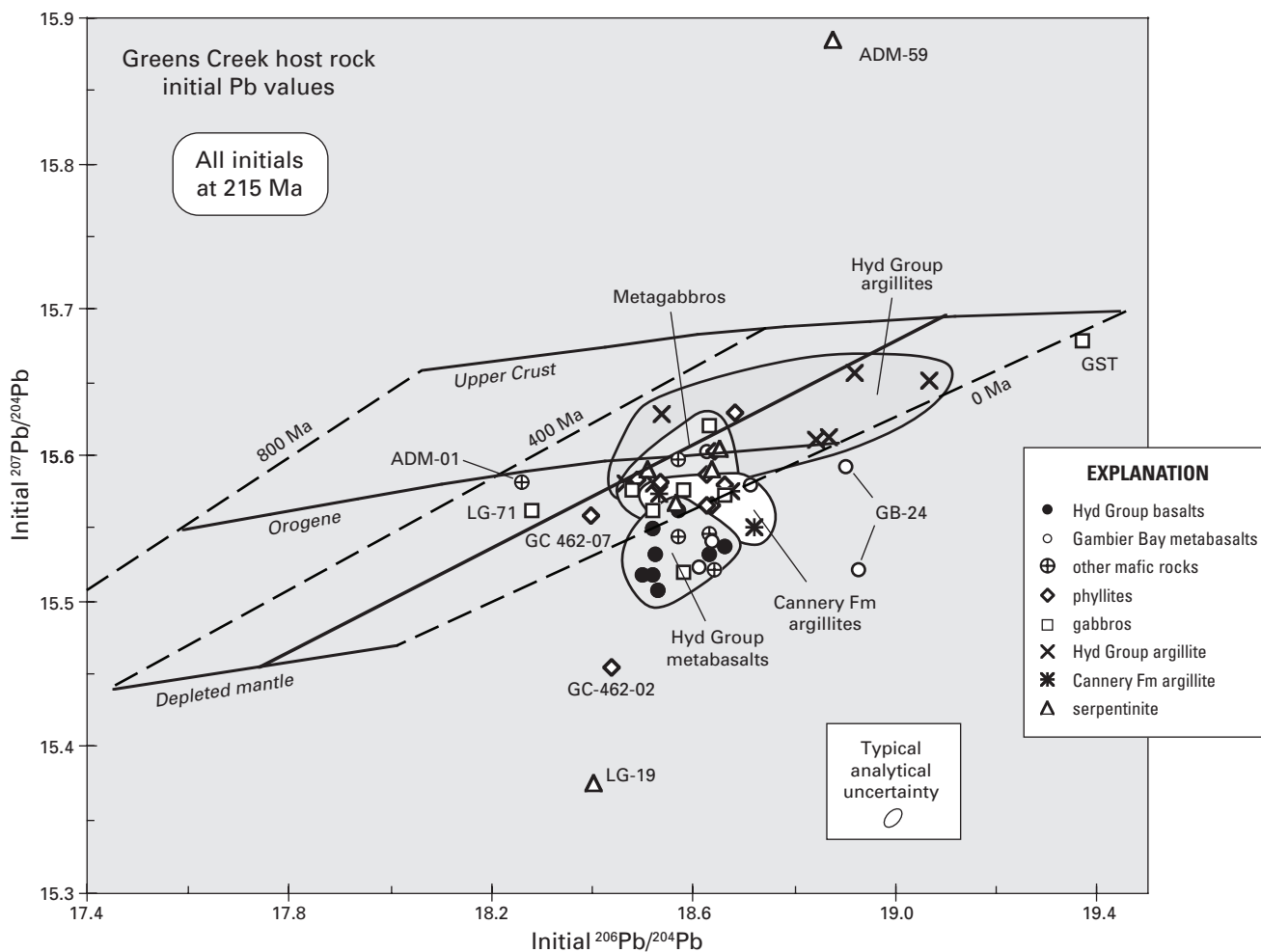


Figure 10. Pb-Pb correlation diagram ($^{206}\text{Pb}/^{204}\text{Pb}$ versus $^{207}\text{Pb}/^{204}\text{Pb}$) showing the distribution of initial Pb compositions of Greens Creek host rocks relative to model lead evolution curves and fields for modern petrotextonic environments (Zartman, 1984). Most mafic lithologies have initial lead values (at 215 Ma) between the “orogene” and “depleted mantle” curves, however, plotting at younger model lead ages (dashed isochrons). Scatter in the isotopic data may be due to postemplacement U-Pb fractionations caused by either low-grade metamorphism or subsequent alteration, particularly within the metagabbros. The field defined by metabasalts, largely those of the Hyd Group, is more discrete (less variation), plotting midway between the “orogene” and “depleted mantle” curves. Their altered equivalents, the phyllites plot just to the left, implying slight U-Pb fractionations during alteration. Argillites also define a wide field (see text for discussion) but basically plot at or near the “orogene” and trending toward the “upper crust” curve, suggesting some older, more radiogenic crustal input.

advantage is that evaluation of lead isotopic data in comparison to them is more definitive. Henceforth, lead isotopic data from Greens Creek will be displayed and discussed mainly using the $^{206}\text{Pb}/^{204}\text{Pb} - ^{207}\text{Pb}/^{204}\text{Pb}$ correlation diagram.

Notably, all fields of initial $^{206}\text{Pb}/^{204}\text{Pb} - ^{207}\text{Pb}/^{204}\text{Pb}$ values at 215 Ma for Greens Creek host rocks do not plot on model lead compositions at the 200-Ma isochron (fig. 10). Nearly all of these initial lead values plot beyond — to younger model ages, indicating derivation from sources more enriched than average model reservoirs — and cluster nearer to the orogene curve than

to either of the other two curves. This lead isotopic behavior is not unusual for arc-related VMS deposits, as pointed out by Newberry and others (1997), and discussed further by Kerrick (1991) and Dickin (1995).

Also, there are profound differences between the $^{206}\text{Pb}/^{204}\text{Pb} - ^{207}\text{Pb}/^{204}\text{Pb}$ correlation (U-derived only) and the $^{206}\text{Pb}/^{204}\text{Pb} - ^{208}\text{Pb}/^{204}\text{Pb}$ correlation (or lack thereof). In figure 11, model lead evolution curves for “mantle,” “orogene,” and “upper crust” are subparallel and adjacent such that initial $^{206}\text{Pb}/^{204}\text{Pb} - ^{208}\text{Pb}/^{204}\text{Pb}$ signatures from Greens Creek host

rocks overlap both the upper crust and the orogene model lead evolution curves. However, the data do mainly cluster about the upper-crust model lead curve, and are unlike lead signatures for either the lower crust or a depleted mantle.

Metabasalts

Although the lead contents in the metabasalts are more variable (2 to 12 ppm), the uranium contents are between 0.2 and 1 ppm, and thorium between 0.5 and 3 ppm (table 4, chap. 11) typical of modern-day basalts. Two exceptions, LG-17 and GB-24, are much more depleted and exhibit uranium and thorium concentrations similar to ultramafic rocks and Greens Creek serpentinite.

The U-Pb isotopic data for the Hyd Group metabasalts define an apparent isochron age of 218 ± 16 Ma with initial leads value of 18.515 (fig. 11; chap. 11) that, while not very precise, lends confidence to their calculated initial lead signatures at 215 Ma. These metabasalts (and related phyllites – altered mafic volcanics) plot between average lead compositions for “orogene” and “mantle,” consistent with their derivation from mainly mantle sources (fig. 10) but probably in a volcanic arc setting (Zartman and Doe, 1981; Zartman, 1984). Initial lead values for the Hyd Group metabasalts (mainly from Gambier Bay; fig. 3) plot within the metagabbroic/ultramafic field, but in a much more discrete area, perhaps indicative of their higher degree of preservation and isotopic stability. A notable exception, two analyses of metabasalt GB-24 plot to

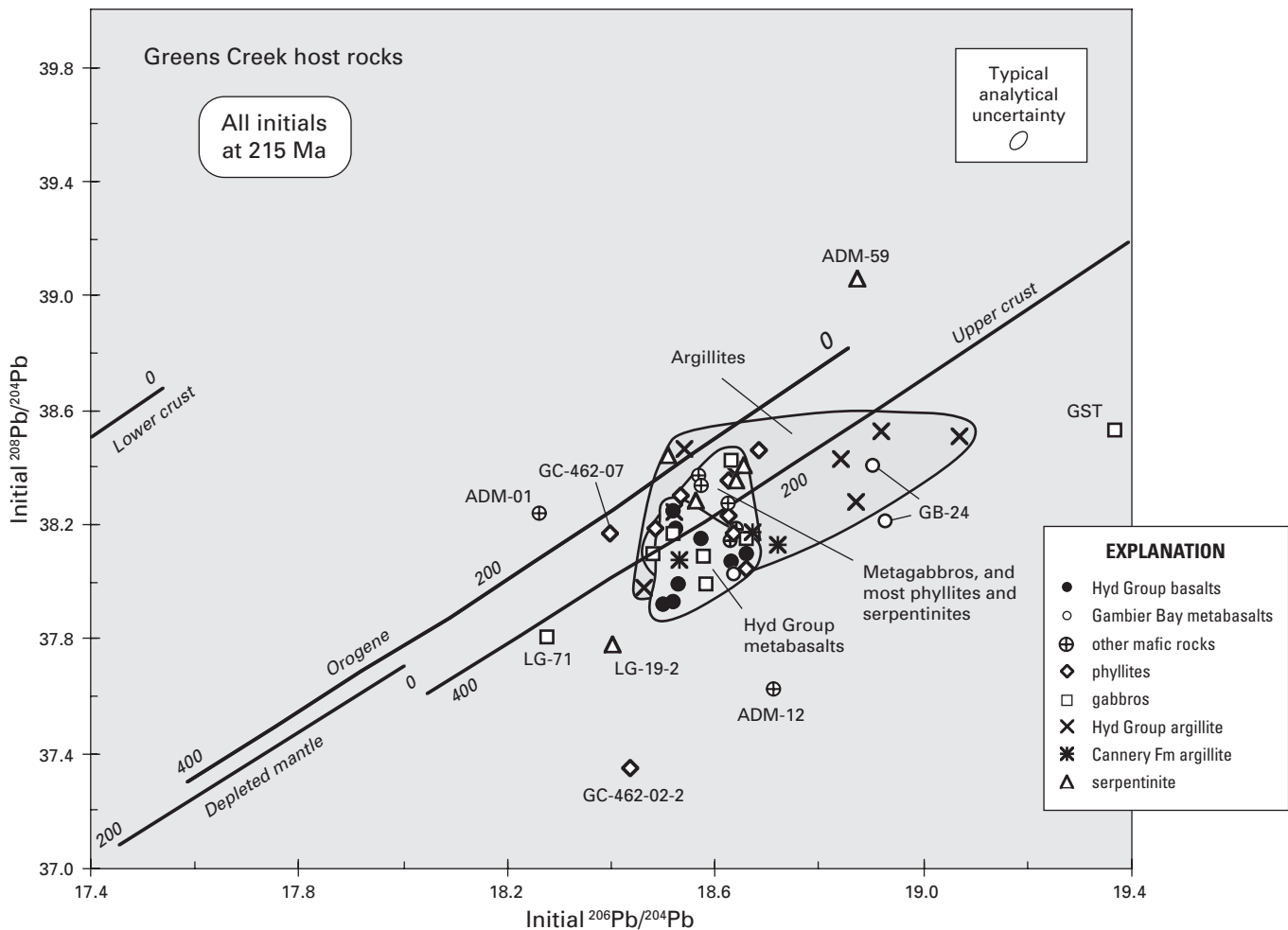


Figure 11. Pb-Pb correlation diagram ($^{206}\text{Pb}/^{204}\text{Pb}$ versus $^{208}\text{Pb}/^{204}\text{Pb}$) showing the distribution of initial lead compositions of Greens Creek host rocks relative to model lead evolution curves and fields for modern petrotectonic environments (Zartman, 1984). Model lead evolution curves for “mantle,” “orogene,” and “upper crust” are subparallel and adjacent such that modern-day isotopic fields for petrotectonic environments (for example, OIB, MORB, IAB) overlap grossly. Initial lead signatures from Greens Creek host rocks unfortunately overlap two of the model lead evolution curves and therefore are not uniquely interpretable using these model lead discriminators.

the right with a higher $^{206}\text{Pb}/^{204}\text{Pb}$ relative to the other Gambier Bay Formation metabasalt (figs. 10 and 11).

Rubidium and strontium concentrations in metabasalts vary widely and apparently are not correlated with degree of alteration or metamorphism (tables 3 and 6). Typical unaltered basalts have Rb contents around 30 ppm and relatively high Sr contents (about 450 ppm) due to their more calcic mineral assemblages. Greens Creek metabasalts have variable Rb (3 – 41 ppm) and low average Sr (125 – 250 ppm) contents, indicating either derivation from a less mafic source or mobility during subsequent metamorphism and/or alteration. A metabasalt, GB-24, from the Gambier Bay Formation is altered and exhibits extremely depleted Rb-Sr contents, similar to serpentinites. Two other metabasalts, GB-42 and GB-55, have high Sr contents (540 – 700 ppm). High Sr contents (>600 ppm) are indicative of carbonates.

Samarium and neodymium contents from the metabasalts are much less scattered (2–5 ppm and 5–21 ppm, respectively; table 6 in chap. 11) and are typical of tholeiites, although slightly more enriched than MORB and less enriched than continental tholeiites (for example, Faure, 1986). Metabasalt, LG-17, from Gallagher Ridge (fig. 5) is highly altered and exhibits more depleted Sm-Nd contents (0.7 and 3 ppm, respectively).

Sm-Nd isotopic data for the Hyd Group metabasalts define an apparent isochron age of 215 ± 95 Ma (fig. 12, chap. 11) and, while not very precise, they do indicate that calculated initial neodymium signatures at 215 Ma are accurate. The Rb-Sr isotopic data for the same suite of Hyd Group metabasalts are not as well defined, but two separate arrays indicate ages at about 190 to 170 Ma but with slightly different initial strontium values of 0.7041 and 0.7049 (fig. 13; chap. 11). Therefore, their calculated initial strontium values are probably slightly lower than they should be. However, this small difference does not alter any of our interpretations regarding the Rb-Sr isotopic systematics for these metabasalts.

With respect to their Nd-Sr isotopic systematics, the metabasalts can be subdivided into at least two groups: a high-Nd ($\epsilon_{\text{Nd}} = +7$ to 9) group that includes most Hyd Group metabasalts from Gambier Bay, southeastern Admiralty Island (fig. 3), and a lower-Nd ($\epsilon_{\text{Nd}} = +4$ to 5) group (fig. 12). Some of the high-Nd metabasalts exhibit low-Sr values (for example, GB-42; $^{87}\text{Sr}/^{86}\text{Sr}_i$ about 0.704), whereas, others have more elevated Sr values ($^{87}\text{Sr}/^{86}\text{Sr}_i = 0.7049$ to 0.7056), possibly due to alteration. Samples GB-24 and GB-80 are in this category. Lower Nd and lower Sr values ($\epsilon_{\text{Nd}} = +4$ to 5, and $^{87}\text{Sr}/^{86}\text{Sr}_i = 0.07038$, respectively) are exemplified by sample GB-55, a chloritized greenstone from the Gambier Bay Formation at Gambier Bay, and a similarly lower-Nd metabasalt, GB-59, has an elevated Sr value ($^{87}\text{Sr}/^{86}\text{Sr}_i$ about 0.7043). Other lower-Nd metabasalts include LG-17 from Gallagher Ridge ($\epsilon_{\text{Nd}} = +5$) and ADM-12 ($\epsilon_{\text{Nd}} = +4.3$) from Staunch Point (fig. 3). Although this last sample is described as a microgabbro (table 3), it is highly altered and could have a basaltic protolith.

All of the metabasalt data lie well within the modern “island arc” field with elevated $^{87}\text{Sr}/^{86}\text{Sr}$ relative to OIB or

MORB (fig. 12). Time-corrected values (at 215 Ma) for the OIB and MORB fields plot slightly farther to the left in the diagram, enhancing the difference between initial Nd-Sr values for Greens Creek samples and those for different petro-tectonic environments at 215 Ma.

A comparison of initial neodymium and lead (fig. 13) for Greens Creek metabasalts is even more discrete than that for Nd-Sr initial signatures. Lower-Nd metabasalts are also characterized by slightly higher average initial $^{206}\text{Pb}/^{204}\text{Pb}$ values than the more depleted, high-Nd metabasalts. Elevated initial $^{206}\text{Pb}/^{204}\text{Pb}$ values relative to MORB and OIB like $^{87}\text{Sr}/^{86}\text{Sr}$ are indicative of some modern oceanic island arc settings (for example, Ellam and Hawkesworth, 1988; Ben Othman and others, 1989). Again, metabasalt GB-24 is notably an outlier with a significantly higher initial $^{206}\text{Pb}/^{204}\text{Pb}$ value similar to serpentinite, ADM-59 (fig. 13).

Metagabbros

Metagabbro lead contents are depleted (less than 1 ppm) relative to metabasalt values, as are uranium contents (0.08–0.5 ppm) and thorium (0.25–2.5 ppm). All of these concentrations are at least half as depleted relative to typical, modern-day values for gabbro (for example, Faure, 1986). Th/U ratios are relatively uniform at about 3.3; a highly altered, massive microgabbro, LG-45, is the only exception.

The U-Pb isotopic data for the metagabbro data define an apparent isochron age of 206 ± 35 Ma indicating an initial $^{206}\text{Pb}/^{204}\text{Pb}$ value of 18.61 (fig. 14; chap. 11) and again, while not very precise, these results do lend confidence in the calculated initial lead signatures at 215 Ma for these metagabbros.

The wide array of initial Pb values for metagabbros and serpentinites more than likely represents slight, yet significant U/Pb fractionations since their emplacement and crystallization. It should be noted, however, that average composition(s) for metagabbroic-serpentinitic magmatic source(s) are very similar to those for metabasalts and phyllites and lie between the “mantle” and “orogene” averages (fig. 10), again indicative of their partial derivation from a depleted mantle source.

Rb-Sr contents for the metagabbros (0.5–23 and 120–330 ppm, respectively) are lower and less scattered than those for the metabasalts, and most lie along a Rb/Sr trend of about 0.01; the highly altered metagabbros, LG-45 and LG-71, are the only exceptions. Samarium and neodymium concentrations (1–4.5 and 3–16 ppm, respectively), like Rb-Sr, are on average lower than those for metabasalts and more similar to typical average modern-day MORB concentrations.

Sm-Nd isotopic data for the Greens Creek metagabbros define an apparent isochron age of 200 ± 27 Ma (fig. 15; chap. 11) and, while not very precise, they do indicate that calculated initial neodymium signatures at 215 Ma are accurate.

Metagabbros plot between the two groups of metabasalt (figs. 12 and 13) with initial $\epsilon_{\text{Nd}} = +5$ to 7, initial $^{87}\text{Sr}/^{86}\text{Sr} = 0.07037$ to 0.7048, and initial $^{206}\text{Pb}/^{204}\text{Pb} = 18.45$ to 18.66, slightly more depleted than the lower-Nd metabasalts and slightly more enriched than the high-Nd metabasalts.

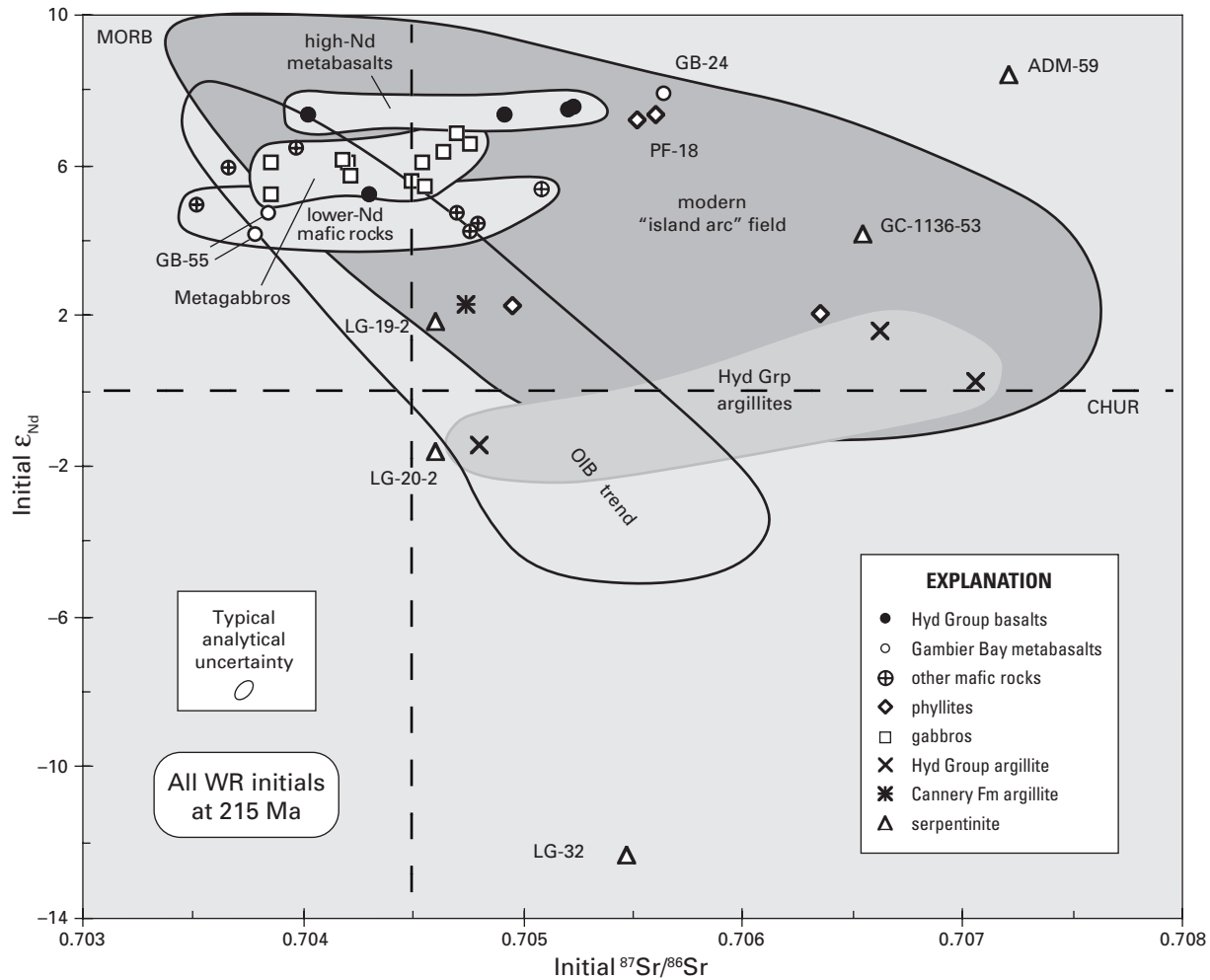


Figure 12. Initial strontium versus initial neodymium correlation diagram showing the distribution of initial Sr-Nd values for Greens Creek host rocks relative to model Sr-Nd fields for modern petro-tectonic environments (for example, Zartman, 1984). Again, most initial Sr-Nd data for these host rocks plot between mid-ocean ridge basalt (MORB) and more enriched values, and mostly displaced to the right in the “island-arc” field relative to the oceanic-island basalt (OIB) trend. Serpentinite data vary widely. See text for more discussion. CHUR, chondritic uniform reservoir.

Initial Sr and Nd values (at 215 Ma) for mafic igneous rocks from Greens Creek have higher ϵ_{Nd} (+4 to +9) and lower $^{87}Sr/^{86}Sr$ (0.7035 to 0.7058) than phyllites and argillites, values indicating mainly mantle derivation (fig. 12). All samples are enriched in $^{87}Sr/^{86}Sr$ and $^{206}Pb/^{204}Pb$ compared to MORB (mid-ocean ridge basalt) or OIB (oceanic island basalt), a characteristic indicative of island arc rocks (Hawkesworth and others, 1977, 1979; Zartman, 1984; Ellam and Hawkesworth, 1988; Ben Othman and others, 1989). Metagabbro LG-71 and metabasalt ADM-01 plot to the left with unusually low $^{206}Pb/^{204}Pb$ values of about 18.27 (fig. 13). We suspect that the U-Th-Pb isotopic systematics from these whole-rock samples may be disturbed (fig. 7A), and caution is advised to the reader regarding some of these data.

Phyllites

Uranium, thorium, and lead concentrations for phyllites (0.1–2 ppm, 0.4–9.3 ppm, and 4–100 ppm, respectively) have a much broader range than the metabasalts, their less altered equivalents. On average, however, the phyllite concentrations are not significantly different. One sample, GC-462-02-2, produced an unusually high thorium concentration of 9.3 ppm; otherwise, thorium contents range between 0.4 and 2.4 ppm. Lead contents from two mine phyllites, GC-1103-16 and GC-1637-44, were uncharacteristically high (60 and 98 ppm, respectively); otherwise, the lead contents ranged between 4 and 13 ppm, almost exactly that of the metabasalts. Th/U ratios for phyllites are variable and typically have lower values than the main mafic trend of about 3.3 (with the exception of PF-18).

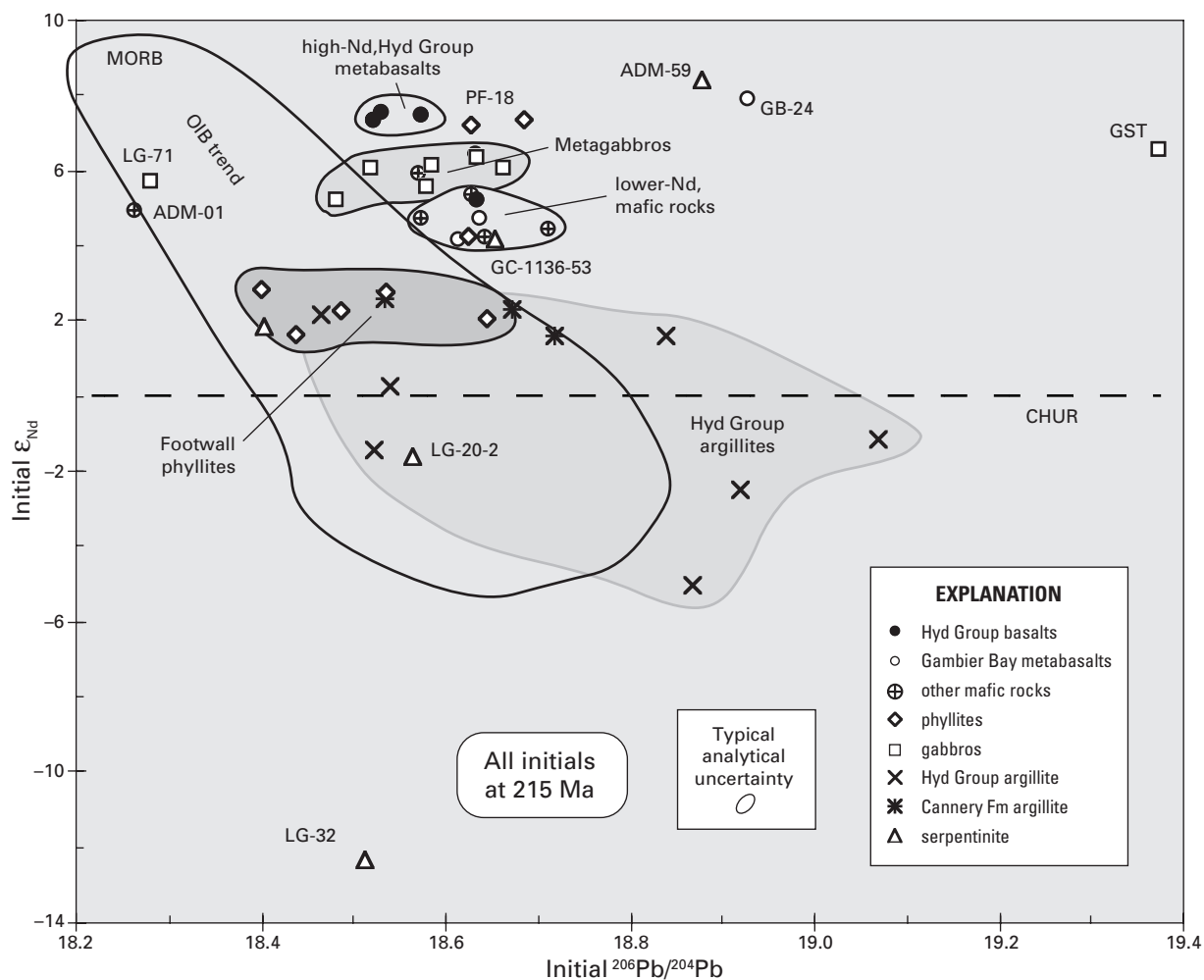


Figure 13. Initial lead versus initial neodymium correlation diagram showing the distribution of initial Pb-Nd values for Greens Creek host rocks relative to model Pb-Nd fields for modern petrotectonic environments (for example, Zartman, 1984). Fields representing different lithologic units of Greens Creek host rocks are more discrete than those shown in figure 12, and a field for most of the phyllites is somewhat discernible from values for argillites. Although a field for modern “island arcs” is not shown, elevated $^{206}\text{Pb}/^{204}\text{Pb}$ values for most Greens Creek mafic rocks relative to the ocean-arc basalt (OIB) trend is indicative of some modern island-arc rock suites (Ellam and Hawkesworth, 1988; Ben Othman and others, 1989). Again, serpentinite data vary widely (although ADM-59 is joined by metabasalt GB-24). MORB, mid-ocean ridge basalt; OIB, oceanic-island basalt; CHUR, chondritic uniform reservoir.

The phyllites, interpreted as altered mafic volcanic rocks, exhibit initial Pb isotopic compositions similar to the meta-basalt and metagabbro initial Pb compositions (figs. 10 and 11), although more scatter is evident — an indication of U-Pb fractionations during subsequent alteration (fig. 11, chap. 11). Although the phyllites plot mostly within the metagabbro field, this field significantly overlaps fields for both the metabasalts and the argillites.

Rubidium and strontium concentrations vary somewhat (1–55 ppm and 26–112 ppm, respectively), notably lower in strontium and slightly higher in rubidium contents than associated metabasalts, perhaps due to alteration. Samarium and neodymium contents are less variable (0.6–4.4 ppm and 3–18.4 ppm, respectively) and very similar to their less-altered equivalents, the metabasalts.

Although the calculated initial lead values for phyllite samples mimic those of the metabasalts and metagabbros, calculated initial Sr-Nd and Pb-Nd values of phyllites are more scattered (figs. 12 and 13). The difference in initial strontium in phyllites can be explained by alteration due to seawater interaction or incorporation of carbonate ($^{87}\text{Sr}/^{86}\text{Sr} = 0.707$ to 0.708), as is probably the case with some of the argillites, metabasalts, and serpentinites. Two phyllites (PF-09 and GC-1637-44) plot with very low initial strontium values (less than 0.703) are not within the scale of the diagram (fig. 12), and are suspected of containing secondary rubidium (see fig. 7B). Two analyses of phyllite PF-18 from the Portal Face are similar to the high-Nd metabasalt signature ($\epsilon_{\text{Nd}} = +8$), but with slightly more enriched strontium (0.7056) and lead (18.67) signatures. Other phyllites

plot toward initial signatures for argillites with ϵ_{Nd} about +2, higher initial strontium and lower initial lead, consistent with their lower Th/U, increased uranium content (leading to over-corrected initial lead values).

Differences in initial neodymium are not easily explained or well understood. Because the initial neodymium values of some phyllites tend toward values for argillites, one might suggest that hydrothermal fluids circulating through both the argillitic and older mafic volcanic packages (phyllites) mobilized rare-earth elements (REE) and therefore altered neodymium compositions. Nevertheless, lower ϵ_{Nd} and higher $^{87}\text{Sr}/^{86}\text{Sr}$ values in some Greens Creek samples probably indicate the addition of older, more enriched crustal components either during sedimentation or subsequent alteration (figs. 7 and 8).

Argillites

Argillite samples are of two known ages: an older Permian suite from the Cannery Formation (LG-78, ADM-29, and ADM-34), and a younger, Late Triassic, Greens Creek-contemporary suite from the Hyd Group sequence (table 3, chap. 11). A comparison of uranium, thorium, and lead concentrations from the two suites reveals no differences (0.7–4, 0.2–4.5, and 1.7–20 ppm, respectively), nor do Th/U ratios show any distinction. As mentioned previously, the variations in Th/U would suggest variable fractionation either during shale deposition or subsequent alteration. Unusually high uranium contents were found in mine argillite PP-204-01 (7.4 ppm).

The argillites yielded an apparent U-Pb isochron age of 186 ± 100 Ma (chap. 11), and whereas this age is very imprecise, if accurate, it is interestingly similar to U-Pb and Rb-Sr apparent isochron ages for some of the metabasalts and phyllites (about 205 and 182 Ma, respectively) and ages of either intrusion or alteration of the metagabbros (about 206 Ma). Despite slight alteration, these isochron ages lend confidence to calculated initial Pb signatures at 215 Ma for the argillite samples.

On average, a higher ^{207}Pb component can be found in initial lead compositions from some of the argillites (fig. 10). These values range from average “orogene” to “upper crust” compositions, indicating that lead in some of the argillites is derived from an older, slightly more radiogenic source. The same indication is observed in ^{206}Pb – ^{208}Pb space (fig. 11) — argillites plot approximately on the model “upper crust” Pb evolution curve at 200 Ma.

Argillite Pb signatures can be subdivided into two fields (see fig. 15, chap. 10). The least radiogenic argillite field is compatible with some phyllites, but also galena Pb from Kennecott-Rand. And the most radiogenic argillite field appears as a possible endmember composition consistent with some Greens Creek pyrite and sphalerite Pb compositions. In general, the older Cannery Formation argillites plot under the Hyd Group argillites (lower $^{206}\text{Pb}/^{204}\text{Pb}$ and $^{207}\text{Pb}/^{204}\text{Pb}$) and within the upper section for the metabasalts and phyllites. The Hyd Group argillites, on the other hand, plot either to the low $^{206}\text{Pb}/^{204}\text{Pb}$ side, similar to values for galena Pb from Kennecott-Rand, some phyllites and some metagabbros, or to the

high $^{206}\text{Pb}/^{204}\text{Pb}$ side, similar to some Greens Creek pyrite and sphalerite Pb compositions that may contain more evolved, younger lead (Cretaceous pyrite formation?).

Rb-Sr concentrations from argillites vary widely (1–60 ppm and 1–135 ppm, respectively), although in general Rb/Sr ratios are quite high (0.2–20). These concentrations are considerably below the typical average shale concentrations for Rb and Sr (about 140 and 300 ppm, respectively). Sm-Nd contents in typical modern shales are 10 and 50 ppm, respectively (for example, Faure, 1986), far greater than those exhibited by Greens Creek argillites (0.7–4 ppm and 3.2–18.2 ppm, respectively); however, Greens Creek argillites have Sm-Nd contents near exactly the same as associated phyllites and metabasalts from which they were supposedly derived.

Rb-Sr isotopic age data for the argillite samples suggest a single resetting age of 91.4 ± 2.6 Ma (fig. 16, chap. 11) that includes Hyd Group and Cannery Formation alike. It is essentially a three-point isochron controlled by two Hyd Group argillites, LG-66 and NAD-T4-2, neither of which is carbonaceous. Omission of the Cannery Formation data alters the Rb-Sr apparent isochron age to 90.8 ± 2.2 Ma with initial $^{87}\text{Sr}/^{86}\text{Sr}$ at 0.70733 for the Hyd Group argillites, a value that approaches Cretaceous seawater strontium composition (figs. 7 and 8).

Correctable initial Nd-Sr-Pb isotopic data for argillites (only four analyses) lie in fields with lower initial Nd (ϵ_{Nd} about –2 to +2), higher initial $^{206}\text{Pb}/^{204}\text{Pb}$ (18.45–19.08), and higher initial $^{87}\text{Sr}/^{86}\text{Sr}$ (0.7048 to 0.7070) than other host rocks (figs. 12 and 13), but typical of values for modern shales (between modern OIB and “orogene”). High ^{207}Pb , low ϵ_{Nd} , and higher Sr values all suggest that the argillites contain older, slightly more radiogenic source material, perhaps indicative of some Paleozoic provenance (Alexander terrane). However, because these Sr-Pb isotopic data may have been altered, even slightly (figs. 7 and 8), an emphasis on the initial Nd values is recommended. Nonetheless, the initial Pb-Sr-Nd isotopic signatures for argillites do plot on average where one might expect from the interpreted tectonic setting — an oceanic arc environment (for example, Zartman, 1984).

Serpentinities

Uranium, thorium, and lead contents in ultramafic rocks average 0.015, 0.05, and 0.3 ppm, respectively, and Greens Creek serpentinites exhibit comparable concentrations of 0.01–0.06, 0.03–0.2, and 0.2–0.75 ppm, respectively. Several outliers are observed; ADM-59 is exceptional with uranium (0.11 ppm), thorium (0.95 ppm), and lead (4.7 ppm); and mine serpentinites GC-1136-53 and GC-1136-59 are enhanced with uranium and lead (0.04–0.07 and 75–26 ppm, respectively). The high lead contents in the latter two are indicative of alteration due to mineralization, and these lead results should therefore be ignored when evaluating the isotopic systematics of the serpentinites.

The initial lead compositions for most serpentinites lie within the mafic igneous field (fig. 10). However, two exceptions exist: an extremely low $^{207}\text{Pb}/^{204}\text{Pb}$ analysis of LG-19-2 and an extremely high $^{207}\text{Pb}/^{204}\text{Pb}$ analysis of ADM-59.

Because of large errors (table 4, chap. 11) and the possibility of difficulties in maintaining stable $^{207}\text{Pb}/^{204}\text{Pb}$ measurements relative to $^{206}\text{Pb}/^{204}\text{Pb}$ (see chap. 10), these two serpentinite analyses are highly tentative. Nonetheless, if these results are even somewhat accurate, they do present interesting speculation.

Typical ultramafic rubidium and strontium concentrations are 0.2 and 1 ppm, respectively, and Greens Creek serpentinites range between 0.15 and 0.32, and 6.8 and 16 ppm, respectively (table 6, chap. 11). Exceptions are noted with mine serpentinites GC-1136-53 and GC-1136-59 that exhibit extreme Rb and Sr contents of 33 to 45 and 68 to 153 ppm, respectively, and these analyses again should be excluded when considering the Rb-Sr isotopic characteristics of the serpentinite protolith(s). Samarium and neodymium concentrations for typical modern ultramafic rocks vary, but generally are below 0.6 and 2.5 ppm, respectively. Greens Creek serpentinites range between 0.017–0.03 and 0.09–2.7 ppm, respectively, excluding the mine serpentinites (table 6, chap. 11).

Although the Rb-Sr isotopic data from serpentinite samples are scattered and do not form well-defined isochrons, an age of about 195 Ma is suggested for serpentinites LG-19 and LG-20 from the Lakes District area (fig. 5), probably an age close to that of alteration. An initial Sr value of 0.70462 ± 6 is calculated from this regression, a value very similar to both metabasalts and some metagabbros (fig. 17, chap. 11).

Another Rb-Sr age of 89 ± 15 Ma (fig. 17, chap. 11) is defined by the two mine serpentinites, GC-1136-53 and GC-1136-59, with an initial Sr value of 0.70767 — a value very similar to that indicated by the data from the Hyd Group argillites (0.70733) with a Rb-Sr age of resetting at 91 Ma (fig. 16, chap. 11). Serpentinite ADM-59 from Gambier Bay plots near this “reset” isochron.

Initial Pb-Sr-Nd isotopic values for serpentinite vary widely (figs. 10 through 13) due in part to the poor quality of the analyses (very low abundances and correspondingly low ion beam intensities). If one can believe the data, however, they suggest highly variable source(s) during emplacement (perhaps over a substantial time period) or isotopic resetting during alteration probably due to Cretaceous deformation. An attempt to date serpentinite sample LG-19 was largely unsuccessful in all isotopic systems, indicating that internal isotopic systematics had been disturbed (chap. 11).

With the hope that any of these serpentinite analyses are accurate, if not precise, their isotopic behavior imply several interesting points. One of the serpentinites (ADM-59) is much different than the rest, with high initial Nd (+8.4), high $^{207}\text{Pb}/^{204}\text{Pb}$ (15.885), and high $^{87}\text{Sr}/^{86}\text{Sr}$ (0.7072), whereas the remainder of the serpentinites exhibit decreasing initial Nd values (GC-1136-53, +4.15; LG-19-2, +1.8; LG-20-2, -1.6; and so forth), indicating increasing crustal involvement in their production (figs. 9, 12, and 13). If these results are accurate, it would suggest that serpentinite LG-32, the most negative (ϵ_{Nd} about -12), was derived from a source enriched with much older crust (Nd model age, $T_{\text{DM}^7} = 1,350$ Ma). Unfortunately, age data for any of these serpentinites do not exist; they may range anywhere in age from Late Triassic to Cretaceous.

Crosscutting Diabases — Diorites

Uranium, thorium, and lead contents for these samples are given in table 4 (chap. 11), initial Pb values are given in table 5 (chap. 11), and they indicate that these sills/intrusions are of two types. Samples LG-64 (diorite) and GC-1704-01 are remarkably similar, especially with respect to their Nd-Sr and Nd-Pb isotopic systematics (not shown), and GC-1701-01 is notably different. All of these samples have uranium contents between 0.84 and 1.35 ppm and thorium contents between 1.6 and 2.6 ppm, but variable lead contents of about 4 ppm to 640 ppm, the latter indicative of contamination by mineralization — sample GC-1701-01. Otherwise, the diabasic intrusions are similar to the metabasalts, metagabbros, and phyllites with respect to their U, Th, and Pb contents.

Without an actual age for these intrusions, accurate initial Pb compositions are not possible. All of these bodies are known to be younger than the Greens Creek ore-forming event, but how much younger has not been established. Assuming reasonably contemporaneous ages for these crosscutting intrusions (from 185 to 90 Ma), initial lead and strontium values do not match Cretaceous lead and strontium model isotopic compositions (for example, Burke and others, 1982; Zartman, 1984), suggesting that the isotopic systematics of these samples are not controlled by Cretaceous deformation and(or) seawater alteration. Initial Nd-Sr and Nd-Pb correlation diagrams (from 215 Ma to 50 Ma) show that these samples, and especially LG-64 and GC-1704-01, are quite similar and depleted; in fact, the most depleted whole-rock samples at Greens Creek had initial $\epsilon_{\text{Nd}} = +7$ to 8, $^{87}\text{Sr}/^{86}\text{Sr} = 0.7033$, and $^{206}\text{Pb}/^{204}\text{Pb} = 18.2$ to 18.45, values slightly less than MORB at 185 to 90 Ma.

Discussion

Geologic Framework at Greens Creek

We know from previous geologic studies that the Greens Creek ore deposit is located in a belt of volcano-sedimentary rocks interpreted to represent a rift-fill sequence formed during a brief period of intra-arc or back-arc rifting in latest Triassic time (Berg and others, 1972; Taylor, 1997; Taylor and others, 1995a, 1995b, 1999, 2000). The stratigraphy within the belt consists of conglomerates, limestones, marine clastic sediments, and tuffs that are intercalated with and overlain by a distinctive unit of mafic pyroclastics and pillowed flows (figs. 3 and 4). Faunal data bracket the age of the host rocks between early Carnian (early Late Triassic) and late Norian (late Late Triassic) time (chap. 11).

The radiogenic isotopic systematics indicate a progressively depleting source for the Upper Triassic Greens Creek rocks, suggesting a rift setting. The oldest argillites have slightly depleted signatures (ϵ_{Nd} about +1.5), consistent with their derivation from mainly oceanic-arc volcanic rocks of the Alexander terrane. These rocks in turn are unconformably overlain by a sequence of mainly altered metabasalts

and related rocks, perhaps similar to metabasalts of either the Halleck Formation or the Gambier Bay Formation that exhibit depleted, island-arc-type isotopic signatures (ϵ_{Nd} about +4 to 5 and elevated $^{87}\text{Sr}/^{86}\text{Sr}$ and $^{206}\text{Pb}/^{204}\text{Pb}$). The metabasalts are then unconformably overlain by conglomerate, dolomite, and more argillites of the Hyd Group. The Hyd Group argillites have slightly depleted to slightly enriched ϵ_{Nd} about -5 to +2, indicating partial incorporation of some older, more enriched source material. The lower metabasaltic sequences are intruded by ultramafic sills and stocks, represented now as highly altered serpentinites that exhibit a wide range of isotopic signatures (ϵ_{Nd} about -12 to +8), suggesting that they may have been early to late rift-forming intrusions, and enriched relative to other igneous rocks. Subsequent mafic volcanism and gabbroic plutonism are characterized by more depleted source signatures (ϵ_{Nd} = +5 to +9). Hyd Group basalts that cap the Triassic section have yet more depleted signatures (ϵ_{Nd} = +8 to +9), and lastly, post-Greens Creek crosscutting diabase dikes are the most depleted (ϵ_{Nd} = +9). This progressive sequence of least to most depleted isotopic signatures implies opening of preexisting crust in a rift setting, most likely within an oceanic arc environment.

Petrotectonic Environment of the Greens Creek VMS Deposit

Scatter in the isotopic data for phyllites, metagabbros, serpentinites, and argillites indicate the likelihood of open-system behavior due to mobilization of either or both elements probably during Cretaceous deformation and metamorphism. However, despite this probable isotopic behavior, average initial Pb-Sr-Nd isotopic data from the mafic rock units (metabasalts, metagabbros, and associated phyllites) plot where one might expect them and indicate derivation from sources similar to those of oceanic-arc environments. Initial Pb signatures for the basaltic-gabbroic-ultramafic magmatic source(s) and related phyllites (altered mafic volcanics?) plot between average Pb compositions for “orogene” and “mantle,” consistent with their derivation from mainly mantle sources (fig. 10), but in a volcanic arc setting (Zartman and Doe, 1981; Zartman, 1984). Likewise, initial Sr and Nd (at 215 Ma) values for mafic igneous rocks from Greens Creek are depleted (higher ϵ_{Nd} and lower $^{87}\text{Sr}/^{86}\text{Sr}$), indicating mainly mantle derivation (fig. 12). All samples are enriched in $^{87}\text{Sr}/^{86}\text{Sr}$ and $^{206}\text{Pb}/^{204}\text{Pb}$ compared to MORB (mid-ocean ridge basalt) or the OIB (oceanic island basalt) trend, a characteristic indicative of island-arc rocks (Hawkesworth and others, 1977, 1979; Ellam and Hawkesworth, 1988; Ben Othman and others, 1989). Explanations for the elevated Sr values include the addition of subducted ^{87}Sr from seawater and/or oceanic sediments (Hawkesworth and others, 1977), or metasomatic contamination of the mantle wedge with high $^{87}\text{Sr}/^{86}\text{Sr}$ derived from subducted ocean crust (Pearce, 1983). Although some of these enriched values may be the result of alteration during Cretaceous deformation, even the most depleted values are slightly more enriched than MORB values.

Initial Nd values for phyllites are bimodal; some have a mafic igneous signature (+8), others trend toward initial signatures for the argillites (+2). Argillites tend to have lower Nd (ϵ_{Nd} about -5 to +2) and higher $^{87}\text{Sr}/^{86}\text{Sr}$ (0.705 to 0.707) than other host rocks and serpentinite data scatter widely, partly due to the questionable quality of the analyses, but also because of post-emplacement alteration. High ^{207}Pb , low ϵ_{Nd} , and higher Sr values all suggest that the argillites contain older, slightly more radiogenic, crustal material, perhaps indicative of a partial Paleozoic provenance. Crosscutting diabase dikes have variable Pb and Sr, but high ϵ_{Nd} values indicate that these dikes are from a depleted source — one sample exhibiting the most depleted isotopic signature of any of the Greens Creek host rocks.

Initial Nd-Sr isotopic signatures for Greens Creek host rocks are compared with other Nd-Sr isotopic results from Alexander and Gravina terranes (fig. 14) that have been interpreted to represent depleted, mantle-derived, oceanic island-arc environments (Samson and others, 1989, 1991a). Initial Nd isotopic compositions for Greens Creek metabasalt and metagabbro are similar to both Alexander and Gravina mafic rock data but vary more widely in Sr isotopic composition. This deviation could be the result of alteration and/or mobilization of Rb and Sr during Cretaceous deformation. Greens Creek argillite and serpentinite signatures vary widely, not unlike values from Alexander and Gravina metasedimentary samples. Sr values for other Alexander terrane samples (Samson and others, 1989) also approach Cretaceous seawater values (about 0.7078).

Interestingly, Alexander terrane felsic igneous rocks are more depleted (higher initial Nd and lower initial Sr) than their relatively coeval mafic counterparts. Two crosscutting bodies in the Greens Creek area, GC-1704-01 and LG-64, plot with the Alexander terrane felsic igneous rocks (fig. 14). A third dike, GC-1701-01, however, does not, but instead plots with the mafic igneous rocks. There were no other samples analyzed that come close to isotopic signatures exhibited by the serpentinites ADM-59 or LG-32, throwing further doubt on their validity.

Initial Lead Isotopes of Greens Creek Host Rocks Compared to Ore Lead Compositions

Lead isotopic data were obtained from many samples of galena, pyrrargyrite, sphalerite, pyrite, chalcopyrite, and tetrahedrite from inside the Greens Creek mine as well as several samples from outside the mine. Their lead isotopic compositions varied only slightly along a ^{207}Pb trend (fig. 11, chap. 10) and were compared to model lead evolutions for different large-scale, global sources or reservoirs (for example, mantle, orogene, upper crust; Zartman and Doe, 1981). The Greens Creek ore lead compositions ($^{206}\text{Pb}/^{204}\text{Pb}$ = 18.6–18.8 and $^{207}\text{Pb}/^{204}\text{Pb}$ = 15.55–15.68) plotted along the “orogene” evolution curve at a model lead age between 0 and 100 Ma. Some lead compositions lie along a high- ^{207}Pb trend, suggesting mixing with older, more radiogenic material, not unlike lead that could be derived from the Paleozoic Alexander terrane.

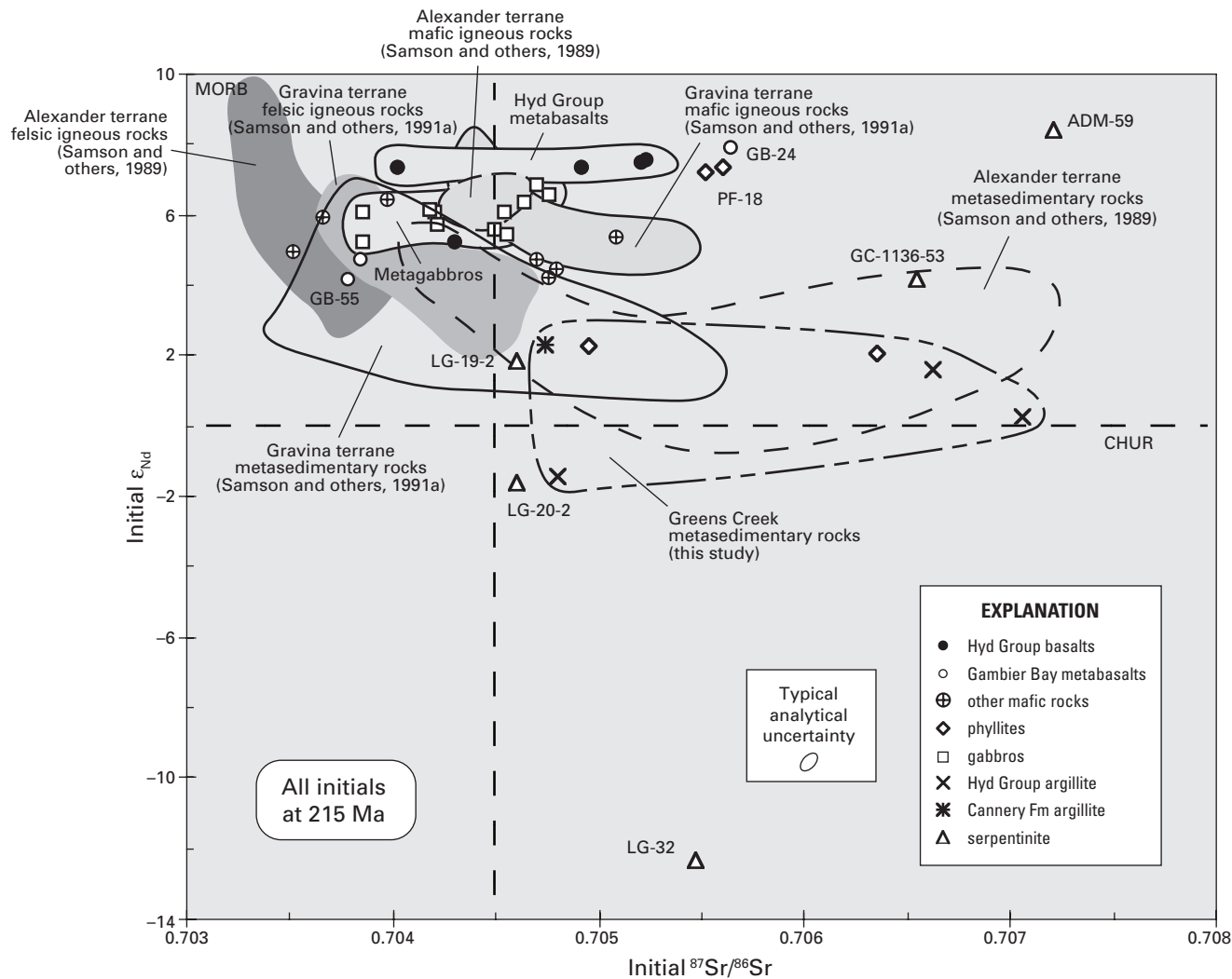


Figure 14. Initial strontium versus initial neodymium correlation diagram showing the distribution of initial Sr-Nd values for Greens Creek host rocks relative to Sr-Nd fields for previously published Alexander and Gravina terrane rocks (Samson and others, 1989, 1991a). Initial isotopic values for Greens Creek host rocks are more scattered than data shown for comparable lithologies of Alexander and Gravina terrane rocks; however, in general, the fields are not too dissimilar with relatively equal initial ϵ_{Nd} values for mafic lithologies and on average equal $^{87}Sr/^{86}Sr$ values. There are no felsic igneous rock data from Greens Creek to compare with the other terranes (except perhaps LG-64), but metasedimentary rock data from Greens Creek are very similar to that reported for other Alexander terrane metasedimentary samples. Again, data from serpentinites do not match any other results from either terrane, supporting the idea that these analyses are not reliable. MORB, mid-ocean ridge basalt; CHUR, chondritic uniform reservoir.

Likewise, initial lead isotopic compositions for host rocks have been compared to model lead compositions to help delineate their petrotectonic derivation (figs. 10 and 11). More important, initial lead compositions can be calculated to match the assumed age of mineralization (215 Ma), such that ore lead compositions can be directly compared to host/source-rock initial lead compositions to evaluate their genetic link, if any (fig. 15). A direct comparison such as this is a powerful tool in determining whether ore is syngenetic or epigenetic.

Lead isotopic data for Greens Creek ore suggest that it was formed through mixing between two main components: mafic magmatic source(s) represented by compositions of the metabasalts, metagabbros, and serpentinites, and compositions

given by the hanging-wall, pyritic, black argillites (fig. 15). The ore Pb field plots at the top of the mafic igneous fields, but not within it. Initial lead values for the various black argillites appear to embody the range of Pb values for the Greens Creek ore, suggesting that the ore Pb may be a homogenization of argillite Pb alone. On closer inspection, Pb values for unmineralized phyllites and argillites do not actually lie within the ore Pb field, but surround it (figs. 10 and 15). Therefore, it would appear that the Pb isotopic composition for Greens Creek ore is unique, and no particular host rock consistently shares that same composition. It is evident that the relatively uniform ore Pb signature may represent a homogenization of Pb derived from host metabasalt, metagabbro, some footwall phyllites, and the hanging-wall argillite(s).

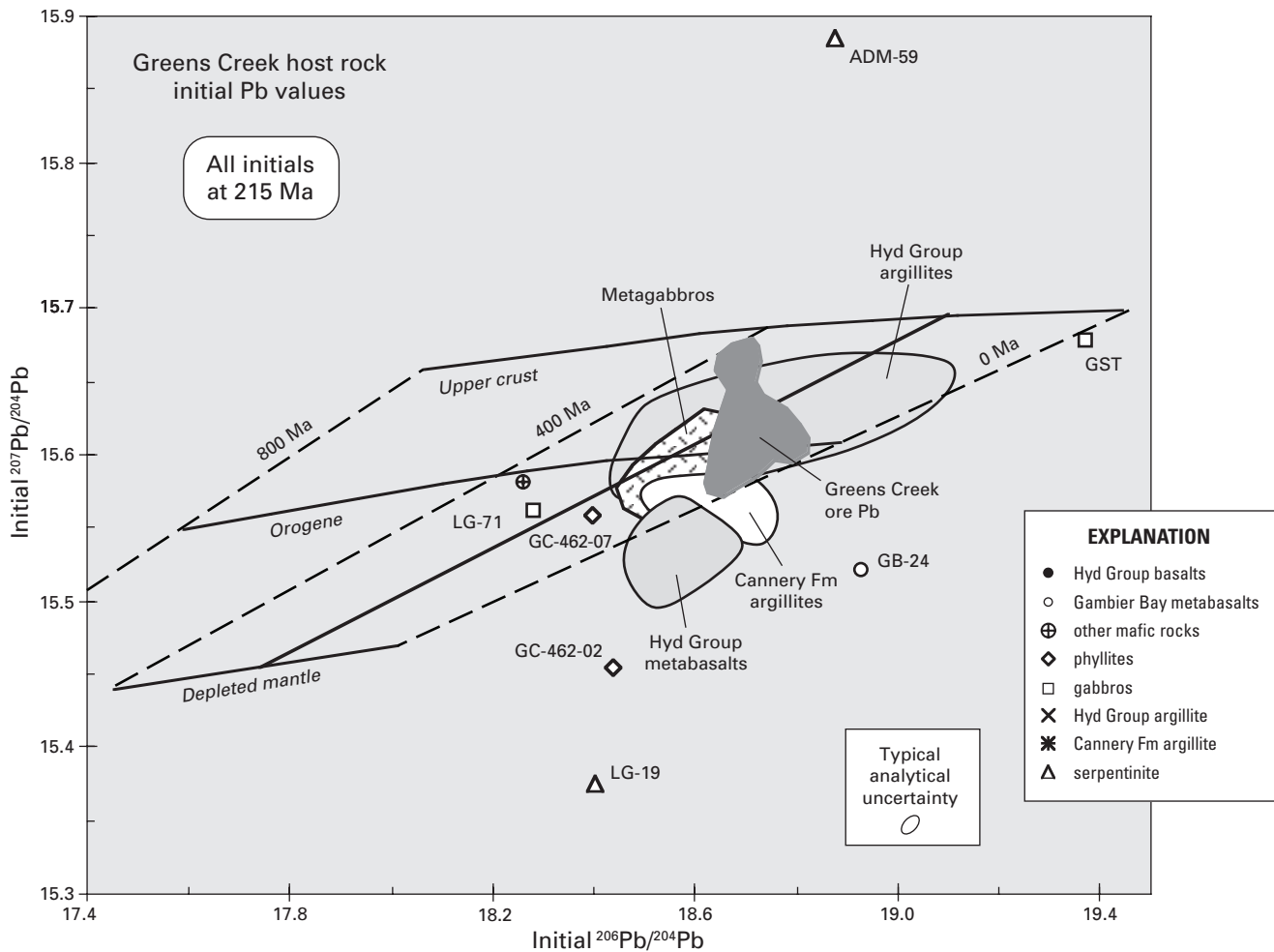


Figure 15. Pb-Pb correlation diagram (²⁰⁶Pb/²⁰⁴Pb versus ²⁰⁷Pb/²⁰⁴Pb) showing the distribution of initial lead compositions of Greens Creek host rocks relative to lead isotopic compositions for Greens Creek sulfides (ore). The Greens Creek ore lead compositions (²⁰⁶Pb/²⁰⁴Pb = 18.6 – 18.8 and ²⁰⁷Pb/²⁰⁴Pb = 15.55 – 15.68) plotted along the “orogene” evolution curve at a model lead age between 0 and 100 Ma. The field for the ore lies within that for the argillites, however, none of the argillite initial lead compositions actually lie on the ore trend, but surround it. Lead isotopic data for Greens Creek ore suggest that it was formed through mixing between two main components: mafic magmatic source(s) represented by compositions of the metabasalts, metagabbros, and serpentinites, and compositions given by the hanging-wall, pyritic, black argillites. See text and chapter 10 for more discussion.

The isotopic data imply that magmatic fluids, emanating from ascending volcanic-arc magmas, mix with overlying marine shales and volcanic sediment. Driven by the heat of the intrusion, hydrothermal circulation of these fluids with high salinity and moderate temperatures through the sediment package, metasomatize the sediment and deposit metals onto the sea floor and into adjacent sediments. The sulfides in this scenario would incorporate the lead isotopic compositions of the magmatic fluid and the marine sediment. This same lead isotopic behavior — ore compositions between basalts and pelagic sediment signatures — has been documented from several modern VMS ore deposits around the world: East Pacific Rise (Dasch and others, 1971; O’Nions and others, 1978; Brevart and others, 1981), Nazca plate MORB (Unruh and Tatsumoto, 1976), Japanese Kuroko deposits (Fehn and others, 1983).

Summary

Initial Pb-Sr-Nd isotopic data indicate a depleted mantle source for Greens Creek host rocks and their associated ore, with very little to no input of any older crustal material. The initial isotopic data scatter somewhat, indicating the likelihood of post-emplacement isotopic disturbances during subsequent metamorphism and(or) alteration by fluid/rock interaction processes. Nonetheless, the isotopic data exhibit elevated $^{206}\text{Pb}/^{204}\text{Pb}$ and $^{87}\text{Sr}/^{86}\text{Sr}$ relative to OIB or MORB trends at 215 Ma and are consistent with isotopic signatures typical of oceanic-arc environments. The Greens Creek host-rock data are similar to other isotopic data from the Alexander and Gravina terranes that support these interpretations.

A sequence of progressively more positive or depleted ϵ_{Nd} and lower $^{87}\text{Sr}/^{86}\text{Sr}$ values throughout the Greens Creek host-rock stratigraphy implies rifting of the preexisting arc crust and emplacement of magmas with progressively higher mantle-derived components. These isotopic data support a genetic model of ore deposition in a rifted oceanic-arc environment.

Lead isotopic values for Greens Creek ore indicate the probability that metals were derived from magmatic fluids emanating from mafic/ultramafic sources and circulating through or mixing with marine shales (argillites).

Acknowledgments

The authors thank the Kennecott Greens Creek Mining Company for their cooperation, hospitality, and special equipment during sample collection on Admiralty Island. Also, thanks to all the workers at the USGS that were responsible for the majority of sample preparation and chemical analysis, especially Elaine Gilman. Special thanks to manuscript reviewers Brian Marshall and Gary Landis for their helpful comments and criticisms. And special thanks to C.D. Taylor and C.A. Johnson, our editors, for having the patience to see this manuscript into review and eventual fruition.

References

- Allegre, C.J., and Luck, J.M., 1980, Osmium isotopes as petrogenetic and geological tracers: *Earth and Planetary Science Letters*, v. 48, p. 148–54.
- Ayuso, R.A., Wooden, J.L., Foley, N.K., Seal, R.R., Sinha, A.K., and Persing, H., 2004, U-Pb zircon ages and Pb isotope geochemistry of gold deposits in the Carolina Slate Belt of South Carolina: *Economic Geology*, v. 100, p. 225–252.
- Barovich, K.M., and Patchett, P.J., 1992, Behavior of isotopic systematics during deformation and metamorphism—A Hf, Nd and Sr isotopic study of mylonitized granite: *Contributions to Mineralogy Petrology*, v. 109, p. 386–393.
- Ben Othman, Dalila, White, W.M., and Patchett, J., 1989, The geochemistry of marine sediments, island arc magma genesis, and crust-mantle recycling: *Earth and Planetary Science Letters*, v. 94, p. 1–21.
- Berg, H.C., Jones, D.L., and Richter, D.H., 1972, Gravina-Nutzotin Belt — Tectonic significance of an upper Mesozoic sedimentary and volcanic sequence in southern and southeastern Alaska: *U.S. Geological Survey Professional Paper 800-D*, p. D1–D24.
- Brevart, Olivier, Dupre, B., and Allegre, C.J., 1981, Metallogenesis at spreading centers — Lead isotope systematics for sulfides, manganese-rich crusts, basalts, and sediments from the Cyamex and Alvin areas (East Pacific Rise): *Economic Geology*, v. 76, p. 1205–1210.
- Burke, W.H., Denison, R.E., Hetherington, E.A., Koepnick, R.B., Nelson, H.F., and Otto, J.B., 1982, Variations of seawater $^{87}\text{Sr}/^{86}\text{Sr}$ throughout Phanerozoic time: *Geology*, v. 10, p. 516–519.
- Dasch, E.J., Dymond, J.R., and Heath, G.R., 1971, Isotopic analysis of metalliferous sediment from the East Pacific Rise: *Earth and Planetary Science Letters*, v. 13, p. 175–180.
- DePaolo, D.J., 1981, Neodymium isotopes in the Colorado Front Range and crust-mantle evolution in the Proterozoic: *Nature*, v. 291, p. 193–196.
- Dickin, Alan, 1995, *Radiogenic isotope geology*: Cambridge, England, Cambridge University Press, 490 p.
- Ellam, R.M., and Hawkesworth, C.J., 1988, Elemental and isotopic variations in subduction related basalts — Evidence for a three component model: *Contributions to Mineralogy and Petrology*, v. 98, pp. 72–80.
- Farmer, G. Lang, Ayuso, R., and Plafker, G., 1993, A Coast Mountains provenance for the Valdez and Orca Groups, southern Alaska, based on Nd, Sr, and Pb isotopic evidence: *Earth and Planetary Science Letters*, v. 116, pp. 9–21.

- Faure, Gunther, 1986, Principles of isotope geology: New York, John Wiley and Sons, 589 p.
- Fehn, Udo, Doe, B.R., and Delevaux, M.H., 1983, The distribution of lead isotopes and the origin of Kuroko ore deposits in the Hokuroku district, Japan: Economic Geology Monograph no. 5, p. 488–506.
- Gaccetta, J.D., and Church, S.E., 1989, Lead isotope data base for sulfide occurrences from Alaska, December, 1989: U.S. Geological Survey Open-File Report 89–688, 60 p.
- Gehrels, G.E., and Berg, H.C., 1992, Geologic map of southeastern Alaska: U.S. Geological Survey Investigation Series Map I–1867, scale 1:600,000.
- Hart, S.R., and Kinloch, E.D., 1989, Osmium isotope systematics in Witwatersrand and Bushveld ore deposits: Economic Geology, v. 84, p. 1651–1655.
- Hawkesworth, C.J., O’Nions, R.K., Pankhurst, R.J., Hamilton, P.J., and Evensen, N.M., 1977, A geochemical study of island-arc and back-arc tholeiites from the Scotia Sea: Earth and Planetary Science Letters, v. 36, pp. 253–262.
- Hawkesworth, C.J., O’Nions, R.K., and Arculus, R.J., 1979, Nd and Sr isotope geochemistry of island arc volcanics, Grenada, Lesser Antilles: Earth and Planetary Science Letters, v. 45, p. 237–248.
- Hess, Jennifer, Bender, M.L., and Schilling, J.G., 1986, Evolution of the ratio of strontium–87 to strontium–86 in seawater from Cretaceous to present: Science, v. 231, p. 979–984.
- Kerrick, Robert, 1991, Radiogenic isotope systems applied to ore deposits, *in* Heaman, L., and Ludden, J.N., eds., Applications of radiogenic isotopes systems to problems in geology, Mineralogical Association of Canada, Short Course 19, p. 365–421.
- Lambert, D.D., Morgan, J.W., Walker, R.J., Shirey, S.B., Carlson, R.W., Zientek, M.L., and Koski, M.S., 1989, Rhenium–osmium and samarium–neodymium isotopic systematics of the Stillwater Complex: Science, v. 244, p. 1169–1174.
- Martin, C.E., 1991, Osmium isotopic characteristics of mantle-derived rocks: Geochimica et Cosmochimica Acta, v. 55, p. 1421–1434.
- Newberry, R.J., and Brew, D.A., 1997, Chemical and isotopic data for rocks and ores from the Upper Triassic Greens Creek and Woewodski Island volcanogenic massive sulfide deposits, southeastern Alaska, *in* Geologic studies in Alaska by the U.S. Geological Survey: U.S. Geological Survey Professional Paper 1614, p. 35–55.
- Newberry, R.J., Brew, D.A., and Crafford, T.C., 1990, Genesis of the Greens Creek volcanogenic massive sulfide deposit, S.E. Alaska — A geochemical study, [abs.]: Geological Association of Canada Program with Abstracts, v. 15, p. A96.
- Newberry, R.J., Crafford, T.C., Newkirk, S.R., Young, L.E., Nelson, S.W., and Duke, N.A., 1997, Volcanogenic massive sulfide deposits of Alaska: Economic Geology Monograph no. 9, p. 120–150.
- O’Nions, R.K., Carter, S.R., Cohen, R.S., Evensen, N.M., and Hamilton, P.J., 1978, Pb, Nd and Sr isotopes in oceanic ferromanganese deposits and ocean floor basalts: Nature, v. 273, p. 435–438.
- Pearce, J.A., 1983, The role of sub-continental lithosphere in magma genesis at destructive plate margins, *in* Hawkesworth, C.J., and Norry, M.J., eds., Continental basalts and mantle xenoliths, p. 230–249: Nantwich, United Kingdom, Shiva Publications, Ltd.
- Premo, W.R., and Tatsumoto, M., 1991, U-Th-Pb isotopic systematics of lunar norite 78235, *in* Proceedings of Lunar and Planetary Science Conference, v. 21, p. 89–100: Houston, Texas, The Lunar and Planetary Institute.
- Premo, W.R., and Tatsumoto, M., 1992, U-Th-Pb, Rb-Sr, and Sm-Nd isotopic systematics of lunar troctolitic cumulate 76535: Implications on the age and origin of this early lunar, deep-seated cumulate, *in* Proceedings of Lunar and Planetary Science Conference, v. 22, p. 381–397: Houston, Texas, The Lunar and Planetary Institute.
- Rubin, C.M., and Saleeby, J.B., 1992, Tectonic history of the eastern edge of the Alexander Terrane, southeast Alaska: Tectonics, v. 11, p. 586–602.
- Rubin, C.M., Saleeby, J.B., Cowan, D.S., Brandon, M.T., and McGroder, M.F., 1990, Regionally extensive mid-Cretaceous west-vergent thrust system in the northwestern Cordillera — Implications for continent-margin tectonism: Geology, v. 18, p. 276–280.
- Samson, S.D., McClelland, W.C., Patchett, P.J., Gehrels, G.E., and Anderson, R.G., 1989, Evidence from neodymium isotopes for mantle contributions to Phanerozoic crustal genesis in the Canadian Cordillera: Nature, v. 337, p. 705–709.
- Samson, S.D., Patchett, P.J., Gehrels, G.E., and Anderson, R.G., 1990, Nd and Sr isotopic characterization of the Wrangellia Terrane and implications for crustal growth of the Canadian Cordillera: Journal of Geology, v. 98, p. 749–762.
- Samson, S.D., Patchett, P.J., McClelland, W.C., and Gehrels, G.E., 1991a, Nd isotopic characterization of metamorphic rocks in the Coast Mountains, Alaskan and Canadian Cordillera — Ancient crust bounded by juvenile terranes: Tectonics, v. 10, p. 770–780.
- Samson, S.D., Patchett, P.J., McClelland, W.C., and Gehrels, G.E., 1991b, Nd and Sr isotopic constraints on the petrogenesis of the west side of the northern Coast Mountains batholith, Alaskan and Canadian Cordillera: Canadian Journal of Earth Science, v. 28, p. 939–946.

- Stacey, J.S., and Kramers, J.D., 1975, Approximation of terrestrial lead isotope evolution by a two stage model: *Earth and Planetary Science Letters*, v. 26, p. 207–221.
- Tatsumoto, Mitsunobu, and Unruh, D.M., 1976, KREEP basalt age — Grain by grain U-Th-Pb systematics study of the quartz monzodiorite clast 15405, 88, *in* Proceedings of the 7th Lunar Science Conference, p. 2107–2129: Houston, Texas, The Lunar Planetary Institute.
- Taylor, C.D., 1997, An arc-flank to back-arc transect — Metallogeny of Late Triassic volcanogenic massive sulfide occurrences of the Alexander terrane, southeastern Alaska and British Columbia: [extended abs.], *in* Society of Economic Geologists Neves Corvo Field Conference, May 7–17, 1997, Lisbon, Portugal, Abstracts and Programs, p. 68.
- Taylor, C.D., Philpotts, J.A., Hall, T.E., and Wakeman, B.W., 1995b, New information on the geochemistry, age, and tectonic history of Late Triassic volcanic host rocks and associated massive sulfide occurrences of the Alexander terrane, southeast Alaska: Alaska Miners Association Conference Juneau, Program with Abstracts, p. 31–32.
- Taylor, C.D., Philpotts, J., Sutley, S., Gent, C., Harlan, S., Premo, W., Tatsumoto, M., Emsbo, P., and Meier, A., 1995a, Geochemistry of late Triassic volcanic rocks and age of alteration associated with volcanogenic massive sulfide occurrences, Alexander terrane, southeast Alaska, *in* *Geology and Ore Deposits of the American Cordillera, A Symposium*, Reno, Nev., 1995: Reno, Nev., Geological Society of Nevada, p. A74.
- Taylor, C.D., Premo, W.R., and Meier, A.L., 1999, The Late Triassic metallogeny of the Alexander terrane, southeastern Alaska and British Columbia: *Geological Society of America Abstracts with Programs*, v. 31, no. 6, p. A–101.
- Taylor, C.D., Premo, W.R., and Lear, K.G., 2000, The Greens Creek massive sulfide deposit — Premier example of the Late Triassic metallogeny of the Alexander terrane, southeastern Alaska and British Columbia: *Geological Society of America Abstracts with Programs*, v. 32, no. 6, p. A–71.
- Unruh, Daniel M., and Tatsumoto, M., 1976, Lead isotopic composition and uranium, thorium and lead concentrations in sediments and basalts from the Nazca plate: Initial Report of Deep Sea Drilling Project, v. 34, p. 341–347.
- Walker, R.J., Morgan, J.W., Naldrett, A.J., and Li C., 1991, Re-Os isotopic systematics of Ni-Cu sulfide ores, Sudbury Igneous Complex, Ontario — Evidence for a major crustal component: *Earth and Planetary Science Letters*, v. 105, p. 416–429.
- Whitehouse, M.J., 1988, Granulite facies Nd-isotopic homogenization in the Lewisian complex of northwest Scotland: *Nature*, v. 331, p. 705–707.
- Zartman, R.E., 1984, Lead, strontium, and neodymium isotopic characterization of mineral deposits relative to their geologic environments, *in* Proceedings of the 27th International Geological Congress, Moscow, v. 12, p. 83–106, *Metallogenesis and mineral ore deposits: Utrecht, The Netherlands*, VNU Science Press.
- Zartman, R.E., and Doe, B.R., 1981, Plumbotectonics — The model: *Tectonophysics*, v. 75, p. 135–162.

Structure of the Lower Southwest Orebody, Structural Comparison to Neighboring Orebodies, and Tectonic Model for the Greens Creek Deposit

By Katja Freitag

Chapter 13 of

**Geology, Geochemistry, and Genesis of the Greens Creek Massive
Sulfide Deposit, Admiralty Island, Southeastern Alaska**

Edited by Cliff D. Taylor and Craig A. Johnson

Professional Paper 1763

**U.S. Department of the Interior
U.S. Geological Survey**

Contents

Abstract.....	371
Introduction.....	371
Structural Background.....	374
Methodology.....	375
Structure of the Lower Southwest Orebody	375
D _{mineral} Deformation.....	375
D0 Deformation.....	375
D1 Deformation.....	375
D2 Deformation.....	375
D3 Deformation.....	378
D4 Deformation.....	386
D5 Deformation.....	388
Structural Transition and Comparison to Neighboring Orebodies	389
Model of the Structural and Tectonic Evolution of the Greens Creek Deposit.....	399
Summary and Conclusions.....	401
Acknowledgments.....	401
References Cited.....	401

Figures

1. Location map of the Greens Creek deposit.....	372
2. Cross section 2400 of the Greens Creek deposit looking north	373
3. Plan of Greens Creek orebodies (A) and Lower Southwest orebody located on the mine grid (B).....	376
4. Drawing and photograph of typical structures in massive argillite beds in the stratigraphic hanging wall of the Lower Southwest orebody.....	377
5. Rib map of siliceous rock showing well-developed S2 and S3 foliation	377
6. Cross section 2500 of the Lower Southwest orebody	378
7. Plan map of the 224 level, Lower Southwest orebody.....	379
8. Photomicrograph of a quartz-carbonate “ladder” vein offset along a stylolite	380
9. Cross section illustrating early east-directed thrust faults in massive argillite beds after removing effects of F2 and F3 folding	380
10. Rib map showing argillite forming the core of a major isoclinal F2 syncline, Lower Southwest orebody	380
11. Plan map of level 224 onto which the locations of F2 fold axes are projected to show the axis trends.....	381
12. Cross section 2400 onto which the locations of F2 fold axes are projected to show the axis plunges	383
13. Photomicrograph of S2 stylolitic foliation in stratigraphic footwall siliceous rocks.....	383
14. Photomicrograph of white mica forming penetrative S2 foliation. S2 foliation is folded S3 crenulation cleavage.....	383
15. Cross-sectional model showing the development of shears along F2 anticlines during progressive D2 deformation	384

16. Rib map of F3 folds.....	385
17. Schematic cross section illustrating the “ripple and fall” model of F3 fold distributions at the Greens Creek deposit.....	386
18. Ramsay and Huber’s (1987) principal type-3 three-dimensional fold.....	387
19. Photomicrograph of S3 stylolites in siliceous rock.....	388
20. Photomicrograph and sketch of spaced S3 crenulation cleavage in sericitic phyllite, defined by S3 cleavage domains and microlithons	389
21. Rib map depicting intermediate to steeper sections along the upper thrust of the Lower Southwest thrust system	390
22. Rose diagram comparing strikes of left-slip faults (n=8) with right-slip high-angle faults	390
23. Map of the various terranes and their bounding regional strike-slip faults, southeast Alaska and the structural setting of the Greens Creek deposit	391
24. Schematic cross section illustrating the sequence of brittle deformation events	392
25. Block diagram representing two fault blocks of massive sulfide of the Lower Southwest orebody offset across right-slip faults, with an intensely fractured fault zone	393
26. Schematic model for the transition from the Lower Southwest to the Upper Southwest and 224 West Bench orebodies based on F2 fold geometry	394
27. Lower hemisphere equal area projections of F3 fold axes of the (a) Lower Southwest and (b) Upper Southwest and 200 South orebodies	396
28. Lower hemisphere equal area projections of L3 crenulation lineations of the (a) Lower Southwest (n=22) and (b) Upper Southwest (triangles; n=16), 224 West Bench (square; n=1), and 200 South (star; n=1) orebodies	396
29. Lower hemisphere equal-area projections of poles to S2 foliation planes measured in footwall rocks of the (a) Lower Southwest (b) Upper Southwest, and (c) 224 West Bench orebodies.....	397
30. Lower hemisphere equal area projections of poles to S3 cleavage in the (a) Lower Southwest, 200 South, (b) Upper Southwest, and (c) 224 West Bench orebodies	398
31. Schematic representation of polyharmonic folds developed in competent layers of varying thickness and incompetent host materials showing the effect of the thickness of the mineralized horizon during folding	399
32. Model of the structural and tectonic evolution of the Greens Creek deposit.....	400

Tables

1. Deformation nomenclature (taken from chap. 7)	374
2. Deformation nomenclature used in this study.....	374
3. Comparison of orientations of structural features in the Lower Southwest, Upper Southwest, 224 West Bench and 200 South orebodies.....	395
4. Comparison of orebody thickness and orientations of structural features	395

Structure of the Lower Southwest Orebody, Structural Comparison to Neighboring Orebodies, and Tectonic Model for the Greens Creek Deposit

By Katja Freitag

Abstract

Greens Creek is a Zn-Pb-Ag-(Cu-Au) volcanogenic massive sulfide deposit that formed in a back-arc basin in the Alexander terrane, southeastern Alaska. Numerous sulfide orebodies are located discontinuously along the contact between highly altered mafic volcanic/volcaniclastic stratigraphic footwall rocks and stratigraphically overlying graphitic metasilstones and metashales. The orebodies were deformed several times during accretionary and subsequent wrench tectonic activity. The structurally complex deposit includes open to isoclinal folds that are refolded by open to closed folds, low-angle faults, and high-angle strike-slip faults.

Detailed rib maps, plan maps, cross sections, and long sections were used to define the structural geometry and style of the Lower Southwest orebody. The earliest deformational features are inferred Late Triassic, syndepositional normal (?) faults (D_{mineral} deformation). Hydrothermal fluids are interpreted to have flowed along these inferred faults and resulted in spatially distinct distributions of mineralized dolomite and massive sulfide. During diagenesis (D_0 deformation), early “ladder” veins formed perpendicular to metasilstone beds and, during partial subduction of the Alexander terrane in the Jurassic, these beds were offset along small thrust faults (D_1 deformation). Late Jurassic to early Tertiary accretion of the Alexander terrane resulted in south-southwest- to southeast-plunging, open to isoclinal folds (D_2 deformation), and southeast-plunging open folds (D_3 deformation), with orebody thickness and footwall and ore lithologies controlling fold geometry. Thicker sulfide horizons are not as complexly folded as thinner sulfide horizons, resulting in a polyharmonic style of fold geometry for the orebody. The D_4 deformation event signified a change from ductile to brittle deformation and formed gentle folds and thrust faults. Starting in the Eocene, wrench tectonics resulted in high-angle faults (D_5), which locally reactivated the thrust faults.

Introduction

The Greens Creek zinc-lead-silver (copper-gold) volcanogenic massive sulfide deposit, in the Alexander terrane,

southeastern Alaska (fig. 1), formed by structurally controlled hydrothermal activity in a back-arc basin environment. Numerous sulfide orebodies are located discontinuously along the contact between highly altered mafic volcanic/volcaniclastic stratigraphic footwall rocks (“phyllite”) and stratigraphically overlying graphitic metasilstones and metashales (“argillite” unit) (chap. 6). The orebodies were multiply deformed during accretionary and subsequent wrench fault tectonic activity (fig. 2).

Stratigraphic footwall phyllites are quartz-carbonate-mica-rich rocks, with variable contents of carbonate (dolomite, ankerite, magnesite, calcite), white mica, chlorite, mariposite, pyrite, titanium oxides, and graphite (Newberry and others, 1997). Footwall phyllites are more varied than hanging-wall argillites but are typically yellowish grey and contain abundant, very fine grained quartz, white mica, pyrite, and minor mariposite. Pyrite can occur as 0.5- to 10-cm-wide bands oriented subparallel to the mineralized horizon contact.

The stratigraphic hanging-wall argillites are metasedimentary rocks that consist of dark brown to black, graphitic and calcareous metasilstones and metashales, which probably represent distal turbidite sequences rather than true argillites, as well as occasional nonfossiliferous, argillaceous limestone beds. The limestone beds consist of calcite and dark brown to black, soft, opaque, organic material. The metasilstones and metashales, hereinafter referred to as massive and slaty argillite (mine nomenclature), also have a simple mineralogy, consisting of varying amounts of very fine grained quartz, calcite, white mica, and organic material. Disseminated, frequently framboidal pyrite is ubiquitous. Slaty argillite beds (metashales) are thinly laminated, whereas massive argillites (metasilstone) are slightly coarser grained than slaty argillites and form 10-cm- to 0.5-m-thick beds. The massive argillite beds are usually characterized by abundant quartz-calcite veins (“ladder” veins in mine terminology), which typically have a core of ribbon quartz oriented perpendicular to the vein walls.

The high degree of structural complexity of the Greens Creek deposit was recognized when mining of the Southwest orebody began. The Southwest orebody, which contains high

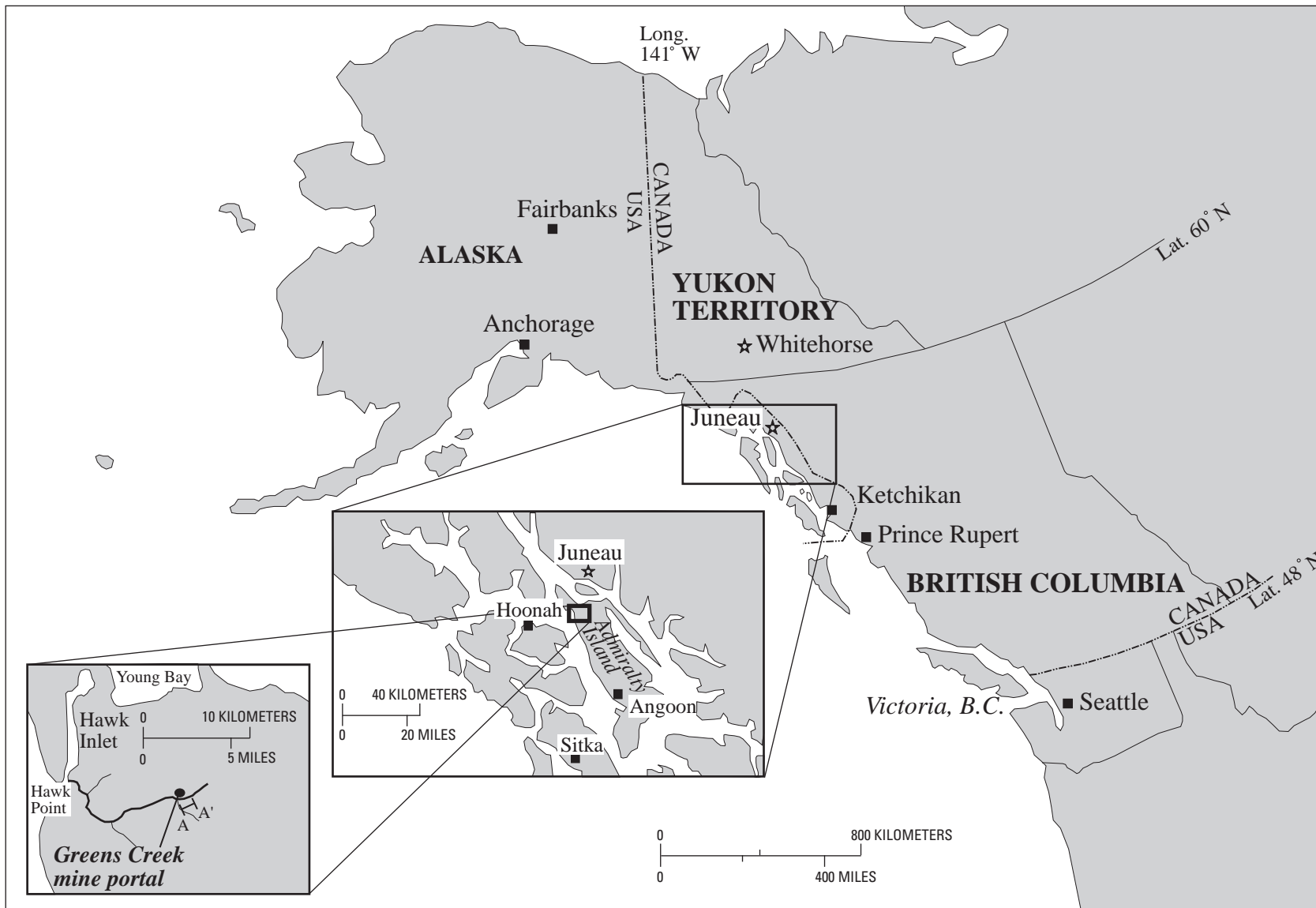
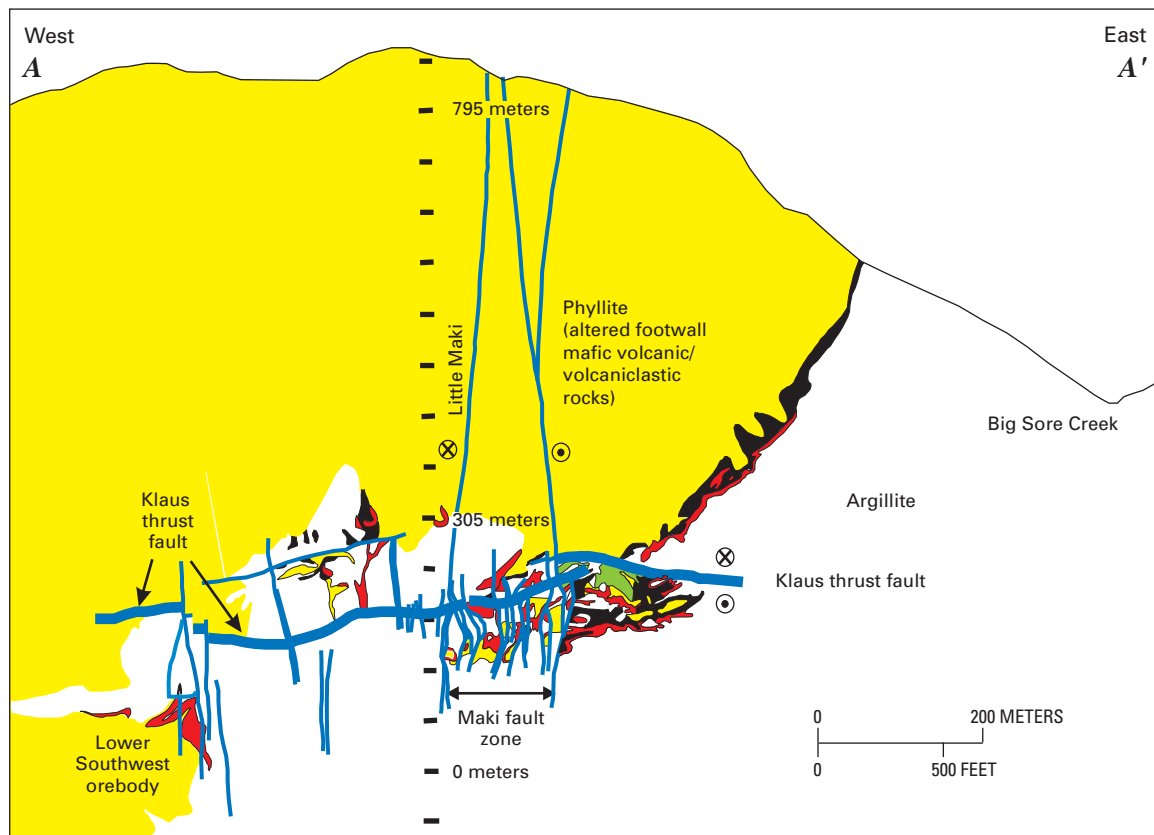


Figure 1. Location map of the Greens Creek deposit (modified after Freitag, 2000). A–A' is line of cross section shown in figure 2.



EXPLANATION

- | | |
|--------------------------------------|--|
| Stratigraphic hanging-wall argillite | Fault |
| Mineralized rocks | Klaus shear |
| Siliceous rock | Displacement to north (into plane of figure) |
| Stratigraphic footwall phyllite | Displacement to south (out of plane of figure) |
| Serpentinite | |

Figure 2. Cross section 2400 of the Greens Creek deposit looking north (modified after P.A. Lindberg, written commun., 1996).

precious-metal grades, is divided into an upper part, the Upper Southwest orebody, and a lower part, the Lower Southwest orebody. The Upper Southwest orebody comprises massive sulfide bands that are generally less than 5 m thick. The Lower Southwest orebody, the focus of this study, is characterized by up to 25-m-thick massive sulfide and mineralized dolomite sections, which thin toward the periphery of the orebody (Freitag, 2000).

This detailed structural study of the Lower Southwest orebody is the first complete study of a Greens Creek deposit orebody. The objective was to understand the structure of the orebody through detailed stope mapping and to develop a model of the geometry and structural development of the Lower

Southwest orebody. The results of this study may be used to understand the structure of other orebodies at the deposit and to understand local details of the regional structural development. A structural comparison and model for the transition between adjoining orebodies enabled the prediction of structural style to be encountered at other Greens Creek orebodies. The project built on existing structural studies and models developed by Proffett (chap. 7) and P.A. Lindberg (written commun., 1996). The tectonic history derived from the study of the Lower Southwest orebody was put in a regional context by comparing Lower Southwest structures to regional structures in this portion of southeastern Alaska. There are strong similarities between deposit-scale and regional structures.

Structural Background

At least three folding and two faulting events deformed the Greens Creek deposit (chap. 7; P.A. Lindberg, oral commun., 1997). The postmineralization deformation nomenclature that is currently used at the mine, which is based on the work of Proffett (chap. 7), is summarized in table 1. For this study, the same basic nomenclature was used, but in a slightly modified form (table 2).

D1 deformation is poorly documented. Evidence for D1 deformation is a bedding-cleavage intersection lineation (L1) recognized in the vicinity of the mine area (K.G. Lear, oral commun., 1999). This lineation is found in rocks similar to stratigraphic footwall rocks at the deposit, although it is not known whether these rocks are the same age as footwall rocks of the Greens Creek deposit.

The deposit was ductilely deformed into tight to isoclinal F2 folds that are recognized throughout the mine. Structurally thickened sulfide sections occur in hinge zones of major F2 synclines. Thin (less than 3 m) sulfide sections commonly were attenuated in hinges of F2 anticlines (chap. 7). Locally,

F2 folds were refolded by open to tight F3 and open F4 folds (chap. 7; P.A. Lindberg, written commun., 1996, 1997).

Two major fault systems are recognized at the Greens Creek deposit. A thrust fault, known as the Klaus "shear" (P.A. Lindberg, written commun., 1996) at the mine, separates the East and the West orebodies and has approximately 213 m of reverse offset across the fault, with the hanging wall displaced in a N. 60° W. direction (P.A. Lindberg, oral commun., 1998). The Maki fault zone (fig. 2) is a wide (about 150 m) zone of anastomosing, high-angle, right-slip faults that offset the deposit approximately 600 m (P.A. Lindberg, written commun., 1996). Two minor low-angle thrust faults are interpreted to have developed subparallel to the Klaus thrust fault (chap. 7; Freitag, 2000), and numerous high-angle faults formed subparallel to the Maki fault zone.

The only attempt at dating deformation episodes is the study reported by Premo and others (chap. 11), who determined ⁴⁰Ar/³⁹Ar spectra from white micas in the mine area. These spectra record the uplift and cooling of the area during mid-Cretaceous time. The uplift and cooling are interpreted to have followed accretion of the South Alaska superterrane to the North American margin (chap. 11).

Table 1. Deformation nomenclature (taken from chap. 7).

Deformation event	First	Second	Third	Fourth	Fifth
Symbol	D1	D2	D3	D4	D5
Folds		F2	F3	F4	
Cleavage		S2	S3	S4	
Lineation	L1 (?)	L2	L3	L4	
Faults		Low-angle and cleavage plane shear	Cleavage plane shear	Low-angle faults	Brittle, high-angle strike-slip faults

Table 2. Deformation nomenclature used in this study.

Deformation event	Syndepositional faulting	Diagenesis	First	Second	Third	Fourth	Fifth
Symbol	D _{mineral}	D0	D1	D2	D3	D4	D5
Folds				F2 (open to isoclinal)	F3 (open to closed)	F4 (gentle)	
Cleavage		S0 stylolites		S2 stylolitic foliation	S3 crenulation cleavage and stylolites		
Lineation				L2	L3		
Shears, faults and fractures	Syndepositional normal (?) faults	Diagenetic veins along extensional fractures	Low-angle thrust	F2 axial plane shear		Low-angle faults	High-angle strike-slip faults

Methodology

This study is based on detailed underground mapping of the Lower Southwest orebody, and parts of the Upper Southwest, 224 West Bench, and 200 South orebodies (fig. 3). Detailed maps were prepared by setting up a 33-cm (1-ft) grid along sidewalls (“ribs”) in ore accesses and stopes, and recording geological and structural data at a scale of 1 cm = 98 cm (1 inch = 8 feet). Structural analysis of the Lower Southwest, Upper Southwest, 224 West Bench, and 200 South orebodies included orientations of bedding measured in the stratigraphic hanging-wall units, contacts between the mineralized horizon and footwall and hanging-wall units, F2 fold hinges, S2 stylolitic foliation, L2 bedding-cleavage intersection lineation, F3 fold hinges, S3 stylolitic spaced crenulation cleavage, L3 crenulation lineation, and low- and high-angle fault surfaces (table 2). Pre-D2 structural elements include inferred synmineralization faults, which were interpreted after reconstruction of the Lower Southwest orebody (Freitag, 2000), and diagenetic stylolites and veins, which were examined in petrographic studies. Early L1 lineations were not recognized, and F4 folds were identified using plan and rib map patterns. Most measurements were taken in the stratigraphic hanging-wall argillite (fig. 4) and highly strained stratigraphic footwall phyllites (fig. 5) because they best reveal well-developed microfabrics. Petrographic studies of the host rocks were used to characterize structural elements.

Structure of the Lower Southwest Orebody

Structural analysis of the complexly deformed Lower Southwest orebody revealed structural elements similar to those described in studies by Lindberg (P.A. Lindberg, written commun., 1996) and Proffett (chap. 7) in other parts of the Greens Creek deposit, including F2 folds, S2 foliation, L2 lineation, F3 folds, S3 cleavage, L3 lineation, low-angle thrust faults, and high-angle faults. Detailed underground mapping of stopes and construction of plan view maps, cross sections, and long sections show that three major folds can be traced through the Lower Southwest orebody. These are an open F2 anticline, a tight to isoclinal F2 syncline, and a tight to isoclinal F2 anticline (figs. 6 and 7). The Lower Southwest orebody is refolded by stope-scale, open to closed F3 and gentle F4 folds, which locally complicate the structure. Displacement of the Lower Southwest orebody along low-angle thrust faults and high-angle strike-slip faults is minor. The thrust faults are interpreted as minor slip planes that formed below the Klaus thrust fault, and the high-angle faults are interpreted to have developed subparallel to and east of the Maki fault zone. Domain analysis indicates that the Lower Southwest orebody falls into a single structural domain.

D_{mineral} Deformation

Although pre- to synmineralization faults have not been mapped, Freitag (2000) interprets early faults on the basis of the original distributions of ore lithologies revealed by unfolding the Lower Southwest orebody to its predeformed state. Palinspastic reconstruction of the Lower Southwest orebody revealed very distinct ore lithology distributions on an orebody scale. Isopach maps of these ore lithologies, constructed on a restored base, showed spatially separate, north-south-elongated accumulations of massive sulfide and mineralized dolomite (Freitag, 2000). Freitag interpreted the linear morphologies of the accumulations to reflect primary depositional thicknesses and interpreted that the thickest accumulations formed above, or adjacent to, inferred, normal faults. The interpreted synmineralizing faults would trend north, although no further evidence for these faults was found, and may have formed in a back-arc basin environment.

D0 Deformation

Quartz-carbonate veins (“ladder veins”) are in massive argillite beds in the hanging wall of the Lower Southwest orebody. The veins are oriented perpendicular to massive argillite beds and are interpreted to have formed during burial and diagenesis (D0). The veins are commonly offset along early (S0) stylolites (fig. 8).

D1 Deformation

Evidence for D1 deformation is recorded by small thrust faults that offset hanging-wall massive argillite beds in the Lower Southwest orebody (fig. 4). Beds offset by these small (less than 1 m) displacement thrust faults have subsequently been folded by ductile D2 and D3 events. In the studied areas, unfolding of later structures indicates offset is unidirectional, with the hanging wall offset to the east (fig. 9). Evidence of early thrust faulting at an orebody scale (greater than 100 m) was not recognized.

D2 Deformation

The earliest postmineralization ductile event (D2) to deform the Lower Southwest orebody led to the development of tight to isoclinal (interlimb angle 0–30°; Ramsay and Huber, 1987) F2 folds (fig. 6). These F2 folds are important features of the Lower Southwest orebody, as they structurally thickened parts of the orebody. Rarely, open F2 folds were recognized.

Small-scale F2 folds with amplitudes of up to 2 m are easily recognized in folded massive argillite beds (fig. 4). On a stope scale, major F2 folds with amplitudes greater than 9 m can be traced on rib and plan maps (fig. 10); on an orebody scale, these major F2 folds are more easily recognized on cross sections (fig. 6).

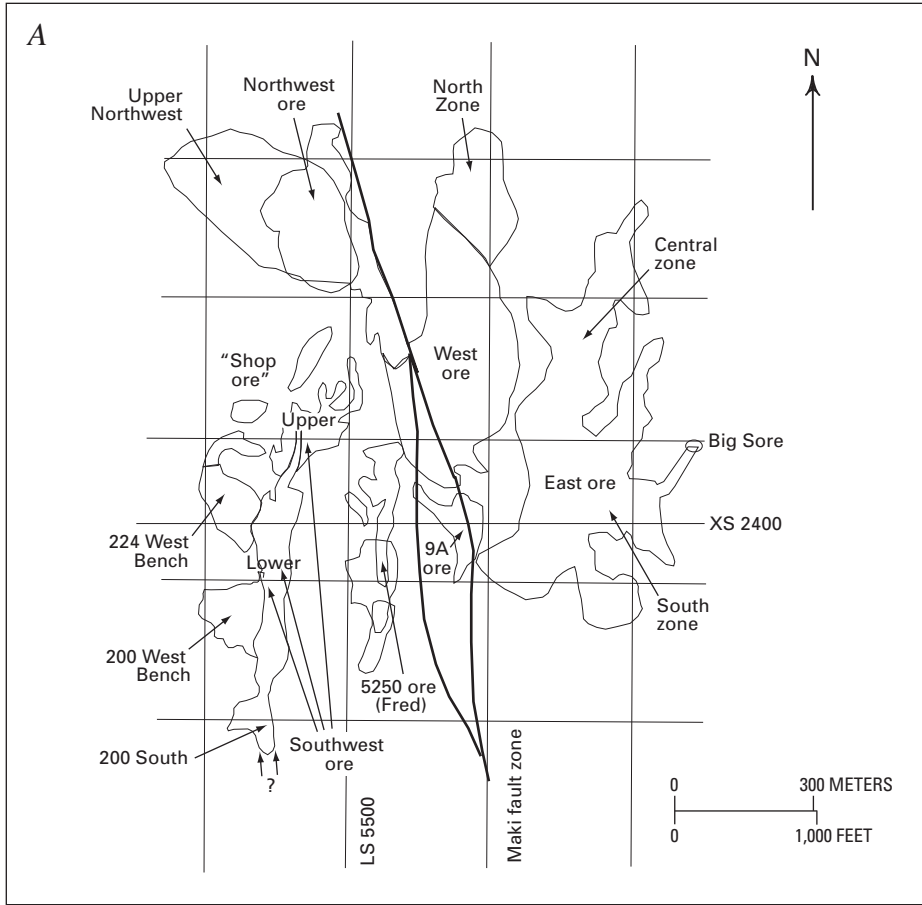
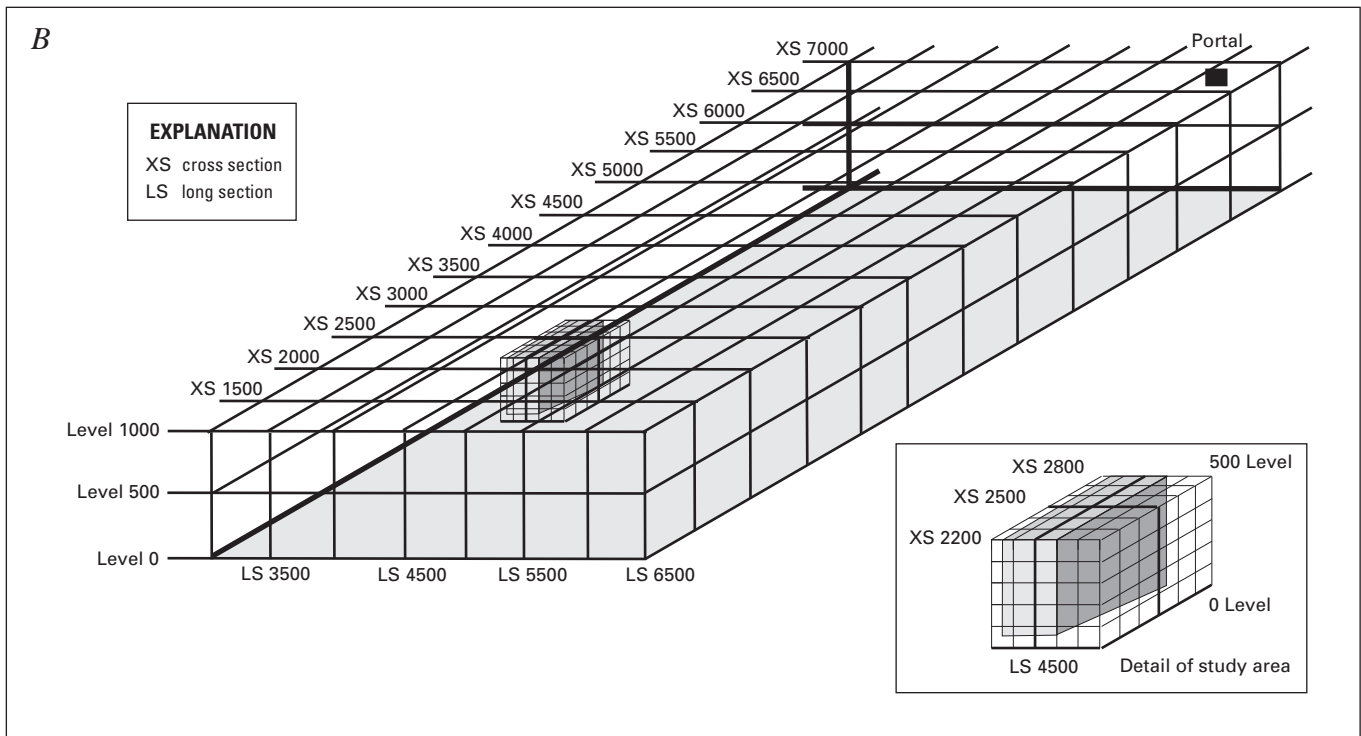


Figure 3. Plan of Greens Creek orebodies (A) and Lower Southwest orebody located on the mine grid (B).



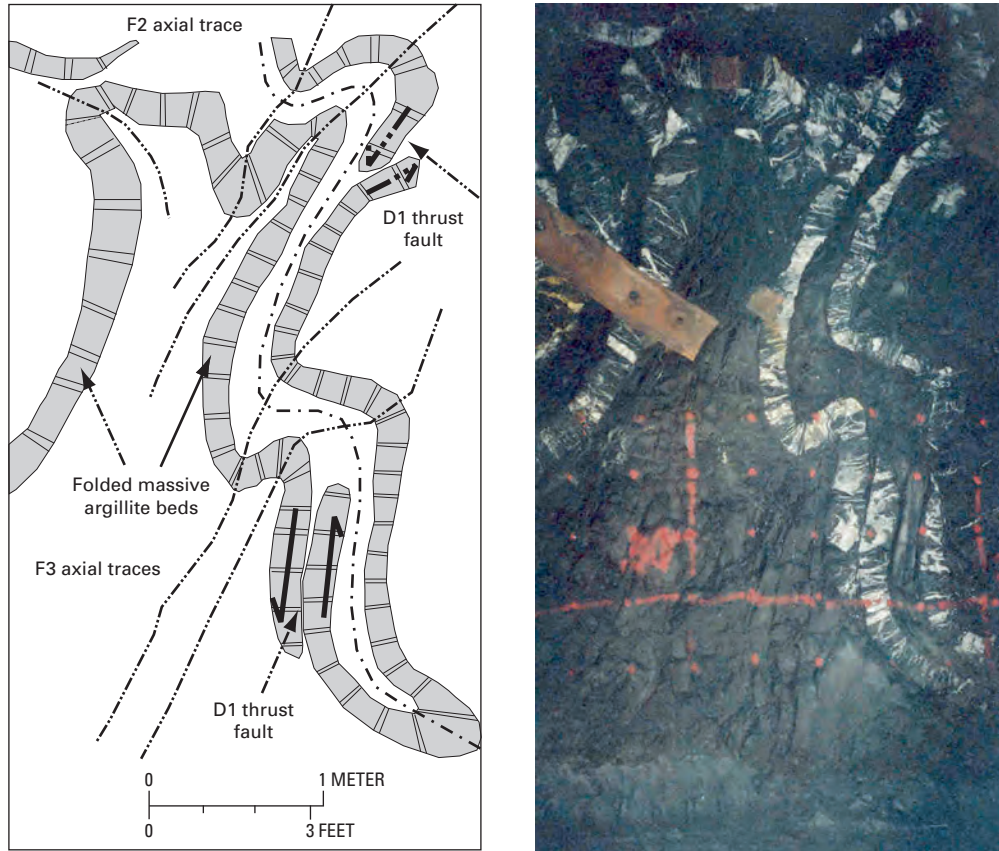


Figure 4. Drawing and photograph of typical structures in massive argillite beds in the stratigraphic hanging wall of the Lower Southwest orebody (284 ore access, looking south).

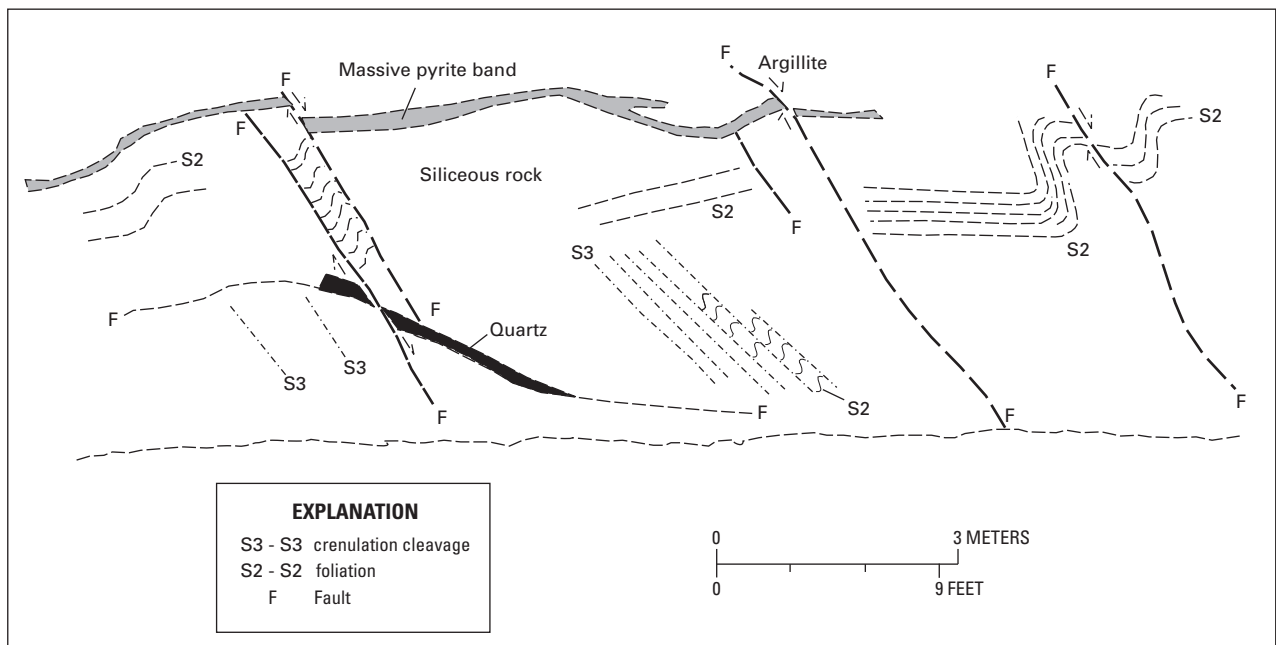


Figure 5. Rib map of siliceous rock showing well-developed S2 and S3 foliation (224 West 1 access, looking north).

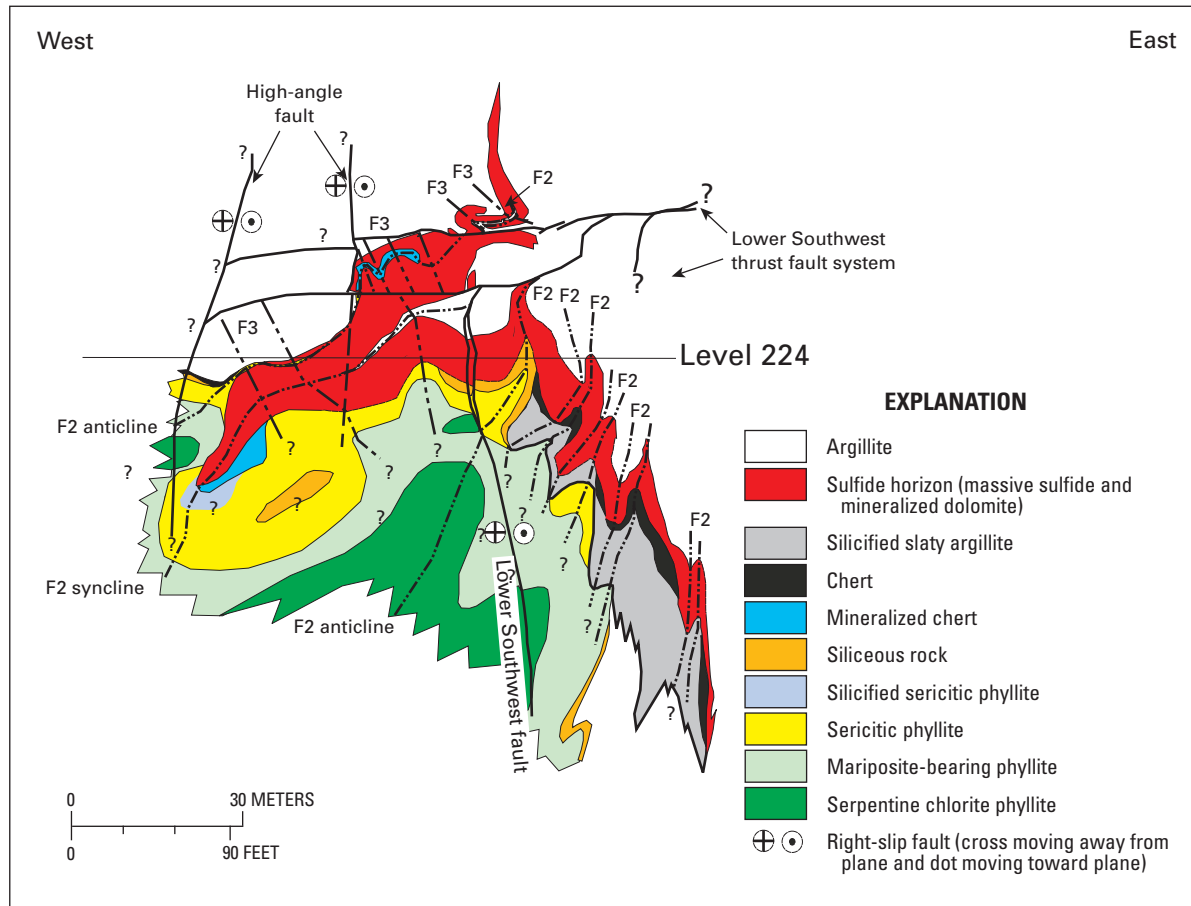


Figure 6. Cross section 2500 of the Lower Southwest orebody. Section line is shown in figure 7.

A plan projection of major F2 folds of the Lower Southwest orebody (fig. 11) shows that the general trend of these is to the south-southwest. The plunge of F2 axes varies along trend due to later F4 folding but generally ranges from 0° to 22° (fig. 12).

S2 foliation of footwall siliceous rocks is formed by closely spaced, thin (less than 25–50 μm) stylolitic foliation planes composed of dark brown to black, soft, opaque, organic material (fig. 13). Some stylolites truncate small quartz veinlets. In mica-rich sericitic phyllites, white micas are aligned and form a penetrative S2 foliation (fig. 14).

The orientations of S2 foliation planes were measured in footwall rocks (sericitic phyllite, siliceous rock, chert). These S2 foliation planes strike north to northwest in the Lower Southwest orebody, with a subordinate strike to the northeast, and vary in dip from almost vertical to almost horizontal.

The author interprets cross-section patterns, such as mapped in the rib map of level 315 (fig. 15), to indicate that D2 shears formed during later stages of D2 deformation. The combination of mica-rich, incompetent footwall rocks and a

thin, thus relatively incompetent, massive sulfide layer probably enabled a slip plane to form along axial planes of F2 isoclines, which developed into D2 shears.

D3 Deformation

The ductile D3 deformation event led to the development of open to closed ($120\text{--}30^\circ$; Ramsay and Huber, 1987) F3 folds throughout the argillite unit. The wavelength of F3 folds in argillite varies but is generally about 5 m, and the F3 axial planes are inclined 45° to 60° to the east (fig. 16). Proffett (chap. 7) describes the distribution of F3 folds in a “ripple and fall” model, which suggests that F3 folds are locally developed (fig. 17).

Hinges of F3 folds plunge 5° to 55° (average about 35°) to the southeast, although a few F3 fold hinges plunge to the northwest. The author interprets the northwest plunge to be due to later folding perpendicular to the trend of F3 fold hinges.

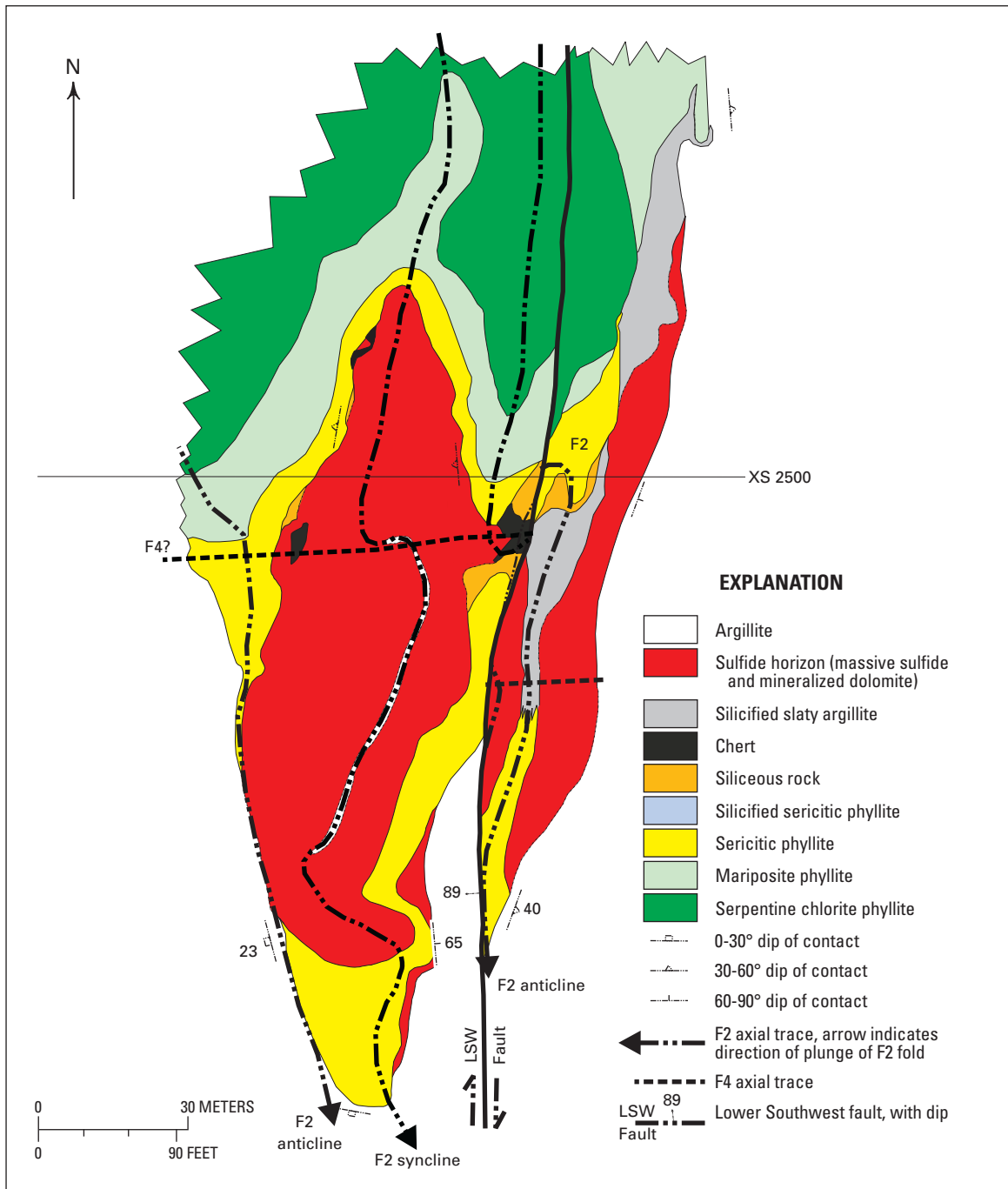


Figure 7. Plan map of the 224 level, Lower Southwest orebody. Level is shown in figure 6.

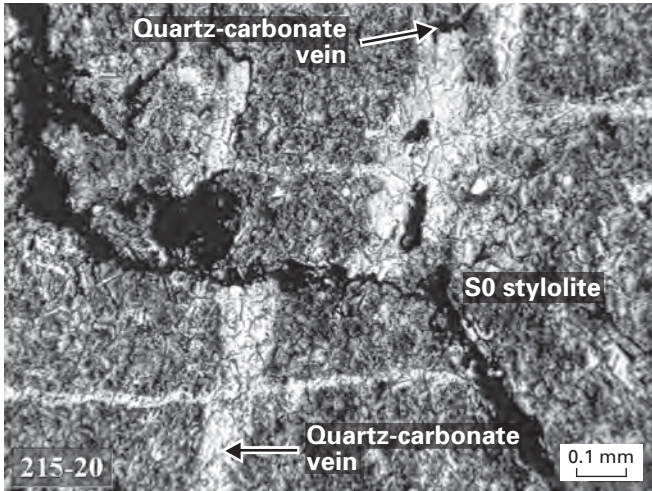


Figure 8. Photomicrograph of a quartz-carbonate “ladder” vein offset along a (S0) stylolite. Both “ladder” vein and stylolite were probably formed during burial and diagenesis (D0). mm, millimeters.

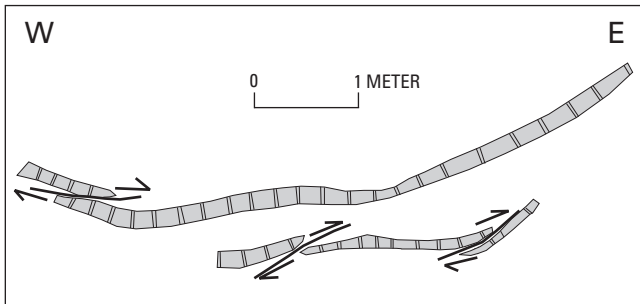


Figure 9. Cross section illustrating early east-directed thrust faults (D1) in massive argillite beds after removing effects of F2 and F3 folding (reconstructed from figure 4).

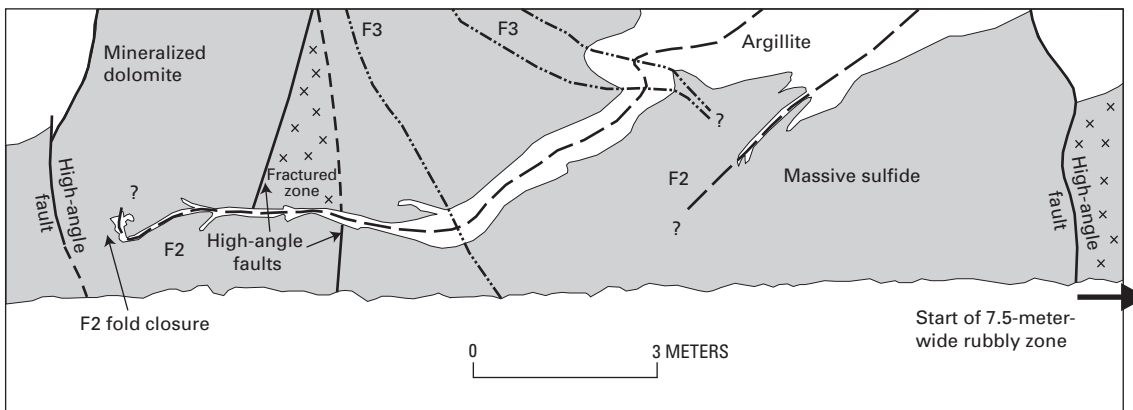


Figure 10. Rib map showing argillite forming the core of a major isoclinal F2 syncline, Lower Southwest orebody (level 224, looking north).

The L3 intersection lineations, which formed at the intersection between S2 foliation and S3 cleavage, are fine, tightly spaced to almost penetrative, linear features on S2 foliation surfaces. The L3 lineations primarily plunge 10–50° to the southeast, though a few plunge to the northeast, similar to F3 fold hinge orientations.

Although F2 fold hinges plunge steeper to the south-southwest and southeast than F3 fold hinges, both F2 and F3 fold hinges in the Lower Southwest orebody are approximately coaxial. Ramsay and Huber (1987) developed patterns arising from superposition of different fold generations, and their principal type 3 fold pattern describes the observed geometry of the superposition of F2 and F3 folds in the Lower Southwest orebody (fig. 18).

A strongly developed S3 cleavage deforms footwall rocks, especially sericitic phyllites and siliceous rocks. In siliceous rocks, S3 forms a spaced dissolution and crenulation cleavage, which offsets or crenulates the S2 foliation. In thin section, this spaced cleavage is recognizable as thick (greater than 0.1 mm) stylolites composed of dark brown to black, soft, nontranslucent, and nonreflecting organic material (fig. 19). In phyllitic rocks, S3 crenulation cleavage is defined by spaced cleavage domains composed of both stylolites of opaque, organic material, and white mica, that have gradational transitions with microlithons (Passchier and Trouw, 1996) (fig. 20). The S3 cleavage strikes north-northwest and dips moderately to steeply to the east.

Structural analyses incorporated measurements from the entire Lower Southwest orebody. This was done because the Lower Southwest orebody belongs to a single structural domain, which was determined by Freitag (2000), who undertook a π -analysis of orientations of massive argillite beds for individual mapped levels and compared combined F2/F3 π -axes. Because the beds are assumed to have been subparallel prior to deformation, F2/F3 π -axes of the same structural domain should show similar orientations, which is generally true for F2/F3 π -axes of massive argillite beds of each mapped level in the Lower Southwest orebody.

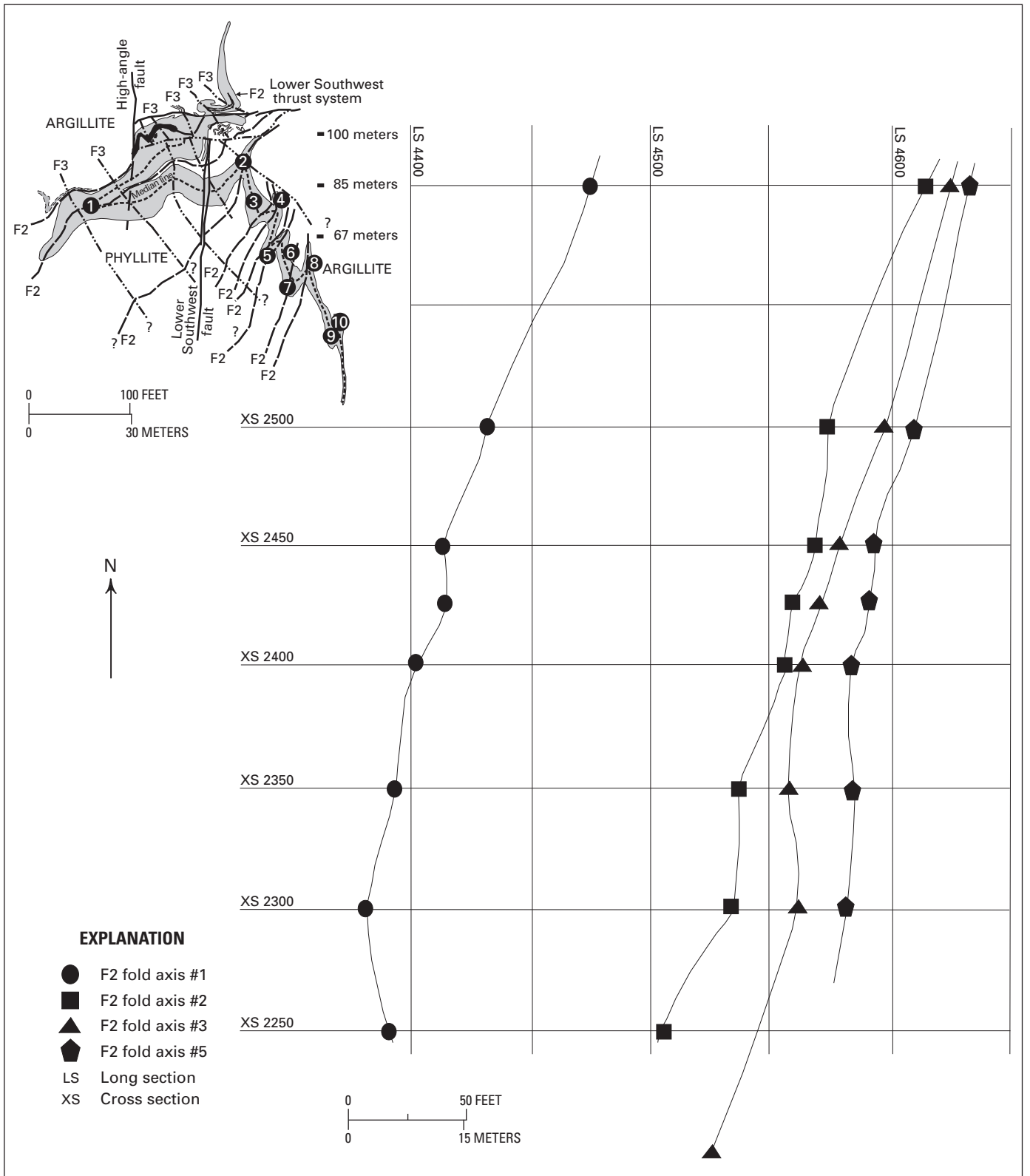


Figure 11. Plan map of level 224 onto which the locations of F2 fold axes are projected to show the axis trends. Inset map, which is a simplification of figure 6, gives the numbering of the fold hinges.

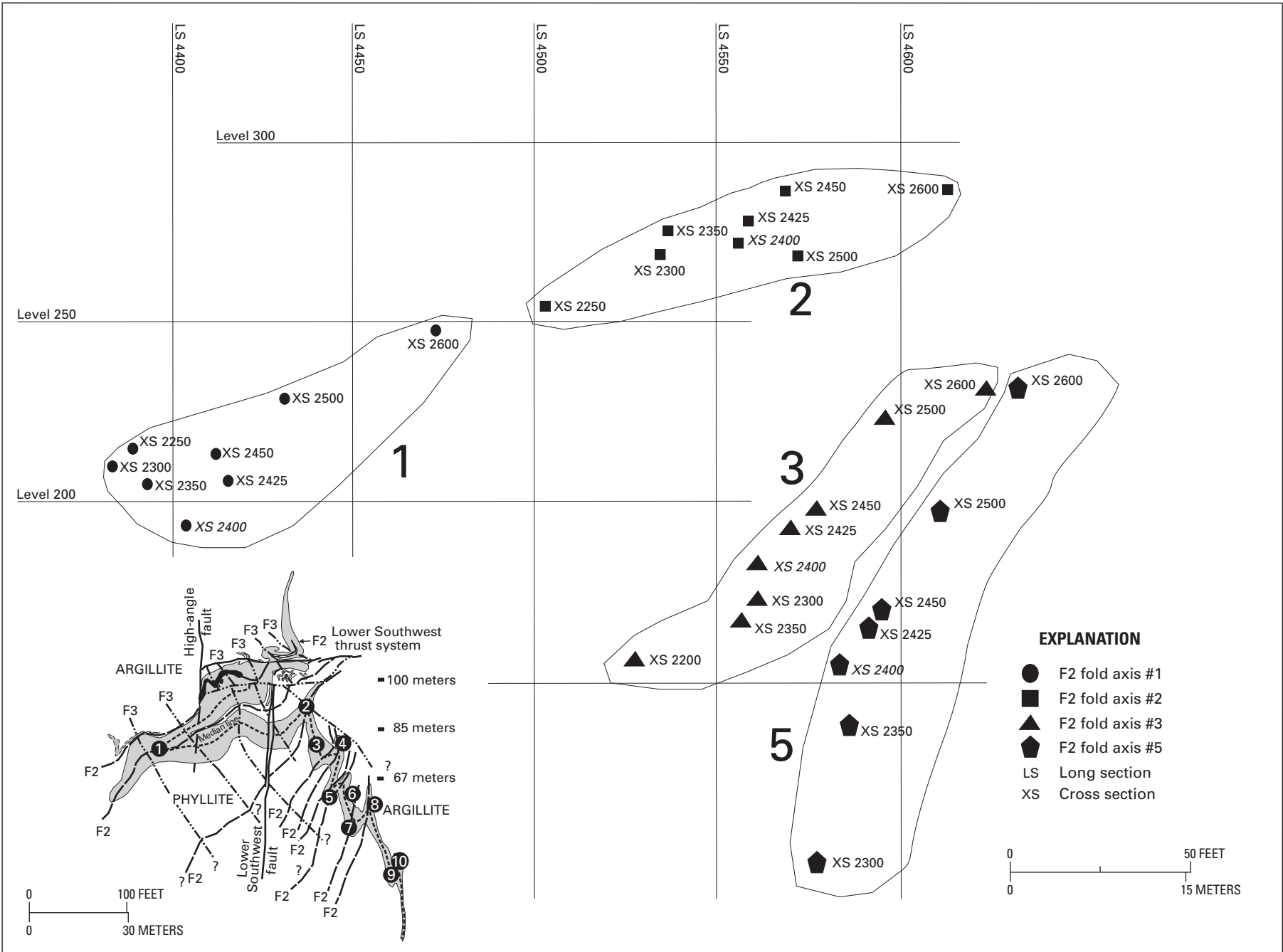


Figure 12 (facing page). Cross section 2400 (looking north) onto which the locations of F2 fold axes are projected to show the axis plunges. Inset map, which is a simplification of figure 6, gives the numbering of the fold hinges.

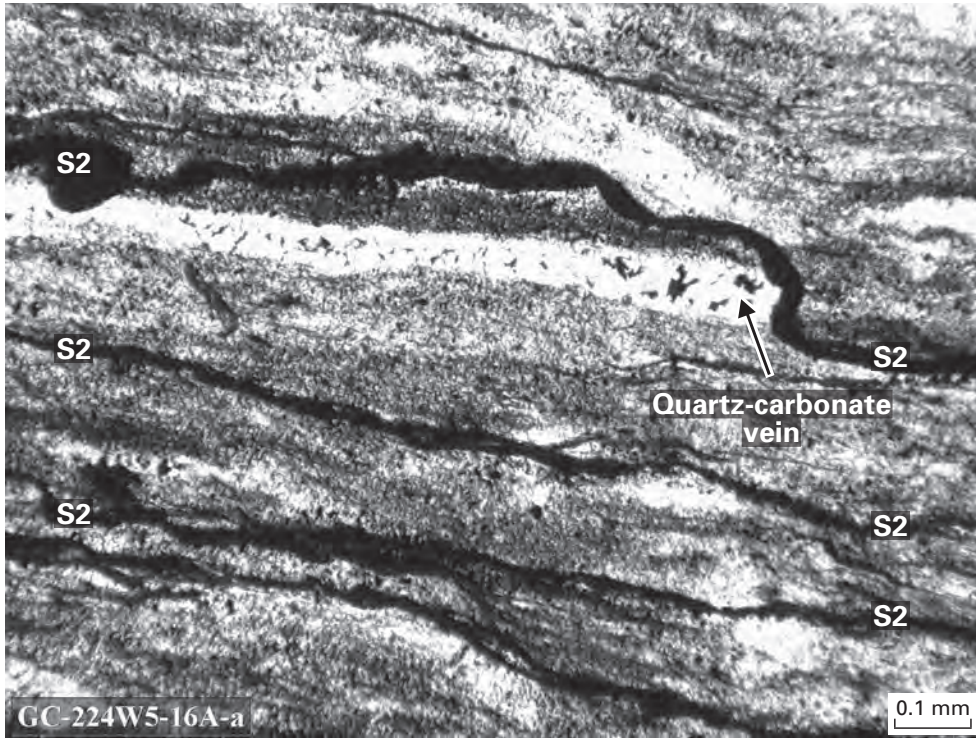


Figure 13. Photomicrograph of S2 stylonitic foliation in stratigraphic footwall siliceous rocks. mm, millimeters.

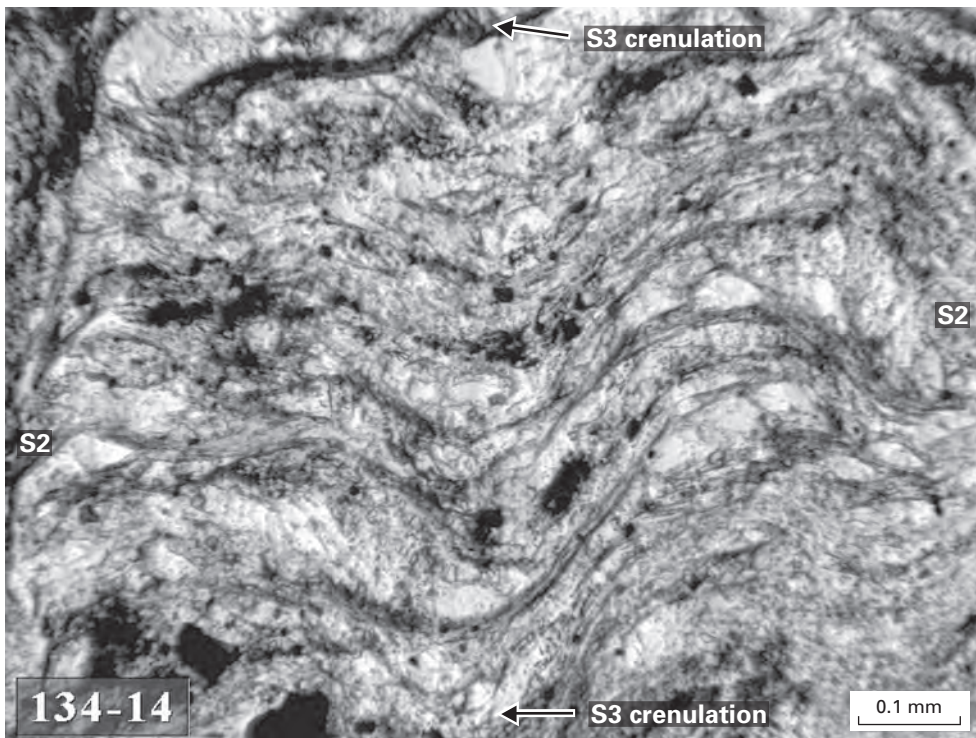


Figure 14. Photomicrograph of white mica forming penetrative S2 foliation. S2 foliation is folded S3 crenulation cleavage. mm, millimeters.

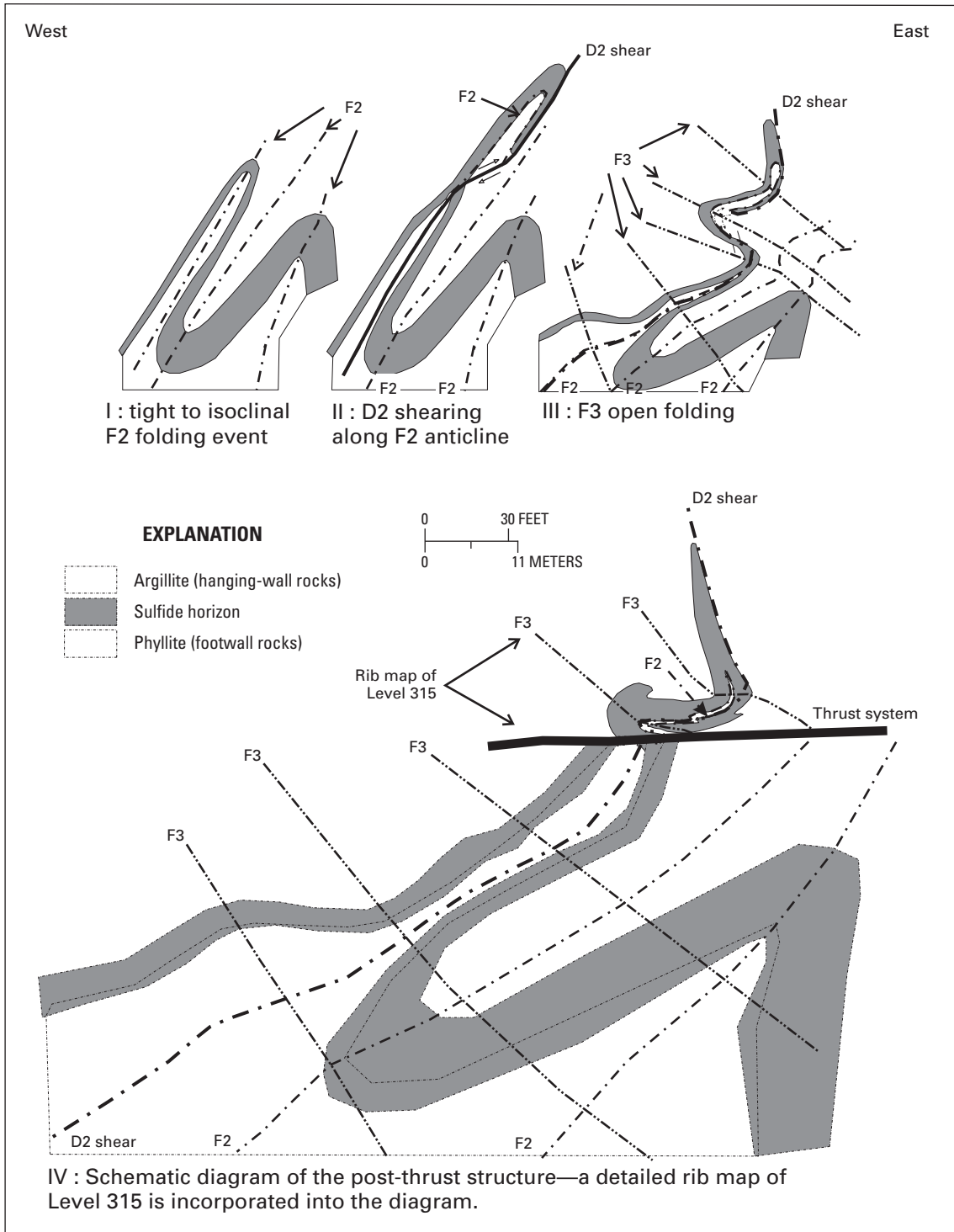


Figure 15. Cross-sectional model showing the development of shears along F2 anticlines during progressive D2 deformation. Subsequent D3 deformation and late faulting resulted in the geometry of the Lower Southwest orebody mapped on level 315.

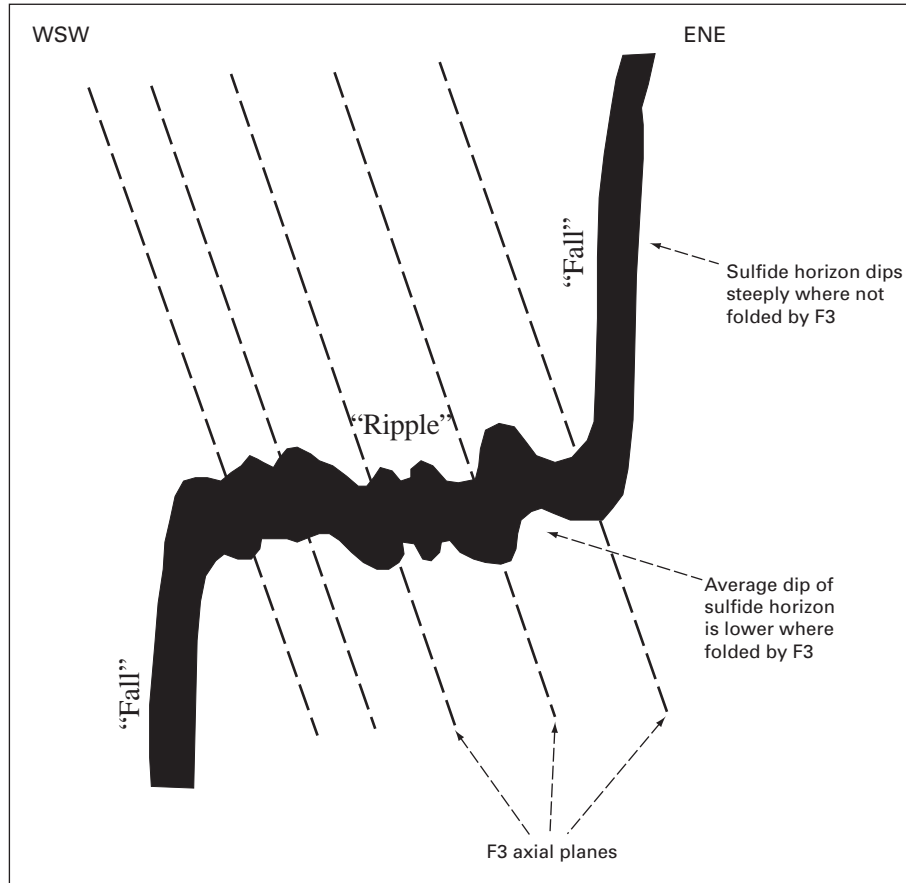


Figure 17. Schematic cross section illustrating the “ripple and fall” model of F3 fold distributions at the Greens Creek deposit (modified after Proffett, written commun., 1997).

D4 Deformation

Two low-angle fault systems, the Klaus thrust fault (fig. 2), which has a northeasterly strike and dips 30° to 50° toward the southeast, and the Lower Southwest thrust faults, (fig. 6) deform the Greens Creek deposit. These low-angle faults post-date F3 folds as they truncate F3 folds. High-angle faults offset these low-angle thrust faults, which are therefore assigned to a D4 deformation event (P.A. Lindberg, written commun., 1997; oral commun., 1998; Freitag, 2000; Freitag, unpub. data, 1997). The low-angle faults mark the change from ductile to brittle deformation.

The Lower Southwest thrust fault system is a feature in the Lower Southwest orebody, which has brecciated a zone and weakened rocks, thus causing rock failure during mining. The thrust faults are of minor importance geologically because the offset along the faults is small (approximately 24 m). The Lower Southwest thrust fault system consists of two subparallel thrust faults (upper and lower) that are less than

3 m apart in the southern part and about 10 m apart in the northern part of the Lower Southwest orebody. Characteristically, a brecciated zone of about 15 cm, containing quartz and dolomite matrix, is present on both sides of the fault planes, and carbonate is locally abundant. The fault surfaces commonly contain a thin (less than 14 mm) layer of gouge.

These thrust fault systems generally dip gently (5 – 20°) southeast, southwest, or northwest; however, locally, they dip moderately to steeply (up to 85°). Steeper segments have the appearance of having been folded by F3 folds (fig. 21). But because the thrust faults generally cut F3 folds, the flexures are not considered the result of F3 folding, and the author suggests they formed after the F3 folding event. Furthermore, the frequency of F3 folds in argillite (three folds per 15 m) differs from the frequency of steeper sections of the thrust faults in argillite (1 steeper section per 15 m) (Katja Freitag, written commun., 1998). The author therefore interprets steeper thrust fault sections as transfer faults between thrust and high-angle faults (see subsequent sections).

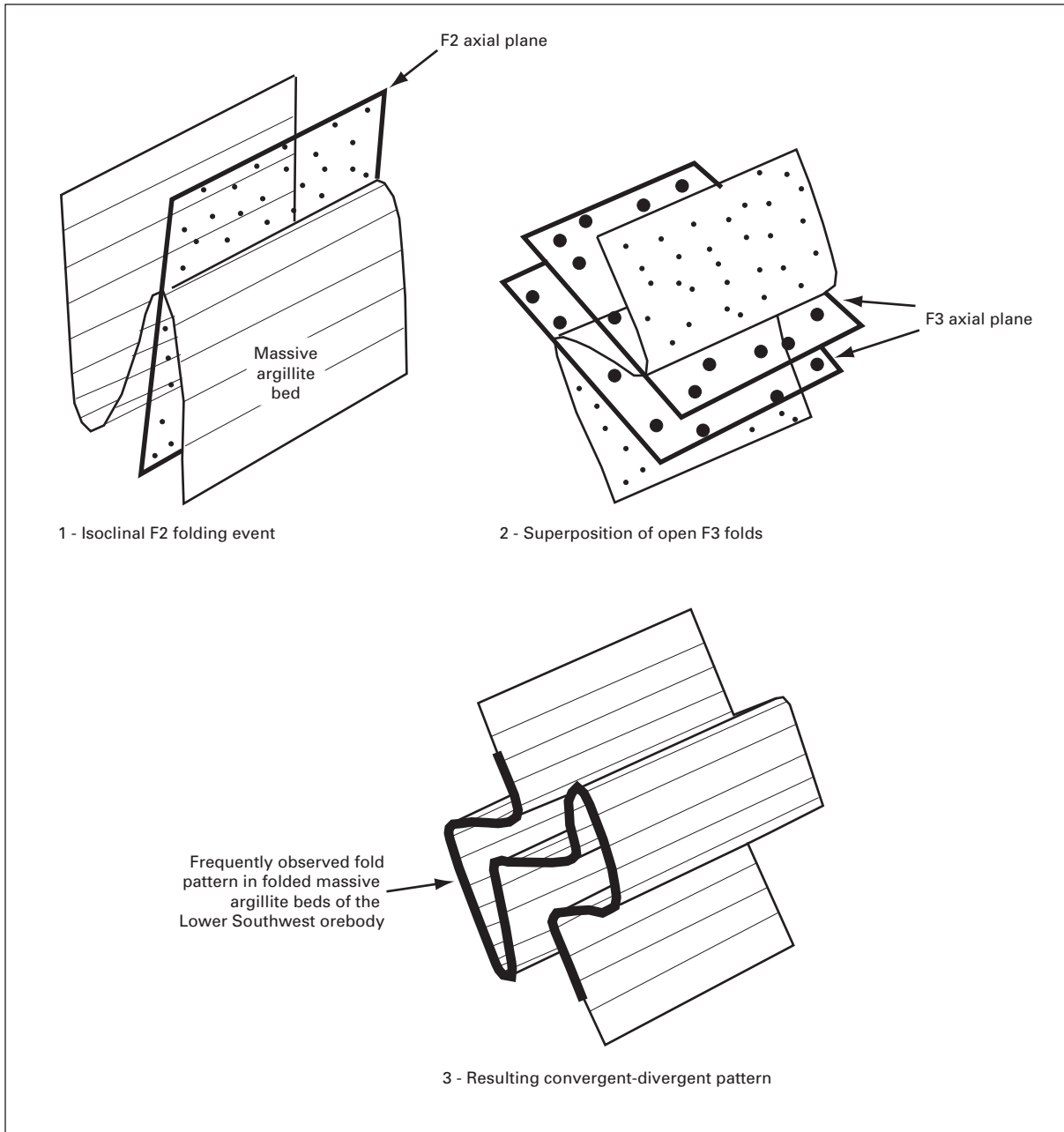


Figure 18. Ramsay and Huber's (1987) principal type-3 three-dimensional fold. The form arises by the superposition of shear folds on preexisting fold forms. This leads to a convergent-divergent pattern. Although the first fold axial surfaces become curved, the first fold hinges are not markedly deflected, and all fold axial directions, both first and second phase, tend to be subparallel (modified after Ramsay and Huber, 1987).

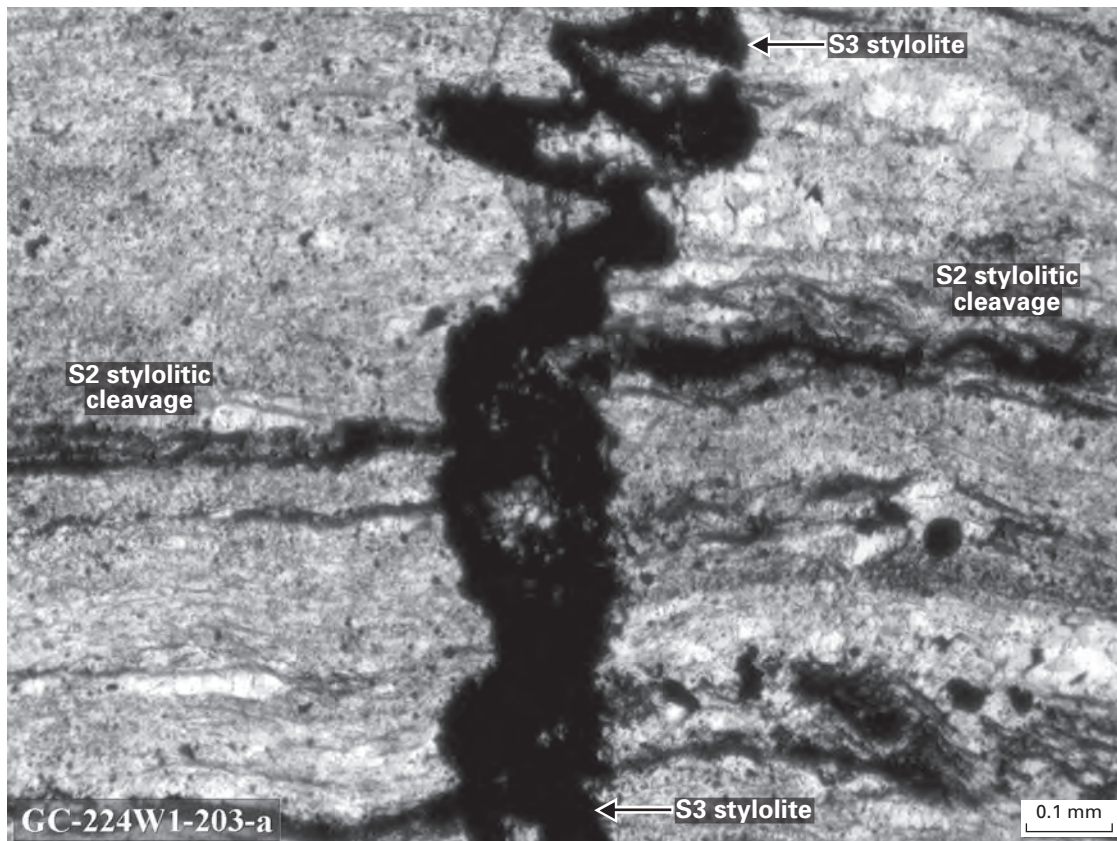


Figure 19. Photomicrograph of S3 stylolites in siliceous rock. mm, millimeters.

Offset along the thrust faults was determined using F2 and F3 fold hinges as piercing points. To do this, the geology above and below the thrust faults was projected downward and upward, respectively, onto plan view maps (Freitag, 2000). In general, the geology on the hanging wall and footwall of the fault system could be correlated, with a maximum offset of 22 m determined across the faults. There was little deformation of hanging wall and footwall during or after faulting.

Small-scale D4 fabrics, such as F4 hinges and S4 foliation, were not recognized in the Lower Southwest orebody. However, gentle (interlimb angle 180–120°; Ramsay and Huber, 1987) F4 folds were recognized on a stope scale as undulations of the orebody about east-west-oriented axes. The F4 folds resulted in local north-plunging F2 and F3 fold axes and are recognized on plan maps where stratigraphic footwall rocks are exposed along the southern part of the generally south- to southeast-plunging Lower Southwest orebody (fig. 7).

D5 Deformation

The final stage of deformation in the Lower Southwest orebody resulted in high-angle strike-slip faults referred to as Maki-type faults. The faults mostly show right-slip, although a

few faults with left-slip were recognized. High-angle, right-slip faults strike northwest to north-northwest and dip 80–90°. Faults are commonly narrow (less than 10 cm) but widen locally to 2 m. In phyllitic rocks, faults are characterized by zones of soft, gougy, bleached phyllite. Massive sulfide and argillite in fault zones are brecciated, and discrete fault surfaces bounding the zone contain thin gouge (less than 14 mm).

The Lower Southwest orebody is offset along the Lower Southwest fault (Katja Freitag, written commun., 1998), which has a map separation of less than 30 m (fig. 7). An oblique-slip component is documented by slickenlines in calcite that plunge as much as 20°; however, this is of minor importance in the Lower Southwest orebody, as the map separation along the fault is less than 30 m.

Right-slip faults generally strike northwest, and left-lateral faults strike north (fig. 22). These two fault sets intersect at an angle of about 35°, suggesting they may be conjugate faults (Ramsay and Huber, 1987). The strike of both sets of high-angle faults is similar to that of regional high-angle faults in southeast Alaska (fig. 23).

Faults with intermediate dips are not well understood. They are distinguished from the high-angle faults and low-angle thrust faults by having dips of approximately 40–50°

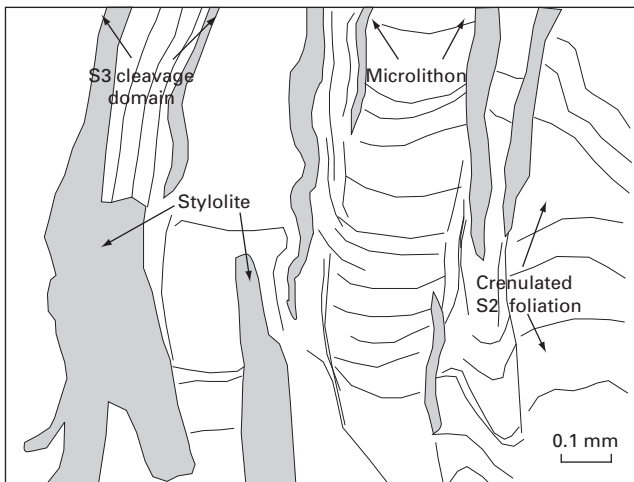
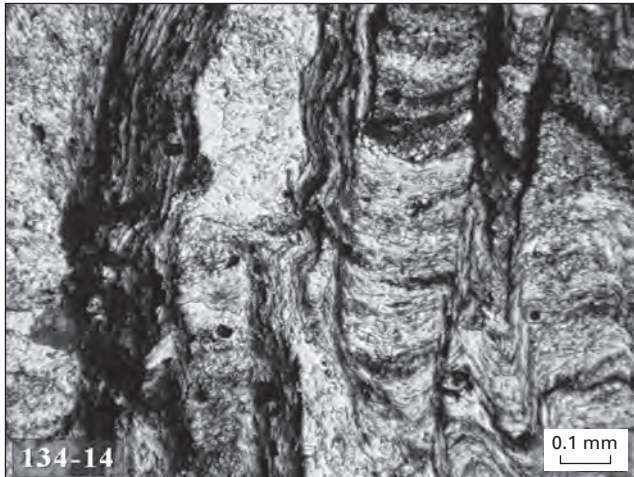


Figure 20. Photomicrograph and sketch of spaced S3 crenulation cleavage in sericitic phyllite, defined by S3 cleavage domains and microlithons. mm, millimeter.

and apparent normal offset of approximately 1 m. In addition, the faults may offset high-angle faults, which suggests they developed later than the high-angle faults. The author postulates that relaxation of the stress regime under which the high-angle faults developed resulted in small normal faults with minor (less than 1 m) offset.

Although the thrust faults of the Lower Southwest orebody are truncated by high-angle faults, they also splay into the high-angle faults. In such cases, propagation of the high-angle faults across the thrust fault resulted in fractured, but not offset, rock units. Lear (K.G. Lear, oral commun., 1997) and Proffett (chap. 7) have suggested that the Lower Southwest thrust faults are kinematically related to high-angle faults. The author interprets the thrust faults to predate the high-angle faults, however, because quartz-calcite only precipitated along the thrust faults but not in the high-angle faults, and the thrust faults commonly are truncated by the high-angle faults.

In addition, the author suggests that the lower thrust fault of the Lower Southwest thrust fault system was locally reactivated during high-angle faulting. The author proposes a model where high-angle, right-slip faults transferred strain to the thrust fault along splaying faults and locally reactivated sections of the thrust fault (fig. 24). A three-dimensional block model (fig. 25) shows the geometry of fault blocks and indicates that an intensely fractured zone developed between fault blocks.

Structural Transition and Comparison to Neighboring Orebodies

Understanding the transition between adjacent orebodies at Greens Creek is complicated by the complex structure of the deposit. A geometry of the transition between the Lower Southwest orebody and the Upper Southwest and 224 West Bench orebodies was developed by the author (fig. 26) based on plan map and cross-section patterns.

The orientations of bedding and ductile deformation structures of the Lower Southwest, Upper Southwest, 224 West Bench, and 200 South orebodies were compared by the author (table 3) and used to develop the following model explaining the difference in deformation style between thick orebodies (Lower Southwest and 200 South orebodies; greater than 10 m) and thin orebodies (Upper Southwest and 224 West Bench orebodies; less than 3 m).

The Upper Southwest orebody is folded by isoclinal F2 folds, which have steeply plunging axes that are located approximately at cross section 2700 (fig. 3) and are less apparent farther to the south. The orebody is located along the eastern limbs of two F2 anticlines. Toward the south, the Lower Southwest orebody is also deformed by F2 folds. The hinge lines of the F2 anticlines and synclines of both orebodies can be interpolated to form continuous hinge lines between the orebodies. The model suggested for the change in plunge of F2 fold axes between the Upper and Lower Southwest orebodies is that an F4 fold axis is located in the area of cross section 2700 (fig. 3), trending perpendicular to the F2 fold axes.

The 224 West Bench orebody is located to the west of the Lower Southwest and Upper Southwest orebodies. The Lower Southwest orebody is characterized thin (less than 1 m), usually discontinuous layers of stratigraphic footwall phyllite close to the western limb of a D2 shear that developed from an isoclinal F2 anticline. The author interprets phyllite as the core of this sheared anticline. The 224 West Bench orebody forms the continuation of the mineralized horizon toward the west and lies along the upper western limb of the sheared anticline. The mineralized horizon thins to form a barren contact between phyllite and argillite. The barren contact is interpreted by the author to be folded into a syncline. Proximal to the Upper Southwest orebody, which lies toward the northeast of the 224 West Bench orebody, the contact becomes mineralized, with the Upper Southwest orebody located on the eastern limb of the sheared anticline recognized in the Lower Southwest orebody.

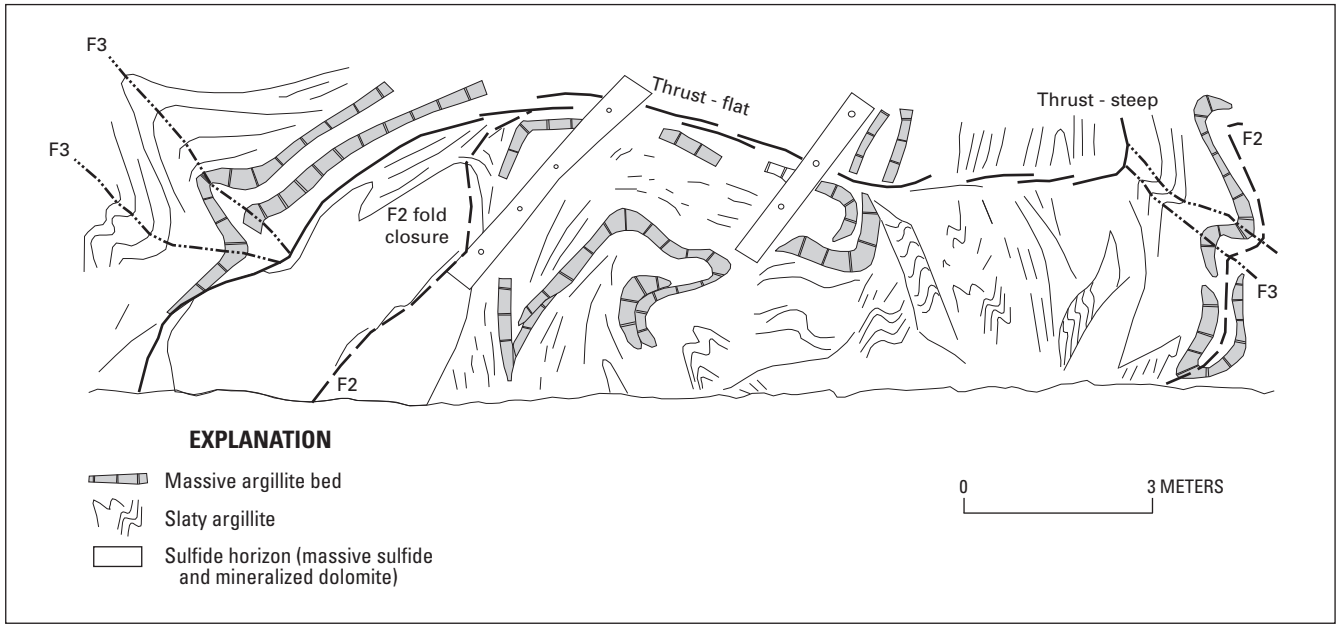


Figure 21. Rib map depicting intermediate to steeper sections along the upper thrust of the Lower Southwest thrust system (284 level, looking north).

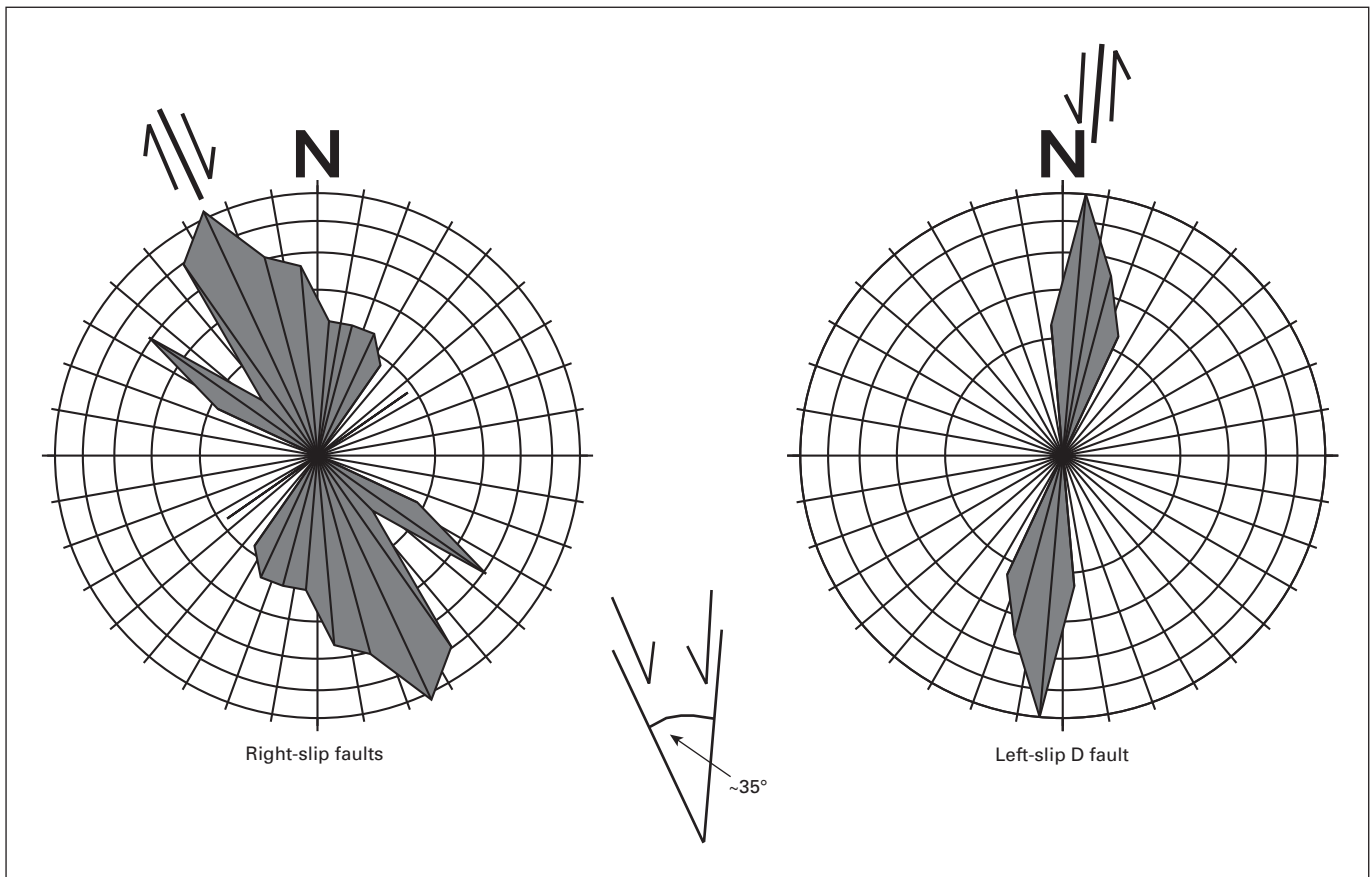


Figure 22. Rose diagram comparing strikes of left-slip faults (n=8) with right-slip high-angle faults (n=57). The difference in strike is about 40°, suggesting these are conjugate faults.

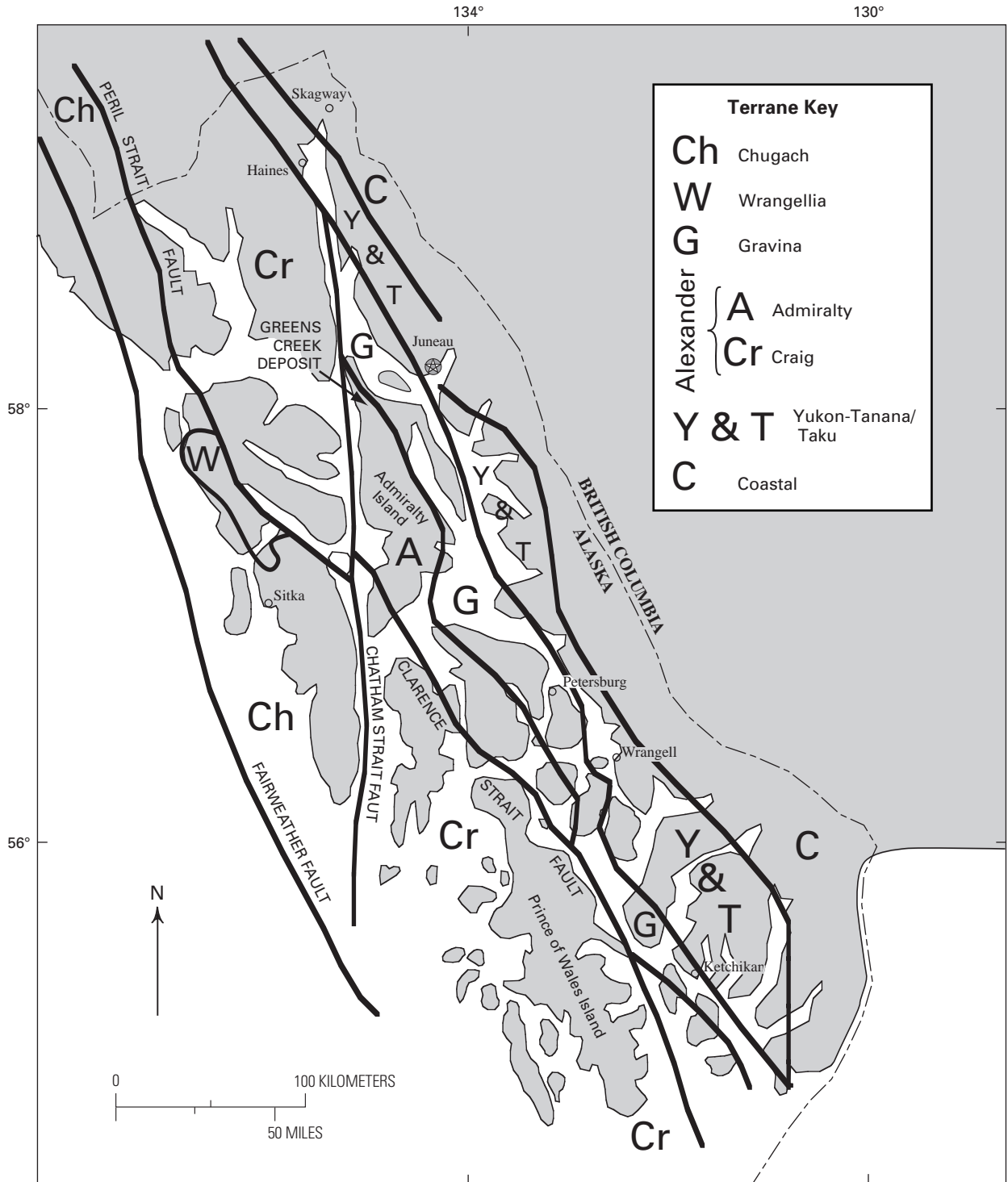


Figure 23. Map of the various terranes and their bounding regional strike-slip faults, southeast Alaska (modified from Sutley and others, 1990, and Newberry and others, 1997), and the structural setting of the Greens Creek deposit.

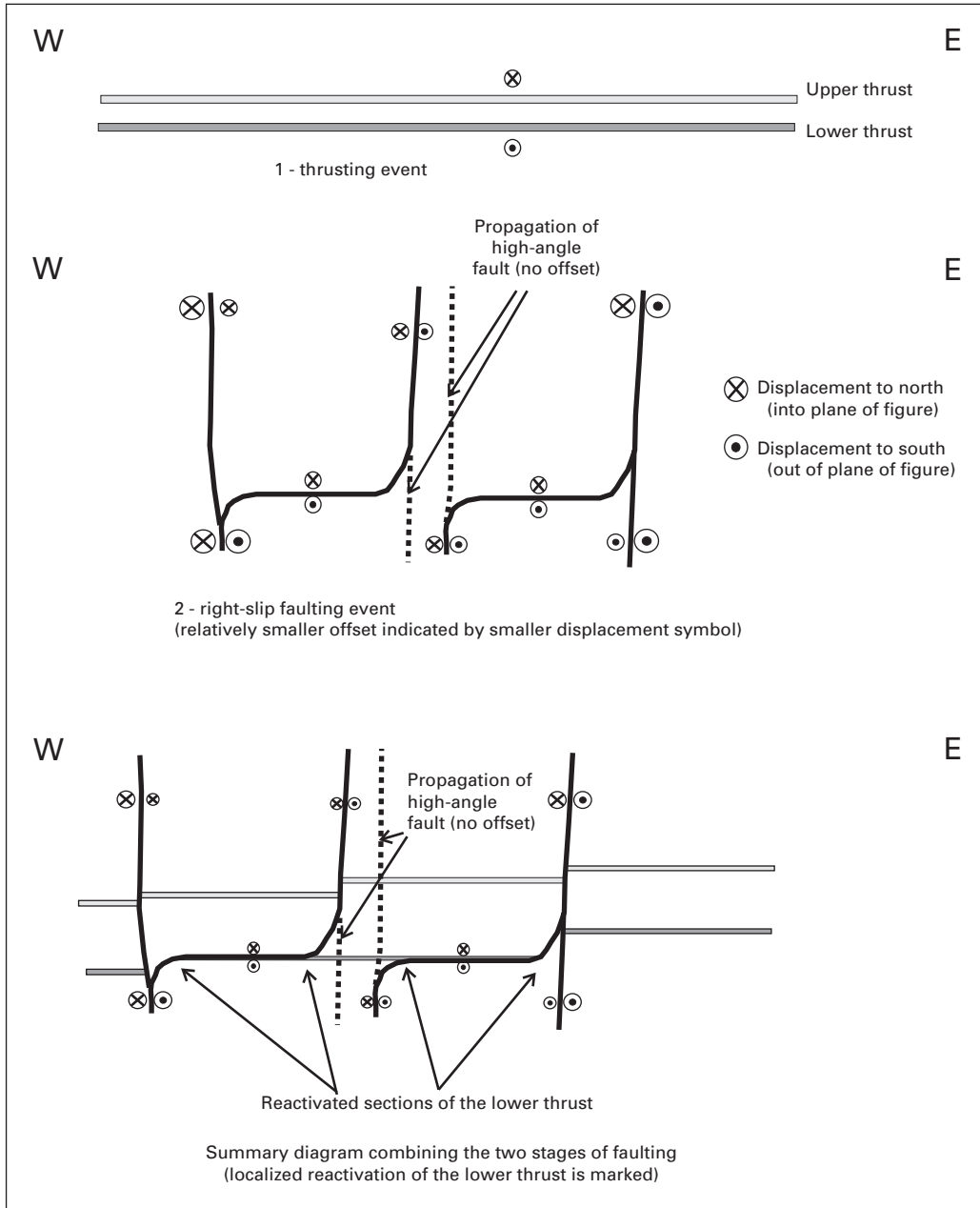


Figure 24. Schematic cross section illustrating the sequence of brittle deformation events, looking north.

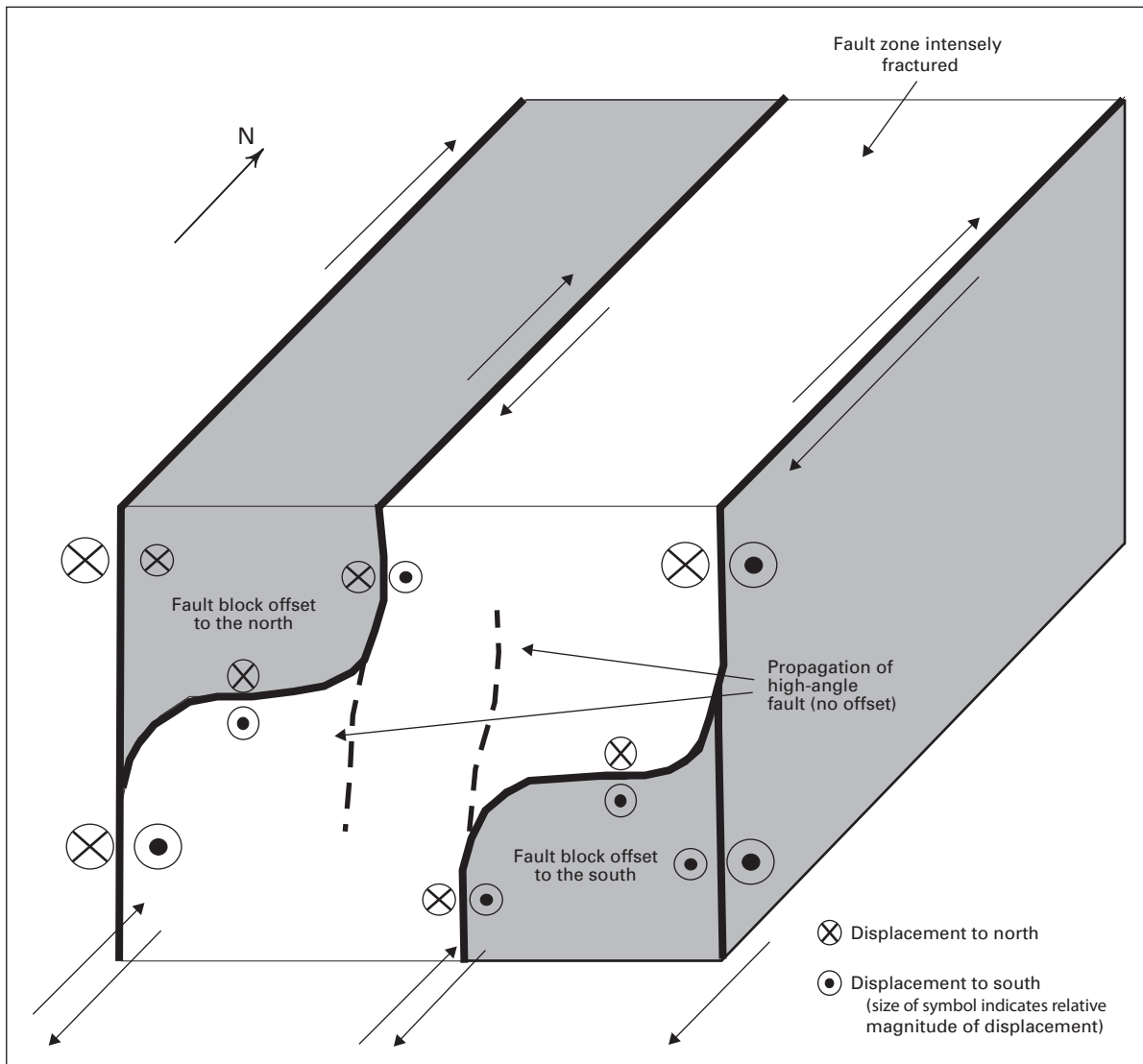


Figure 25. Block diagram representing two fault blocks of massive sulfide of the Lower Southwest orebody offset across right-slip faults, with an intensely fractured fault zone.

A simplification of the structural similarities and differences (table 4) shows that bedding, F2/L2, and F3/L3 orientations are similar in all of the examined orebodies (figs. 27, 28). The S2 foliation (fig. 29) and S3 cleavage (fig. 30) have consistent dips in the Lower Southwest and 200 South orebodies. In contrast, S2 foliation and S3 cleavage in the Upper Southwest and 224 West Bench orebodies have variable strikes and dips.

The author uses a modified schematic representation of polyharmonic folds (fig. 31) after Ramsay and Huber (1987) to explain the difference in orientation of S3 cleavage between the orebodies as a function of the relative

competency of the orebody. The schematic representation of polyharmonic folds suggests that during ductile deformation of the Greens Creek deposit, the effect of folding was more pronounced in relatively less competent, thin orebody sections, resulting in higher frequencies and amplitudes of F2 and F3 folds and variable orientations of S2 foliation and S3 cleavage. In contrast, relatively competent, thick orebodies formed consistently oriented folds, with consistently oriented S2 foliation and S3 cleavage. The fold structure, therefore, is more complex in the thinner orebodies. The least competent rocks, slaty argillite and sericitic phyllites, show the highest degree of deformation.

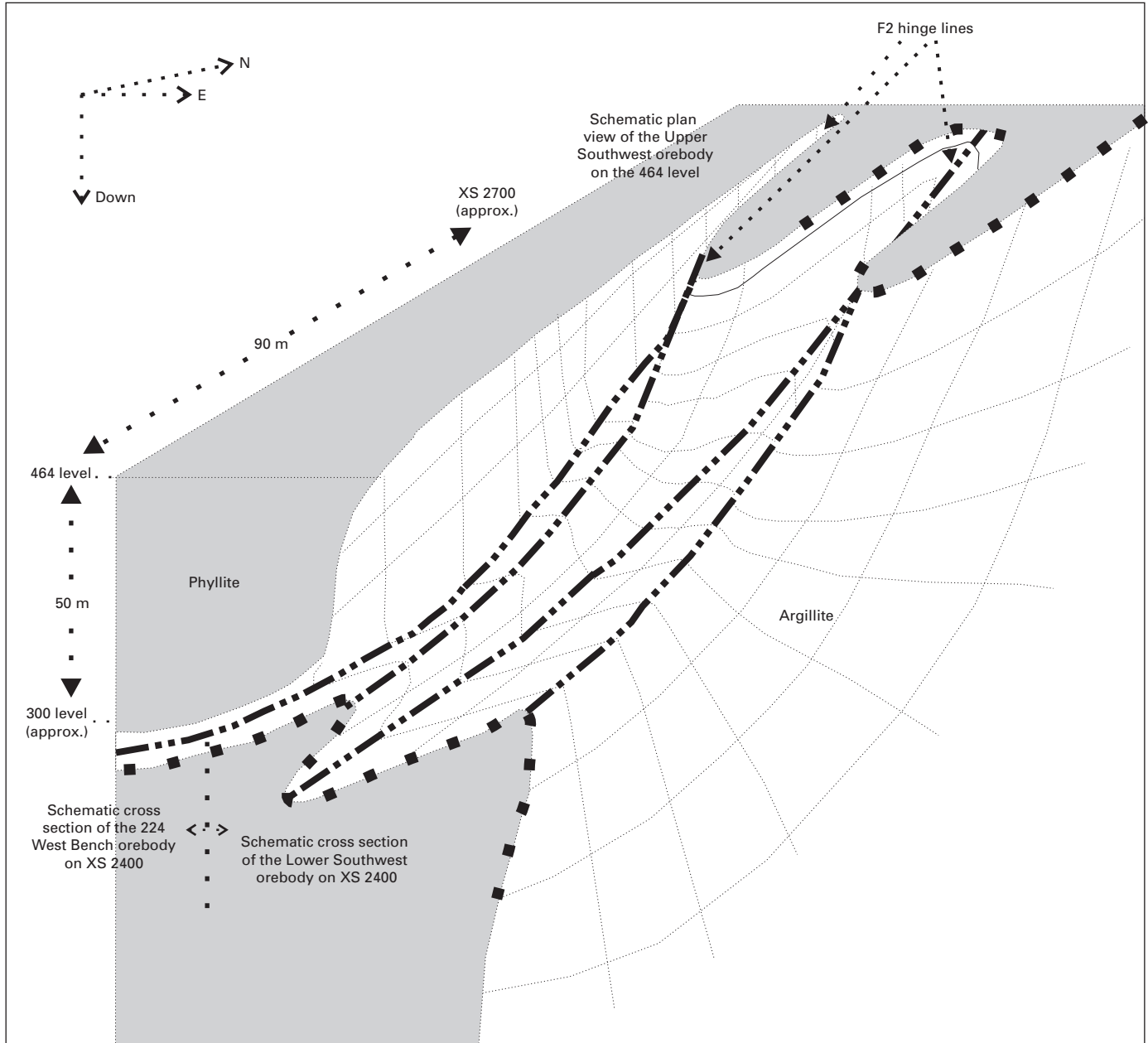


Figure 26. Schematic model for the transition from the Lower Southwest to the Upper Southwest and 224 West Bench orebodies based on F2 fold geometry. F3 folds, which have a similar trend to F2 folds, are unfolded to simplify the model (thin black lines contour the surface of footwall phyllites).

Table 3. Comparison of orientations of structural features in the Lower Southwest, Upper Southwest, 224 West Bench and 200 South orebodies. The notations “thick” and “thin” refer to relative thickness (greater than 10 meters and less than 3 meters, respectively) of the orebodies.

Structural feature	Lower Southwest (thick)	Upper Southwest (thin)	224 West Bench (thin)	200 South (thick)
Bedding	F2/F3 π -axes similar		No data	No data
F2/L2	Similar orientation, trend generally to southeast, variable plunge		No data	No data
S2	General strike northwest, general dip to southwest	Varied strike and dip		No data
F3	5–55° to southeast, minor northwest trend	10–66° to southeast	No data	10–40° to south-southeast
L3	5–50° to southeast, minor northwest trend	10–50° to southeast	10° to south-southeast	45° to southeast
S3	Consistent dip of 40–90° to east	Variable dip of 40–90° to east, southeast, south and southwest		Consistent dip of 50–65° to east

Table 4. Comparison of orebody thickness and orientations of structural features.

Structural feature	Thick orebody (Lower Southwest, 200 South orebodies)	Thin orebody (Upper Southwest, 224 West Bench orebodies)
Bedding		Same
F2/L2		Same
S2	Dip to the west	Variable dip direction to northeast or southwest
F3		Same
L3		Same
S3	Moderate to steep dip to east	Variable—east-northeast and southeast dips dominant

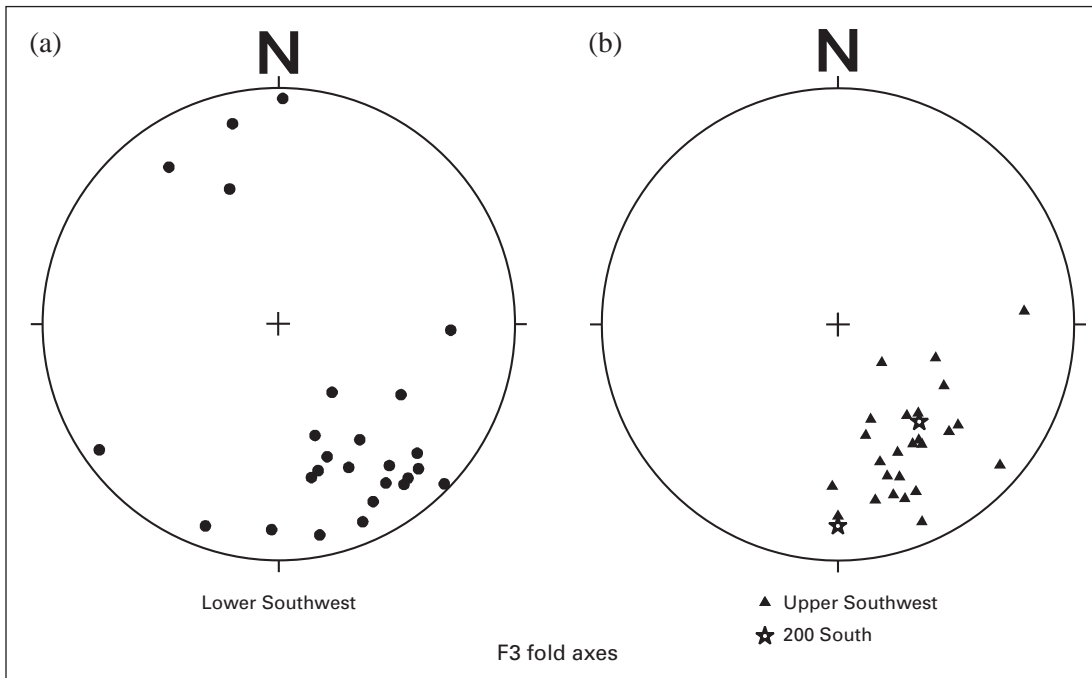


Figure 27. Lower hemisphere equal area projections of F3 fold axes of the (a) Lower Southwest (circles; n=26) and (b) Upper Southwest (triangles; n=25) and 200 South (stars; n=2) orebodies.

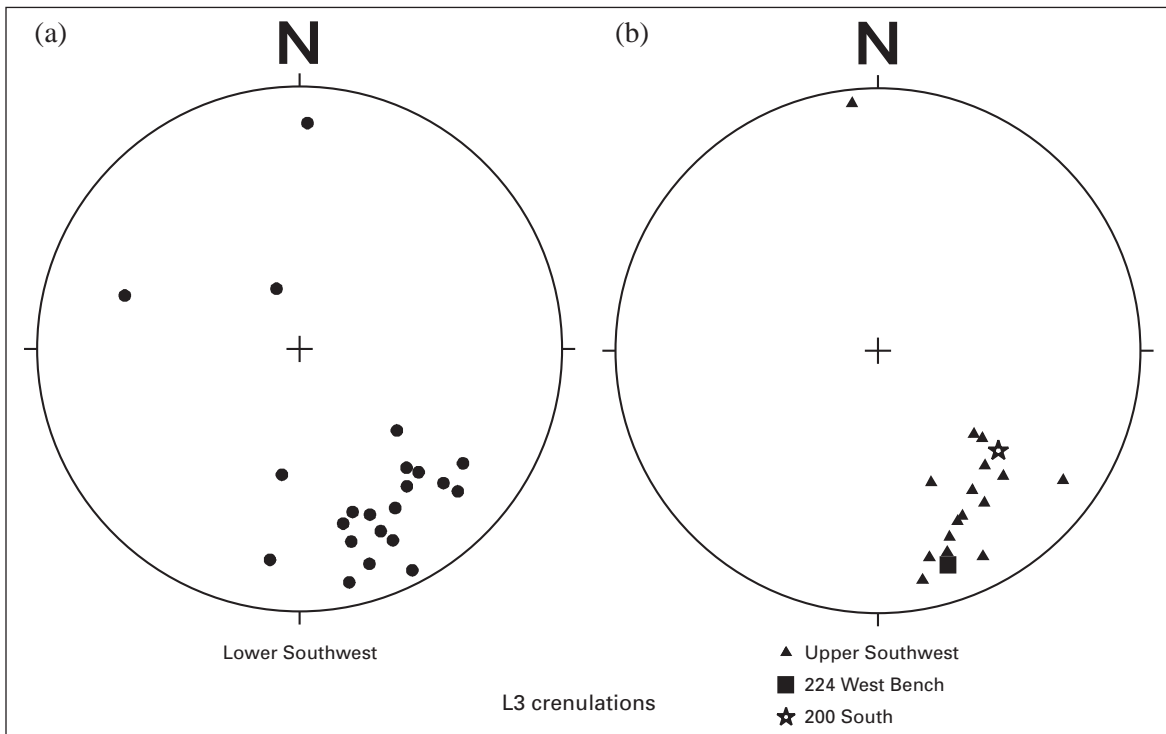


Figure 28. Lower hemisphere equal area projections of L3 crenulation lineations of the (a) Lower Southwest (n=22) and (b) Upper Southwest (triangles; n=16), 224 West Bench (square; n=1), and 200 South (star; n=1) orebodies.

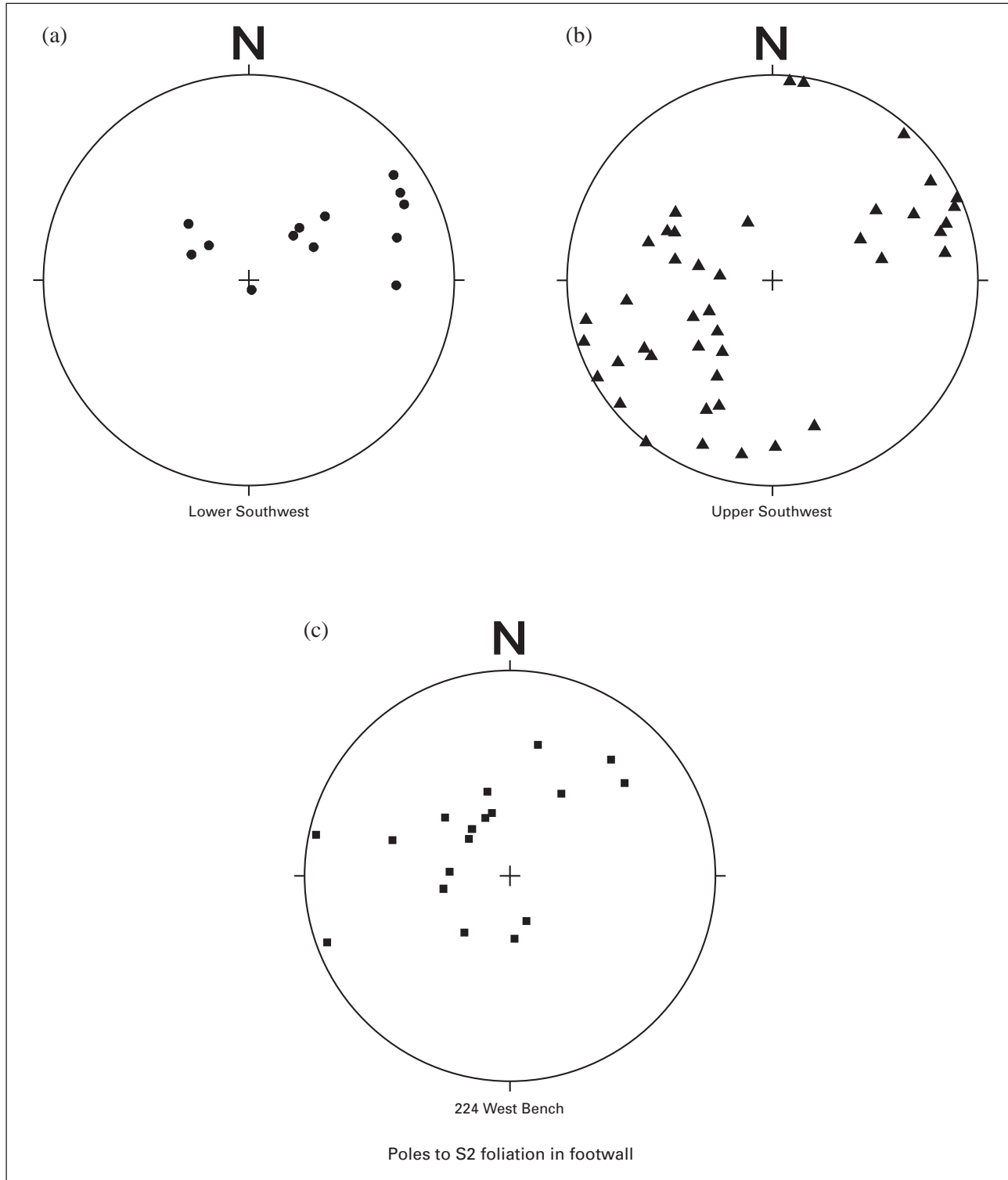


Figure 29. Lower hemisphere equal-area projections of poles to S2 foliation planes measured in footwall rocks of the (a) Lower Southwest (circles; n=13), (b) Upper Southwest (triangles; n=42), and (c) 224 West Bench (squares; n=18) orebodies.

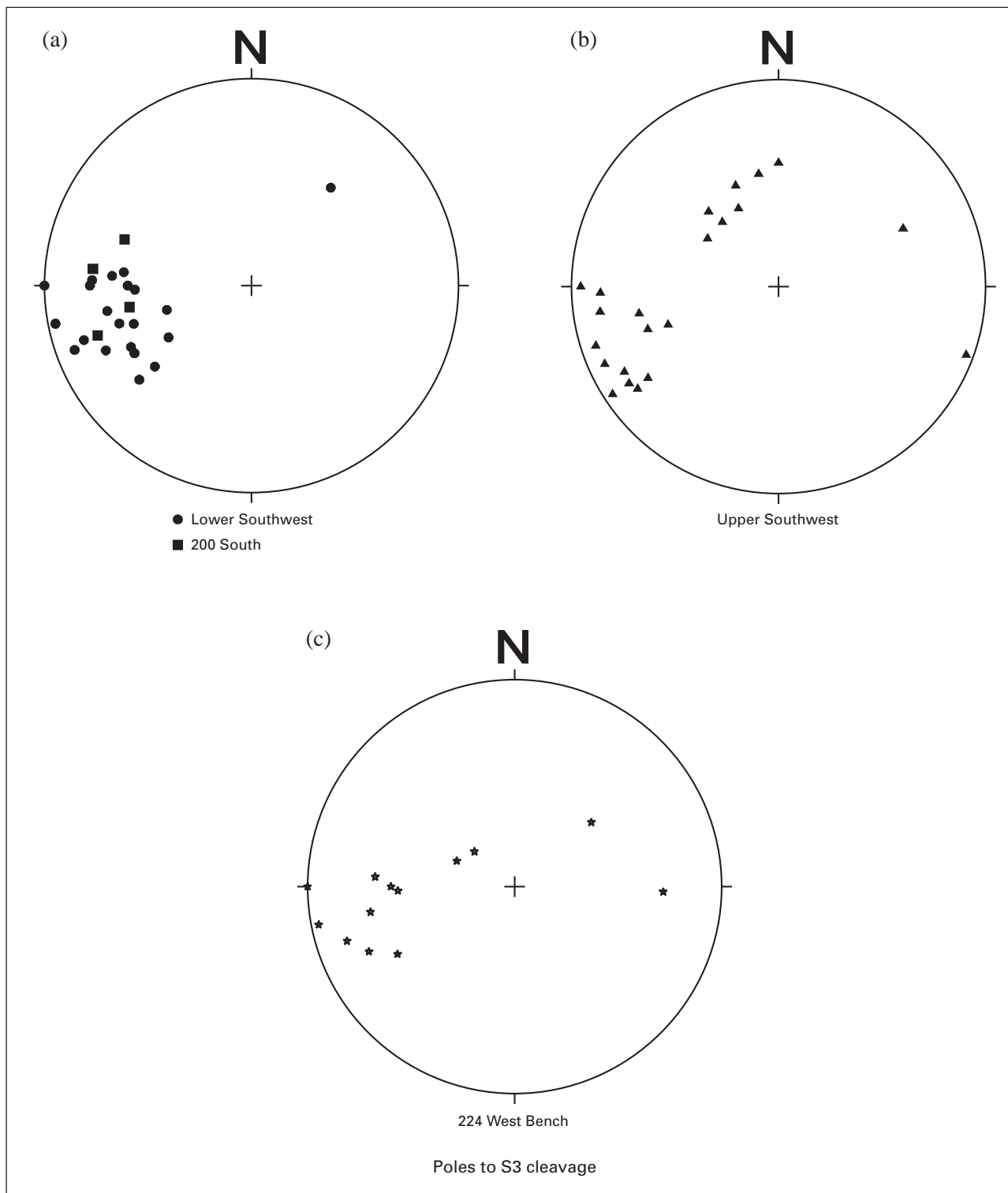


Figure 30. Lower hemisphere equal area projections of poles to S3 cleavage in the (a) Lower Southwest (circles; n=21), 200 South (squares; n=4), (b) Upper Southwest (triangles; n=22), and (c) 224 West Bench (stars; n=13) orebodies.

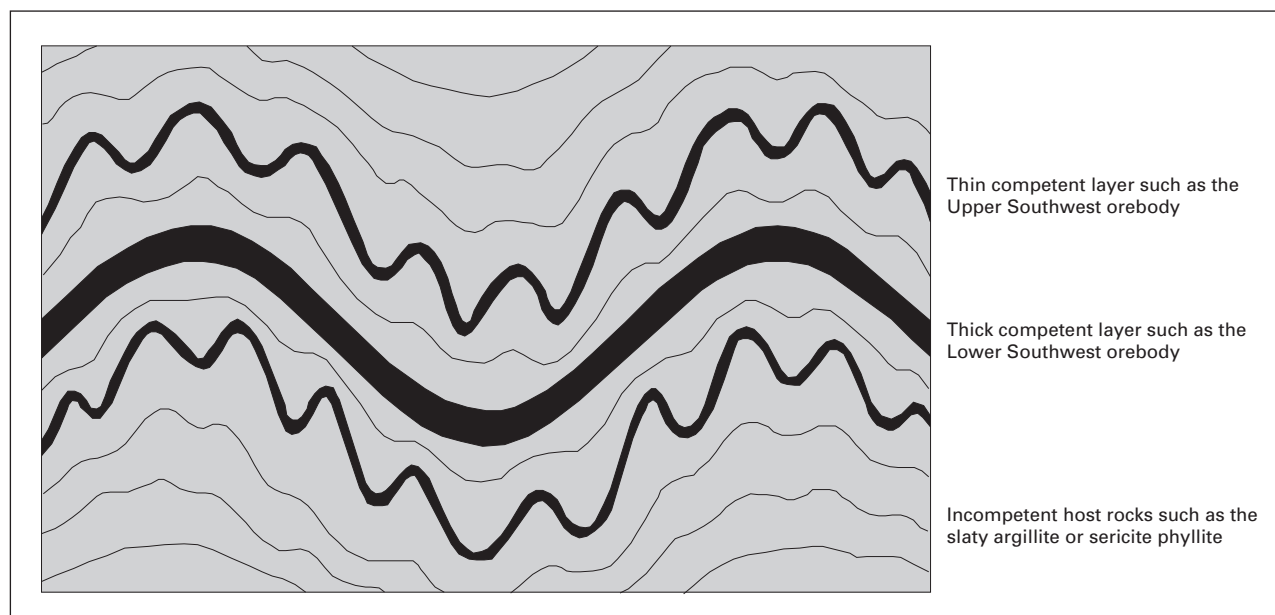


Figure 31. Schematic representation of polyharmonic folds developed in competent layers of varying thickness (black) and incompetent host materials (grey) showing the effect of the thickness of the mineralized horizon during folding (modified after Ramsay and Huber, 1987).

Model of the Structural and Tectonic Evolution of the Greens Creek Deposit

The following model outlines the structural evolution of the Greens Creek deposit on both a local and regional scale (fig. 32). The basis for the model is structural data from, and interpretations of, the Lower Southwest orebody and limited data from adjacent orebodies (Upper Southwest, 224 West Bench, and 200 South orebodies).

A Late Triassic, inferred structural event (D_{mineral}) is interpreted to have formed pre- to synmineralization, normal (?) faults in a back-arc basin environment. Subsequent to sulfide, carbonate, and argillite deposition, compaction during diagenesis (D_0) led to the formation of quartz-carbonate “ladder” veins oriented perpendicular to massive argillite beds and offset by S_0 pressure solution seams.

Late Jurassic to Early Cretaceous small-scale thrust faults, which offset massive argillite beds and are attributed to a D_1 deformation event by the author, may have formed during partial subduction of the Alexander terrane under the North American plate along an east-dipping subduction zone (Plafker and Berg, 1994). Late Cretaceous to early Tertiary accretion of the Alexander terrane to the North American plate (Gehrels and Saleeby, 1987) folded the Greens Creek deposit into early

open to isoclinal F_2 and later open to closed F_3 folds. Both F_2 and F_3 folds have northerly oriented fold hinges, indicating east-west contraction. F_3 folds whose axial planes dip easterly are interpreted to have formed during back-thrusting of the Alexander terrane during later stages of accretion. The F_2 and F_3 folds at Greens Creek may reflect two regionally recognized fold generations along the eastern edge of the Alexander terrane. The earlier folds (probably correlative to F_2 folds at Greens Creek) are tight to isoclinal, with attenuated fold limbs, moderately southeast-plunging fold axes, and associated, steeply (70° to 90°) northeast-dipping foliation planes (for example, Rubin and Saleeby, 1992). These were crenulated by a northeast-trending, spaced cleavage and folded by west- to northwest-vergent folds (probably correlative to F_3 folds at Greens Creek) (for example, Rubin and Saleeby, 1992).

A change in the stress regime from east-west to northeast-southwest and from ductile to brittle deformation resulted in the development of low-angle D_4 faults (Klaus and Lower Southwest thrust fault systems), which offset the Greens Creek deposit to the north, and gentle F_4 folds, which have east-west-trending fold axes. Finally, dextral transpression along the transform plate margin of southeastern Alaska resulted in right-slip faulting, starting in Eocene time, and probably formed high-angle, strike-slip faults (for example, Maki fault) at Greens Creek.

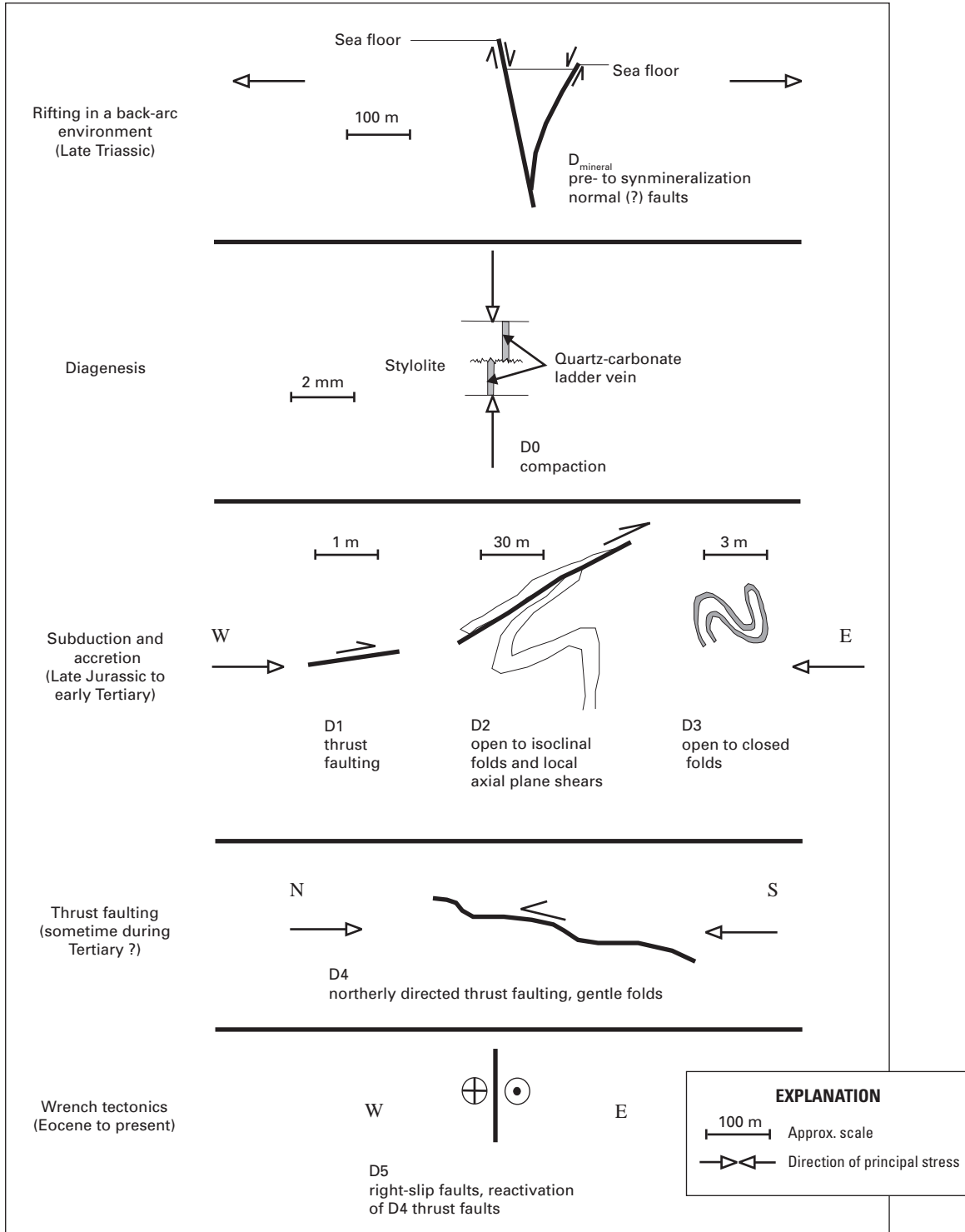


Figure 32. Model of the structural and tectonic evolution of the Greens Creek deposit. All views are cross sectional.

Summary and Conclusions

Detailed mapping of the Lower Southwest orebody revealed structural elements throughout the Greens Creek deposit, including F2 folds, S2 foliation, L2 lineation, F3 folds, S3 cleavage, L3 lineation, and brittle faults. However, L1 lineations and D4 fabrics were not recognized. Analysis of structural elements led to a structural model for the Lower Southwest orebody and a tectonic model for the Greens Creek deposit.

Pre- to syndepositional faults are inferred from reconstructed ore lithology morphologies and may have formed in an extensional back-arc basin environment. The faults are inferred to have focused hydrothermal fluids, resulting in separate accumulations of massive sulfide and mineralized dolomite. Burial and diagenesis of the deposit are recognized in diagenetic quartz-carbonate “ladder” veins and stylolites in massive argillite beds and were followed by early post-depositional thrust faulting during Late Jurassic (?) subduction of the Alexander terrane, determined in offset of massive argillite beds. Ductile deformation features of the Lower Southwest orebody, including open to isoclinal F2 and open to closed F3 folds, probably developed during Late Jurassic to early Tertiary accretion of the Alexander terrane to the North American continent. Major F2 fold hinges, which coincide with the inferred syndepositional faults, is interpreted to have developed in zones of weakness created by these inferred early faults. Ore type, thickness of orebodies, and silicification of the stratigraphic footwall rocks determined the geometry of F2 folds. Tight to isoclinal F2 folds deformed and structurally thickened the relatively ductile massive sulfide layers and, locally, isoclinal F2 anticlines developed into D2 shear zones along the F2 axial planes. Open F2 folds formed where stratigraphic footwall argillites were silicified and where competent mineralized dolomite was the predominant ore lithology. The F3 folds, prevalent in thin (less than 2.5 m) massive sulfide layers, refolded open to isoclinal F2 folds. Because F3 axial planes are inclined to the east, these may have formed during back-thrusting in later stages of accretion. The S2 stylolitic foliation, S3 stylolites, and locally remobilized ductile sulfide and sulfosalt minerals indicate that pressure solution was an important mechanism during both F2 and F3 folding.

The main structural features of the D4 event are the Lower Southwest thrust faults, which show small offsets (generally to the northwest), and gentle F4 folds oriented perpendicular to the F2 and F3 axial planes. These D4 structures represent a change from ductile to brittle deformation and a change from east-west compression during accretion to northeast oriented, dextral transpression along the transform plate margin of southeastern Alaska. The youngest D5 deformation features are high-angle, strike-slip faults that locally reactivated D4 thrust faults.

Acknowledgments

This paper formed a major part of my Ph.D. dissertation and is the result of fieldwork done at the Greens Creek mine and research undertaken at the Colorado School of Mines. I acknowledge my thesis advisors, M.W. Hitzman and E.P. Nelson, for their support and guidance throughout the study. I thank the Kennecott Greens Creek Mining Company for supporting my fieldwork and the mine geologists for their input on my interpretations. Invaluable discussions on the geology and structure of the Lower Southwest orebody and the Greens Creek deposit in general were provided by P. Lindberg, J. Proffett, C. Taylor, and N. Duke. Financial support came from an SEG Student Research Grant. Rick Allmendinger is acknowledged for the use of his Stereonet program. Finally, I thank the reviewers C. Thorman and P. Haeussler for their constructive criticism, which resulted in a much improved final manuscript.

References Cited

- Freitag, Katja, 2000, Geology and structure of the Lower Southwest orebody, Greens Creek mine, Alaska: Golden, Colorado School of Mines, Ph.D. dissertation, 248 p.
- Gehrels, G.E., and Saleeby, J.B., 1987, Geologic framework, tectonic evolution and displacement history of the Alexander Terrane: *Tectonics*, v. 6, no. 2, p. 151–173.
- Newberry, R.J., Crafford, T.C., Newkirk, S.R., Young, L.E., Nelson, S.W., and Duke, N.A., 1997, Volcanogenic massive sulfide deposits of Alaska: *Economic Geology Monograph* 9, p. 120–150.
- Passchier, C.W., and Trouw, R.A.J., 1996, *Microtectonics*: Berlin, Springer-Verlag, 289 p.
- Plafker, George, and Berg, H.C., 1994, Overview of the geology and tectonic evolution of Alaska, *in* Plafker, George, and Berg, H.C., eds., *The geology of Alaska: Geological Society of America, The geology of North America G-1*, p. 989–1021.
- Ramsay, J.G., and Huber, M.I., 1987, *The techniques of modern structural geology, volume 2—folds and fractures*: London, Academic Press, 400 p.
- Rubin, C.M., and Saleeby, J.B., 1992, Tectonic history of the eastern edge of the Alexander terrane, southeast Alaska: *Tectonics*, v. 11, no. 3, p. 586–602.
- Sutley, S.J., Goldfarb, R.J., O’Leary, R.M., and Tripp, R.B., 1990, A comparison of geochemical exploration techniques and sample media within accretionary continental margins—An example from the Pacific Border Ranges, Southern Alaska, USA: *Journal of Geochemical Exploration*, v. 37, p. 255–275.

Three-Dimensional Modeling and Visualization of Greens Creek Drill-Hole Data

By Gregory K. Lee and Cliff D. Taylor

Chapter 14 of

**Geology, Geochemistry, and Genesis of the Greens Creek Massive
Sulfide Deposit, Admiralty Island, Southeastern Alaska**

Edited by Cliff D. Taylor and Craig A. Johnson

Professional Paper 1763

**U.S. Department of the Interior
U.S. Geological Survey**

Contents

Abstract.....	405
Introduction.....	405
Description of the Dataset.....	405
Data-Processing Procedures.....	405
Modeling.....	406
Minimum-Tension Gridding.....	406
Topographic Model.....	408
Ore Model.....	408
Geochemical Models.....	408
Geologic Structure Models.....	410
Visualization.....	410
Conclusions.....	416
Reference Cited.....	416

Figures

1. Drill-hole locations, Greens Creek mine area.....	407
2. Greens Creek mine orebodies, showing major workings.....	409
3. Faults, shear zones, and gold distribution within orebodies, Greens Creek mine.....	410
4. Chair cut display of silver in orebodies, Greens Creek mine.....	411
5. Isovalue shell display of silver greater than 10 parts per million in orebodies, Greens Creek mine.....	412
6. Isovalue shell display of zinc greater than 10 percent in orebodies, Greens Creek mine.....	413
7. Isovalue shell display of antimony greater than 600 parts per million in orebodies, Greens Creek mine.....	414
8. Isovalue shell display of arsenic: antimony ratios greater than 10 in orebodies, Greens Creek mine.....	415

Three-Dimensional Modeling and Visualization of Greens Creek Drill-Hole Data

By Gregory K. Lee and Cliff D. Taylor

Abstract

Three-dimensional modeling and visualization provide powerful tools for evaluating and interpreting chemical and physical properties in space, including subsurface domains. These tools were applied to drill-hole data provided by the Kennecott Greens Creek Mining Company for the Greens Creek mine on Admiralty Island, southeast Alaska. Three-dimensional models of subsurface data from drill-core chemical assays, ore lithology logs, mine workings, digitized faults, and digital terrain were produced and combined to create visual displays that could be manipulated and rendered as images for this report. The validity of the model showing the distribution of orebodies is confirmed by comparisons with plan and cross-section drawings produced by geologists at the mine. The three-dimensional models should therefore be useful to guide mining development efforts and could also be effectively used to revisit previously developed mine areas to determine where additional production might be targeted.

Introduction

This chapter describes methods that were used to render Greens Creek mine drill-hole information into three-dimensional models of the distribution of orebodies and of geochemical concentrations within the orebodies. Geologic structures, mine workings, and a topographic surface were also modeled and were integrated with the other models for purposes of scientific visualization. Data descriptions, coordinate transformation procedures, and modeling techniques are included. Dynamic Graphics, Inc., EarthVision software was used to successfully calculate and display the three-dimensional models, and several graphical images of the modeling results are included in this report.

Description of the Dataset

In 1997, the Kennecott Greens Creek Mining Company provided core log data for 1,895 exploration drill holes in the Greens Creek mine vicinity. There are 12,764 deviated

segments in these holes and more than a million observations and analytical determinations at 75,291 locations along the core segments. These data include measured depths, geochemical concentrations, lithologic and ore-type classifications, and inclinations and orientations of drill-hole segments. The spatial coordinates of the drill-hole collars (origins) and the azimuths of the holes were relative to a local surface grid of northings and eastings, measured in feet. The origin of this grid, relative to the Alaska State Plane projection, Zone 1, Clarke 1866 spheroid, NAD 1927 datum, also in units of feet, is 2262748.50N; 2479273.89E. These coordinates correspond to lat 58.0234985°N., long 134.7311267°W.

The spatial reference for the mine workings, however, is a local grid of cross-section (*XS*) and long-section (*LS*) coordinates whose origin is given as northing 12635.93 ft and easting 17438.42 ft in terms of the surface grid coordinates. Therefore, the mine grid origin is at Alaska State Plane Zone 1 coordinates of 2275384.43N and 2496712.31E. The mine grid is rotated 26.5651 degrees counterclockwise from due north. The mine coordinate elevations are 60 ft higher than true above-sea-level elevations (chap. 7).

Data-Processing Procedures

Although the data were provided with spatial coordinates in terms of the local surface grid, it was felt that three-dimensional modeling and visualization of the subsurface data would be most useful if rendered in terms of the mine coordinates. This necessitated the task of mathematically describing the paths of every drill hole in mine-coordinate space. From a computational perspective, there are complicating factors presented by the Greens Creek drill-hole data in addition to the offset and rotation of the mine grid relative to the surface grid. First, the paths of the drill holes are deviated. That is, each hole may be composed of numerous segments with varying azimuths and inclinations. Furthermore, because the origins of most of the drill holes are underground, the inclinations of the many boreholes vary from downward to upward (fig. 1).

Path calculations were performed by first converting the surface grid northing and easting coordinates, given for the collar (origin) locations of the drill holes, into mine cross section and long section coordinates, respectively. After revisiting

previous lessons in geometry and trigonometry, the following formulas were derived:

$$XS = [(N - N_0) - (E - E_0) \tan \alpha] \cos \alpha, \quad (1)$$

and

$$LS = \frac{(E - E_0)}{\cos \alpha} + [(N - N_0) - (E - E_0) \tan \alpha] \sin \alpha, \quad (2)$$

where E_0 is the surface grid easting of the origin of the mine grid,
 E is the surface grid easting coordinate of the drill-hole collar (origin),
 N_0 is the surface grid northing of the origin of the mine grid,
 N is the surface grid northing coordinate of the drill-hole collar (origin),
 α is the angle of axis rotation.

The next step was to calculate the three-dimensional location of each deviation in every drill hole, given the measured downhole depth of each inflection and the inclination and azimuth of the drill hole at each of these points. The following calculation framework was derived:

$$LS = LS_0 + (MD \cos n\phi \sin \theta), \quad (3)$$

$$XS = XS_0 + (MD \cos \phi \cos \theta), \quad (4)$$

$$TVDSS = [Z_0 + (MD \sin \phi)] - 60, \quad (5)$$

where MD is the measured downhole distance from the origin of the core segment,
 LS_0 is the long section coordinate of the origin of the core segment,
 XS_0 is the cross-section coordinate of the origin of the core segment,
 Z_0 is the mine elevation coordinate,
 ϕ is the inclination of the drill-hole segment from horizontal, in radians,
 θ is the azimuth (relative to LS - XS axes) of the drill-hole segment, in radians,
 $TVDSS$ is true vertical distance above sea level (elevation).

Because the azimuths and inclinations of the boreholes change at inflection points, or deviations, along the paths, the application of these formulas is somewhat involved. Each time a point of inflection is encountered along a hole, the 3-D coordinates must be calculated for the inflection point and then reintroduced into formulas 3–5 as a new origin for the next

section of core, until another deviation is encountered, and so on. To apply the required series of successive calculations for each of the drill holes with thousands of deviated segments, Robert McFaul of Dynamic Graphics, Inc. (DGI), wrote and provided programming code to accomplish the task. Bob Belcher of DGI also assisted with subsequent modeling tasks.

The log and assay data were recorded for core segments defined by a top (first) measured downhole depth and a bottom (second) measured depth. It was felt that a reasonable single measured distance to attach to each data point is the midpoint of the core segment from which the data were obtained. This midpoint was calculated for each core segment and was used as the measured downhole depth for each data point.

Modeling

For three-dimensional modeling of the drill-hole data, it was necessary to calculate the coordinates of each of the observation locations in three-dimensional space, in this case LS , XS , and $TVDSS$ (elevation). This task was performed using Dynamic Graphics, Inc., EarthVision software. By incorporating core logs and assay data with the drill-hole paths, the software calculated the three-dimensional coordinates of each data point. The result was a file of data with associated drill-hole identifiers, three-dimensional coordinates, and associated physical and chemical properties. These property data were used as input for three-dimensional EarthVision modeling calculations.

This procedure produces a three-dimensional grid depicting the calculated distribution of the measured property throughout a defined volume. The calculated models are grids in the shape of rectangular prisms containing grid nodes at regularly spaced intervals in each dimension. The calculated value of the property being modeled is stored for each grid node location and used for subsequent display and analysis. The drill-hole data locations (fig. 1) are most densely distributed within a volume bounded by cross-section coordinates of 2000 to 5200, long-section coordinates of 4200 to 7100, and true elevations between -400 and 3,000 feet. The rest of the three-dimensional models produced in this study are confined to the rectangular prism defined by those limits. The displays of these models were also clipped by the two-dimensional topographic surface grid discussed below.

Minimum-Tension Gridding

To produce spatially continuous two- and three-dimensional models that are representative of data associated with scattered points along drill holes, topographic maps, and digitized cross sections, interpolated grid values were calculated using 2-D and 3-D minimum-tension gridding algorithms in the EarthVision software suite. The following discussion is derived from EarthVision documentation by Dynamic Graphics, Inc. (Dynamic Graphics, Inc., 1997).

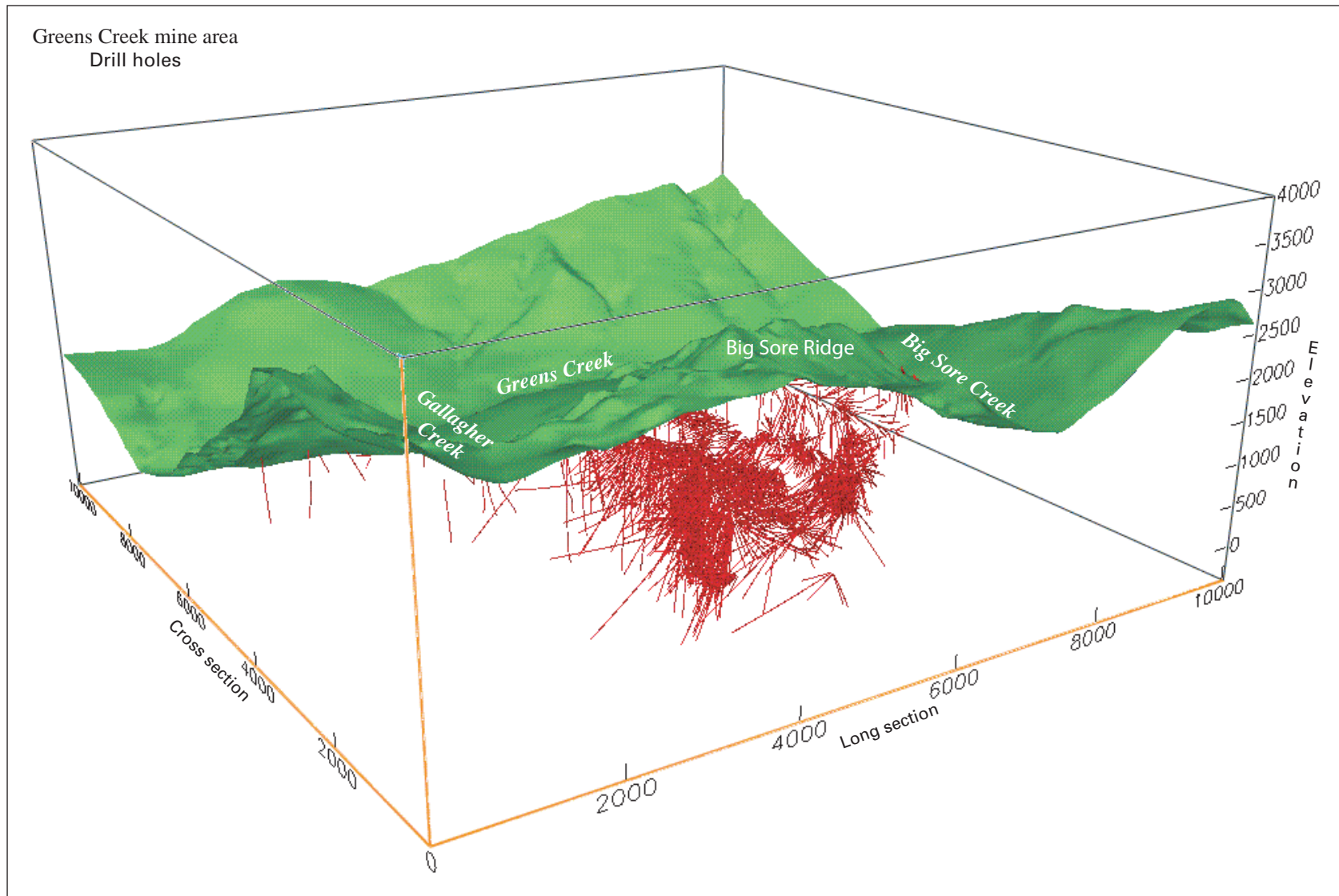


Figure 1. Drill-hole locations, Greens Creek mine area. The bearing of the cross-section axis is N. 26.5651° W. Cross-section and long-section coordinates and elevation shown in feet.

The main goals of representational gridding are to honor the values of the input data as closely as possible and to calculate a reasonable-looking model for grid nodes that are not on or adjacent to input data points. Minimum tension is the distribution of the second derivative or curvature of the property variation among the nodes such that the sum of the squares of the second derivative (tension) is minimized.

The EarthVision two-stage minimum-tension gridding method reconciles these two, sometimes conflicting, goals. The two stages of minimum-tension gridding are (1) the initial estimate, and (2) cubic iteration functions with scattered data feedback.

The initial grid estimation process calculates a property value for every grid node in an extremely coarse grid that is used in the initial stages of gridding. Next, iterations begin, each a calculation of a new property value for each grid node with neighboring grid nodes providing input values to a cubic function that determines the new value. Once the new value is calculated for a node, the scattered data are used for the feedback process. Each set of iterations produces a finer grid, and this process is repeated until the desired grid size is produced.

To ensure that the original data values are honored, each iterative reevaluation of grid nodes is followed by a feedback process that compares the calculated property values to the input scattered data values that fall within a one-cell zone around the grid nodes. If the difference is less than with the preceding iteration, the program accepts the new function-derived grid node value and proceeds to recalculate the next grid node. If, however, the difference has increased, the node is reset to a value closer to the input scattered data point. Through this process, the scattered data feedback keeps grid nodes tied to neighboring scattered data while allowing the cubic function to distribute tension in a reasonable fashion. The result of these operations is a continuous data distribution that honors the values of the original scattered points and that can be displayed and manipulated in 2- and 3-D visualizations.

Topographic Model

Terrain data were digitized from topographic contour maps by the Kennecott Greens Creek Mining Company and were made available in Alaska State Plane Zone 1 coordinates by Andy West. The State Plane coordinates were first translated to the Greens Creek mine local surface grid reference system by subtracting the 2262748.50N, 2479273.89E grid origin offsets described earlier. The resulting local surface grid coordinates were then transformed to mine grid long-section and cross-section coordinates by applying equations 1 and 2, so that a terrain model calculated from the data would be correctly geographically referenced with respect to the subsurface ore, geochemical, and structural models. EarthVision two-dimensional minimum-tension gridding was applied to the transformed data to produce the topographic surface model that is included in figures 1–4. It can be seen that this model, when rendered in three-dimensional space, appears as a thin floating wafer, similar to the fault planes in this respect.

The topographic surface was also used to constrain, or clip, the ore, geochemical, and fault models at the ground surface. Otherwise, the models would be unrealistically extrapolated to fill the entire extent of the volume defined by the model limits of *LS*, *XS*, and *TVDSS*.

Ore Model

The core log data include lithologic codes that permit the identification of five types of ore in the Greens Creek mine. Because goals of the three-dimensional modeling in this study were not only to model and visualize the distribution of orebodies, but also to depict geochemical distributions within those orebodies, it was necessary to derive a numeric variable to designate each lithologic log observation as ore or “non-ore.” The samples designated as ore were given an ore value of 1; non-ore samples were assigned an ore value of 0. A three-dimensional minimum-distance gridding algorithm was first applied to the derived ore value variable, by which grid cells within a prescribed distance from data points were assigned the value of the nearest data point. The appearance of this ore model, however, was found to be somewhat unsatisfactory because the display routine imposed continuously varying ore values to the desired binary distribution. Instead, although minimum-tension gridding is more typically used for continuously varying properties, a somewhat unconventional application of the technique was used in this study to create 3-D models of ore distribution (fig. 2).

Minimum-tension gridding calculations were applied to the ore value variable, and the resulting continuously varying model values were converted to binary form. All model values of 0.5 or greater were converted to 1. All model values less than 0.5 were converted to 0.

The validity of the results was tested by comparing this binary ore model with views of various cross sections and plan views of ore distributions as shown by Proffett (chap. 7) and other maps created and provided by the Kennecott Greens Creek Mining Company. Close agreement was noted between the results of the three-dimensional ore model and geologist-drawn cross sections showing ore delineation. Although the cross-section profiles of orebodies mapped by geologists were rendered in greater detail, the 3-D model shows similar orebody shapes and precise spatial concordance at locations where comparative drawings are available to be examined.

Geochemical Models

EarthVision minimum-tension 3-D gridding was applied to geochemical variables in the scattered point data of the drill-core assays, and to derived variables such as element concentration ratios. To produce models that could readily be related to modeled orebody distributions derived from geologic interpretations rendered by mine geologists, the three-dimensional geochemical grids were constrained by the interpreted orebodies (fig. 2). To do so, each of the

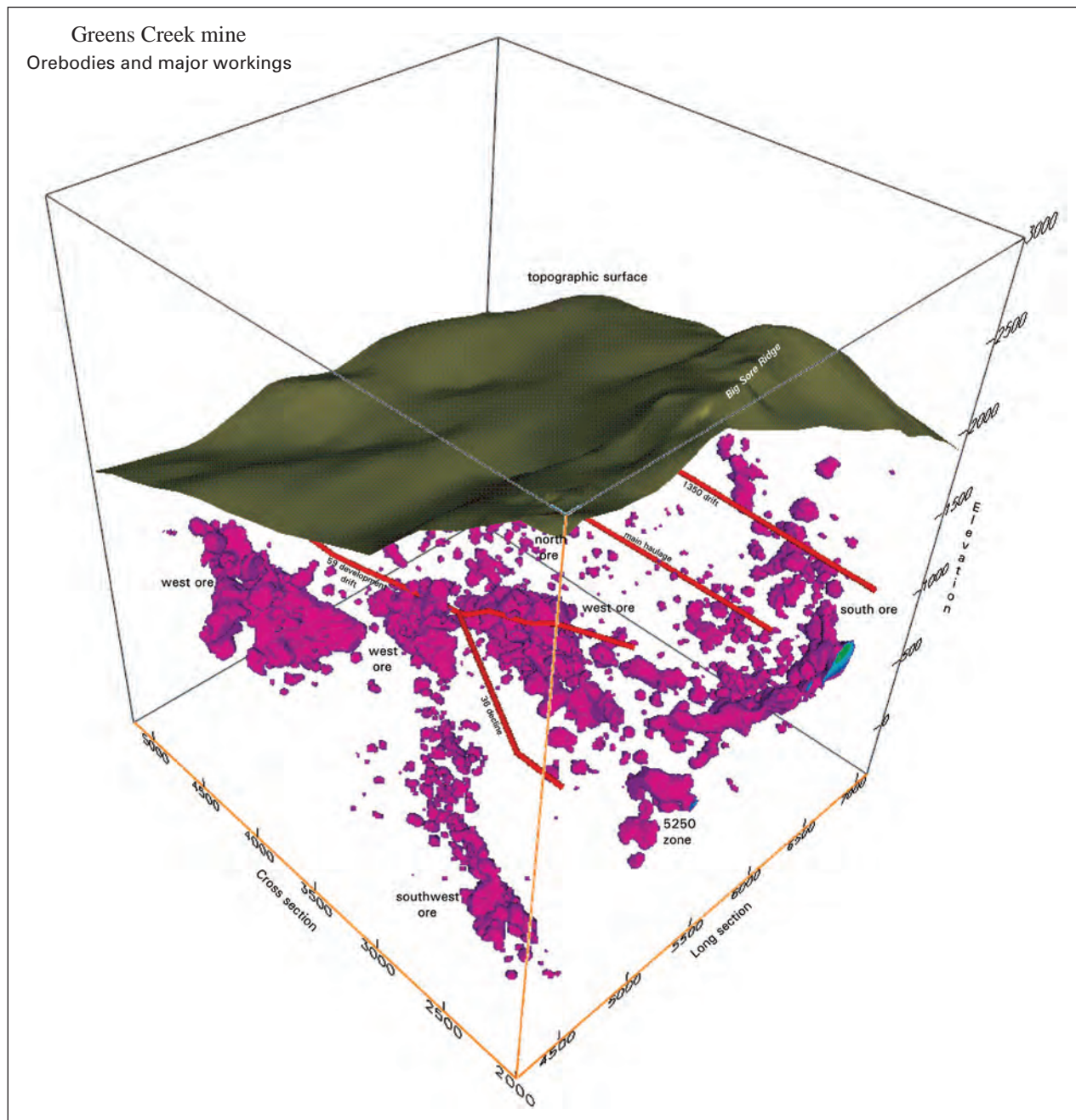


Figure 2. Greens Creek mine orebodies, showing major workings. The bearing of the cross-section axis is $N. 26.5651^\circ W$. Cross-section and long-section coordinates and elevation shown in feet.

three-dimensional geochemical grids was multiplied by the binary ore grid to produce models of geochemical variables within interpreted orebodies. The multiplication operation left the geochemical distributions unchanged in the presence of ore (ore value=1) but changed the geochemical grid values to 0 in the presence of non-ore (ore value=0). Some of the resulting geochemical models are shown in figures 3–8.

It had also been intended to model the lithologic horizons of the mine and to conformably model geochemical distributions among these units as well, but intractable difficulties were encountered in the form of numerous discontinuous repetitions of lithologies down the same drill holes. Additional information pertaining to dip and azimuth of the bedding planes would have been required to successfully create lithologic horizon models.

Geologic Structure Models

Several of the most important geologic structures in the area were modeled to provide three-dimensional visualization of these features. Cross sections and surface maps produced by Proffett (chap. 7) were used to digitize locations along the Klaus shear, the Maki and Little Maki faults, and the Upper Shear Zone. The *LS*, *XS*, and *TVDSS* coordinates of plan and cross-section traces of these structures were recorded and used as input to EarthVision's fault-modeling program. The modeled structures appear as thin wafers, floating in space, and can be combined with geochemical and ore models as shown in fig. 3.

Visualization

A significant advantage of three-dimensional modeling is that it makes available practically unlimited perspectives from which to view or visualize the results. The models may be sliced, rotated, panned, and zoomed in countless ways. Isovalue shells, equivalent to three-dimensional contour surfaces and analogous to two-dimensional contour lines, may be chosen for display, and volumetric statistics can be readily calculated and displayed for each variation of the property models. In addition, various 3-D models may be combined for simultaneous display and visualization.

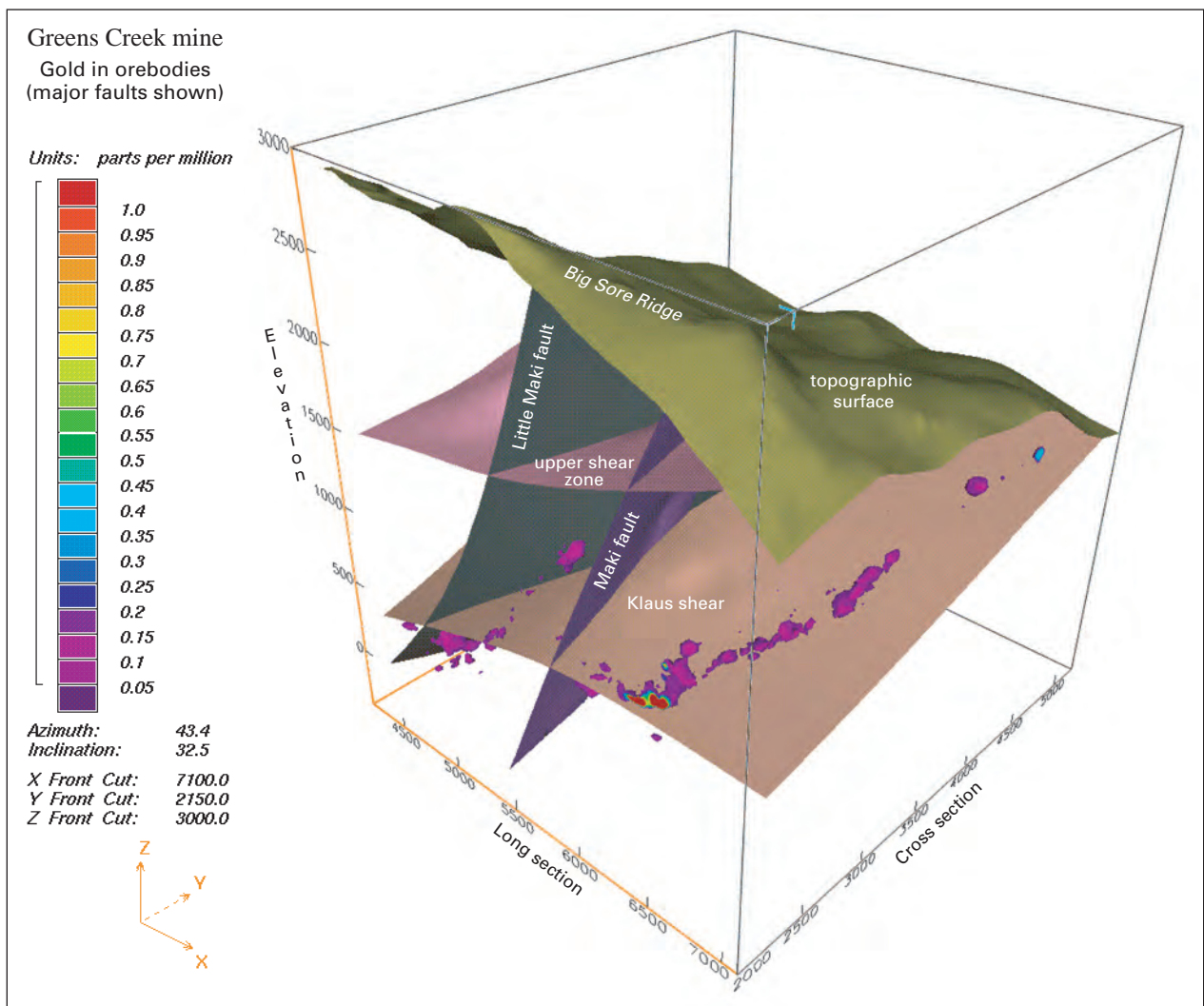


Figure 3. Faults, shear zones, and gold distribution within orebodies, Greens Creek mine. Only gold concentrations greater than 0.05 part per million are shown. The bearing of the cross-section axis is N. 26.5651° W. Cross-section and long-section coordinates and elevation shown in feet.

A few of the myriad visualization possibilities for the three-dimensional models produced for the Greens Creek mine are included here. Figure 4 shows a chair cut display of the three-dimensional distribution of silver within ore bodies, clipped by the topographic surface above. It can be seen that

parts of five different cross sections are shown in the same image, and that a sixth is possible if the top slice of the model were lowered to be below the topography. Figures 5–7 show iso-value shells of silver, zinc, and antimony, and figure 8 shows iso-value shells of the arsenic:antimony ratios.

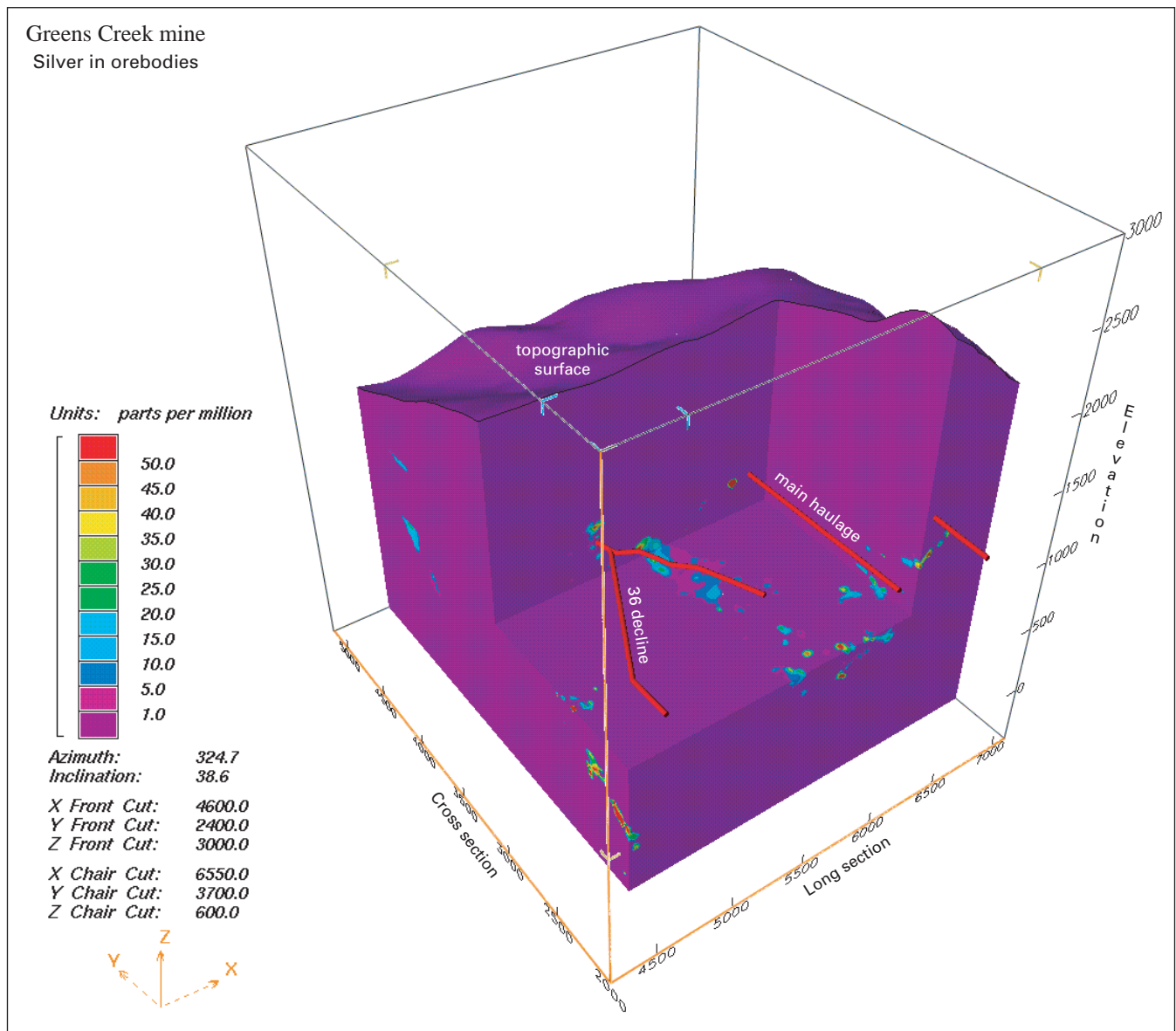


Figure 4. Chair cut display of silver in orebodies, Greens Creek mine. The bearing of the cross-section axis is N. 26.5651° W. Cross-section and long-section coordinates and elevation shown in feet.

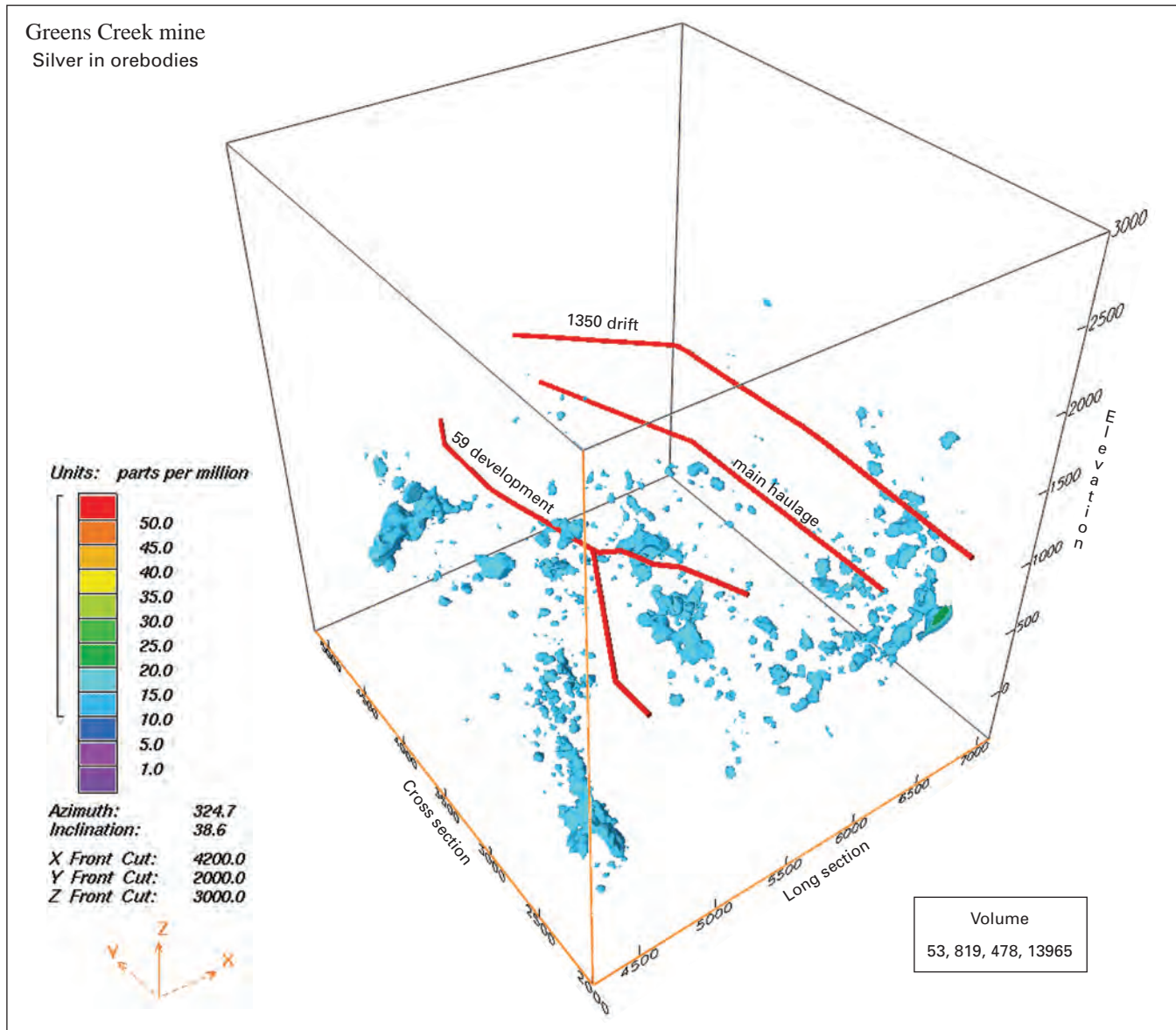


Figure 5. Isovvalue shell display of silver greater than 10 parts per million in orebodies, Greens Creek mine. Volume calculated in cubic feet. The bearing of the cross-section axis is N. 26.5651° W. Cross-section and long-section coordinates and elevation shown in feet.

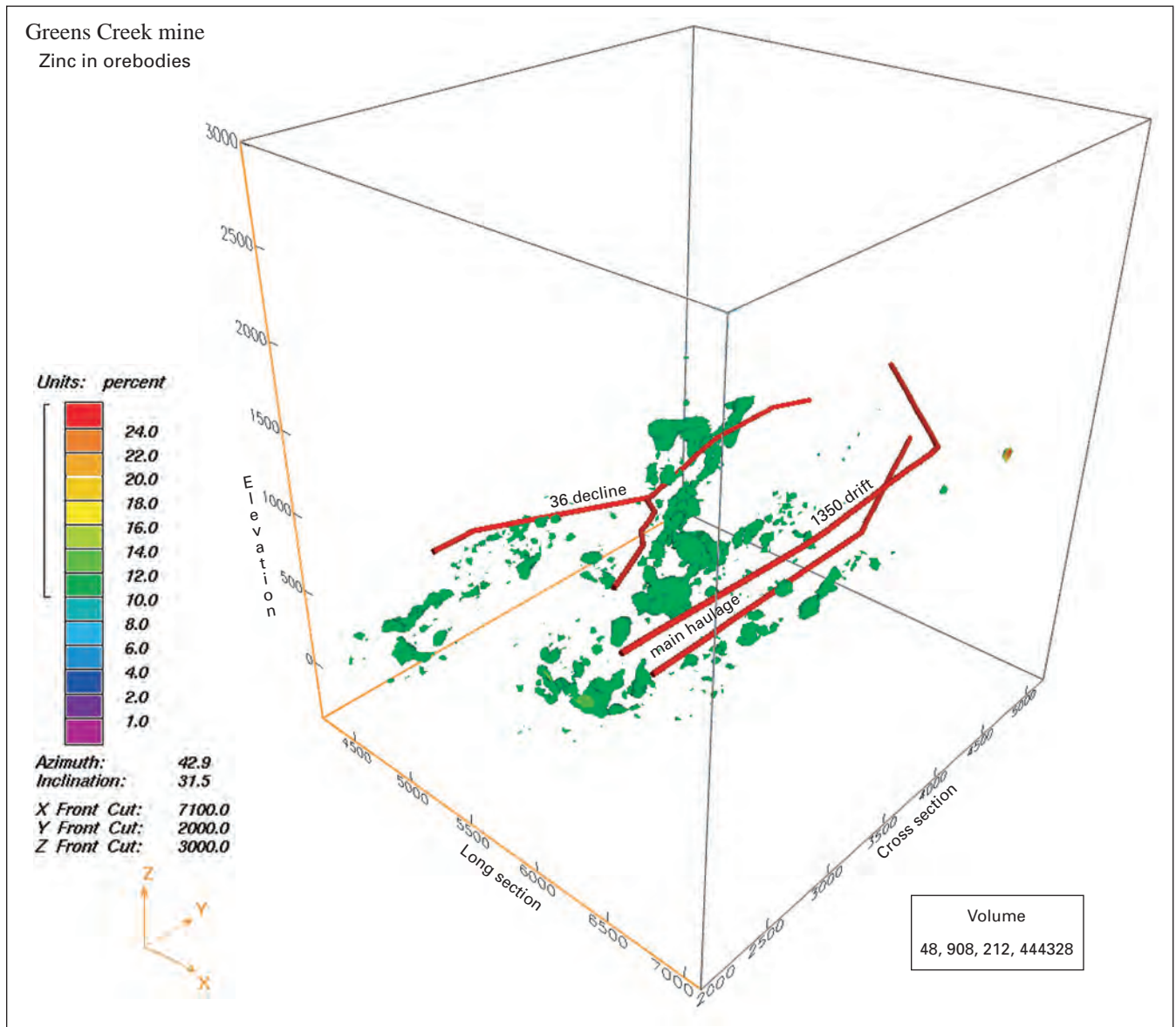


Figure 6. Isovvalue shell display of zinc greater than 10 percent in orebodies, Greens Creek mine. Volume calculated in cubic feet. The bearing of the cross-section axis is N. 26.5651° W. Cross-section and long-section coordinates and elevation shown in feet.

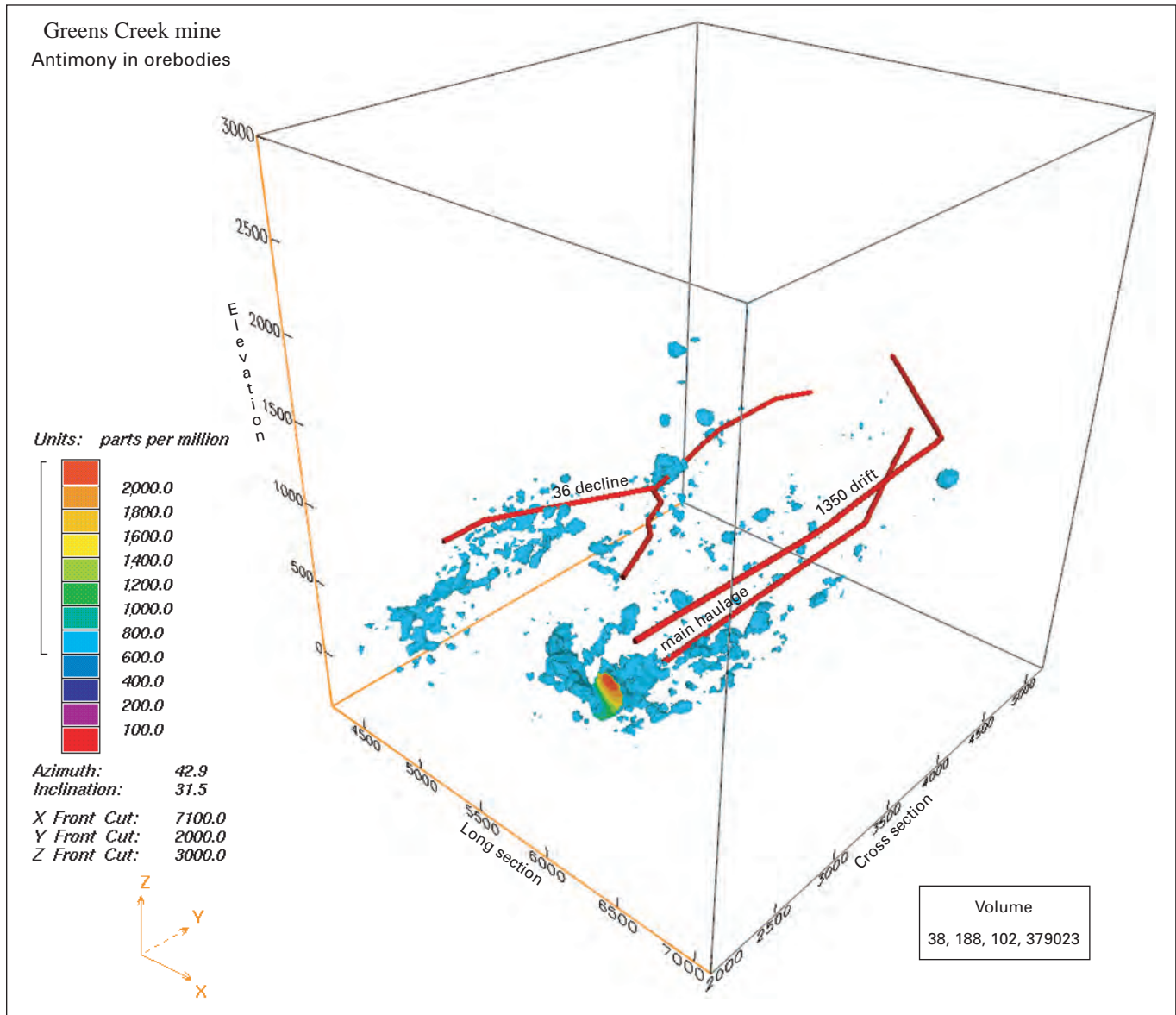


Figure 7. Isovallu shell display of antimony greater than 600 parts per million in orebodies, Greens Creek mine. Volume calculated in cubic feet. The bearing of the cross-section axis is N. 26.5651° W. Cross-section and long-section coordinates and elevation shown in feet.

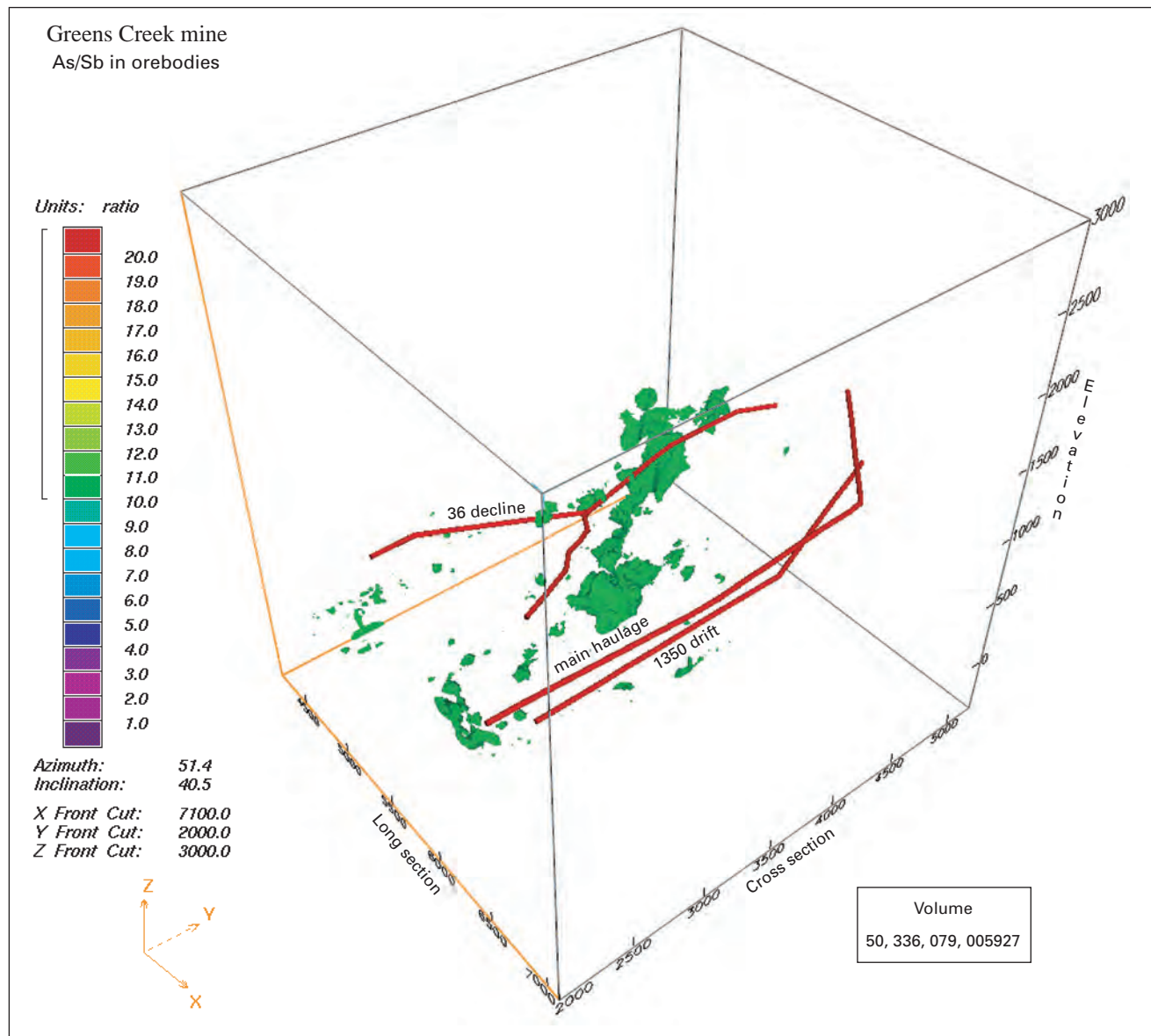


Figure 8. Isovale shell display of arsenic: antimony ratios greater than 10 in orebodies, Greens Creek mine. Volume calculated in cubic feet. The bearing of the cross-section axis is N. 26.5651° W. Cross-section and long-section coordinates and elevation shown in feet.

Conclusions

The modeling efforts have been successful in producing reasonable three-dimensional renderings of the ore and geochemical information included in the drill-hole data. Verification has been obtained from geologist-drawn plan and cross-section views of the mine. Although the drawn cross sections may provide greater detail in delineating the shapes of the orebodies, the 3-D models provide great flexibility in readily displaying and manipulating unlimited perspectives of the locations, shapes, and volumes of orebodies along with their associated metal content throughout the region of data. These capabilities are potentially valuable tools for examining issues of not only scientific interest, but also of mining development and redevelopment strategies. The three-dimensional models and visualization can be used to guide development as it progresses but might also be used to consider and devise effective strategies for revisiting previously explored areas for the purpose of ancillary production efforts if warranted by changing economic conditions.

Reference Cited

Dynamic Graphics, Inc., 1997, EarthVision user's guide 5.1: Alameda, Calif., Dynamic Graphics, Inc.

A Genetic Model for the Greens Creek Polymetallic Massive Sulfide Deposit, Admiralty Island, Southeastern Alaska

By Cliff D. Taylor, Kerry G. Lear, and Steven R. Newkirk

Chapter 15 of

**Geology, Geochemistry, and Genesis of the Greens Creek Massive
Sulfide Deposit, Admiralty Island, Southeastern Alaska**

Edited by Cliff D. Taylor and Craig A. Johnson

Professional Paper 1763

**U.S. Department of the Interior
U.S. Geological Survey**

Contents

Abstract.....	419
Introduction.....	419
Genetic Model for the Greens Creek Deposit.....	420
Tectonic Setting	420
Style and Timing of Mineralization.....	421
Post-Mineral Modifications to the Greens Creek Orebodies.....	424
Discussion.....	425
References Cited.....	427

Figure

1. Graphic illustrations of the: (a) early, (b) main-stage, and (c) late periods of the development, growth, and death of the Greens Creek ore-forming environment.....422

A Genetic Model for the Greens Creek Polymetallic Massive Sulfide Deposit, Admiralty Island, Southeastern Alaska

By Cliff D. Taylor,¹ Kerry G. Lear,² and Steven R. Newkirk^{2*}

Abstract

The Greens Creek deposit (global resource of 24.2 million tons at an average grade of 13.9 percent zinc, 5.1 percent lead, 0.15 troy ounce per ton gold, and 19.2 troy ounces per ton silver at zero cutoff) formed in latest Triassic time during a brief period of rifting of the Alexander terrane. The deposit exhibits a range of syngenetic, diagenetic, and epigenetic features that are typical of volcanogenic (VMS), sedimentary exhalative (SEDEX), and Mississippi Valley-type (MVT) genetic models. In the earliest stages of rifting, formation of precious-metal-rich silica-barite-carbonate white ores began at low temperature in a shallow, subaqueous setting, probably a thin carbonate shelf on the flanks of the Alexander landmass. Epigenetic carbonate replacement textures in the footwall dolostones are overlain by stratiform silica-carbonate-barite-rich ores and indicate that early mineralization formed at and just beneath the paleo sea floor by mixing of a reduced, precious-metal-rich, base-metal-poor hydrothermal fluid with oxygenated seawater. As rifting intensified, the shelf was downfaulted and isolated as a graben. Isolation of the basin and onset of starved-basin shale sedimentation was concurrent with emplacement of mafic-ultramafic intrusives at shallow levels in the rift, resulting in an increasingly higher temperature and progressively more anoxic ore-forming environment. The formation of the main stage of massive sulfide ores began as the supply of bacterially reduced sulfur increased in the accumulating shales. As the main-stage mineralization intensified, shale sedimentation inundated the hydrothermal system, eventually forming a cap. Biogenic sulfate reduction supplied reduced sulfur to the base of the shales where mixing occurred with hot, base-metal-rich hydrothermal fluids. Ore deposition continued by destruction and epigenetic replacement of the early white ores in proximal areas and by inflation and diagenetic replacement of unlithified shale at the interface

between the white ores and the base of the shale cap. Ore deposition waned as the shales became lithified and as the supply of bacterially reduced sulfur to the site of ore deposition ceased. The final stages of rifting resulted in the emplacement of mafic-ultramafic intrusive rocks into the Greens Creek system and extrusion of voluminous basaltic flows at the top of the Triassic section. Greenschist facies metamorphism during the Jurassic-Cretaceous accretion of the Alexander terrane to the continental margin resulted in recrystallization, remobilization, and significant upgrading of the Greens Creek orebody.

Current ore-genetic models are inadequate to explain the diverse characteristics of the Greens Creek deposit. We suggest that Greens Creek represents a transitional type of deposit that formed as a result of its evolving metallogenic setting in a propagating intra-arc rift. It is therefore a hybrid deposit within a spectrum of exhalative to replacement-style deposits.

Introduction

The Greens Creek deposit provides an opportunity to examine the relationship between VMS, SEDEX, and MVT massive sulfide genetic models. VMS characteristics (Hutchinson, 1973; Franklin and others, 1981; Large, 1992) of the Greens Creek deposit include a zinc-lead-silver-gold-copper metal endowment similar to the Kuroko-type, a mafic volcanic footwall, a zoned alteration profile, and mineralogy similar to that of white smoker systems of the southwestern Pacific Ocean (Halbach and others, 1993). However, the deposit also has numerous characteristics usually associated with the SEDEX class (Goodfellow and others, 1993; Solomon and Groves, 1994) including: a metal assemblage dominated by zinc, lead, and silver; the absence of felsic igneous rocks and the presence of altered mafic-ultramafic intrusives in the footwall; lack of a focused feeder system and presence of a huge alteration envelope containing chromium and barium-rich silicates and complex carbonate alteration mineralogy; a hanging wall consisting of graphitic, pyritic argillites; geochronologic and isotopic evidence suggesting that ore formation occurred during and after deposition of the shale cap; and location in an

¹U.S. Geological Survey, Denver, Colorado, USA.

² Kennecott Greens Creek Mining Company, Juneau, Alaska, USA.

*Present address: Department of Earth Sciences, University of Memphis, Memphis, Tennessee, USA 38152.

intra-arc setting consistent with the rift tectonics model common to most SEDEX deposits. Crosscutting relationships and ore textures are consistent with growth by inflation beneath, and syndiagenetic replacement of, the shales during sedimentation. Additionally, MVT mineral-forming processes (Leach and Sangster, 1993) are suggested by the presence of a thin, discontinuous, platform carbonate unit in the footwall. The footwall carbonate is host to an epigenetic ore and gangue mineral assemblage that occurs in veins, replacements, and open space fillings similar to the carbonate-hosted deposits of the Irish Midlands and the U.S. Midcontinent regions. Sulfur isotope values are unusually low and are unlike sulfur isotope compositions typical of either VMS or SEDEX deposits. They most closely resemble the range of values exhibited by a subset of deposits in the Irish Midlands. Greens Creek, therefore, is a hybrid or transitional type of mineral deposit, with characteristics of VMS, MVT, and SEDEX deposits.

In this chapter we present an interpretive genetic model for the formation of the deposit based on the cumulative information presented in the preceding chapters of this volume. We then discuss the genetic model with regard to the proposed tectonic setting and examine whether the Greens Creek deposit fits into existing ore-genetic classification schemes.

Genetic Model for the Greens Creek Deposit

Tectonic Setting

Development of a genetic model for the Greens Creek deposit requires the consideration of the data presented in the preceding chapters in the context of the tectonic environment that was extant at the time of mineralization. The well-established age of the immediate hanging-wall argillites of 220.7 ± 4.4 Ma (latest Carnian-earliest Norian stages of the latest Triassic; chap. 11) places Greens Creek into the allochthonous, oceanic portion of the Alexander terrane's history prior to the Jurassic-early Tertiary accretion to the continental margin. The geologic history of the Alexander terrane from middle Paleozoic through Middle (?) Permian is thought to have been largely a period of relative quiescence marked by erosion of uplifts formed during the Middle Silurian to earliest Devonian Klakas orogeny, development of large areas of platform carbonates, and shale sedimentation in open marine depositional basins (Gehrels and Berg, 1994). Minor mafic volcanism and tectonism during Early Permian (?) time is marked by the volumetrically minor and poorly preserved Halleck Formation. This unit occurs between the Mississippian to Permian Cannery Formation shales and the Lower to Upper Permian Pybus dolomite.

The Permian depositional setting is marked by progressive emergence of the Alexander terrane. The siliceous black shales and interbedded cherts of the Cannery Formation, indicative of sedimentation below the carbonate compensation depth, are overlain by shallow-water, dolomitic carbonates

of the Pybus Formation. Preservation of ooid grainstones and fossil debris provides evidence that the Pybus Formation was deposited at or close to wave base. Nondeposition (erosion) is indicated by the absence of Late (?) Permian through Middle Triassic strata throughout southeastern Alaska. This hiatus is significant and probably indicates emergence of the Alexander landmass. However, it is surprising that there is no evidence for prolonged exposure in the form of extensive karsting of the Pybus Formation or the development of a regolith horizon. These lines of evidence may suggest that the hiatus was a prolonged period of exposure marked by erosion and removal rather than nondeposition of pre-Late Permian units (chap. 2).

Deposition of the polymictic conglomerates at the base of the Hyd Group provides the earliest indication of the onset of rift tectonic activity that ultimately resulted in the formation of the Greens Creek deposit. Although not directly dated, their presence immediately underlying the 225 ± 3 Ma Puppets Formation rhyolite (uranium-lead zircon, Gehrels and others, 1987) on Gravina Island provides a minimum age for the initiation of graben formation and rift-filling volcano-sedimentary activity in southeastern Alaska. The earliest known intrusive rocks related to rifting in southeastern Alaska are mafic-ultramafic intrusions on Duke Island that yield a similar age of 226 ± 3 Ma (uranium-lead zircon, Gehrels and others, 1987). The absence of a well-defined basal conglomerate horizon at the latitude of Greens Creek indicates that the mine area was distal to the locations where normal faulting first occurred. This period of tectonic readjustment and associated gravity sliding was immediately followed by the extrusion of the first of two major pulses of volcanic rocks into the nascent rift; the first pulse was bimodal and consists of voluminous rhyolites in the southern part of the rift and relatively minor basaltic volcanic rocks in the central and northern portions (where Greens Creek is located). The second pulse consists of voluminous basaltic flows that cap most exposures of Late Triassic rocks throughout southeast Alaska. The geochemical character of these volcanic rocks changes northward from arc-contaminated calc alkaline rhyolites to peralkaline rhyolites and then to arc-contaminated tholeiites and minor alkaline basalts by the latitude of Admiralty Island. This geochemical evolution of the volcanic rocks, coupled with the northward thinning of the underlying conglomerates, suggests that the developing rift may have been oblique to, and propagating southward into, the Alexander terrane landmass (Taylor, 1997; Taylor, Philpotts, Sutley, and others, 1995; Taylor, Philpotts, Hall, and Wakeman, 1995; Taylor, Premo, and Meier, 1999; Taylor 2000; chap. 2). Indications of the depositional setting at the time of extrusion of the bimodal first pulse of volcanic rocks are scarce due to their predominantly volcanoclastic character; however, minor pillow basalts exposed on Admiralty Island indicate that at least at the latitude of Greens Creek the environment was subaqueous. Conodont data from the overlying Hyd Group argillites at Greens Creek constrain the cessation of the first extrusive episode to sometime before the onset of shale sedimentation at 220.7 ± 4.4 Ma (chap. 12).

Following the first period of magmatism, a period of quiescence ensued during which a thin carbonate platform developed in the newly formed rift. On Annette, Gravina, and Kuiu Islands (see fig. 1 in chap. 2) this unit consists primarily of a light gray, fossiliferous, massive, fine to coarse crystalline, cliff-forming, dolomitic metalimestone with minor reef-forming communities (George Stanley, oral commun., 2000) and oolitic shoals (Muffler, 1967; Berg, 1973) that indicate a shallow-water depositional setting. The carbonate platform thins northward to Gambier Bay on southern Admiralty Island where it is discontinuously exposed as hackly textured thick-bedded blocks of alternating limestone and dolomite. Discontinuous bodies of heavily altered, coarse crystalline dolomite and dolomitic breccia rest on the phyllites in the immediate footwall of the Greens Creek deposit and contain relict fragments of *Halobia* and crinoid stems. Their presence indicates that the depositional environment just prior to mineralization was a shallow-water carbonate platform or possibly a proximal carbonate ramp setting.

Resumption of rifting resulted in the cessation of carbonate deposition and the initiation of hydrothermal fluid flow at Greens Creek. Foundering of the carbonate platform and tectonic readjustment of various subbasins within what was probably a segmented rift is indicated by the localized presence of carbonate debris flows and more distal, graded, carbonate turbidites. Carbonate breccias in the footwall at Greens Creek are highly altered, which makes it difficult to distinguish between tectonic and sedimentary origins. However, a subset of the carbonate breccias displays rounded clasts, suggesting that carbonate debris flows are present.

Style and Timing of Mineralization

As described in detail in chapters 6 and 9, ore lithologies at Greens Creek are divided into two major groups. The first group of early white ores, consisting of silica-, carbonate-, and barite-rich subtypes, rests on the footwall phyllite and platform carbonate units beneath and(or) distal to the second group of main stage, massive, pyritic and base-metal-rich sulfides. The gradation from white ores into massive ores is fairly abrupt, and the metal endowments are distinct. White ores are base-metal-poor and precious-metal-rich with a gangue-rich mineral assemblage marked by a distinctive yellow, low-iron sphalerite, pyrite, galena, tetrahedrite, pyrargyrite, free gold, and a host of lead-antimony-sulfosalt minerals, whereas the massive ores are markedly enriched in base metals in addition to significantly elevated precious-metal concentrations. The main-stage ores are dominated by pyrite, sphalerite, galena, and tetrahedrite and contain chalcopyrite, arsenian pyrite/arsenopyrite, free gold, and electrum in proximal areas of the deposit.

In the absence of any direct geochronological evidence from this ore assemblage, the timing of the onset of mineralization is an arguable point. The ore stratigraphic succession from the basal and peripheral early white ores up into massive sulfides, and the silica-carbonate-barite-dominated mineral assemblage of the early white ores, indicate that mineralization

began by exhalation of low-temperature, hydrogen sulfide-dominated hydrothermal fluids onto or near the sea floor (fig. 1A). The presence of epigenetic mineral textures dominated by low iron sphalerite, lead-antimony, and silver sulfosalts associated with dolomite and quartz-infilled solution cavities is consistent with percolation of hydrothermal fluids through, and replacement of, the footwall sedimentary carbonate units. Precipitation of the baritic ores as blankets occurred at or just below the sediment/water interface. Sulfur isotopic values from these baritic ores are equivalent to Triassic seawater values and suggest that initially the hydrothermal fluids mixed with oxygenated marine water (chap. 10). The high arsenic, antimony, and mercury content of the white ores in the form of minor realgar, arsenian pyrite, and mercurian tetrahedrites and electrum represents additional evidence of the low-temperature, reduced state of the initial ore fluid. Recent studies of active shallow and(or) low-temperature white smoker systems on the sea floor (Hannington and others, 1986; Halbach and others, 1993; Binns and others, 1993; Fouquet and others, 1993; Stoffers and others, 1999) have documented the existence of mineral assemblages and metal endowments very similar to those observed in the early white ores at Greens Creek. The very large size of the footwall alteration envelope (Taylor, Newkirk, and others, 1999; Anderson and Taylor, 2000; Anderson and Taylor, unpub. data, 2000) and the absence of any evidence suggestive of white smoker chimneys or focused upflow zones indicate that fluid upwelling was diffuse and occurred over a large area of the sea floor. Another feature that suggests fluid upwelling occurred by diffuse flow over a relatively large area is the dominantly volcanoclastic nature of the footwall. Mafic volcanoclastic rocks extruded during the first period of rift-related tectonic activity, overlain by sedimentary carbonate breccias in the mine area, resulted in a permeable substrate through which hydrothermal fluids passed. The presence of a highly permeable footwall at Greens Creek precluded the development of a focused feeder system and probably contributed to the large size of the deposit. Similar relationships have been observed in Canada, where many of the larger massive sulfide deposits are associated with volcanoclastic sequences (Morton and Franklin, 1987; Kerr and Gibson, 1993; Hannington and others, 1999).

As rifting progressed, the graben continued to deepen, resulting in shale sedimentation and the gradual isolation of the immediate Greens Creek depositional system (fig. 1B). A variety of evidence suggests that the accumulation of the shales over the diffuse vent system happened rapidly enough to prevent vertical growth of the orebody through the un lithified sediments. As the rising hydrothermal fluids came in contact with the growing shale cap, physical and(or) chemical conditions were such that ore precipitation occurred at the contact between the footwall greenstones and carbonates and the overlying shales. The absence of significant shale interbedding at the top of the orebodies and the lack of stacked massive sulfide lenses in the shales suggest that the majority of ore formation occurred by inflation beneath and replacement of the shales at the base of the sedimentary pile. The shales also

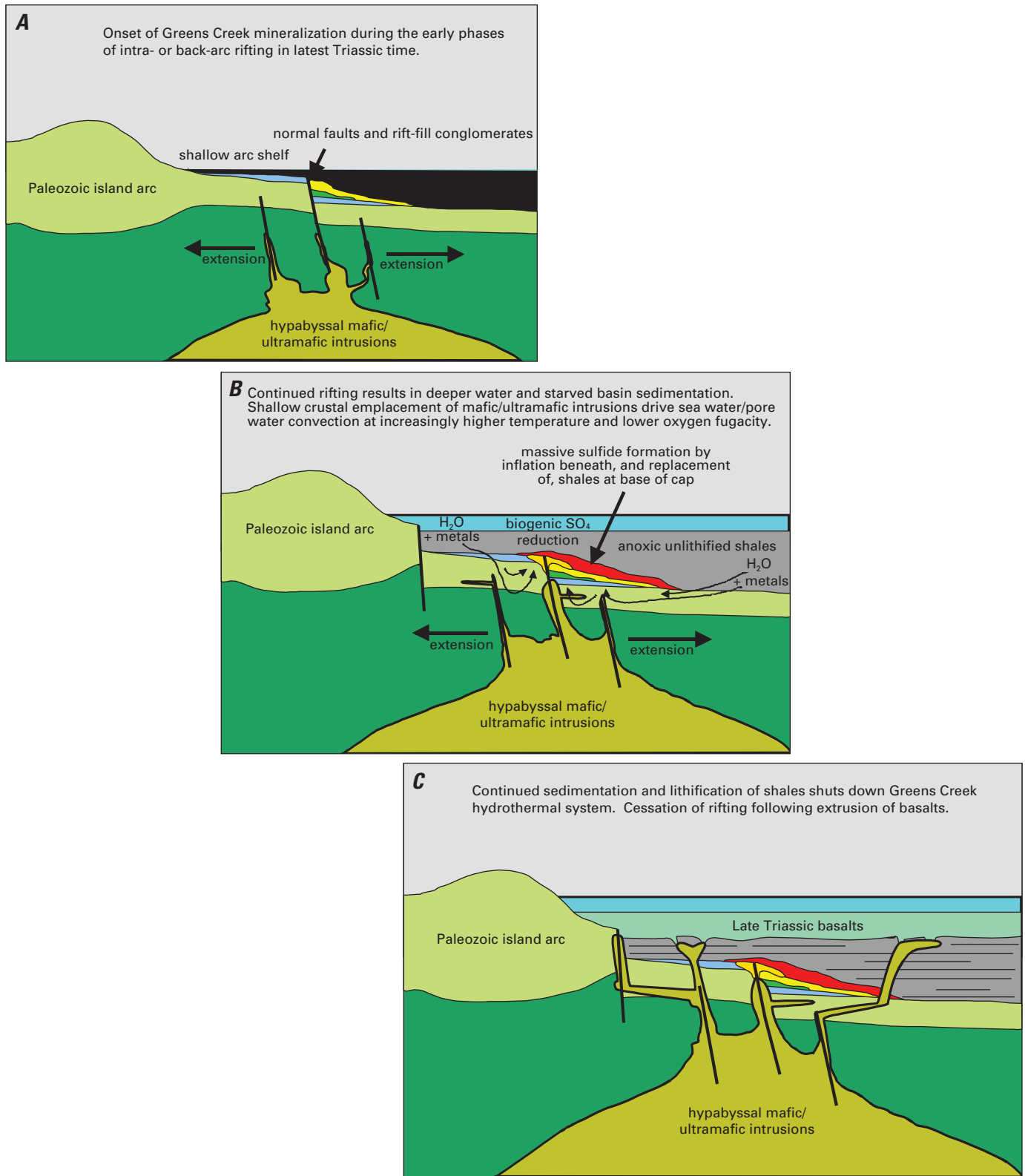


Figure 1A–C. Graphic illustrations of the: (A) early, (B) main-stage, and (C) late periods of the development, growth, and death of the Greens Creek ore-forming environment.

are characterized by high organic carbon content and contain abundant diagenetic pyrite. These features indicate that, as the bottom dropped out of the rift basin, the local depositional setting at Greens Creek quickly evolved into a restricted, anoxic marine basin (chap. 8). Although direct indications of water depth are lacking, the conodont assemblages recovered from the hanging-wall shales are consistent with a shallow marine shelf or possibly of a shelf-slope setting (chap. 12). The interbedded massive and slaty argillites were originally deposited as relatively quiescent silty, organic-rich dolomitic muds above the carbonate compensation depth, which received periodic influxes of very fine grained clastic sediments.

Once restricted, anoxic, bottom-water conditions were established, the Greens Creek area became a locus of intense microbial activity. Supporting evidence of bacterial sulfate reduction includes the high organic carbon content and the locally enriched sulfur and carbonate content of the shales, as well as the anomalously light sulfur and carbon isotope values of sulfides and carbonates in the shales (chaps. 8, 10). This supplied a steadily increasing component of biogenically reduced sulfur to the ore-forming system at the base of the shales. As the pore water being supplied at the base of the shales became dominated by biogenically reduced hydrogen sulfide (H_2S), barite precipitation ceased, marking the onset of the main stage of sulfide ore formation. Concurrent with the change of the pore fluids in the shales to more reduced conditions, the accumulation of the shale cap acted as an insulating blanket to the hydrothermal system. As the shale cap grew and the hydrothermal system intensified, temperatures in the footwall rose to the point where significant quantities of iron, lead, and zinc were carried in the ore fluid as chloride complexes. The striking ore stratigraphic shift from early precious-metal-rich and base-metal-poor white ores to the main-stage massive pyritic and base-metal-rich ores requires the shift from an initial low-temperature ore fluid with H_2S -complexed metals to a higher temperature fluid in which base metals, carried as chloride complexes, predominate. The presence of sedimentary carbonate bodies in the footwall and the abundance of carbonate alteration at Greens Creek further require that the fluid was buffered to near neutral pH. Numerous studies on metal solubility in volcanogenic massive sulfide deposits and recent sea-floor hydrothermal systems indicate that the cross-over temperature of H_2S -complex-dominated to Cl^- -complex-dominated fluids at salinities and H_2S contents typical of volcanogenic massive sulfide deposits, occurs at roughly 300°C (Hannington and Scott, 1989; Huston and Large, 1989; Large and others, 1989; Herzig and others, 1993). A variety of indirect constraints on temperature ($^{40}Ar/^{39}Ar$ closure temperature of $2M_1$ muscovite, conodont CAIs of 5 to 5.5, lack of carbonate and organic carbon isotopic re-equilibration, sphalerite-galena sulfur isotope pairs; chaps. 8, 10, 12) at Greens Creek suggest that maximum temperature during either the mineralizing event or Cretaceous regional metamorphism was no greater than about 275–350°C.

As the temperature of the ore fluid increased, a greater dissolved load of base metals percolated upward to the base

of the shale cap where it mixed with much cooler pore water containing abundant biogenically reduced sulfur. During this main stage of massive sulfide formation, massive pyritic and base-metal-rich sulfides grew by inflation beneath the shales. The very low aspect ratio of the deposit (great length to thickness) and the exceptionally large and diffuse nature of the footwall alteration zone (Taylor, Newkirk, and others, 1999; Anderson and Taylor, 2000; Anderson and Taylor, unpub. data, 2000), suggest that the precipitation of massive sulfides by mixing and cooling occurred over a broad area. Thus, the tabular, sheetlike morphology of the orebodies is a result of unfocused upflow of the hydrothermal fluids and probably multiple centers of thermal activity.

As described for the West orebody (chap. 6), areas with the hottest temperatures and greatest fluid flow are characterized by greater accumulations of copper-arsenic-rich pyritic ores centered over thick footwall sections of intensely silica-sericite flooded proximal alteration. Within these higher temperature centers, mineral textures and metal zonation suggest that any early white ores were completely destroyed and that zone refining of metals within the growing sulfide blanket occurred (chap. 9). The presently observed footwall to hanging-wall progression of white, to massive pyritic, to massive base-metal-rich ore types, therefore, reflects the transgression and destruction of the early white ores by the main-stage sulfide ores as the hydrothermal system reached its thermal maximum. Such a progression is consistent with an early, H_2S -dominated, precious-metal and barium-rich fluid evolving to a higher temperature main-stage fluid characterized by much higher base-metal and lower precious-metal contents. The steady increase in the proportion of biogenically reduced sulfur supplied to the locus of sulfide precipitation is supported by the upward progression from isotopically heavy to light $\delta^{34}S$ values through the ore stratigraphy (chap. 10). As peak thermal conditions were attained, metals such as Au, Sb, Hg, Tl, Mo, and Ag were zone refined upward and outward into the base-metal-rich massive sulfides against the hanging wall, leaving proximal pyritic massive sulfides enriched in copper, arsenic, nickel, and cobalt (chap. 9). Mineralogically, this resulted in the development of subhedral to euhedral arsenian pyrite-arsenopyrite along the fringes of clasts and in areas of greater permeability in the proximal ores and expulsion of the base-metal sulfides outward in the pile.

As the Greens Creek hydrothermal system matured, ongoing sedimentation and lithification of the shales, coupled with precipitation of gangue minerals, gradually choked off fluid flow through the accumulated sulfide body (fig. 1C). Additionally, the eventual depletion of palatable organic matter in the hanging-wall shales may have decreased the supply of organically reduced sulfur. A combination of these factors led to the final decline in ore formation. As temperatures decreased after peak ore deposition, the system was swamped with paragenetically late hydrothermal carbonate gangue. Outward zonation from stoichiometric dolomite to more iron- and manganese-rich dolomite (Taylor, Newkirk, and others, 1999; Anderson and Taylor, 2000; Anderson and Taylor, unpub.

data, 2000) occurred as the supply of H_2S to the hydrothermal system waned. In the final stages of Late Triassic rifting, tapping of the underlying mafic-ultramafic heat sources occurred, resulting in the voluminous extrusion of the Hyd Group basalt flows onto the argillites.

Although efforts to establish an absolute age of mineral formation at Greens Creek failed, an age of alteration of an ultramafic sill with associated Greens Creek-like mineralogy and metal geochemistry was obtained for an occurrence in the Triassic belt on the south end of Admiralty Island. The 210.7 ± 0.3 Ma ($^{40}Ar/^{39}Ar$ – fuchsite) age of alteration at this occurrence (Taylor, Philpotts, Sutley, and others, 1995; Taylor, Philpotts, Hall, and Wakeman, 1995; chaps. 2, 12) represents the closest available estimate for the age of main-stage hydrothermal fluid flow at Greens Creek. Our best constraint for the age of extrusion of the Hyd basalts onto the Hyd argillites comes from whole-rock radiogenic isotope data and indicates an approximately 215 Ma age of emplacement (chap. 12). Figures 1A–C represent graphic illustrations of the early, main-stage, and late periods of the development, growth, and death of the Greens Creek ore-forming environment.

Post-Mineral Modifications to the Greens Creek Orebodies

The final event to affect the Greens Creek deposit was the Jurassic through Cretaceous regional mid-greenschist facies metamorphism that occurred during accretion of the Alexander terrane to the North American margin. During this event the morphology, mineralogy, and tenor of the orebody was significantly modified. Tight isoclinal F2 folding resulted in significant shortening and local thickening of the orebody. These were followed by open F3 folds, which further thickened ore in fold axes (see chap. 7). The absolute age of these two deformation events is unknown; however, folding is clearly younger than the Norian Triassic argillites of the hanging wall. The orientation of these fabrics is consistent with regional northwest-vergent thrust faults that are thought to have formed during Jurassic–Cretaceous collision of the Alexander terrane with the continental margin (Haeussler and others, 1999). High-angle strike-slip movement along the Maki fault and its subsidiaries is generally thought to have occurred during transcurrent movement of the terrane during early Tertiary time. Although Maki faulting significantly complicated the morphology of the deposit, little modification of the mineralogy or tenor of the ore occurred.

Textural studies indicate that semiductile shearing of the ores occurred during Jurassic–Cretaceous metamorphism. Rigid blocks of massive pyritic ore acted as buttresses around which the more ductile base-metal-rich ores flowed. This resulted in near-complete (about 70 percent) recrystallization of pyrite and base-metal sulfides and imparted a tectonic banding to the base-metal-rich ores. Brittle failure occurred within the rigid blocks of massive pyritic ore, producing breccia textures consisting of angular clasts of massive pyrite in matrix of pyrite, base-metal sulfides, and gangue. Recrystallization of the

sulfides also occurred within the sulfide clasts, but to a much lesser degree than in the plastically deformed and banded base-metal-rich ores. Thus, a full range of primary, partially recrystallized, fully recrystallized, and remobilized sulfide textures are preserved (chap. 9).

Mineralogically, the primary ores consist of very fine grained, framboidal, colloform, dendritic, and botryoidal, brassy-colored pyrite intimately intergrown with sphalerite, galena, tetrahedrite, rarely chalcopyrite, and an unidentified and probably variable suite of lead-antimony sulfosalts. Partial recrystallization results in an increase in crystal size and coalescence of the primary pyrite into large, spongy-textured masses. The base-metal sulfides begin to form mineralogically discrete anhedral masses, and pyrite aggregates form subhedral masses of pyrite with spongy interiors and inclusion-free, growth-zoned margins. Complete recrystallization results in a metamorphic “cleaning” of the primary- and spongy-textured pyrite and formation of very large, bright-colored, inclusion-free, euhedral pyrites in matrix of anhedral tetrahedrite, sphalerite, chalcopyrite, and galena, argentite, and acanthite. In the extreme case, polygonal aggregates of near-monomineralic pyrite are formed. Grains of yellow gold appear entirely included within pyrite masses or on the margins of crystals, and the exotic lead-antimony sulfosalts are absent. Metamorphic remobilization is characterized by cross-cutting veinlets and fractures filled with chalcopyrite, sphalerite, galena, tetrahedrite, pyrargyrite, argentite, acanthite, free gold, and electrum and an increased abundance of quartz and dolomite gangue.

The process of metamorphic recrystallization and remobilization of the primary ores is reflected in the correlation between the variety and abundance of trace metals in sulfides and the textural state of the sulfides. The primary-textured ores, and specifically pyrite, contain elevated abundances of Sb, As, Hg, Mo, Tl, Ni, Co, V, Ag, and Au, whereas in the recrystallized and remobilized ores, the number of trace metals in pyrite decreases and the post-recrystallization mineral residence of a given trace metal becomes predictable based on the stoichiometry of the major sulfide phases. For example, pyrite becomes almost trace-metal free; mercury resides in sphalerite; antimony, arsenic, and silver reside predominantly in tetrahedrite and pyrargyrite; and gold forms discrete grains.

Although the Jurassic–Cretaceous metamorphism is not related to the genetic origin of the Greens Creek deposit, it is of major importance with regard to the distribution of metal grades throughout the deposit as well as the recoverability of those metals during the beneficiation process. The highest-grade ore intercepts in the mine occur where high-grade primary-textured ores are shot through with densely packed, remobilized veinlets consisting of electrum and silver sulfosalts minerals. Recrystallization of the ores greatly improves the recovery of metals in the mill and allows for blending of ore types, which decreases the content of deleterious trace metals in the resulting concentrates. Unblended primary ores result in concentrates with high trace-metal contents and poor recovery of precious metals.

Discussion

Greens Creek presents an interesting case of a poly-metallic massive sulfide deposit at which the immediate footwall was a cold, basaltic volcanoclastic pile irregularly mantled by carbonate rocks at the time of ore formation. In contrast to the commonly modeled case in VMS deposits where the heat source is attributed to subvolcanic intrusions and related active volcanism, at Greens Creek the heat source(s) for the hydrothermal system were hypabyssal mafic-ultramafic intrusions associated with Late Triassic rifting (chap. 12). The rift succession in southeastern Alaska contains a number of Triassic-aged trondhjemite and gabbro-peridotite intrusions (Gehrels and Berg, 1992; Haeussler and others, 1999), and there is a striking spatial correlation between mafic-ultramafic dikes, sills, serpentinite bodies, and mineral occurrences in the Late Triassic mineral belt (Taylor and others, 2000). Several of these occurrences provide evidence that some of the mafic-ultramafic intrusions were emplaced at very shallow levels. A basaltic dike of probable Late Triassic age associated with the Keku Inlet Ladder Vein occurrence (see fig. 2 in chap. 2) has peperitic margins indicative of intrusion into wet sediments. Similarly, mineralized basaltic dikes in Gambier Bay (see fig. 2 in chap. 2) display a composite texture in the form of chilled margins and vesicular interiors. One dike pinches from about 2-m thickness down to 0.2-m thickness, at which point the dike spreads horizontally to the enclosing host rocks and forms bulbous structures similar to pillow basalts. Presumably the dike rose to a position at or very near the paleo sea floor where it then spread laterally due to a lack of confinement.

Both of these examples suggest that during Late Triassic rifting, mafic-ultramafic intrusives were emplaced near the sediment/water interface. We believe that gabbroic sills significantly thicken the footwall phyllite at Greens Creek, and both altered and fresh serpentinites are present in the immediate footwall and at depth. Significantly, compared to other Late Triassic mineral occurrences, outcrop (chap. 4) and geophysical data (chap. 5) indicate that the Greens Creek mine area contains a high concentration of gabbro and serpentinite intrusive bodies. The gabbros are linked geochronologically and geochemically to Late Triassic igneous suites, as are the altered ultramafic bodies underground and on Mariposite Ridge (see fig. 1 in chap. 2) immediately north of the mine (chaps. 11, 12). The combination of the concentration of intrusive heat sources emplaced into a locally restricted, anoxic, organic-rich, shale-filled rift basin may represent the key conditions required for the development of a world-class deposit at Greens Creek.

Taking into account the wide error bars, we note that the available geochronological constraints on the timing of mineralization and emplacement of both the igneous and sedimentary rocks are broadly consistent with the progression of events previously outlined. The onset of rifting at 225 ± 3 Ma, as established by the first extrusive event, and sedimentation of the hanging wall shales at 220.7 ± 4.4 Ma (based on conodonts)

followed by alteration of serpentinite at 210.7 ± 0.3 Ma (Taylor, Philpotts, Sutley, and others, 1995; Taylor, Philpotts, Hall, and Wakeman, 1995) provides the window of time during which the Greens Creek deposit must have formed (chap. 12). Considered independently of geologic constraints, our strontium-neodymium-lead isotopic age data are not precise enough to provide resolution to the emplacement sequence of the gabbros and serpentinites into the footwall and extrusion of the Hyd Group basalts above the argillites. Geologic relationships are consistent with emplacement of gabbros into the footwall as sediments accumulated, causing leaching and alteration of associated serpentinites. Extrusion of the Hyd basalts marks the end of sediment accumulation. Igneous activity ceased following stoping of the gabbros up to the base of the Hyd basalt flows. Our mineral and whole-rock samarium-neodymium data on gabbros in the mine area and the ~ 215 -Ma age of extrusion of the Hyd basalts at the top of the section (chap. 12) are broadly consistent with geologic relationships.

Another enigmatic feature of the Greens Creek deposit that is contrary to conventional thinking is the relationship between the tectonic setting, the geochemical nature of the observed host rocks, and the metal endowment of the ores. Comparisons of metal content at Greens Creek to other volcanic-associated massive sulfide deposits worldwide suggest that the zinc-lead-rich polymetallic metal suite present at Greens Creek is most like the metal suites found in the Kuroko district of Japan, the Bathurst district of Canada, and the deposits of the Mt. Read volcanic belt in Tasmania (Franklin and others, 1981; Large, 1992). However, in marked contrast to Greens Creek, which has a dominantly basaltic footwall, all of these districts are dominated by the presence of thick rhyolitic volcanic piles and associated felsic subvolcanic intrusions that are generally considered to be the major sources of metals. Long-established classification schemes, based on metal endowments of VMS deposits of all ages, equate high zinc/copper and lead/copper ratios to felsic igneous source rocks. Copper-rich deposits with high gold/silver ratios are attributed to basaltic source rocks (Hutchinson, 1973; Franklin and others, 1981; Ohmoto and others, 1983). Similarly, a recently suggested classification scheme based on dominant host-rock compositions (Barrie and Hannington, 1999) does not apply well to Greens Creek. All three of the host-rock classes that involve a major mafic component (their mafic, bimodal-mafic, and mafic siliciclastic divisions) are characterized by districts and deposits that contain copper- or copper-zinc-rich metal assemblages. It is noteworthy that the mafic siliciclastic division describes the major host-rock lithologies present at Greens Creek. Further, the mafic siliciclastic division includes the Windy Craggy deposit (the world's largest Besshi-type deposit; Peter and Scott, 1999), which we suggest is metallogenically related to Greens Creek and occupies a position in the northernmost, deepest portion of the Late Triassic rift. However, Greens Creek is out of place in a division that is dominated by copper-rich deposits characterized by the Besshi-type of volcanic-associated massive sulfides.

Perhaps the reason for the unusual nature of the Greens Creek deposit is that the hydrothermal fluids may have derived the majority of their metals from the mafic-ultramafic intrusive rocks in the footwall and from the immediately overlying shales, rather than from the cold basaltic volcanoclastic pile. Available trace metal (chap. 9) and sulfur and lead isotopic data (chap. 10) appear to suggest this possibility. The extreme alteration of serpentinites in the mine area and the cobalt-nickel-chromium enrichments of the massive pyritic ores point to leaching of the mafic-ultramafic intrusive rocks. Sulfur isotopic studies implicate a major contribution of reduced sulfur-bearing fluids from the hanging-wall shales, as do the strong arsenic, antimony, mercury, molybdenum, and vanadium enrichments of the ores. Finally, the radiogenic isotopic data show that ore metals were derived from two major sources, an unradiogenic source similar to the mafic-ultramafic rocks in the mine area, and an undetermined radiogenic source. The ore-lead isotopic array clearly shows derivation of unradiogenic lead from a field of whole-rock lead determinations defined by the comagmatic, Late Triassic gabbros and basalts of the Hyd Group (chap. 10). Samarium-neodymium isotopic data also suggest a comagmatic relationship for the entire mafic-ultramafic suite (chap. 11). Derivation of the radiogenic lead component of the ores remains inconclusive. The data are permissive of the contribution of radiogenic lead from the hanging-wall argillites. However, contributions from serpentinites, the Permian Canyery Formation shales, or from older Paleozoic rocks lower in the section cannot be ruled out at this time.

We believe the major reason why Greens Creek is difficult to reconcile with currently favored models for VMS deposits is because it represents a transitional type of massive sulfide (Taylor, Newkirk, and others, 1999). Early genetic descriptions for Greens Creek included proponents of a SEDEX model (Dressler and Dunbire, 1981) as well as of a VMS model (Newberry and others, 1997). As previously discussed, attempts to classify Greens Creek based on metal ratios or on composition of the host rocks leads to ambiguities. A review of the major features of the Greens Creek deposit shows that many of its distinctive characteristics can be placed in either the VMS or SEDEX classes. VMS characteristics include a zinc-lead-silver-gold-copper-rich metal endowment similar to the Kuroko-type in an essentially continuous, single orebody. Ore types display distinct lateral and vertical zonation that indicate thermal and geochemical evolution of a fluid during a single mineralizing event. The thickest portions of the orebody are dominated by massive pyritic ores that retain primary textures indicative of growth by zone refining and replacement of earlier formed minerals. Further, both the ore and gangue mineral assemblages at Greens Creek are strikingly similar to recent descriptions of active sea-floor systems generally described as modern analogues to the Kuroko-type of deposits.

Although volcanism was not active immediately before or during ore formation, Greens Creek sits on an intensely altered mafic volcanic footwall that has a zoned alteration profile typical of VMS systems (Taylor, Newkirk, and others, 1999; Anderson and Taylor, 2000; Anderson and Taylor,

unpub. data, 2000). However, the deposit also has numerous characteristics usually associated with the SEDEX class. The complete absence of felsic igneous rocks is striking, and the intrusion of mafic-ultramafic stocks and sills into a cold footwall is more typical of SEDEX deposits. Similarly, the lack of a focused feeder system and presence of a huge alteration envelope containing chromium and barium-rich silicates such as fuchsite, oellacherite, and celsian, and a complexly zoned carbonate alteration assemblage are more typical of SEDEX. Perhaps even more striking is the abundant evidence that suggests Greens Creek formed primarily during diagenesis of the graphitic, pyritic, hanging-wall argillite; geochronologic and isotopic evidence suggests that ore formation occurred during and after deposition of the shale cap. Crosscutting relationships and ore textures are consistent with growth by inflation beneath, and diagenetic replacement of, the shales during sedimentation. Additionally, sulfur isotope values are unusually low and are unlike either VMS or SEDEX values. Indeed, the epigenetic replacement textures in the footwall sedimentary carbonate bodies and the sulfur isotopic characteristics of the ores are most similar to the carbonate-hosted massive sulfide deposits of the Irish Midlands ore field and of the MVT deposits of the U.S. Midcontinent. Greens Creek, therefore, exhibits a hybrid set of characteristics that places it within a spectrum of exhalative- to replacement-style deposits rather than within a single general category.

A major reason for the hybrid characteristics of the Greens Creek deposit may be reconciled by examination of the Late Triassic tectonic setting. If, as proposed, the Late Triassic rift in southeastern Alaska formed by oblique propagation into the Alexander terrane (Taylor, 1997; Taylor, Philpotts, Sutley, and others, 1995; Taylor, Philpotts, Hall, and Wakeman, 1995; Taylor, Premo, and Meier, 1999; Taylor, 2000), then a metallogenic environment would have existed that is common to both VMS and SEDEX environments. Recent work relating the specific nature of both ancient (Barrett and MacLean, 1999) and modern (Hannington and others, 1986; Halbach and others, 1993; Binns and others, 1993; Fouquet and others, 1993; Stoffers and others, 1999) VMS deposits to the location (continental margin, oceanic) and maturity level of the rift basin may explain the variation in the mineral occurrences of the Late Triassic belt in southeastern Alaska. For example, deposits that form at the tip of rifts propagating into mature arcs (Binns and others, 1993; Fouquet and others, 1993) or where nascent intra-continental rifts split arcs, such as Japan, are generally Kuroko-type and are associated with arc-type or heavily calc-alkaline-contaminated tholeiitic lavas (Barrett and MacLean, 1999). Deposits that form in this setting correspond to the bimodal-mafic division of Barrie and Hannington (1999). Deposits that form landward from the propagating rift or on land in the early stages of rifting have an epithermal or hot springs style of expression (for example, Stoffers and others, 1999; deposits of the Taupo volcanic zone). Deposits that form in the deeper, seaward portion of propagating rifts or in mature rifts are more likely to be copper-zinc-rich and may be associated with distal clastic sediments such as Windy Craggy (Peter and Scott,

1999) and the Besshi deposits. The deposits in the mature rift settings are usually associated with primitive mafic melts that are forming segments of new oceanic crust that may or may not show contamination by melting and incorporation of the rifted crust (Barrett and MacLean, 1999; the mafic-siliciclastic division of Barrie and Hannington, 1999). That such a variation of deposit styles, associated with predictably varying suites of igneous rocks, can be found in a single rift propagating into a mature arc or continental margin provides confirmation for the lithochemical and deposit variability of the occurrences in southeastern Alaska.

The segment of a propagating rift that we feel is analogous to the Greens Creek tectonic setting is that portion seaward of the propagating tip of the rift basin and landward of the point at which new oceanic crust begins to form. Within this segment, bimodal volcanism is characterized by peralkaline rhyolites and tholeiitic basalts that exhibit varying degrees of crustal contamination (chap. 2). Moving seaward, the rhyolites disappear from the section and the mafic melts become less arc-contaminated and more similar to ocean-ridge basalts, commonly EMORB or “transitional” basalts. The seaward transition may or may not evolve into a sediment-covered ridge; however, the transition represents the change from a bimodal-mafic to a mafic-siliciclastic metallogenic environment. This transition is exactly like the observed changes in the tectonostratigraphic setting described between the Keku Inlet, where Greens Creek-like occurrences are hosted in dolomitic limestone overlying peralkaline rhyolites, and Greens Creek, where rhyolites are absent, the rift has become sediment-covered, and mafic-ultramafic melts are still heavily contaminated by the Alexander terrane basement that they rise through (chap. 2).

We suggest that the specific portion or period of an evolving rift—where lithologies have transitioned to mafic-ultramafic rocks intruding through and being heavily contaminated by a mature arc, covered by distal clastic sedimentation—is strikingly similar to the failed epicontinental rift tectonic setting common to most SEDEX deposits. At the time of Late Triassic rifting, the Alexander terrane was an inactive continent-sized landmass of wholly oceanic affinities, cored by sialic Proterozoic and lower Paleozoic crust. At the latitude of Greens Creek, rifting resulted in the formation of a small (second order?), restricted, anoxic, and very organic rich sedimentary basin, which was intruded by rift-related mafic-ultramafic intrusive rocks. This specific, SEDEX-like metallogenic setting occurred within a propagating rift, which on a larger scale is more akin to the metallogenic setting common to many VMS deposits.

References Cited

- Anderson, V.M., and Taylor, C.D., 2000, Alteration mineralogy and zonation in host rocks to the Greens Creek deposit, southeastern Alaska: Geological Society of America Cordilleran Section Meeting, Abstracts with Programs, v. 32, no. 6, p. A-2.
- Barrett, T.J., and MacLean, W.H., 1999, Volcanic sequences, lithochemistry, and hydrothermal alteration in some bimodal volcanic-associated massive sulfide systems, *in* Barrie, C.T., and Hannington, M.D., eds., Volcanic-associated massive sulfide deposits—Processes and examples in modern and ancient settings: Society of Economic Geologists Reviews in Economic Geology, v. 8, p. 101–127.
- Barrie, C.T., and Hannington, M.D., 1999, Classification of volcanic-associated massive sulfide deposits based on host-rock composition, *in* Barrie, C.T., and Hannington, M.D., eds., Volcanic-associated massive sulfide deposits—Processes and examples in modern and ancient settings: Society of Economic Geologists Reviews in Economic Geology, v. 8, p. 1–11.
- Berg, H.C., 1973, Geology of Gravina Island, Alaska: U.S. Geological Survey Bulletin 1373, 41 p.
- Binns, R.A., Scott, S.D., Bogdanov, Y.A., Lisitzin, A.P., Gordeev, V.V., Gurvich, E.G., Finlayson, E.J., Boyd, T., Dotter, L.E., Wheller, G.E., and Muravyev, K.G., 1993, Hydrothermal oxide and gold-rich sulfate deposits of Franklin Seamount, western Woodlark basin, Papua New Guinea: Economic Geology, v. 88, p. 2122–2153.
- Dressler, J.S., and Dunbire, J.C., 1981, The Greens Creek ore deposit, Admiralty Island, Alaska: Canadian Institute of Mining and Metallurgy Bulletin, v. 74, no. 833, p. 57.
- Fouquet, Yves, Von Stackelberg, U., Charlou, J.L., Erzinger, J., Herzig, P.M., Muhe, R., and Wiedicke, M., 1993, Metallogensis in back-arc environments—The Lau basin example: Economic Geology, v. 88, p. 2154–2181.
- Franklin, J.M., Lydon, J.W., and Sangster, D.F., 1981, Volcanic-associated massive sulfide deposits, *in* Skinner, B.J., ed., Economic geology: Seventy-fifth anniversary volume, 1905–1980, p. 485–627.
- Gehrels, G.E., and Berg, H.C., 1992, Geologic map of southeastern Alaska: U.S. Geological Survey Miscellaneous Investigations Series Map I-1867, scale 1:600,000.
- Gehrels, G.E., and Berg, H.C., 1994, Geology of southeastern Alaska, *in* Plafker, George, and Berg, H.C., eds., The geology of Alaska: Boulder, Colorado, Geological Society of America, Decade of North American Geology, v. G1, p. 451–468.
- Gehrels, G.E., Saleeby, J.B., and Berg, H.C., 1987, Geology of Annette, Gravina, and Duke Islands, southeastern Alaska: Canadian Journal of Earth Sciences, v. 24, p. 866–881.
- Goodfellow, W.D., Lydon, J.W., and Turner, R.J.W., 1993, Geology and genesis of stratiform sediment-hosted (SEDEX) zinc-lead-silver sulphide deposits, *in* Kirkham, R.V., Sinclair, W.D., Thorpe, R.I., and Duke, J.M., eds., Mineral deposit modeling: Geological Association of Canada, Special Paper 40, p. 201–251.

- Haeussler, P.J., Karl, S.M., Mortensen, J.K., Layer, Paul, and Himmelberg, G.R., 1999, Permian and mid-Cretaceous deformation of the Alexander terrane on Admiralty and Kupreanof Islands, southeastern Alaska [abs.]: Geological Society of America Abstracts with Programs v. 31, no. 6, p. A-60.
- Halbach, Peter, Pracejus, B., and Marten, A., 1993, Geology and mineralogy of massive sulfide ores from the central Okinawa trough, Japan: *Economic Geology*, v. 88, p. 2210-2225.
- Hannington, M.D., Bleeker, W., and Kjarsgaard, I., 1999, Sulfide mineralogy, geochemistry, and ore genesis of the Kidd Creek deposit—Part I, North, Central, and South orebodies: *Economic Geology Monograph 10*, p. 163-224.
- Hannington, M.D., Peter, J.M., and Scott, S.D., 1986, Gold in sea-floor polymetallic sulfide deposits: *Economic Geology*, v. 81, p. 1867-1883.
- Hannington, M.D., and Scott, S.D., 1989, Gold mineralization in volcanogenic massive sulfides—Implications of data from active hydrothermal vents on the modern sea floor: *Economic Geology Monograph 6*, p. 491-507.
- Herzig, P.M., Hannington, M.D., Fouquet, Y., Von Stackelberg, U., and Petersen, S., 1993, Gold-rich polymetallic sulfides from the Lau back-arc and implications for the geochemistry of gold in sea-floor hydrothermal systems of the southwest Pacific: *Economic Geology*, v. 88, p. 2182-2209.
- Huston, D.L., and Large, R.R., 1989, A chemical model for the concentration of gold in volcanogenic massive sulphide deposits: *Ore Geology Reviews*, v. 4, p. 171-200.
- Hutchinson, R.W., 1973, Volcanogenic sulfide deposits and their metallogenic significance: *Economic Geology*, v. 68, p. 1223-1246.
- Kerr, D.J., and Gibson, H.L., 1993, A comparison of the Horne volcanogenic massive sulfide deposit and intracauldron deposits of the mine sequence, Noranda, Quebec: *Economic Geology*, v. 88, p. 1419-1442.
- Large, R.R., 1992, Australian VHMS deposits—Features, styles, models: *Economic Geology*, v. 87, p. 471-510.
- Large, R.R., Huston, D.L., McGoldrick, P.J., and Ruxton, P.A., 1989, Gold distribution and genesis in Australian volcanogenic massive sulfide deposits and their significance for gold transport models: *Economic Geology Monograph 6*, p. 520-536.
- Leach, D.L., and Sangster, D.F., 1993, Mississippi Valley-type lead-zinc deposits, in Kirkham, R.V., Sinclair, W.D., Thorpe, R.I., and Duke, J.M., eds., *Mineral deposit modeling: Geological Association of Canada, Special Paper 40*, p. 289-314.
- Morton, R.L., and Franklin, J.M., 1987, Two-fold classification of Archean volcanic-associated massive sulfide deposits: *Economic Geology*, v. 82, p. 1057-1064.
- Muffler, L.J.P., 1967, Stratigraphy of the Keku Islets and neighboring parts of Kuiu and Kupreanof Islands southeastern Alaska: U.S. Geological Survey Bulletin 1241-C, 52 p.
- Newberry, R.J., Crafford, T.C., Newkirk, S.R., Young, L.E., Nelson, S.W., and Duke, N.A., 1997, Volcanogenic massive sulfide deposits of Alaska, in Goldfarb, R.J., and Miller, L.E., eds., *Mineral deposits of Alaska: Economic Geology Monograph 9*, p. 120-150.
- Ohmoto, Hiroshi, Mizukami, M., Drummond, S.E., Eldridge, C.S., Pisutha-Arnond, V., and Lenagh, T.C., 1983, Chemical processes of Kuroko formation, in Ohmoto, Hiroshi, and Skinner, B.J., eds., *The Kuroko and related volcanogenic massive sulfide deposits: Economic Geology Monograph 5*, p. 570-604.
- Peter, J.M., and Scott, S.D., 1999, Windy Craggy, northwestern British Columbia—The world's largest Besshi-type deposit, in Barrie, C.T., and Hannington, M.D., eds., *Volcanic-associated massive sulfide deposits—Processes and examples in modern and ancient settings: Society of Economic Geologists Reviews in Economic Geology*, v. 8, p. 261-295.
- Solomon, Michael, and Groves, D.I., 1994, *The geology and origin of Australia's mineral deposits: Oxford, Oxford Science Publications*, 951 p.
- Stoffers, Peter, Hannington, M., Wright, I., Herzig, P., de Ronde, C., and Shipboard Scientific Party, 1999, Elemental mercury at submarine hydrothermal vents in the Bay of Plenty, Taupo volcanic zone, New Zealand: *Geology*, v. 27, no. 10, p. 931-934.
- Taylor, C.D., 1997, An arc-flank to back-arc transect—Metallogeny of Late Triassic volcanogenic massive sulfide occurrences of the Alexander terrane, southeastern Alaska and British Columbia: [extended abs.] in *Society of Economic Geologists Neves Corvo Field Conference, May 7-17, 1997, Lisbon, Portugal, Abstracts and Programs volume*, p. 68.
- Taylor, C.D., Newkirk, S.R., Hall, T.E., Lear, K.G., Premo, W.R., Leventhal, J.S., Meier, A.L., Johnson, C.A., and Harris, A.G., 1999, The Greens Creek deposit, southeastern Alaska—A VMS-SEDEX hybrid, in Stanley, C.J., and others, eds., *Mineral deposits—Processes to processing: Rotterdam, Balkema*, v. 1, p. 597-600.
- Taylor, C.D., Philpotts, J.A., Hall, T.E., and Wakeman, B.W., 1995, New information on the geochemistry, age, and tectonic history of Late Triassic volcanic host rocks and associated massive sulfide occurrences of the Alexander terrane, southeast Alaska [abs.]: *Alaska Miners Association Conference, Juneau, Program with Abstracts*, p. 31-32.

Taylor, C.D., Philpotts, J., Sutley, S., Gent, C., Harlan, S., Premo, W., Tatsumoto, M., Emsbo, P., and Meier, A., 1995, Geochemistry of Late Triassic volcanic rocks and age of alteration associated with volcanogenic massive sulfide occurrences, Alexander terrane, southeast Alaska, *in* Geology and ore deposits of the American Cordillera, A Symposium, Reno, Nev., 1995: Reno, Nev., Geological Society of Nevada, p. A74.

Taylor, C.D., Premo, W.R., and Lear, K.G., 2000, The Greens Creek massive sulfide deposit—Premier example of the Late Triassic metallogeny of the Alexander terrane, southeastern Alaska and British Columbia [abs.]: Geological Society of America Abstracts with Programs, v. 32, no. 6, p. A-71.

Taylor, C.D., Premo, W.R., and Meier, A.L., 1999, The Late Triassic metallogeny of the Alexander terrane, southeastern Alaska and British Columbia [abs.]: Geological Society of America Abstracts with Programs, v. 31, no. 6, p. A-101.

Publishing support provided by:
Denver Publishing Service Center

For more information concerning this publication, contact:
Team Chief Scientist, USGS Central Mineral Resources
Box 25046, Mail Stop 973
Denver, CO 80225
(303) 236-1562

Or visit the Central Mineral Resources Team Web site at:
<http://minerals.cr.usgs.gov/>



ISBN 978-141132622-4



9 781411 326224